Attachment 3

Evaluation of Sea Level Rise Effects using UNTRIM San Francisco Bay-Delta Model

BAY DELTA CONSERVATION PLAN

UnTRIM San Francisco Bay-Delta Model Sea Level Rise Scenario Modeling Report

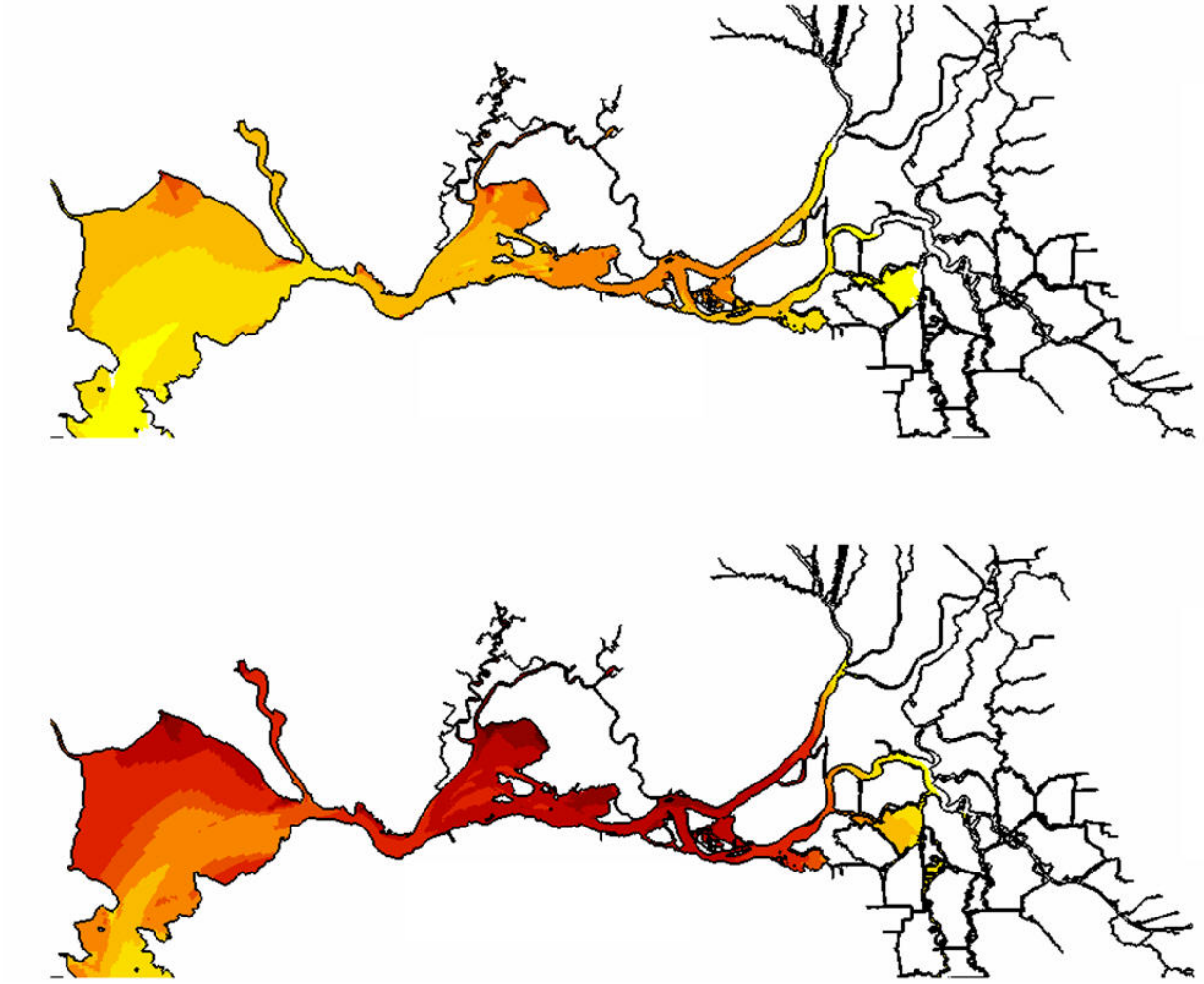

Prepared For:

Science Applications International Corporation
and
California Department of Water Resources

Prepared By:

Michael L. MacWilliams, Ph.D.

Edward S. Gross, Ph.D.

FINAL REPORT

July 16, 2010

[This page intentionally left blank.]

Executive Summary

As part of the Bay Delta Conservation Plan (BDCP), future conditions simulations are planned which will need to incorporate the potential effects of sea level rise on salinity intrusion in the Sacramento-San Joaquin Delta. In support of this effort, three-dimensional hydrodynamic and salinity simulations using the UnTRIM Bay-Delta model were made to provide a reference condition for re-calibration of appropriate dispersion factors for the 1-D and 2-D models which are the primary tools being used in the BDCP planning process. The 3-D UnTRIM Bay-Delta model provides an already established and well-documented hydrodynamic model which is suitable for a detailed assessment of the potential salinity impacts of Sea Level Rise (SLR) in San Francisco Bay and the Sacramento-San Joaquin Delta.

The UnTRIM Bay-Delta model used for this project builds on previous applications (e.g., MacWilliams et al., 2007; MacWilliams et al., 2008; MacWilliams et al., 2009), and was further refined as part of this study to increase the model grid resolution in Suisun Marsh. The UnTRIM Bay-Delta model was used to simulate hydrodynamics and salinity under baseline conditions and for six levels of SLR. The baseline simulation period spans from October 15, 2001 through January 1, 2003. The analysis of sea level rise impacts spans a one-year period from January 1, 2002 through January 1, 2003. This report presents the results of the sea level rise impacts on salinity in San Francisco Bay and the Sacramento-San Joaquin Delta that were predicted using the UnTRIM Bay-Delta model. The relative contributions of different transport processes, including gravitational circulation and tidal dispersion, to salt intrusion were investigated with a salt flux analysis. A full set of hydrodynamic and salinity model results were also provided to CH2M Hill for use in recalibration of the DSM2 and RMA2 models to incorporate the effects of SLR into the lower dimensional models being used as part of the BDCP technical studies.

Questions, comments, or suggestions for future improvements to the UnTRIM Bay-Delta model should be addressed to Michael MacWilliams at: michael@rivermodeling.com.

Table of Contents

Abbreviations

1D	One-Dimensional
2D	Two-Dimensional
3D	Three-Dimensional
BBID	Byron Bethany Irrigation District
BDCP	Bay Delta Conservation Plan
CCWD	Contra Costa Water District
CDEC	California Data Exchange Center
CVP	Central Valley Project
DICU	Delta Island Consumptive Use
DFG	Department of Fish and Game
DRMS	Delta Risk Management Strategy
DSS	Data Storage System
DWR	Department of Water Resources
DWSC	Deep Water Ship Channel
EC	Electrical Conductivity
GLS	Generic Length Scale
IEP	Interagency Ecological Program
NOAA	National Oceanic & Atmospheric Administration
PSU	Practical Salinity Unit
SLR	Seal Level Rise
SMSCG	Suisun Marsh Salinity Control Gates
SWP	State Water Project
TRIM	Tidal, Residual, Intertidal & Mudflat Model
UnTRIM	Unstructured Tidal, Residual, Intertidal & Mudflat Model
USACE	United States Army Corps of Engineers
USBR	United States Bureau of Reclamation
USGS	United States Geological Survey
WPCP	Water Pollution Control Plant

1. Introduction

As part of the Bay Delta Conservation Plan (BDCP), future conditions simulations are planned which will need to incorporate the potential effects of sea level rise on salinity intrusion in the Sacramento-San Joaquin Delta. This report presents the results of the UnTRIM Bay-Delta model simulations of sea level rise impacts on salinity in San Francisco Bay and the Sacramento-San Joaquin Delta. The UnTRIM Bay-Delta model used for this project builds on previous applications (e.g., MacWilliams et al., 2007; MacWilliams et al., 2008; MacWilliams et al., 2009).

The report includes a brief overview of the UnTRIM Bay-Delta model, a description of the sea level rise scenarios and the sea level rise scenario results, a discussion of the regression relationships used to characterize the effects of SLR at the DSM2 and RMA2 model boundaries, and a brief summary and conclusions section. Hydrodynamic and salinity comparison figures for the 2002 baseline simulation period are included as an appendix.

This report is divided into nine major sections and one appendix:

- **Section 1. Introduction.** This section presents the project approach and objectives, as well as a summary of the scope and organization of the report.

- **Section 2. UnTRIM Bay-Delta Model Description.** This section provides a description of the UnTRIM hydrodynamic model, and an overview of the UnTRIM Bay-Delta model.

- **Section 3. Sea Level Rise Scenario Descriptions.** This section describes the sea level rise scenarios that were simulated for this study.

- **Section 4. Sea Level Rise Impacts on Daily-averaged Depth-average Salinity.** This section evaluates the impacts of sea level rise on daily-averaged depth-average salinity in San Francisco Bay and the Sacramento-San Joaquin Delta.

- **Section 5. Evaluation of Impact of Sea Level Rise on X2.** This section evaluates the impacts of sea level rise on X2.

- **Section 6. Sea Level Rise Impacts on Salinity at Continuous Monitoring Locations.** This section evaluates the impacts of sea level rise on salinity at a set of continuous monitoring stations in San Francisco Bay and the Sacramento-San Joaquin Delta.

- **Section 7. Stage and Salinity Relationships for SLR at Fort Point and Martinez.** This section presents the regression relationships developed to characterize the effects of SLR on stage and salinity at Fort Point and Martinez.

- **Section 8. Analysis of Salt Flux Mechanisms.** This section presents a detailed analysis of the effect of SLR on the mechanisms responsible for salt transport in San Francisco Bay and the Sacramento-San Joaquin Delta.

- **Section 9. Summary and Conclusions.** This section presents a brief summary of the simulation results and analysis presented in this report.

- **Appendix A. Model Comparison Figures for 2002 simulation period.** This section presents a set of hydrodynamic and salinity validation figures for the 2002 simulation period.

2. UnTRIM Bay-Delta Model Description

The primary tool used in this technical study was the three-dimensional hydrodynamic model UnTRIM (Casulli and Zanolli, 2002). A complete description of the governing equations, numerical discretization, and numerical properties of UnTRIM is presented in Casulli and Zanolli (2002; 2005), Casulli (1999), and Casulli and Walters (2000). A complete description of the UnTRIM Bay-Delta model can be found in MacWilliams et al. (2009). This section provides a brief summary of the UnTRIM hydrodynamic model formulation and a brief description of the UnTRIM Bay-Delta model.

The UnTRIM model solves the three-dimensional Navier-Stokes equations on an unstructured grid in the horizontal plane. The boundaries between vertical layers are at fixed elevations, and cell heights can be varied vertically to provide increased resolution near the surface or other vertical locations. Volume conservation is satisfied by a volume integration of the incompressible continuity equation, and the free-surface is calculated by integrating the continuity equation over the depth, and using a kinematic condition at the free-surface as described in Casulli (1990). The numerical method allows full wetting and drying of cells in the vertical and horizontal directions. The governing equations are discretized using a finite difference – finite volume algorithm. Discretization of the governing equations and model boundary conditions are presented in detail by Casulli and Zanolli (2002). All details and numerical properties of this state-of-the-art three-dimensional model are well-documented in peer reviewed literature (Casulli and Zanolli, 2002; Casulli and Zanolli, 2005).

The UnTRIM San Francisco Bay-Delta model (UnTRIM Bay-Delta model) is a three-dimensional hydrodynamic model of San Francisco Bay and the Sacramento-San Joaquin Delta, which has been developed using the UnTRIM hydrodynamic model (MacWilliams et al., 2007; MacWilliams et al., 2008; MacWilliams et al., 2009). The UnTRIM Bay-Delta model extends from the Pacific Ocean through the entire Sacramento-San Joaquin Delta (Figure 2-1). The UnTRIM Bay-Delta model takes advantage of the grid flexibility allowed in an unstructured mesh by gradually varying grid cell sizes, beginning with large grid cells in the Pacific Ocean and gradually transitioning to finer grid resolution in the smaller channels of the Sacramento-San Joaquin Delta. This approach offers significant advantages both in terms of numerical efficiency and accuracy, and allows for local grid refinement for detailed analysis of local hydrodynamics, while still incorporating the overall hydrodynamics of the larger estuary in a single model. The UnTRIM Bay-Delta model has been calibrated using water level, flow, and salinity data collected in San Francisco Bay and the Sacramento-San Joaquin Delta (MacWilliams et al., 2008; MacWilliams et al., 2009).

The model calibration and validation results (MacWilliams et al., 2008; MacWilliams et al., 2009) demonstrate that the UnTRIM Bay-Delta model is accurately predicting flow, stage, and salinity in San Francisco Bay and the Sacramento-San Joaquin Delta under a wide range of hydrologic conditions and is suitable for evaluating the potential salinity impacts resulting from sea level rise.

Some aspects of the boundary conditions used in the application of the UnTRIM Bay-Delta model in this study differ from the commonly used boundary conditions described by

MacWilliams et al. (2008; 2009). In general, these modifications were made so that the boundary conditions used in this application of the UnTRIM Bay-Delta model were as close to identical as possible to the boundary conditions used in DSM2 for the DSM2 recalibration (CH2M Hill, 2009). The most significant change was that the flow though the radial gates into Clifton Court Forebay were applied using the exact flows calculated by DSM2. This modification results in a much lower level of agreement between observed and predicted water levels inside Clifton Court Forebay, than in previous applications of the UnTRIM Bay-Delta model (e.g., MacWilliams et al., 2009). In addition, the agreement between observed and predicted tidal time scale flows in Old River is decreased relative to the three periods simulated by MacWilliams et al. (2008) or the three periods simulated by MacWilliams et al. (2009). This largely results because the gate equations used in DSM2 are not nearly as accurate at determining the instantaneous flow through the radial gates as the historical SWP flow values which are based in part the daily change in volume inside Clifton Court Forebay. Additionally, the time interpolation of inflow boundaries was modified to reflect the stepwise application of these boundaries in DSM2. The effect of this change is evident in the stage comparisons at Verona and Vernalis, and some of the computed phase differences in the calibration, but this change is not expected to have a significant impact on the overall model results. Lastly, additional inflows were applied in Suisun Marsh to be consistent with the flows used in the RMA2 model.

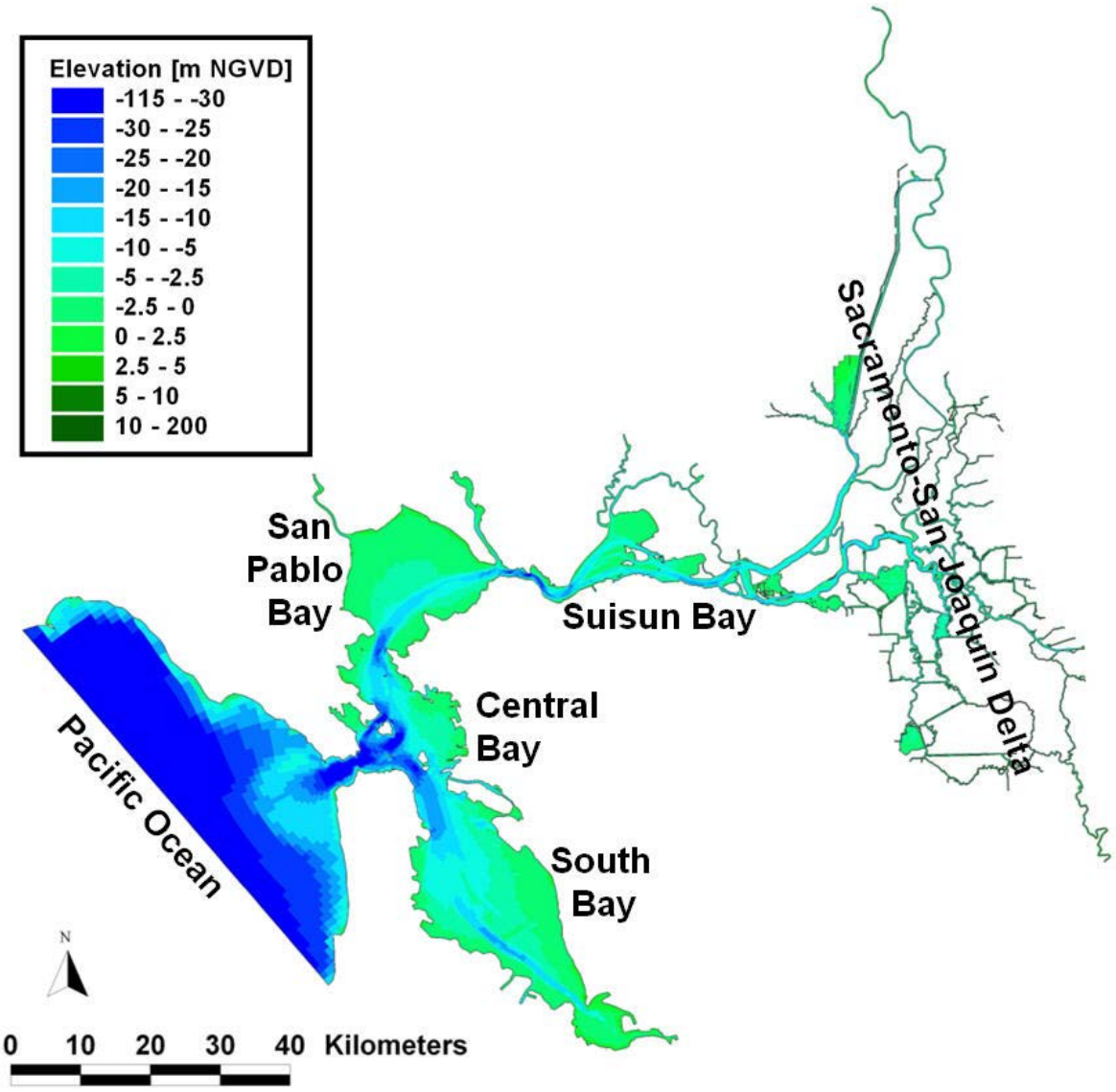

Figure 2-1 Model domain for the UnTRIM Bay-Delta model.

3. Sea Level Rise Scenario Descriptions

3.1 UnTRIM Bay-Delta Model Approach

The UnTRIM Bay-Delta model was used to simulate a 14.5 month period spanning from October 15, 2001 through January 1, 2003. The model was allowed to spin-up from the initial condition for 2.5 months and the analysis period used in the SLR comparisons spans from January 1, 2002 through January 1, 2003.

The specification of the Delta boundary conditions and operations were modified from the standard approach described by MacWilliams et al. (2008; 2009) in order to more closely match the exact boundary conditions and time interpolation of daily values used in DSM2 for the DSM2 Recalibration (CH2M Hill, 2009). The most significant change was that the flow though the radial gates into Clifton Court Forebay were applied using the exact flows calculated by DSM2, and daily inflow values were specified uniformly across each day. Additional inflows were also applied in Suisun Marsh to be consistent with the flows used in the RMA2 model. These changes to the standard UnTRIM Bay-Delta model implementation were all made to facilitate inter-comparisons between the UnTRIM Bay-Delta model, RMA2, and DSM2, and to facilitate the recalibration of dispersion factors in DSM2.

In regions of the UnTRIM Bay-Delta model that are not included in the DSM2 model domain, the standard boundary conditions described by MacWilliams et al. (2008; 2009) were applied. These include spatially variable evaporation and precipitation in the non-Delta portion of the San Francisco Estuary (evaporation and precipitation are included as part of DICU in the Delta), spatially variable wind, and other non-Delta inflows, including Napa River, Sonoma Creek, Petaluma River, Novato River, San Lorenzo Creek, Alameda Creek, San Francisquito Creek, Matadero Creek, Saratoga Creek, Guadalupe River, Coyote Creek, and flows from the San Jose/Santa Clara WPCP.

3.2 Baseline Scenario Validation

Detailed calibration and validation of the UnTRIM Bay-Delta model has been conducted over a range of simulation periods as part of previous studies (e.g., MacWilliams et al., 2007; MacWilliams et al., 2008; MacWilliams et al., 2009). As a result, no additional calibration was conducted as part of this study. MacWilliams et al. (2008) provide flow and stage comparisons for the summer 2002 period, however salinity validation of the UnTRIM Bay-Delta model for 2002 period has not been previously conducted.

Because some boundary conditions have been changed from the standard UnTRIM Bay-Delta implementation, comparison of observed and predicted stage, flow, and salinity for this study may differ from the standard implementation. Flow, stage and salinity comparisons were made for the 2002 analysis period to verify that the modified implementation of the UnTRIM Bay-Delta model used in this study accurately predicted stage, flow, and salinity in San Francisco Bay and the Sacramento-San Joaquin Delta. In this context, comparison of predicted water

levels, flows, and salinity with observations during this simulation provides an additional validation of the previous calibration and validation studies.

Appendix A provides a set of validation figures that provide a measure of the ability of the UnTRIM Bay-Delta model to accurately predict water levels (stage), flows, and salinity in San Francisco Bay and the Sacramento-San Joaquin Delta. For the 2002 simulation period, observed and predicted stage were compared at 56 continuous stage monitoring locations, flow was compared at 25 flow monitoring stations, and predicted salinity was compared to observed salinity at 59 continuous salinity monitoring locations. Predicted salinity was also compared to observed salinity along the axis of San Francisco Bay on each of the days during the analysis period when the USGS collected synoptic salinity profiles.

Accurate prediction of water levels in San Francisco Bay demonstrates that tides are accurately propagating through the Bay and into the Delta. Comparison of predicted flows to observations in the Delta demonstrate the degree that the model captures both the instantaneous and net flows in specific channels within the Delta. Accurate prediction of salinity in San Francisco Bay and the western Delta demonstrate the degree to which the model is accurately predicting salinity intrusion due to gravitational circulation and other processes. Within the Sacramento-San Joaquin Delta, prediction of salinity is strongly dependent on consumptive use and the outflow salinity from agricultural diversions, both of which introduce a significant level of uncertainty.

3.3 Sea Level Rise Scenario Descriptions

The Baseline (0 cm SLR) simulation was made assuming historic operations and inflows, as applied in the DSM2 recalibration (CH2M Hill, 2009). Tides at the Pacific Ocean boundary of the UnTRIM Bay-Delta model were applied using observed stage at Fort Point (NOAA 9454290), with a phase and amplitude offset applied to account for phase differences between the ocean boundary and Fort Point. These offsets were calibrated by MacWilliams et al. (2009) to achieve nearly exact agreement between observed and predicted stage at Fort Point, in terms of mean water level, tidal amplitude, and tidal phase as seen in Figure A.3-2.

Six sea level rise scenarios were simulated. For the sea level rise scenarios, a constant offset was added to the tides applied at the Pacific Ocean boundary for the Baseline (0 cm SLR) scenario. For the 15 cm SLR scenario, a constant offset of 15 cm was applied at the ocean boundary; for the 30 cm SLR scenario, a constant offset of 45 cm was applied at the ocean boundary; for the 45 cm SLR scenario, a constant offset of 45 cm was applied at the ocean boundary; for the 60 cm SLR scenario, a constant offset of 60 cm was applied at the ocean boundary; for the 140 cm SLR scenario, a constant offset of 140 cm was applied at the ocean boundary. For the sixth scenario, 140 cm SLR with 5% Amplification, a constant offset of 140 cm was applied at the ocean boundary and the tidal range was amplified by 5%. All other boundary conditions were identical between the six sea level rise scenarios and the Baseline scenario. Thus, the simulations assume historical operations, with no re-operation to account for changes in water quality resulting from SLR.

3.4 Sea Level Rise Scenario Analysis Approach

The impacts are evaluated through comparison of daily-averaged depth-average salinity maps (Section 4), comparison of X2 (Section 5), and comparison of predicted salinity at a set of fixed monitoring locations (Section 6). Relationships between predicted stage and salinity between the Baseline scenario and each of the sea level rise scenarios are developed at both Martinez and the Golden Gate (Section 7) to facilitate the implementation of appropriate boundary conditions for sea level rise scenarios in DSM2 and the RMA2 models. Lastly, a detailed analysis of salt flux is included (Section 8) to evaluate the mechanisms responsible for increase salt intrusion with sea level rise.

A full set of flow and section averaged salinity predictions for the Baseline scenario, the 15 cm SLR scenario, and the 45 cm SLR scenario at stations throughout the Delta were provided to CH2M Hill for comparison to predicted flow and salinity from DSM2. These output include the section averaged salinity at the locations shown on Figure 3-1, depth-averaged and surface point salinity data, daily-averaged depth-average salinity transects along the axis of San Francisco Bay, the Sacramento River and the San Joaquin River, and instantaneous flow data at a set of 36 cross-sections. A similar set of model predictions was provided to RMA, Inc. for recalibration of the RMA2 model for the 140 cm sea level rise scenario.

The UnTRIM Bay-Delta model simulates salinity in Practical Salinity Units (psu), while DSM2 simulates salinity electrical conductivity (EC). Salinity is a conservative quantity, whereas electrical conductivity is not conservative (as seen in Table 3-1). For example if a volume of water with salinity of 25 psu were mixed with an equal volume of water with salinity of 5 psu, the resulting salinity in UnTRIM would be 15 psu. However if the same volume of water with EC 39269 [µmhos cm^{-1}] (corresponding to 25 psu) were mixed with an equal volume of water with EC 8961 [µmhos cm^{-1}] (corresponding to 5 psu), the resulting EC in DSM2 would be 24115 [µmhos cm^{-1}], which corresponds to 14.61 psu. Thus, the non-conservative nature of EC introduces a 2.4% error in this case if EC is simulated instead of salinity. As a result, there are significant advantages to simulating salinity in psu as opposed to simulating EC. Because water quality standards in the Delta are typically based on EC, salinity can be converted to EC following the inverse of the approach used by the USGS in San Francisco Bay to convert from measured specific conductance (EC at 25 degrees Celsius) to salinity (Schoellhamer and Buchanan, 2010). The measured electrical conductivity (EC) and temperature data collected in the field are converted to electrical conductance, which is the EC at 25 degrees Celsius. The specific conductance data is converted to salinity using the 1985 UNESCO standard (UNESCO, 1985) in the range of 2-42 practical salinity units (psu). Salinities below 2 psu are computed using the extension of the practical salinity scale proposed by Hill et al. (1986). For reference, conversions between salinity in psu and electrical conductivity in [µmhos cm^{-1}] are provided in Table 3-1. In this table and throughout the report, EC refers to EC at 25 degrees Celsius.

Table 3-1 Electrical Conductivity values corresponding to a range of salinity values.

Salinity [psu]	Electrical Conductivity [µmhos cm-1]
0.05	108
0.10	213
0.20	418
0.30	620
0.50	1015
0.75	1497
1.0	1970
5.0	8961
10.0	17025
15.0	24697
20.0	32093
25.0	39269
30.0	46256

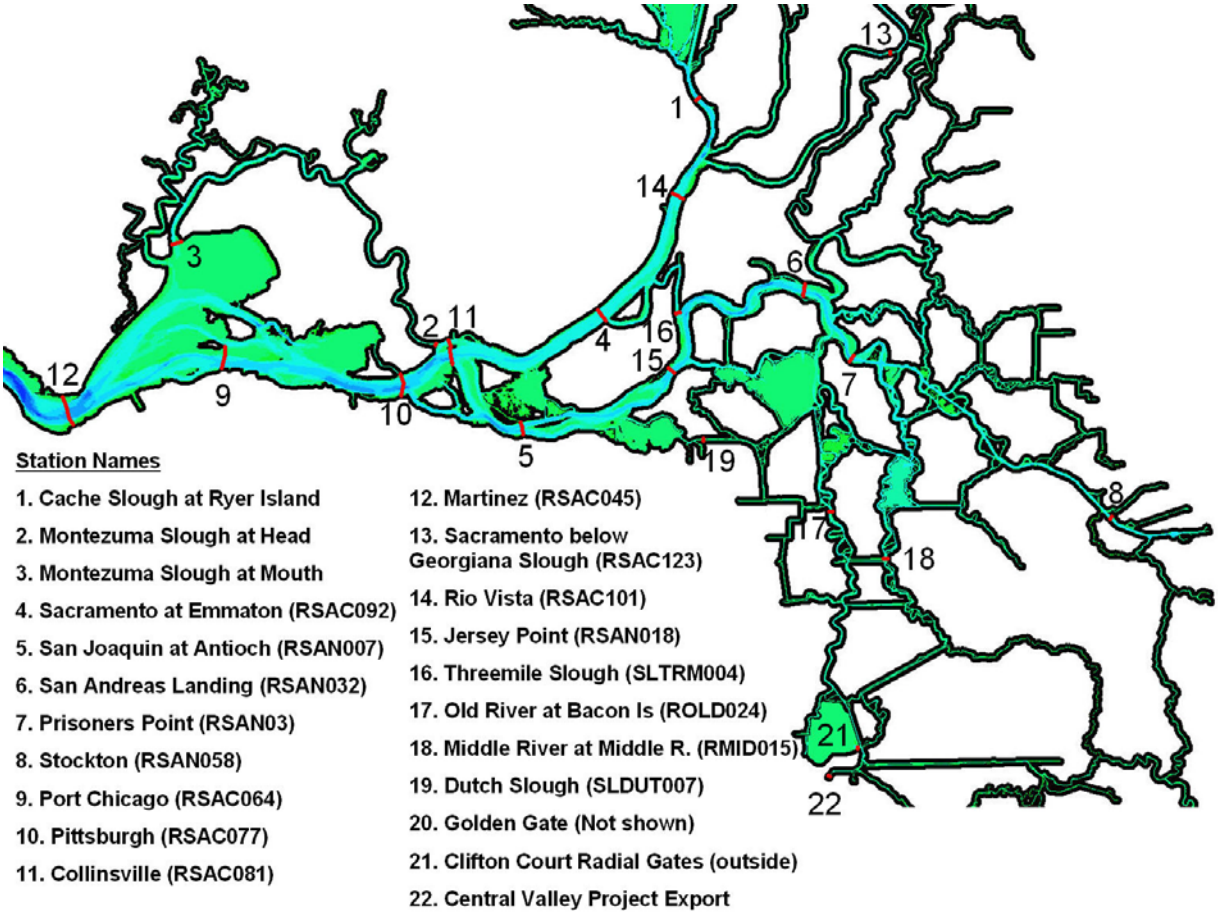

Figure 3-1 Locations of section averaged salinity output provided to CH2M Hill for DSM2 comparisons.

4. Sea Level Rise Impacts on Daily-averaged Depth-average Salinity

Daily-averaged depth-average salinity maps provide an effective way to make visual comparisons between predicted salinity under a range of scenarios. For each sea level rise scenario, the depth-averaged salinity is computed at each model time step and then averaged over each day. The resulting daily-averaged depth-average salinity maps for each sea level rise scenario can then be compared to the Baseline salinity to show the spatial distribution of the predicted increase in daily-average salinity. In the following sections, the salinity map comparisons are made on the first day of each month during the simulation period, spanning from January 1, 2002 through January 1, 2003.

4.1 Predicted Increase in Salinity for 15 cm SLR Scenario

Figure 4.1-1 through 4.1-13 show the predicted salinity along the northern portion of the San Francisco Estuary, spanning from San Pablo Bay through the Sacramento-San Joaquin Delta for the 15 cm SLR scenario. The top panel of each figure shows the predicted daily-averaged depth-average salinity for the 15 cm SLR scenario. The lower panel shows the predicted salinity increase computed by subtracting the predicted daily-averaged depth-average salinity for the Baseline (0 cm SLR) scenario from the predicted daily-averaged depth-average salinity for the 15 cm SLR scenario. Figures 4.1-14 through 4.1-26 show the predicted salinity increases resulting from the 15 cm SLR scenario in the Sacramento-San Joaquin Delta.

At the beginning of the analysis period on January 1, 2002, salinity increases between 0.05 and 0.10 psu are predicted between Chipps Island and Collinsville and predicted salinity increases are less than 0.05 psu throughout the remaining portions of the Delta. Salinity increases between 0.20 and 0.50 psu are predicted through Carquinez Strait and salinity increases between 0.05 and 0.35 psu are predicted throughout Suisun Bay. Larger salinity increases of up to more than 1.5 psu are predicted in San Pablo Bay. During the first half of the year, predicted salinity increases in Suisun Bay and the Delta remain similar to the predicted salinity increases seen on January 1, 2002, though the predicted salinity is increasing throughout this period. Larger salinity increases are predicted in the Delta between July and December, with the largest predicted salinity increases in December prior to the first flush. In December, salinity increases of between 0.20 and 0.50 psu are predicted between Chipps Island and Emmaton, and salinity increases of between 0.05 and 0.10 psu are predicted in Franks Tract. Following high flows which occurred in December, predicted salinity on January 1, 2003 shows that the 0.50 psu isohaline is on the western side of Suisun Bay near Martinez, and predicted salinity increases are less than 0.05 psu throughout the Delta.

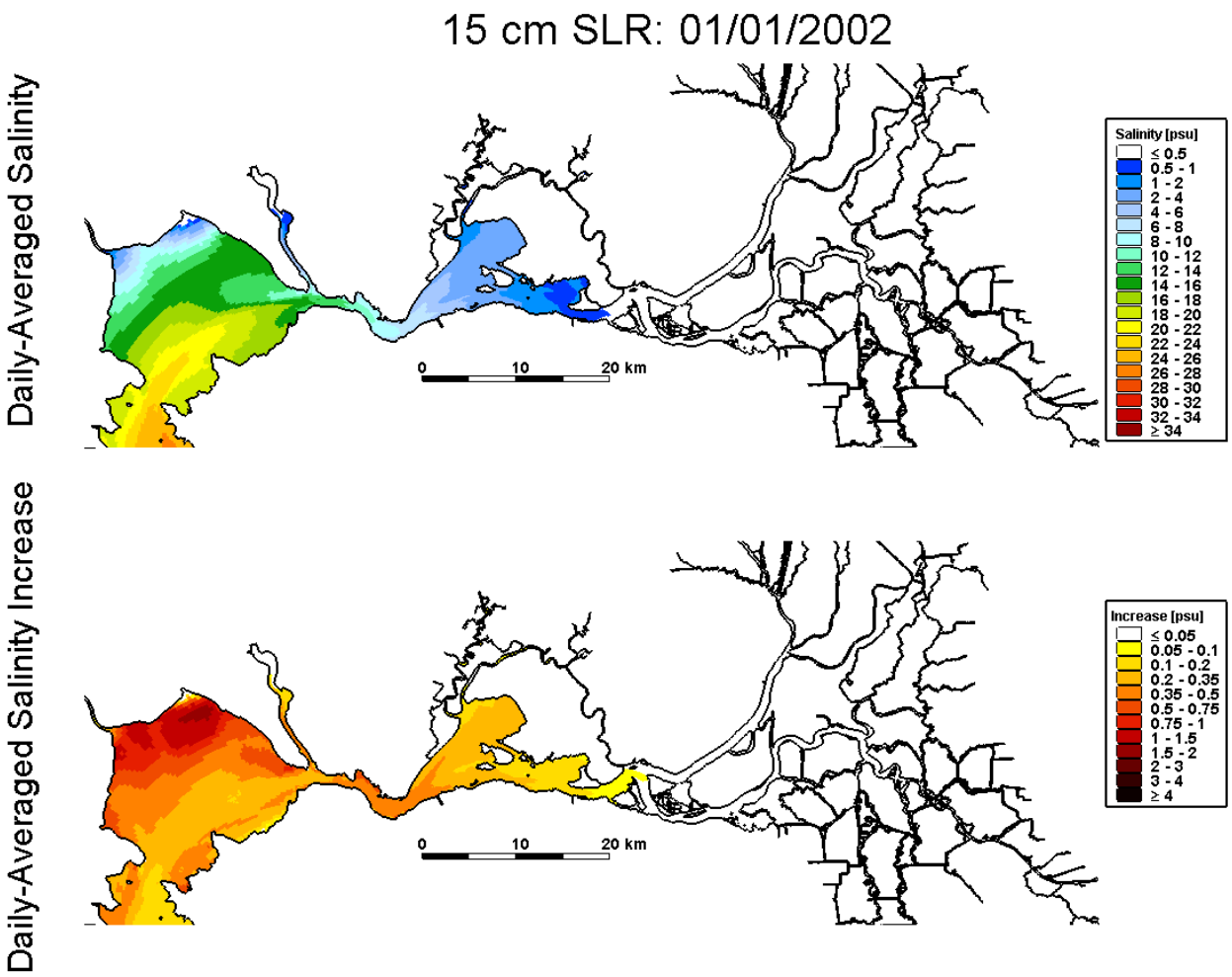

Figure 4.1-1 Predicted daily-averaged depth-average salinity on January 1, 2002 for the 15 cm SLR scenario (top); predicted increase in daily-averaged depth-average salinity on January 1, 2002 relative to the Baseline (0 cm SLR) scenario for the 15 cm SLR scenario.

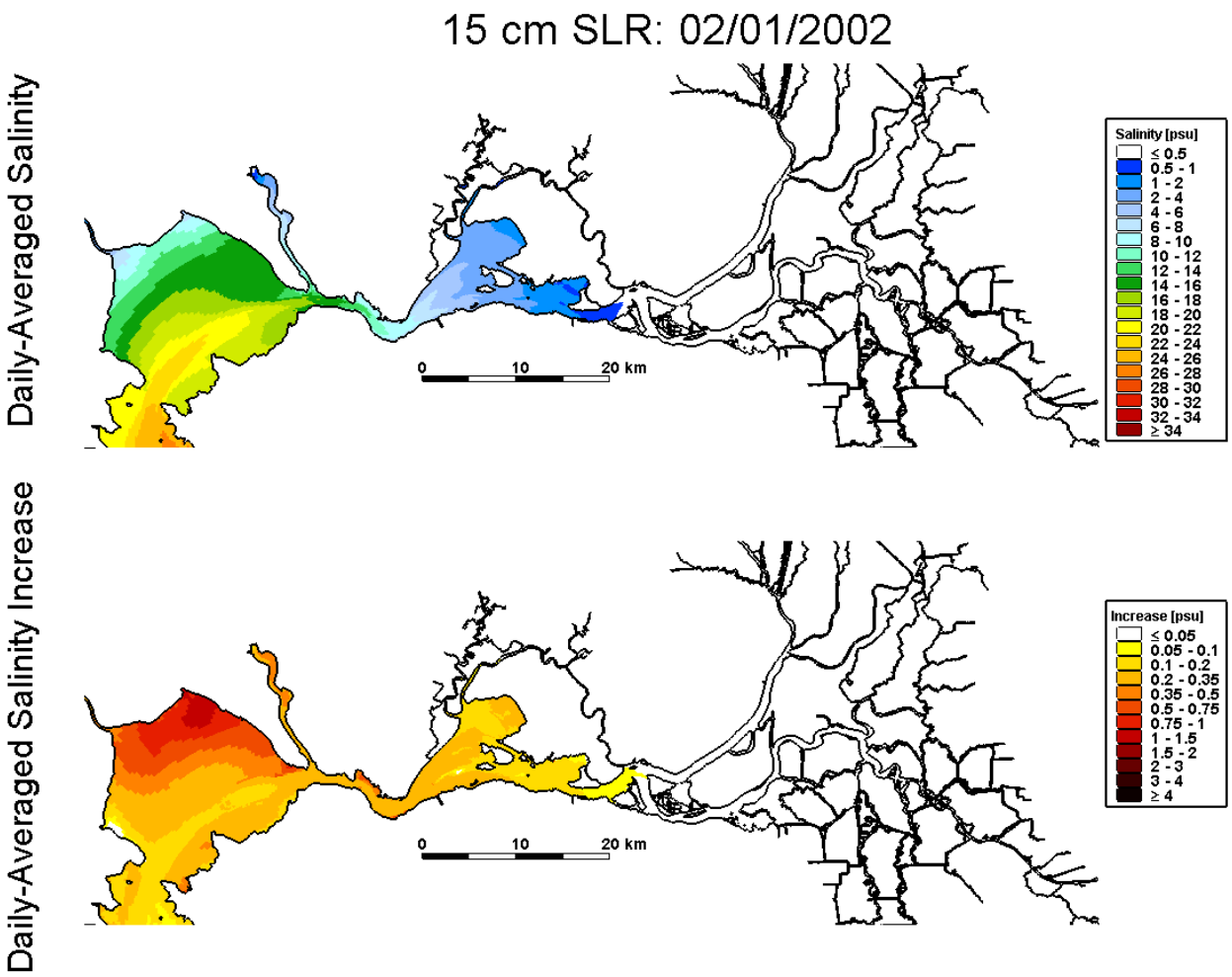

Figure 4.1-2 Predicted daily-averaged depth-average salinity on February 1, 2002 for the 15 cm SLR scenario (top); predicted increase in daily-averaged depth-average salinity on February 1, 2002 relative to the Baseline (0 cm SLR) scenario for the 15 cm SLR scenario.

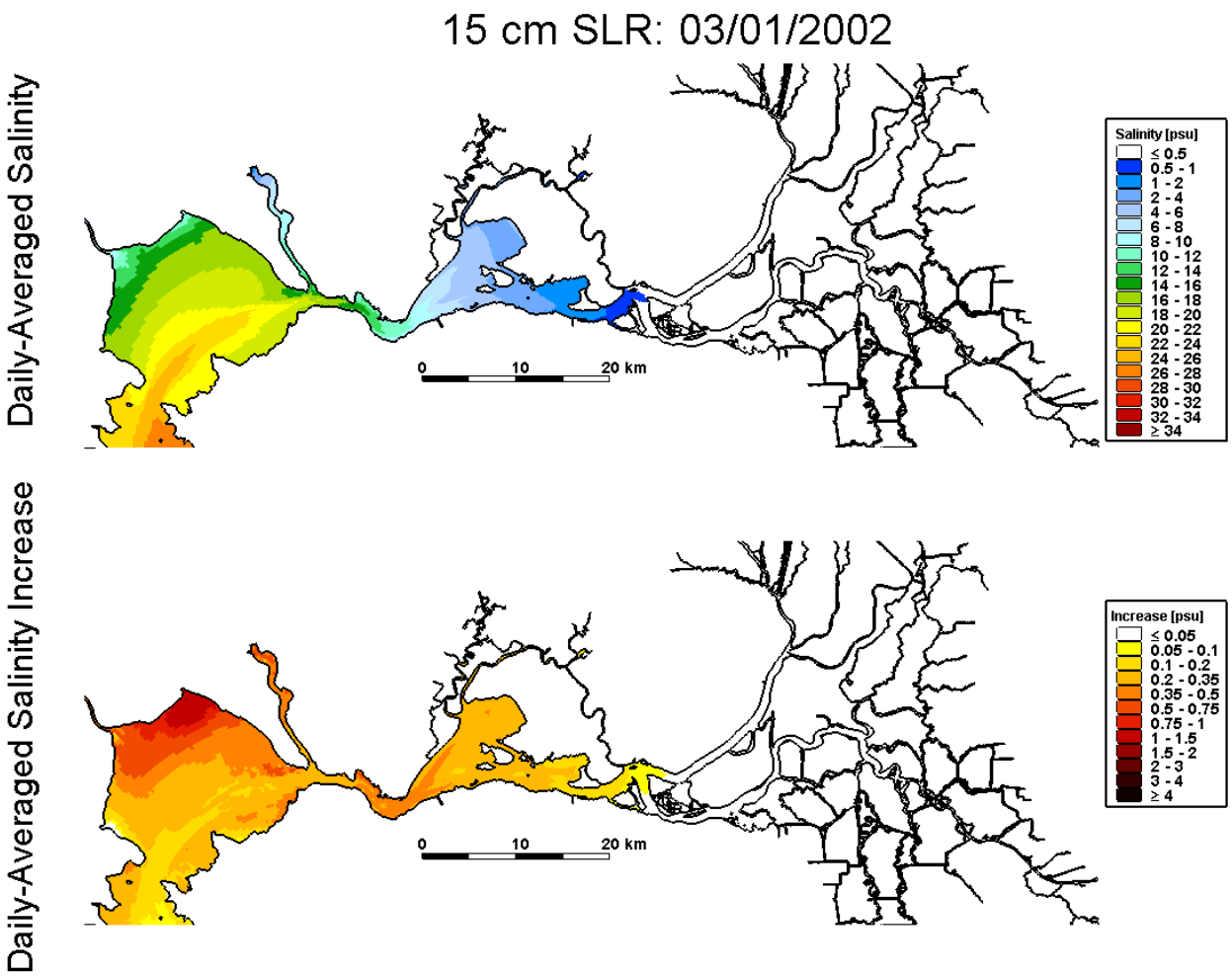

Figure 4.1-3 Predicted daily-averaged depth-average salinity on March 1, 2002 for the 15 cm SLR scenario (top); predicted increase in daily-averaged depth-average salinity on March 1, 2002 relative to the Baseline (0 cm SLR) scenario for the 15 cm SLR scenario.

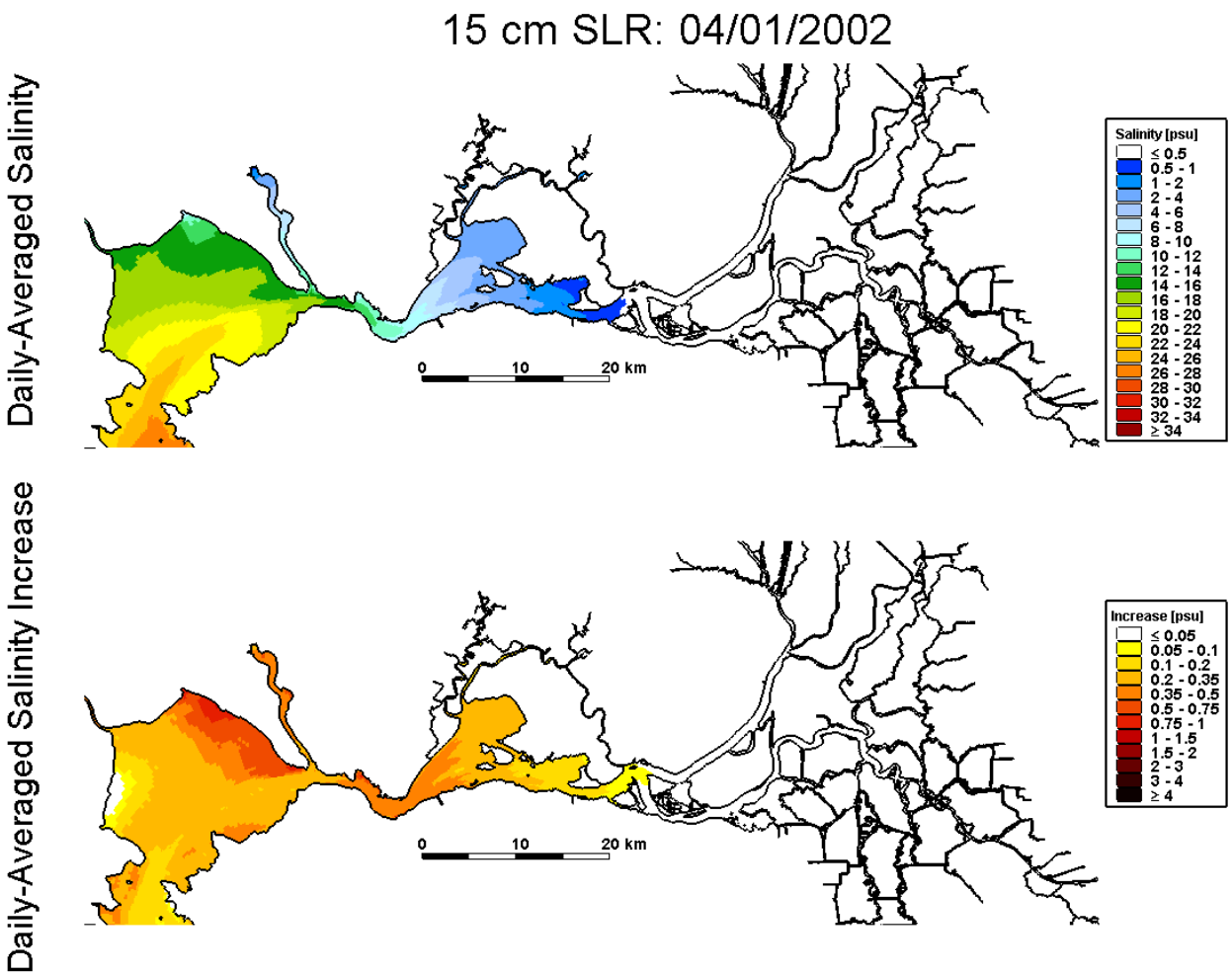

Figure 4.1-4 Predicted daily-averaged depth-average salinity on April 1, 2002 for the 15 cm SLR scenario (top); predicted increase in daily-averaged depth-average salinity on April 1, 2002 relative to the Baseline (0 cm SLR) scenario for the 15 cm SLR scenario.

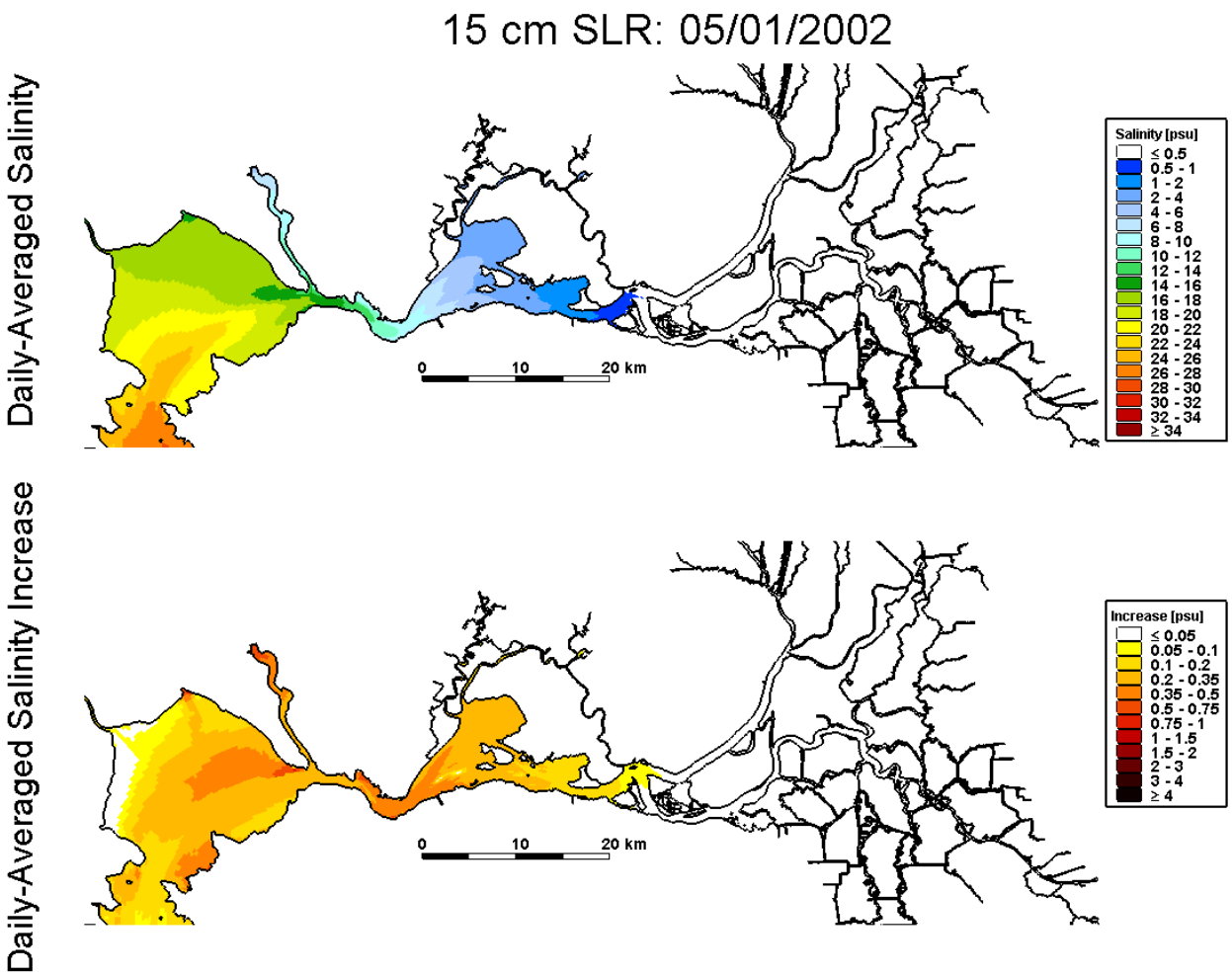

Figure 4.1-5 Predicted daily-averaged depth-average salinity on May 1, 2002 for the 15 cm SLR scenario (top); predicted increase in daily-averaged depth-average salinity on May 1, 2002 relative to the Baseline (0 cm SLR) scenario for the 15 cm SLR scenario.

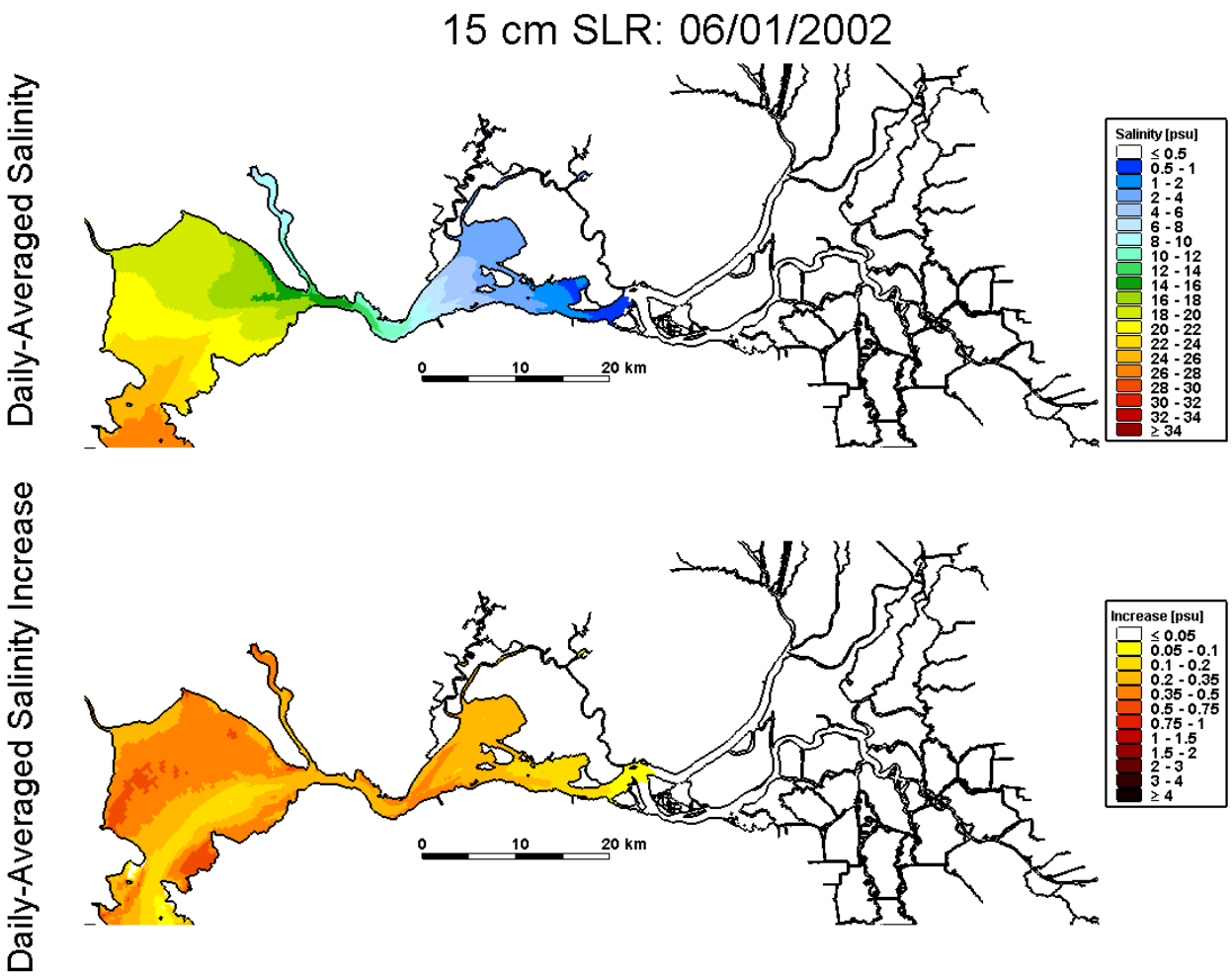

Figure 4.1-6 Predicted daily-averaged depth-average salinity on June 1, 2002 for the 15 cm SLR scenario (top); predicted increase in daily-averaged depth-average salinity on June 1, 2002 relative to the Baseline (0 cm SLR) scenario for the 15 cm SLR scenario.

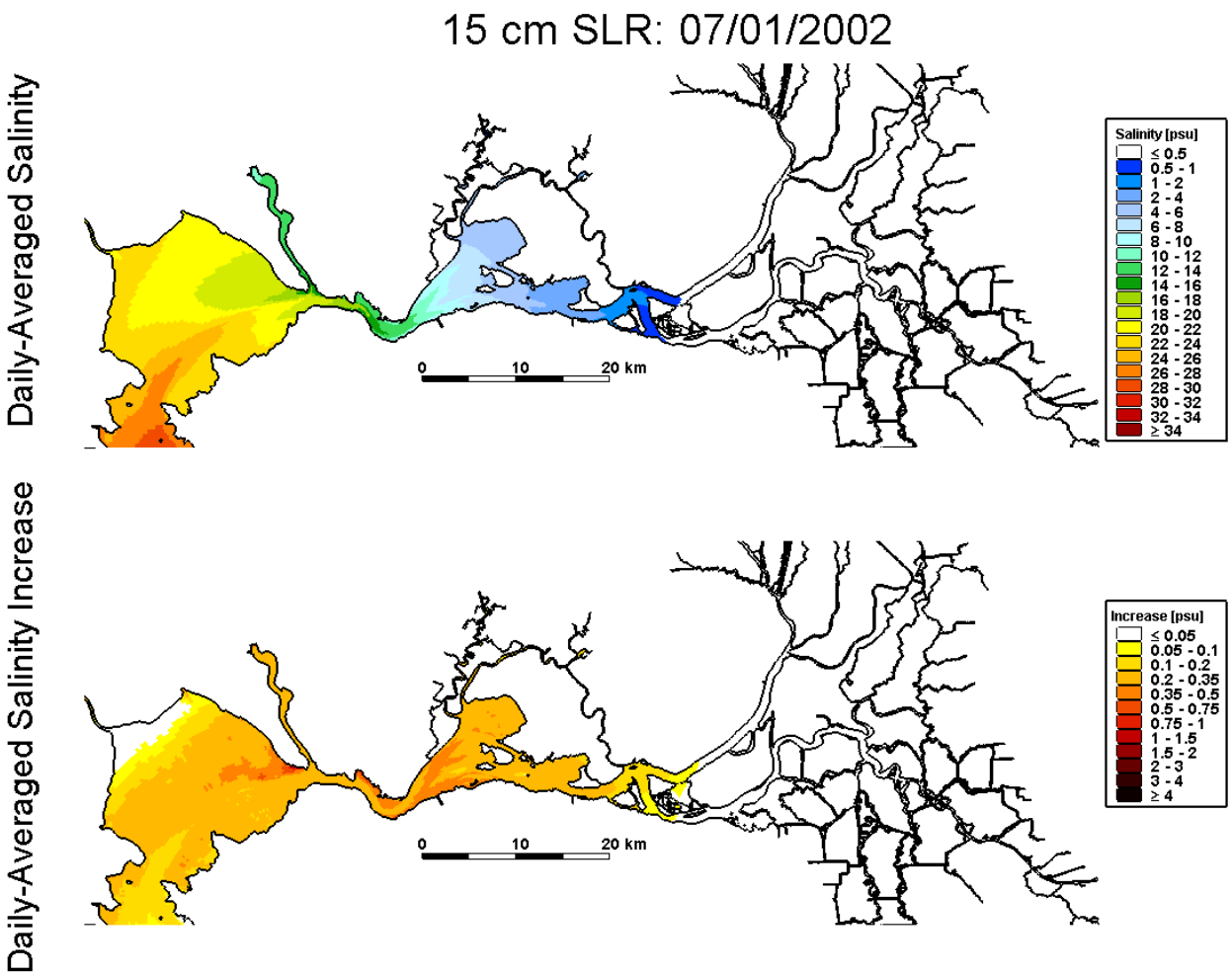

Figure 4.1-7 Predicted daily-averaged depth-average salinity on July 1, 2002 for the 15 cm SLR scenario (top); predicted increase in daily-averaged depth-average salinity on July 1, 2002 relative to the Baseline (0 cm SLR) scenario for the 15 cm SLR scenario.

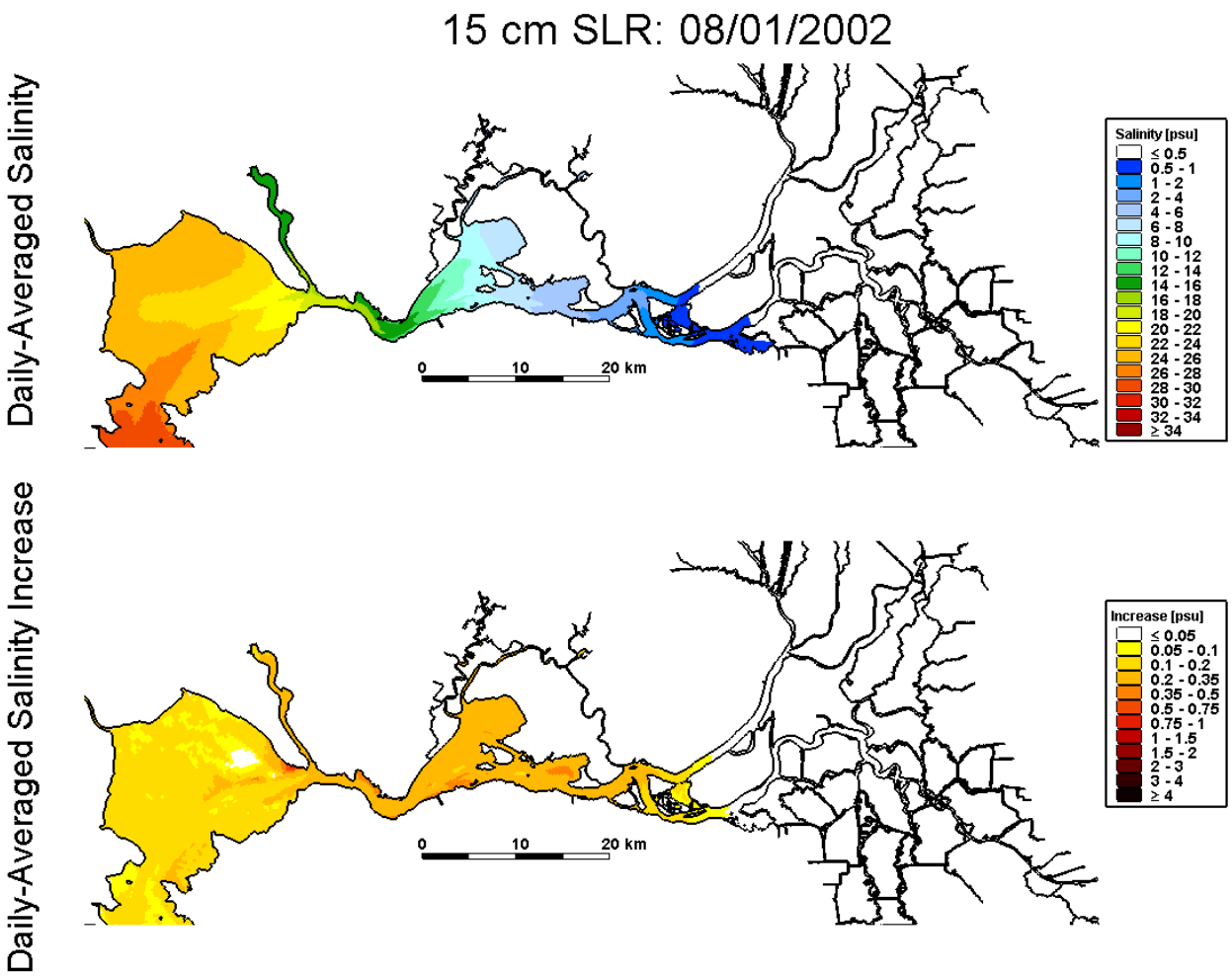

Figure 4.1-8 Predicted daily-averaged depth-average salinity on August 1, 2002 for the 15 cm SLR scenario (top); predicted increase in daily-averaged depth-average salinity on August 1, 2002 relative to the Baseline (0 cm SLR) scenario for the 15 cm SLR scenario.

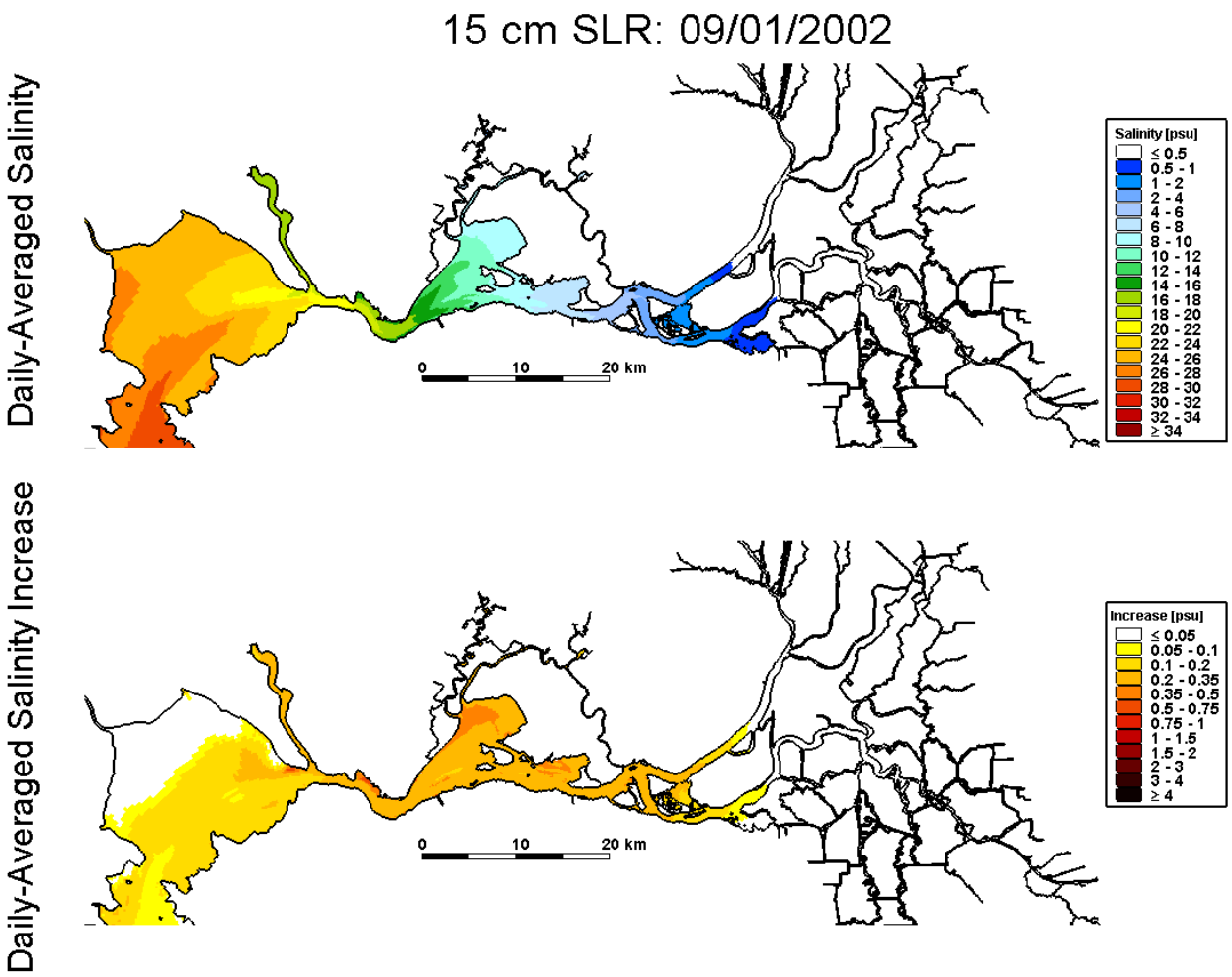

Figure 4.1-9 Predicted daily-averaged depth-average salinity on September 1, 2002 for the 15 cm SLR scenario (top); predicted increase in daily-averaged depth-average salinity on September 1, 2002 relative to the Baseline (0 cm SLR) scenario for the 15 cm SLR scenario.

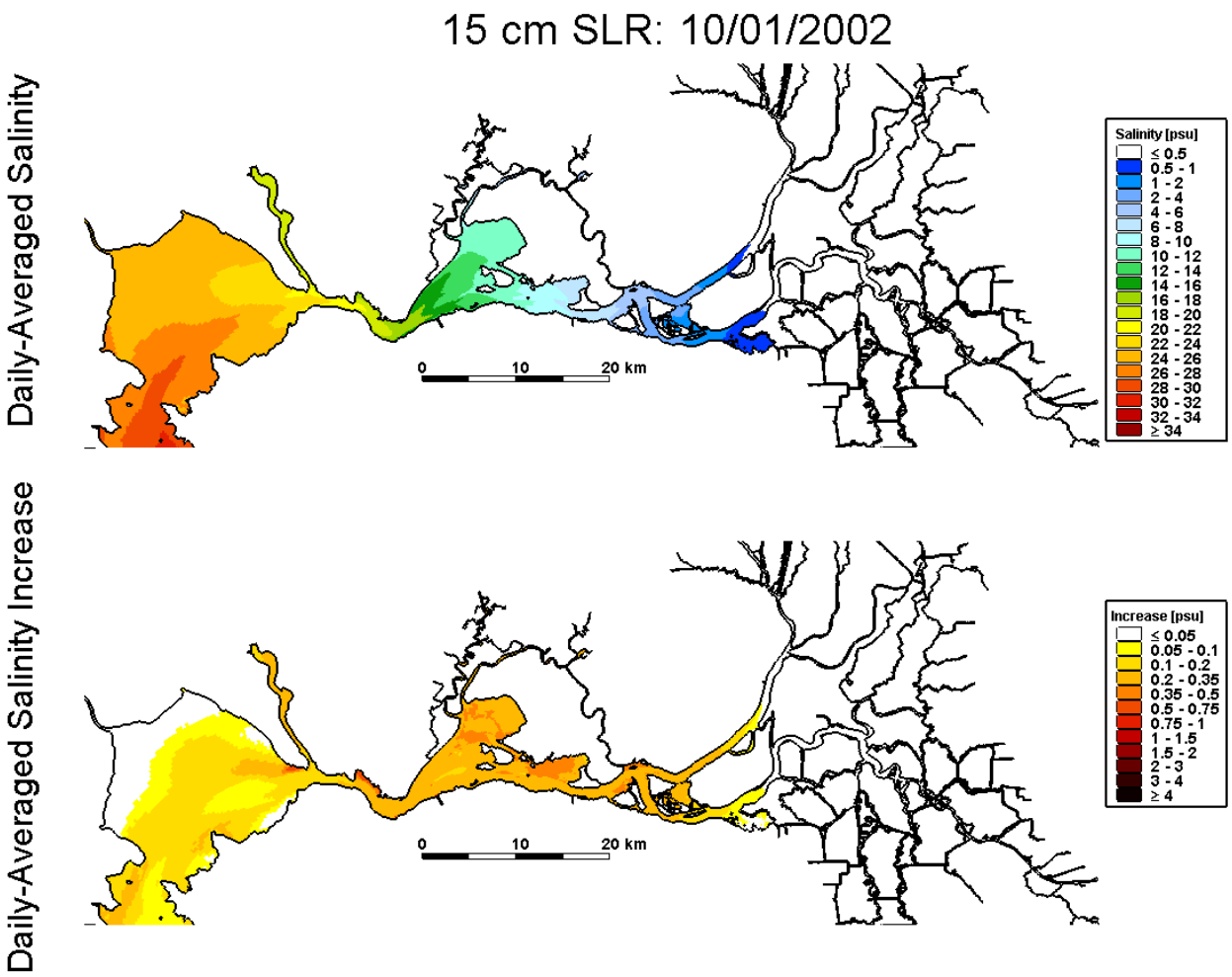

Figure 4.1-10 Predicted daily-averaged depth-average salinity on October 1, 2002 for the 15 cm SLR scenario (top); predicted increase in daily-averaged depth-average salinity on October 1, 2002 relative to the Baseline (0 cm SLR) scenario for the 15 cm SLR scenario.

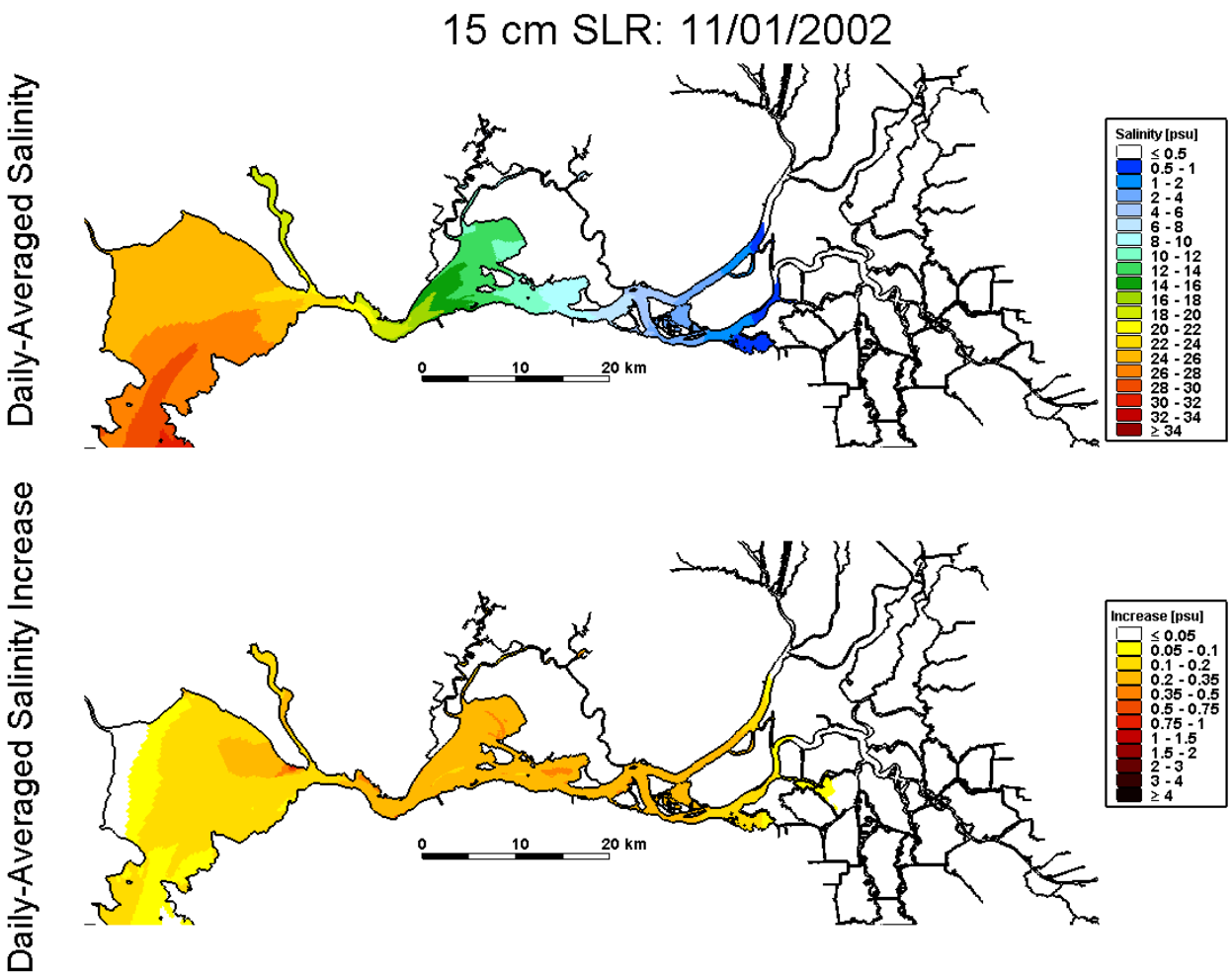

Figure 4.1-11 Predicted daily-averaged depth-average salinity on November 1, 2002 for the 15 cm SLR scenario (top); predicted increase in daily-averaged depth-average salinity on November 1, 2002 relative to the Baseline (0 cm SLR) scenario for the 15 cm SLR scenario.

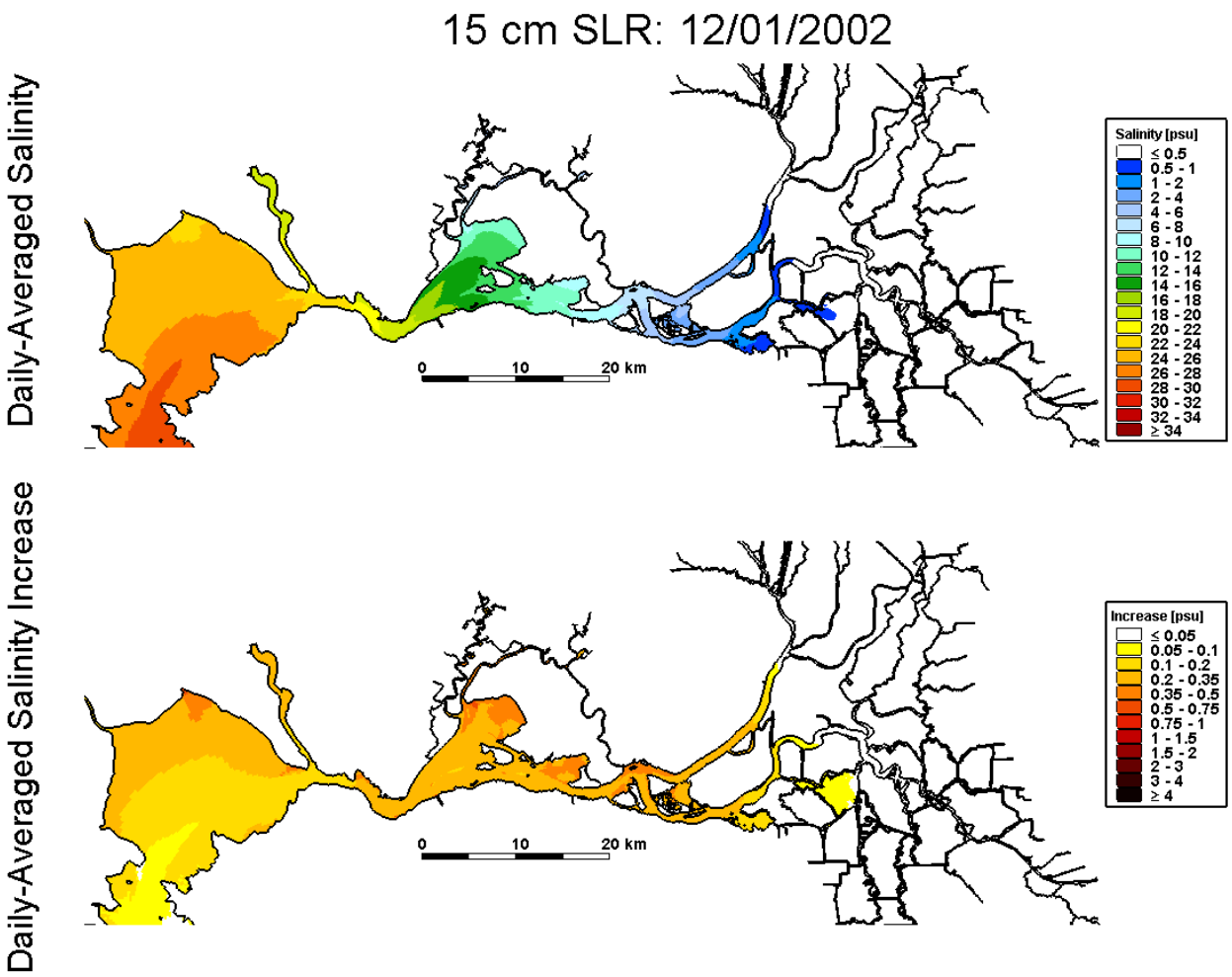

Figure 4.1-12 Predicted daily-averaged depth-average salinity on December 1, 2002 for the 15 cm SLR scenario (top); predicted increase in daily-averaged depth-average salinity on December 1, 2002 relative to the Baseline (0 cm SLR) scenario for the 15 cm SLR scenario.

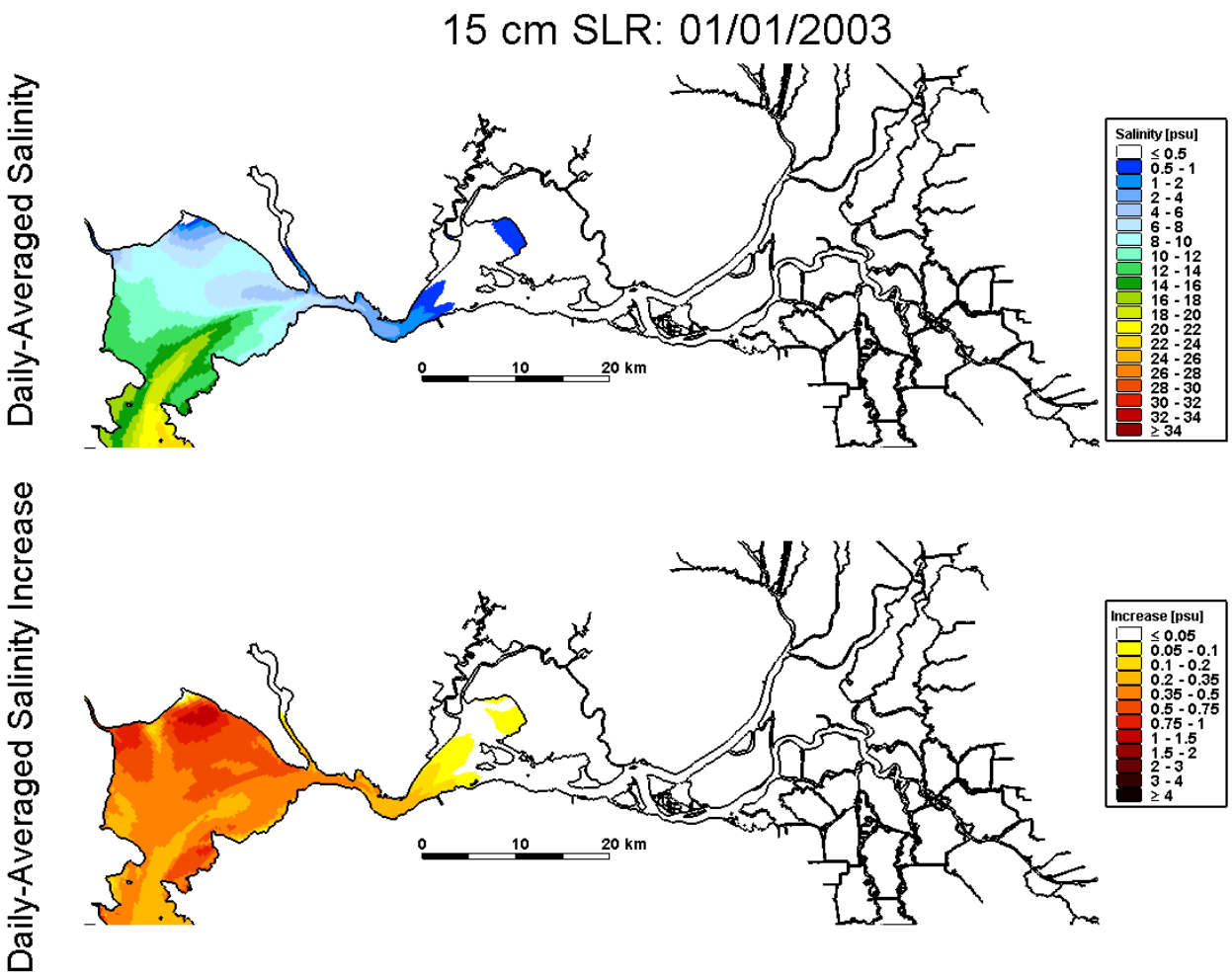

Figure 4.1-13 Predicted daily-averaged depth-average salinity on January 1, 2003 for the 15 cm SLR scenario (top); predicted increase in daily-averaged depth-average salinity on January 1, 2003 relative to the Baseline (0 cm SLR) scenario for the 15 cm SLR scenario.

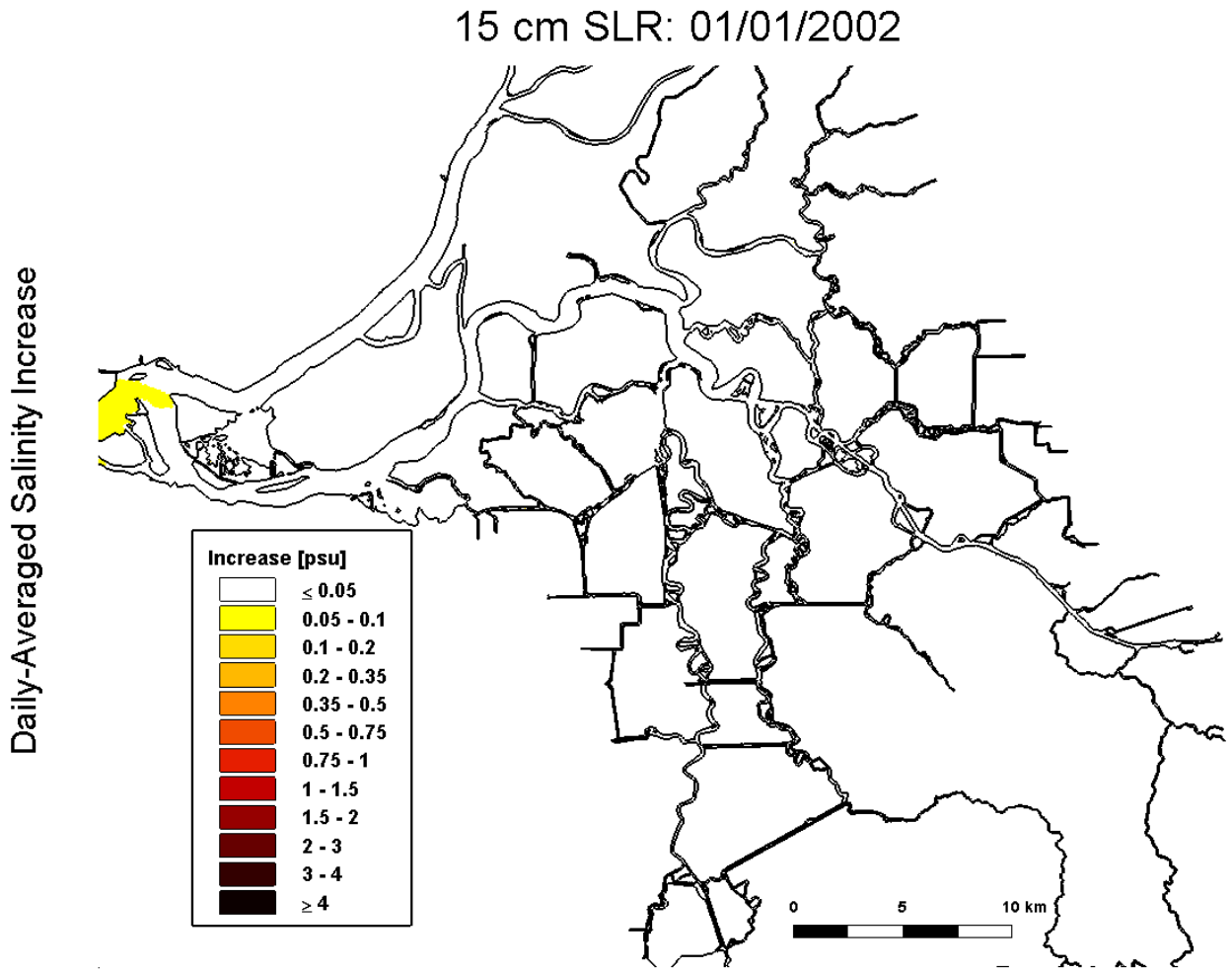

Figure 4.1-14 Predicted increase in daily-averaged depth-average salinity in the Sacramento-San Joaquin Delta on January 1, 2002 relative to the Baseline (0 cm SLR) scenario for the 15 cm SLR scenario.

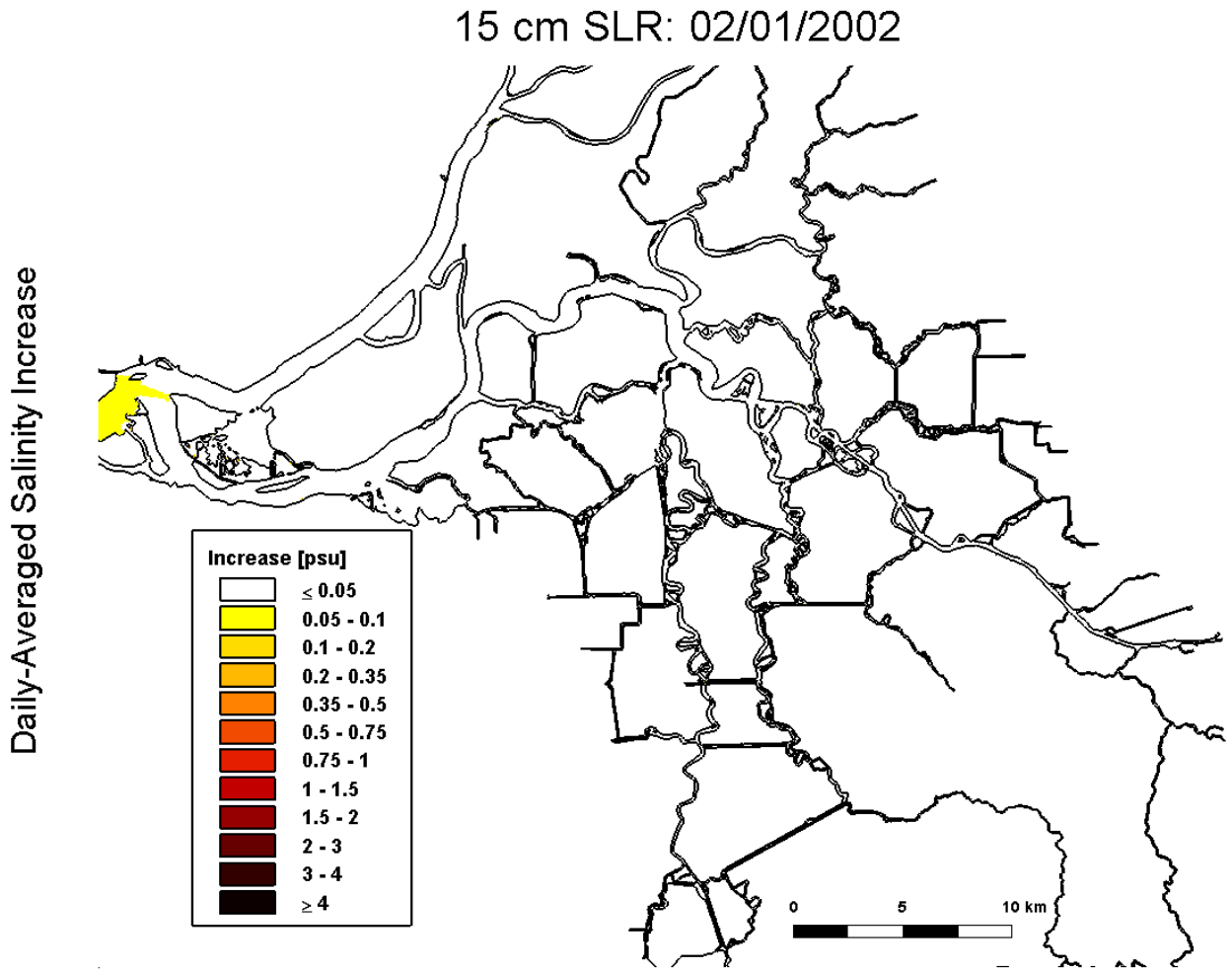

Figure 4.1-15 Predicted increase in daily-averaged depth-average salinity in the Sacramento-San Joaquin Delta on February 1, 2002 relative to the Baseline (0 cm SLR) scenario for the 15 cm SLR scenario.

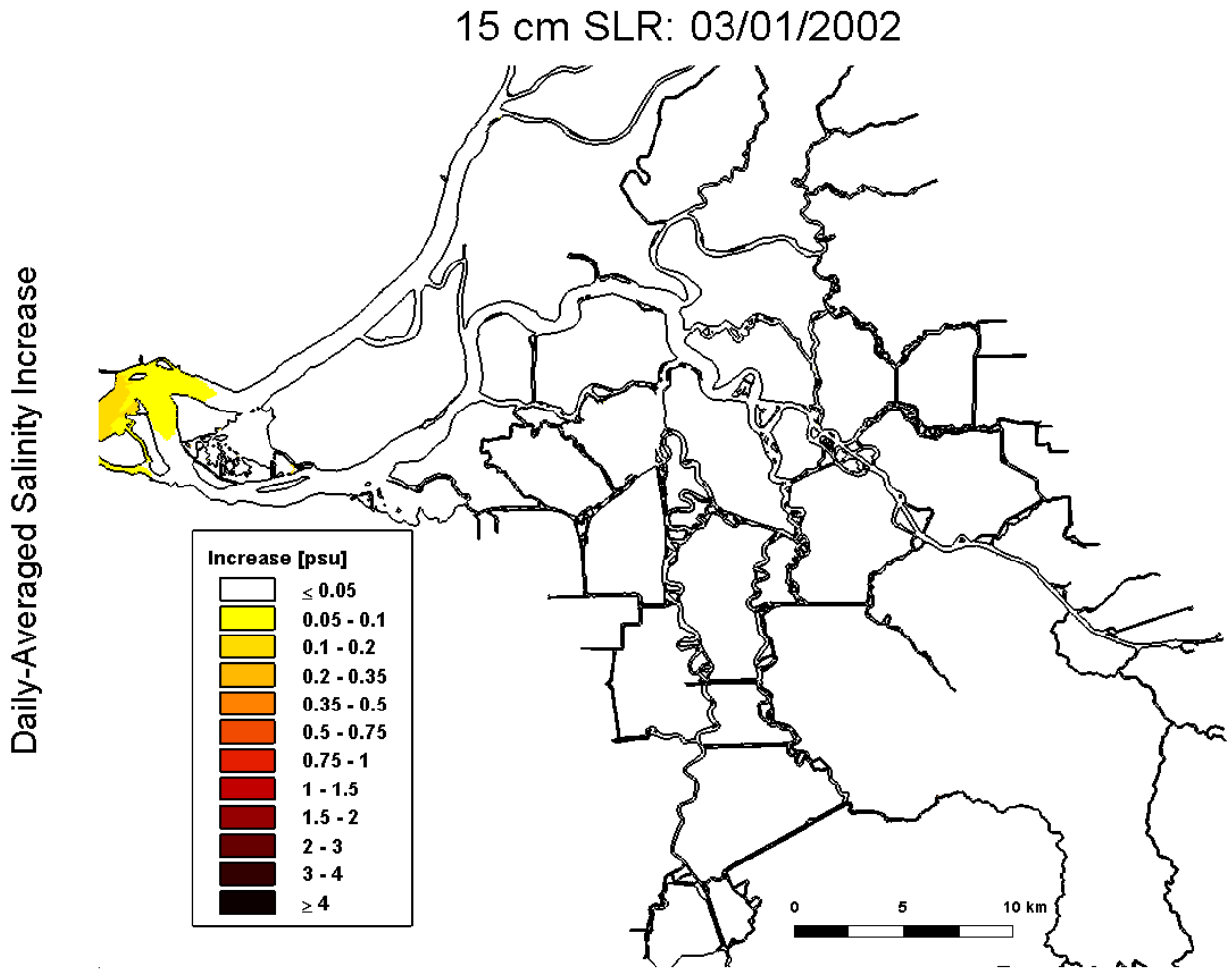

Figure 4.1-16 Predicted increase in daily-averaged depth-average salinity in the Sacramento-San Joaquin Delta on March 1, 2002 relative to the Baseline (0 cm SLR) scenario for the 15 cm SLR scenario.

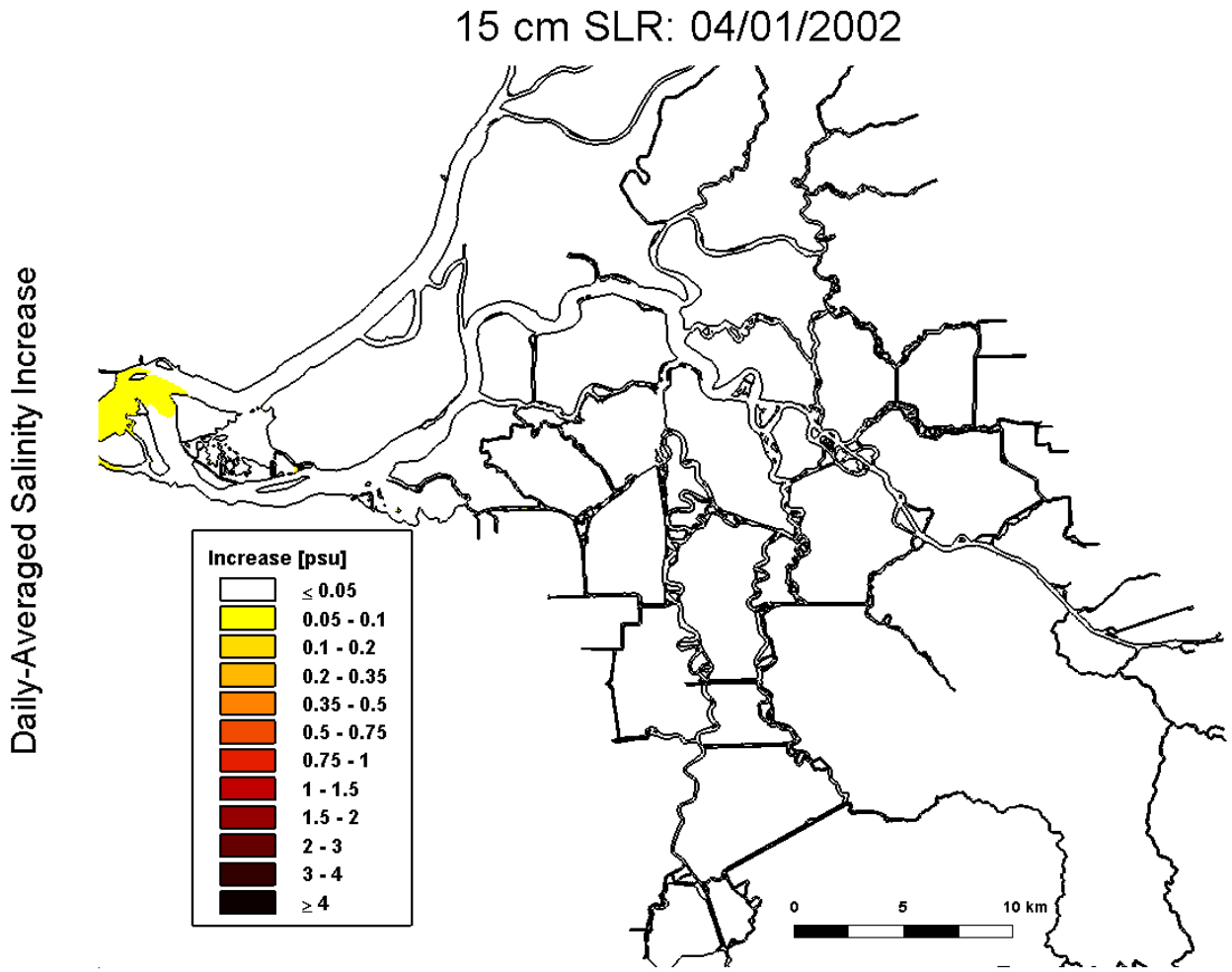

Figure 4.1-17 Predicted increase in daily-averaged depth-average salinity in the Sacramento-San Joaquin Delta on April 1, 2002 relative to the Baseline (0 cm SLR) scenario for the 15 cm SLR scenario.

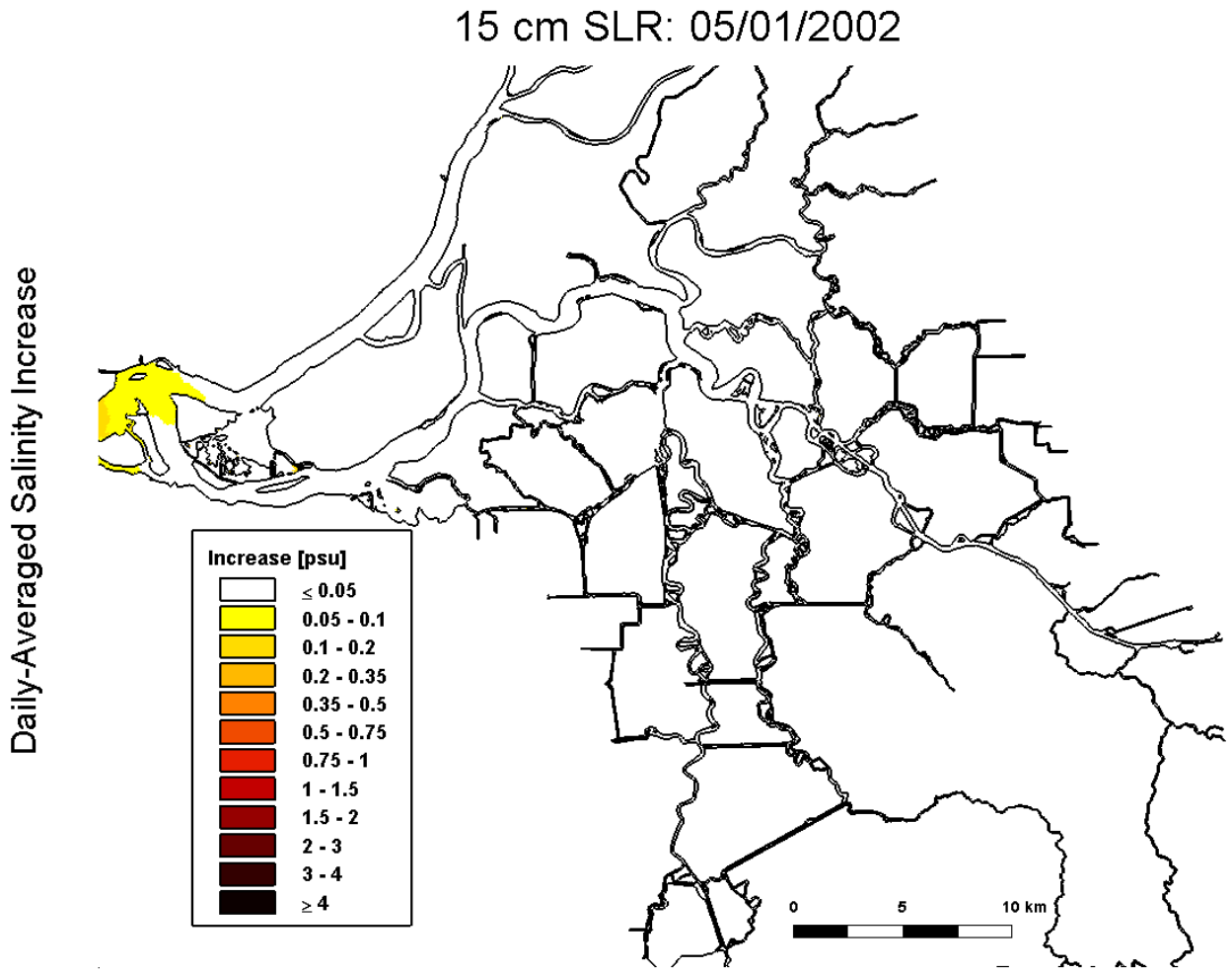

Figure 4.1-18 Predicted increase in daily-averaged depth-average salinity in the Sacramento-San Joaquin Delta on May 1, 2002 relative to the Baseline (0 cm SLR) scenario for the 15 cm SLR scenario.

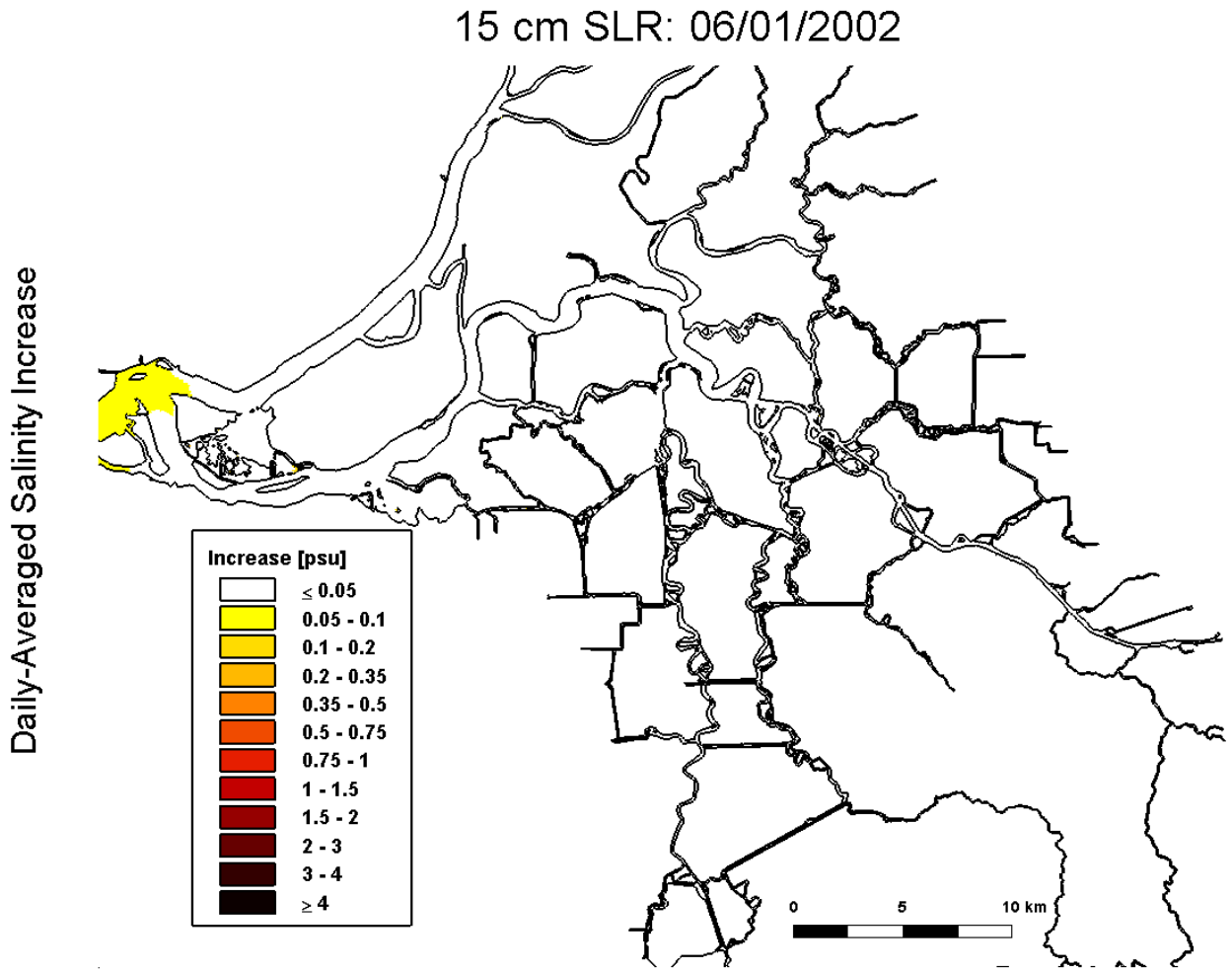

Figure 4.1-19 Predicted increase in daily-averaged depth-average salinity in the Sacramento-San Joaquin Delta on June 1, 2002 relative to the Baseline (0 cm SLR) scenario for the 15 cm SLR scenario.

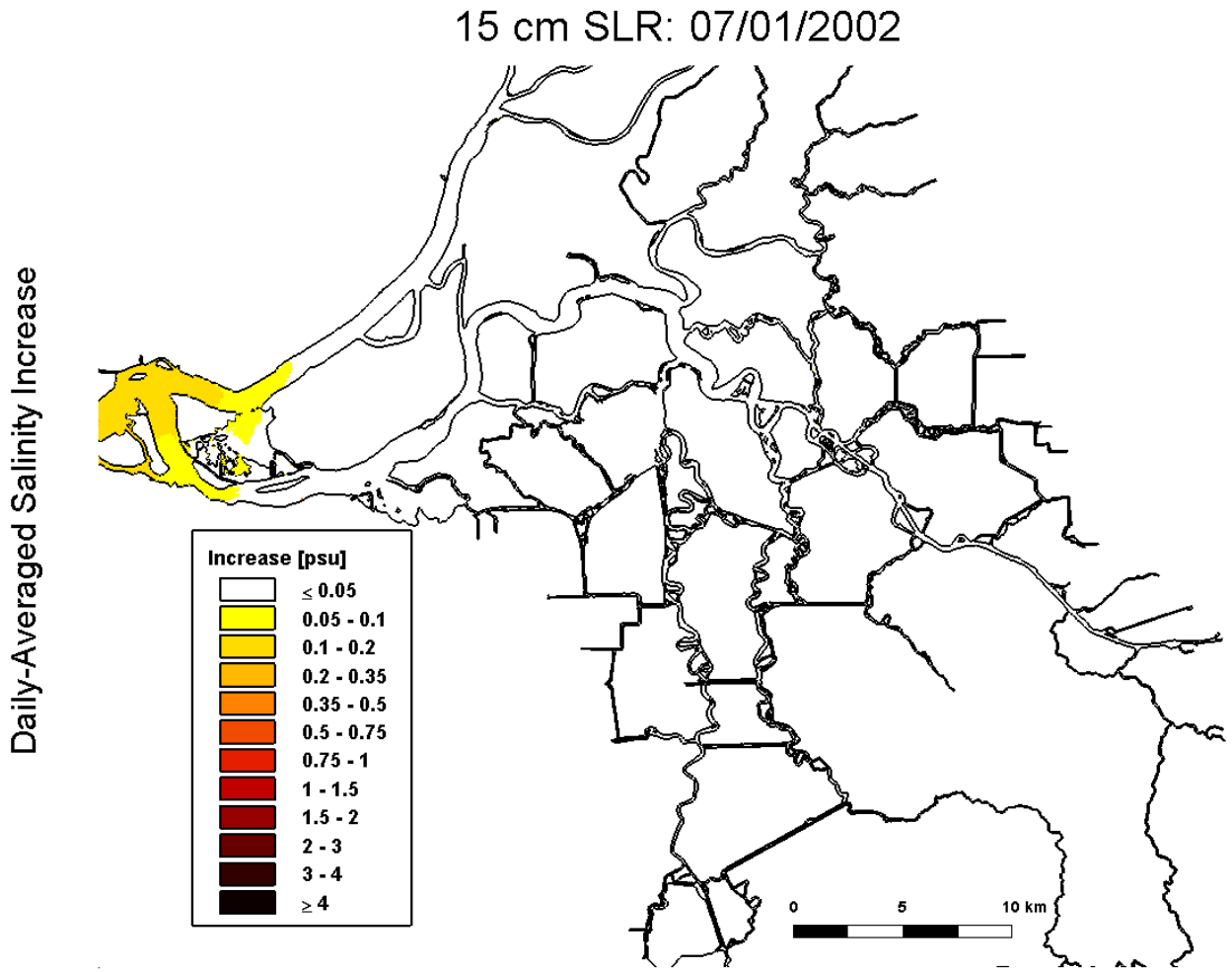

Figure 4.1-20 Predicted increase in daily-averaged depth-average salinity in the Sacramento-San Joaquin Delta on July 1, 2002 relative to the Baseline (0 cm SLR) scenario for the 15 cm SLR scenario.

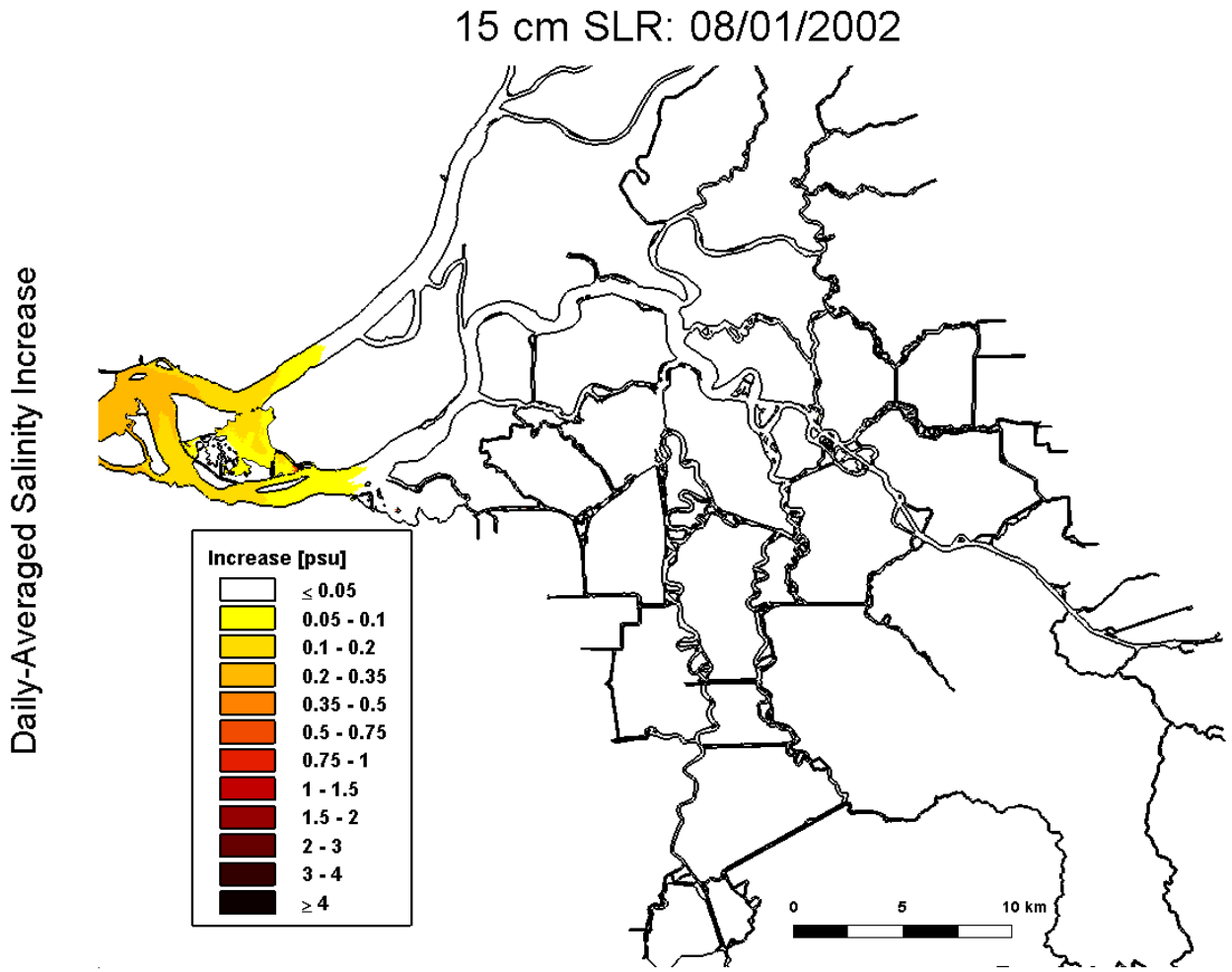

Figure 4.1-21 Predicted increase in daily-averaged depth-average salinity in the Sacramento-San Joaquin Delta on August 1, 2002 relative to the Baseline (0 cm SLR) scenario for the 15 cm SLR scenario.

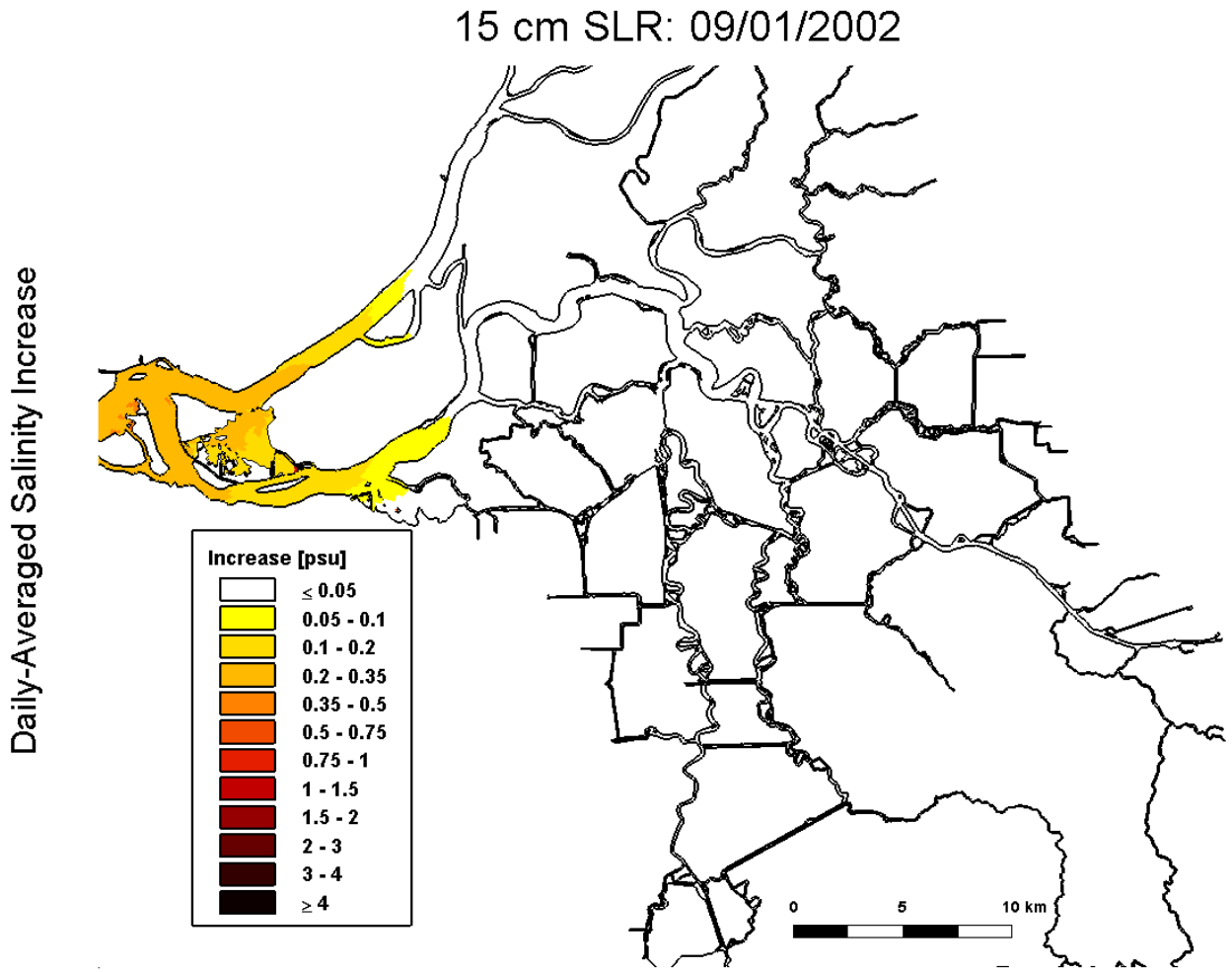

Figure 4.1-22 Predicted increase in daily-averaged depth-average salinity in the Sacramento-San Joaquin Delta on September 1, 2002 relative to the Baseline (0 cm SLR) scenario for the 15 cm SLR scenario.

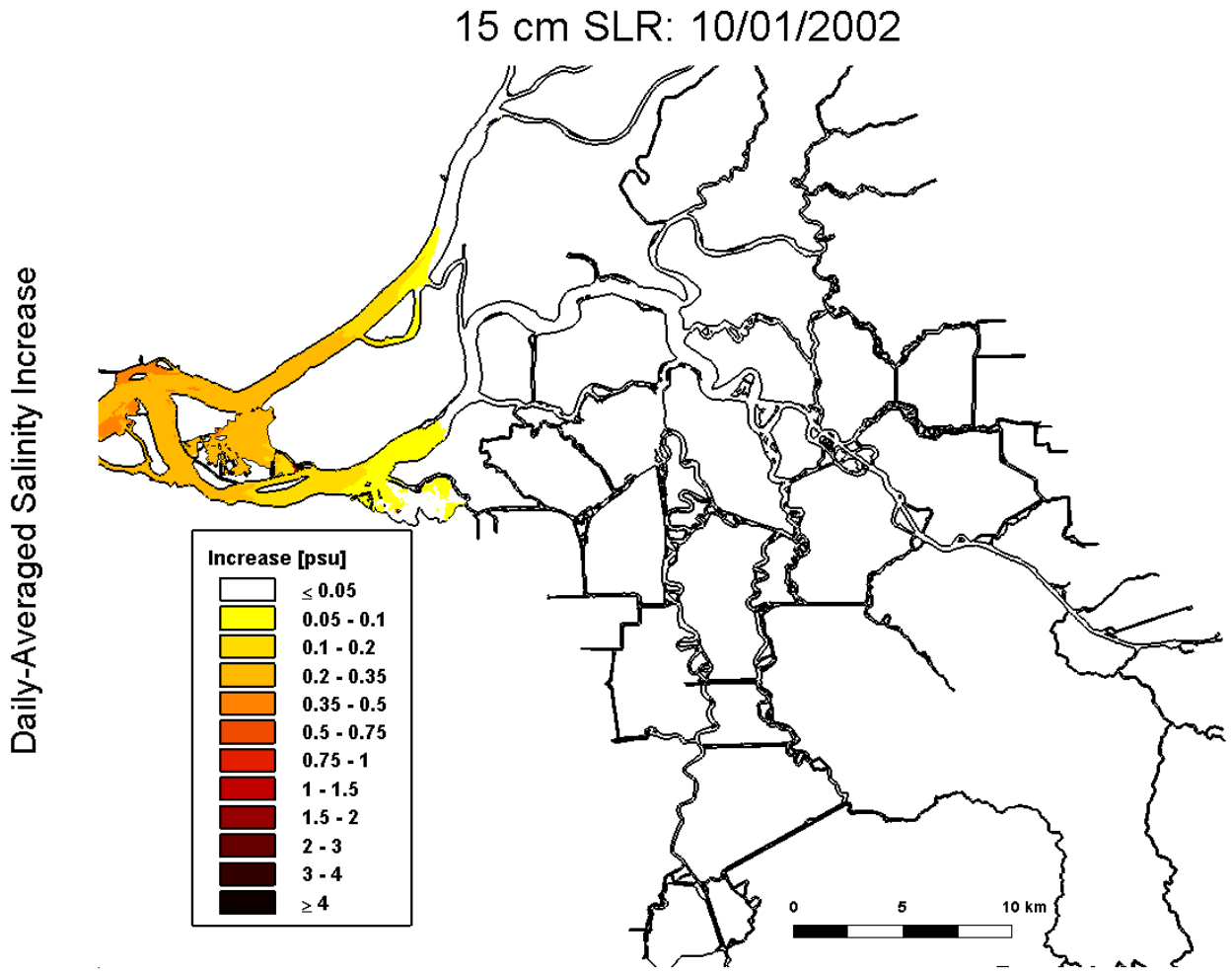

Figure 4.1-23 Predicted increase in daily-averaged depth-average salinity in the Sacramento-San Joaquin Delta on October 1, 2002 relative to the Baseline (0 cm SLR) scenario for the 15 cm SLR scenario.

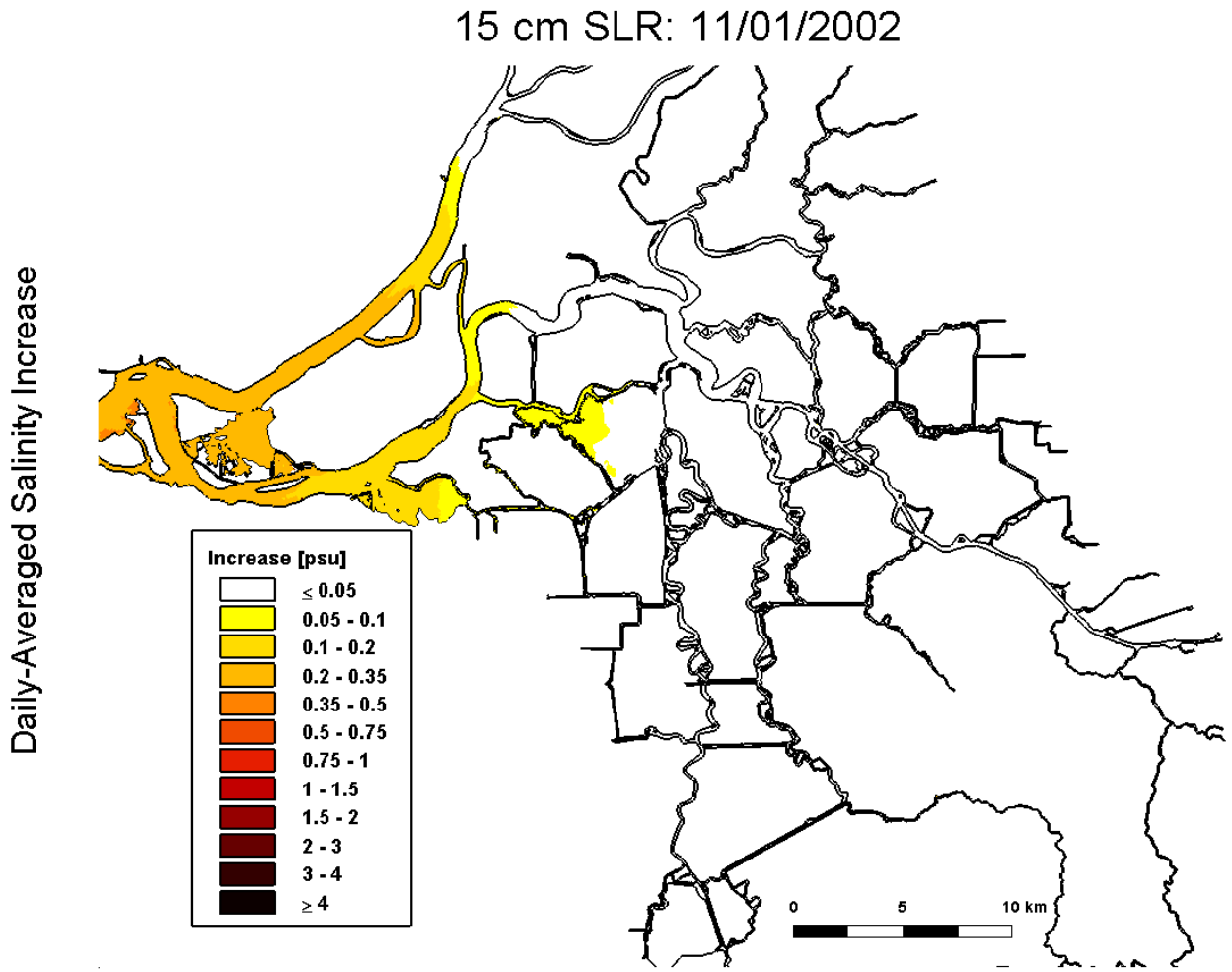

Figure 4.1-24 Predicted increase in daily-averaged depth-average salinity in the Sacramento-San Joaquin Delta on November 1, 2002 relative to the Baseline (0 cm SLR) scenario for the 15 cm SLR scenario.

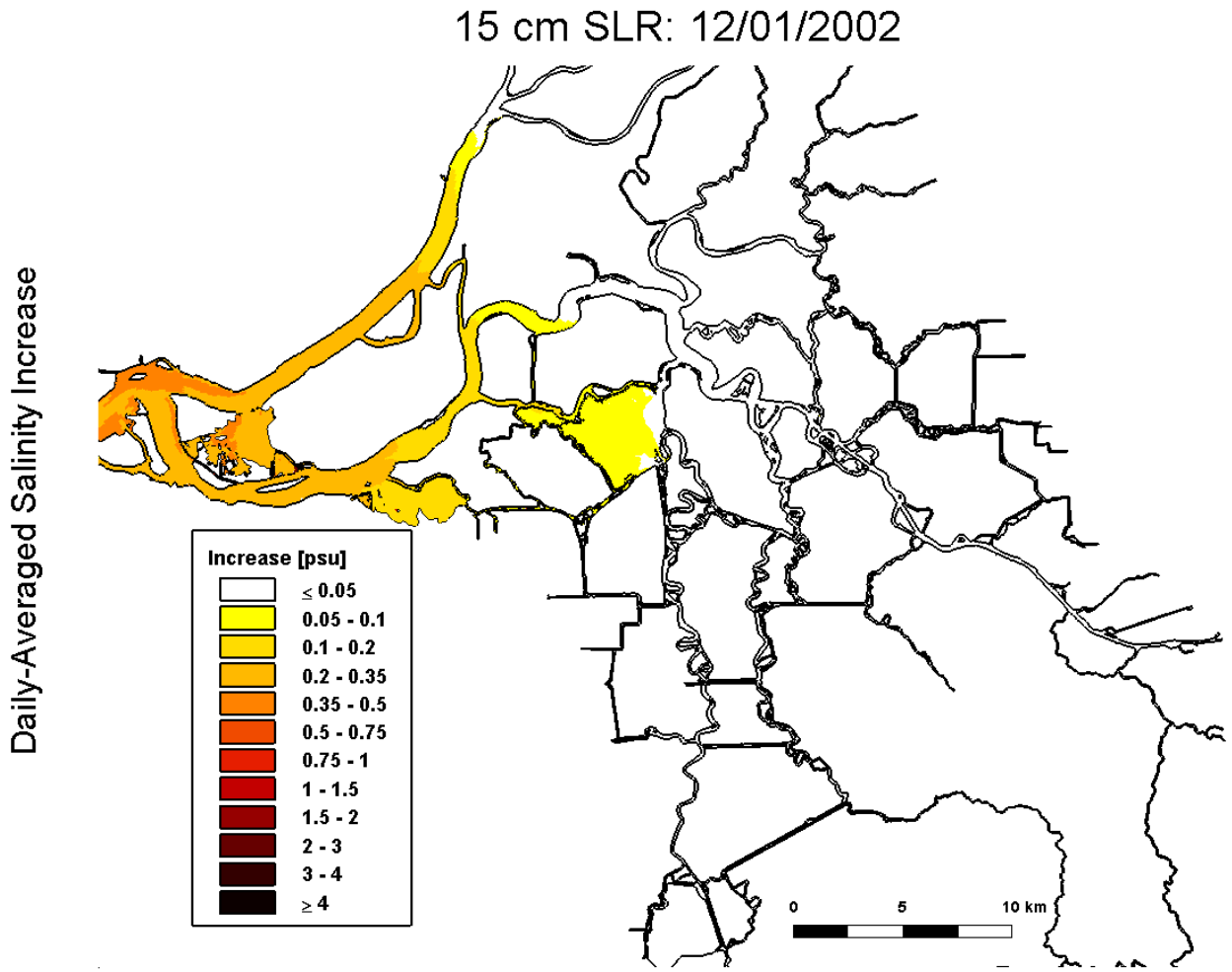

Figure 4.1-25 Predicted increase in daily-averaged depth-average salinity in the Sacramento-San Joaquin Delta on December 1, 2002 relative to the Baseline (0 cm SLR) scenario for the 15 cm SLR scenario.

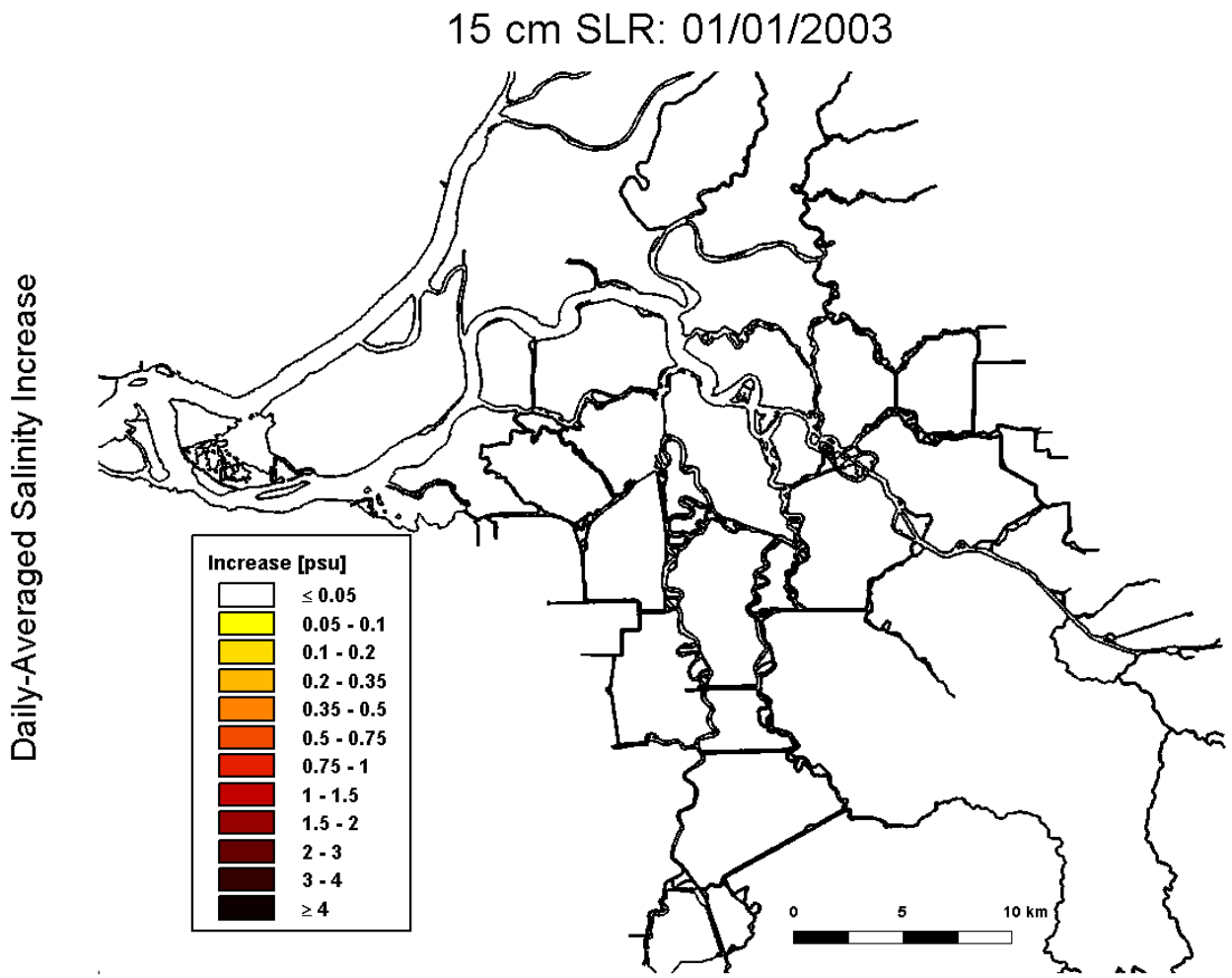

Figure 4.1-26 Predicted increase in daily-averaged depth-average salinity in the Sacramento-San Joaquin Delta on January 1, 2003 relative to the Baseline (0 cm SLR) scenario for the 15 cm SLR scenario.

4.2 Predicted Increase in Salinity for 30 cm SLR Scenario

Figure 4.2-1 through 4.2-13 show the predicted salinity along the northern portion of the San Francisco Estuary, spanning from San Pablo Bay through the Sacramento-San Joaquin Delta for the 30 cm SLR scenario. The top panel of each figure shows the predicted daily-averaged depth-average salinity for the 30 cm SLR scenario. The lower panel shows the predicted salinity increase computed by subtracting the predicted daily-averaged depth-average salinity for the Baseline (0 cm SLR) scenario from the predicted daily-averaged depth-average salinity for the 30 cm SLR scenario. Figures 4.2-14 through 4.2-26 show the predicted salinity increases resulting from the 30 cm SLR scenario in the Sacramento-San Joaquin Delta.

At the beginning of the analysis period on January 1, 2002, salinity increases between 0.10 and 0.35 psu are predicted between Chipps Island and Collinsville and predicted salinity increases of up to 0.05 psu are predicted upstream to the western end of Sherman Lake. Predicted salinity increases are less than 0.05 psu throughout the remaining portions of the Delta. Salinity increases between 0.75 and 1.0 psu are predicted through Carquinez Strait and salinity increases between 0.35 and 1.0 psu are predicted throughout Suisun Bay. Larger salinity increases of more than 1.0 psu are predicted in much of San Pablo Bay, and more than 3 psu in northern San Pablo Bay. During the first half of the year, predicted salinity increases in Suisun Bay and the Delta remain similar to the predicted salinity increases seen on January 1, 2002, though the predicted salinity is increasing throughout this period. Larger salinity increases are predicted in the Delta between July and December, with the largest predicted salinity increases in December prior to the first flush. In December, salinity increases of between 0.50 and 0.75 psu are predicted between Chipps Island and Emmaton, and salinity increases of between 0.05 and 0.20 psu are predicted in Franks Tract. South of Franks Tract, predicted salinity increases between 0.05 and 0.10 psu extend down Old River to Italian Slough. Following high flows which occurred in December, predicted salinity on January 1, 2003 shows that the 0.50 psu isohaline is on the western side of Suisun Bay near Martinez. Predicted salinity increases of between 0.05 and 0.10 psu persist in Big Break, a portion of Little Mandeville Island, and some reaches of Dutch Slough. Predicted salinity increases are less than 0.05 psu throughout the remaining portions of the Delta.

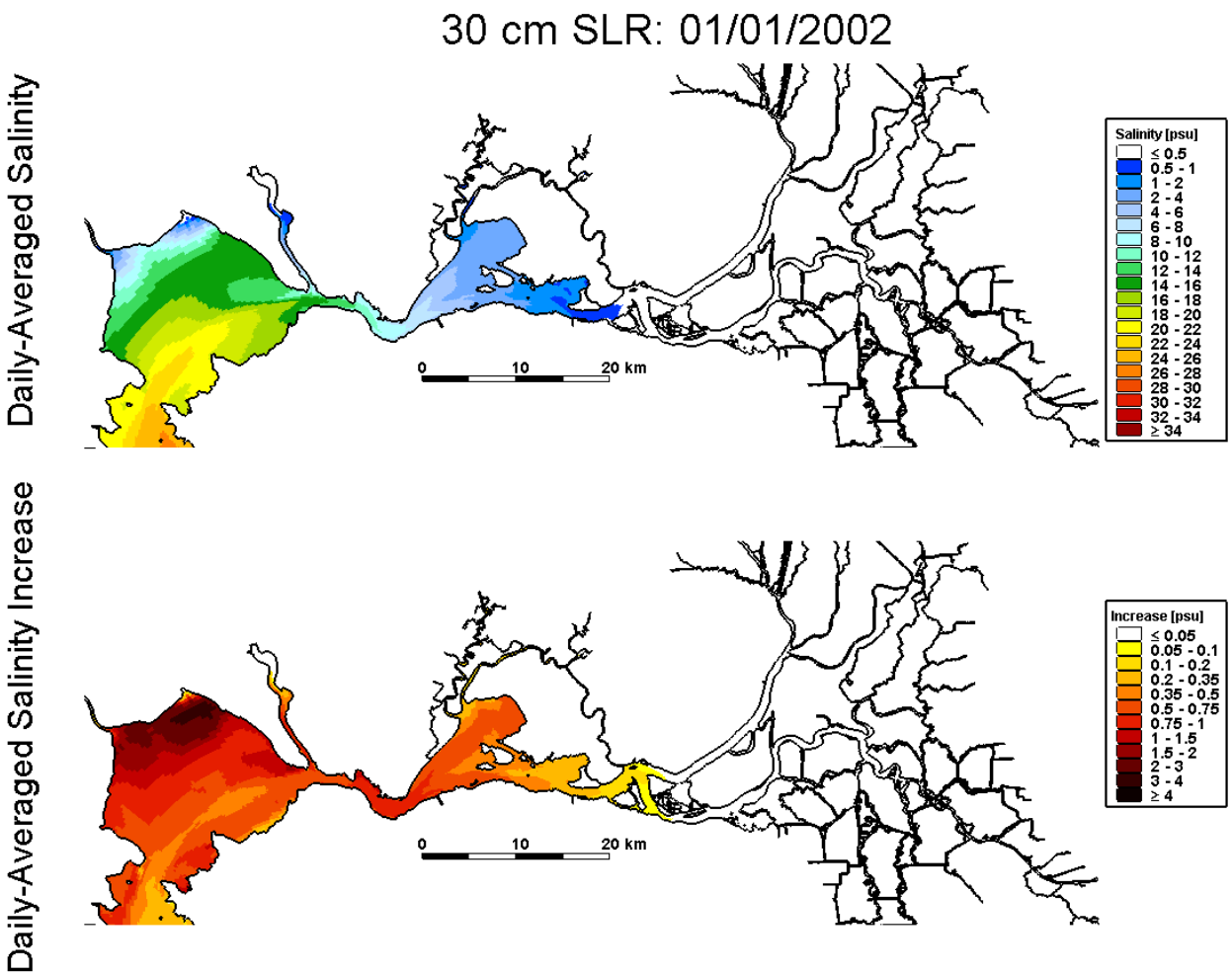

Figure 4.2-1 Predicted daily-averaged depth-average salinity on January 1, 2002 for the 30 cm SLR scenario (top); predicted increase in daily-averaged depth-average salinity on January 1, 2002 relative to the Baseline (0 cm SLR) scenario for the 30 cm SLR scenario.

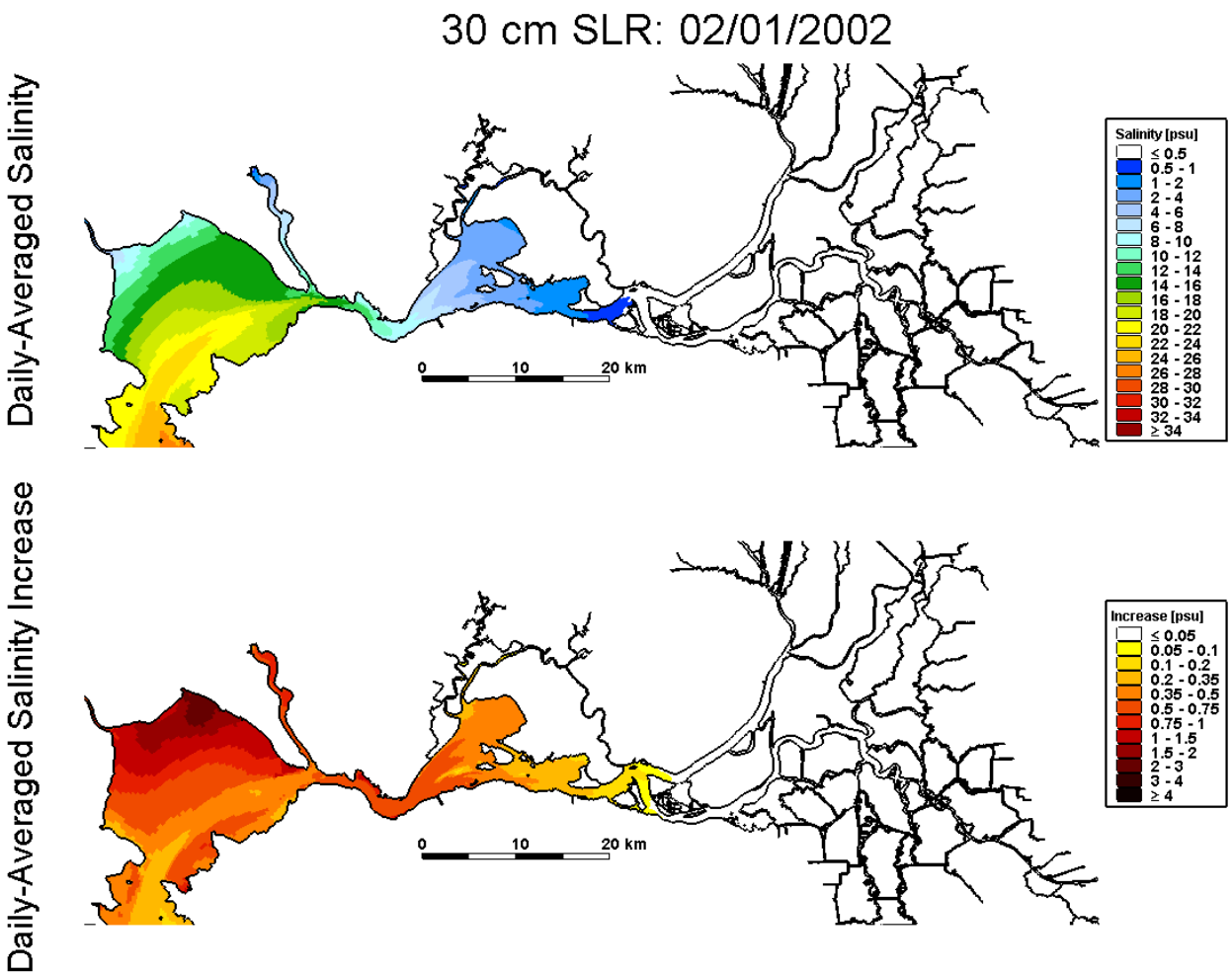

Figure 4.2-2 Predicted daily-averaged depth-average salinity on February 1, 2002 for the 30 cm SLR scenario (top); predicted increase in daily-averaged depth-average salinity on February 1, 2002 relative to the Baseline (0 cm SLR) scenario for the 30 cm SLR scenario.

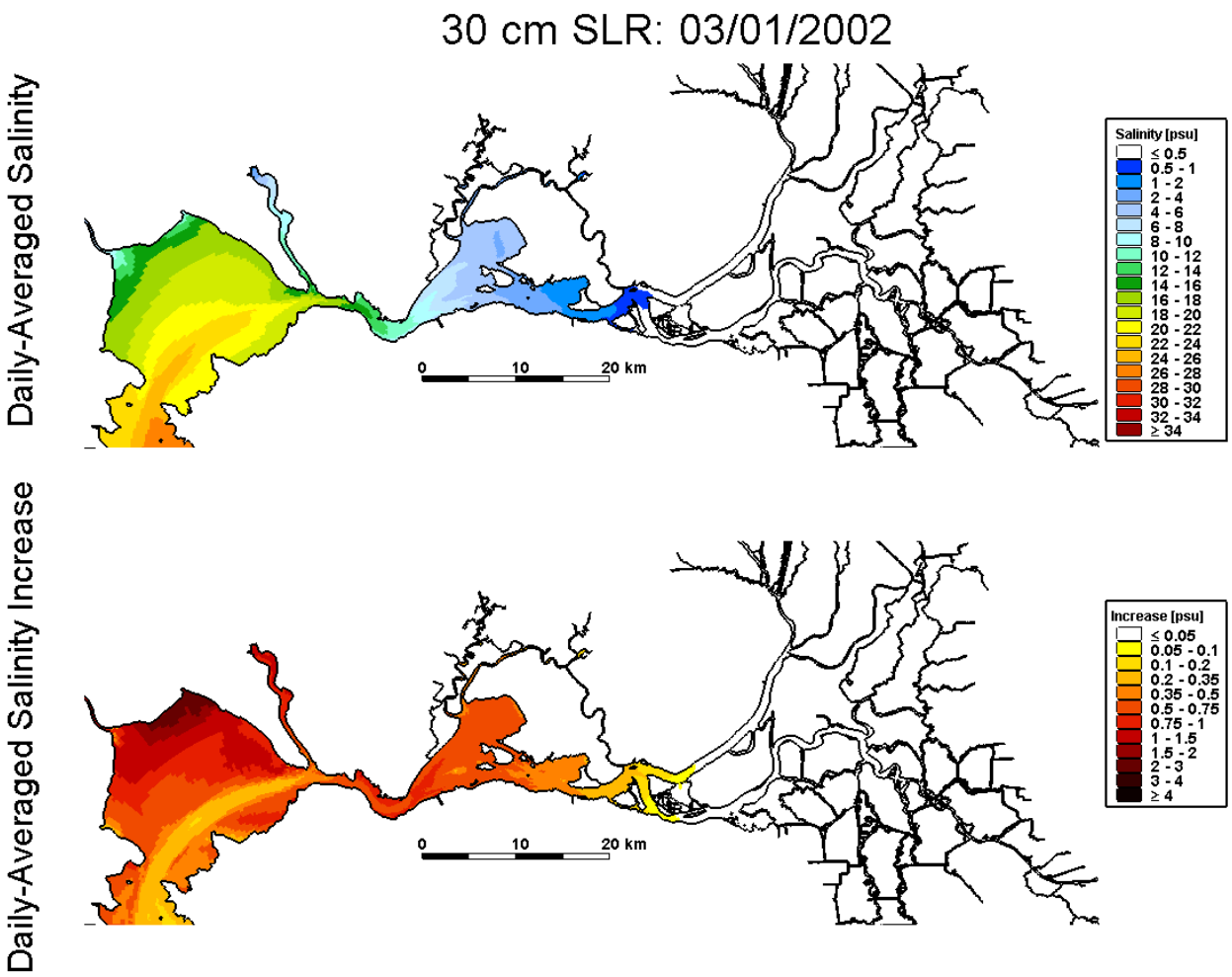

Figure 4.2-3 Predicted daily-averaged depth-average salinity on March 1, 2002 for the 30 cm SLR scenario (top); predicted increase in daily-averaged depth-average salinity on March 1, 2002 relative to the Baseline (0 cm SLR) scenario for the 30 cm SLR scenario.

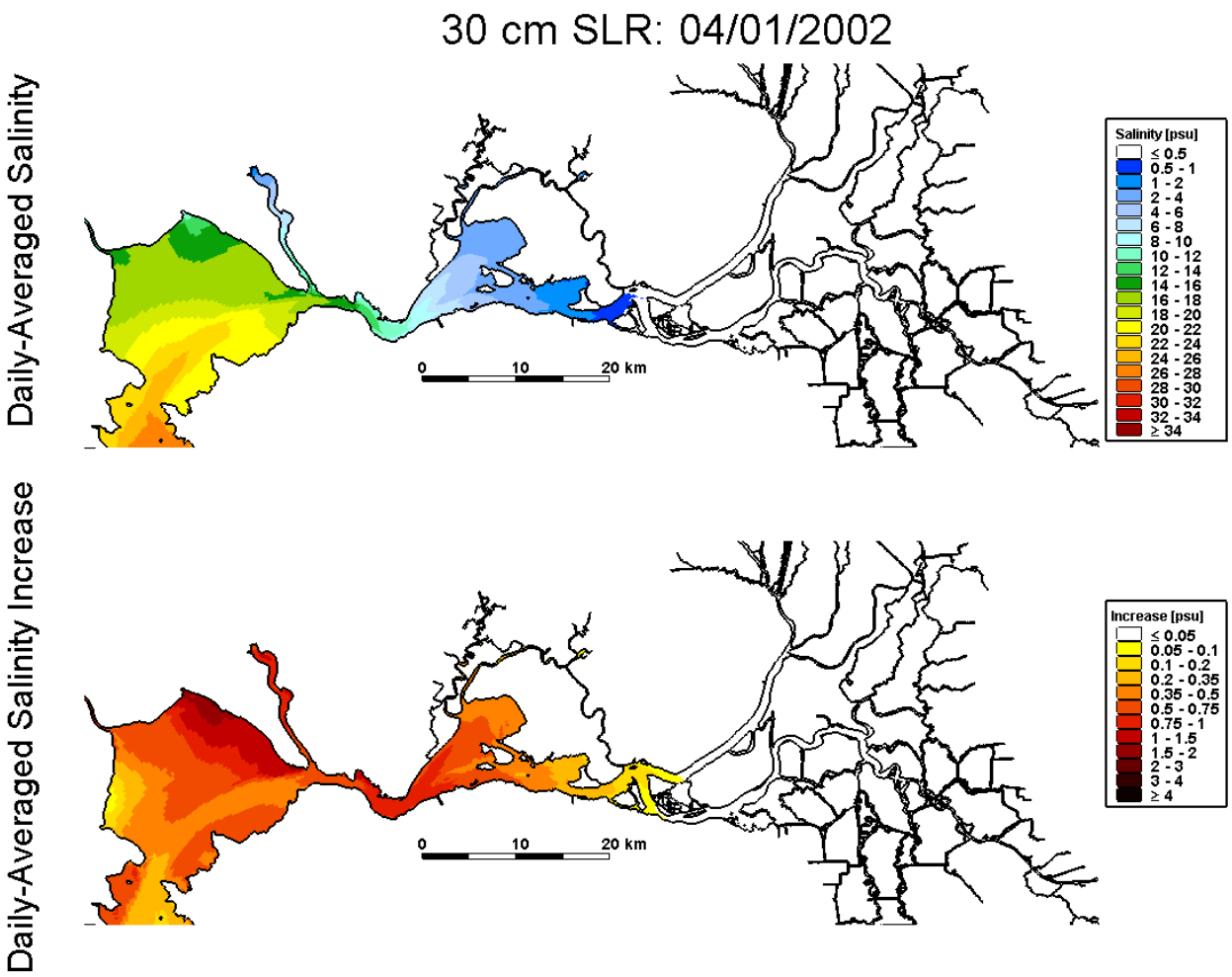

Figure 4.2-4 Predicted daily-averaged depth-average salinity on April 1, 2002 for the 30 cm SLR scenario (top); predicted increase in daily-averaged depth-average salinity on April 1, 2002 relative to the Baseline (0 cm SLR) scenario for the 30 cm SLR scenario.

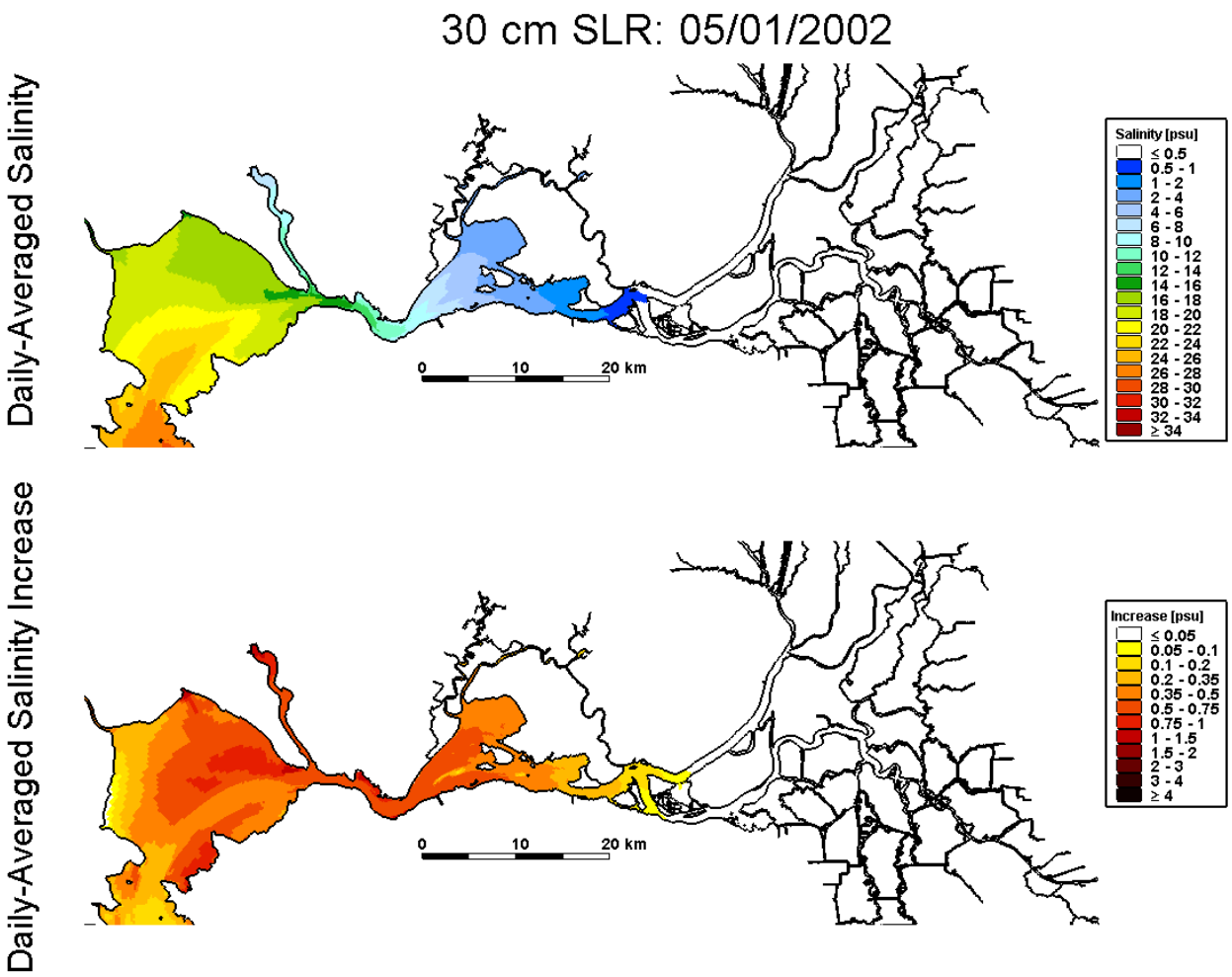

Figure 4.2-5 Predicted daily-averaged depth-average salinity on May 1, 2002 for the 30 cm SLR scenario (top); predicted increase in daily-averaged depth-average salinity on May 1, 2002 relative to the Baseline (0 cm SLR) scenario for the 30 cm SLR scenario.

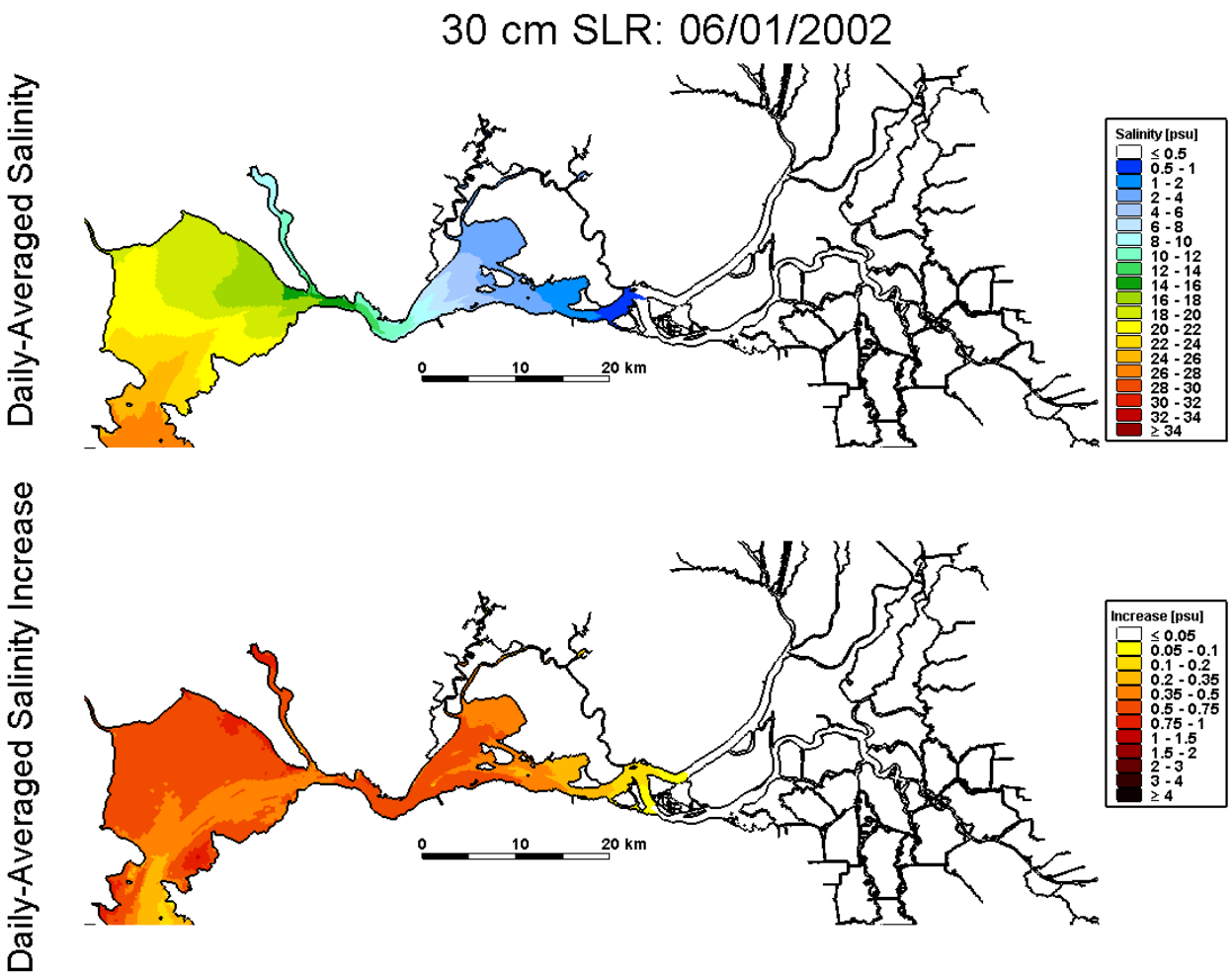

Figure 4.2-6 Predicted daily-averaged depth-average salinity on June 1, 2002 for the 30 cm SLR scenario (top); predicted increase in daily-averaged depth-average salinity on June 1, 2002 relative to the Baseline (0 cm SLR) scenario for the 30 cm SLR scenario.

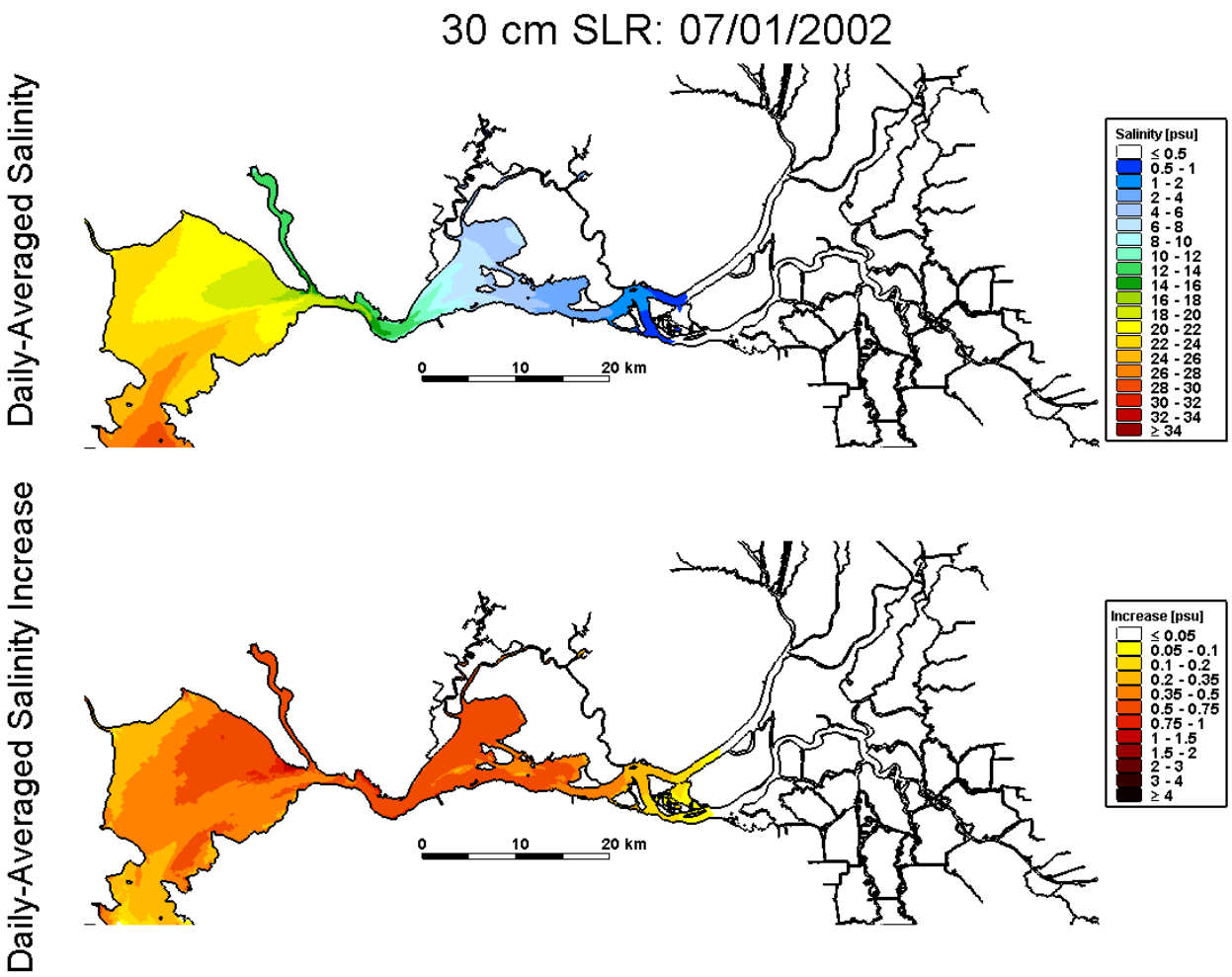

Figure 4.2-7 Predicted daily-averaged depth-average salinity on July 1, 2002 for the 30 cm SLR scenario (top); predicted increase in daily-averaged depth-average salinity on July 1, 2002 relative to the Baseline (0 cm SLR) scenario for the 30 cm SLR scenario.

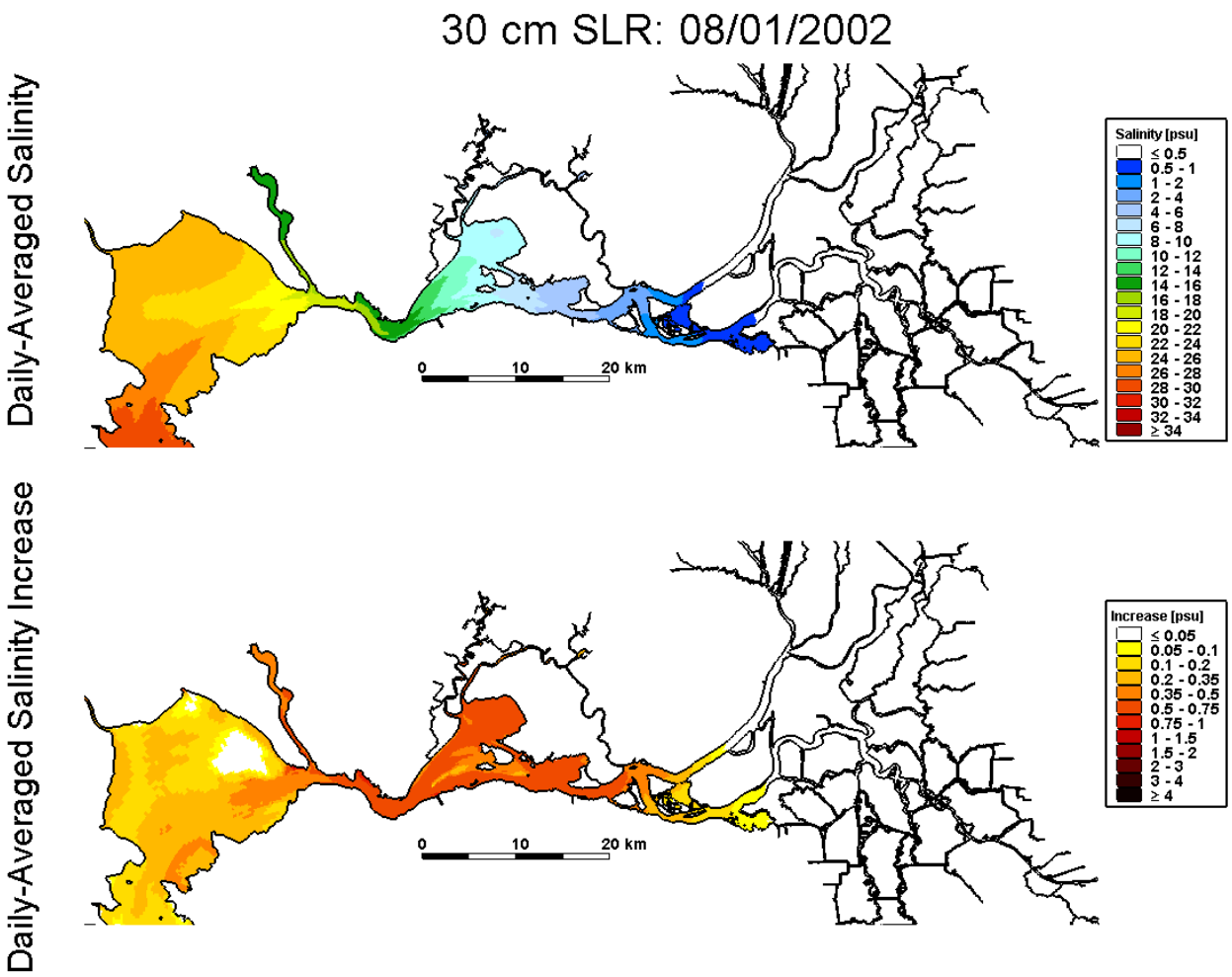

Figure 4.2-8 Predicted daily-averaged depth-average salinity on August 1, 2002 for the 30 cm SLR scenario (top); predicted increase in daily-averaged depth-average salinity on August 1, 2002 relative to the Baseline (0 cm SLR) scenario for the 30 cm SLR scenario.

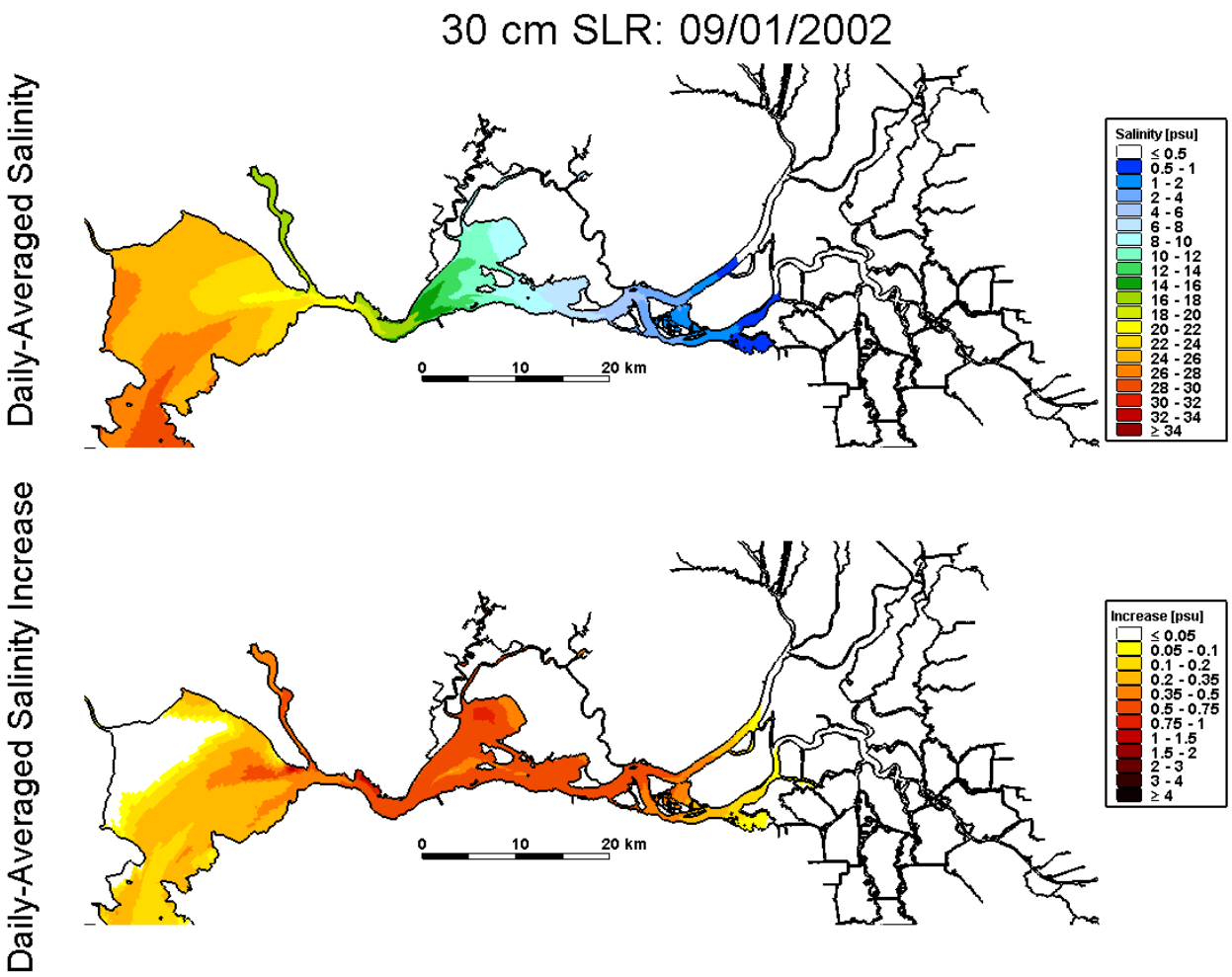

Figure 4.2-9 Predicted daily-averaged depth-average salinity on September 1, 2002 for the 30 cm SLR scenario (top); predicted increase in daily-averaged depth-average salinity on September 1, 2002 relative to the Baseline (0 cm SLR) scenario for the 30 cm SLR scenario.

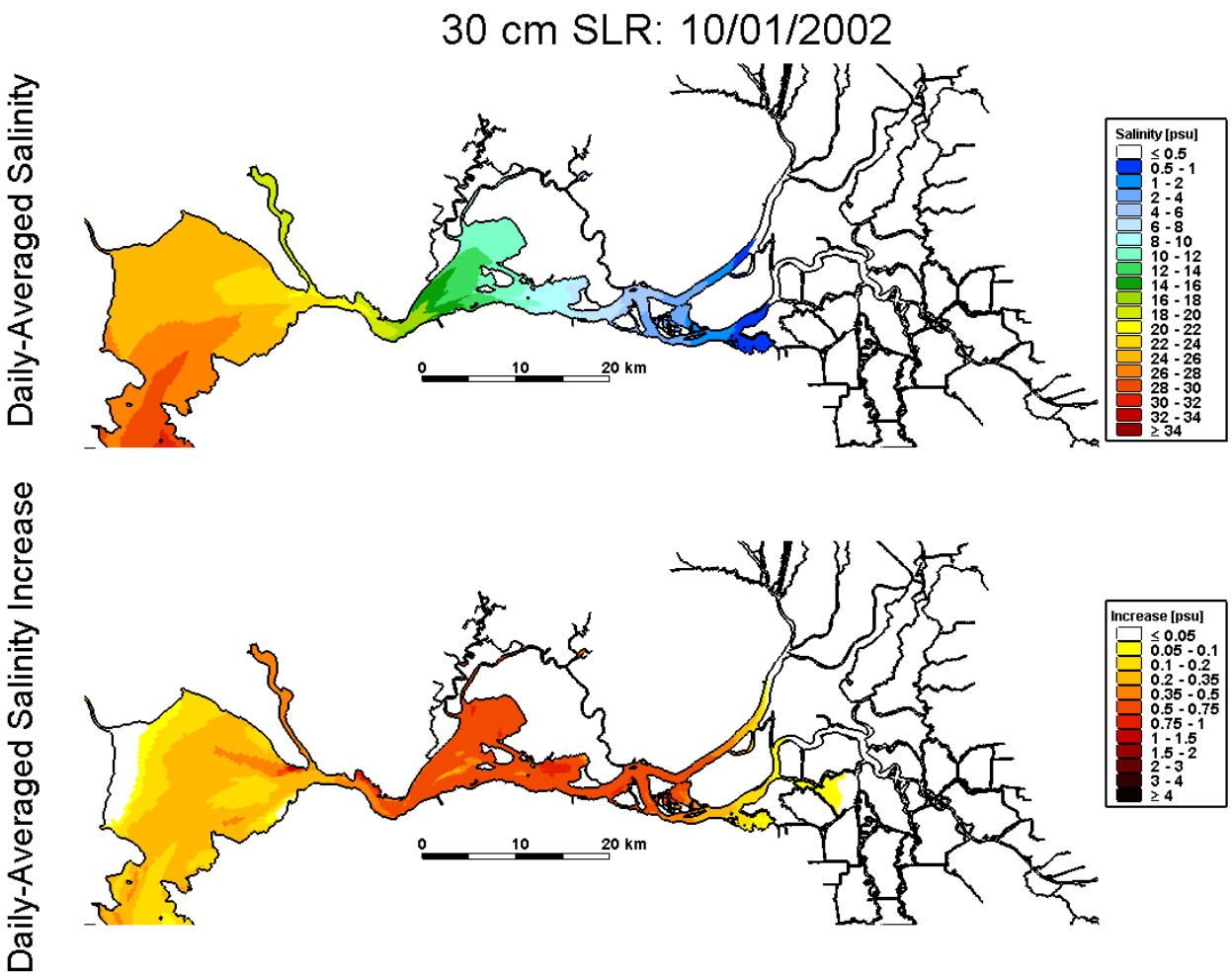

Figure 4.2-10 Predicted daily-averaged depth-average salinity on October 1, 2002 for the 30 cm SLR scenario (top); predicted increase in daily-averaged depth-average salinity on October 1, 2002 relative to the Baseline (0 cm SLR) scenario for the 30 cm SLR scenario.

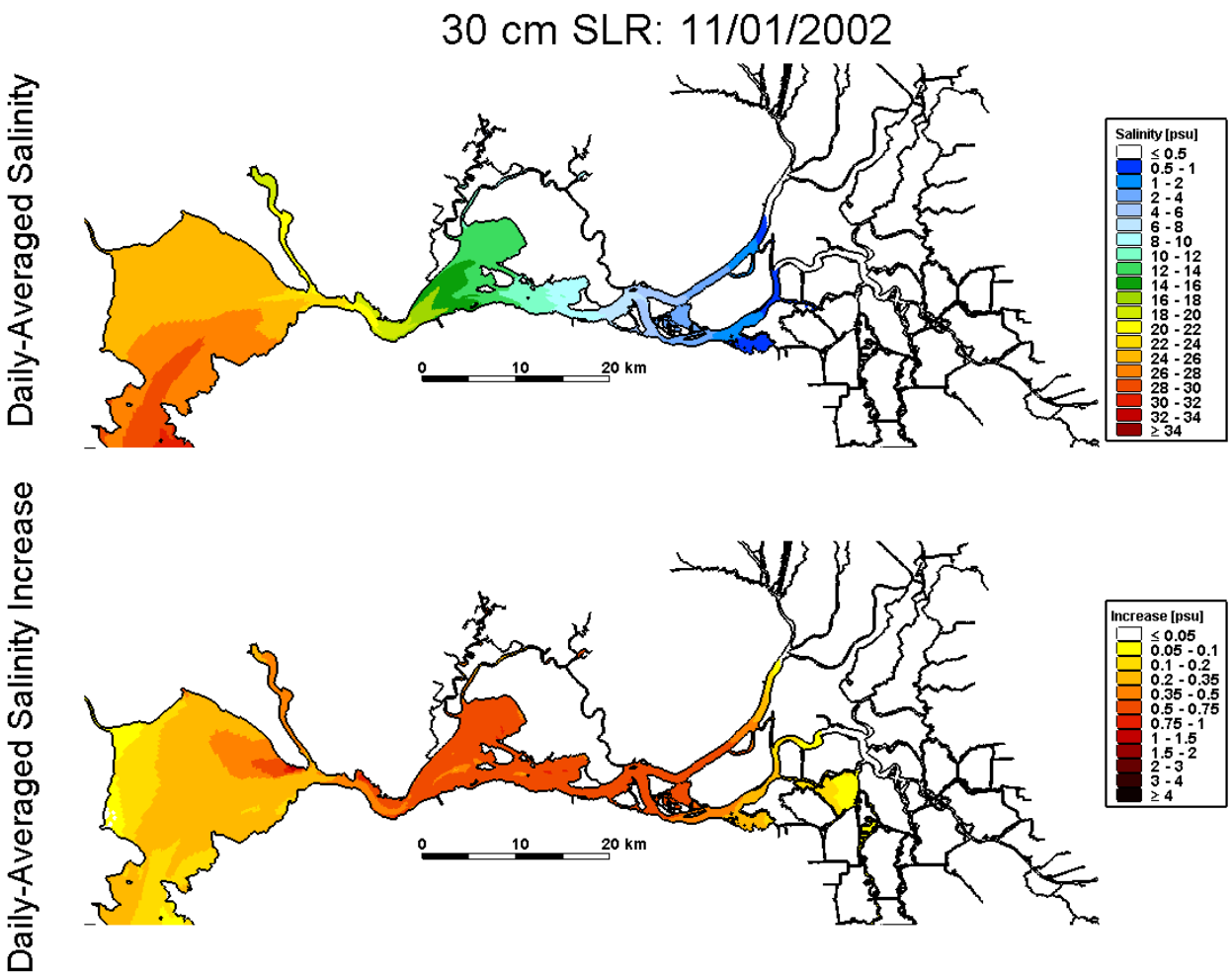

Figure 4.2-11 Predicted daily-averaged depth-average salinity on November 1, 2002 for the 30 cm SLR scenario (top); predicted increase in daily-averaged depth-average salinity on November 1, 2002 relative to the Baseline (0 cm SLR) scenario for the 30 cm SLR scenario.

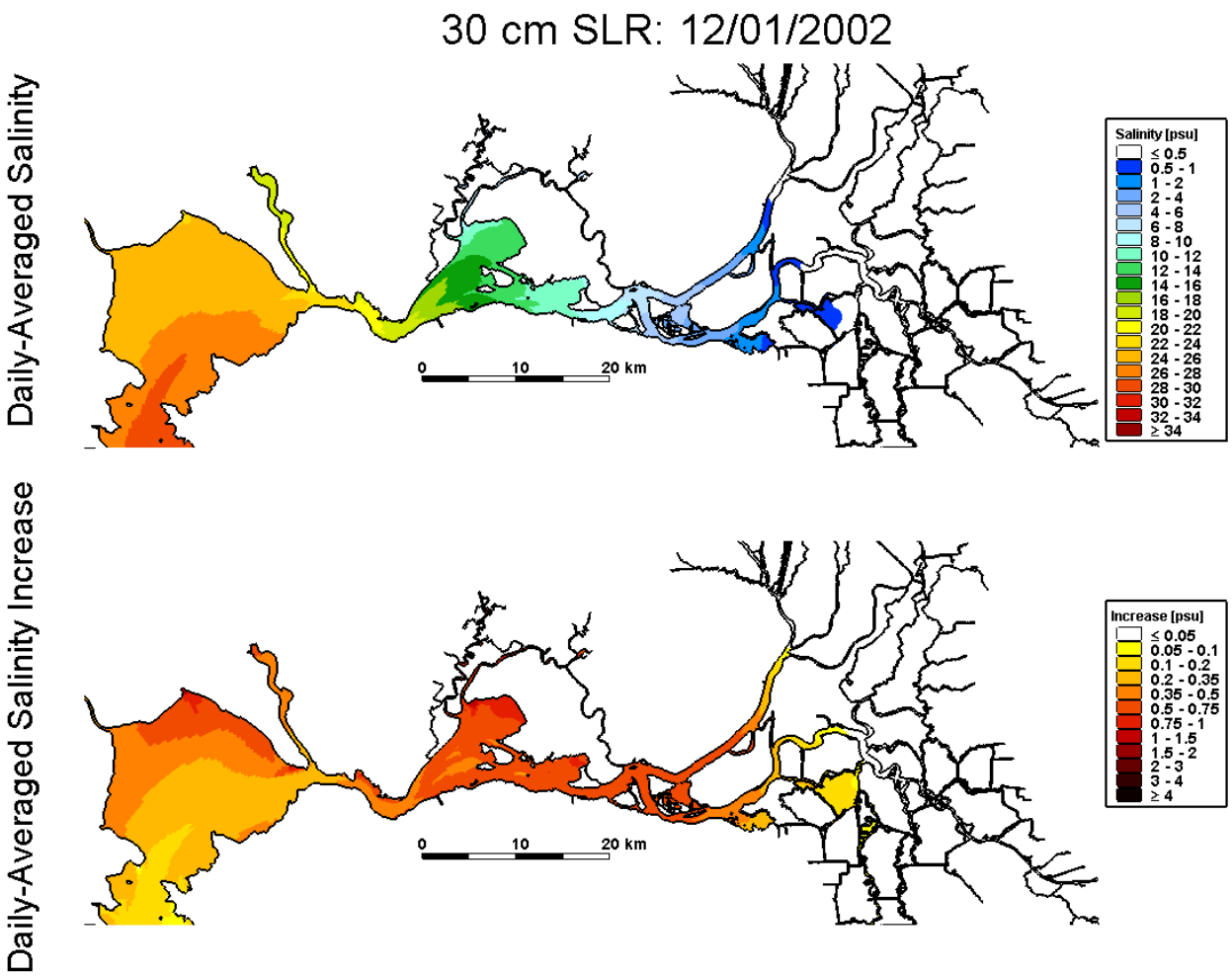

Figure 4.2-12 Predicted daily-averaged depth-average salinity on December 1, 2002 for the 30 cm SLR scenario (top); predicted increase in daily-averaged depth-average salinity on December 1, 2002 relative to the Baseline (0 cm SLR) scenario for the 30 cm SLR scenario.

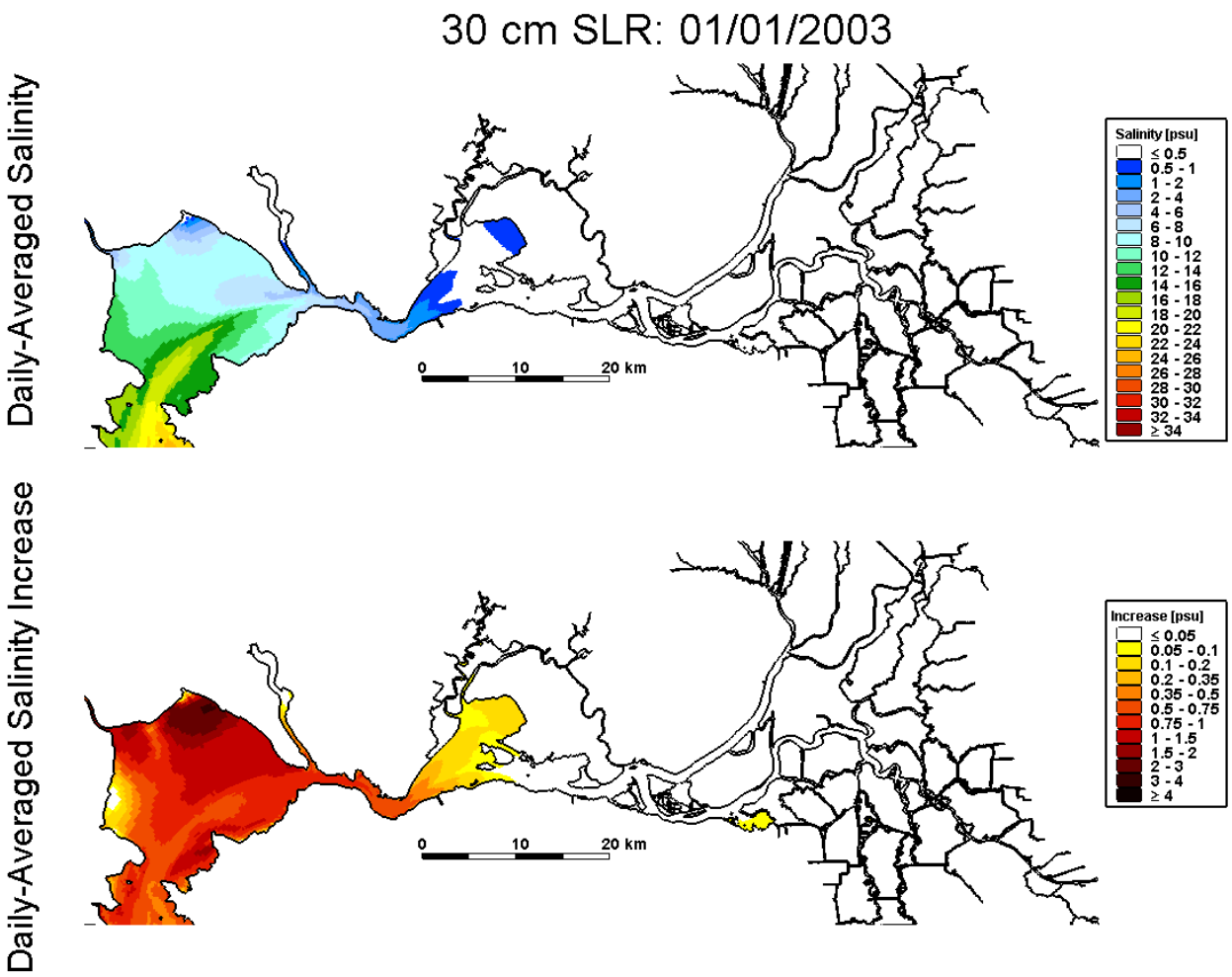

Figure 4.2-13 Predicted daily-averaged depth-average salinity on January 1, 2003 for the 30 cm SLR scenario (top); predicted increase in daily-averaged depth-average salinity on January 1, 2003 relative to the Baseline (0 cm SLR) scenario for the 30 cm SLR scenario.

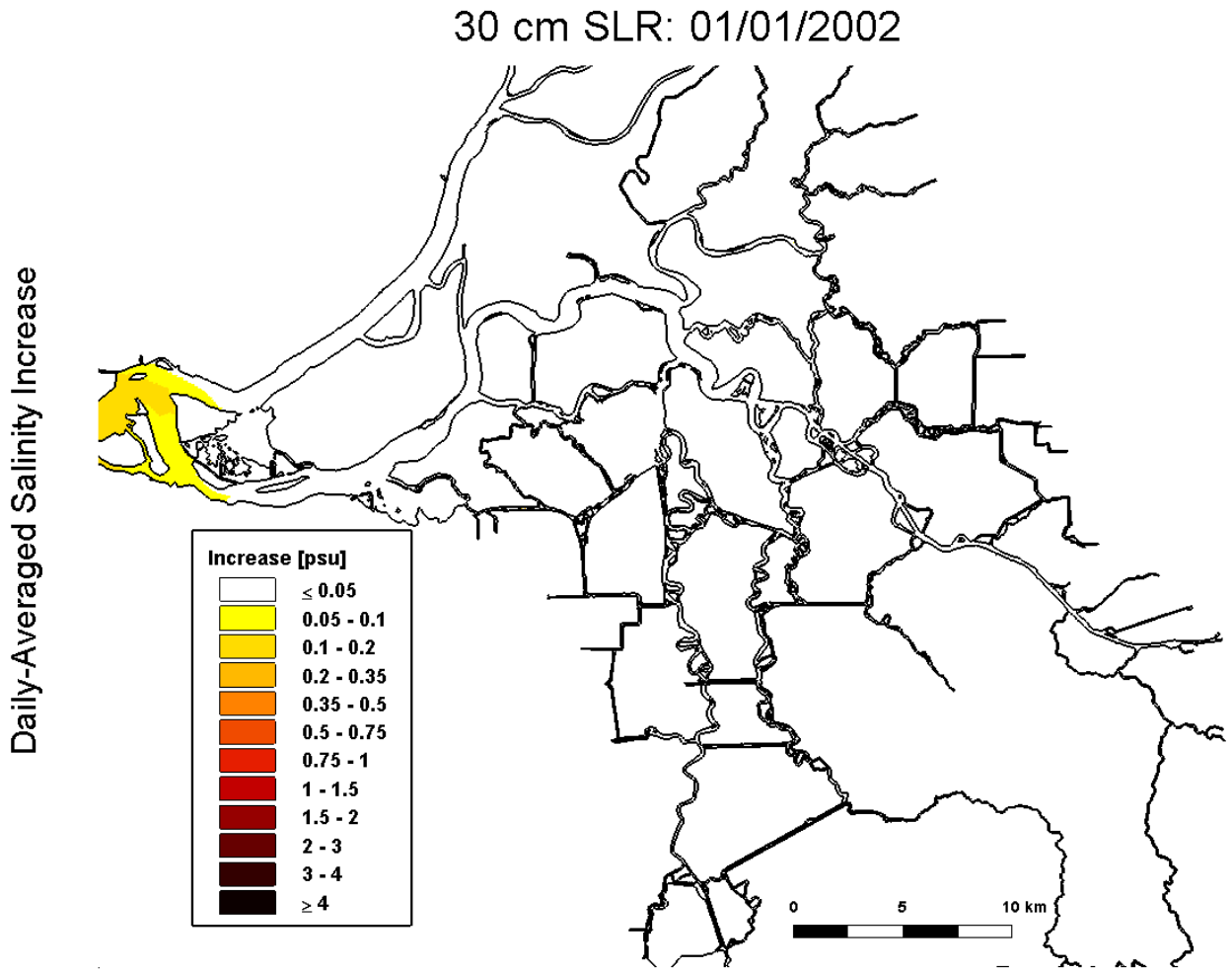

Figure 4.2-14 Predicted increase in daily-averaged depth-average salinity in the Sacramento-San Joaquin Delta on January 1, 2002 relative to the Baseline (0 cm SLR) scenario for the 30 cm SLR scenario.

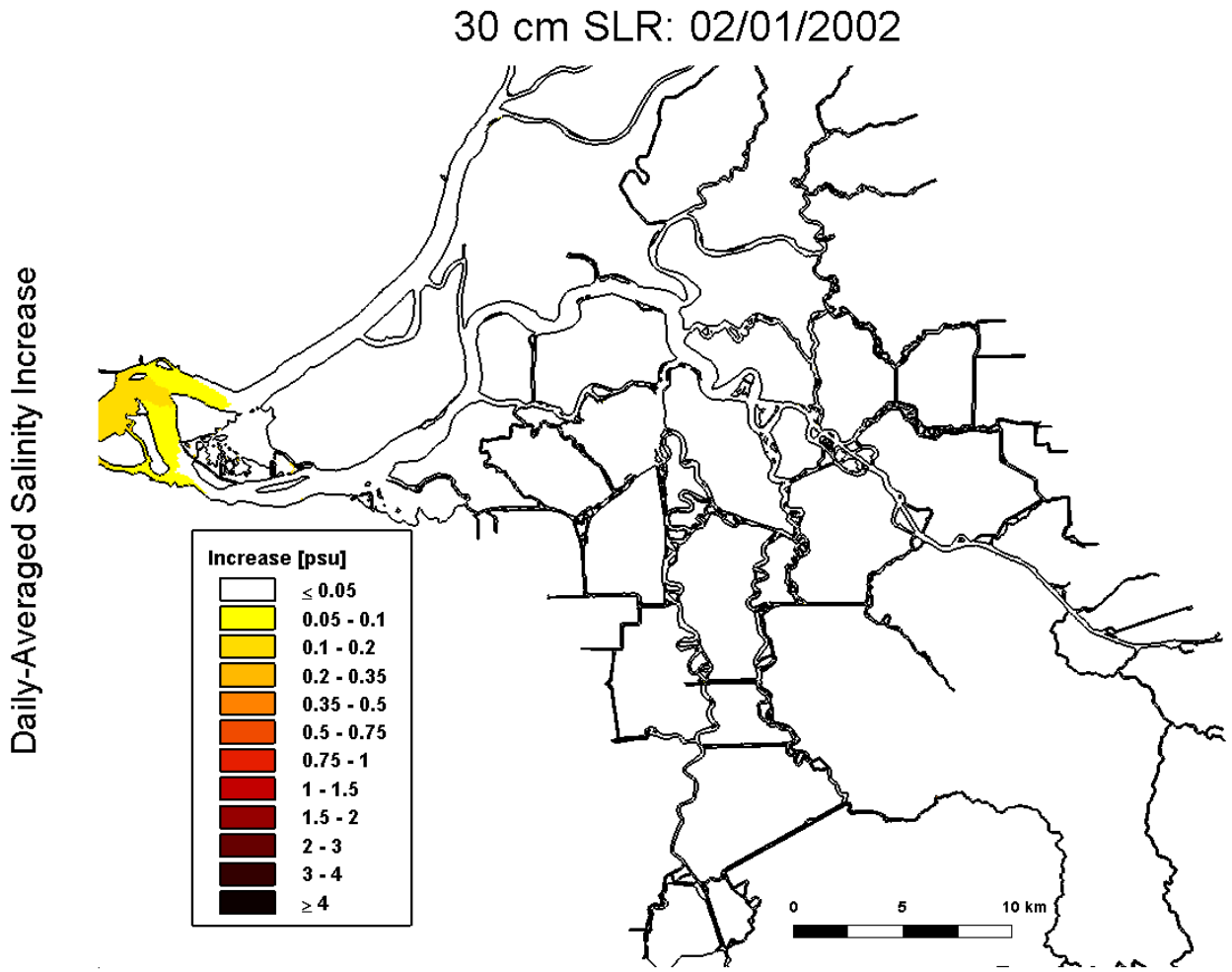

Figure 4.2-15 Predicted increase in daily-averaged depth-average salinity in the Sacramento-San Joaquin Delta on February 1, 2002 relative to the Baseline (0 cm SLR) scenario for the 30 cm SLR scenario.

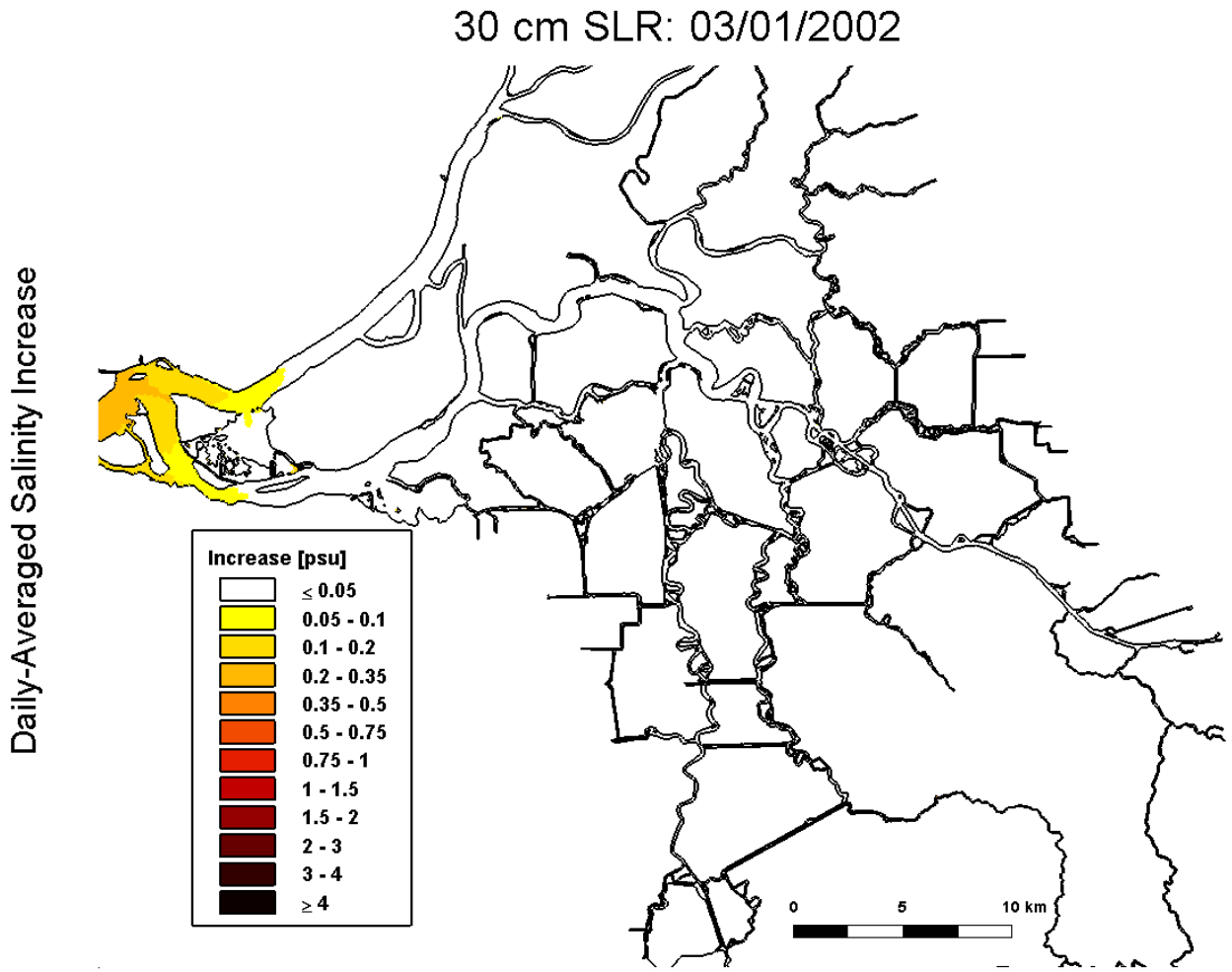

Figure 4.2-16 Predicted increase in daily-averaged depth-average salinity in the Sacramento-San Joaquin Delta on March 1, 2002 relative to the Baseline (0 cm SLR) scenario for the 30 cm SLR scenario.

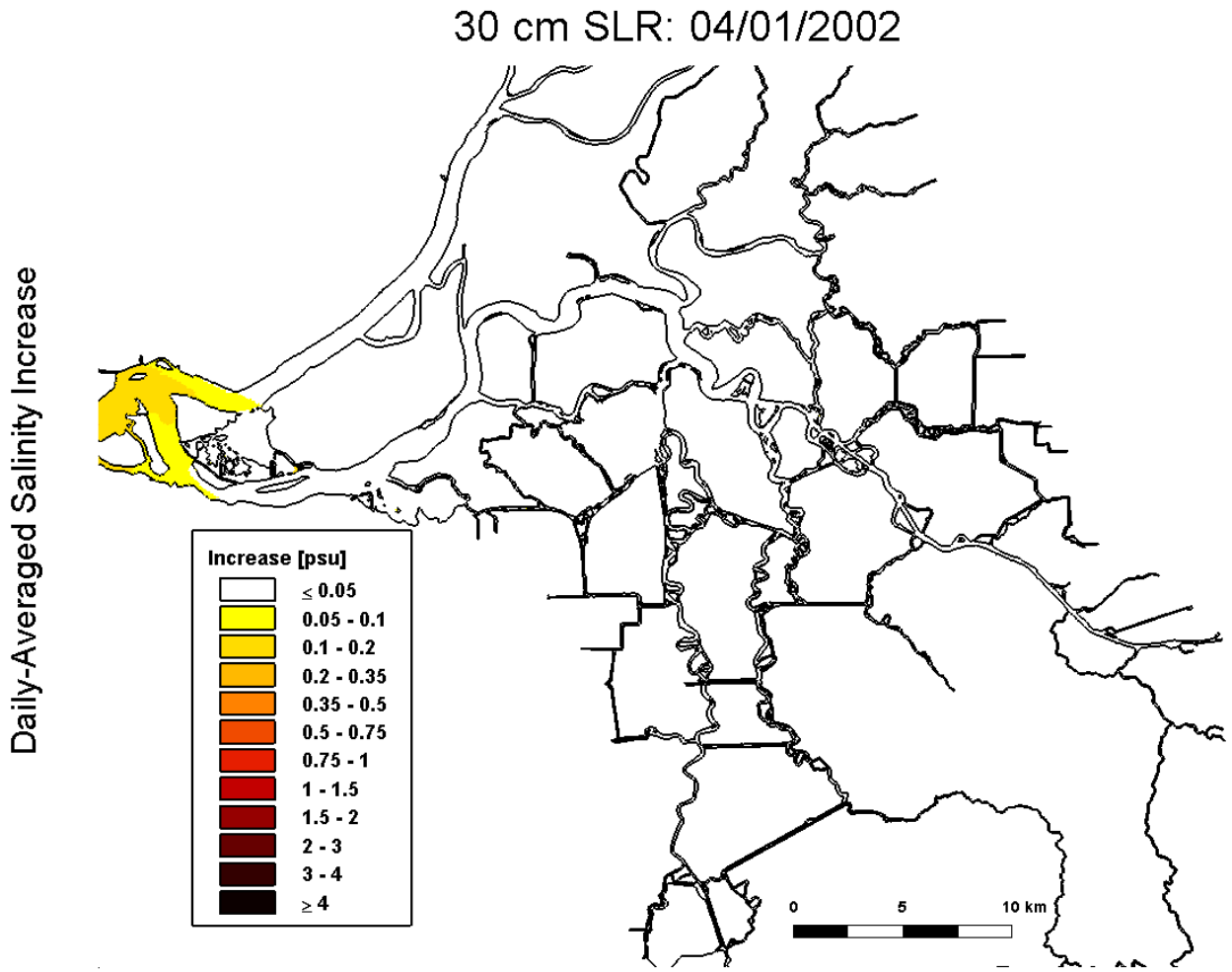

Figure 4.2-17 Predicted increase in daily-averaged depth-average salinity in the Sacramento-San Joaquin Delta on April 1, 2002 relative to the Baseline (0 cm SLR) scenario for the 30 cm SLR scenario.

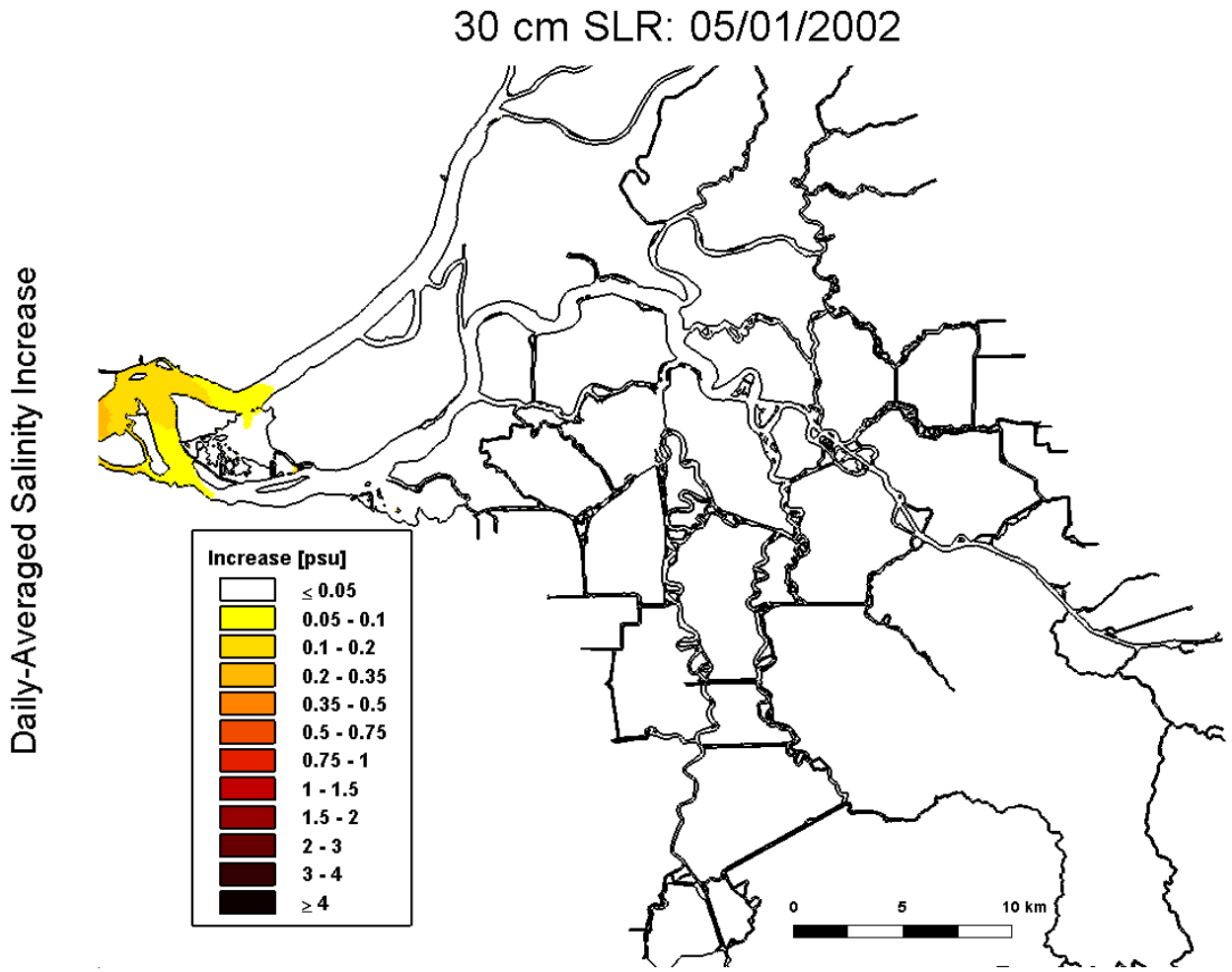

Figure 4.2-18 Predicted increase in daily-averaged depth-average salinity in the Sacramento-San Joaquin Delta on May 1, 2002 relative to the Baseline (0 cm SLR) scenario for the 30 cm SLR scenario.

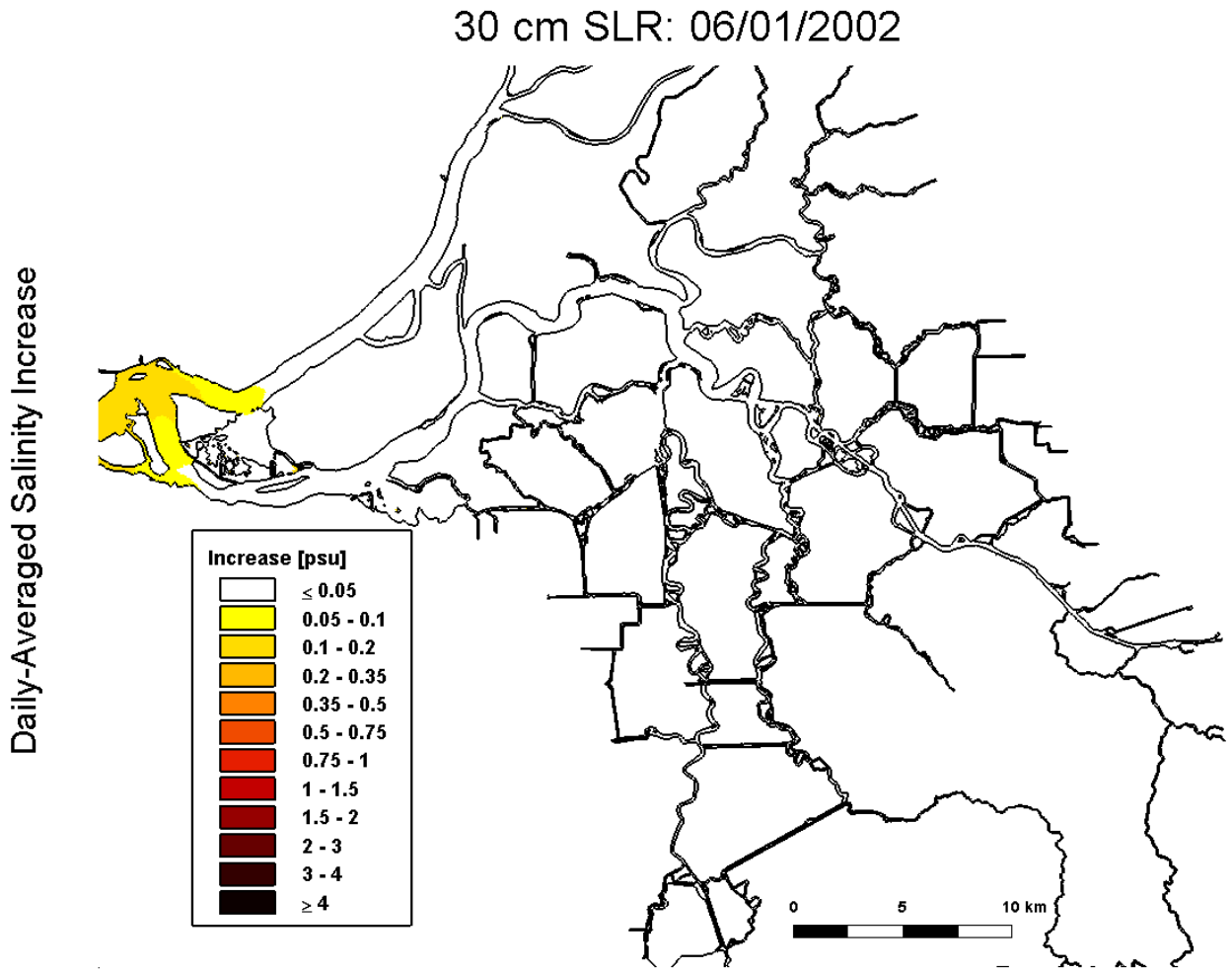

Figure 4.2-19 Predicted increase in daily-averaged depth-average salinity in the Sacramento-San Joaquin Delta on June 1, 2002 relative to the Baseline (0 cm SLR) scenario for the 30 cm SLR scenario.

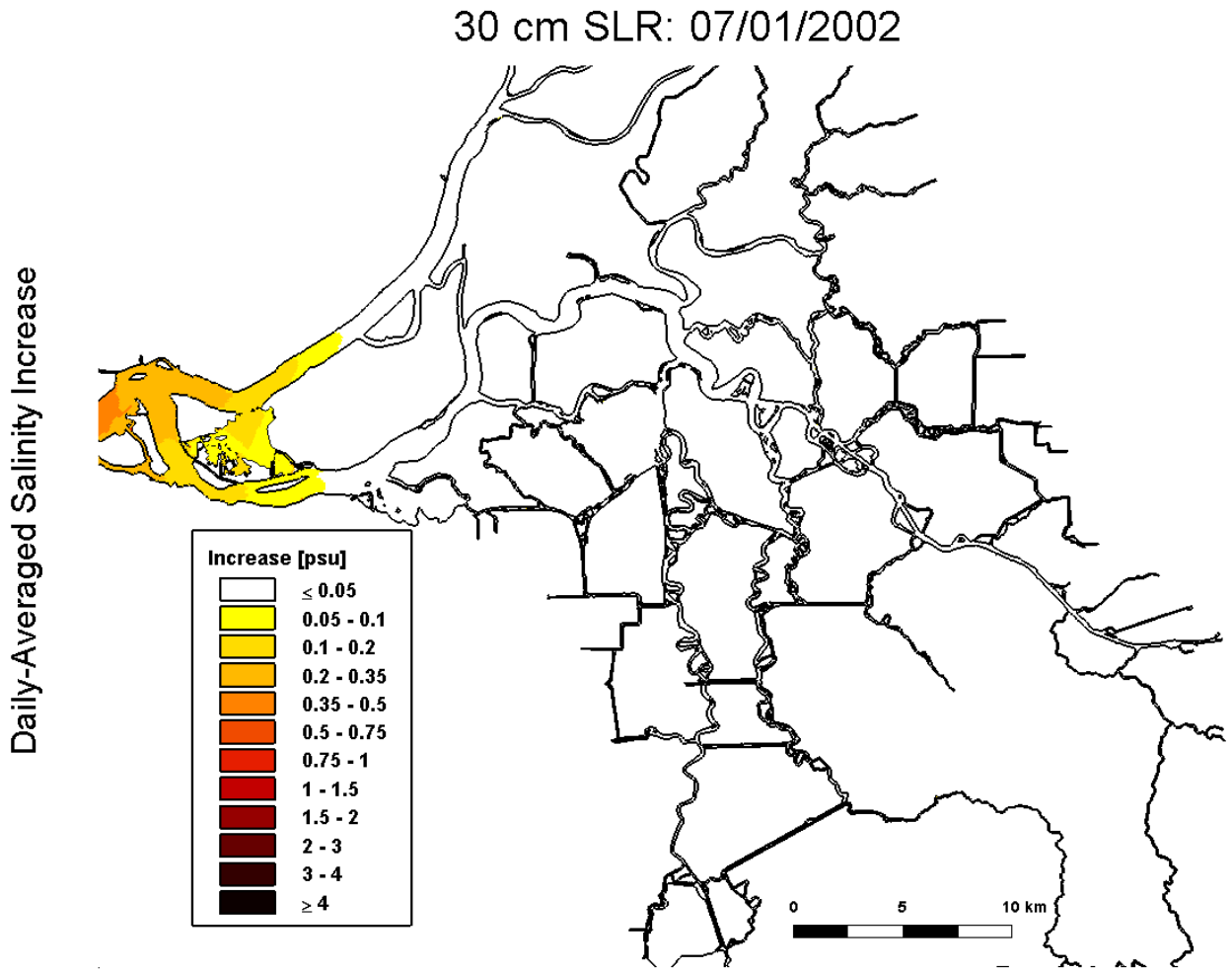

Figure 4.2-20 Predicted increase in daily-averaged depth-average salinity in the Sacramento-San Joaquin Delta on July 1, 2002 relative to the Baseline (0 cm SLR) scenario for the 30 cm SLR scenario.

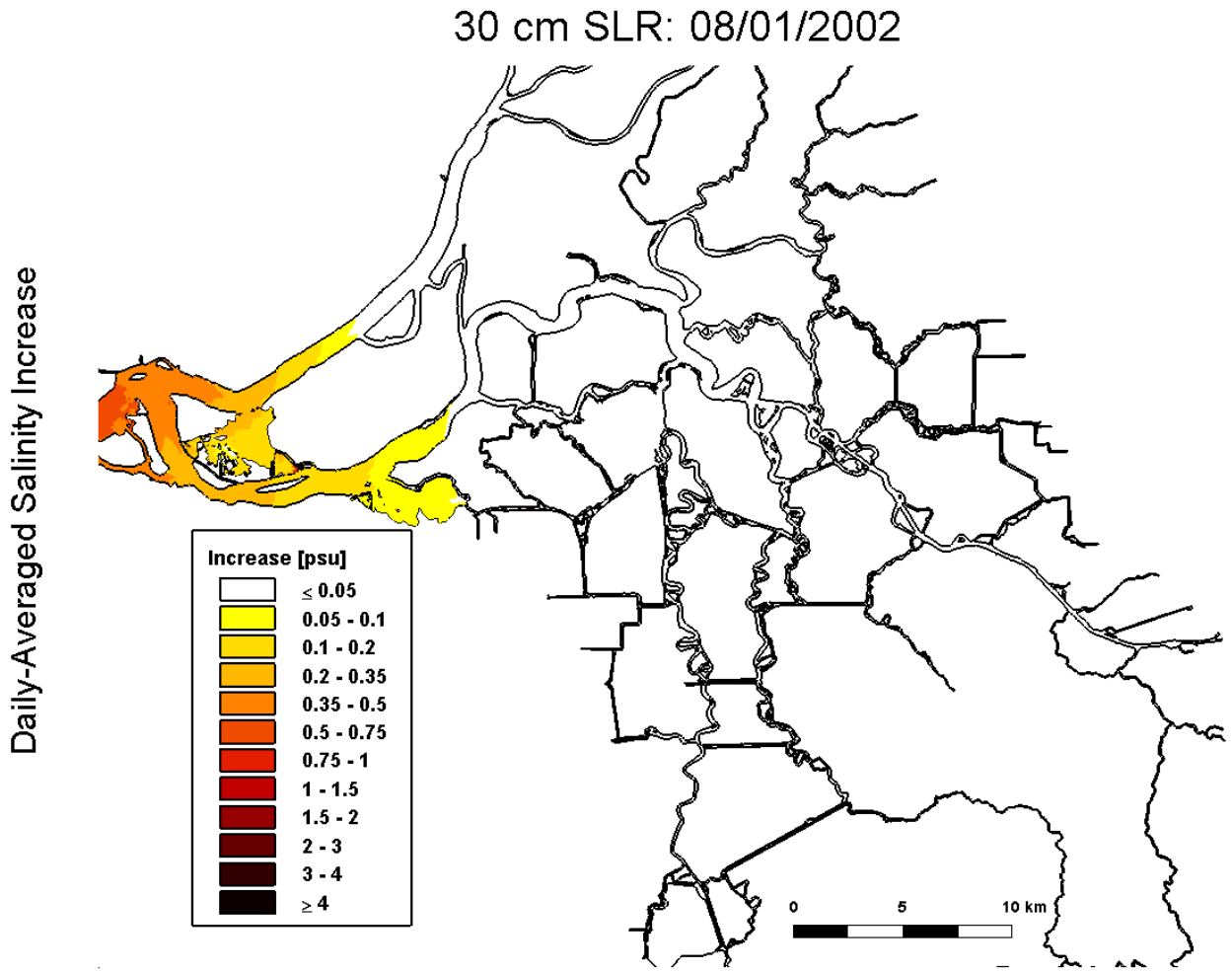

Figure 4.2-21 Predicted increase in daily-averaged depth-average salinity in the Sacramento-San Joaquin Delta on August 1, 2002 relative to the Baseline (0 cm SLR) scenario for the 30 cm SLR scenario.

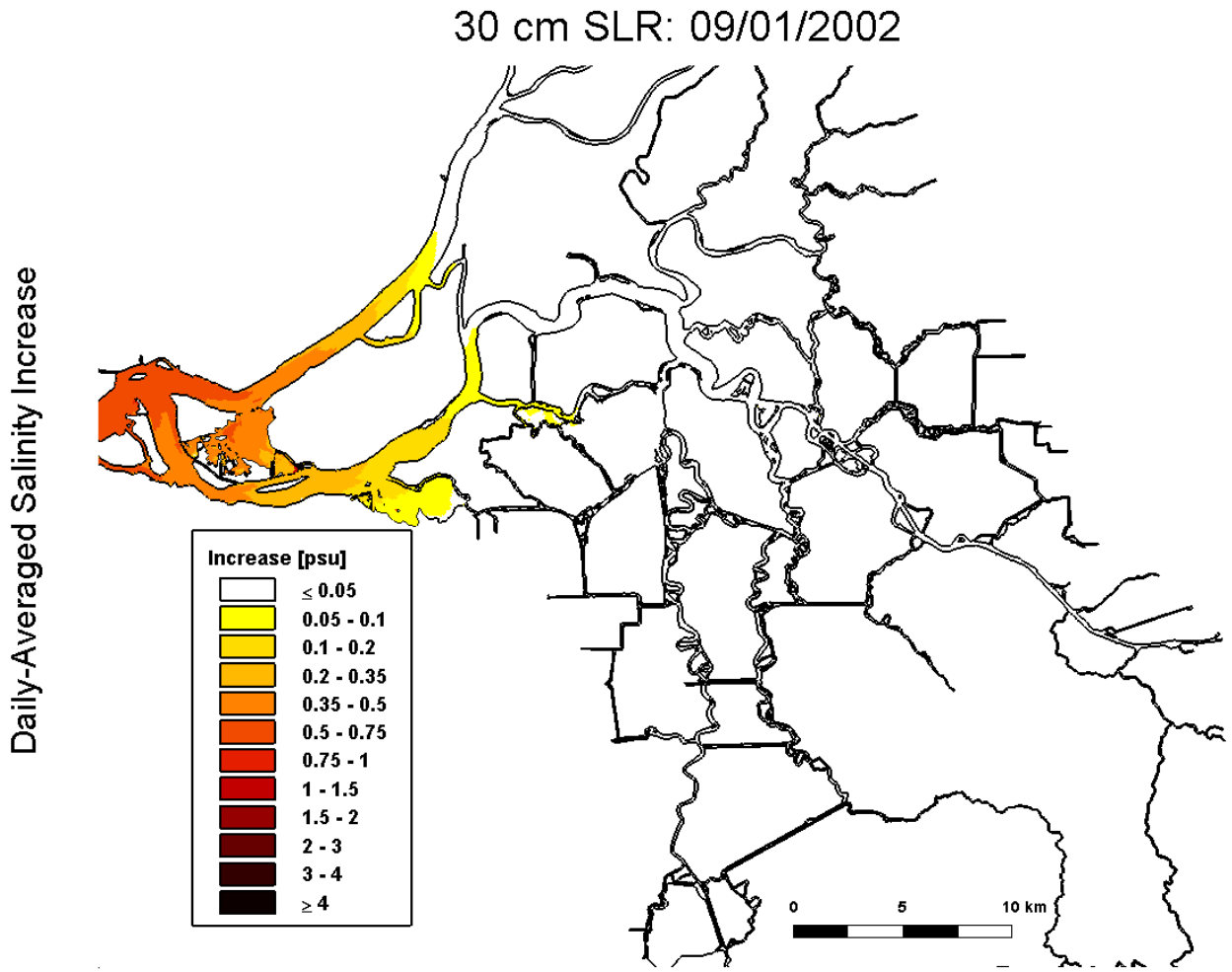

Figure 4.2-22 Predicted increase in daily-averaged depth-average salinity in the Sacramento-San Joaquin Delta on September 1, 2002 relative to the Baseline (0 cm SLR) scenario for the 30 cm SLR scenario.

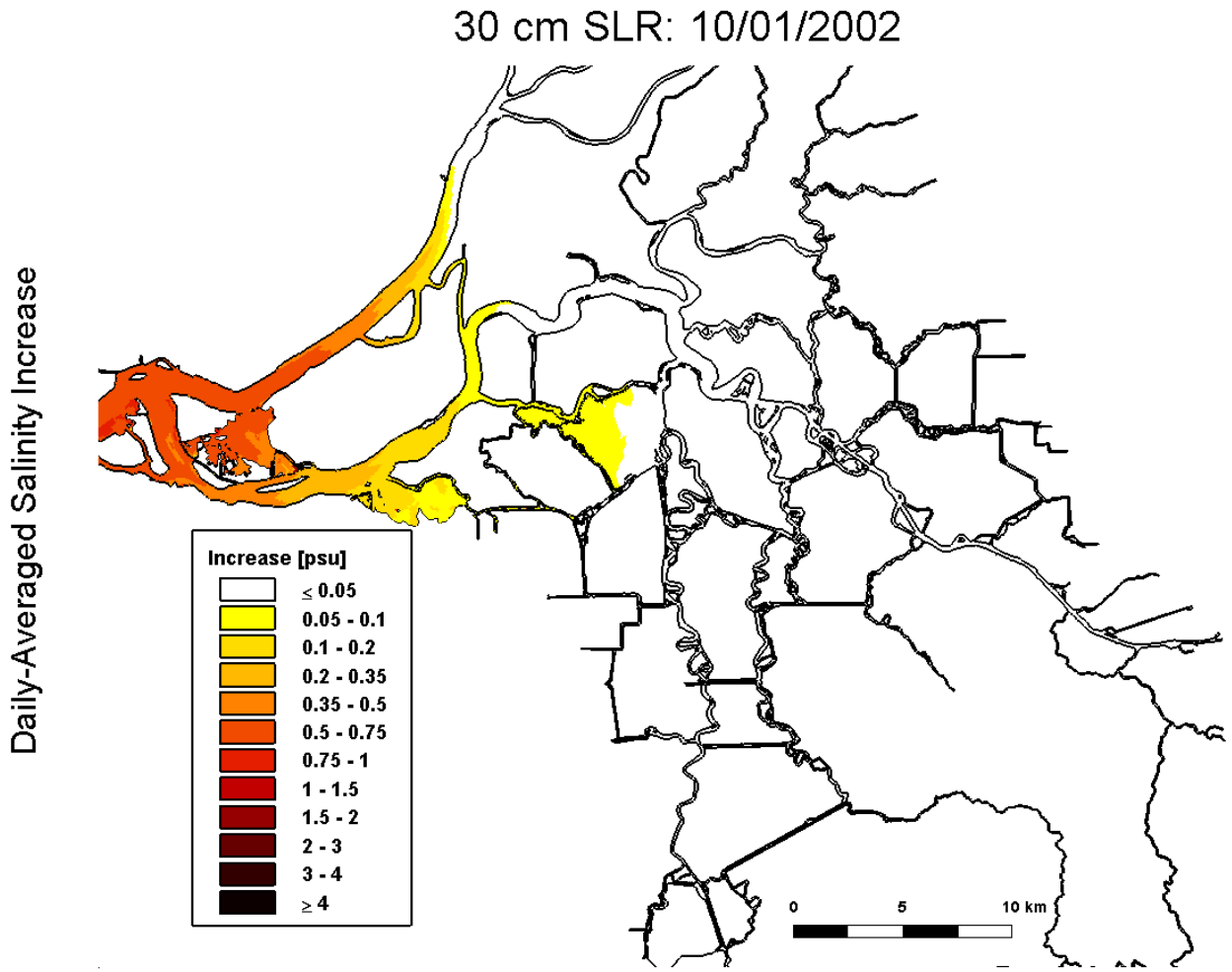

Figure 4.2-23 Predicted increase in daily-averaged depth-average salinity in the Sacramento-San Joaquin Delta on October 1, 2002 relative to the Baseline (0 cm SLR) scenario for the 30 cm SLR scenario.

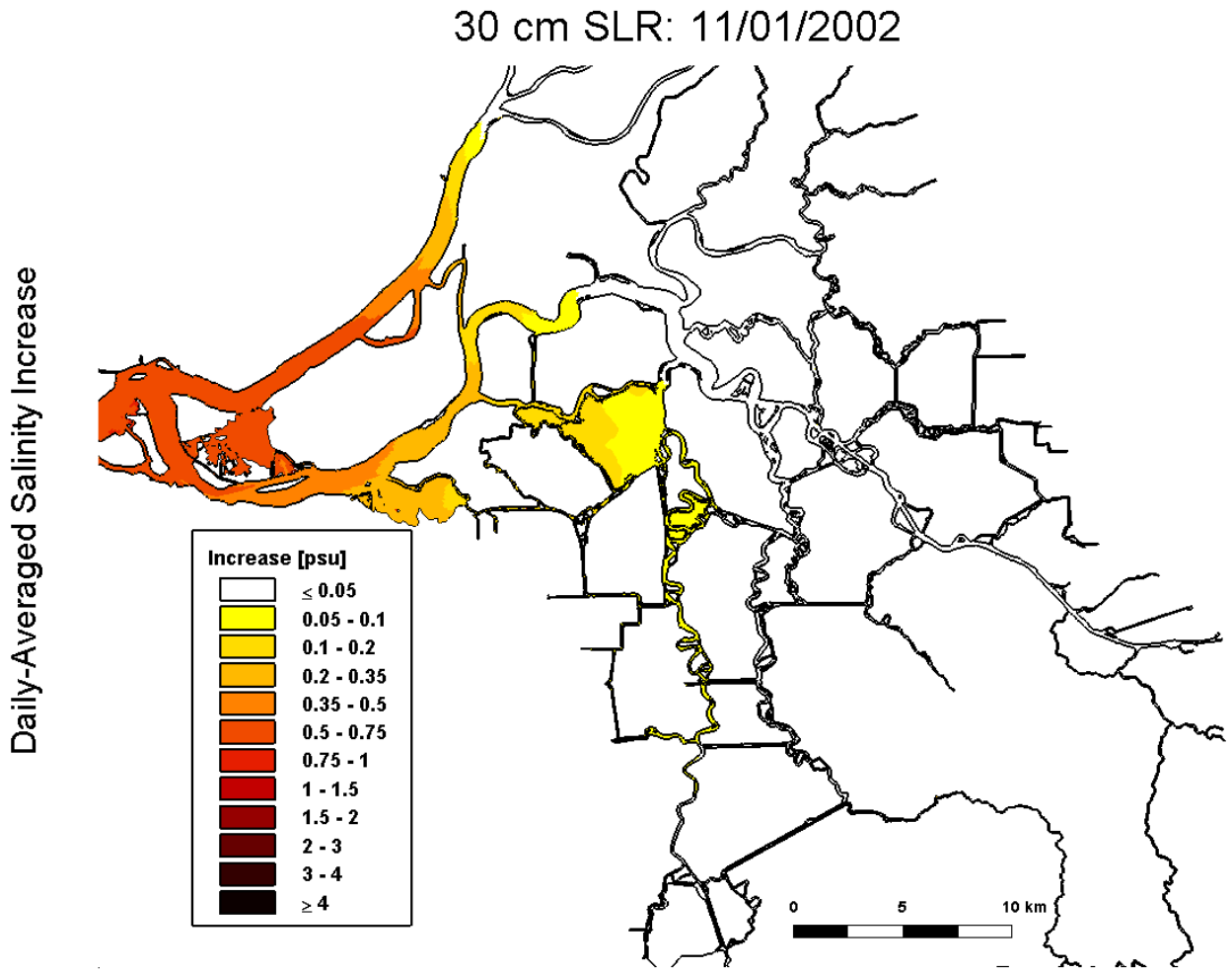

Figure 4.2-24 Predicted increase in daily-averaged depth-average salinity in the Sacramento-San Joaquin Delta on November 1, 2002 relative to the Baseline (0 cm SLR) scenario for the 30 cm SLR scenario.

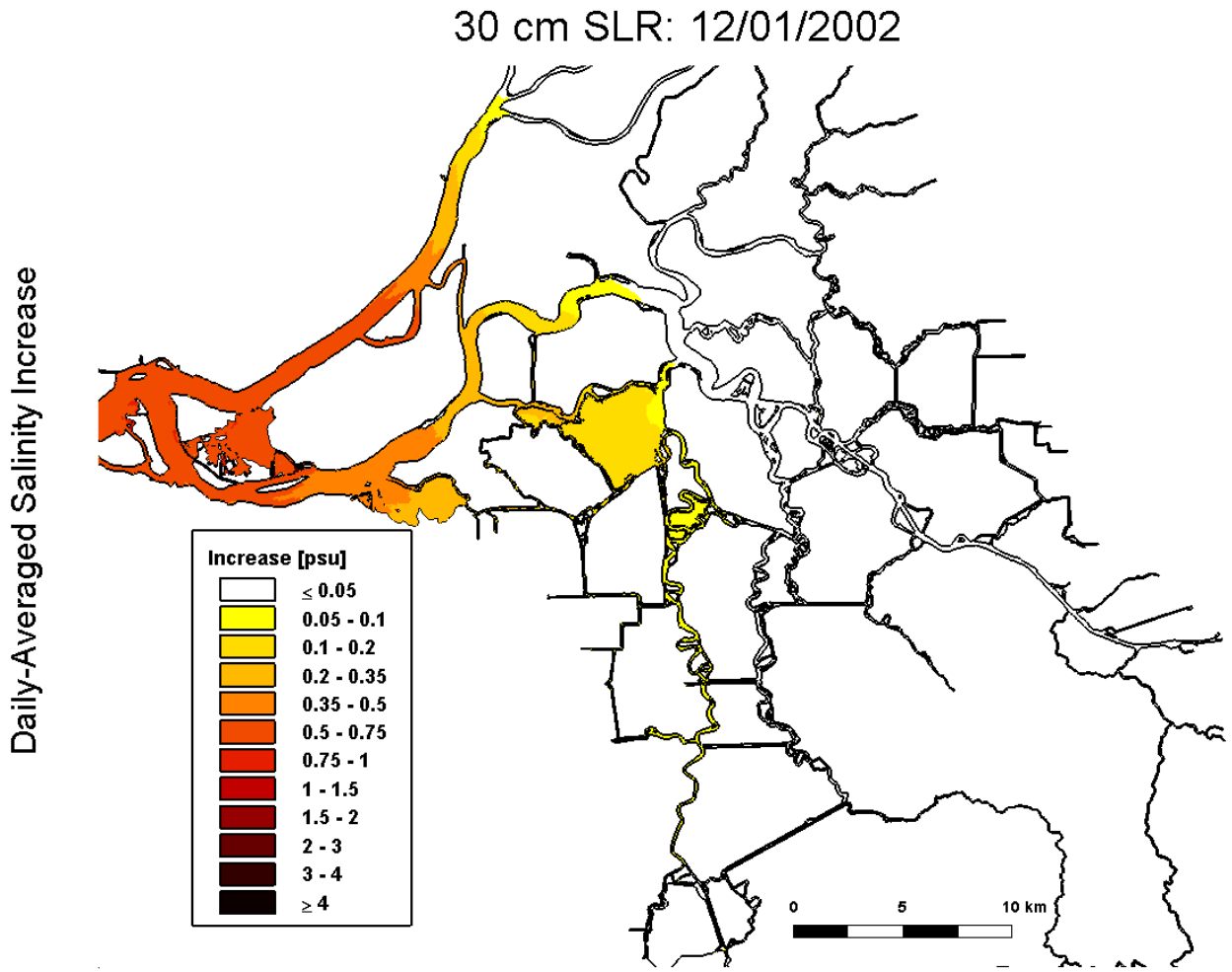

Figure 4.2-25 Predicted increase in daily-averaged depth-average salinity in the Sacramento-San Joaquin Delta on December 1, 2002 relative to the Baseline (0 cm SLR) scenario for the 30 cm SLR scenario.

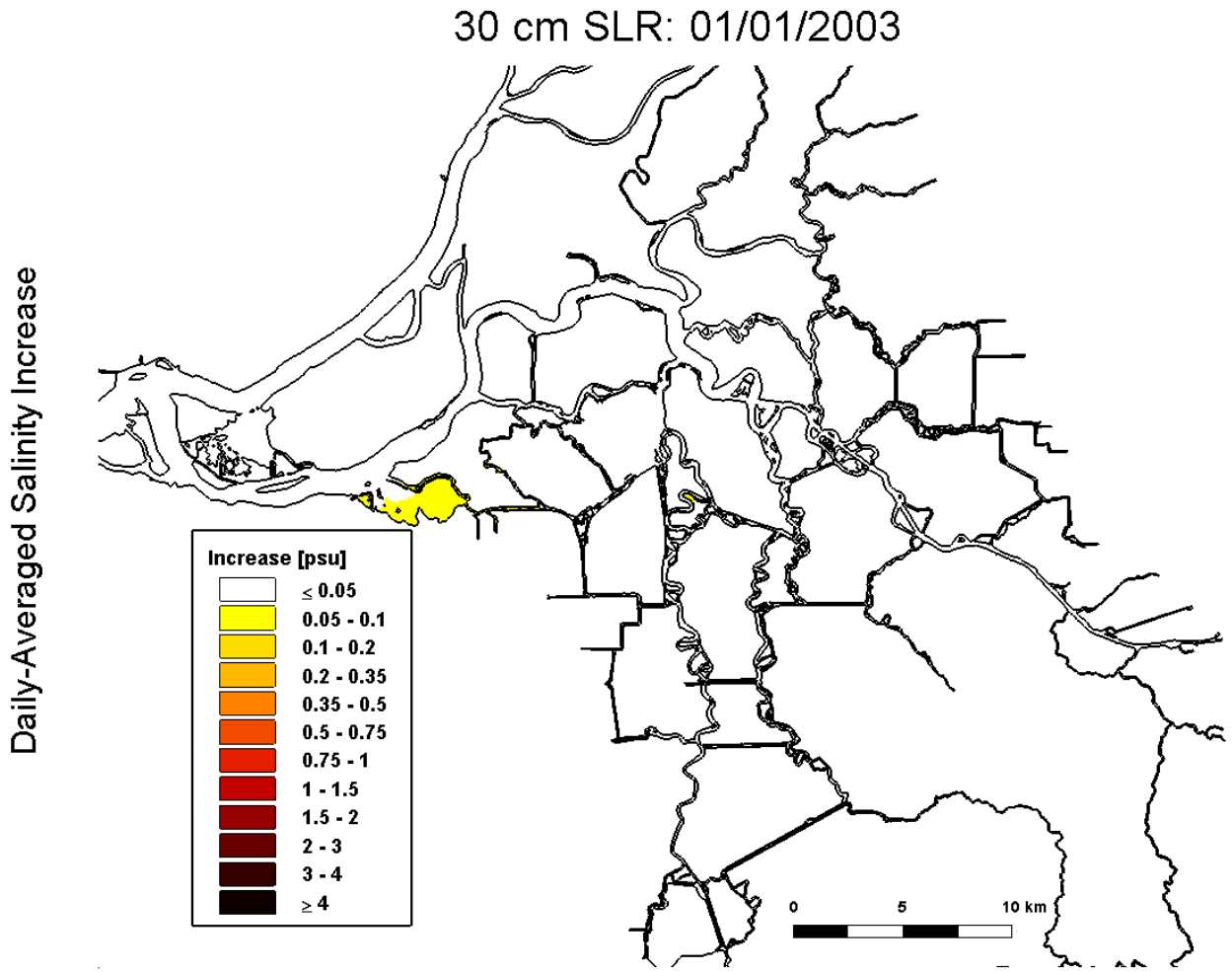

Figure 4.2-26 Predicted increase in daily-averaged depth-average salinity in the Sacramento-San Joaquin Delta on January 1, 2003 relative to the Baseline (0 cm SLR) scenario for the 30 cm SLR scenario.

4.3 Predicted Increase in Salinity for 45 cm SLR Scenario

Figure 4.3-1 through 4.3-13 show the predicted salinity along the northern portion of the San Francisco Estuary, spanning from San Pablo Bay through the Sacramento-San Joaquin Delta for the 45 cm SLR scenario. The top panel of each figure shows the predicted daily-averaged depth-average salinity for the 45 cm SLR scenario. The lower panel shows the predicted salinity increase computed by subtracting the predicted daily-averaged depth-average salinity for the Baseline (0 cm SLR) scenario from the predicted daily-averaged depth-average salinity for the 45 cm SLR scenario. Figures 4.3-14 through 4.3-26 show the predicted salinity increases resulting from the 45 cm SLR scenario in the Sacramento-San Joaquin Delta.

At the beginning of the analysis period on January 1, 2002, salinity increases between 0.20 and 0.35 psu are predicted between Chipps Island and Collinsville and predicted salinity increases of up to 0.05 psu are predicted upstream to the western end of Sherman Island. Predicted salinity increases are less than 0.05 psu throughout the remaining portions of the Delta. Salinity increases between 1.0 and 1.50 psu are predicted through Carquinez Strait and salinity increases between 0.35 and 1.50 psu are predicted throughout Suisun Bay. Larger salinity increases of more than 1.0 psu are predicted in much of San Pablo Bay, with increase of more than 4.0 psu predicted in northern San Pablo Bay. During the first half of the year, predicted salinity increases in Suisun Bay and the Delta remain similar to the predicted salinity increases seen on January 1, 2002, though the predicted salinity is increasing throughout this period. Larger salinity increases are predicted in the Delta between July and December, with the largest predicted salinity increases in December prior to the first flush. In December, salinity increases of between 0.75 and 1.50 psu are predicted between Chipps Island and Emmaton, and salinity increases of between 0.10 and 0.35 psu are predicted in Franks Tract. South of Franks Tract, predicted salinity increases between 0.10 and 0.20 psu extend down Old River to Clifton Court Forebay, and salinity increases of between 0.05 and 0.10 psu are predicted inside Clifton Court Forebay. These simulations assumed no operational response to sea level rise, however it is expected significant operational response will be required to maintain water quality standards for 45 cm of sea level rise. Following high flows which occurred in December, predicted salinity on January 1, 2003 shows that the 0.50 psu isohaline is on the western side of Suisun Bay near Martinez. Predicted salinity increases of between 0.05 and 0.10 psu persist in some regions of the Delta, primarily in Big Break and south of Franks Tract.

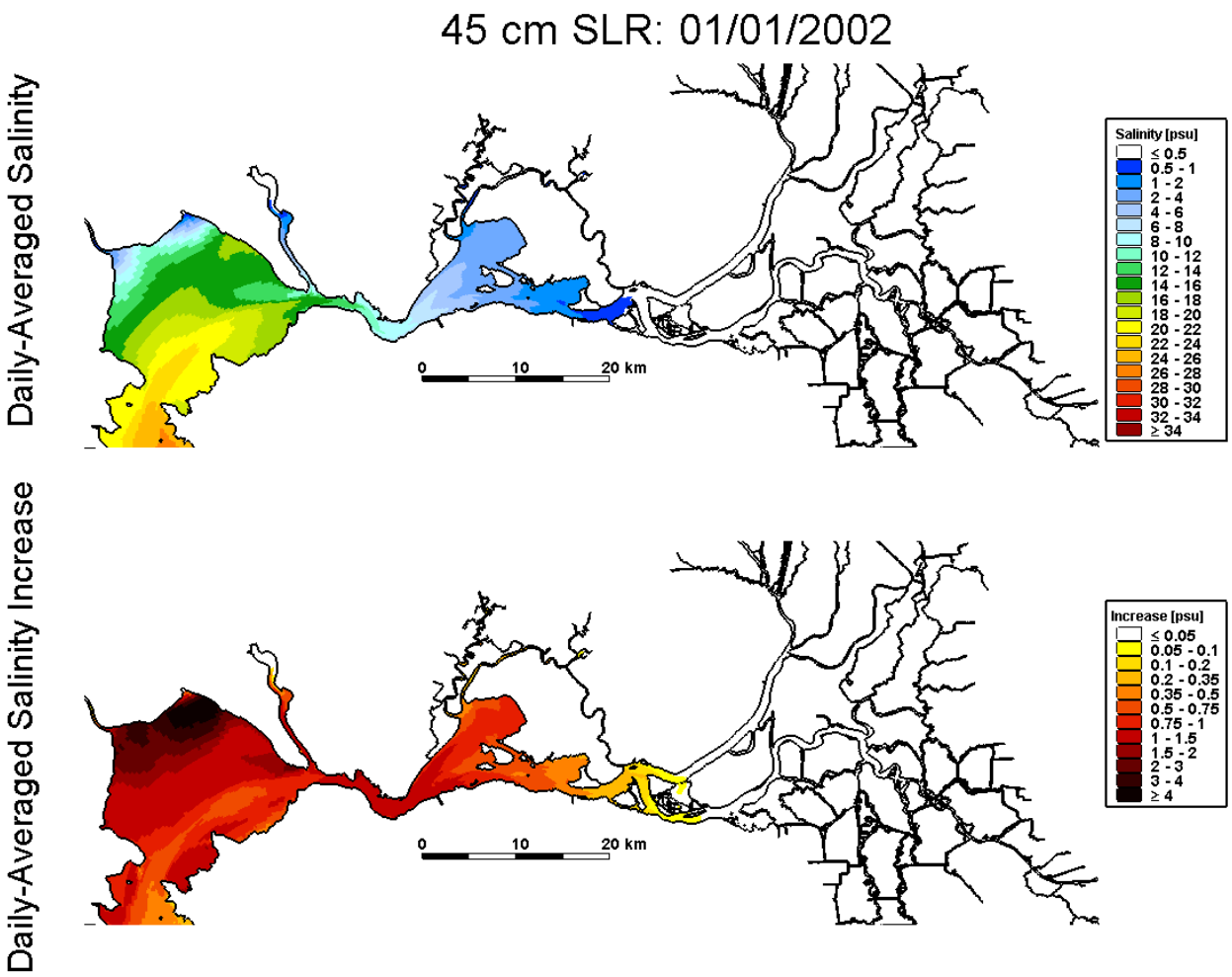

Figure 4.3-1 Predicted daily-averaged depth-average salinity on January 1, 2002 for the 45 cm SLR scenario (top); predicted increase in daily-averaged depth-average salinity on January 1, 2002 relative to the Baseline (0 cm SLR) scenario for the 45 cm SLR scenario.

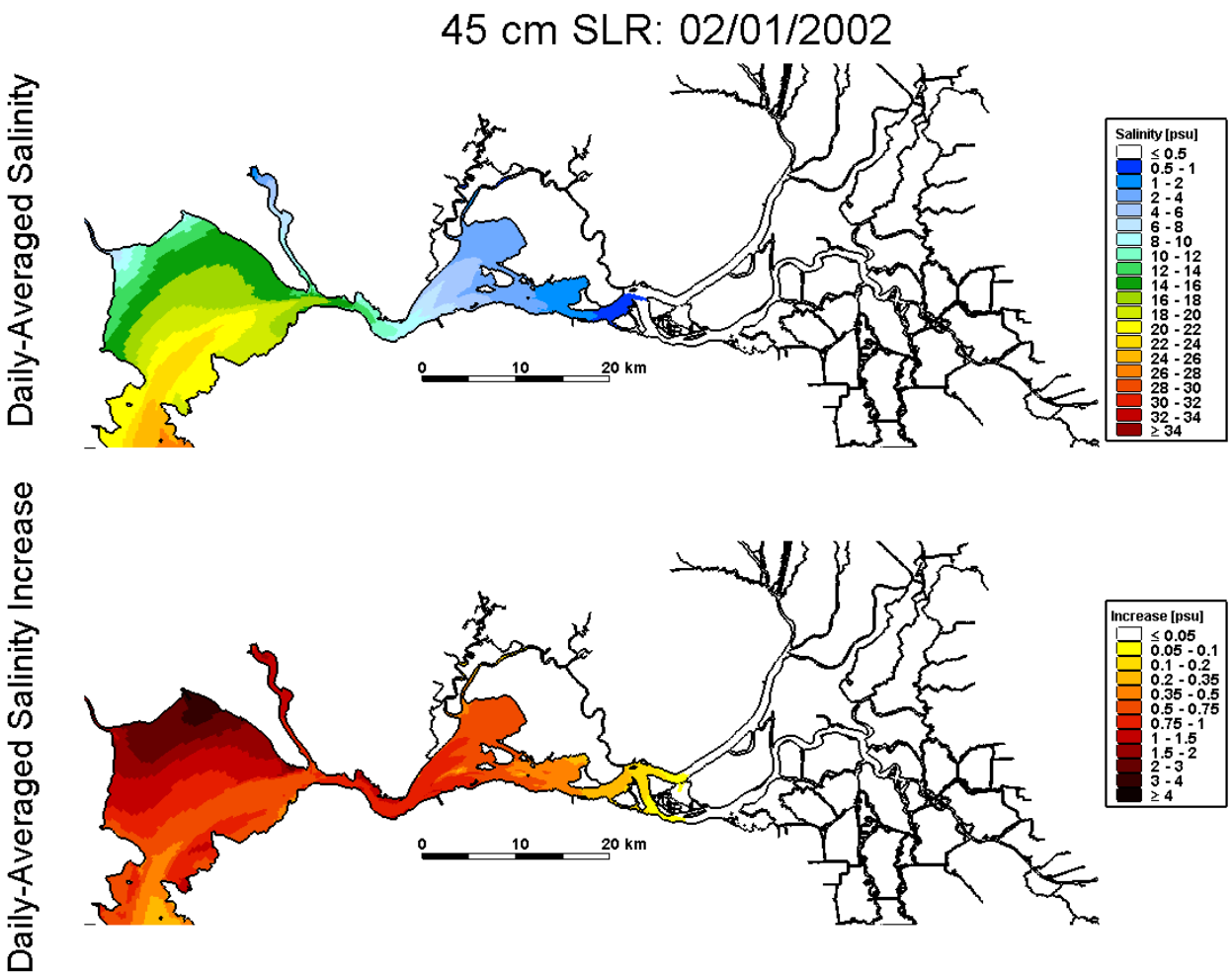

Figure 4.3-2 Predicted daily-averaged depth-average salinity on February 1, 2002 for the 45 cm SLR scenario (top); predicted increase in daily-averaged depth-average salinity on February 1, 2002 relative to the Baseline (0 cm SLR) scenario for the 45 cm SLR scenario.

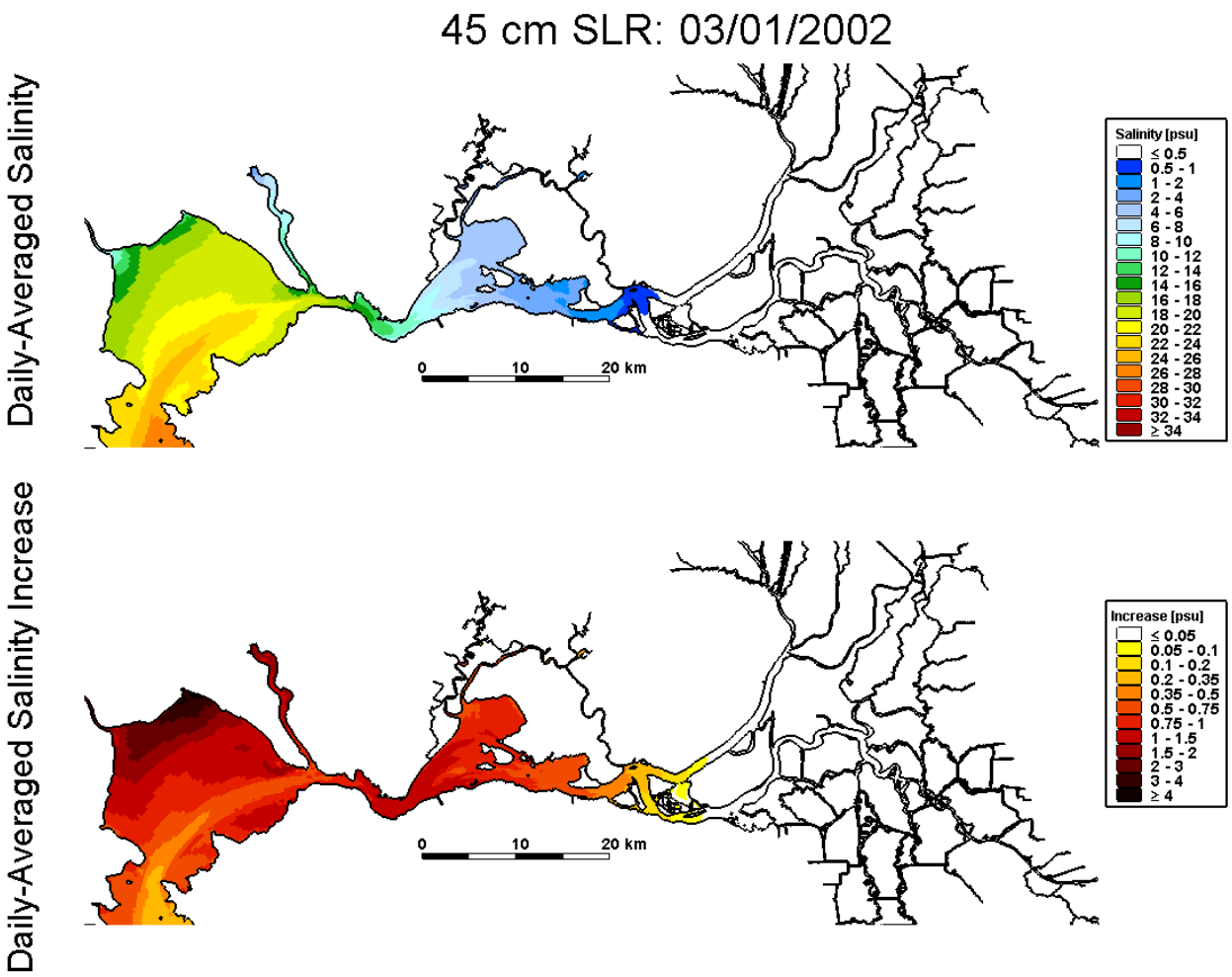

Figure 4.3-3 Predicted daily-averaged depth-average salinity on March 1, 2002 for the 45 cm SLR scenario (top); predicted increase in daily-averaged depth-average salinity on March 1, 2002 relative to the Baseline (0 cm SLR) scenario for the 45 cm SLR scenario.

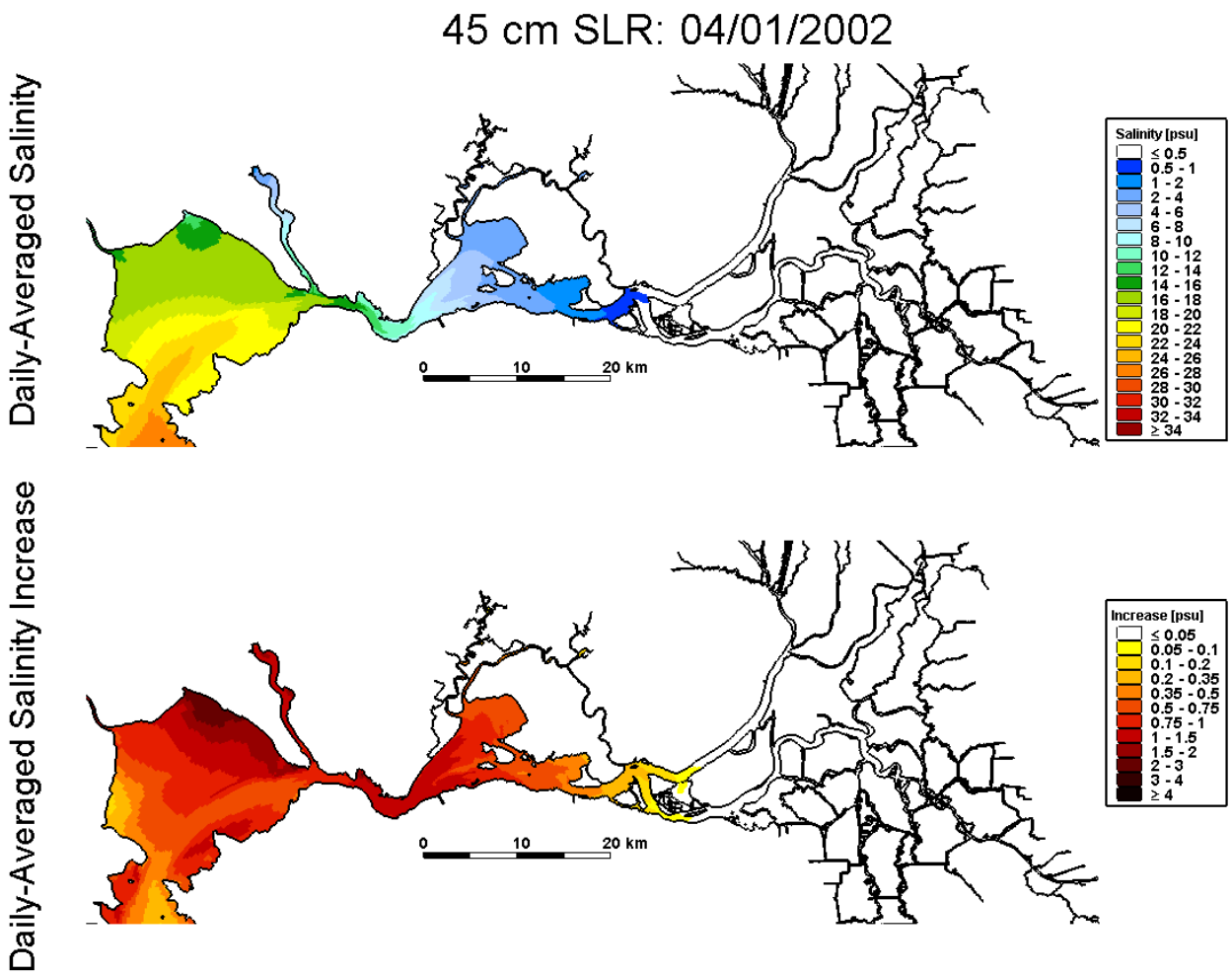

Figure 4.3-4 Predicted daily-averaged depth-average salinity on April 1, 2002 for the 45 cm SLR scenario (top); predicted increase in daily-averaged depth-average salinity on April 1, 2002 relative to the Baseline (0 cm SLR) scenario for the 45 cm SLR scenario.

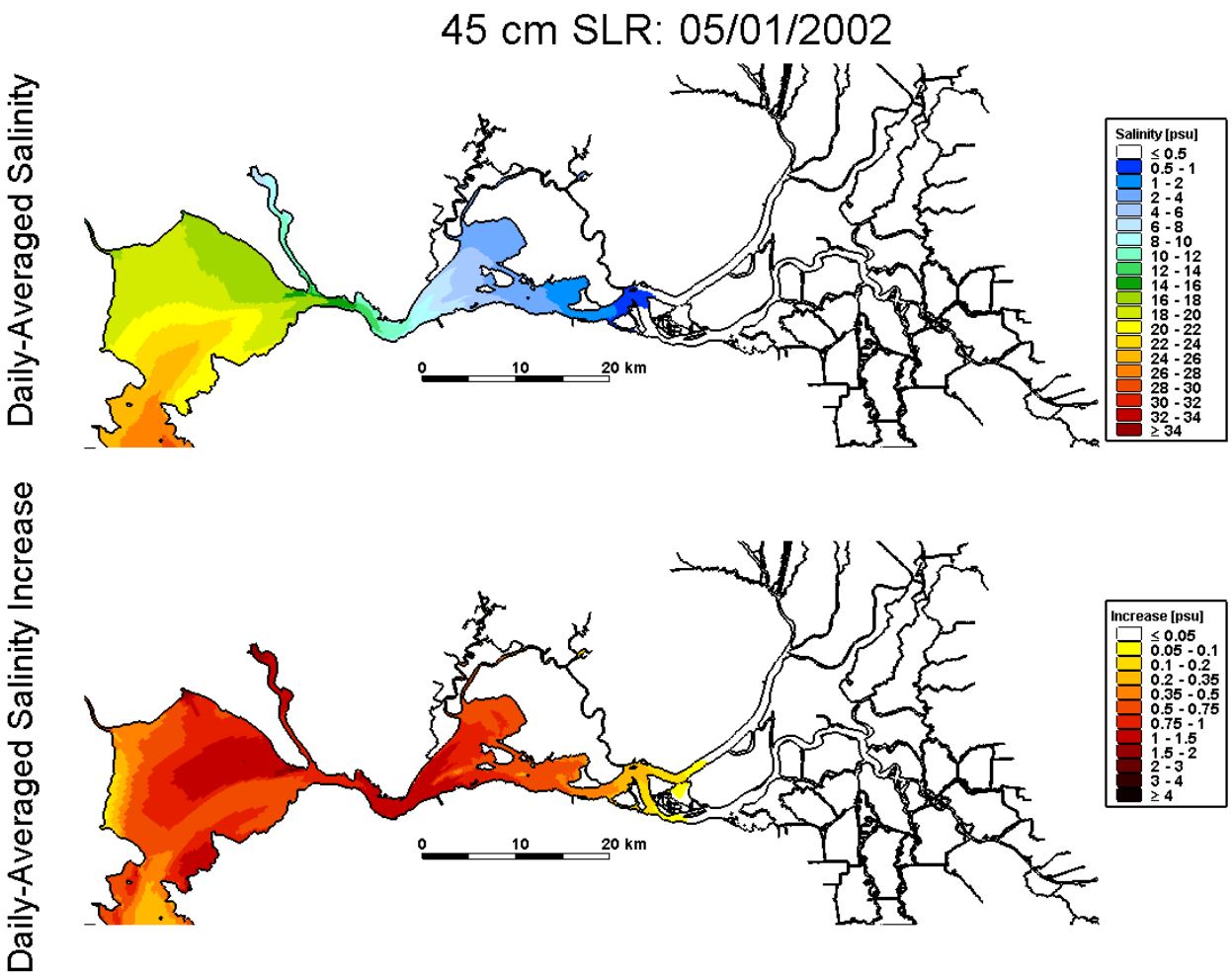

Figure 4.3-5 Predicted daily-averaged depth-average salinity on May 1, 2002 for the 45 cm SLR scenario (top); predicted increase in daily-averaged depth-average salinity on May 1, 2002 relative to the Baseline (0 cm SLR) scenario for the 45 cm SLR scenario.

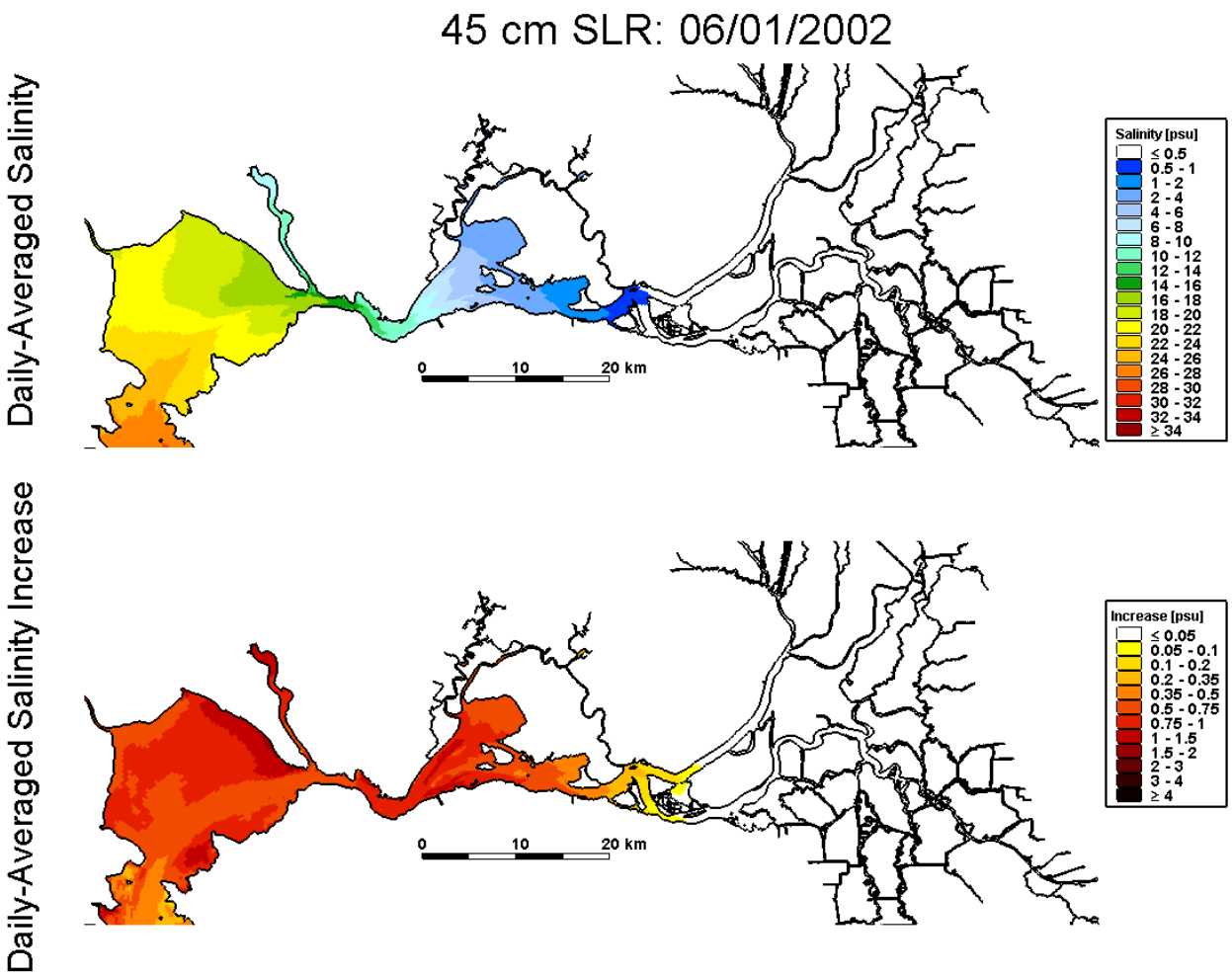

Figure 4.3-6 Predicted daily-averaged depth-average salinity on June 1, 2002 for the 45 cm SLR scenario (top); predicted increase in daily-averaged depth-average salinity on June 1, 2002 relative to the Baseline (0 cm SLR) scenario for the 45 cm SLR scenario.

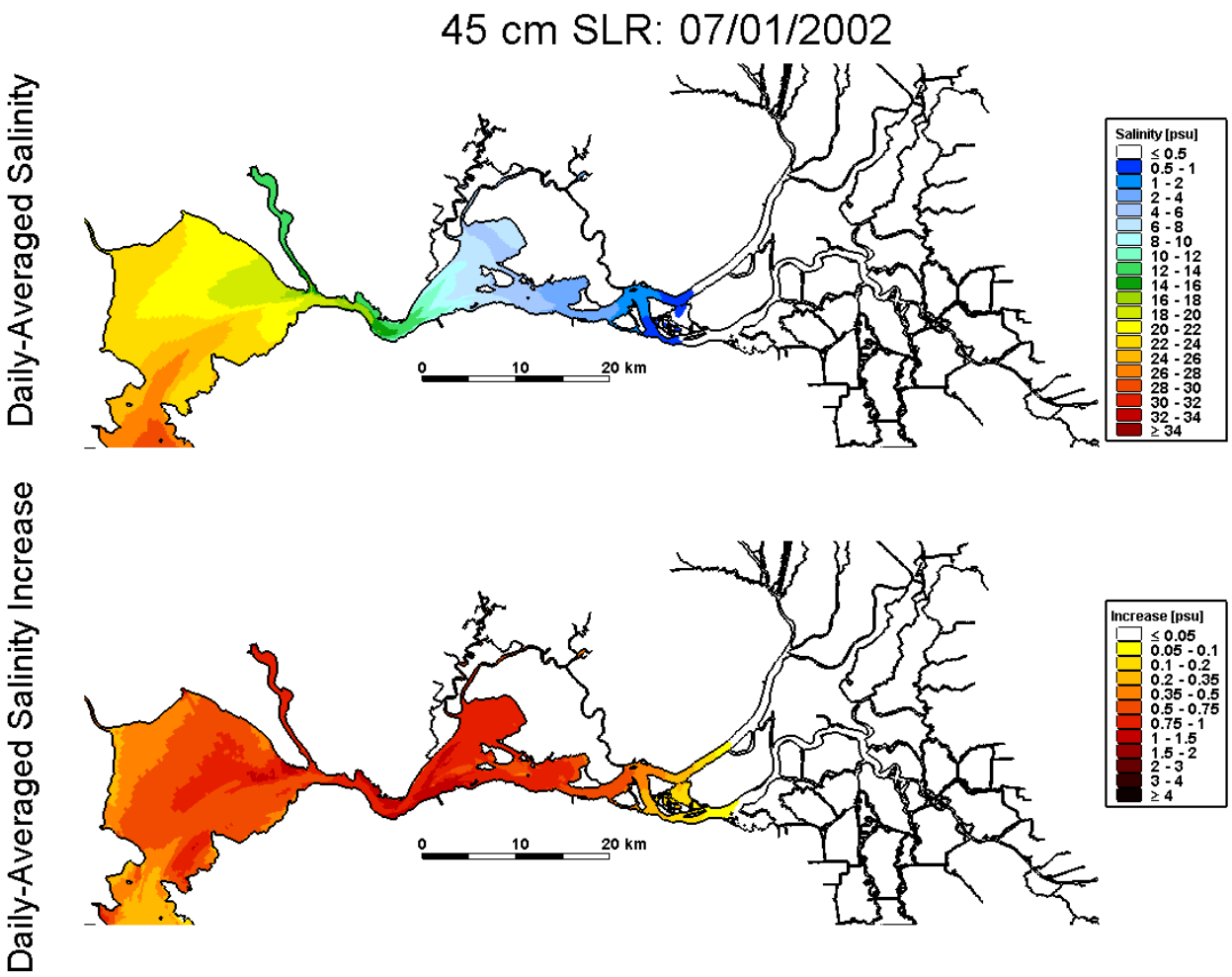

Figure 4.3-7 Predicted daily-averaged depth-average salinity on July 1, 2002 for the 45 cm SLR scenario (top); predicted increase in daily-averaged depth-average salinity on July 1, 2002 relative to the Baseline (0 cm SLR) scenario for the 45 cm SLR scenario.

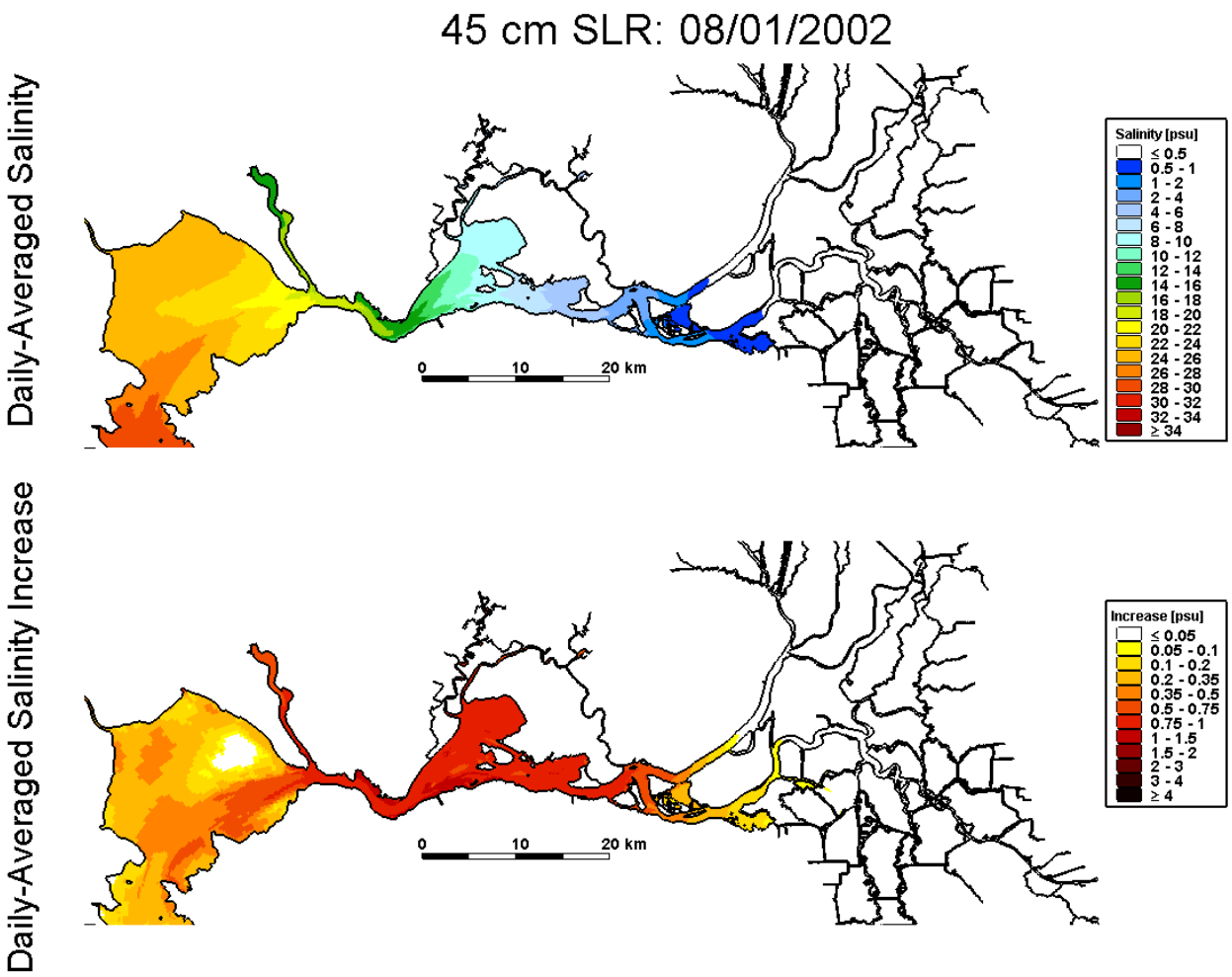

Figure 4.3-8 Predicted daily-averaged depth-average salinity on August 1, 2002 for the 45 cm SLR scenario (top); predicted increase in daily-averaged depth-average salinity on August 1, 2002 relative to the Baseline (0 cm SLR) scenario for the 45 cm SLR scenario.

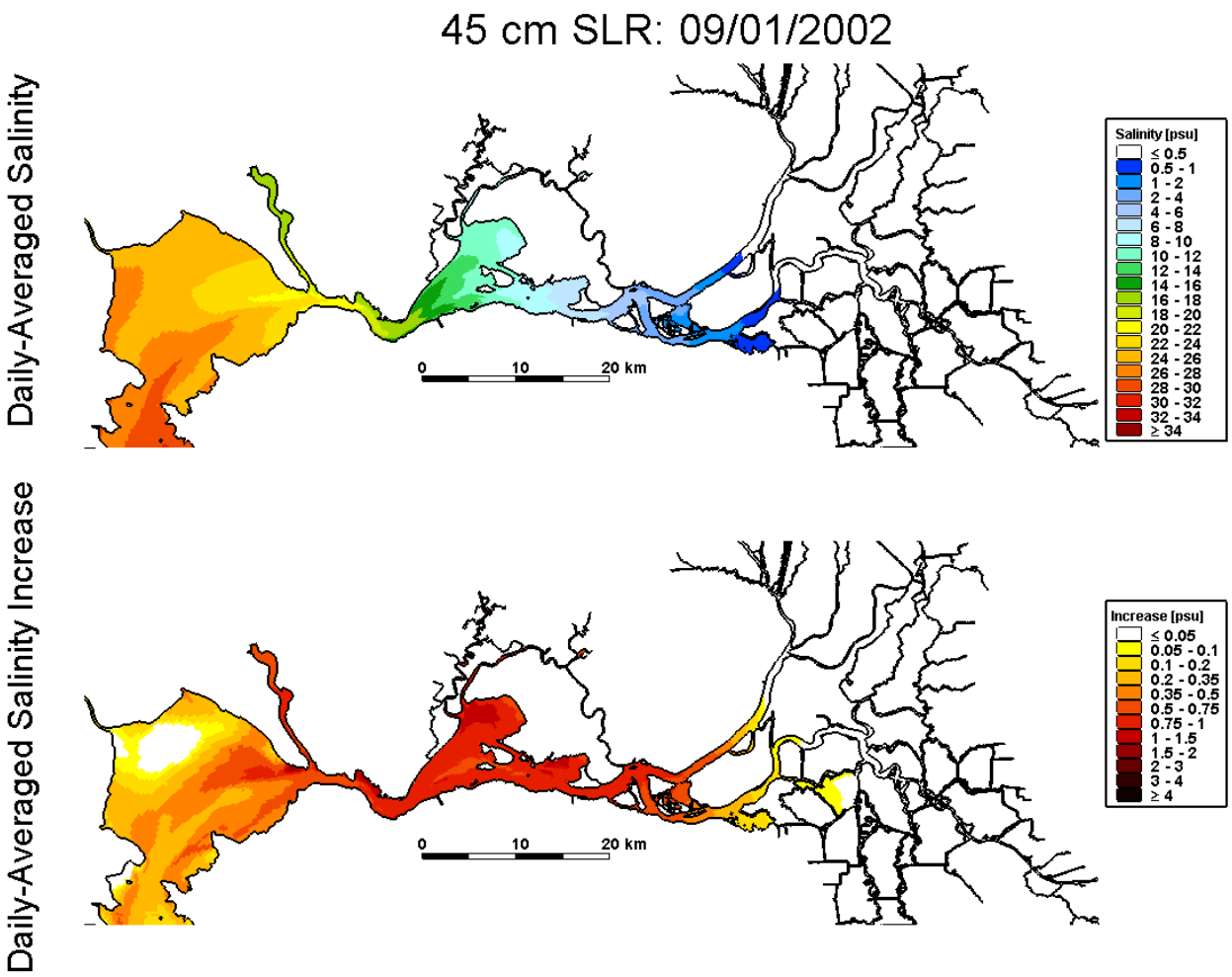

Figure 4.3-9 Predicted daily-averaged depth-average salinity on September 1, 2002 for the 45 cm SLR scenario (top); predicted increase in daily-averaged depth-average salinity on September 1, 2002 relative to the Baseline (0 cm SLR) scenario for the 45 cm SLR scenario.

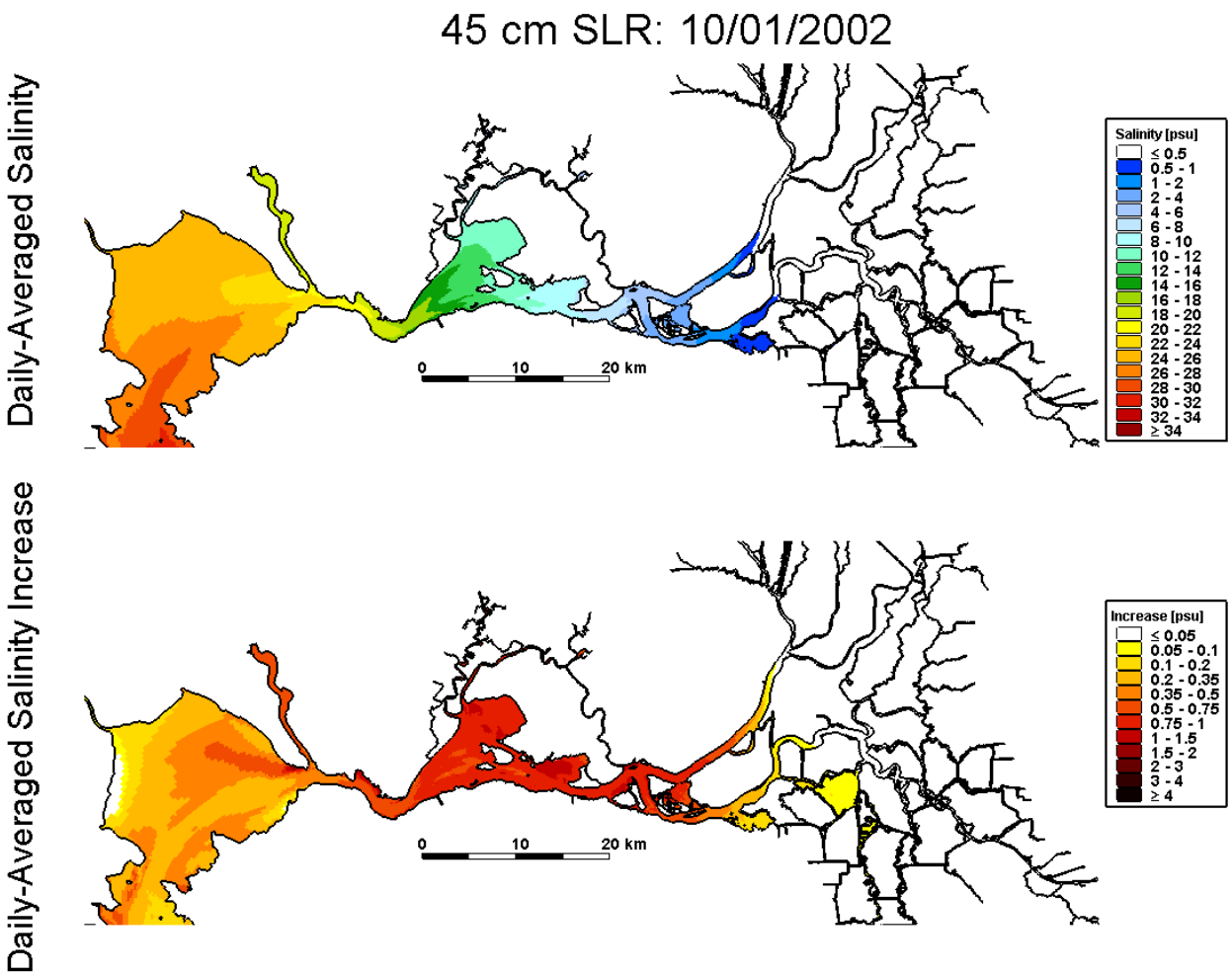

Figure 4.3-10 Predicted daily-averaged depth-average salinity on October 1, 2002 for the 45 cm SLR scenario (top); predicted increase in daily-averaged depth-average salinity on October 1, 2002 relative to the Baseline (0 cm SLR) scenario for the 45 cm SLR scenario.

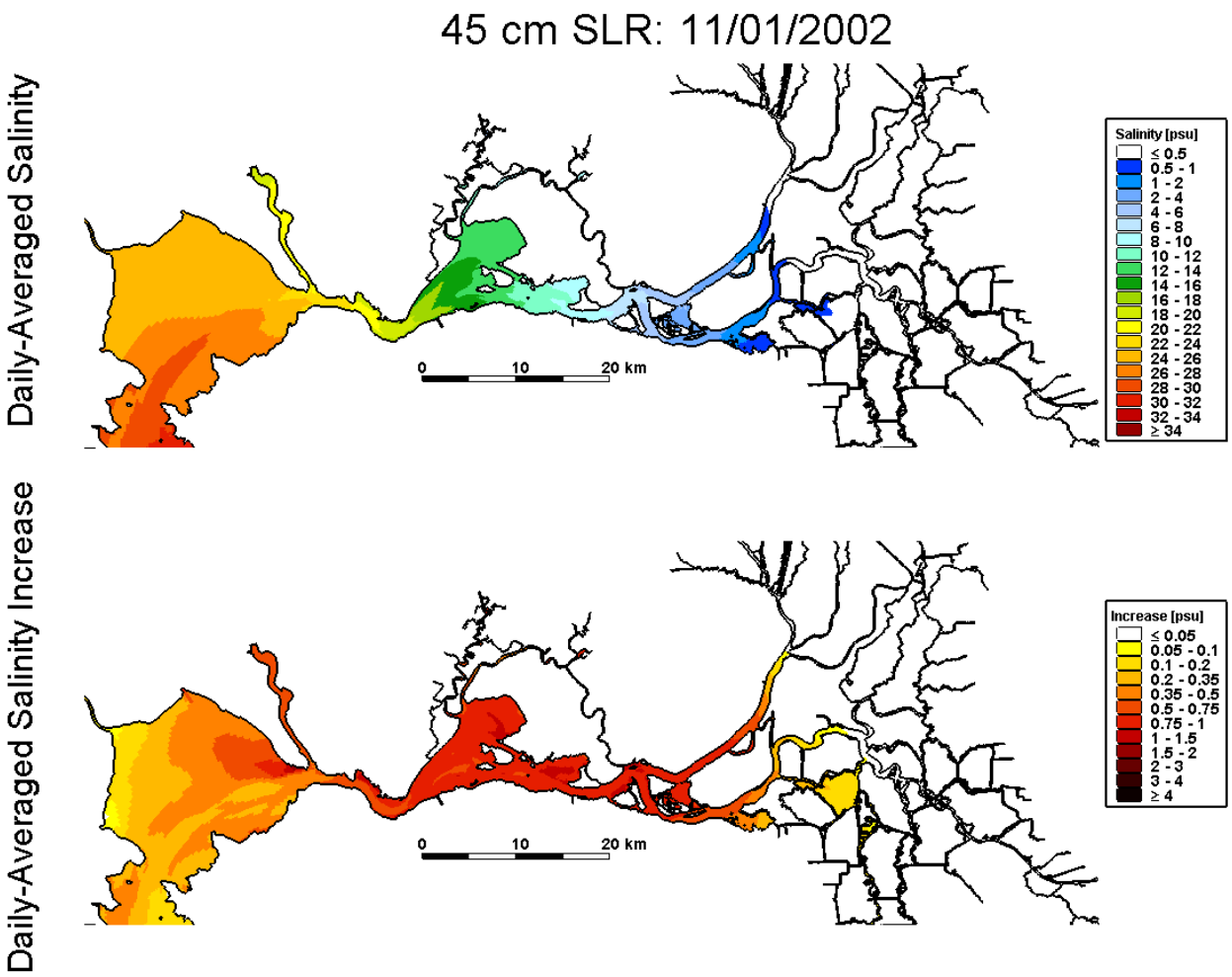

Figure 4.3-11 Predicted daily-averaged depth-average salinity on November 1, 2002 for the 45 cm SLR scenario (top); predicted increase in daily-averaged depth-average salinity on November 1, 2002 relative to the Baseline (0 cm SLR) scenario for the 45 cm SLR scenario.

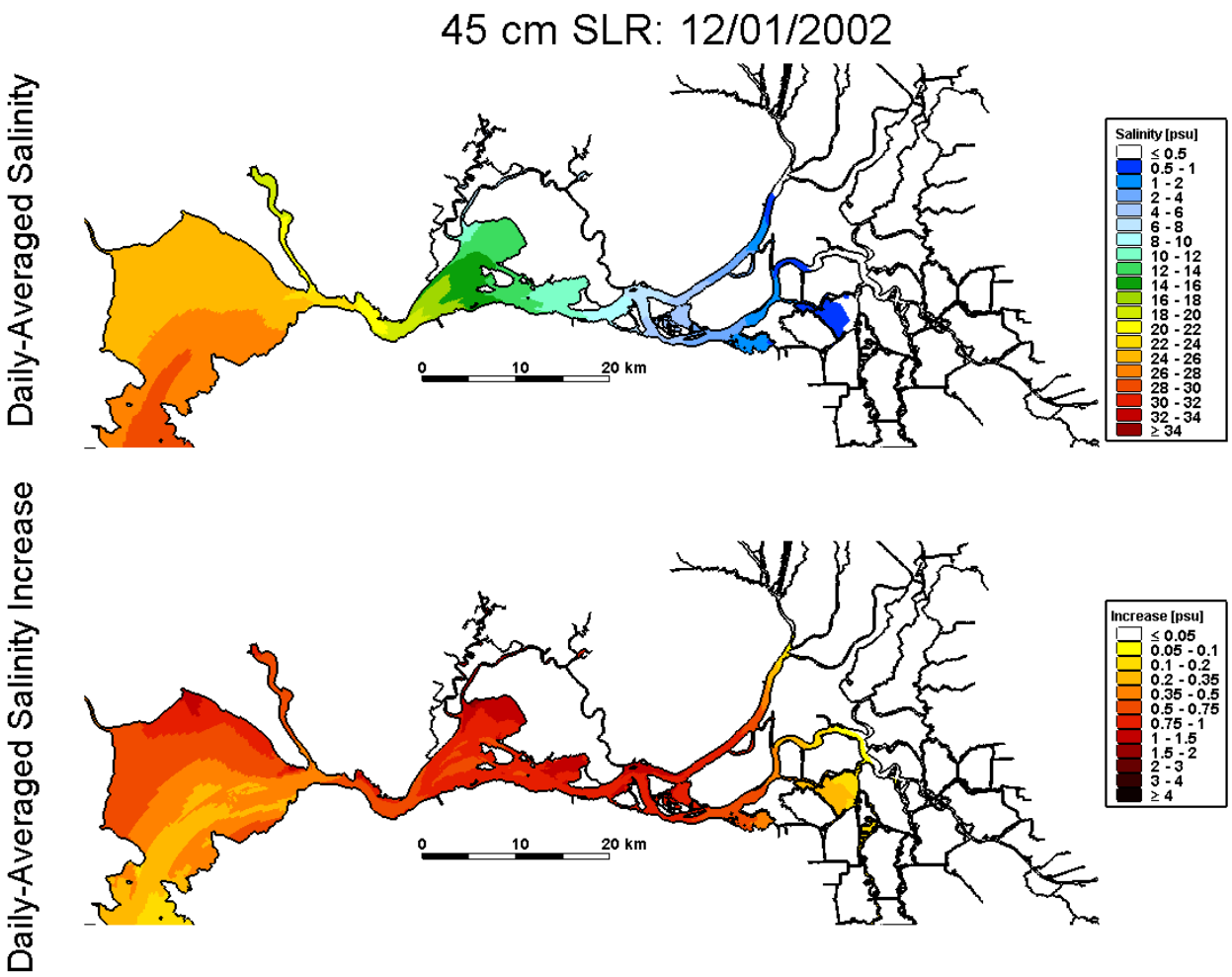

Figure 4.3-12 Predicted daily-averaged depth-average salinity on December 1, 2002 for the 45 cm SLR scenario (top); predicted increase in daily-averaged depth-average salinity on December 1, 2002 relative to the Baseline (0 cm SLR) scenario for the 45 cm SLR scenario.

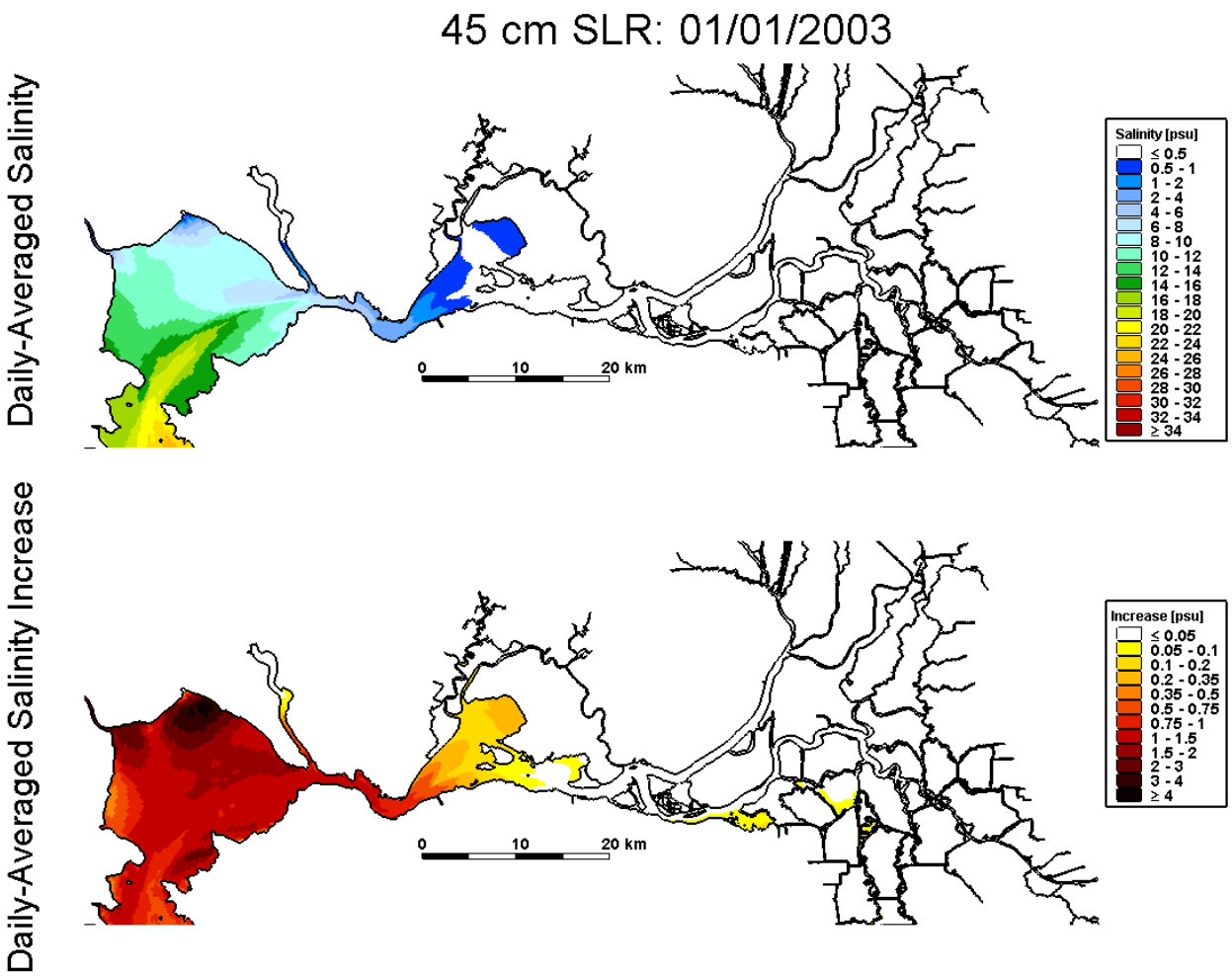

Figure 4.3-13 Predicted daily-averaged depth-average salinity on January 1, 2003 for the 45 cm SLR scenario (top); predicted increase in daily-averaged depth-average salinity on January 1, 2003 relative to the Baseline (0 cm SLR) scenario for the 45 cm SLR scenario.

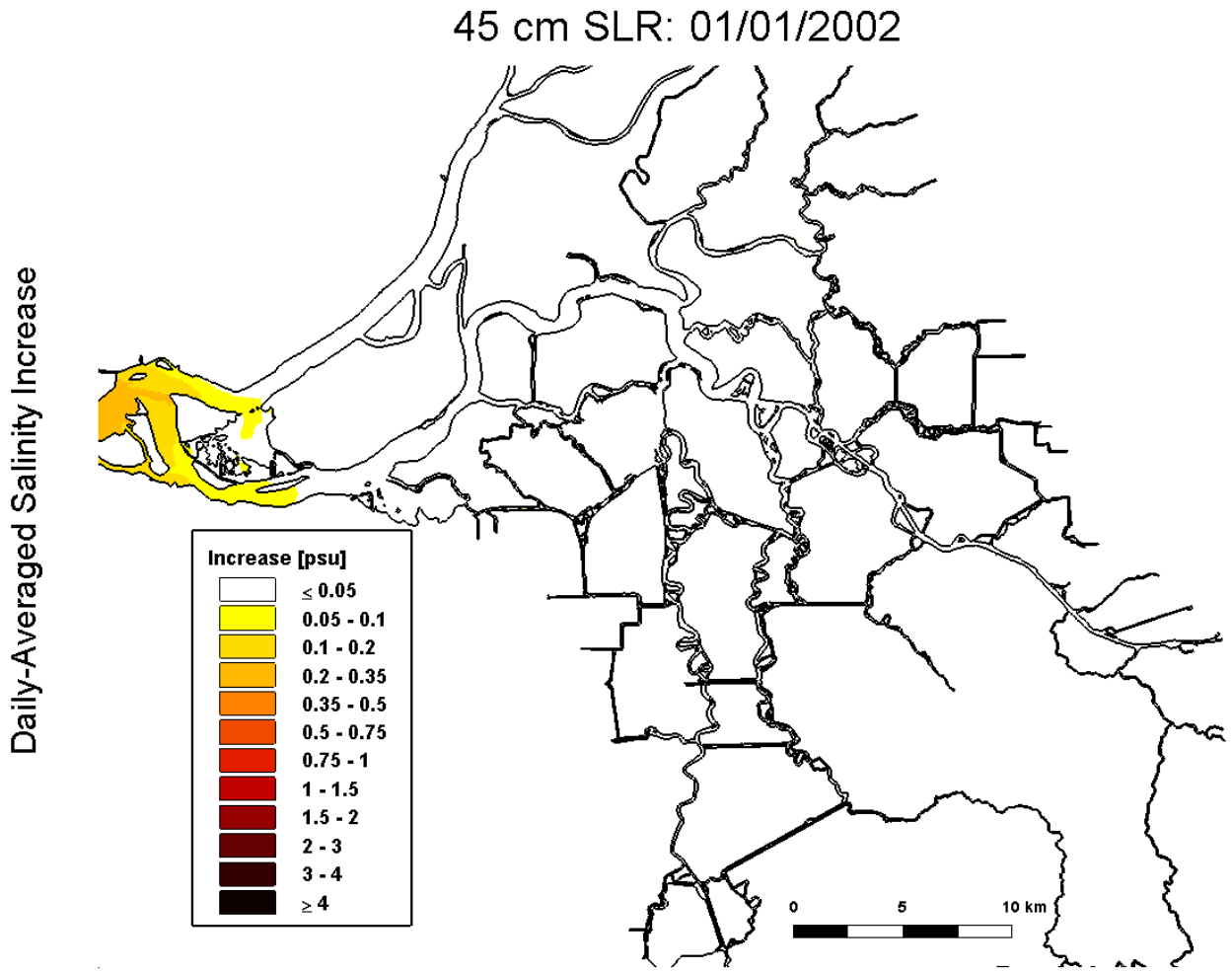

Figure 4.3-14 Predicted increase in daily-averaged depth-average salinity in the Sacramento-San Joaquin Delta on January 1, 2002 relative to the Baseline (0 cm SLR) scenario for the 45 cm SLR scenario.

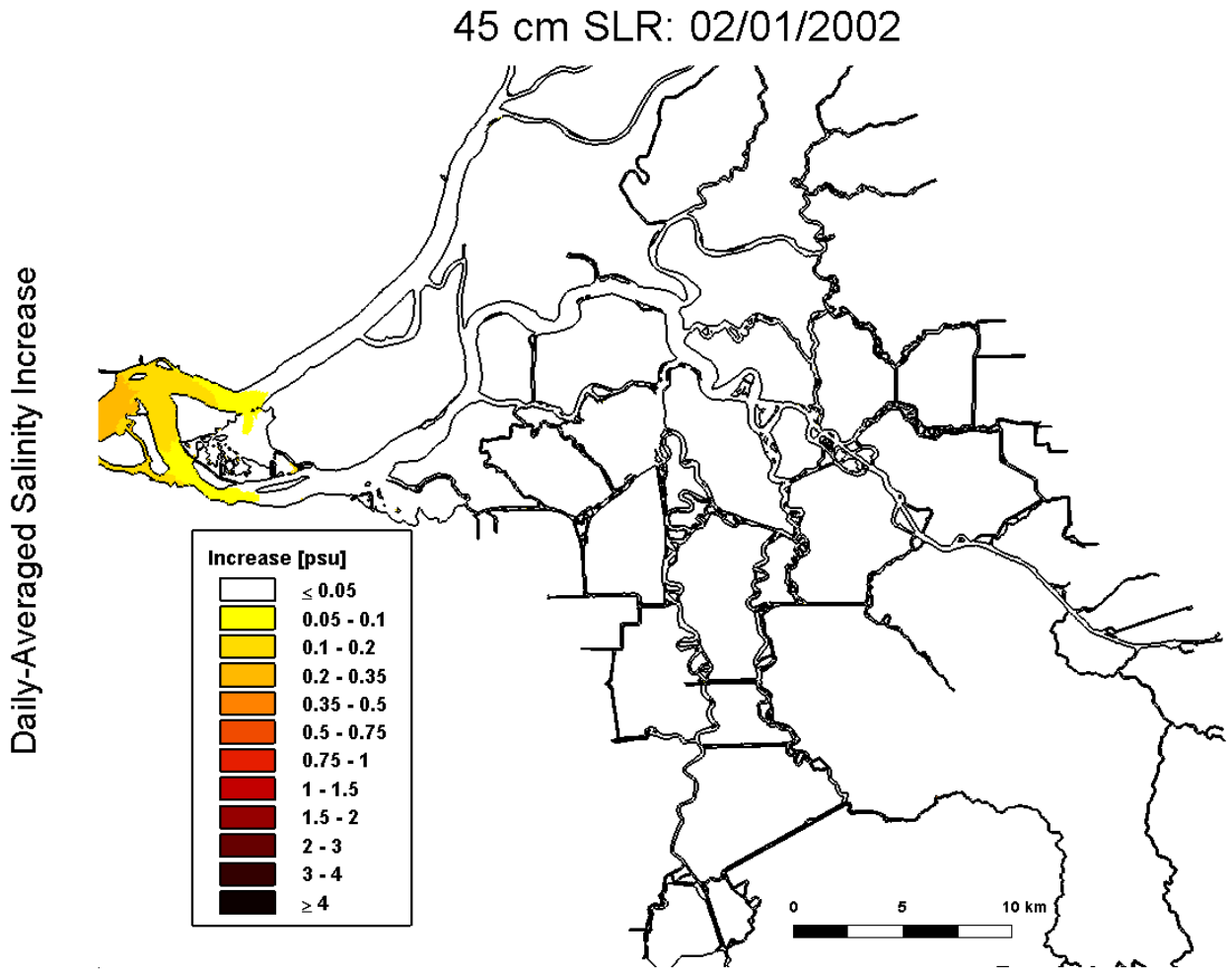

Figure 4.3-15 Predicted increase in daily-averaged depth-average salinity in the Sacramento-San Joaquin Delta on February 1, 2002 relative to the Baseline (0 cm SLR) scenario for the 45 cm SLR scenario.

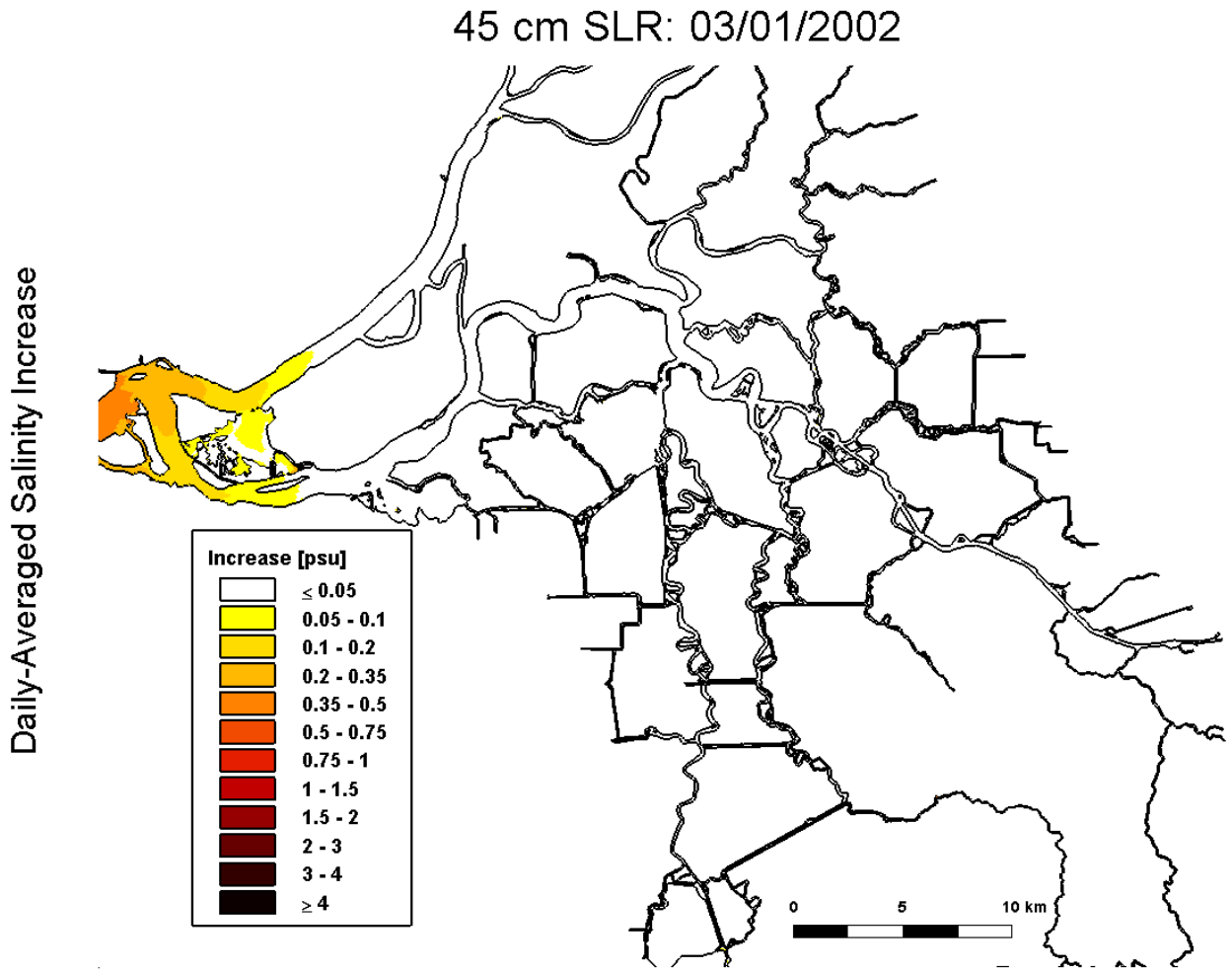

Figure 4.3-16 Predicted increase in daily-averaged depth-average salinity in the Sacramento-San Joaquin Delta on March 1, 2002 relative to the Baseline (0 cm SLR) scenario for the 45 cm SLR scenario.

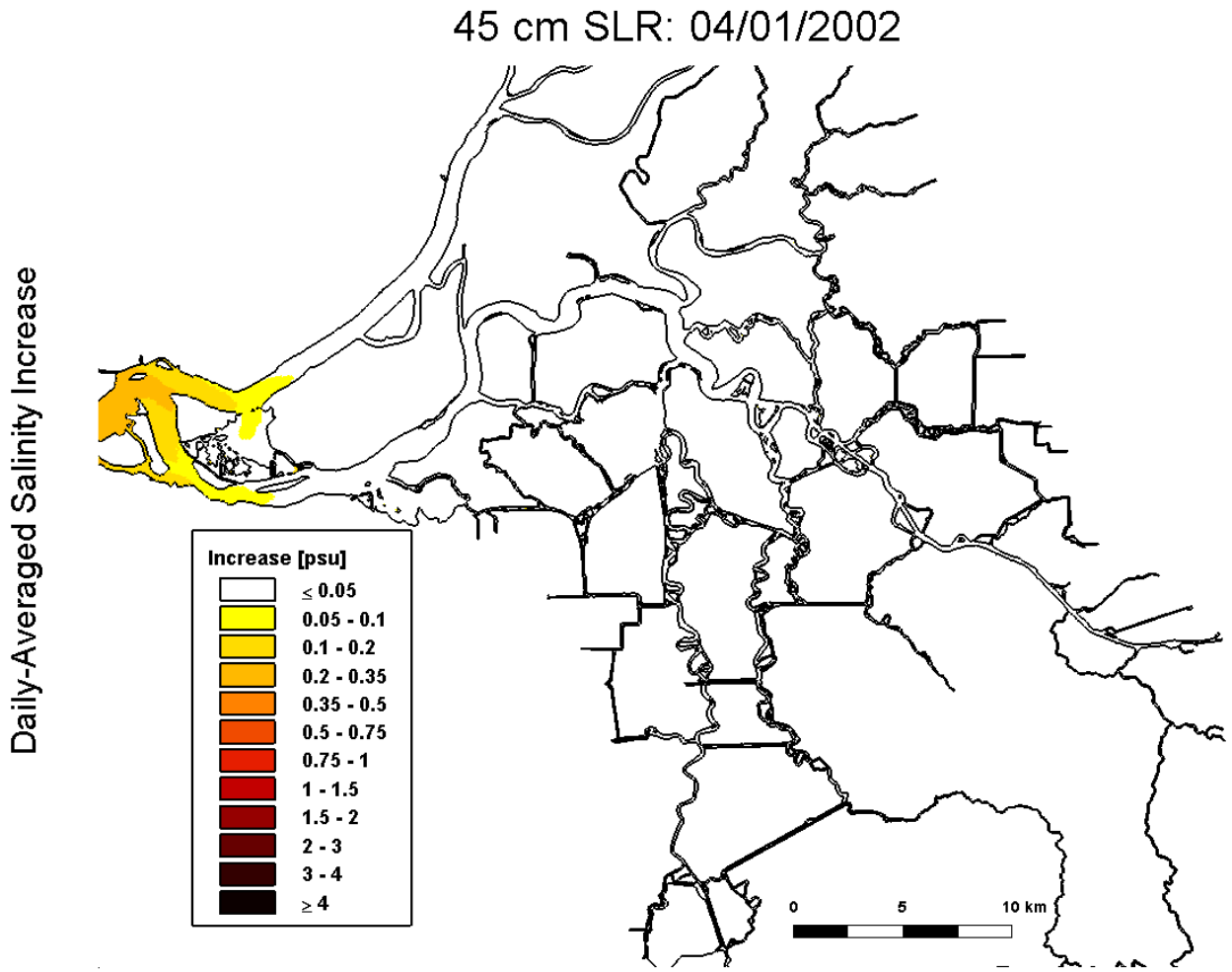

Figure 4.3-17 Predicted increase in daily-averaged depth-average salinity in the Sacramento-San Joaquin Delta on April 1, 2002 relative to the Baseline (0 cm SLR) scenario for the 45 cm SLR scenario.

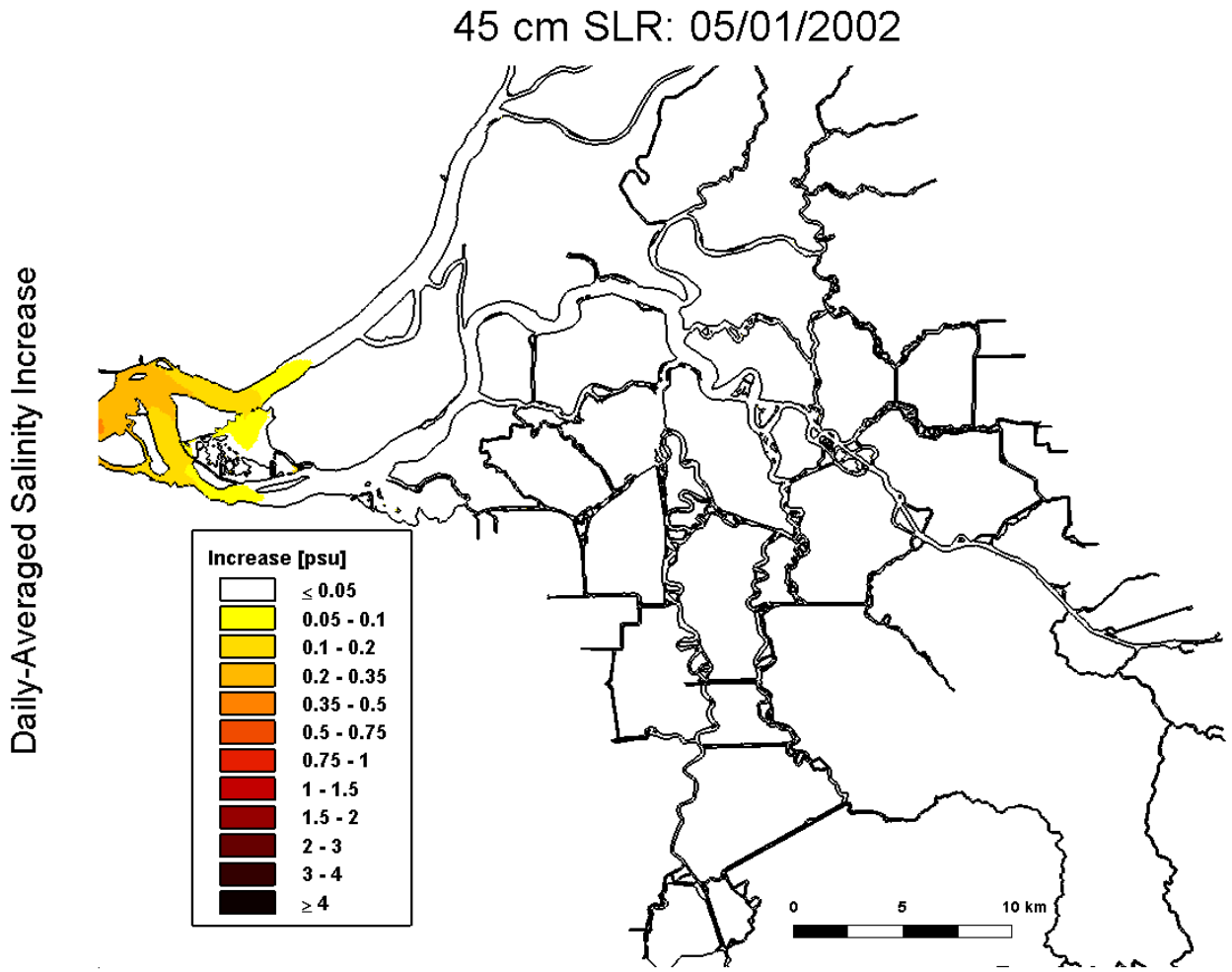

Figure 4.3-18 Predicted increase in daily-averaged depth-average salinity in the Sacramento-San Joaquin Delta on May 1, 2002 relative to the Baseline (0 cm SLR) scenario for the 45 cm SLR scenario.

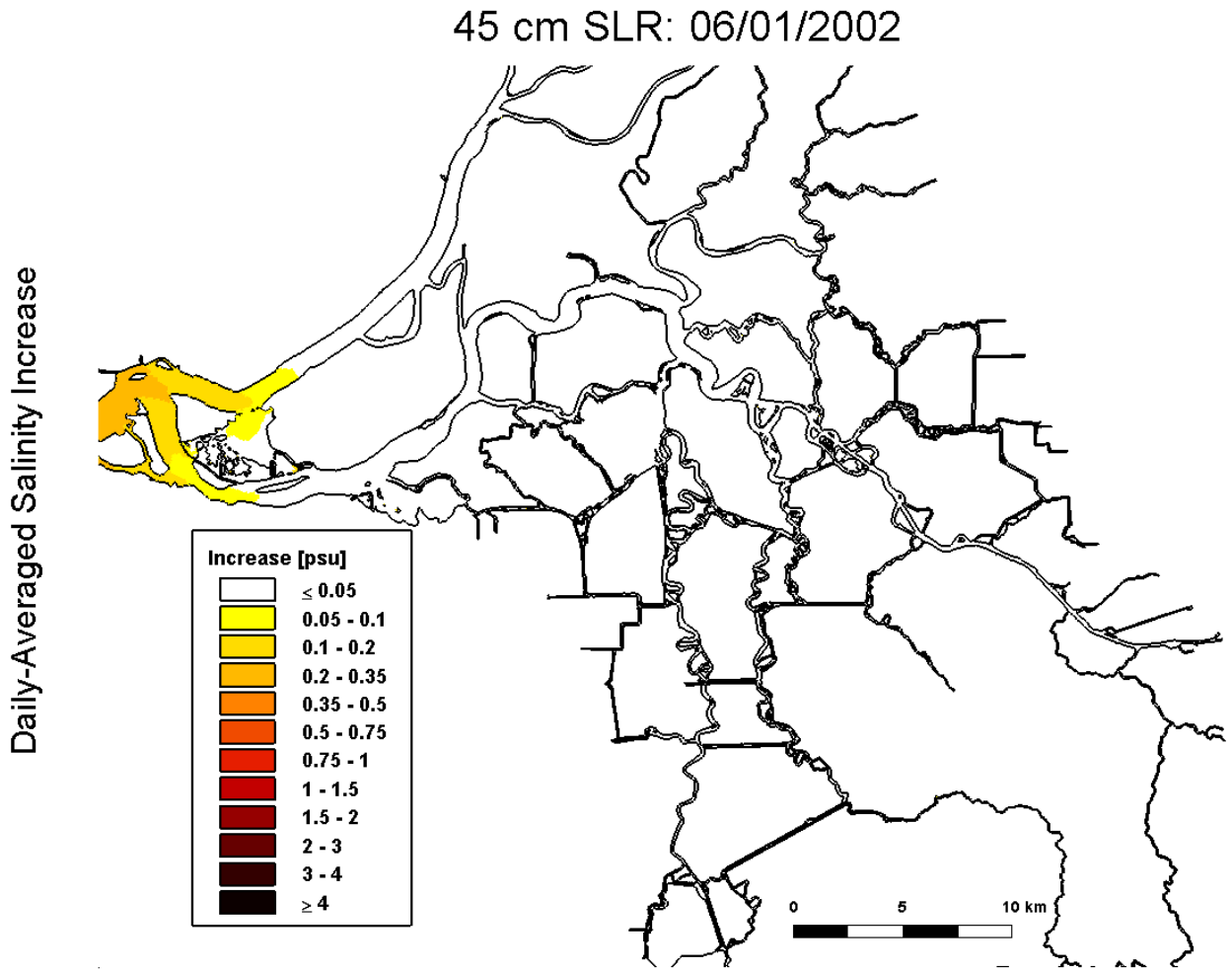

Figure 4.3-19 Predicted increase in daily-averaged depth-average salinity in the Sacramento-San Joaquin Delta on June 1, 2002 relative to the Baseline (0 cm SLR) scenario for the 45 cm SLR scenario.

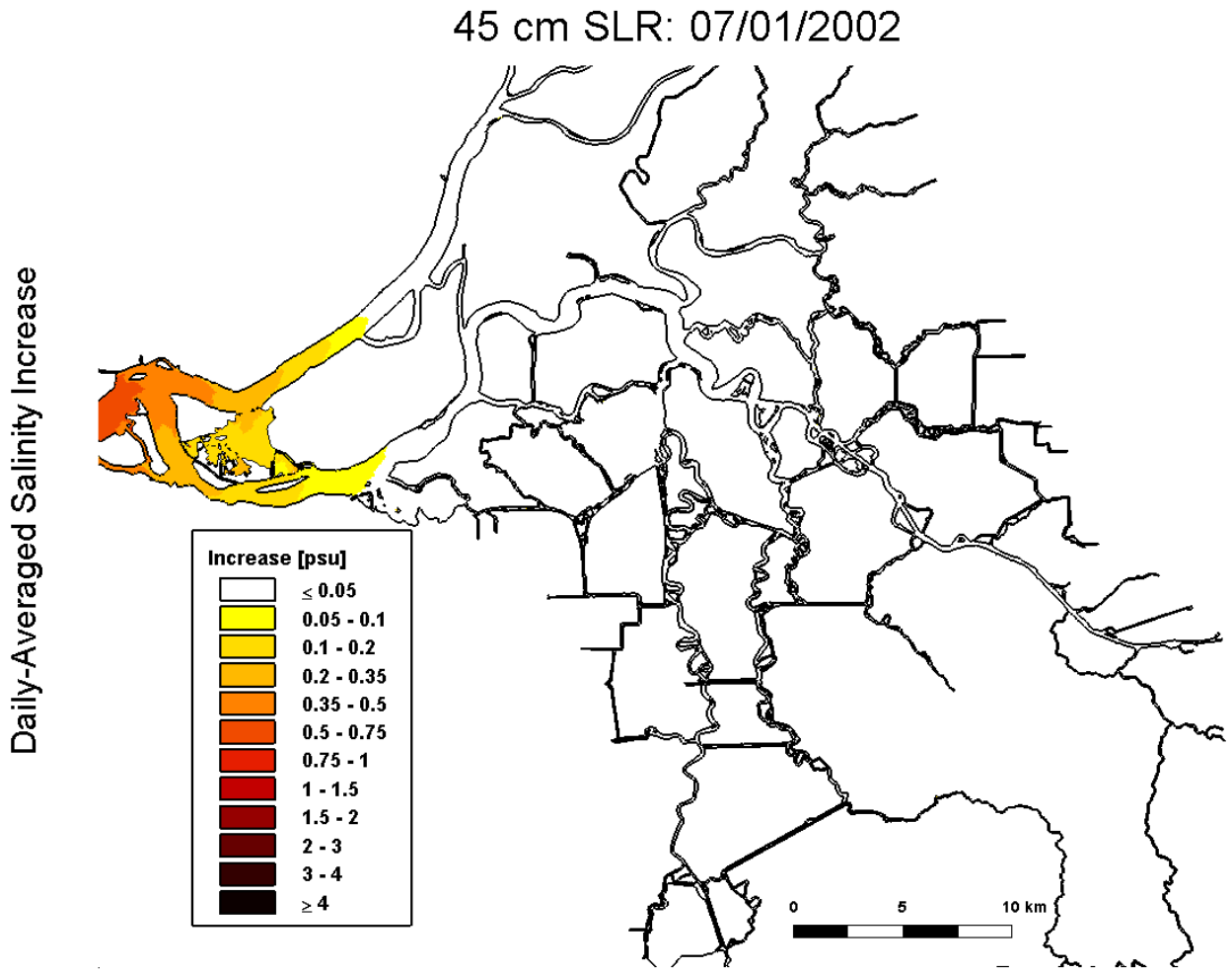

Figure 4.3-20 Predicted increase in daily-averaged depth-average salinity in the Sacramento-San Joaquin Delta on July 1, 2002 relative to the Baseline (0 cm SLR) scenario for the 45 cm SLR scenario.

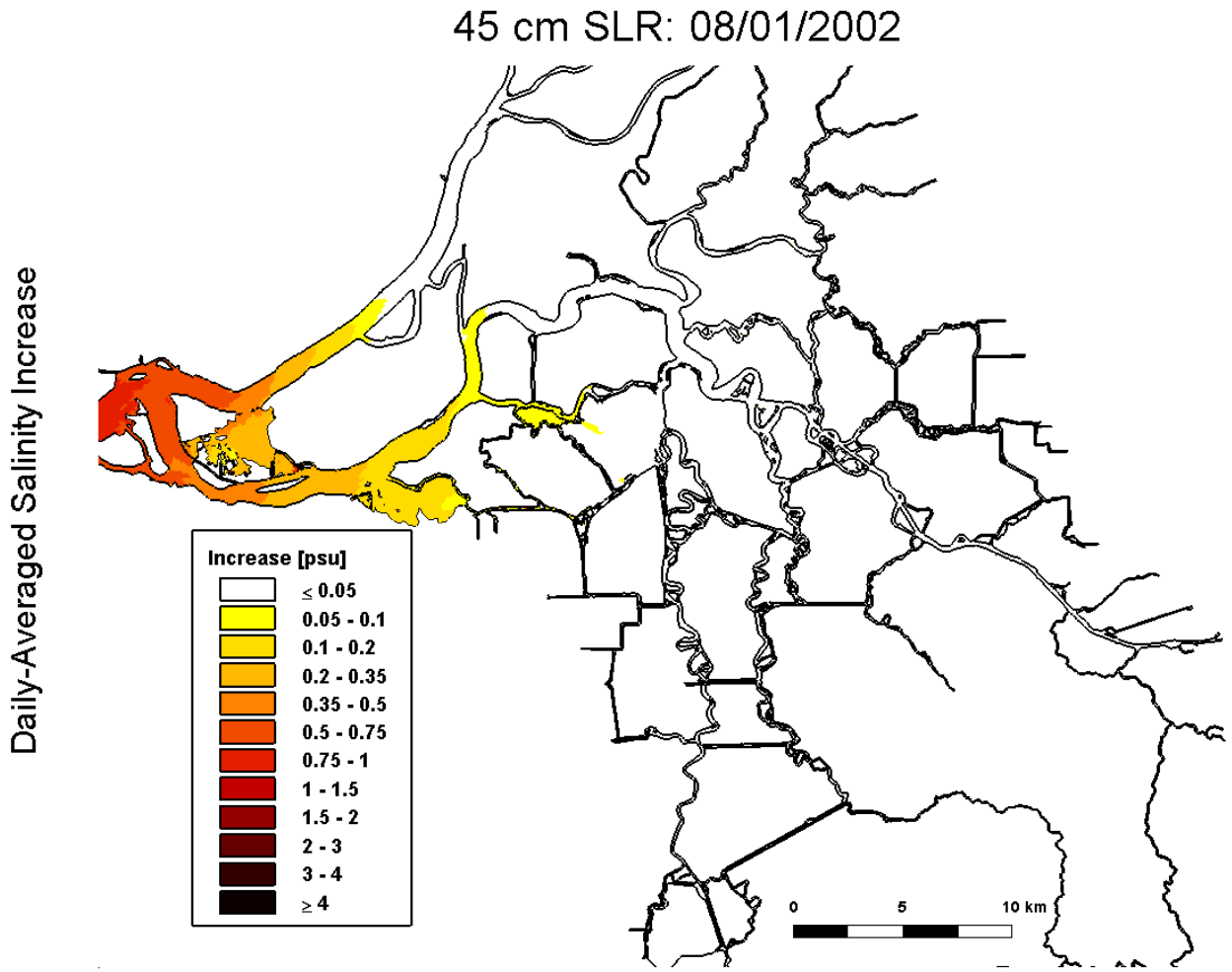

Figure 4.3-21 Predicted increase in daily-averaged depth-average salinity in the Sacramento-San Joaquin Delta on August 1, 2002 relative to the Baseline (0 cm SLR) scenario for the 45 cm SLR scenario.

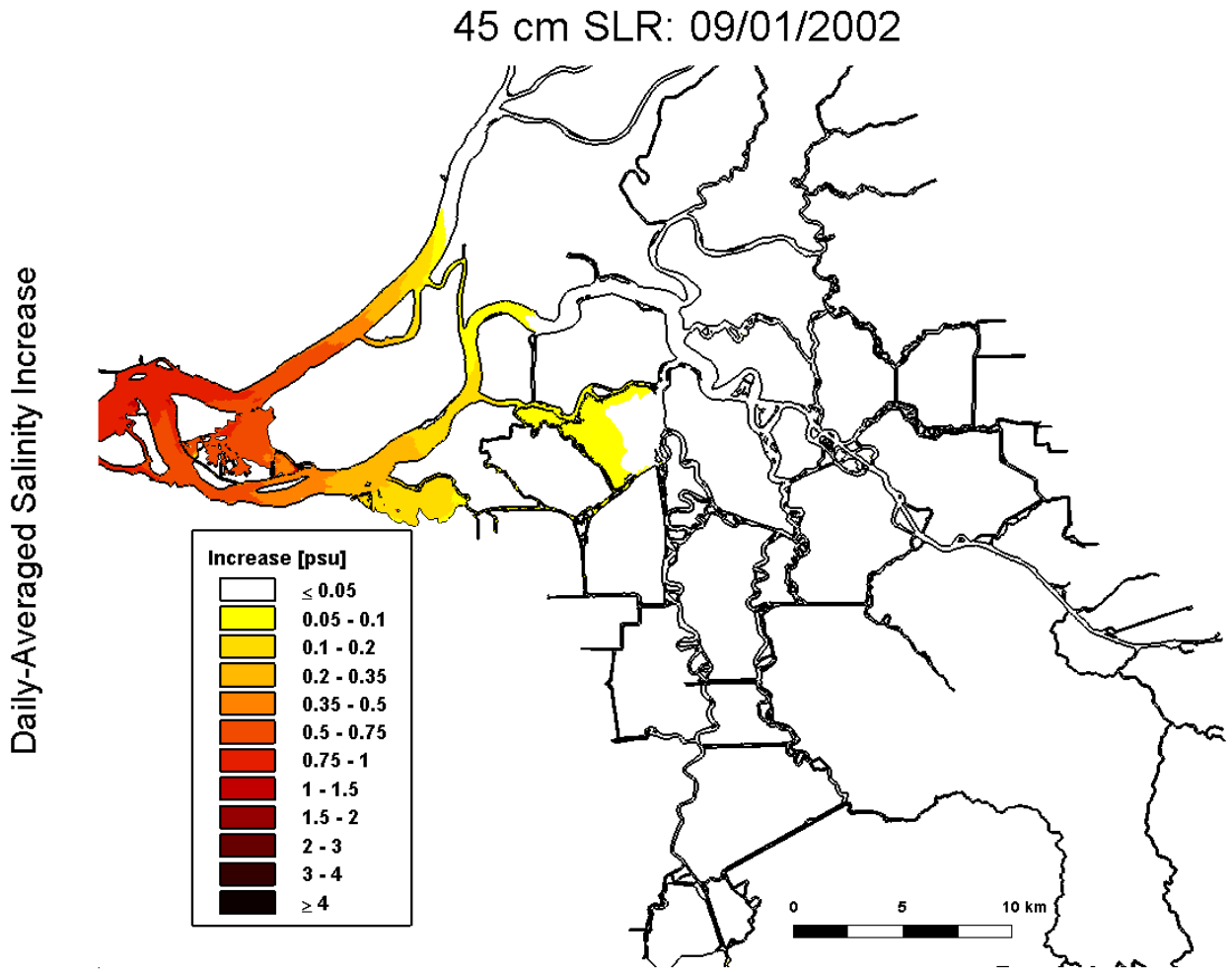

Figure 4.3-22 Predicted increase in daily-averaged depth-average salinity in the Sacramento-San Joaquin Delta on September 1, 2002 relative to the Baseline (0 cm SLR) scenario for the 45 cm SLR scenario.

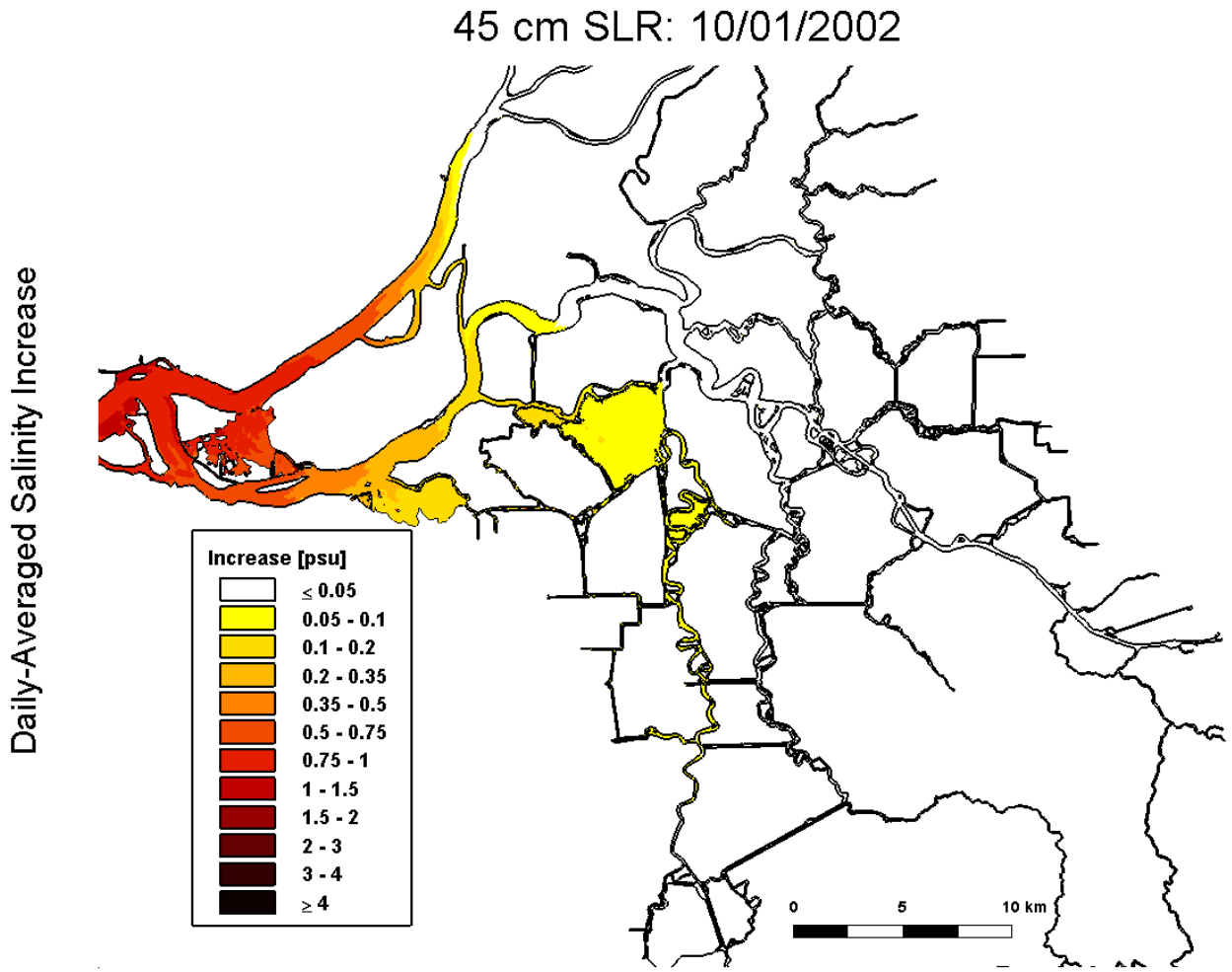

Figure 4.3-23 Predicted increase in daily-averaged depth-average salinity in the Sacramento-San Joaquin Delta on October 1, 2002 relative to the Baseline (0 cm SLR) scenario for the 45 cm SLR scenario.

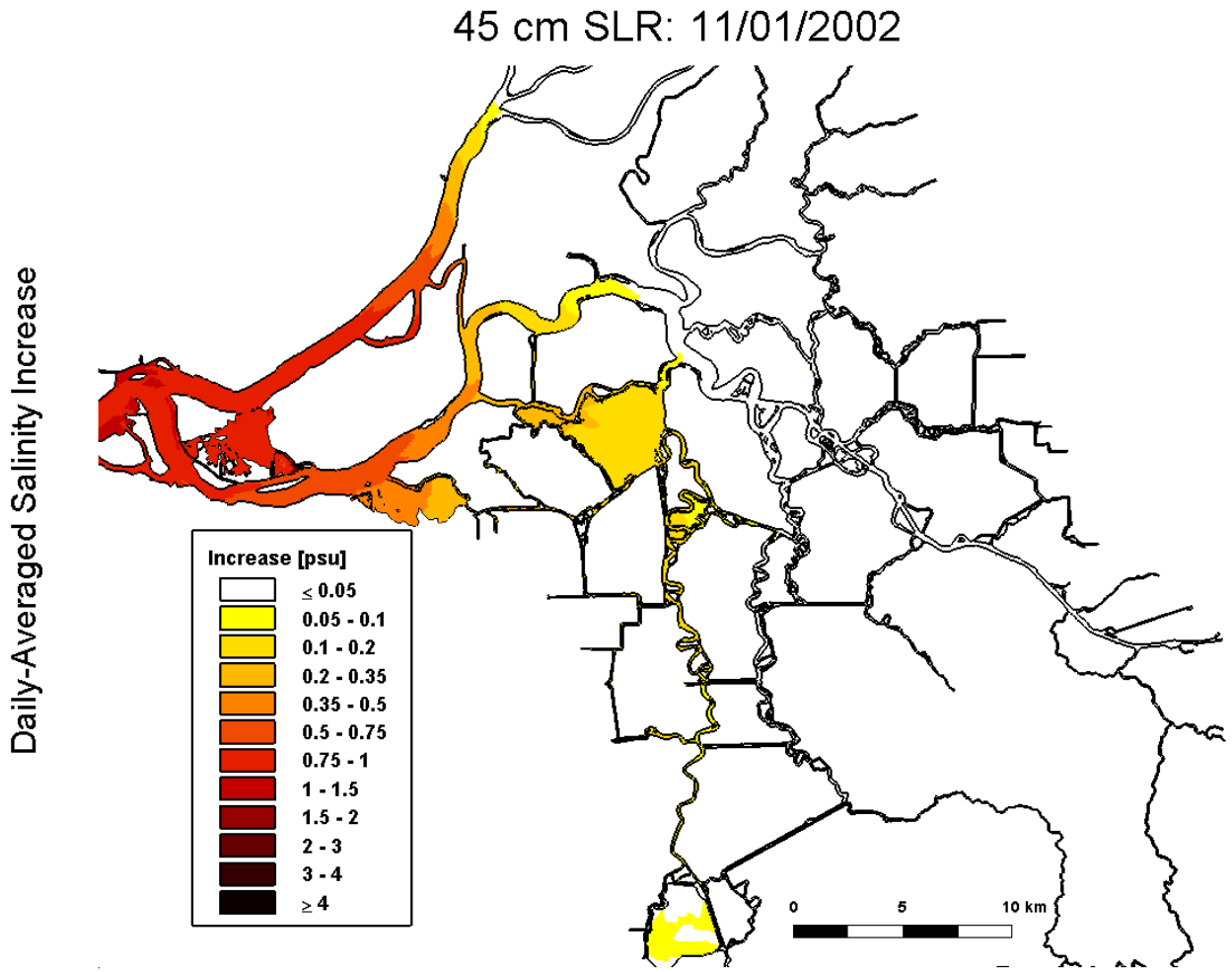

Figure 4.3-24 Predicted increase in daily-averaged depth-average salinity in the Sacramento-San Joaquin Delta on November 1, 2002 relative to the Baseline (0 cm SLR) scenario for the 45 cm SLR scenario.

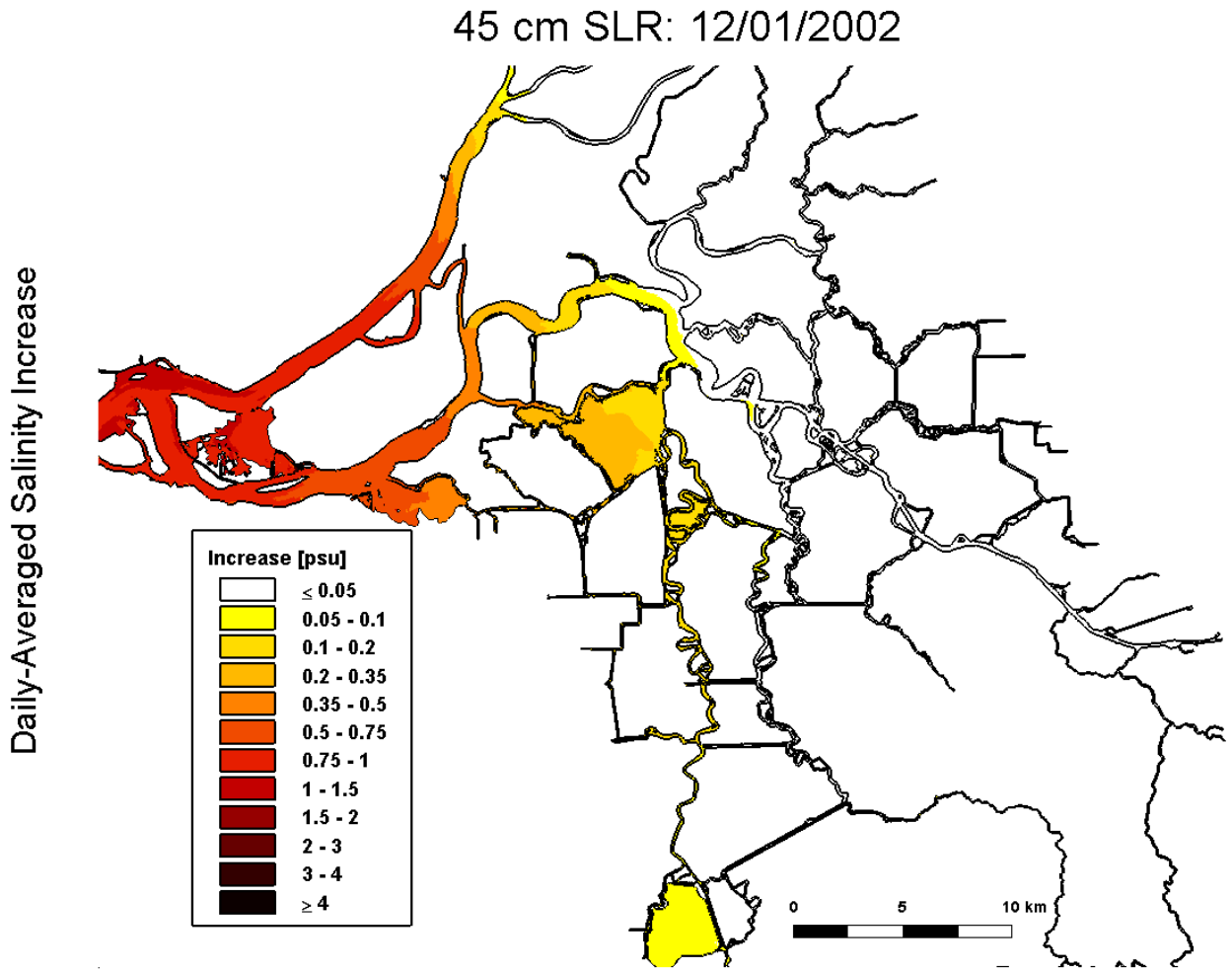

Figure 4.3-25 Predicted increase in daily-averaged depth-average salinity in the Sacramento-San Joaquin Delta on December 1, 2002 relative to the Baseline (0 cm SLR) scenario for the 45 cm SLR scenario.

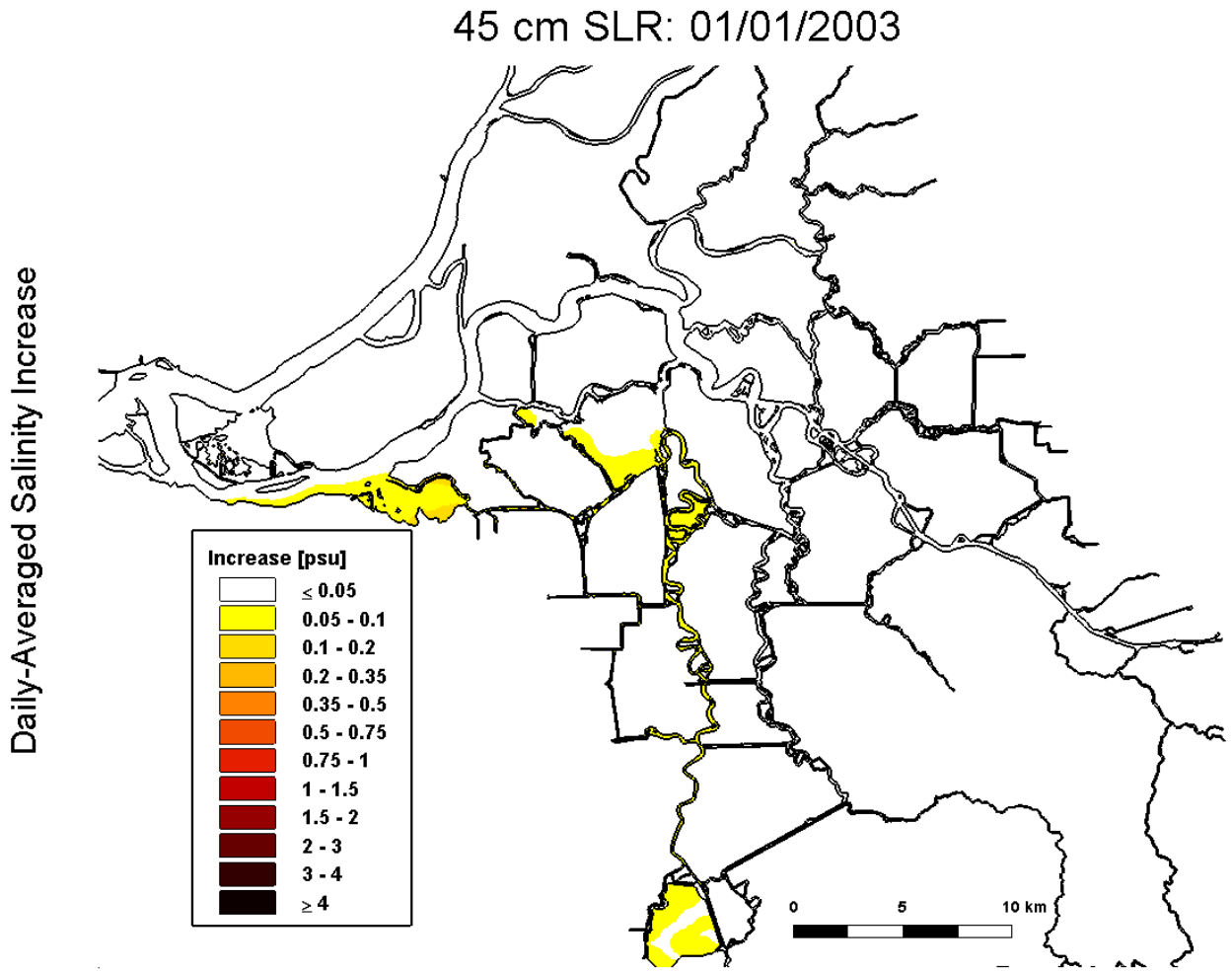

Figure 4.3-26 Predicted increase in daily-averaged depth-average salinity in the Sacramento-San Joaquin Delta on January 1, 2003 relative to the Baseline (0 cm SLR) scenario for the 45 cm SLR scenario.

4.4 Predicted Increase in Salinity for 60 cm SLR Scenario

Figure 4.4-1 through 4.4-13 show the predicted salinity along the northern portion of the San Francisco Estuary, spanning from San Pablo Bay through the Sacramento-San Joaquin Delta for the 60 cm SLR scenario. The top panel of each figure shows the predicted daily-averaged depth-average salinity for the 60 cm SLR scenario. The lower panel shows the predicted salinity increase computed by subtracting the predicted daily-averaged depth-average salinity for the Baseline (0 cm SLR) scenario from the predicted daily-averaged depth-average salinity for the 60 cm SLR scenario. Figures 4.4-14 through 4.4-26 show the predicted salinity increases resulting from the 60 cm SLR scenario in the Sacramento-San Joaquin Delta.

At the beginning of the analysis period on January 1, 2002, salinity increases between 0.35 and 0.50 psu are predicted between Chipps Island and Collinsville and predicted salinity increases of up to 0.05 psu are predicted upstream along the western end of Sherman Island to Big Break. Predicted salinity increases are less than 0.05 psu throughout the remaining portions of the Delta. Salinity increases between 1.5 and 2.0 psu are predicted through Carquinez Strait and salinity increases between 0.50 and 1.5 psu are predicted throughout Suisun Bay. Larger salinity increases of more than 1.0 psu are predicted in much of San Pablo Bay, with salinity increases of more than 4 psu predicted in northern San Pablo Bay. During the first half of the year, predicted salinity increases in Suisun Bay and the Delta remain similar to the predicted salinity increases seen on January 1, 2002, though the predicted salinity is increasing throughout this period. Larger salinity increases are predicted in the Delta between July and December, with the largest predicted salinity increases in December prior to the first flush. In December, salinity increases of between 1.0 and 1.5 psu are predicted between Chipps Island and Emmaton, and salinity increases of between 0.20 and 0.50 psu are predicted in Franks Tract. South of Franks Tract, predicted salinity increases between 0.20 and 0.35 psu extend down Old River to Clifton Court Forebay, and salinity increases of between 0.10 and 0.20 psu are predicted inside Clifton Court Forebay. These simulations assumed no operational response to sea level rise, however it is expected significant operational response will be required to maintain water quality standards for 60 cm of sea level rise. Following high flows which occurred in December, predicted salinity on January 1, 2003 shows that the 0.50 psu isohaline is on the western side of Suisun Bay near Martinez. Predicted salinity increases of between 0.05 and 0.20 psu persist in some regions of the Delta, primarily along the San Joaquin River between Antioch and False River, in Big Break, south of Franks Tract along Old River, and in Clifton Court Forebay.

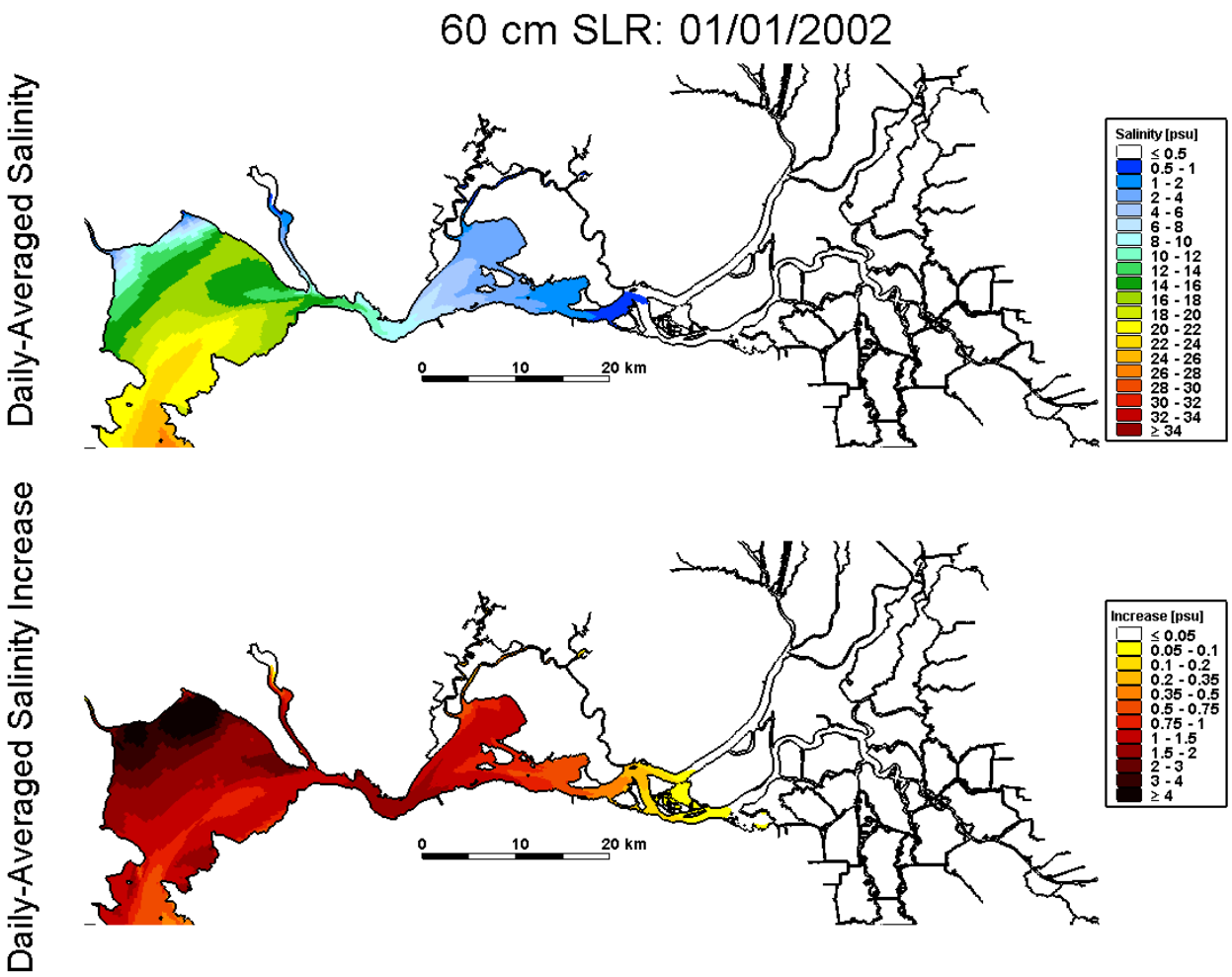

Figure 4.4-1 Predicted daily-averaged depth-average salinity on January 1, 2002 for the 60 cm SLR scenario (top); predicted increase in daily-averaged depth-average salinity on January 1, 2002 relative to the Baseline (0 cm SLR) scenario for the 60 cm SLR scenario.

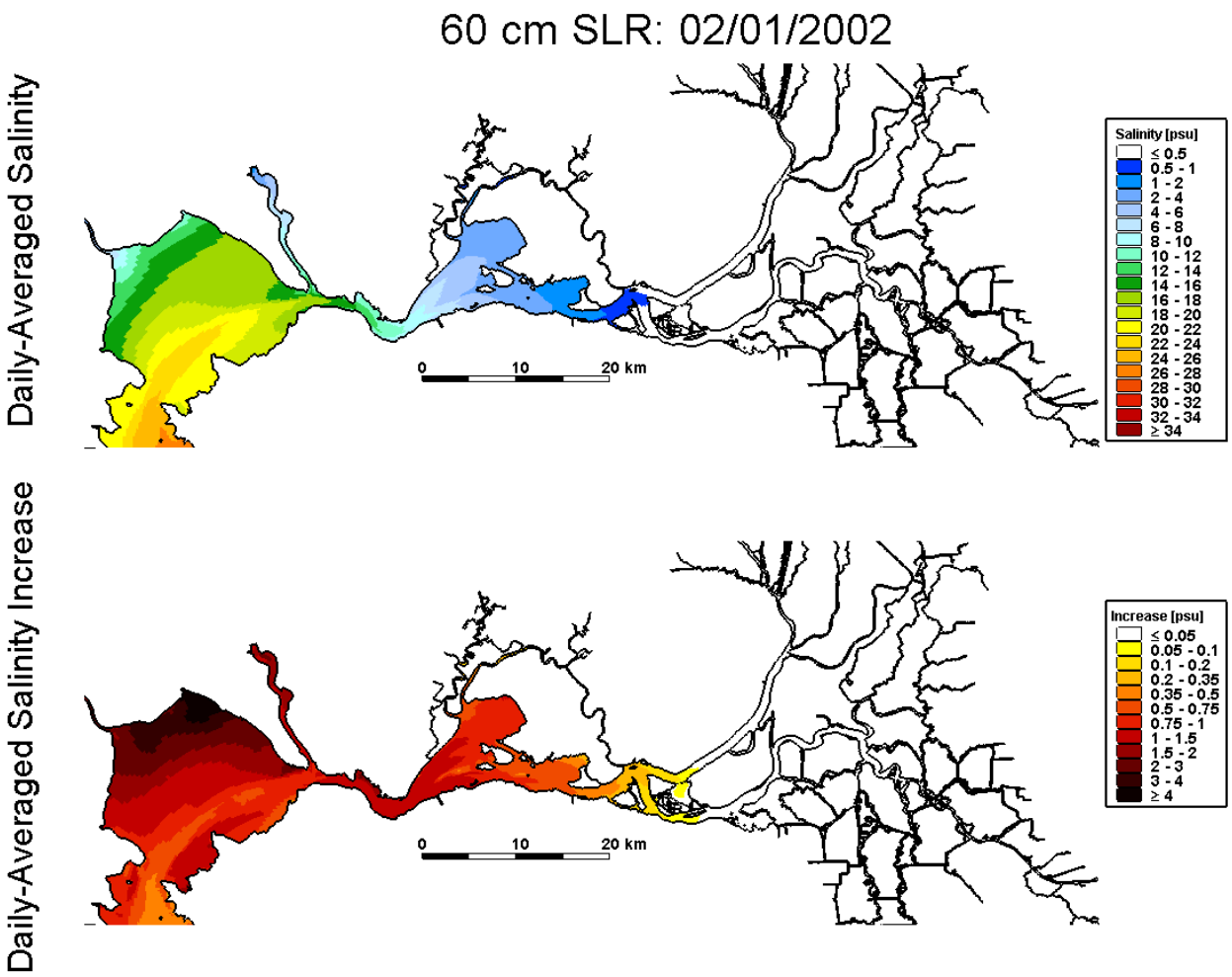

Figure 4.4-2 Predicted daily-averaged depth-average salinity on February 1, 2002 for the 60 cm SLR scenario (top); predicted increase in daily-averaged depth-average salinity on February 1, 2002 relative to the Baseline (0 cm SLR) scenario for the 60 cm SLR scenario.

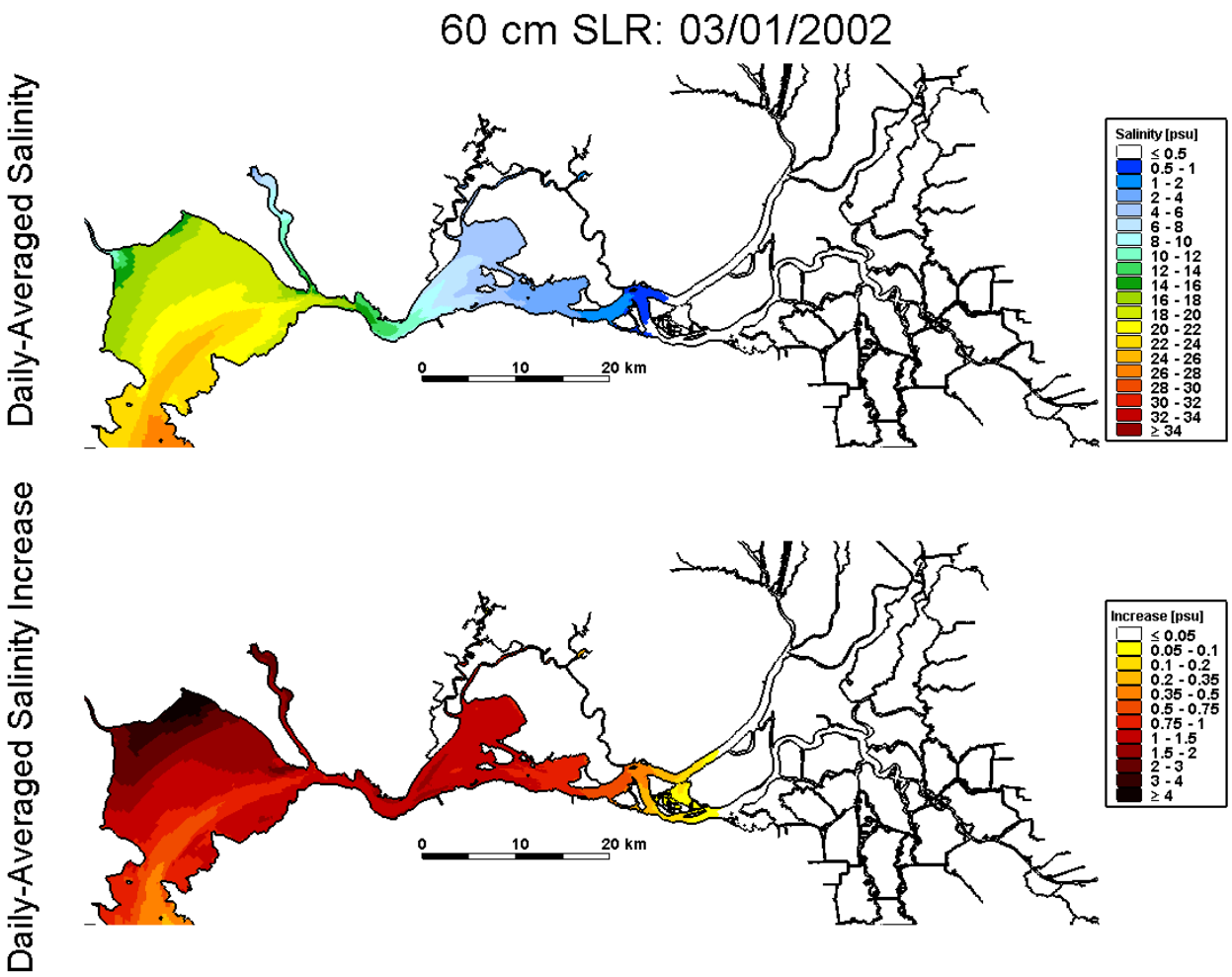

Figure 4.4-3 Predicted daily-averaged depth-average salinity on March 1, 2002 for the 60 cm SLR scenario (top); predicted increase in daily-averaged depth-average salinity on March 1, 2002 relative to the Baseline (0 cm SLR) scenario for the 60 cm SLR scenario.

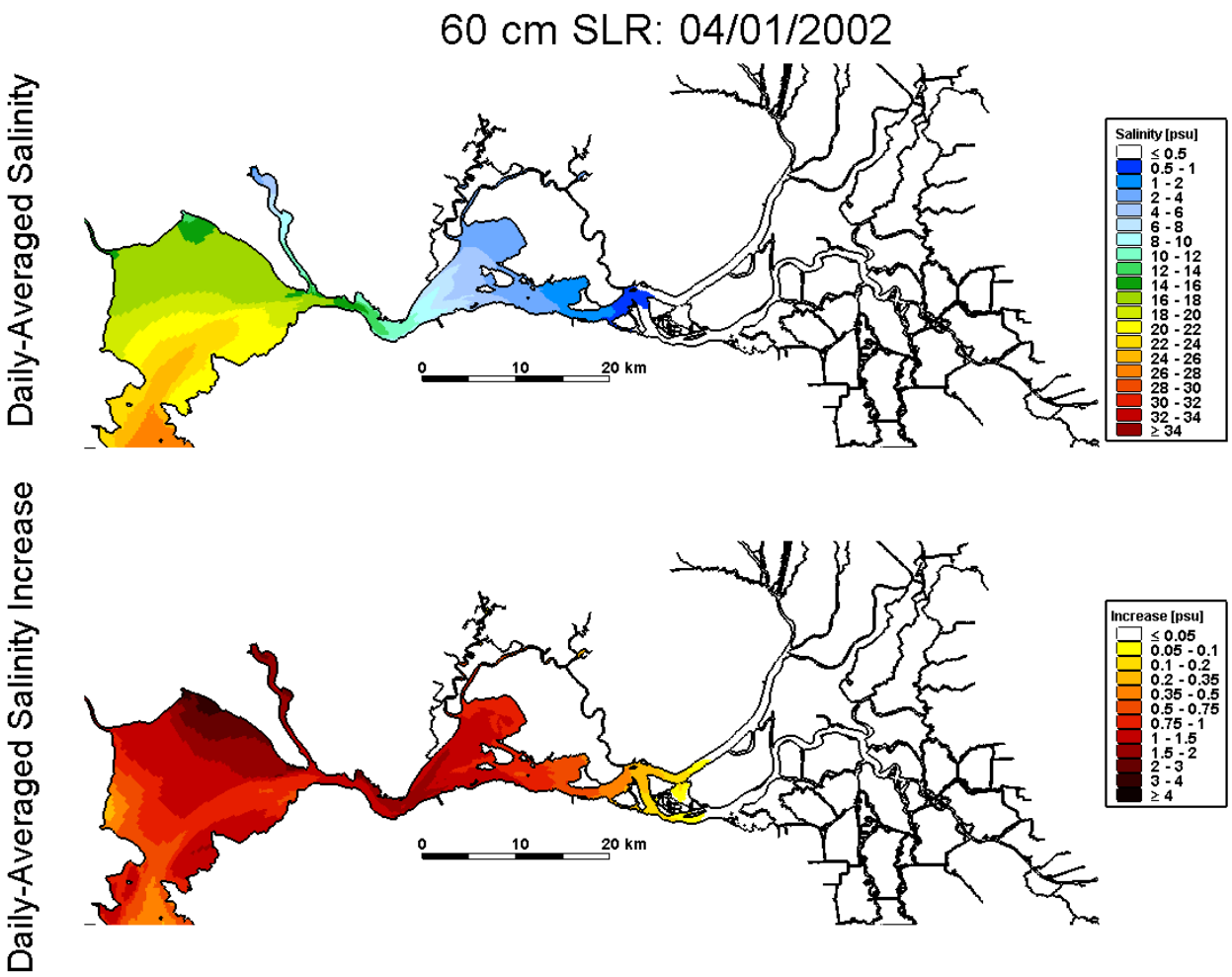

Figure 4.4-4 Predicted daily-averaged depth-average salinity on April 1, 2002 for the 60 cm SLR scenario (top); predicted increase in daily-averaged depth-average salinity on April 1, 2002 relative to the Baseline (0 cm SLR) scenario for the 60 cm SLR scenario.

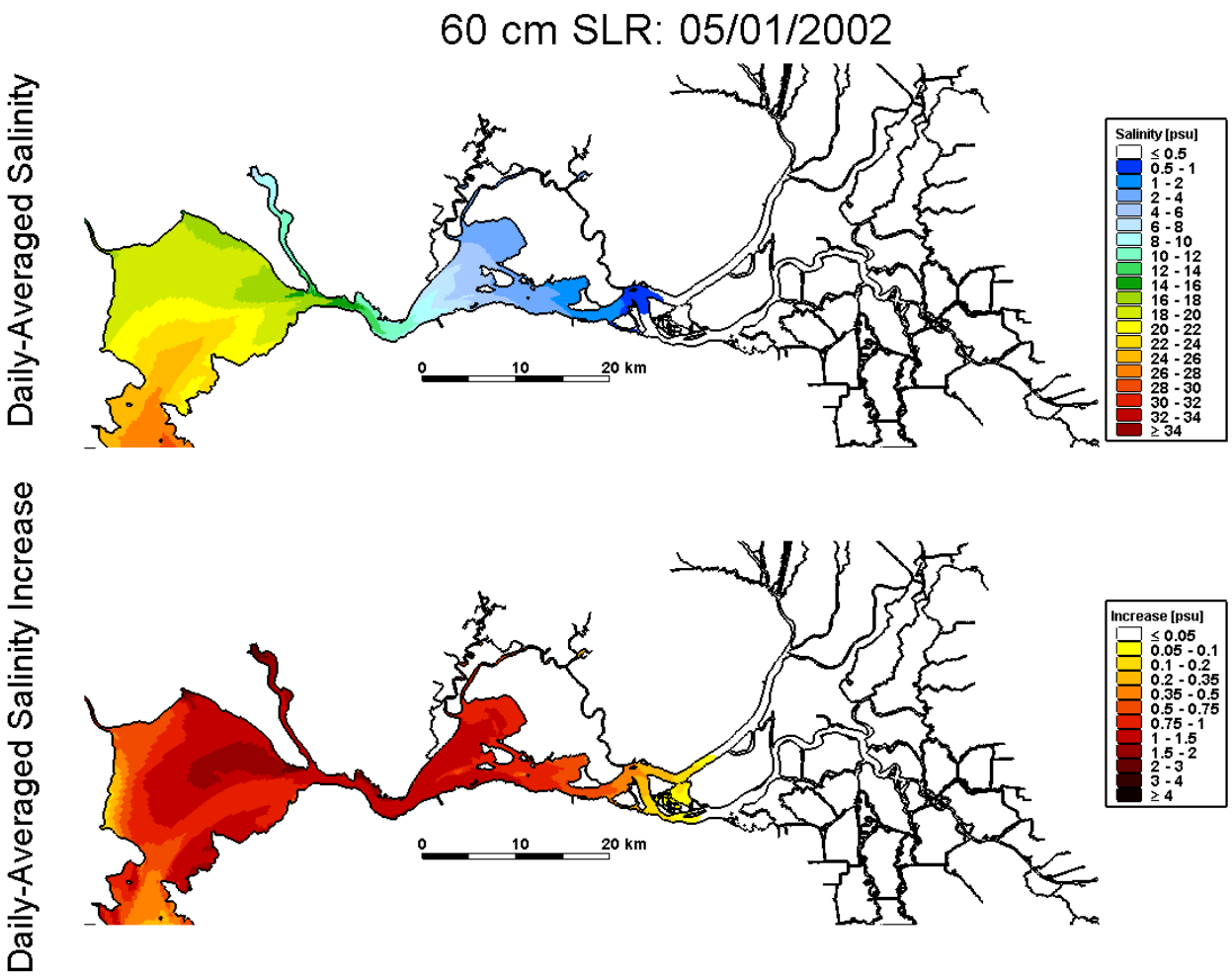

Figure 4.4-5 Predicted daily-averaged depth-average salinity on May 1, 2002 for the 60 cm SLR scenario (top); predicted increase in daily-averaged depth-average salinity on May 1, 2002 relative to the Baseline (0 cm SLR) scenario for the 60 cm SLR scenario.

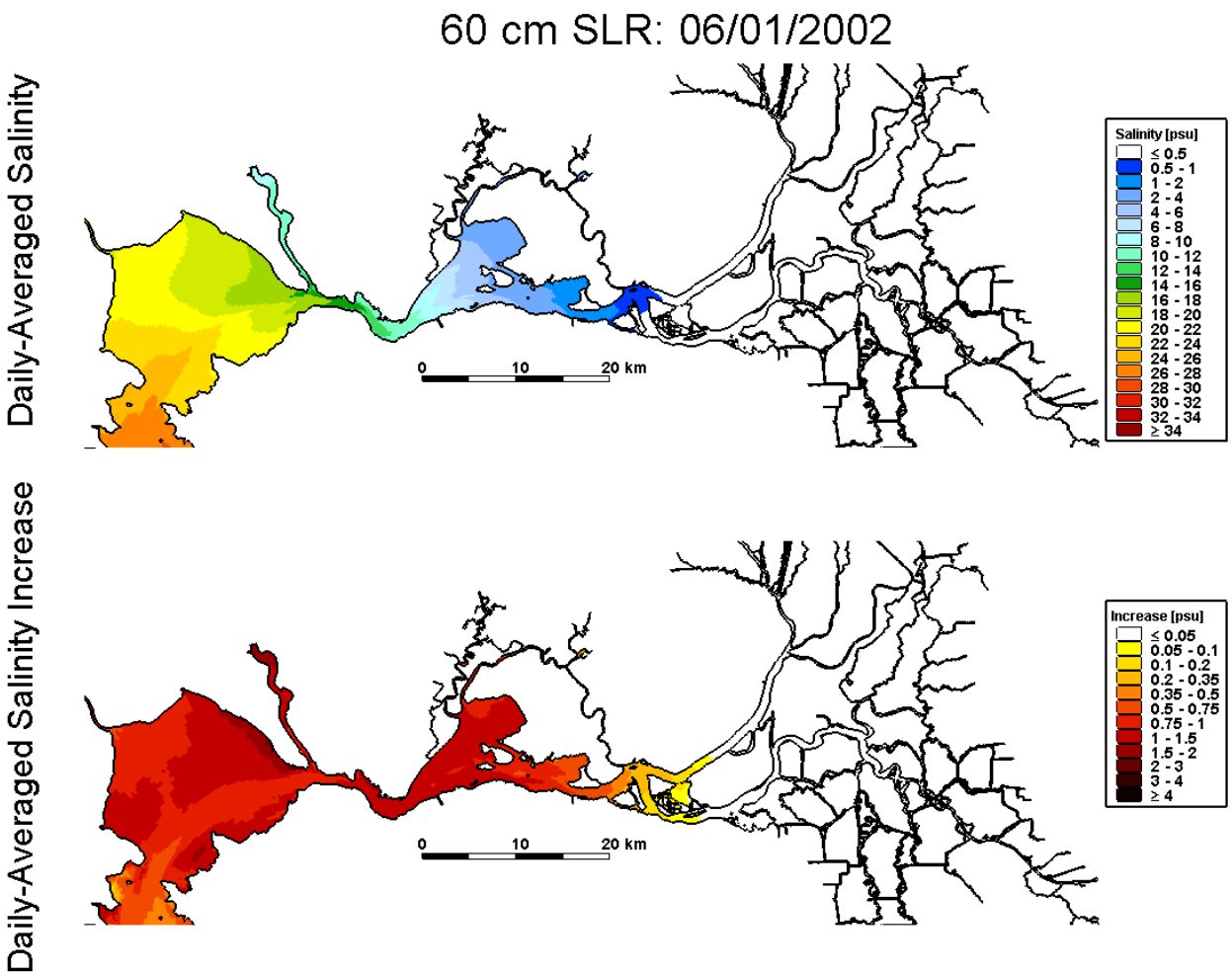

Figure 4.4-6 Predicted daily-averaged depth-average salinity on June 1, 2002 for the 60 cm SLR scenario (top); predicted increase in daily-averaged depth-average salinity on June 1, 2002 relative to the Baseline (0 cm SLR) scenario for the 60 cm SLR scenario.

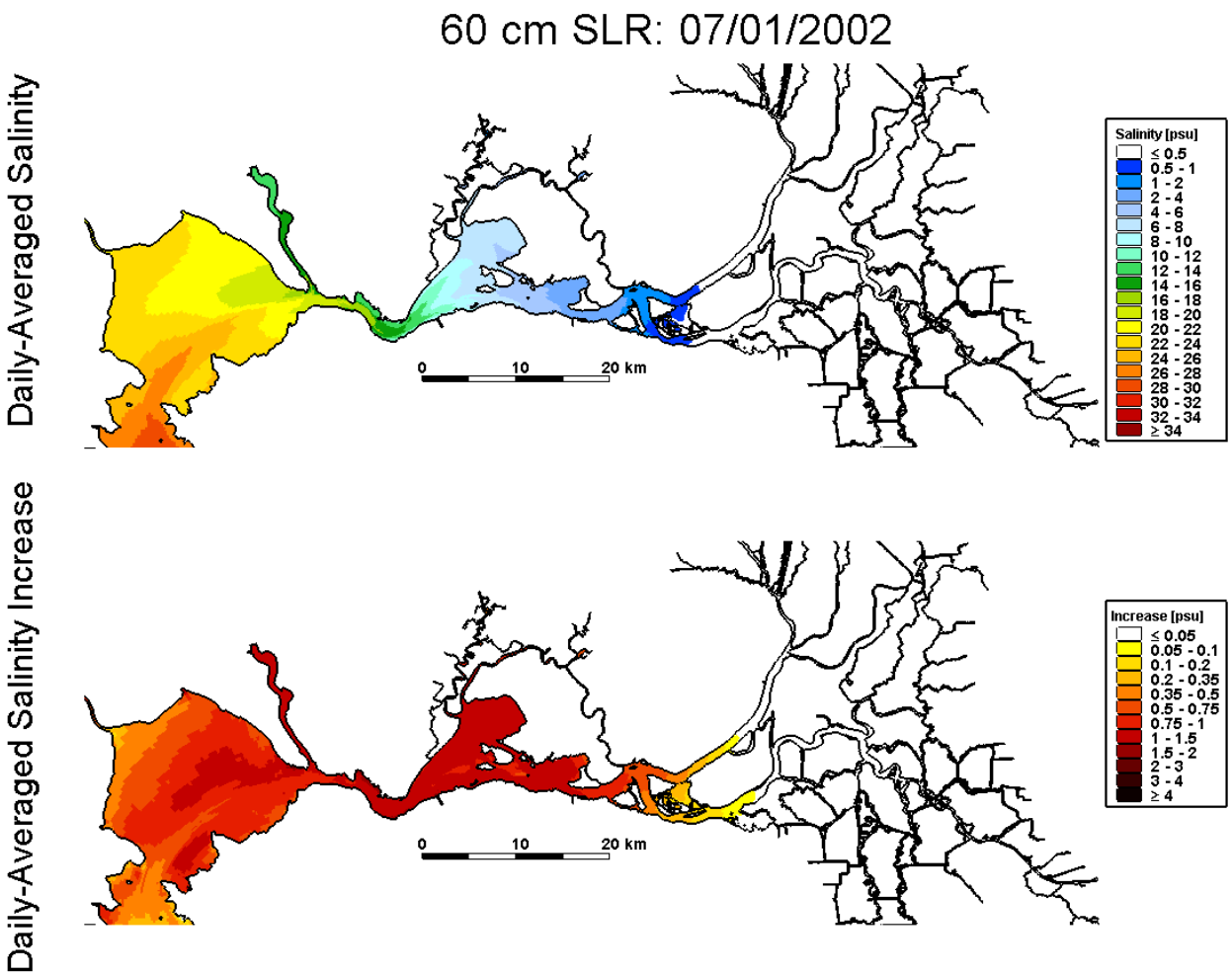

Figure 4.4-7 Predicted daily-averaged depth-average salinity on July 1, 2002 for the 60 cm SLR scenario (top); predicted increase in daily-averaged depth-average salinity on July 1, 2002 relative to the Baseline (0 cm SLR) scenario for the 60 cm SLR scenario.

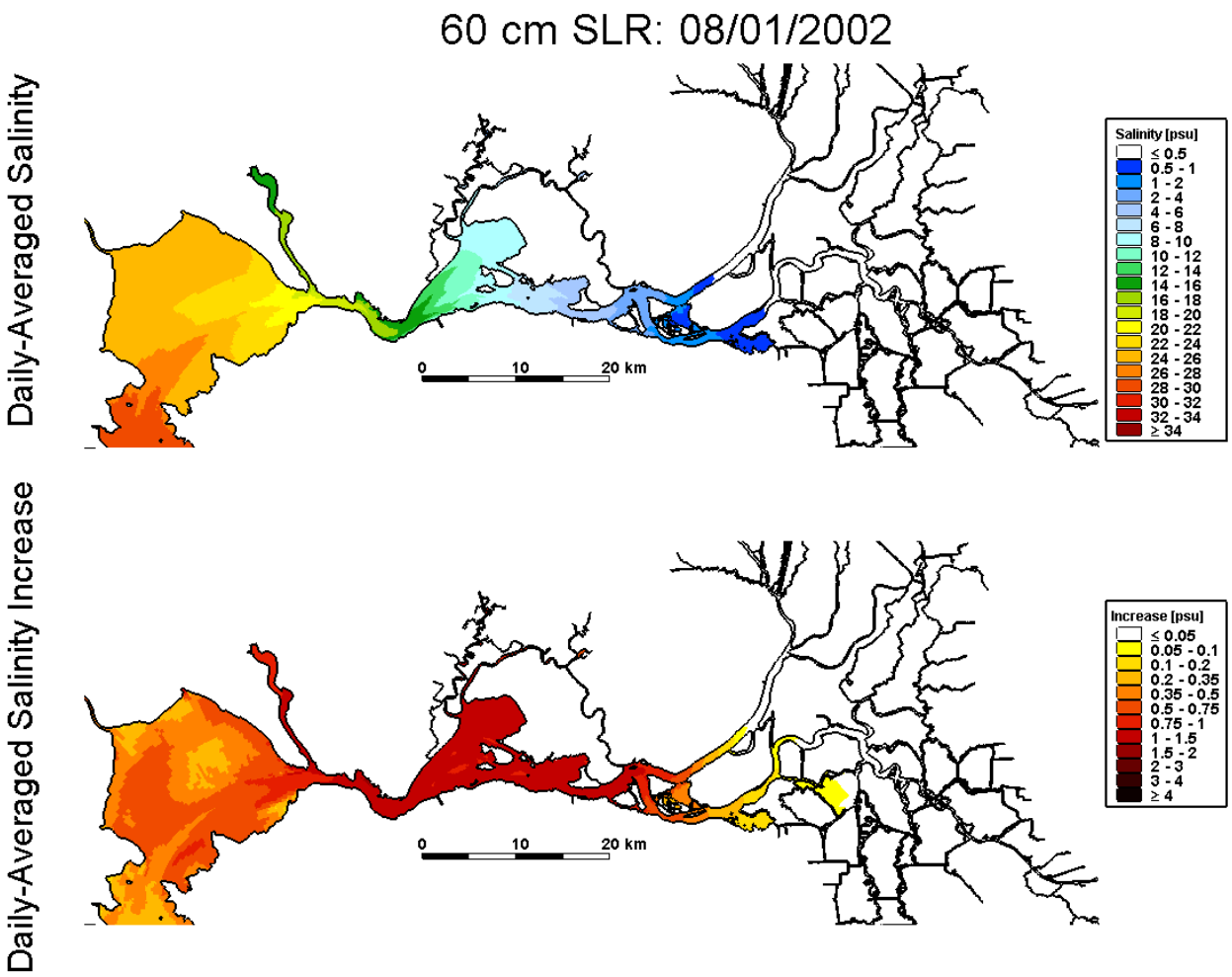

Figure 4.4-8 Predicted daily-averaged depth-average salinity on August 1, 2002 for the 60 cm SLR scenario (top); predicted increase in daily-averaged depth-average salinity on August 1, 2002 relative to the Baseline (0 cm SLR) scenario for the 60 cm SLR scenario.

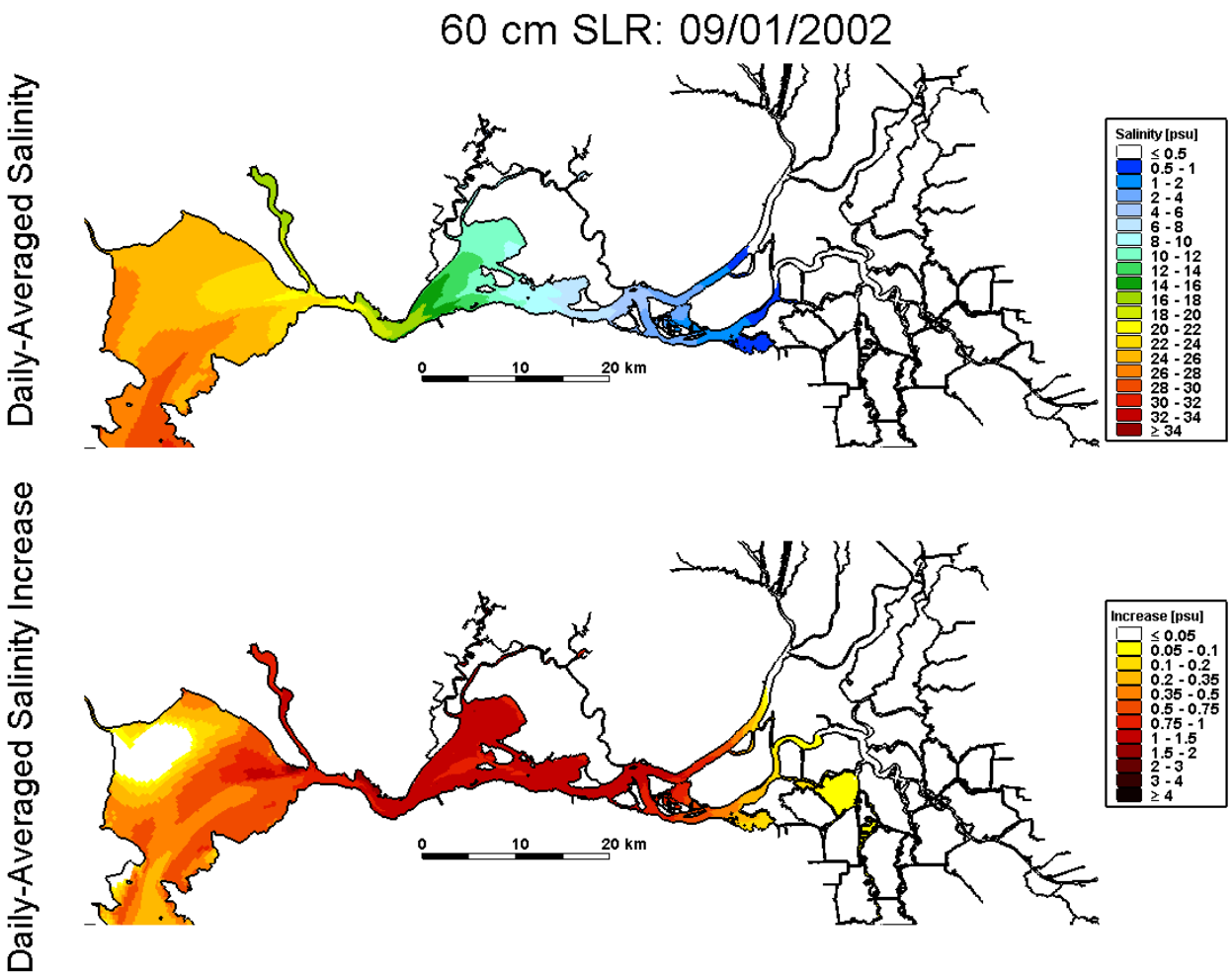

Figure 4.4-9 Predicted daily-averaged depth-average salinity on September 1, 2002 for the 60 cm SLR scenario (top); predicted increase in daily-averaged depth-average salinity on September 1, 2002 relative to the Baseline (0 cm SLR) scenario for the 60 cm SLR scenario.

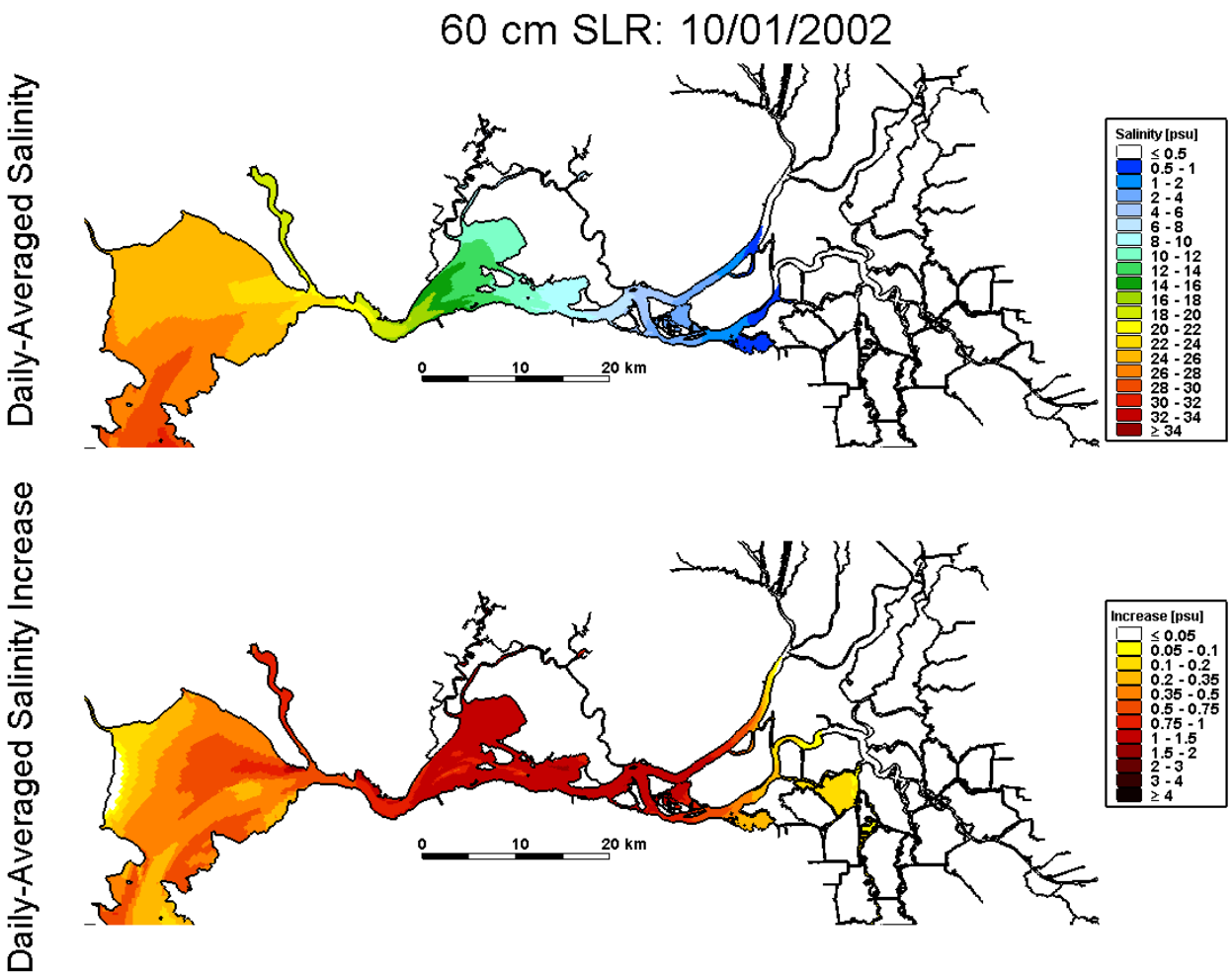

Figure 4.4-10 Predicted daily-averaged depth-average salinity on October 1, 2002 for the 60 cm SLR scenario (top); predicted increase in daily-averaged depth-average salinity on October 1, 2002 relative to the Baseline (0 cm SLR) scenario for the 60 cm SLR scenario.

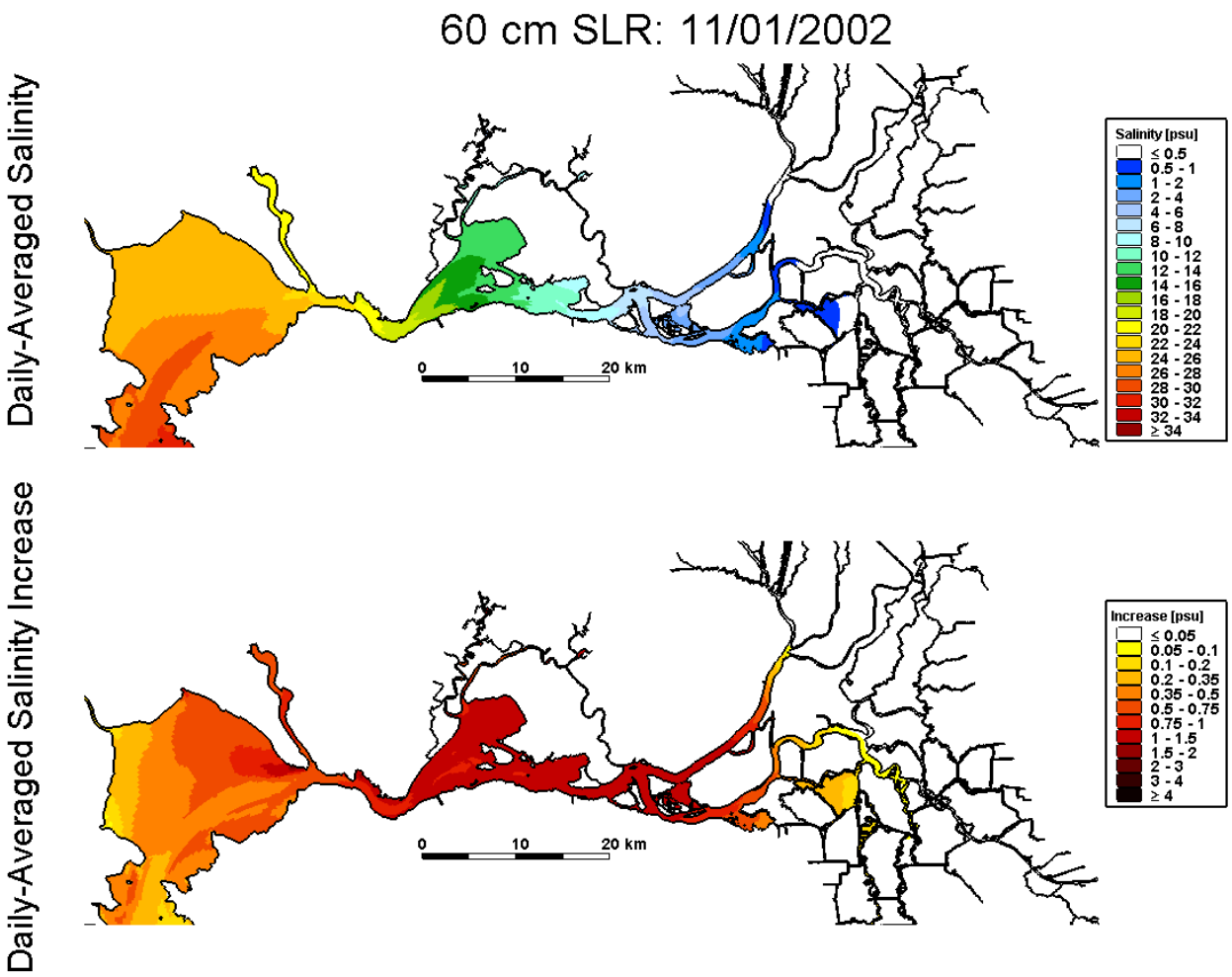

Figure 4.4-11 Predicted daily-averaged depth-average salinity on November 1, 2002 for the 60 cm SLR scenario (top); predicted increase in daily-averaged depth-average salinity on November 1, 2002 relative to the Baseline (0 cm SLR) scenario for the 60 cm SLR scenario.

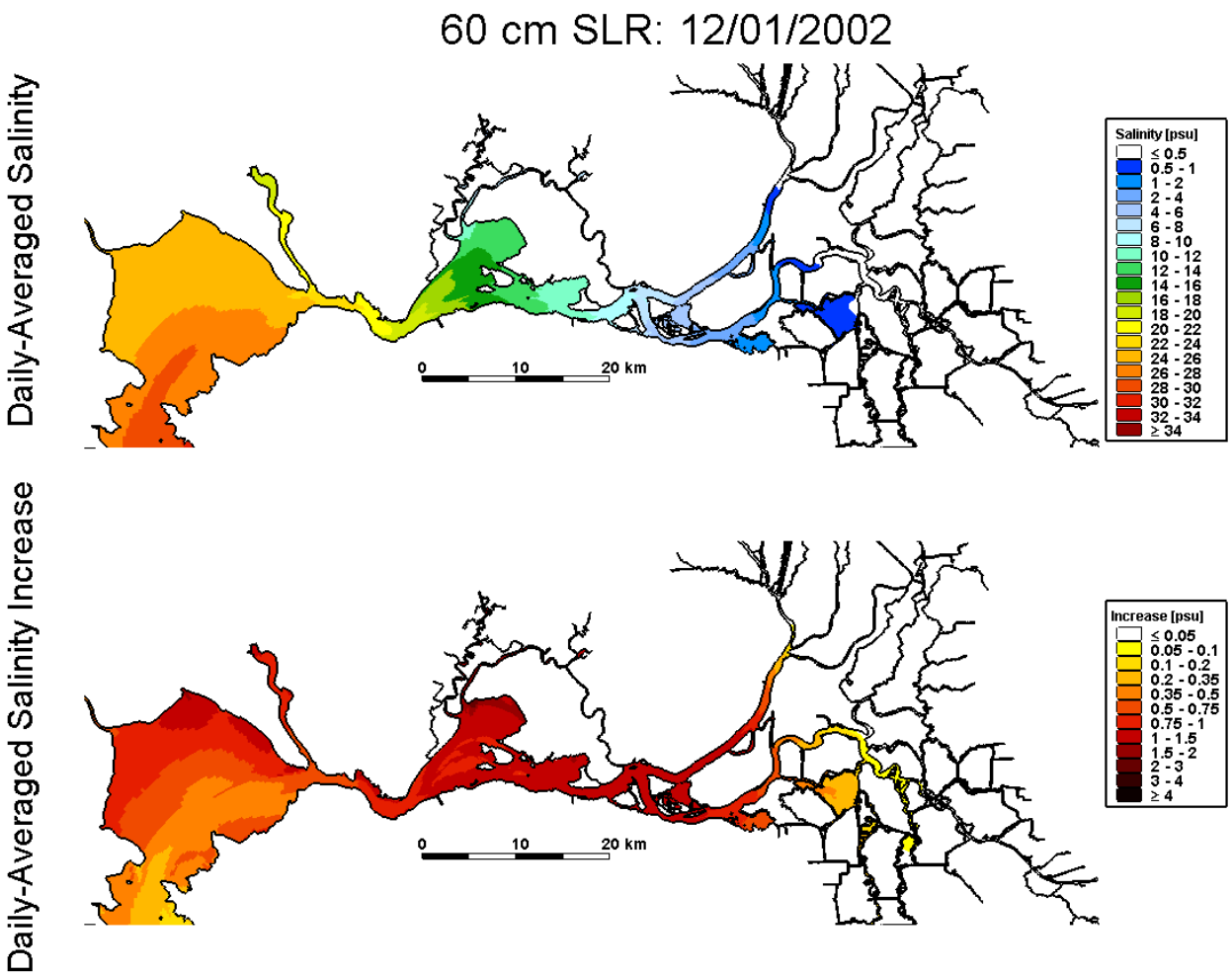

Figure 4.4-12 Predicted daily-averaged depth-average salinity on December 1, 2002 for the 60 cm SLR scenario (top); predicted increase in daily-averaged depth-average salinity on December 1, 2002 relative to the Baseline (0 cm SLR) scenario for the 60 cm SLR scenario.

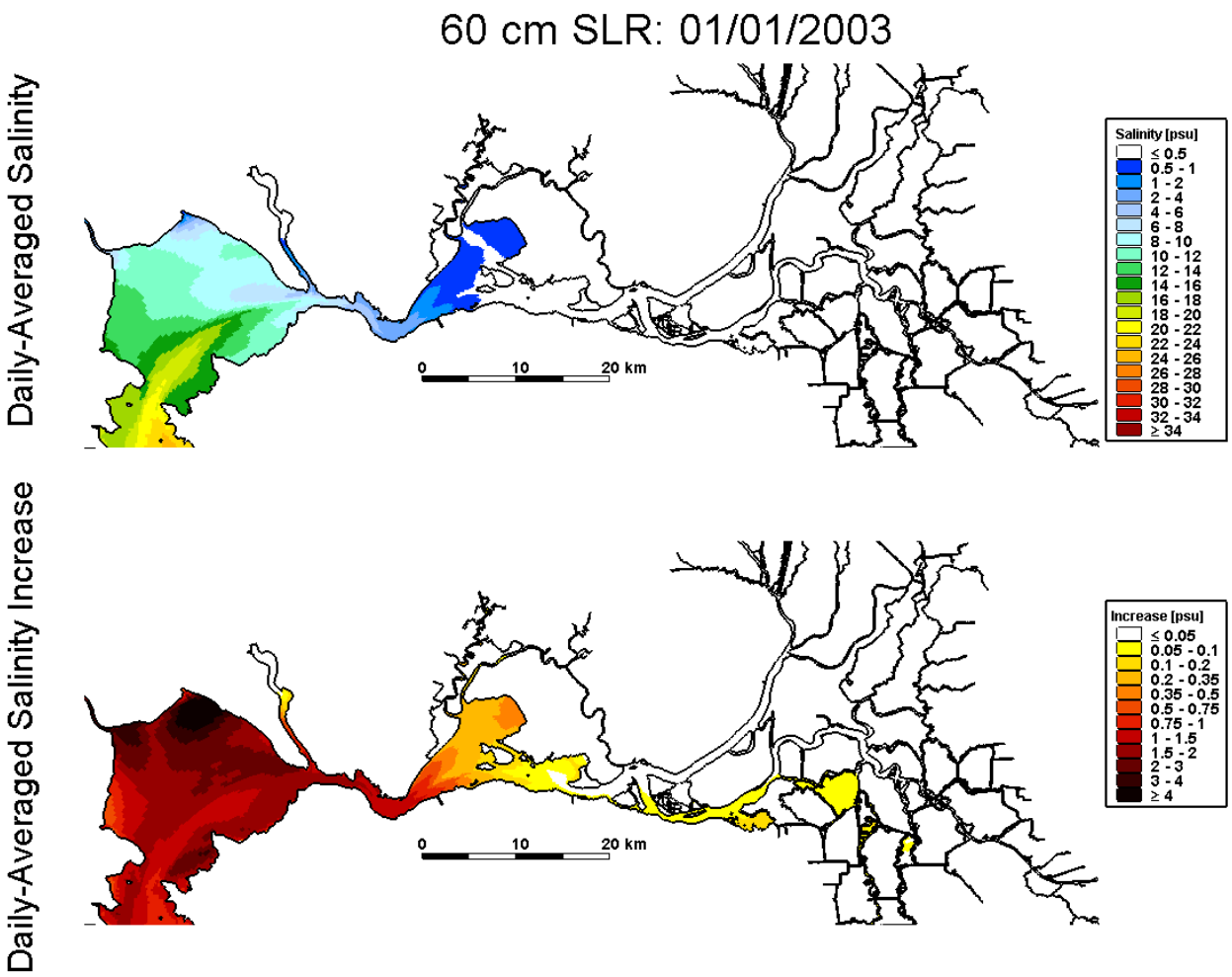

Figure 4.4-13 Predicted daily-averaged depth-average salinity on January 1, 2003 for the 60 cm SLR scenario (top); predicted increase in daily-averaged depth-average salinity on January 1, 2003 relative to the Baseline (0 cm SLR) scenario for the 60 cm SLR scenario.

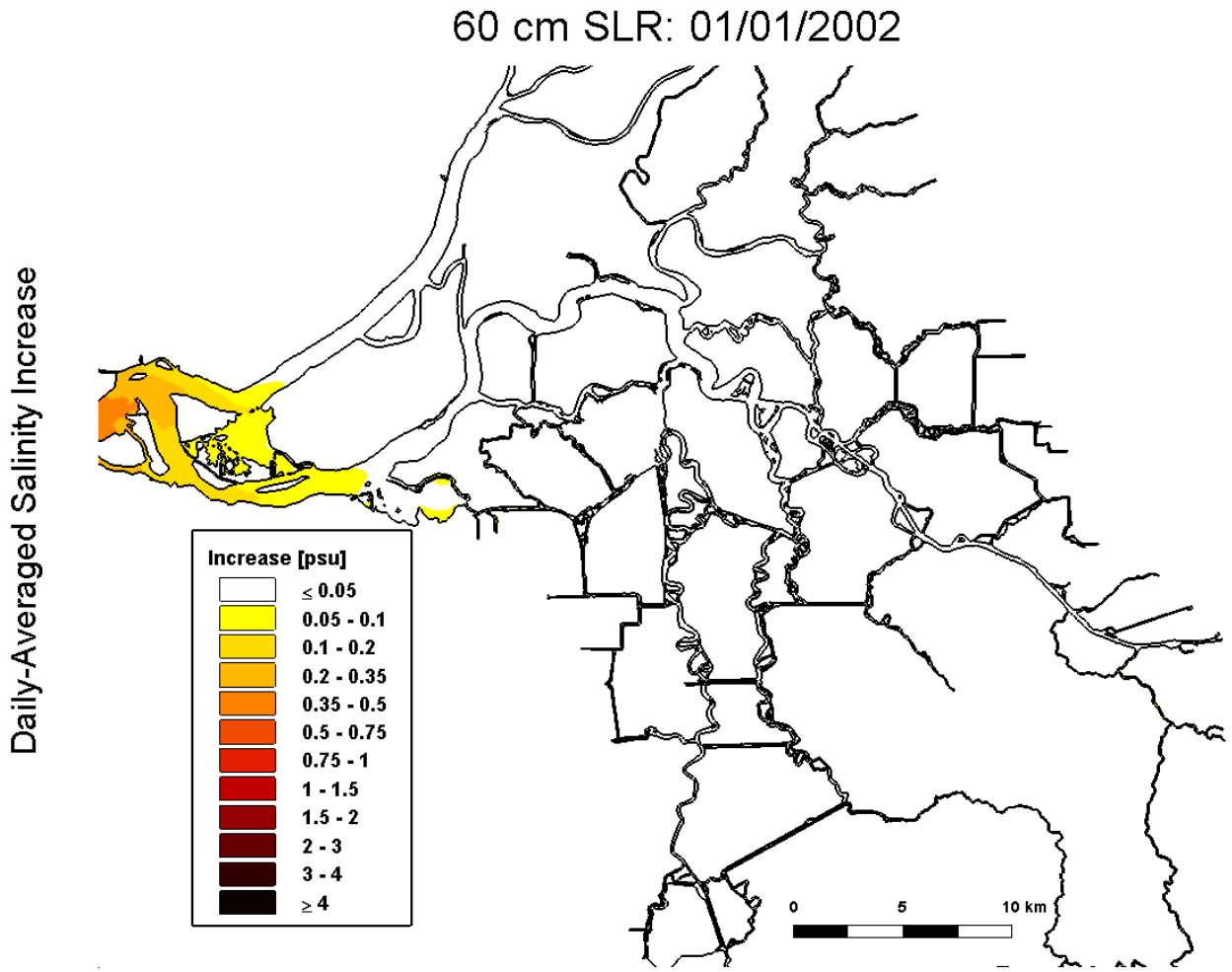

Figure 4.4-14 Predicted increase in daily-averaged depth-average salinity in the Sacramento-San Joaquin Delta on January 1, 2002 relative to the Baseline (0 cm SLR) scenario for the 60 cm SLR scenario.

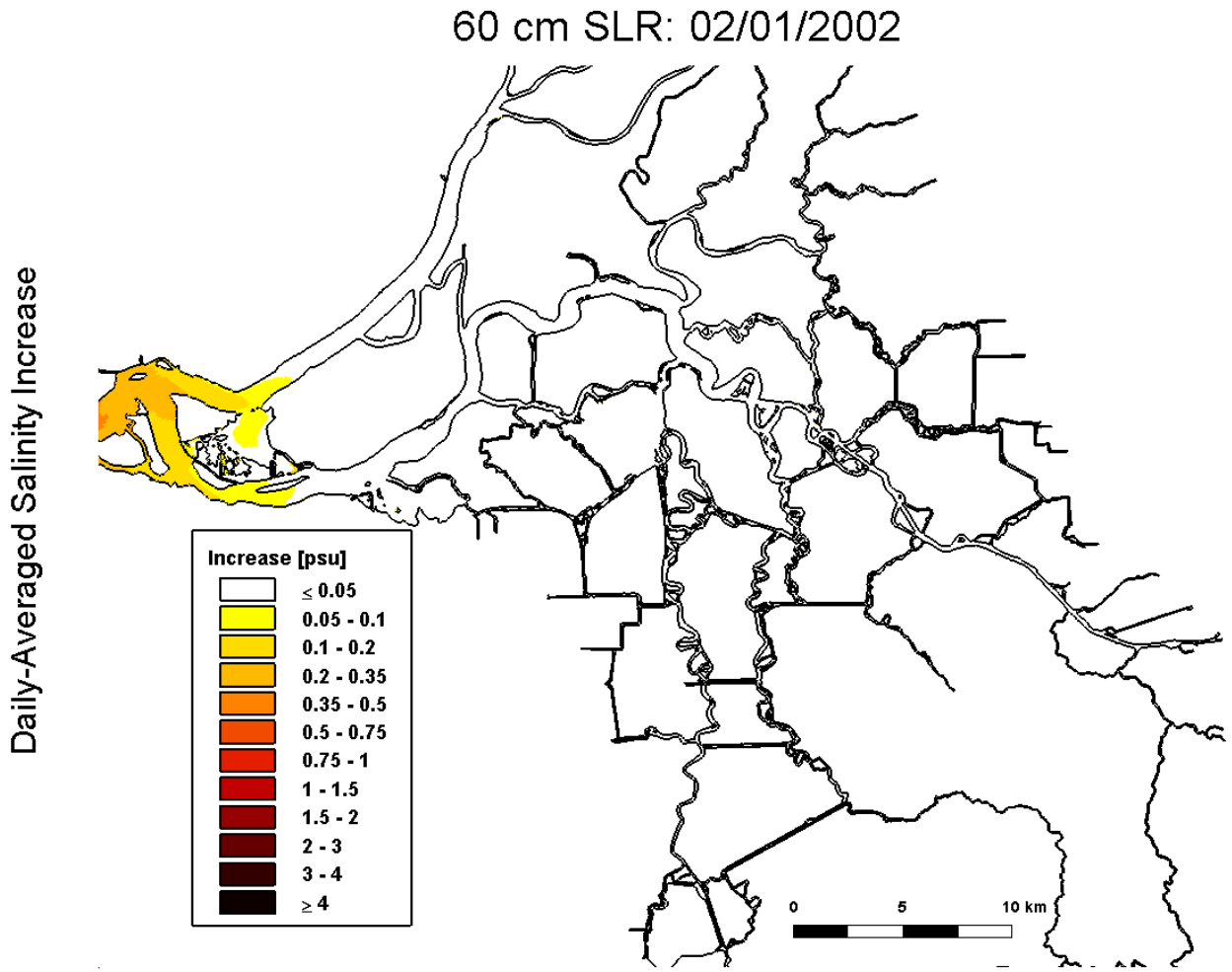

Figure 4.4-15 Predicted increase in daily-averaged depth-average salinity in the Sacramento-San Joaquin Delta on February 1, 2002 relative to the Baseline (0 cm SLR) scenario for the 60 cm SLR scenario.

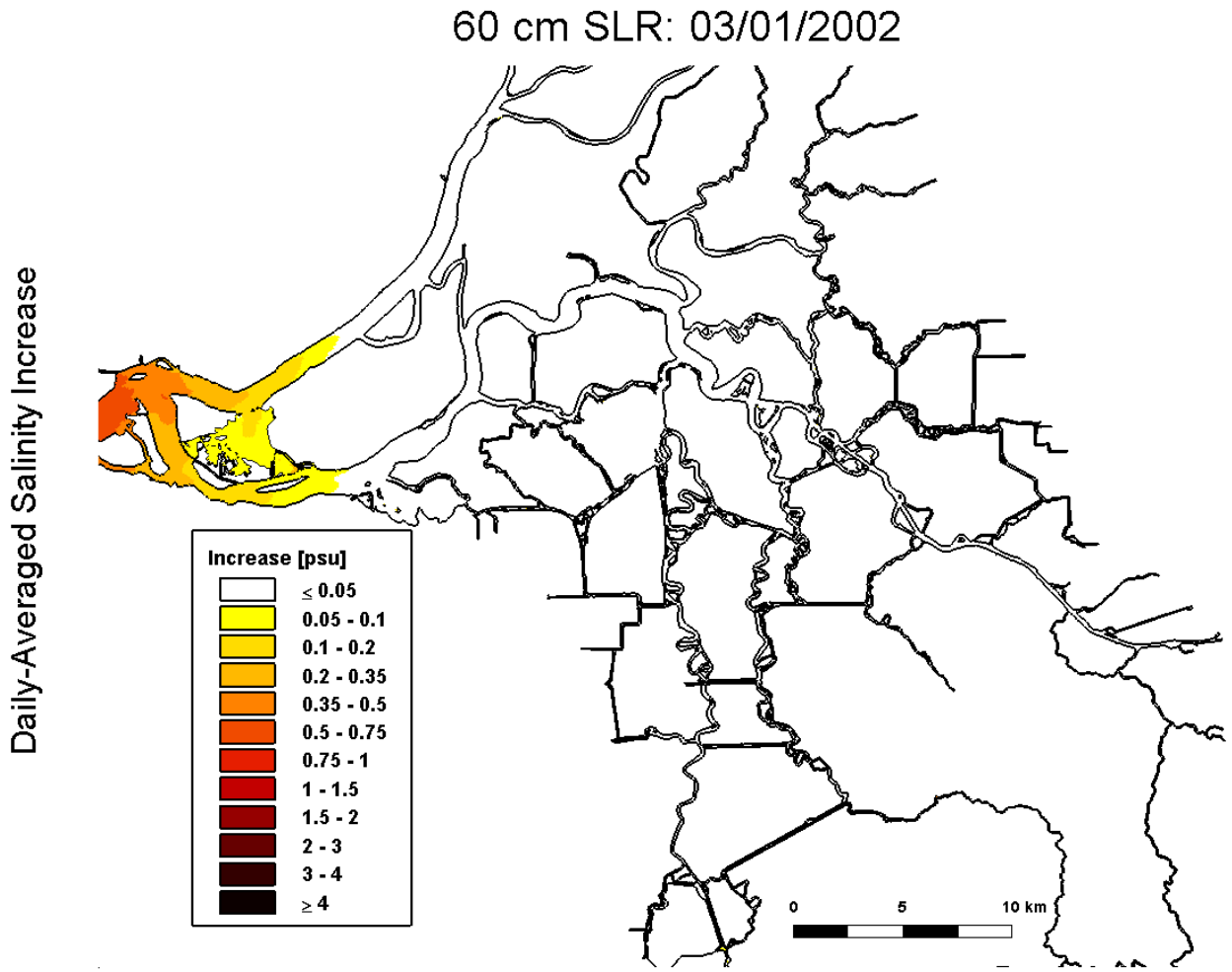

Figure 4.4-16 Predicted increase in daily-averaged depth-average salinity in the Sacramento-San Joaquin Delta on March 1, 2002 relative to the Baseline (0 cm SLR) scenario for the 60 cm SLR scenario.

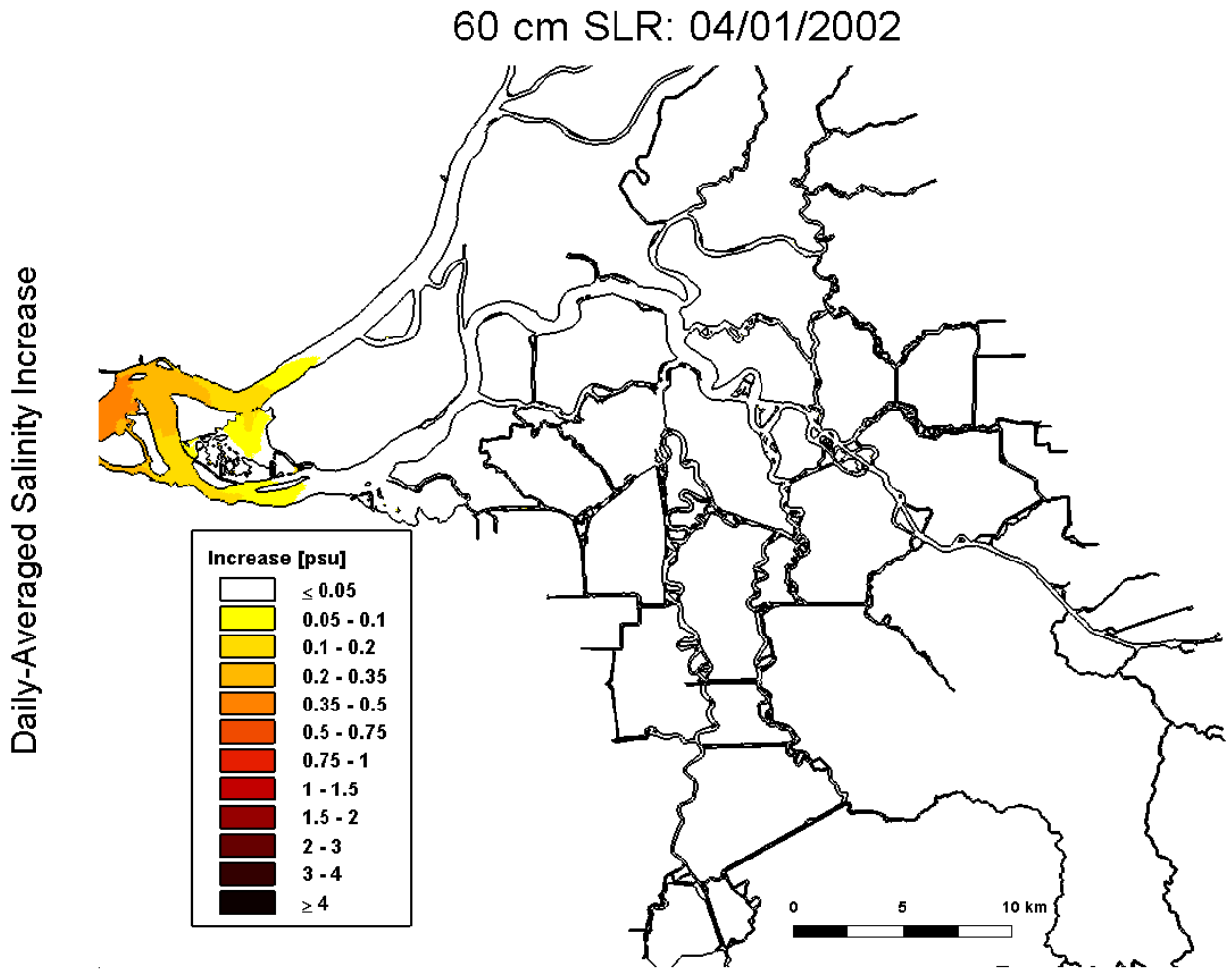

Figure 4.4-17 Predicted increase in daily-averaged depth-average salinity in the Sacramento-San Joaquin Delta on April 1, 2002 relative to the Baseline (0 cm SLR) scenario for the 60 cm SLR scenario.

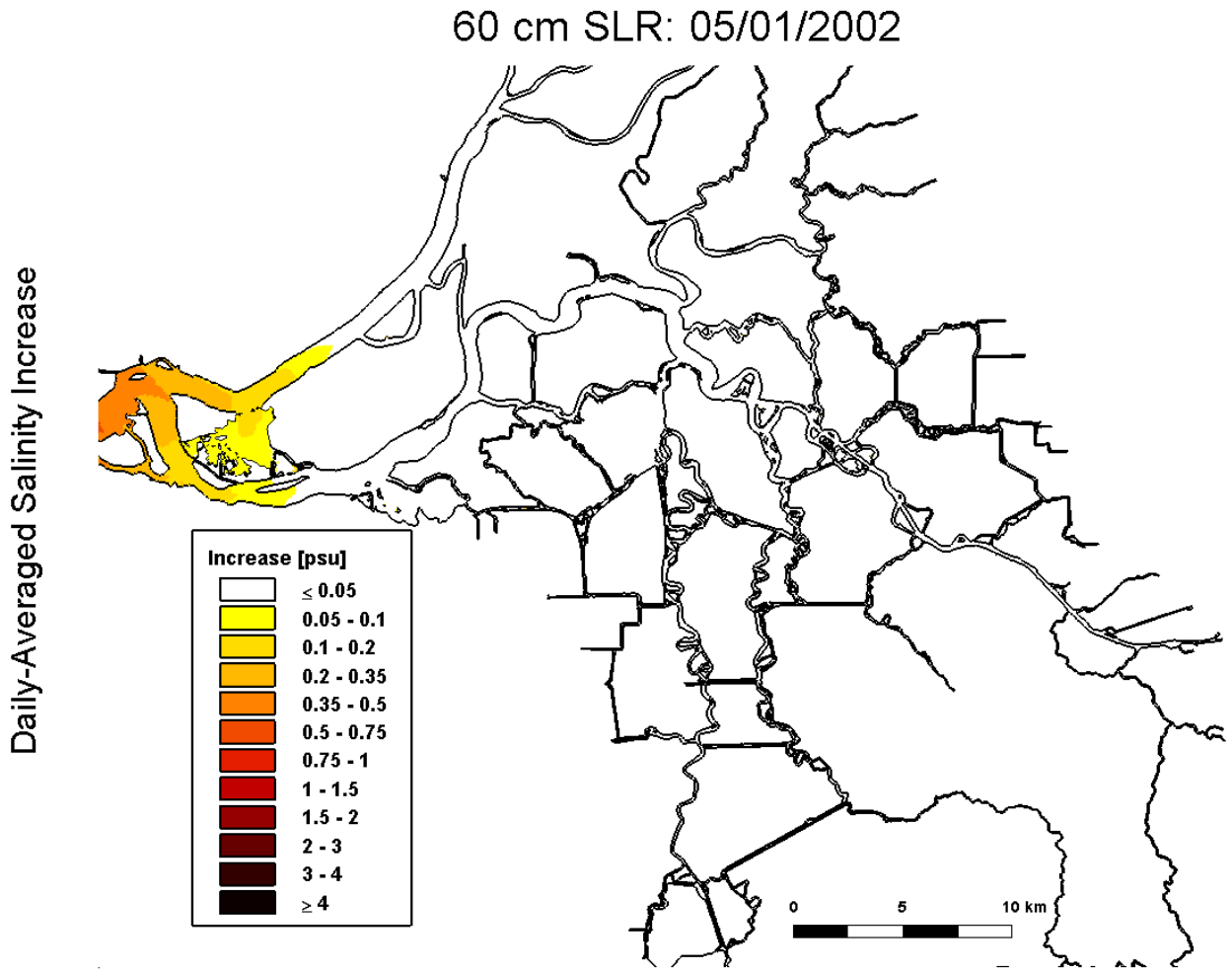

Figure 4.4-18 Predicted increase in daily-averaged depth-average salinity in the Sacramento-San Joaquin Delta on May 1, 2002 relative to the Baseline (0 cm SLR) scenario for the 60 cm SLR scenario.

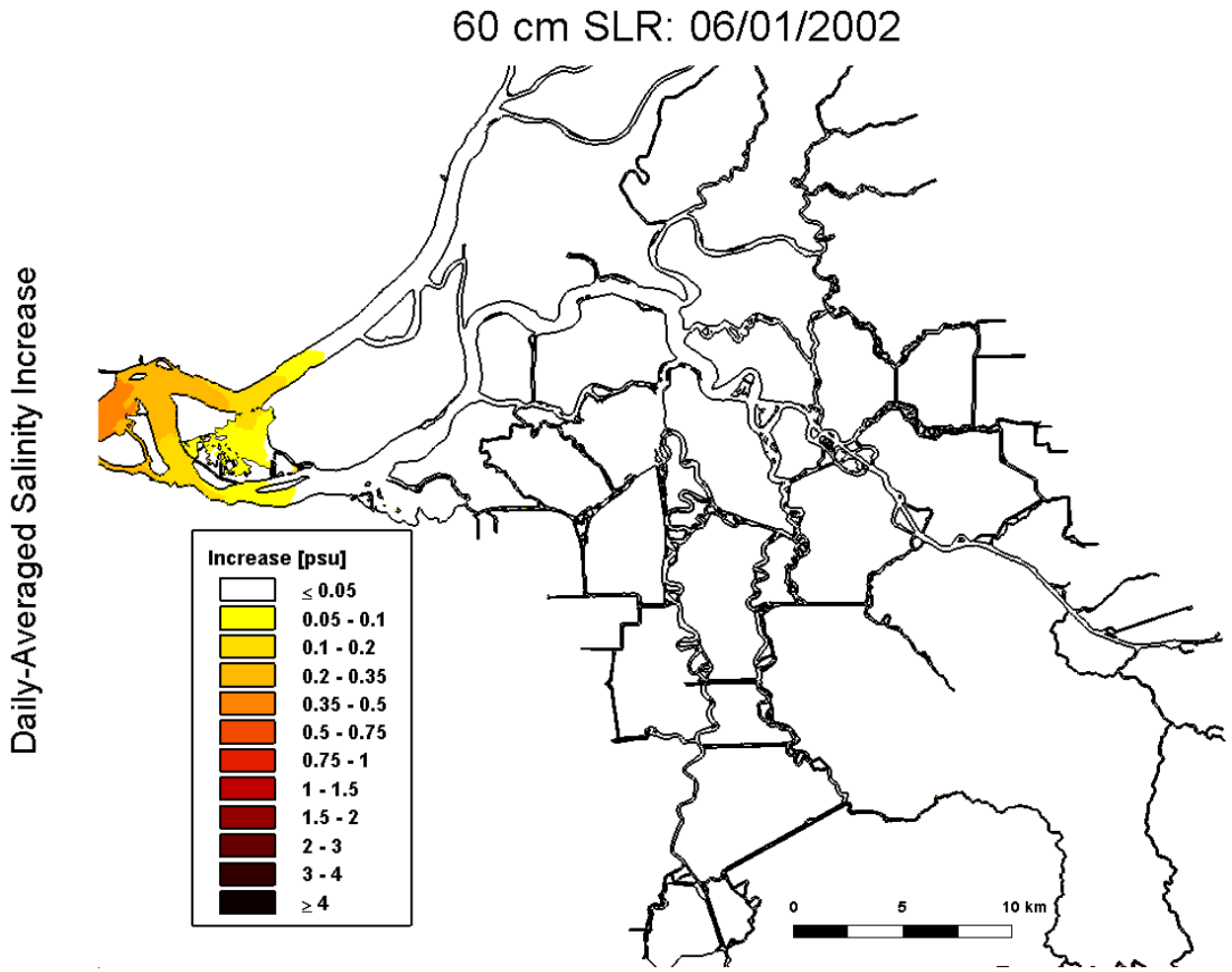

Figure 4.4-19 Predicted increase in daily-averaged depth-average salinity in the Sacramento-San Joaquin Delta on June 1, 2002 relative to the Baseline (0 cm SLR) scenario for the 60 cm SLR scenario.

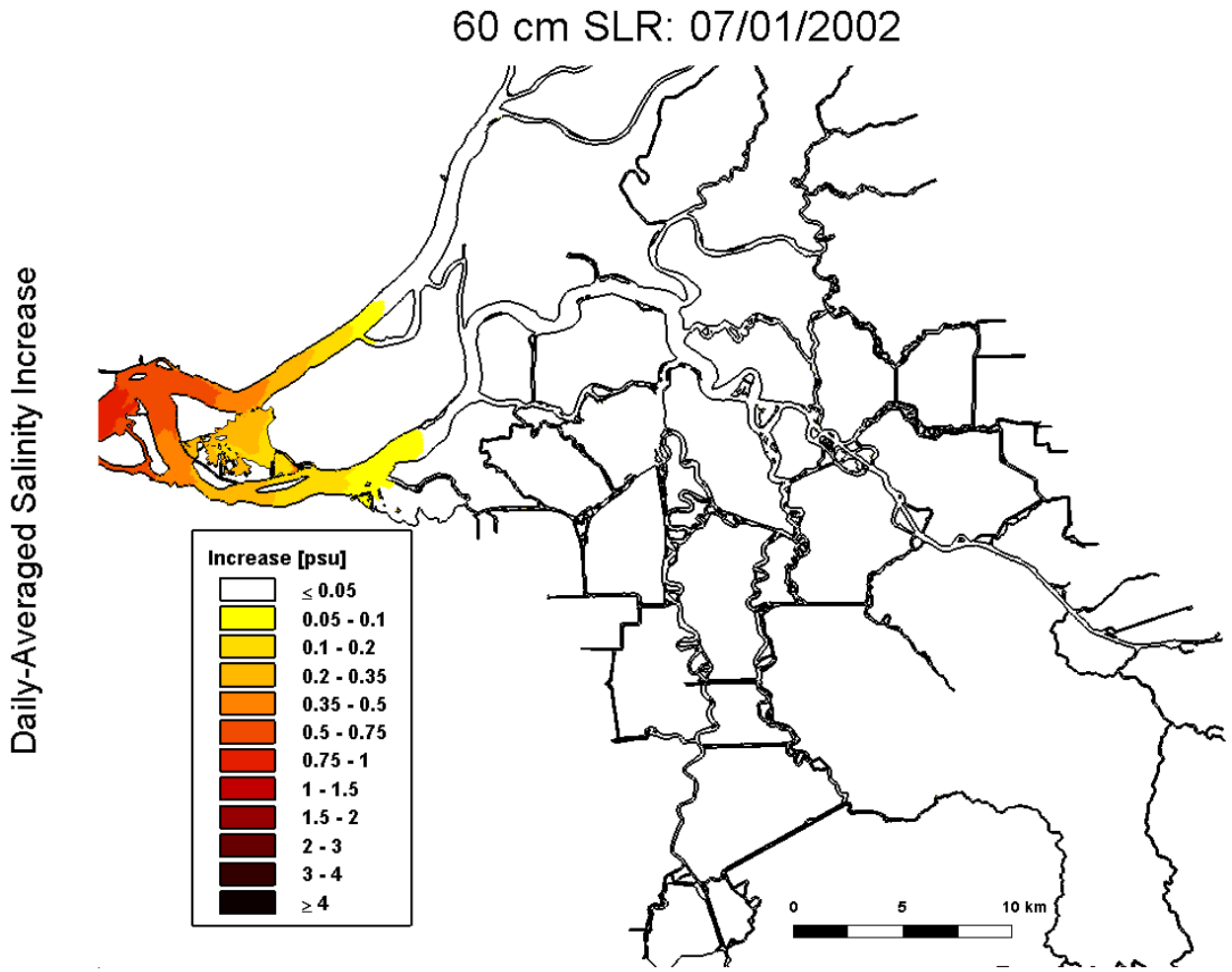

Figure 4.4-20 Predicted increase in daily-averaged depth-average salinity in the Sacramento-San Joaquin Delta on July 1, 2002 relative to the Baseline (0 cm SLR) scenario for the 60 cm SLR scenario.

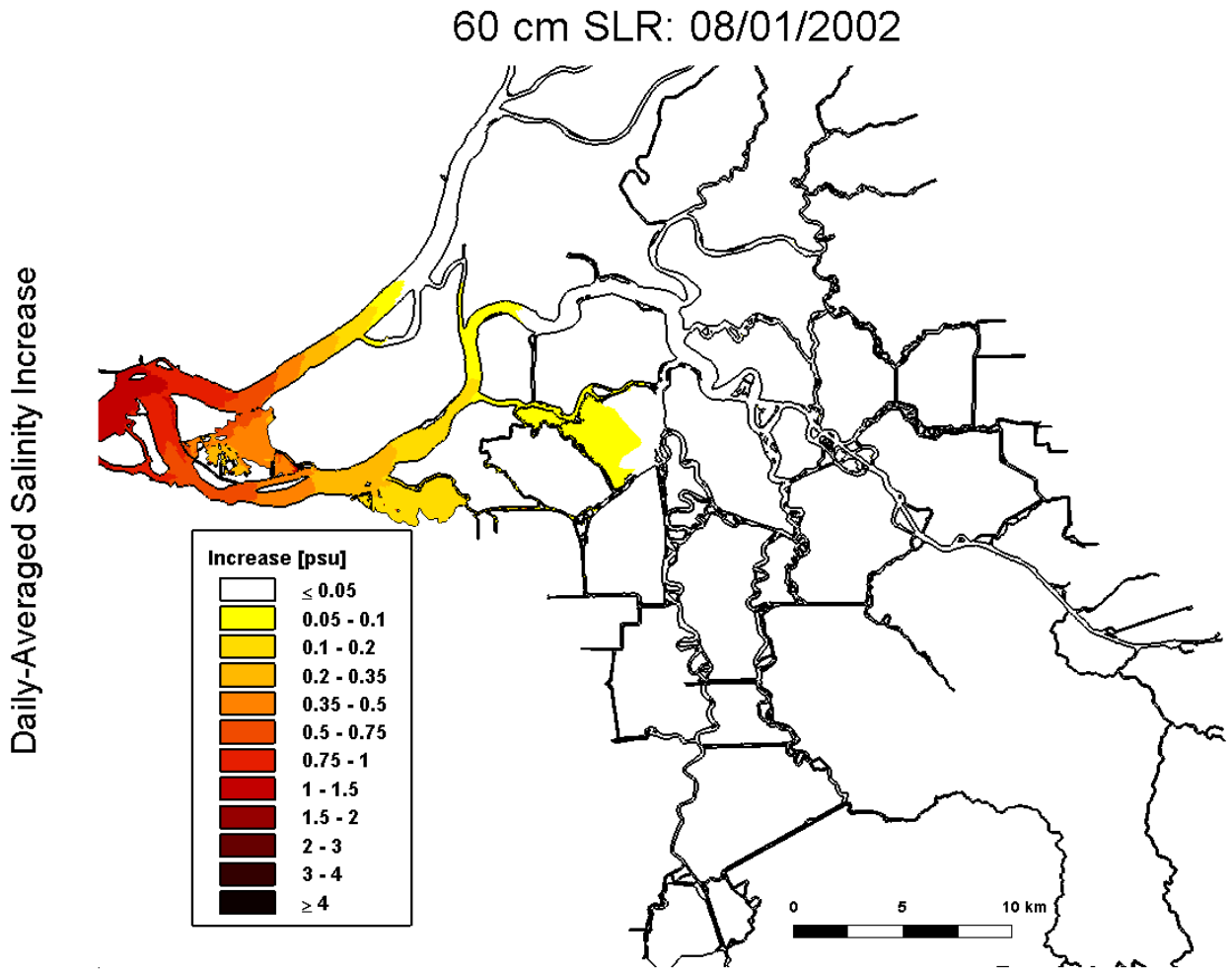

Figure 4.4-21 Predicted increase in daily-averaged depth-average salinity in the Sacramento-San Joaquin Delta on August 1, 2002 relative to the Baseline (0 cm SLR) scenario for the 60 cm SLR scenario.

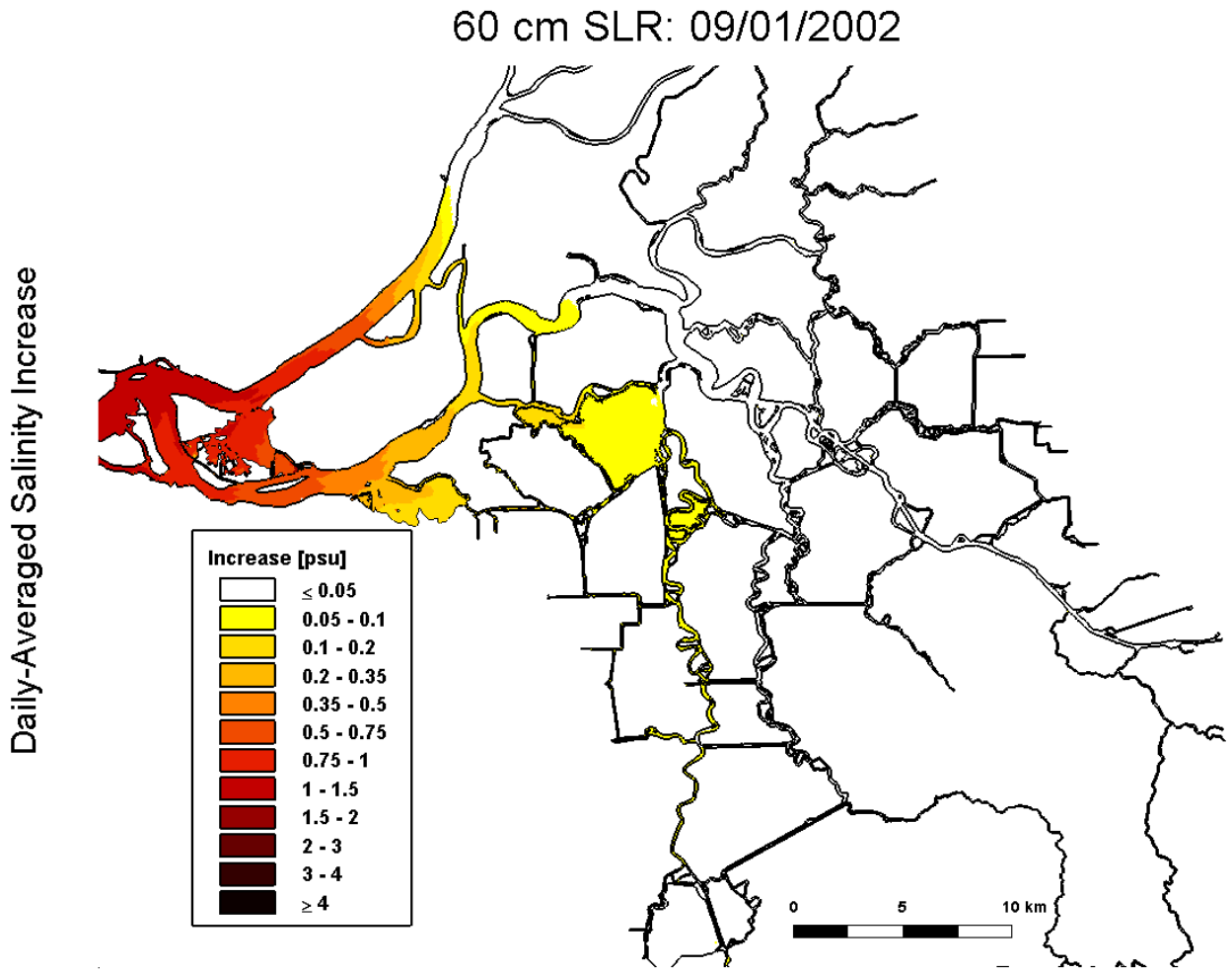

Figure 4.4-22 Predicted increase in daily-averaged depth-average salinity in the Sacramento-San Joaquin Delta on September 1, 2002 relative to the Baseline (0 cm SLR) scenario for the 60 cm SLR scenario.

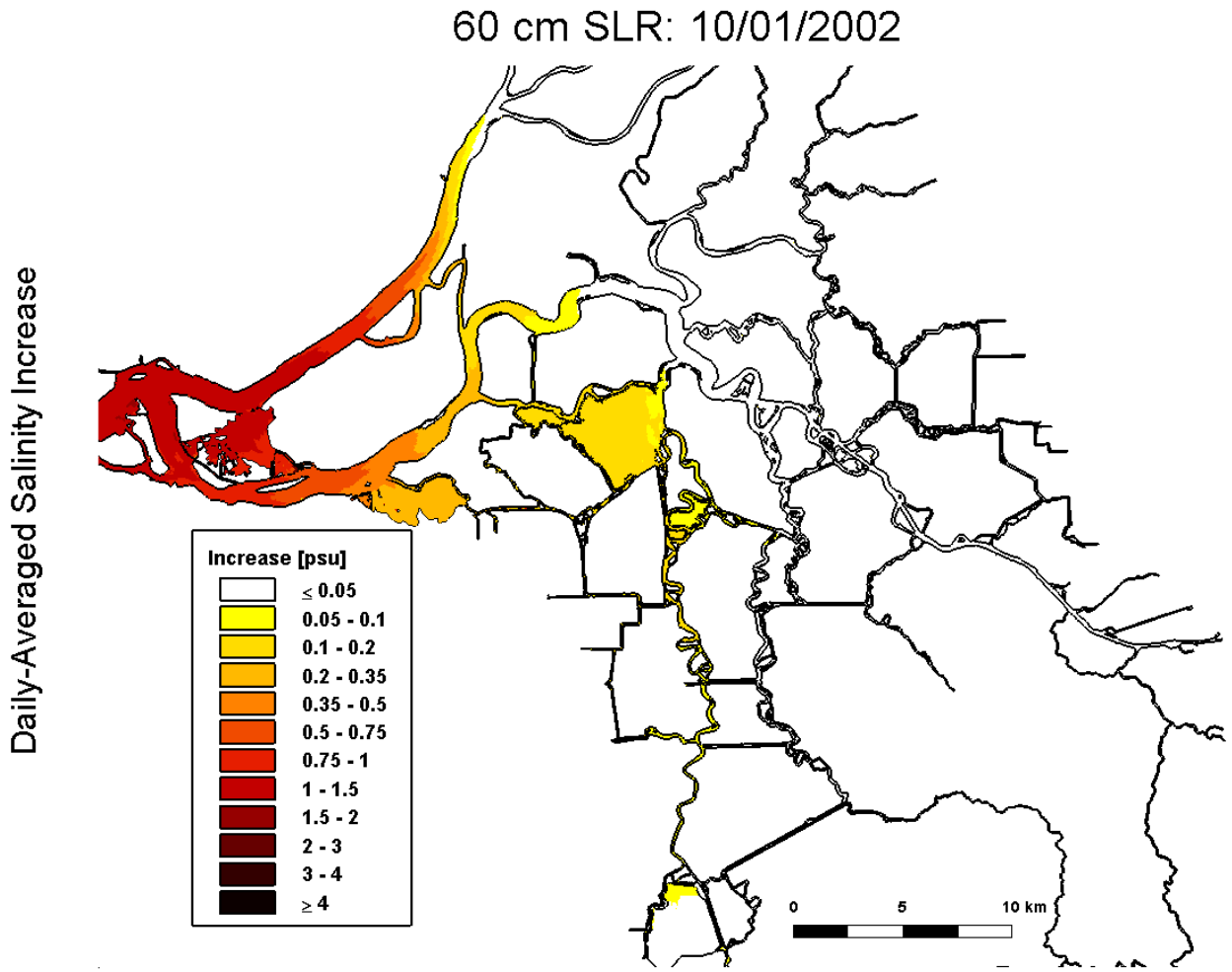

Figure 4.4-23 Predicted increase in daily-averaged depth-average salinity in the Sacramento-San Joaquin Delta on October 1, 2002 relative to the Baseline (0 cm SLR) scenario for the 60 cm SLR scenario.

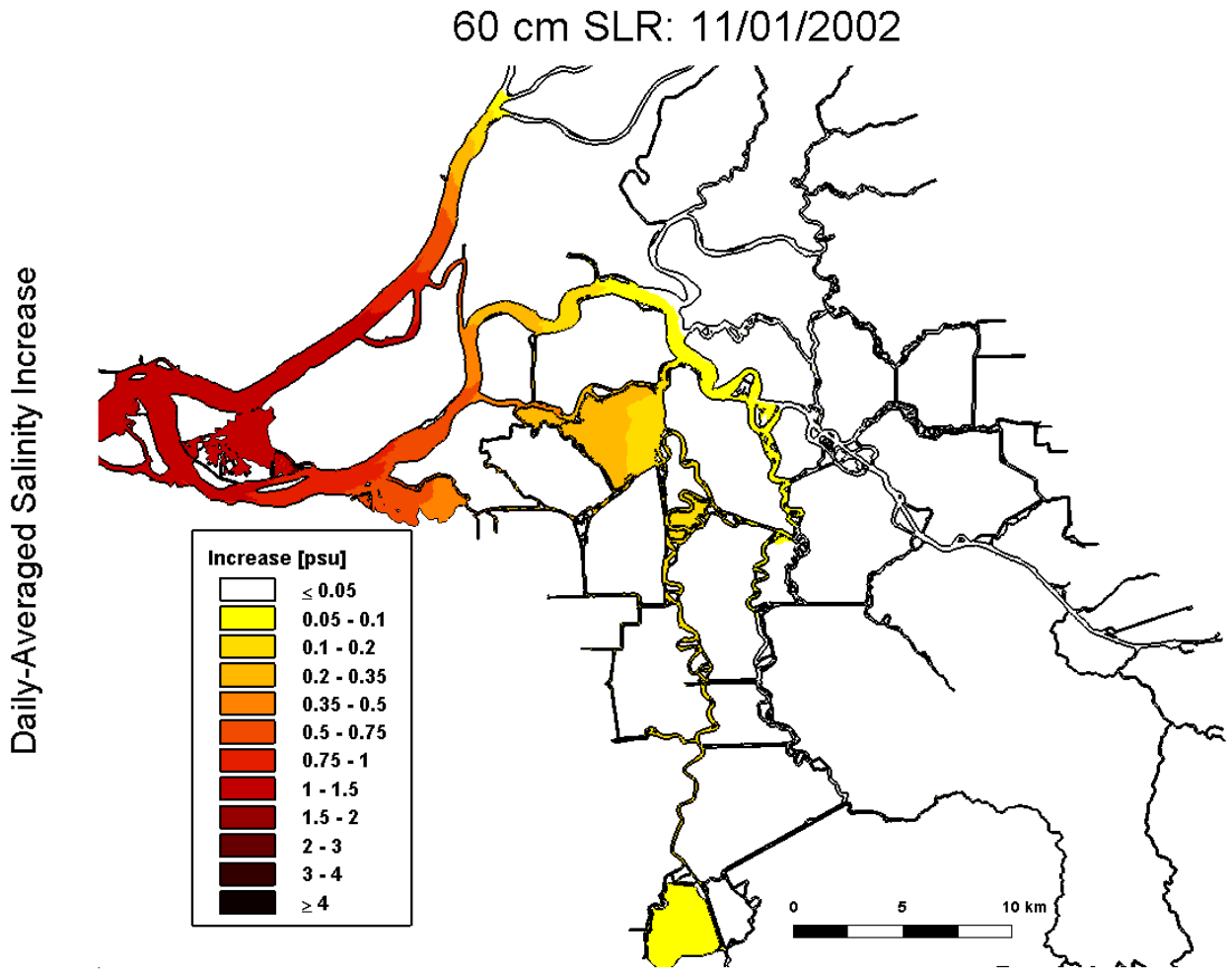

Figure 4.4-24 Predicted increase in daily-averaged depth-average salinity in the Sacramento-San Joaquin Delta on November 1, 2002 relative to the Baseline (0 cm SLR) scenario for the 60 cm SLR scenario.

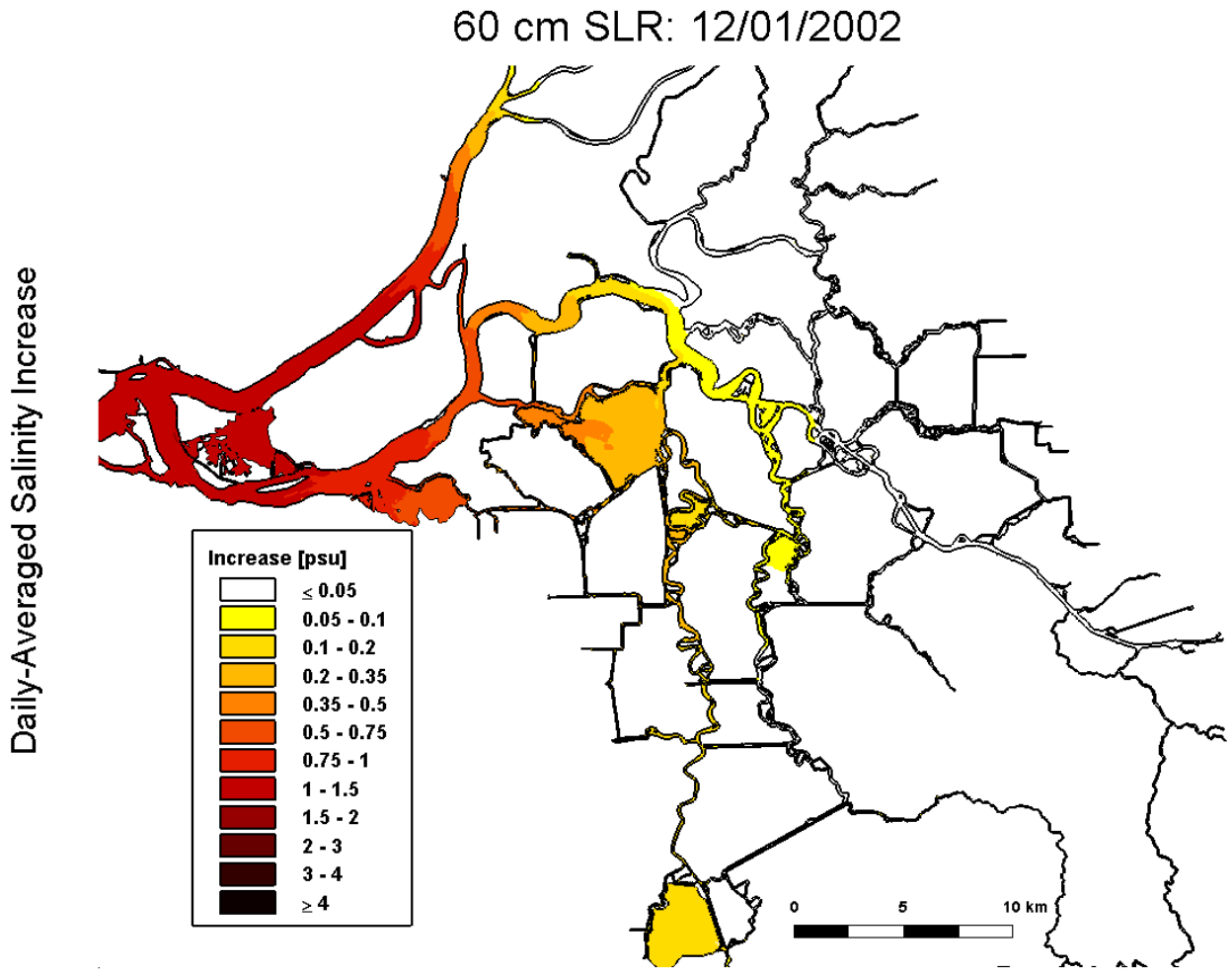

Figure 4.4-25 Predicted increase in daily-averaged depth-average salinity in the Sacramento-San Joaquin Delta on December 1, 2002 relative to the Baseline (0 cm SLR) scenario for the 60 cm SLR scenario.

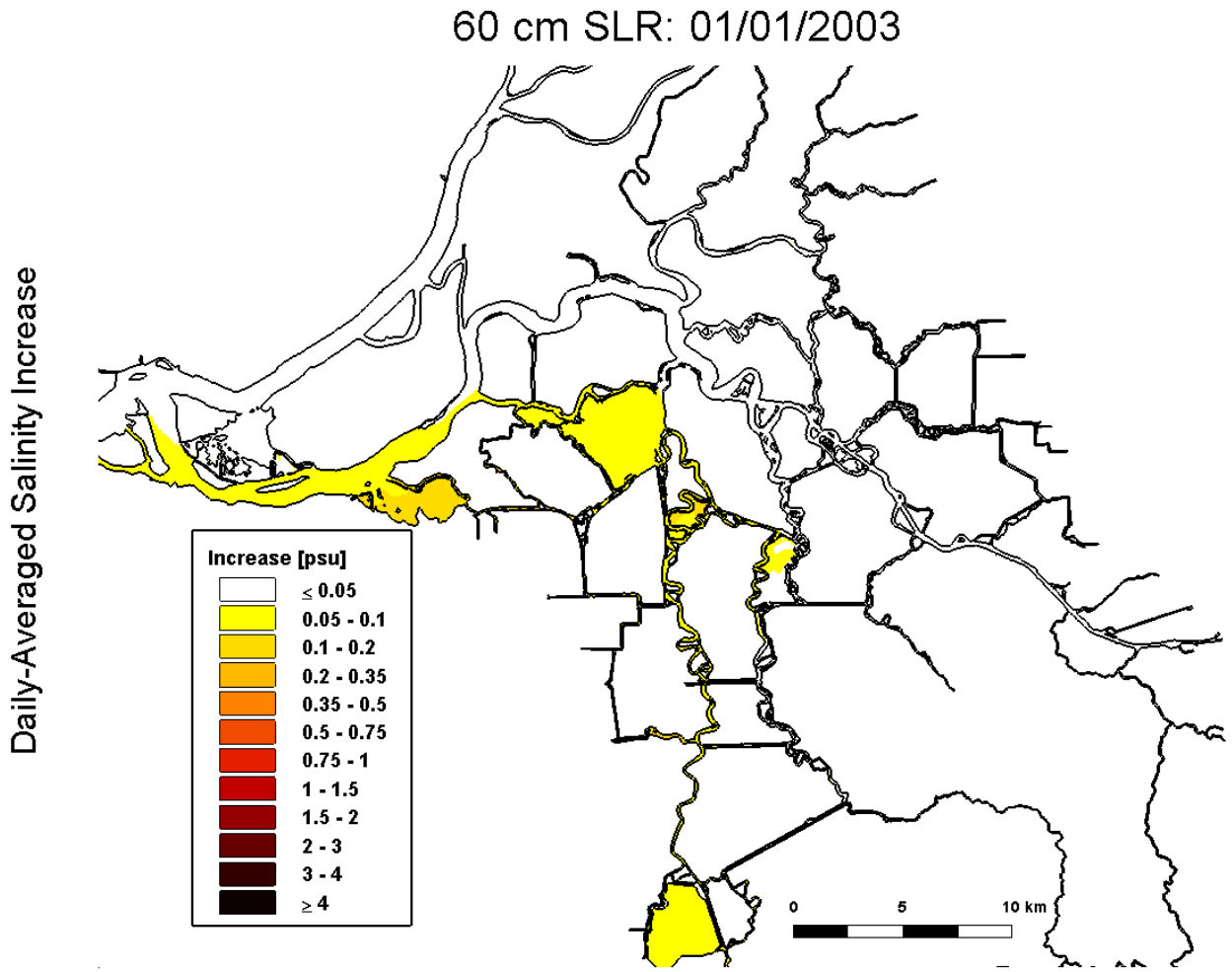

Figure 4.4-26 Predicted increase in daily-averaged depth-average salinity in the Sacramento-San Joaquin Delta on January 1, 2003 relative to the Baseline (0 cm SLR) scenario for the 60 cm SLR scenario.

4.5 Predicted Increase in Salinity for 140 cm SLR Scenario

Figure 4.5-1 through 4.5-13 show the predicted salinity along the northern portion of the San Francisco Estuary, spanning from San Pablo Bay through the Sacramento-San Joaquin Delta for the 140 cm SLR scenario. The top panel of each figure shows the predicted daily-averaged depth-average salinity for the 140 cm SLR scenario. The lower panel shows the predicted salinity increase computed by subtracting the predicted daily-averaged depth-average salinity for the Baseline (0 cm SLR) scenario from the predicted daily-averaged depth-average salinity for the 140 cm SLR scenario. Figures 4.5-14 through 4.5-26 show the predicted salinity increases resulting from the 140 cm SLR scenario in the Sacramento-San Joaquin Delta.

At the beginning of the analysis period on January 1, 2002, significant salinity increases are evident in the Delta, indicating that the salinity increases from the previous fall period have not been fully flushed out. Salinity increases between 1. 0 and 1.50 psu are predicted between Chipps Island and Collinsville and predicted salinity increases of up to 0.05 psu are predicted upstream to Emmaton on the Sacramento River. Along the San Joaquin River predicted salinity increases of 0.1 and 0.2 psu extend from Big Break to False River and predicted salinity increases of between 0.05 psu and 1.0 psu extend upstream to Sevenmile Slough. Salinity increases of between 0.05 and 0.10 psu are predicted in Franks Tract. South of Franks Tract, predicted salinity increases between 0.10 and 0.20 psu extend down Old River to Clifton Court Forebay, and salinity increases of between 0.10 and 0.20 psu are predicted inside Clifton Court Forebay. Predicted salinity increases are less than 0.05 psu throughout the remaining portions of the Delta. Salinity increases between 3.0 and 4.0 psu are predicted through Carquinez Strait and salinity increases between 1.5 and 3.0 psu are predicted throughout Suisun Bay. Larger salinity increases of more than 2.0 psu are predicted in much of San Pablo Bay, with salinity increases of more than 4.0 psu predicted in northern San Pablo Bay. By February 1, 2002 much of the salinity increases have been flushed out of the Delta following the high flows in January. During the first half of the year, predicted salinity increases in Suisun Bay and the Delta remain similar to the predicted salinity increases seen on February 1, 2002, while predicted salinity increases in San Pablo Bay decrease, though the predicted salinity is increasing throughout this period. Larger salinity increases are predicted in the Delta between July and December, with the largest predicted salinity increases in December prior to the first flush. In December, salinity increases of between 1.50 and 3.0 psu are predicted between Chipps Island and Emmaton, and salinity increases of between 0.75 and 1.5 psu are predicted in Franks Tract. South of Franks Tract, predicted salinity increases between 0.50 and 1.0 psu extend down Old River to Clifton Court Forebay, and salinity increases of between 0.35 and 0.50 psu are predicted inside Clifton Court Forebay. Predicted salinity increases extend up the San Joaquin River as far as Turner Cut. These simulations assumed no operational response to sea level rise, however it is expected significant operational response will be required to maintain water quality standards for 140 cm of sea level rise. Following high flows which occurred in December, predicted salinity on January 1, 2003 shows that the 0.50 psu isohaline is in central Suisun Bay near Port Chicago, which is much further east than in the Baseline scenario. On January 1, 2003 (Figure 4.5-26) salinity increases are predicted throughout much of the Delta indicating that the high flows in December were not sufficient to push all of the salt out of the Delta for the 140 cm SLR scenario. Similar incomplete flushing of salt from the Delta for the 140 cm SLR scenario was observed on January 1, 2002 (Figure 4.5-14).

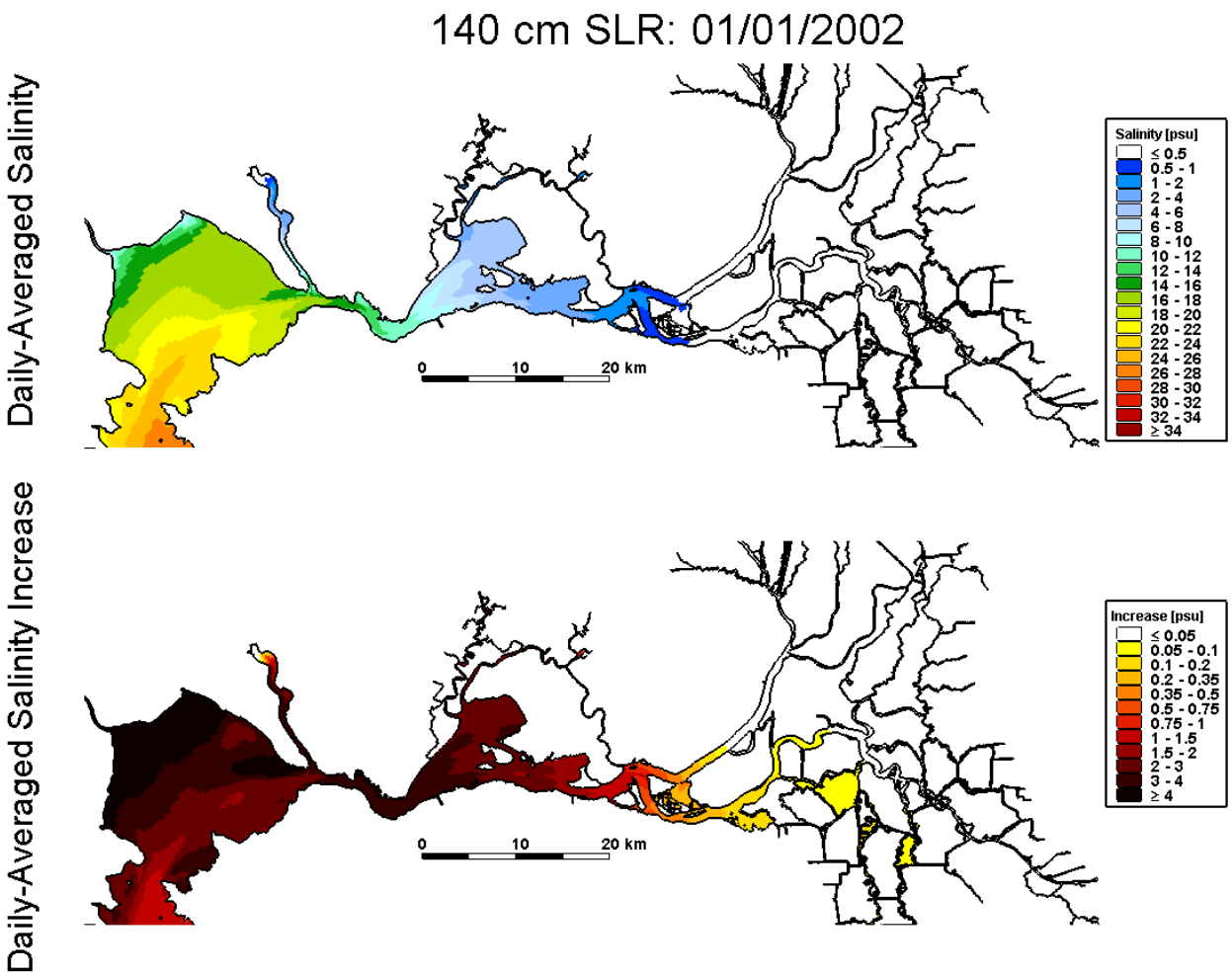

Figure 4.5-1 Predicted daily-averaged depth-average salinity on January 1, 2002 for the 140 cm SLR scenario (top); predicted increase in daily-averaged depth-average salinity on January 1, 2002 relative to the Baseline (0 cm SLR) scenario for the 140 cm SLR scenario.

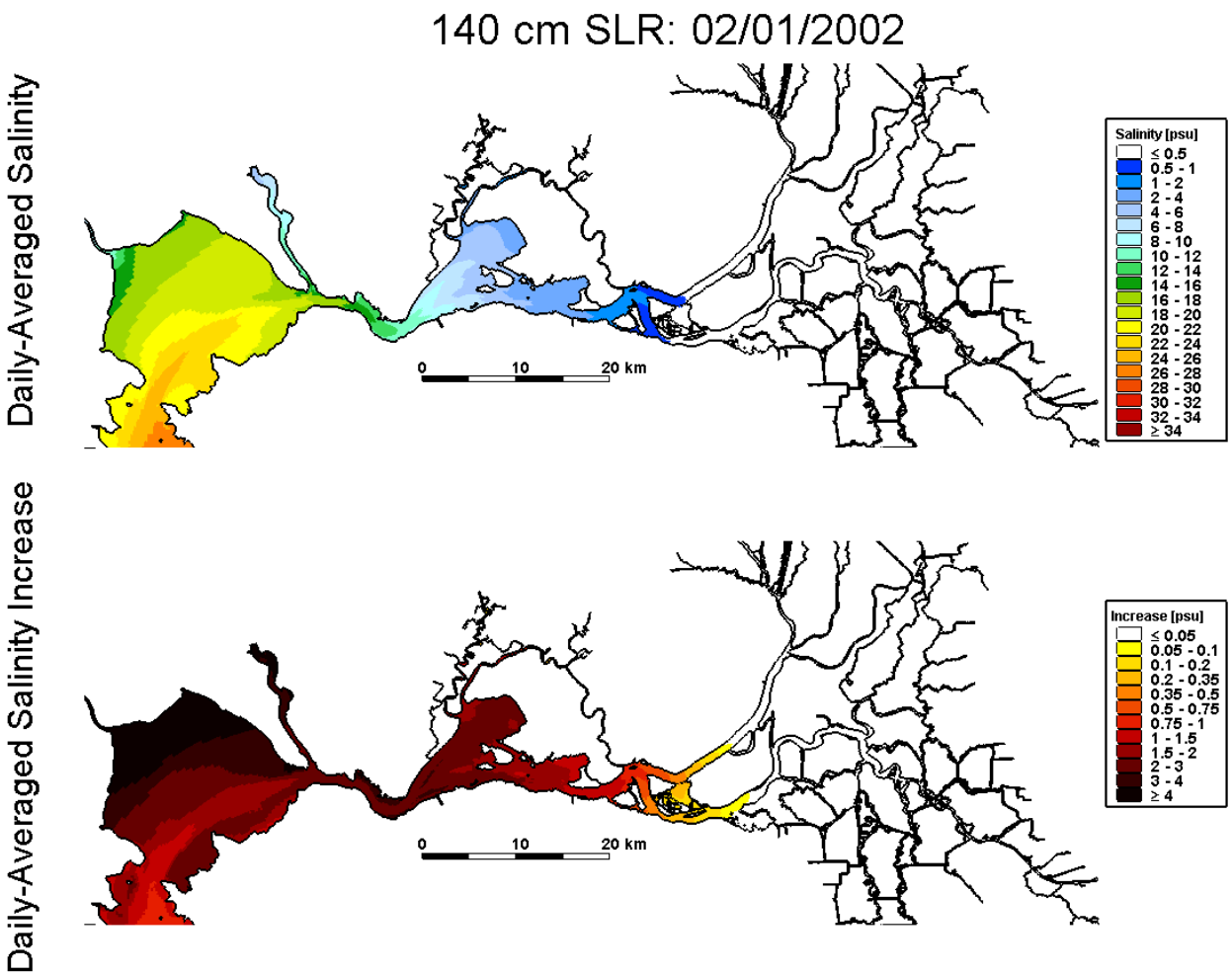

Figure 4.5-2 Predicted daily-averaged depth-average salinity on February 1, 2002 for the 140 cm SLR scenario (top); predicted increase in daily-averaged depth-average salinity on February 1, 2002 relative to the Baseline (0 cm SLR) scenario for the 140 cm SLR scenario.

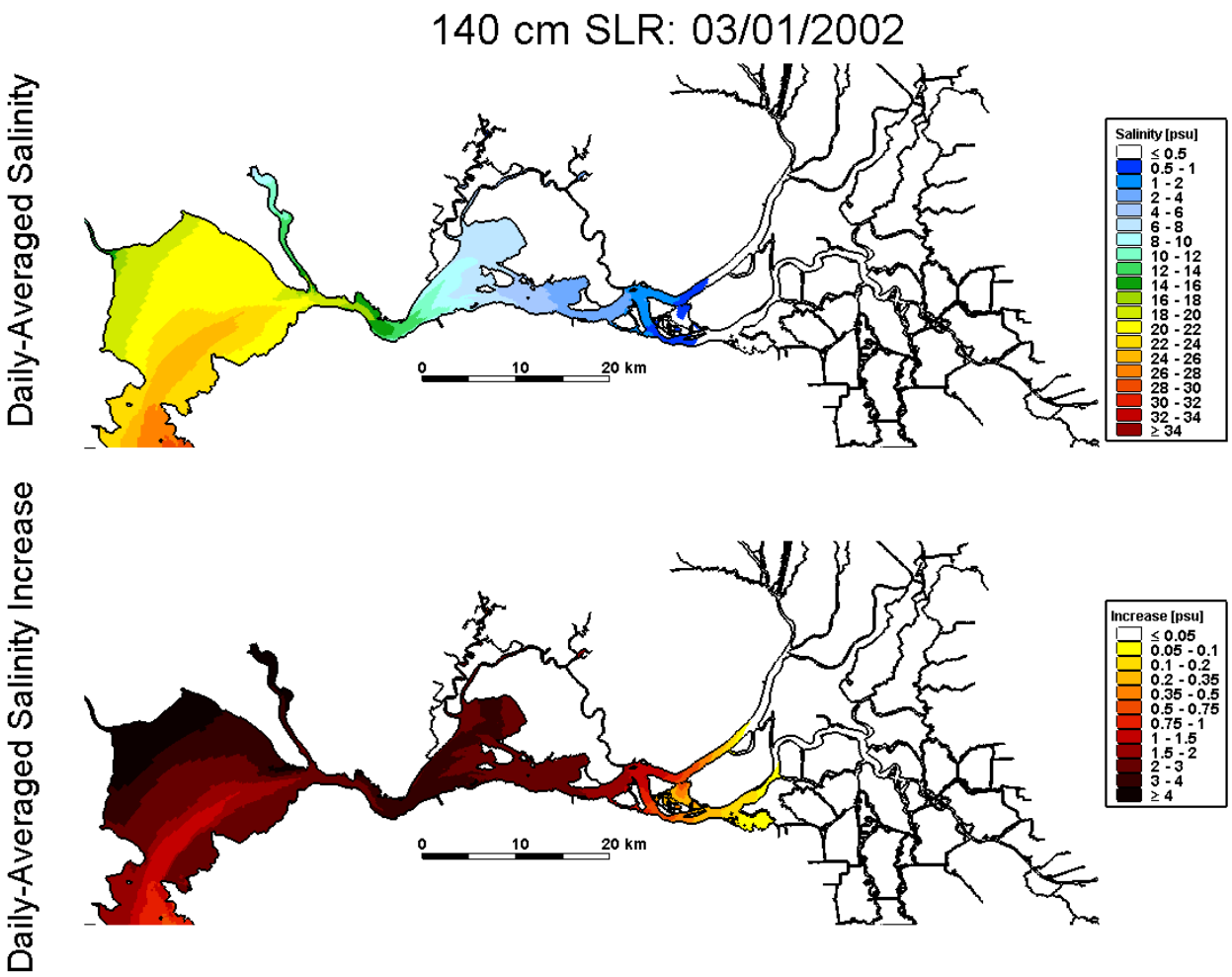

Figure 4.5-3 Predicted daily-averaged depth-average salinity on March 1, 2002 for the 140 cm SLR scenario (top); predicted increase in daily-averaged depth-average salinity on March 1, 2002 relative to the Baseline (0 cm SLR) scenario for the 140 cm SLR scenario.

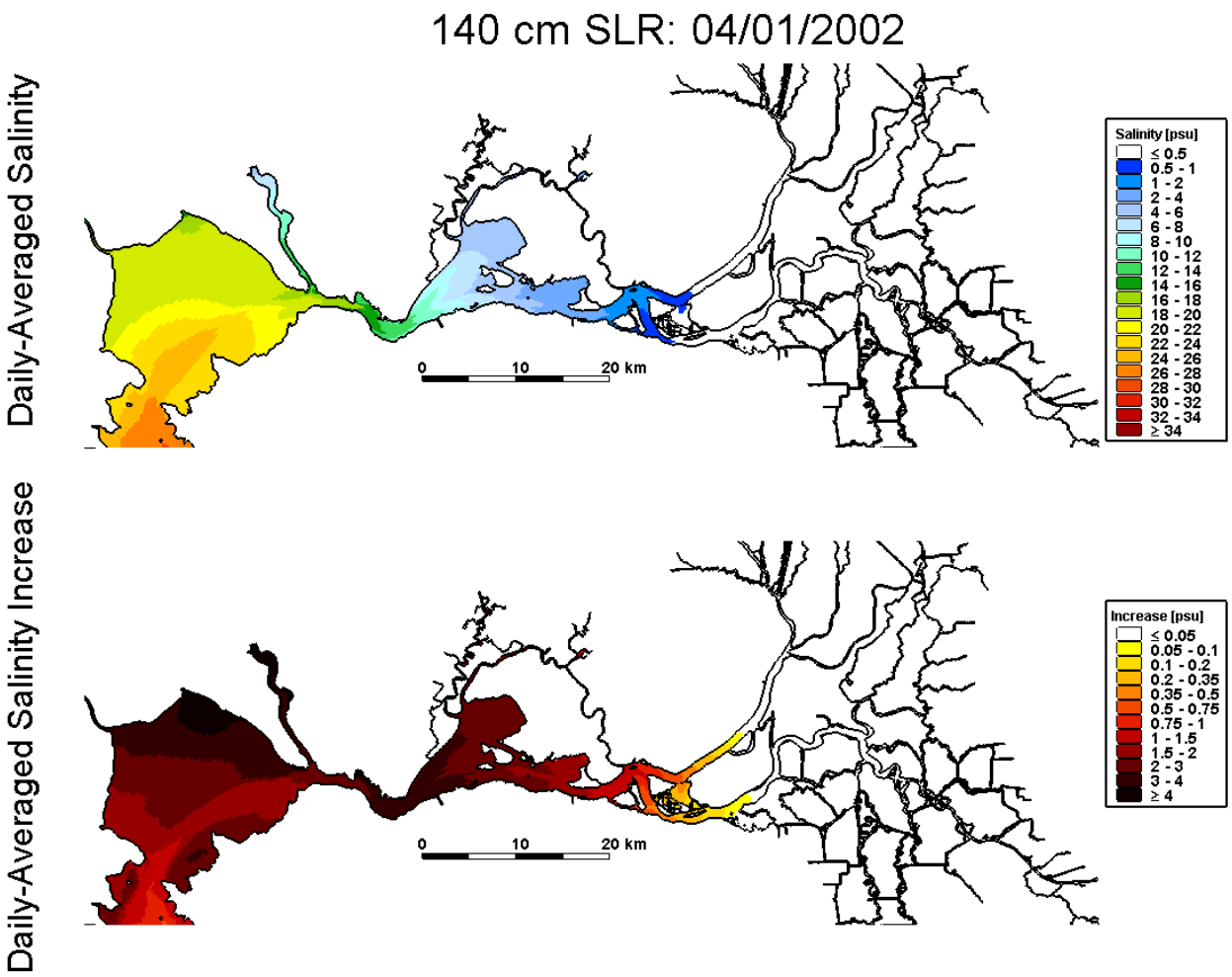

Figure 4.5-4 Predicted daily-averaged depth-average salinity on April 1, 2002 for the 140 cm SLR scenario (top); predicted increase in daily-averaged depth-average salinity on April 1, 2002 relative to the Baseline (0 cm SLR) scenario for the 140 cm SLR scenario.

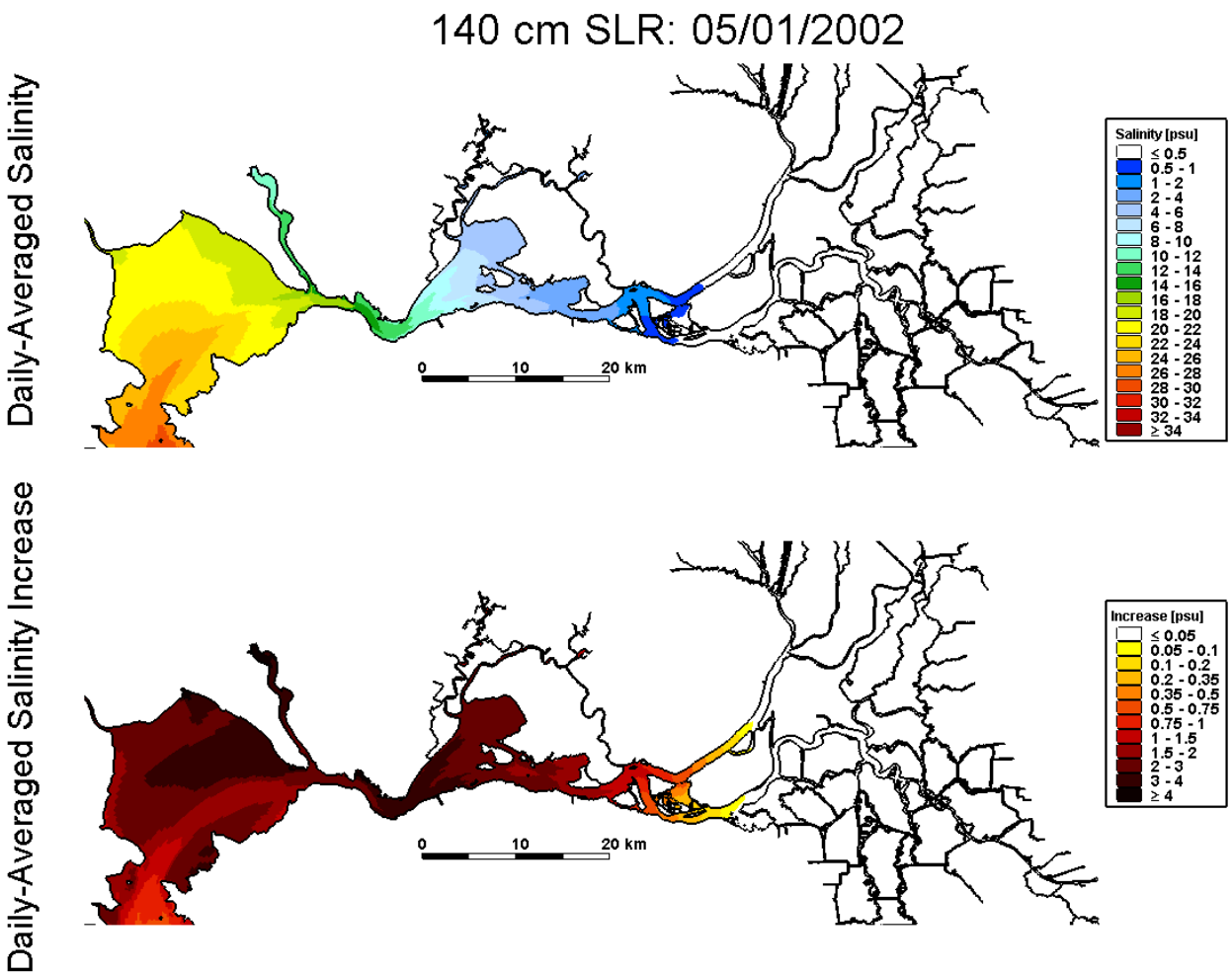

Figure 4.5-5 Predicted daily-averaged depth-average salinity on May 1, 2002 for the 140 cm SLR scenario (top); predicted increase in daily-averaged depth-average salinity on May 1, 2002 relative to the Baseline (0 cm SLR) scenario for the 140 cm SLR scenario.

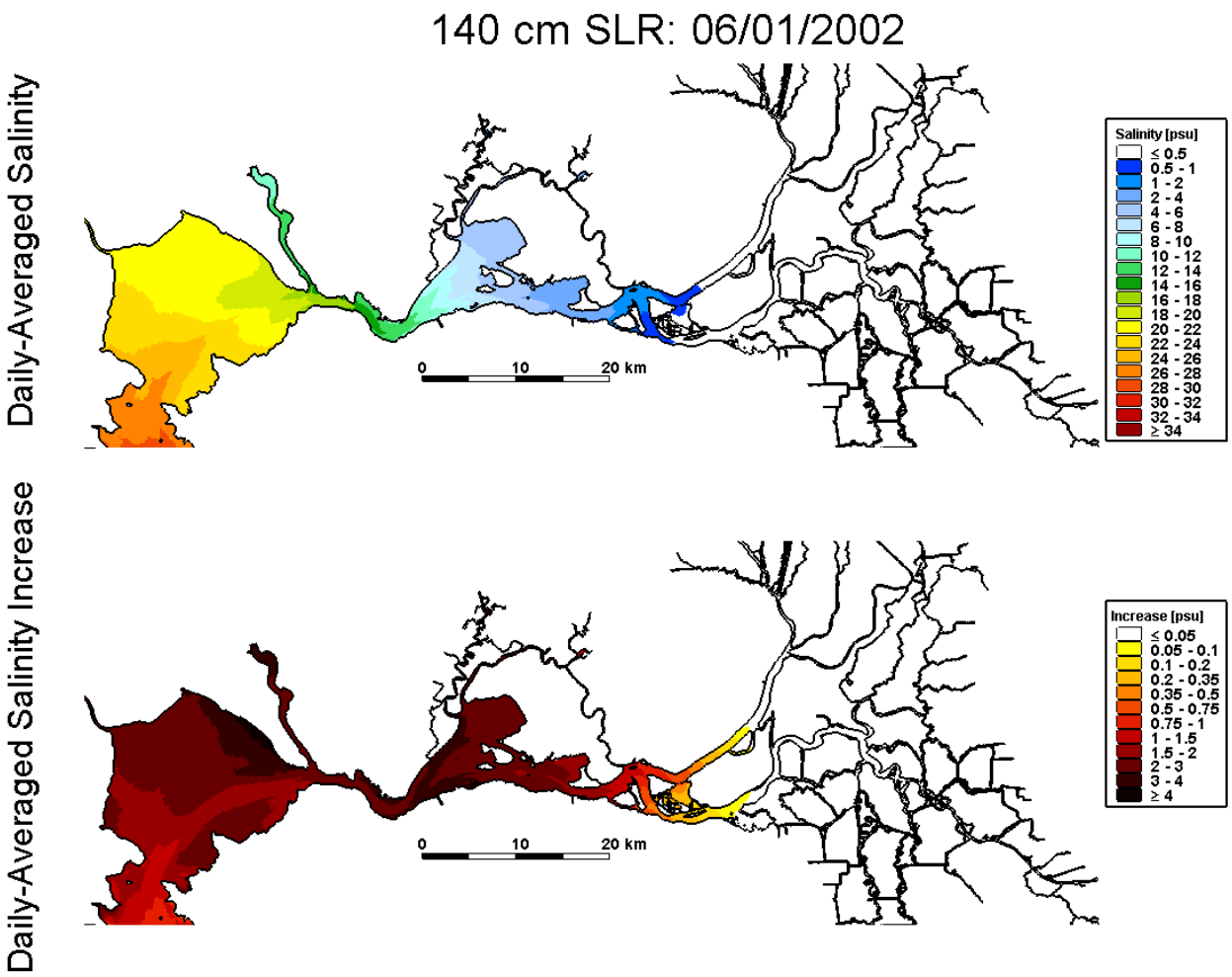

Figure 4.5-6 Predicted daily-averaged depth-average salinity on June 1, 2002 for the 140 cm SLR scenario (top); predicted increase in daily-averaged depth-average salinity on June 1, 2002 relative to the Baseline (0 cm SLR) scenario for the 140 cm SLR scenario.

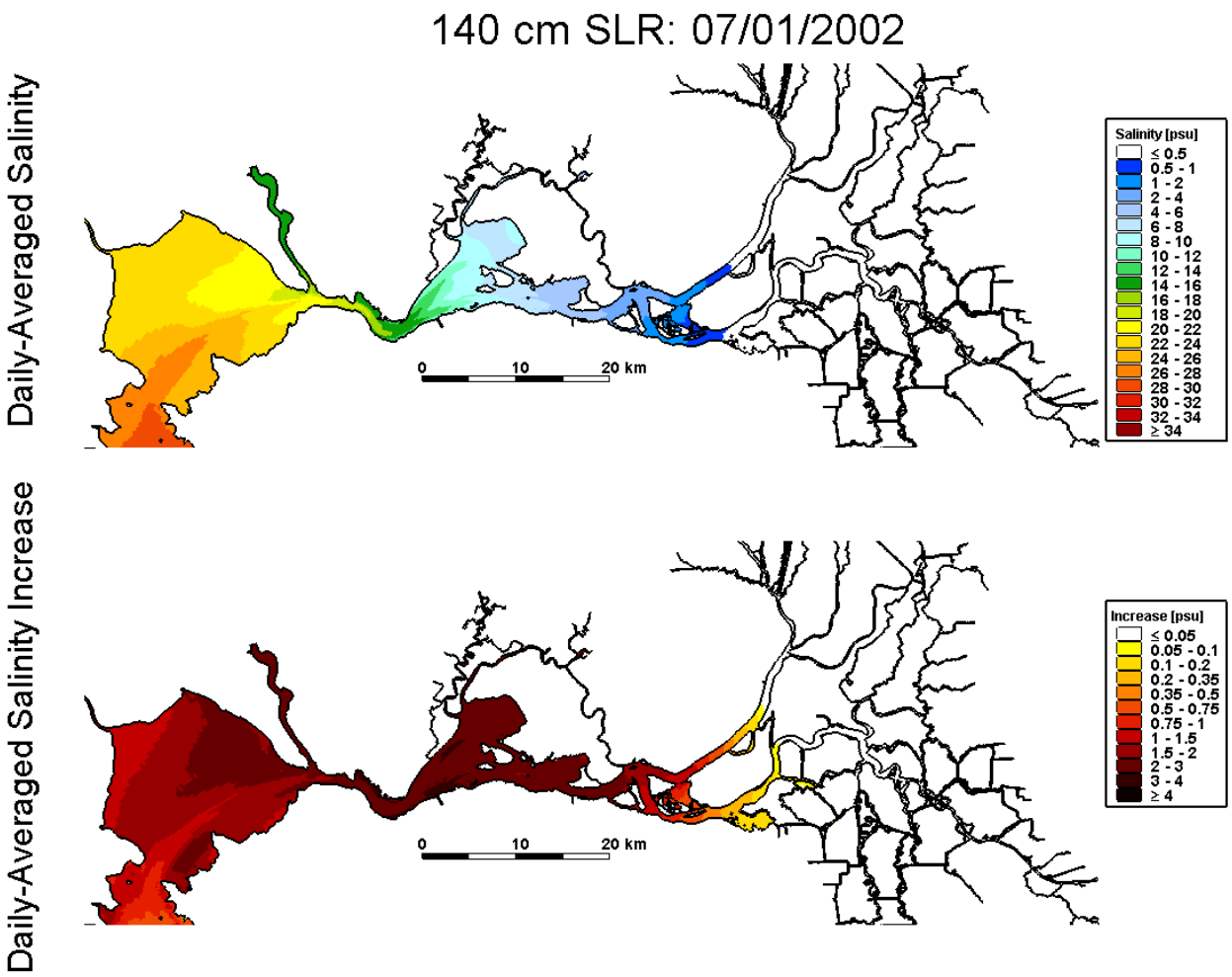

Figure 4.5-7 Predicted daily-averaged depth-average salinity on July 1, 2002 for the 140 cm SLR scenario (top); predicted increase in daily-averaged depth-average salinity on July 1, 2002 relative to the Baseline (0 cm SLR) scenario for the 140 cm SLR scenario.

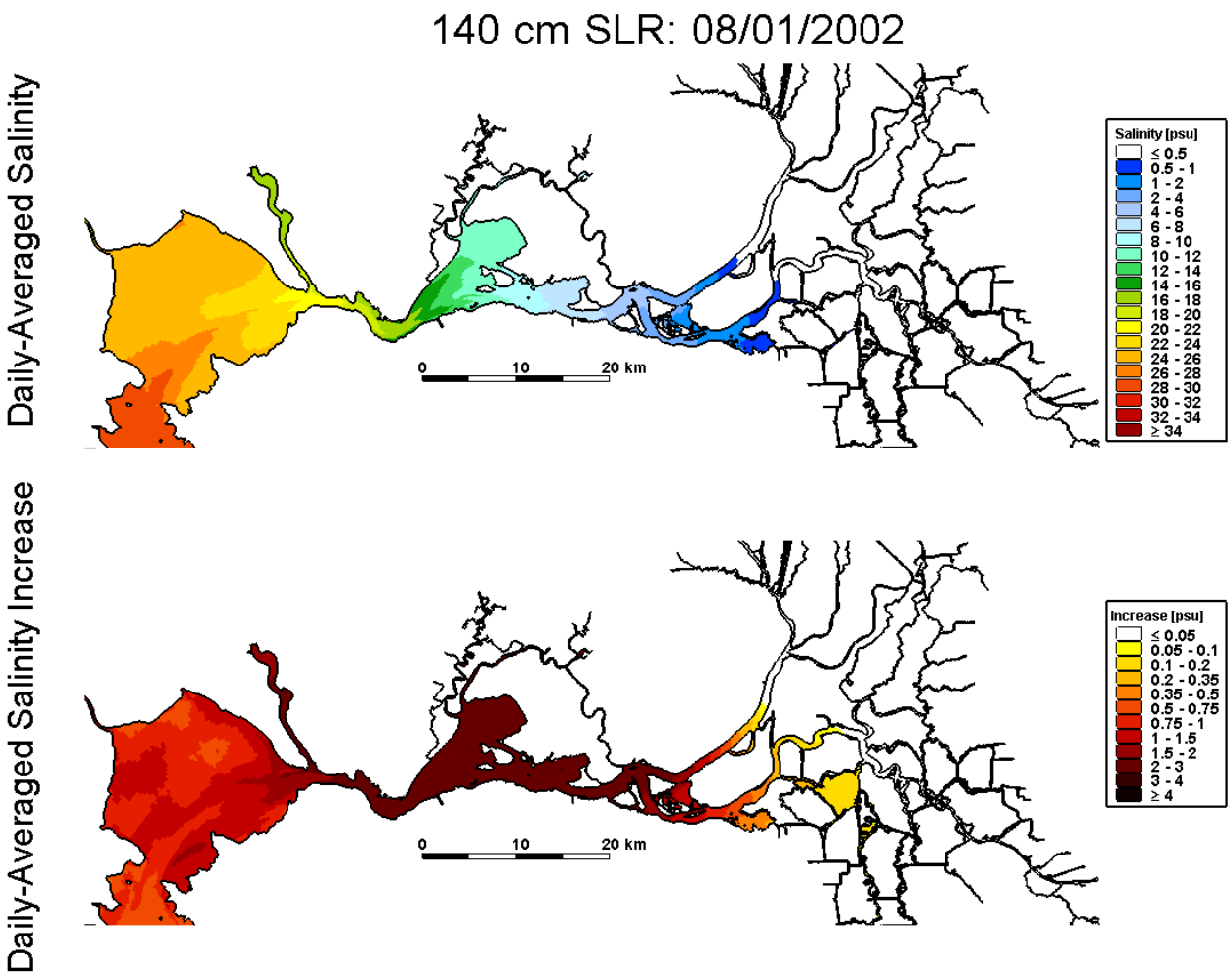

Figure 4.5-8 Predicted daily-averaged depth-average salinity on August 1, 2002 for the 140 cm SLR scenario (top); predicted increase in daily-averaged depth-average salinity on August 1, 2002 relative to the Baseline (0 cm SLR) scenario for the 140 cm SLR scenario.

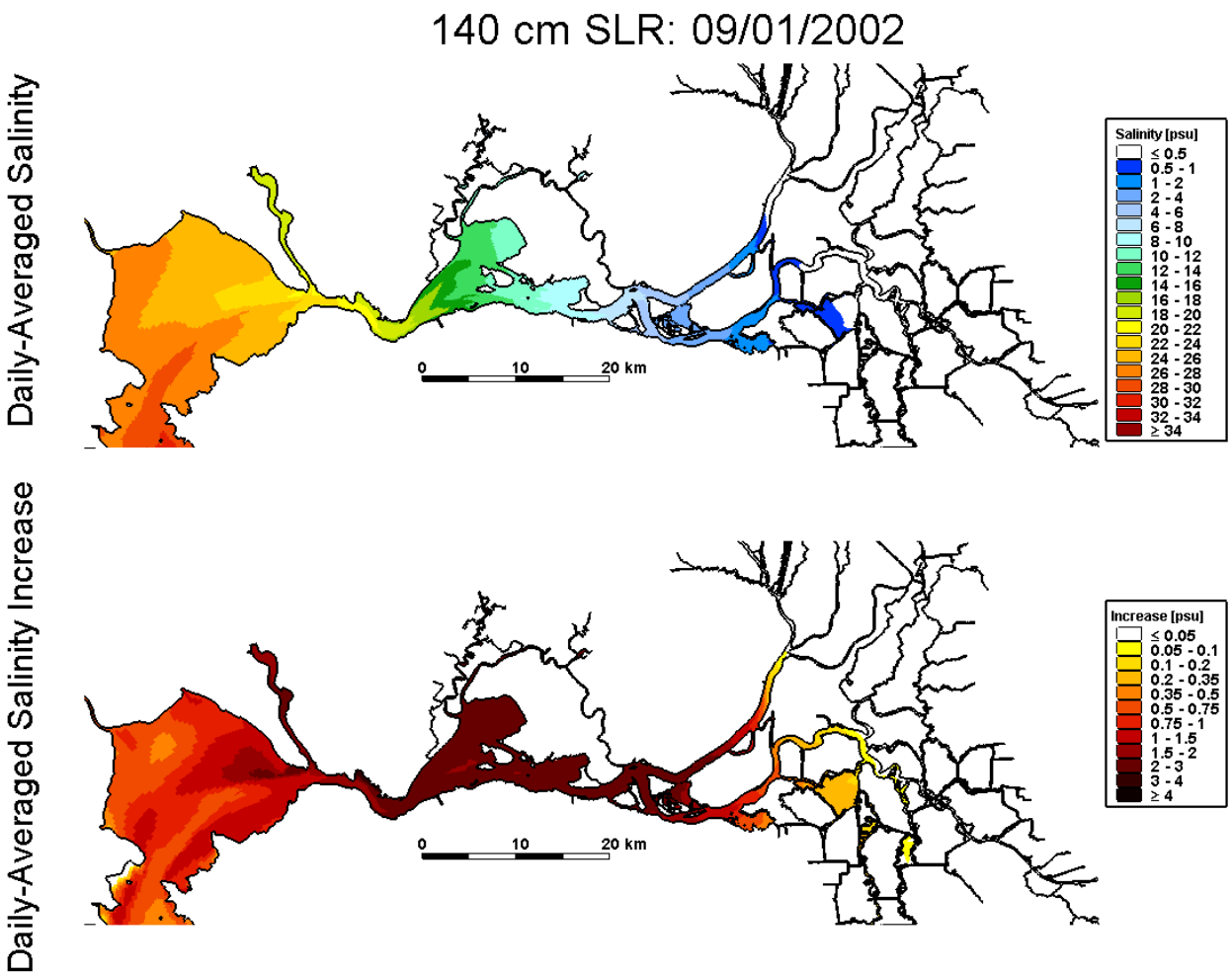

Figure 4.5-9 Predicted daily-averaged depth-average salinity on September 1, 2002 for the 140 cm SLR scenario (top); predicted increase in daily-averaged depth-average salinity on September 1, 2002 relative to the Baseline (0 cm SLR) scenario for the 140 cm SLR scenario.

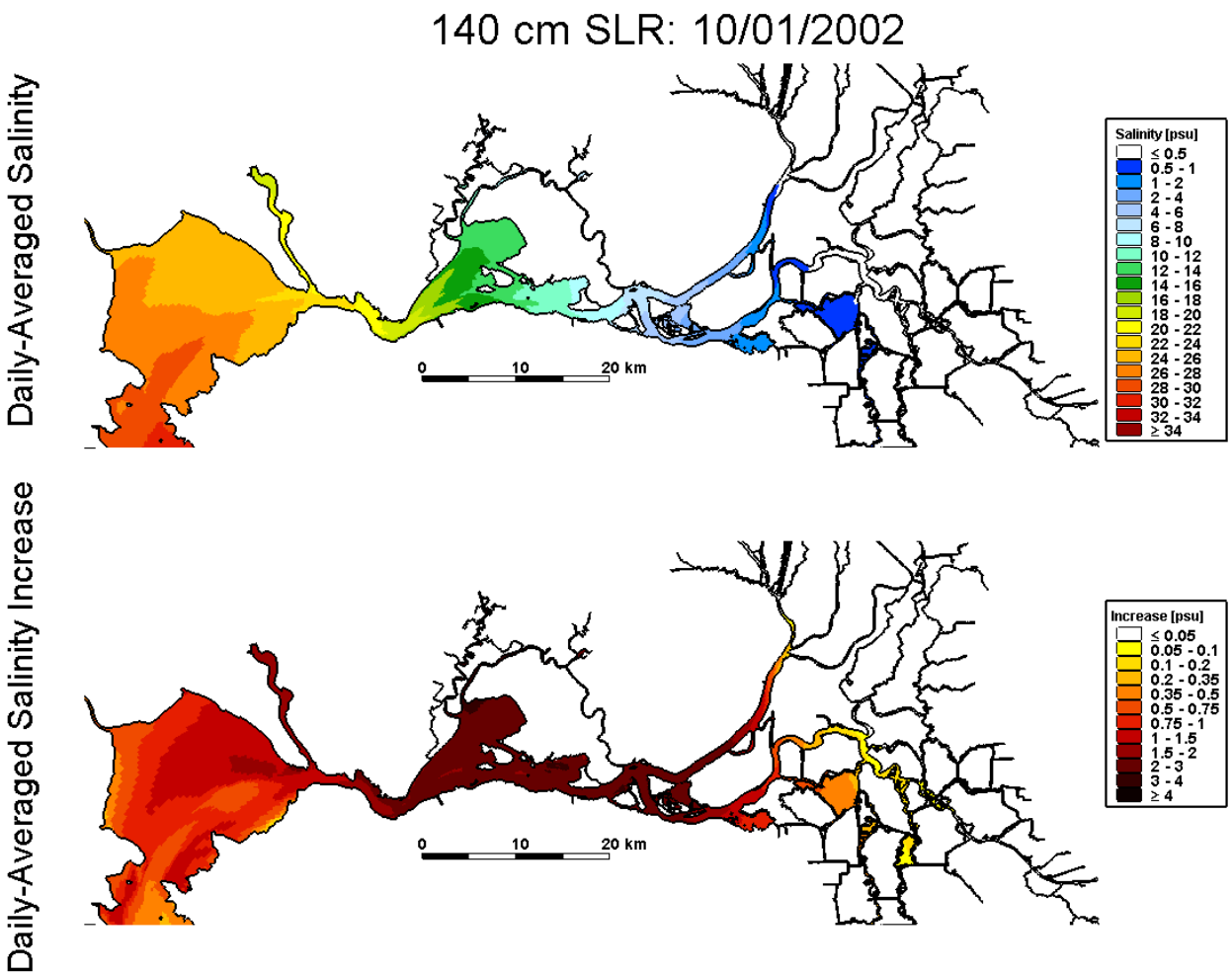

Figure 4.5-10 Predicted daily-averaged depth-average salinity on October 1, 2002 for the 140 cm SLR scenario (top); predicted increase in daily-averaged depth-average salinity on October 1, 2002 relative to the Baseline (0 cm SLR) scenario for the 140 cm SLR scenario.

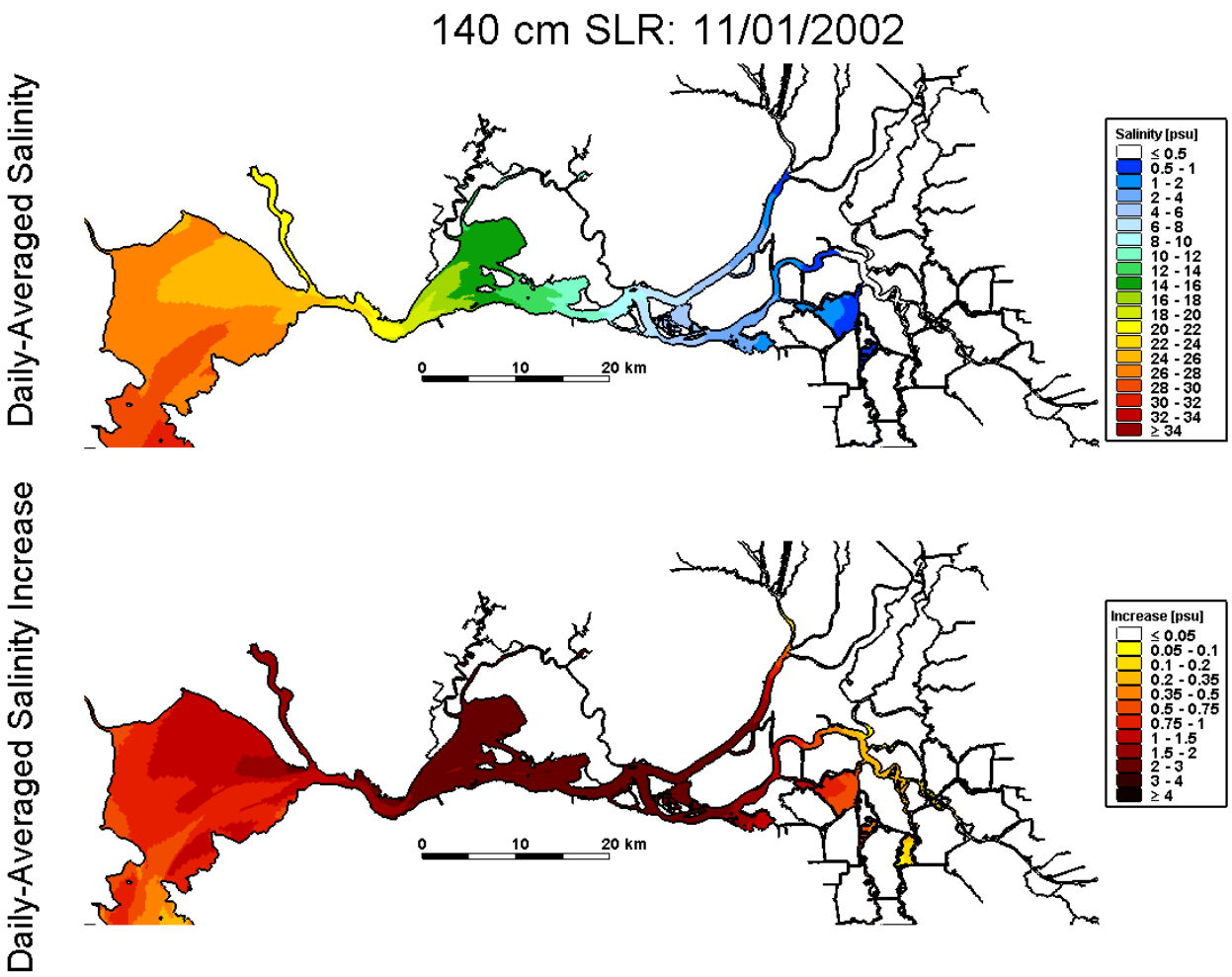

Figure 4.5-11 Predicted daily-averaged depth-average salinity on November 1, 2002 for the 140 cm SLR scenario (top); predicted increase in daily-averaged depth-average salinity on November 1, 2002 relative to the Baseline (0 cm SLR) scenario for the 140 cm SLR scenario.

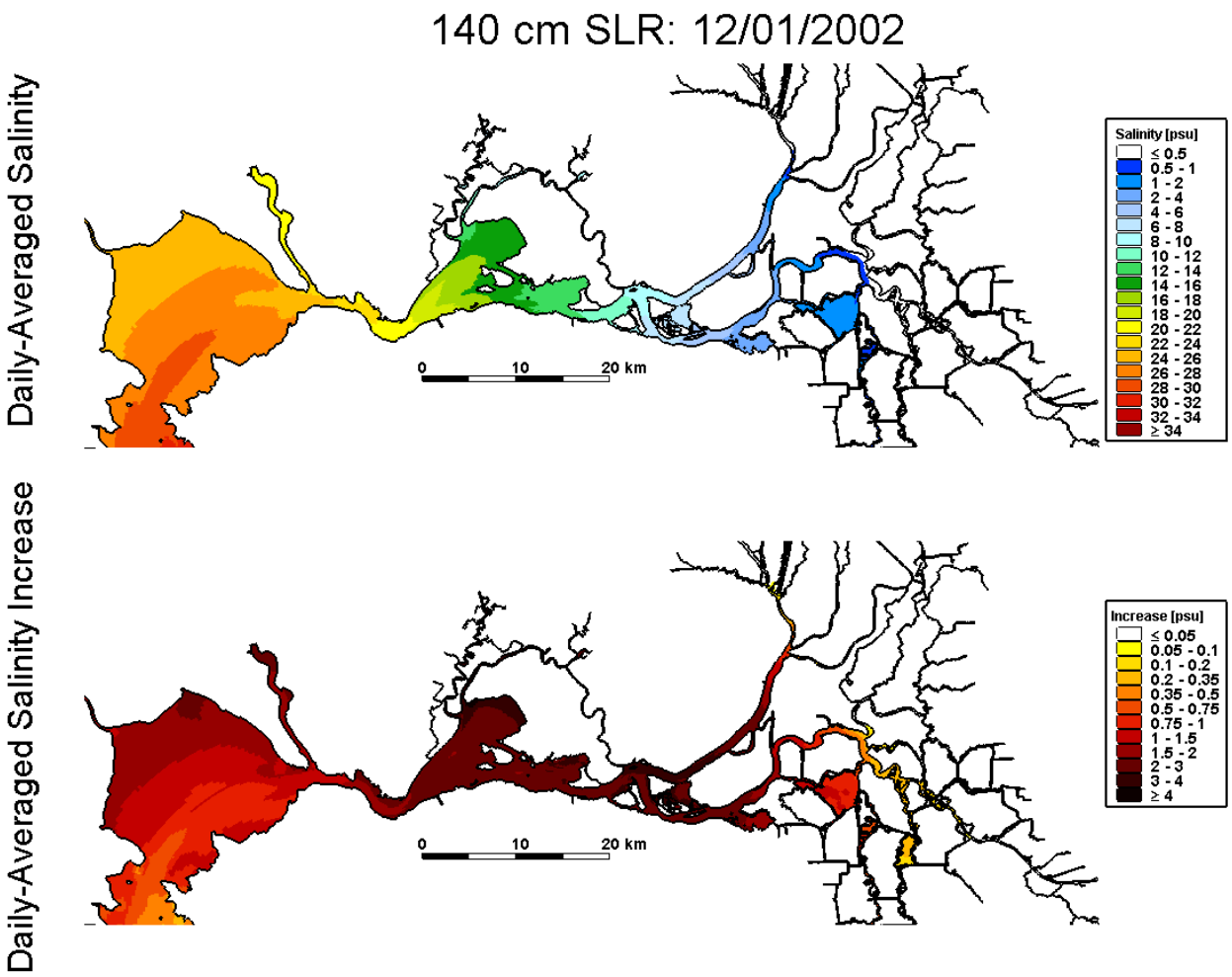

Figure 4.5-12 Predicted daily-averaged depth-average salinity on December 1, 2002 for the 140 cm SLR scenario (top); predicted increase in daily-averaged depth-average salinity on December 1, 2002 relative to the Baseline (0 cm SLR) scenario for the 140 cm SLR scenario.

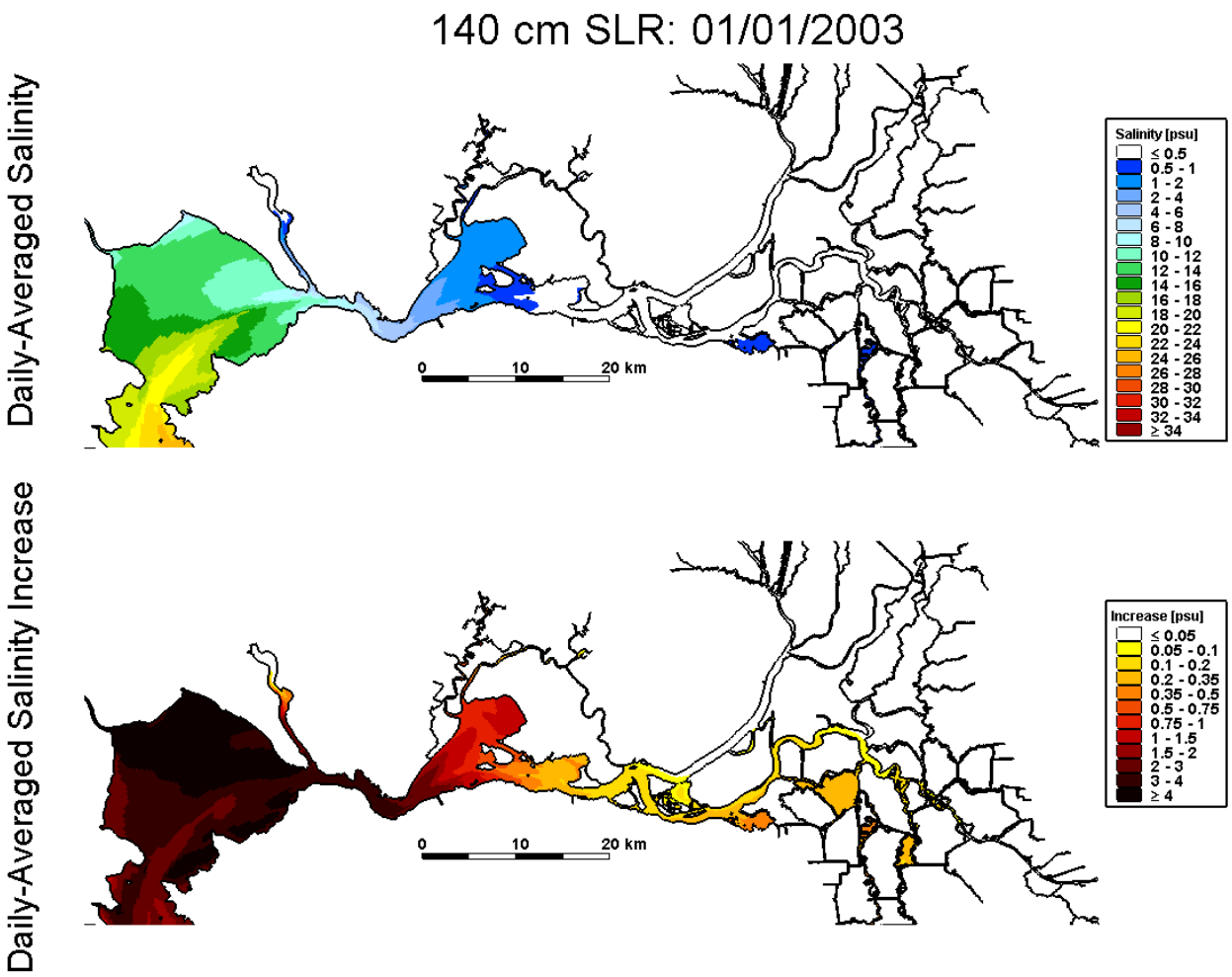

Figure 4.5-13 Predicted daily-averaged depth-average salinity on January 1, 2003 for the 140 cm SLR scenario (top); predicted increase in daily-averaged depth-average salinity on January 1, 2003 relative to the Baseline (0 cm SLR) scenario for the 140 cm SLR scenario.

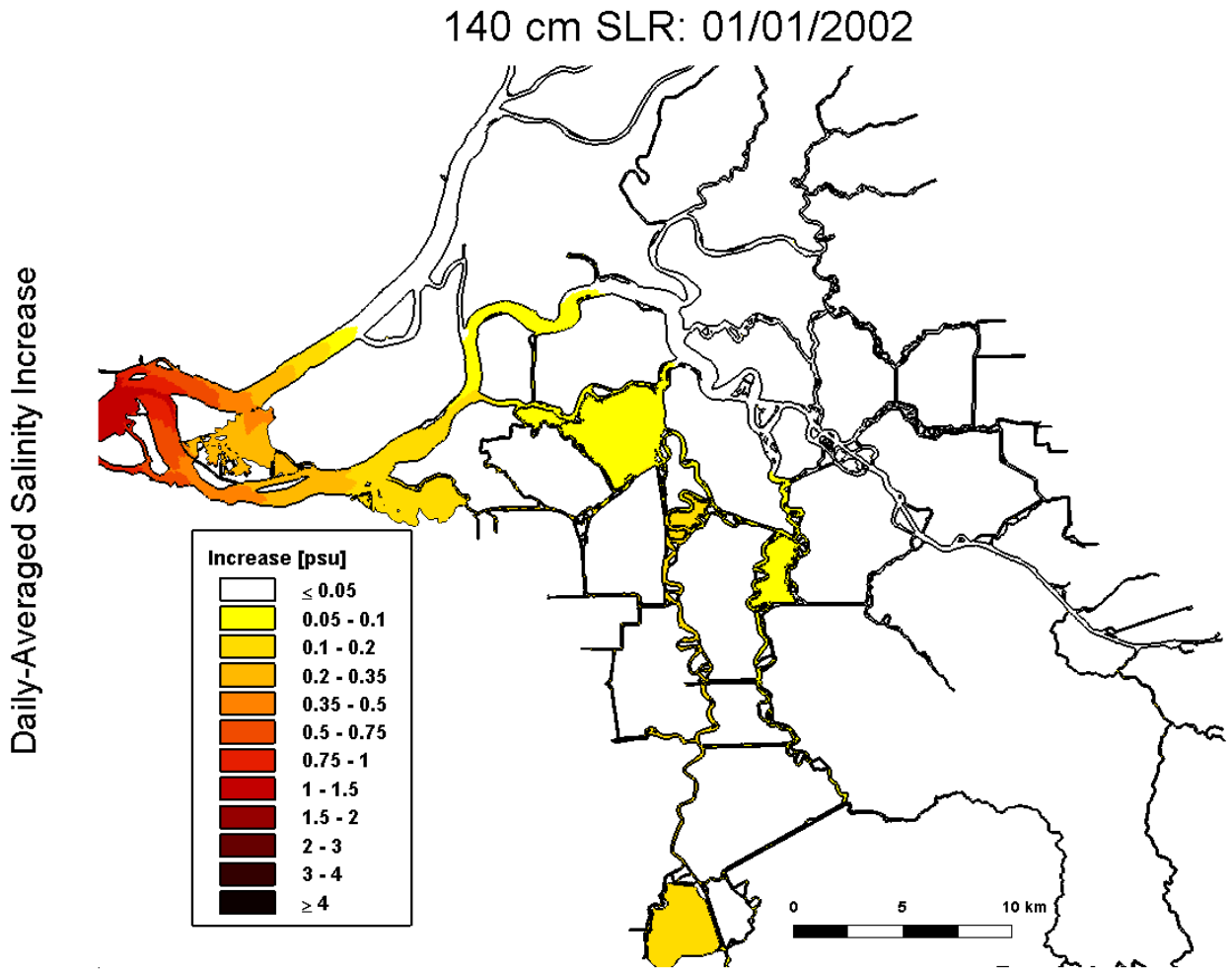

Figure 4.5-14 Predicted increase in daily-averaged depth-average salinity in the Sacramento-San Joaquin Delta on January 1, 2002 relative to the Baseline (0 cm SLR) scenario for the 140 cm SLR scenario.

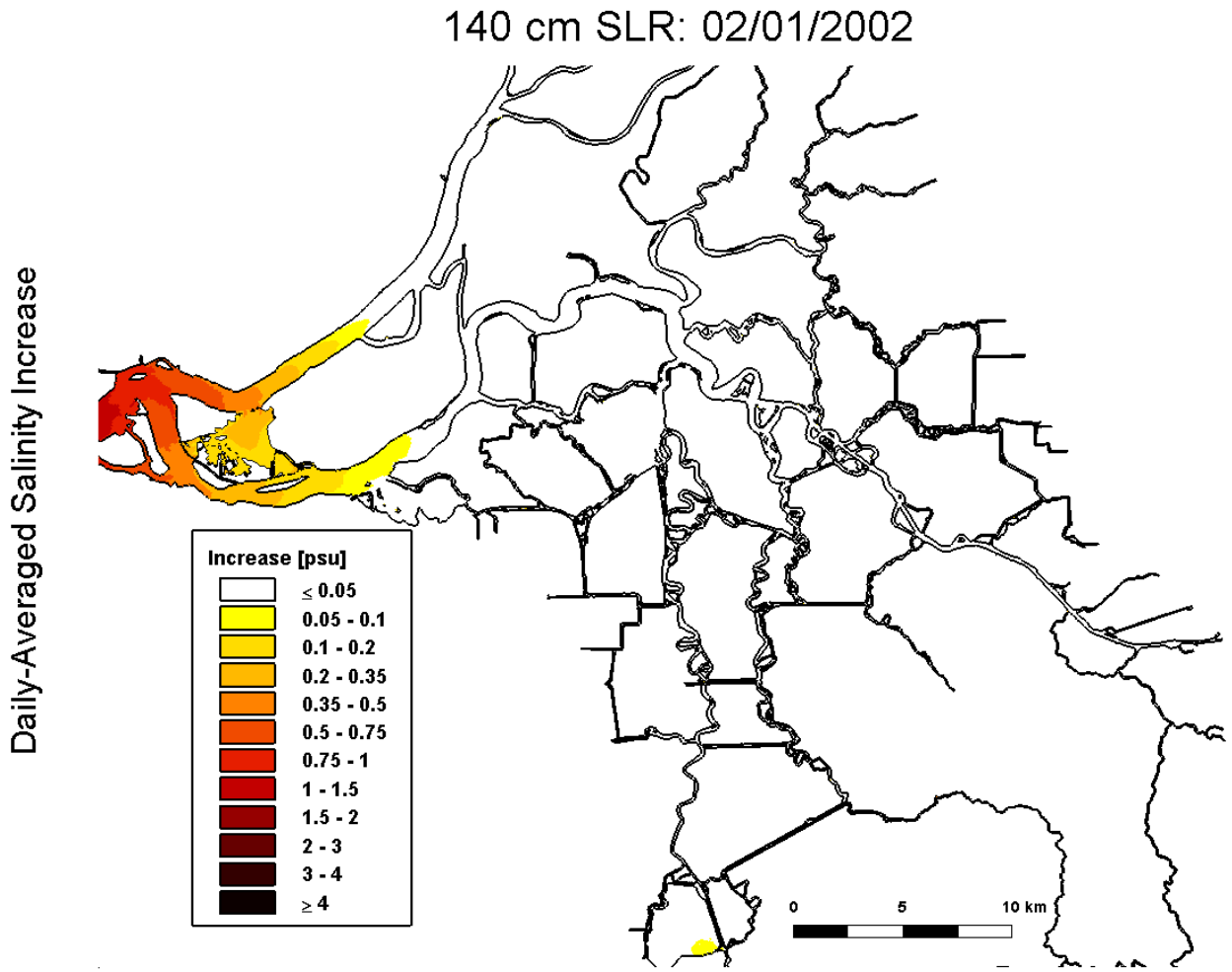

Figure 4.5-15 Predicted increase in daily-averaged depth-average salinity in the Sacramento-San Joaquin Delta on February 1, 2002 relative to the Baseline (0 cm SLR) scenario for the 140 cm SLR scenario.

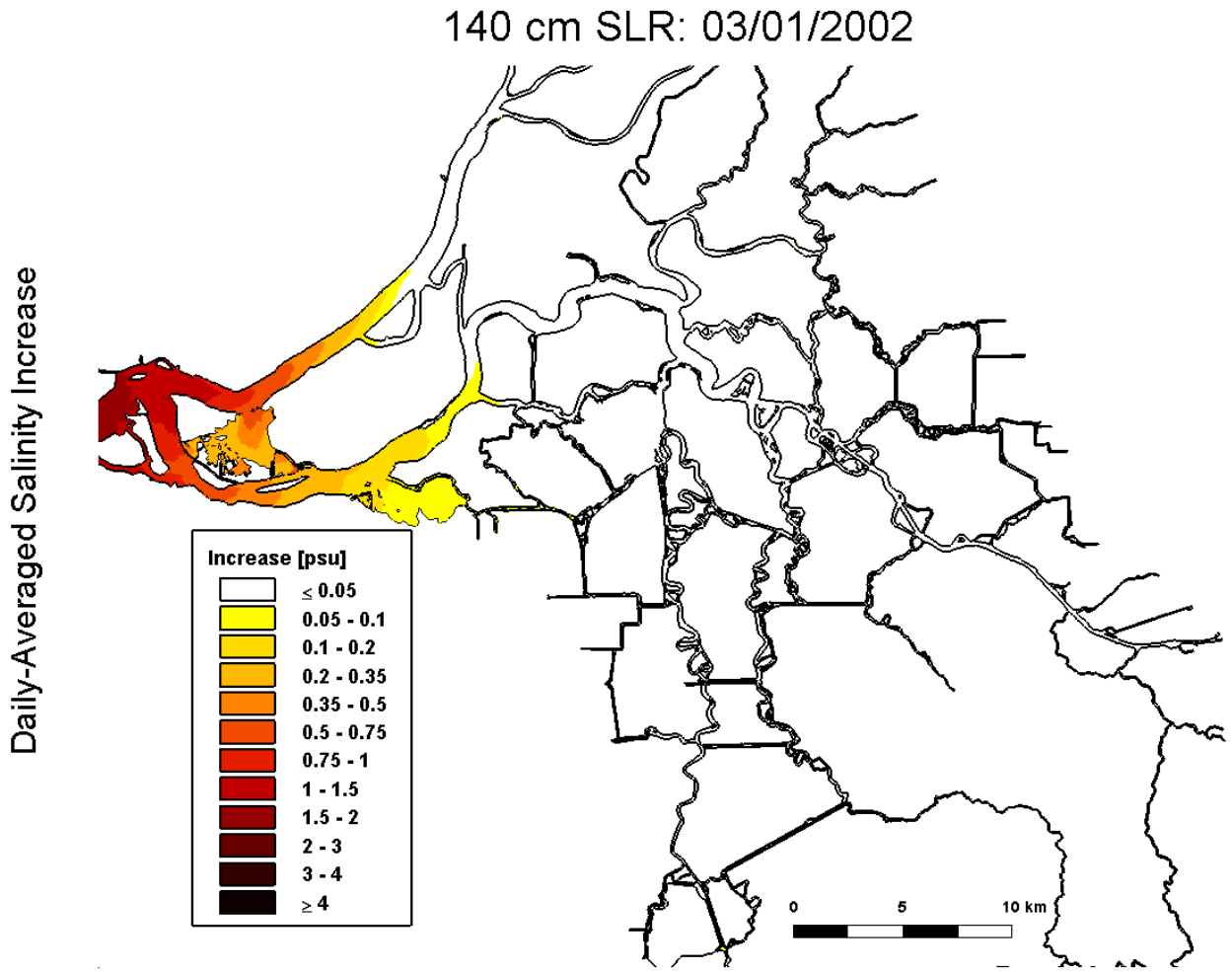

Figure 4.5-16 Predicted increase in daily-averaged depth-average salinity in the Sacramento-San Joaquin Delta on March 1, 2002 relative to the Baseline (0 cm SLR) scenario for the 140 cm SLR scenario.

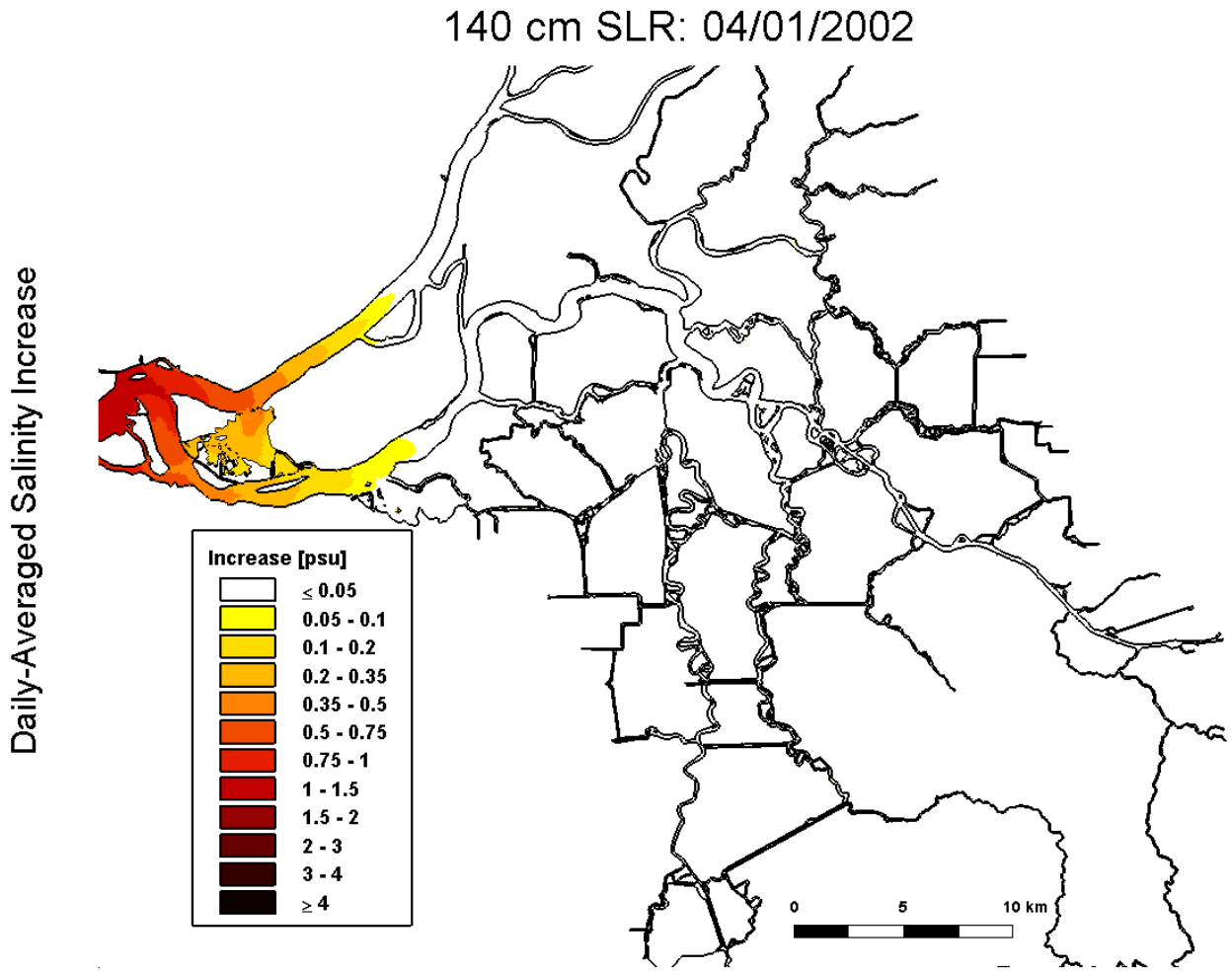

Figure 4.5-17 Predicted increase in daily-averaged depth-average salinity in the Sacramento-San Joaquin Delta on April 1, 2002 relative to the Baseline (0 cm SLR) scenario for the 140 cm SLR scenario.

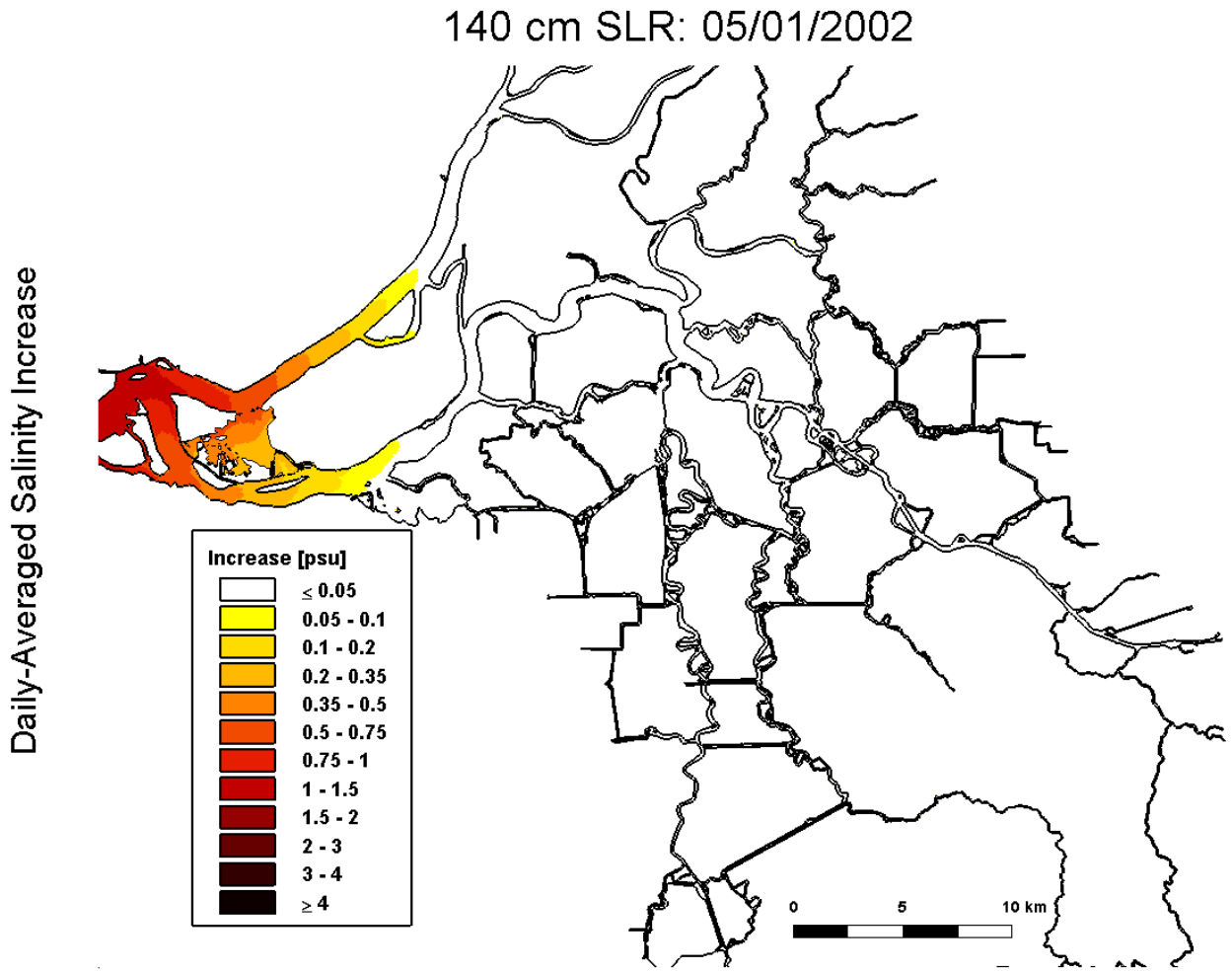

Figure 4.5-18 Predicted increase in daily-averaged depth-average salinity in the Sacramento-San Joaquin Delta on May 1, 2002 relative to the Baseline (0 cm SLR) scenario for the 140 cm SLR scenario.

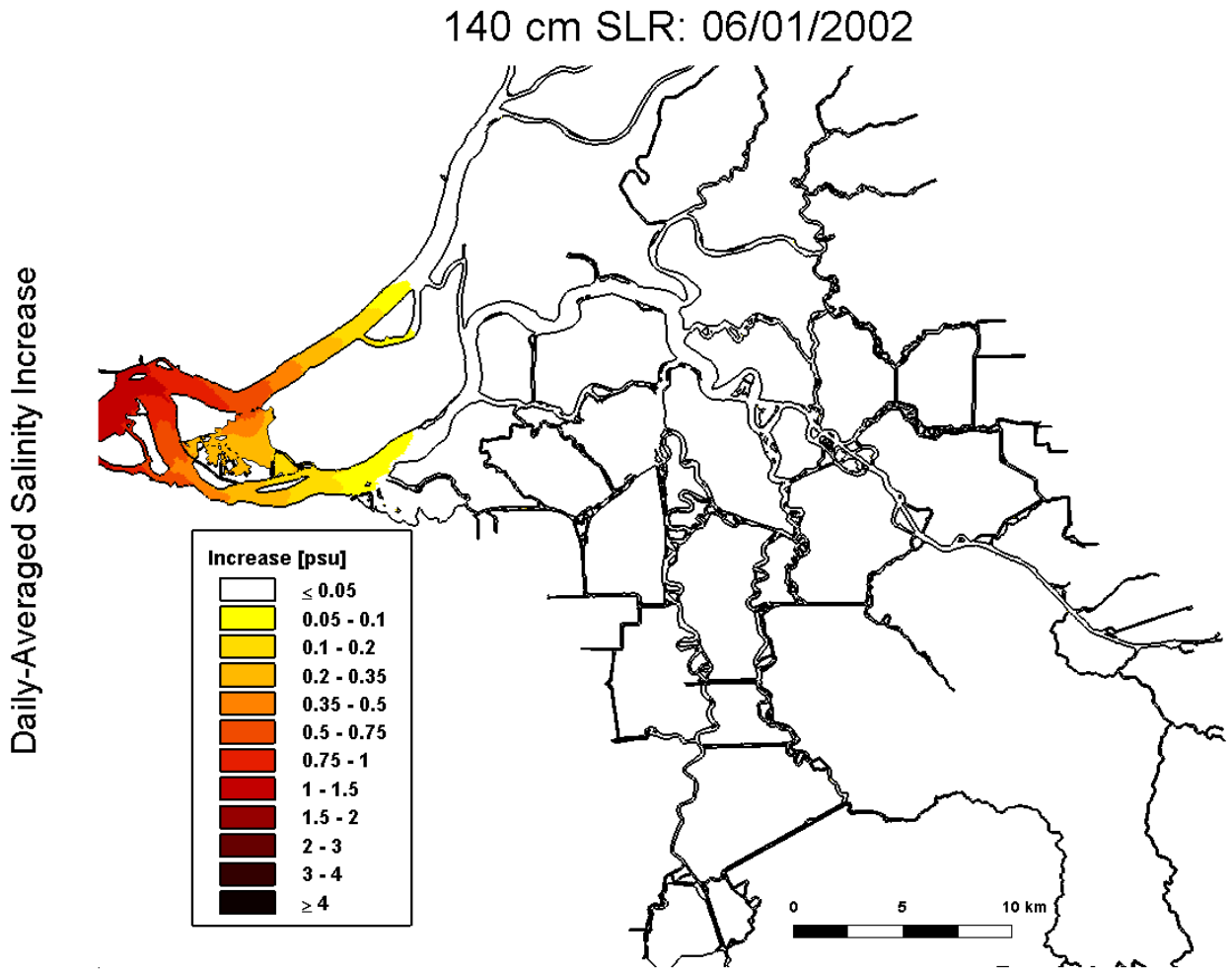

Figure 4.5-19 Predicted increase in daily-averaged depth-average salinity in the Sacramento-San Joaquin Delta on June 1, 2002 relative to the Baseline (0 cm SLR) scenario for the 140 cm SLR scenario.

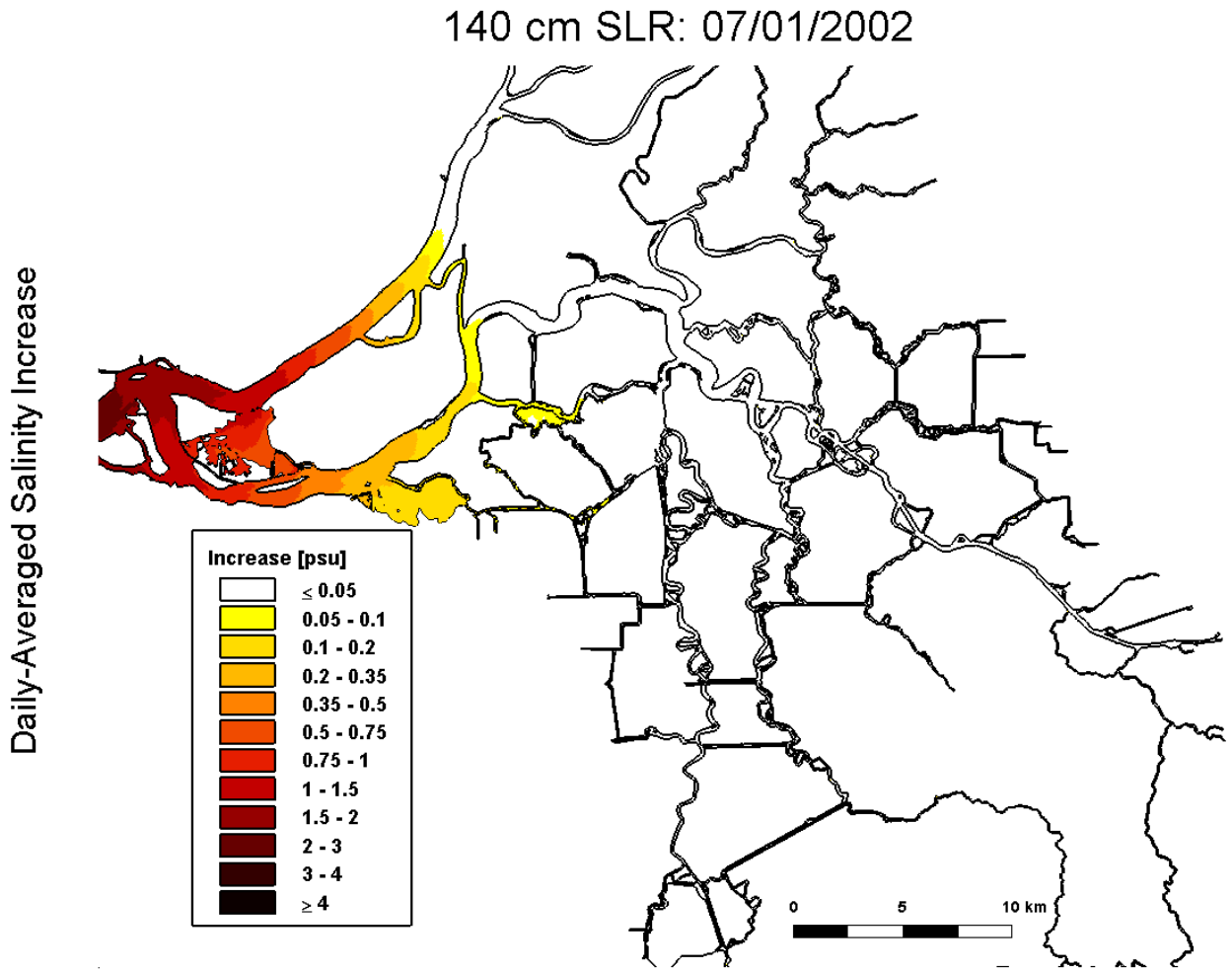

Figure 4.5-20 Predicted increase in daily-averaged depth-average salinity in the Sacramento-San Joaquin Delta on July 1, 2002 relative to the Baseline (0 cm SLR) scenario for the 140 cm SLR scenario.

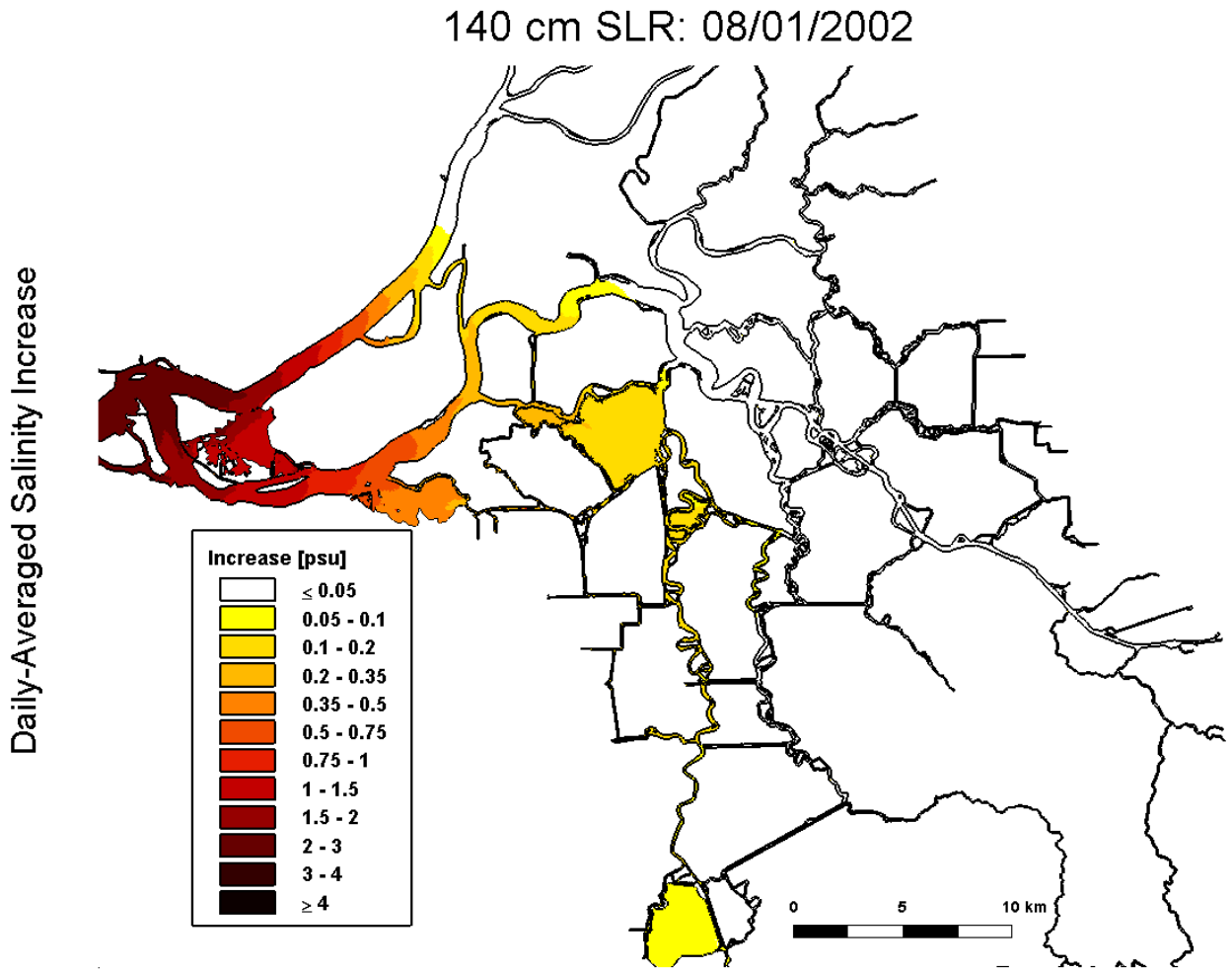

Figure 4.5-21 Predicted increase in daily-averaged depth-average salinity in the Sacramento-San Joaquin Delta on August 1, 2002 relative to the Baseline (0 cm SLR) scenario for the 140 cm SLR scenario.

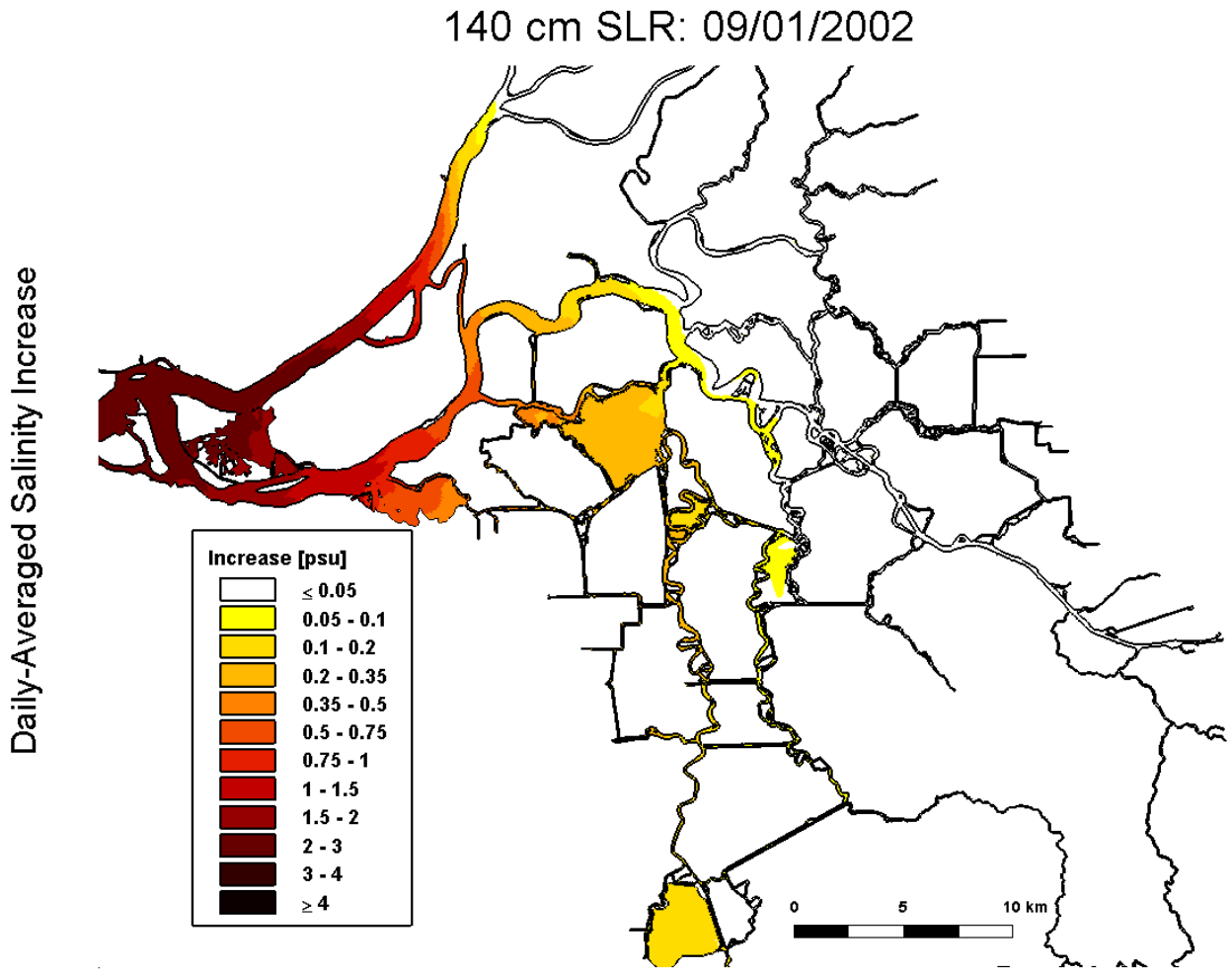

Figure 4.5-22 Predicted increase in daily-averaged depth-average salinity in the Sacramento-San Joaquin Delta on September 1, 2002 relative to the Baseline (0 cm SLR) scenario for the 140 cm SLR scenario.

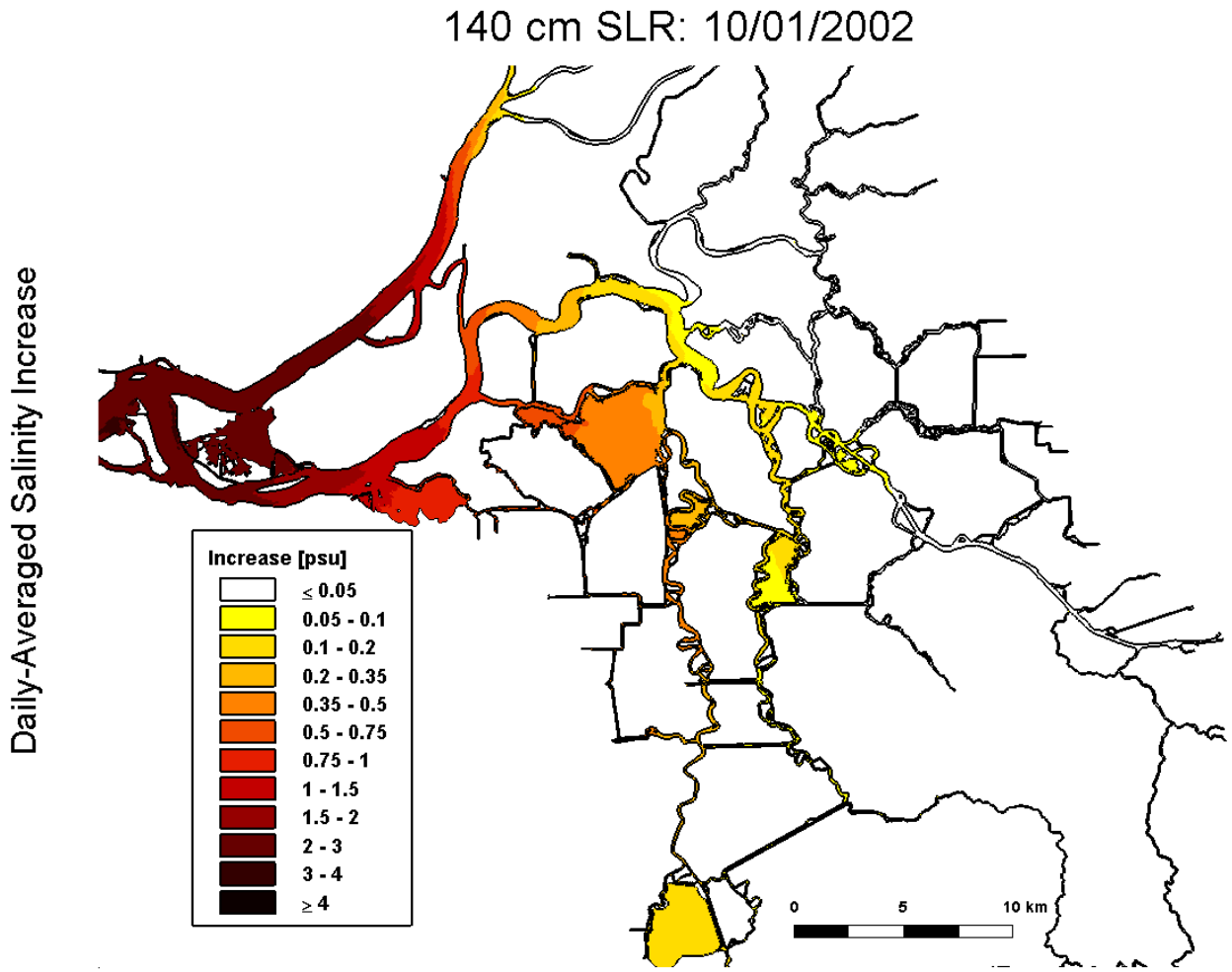

Figure 4.5-23 Predicted increase in daily-averaged depth-average salinity in the Sacramento-San Joaquin Delta on October 1, 2002 relative to the Baseline (0 cm SLR) scenario for the 140 cm SLR scenario.

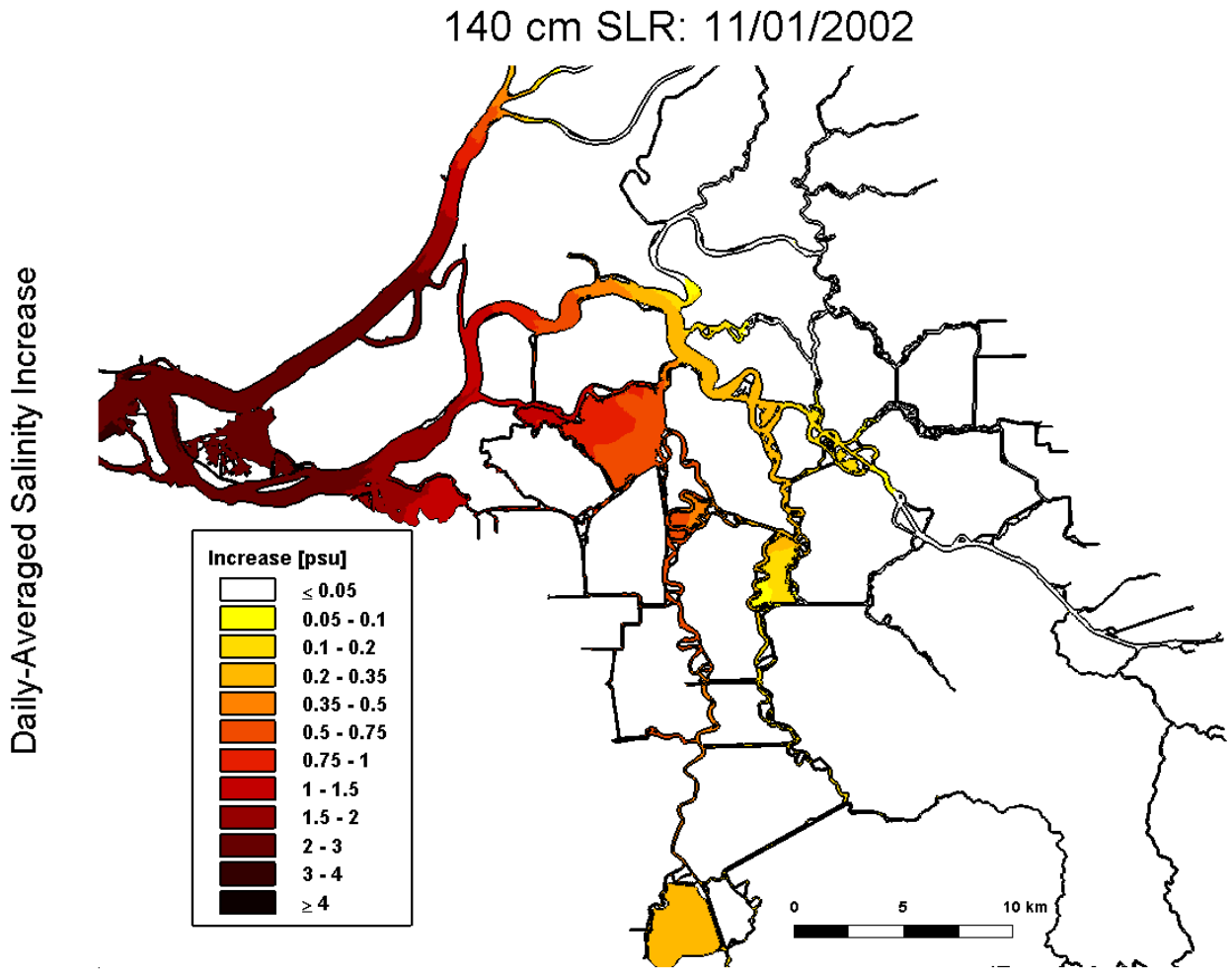

Figure 4.5-24 Predicted increase in daily-averaged depth-average salinity in the Sacramento-San Joaquin Delta on November 1, 2002 relative to the Baseline (0 cm SLR) scenario for the 140 cm SLR scenario.

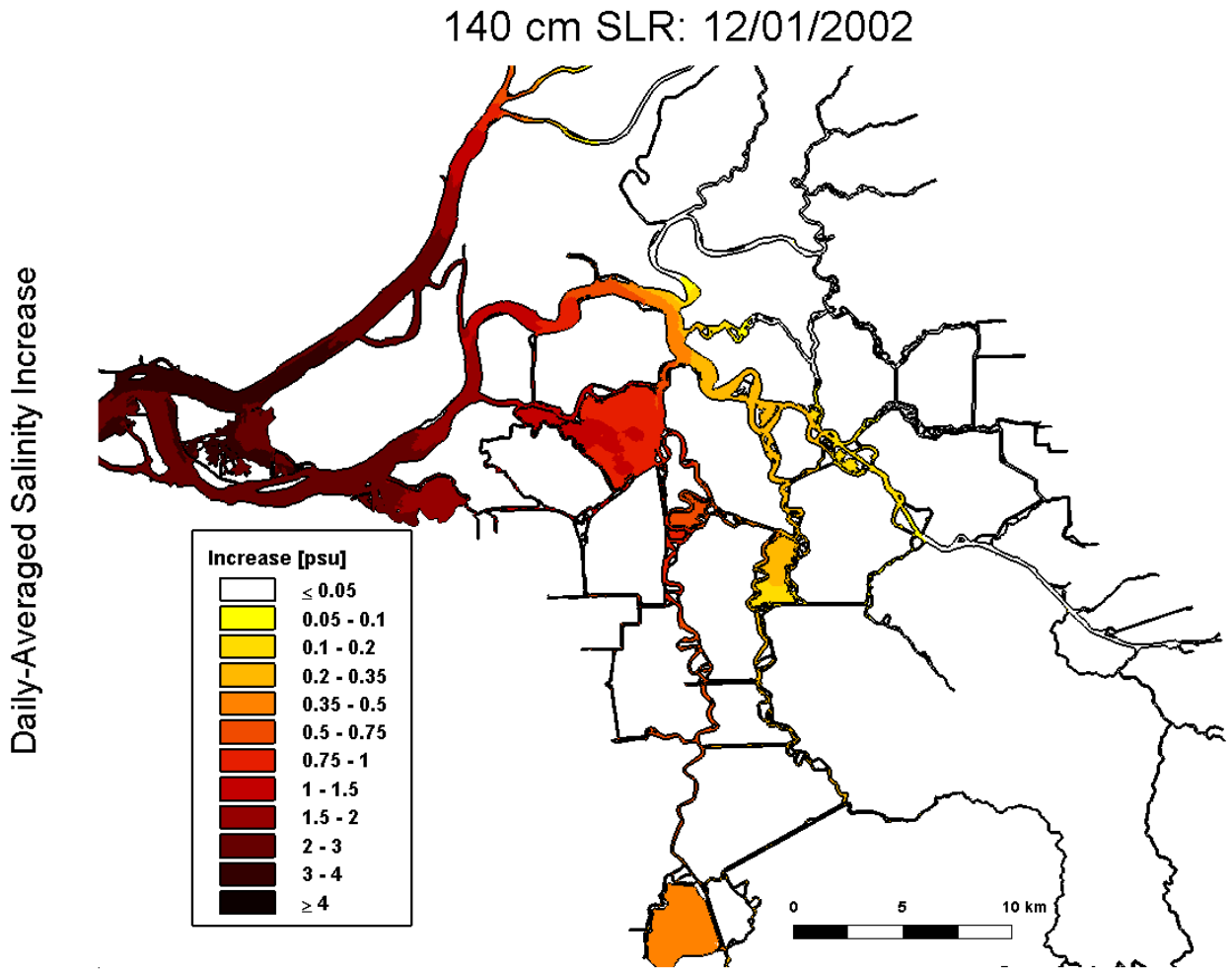

Figure 4.5-25 Predicted increase in daily-averaged depth-average salinity in the Sacramento-San Joaquin Delta on December 1, 2002 relative to the Baseline (0 cm SLR) scenario for the 140 cm SLR scenario.

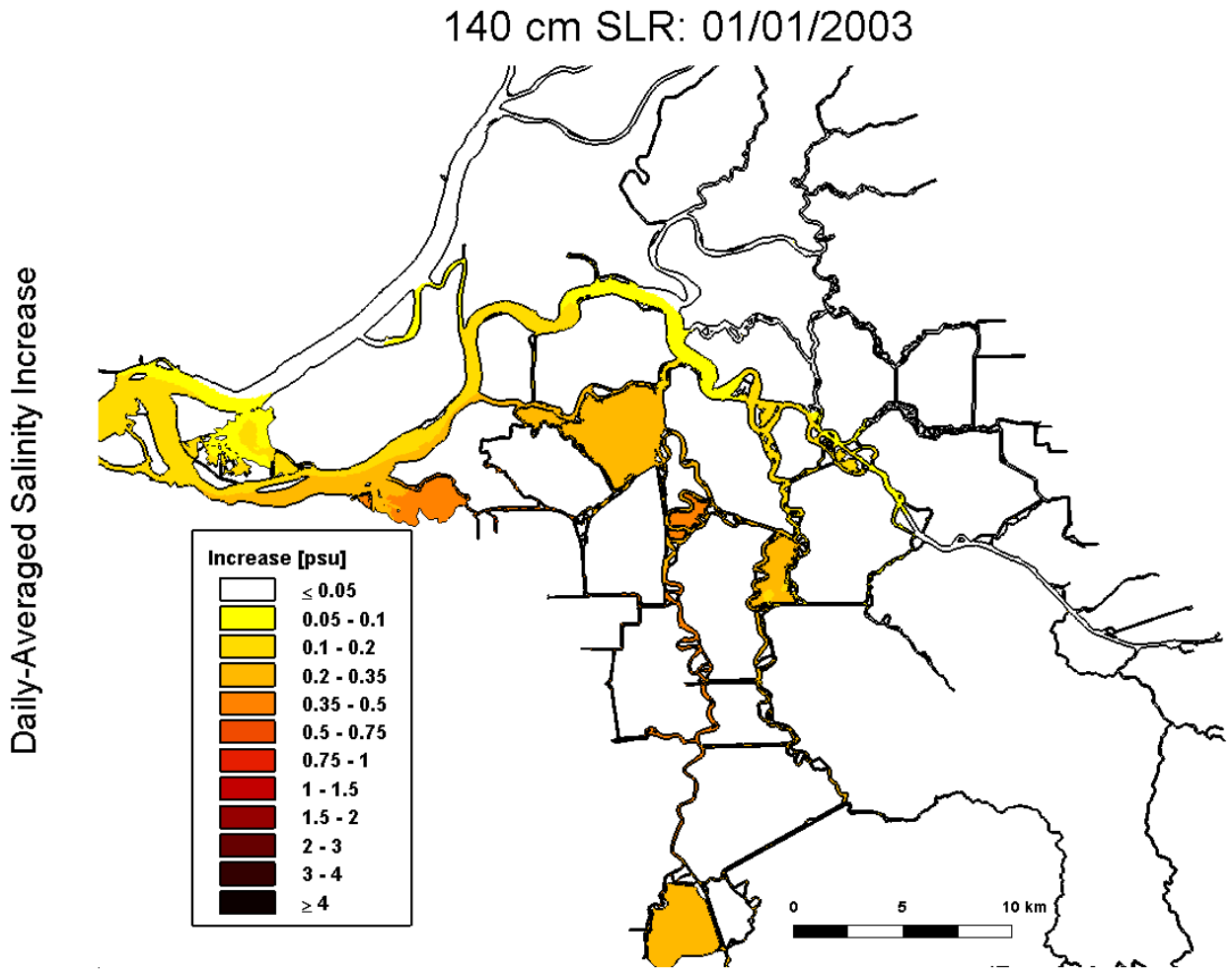

Figure 4.5-26 Predicted increase in daily-averaged depth-average salinity in the Sacramento-San Joaquin Delta on January 1, 2003 relative to the Baseline (0 cm SLR) scenario for the 140 cm SLR scenario.

4.6 Predicted Increase in Salinity for 140 cm SLR with 5% Amplification Scenario

Figure 4.6-1 through 4.6-13 show the predicted salinity along the northern portion of the San Francisco Estuary, spanning from San Pablo Bay through the Sacramento-San Joaquin Delta for the 140 cm SLR with 5% Amplification scenario. The top panel of each figure shows the predicted daily-averaged depth-average salinity for the 140 cm SLR with 5% Amplification scenario. The lower panel shows the predicted salinity increase computed by subtracting the predicted daily-averaged depth-average salinity for the Baseline (0 cm SLR) scenario from the predicted daily-averaged depth-average salinity for the 140 cm SLR with 5% Amplification scenario. Figures 4.6-14 through 4.6-26 show the predicted salinity increases resulting from the 140 cm SLR with 5% Amplification scenario in the Sacramento-San Joaquin Delta.

At the beginning of the analysis period on January 1, 2002, significant salinity increases are evident in the Delta, indicating that the salinity increases from the previous fall period have not been fully flushed out. Salinity increases between 1. 0 and 1.50 psu are predicted between Chipps Island and Collinsville and predicted salinity increases of up to 0.05 psu are predicted upstream to Emmaton on the Sacramento River. Along the San Joaquin River predicted salinity increases of 0.1 and 0.2 psu extend from Big Break to False River and predicted salinity increases of between 0.05 psu and 1.0 psu extend upstream to Sevenmile Slough. salinity increases of between 0.05 and 0.10 psu are predicted in Franks Tract. South of Franks Tract, predicted salinity increases between 0.10 and 0.20 psu extend down Old River to Clifton Court Forebay, and salinity increases of between 0.10 and 0.20 psu are predicted inside Clifton Court Forebay. Predicted salinity increases are less than 0.05 psu throughout the remaining portions of the Delta. Salinity increases between 3.0 and 4.0 psu are predicted through Carquinez Strait and salinity increases between 1.5 and 3.0 psu are predicted throughout Suisun Bay. Larger salinity increases of more than 2.0 psu are predicted in much of San Pablo Bay, with salinity increases of more than 4.0 psu predicted in northern San Pablo Bay. By February 1, 2002 much of the salinity increases have been flushed out of the Delta following the high flows in January. During the first half of the year, predicted salinity increases in Suisun Bay and the Delta remain similar to the predicted salinity increases seen on February 1, 2002, while predicted salinity increases in San Pablo Bay decrease, though the predicted salinity is increasing throughout this period.

Larger salinity increases are predicted in the Delta between July and December, with the largest predicted salinity increases in December prior to the first flush. In December, salinity increases of between 1.50 and 3.0 psu are predicted between Chipps Island and Emmaton, and salinity increases of between 0.75 and 1.5 psu are predicted in Franks Tract. South of Franks Tract, predicted salinity increases between 0.50 and 1.0 psu extend down Old River to Clifton Court Forebay, and salinity increases of between 0.55 and 0.50 psu are predicted inside Clifton Court Forebay. Predicted salinity increases extend up the San Joaquin River as far as Turner Cut. These simulations assumed no operational response to sea level rise, however it is expected significant operational response will be required to maintain water quality standards for 140 cm of sea level rise. Following high flows which occurred in December, predicted salinity on January 1, 2003 shows that the 0.50 psu isohaline is in central Suisun Bay near Port Chicago, which is much further east than in the Baseline scenario. On January 1, 2003 (Figure 4.6-26) salinity increases are predicted throughout much of the Delta indicating that the high flows in

December were not sufficient to push all of the salt out of the Delta for the 140 cm SLR with 5% Amplification scenario. Similar incomplete flushing of salt from the Delta for the 140 cm SLR with 5% Amplification scenario was observed on January 1, 2002 (Figure 4.6-14).

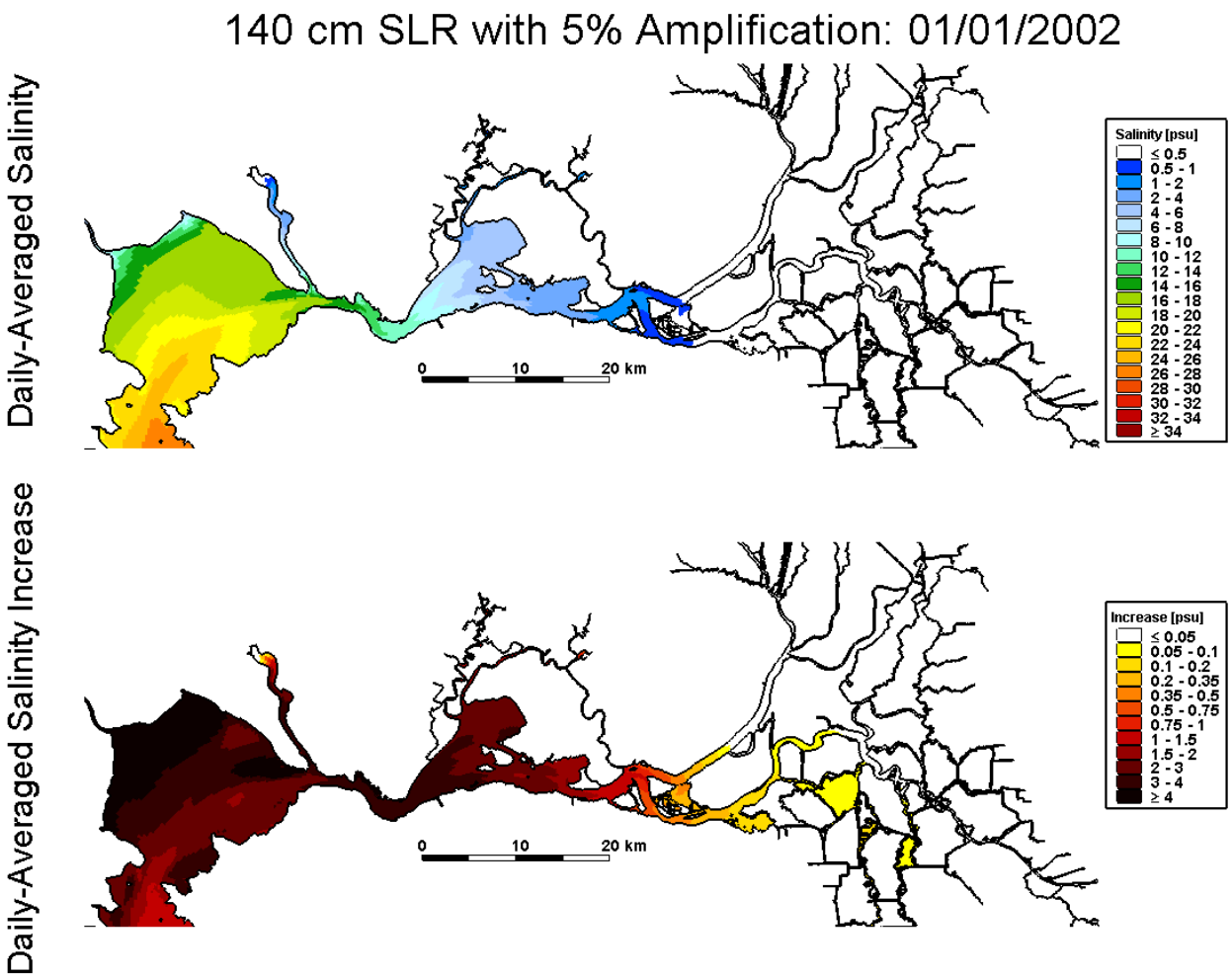

Figure 4.6-1 Predicted daily-averaged depth-average salinity on January 1, 2002 for the 140 cm SLR with 5% Amplification scenario (top); predicted increase in daily-averaged depth-average salinity on January 1, 2002 relative to the Baseline (0 cm SLR) scenario for the 140 cm SLR with 5% Amplification scenario.

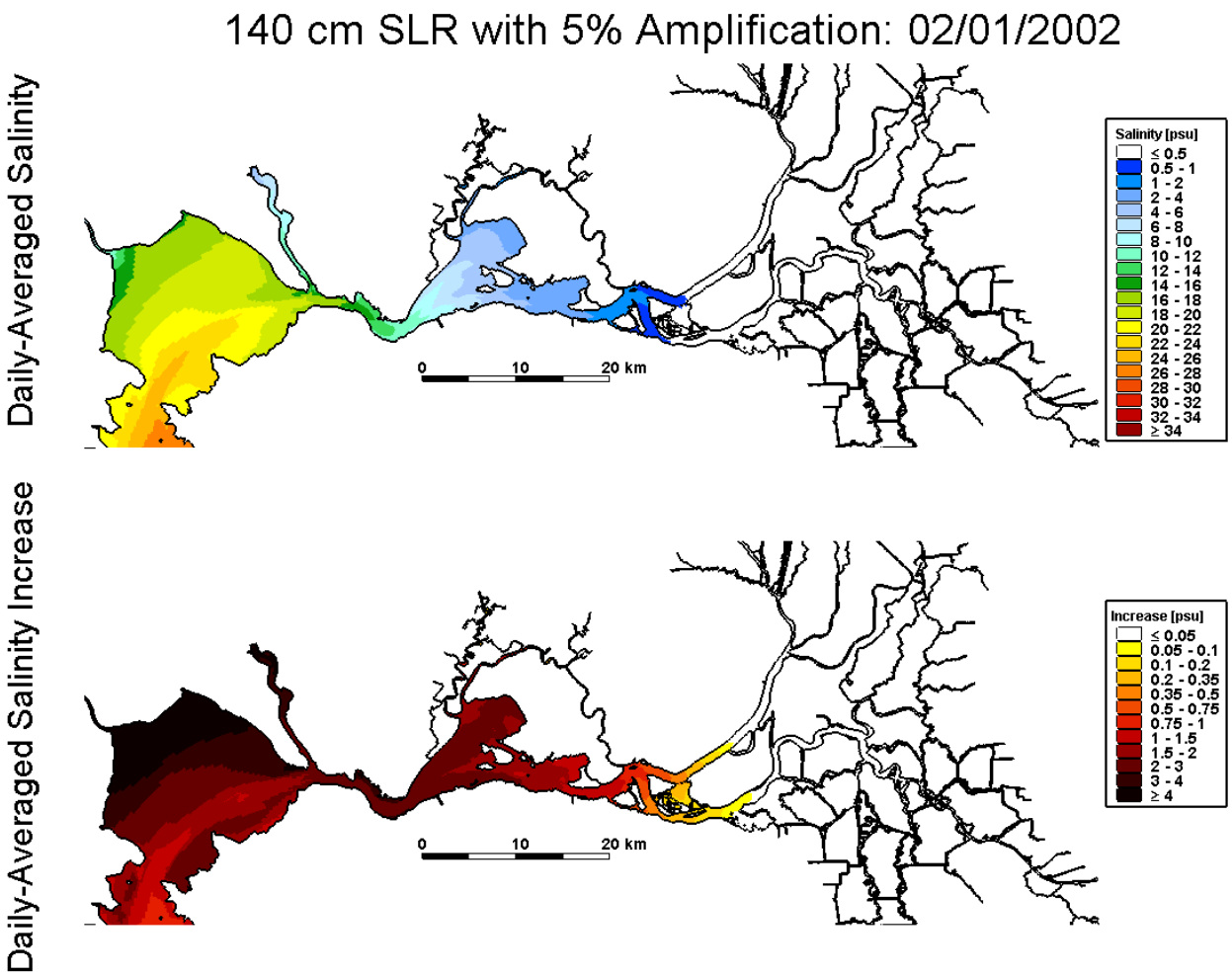

Figure 4.6-2 Predicted daily-averaged depth-average salinity on February 1, 2002 for the 140 cm SLR with 5% Amplification scenario (top); predicted increase in daily-averaged depth-average salinity on February 1, 2002 relative to the Baseline (0 cm SLR) scenario for the 140 cm SLR with 5% Amplification scenario.

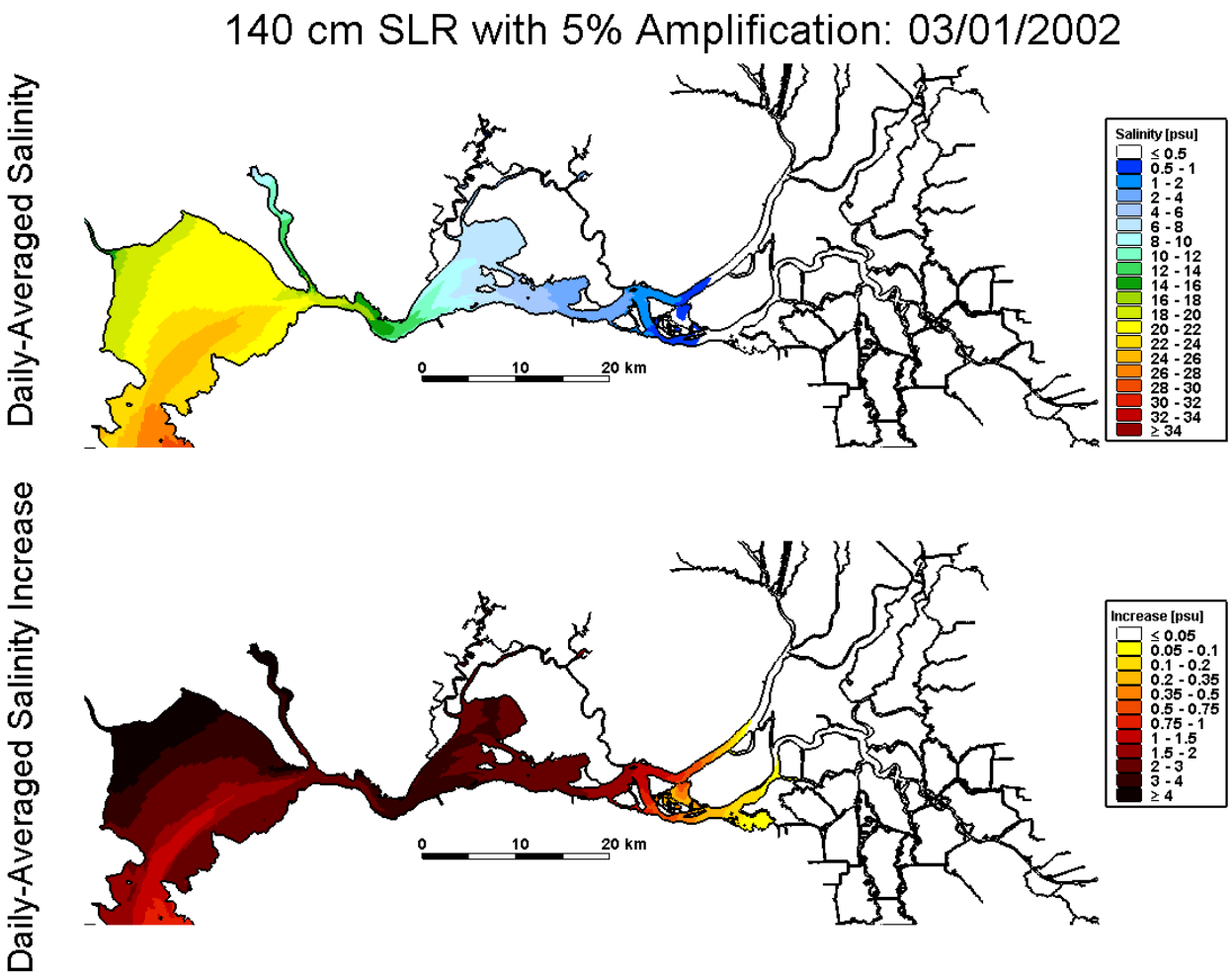

Figure 4.6-3 Predicted daily-averaged depth-average salinity on March 1, 2002 for the 140 cm SLR with 5% Amplification scenario (top); predicted increase in daily-averaged depth-average salinity on March 1, 2002 relative to the Baseline (0 cm SLR) scenario for the 140 cm SLR with 5% Amplification scenario.

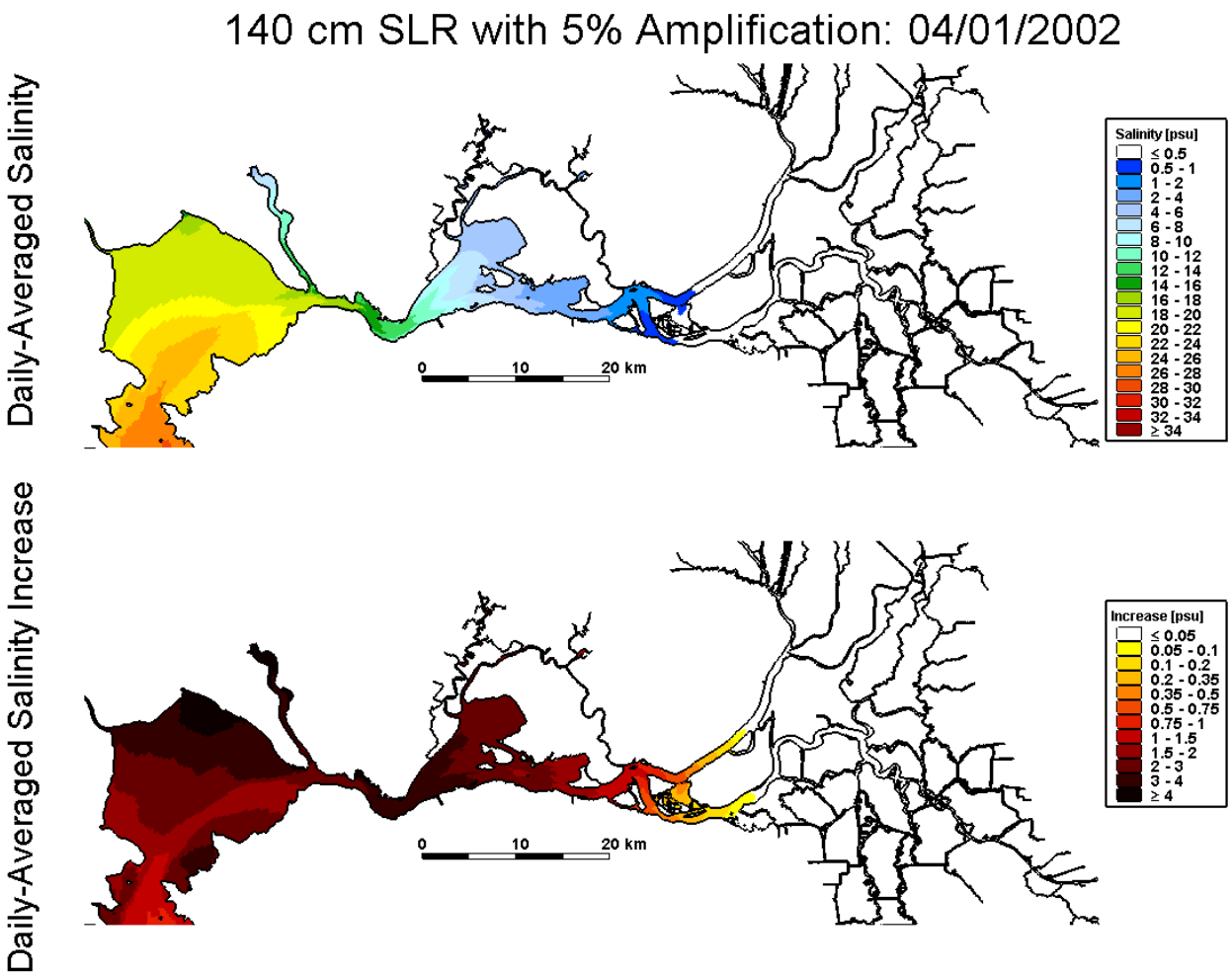

Figure 4.6-4 Predicted daily-averaged depth-average salinity on April 1, 2002 for the 140 cm SLR with 5% Amplification scenario (top); predicted increase in daily-averaged depth-average salinity on April 1, 2002 relative to the Baseline (0 cm SLR) scenario for the 140 cm SLR with 5% Amplification scenario.

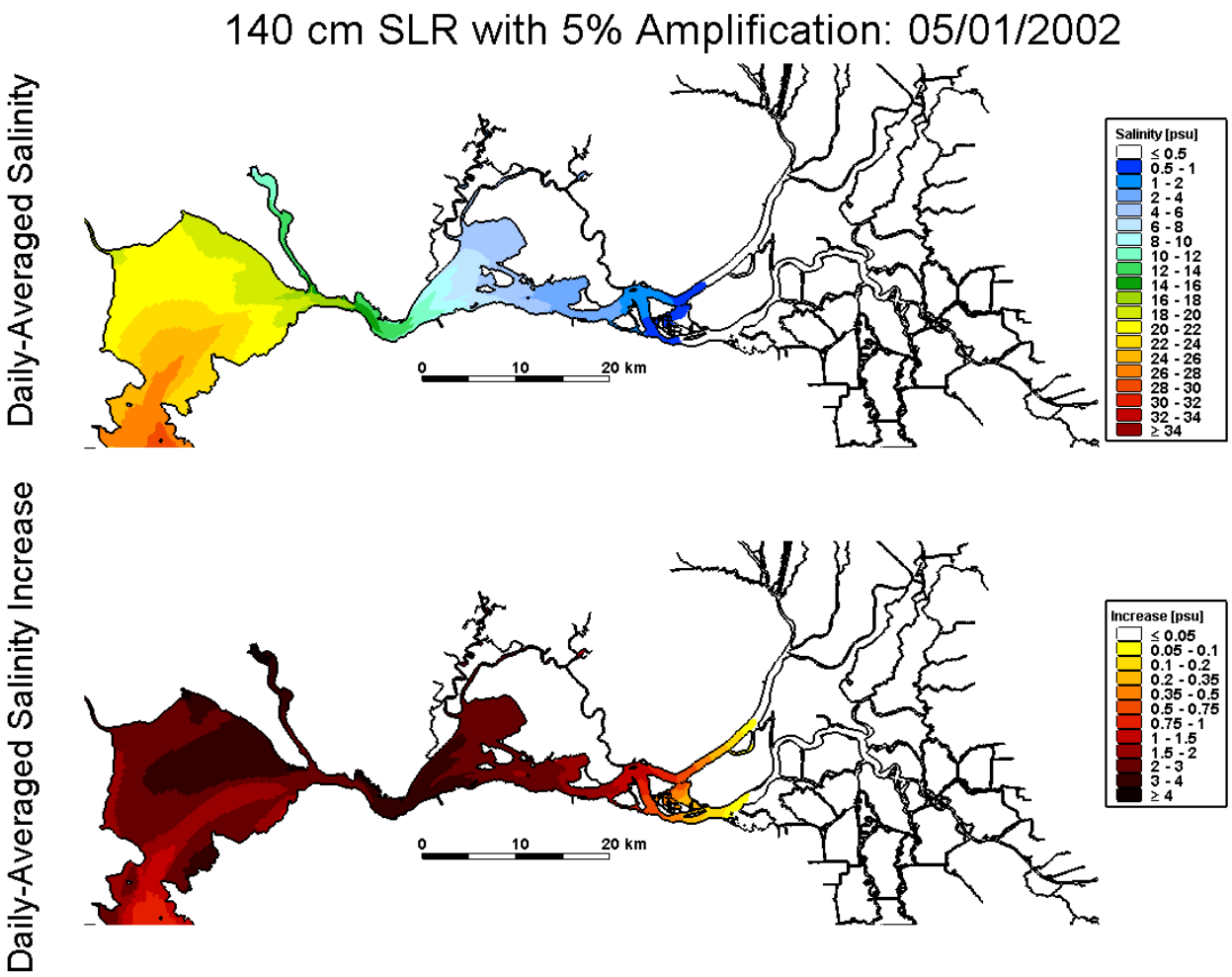

Figure 4.6-5 Predicted daily-averaged depth-average salinity on May 1, 2002 for the 140 cm SLR with 5% Amplification scenario (top); predicted increase in daily-averaged depth-average salinity on May 1, 2002 relative to the Baseline (0 cm SLR) scenario for the 140 cm SLR with 5% Amplification scenario.

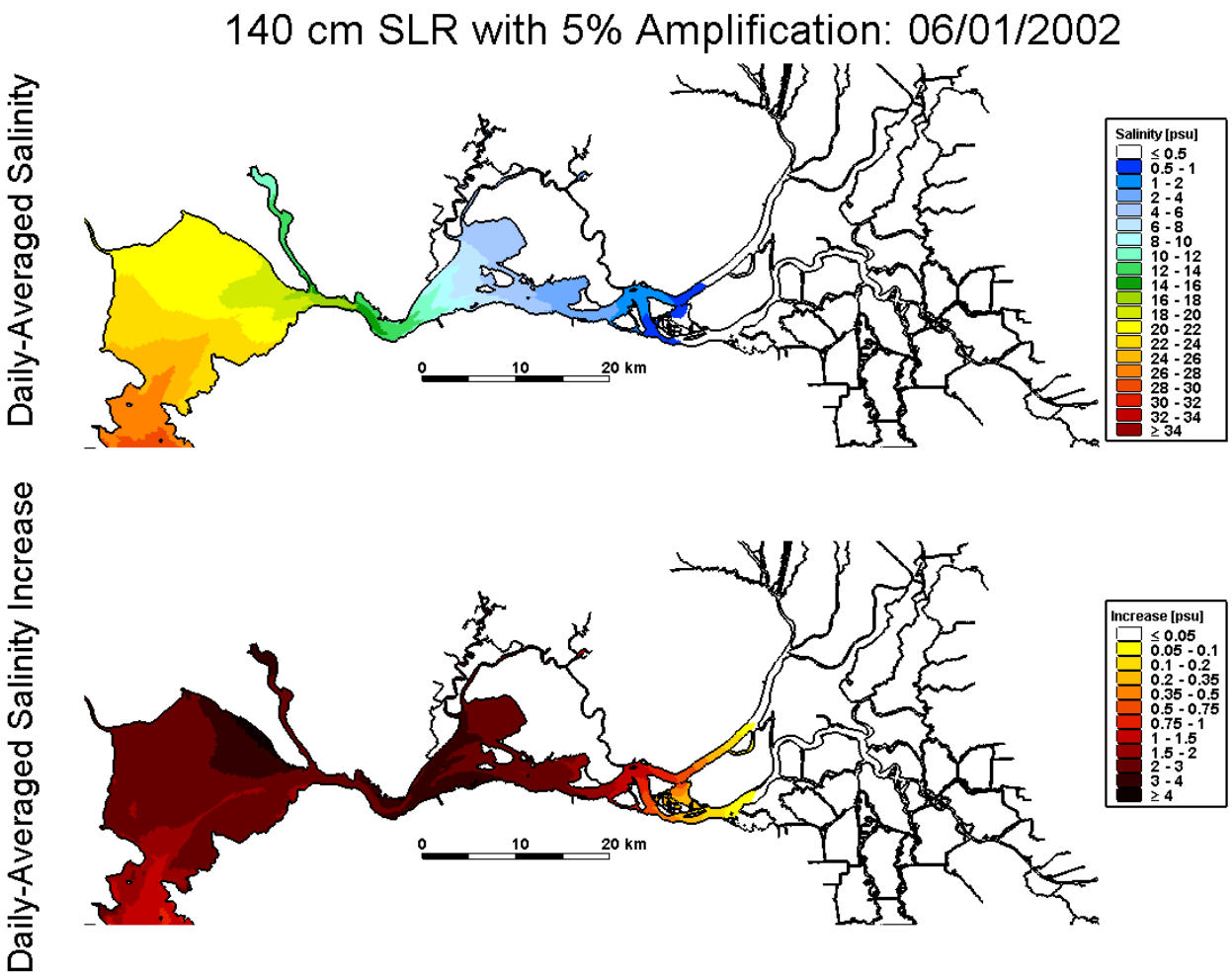

Figure 4.6-6 Predicted daily-averaged depth-average salinity on June 1, 2002 for the 140 cm SLR with 5% Amplification scenario (top); predicted increase in daily-averaged depth-average salinity on June 1, 2002 relative to the Baseline (0 cm SLR) scenario for the 140 cm SLR with 5% Amplification scenario.

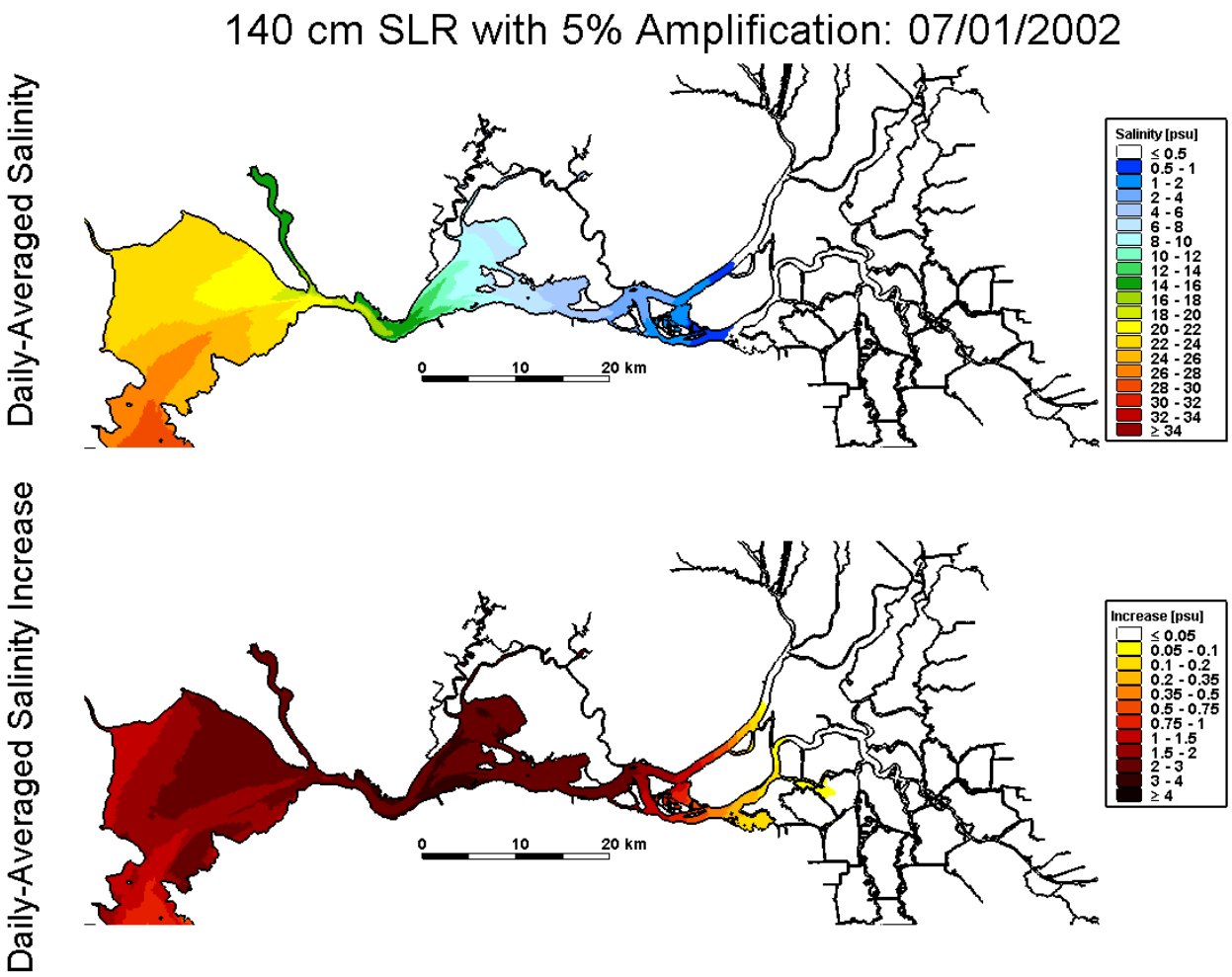

Figure 4.6-7 Predicted daily-averaged depth-average salinity on July 1, 2002 for the 140 cm SLR with 5% Amplification scenario (top); predicted increase in daily-averaged depth-average salinity on July 1, 2002 relative to the Baseline (0 cm SLR) scenario for the 140 cm SLR with 5% Amplification scenario.

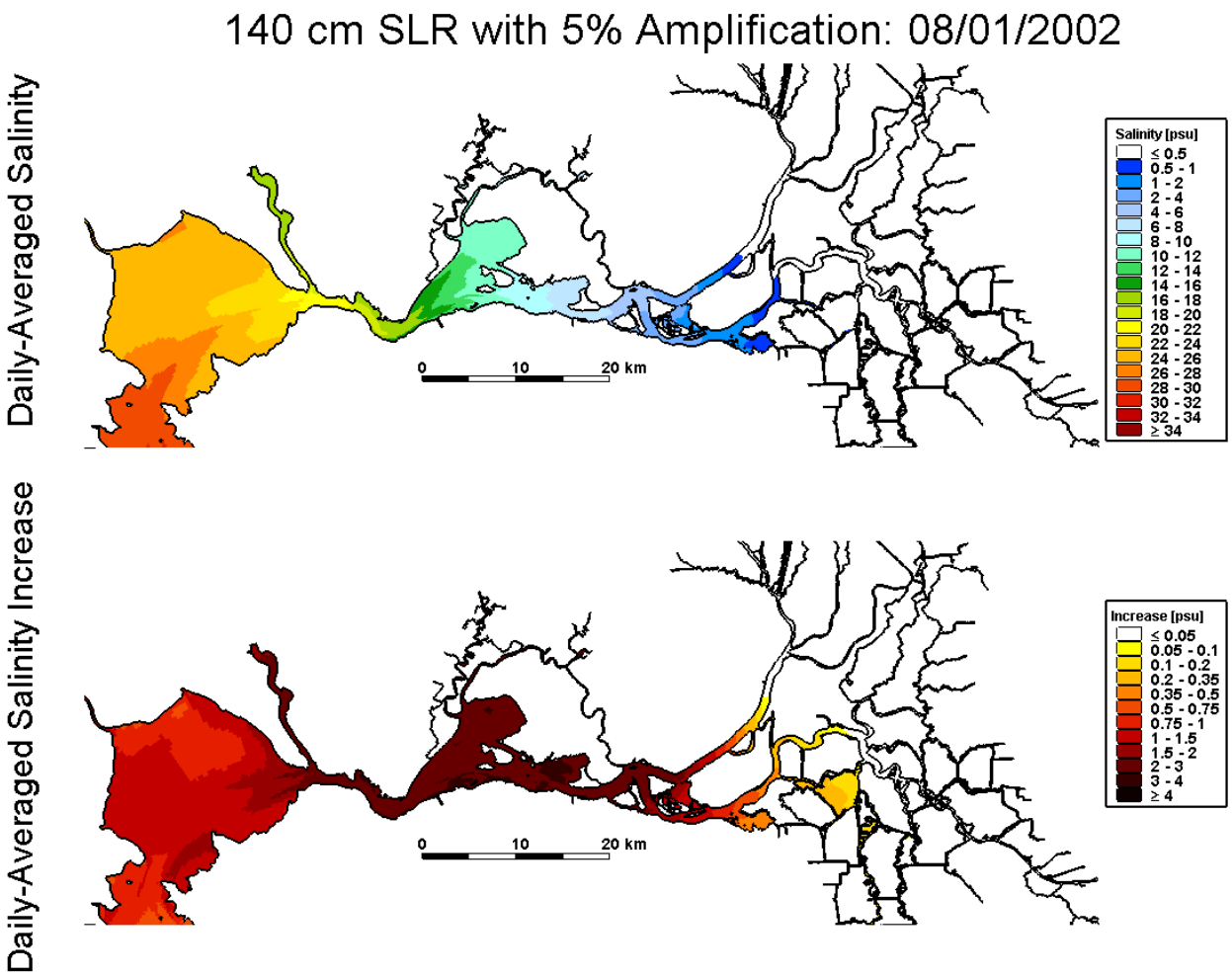

Figure 4.6-8 Predicted daily-averaged depth-average salinity on August 1, 2002 for the 140 cm SLR with 5% Amplification scenario (top); predicted increase in daily-averaged depth-average salinity on August 1, 2002 relative to the Baseline (0 cm SLR) scenario for the 140 cm SLR with 5% Amplification scenario.

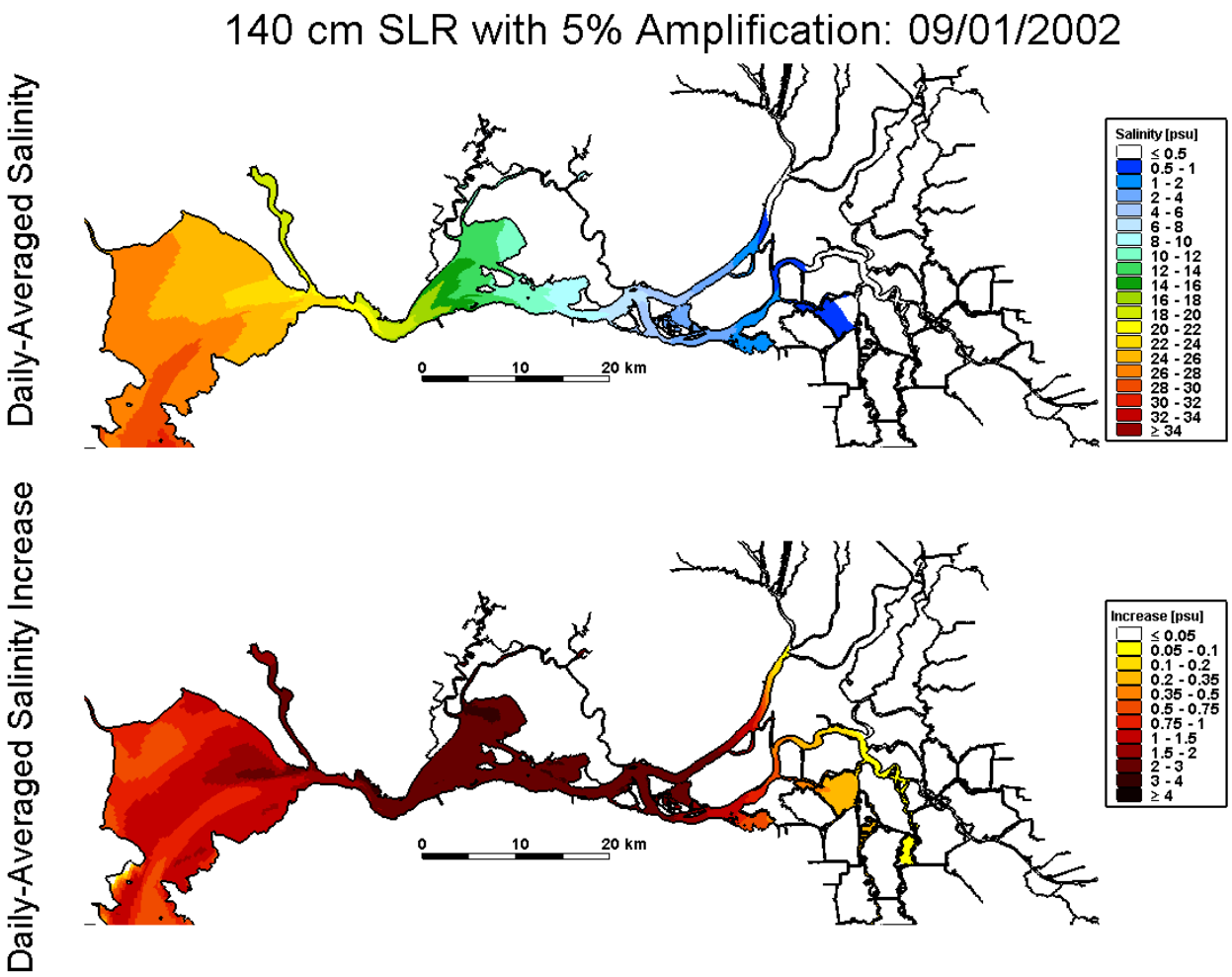

Figure 4.6-9 Predicted daily-averaged depth-average salinity on September 1, 2002 for the 140 cm SLR with 5% Amplification scenario (top); predicted increase in daily-averaged depth-average salinity on September 1, 2002 relative to the Baseline (0 cm SLR) scenario for the 140 cm SLR with 5% Amplification scenario.

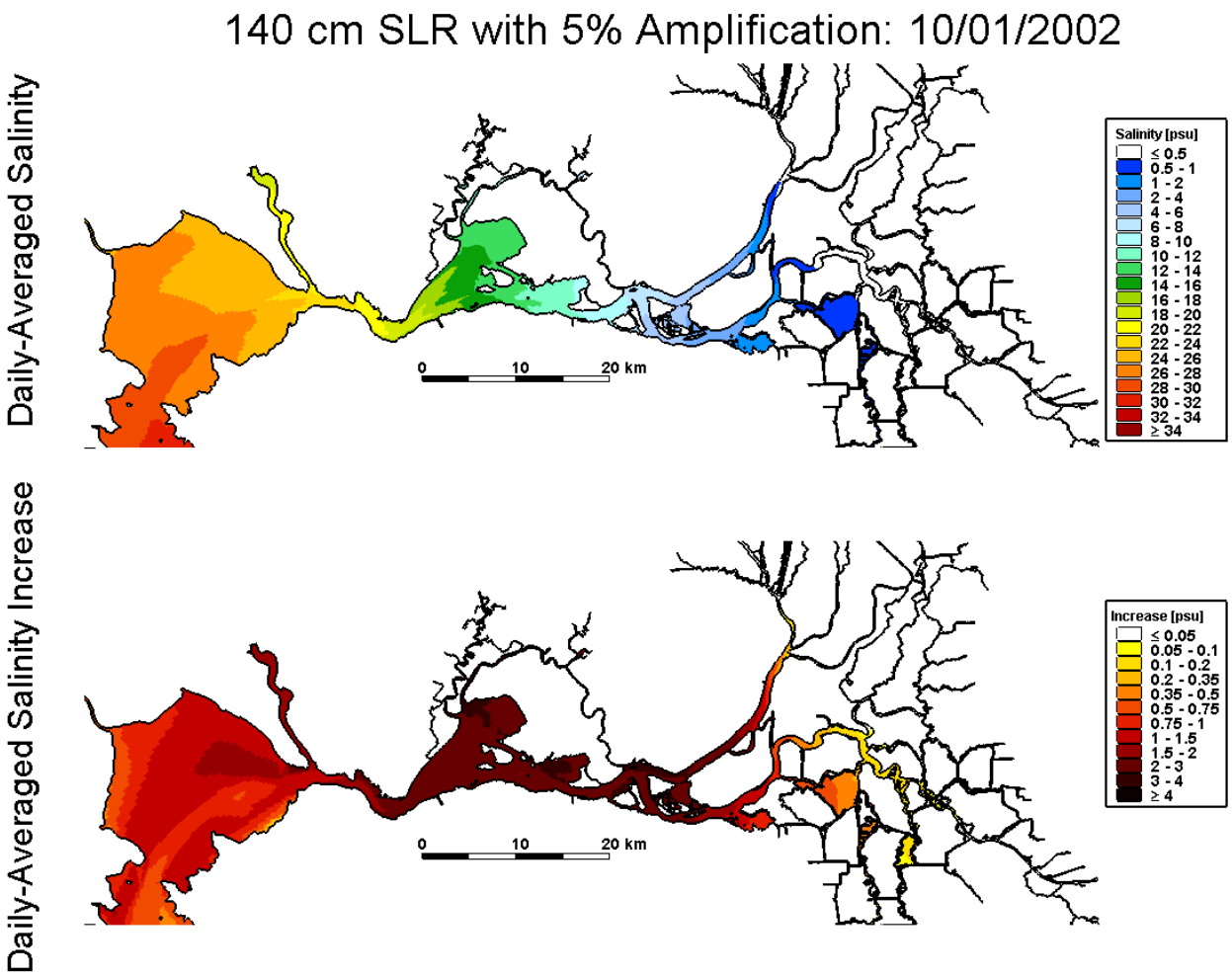

Figure 4.6-10 Predicted daily-averaged depth-average salinity on October 1, 2002 for the 140 cm SLR with 5% Amplification scenario (top); predicted increase in daily-averaged depth-average salinity on October 1, 2002 relative to the Baseline (0 cm SLR) scenario for the 140 cm SLR with 5% Amplification scenario.

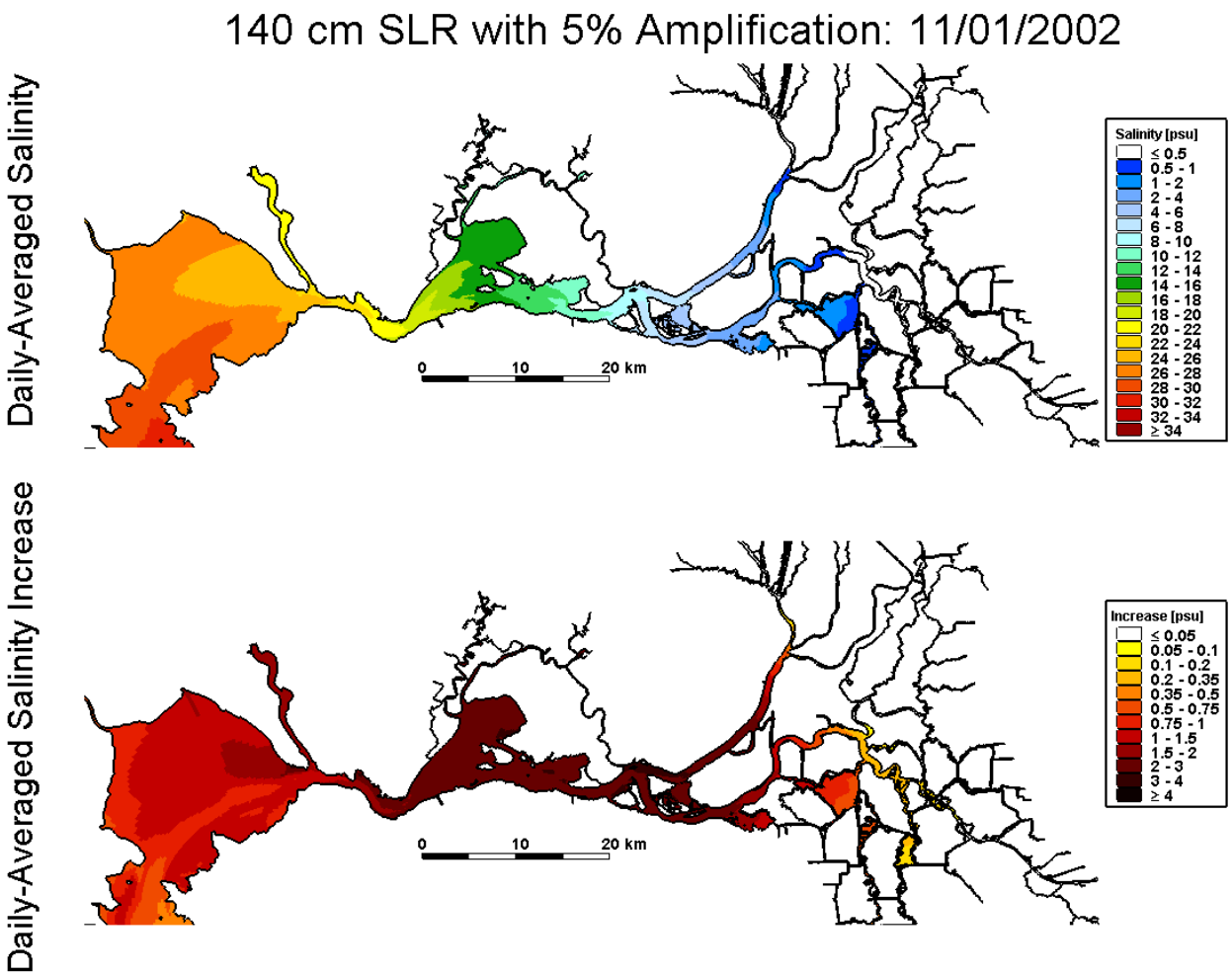

Figure 4.6-11 Predicted daily-averaged depth-average salinity on November 1, 2002 for the 140 cm SLR with 5% Amplification scenario (top); predicted increase in daily-averaged depth-average salinity on November 1, 2002 relative to the Baseline (0 cm SLR) scenario for the 140 cm SLR with 5% Amplification scenario.

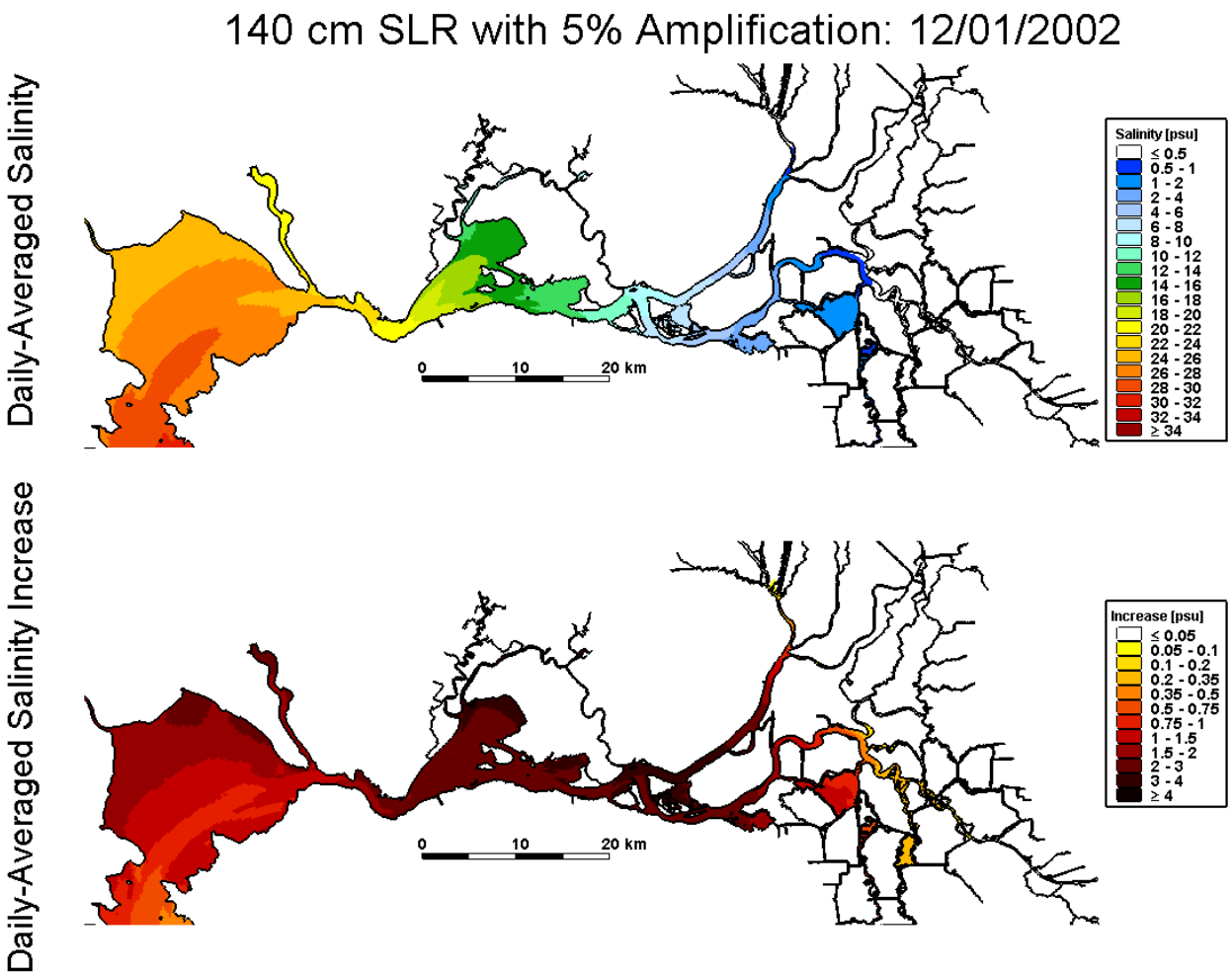

Figure 4.6-12 Predicted daily-averaged depth-average salinity on December 1, 2002 for the 140 cm SLR with 5% Amplification scenario (top); predicted increase in daily-averaged depth-average salinity on December 1, 2002 relative to the Baseline (0 cm SLR) scenario for the 140 cm SLR with 5% Amplification scenario.

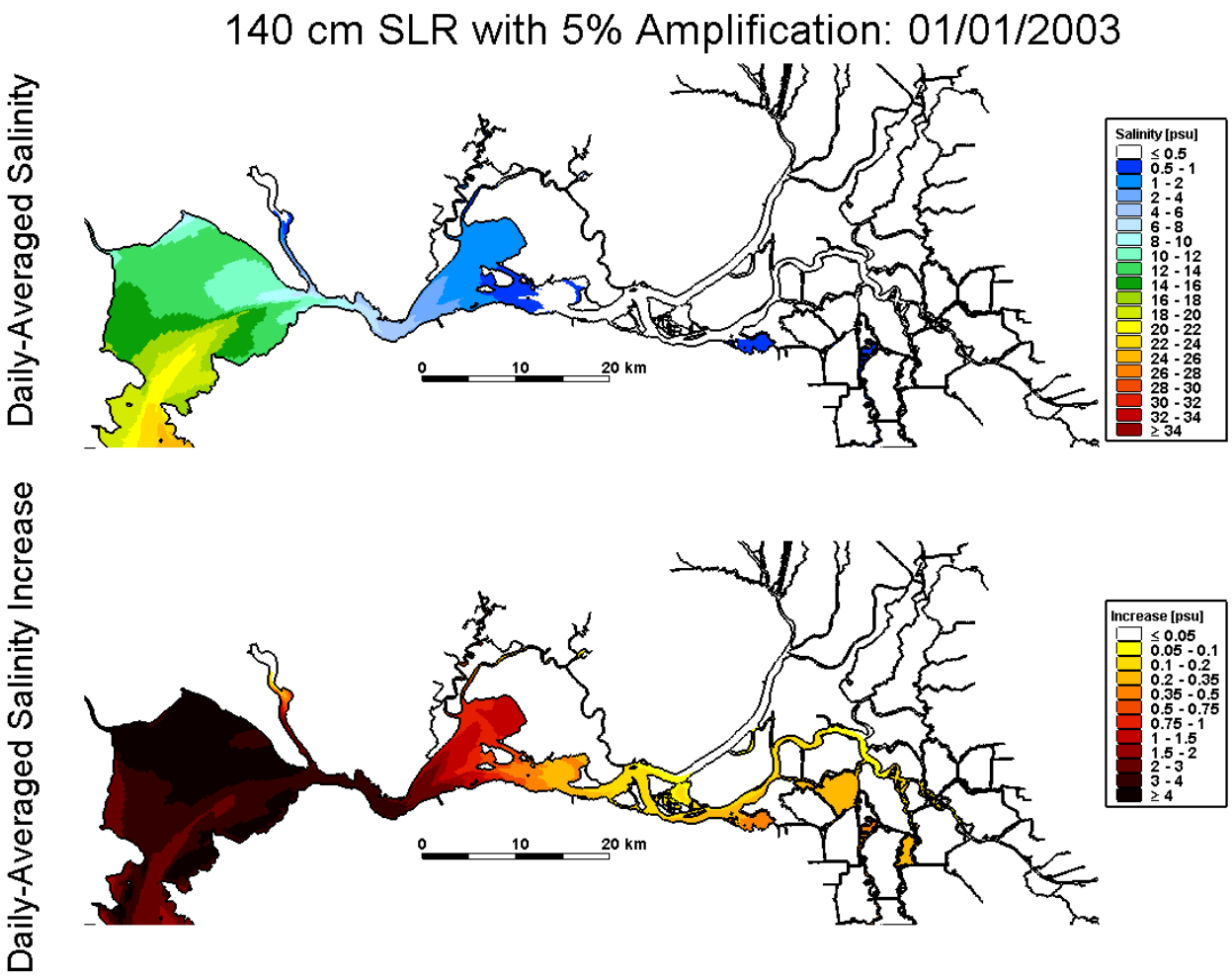

Figure 4.6-13 Predicted daily-averaged depth-average salinity on January 1, 2003 for the 140 cm SLR with 5% Amplification scenario (top); predicted increase in daily-averaged depth-average salinity on January 1, 2003 relative to the Baseline (0 cm SLR) scenario for the 140 cm SLR with 5% Amplification scenario.

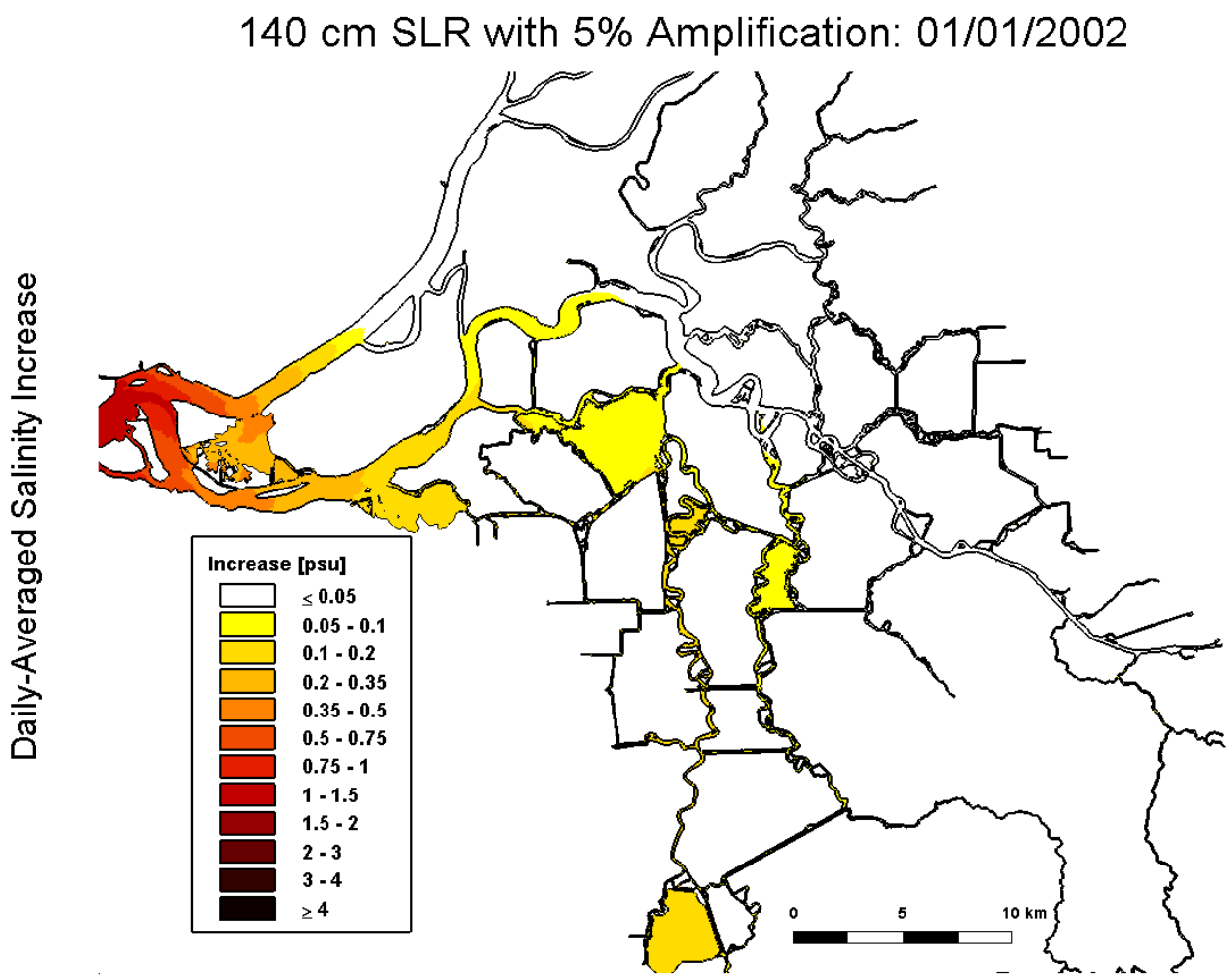

Figure 4.6-14 Predicted increase in daily-averaged depth-average salinity in the Sacramento-San Joaquin Delta on January 1, 2002 relative to the Baseline (0 cm SLR) scenario for the 140 cm SLR with 5% Amplification scenario.

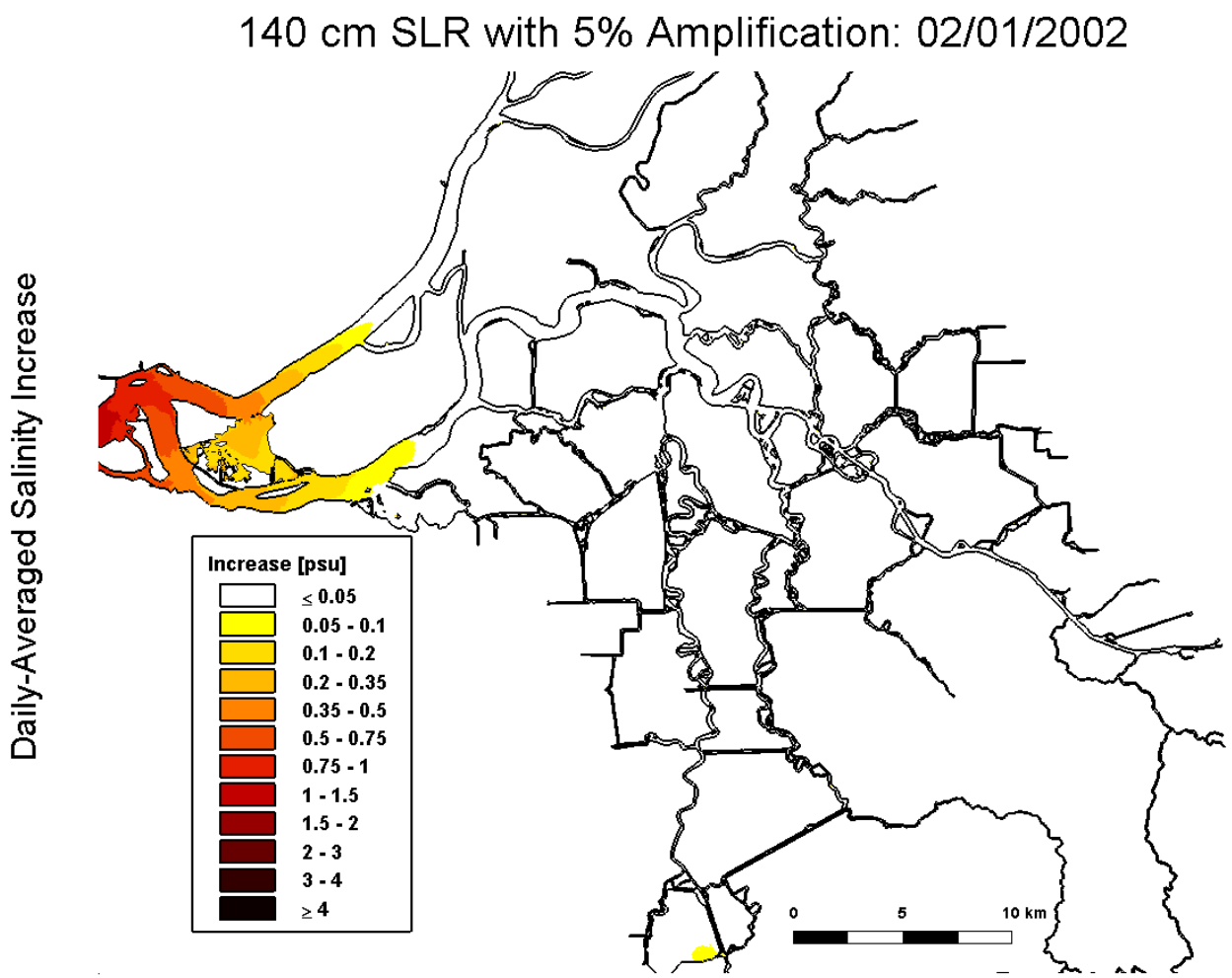

Figure 4.6-15 Predicted increase in daily-averaged depth-average salinity in the Sacramento-San Joaquin Delta on February 1, 2002 relative to the Baseline (0 cm SLR) scenario for the 140 cm SLR with 5% Amplification scenario.

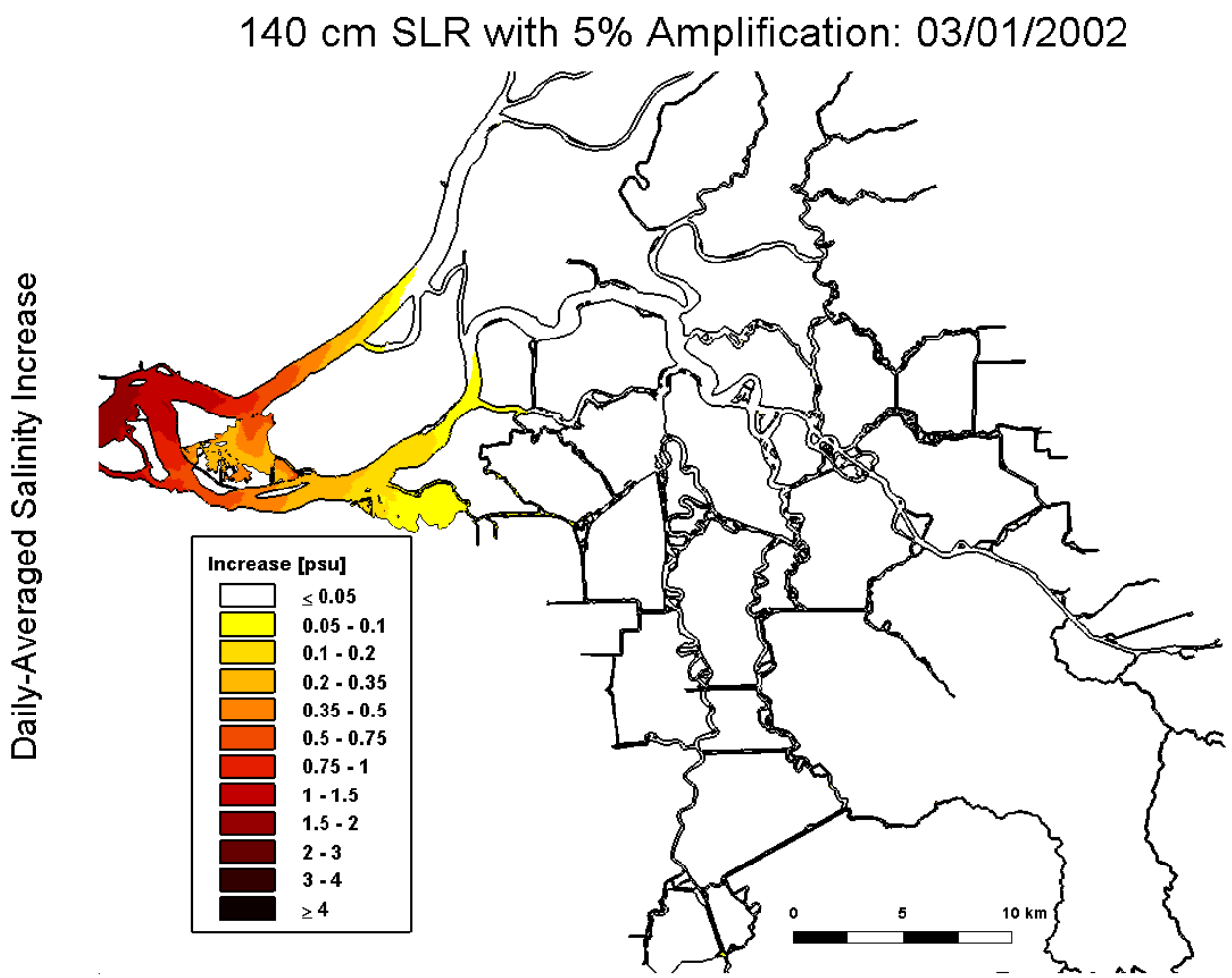

Figure 4.6-16 Predicted increase in daily-averaged depth-average salinity in the Sacramento-San Joaquin Delta on March 1, 2002 relative to the Baseline (0 cm SLR) scenario for the 140 cm SLR with 5% Amplification scenario.

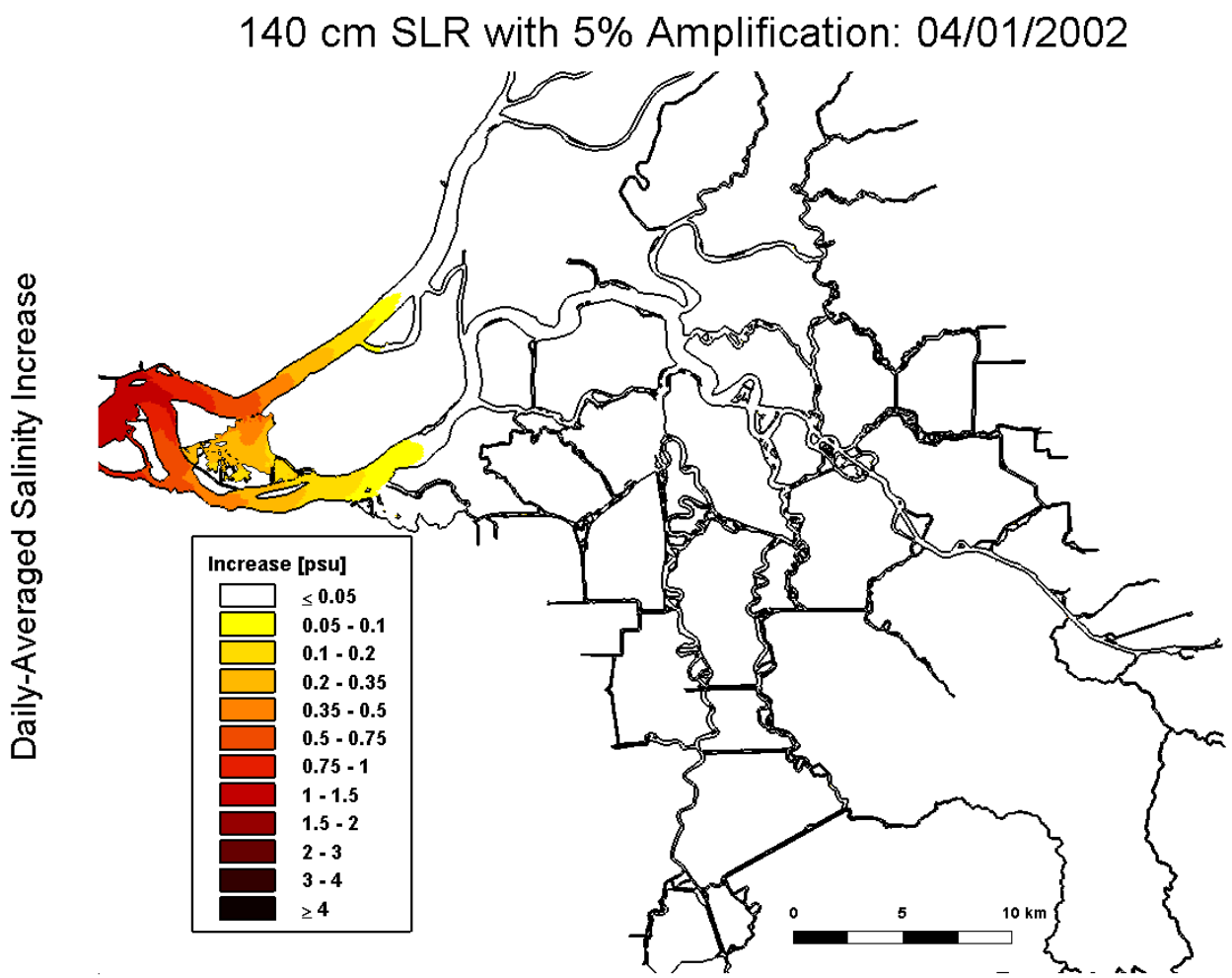

Figure 4.6-17 Predicted increase in daily-averaged depth-average salinity in the Sacramento-San Joaquin Delta on April 1, 2002 relative to the Baseline (0 cm SLR) scenario for the 140 cm SLR with 5% Amplification scenario.

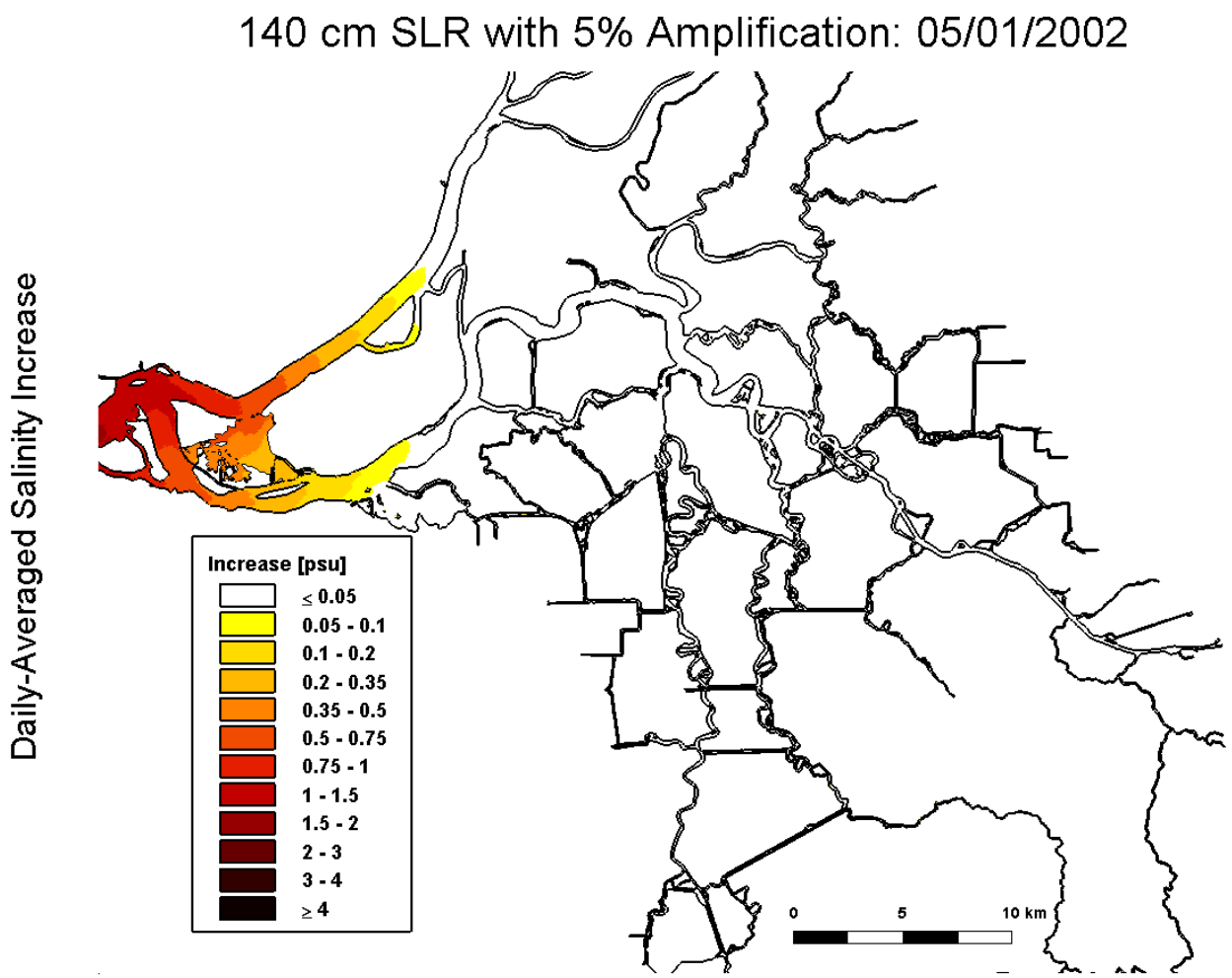

Figure 4.6-18 Predicted increase in daily-averaged depth-average salinity in the Sacramento-San Joaquin Delta on May 1, 2002 relative to the Baseline (0 cm SLR) scenario for the 140 cm SLR with 5% Amplification scenario.

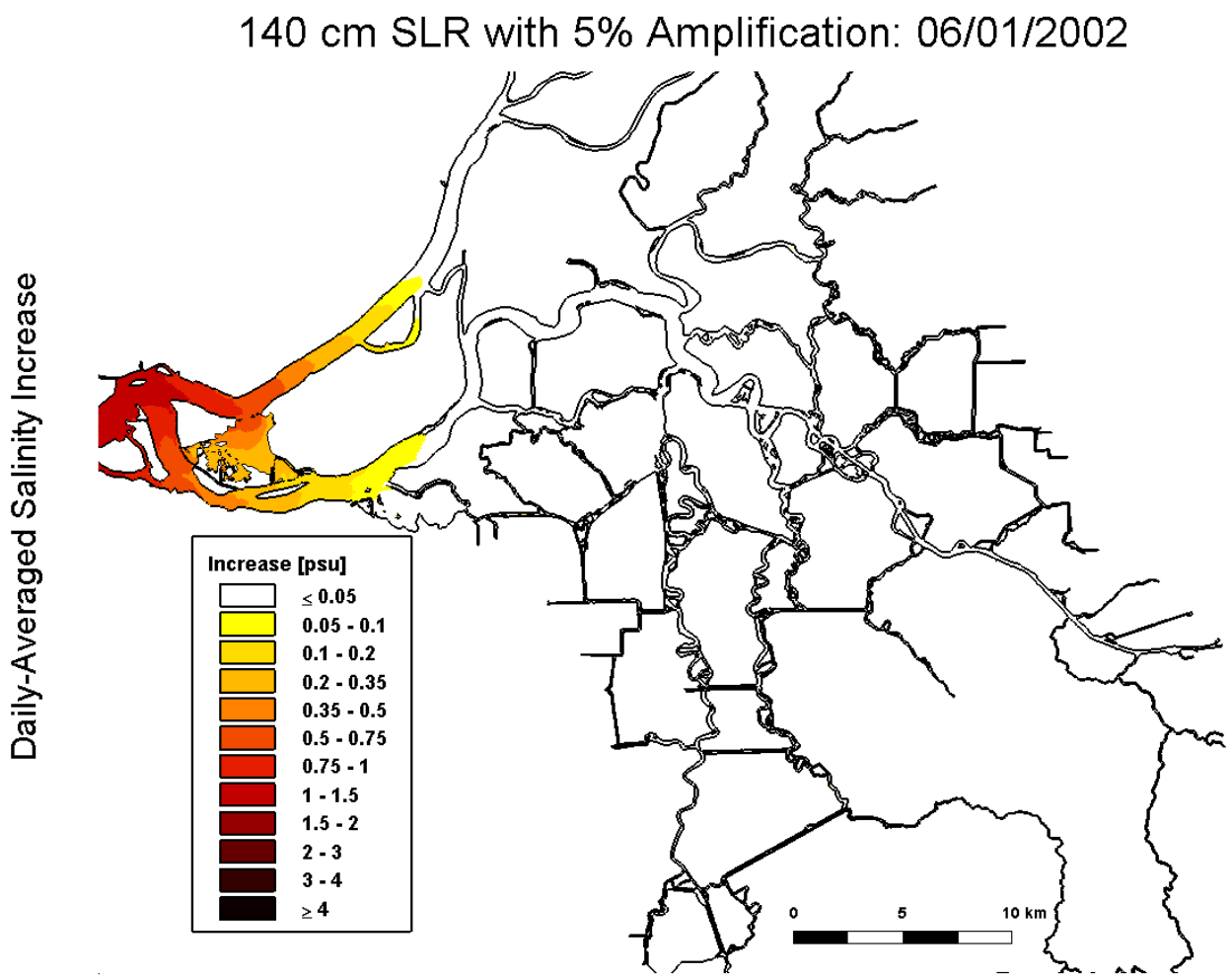

Figure 4.6-19 Predicted increase in daily-averaged depth-average salinity in the Sacramento-San Joaquin Delta on June 1, 2002 relative to the Baseline (0 cm SLR) scenario for the 140 cm SLR with 5% Amplification scenario.

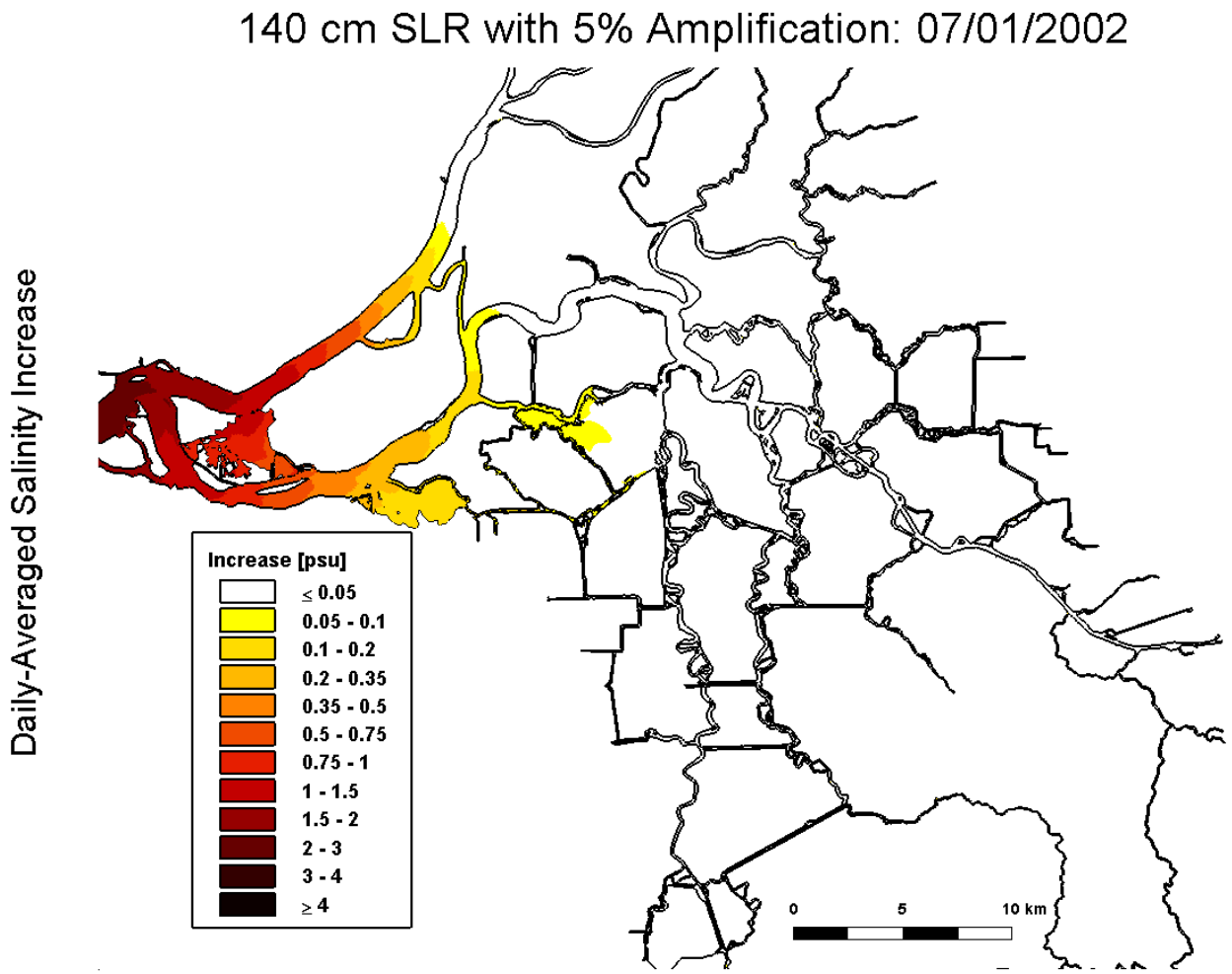

Figure 4.6-20 Predicted increase in daily-averaged depth-average salinity in the Sacramento-San Joaquin Delta on July 1, 2002 relative to the Baseline (0 cm SLR) scenario for the 140 cm SLR with 5% Amplification scenario.

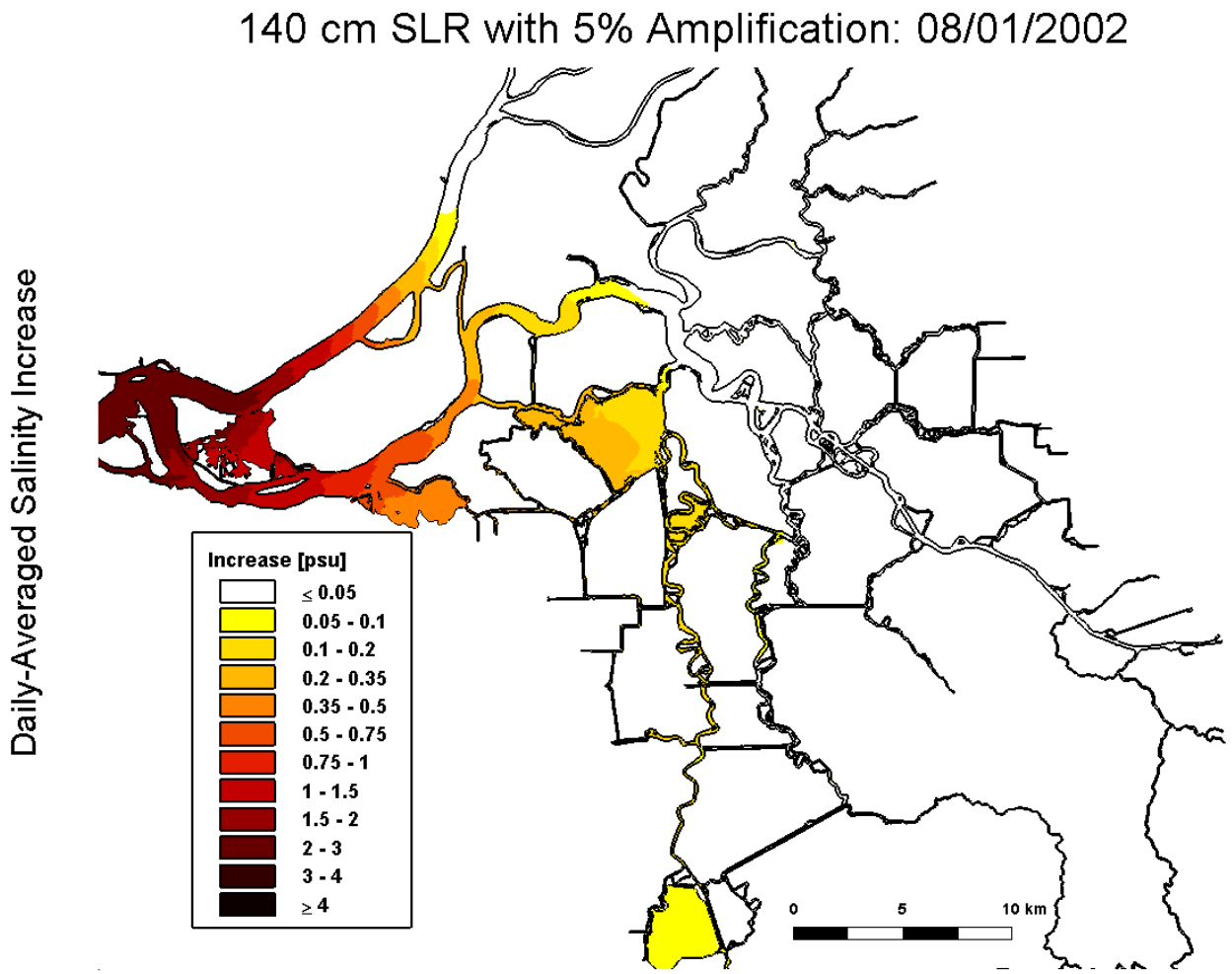

Figure 4.6-21 Predicted increase in daily-averaged depth-average salinity in the Sacramento-San Joaquin Delta on August 1, 2002 relative to the Baseline (0 cm SLR) scenario for the 140 cm SLR with 5% Amplification scenario.

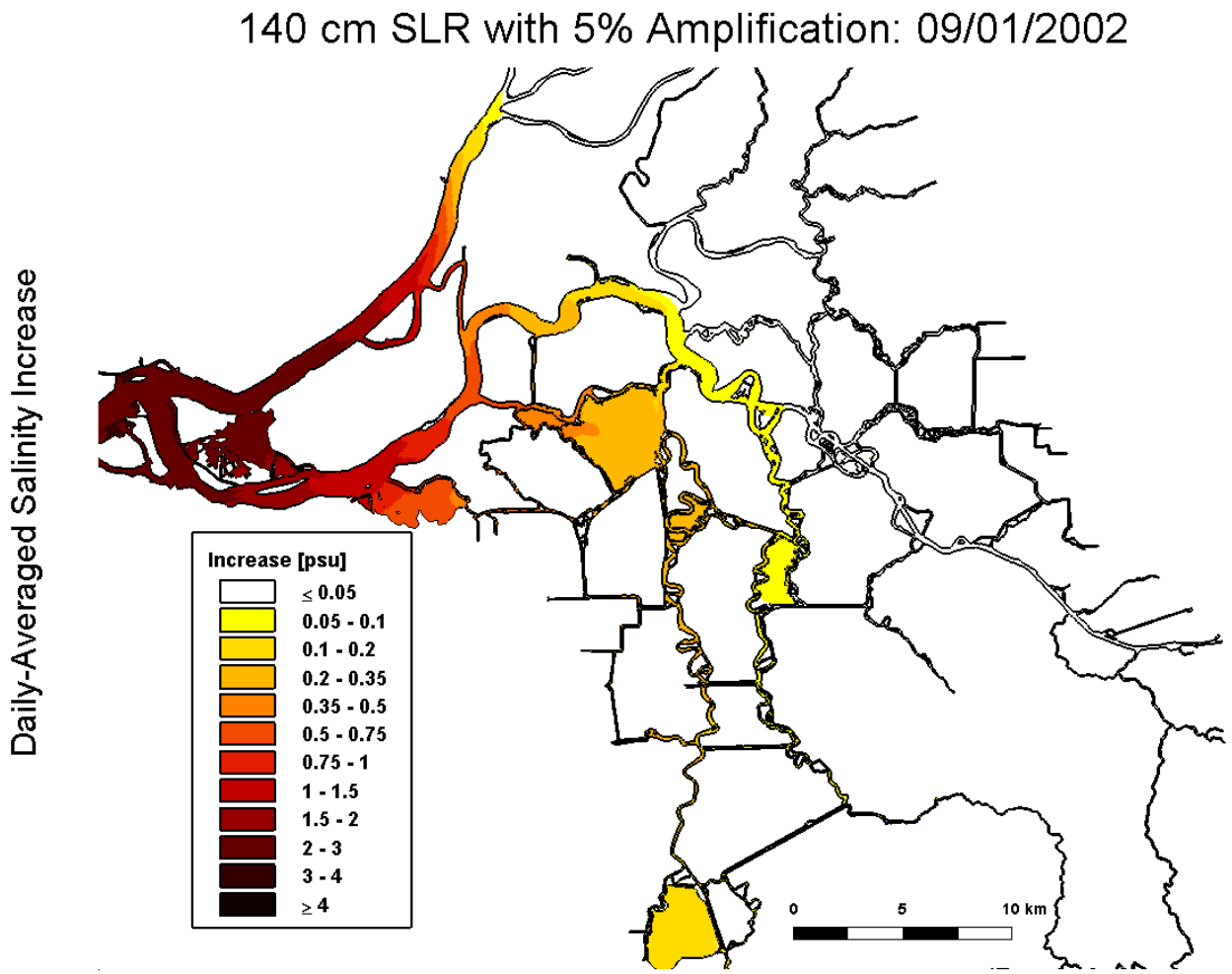

Figure 4.6-22 Predicted increase in daily-averaged depth-average salinity in the Sacramento-San Joaquin Delta on September 1, 2002 relative to the Baseline (0 cm SLR) scenario for the 140 cm SLR with 5% Amplification scenario.

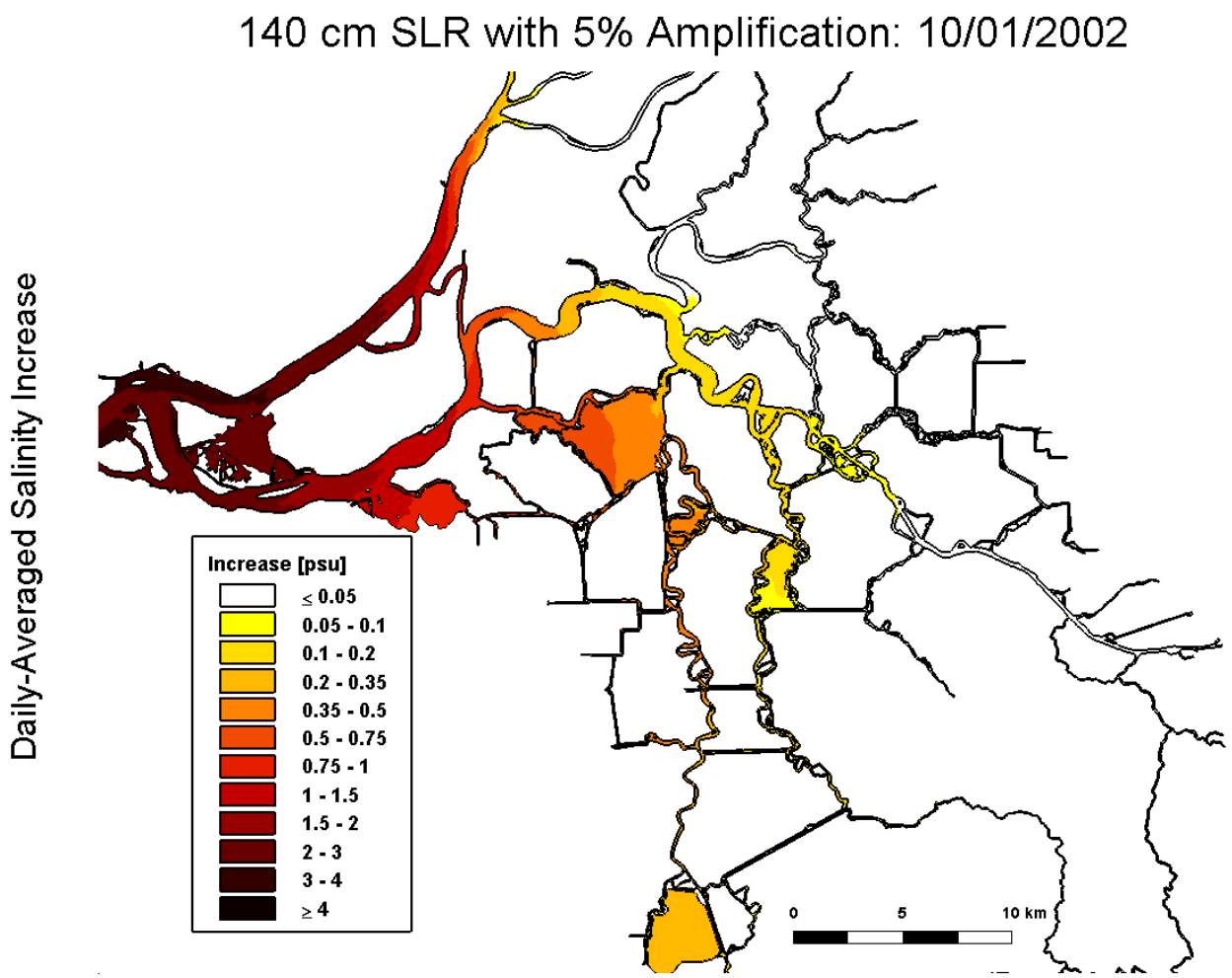

Figure 4.6-23 Predicted increase in daily-averaged depth-average salinity in the Sacramento-San Joaquin Delta on October 1, 2002 relative to the Baseline (0 cm SLR) scenario for the 140 cm SLR with 5% Amplification scenario.

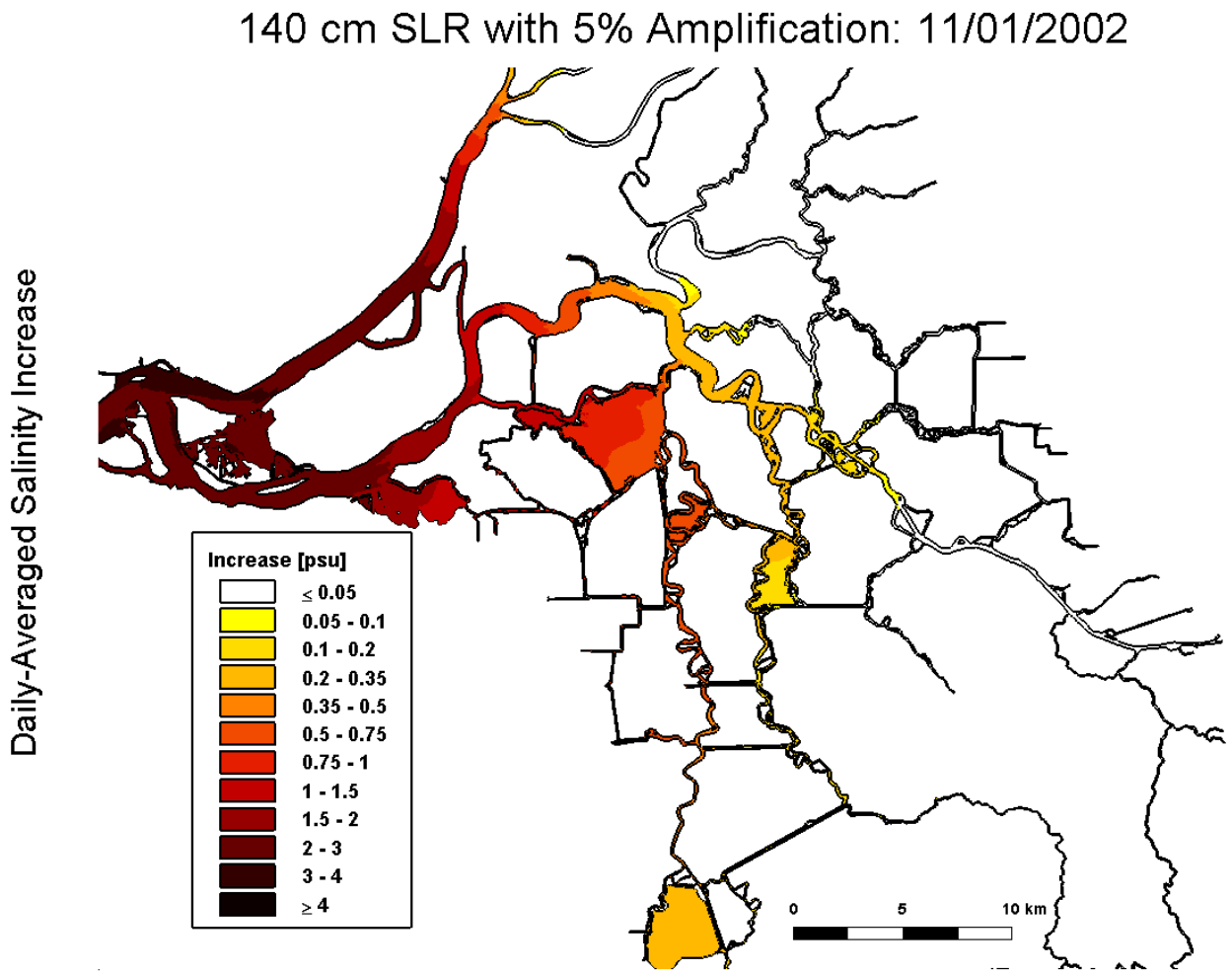

Figure 4.6-24 Predicted increase in daily-averaged depth-average salinity in the Sacramento-San Joaquin Delta on November 1, 2002 relative to the Baseline (0 cm SLR) scenario for the 140 cm SLR with 5% Amplification scenario.

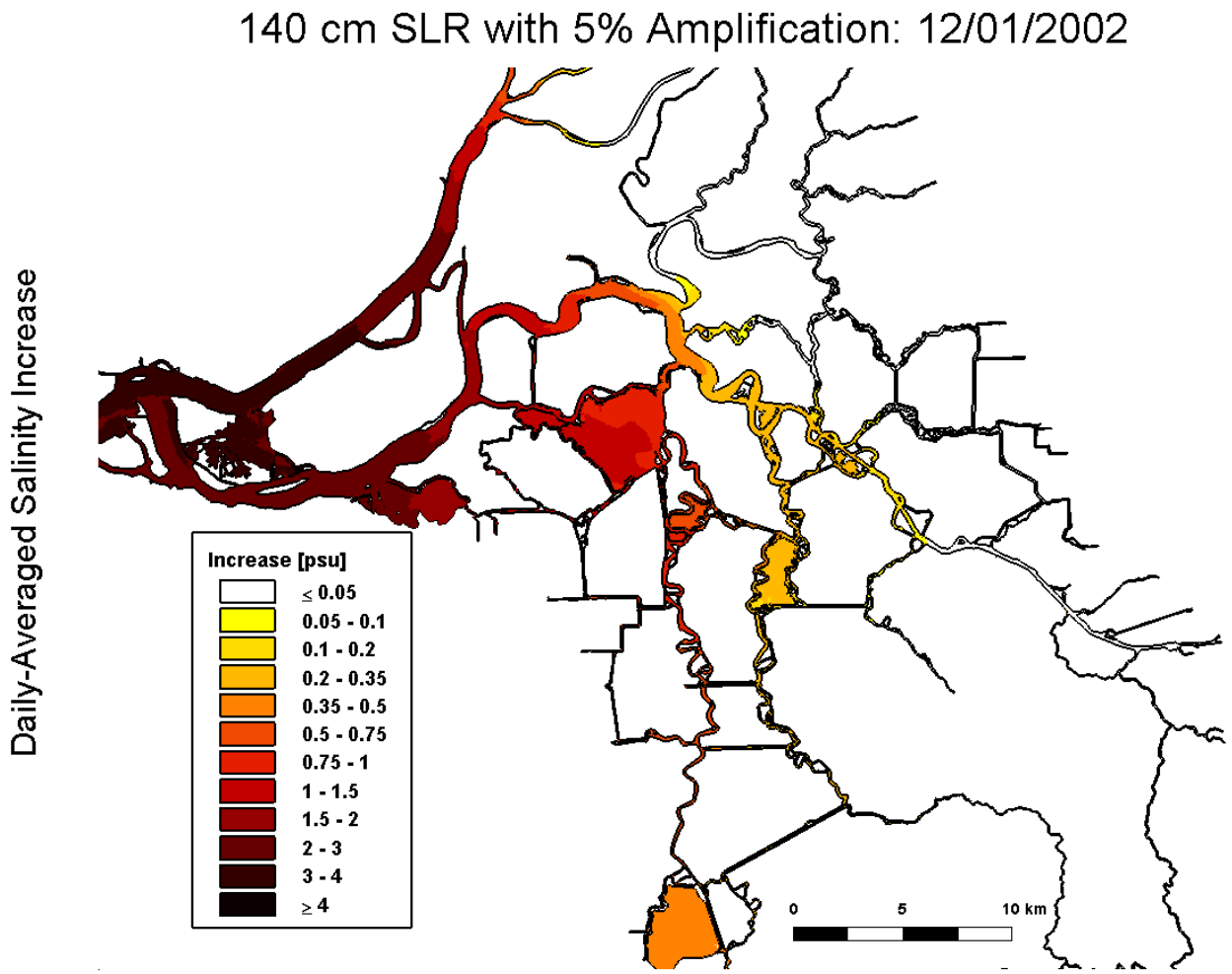

Figure 4.6-25 Predicted increase in daily-averaged depth-average salinity in the Sacramento-San Joaquin Delta on December 1, 2002 relative to the Baseline (0 cm SLR) scenario for the 140 cm SLR with 5% Amplification scenario.

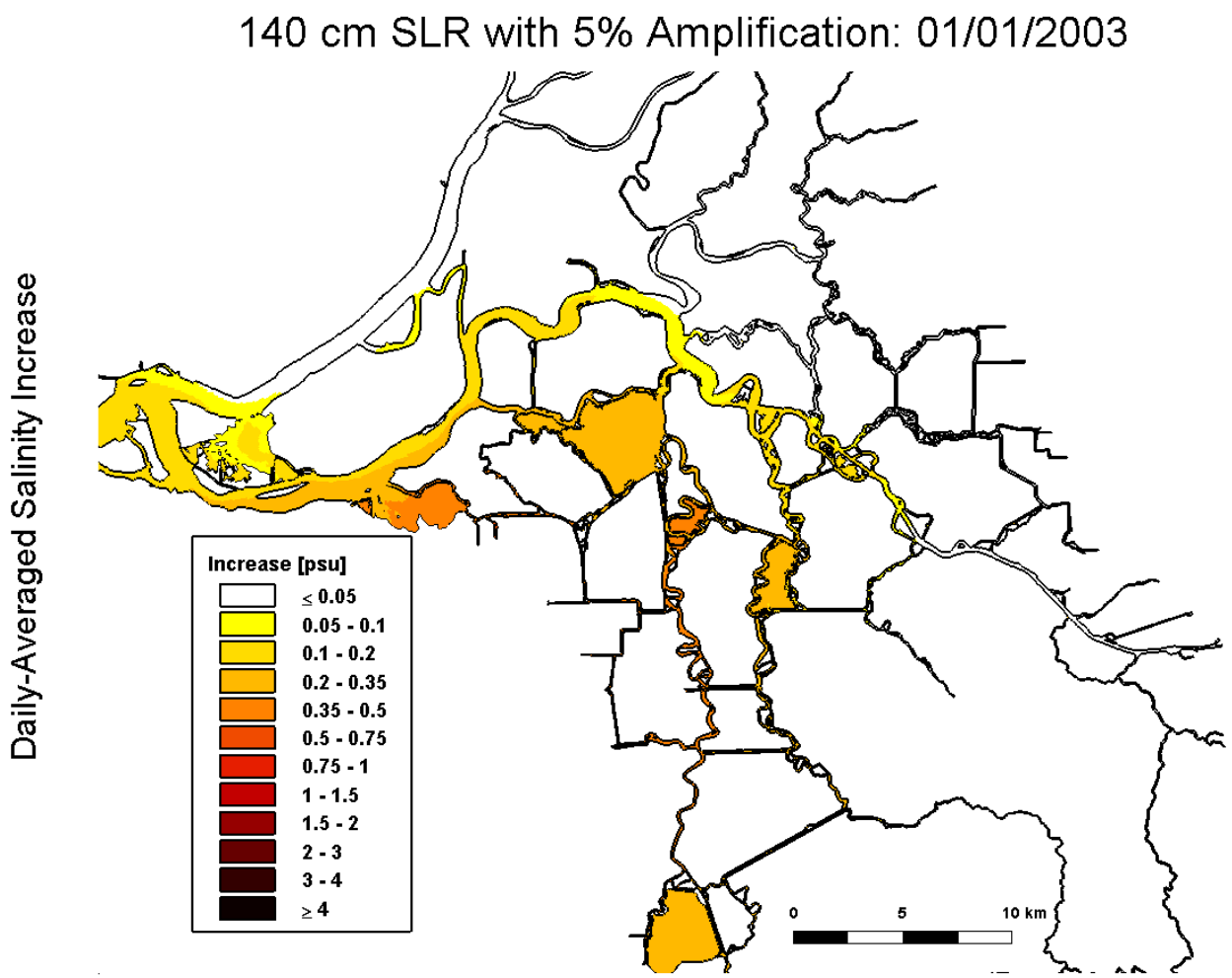

Figure 4.6-26 Predicted increase in daily-averaged depth-average salinity in the Sacramento-San Joaquin Delta on January 1, 2003 relative to the Baseline (0 cm SLR) scenario for the 140 cm SLR with 5% Amplification scenario.

4.7 Effect of Tidal Range Amplification on Daily-averaged Depth-average Salinity

This section evaluates the effect of the amplification of tidal range on daily-averaged depth-average salinity through the comparison of the predicted daily-averaged depth-average salinity for the 140 cm SLR scenario and the 140 cm SLR with 5% Amplification scenario.

The top panel of Figure 4.5-1 through Figure 4.5-13 shows the predicted daily-averaged depth-average salinity for the 140 cm SLR scenario on the first day of each month during the 2002 simulation period. The predicted daily-averaged depth-average salinity for the 140 cm SLR with 5% Amplification scenario on the first day of each month during the 2002 simulation period is shown on the top panel of Figure 4.6-1 through Figure 4.6-13. By subtracting the predicted depth-averaged salinity for the 140 cm SLR scenario from the predicted depth-averaged salinity from the 140 cm SLR with 5% Amplification scenario, the salinity increase resulting from the 5% amplification of tidal range can be computed. Figures 4.7-1 through 4.7-13 show the predicted increase in daily-averaged depth-average salinity for the140 cm SLR with 5% Amplification scenario relative to the 140 cm SLR scenario on the first day of each month during the 2002 simulation period. Note that the color scale shows only salinity increases and not salinity decreases.

On January 1, 2002 (Figure 4.7-1) salinity increases of between 0.05 and 0.2 psu are predicted in western San Pablo Bay and Central Bay. Salinity increases of between 0.05 and 0.10 psu are predicted in small regions of Suisun Bay. Following the high flows in January, smaller salinity increases are predicted on February 1, 2002 (Figure 4.7-2). Predicted salinity increases resulting from the tidal range amplification increase throughout the spring and summer. By June 1, 2002 (Figure 4.7-6), salinity increases of between 0.1 and 0.2 psu are predicted in most of Suisun Bay. By October 1, 2002 (Figure 4.7-10) and November 1, 2002 (Figure 4.7-11) salinity increases of between 0.05 and 0.10 psu extend upstream into Franks Tract and salinity increases of between 0.10 and 0.20 psu are predicted along the Sacramento River between Collinsville and Emmaton. Following the high flows in December, predicted salinity increases throughout the Delta are less than 0.05 psu on January 1, 2003 (Figure 4.7-13). The mechanisms responsible for the increased salt intrusion for the 140 cm SLR with 5% Amplification scenario relative to the 140 cm SLR scenario are discussed in Section 8.5.

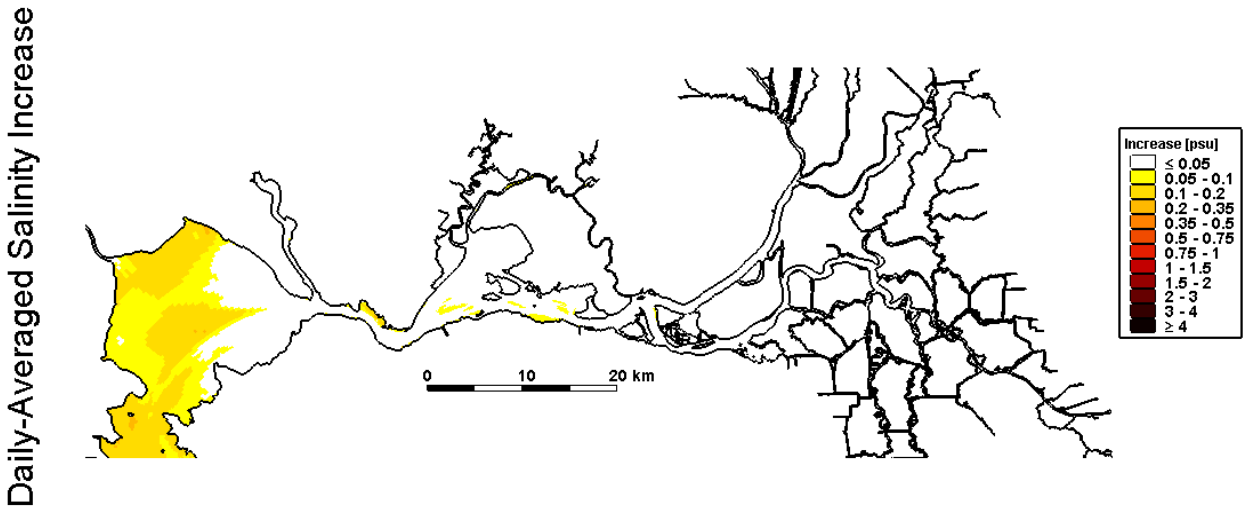

Figure 4.7-1 Predicted increase in daily-averaged depth-average salinity on January 1, 2002 for the 140 cm SLR with 5% Amplification scenario relative to the 140 cm SLR scenario.

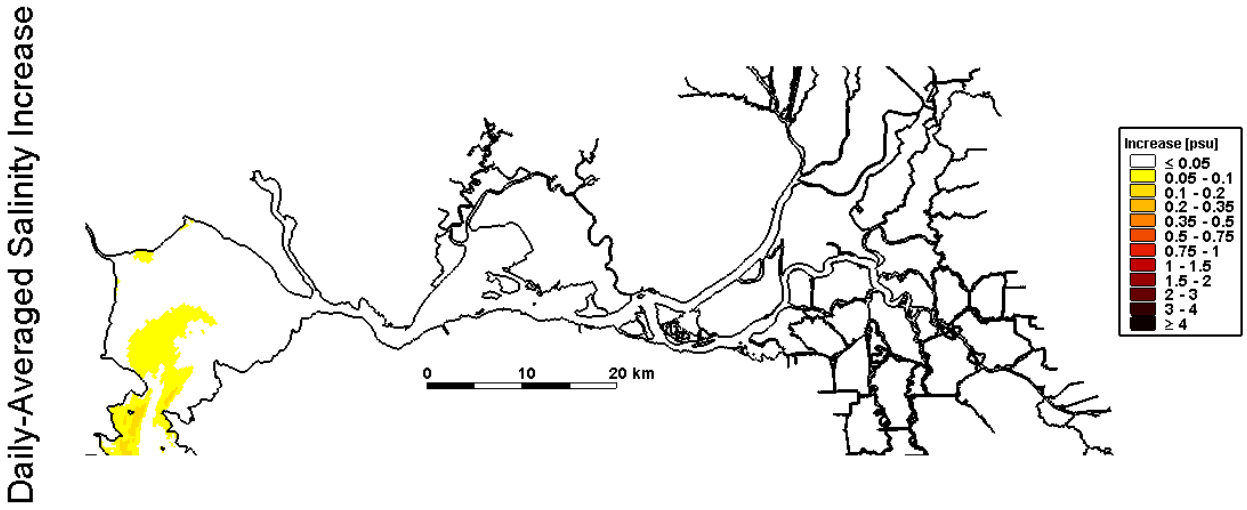

Figure 4.7-2 Predicted increase in daily-averaged depth-average salinity on February 1, 2002 for the 140 cm SLR with 5% Amplification scenario relative to the 140 cm SLR scenario.

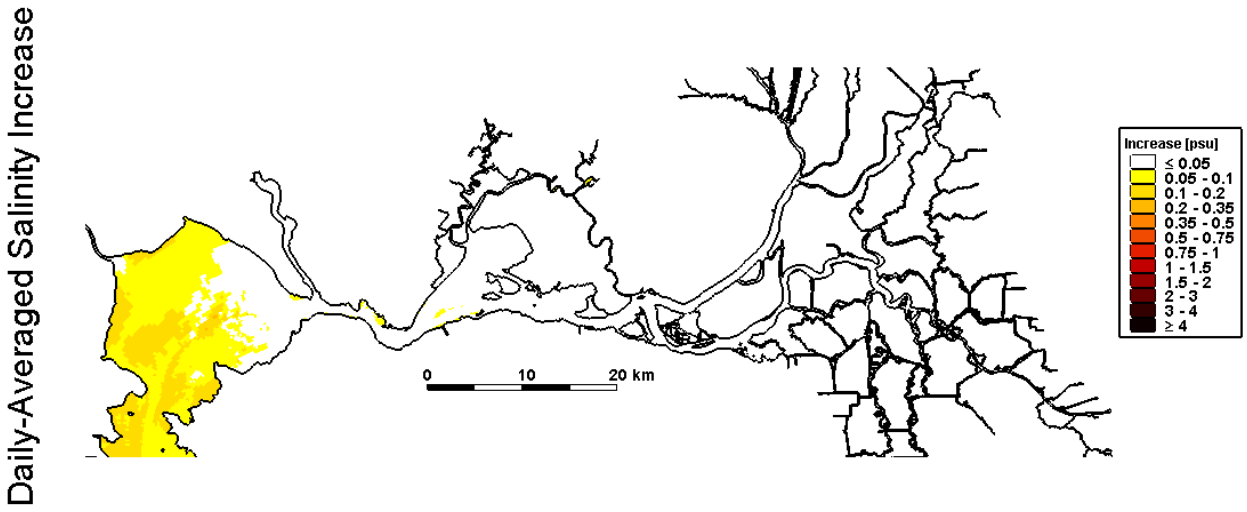

Figure 4.7-3 Predicted increase in daily-averaged depth-average salinity on March 1, 2002 for the 140 cm SLR with 5% Amplification scenario relative to the 140 cm SLR scenario.

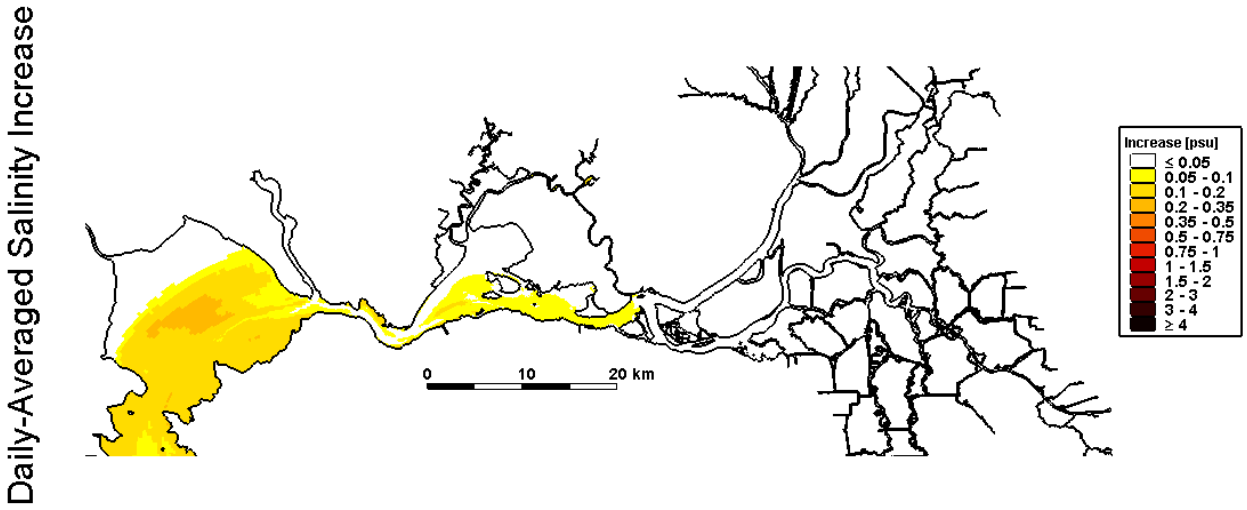

Figure 4.7-4 Predicted increase in daily-averaged depth-average salinity on April 1, 2002 for the 140 cm SLR with 5% Amplification scenario relative to the 140 cm SLR scenario.

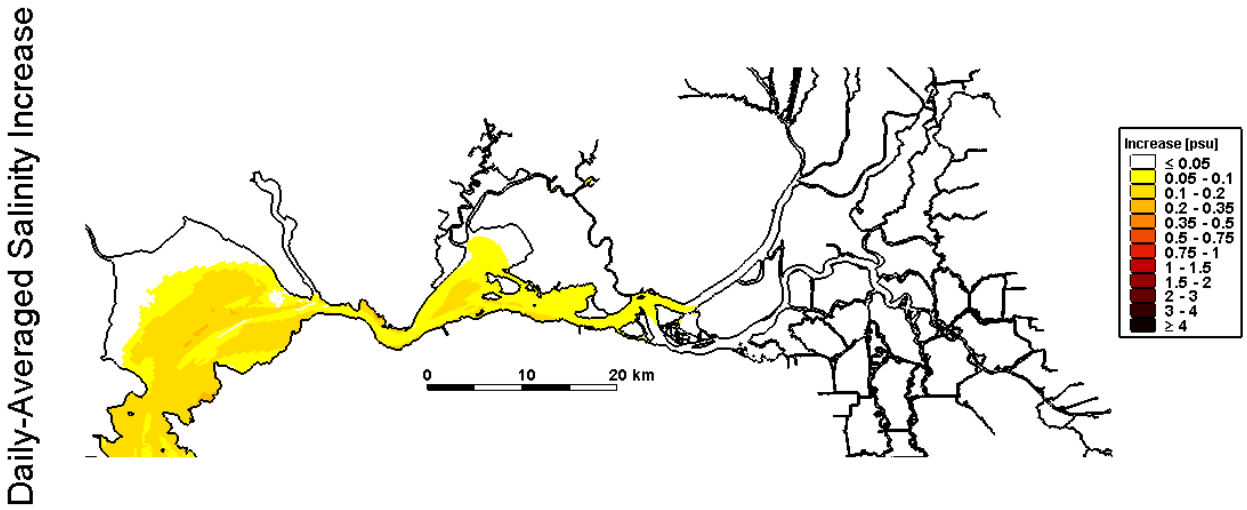

Figure 4.7-5 Predicted increase in daily-averaged depth-average salinity on May 1, 2002 for the 140 cm SLR with 5% Amplification scenario relative to the 140 cm SLR scenario.

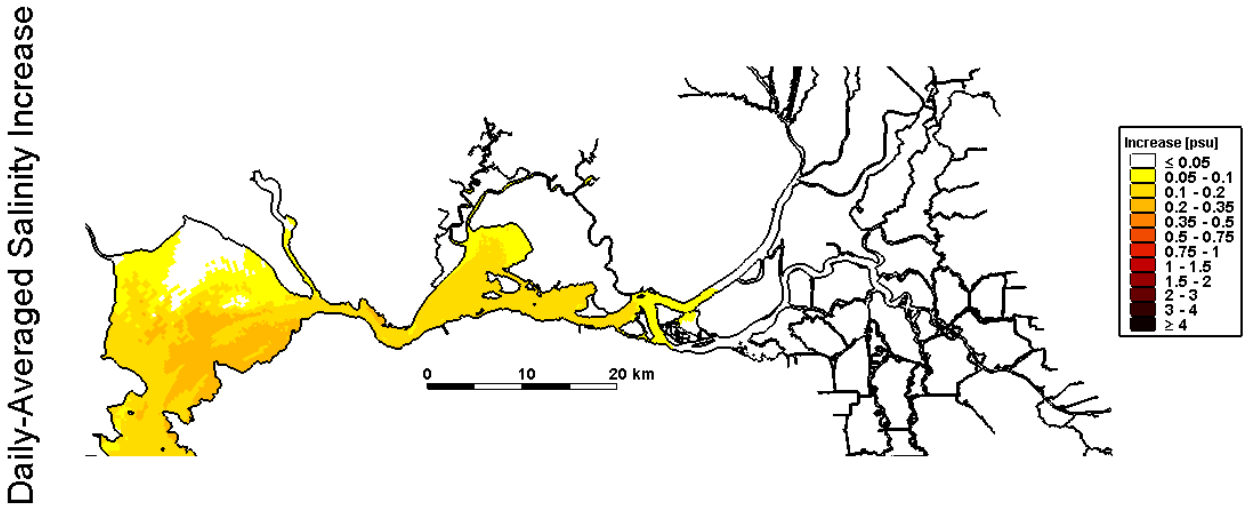

Figure 4.7-6 Predicted increase in daily-averaged depth-average salinity on June 1, 2002 for the 140 cm SLR with 5% Amplification scenario relative to the 140 cm SLR scenario.

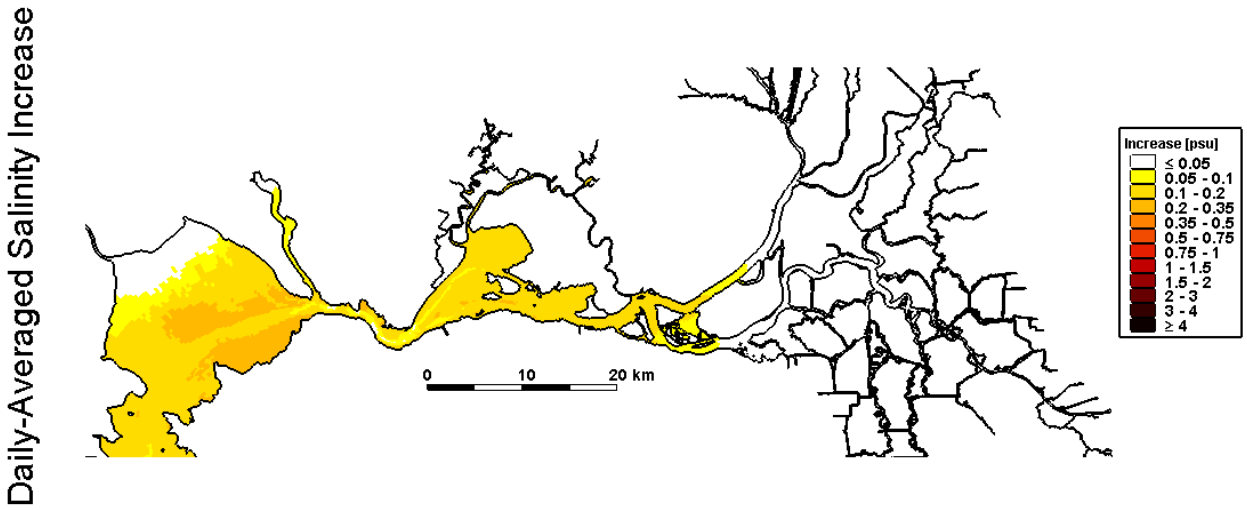

Figure 4.7-7 Predicted increase in daily-averaged depth-average salinity on July 1, 2002 for the 140 cm SLR with 5% Amplification scenario relative to the 140 cm SLR scenario.

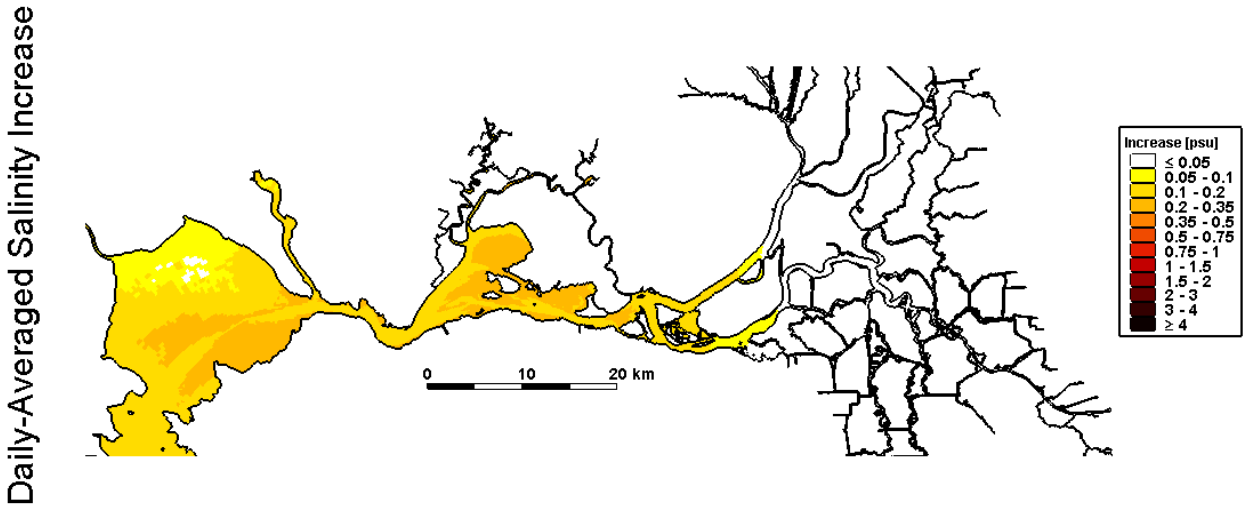

Figure 4.7-8 Predicted increase in daily-averaged depth-average salinity on August 1, 2002 for the 140 cm SLR with 5% Amplification scenario relative to the 140 cm SLR scenario.

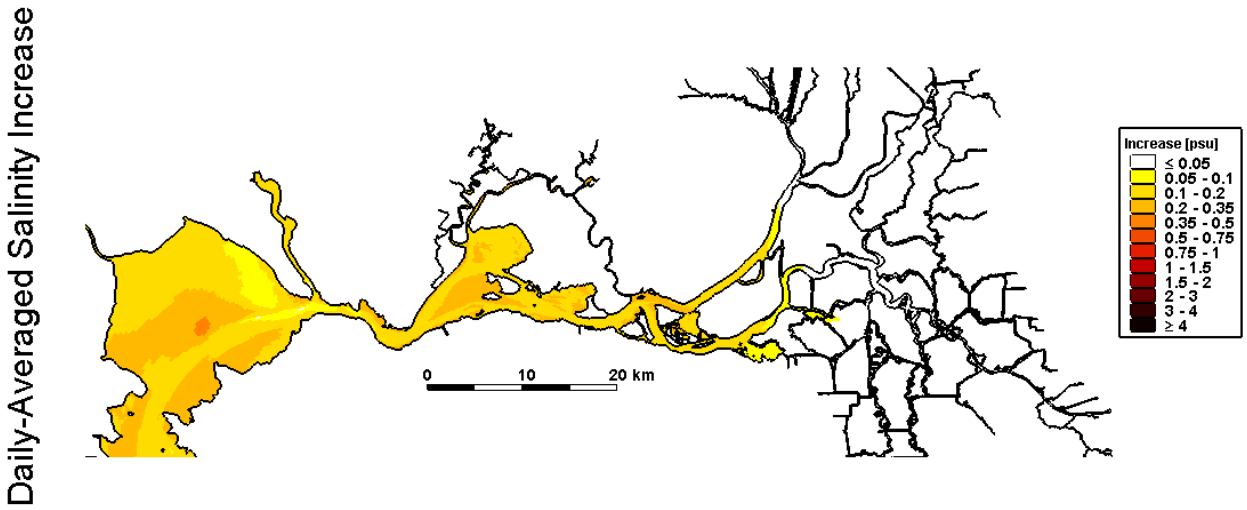

Figure 4.7-9 Predicted increase in daily-averaged depth-average salinity on September 1, 2002 for the 140 cm SLR with 5% Amplification scenario relative to the 140 cm SLR scenario.

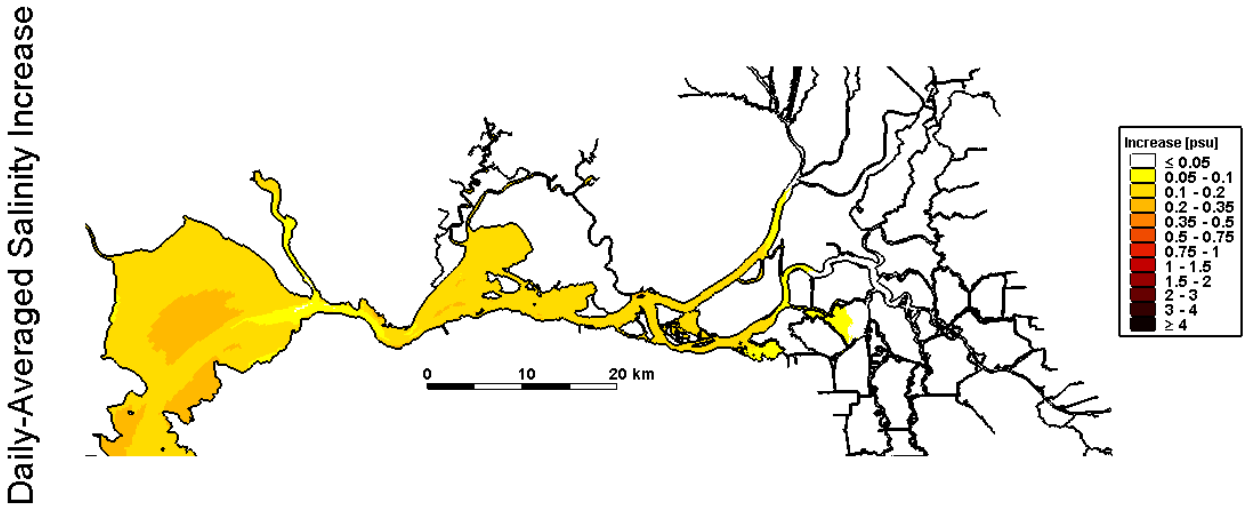

Figure 4.7-10 Predicted increase in daily-averaged depth-average salinity on October 1, 2002 for the 140 cm SLR with 5% Amplification scenario relative to the 140 cm SLR scenario.

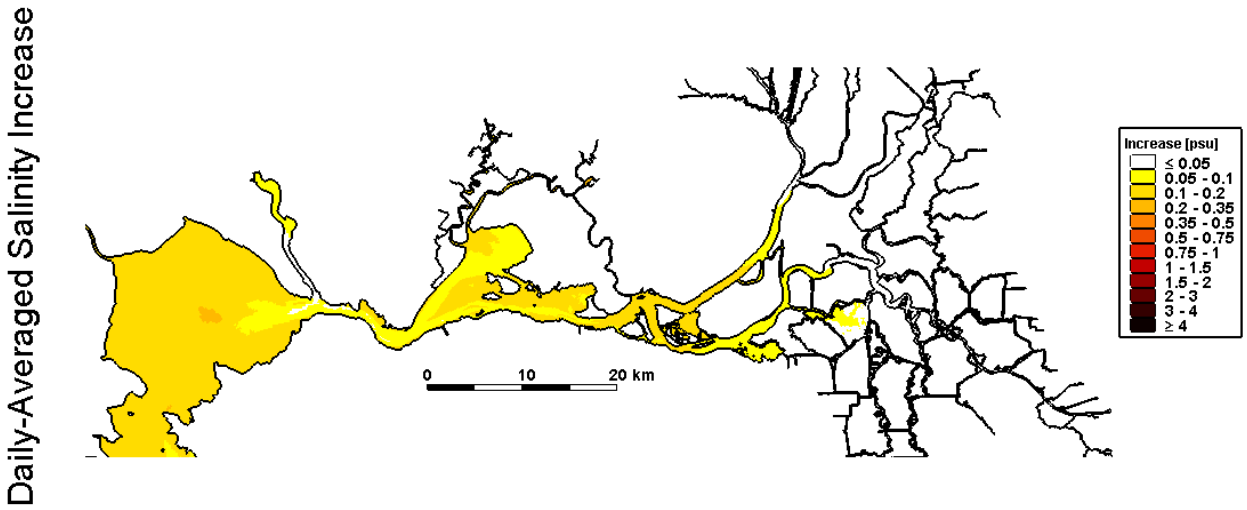

Figure 4.7-11 Predicted increase in daily-averaged depth-average salinity on November 1, 2002 for the 140 cm SLR with 5% Amplification scenario relative to the 140 cm SLR scenario.

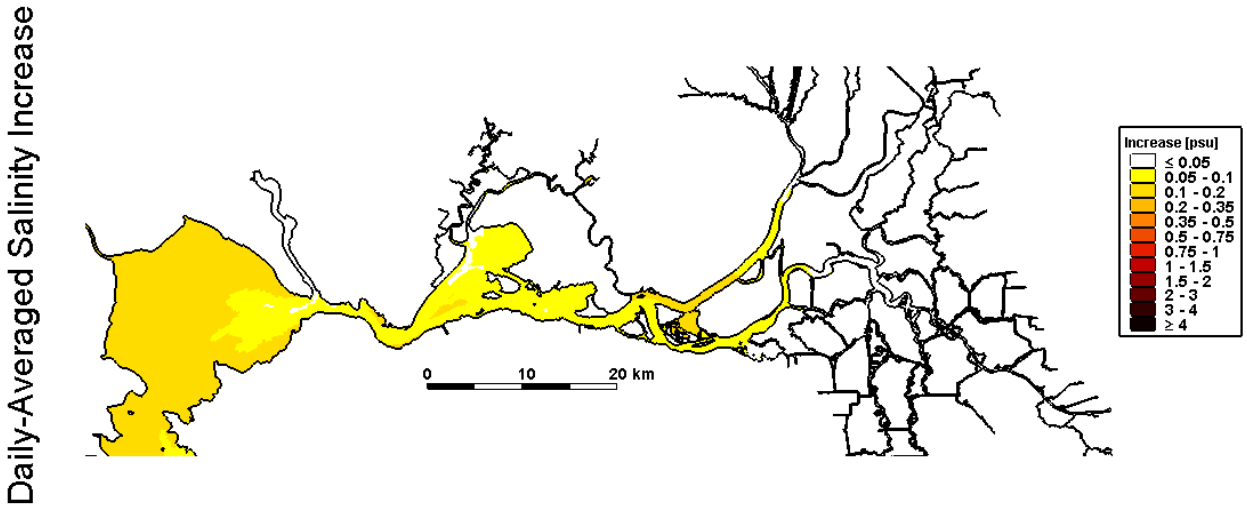

Figure 4.7-12 Predicted increase in daily-averaged depth-average salinity on December 1, 2002 for the 140 cm SLR with 5% Amplification scenario relative to the 140 cm SLR scenario.

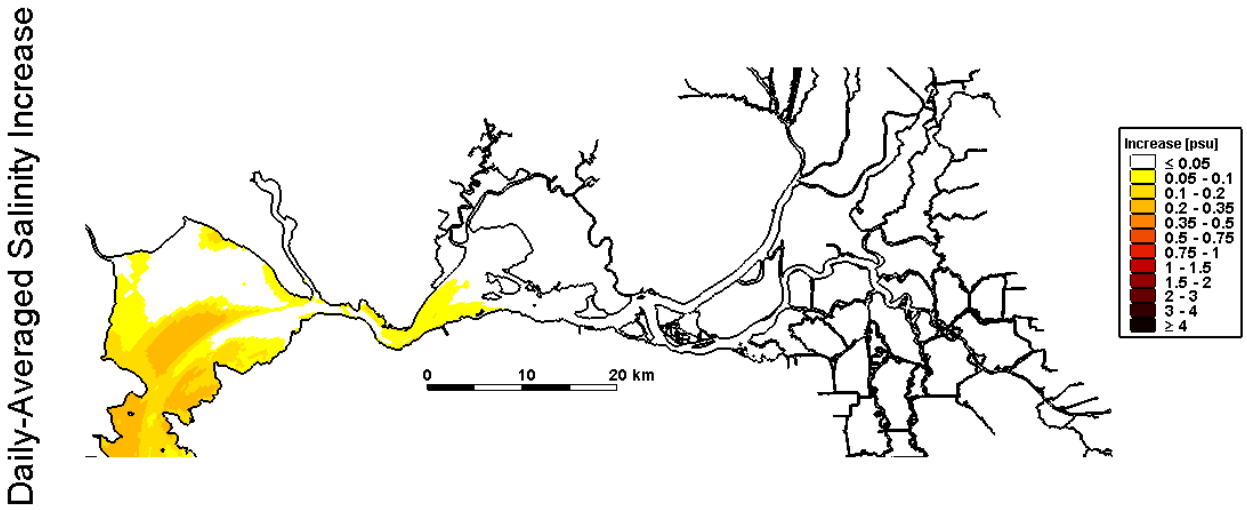

Figure 4.7-13 Predicted increase in daily-averaged depth-average salinity on January 1, 2003 for the 140 cm SLR with 5% Amplification scenario relative to the 140 cm SLR scenario.

5. Evaluation of Impact of Sea Level Rise on X2

5.1 X2 Comparison Approach

By definition X2 is the distance, in kilometers, from the Golden Gate to the tidally averaged near-bed 2 psu isohaline. The 1995 Bay-Delta agreement established standards for salinity in the estuary. Specifically, the standards determine the degree to which salinity is allowed to penetrate up-estuary, with salinity to be controlled through Delta outflow (IEP, 2009). This regulation is based on observations that the abundance or survival of several estuarine biological populations in the San Francisco Estuary is positively related to freshwater flow (Jassby et al. 1995), although recent studies suggest that some of these relationships have changed (Sommer et al. 2007).

As reported in the Water Rights Decision 1641 (D-1641; SWRCB, 2000), diversion by the USBR at Banks Pumping Plant is not authorized when the Delta is in excess conditions (excess conditions exist when upstream reservoir releases plus unregulated natural flow exceed Sacramento Valley in-basin uses, plus exports) and such diversion causes the location of X2 to shift upstream so far that:

> (a) It is east of Chipps Island (75 river kilometers upstream of the Golden Gate) during the months of February through May, or
>
> (b) It is east of Collinsville (81 kilometers upstream of the Golden Gate) during the months of January, June, July, and August, or
>
> (c) During December it is east of Collinsville and delta smelt are present at Contra Costa Water District's point of diversion under Permits 20749 and 20750 (Application 20245).

For the purposes of this standard, X2 is the most downstream location of either the maximum daily-average or the 14-day running average of the 2.64 mmhos/cm isohaline (SWRCB, 2000). Additional restrictions reported in D-1641 restrict CCWD from refilling Los Vaqueros Reservoir during the months of February through May if X2 is east of Chipps Island. In January, June, and August, CCWD is restricted from filling Los Vaqueros if X2 is east of Collinsville. Further restrictions apply in December if delta smelt are present at the intake on Old River and X2 is east of Collinsville (SWRCB, 2000).

Jassby et al. (1995) provide a graphical depiction of X2 locations (Figure 5.1-1), showing X2 distance measured from the Golden Gate. The inset figure shows an X2 of about 75 km at Chipps Island and 81 km at Collinsville. In the UnTRIM Bay-Delta model, X2 is calculated along the axis of the estuary along the transects shown in Figure 5.2-1. For X2 distances greater than 75 km, the distance from the Golden Gate to the location of 2 psu bottom salinity is measured along both the Sacramento and San Joaquin transects, and the reported predicted X2 is the average of the Sacramento and San Joaquin X2 distances.

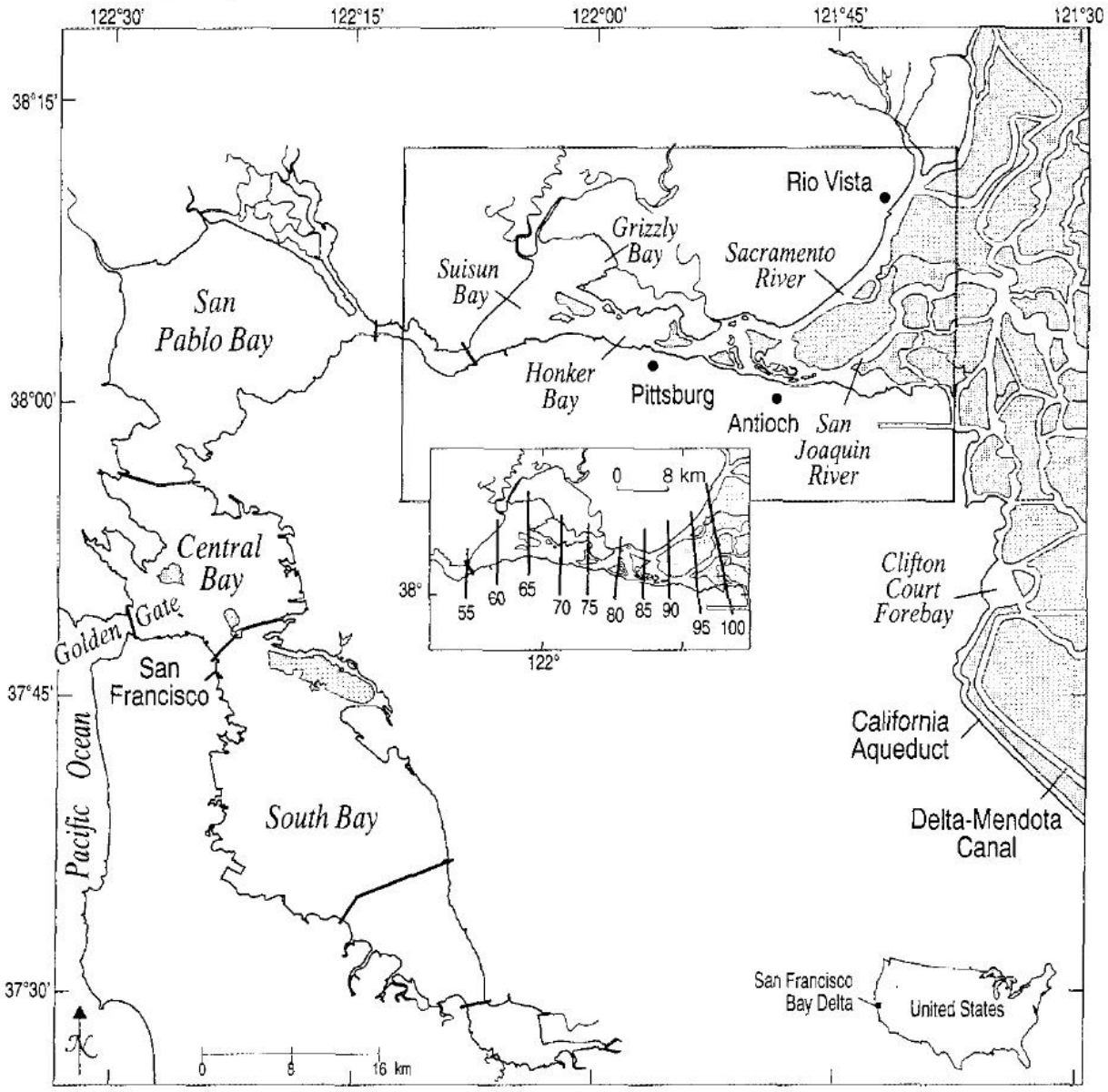

Figure 5.1-1 Map of San Francisco Bay and the Sacramento-San Joaquin Delta, with inset showing X2 locations in Suisun Bay and the western Delta (from Jassby et al., 1995).

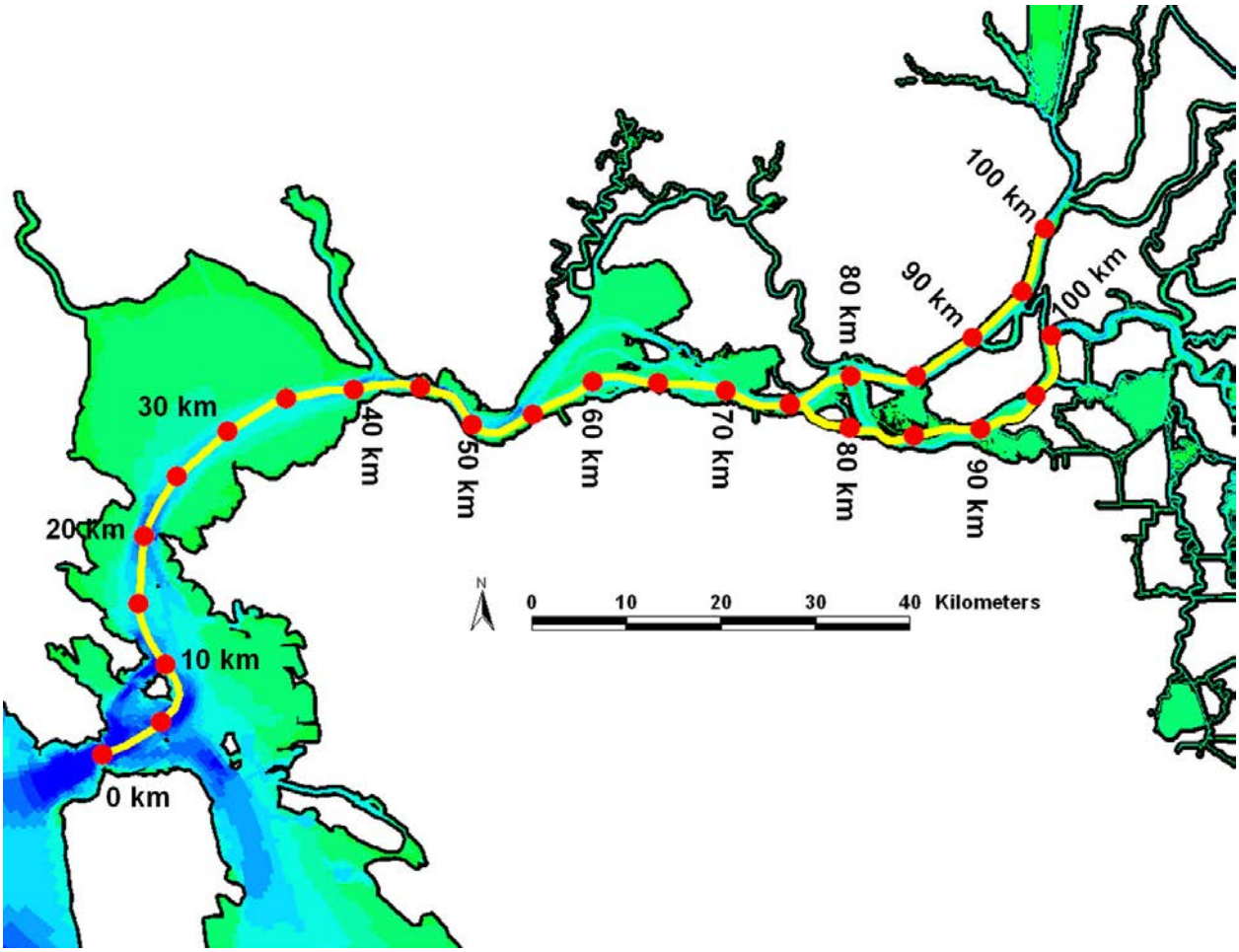

Figure 5.1-2 Transects along the axis of northern San Francisco Bay used to measure X2 in the UnTRIM Bay-Delta model.

5.2 X2 Comparison Results

Figure 5.2-1 shows the predicted X2 distance for the Baseline scenario, the 15 cm SLR scenario, the 30 cm SLR scenario, the 45 cm SLR scenario, the 60 cm SLR scenario, the 140 cm SLR scenario, and the 140 cm SLR with 5% Amplification scenario during the one-year analysis period. The lower panel of Figure 5.2-1 shows the predicted change in X2 relative to the Baseline scenario the 15 cm SLR scenario, the 30 cm SLR scenario, the 45 cm SLR scenario, the 60 cm SLR scenario, the 140 cm SLR scenario, and the 140 cm SLR with 5% Amplification scenario. Relative to the Baseline X2, all six of the sea level ruse scenarios show an increase in X2 throughout the year. For easier visual evaluation of the change in X2 for the SLR scenarios with 60 cm SLR or less, Figure 5.2-2 shows the predicted X2 distance for the Baseline scenario, the 15 cm SLR scenario, the 30 cm SLR scenario, the 45 cm SLR scenario, and the 60 cm SLR scenario.

For the 15 cm SLR scenario, an increase in X2 of between 0.5 km and 1 km is predicted throughout most of the year. X2 increases of up to 1.53 km are predicted in January and December during high flow periods. These increases in X2 indicate that the flushing flows become less efficient at pushing salt out of the estuary with increasing sea level rise. For the 30 cm SLR, an increase in X2 of between 1 km and 2 km is predicted throughout most of the year. X2 increases of up to 2.73 km are predicted in January and December during high flow periods. For the 45 cm SLR scenario, an increase in X2 of between 2 and 3 km is predicted throughout most of the year. The highest predicted increases in X2 occur in January and December during high flows, again indicating that the flushing flows become less efficient at pushing salt out of the estuary with increasing sea level rise. For the 60 cm SLR scenario, an increase in X2 of between 3 km and 4 km is predicted throughout most of the year. X2 increases of up to 4.99 km are predicted in January and December during high flow periods. For the 140 cm SLR scenario and the 140 cm SLR with 5% Amplification scenario, an increase in X2 of between 6 km and 8 km is predicted throughout most of the year. X2 increases of more than 11 km are predicted in January and December during high flow periods. These results show a relatively uniform increase in X2 throughout the year for each of the SLR scenarios, with the exception of the higher flow periods which tend to show the largest increases in X2.

Figure 5.2-3 shows the cumulative number of days during 2002 that the change in predicted X2 for the 15 cm SLR scenario, 30 cm SLR scenario, 45 cm SLR scenario, 60 cm SLR scenario, 140 cm SLR scenario, and 140 cm SLR with 5% Amplification scenario exceeds the corresponding X2 predicted under the Baseline scenario by a specific distance.

The maximum increase in X2 under the 15 cm SLR scenario is 1.53 km and the median predicted change in X2 under the 15 cm SLR scenario is 0.69 km. The median predicted change in X2 indicates that for 182 days during 2002 under the 15 cm SLR scenario the predicted change in average X2 is more than 0.69 km, whereas for 182 days the predicted change in average X2 under the 15 cm SLR scenario is less than 0.69 km. The maximum increase in X2 under the 30 cm SLR scenario is 2.73 km and the median predicted change in X2 under the 30 cm SLR scenario is 1.39 km. The maximum increase in X2 under the 45 cm SLR scenario is 4.00 km and the median predicted change in X2 under the 45 cm SLR scenario is 2.12 km. The maximum increase in X2 under the 60 cm SLR scenario is 4.99 km and the median predicted

change in X2 under the 60 cm SLR scenario is 2.91 km. The maximum increase in X2 under the 140 cm SLR scenario is 11.31 km and the median predicted change in X2 under the 140 cm SLR scenario is 7.03 km. The maximum increase in X2 under the 140 cm SLR with 5% Amplification scenario is 11.64 km and the median predicted change in X2 under the 140 cm SLR with 5% Amplification scenario is 7.32 km. The median and maximum increase in X2 for each of the sea level rise scenarios during 2002 is summarized in Table 5-1.

Figure 5.4-4 shows a scatter plot of the predicted increase in X2 for each day during 2002 for each of the sea level rise scenarios. The median increase and maximum increase are also plotted for each scenario. Both the median and the maximum increase in X2 lines show a nearly linear slope as a function of sea level rise, however the maximum increase has a steeper slope than the median increase.

Table 5-1 Median predicted increase in X2 and maximum predicted increase in X2 during the 2002 simulation period for each SLR scenario.

Scenario Name	**Median Increase in X2 [km]**	**Max Increase in X2 [km]**
15 cm SLR	0.69	1.53
30 cm SLR	1.39	2.73
45 cm SLR	2.12	4.00
60 cm SLR	2.91	4.99
140 cm SLR	7.03	11.31
140 cm SLR with 5% Amp	7.32	11.64

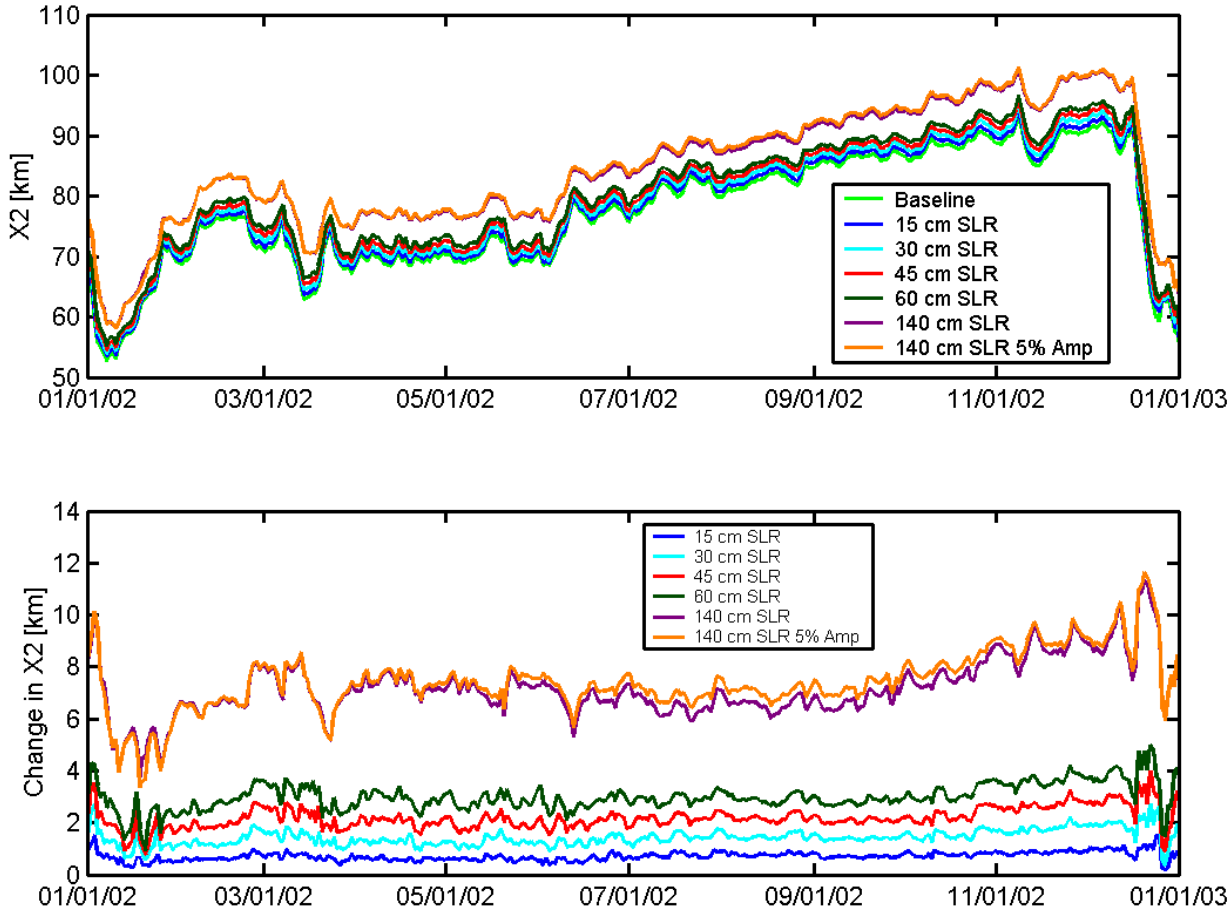

Figure 5.2-1 Predicted X2 for Baseline (0 cm SLR) scenario, 15 cm SLR scenario, 30 cm SLR scenario, 45 cm SLR scenario, 60 cm SLR scenario, 140 cm SLR scenario, and 140 cm SLR with 5% Amplification scenario (top); Predicted change in X2 relative to Baseline scenario for 15 cm SLR scenario, 30 cm SLR scenario, 45 cm SLR scenario, 60 cm SLR scenario, 140 cm SLR scenario, and 140 cm SLR with 5% Amplification scenario (bottom).

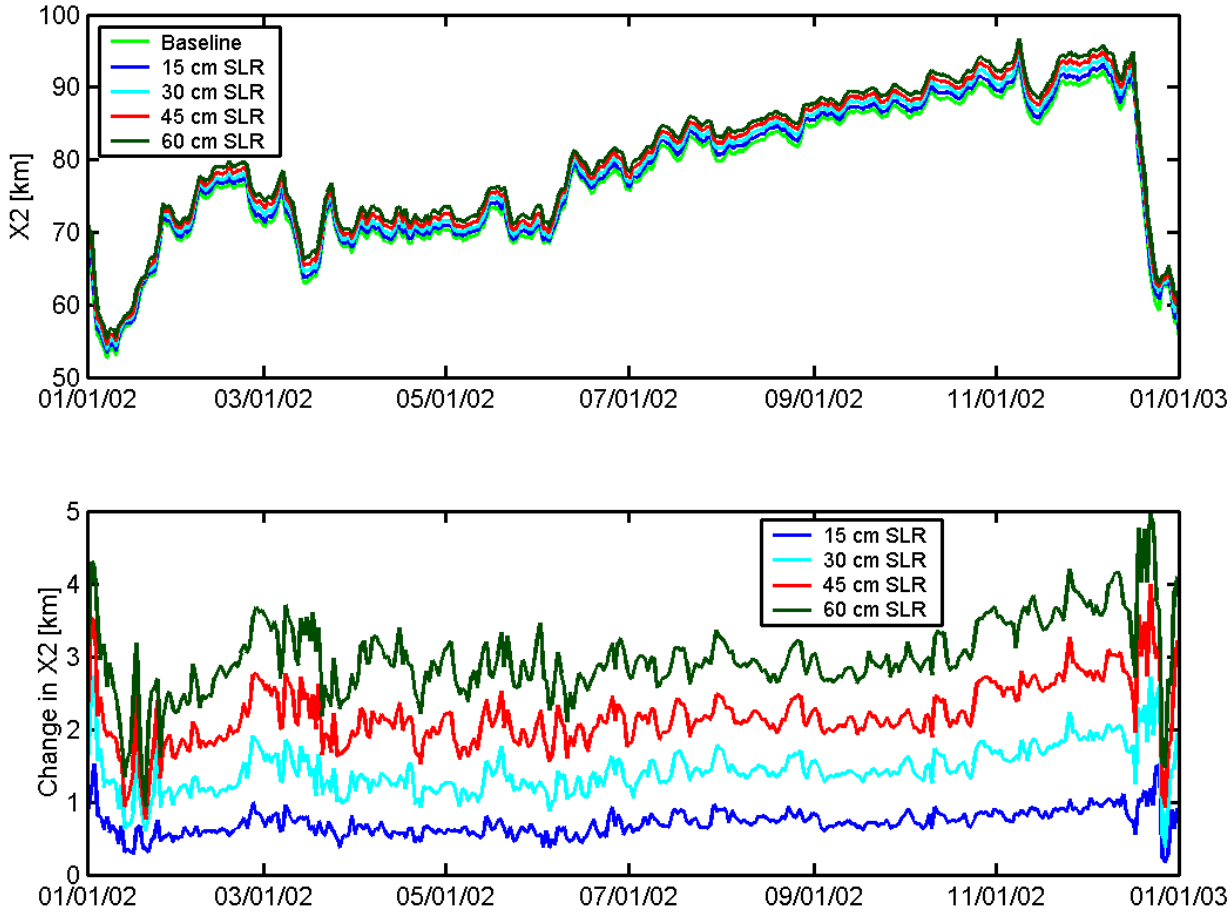

Figure 5.2-2 Predicted X2 for Baseline (0 cm SLR) scenario, 15 cm SLR scenario, 30 cm SLR scenario, 45 cm SLR scenario, and 60 cm SLR scenario (top); Predicted change in X2 relative to Baseline scenario for 15 cm SLR scenario, 30 cm SLR scenario, 45 cm SLR scenario, and 60 cm SLR scenario (bottom).

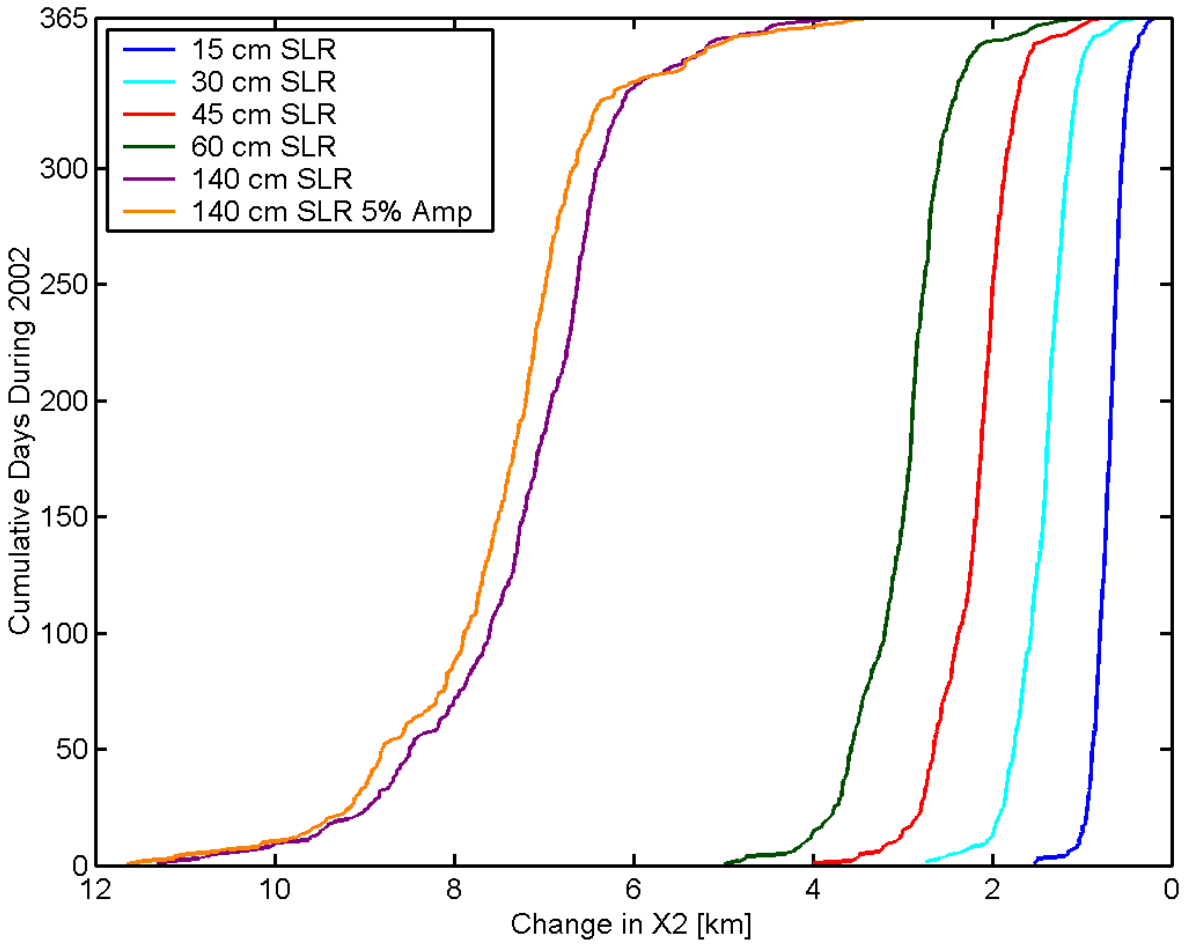

Figure 5.2-3 Cumulative number of days during 2002 that the change in predicted X2 for the 15 cm SLR scenario, 30 cm SLR scenario, 45 cm SLR scenario, 60 cm SLR scenario, 140 cm SLR scenario, and 140 cm SLR with 5% Amplification scenario exceeds the corresponding X2 predicted under the Baseline (0 cm SLR) scenario by a specific distance.

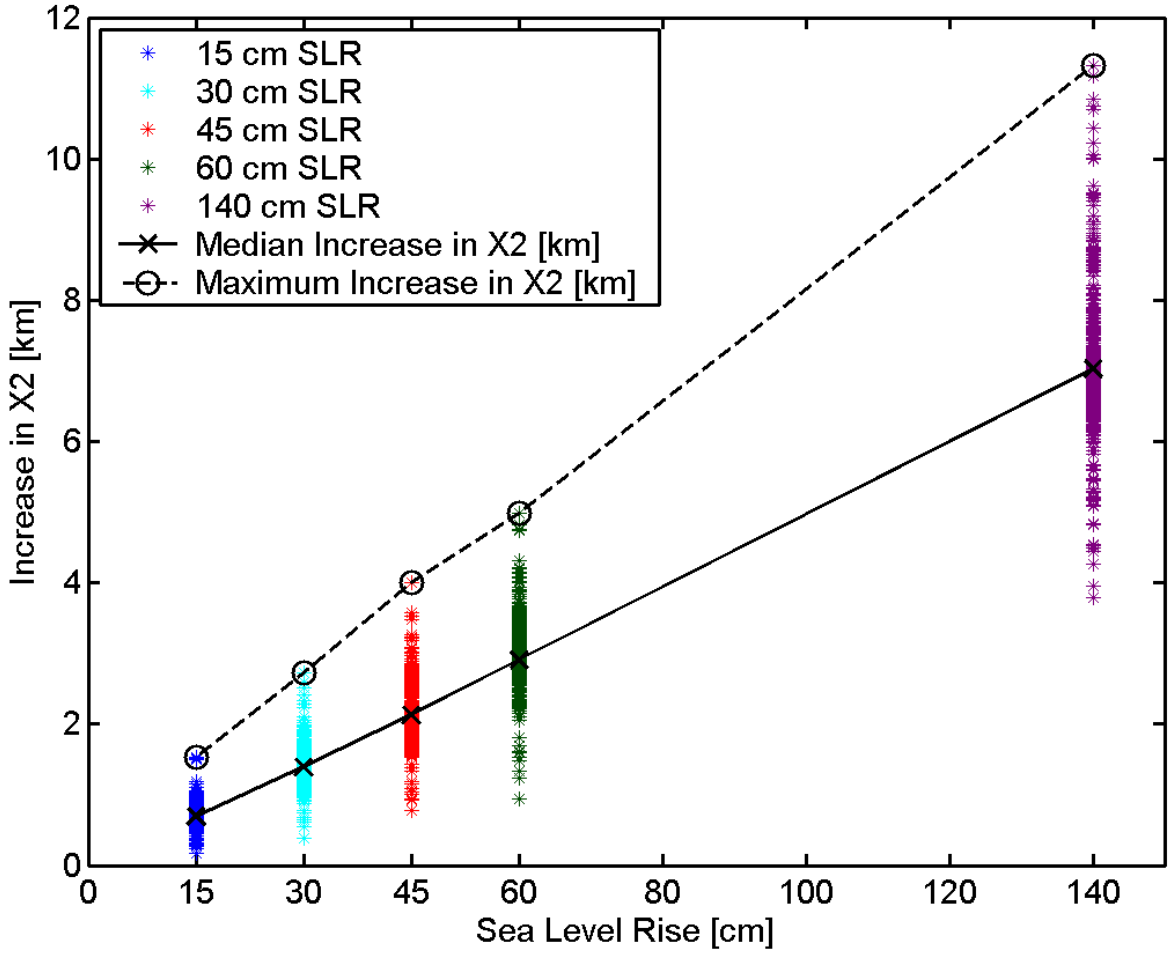

Figure 5.2-4 Scatter plot of the predicted increase in X2 for each day during 2002 for each of the sea level rise scenarios; solid black line shows the median increase in X2 for each SLR scenario and the dashed black line shows the maximum increase in X2 for each SLR scenario.

5.3 Effect of Tidal Range Amplification on X2

This section evaluates the effect of the amplification of tidal range on X2 through the comparison of X2 for the 140 cm SLR scenario and X2 for the the 140 cm SLR with 5% Amplification scenario.

Figure 5.3-1 shows the predicted X2 for 140 cm SLR scenario and 140 cm SLR with 5% Amplification scenario and the predicted change in X2 for the 140 cm SLR with 5% Amplification scenario relative to the 140 cm SLR scenario. During the high flow period during January, the predicted X2 for the 140 cm SLR with 5% Amplification scenario is less than the X2 for the 140 cm SLR scenario resulting in a decrease in X2 with tidal amplification (shown as a negative change in X2 on Figure 5.3-1). During periods when the change in X2 is negative, X2 is typically between Martinez and Port Chicago, and strong stratification is present in Carquinez Strait, as is typical during high flows. The increased tidal prism resulting from the 140 cm SLR with 5% Amplification scenario (see Section 8.4) results in higher tidal currents and, therefore, stronger vertical mixing and less stratification. Since gravitational circulation associated with this strong stratification is responsible for much of the salt intrusion during high flows (see Section 8), the reduced strength of stratification resulting from the stronger vertical mixing results in a decrease in X2 during high flows as a result of the amplification of tidal range. During summer and fall conditions, the predicted X2 for the 140 cm SLR with 5% Amplification scenario is greater than the X2 for the 140 cm SLR scenario resulting in an increase in X2 with tidal amplification. From July through November an increase of X2 of approximately 0.5 km is predicted as a result of the 5% tidal amplification. The mechanisms responsible for the increased salt intrusion for the 140 cm SLR with 5% Amplification scenario relative to the 140 cm SLR scenario are discussed in Section 8.5.

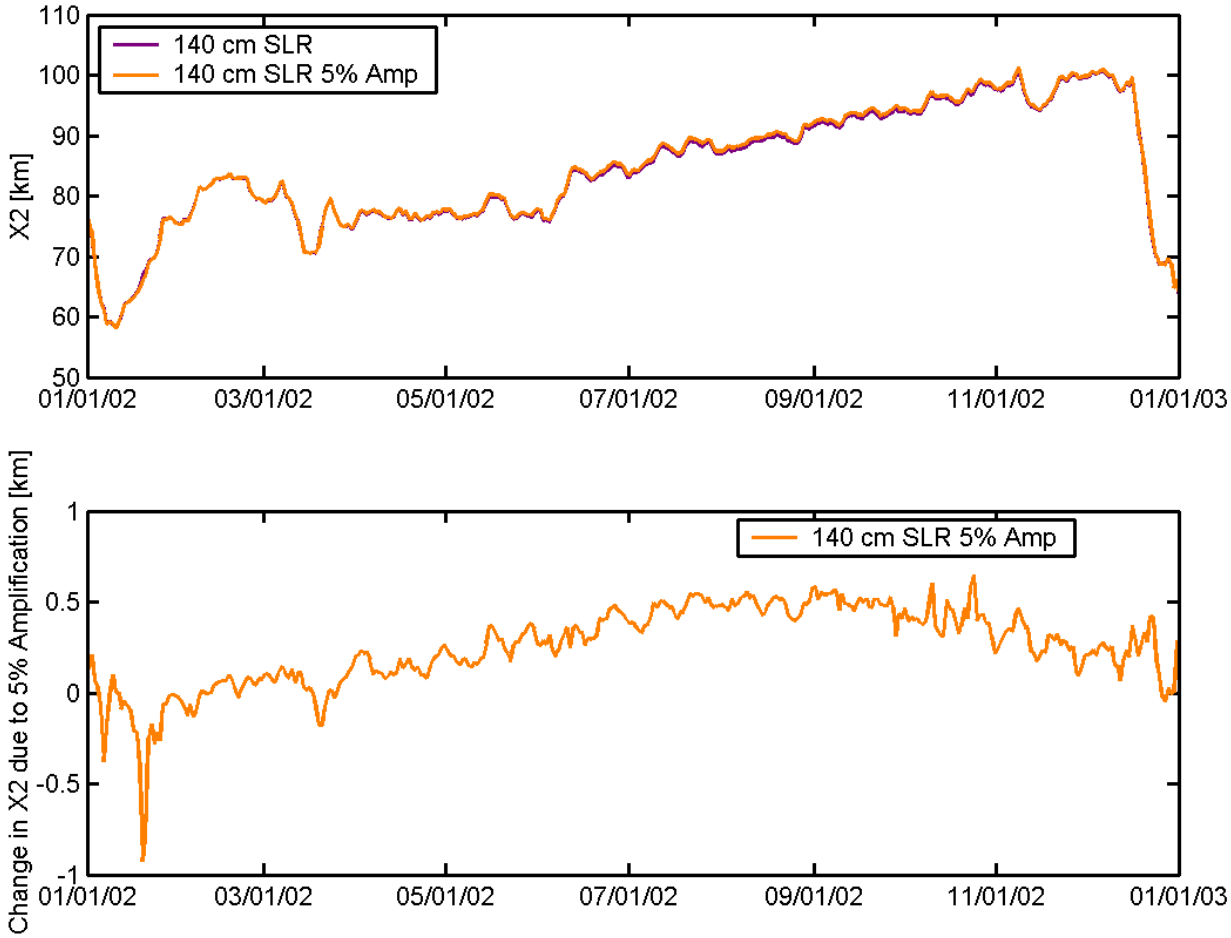

Figure 5.3-1 Predicted X2 for 140 cm SLR scenario and 140 cm SLR with 5% Amplification scenario (top); Predicted change in X2 relative to 140 cm SLR scenario for 140 cm SLR with 5% Amplification scenario (bottom).

6. Sea Level Rise Impacts on Salinity at Continuous Monitoring Locations

Salinity time series provide information about potential salinity impacts over time at a fixed location. Time series comparisons of predicted salinity were made at ten continuous salinity monitoring stations in San Francisco Bay and the Sacramento-San Joaquin Delta.

6.1 Salinity Time Series Comparisons

For each sea level rise scenario, salinity time series comparisons were made at ten continuous salinity monitoring stations in San Francisco Bay and the Sacramento-San Joaquin Delta, shown on Figure 6.1-1. For each comparison, three separate plots are shown. The top plot shows the tidal time-scale variability over a 15-day period for each sea level rise scenario. The middle plot shows daily-average salinity during the full simulation year for each sea level rise scenario. The bottom plot shows the predicted change in daily-average salinity for each of the sea level rise scenarios relative to the Baseline (0 cm SLR) scenario. The figures provide a quantitative measure of potential impacts of sea level rise on salinity in San Francisco Bay and the Sacramento-San Joaquin Delta on both tidal and annual time scales.

Figure 6.1-2 shows the predicted salinity at the Presidio for the Baseline scenario and the six sea level rise scenarios. The increase in salinity at the Presidio resulting from sea level rise is relatively small, with predicted increases in daily-average salinity of less than 0.5 psu during the entire year for the 15 cm SLR scenario and the 30 cm SLR scenario. The largest increases in daily-average salinity under all of the sea level rise scenarios occur during the high flow periods in January and December, due to the decreased ability of high flows to flush salt out of the estuary with increasing sea level rise.

Figure 6.1-3 shows the predicted salinity at Point San Pablo Upper Sensor for the Baseline scenario and the six sea level rise scenarios. The predicted increases in daily-average salinity at Point San Pablo show a similar pattern to the predicted salinity increases at the Presidio, with the largest predicted increases in daily-average salinity during the high flows during January and December. The predicted increases in daily-average salinity at Point San Pablo are larger than the predicted salinity increases at the Presidio.

Figure 6.1-4 shows the predicted salinity at the Sacramento River at the Martinez Surface Sensor (RSAC054) for the Baseline scenario and the six sea level rise scenarios. In each of the scenarios, the predicted increase in daily-average salinity at the Martinez Surface Sensor is relatively constant throughout the year, with the exception of the high flow periods.

Figure 6.1-5 shows the predicted salinity at the Sacramento River near Mallard Island Surface Sensor (RSAC075) for the Baseline scenario and the six sea level rise scenarios. The predicted increase in daily-average salinity is close to zero during January following the high flows and gradually increases throughout the summer. The predicted salinity increase for all scenarios approaches zero during December as salt is pushed out of Suisun Bay by high Delta outflows.

Figure 6.1-6 shows the predicted salinity at the Sacramento River at Emmaton Surface Sensor (RSAC092) for the Baseline scenario and the six sea level rise scenarios. With the exception of the 140 cm SLR and 140 cm SLR with 5% Amplification scenarios, the predicted increase in daily-average salinity at Emmaton is close to 0 psu from January through May, and following the high flows in December. The predicted increase in daily-average salinity gradually increases throughout the summer for all scenarios, with larger increases predicted with increasing SLR.

Figure 6.1-7 shows the predicted salinity at Sacramento River at Rio Vista (RSAC101) for the Baseline scenario and the six sea level rise scenarios. The predicted increase in daily-average salinity at Rio Vista is close to 0 psu from January through May for all scenarios. The predicted increase in daily-average salinity gradually increases throughout the summer, beginning in July for the 140 cm SLR and 140 cm SLR with 5% Amplification scenarios, and beginning in September for the other SLR scenarios. The largest predicted increases in daily-average salinity for all scenarios occur in November.

Figure 6.1-8 shows the predicted salinity at San Joaquin River at Jersey Point (RSAN018) for the Baseline scenario and the six sea level rise scenarios. The predicted increase in daily-average salinity at Jersey Point is close to 0 psu from January through May for all scenarios. The predicted increase in daily-average salinity gradually increases throughout the summer, beginning in June for the 140 cm SLR and 140 cm SLR with 5% Amplification scenarios, and beginning later in the summer for the other SLR scenarios. The largest predicted increases in daily-average salinity for all scenarios occur in November and December.

Figure 6.1-9 shows the predicted salinity at San Joaquin River before Prisoner's Point (RSAN037) for the Baseline scenario and the six sea level rise scenarios. The predicted increase in daily-average salinity at Prisoner's Point is close to 0 psu from January through June for all scenarios. The predicted increase in daily-average salinity gradually increases throughout the late-summer and fall, beginning in July for the 140 cm SLR and 140 cm SLR with 5% Amplification scenarios, and beginning later in the summer for the other SLR scenarios. The largest predicted increases in daily-average salinity for all scenarios occur in early December.

Figure 6.1-10 shows the predicted salinity at Old River at Bacon Island (ROLD024) for the Baseline scenario and the six sea level rise scenarios. The predicted increase in daily-average salinity at Old River at Bacon Island is close to 0 psu from January through June for all scenarios. The predicted increase in daily-average salinity gradually increases throughout the late-summer and fall, beginning in July for the 140 cm SLR and 140 cm SLR with 5% Amplification scenarios, and beginning later in the summer for the other SLR scenarios. The largest predicted increases in daily-average salinity for all scenarios occur in early December.

Figure 6.1-11 shows the predicted salinity at Clifton Court Forebay Radial Gates (CHWST000) for the Baseline scenario and the six sea level rise scenarios. The predicted increase in daily-average salinity at the Clifton Court Forebay Radial gates is close to 0 psu from January through June for all scenarios except for the 140 cm SLR scenario and the 140 cm SLR with 5 % Amplification scenarios. The predicted increase in daily-average salinity gradually increases throughout the late-summer and fall, beginning in July for the 140 cm SLR and 140 cm SLR with 5% Amplification scenarios, and beginning later in the summer for the other SLR scenarios.

The largest predicted increases in daily-average salinity for all scenarios occur in early December.

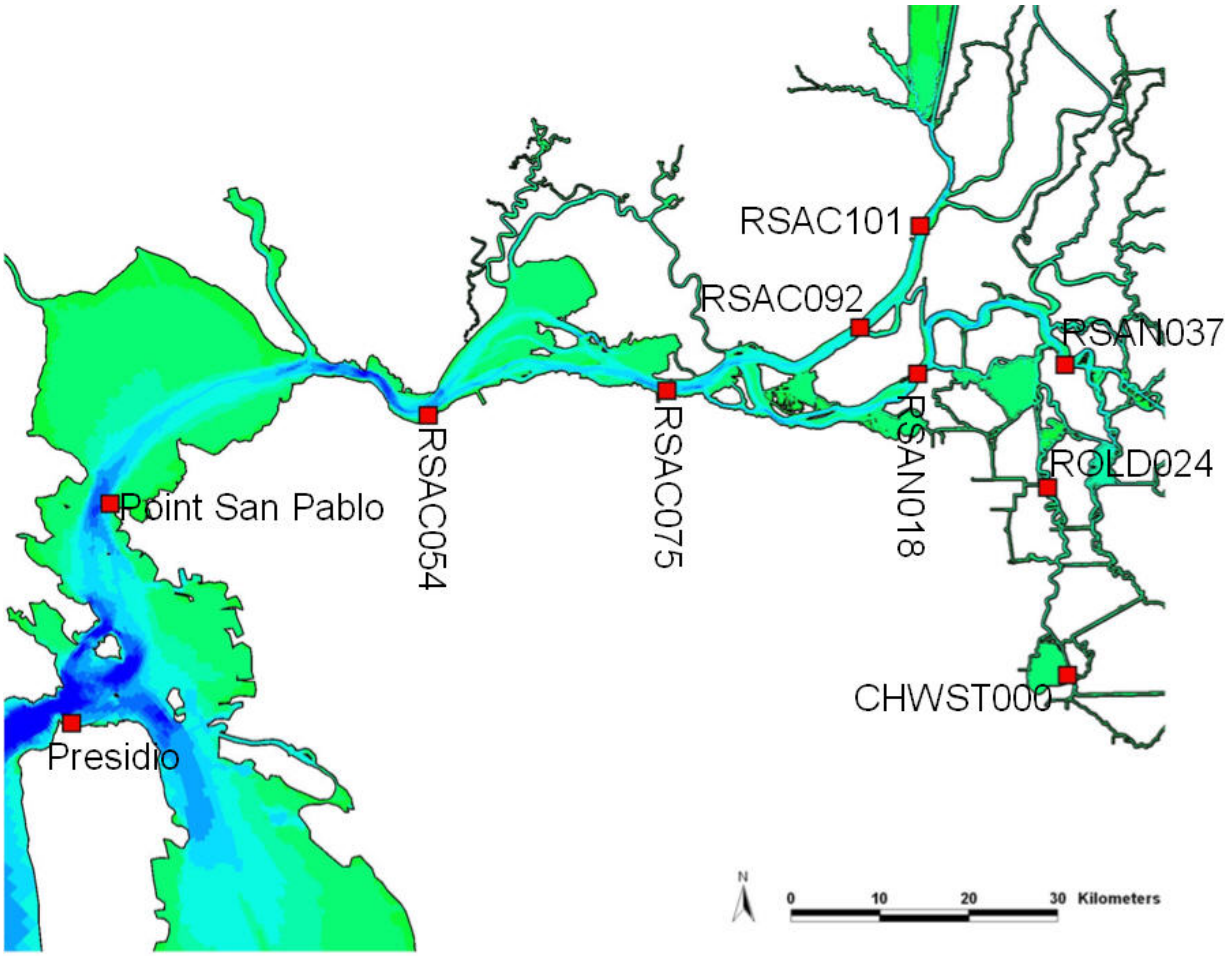

Station Names

RSAC054, Sacramento River at Martinez

RSAN007, Sacramento River near Mallard Island

RSAC092, Sacramento River at Emmaton

RSAC101, Sacramento River at Rio Vista

RSAN018, San Joaquin River at Jersey Point

RSAN037, San Joaquin River before Prisoners Point

ROLD024, Old River at Bacon Island

CHWST000, Clifton Court Forebay

Figure 6.1-1 Location of continuous monitoring stations in San Francisco Bay and the Sacramento-San Joaquin Delta where time series comparisons were made to evaluate potential salinity impacts resulting from sea level rise scenarios.

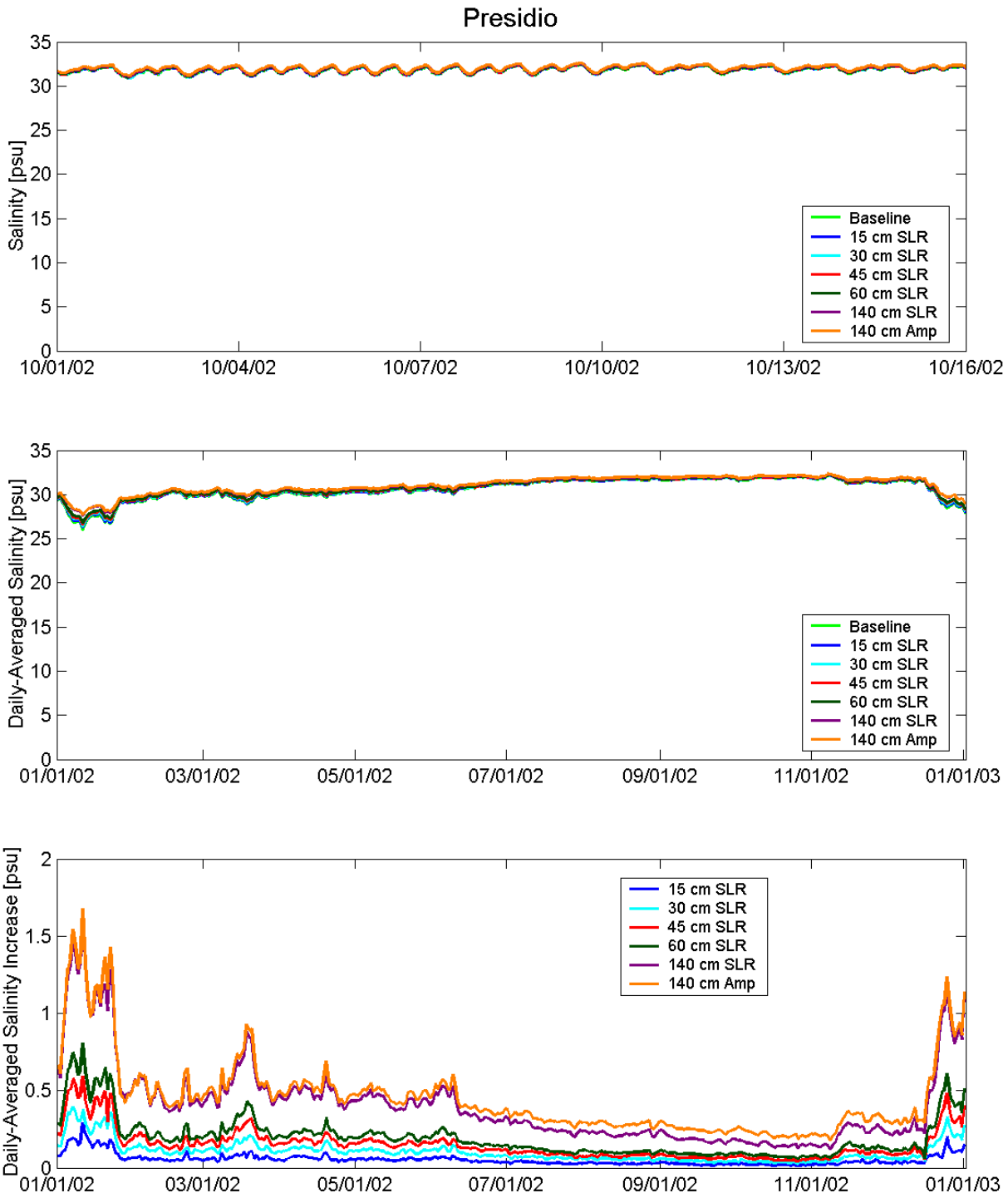

Figure 6.1-2 Predicted salinity at the Presidio for each of the sea level rise scenarios: tidal time-scale variability over a 15-day period (top); daily-average salinity during the 2002 simulation period (middle); predicted increase in daily-average salinity for each of the sea level rise scenarios relative to the Baseline scenario (bottom).

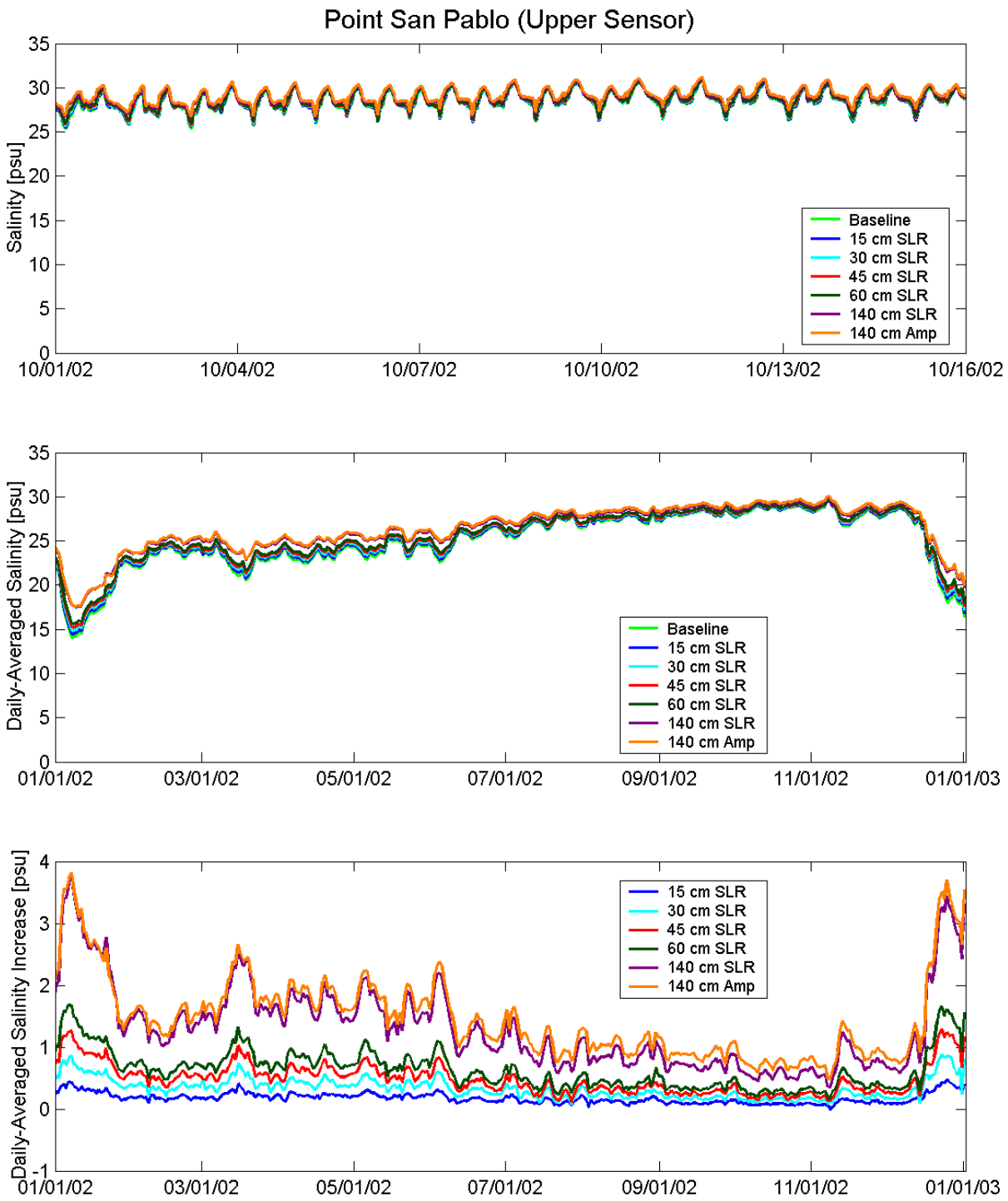

Figure 6.1-3 Predicted salinity at Point San Pablo for each of the sea level rise scenarios: tidal time-scale variability over a 15-day period (top); daily-average salinity during the 2002 simulation period (middle); predicted increase in daily-average salinity for each of the sea level rise scenarios relative to the Baseline scenario (bottom).

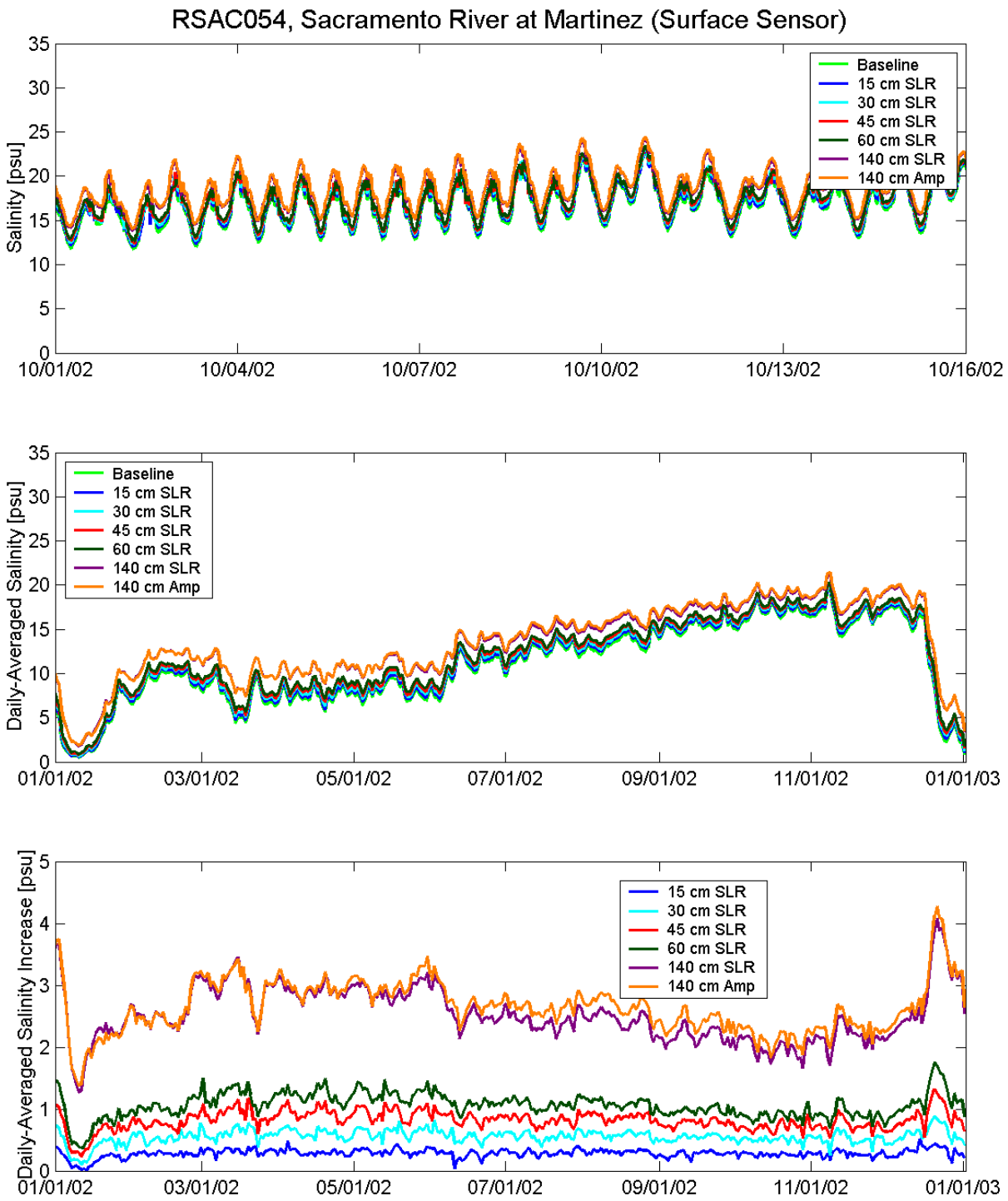

Figure 6.1-4 Predicted salinity at Sacramento River at Martinez (RSAC054) for each of the sea level rise scenarios: tidal time-scale variability over a 15-day period (top); daily-average salinity during the 2002 simulation period (middle); predicted increase in daily-average salinity for each of the sea level rise scenarios relative to the Baseline scenario (bottom).

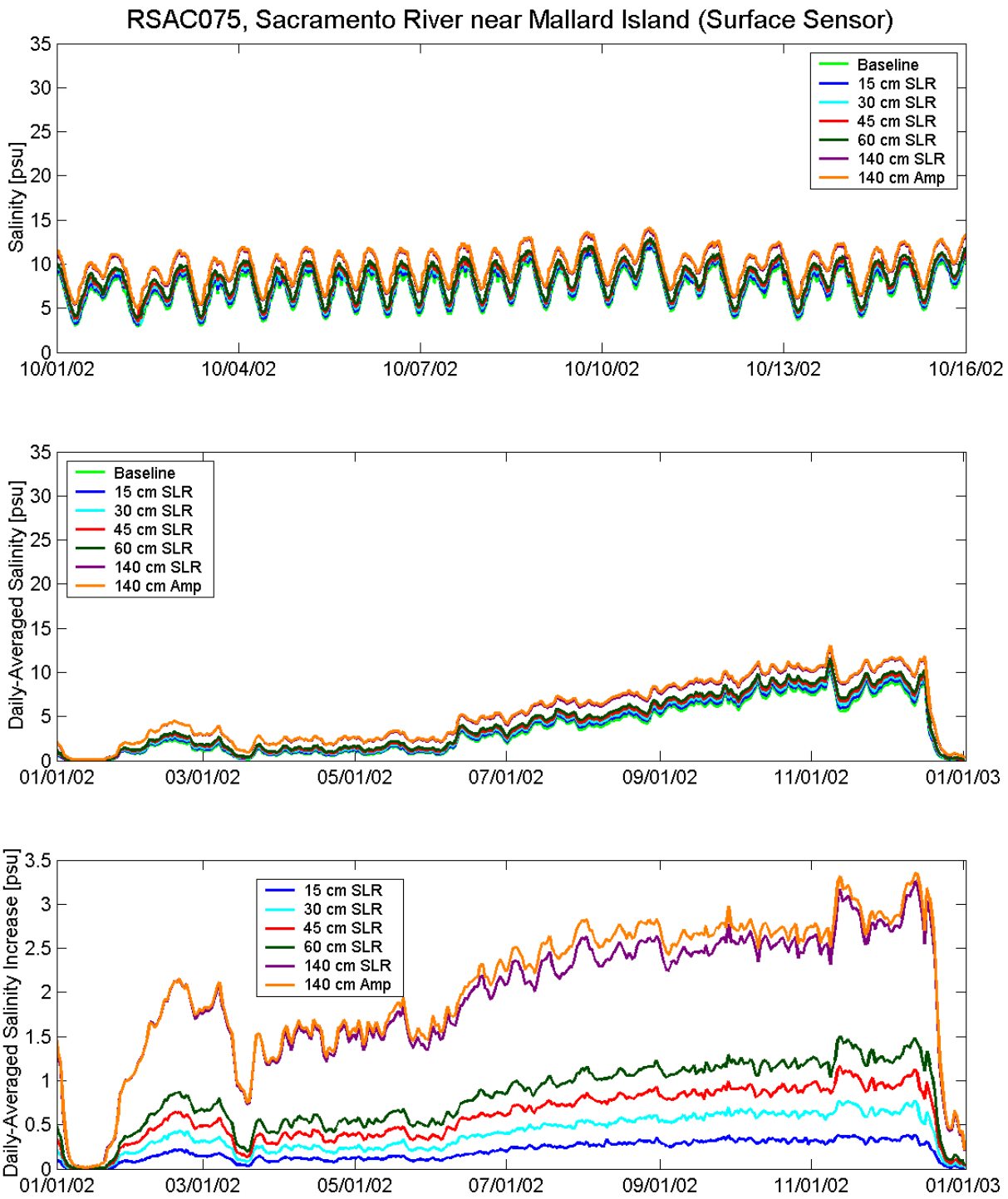

Figure 6.1-5 Predicted salinity at Sacramento River near Mallard Island (RSAC075) for each of the sea level rise scenarios: tidal time-scale variability over a 15-day period (top); daily-average salinity during the 2002 simulation period (middle); predicted increase in daily-average salinity for each of the sea level rise scenarios relative to the Baseline scenario (bottom).

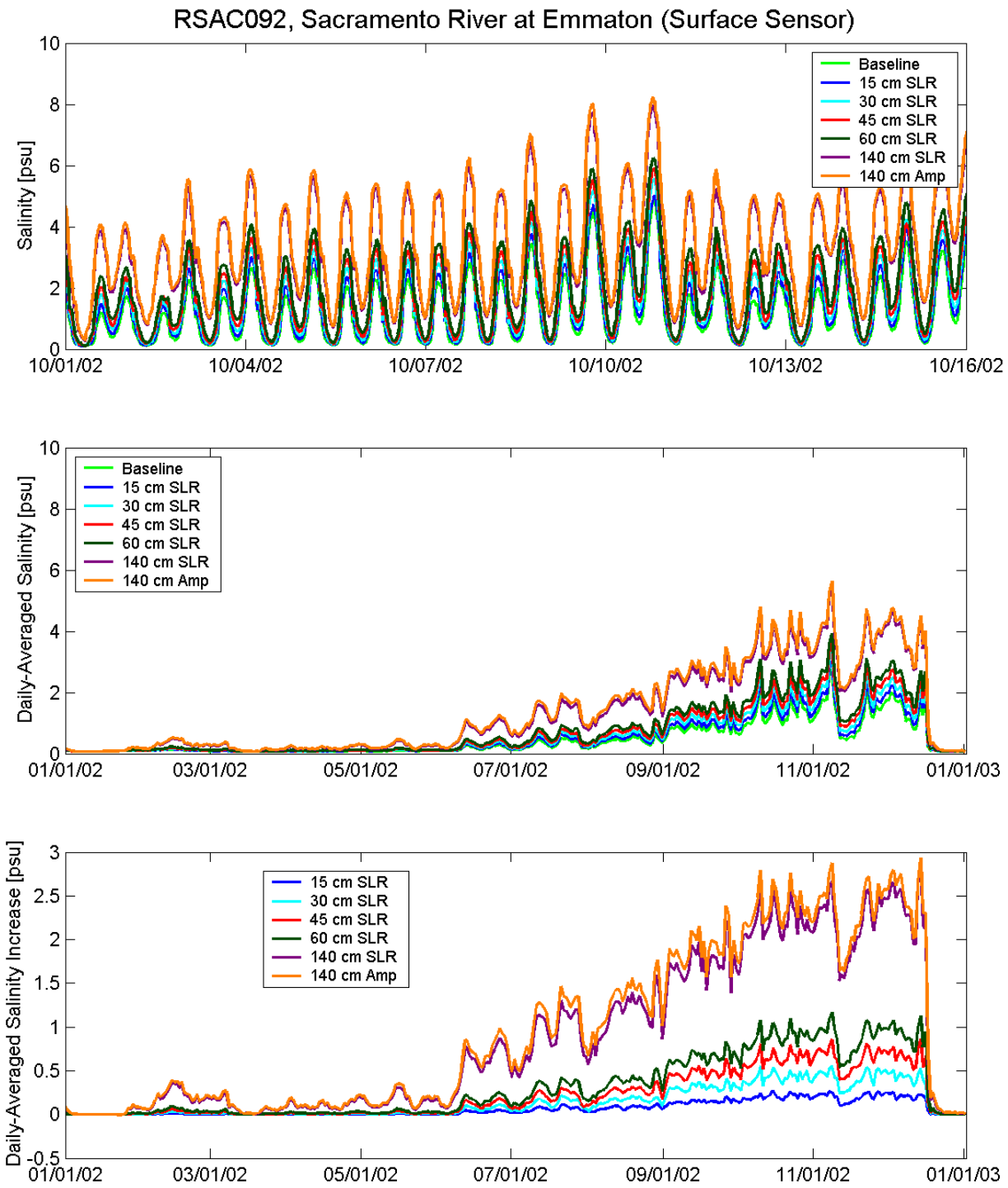

Figure 6.1-6 Predicted salinity at Sacramento River at Emmaton (RSAC092) for each of the sea level rise scenarios: tidal time-scale variability over a 15-day period (top); daily-average salinity during the 2002 simulation period (middle); predicted increase in daily-average salinity for each of the sea level rise scenarios relative to the Baseline scenario (bottom).

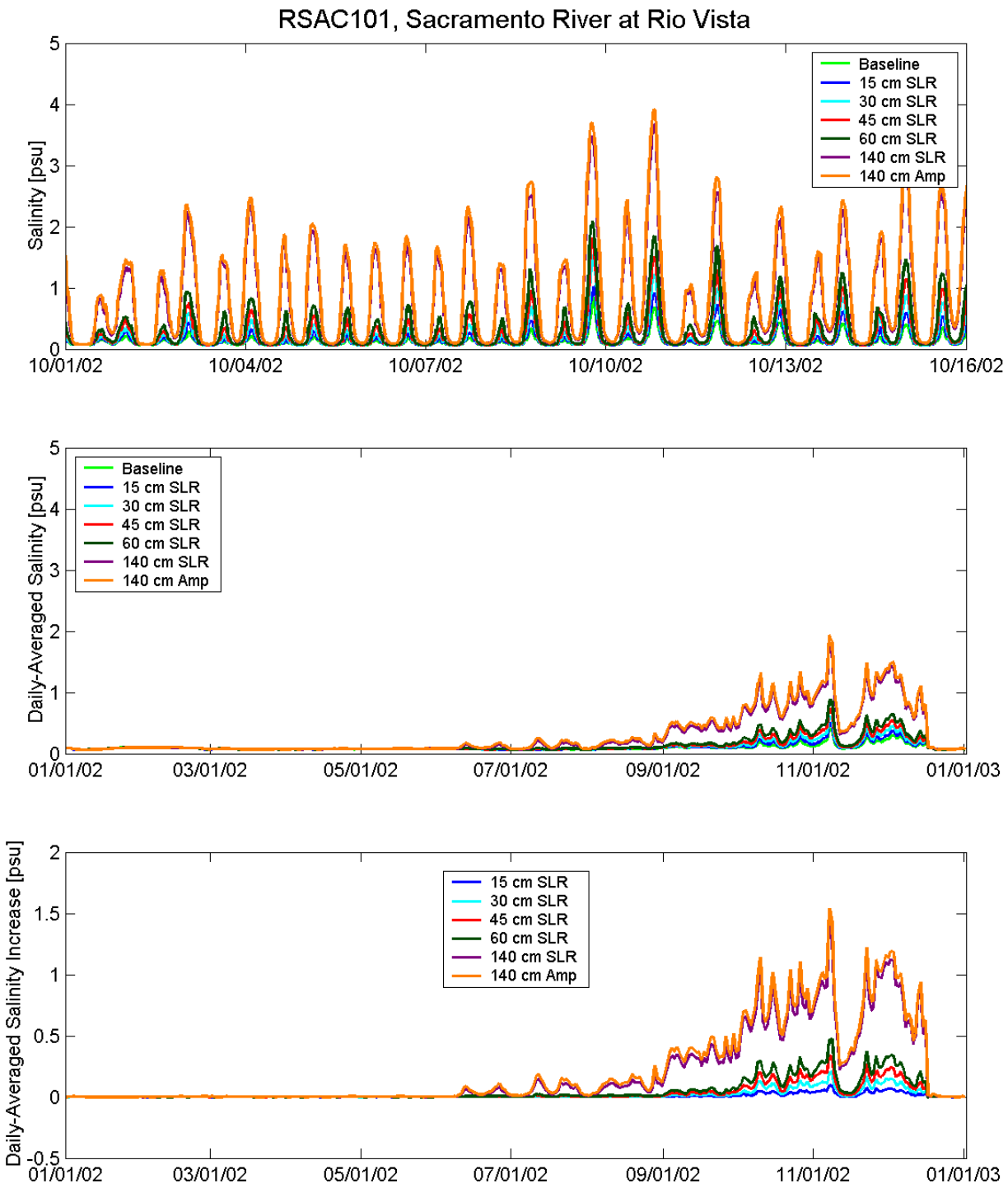

Figure 6.1-7 Predicted salinity at Sacramento River at Rio Vista (RSAC101) for each of the sea level rise scenarios: tidal time-scale variability over a 15-day period (top); daily-average salinity during the 2002 simulation period (middle); predicted increase in daily-average salinity for each of the sea level rise scenarios relative to the Baseline scenario (bottom).

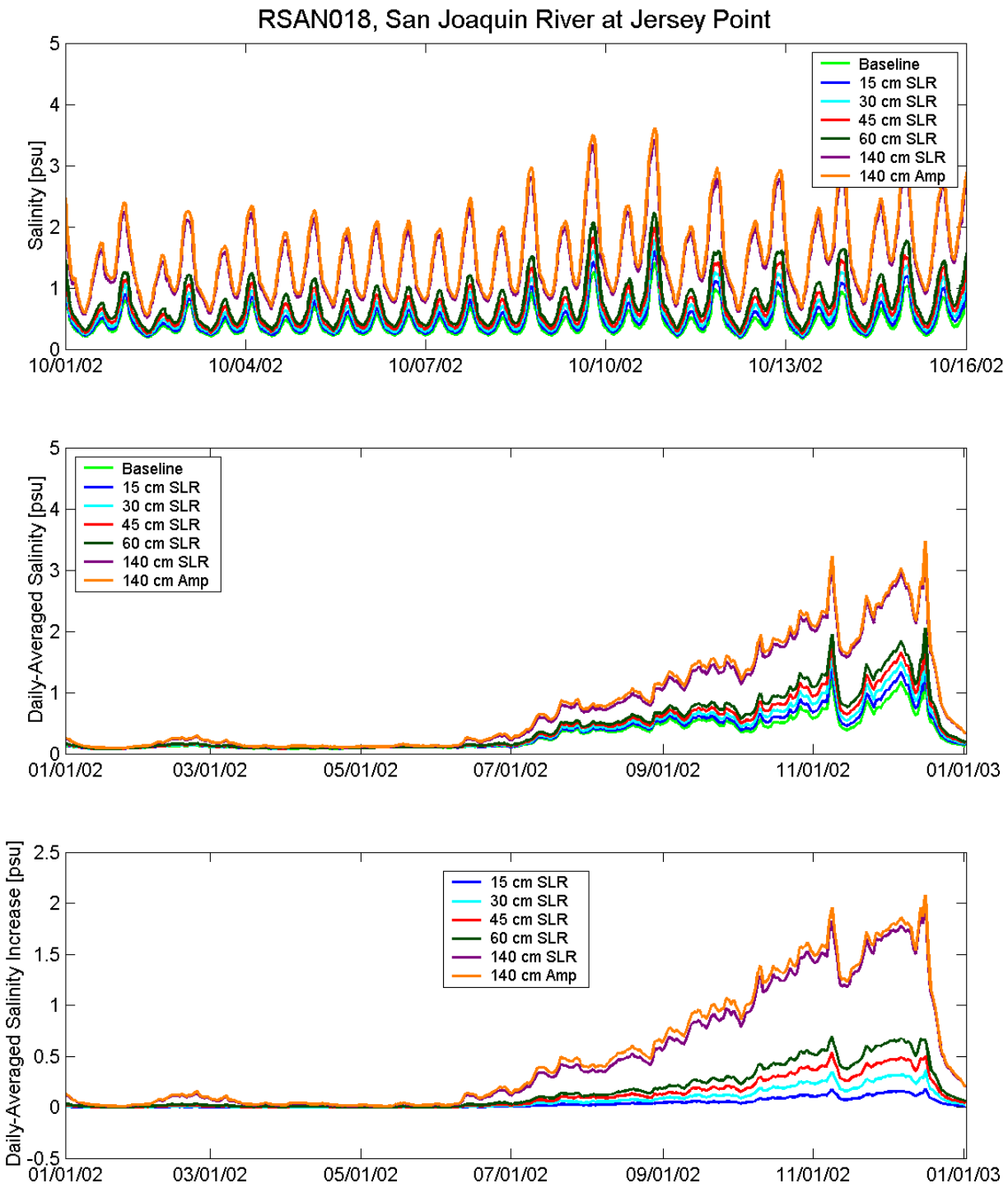

Figure 6.1-8 Predicted salinity at San Joaquin River at Jersey Point (RSAN018) for each of the sea level rise scenarios: tidal time-scale variability over a 15-day period (top); daily-average salinity during the 2002 simulation period (middle); predicted increase in daily-average salinity for each of the sea level rise scenarios relative to the Baseline scenario (bottom).

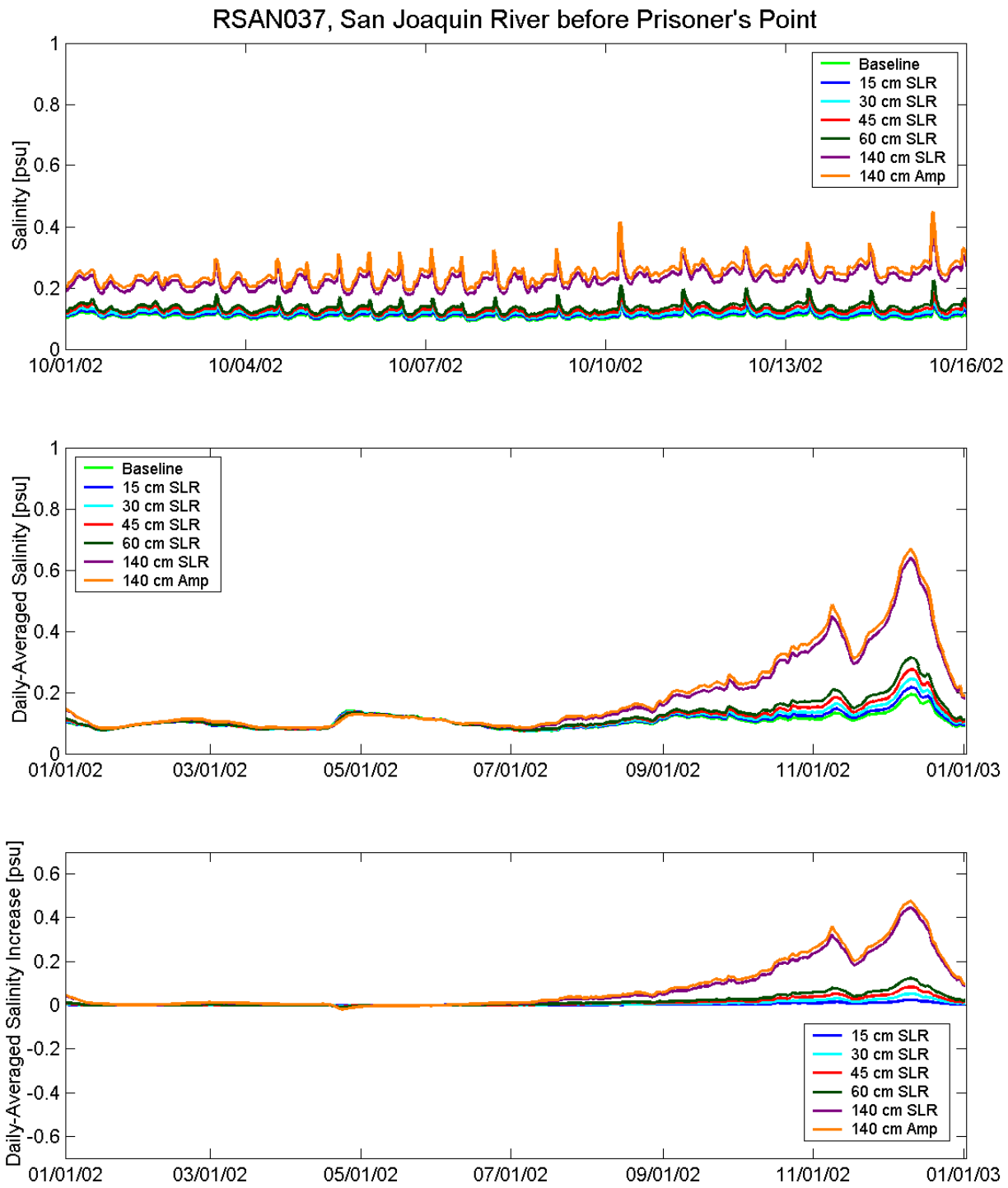

Figure 6.1-9 Predicted salinity at San Joaquin River before Prisoner's Point (RSAN037) for each of the sea level rise scenarios: tidal time-scale variability over a 15-day period (top); daily-average salinity during the 2002 simulation period (middle); predicted increase in daily-average salinity for each of the sea level rise scenarios relative to the Baseline scenario (bottom).

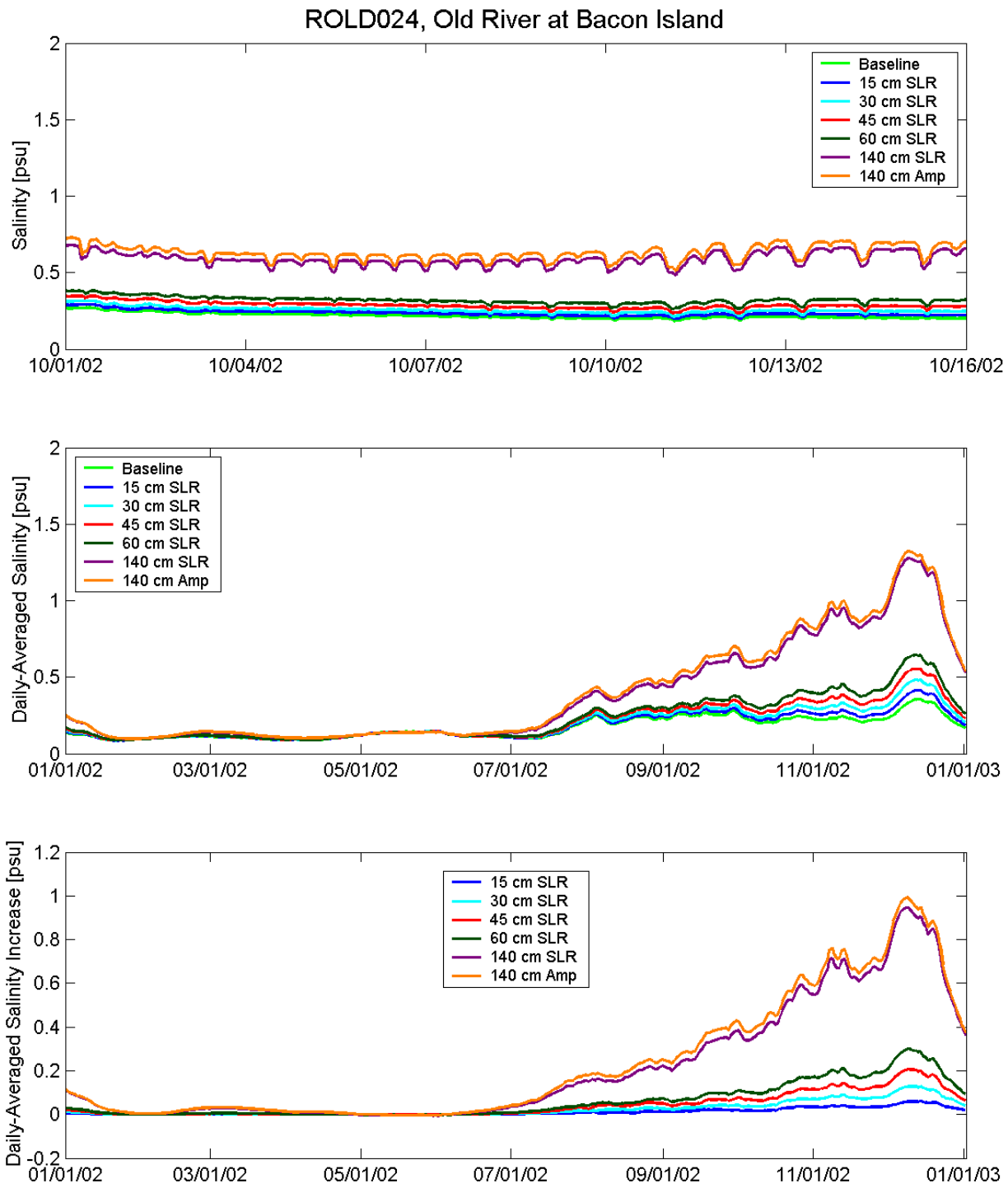

Figure 6.1-10 Predicted salinity at Old River at Bacon Island (ROLD024) for each of the sea level rise scenarios: tidal time-scale variability over a 15-day period (top); daily-average salinity during the 2002 simulation period (middle); predicted increase in daily-average salinity for each of the sea level rise scenarios relative to the Baseline scenario (bottom).

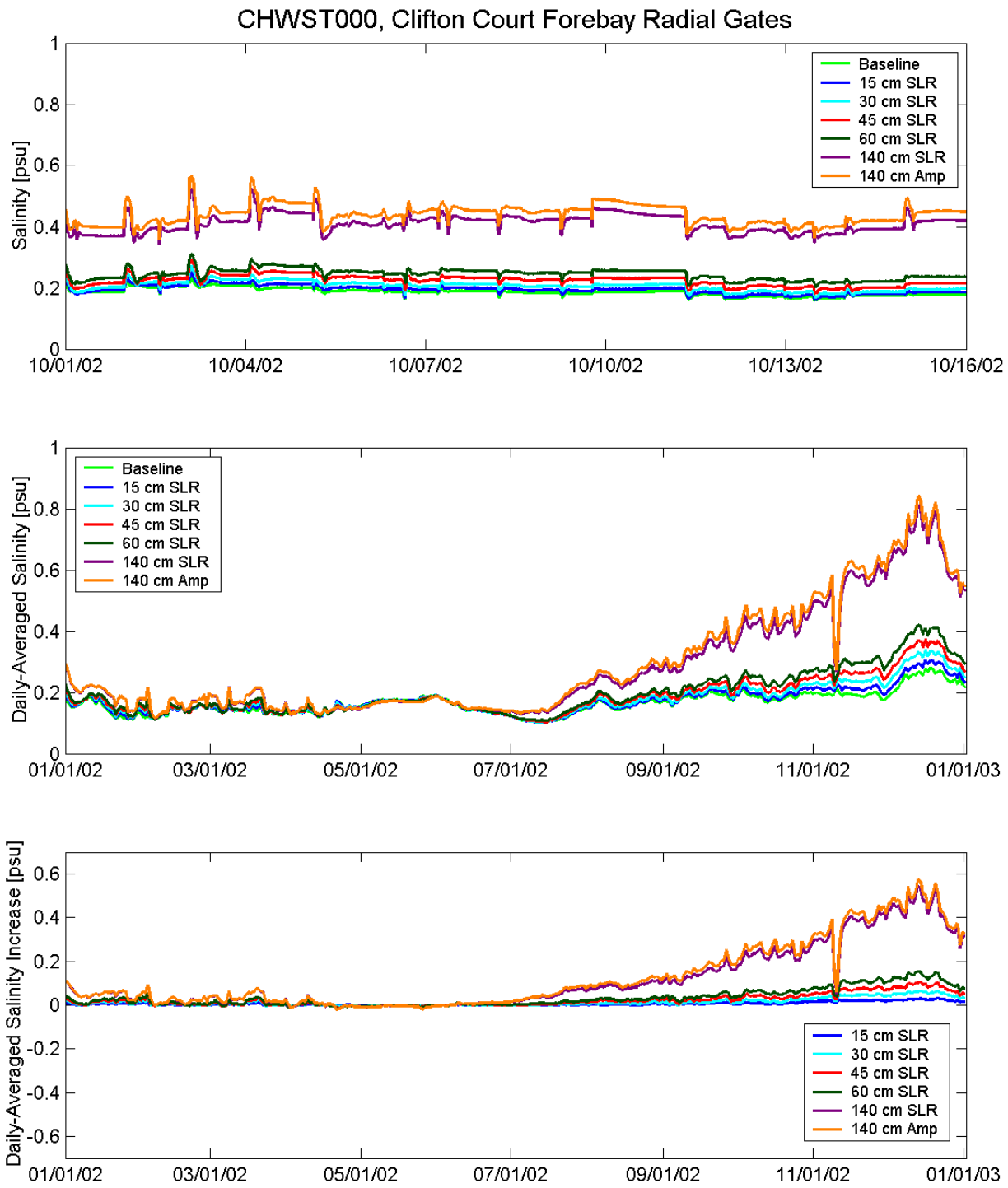

Figure 6.1-11 Predicted salinity at Clifton Court Forebay Radial Gates (CHWST000) for each of the sea level rise scenarios: tidal time-scale variability over a 15-day period (top); daily-average salinity during the 2002 simulation period (middle); predicted increase in daily-average salinity for each of the sea level rise scenarios relative to the Baseline scenario (bottom).

7. Stage and Salinity Relationships for SLR at Fort Point and Martinez

Because the DSM2 model and the RMA2 Delta models have their downstream boundary at Martinez, the effects of SLR on water levels and salinity at the UnTRIM ocean boundary have to be translated to Martinez in order to allow for simulation of SLR scenarios using the DSM2 or the RMA2 Delta model. Similarly, the RMA2 Bay-Delta model has its boundary at the Golden Gate, so it is necessary to translate predicted changes in water levels and salinity at the Golden Gate to the boundary conditions used in the RMA2 Bay-Delta model. Additionally, because the UnTRIM Bay-Delta model SLR simulations only span one year, these relationships allow for simulation of SLR affects using either DSM2 or RMA2 over either longer or different time periods. This section presents some regression relationships developed using the cross-correlation procedure described in section A.1. Further development of these relationships is being conducted by CH2M Hill. Anderson and Miller (2005) used a similar approach to develop relationships to estimate electrical conductivity at Martinez for sea level rise conditions simulated using the RMA2 Bay-Delta model for 1 foot of SLR. The relationships developed in this section apply to 15 cm of SLR, 30 cm SLR, 45 cm of SLR, 60 cm SLR, 140 cm SLR, and 140 cm SLR with 5% Amplification. Because the impact on salinity due to SLR is non-linear, additional simulations would be required to estimate these relationships for other levels of SLR or for simulations that included either an operational response to SLR or significant changes to the structure or operation of the Delta.

7.1 Establishing Stage Relationships for Sea Level Rise at Fort Point and Martinez

This section presents linear regression relationships developed using the cross-correlation procedure described in section A.1 to describe the effect of SLR at the ocean boundary on predicted stage at Fort Point and Martinez.

7.1.1 Stage Relationships for Sea Level Rise at Fort Point

Figure 7.1-1 shows the predicted stage and tidally averaged stage at Fort Point for the Baseline and 15 cm SLR scenarios. The cross-correlation yields a best linear fit of

$$[\text{Stage 15 cm SLR}] = 0.9993 \times [\text{Stage Baseline}] + 0.1500 \qquad (7\text{-}1)$$

with an R^2 value of 1.000 and no phase difference. Because this relationship is linear with a slope very close to 1.000, this shows that the 15 cm stage offset applied at the ocean boundary is translating almost exactly to a 15 cm stage offset at Fort Point. This is also reflected by the difference between the annual mean stage for the Baseline scenario and the annual mean stage of 15 cm SLR scenario which is 14.9 cm.

Figure 7.1-2 shows the predicted stage and tidally averaged stage at Fort Point for the Baseline and 30 cm SLR scenarios. The cross-correlation yields a best linear fit of

[Stage 30 cm SLR] = 0.9986 x *[Stage Baseline] + 0.3001* (7-2)

with an R^2 value of 1.000 and a phase lag of 1 minute. Because this relationship is linear with a slope very close to 1.000, this shows that the 30 cm stage offset applied at the ocean boundary is translating almost exactly to a 30 cm stage offset at Fort Point. This is also reflected by the difference between the annual mean stage for the Baseline scenario and the annual mean stage of 30 cm SLR scenario which is 29.9 cm.

Figure 7.1-3 shows the predicted stage and tidally averaged stage at Fort Point for the Baseline and 45 cm SLR scenarios. The cross-correlation yields a best linear fit of

[Stage 45 cm SLR] = 0.9987 x *[Stage Baseline] + 0.4494* (7-3)

with an R^2 value of 1.000 and a phase lag of 1 minute. Because this relationship is linear with a slope very close to 1.000, this shows that the 45 cm stage offset applied at the ocean boundary is translating almost exactly to a 45 cm stage offset at Fort Point. This is also reflected by the difference between the annual mean stage for the Baseline scenario and the annual mean stage of 45 cm SLR scenario which is 44.8 cm.

Figure 7.1-4 shows the predicted stage and tidally averaged stage at Fort Point for the Baseline and 60 cm SLR scenarios. The cross-correlation yields a best linear fit of

[Stage 60 cm SLR] = 0.9992 x *[Stage Baseline] + 0.5986* (7-4)

with an R^2 value of 1.000 and a phase lag of 1 minute. Because this relationship is linear with a slope very close to 1.000, this shows that the 60 cm stage offset applied at the ocean boundary is translating almost exactly to a 60 cm stage offset at Fort Point. This is also reflected by the difference between the annual mean stage for the Baseline scenario and the annual mean stage of 60 cm SLR scenario which is 59.8 cm.

Figure 7.1-5 shows the predicted stage and tidally averaged stage at Fort Point for the Baseline and 140 cm SLR scenarios. The cross-correlation yields a best linear fit of

[Stage 140 cm SLR] = 1.0050 x *[Stage Baseline] + 1.3915* (7-5)

with an R^2 value of 1.000 and a phase lag of 1 minute. Because this relationship is linear with a slope very close to 1.000, this shows that the 140 cm stage offset applied at the ocean boundary is translating almost exactly to a 140 cm stage offset at Fort Point. This is also reflected by the difference between the annual mean stage for the Baseline scenario and the annual mean stage of 140 cm SLR scenario which is 139.6 cm.

Figure 7.1-6 shows the predicted stage and tidally averaged stage at Fort Point for the Baseline and 140 cm SLR with 5% Amplification scenarios. The cross-correlation yields a best linear fit of

[Stage 140 cm SLR with 5% Amplification] = 1.0470 x *[Stage Baseline] + 1.3497* (7-6)

with an R^2 value of 1.000 and a phase lag of 2 minute. Because this scenario includes both an offset and amplification of tidal range at the ocean boundary, the slope of the linear fit is not as close to 1.000 as in the other scenarios, and is closer to 1.05 indicating the higher amplitude of tidal range. However the offset in the linear fit is 1.3497 m which is not as similar to the 140 cm stage offset applied at the ocean boundary as the corresponding offset in Equation 7-5 for the 140 cm SLR scenario.

7.1.2 Stage Relationships for Sea Level Rise at Martinez

Figure 7.1-7 shows the predicted stage and tidally averaged stage at Martinez for the Baseline and 15 cm SLR scenarios. The cross-correlation yields a best linear fit of

[Stage 15 cm SLR] = 1.0033 x *[Stage Baseline] + 0.1435* (7-7)

with an R^2 value of 1.000 and a phase lead of 1 minute. Because this relationship is linear with a slope very close to 1.000 and an offset of 0.1435 m, this shows that the 15 cm stage offset applied at the ocean boundary is translating to slightly less than 15 cm of stage offset at Martinez. This is also reflected by the difference between the annual mean stage for the Baseline scenario and the annual mean stage of 15 cm SLR scenario which is 14.7 cm.

Figure 7.1-8 shows the predicted stage and tidally averaged stage at Martinez for the Baseline and 30 cm SLR scenarios. The cross-correlation yields a best linear fit of

[Stage 30 cm SLR] = 1.0074 x *[Stage Baseline] + 0.2862* (7-8)

with an R^2 value of 1.000 and a phase lead of 1 minute. Because this relationship is linear with a slope very close to 1.000 and an offset of 0.2862 m, this shows that the 30 cm stage offset applied at the ocean boundary is translating to slightly less than 30 cm of stage offset at Martinez. This is also reflected by the difference between the annual mean stage for the Baseline scenario and the annual mean stage of 30 cm SLR scenario which is 29.4 cm.

Figure 7.1-9 shows the predicted stage and tidally averaged stage at Martinez for the Baseline and 45 cm SLR scenarios. The cross-correlation yields a best linear fit of

[Stage 45 cm SLR] = 1.0113 x *[Stage Baseline] + 0.4290* (7-9)

with an R^2 value of 1.000 and a phase lead of 2 minutes. Because this relationship is linear with a slope very close to 1.000 and an offset of 0.4290 m, this shows that the 45 cm stage offset applied at the ocean boundary is translating to slightly less than 45 cm of stage offset at Martinez. This is also reflected by the difference between the annual mean stage for the Baseline scenario and the annual mean stage of 45 cm SLR scenario which is 44.1 cm.

Figure 7.1-10 shows the predicted stage and tidally averaged stage at Martinez for the Baseline and 60 cm SLR scenarios. The cross-correlation yields a best linear fit of

[Stage 60 cm SLR] = 1.0156 x *[Stage Baseline] + 0.5714* (7-10)

with an R^2 value of 1.000 and a phase lead of 3 minute. Because this relationship is linear with a slope close to 1.000 and an offset of 0.5714 m, this shows that the 60 cm stage offset applied at the ocean boundary is translating to slightly less than 60 cm of stage offset at Martinez. This is also reflected by the difference between the annual mean stage for the Baseline scenario and the annual mean stage of 60 cm SLR scenario which is 58.9 cm.

Figure 7.1-11 shows the predicted stage and tidally averaged stage at Martinez for the Baseline and 140 cm SLR scenarios. The cross-correlation yields a best linear fit of

[Stage 140 cm SLR] = 1.0382 x *[Stage Baseline] + 1.3361* (7-11)

with an R^2 value of 0.999 and a phase lead of 10 minutes. Because this relationship is linear with a slope greater than 1.000 and an offset of 1.3361 m, this shows that the 140 cm stage offset applied at the ocean boundary is translating to slightly less than 140 cm of stage offset at Martinez, and resulting in some differences in both phase and amplitude at Martinez. The difference between the annual mean stage for the Baseline scenario and the annual mean stage of 140 cm SLR scenario is 137.8 cm.

Figure 7.1-12 shows the predicted stage and tidally averaged stage at Martinez for the Baseline and 140 cm SLR with 5% Amplification scenarios. The cross-correlation yields a best linear fit of

[Stage 140 cm SLR with 5% Amplification] = 1.0718 x *[Stage Baseline] + 1.3013* (7-12)

with an R^2 value of 0.999 and a phase lead of 9 minutes. Because this relationship is linear with a slope greater than 1.000 and an offset of 1.3013 m, this shows that the 140 cm stage offset with 5% tidal range amplification applied at the ocean boundary is translating to slightly less than 140 cm of stage offset at Martinez and is resulting in differences in both phase and amplitude at Martinez. The difference between the annual mean stage for the Baseline scenario and the annual mean stage of 140 cm SLR scenario is 138.0 cm. These results suggest that a linear fit is not appropriate for developing a tidal stage relationship at Martinez for a scenario which includes amplification of the tidal range in addition to sea level rise.

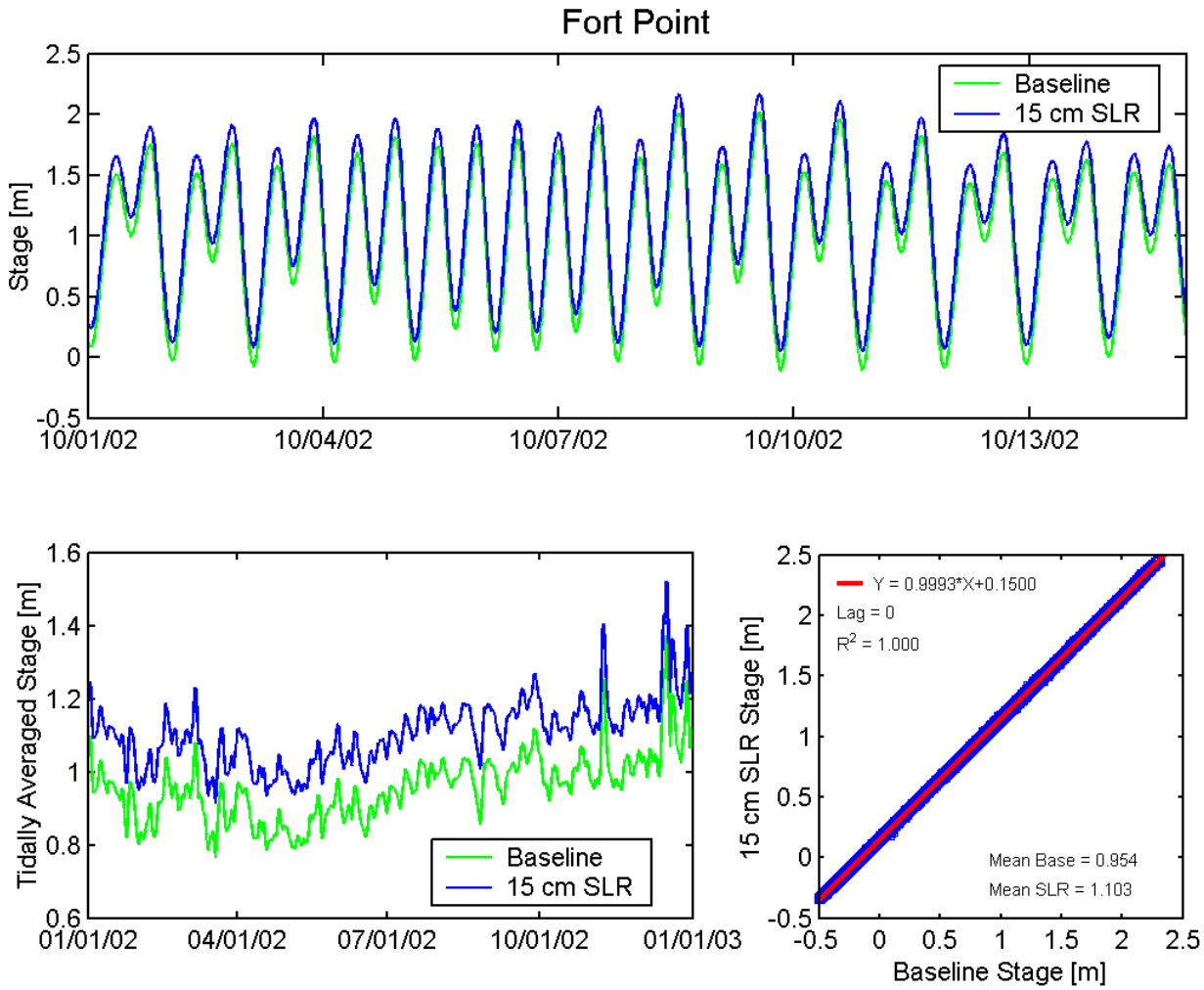

Figure 7.1-1 Predicted stage (top) and tidally averaged stage (lower left) at Fort Point for Baseline and 15 cm SLR scenarios. Regression (lower right) shows the best linear fit for the effect on stage at Fort Point resulting from 15 cm of SLR at the Pacific Ocean boundary.

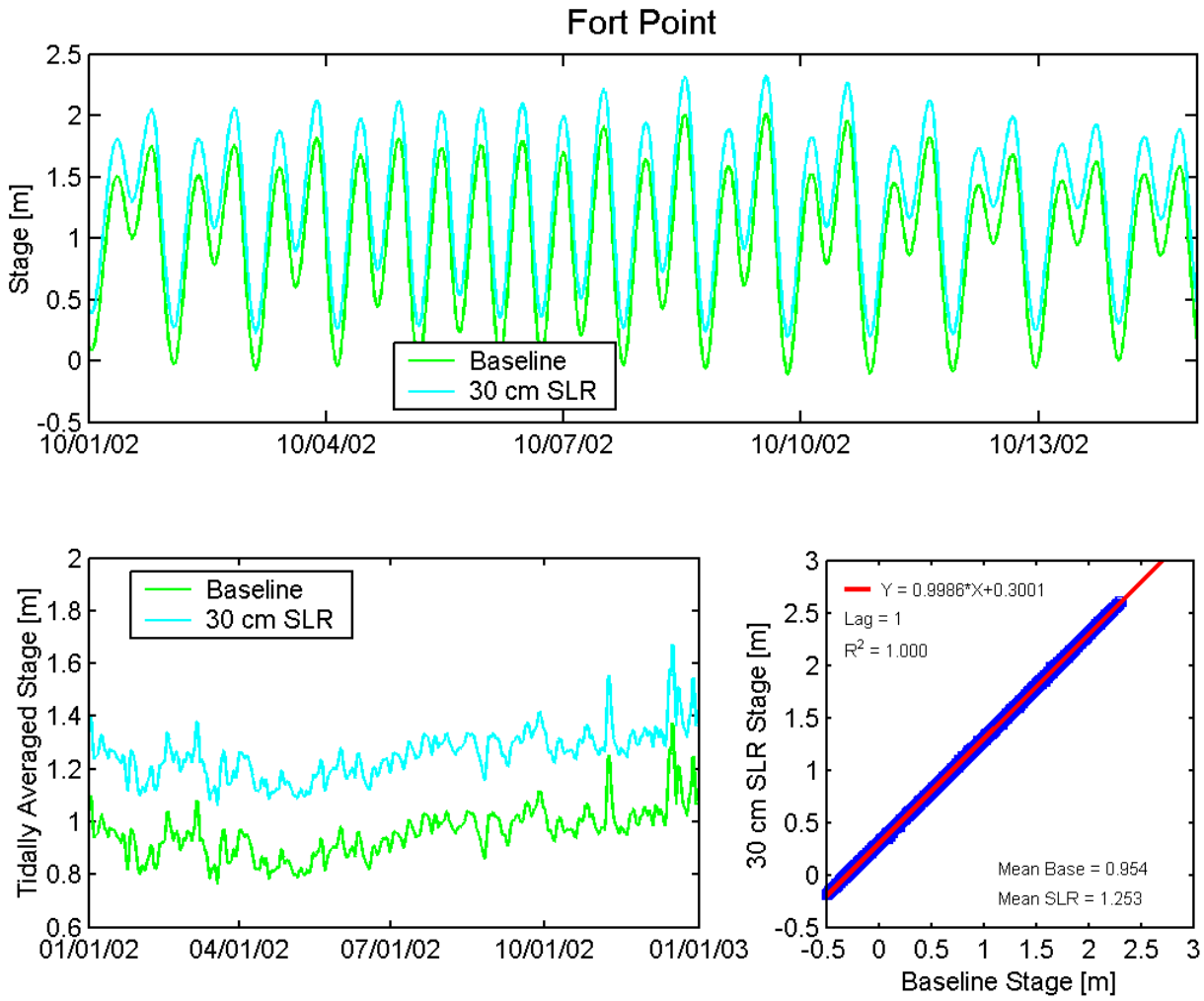

Figure 7.1-2 Predicted stage (top) and tidally averaged stage (lower left) at Fort Point for Baseline and 30 cm SLR scenarios. Regression (lower right) shows the best linear fit for the effect on stage at Fort Point resulting from 30 cm of SLR at the Pacific Ocean boundary.

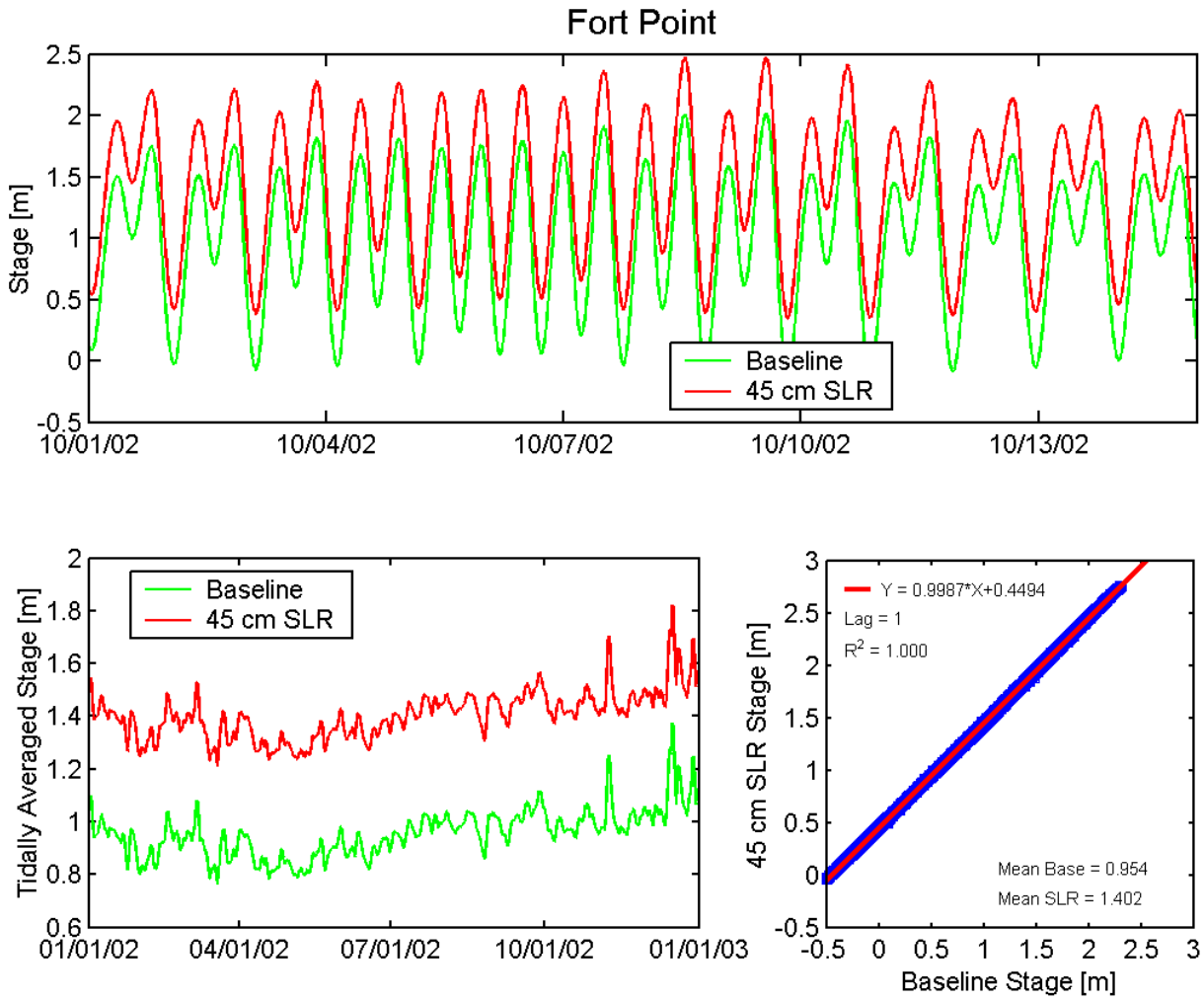

Figure 7.1-3 Predicted stage (top) and tidally averaged stage (lower left) at Fort Point for Baseline and 45 cm SLR scenarios. Regression (lower right) shows the best linear fit for the effect on stage at Fort Point resulting from 45 cm of SLR at the Pacific Ocean boundary.

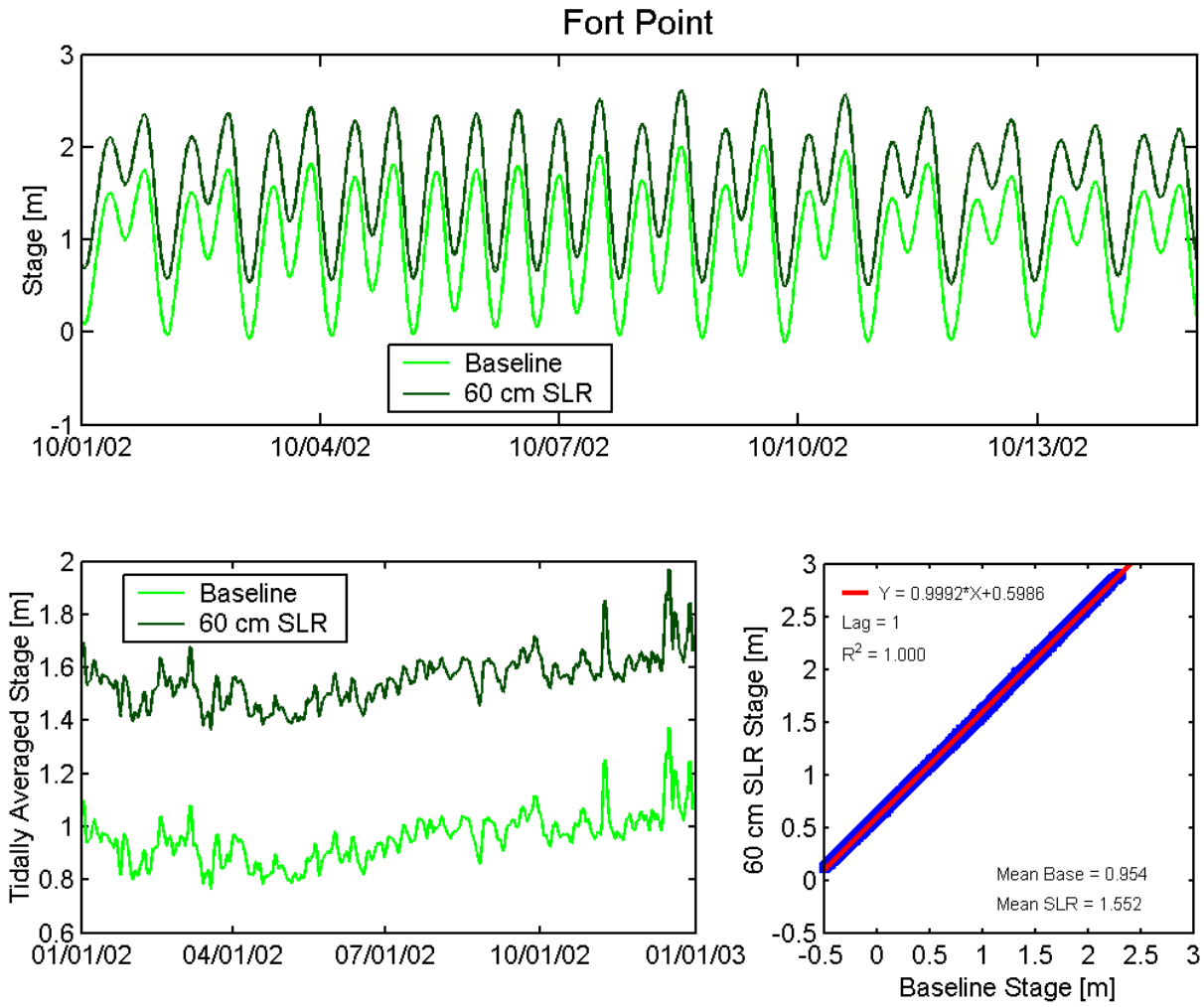

Figure 7.1-4 Predicted stage (top) and tidally averaged stage (lower left) at Fort Point for Baseline and 60 cm SLR scenarios. Regression (lower right) shows the best linear fit for the effect on stage at Fort Point resulting from 60 cm of SLR at the Pacific Ocean boundary.

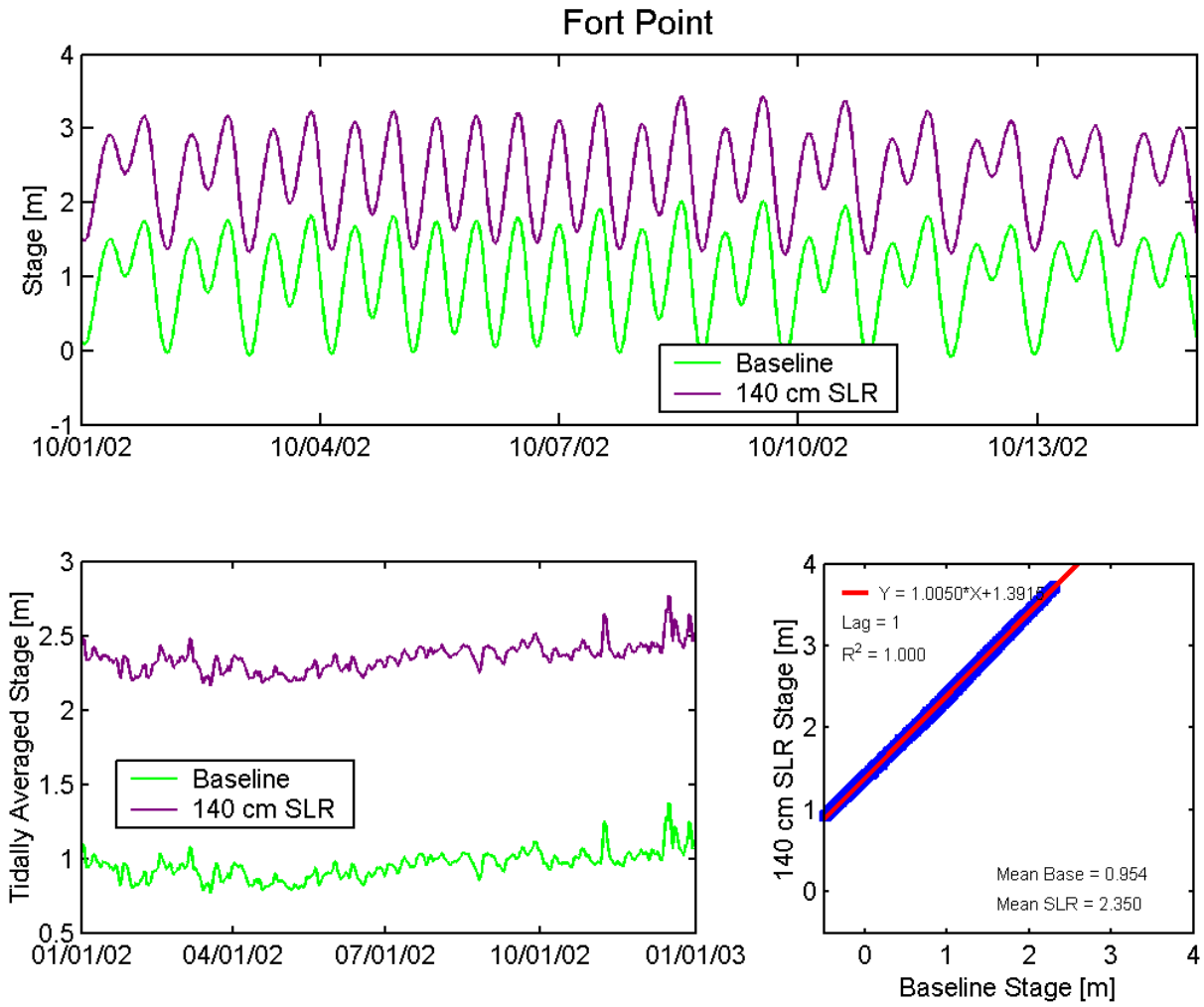

Figure 7.1-5 Predicted stage (top) and tidally averaged stage (lower left) at Fort Point for Baseline and 140 cm SLR scenarios. Regression (lower right) shows the best linear fit for the effect on stage at Fort Point resulting from 140 cm of SLR at the Pacific Ocean boundary.

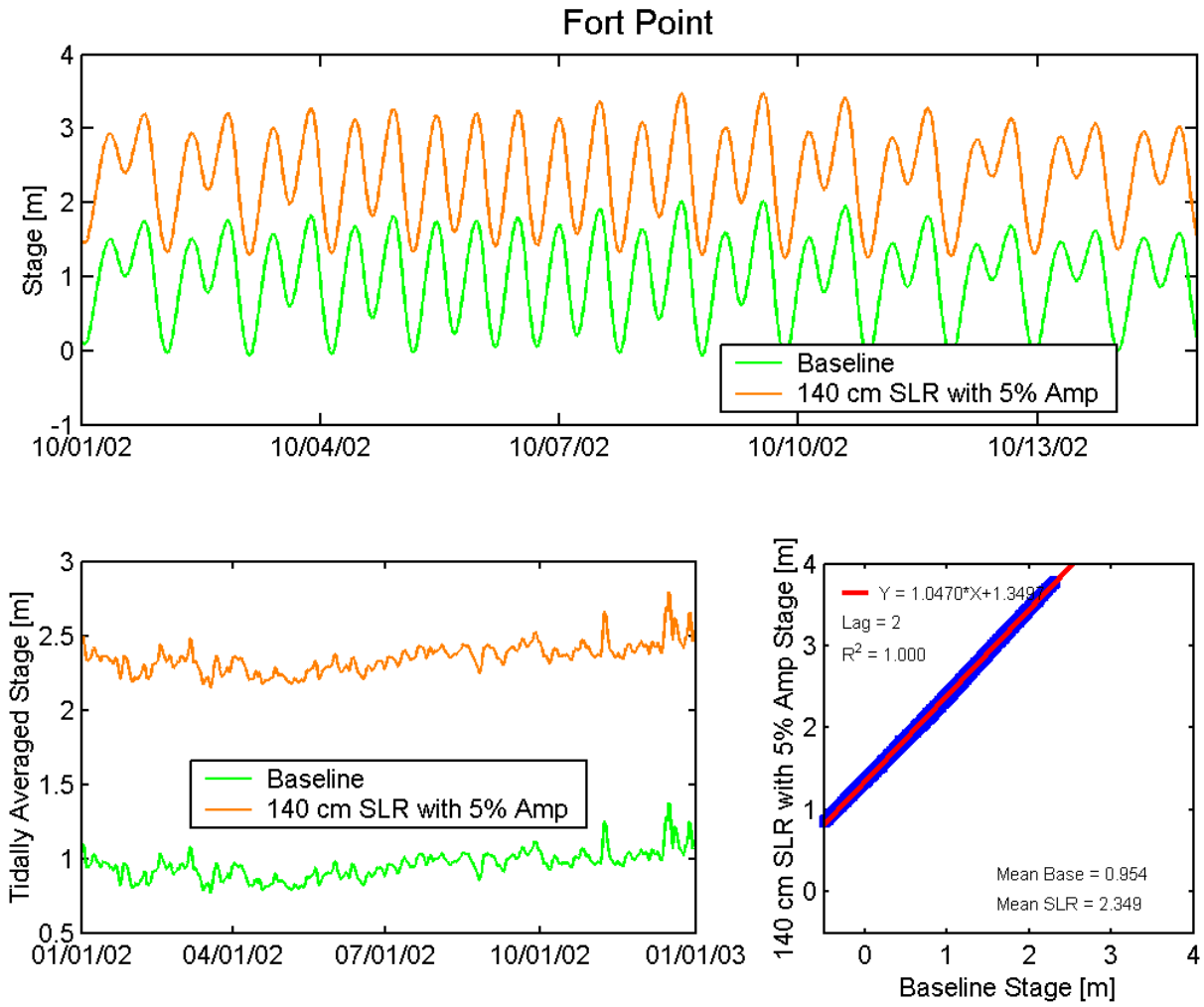

Figure 7.1-6 Predicted stage (top) and tidally averaged stage (lower left) at Fort Point for Baseline and 140 cm of SLR with 5% Amplification scenarios. Regression (lower right) shows the best linear fit for the effect on stage at Fort Point resulting from 140 cm of SLR with 5% Amplification at the Pacific Ocean boundary.

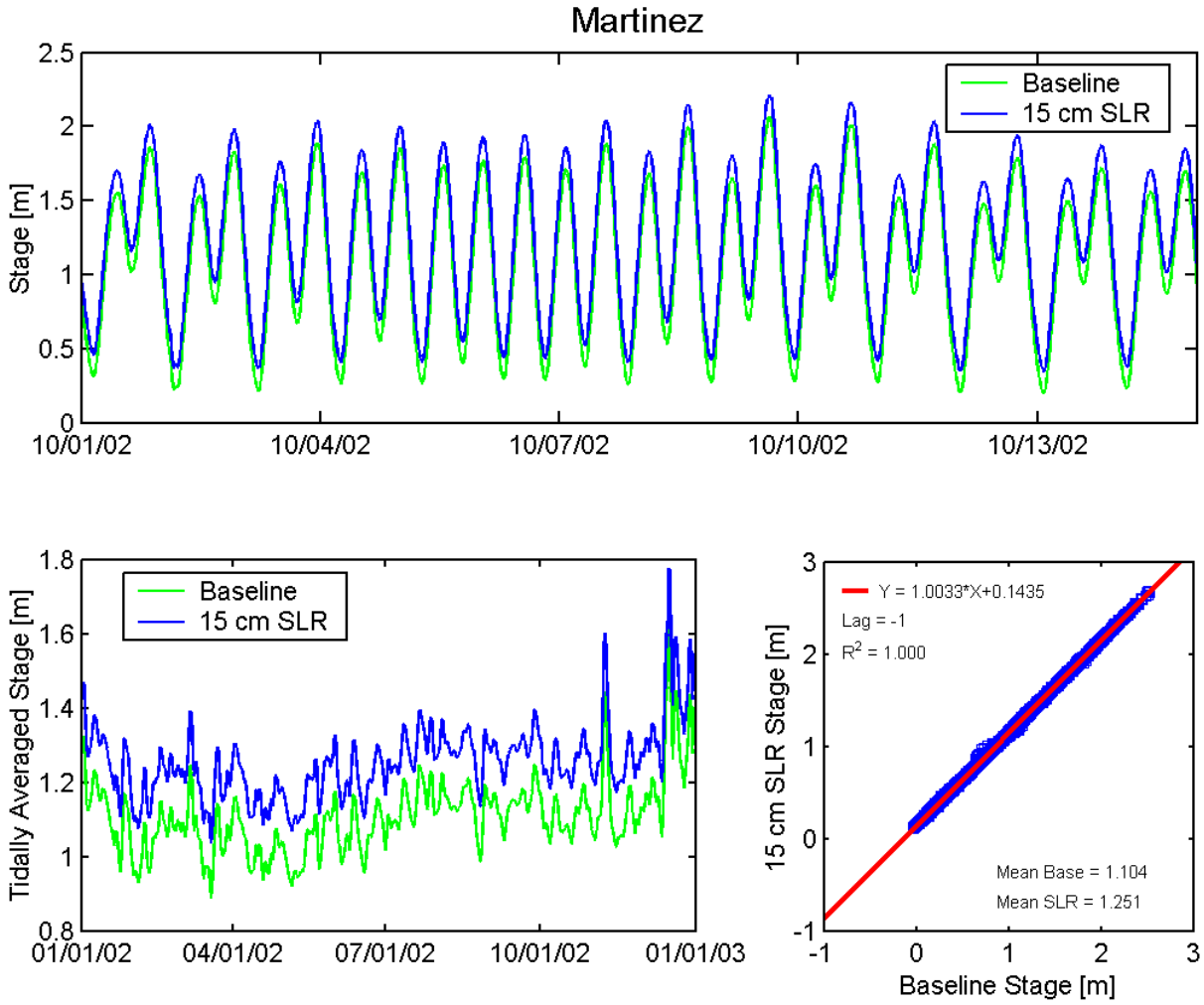

Figure 7.1-7 Predicted stage (top) and tidally averaged stage (lower left) at Martinez for Baseline and 15 cm SLR scenarios. Regression (lower right) shows the best linear fit for the effect on stage at Martinez resulting from 15 cm of SLR at the Pacific Ocean boundary.

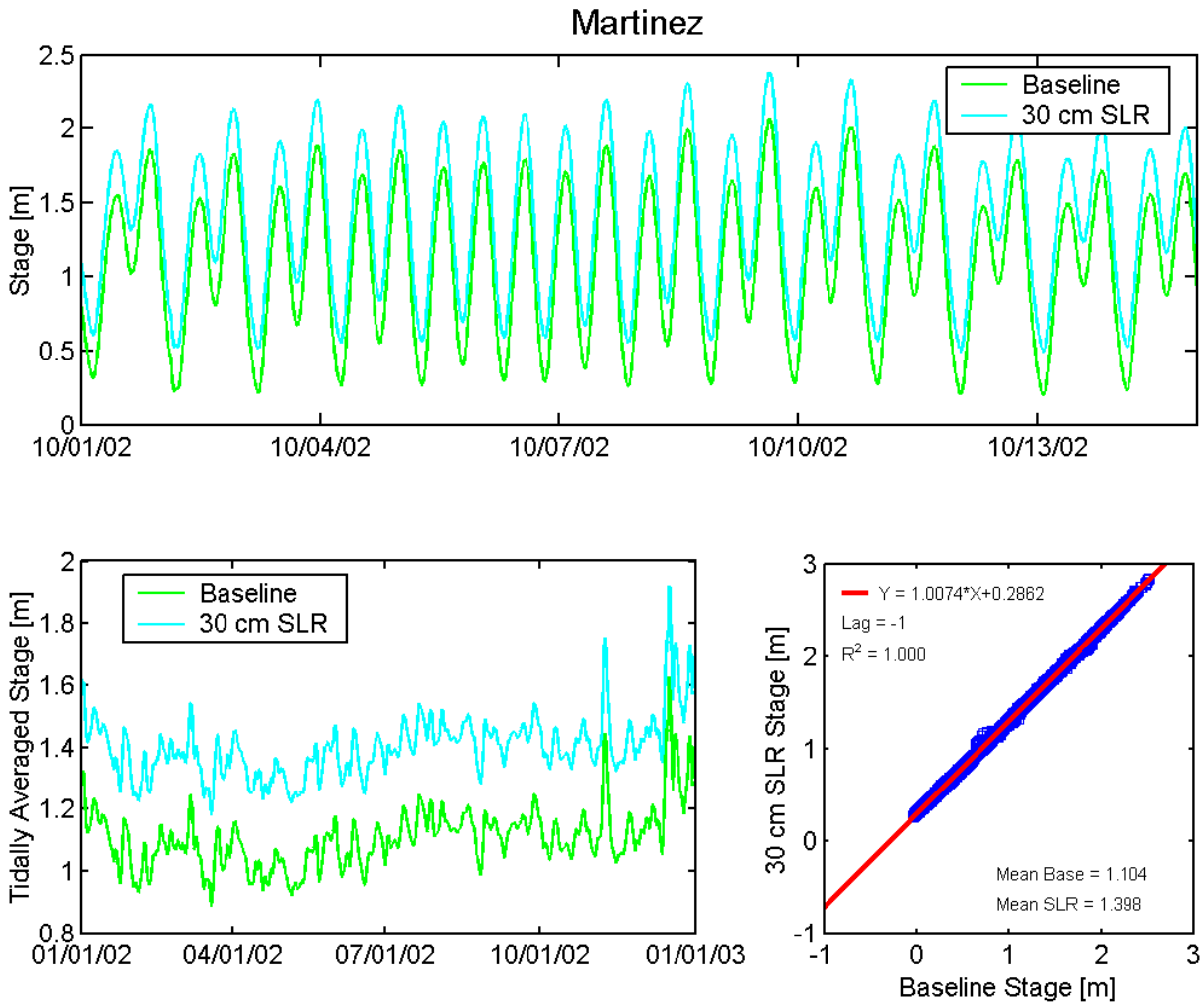

Figure 7.1-8 Predicted stage (top) and tidally averaged stage (lower left) at Martinez for Baseline and 30 cm SLR scenarios. Regression (lower right) shows the best linear fit for the effect on stage at Martinez resulting from 30 cm of SLR at the Pacific Ocean boundary.

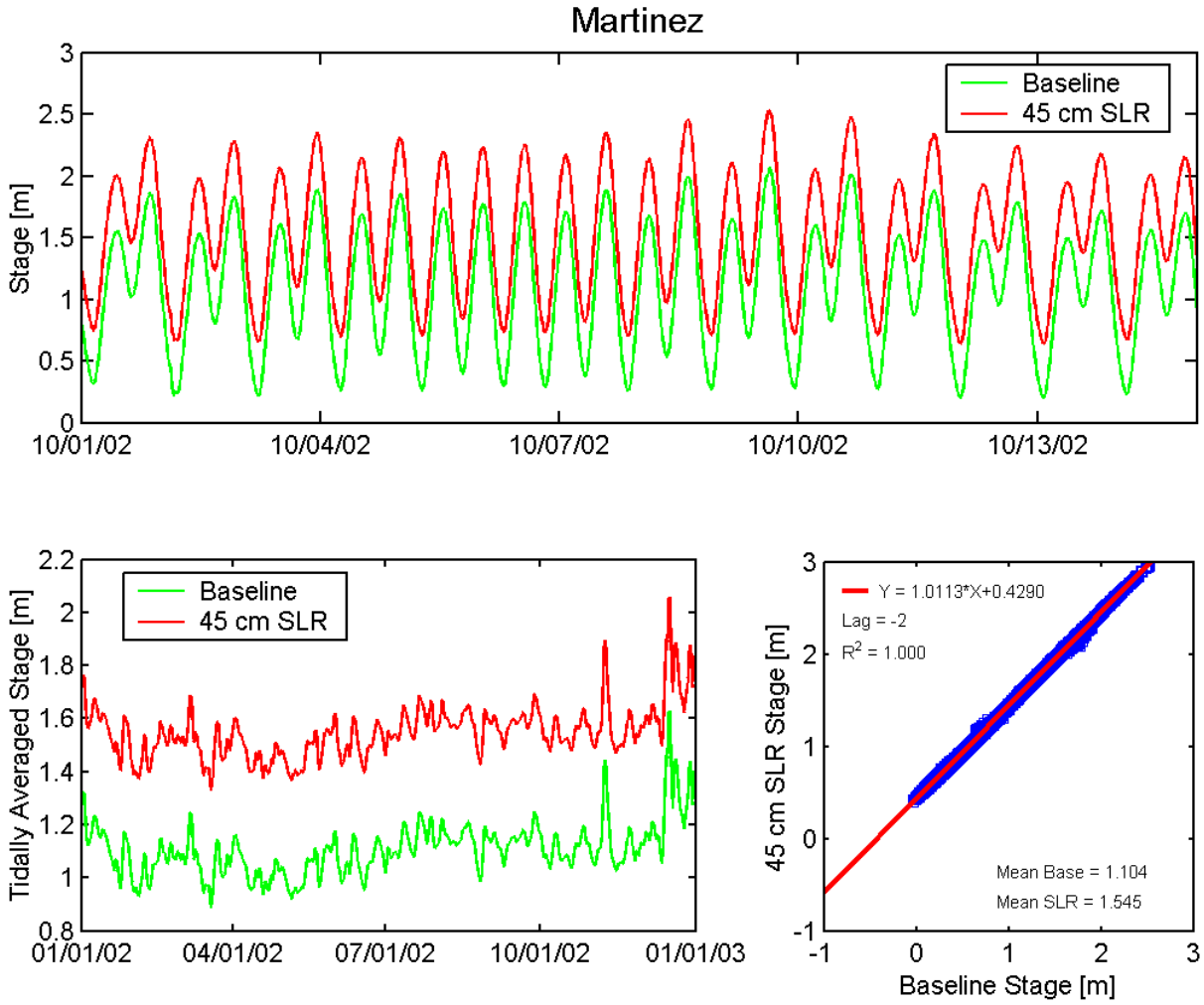

Figure 7.1-9 Predicted stage (top) and tidally averaged stage (lower left) at Martinez for Baseline and 45 cm SLR scenarios. Regression (lower right) shows the best linear fit for the effect on stage at Martinez resulting from 45 cm of SLR at the Pacific Ocean boundary.

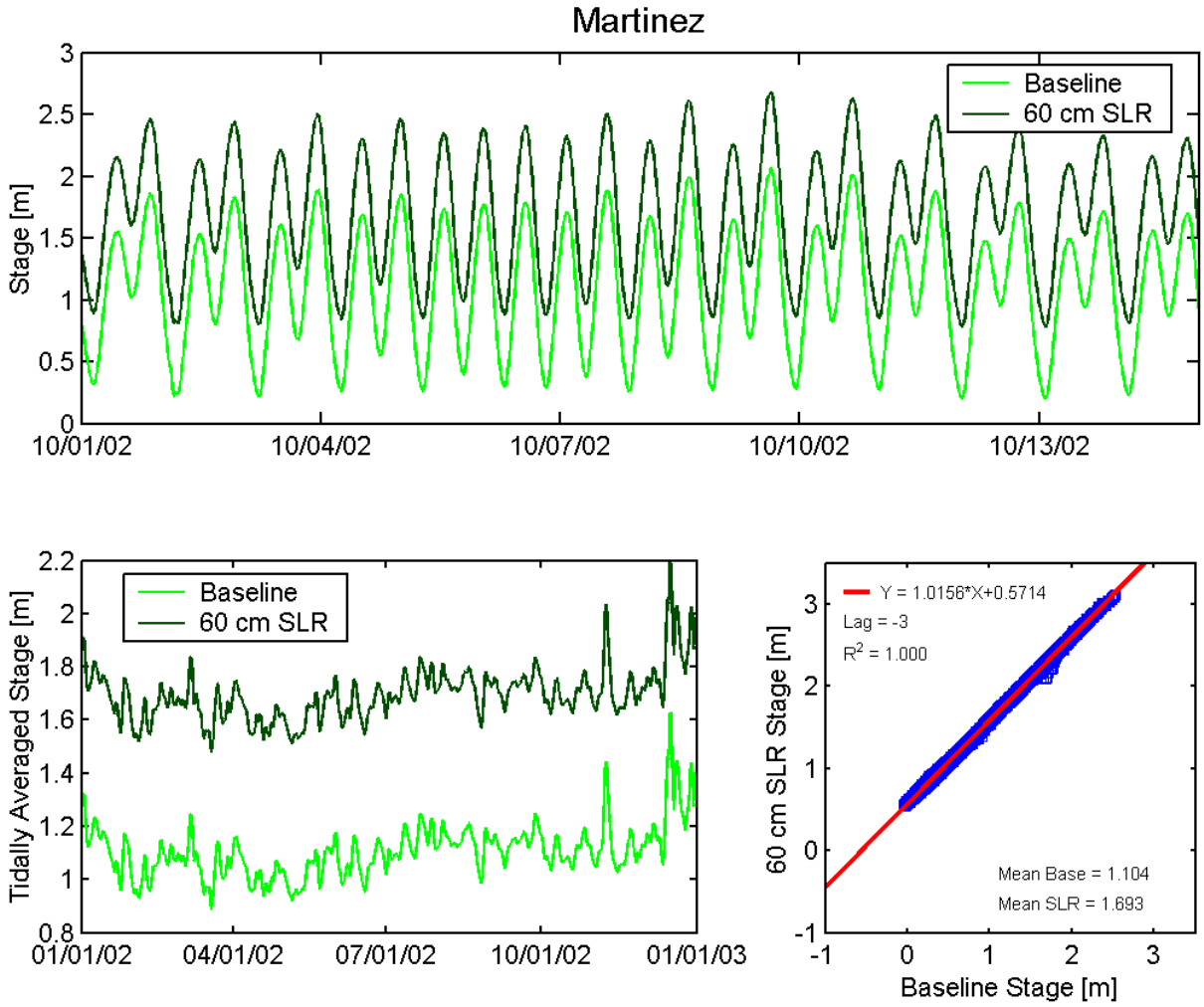

Figure 7.1-10 Predicted stage (top) and tidally averaged stage (lower left) at Martinez for Baseline and 60 cm SLR scenarios. Regression (lower right) shows the best linear fit for the effect on stage at Martinez resulting from 60 cm of SLR at the Pacific Ocean boundary.

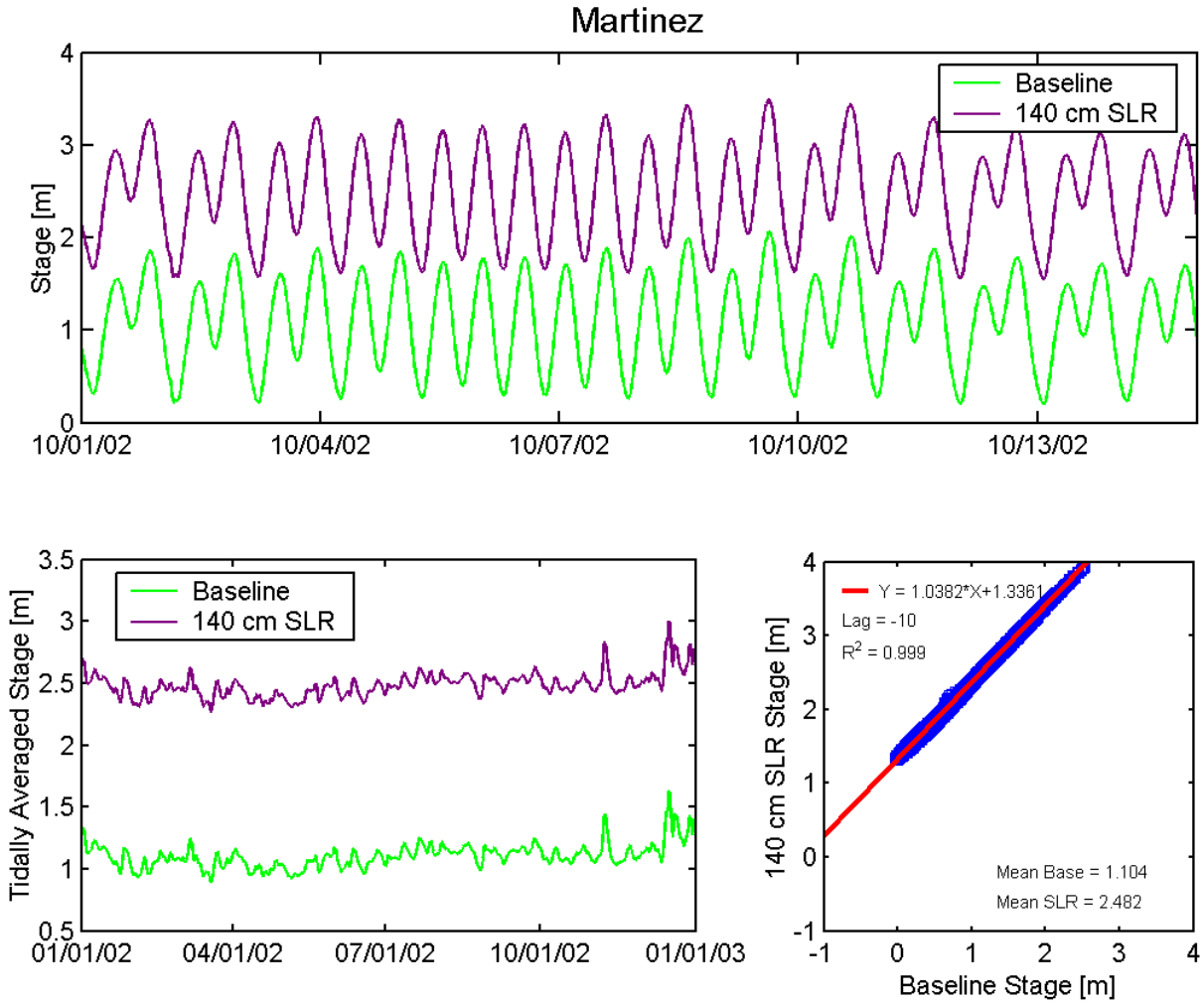

Figure 7.1-11 Predicted stage (top) and tidally averaged stage (lower left) at Martinez for Baseline and 140 cm SLR scenarios. Regression (lower right) shows the best linear fit for the effect on stage at Martinez resulting from 140 cm of SLR at the Pacific Ocean boundary.

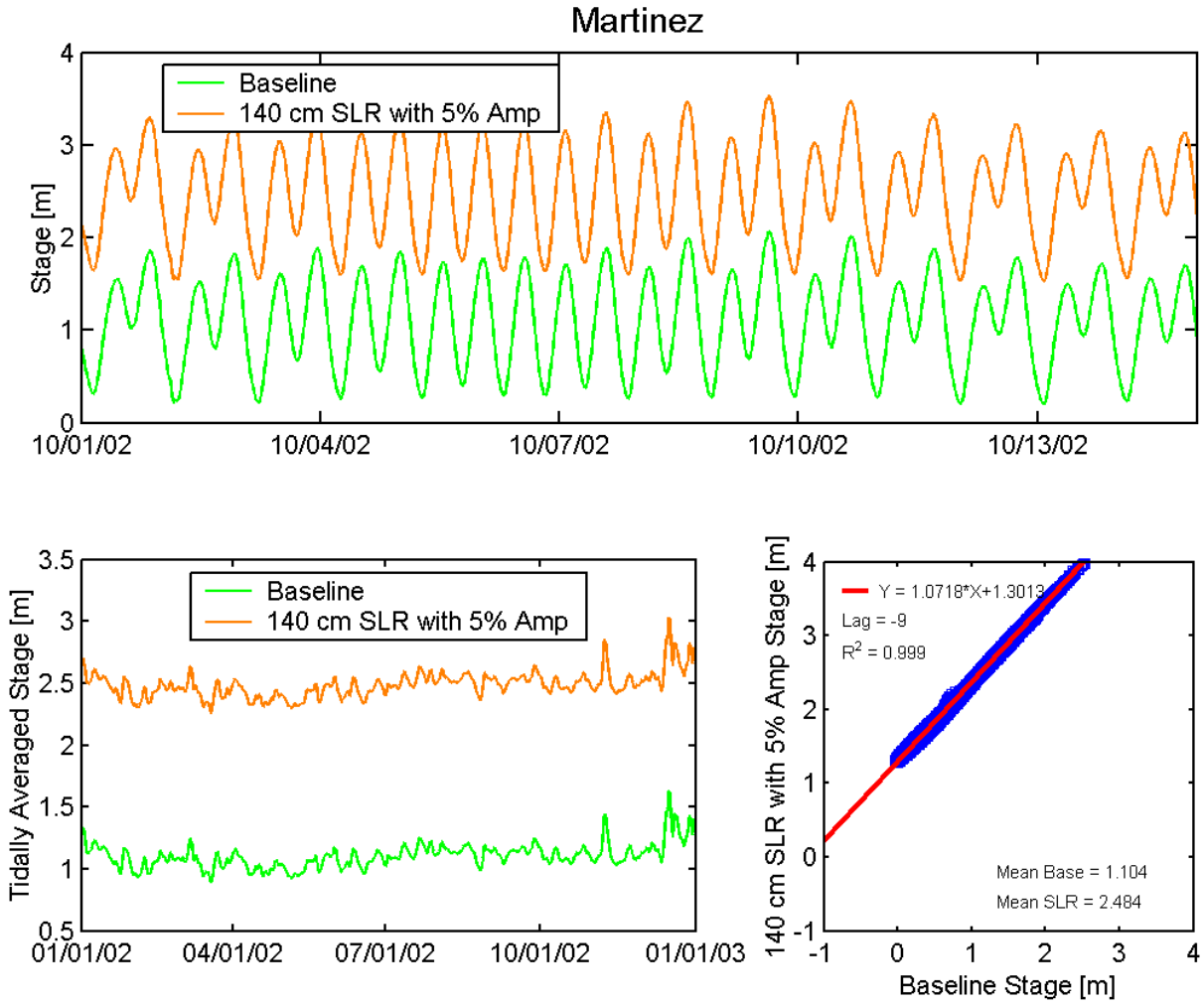

Figure 7.1-12 Predicted stage (top) and tidally averaged stage (lower left) at Martinez for Baseline and 140 cm of SLR with 5% Amplification scenarios. Regression (lower right) shows the best linear fit for the effect on stage at Martinez resulting from 140 cm of SLR with 5% Amplification at the Pacific Ocean boundary.

7.2 Establishing Salinity Relationships for Sea Level Rise at the Golden Gate and Martinez

This section presents linear regression relationships developed using the cross-correlation procedure described in section A.1 to describe the effect of SLR at the ocean boundary on predicted salinity the Golden Gate and at Martinez. No change was made to the ocean boundary salinity for the sea level rise scenarios; a constant salinity of 33.5 psu was applied at the ocean boundary for all scenarios.

7.2.1 Salinity Relationships for Sea Level Rise at the Golden Gate

Figure 7.2-1 shows the predicted cross-section average salinity and tidally averaged cross-section average salinity at the Golden Gate for the Baseline and 15 cm SLR scenarios. The cross-correlation yields a best linear fit of

[Salinity 15 cm SLR] = 0.9883 x *[Salinity Baseline] + 0.3973* (7-13)

with an R^2 value of 1.000 and no phase difference. The slope of the salinity relationship at the Golden Gate for 15 cm SLR is 0.9883 which is not as close to 1.00 as for the stage relationship suggesting that the salinity difference is not accurately represented by a constant offset. This is also reflected by the difference between the annual mean salinity for the Baseline scenario and the annual mean salinity for the 15 cm SLR scenario which is 0.032 psu; this difference is significantly less than the offset of 0.3973 psu in Equation 7-13.

Figure 7.2-2 shows the predicted cross-section average salinity and tidally averaged cross-section average salinity at the Golden Gate for the Baseline and 30 cm SLR scenarios. The cross-correlation yields a best linear fit of

[Salinity 30 cm SLR] = 0.9765 x *[Salinity Baseline] + 0.7960* (7-14)

with an R^2 value of 1.000 and no phase difference. The slope of the salinity relationship at the Golden Gate for 30 cm SLR is 0.9765 which is not as close to 1.00 as for the stage relationship suggesting that the salinity difference is not accurately represented by a constant offset. This is also reflected by the difference between the annual mean salinity for the Baseline scenario and the annual mean salinity for the 30 cm SLR scenario which is 0.063 psu; this difference is significantly less than the offset of 0.7960 psu in Equation 7-14.

Figure 7.2-3 shows the predicted cross-section average salinity and tidally averaged cross-section average salinity at the Golden Gate for the Baseline and 45 cm SLR scenarios. The cross-correlation yields a best linear fit of

[Salinity 45 cm SLR] = 0.9640 x *[Salinity Baseline] + 1.2153* (7-15)

with an R^2 value of 1.000 and a phase lead of 1 minute. The slope of the salinity relationship at the Golden Gate for 45 cm SLR is 0.9640 which is not as close to 1.00 as for the stage

relationship suggesting that the salinity difference is not accurately represented by a constant offset. This is also reflected by the difference between the annual mean salinity for the Baseline scenario and the annual mean salinity for the 15 cm SLR scenario which is 0.092 psu; this difference is significantly less than the offset of 1.2153 psu in Equation 7-15.

Figure 7.2-4 shows the predicted cross-section average salinity and tidally averaged cross-section average salinity at the Golden Gate for the Baseline and 60 cm SLR scenarios. The cross-correlation yields a best linear fit of

[Salinity 60 cm SLR] = 0.9519 x *[Salinity Baseline] + 1.6210* (7-16)

with an R^2 value of 0.999 and a phase lead of 1 minute. The slope of the salinity relationship at the Golden Gate for 60 cm SLR is 0.9519 which is not as close to 1.00 as for the stage relationship suggesting that the salinity difference is not accurately represented by a constant offset. This is also reflected by the difference between the annual mean salinity for the Baseline scenario and the annual mean salinity for the 60 cm SLR scenario which is 0.120 psu; this difference is significantly less than the offset of 1.6210 psu in Equation 7-16.

Figure 7.2-5 shows the predicted cross-section average salinity and tidally averaged cross-section average salinity at the Golden Gate for the Baseline and 140 cm SLR scenarios. The cross-correlation yields a best linear fit of

[Salinity 140 cm SLR] = 0.8871 x *[Salinity Baseline] + 3.7768* (7-17)

with an R^2 value of 0.998 and a phase lead of 6 minutes. The slope of the salinity relationship at the Golden Gate for 140 cm SLR is 0.0.8871 which is much less than 1.00, suggesting that the salinity difference is not accurately represented by a constant offset. This is also reflected by the difference between the annual mean salinity for the Baseline scenario and the annual mean salinity for the 140 cm SLR scenario which is 0.254 psu; this difference is significantly less than the offset of 3.7768 psu in Equation 7-17.

Figure 7.2-6 shows the predicted cross-section average salinity and tidally averaged cross-section average salinity at the Golden Gate for the Baseline and 140 cm SLR with 5% Amplification scenarios. The cross-correlation yields a best linear fit of

[Salinity 140 cm SLR with 5% Amplification] = 0.9037 x *[Salinity Baseline] + 3.2957* (7-18)

with an R^2 value of 0.997 and a phase lead of 4 minutes. The slope of the salinity relationship at the Golden Gate for 140 cm SLR with 5% Amplification is 0.9037 which is much less than 1.00, suggesting that the salinity difference is not accurately represented by a constant offset. This is also reflected by the difference between the annual mean salinity for the Baseline scenario and the annual mean salinity for the 140 cm SLR with 5% Amplification scenario which is 0.290 psu; this difference is significantly less than the offset of 3.2957 psu in Equation 7-18.

7.2.2 Salinity Relationships for Sea Level Rise at Martinez

Salinity relationships at Martinez were developed using both the predicted surface salinity at the location of the DWR Martinez surface salinity sensor (RSAC054), and for predicted cross-sectional average salinity at the location shown on Figure 3-1. The reason for these two different relationships are that observed surface salinity at Martinez is typically used for historical DSM2 simulations, whereas the predicted cross-section averaged salinity from the UnTRIM Bay-Delta model is more representative of the salinity at Martinez as represented by a 1-D model such as DSM2.

Figure 7.2-7 shows the predicted surface salinity and tidally averaged surface salinity at Martinez (RSAC054) for the Baseline and 15 cm SLR scenarios. The cross-correlation yields a best linear fit of

[Salinity 15 cm SLR] = 1.0001 x *[Salinity Baseline] + 0.2778* (7-19)

with an R^2 value of 0.999 and a phase lag of 1 minute. Because this relationship is linear with a slope very close to 1.000, this shows that the 15 cm stage offset applied at the ocean boundary is translating almost exactly to 0.2778 psu salinity increase at the Martinez surface salinity sensor. This is also reflected by the difference between the annual mean salinity for the Baseline scenario and the annual mean salinity for the 15 cm SLR scenario which is 0.279 psu. This suggests that a constant salinity offset between 0.278 and 0.279 psu would fairly accurately represent the salinity increase at Martinez for the 15 cm SLR scenario. The largest expected errors using this approach are likely to occur for low salinity values at Martinez, when salinity in the Delta is expected to be low.

Figure 7.2-8 shows the predicted cross-section average salinity and tidally averaged cross-section average salinity at Martinez (location shown on Figure 3-1) for the Baseline and 15 cm SLR scenarios. The cross-correlation yields a best linear fit of

[Salinity 15 cm SLR] = 0.9969 x *[Salinity Baseline] + 0.3416* (7-20)

with an R^2 value of 1.000 and no phase difference. Because this relationship is linear with a slope very close to 1.000, this shows that the 15 cm stage offset applied at the ocean boundary is translating to approximately a 0.3416 psu increase in cross-section average salinity at Martinez. This is also reflected by the difference between the annual mean salinity for the Baseline scenario and the annual mean salinity for the 15 cm SLR scenario which is 0.301 psu. This suggests that a constant salinity offset between 0.3010 and 0.3416 psu would fairly accurately represent the salinity increase at Martinez for the 15 cm SLR scenario. The relationship derived from the predicted cross-section averaged salinity suggests a larger increase than the relationship derived from the predicted surface salinity.

Figure 7.2-9 shows the predicted surface salinity and tidally averaged surface salinity at Martinez (RSAC054) for the Baseline and 30 cm SLR scenarios. The cross-correlation yields a best linear fit of

[Salinity 30 cm SLR] = 0.9968 x *[Salinity Baseline] + 0.5853* (7-21)

with an R^2 value of 0.998 and a phase lead of 3 minutes. Because this relationship is linear with a slope very close to 1.000, this shows that the 30 cm stage offset applied at the ocean boundary is translating almost exactly to 0.5853 psu salinity increase at the Martinez surface salinity sensor. This is also reflected by the difference between the annual mean salinity for the Baseline scenario and the annual mean salinity for the 30 cm SLR scenario which is 0.550 psu. This suggests that a constant salinity offset between 0.550 and 0.585 psu would fairly accurately represent the salinity increase at Martinez for the 30 cm SLR scenario. The largest expected errors using this approach are likely to occur for low salinity values at Martinez, when salinity in the Delta is expected to be low.

Figure 7.2-10 shows the predicted cross-section average salinity and tidally averaged cross-section average salinity at Martinez (location shown on Figure 3-1) for the Baseline and 30 cm SLR scenarios. The cross-correlation yields a best linear fit of

[Salinity 30 cm SLR] = 0.9912 x *[Salinity Baseline] + 0.7044* (7-22)

with an R^2 value of 1.000 and a phase lead of 1 minute. Because this relationship is linear with a slope very close to 1.000, this shows that the 30 cm stage offset applied at the ocean boundary is translating to approximately a 0.7044 psu increase in cross-section average salinity at Martinez. This is also reflected by the difference between the annual mean salinity for the Baseline scenario and the annual mean salinity for the 30 cm SLR scenario which is 0.602 psu. This suggests that a constant salinity offset between 0.602 and 0.7044 psu would fairly accurately represent the salinity increase at Martinez for the 30 cm SLR scenario. The relationship derived from the predicted cross-section averaged salinity suggests a larger increase than the relationship derived from the predicted surface salinity.

Figure 7.2-11 shows the predicted surface salinity and tidally averaged surface salinity at Martinez (RSAC054) for the Baseline and 45 cm SLR scenarios. The cross-correlation yields a best linear fit of

[Salinity 45 cm SLR] = 0.9919 x *[Salinity Baseline] + 0.9024* (7-23)

with an R^2 value of 0.997 and a phase lead of 4 minutes. Because this relationship is linear with a slope very close to 1.000, this shows that the 45 cm stage offset applied at the ocean boundary is translating to approximately a 0.9024 psu salinity increase at the Martinez surface salinity sensor. This is also reflected by the difference between the annual mean salinity for the Baseline scenario and the annual mean salinity for the 45 cm SLR scenario which is 0.814 psu. This suggests that a constant salinity offset between 0.814 and 0.9024 psu would fairly accurately represent the salinity increase at Martinez for the 45 cm SLR scenario. The largest expected errors using this approach are likely to occur for low salinity values at Martinez, when salinity in the Delta is expected to be low.

Figure 7.2-12 shows the predicted cross-section average salinity and tidally averaged cross-section average salinity at Martinez (location shown on Figure 3-1) for the Baseline and 45 cm SLR scenarios. The cross-correlation yields a best linear fit of

[Salinity 45 cm SLR] = 0.9842 x *[Salinity Baseline] + 1.0914* (7-24)

with an R^2 value of 0.999 and a phase lead of 2 minutes. The slope of the section averaged salinity relationship at Martinez for the 45 cm SLR is 0.9842 which is not as close to 1.00 as for the surface salinity relationship suggesting that the cross-section average salinity difference is not accurately represented by a constant offset. This is also reflected by the difference between the annual mean cross-section average salinity for the Baseline scenario and the annual mean salinity for the 45 cm SLR scenario which is 0.8890 psu; this difference is significantly less than the offset of 1.0914 psu in Equation 7-24. This suggests that with increasing sea level rise, applying a constant salinity offset is less appropriate than for the 15 cm SLR scenario, however the linear fit given by Equation 7-24 shows a high correlation.

Figure 7.2-13 shows the predicted surface salinity and tidally averaged surface salinity at Martinez (RSAC054) for the Baseline and 60 cm SLR scenarios. The cross-correlation yields a best linear fit of

[Salinity 60 cm SLR] = 0.9866 x *[Salinity Baseline] + 1.2019* (7-25)

with an R^2 value of 0.996 and a phase lead of 6 minutes. Because this relationship is linear with a slope relatively close to 1.000, this shows that the 60 cm stage offset applied at the ocean boundary is translating to approximately a 1.2019 psu salinity increase at the Martinez surface salinity sensor. However, the deviation of the slope from 1.000 suggests that the linear fit rather than a constant offset is more appropriate for higher levels of sea level rise. This is also reflected by the difference between the annual mean salinity for the Baseline scenario and the annual mean salinity for the 60 cm SLR scenario which is 1.056 psu; this difference is significantly less than the constant offset of 1.2019 psu in Equation 7-25.

Figure 7.2-14 shows the predicted cross-section average salinity and tidally averaged cross-section average salinity at Martinez (location shown on Figure 3-1) for the Baseline and 60 cm SLR scenarios. The cross-correlation yields a best linear fit of

[Salinity 60 cm SLR] = 0.9769 x *[Salinity Baseline] + 1.4848* (7-26)

with an R^2 value of 0.999 and a phase lead of 3 minutes. Because this relationship is linear with a slope relatively close to 1.000, this shows that the 60 cm stage offset applied at the ocean boundary is translating to approximately a 1.4848 psu increase in cross-section average salinity at Martinez. However, the deviation of the slope from 1.000 suggests that the linear fit rather than a constant offset is more appropriate for higher levels of sea level rise. This is also reflected by the difference between the annual mean salinity for the Baseline scenario and the annual mean salinity for the 60 cm SLR scenario which is 1.177 psu; this difference is significantly less than the constant offset of 1.4848 psu in Equation 7-26. The relationship derived from the predicted cross-section averaged salinity suggests a larger increase than the relationship derived from the predicted surface salinity.

Figure 7.2-15 shows the predicted surface salinity and tidally averaged surface salinity at Martinez (RSAC054) for the Baseline and 140 cm SLR scenarios. The cross-correlation yields a best linear fit of

[Salinity 140 cm SLR] = 0.9633 x *[Salinity Baseline] + 2.9195* (7-27)

with an R^2 value of 0.992 and a phase lead of 12 minutes. Because this relationship is linear with a slope somewhat less than 1.000, this shows that the 140 cm stage offset applied at the ocean boundary does not translate accurately to a constant salinity offset at the Martinez surface salinity sensor. The deviation of the slope from 1.000 suggests that the linear fit rather than a constant offset is more appropriate for higher levels of sea level rise. This is also reflected by the difference between the annual mean salinity for the Baseline scenario and the annual mean salinity for the 140 cm SLR scenario which is 2.520 psu; this difference is significantly less than the constant offset of 2.9195 psu in Equation 7-27.

Figure 7.2-16 shows the predicted cross-section average salinity and tidally averaged cross-section average salinity at Martinez (location shown on Figure 3-1) for the Baseline and 140 cm SLR scenarios. The cross-correlation yields a best linear fit of

[Salinity 140 cm SLR] = 0.9231 x *[Salinity Baseline] + 3.5618* (7-28)

with an R^2 value of 0.994 and a phase lead of 9 minutes. Because this relationship is linear with a slope somewhat less than 1.000, this shows that the 140 cm stage offset applied at the ocean boundary does not translate accurately to a constant salinity offset to cross-section average salinity at Martinez. The deviation of the slope from 1.000 suggests that the linear fit rather than a constant offset is more appropriate for higher levels of sea level rise. This is also reflected by the difference between the annual mean salinity for the Baseline scenario and the annual mean salinity for the 140 cm SLR scenario which is 2.579 psu, , which is significantly less than the constant offset of 3.5618 psu in Equation 7-28. The relationship derived from the predicted cross-section averaged salinity suggests a larger increase than the relationship derived from the predicted surface salinity.

Figure 7.2-17 shows the predicted surface salinity and tidally averaged surface salinity at Martinez (RSAC054) for the Baseline and 140 cm SLR with 5% Amplification scenarios. The cross-correlation yields a best linear fit of

[Salinity 140 cm SLR with 5% Amplification] = 0.9797 x *[Salinity Baseline] + 2.8654* (7-29)

with an R^2 value of 0.991 and a phase lead of 12 minutes. Because this relationship is linear with a slope relatively close to 1.000, this shows that the 140 cm stage offset with 5% amplification applied at the ocean boundary is translating to approximately a 2.8654 psu salinity increase at the Martinez surface salinity sensor. This is also reflected by the difference between the annual mean salinity for the Baseline scenario and the annual mean salinity for the 140 cm SLR with 5% Amplification scenario which is 2.645 psu; this difference is relatively similar to the offset of 2.8654 psu in Equation 7-29. However, it is likely that the linear fit would produce better results than a constant for higher levels of sea level rise.

Figure 7.2-18 shows the predicted cross-section average salinity and tidally averaged cross-section average salinity at Martinez (location shown on Figure 3-1) for the Baseline and 140 cm SLR with 5% Amplification scenarios. The cross-correlation yields a best linear fit of

[Salinity 140 cm SLR with 5% Amplification] = 0.9405 x *[Salinity Baseline] + 3.4103* (7-30)

with an R^2 value of 0.994 and no phase difference. Because this relationship is linear with a slope somewhat less than 1.000, this shows that the 140 cm stage offset with 5% amplification applied at the ocean boundary does not translate accurately to a constant salinity offset in cross-section average salinity at Martinez. This is also reflected by the difference between the annual mean salinity for the Baseline scenario and the annual mean salinity for the 140 cm SLR with 5% Amplification scenario which is 2.650 psu; this difference is significantly less than the constant offset of 3.4103 psu in Equation 7-30. The relationship derived from the predicted cross-section averaged salinity suggests a larger salinity increase than the relationship derived from the predicted surface salinity.

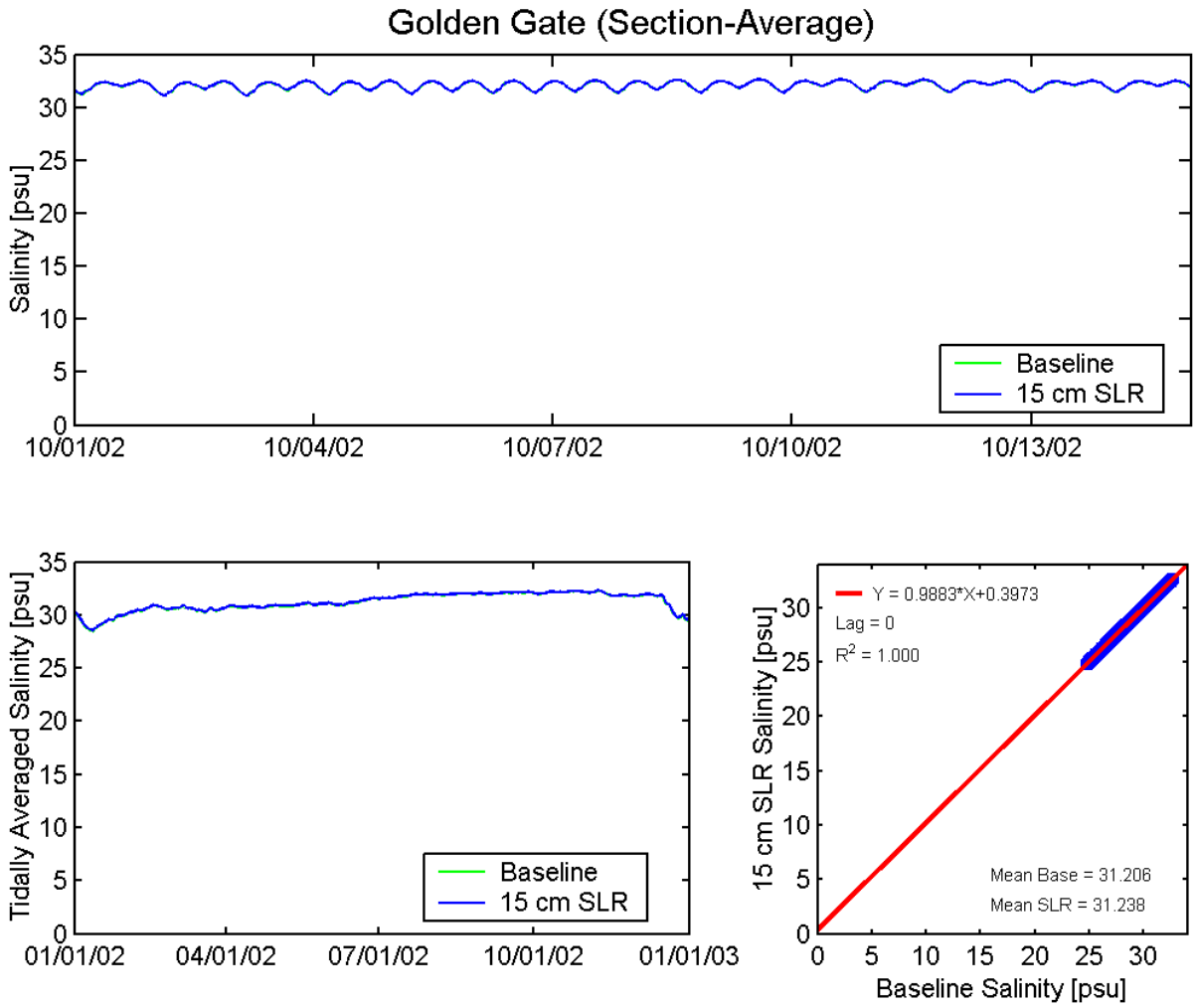

Figure 7.2-1 Predicted salinity (top) and tidally averaged salinity (lower left) at the Golden Gate for Baseline and 15 cm SLR scenarios. Regression (lower right) shows the best linear fit for the effect on salinity at the Golden Gate resulting from 15 cm of SLR at the Pacific Ocean boundary.

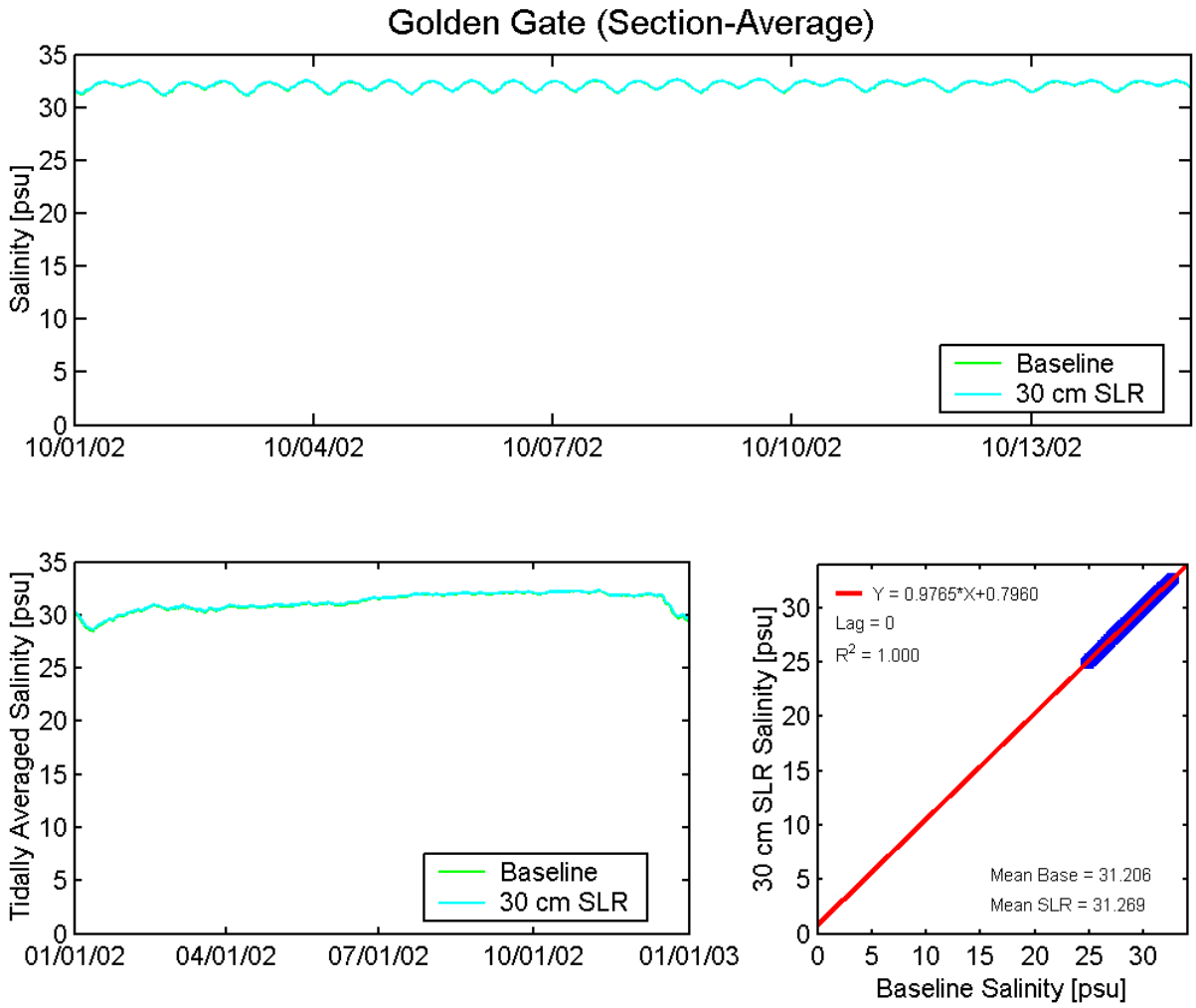

Figure 7.2-2 Predicted salinity (top) and tidally averaged salinity (lower left) at the Golden Gate for Baseline and 30 cm SLR scenarios. Regression (lower right) shows the best linear fit for the effect on salinity at the Golden Gate resulting from 30 cm of SLR at the Pacific Ocean boundary.

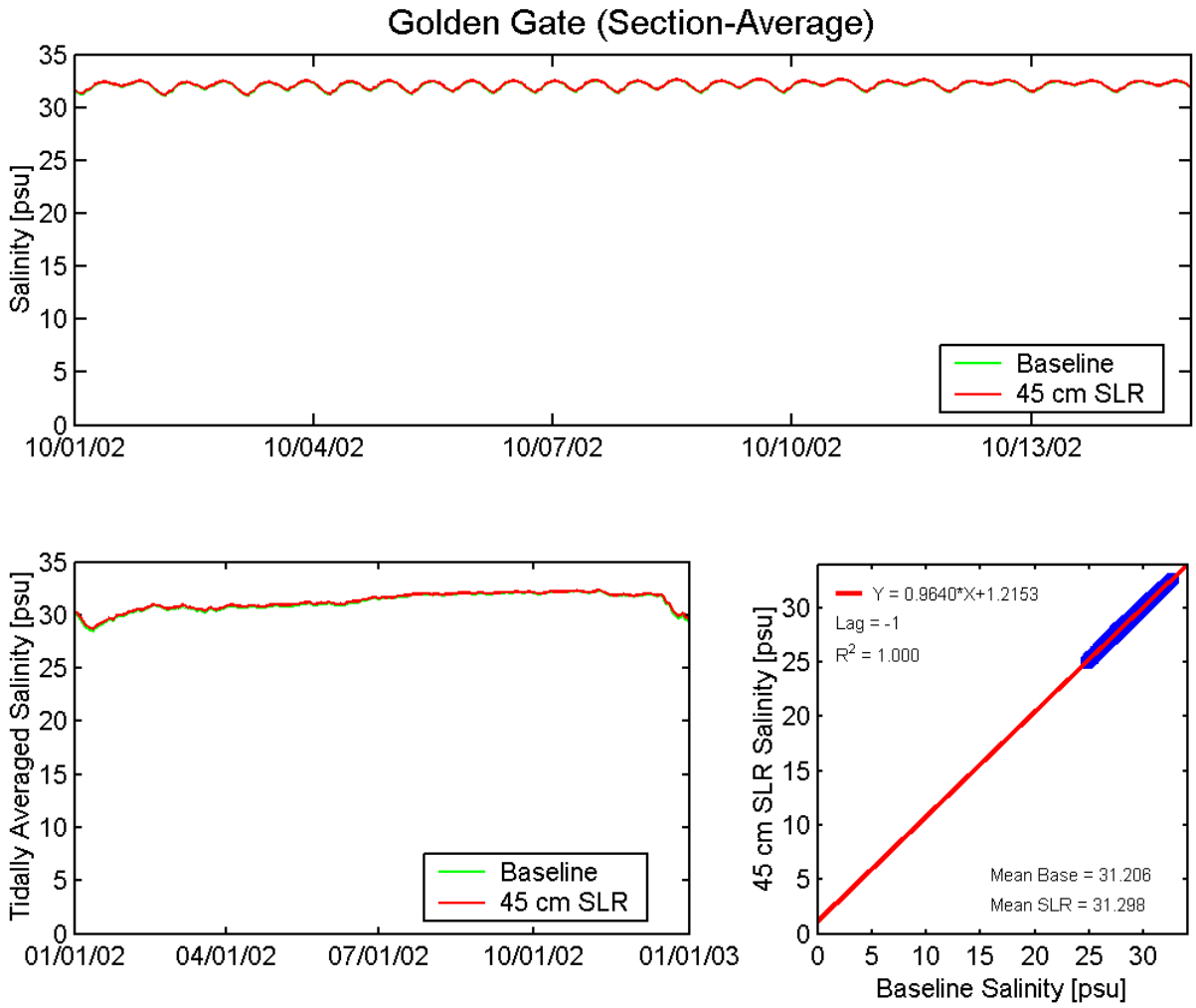

Figure 7.2-3 Predicted salinity (top) and tidally averaged salinity (lower left) at the Golden Gate for Baseline and 45 cm SLR scenarios. Regression (lower right) shows the best linear fit for the effect on salinity at the Golden Gate resulting from 45 cm of SLR at the Pacific Ocean boundary.

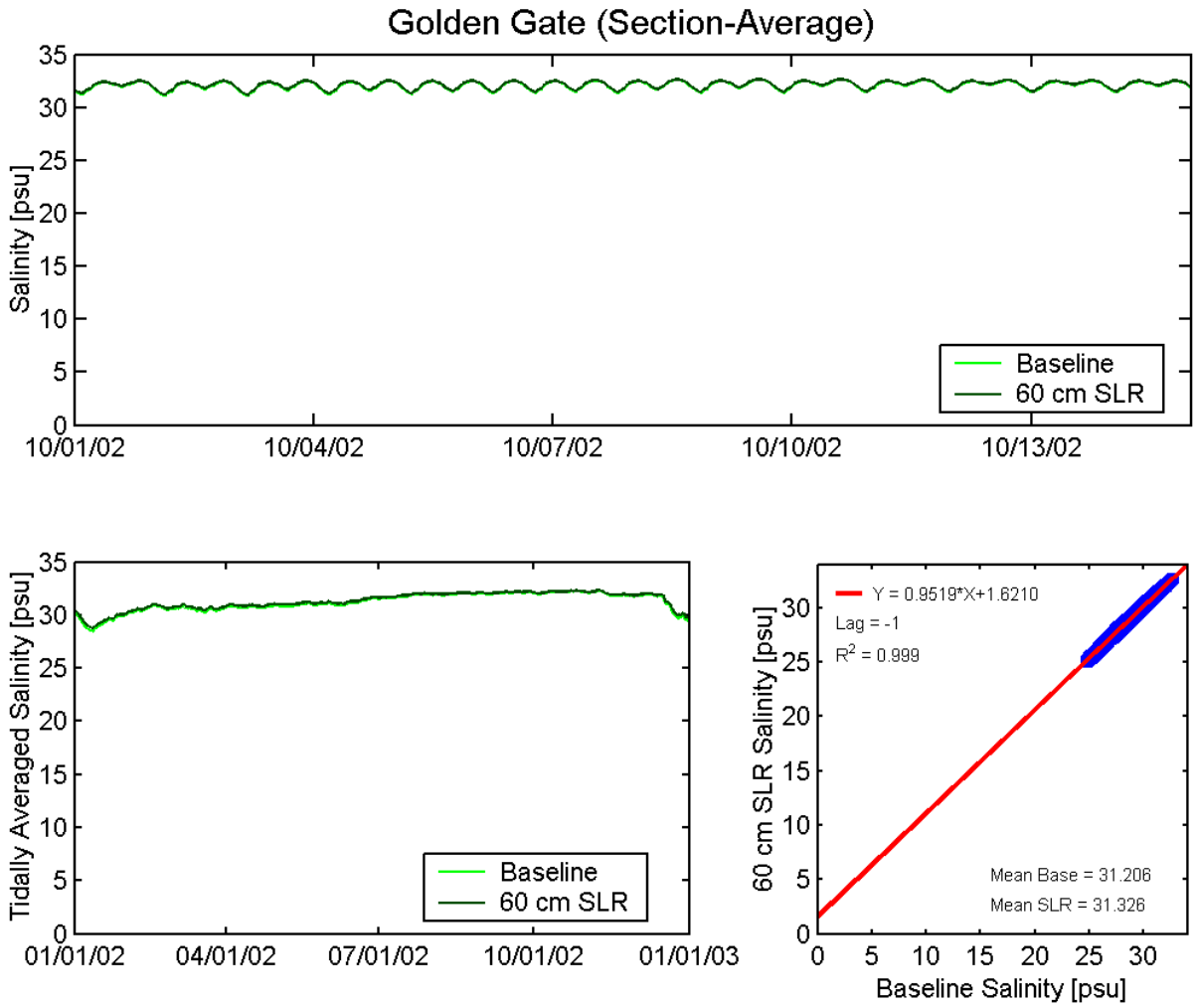

Figure 7.2-4 Predicted salinity (top) and tidally averaged salinity (lower left) at the Golden Gate for Baseline and 60 cm SLR scenarios. Regression (lower right) shows the best linear fit for the effect on salinity at the Golden Gate resulting from 60 cm of SLR at the Pacific Ocean boundary.

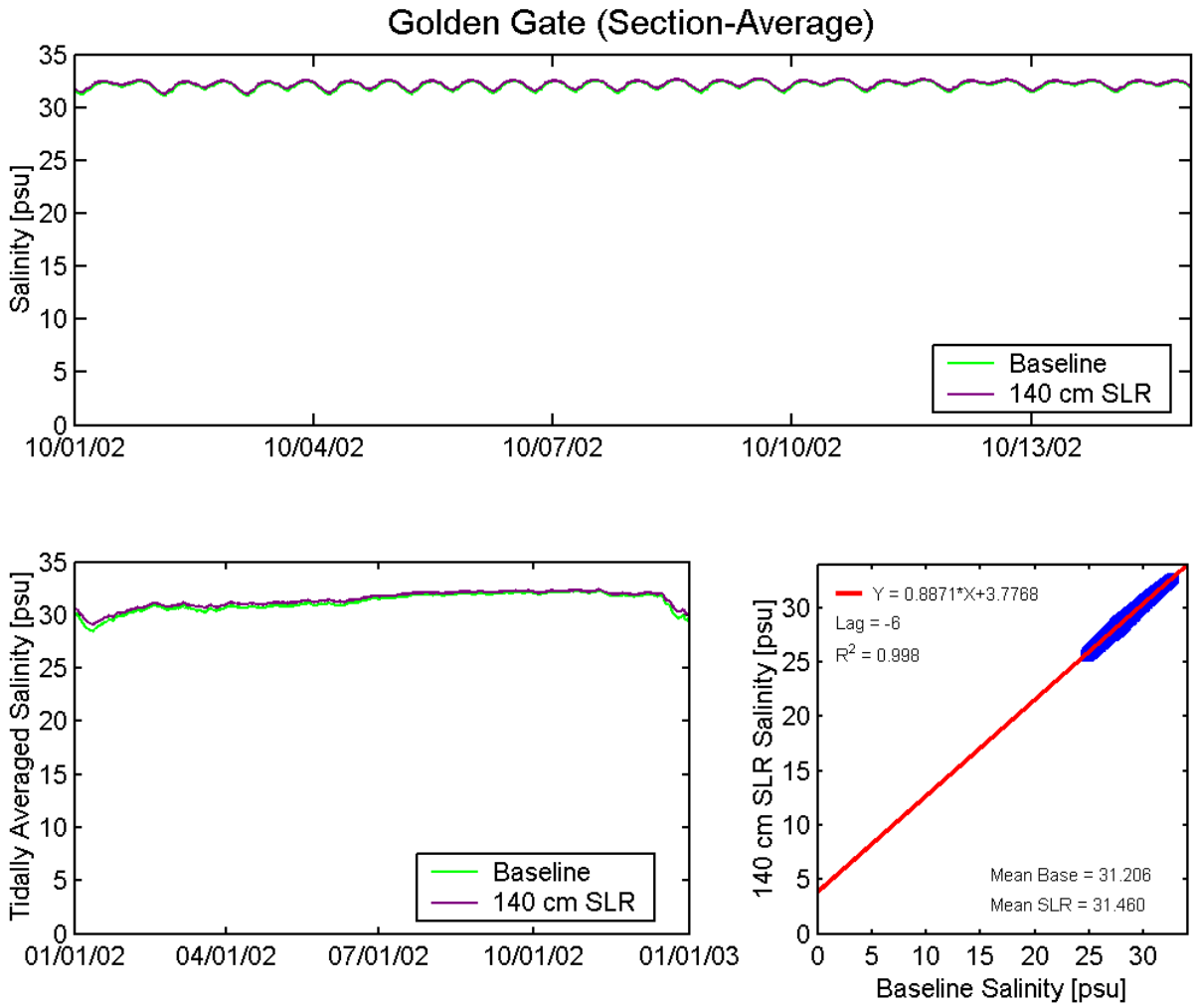

Figure 7.2-5 Predicted salinity (top) and tidally averaged salinity (lower left) at the Golden Gate for Baseline and 140 cm SLR scenarios. Regression (lower right) shows the best linear fit for the effect on salinity at the Golden Gate resulting from 140 cm of SLR at the Pacific Ocean boundary.

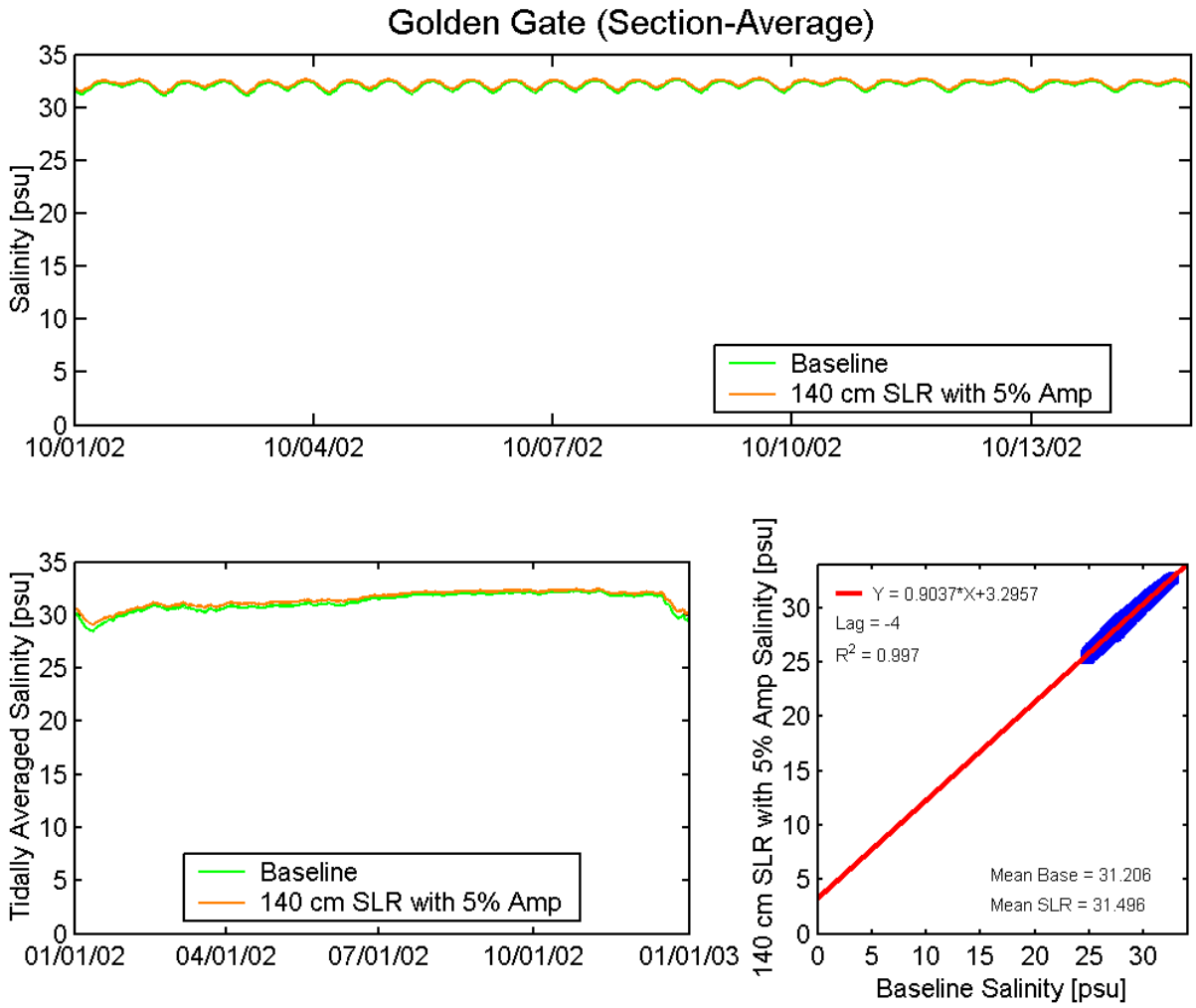

Figure 7.2-6 Predicted salinity (top) and tidally averaged salinity (lower left) at the Golden Gate for Baseline and 140 cm of SLR with 5% Amplification scenarios. Regression (lower right) shows the best linear fit for the effect on salinity at the Golden Gate resulting from 140 cm of SLR with 5% Amplification at the Pacific Ocean boundary.

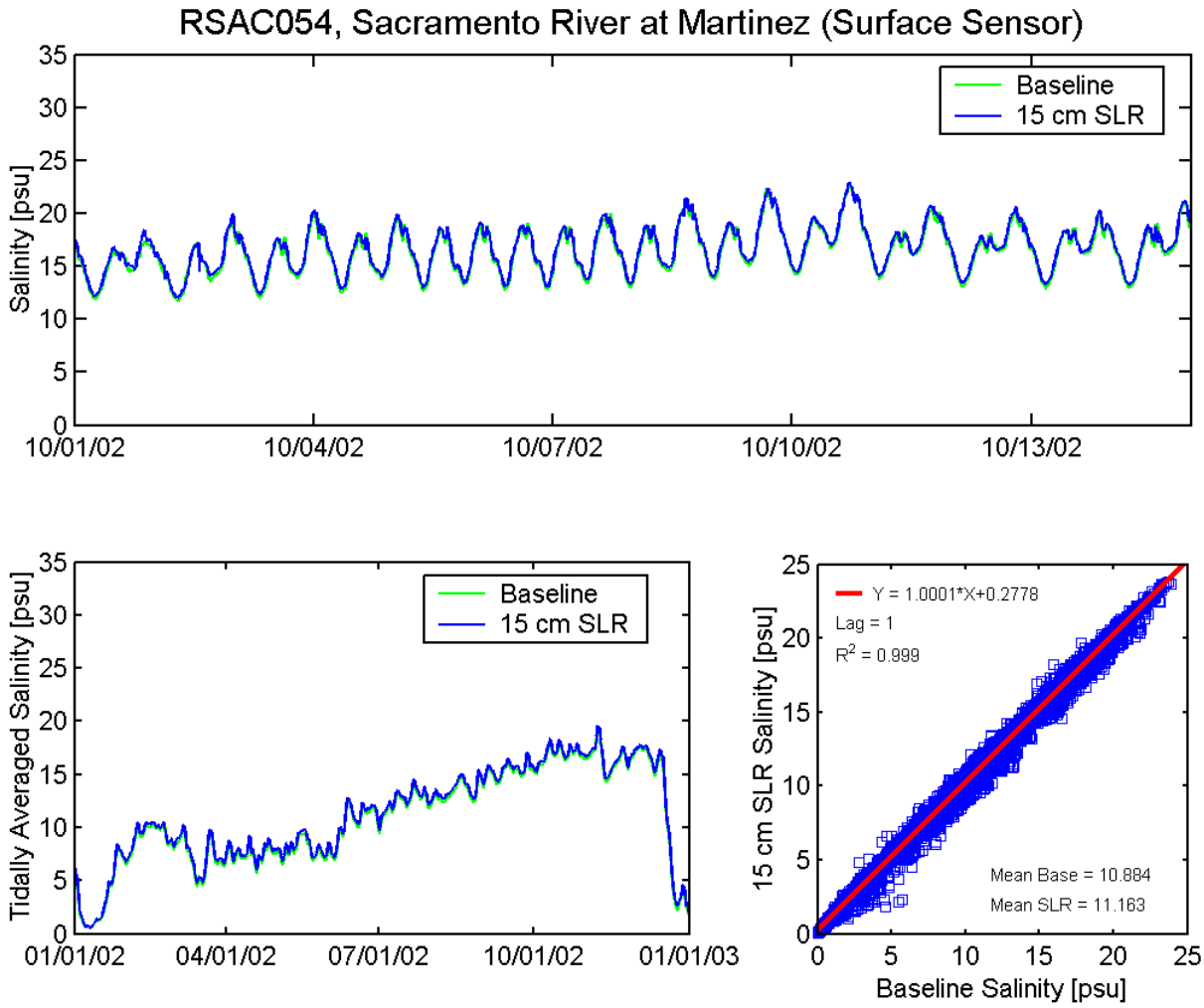

Figure 7.2-7 Predicted salinity (top) and tidally averaged salinity (lower left) at the Martinez surface salinity sensor (RSAC054) for Baseline and 15 cm SLR scenarios. Regression (lower right) shows the best linear fit for the effect on salinity at the Martinez surface salinity sensor resulting from 15 cm of SLR at the Pacific Ocean boundary.

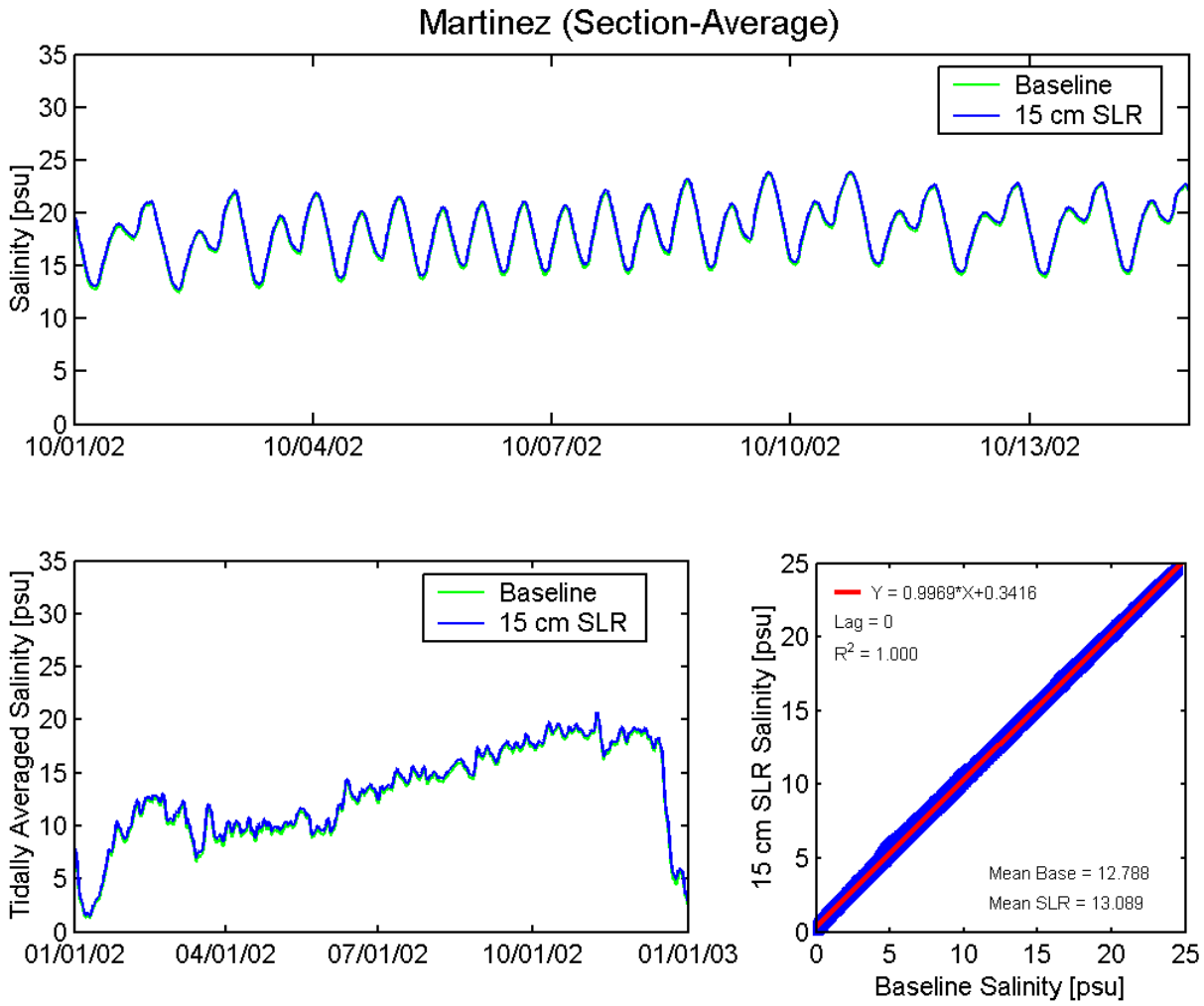

Figure 7.2-8 Predicted cross-section average salinity (top) and tidally averaged cross-section average salinity (lower left) at Martinez for Baseline and 15 cm SLR scenarios. Regression (lower right) shows the best linear fit for the effect on cross-section average salinity at Martinez resulting from 15 cm of SLR at the Pacific Ocean boundary.

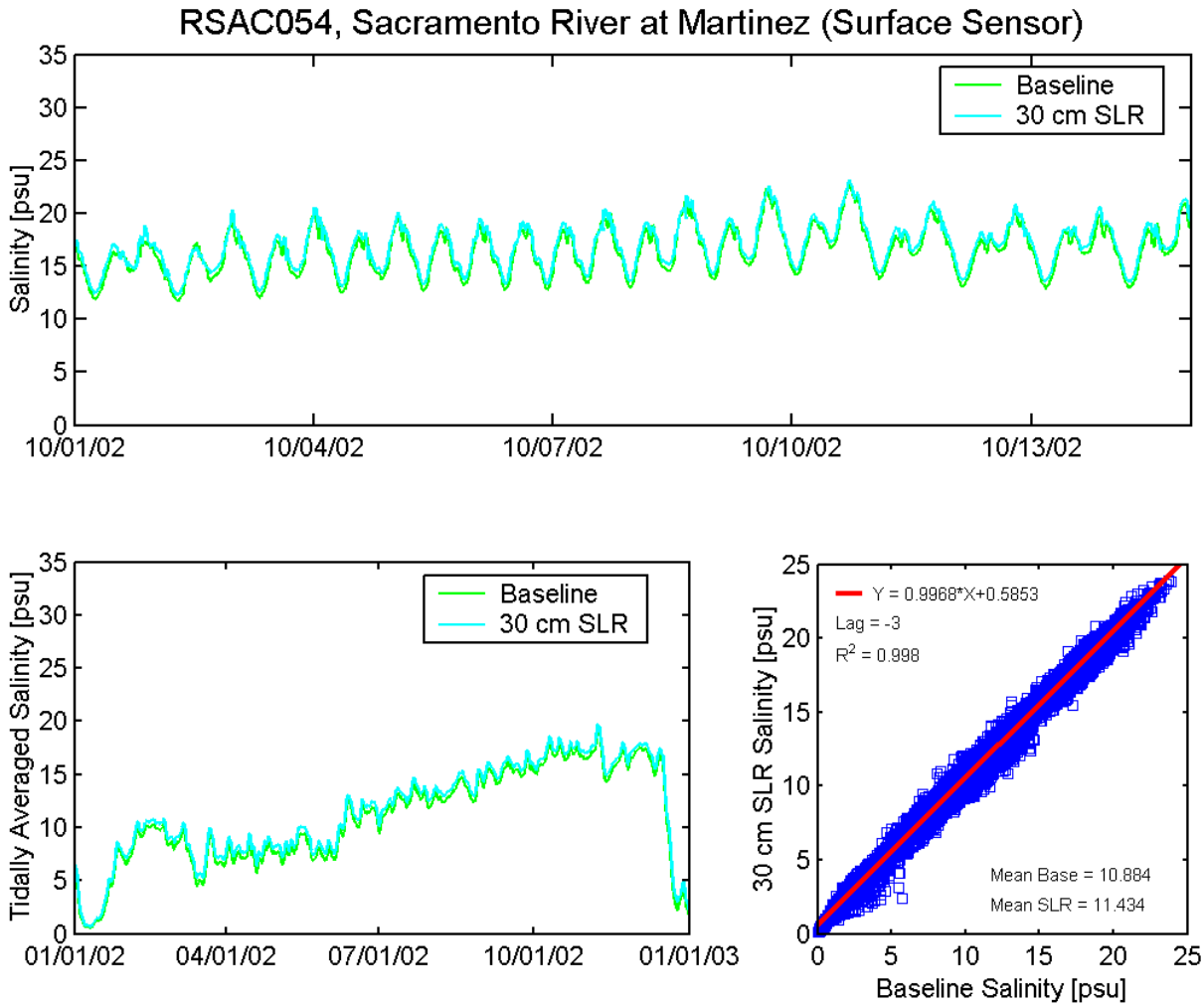

Figure 7.2-9 Predicted salinity (top) and tidally averaged salinity (lower left) at the Martinez surface salinity sensor (RSAC054) for Baseline and 30 cm SLR scenarios. Regression (lower right) shows the best linear fit for the effect on salinity at the Martinez surface salinity sensor resulting from 30 cm of SLR at the Pacific Ocean boundary.

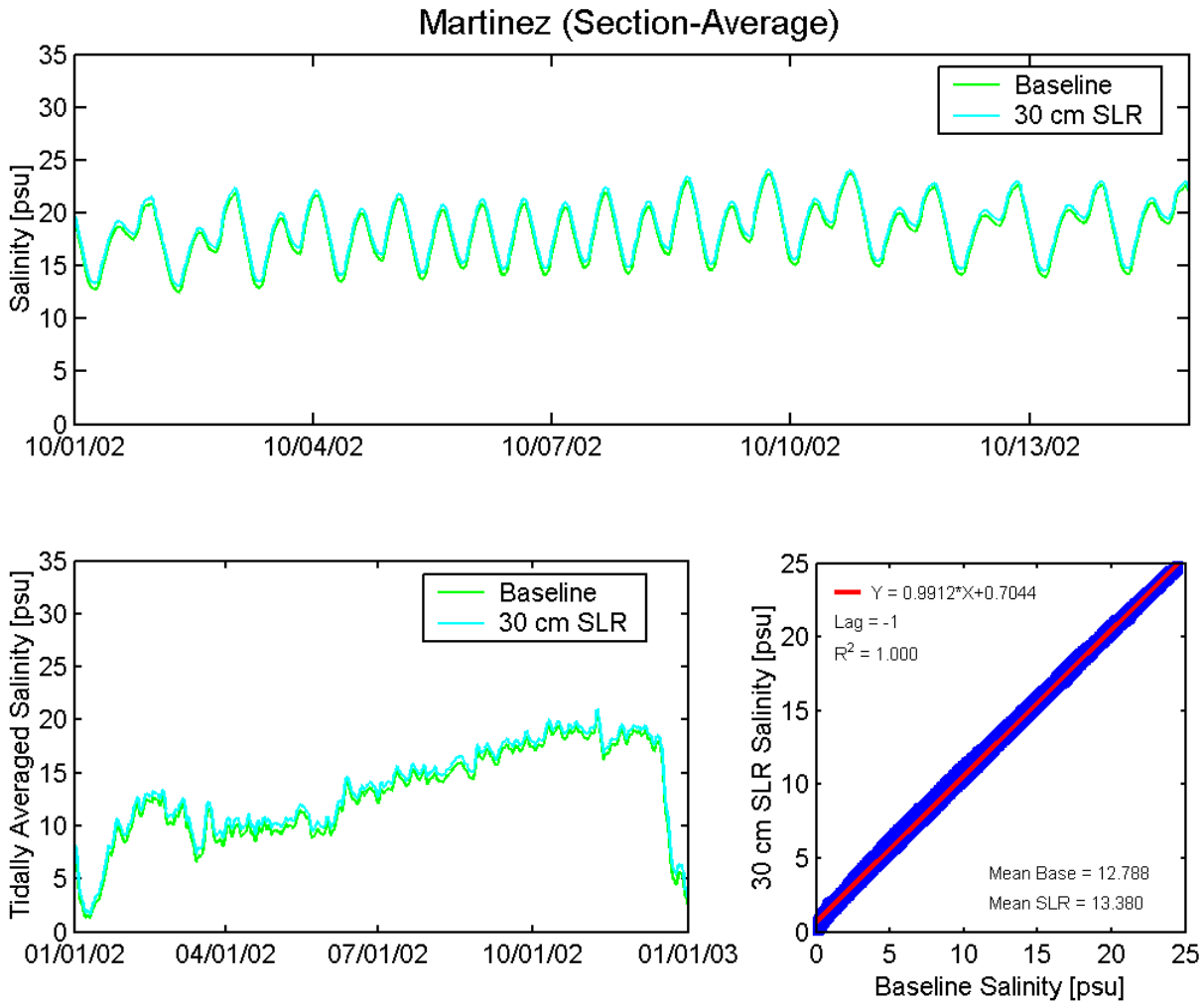

Figure 7.2-10 Predicted cross-section average salinity (top) and tidally averaged cross-section average salinity (lower left) at Martinez for Baseline and 30 cm SLR scenarios. Regression (lower right) shows the best linear fit for the effect on cross-section average salinity at Martinez resulting from 30 cm of SLR at the Pacific Ocean boundary.

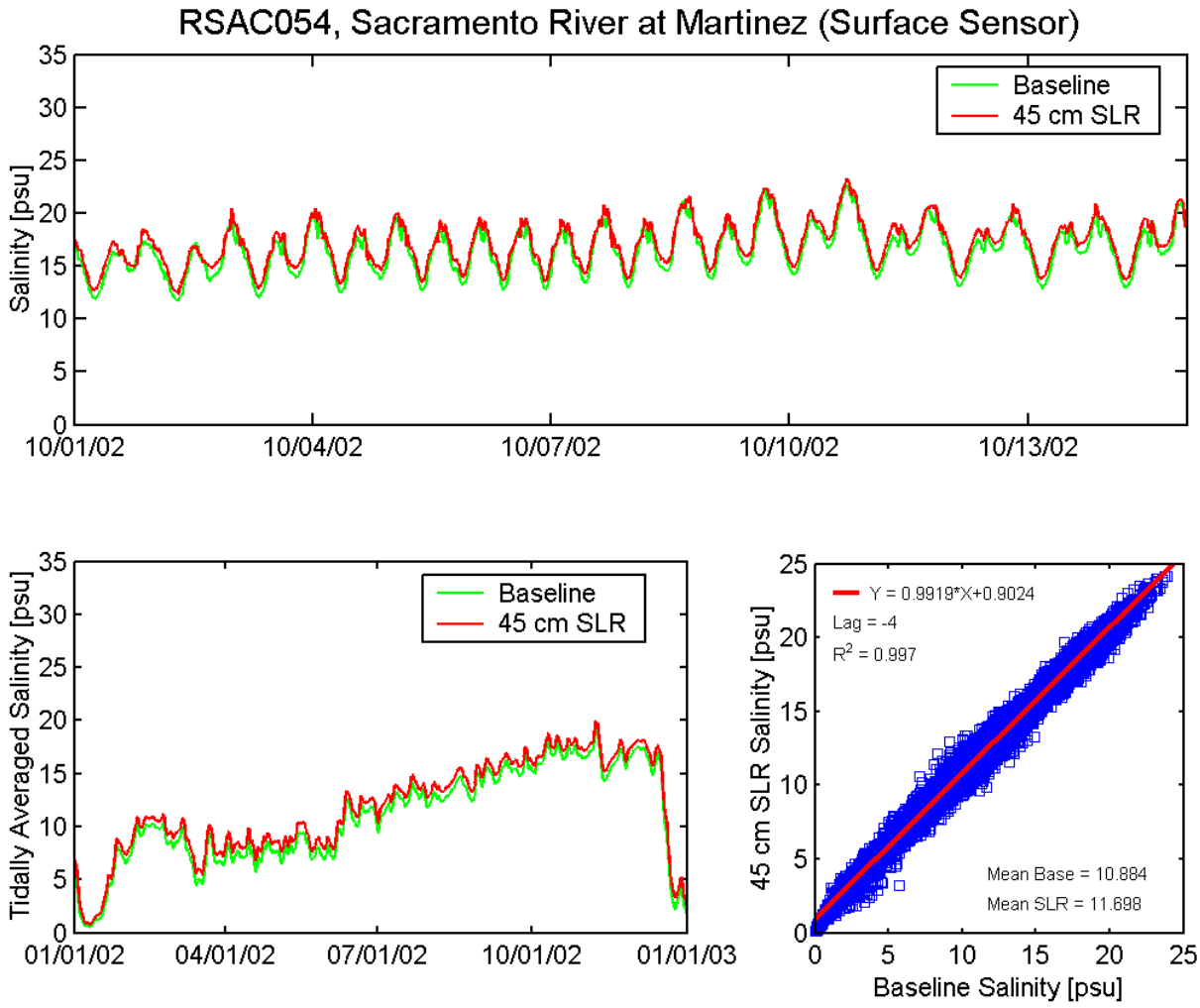

Figure 7.2-11 Predicted salinity (top) and tidally averaged salinity (lower left) at the Martinez surface salinity sensor (RSAC054) for Baseline and 45 cm SLR scenarios. Regression (lower right) shows the best linear fit for the effect on salinity at the Martinez surface salinity sensor resulting from 45 cm of SLR at the Pacific Ocean boundary.

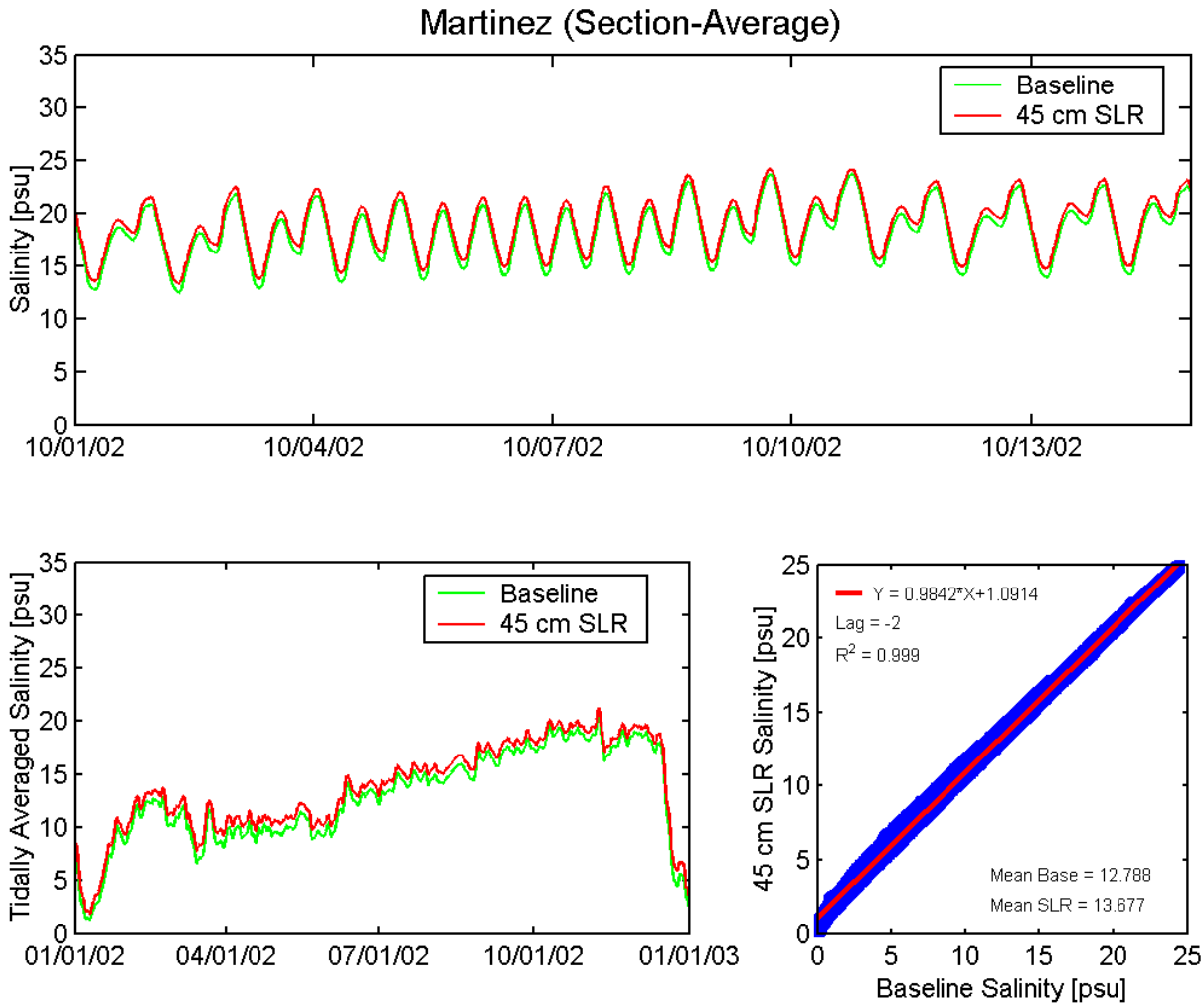

Figure 7.2-12 Predicted cross-section average salinity (top) and tidally averaged cross-section average salinity (lower left) at Martinez for Baseline and 45 cm SLR scenarios. Regression (lower right) shows the best linear fit for the effect on cross-section average salinity at Martinez resulting from 45 cm of SLR at the Pacific Ocean boundary.

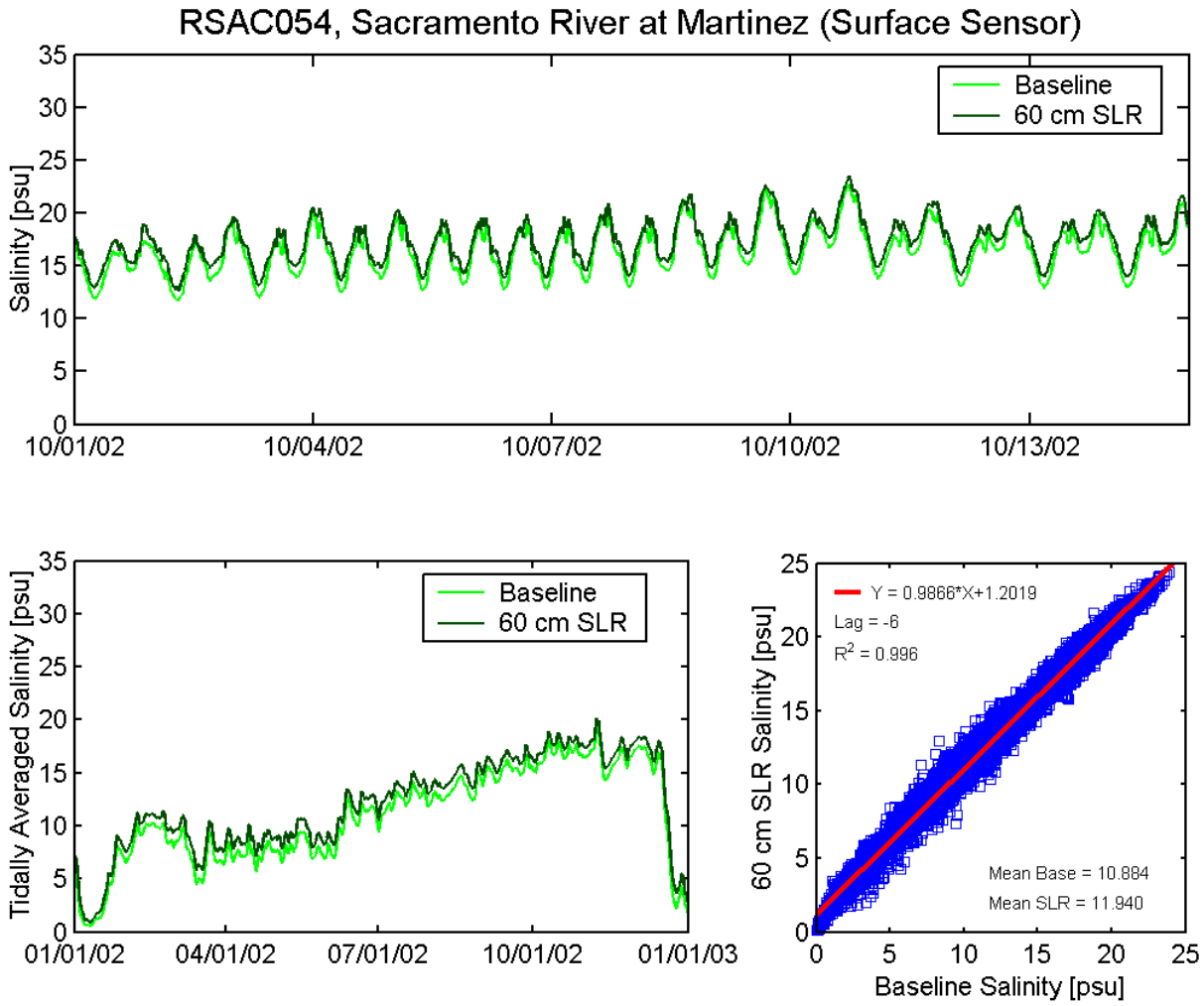

Figure 7.2-13 Predicted salinity (top) and tidally averaged salinity (lower left) at the Martinez surface salinity sensor (RSAC054) for Baseline and 60 cm SLR scenarios. Regression (lower right) shows the best linear fit for the effect on salinity at the Martinez surface salinity sensor resulting from 60 cm of SLR at the Pacific Ocean boundary.

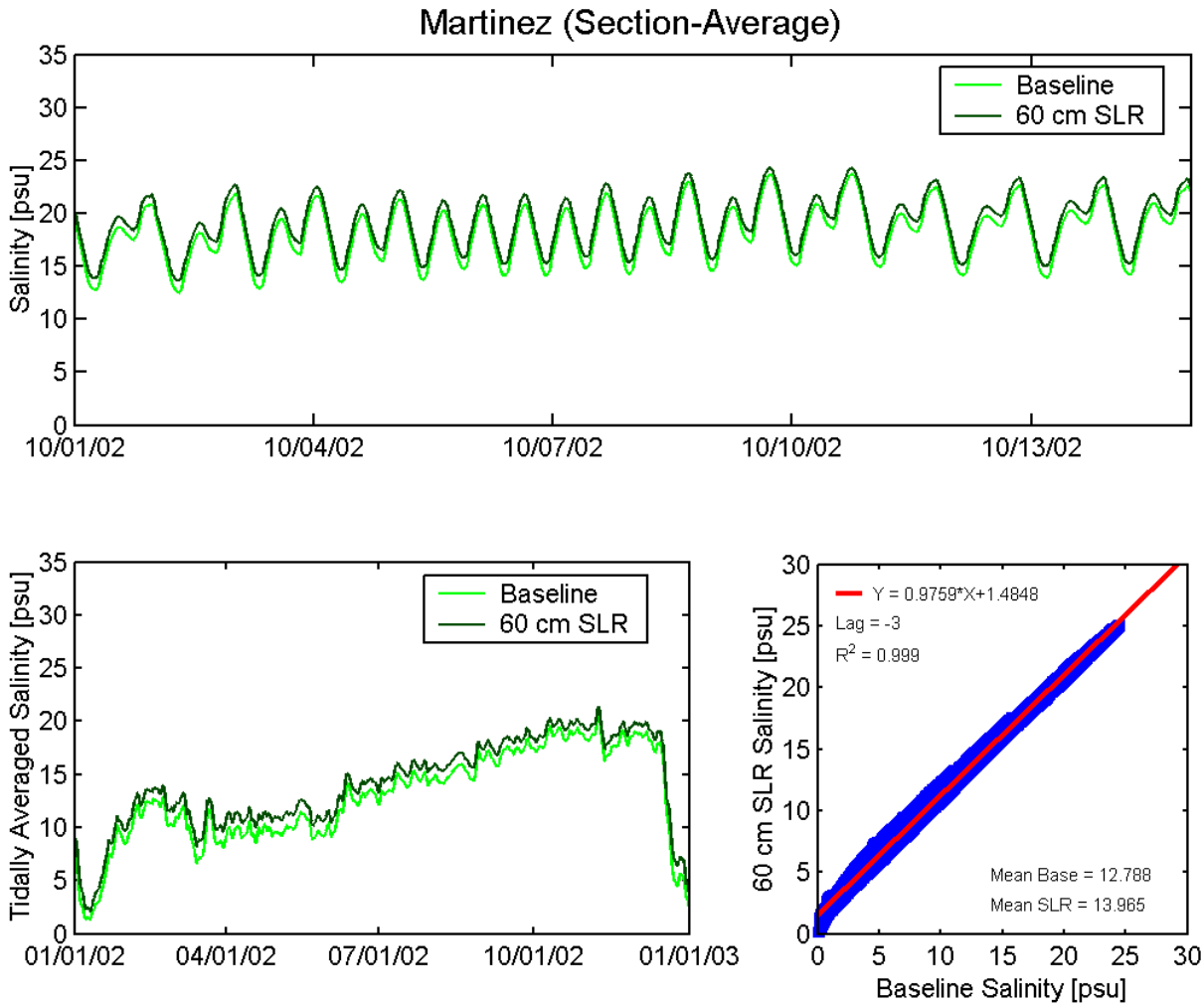

Figure 7.2-14 Predicted cross-section average salinity (top) and tidally averaged cross-section average salinity (lower left) at Martinez for Baseline and 60 cm SLR scenarios. Regression (lower right) shows the best linear fit for the effect on cross-section average salinity at Martinez resulting from 60 cm of SLR at the Pacific Ocean boundary.

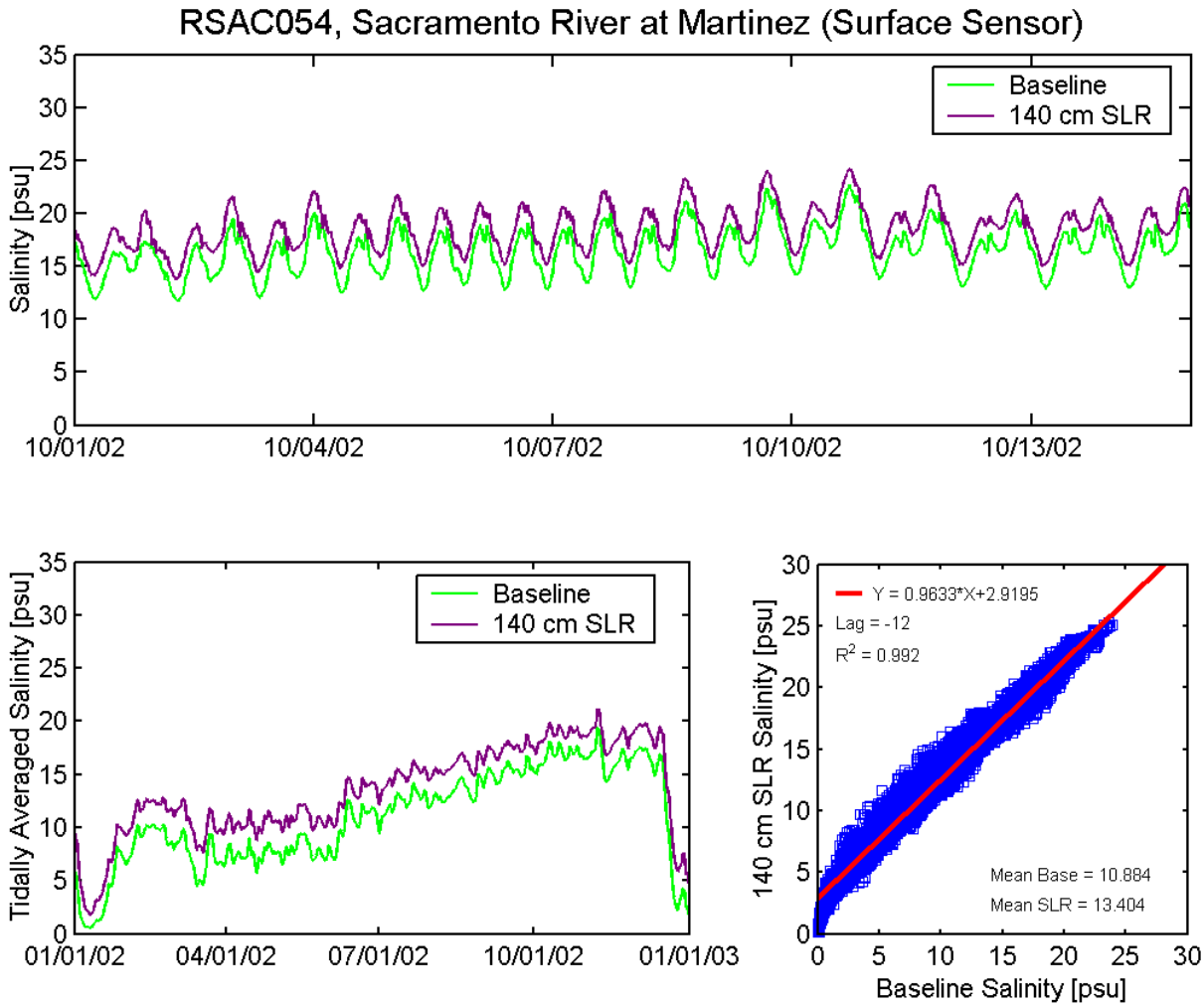

Figure 7.2-15 Predicted salinity (top) and tidally averaged salinity (lower left) at the Martinez surface salinity sensor (RSAC054) for Baseline and 140 cm SLR scenarios. Regression (lower right) shows the best linear fit for the effect on salinity at the Martinez surface salinity sensor resulting from 140 cm of SLR at the Pacific Ocean boundary.

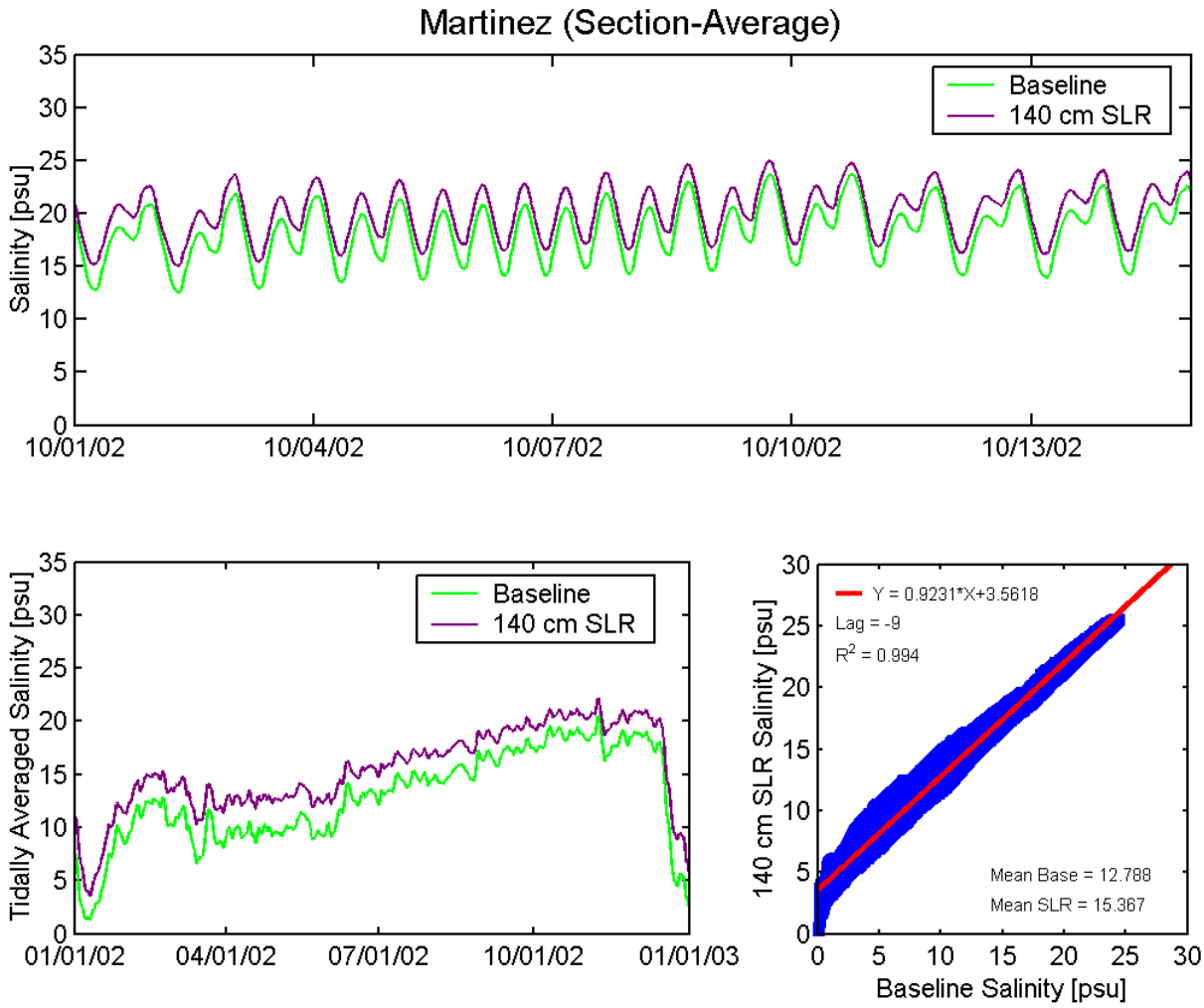

Figure 7.2-16 Predicted cross-section average salinity (top) and tidally averaged cross-section average salinity (lower left) at Martinez for Baseline and 140 cm SLR scenarios. Regression (lower right) shows the best linear fit for the effect on cross-section average salinity at Martinez resulting from 140 cm of SLR at the Pacific Ocean boundary.

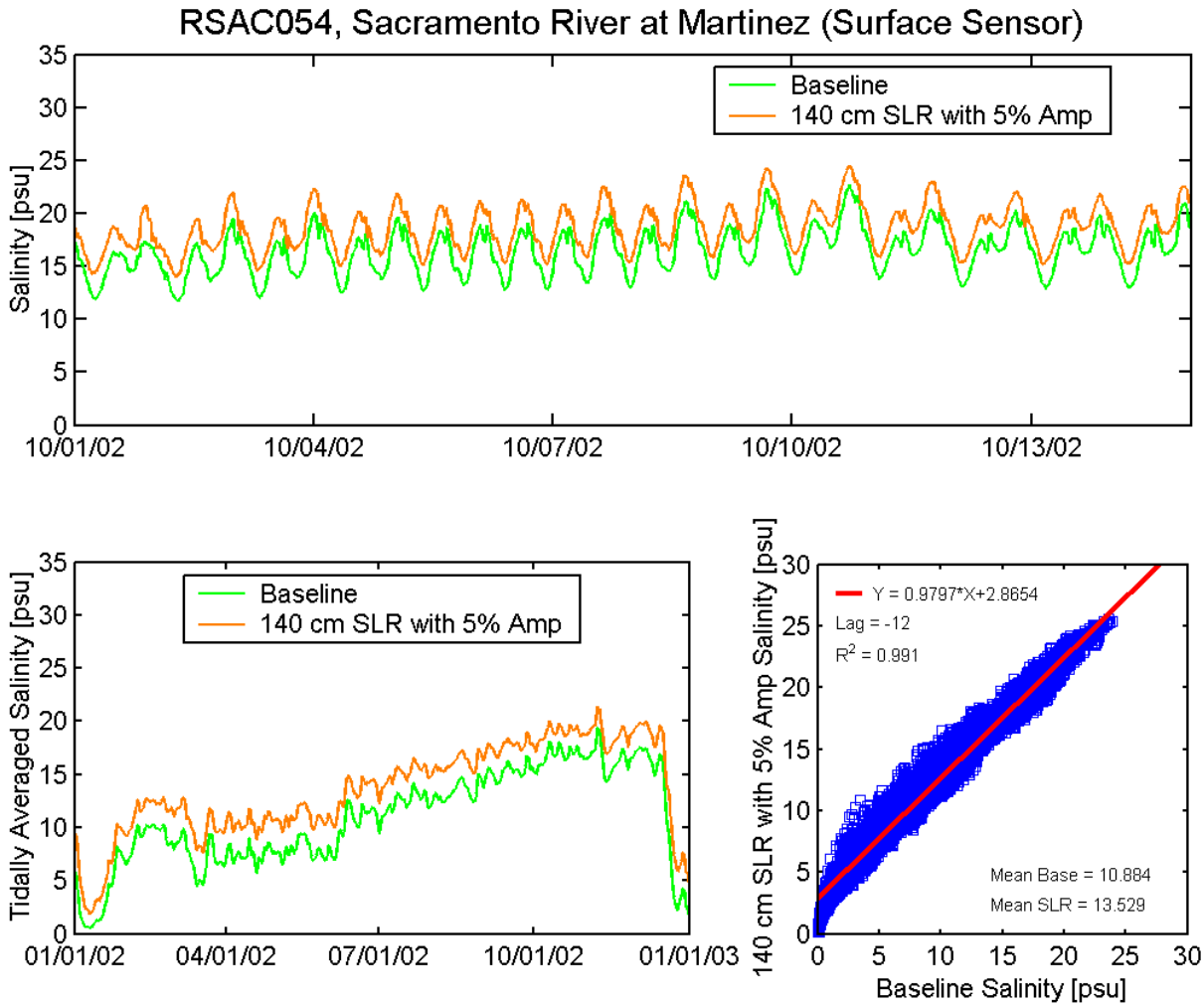

Figure 7.2-17 Predicted salinity (top) and tidally averaged salinity (lower left) at the Martinez surface salinity sensor (RSAC054) for Baseline and 140 cm of SLR with 5% Amplification scenarios. Regression (lower right) shows the best linear fit for the effect on salinity at the Martinez surface salinity sensor resulting from 140 cm of SLR with 5% Amplification at the Pacific Ocean boundary.

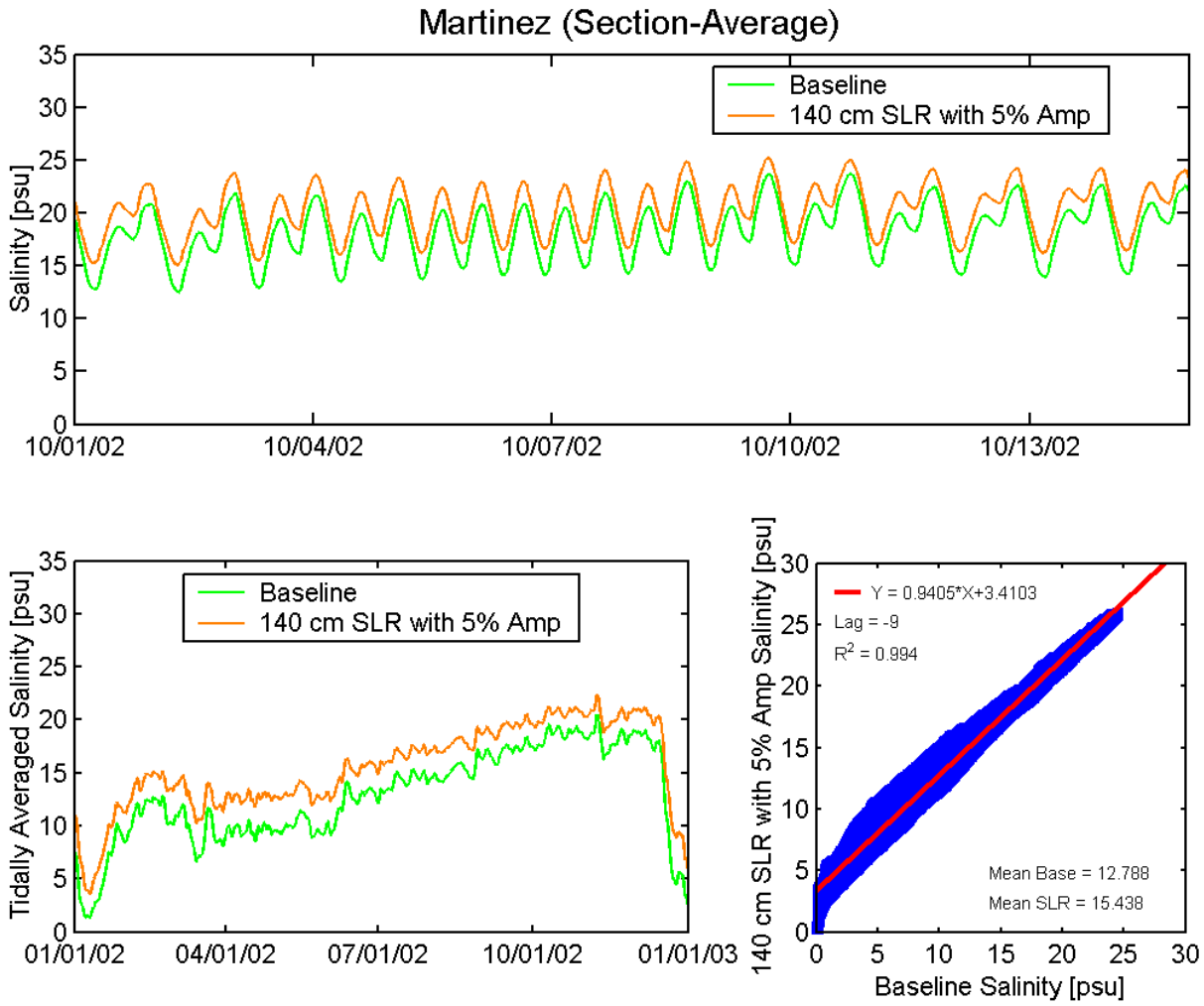

Figure 7.2-18 Predicted cross-section average salinity (top) and tidally averaged cross-section average salinity (lower left) at Martinez for Baseline and 140 cm of SLR with 5% Amplification scenarios. Regression (lower right) shows the best linear fit for the effect on cross-section average salinity at Martinez resulting from 140 cm of SLR with 5% Amplification at the Pacific Ocean boundary.

7.3 Summary of Stage and Salinity Relationships for SLR at Fort Point and Martinez

The linear relationships between stage and salinity for the Baseline scenario and each of the sea level rise scenarios at Fort Point and Martinez were developed to facilitate the development of appropriate sea level rise boundary conditions for models that use Martinez as the downstream boundary (such as DMS2 or the RMA2 Delta model) or the Golden Gate as the downstream boundary (such as the RMA2 San Francisco Bay model).

The stage relationships developed at Fort Point (Section 7.1.1) indicate that the sea level rise offset applied at the ocean boundary is translating almost exactly to a similar offset at Fort Point. This suggests that for a Golden Gate boundary a constant sea level rise offset is appropriate. The stage relationships developed at Martinez (Section 7.1.2) indicate that the predicted change in mean sea level at Martinez is slightly less than the offset applied at the ocean boundary. This difference increases with sea level rise. For the 60 cm and 140 cm SLR scenario, both phase and amplitude differences are evident in the stage correlations at Martinez, indicating the complexity of translating a sea level rise offset at the ocean boundary to Martinez when both changes to wave speed propagation with depth and changes to tidal prism in the Delta resulting from sea level rise are influencing stage at Martinez.

The salinity relationships developed at the Golden Gate (Section 7.2.1) show that a constant offset is not appropriate to account for the change in salinity at the Golden Gate as a result of sea level rise. The salinity relationships for 15 cm SLR and 30 cm SLR at Martinez have a slope of almost exactly 1.000 indicating that a constant salinity offset is appropriate at Martinez. however, for higher levels of sea level rise the slope of the best fit line is somewhat less than 1.000 indicating that a constant salinity offset is not appropriate at Martinez for higher levels of sea level rise.

Anderson and Miller (2005) used a similar approach to develop relationships to estimate electrical conductivity at Martinez for sea level rise conditions simulated using the RMA2 Bay-Delta model for 1 foot (30.48 cm) of SLR. The relationship they derived using the G-model for EC at Martinez for 1 foot of SLR is given by (Anderson and Miller, 2005)

$$[EC\ 1ft\ SLR] = 1.0022 \times [EC\ Baseline] + 840.87 \quad (7\text{-}31)$$

The most similar relationship from this study is the relationship for surface salinity at Martinez for the 30 cm SLR scenario given by Equation 7-21 as

$$[Salinity\ 30\ cm\ SLR] = 0.9968 \times [Salinity\ Baseline] + 0.5853 \quad (7\text{-}32)$$

The comparison between the difference of the annual mean and the offset from the best linear fit suggested that a constant salinity offset between 0.550 and 0.585 psu would fairly accurately represent the salinity increase at Martinez for the 30 cm SLR scenario. This corresponds approximately to an offset of between 1112.14 and 1180.53 [µmhos cm^{-1}]. When the Baseline salinity and the predicted salinity for the 30 cm SLR scenario were converted to EC and the cross-correlation was applied, the best fit relationship is given by

[EC 30 cm SLR] = 0.9924 x *[EC Baseline] + 1001.45* (7-33)

which suggests an offset of 1001.45 [µmhos cm-1]. While this type of comparison is somewhat problematic (as discussed below) due to the nonlinear relationship between EC and salinity, these comparisons show that the predicted EC increase at Martinez for 30 cm SLR is between 19% and 40% higher than the EC offset derived from the G-model for 30.48 cm (1 foot) of SLR.

The salinity relationships for the Golden Gate and Martinez were developed for salinity (psu). The salinity predicted by UnTRIM was converted to EC for some of the sea level rise scenarios and the same cross-correlation was applied (as in Equations 7-32 and 7-33). The resulting linear fit equations for EC were significantly different than the fit equations derived from converting the offset in Equations 7-13 through 7-30 from psu to EC, in part because the slope of the lines for the EC derived curves deviated from 1.000. Part of these differences arise because the relationship between salinity and EC is not linear, and also because EC is not a conservative quantity. As a result, the appropriate method to apply Equations 7-13 through 7-30 for EC boundary conditions would be to convert an EC boundary time series to salinity, apply the appropriate linear relationship to account for sea level rise on salinity, and then convert the resulting salinity back to EC to use for a boundary condition for a model simulating EC instead of salinity. However, as discussed in Section 3.4, there are significant disadvantages to simulating EC since EC is not a conservative quantity.

8. Analysis of Salt Flux Mechanisms

The salt flux analysis presented in this section quantitatively estimates the contributions of individual transport processes to predicted increased salt intrusion resulting from sea level rise. Distinguishing the relative contributions of individual processes responsible for salt intrusion will have several practical benefits. First, it will improve the conceptual model of how salinity is expected to change with different modifications to the Delta, including sea level rise. Second, this analysis may provide insight to the effectiveness of potential management actions to address salt intrusion. Third, this salt flux analysis will provide guidance to the representation of salt intrusion processes in one-dimensional and two-dimensional models for sea level rise scenarios.

As part of the Delta Risk Management Strategy (DRMS) project, the transport processes associated with salt flux were estimated for a Baseline scenario and 4 different sea level rise scenarios simulated with UnTRIM (Gross et al. 2007b). The goal of the study was to parameterize the effects of sea level rise on salt intrusion in a one-dimensional tidally averaged salinity model. The three-dimensional hydrodynamic model applied in the DRMS sea level rise analysis was the first generation of the UnTRIM Bay-Delta model (MacWilliams and Gross, 2007), which resolved only a limited portion of the Delta. The DRMS project scenarios used repeating tides and steady Delta outflow to simplify analysis and interpretation of results. The analysis was limited to a single period (e.g., single Delta outflow) for each SLR scenario. Another DRMS report documented a salt flux analysis for a large range of Delta outflow values to estimate dispersion coefficients as a function of Delta outflow (Gross et al., 2007a). The dispersion coefficients were found to vary strongly with Delta outflow. In particular, the gravitational circulation component increased strongly with increased Delta outflow.

The salt flux analysis presented here is distinct from the previous DRMS analysis and has several advantages. First of all, this analysis uses the UnTRIM Bay-Delta model that was applied to the BDCP scenarios, which uses an updated, more accurate computational method, a model domain covering all of San Francisco Bay and the entire Sacramento-San Joaquin Delta, and has been more thoroughly calibrated. Second, a more complex analysis is performed using real tides. In contrast, the DRMS study used idealized “average” tides that repeated the same pattern each day. Therefore, the salt flux analysis in the DRMS study assumed that the salt flux and dispersion associated with the idealized tides was similar to the average salt flux and dispersion over a spring-neap cycle. Third, more sea level rise scenarios are explored in this analysis. Fourth, the analysis discussed here is performed for two different periods for each scenario. Lastly, the salt flux analysis is discussed in a more accessible (less technical) manner in this report.

8.1 Overview of Dispersion Processes

Salinity in the San Francisco Estuary depends primarily on:

- freshwater input to the Delta;
- salinity in the coastal ocean and exchange between the ocean and the estuary;
- salt transport processes;
- pumping, consumptive use and operations in the Delta;

- salt input from agricultural drainage and other sources; and
- evaporation and precipitation.

Seasonal and yearly variations in salinity are driven primarily by variability in freshwater flow. Mixing of ocean water and salt into an estuary results "from a combination of small-scale turbulent diffusion and larger scale variation of … velocities" (Fischer et al. 1979) which are primarily forced by astronomical tides in the San Francisco Estuary (Walters et al. 1985). The combination of differential advection and turbulent mixing is referred to as dispersive transport. Dispersive transport in estuaries is a complex topic due to the large range of spatial and temporal scales associated with different physical processes.

One key transport process is gravitational circulation, also referred to as estuarine circulation. This process results from longitudinal density gradients and is a form of vertical exchange process. Gravitational circulation results in differential advection in which the more saline near-bed flow has a net landward (up-estuary) direction, while the near-surface flow has a net seaward (down-estuary) direction. Gravitational circulation can result in stratification and is strengthened by stratification, providing a form of positive feedback. Due to the increase in gravitational circulation with stratification, Monismith et al. (2002) predicted that dispersion from gravitational circulation can increase by several orders of magnitude from low Delta outflow to high Delta outflow. The salt flux analysis performed as part of the DRMS studies (Gross et al. 2007a) also showed this strong increase in gravitational circulation with increased Delta outflow. Another vertical exchange process is Strain Induced Periodic Stratification (SIPS), which results from ebb-flood asymmetries in velocity profiles (Simpson et al. 1990). These tidal-asymmetries are a result of different stratification and vertical shear during ebb and flood. Asymmetries occur because stratification decreases turbulent mixing leading to more vertical shear in velocity and stratification. Due to tidal straining, stratification is typically stronger on ebb tides than flood tides, and therefore the velocity profile is more strongly sheared during ebb tides. The effect of SIPS on salt transport is an exchange flow with net transport of salt landward near the bed and seaward near the surface, similar to the exchange flow associated with gravitational circulation. Stacey et al. (2001) found the SIPS process to be active in a Suisun Bay field study.

Another important dispersive transport process in the Estuary is tidal dispersion, including the processes of "tidal trapping" and "tidal pumping." Tidal trapping is a term used by Fischer et al. (1979) to describe one simple process by which tidal dispersion can cause landward transport of salt. The classic case of tidal trapping occurs in an estuary with side embayments when some of the salt mass that enters the side embayments on the flood tide remains "trapped" in the subembayment for a large portion of the ebb tide. More generally, tidal dispersion occurs as a result of tidal flows over bathymetric features such as side embayments, junctions, mudflats and marshes. Tidal dispersion is typically significant when substantial variability in bathymetry and geometry is experienced over the distance of a tidal excursion.

8.2 Analysis of Dispersion Processes

The "salt balance" equation (Fischer et al. 1979) is a simplified but useful description of salt transport:

$$QS = -KA\frac{\partial S}{\partial x} \tag{8-1}$$

where Q is the tidally averaged flow, S is tidally and cross-sectionally averaged salinity, K is the longitudinal dispersion coefficient, A is the cross-sectional area, and x is the longitudinal position. The salt balance equation applies to the longitudinal salinity distribution under tidally averaged steady state conditions. If these conditions are met, Equation 8-1 can be used to estimate dispersion coefficients.

Estimating the portion of the salt flux and dispersion coefficient associated with gravitational circulation and other individual processes requires detailed analysis of the simulation results. The salt flux associated with individual physical processes can be estimated at any cross-section by an analysis method described in Fischer et al. (1979). The longitudinal velocity (u) is decomposed into several components

$$u(x,y,z,t) = U_a(x) + U_c(x,t) + u_s(x,y,z) + u'(x,y,z,t) \tag{8-2}$$

where x is the longitudinal position of a cross-section, y and z are the lateral and vertical distances within a cross-section, and t is time. The velocity components are the cross-sectional and tidally averaged velocity (U_a= Q/A), the deviation of the cross-sectional average from the cross-sectional and tidally averaged velocity (U_c), the deviation of the tidally averaged velocity from the cross-sectional and tidally averaged velocity (u_s) and the remaining variability (u'). The capital letters refer to depth-averaged quantities. The last two terms of Equation 8-2 are further decomposed into lateral and vertical variability

$$u_s(x,y,z) = U_t(x,y) + u_v(x,y,z) \tag{8-3}$$

$$u'(x,y,z,t) = U'_t(x,y,t) + u'_v(x,y,z,t) \tag{8-4}$$

The same decomposition approach is followed for salinity. The cross-sectional area is decomposed into a tidal cycle average and variation from this average,

$$A(x,t) = A_a(x) + A_c(x,t) \tag{8-5}$$

The salt flux through a cross-section at any time is

$$Flux(x,t) = [u(x,y,z,t)\, s(x,y,z,t)]A(x,t) \tag{8-6}$$

where A is the cross-sectional area and the square brackets represent a cross-sectional average. The average salt flux during a tidal cycle is determined by averaging over the tidal cycle:

$$Flux(x) = \langle Flux(x,t) \rangle = \langle [u(x,y,z,t)\, s(x,y,z,t)]A(x,t) \rangle \tag{8-7}$$

where the angle brackets represent a tidal cycle average. This notation follows Fischer et al. (1979) closely except that the square brackets are used instead of an overbar to represent cross-sectional averages. The decomposed velocity, salinity and area are substituted into Equation 8-7 and the product expanded into individual terms. Many of the terms are zero or negligible (Dyer 1973). Retaining all terms that are expected to be significant in any part of the San Francisco Estuary yields

$$\begin{aligned}\text{Flux}(x) = {} & A_a\, U_a\, S_a + S_a < A_c\, U_c > + A_a < U_c\, S_c > + U_a < A_c\, S_c > + < A_c\, U_c\, S_c > \\ & + A_a\,[U_t\, S_t] + A_a\,[u_v\, u_v] + <[U'_t\, S'_t\,](A_a + A_c) > + <[u'_v\, s'_v\,](A_a + A_c) > \\ & + <[\,U_t\, S'_t\,](A_a + A_c) > + <[\,u_v\, s'_v\,](A_a + A_c) > \\ & + <[\,U'_t\, S_t\,](A_a + A_c) > + <[\,u'_v\, s_v\,](A_a + A_c) >\end{aligned} \tag{8-8}$$

The sum of the first and second terms in this equation is advective transport associated with Delta outflow. All other terms are dispersive flux terms. The dispersive terms in this equation are associated with one or more physical processes. Some particularly important terms for the analysis of transport in the San Francisco Estuary are:

- $A_a\, U_a\, S_a + S_a < A_c\, U_c >$ – advective salt flux (QS in the salt balance equation)
- $A_a\,[u_v\, s_v]$ – steady vertical exchange, primarily associated with gravitational circulation
- $<[u'_v\, s'_v\,](A_a + A_c) >$ – the primary term associated with unsteady vertical shear
- $A_a < U_c\, S_c >$ – the primary term associated with tidal dispersion

Both steady vertical exchange and unsteady vertical shear are vertical exchange processes related to stratification and velocity shear in the water column. The steady vertical exchange is primarily associated with gravitational circulation and therefore is referred to as the gravitational circulation term in this report and other estuarine literature. However, this term can also be substantially affected by wind which can also result in a persistent vertical exchange flow. The unsteady vertical shear term is primarily associated with Strain Induced Period Stratification (SIPS). The 11th and 13th terms in Equation 8-8, also represent vertical exchange processes, but are typically small in magnitude. The remaining terms are associated with tidal dispersion processes, such as “tidal trapping” and “tidal pumping” (Fischer et al., 1979). This grouping of salt flux terms and terminology is consistent with the analysis of fluxes at the Golden Gate by Fram et al. (2007) and somewhat simplified relative to the DRMS salt flux analysis (Gross et al. 2007b).

8.3 Analysis Locations and Periods

The cross-sections numbed 1 through 32 in Figure 8.3-1 are the locations at which salt fluxes and dispersion coefficients were estimated for each scenario. These locations were chosen to capture spatial variability in salt transport processes in the estuary.

Multiple criteria were used to select the salt intrusion flux analysis period. First, a period of relatively steady Delta outflow is preferred so that the flow value used in Equation 8-1 is not ambiguous. Second, the period should span at least one spring-neap cycle to cover a full range of tidal conditions. A 29 day analysis period was chosen to allow a full range of tidal conditions. This is the time period typically used by NOAA for analysis of tides. Third, a fairly good “flux balance” is desired, meaning that advective fluxes and dispersive fluxes should roughly balance during the simulation period.

The analysis periods chosen were July 15, 2002 through August 12, 2002 and October 13, 2002 through November 10, 2002. The analysis periods are identified as grey regions in Figure 8.3-2 which shows Sacramento River flow during 2002. Though the Sacramento River flow varies substantially between the two analysis periods, the average predicted flow past Chipps Island is

similar. During the first analysis period the average predicted flow past Chipps Island is 170 m^3 s^{-1} and during the second period the average predicted flow past Chipps Island is 167 m^3 s^{-1} for the Baseline scenario. The predicted net flows were similar for the other scenarios. Because a fairly steady flow period is required for unambiguous estimates of dispersion coefficients, a high flow period could not be analyzed.

The observed water surface elevation through each 29 day simulation period is shown by the grey shaded regions in Figure 8.3-3. The 29 day period spans two spring-neap cycles and the first period exhibits more diurnal inequality (e.g. higher high water) on average than the second period.

As indicated by Figure 8.3-4 through Figure 8.3-17, the salinity conditions are somewhat different between the two analysis periods, with higher salinity in the October 13, 2002 through November 10, 2002 analysis period than the July 16, 2002 through August 12, 2002 analysis period. As discussed in Section 4, the predicted salinity increases with increased sea level rise.

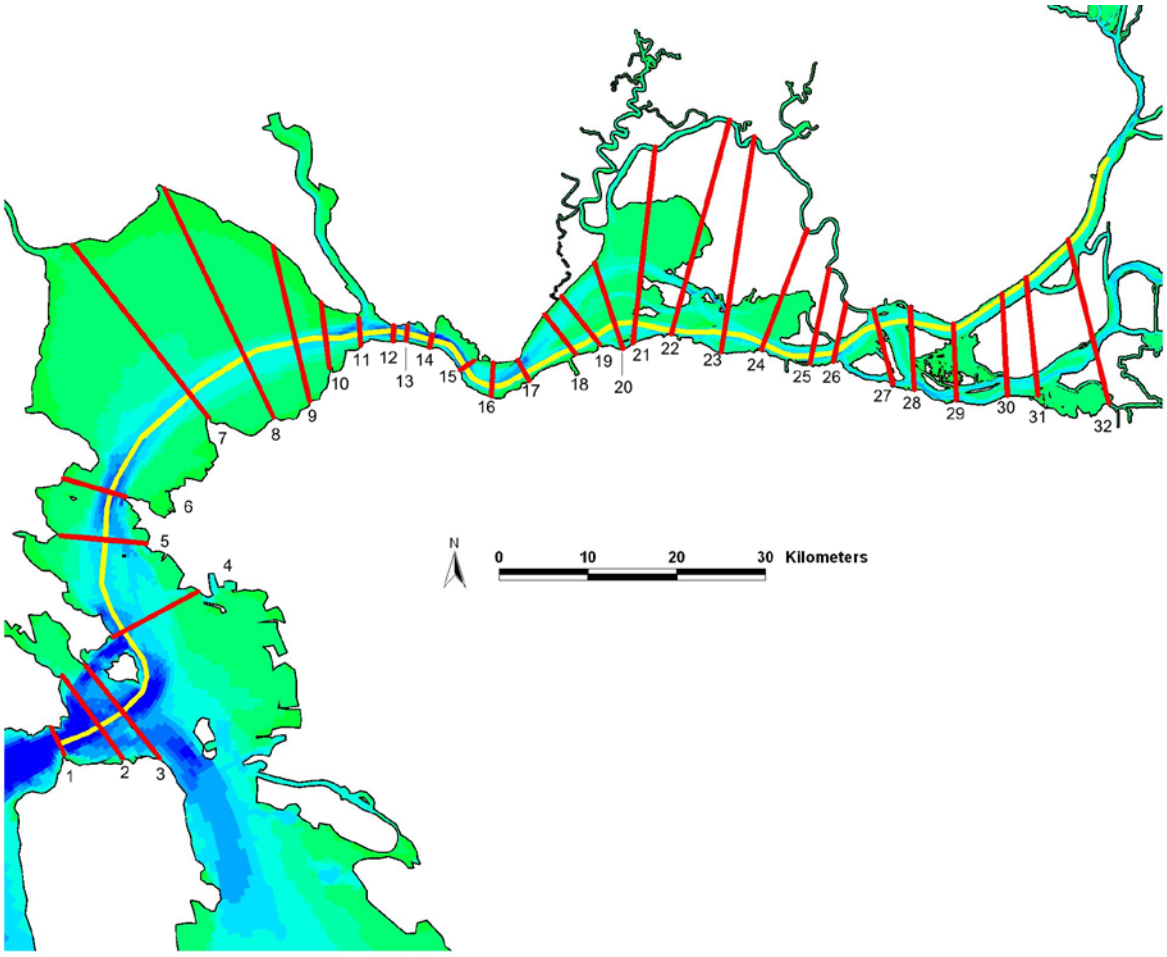

Figure 8.3-1 Locations of cross-sections and centerline transect for salt flux analysis.

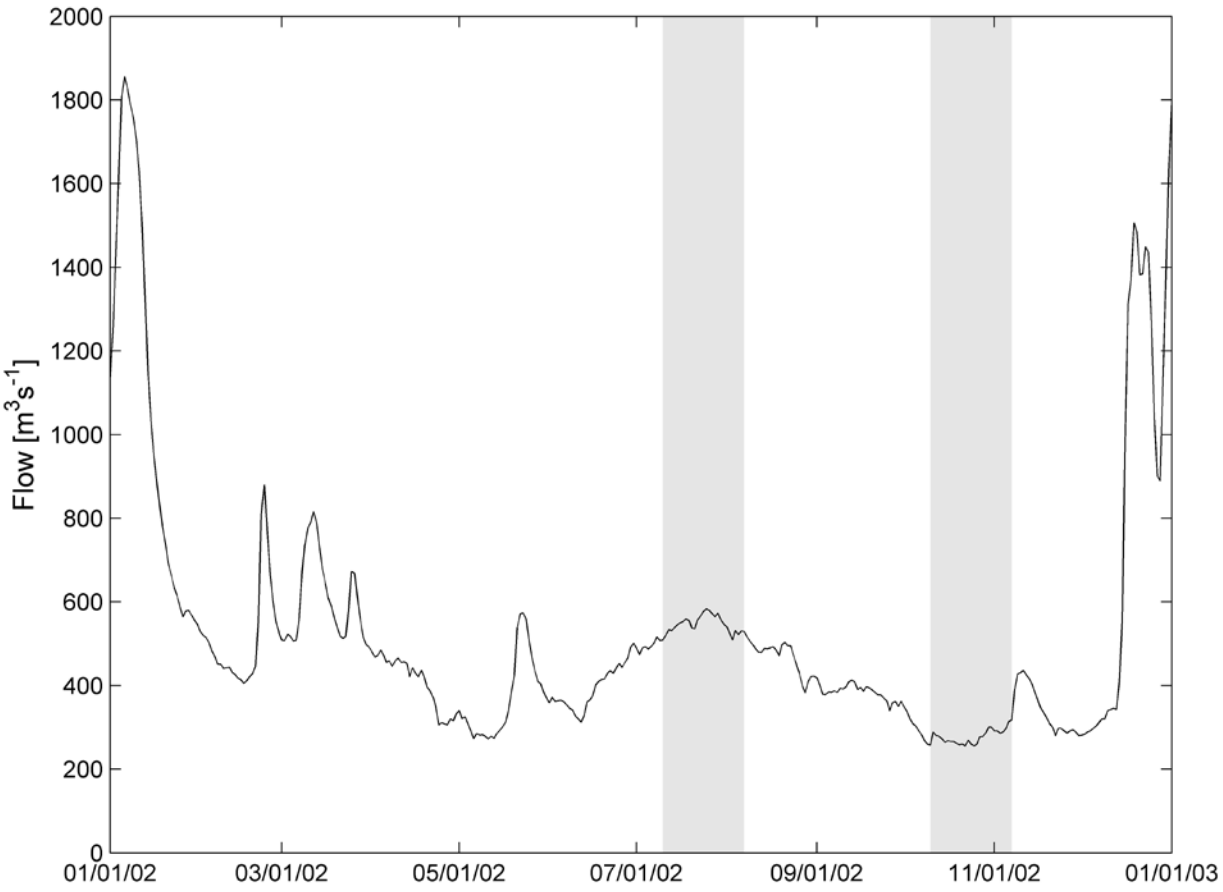

Figure 8.3-2 Observed Sacramento River flow at Freeport during 2002 with salt flux analysis periods identified with grey shading.

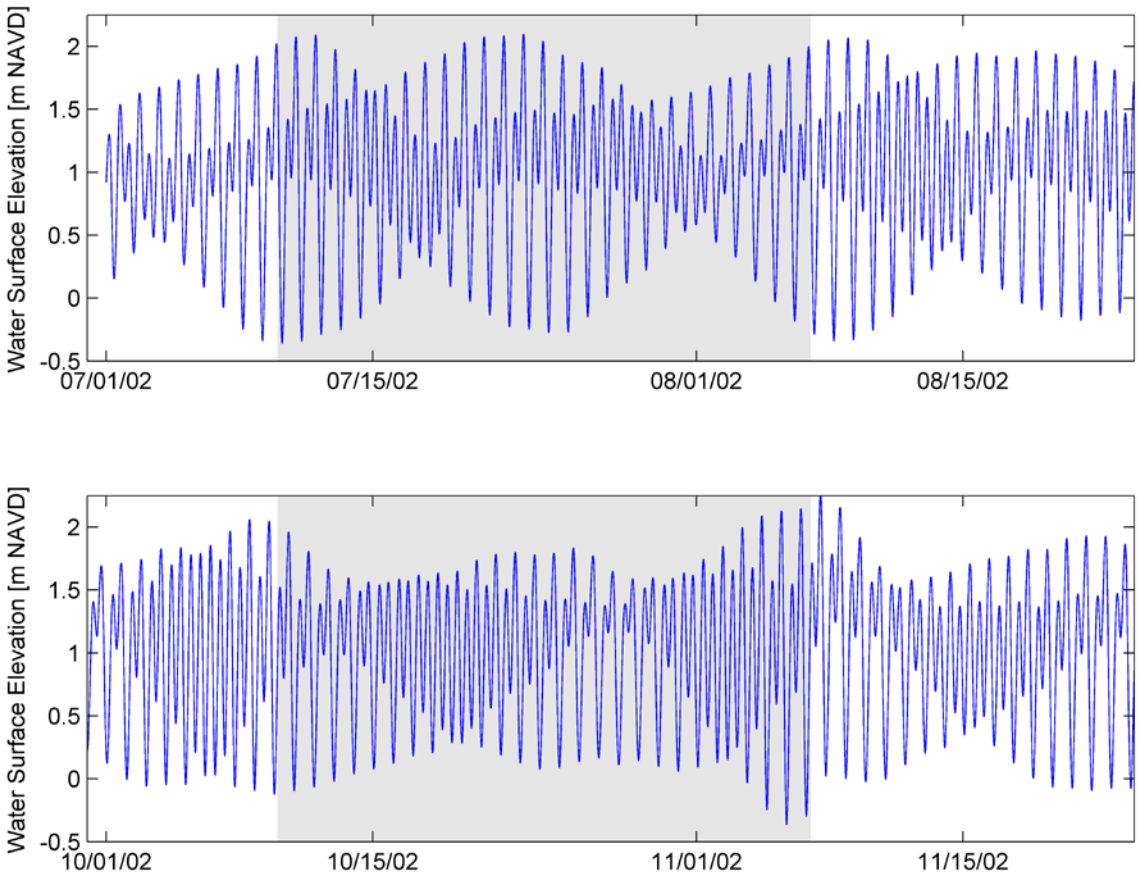

Figure 8.3-3 Observed water surface elevation at the San Francisco Fort Point NOAA station (9414290) during and surrounding the salt flux analysis periods, indicated with grey shading.

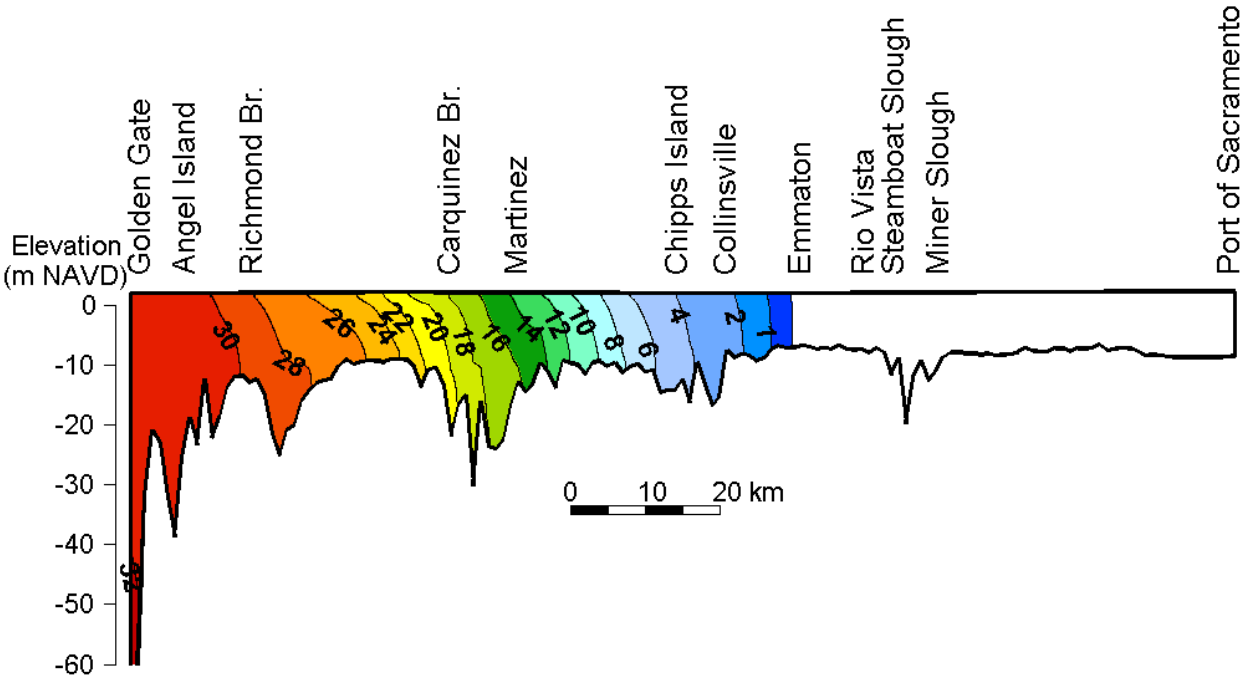

Figure 8.3-4 Period averaged salinity along the centerline transect from the Golden Gate to the Port of Sacramento for the Baseline scenario during the July 15, 2002 through August 12, 2002 analysis period.

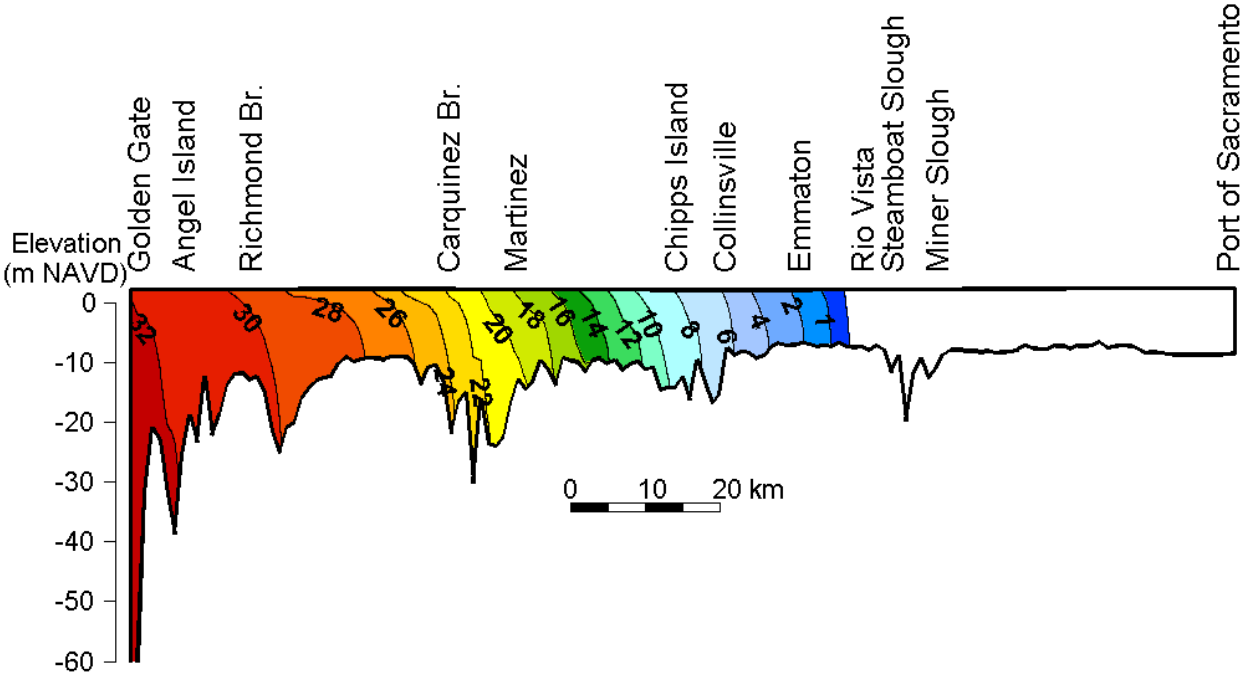

Figure 8.3-5 Period averaged salinity along the centerline transect from the Golden Gate to the Port of Sacramento for the Baseline scenario during the October 13, 2002 through November 10, 2002 analysis period.

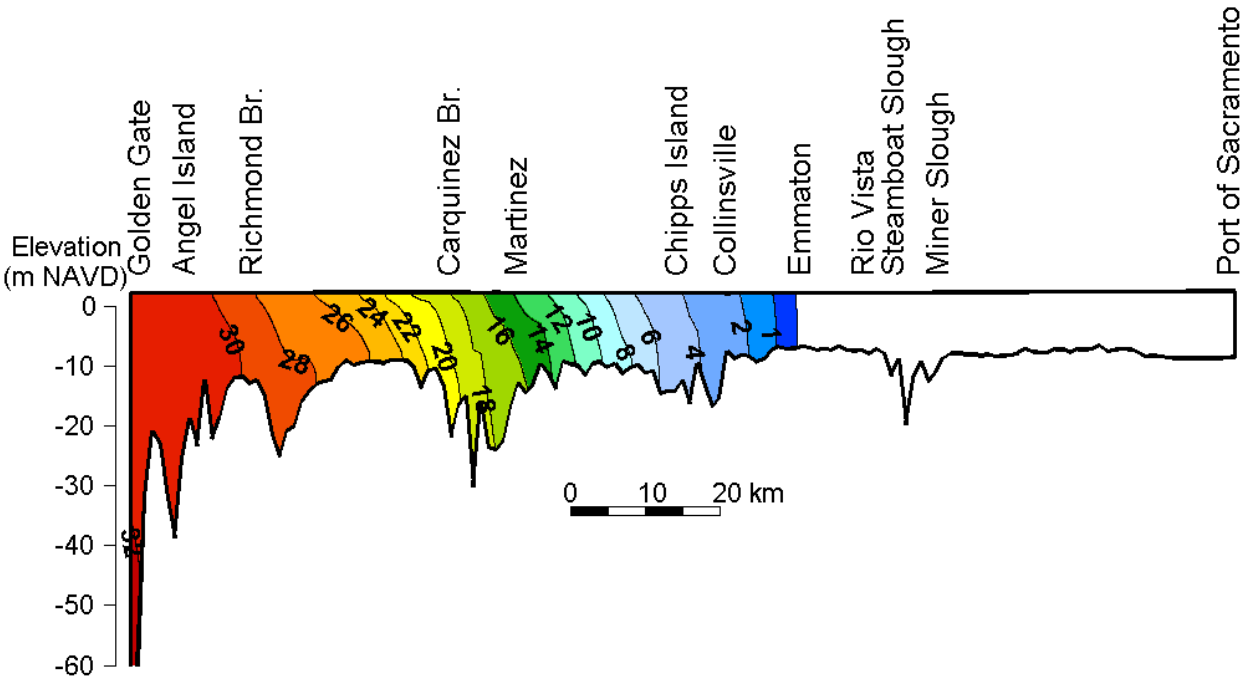

Figure 8.3-6 Period averaged salinity along the centerline transect from the Golden Gate to the Port of Sacramento for the 15 cm SLR scenario during the July 15, 2002 through August 12, 2002 analysis period.

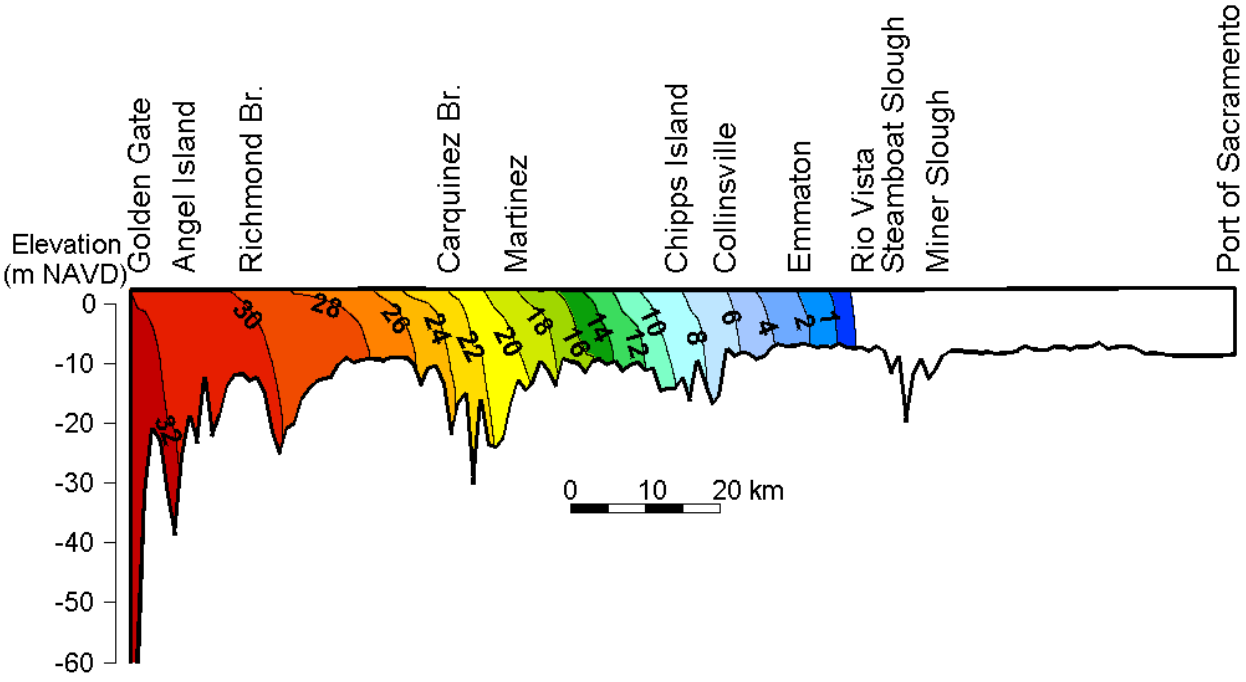

Figure 8.3-7 Period averaged salinity along the centerline transect from the Golden Gate to the Port of Sacramento for the 15 cm SLR scenario during the October 13, 2002 through November 10, 2002 analysis period.

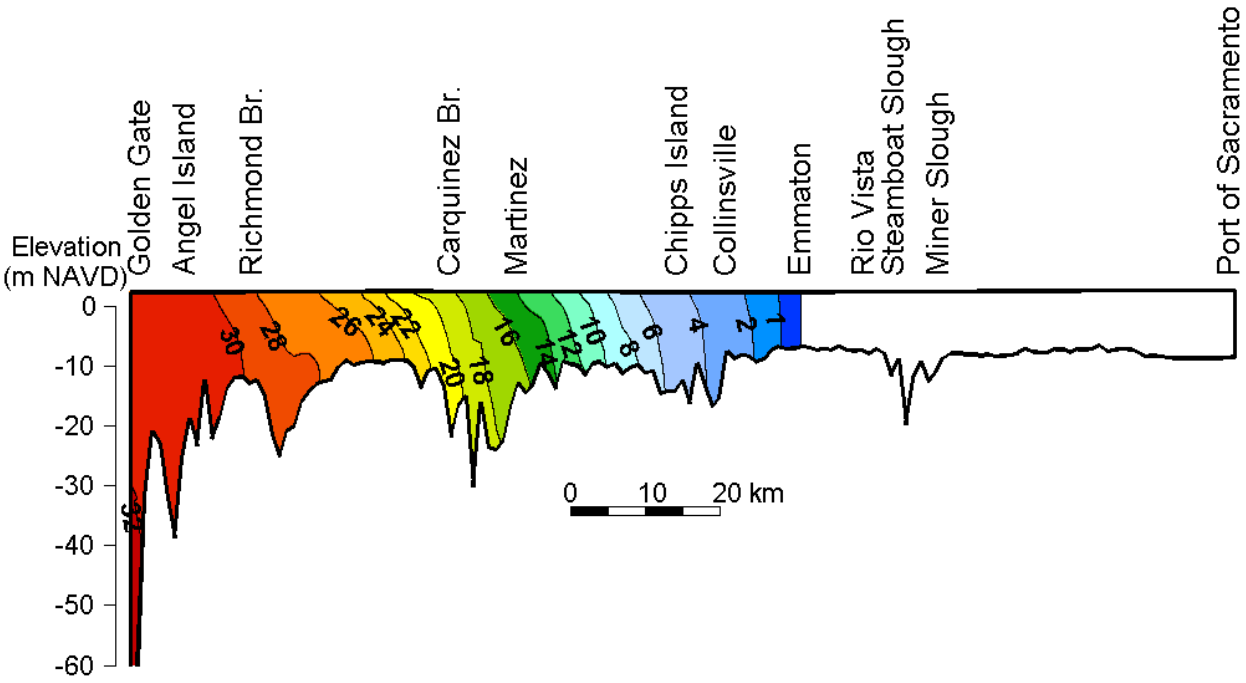

Figure 8.3-8 Period averaged salinity along the centerline transect from the Golden Gate to the Port of Sacramento for the 30 cm SLR scenario during the July 15, 2002 through August 12, 2002 analysis period.

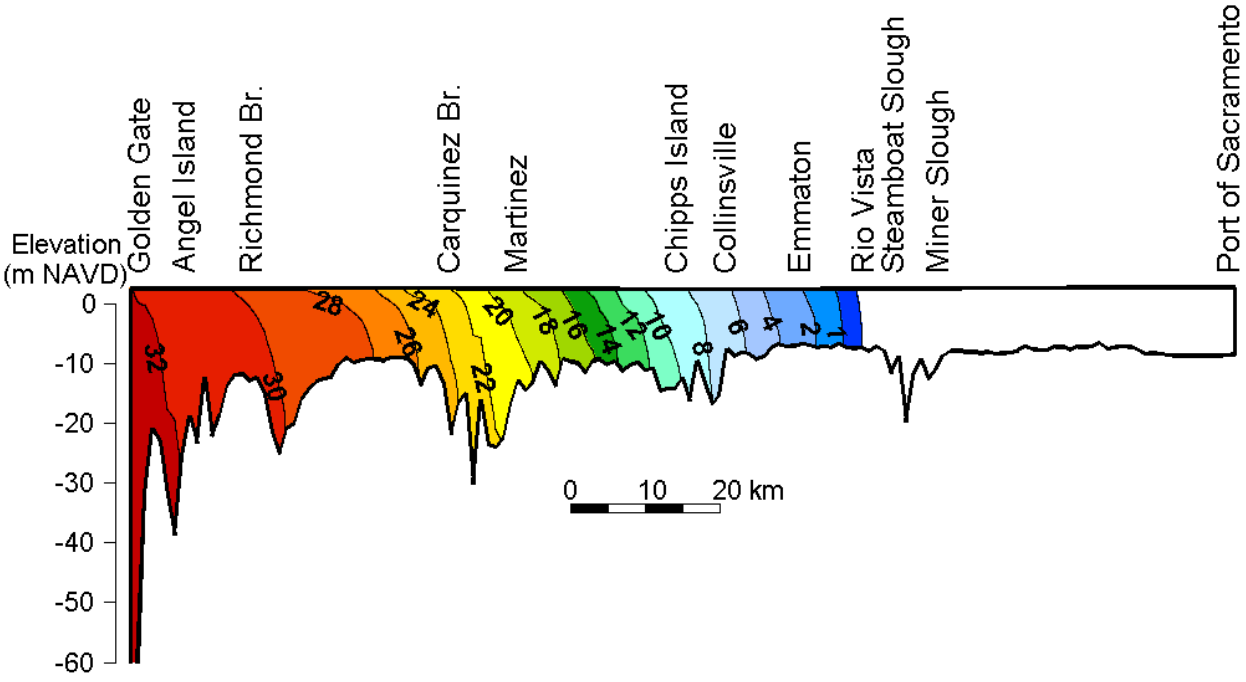

Figure 8.3-9 Period averaged salinity along the centerline transect from the Golden Gate to the Port of Sacramento for the 30 cm SLR scenario during the October 13, 2002 through November 10, 2002 analysis period.

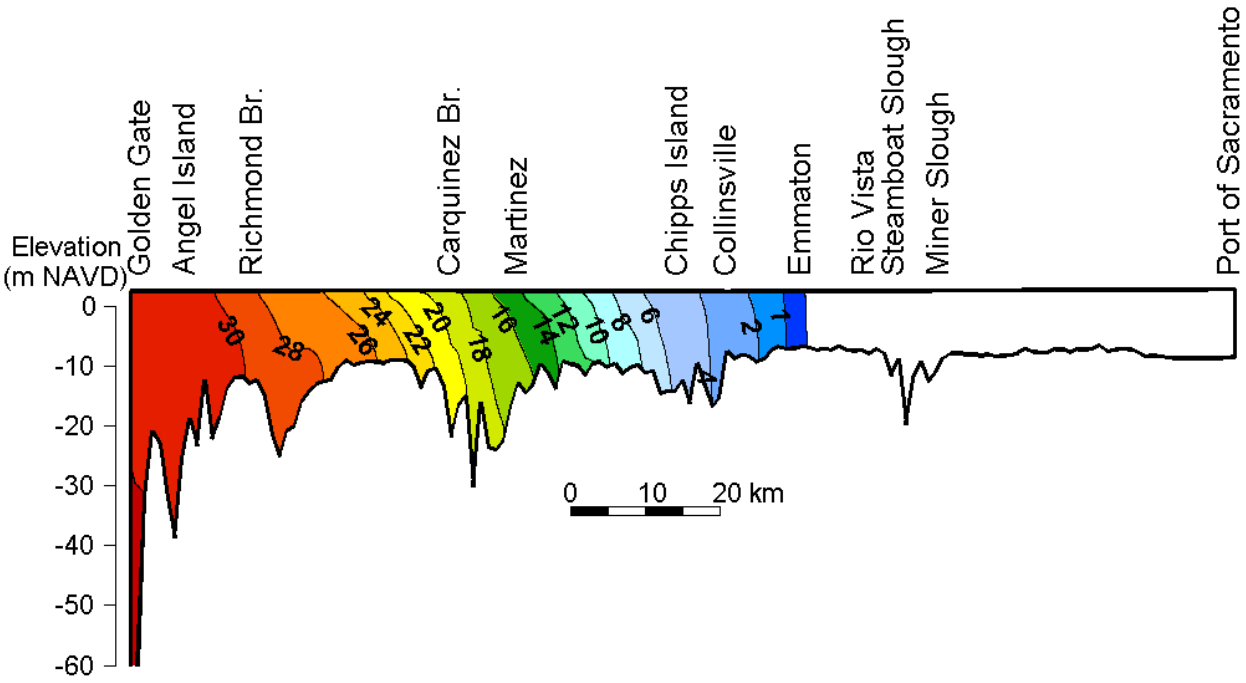

Figure 8.3-10 Period averaged salinity along the centerline transect from the Golden Gate to the Port of Sacramento for the 45 cm SLR scenario during the July 15, 2002 through August 12, 2002 analysis period.

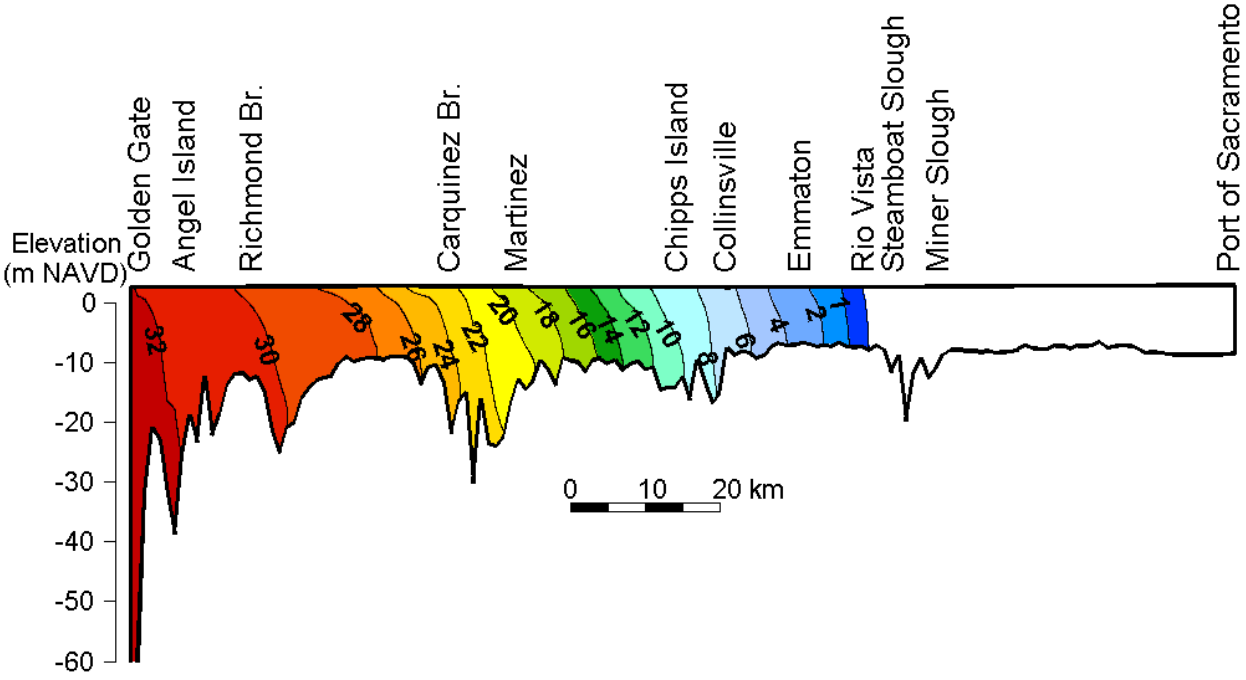

Figure 8.3-11 Period averaged salinity along the centerline transect from the Golden Gate to the Port of Sacramento for the 45 cm SLR scenario during the October 13, 2002 through November 10, 2002 analysis period.

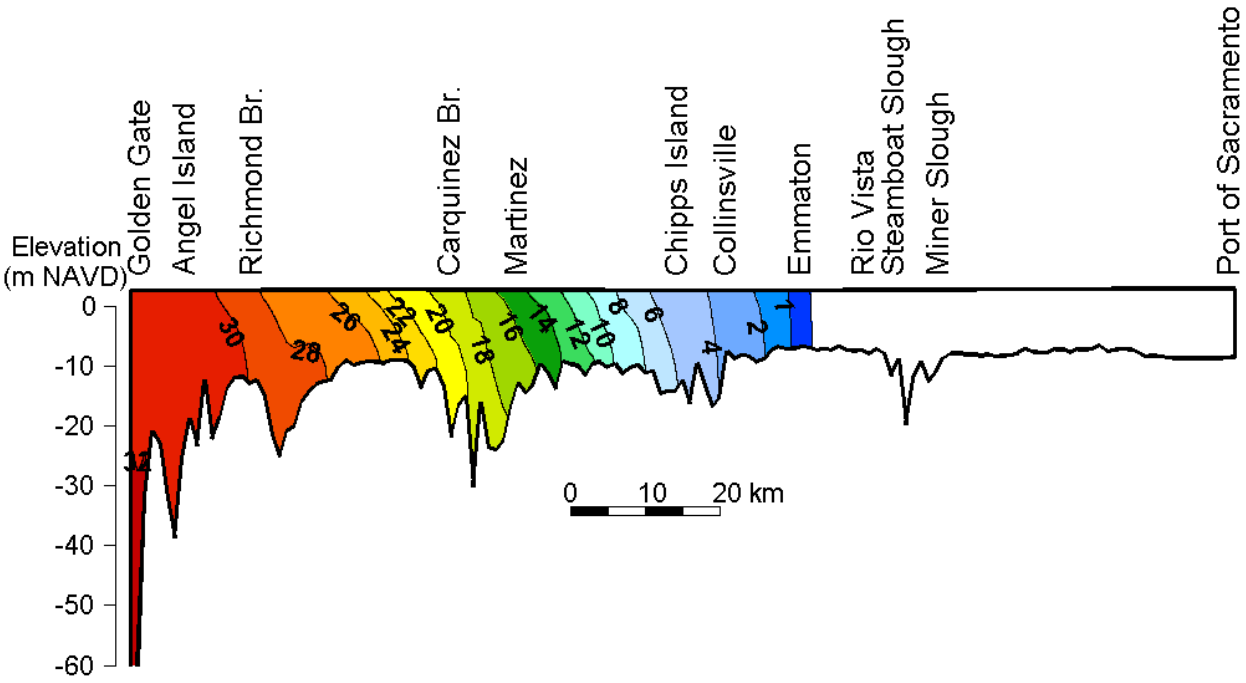

Figure 8.3-12 Period averaged salinity along the centerline transect from the Golden Gate to the Port of Sacramento for the 60 cm SLR scenario during the July 15, 2002 through August 12, 2002 analysis period.

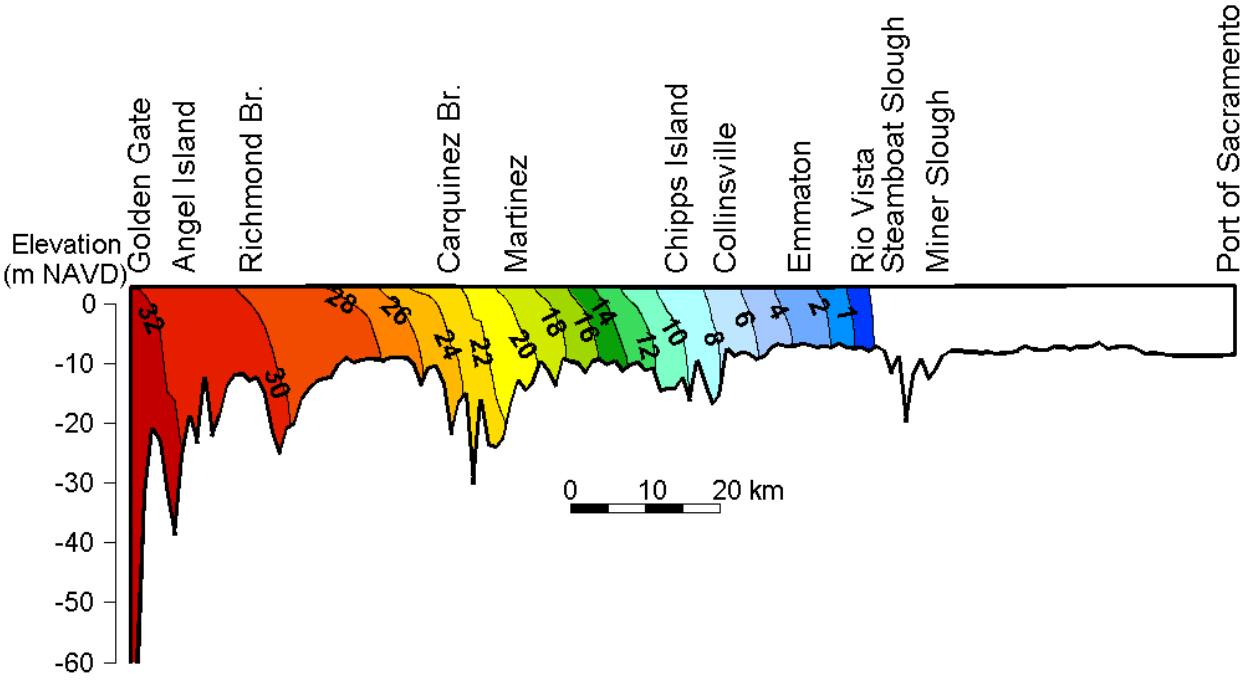

Figure 8.3-13 Period averaged salinity along the centerline transect from the Golden Gate to the Port of Sacramento for the 60 cm SLR scenario during the October 13, 2002 through November 10, 2002 analysis period.

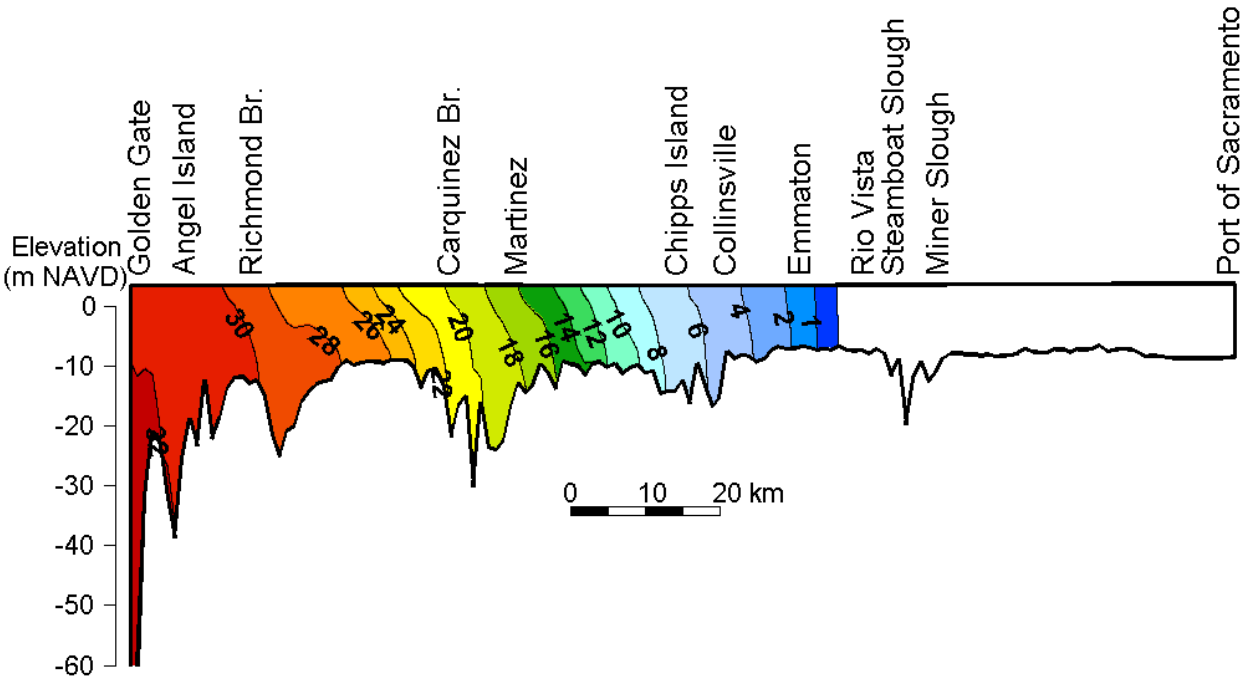

Figure 8.3-14 Period averaged salinity along the centerline transect from the Golden Gate to the Port of Sacramento for the 140 cm SLR scenario during the July 15, 2002 through August 12, 2002 analysis period.

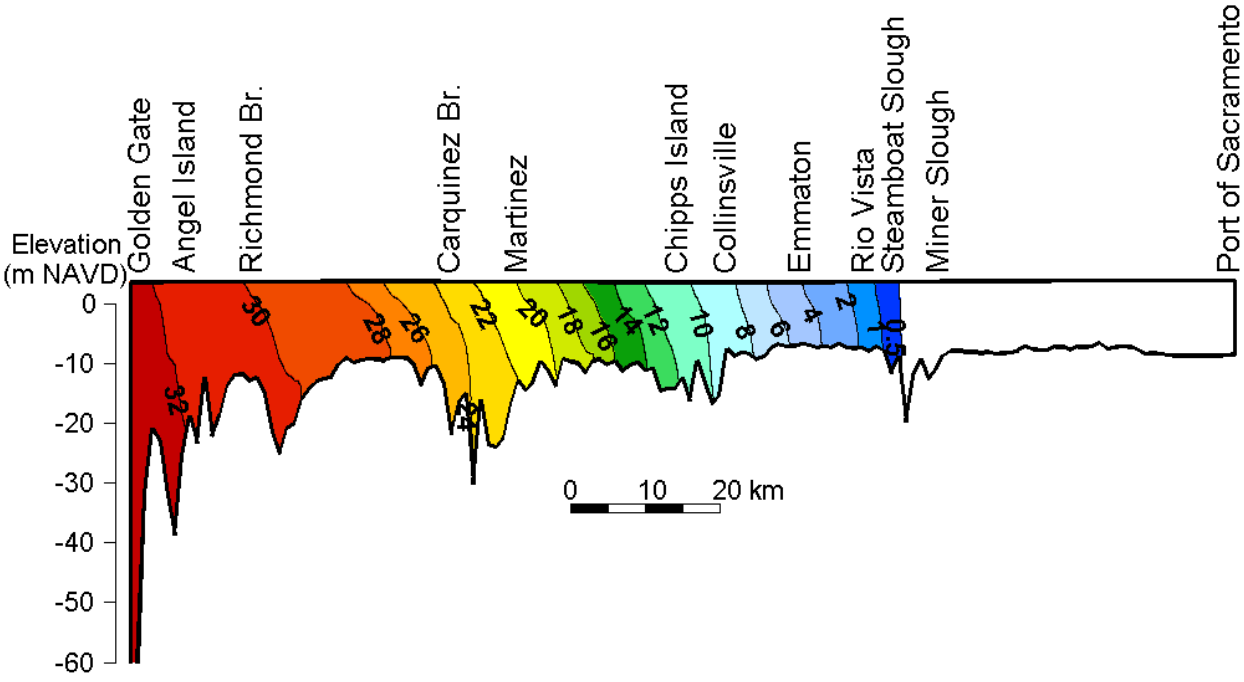

Figure 8.3-15 Period averaged salinity along the centerline transect from the Golden Gate to the Port of Sacramento for the 140 cm SLR scenario during the October 13, 2002 through November 10, 2002 analysis period.

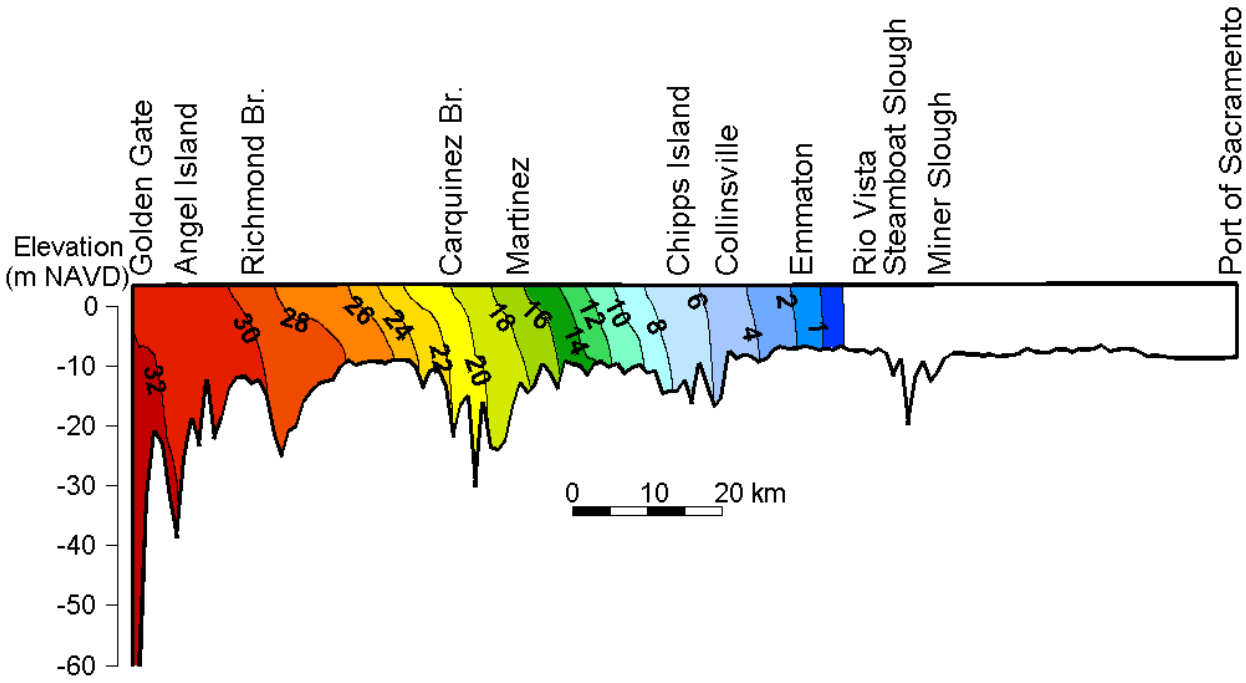

Figure 8.3-16 Period averaged salinity along the centerline transect from the Golden Gate to the Port of Sacramento for the 140 cm SLR with 5% Amplification scenario during the July 15, 2002 through August 12, 2002 analysis period.

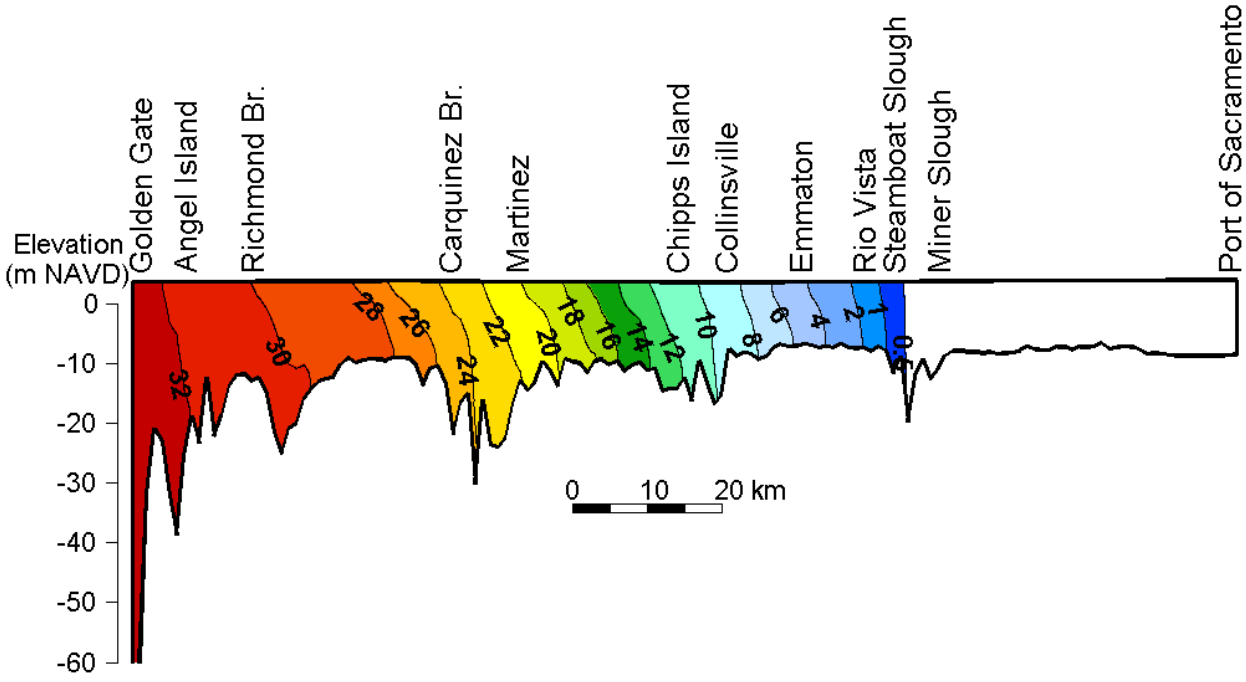

Figure 8.3-17 Period averaged salinity along the centerline transect from the Golden Gate to the Port of Sacramento for the 140 cm SLR with 5% Amplification scenario during the October 13, 2002 through November 10, 2002 analysis period.

8.4 Sea Level Rise Scenario Salt Flux Analysis Results

As discussed in Section 8.3, analysis periods were chosen in part as periods in which advective and dispersive fluxes balance closely. In other words, they are periods of moderate variability in salinity conditions. The total dispersive, advective and net fluxes during each period are shown for both analysis periods of each SLR scenario in Figure 8.4-1 through Figure 8.4-12. The distance shown on the x-axis corresponds to the distances labeled on the Golden Gate to Rio Vista transect in Figure 5.1-2. For each scenario and analysis period, the advective and dispersive fluxes were bigger than the net fluxes at all cross-sections, indicating limited net change in salt mass in the estuary during the analysis period. The net fluxes, indicated with a black x, are generally quite close to the sum of the advective and dispersive fluxes, indicated with a green +. Differences between net fluxes and the sum of the advective and dispersive fluxes are associated with flux terms that are neglected in the flux analysis and other sources of inaccuracies in the analysis but are typically very small.

In Figure 8.4-13 through Figure 8.4-20 the average tidal prism predicted during each analysis period is provided for several cross-sections. The tidal prism increases substantially at all locations with increased sea level rise, with the largest proportional increases with SLR at Chipps Island (cross-section 25). The increase in tidal prism with SLR is likely to explain several trends in the salt flux analysis. It should be noted that the SLR scenarios assume "hard shorelines." As a result of this assumption, the tidal prism is likely to increase more substantially with sea level rise than predicted in this analysis due to inundation of low elevation regions bordering the estuary.

In order to calculate dispersion coefficient using Equation 8-1, the variables Q, S and A are averaged through the analysis period at the individual cross-sections. Salinity is also period averaged along the centerline transect shown in Figure 8.3-1, and is shown for each SLR scenario and analysis period in Figure 8.3-4 through Figure 8.3-15. In order to calculate the longitudinal salinity gradient (dS/dx) at each cross section, the period averaged salinity along the centerline transect is depth-averaged for each scenario to calculate the predicted depth-averaged and period averaged salinity along the centerline of the estuary from the Golden Gate to Rio Vista. The longitudinal salinity gradient at each point is determined by a linear fit of the variability of depth-averaged salinity with distance along the centerline. The longitudinal salinity gradients along the centerline of the estuary are shown in Figure 8.4-21 and Figure 8.4-22.

Salt fluxes and dispersion coefficients were calculated for each cross-section shown in Figure 8.3-1 for the Baseline scenario and for each SLR scenario. Increases in salt fluxes and dispersion coefficients with SLR indicate that increased Delta inflows will be required to meet salinity standards as a result of SLR. The estimated dispersion coefficients (K) are shown in Figure 8.4-23 for the July 15, 2002 through August 12, 2002 analysis period and in Figure 8.4-24 for the October 13, 2002 through November 10, 2002 analysis period. The dispersion coefficients for the two periods show similar trends, but the dispersion coefficients for the October 13, 2002 through November 10, 2002 analysis period are higher in Suisun Bay and the western Delta than the respective dispersion coefficients for the July 15, 2002 through August 12, 2002 analysis period. The calculated dispersion coefficients have limited variability with SLR at most cross-sections in Central Bay and San Pablo Bay. However, dispersion coefficients in Suisun Bay and

the western Delta generally increase substantially with SLR, with more pronounced increases with SLR for the October 13, 2002 through November 10, 2002 analysis period.

The salt flux analysis described in Section 8.2 was used to divide each dispersion coefficient into three components: K_{gc}, $K_{uvs,}$ and K_{td}. K_{gc} represents the strength of gravitational circulation, K_{uvs} represents the strength of all unsteady vertical shear dispersion processes, and K_{td} represents the strength of all tidal dispersion processes. The mixing associated with gravitational circulation and unsteady vertical shear processes are not represented by depth-averaged models. In addition the mixing caused by tidal dispersion processes can be estimated to be quite different among models, particularly between depth-averaged and three-dimensional models.

The estimated dispersion coefficients associated with gravitational circulation (K_{gc}) are shown in Figure 8.4-25 for the July 15, 2002 through August 12, 2002 analysis period and in Figure 8.4-26 for the October 13, 2002 through November 10, 2002 analysis period. Note that this dispersion coefficient component is more variable with location than the overall dispersion coefficient. The dispersion coefficients associated with gravitational circulation drop substantially in Suisun Bay, relative to San Pablo Bay, starting at 55 km from the Golden Gate, near Benicia. These results are consistent with the findings of Burau et al. (1998) in the Entrapment Zone Study. The interpretation in that study is that the reduced depth at the Benicia Shoal reduced the strength of gravitational circulation. The dispersion coefficient components associated with gravitational circulation generally increase strongly with SLR in Suisun Bay and the western Delta, with more pronounced increases with SLR for the October 13, 2002 through November 10, 2002 analysis period than for the July 15, 2002 through August 12, 2002 analysis period. This is consistent with the higher salinity conditions in the October 13, 2002 through November 10, 2002 analysis period than the July 15, 2002 through August 12, 2002 analysis period.

The dispersion coefficients associated with unsteady vertical shear (K_{uvs}) are shown in Figure 8.4-27 for the July 15, 2002 through August 12, 2002 analysis period and in Figure 8.4-28 for the October 13, 2002 through November 10, 2002 analysis period. The unsteady vertical shear component is highly variable but often of similar magnitude as the gravitational circulation component. Some of the dispersion associated with unsteady vertical shear is associated with the SIPS mechanism which is known to be active in portions of Suisun Bay (Stacey et al. 2001). The dispersion associated with unsteady vertical shear varies with sea level rise in Carquinez Strait, Suisun Bay and the western Delta. However, the trend of change in this component with sea level rise varies from cross-section to cross-section. Dispersion coefficient components of less than 1 $m^2 s^{-1}$ are off the y-axis scale and do not appear on the figure.

The dispersion coefficients associated with all tidal dispersion processes (K_{td}) are shown in Figure 8.4-29 for the July 15, 2002 through August 12, 2002 analysis period and in Figure 8.4-30 for the October 13, 2002 through November 10, 2002 analysis period. K_{td} is similar between the two analysis periods and varies over slightly more than one order of magnitude spatially. Since this component of the dispersion coefficient is not expected to have strong variation with stratification, the less pronounced spatial variability was expected. The dispersion coefficient component associated with tidal dispersion generally increases with increased SLR in Carquinez Strait, Suisun Bay and the western Delta. This increase is probably related to the increased tidal prism shown in Figure 8.4-13 through Figure 8.4-20.

In the following sections, the dispersion analysis results in each sub-embayment will be presented.

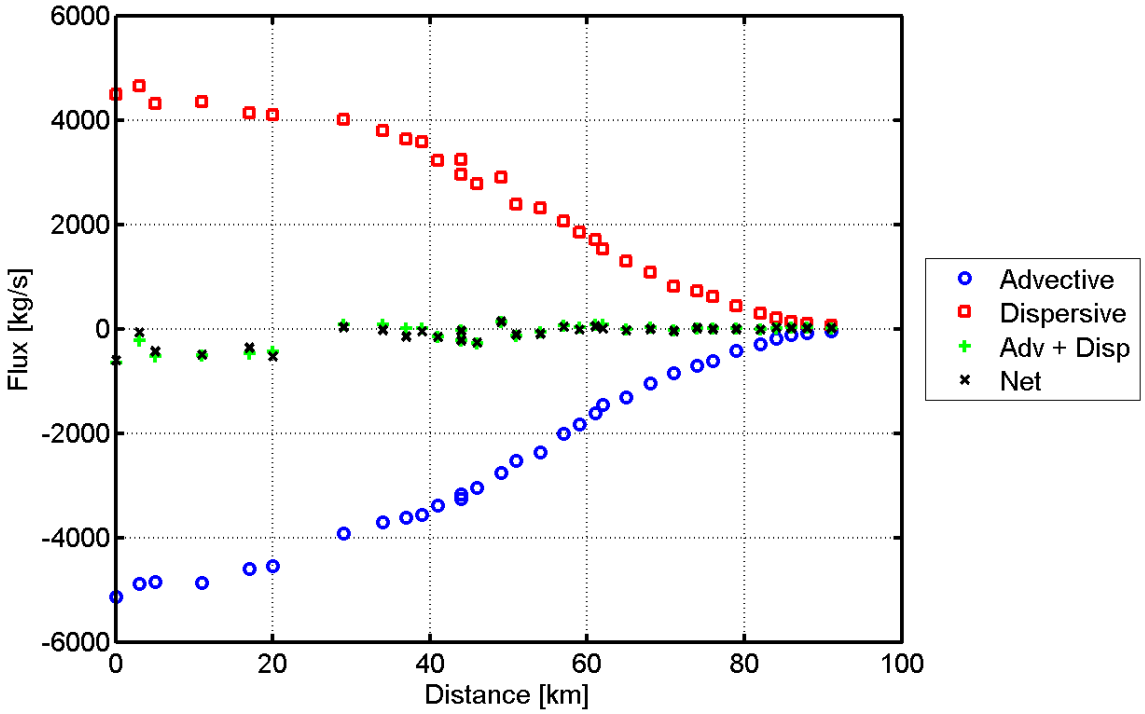

Figure 8.4-1 Predicted advective, dispersive and net salt fluxes for the Baseline scenario during the July 15, 2002 through August 12, 2002 analysis period.

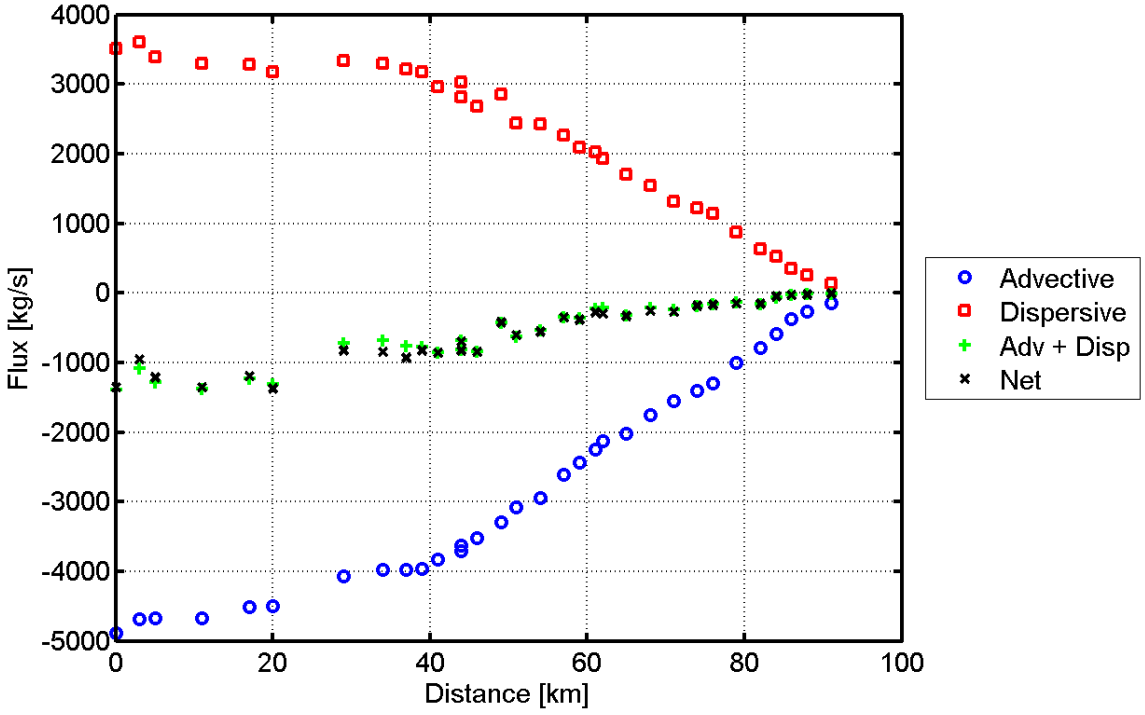

Figure 8.4-2 Predicted advective, dispersive and net salt fluxes for the Baseline scenario during the October 13, 2002 through November 10, 2002 analysis period.

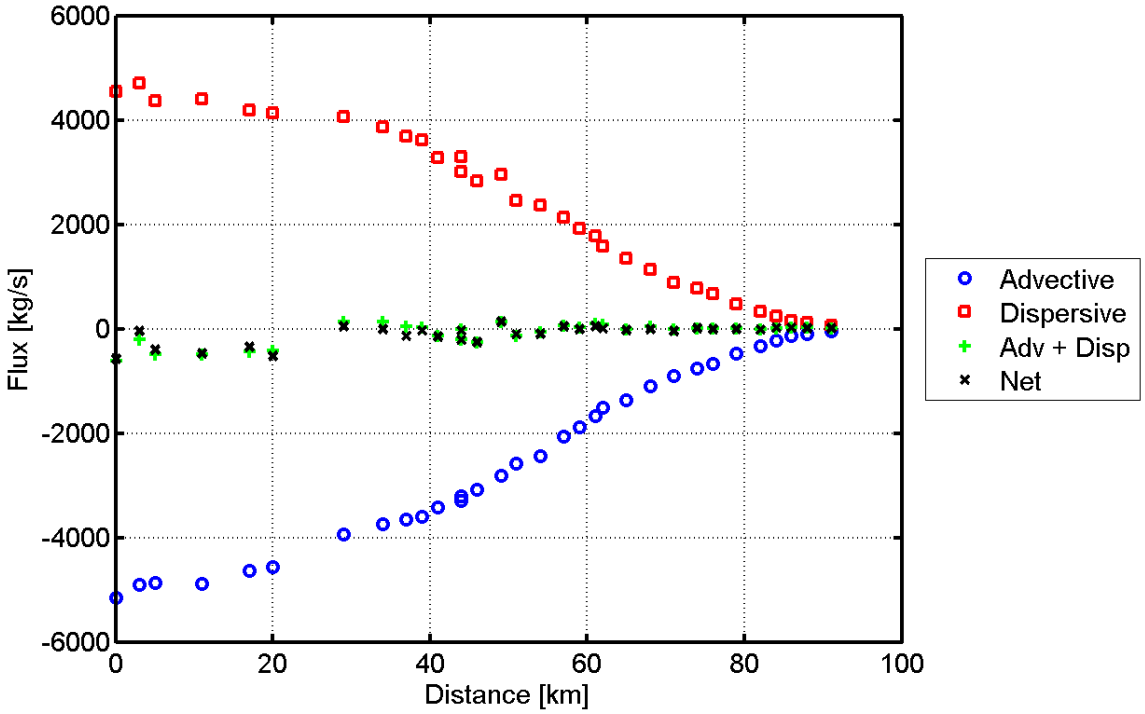

Figure 8.4-3 Predicted advective, dispersive and net salt fluxes for the 15 cm SLR scenario during the July 15, 2002 through August 12, 2002 analysis period.

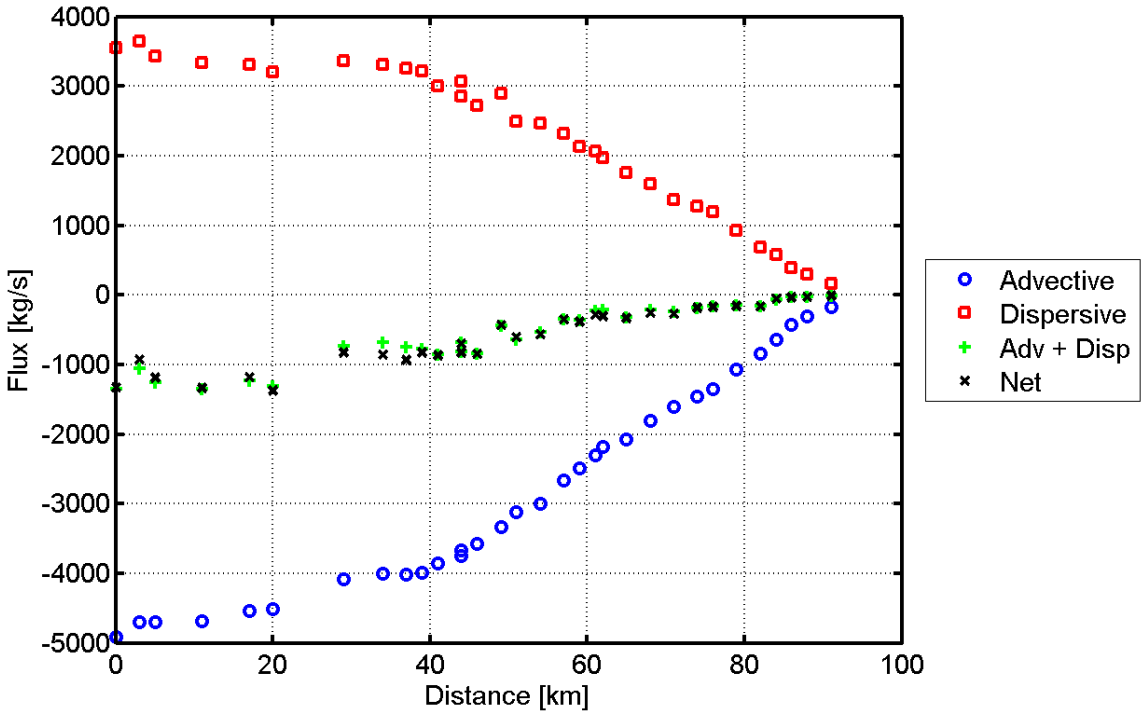

Figure 8.4-4 Predicted advective, dispersive and net salt fluxes for the 15 cm SLR scenario during the October 13, 2002 through November 10, 2002 analysis period.

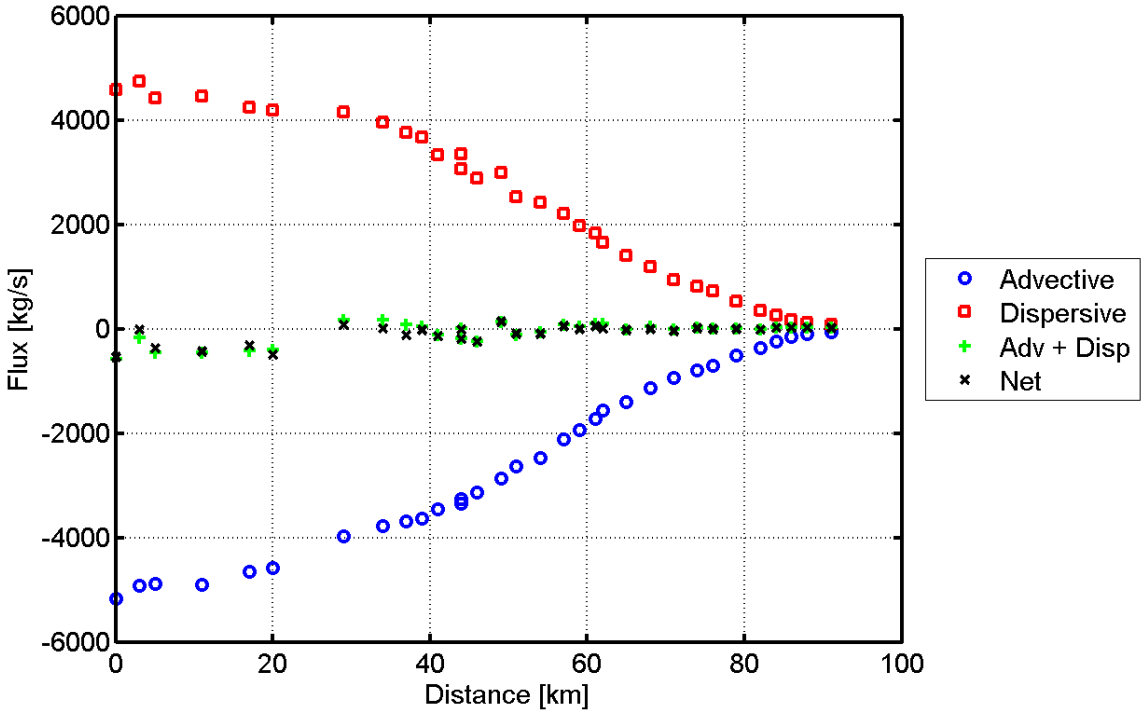

Figure 8.4-5 Predicted advective, dispersive and net salt fluxes for the 30 cm SLR scenario during the July 15, 2002 through August 12, 2002 analysis period.

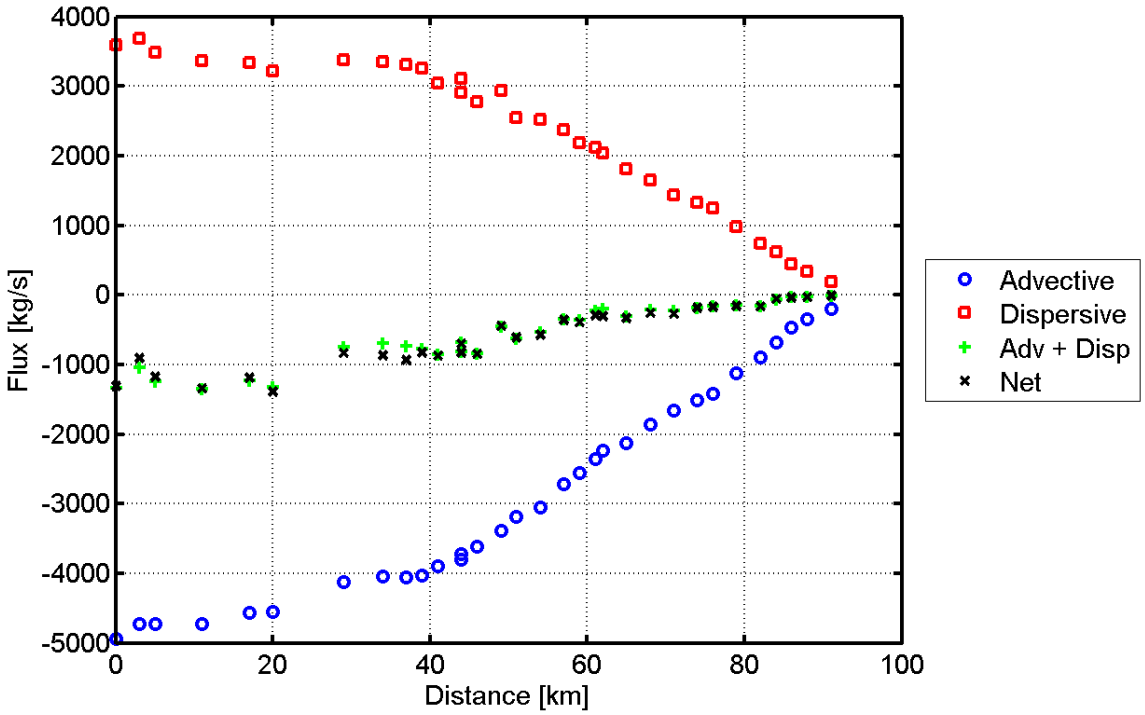

Figure 8.4-6 Predicted advective, dispersive and net salt fluxes for the 30 cm SLR scenario during the October 13, 2002 through November 10, 2002 analysis period.

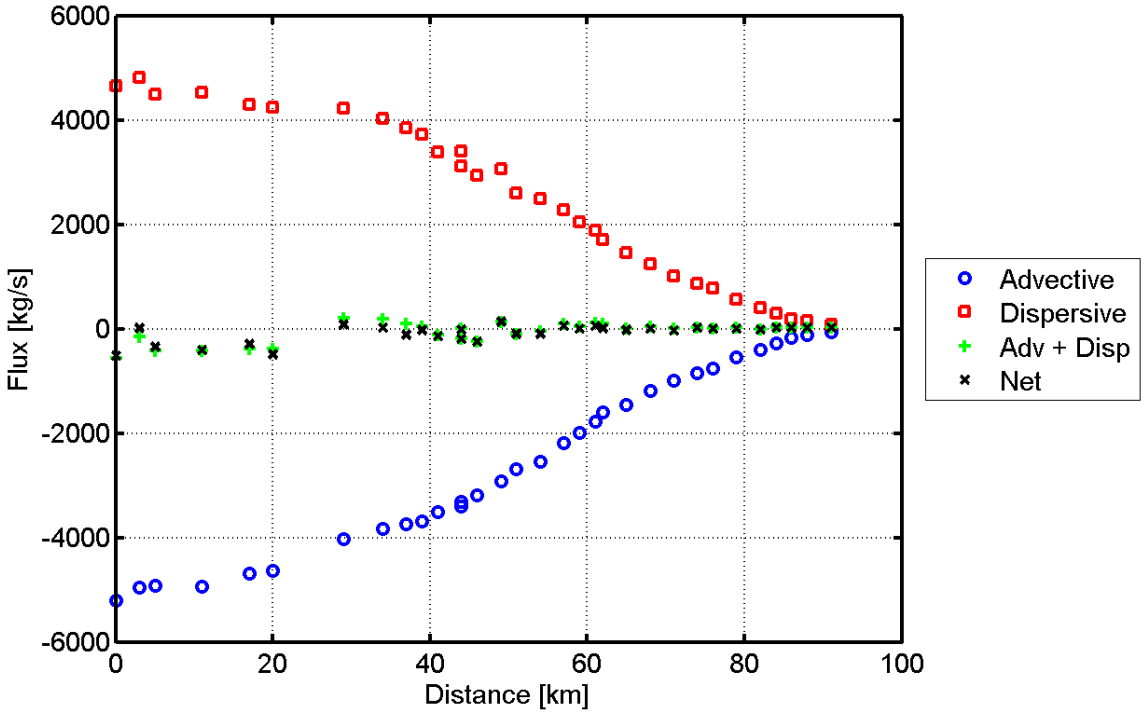

Figure 8.4-7 Predicted advective, dispersive and net salt fluxes for the 45 cm SLR scenario during the July 15, 2002 through August 12, 2002 analysis period.

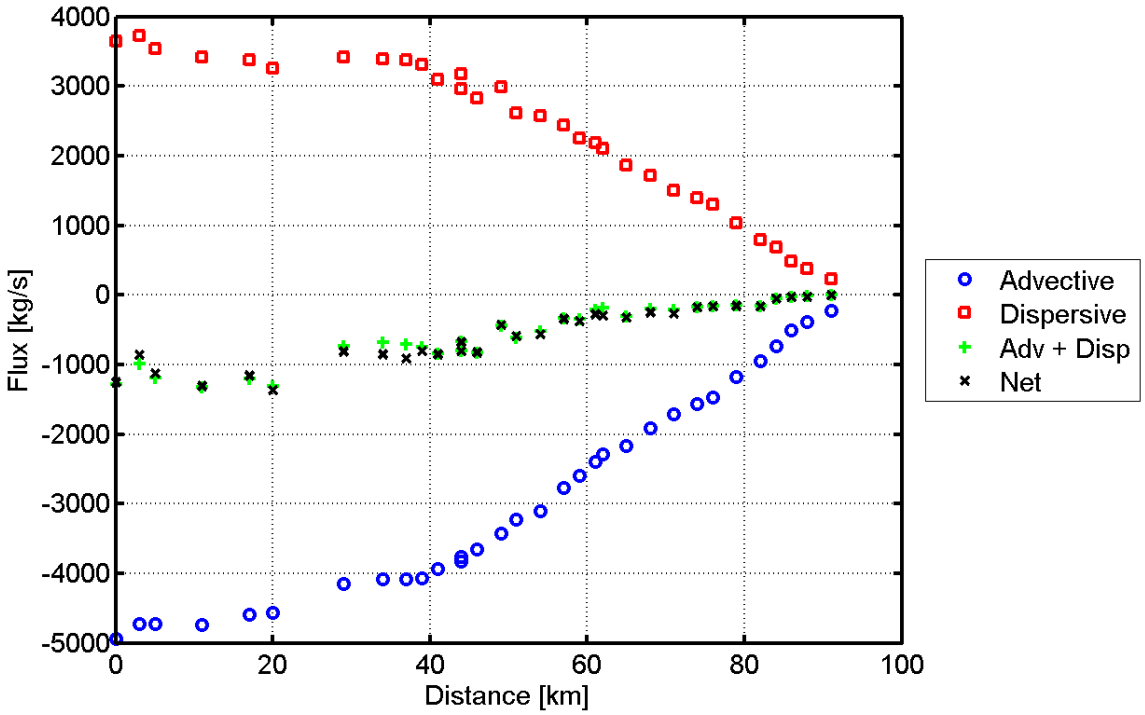

Figure 8.4-8 Predicted advective, dispersive and net salt fluxes for the 45 cm SLR scenario during the October 13, 2002 through November 10, 2002 analysis period.

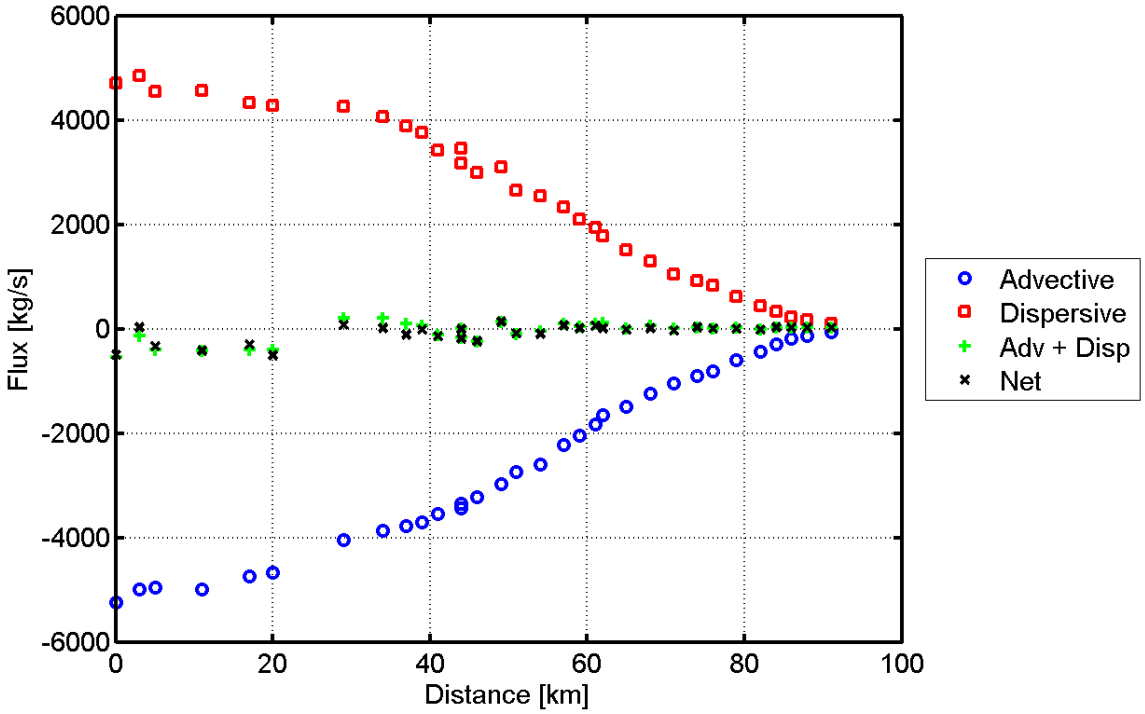

Figure 8.4-9 Predicted advective, dispersive and net salt fluxes for the 60 cm SLR scenario during the July 15, 2002 through August 12, 2002 analysis period.

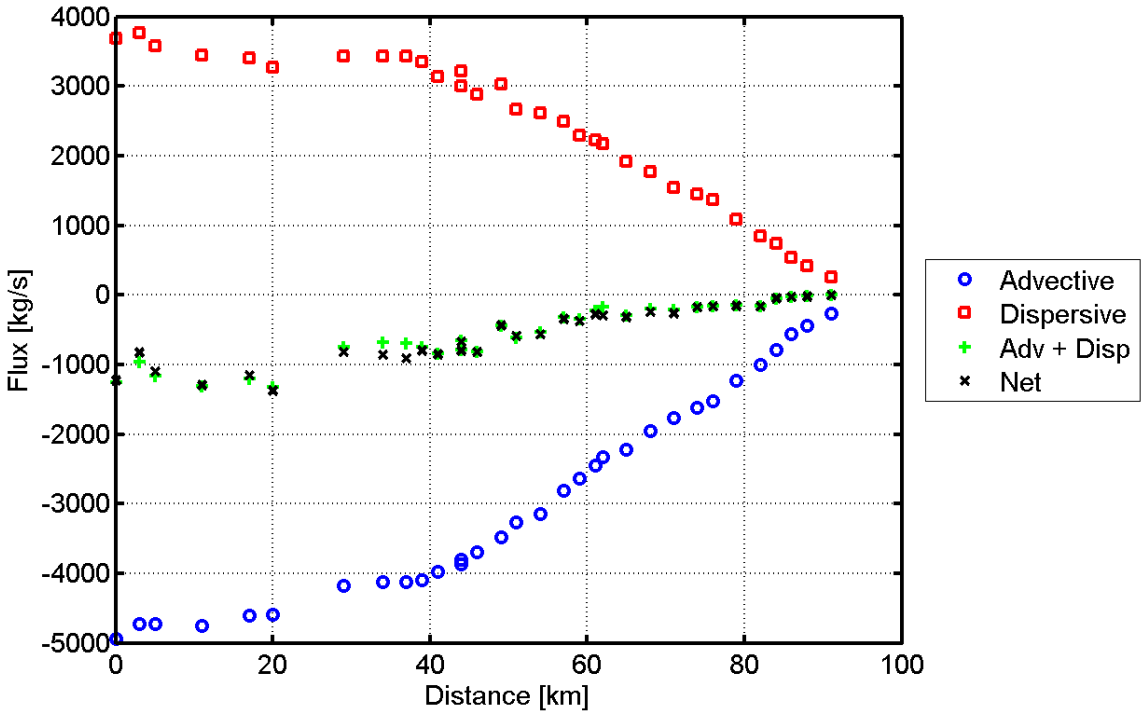

Figure 8.4-10 Predicted advective, dispersive and net salt fluxes for the 60 cm SLR scenario during the October 13, 2002 through November 10, 2002 analysis period.

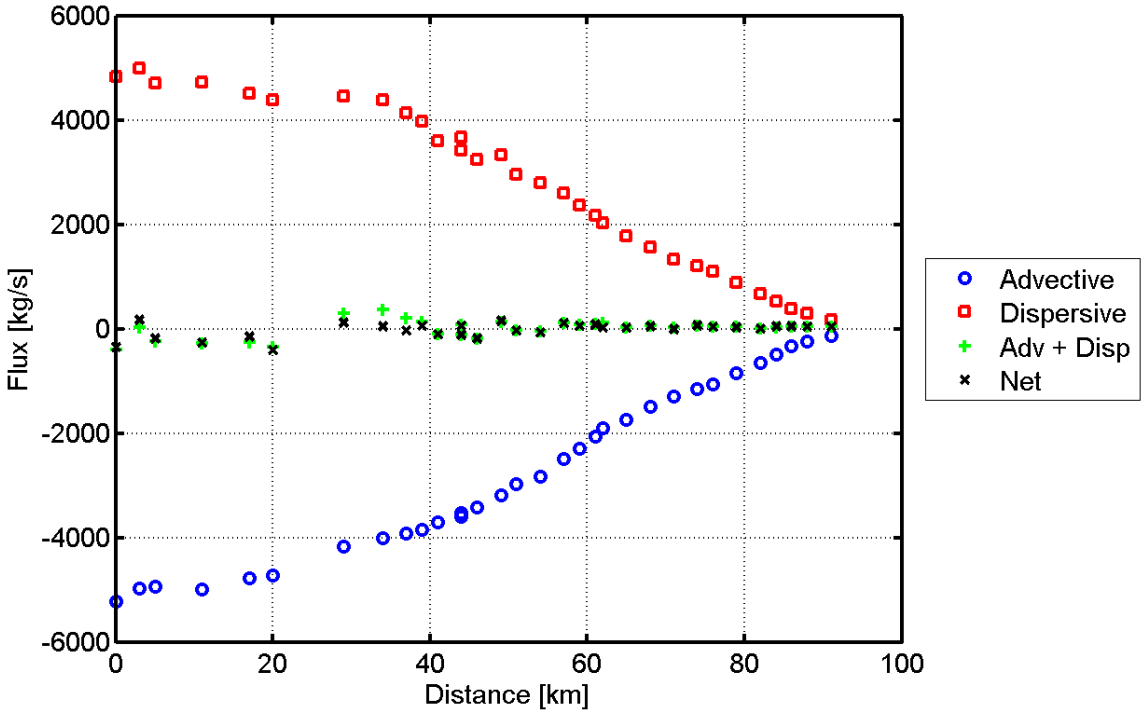

Figure 8.4-11 Predicted advective, dispersive and net salt fluxes for the 140 cm SLR scenario during the July 15, 2002 through August 12, 2002 analysis period.

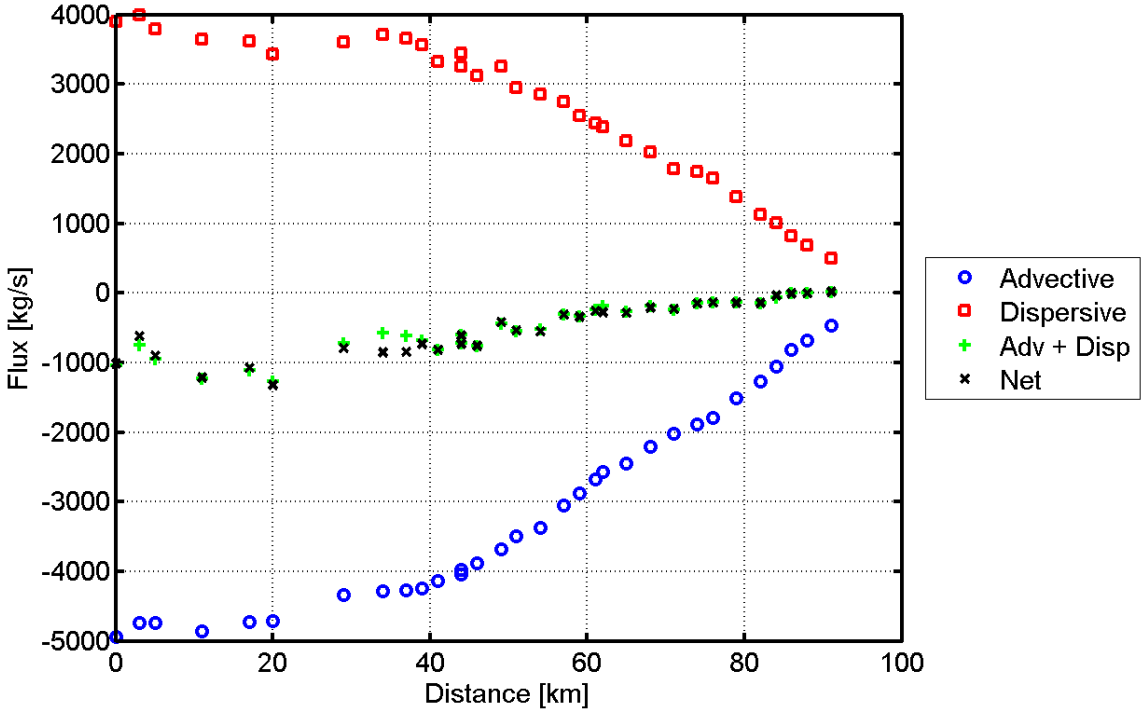

Figure 8.4-12 Predicted advective, dispersive and net salt fluxes for the 140 cm SLR scenario during the October 13, 2002 through November 10, 2002 analysis period.

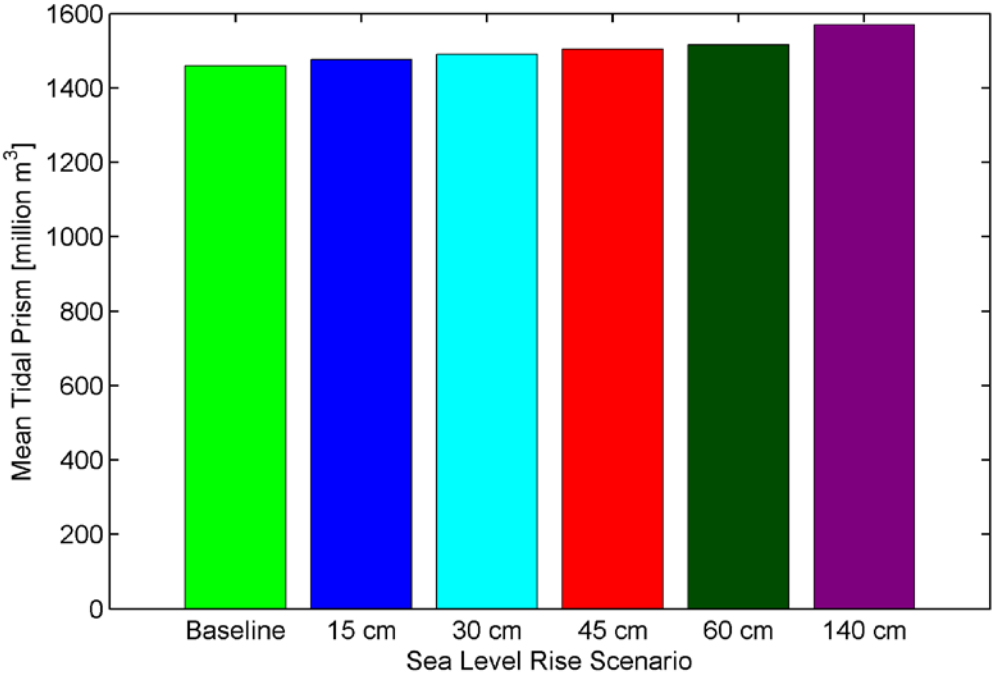

Figure 8.4-13 Average tidal prism at cross-section 1, located at the Golden Gate, for the Baseline and SLR scenarios during the July 15, 2002 through August 12, 2002 analysis period.

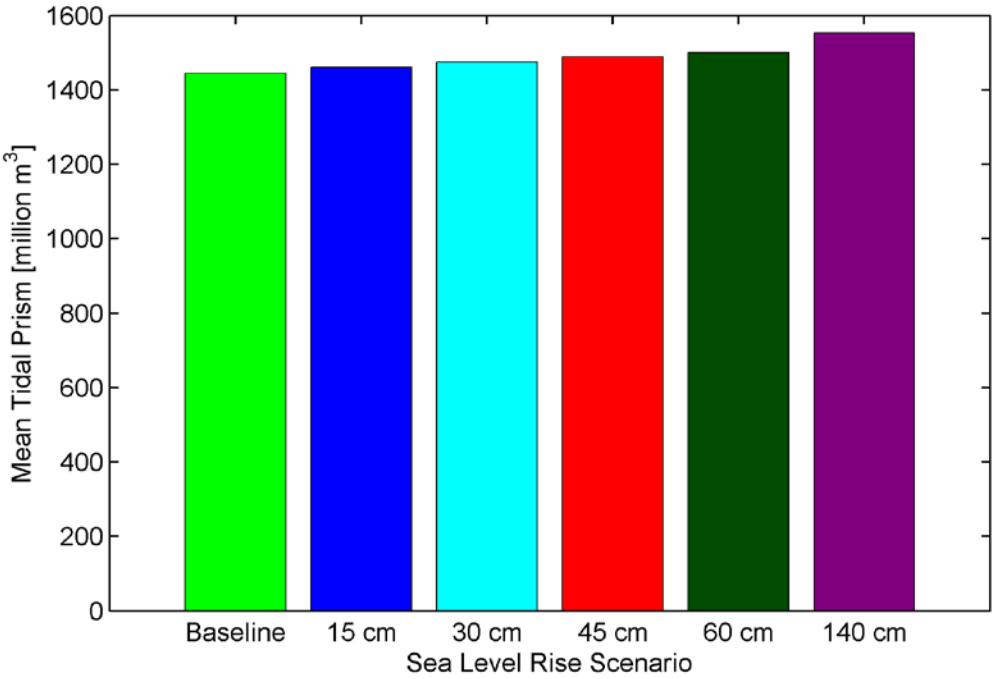

Figure 8.4-14 Average tidal prism at cross-section 1, located at the Golden Gate, for the Baseline and SLR scenarios during the October 13, 2002 through November 10, 2002 analysis period.

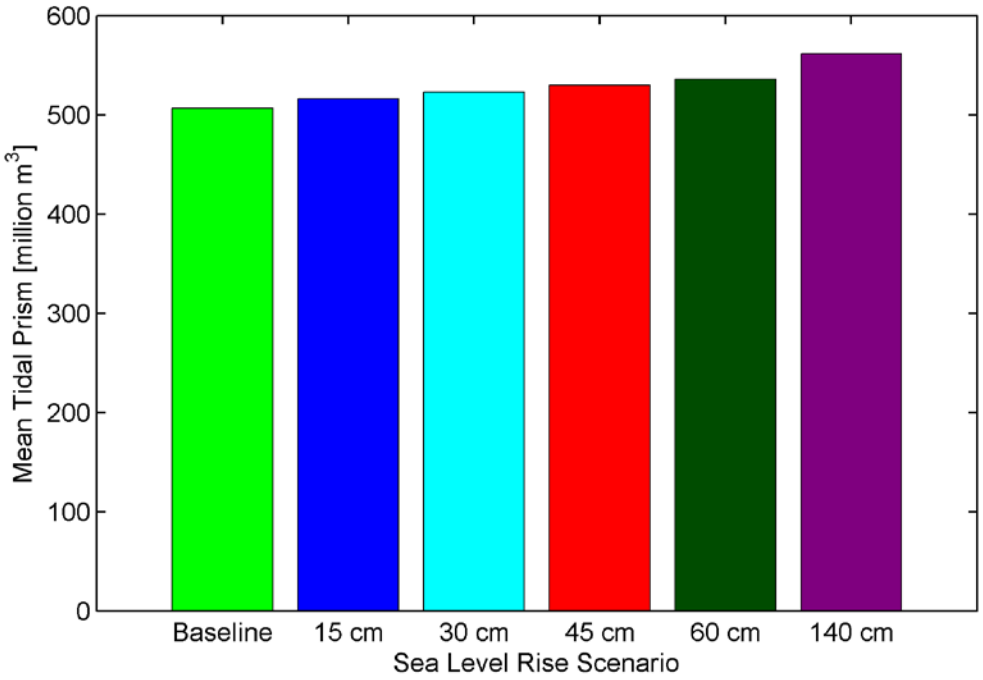

Figure 8.4-15 Average tidal prism at cross-section 5, located at the Richmond-San Rafael Bridge, for the Baseline and SLR scenarios during the July 15, 2002 through August 12, 2002 analysis period.

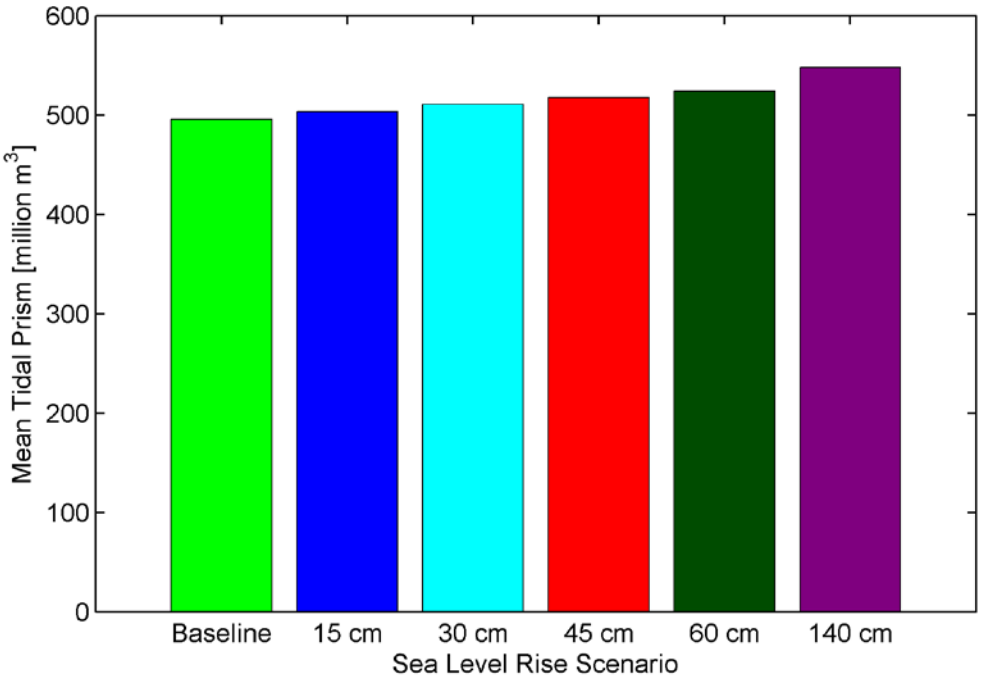

Figure 8.4-16 Average tidal prism at cross-section 5, located at the Richmond-San Rafael Bridge, for the Baseline and SLR scenarios during the October 13, 2002 through November 10, 2002 analysis period.

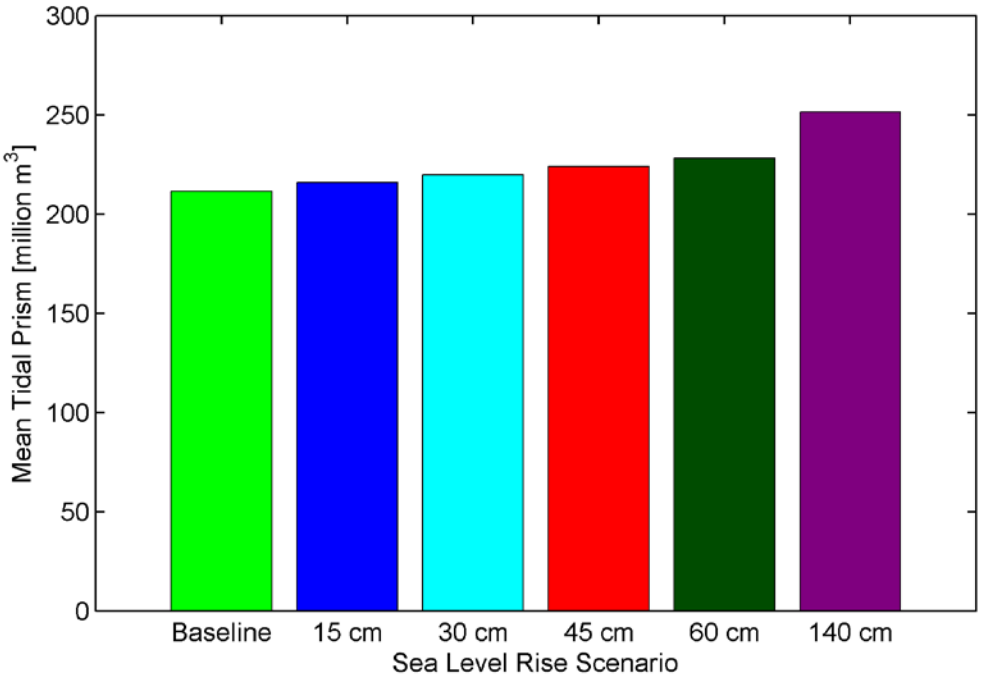

Figure 8.4-17 Average tidal prism at cross-section 12, located at the Carquinez Bridge, for the Baseline and SLR scenarios during the July 15, 2002 through August 12, 2002 analysis period.

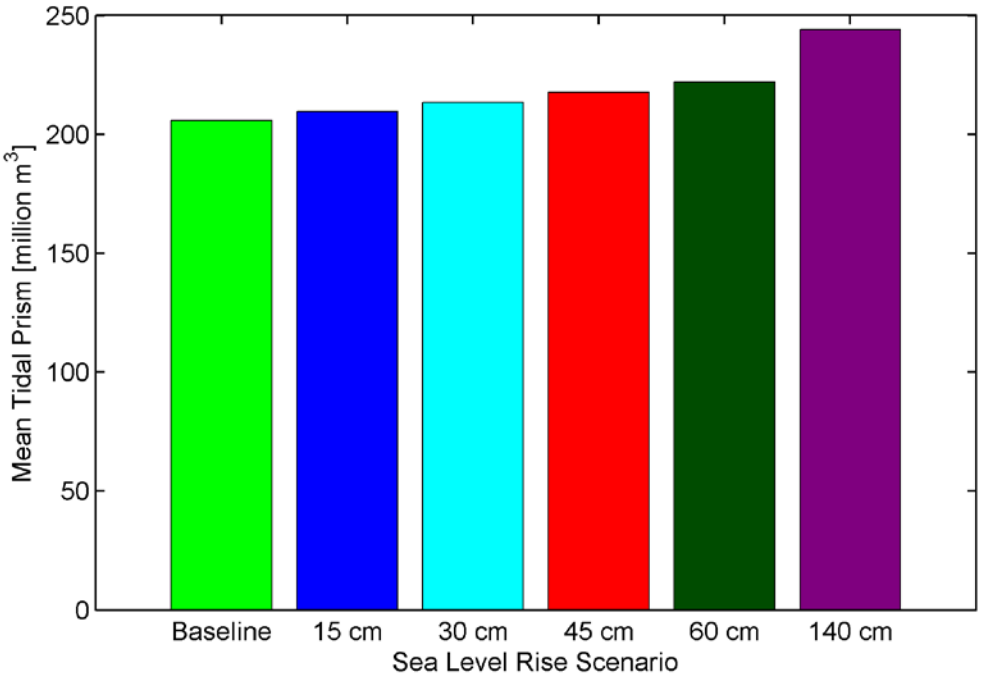

Figure 8.4-18 Average tidal prism at cross-section 12, located at the Carquinez Bridge, for the Baseline and SLR scenarios during the October 13, 2002 through November 10, 2002 analysis period.

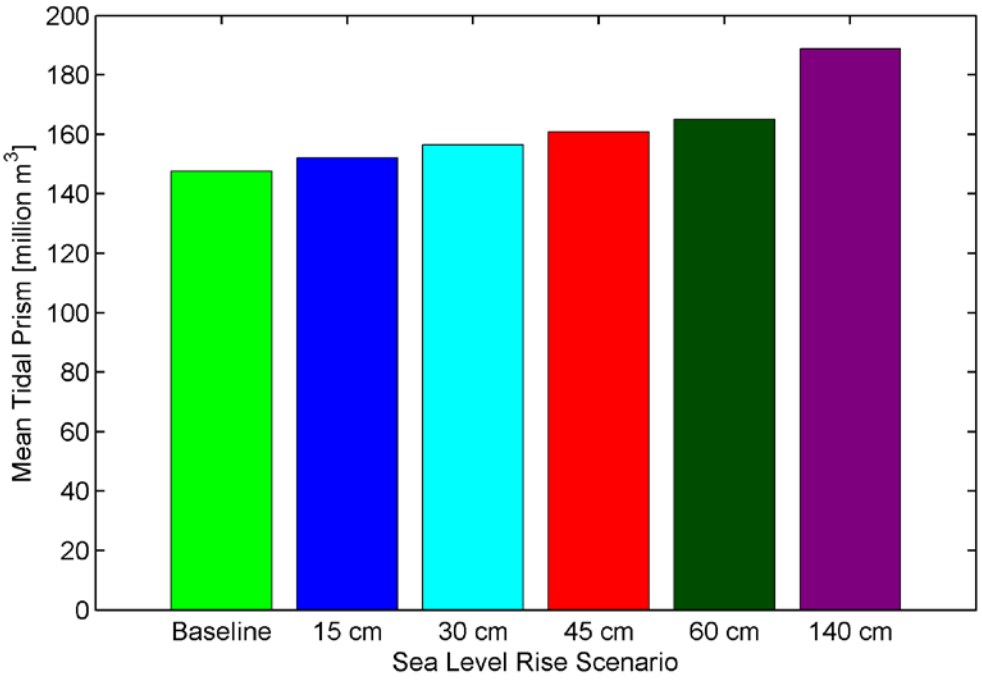

Figure 8.4-19 Average tidal prism at cross-section 25, located at Chipps Island, for the Baseline and SLR scenarios during the July 15, 2002 through August 12, 2002 analysis period.

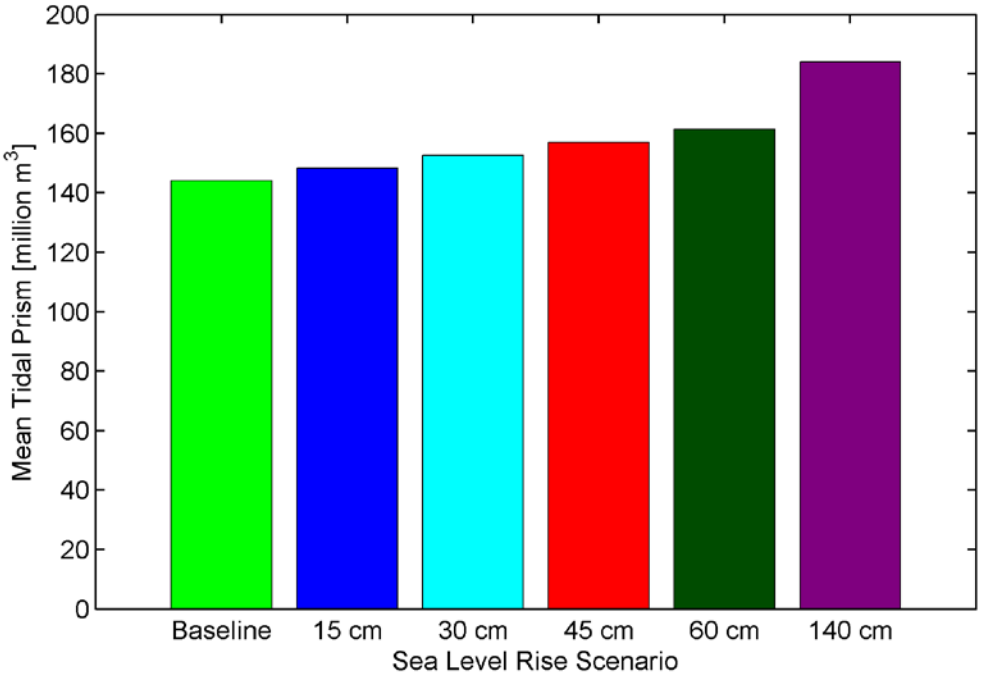

Figure 8.4-20 Average tidal prism at cross-section 25, located at Chipps Island, for the Baseline and SLR scenarios during the October 13, 2002 through November 10, 2002 analysis period.

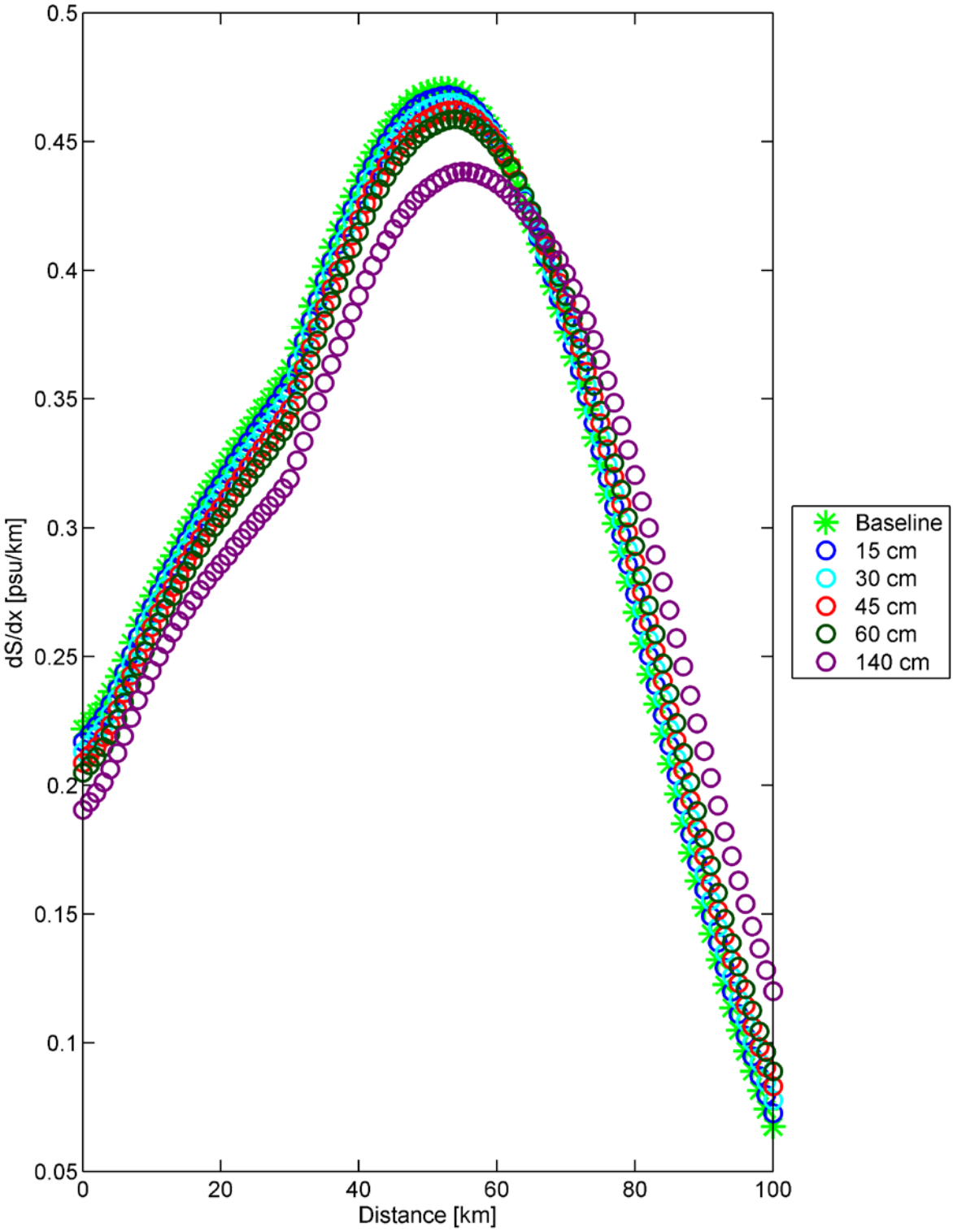

Figure 8.4-21 Estimated depth-averaged salinity gradient for the Baseline and SLR scenarios for the July 15, 2002 through August 12, 2002 analysis period. The horizontal scale is distance along the axis of the estuary from the Golden Gate.

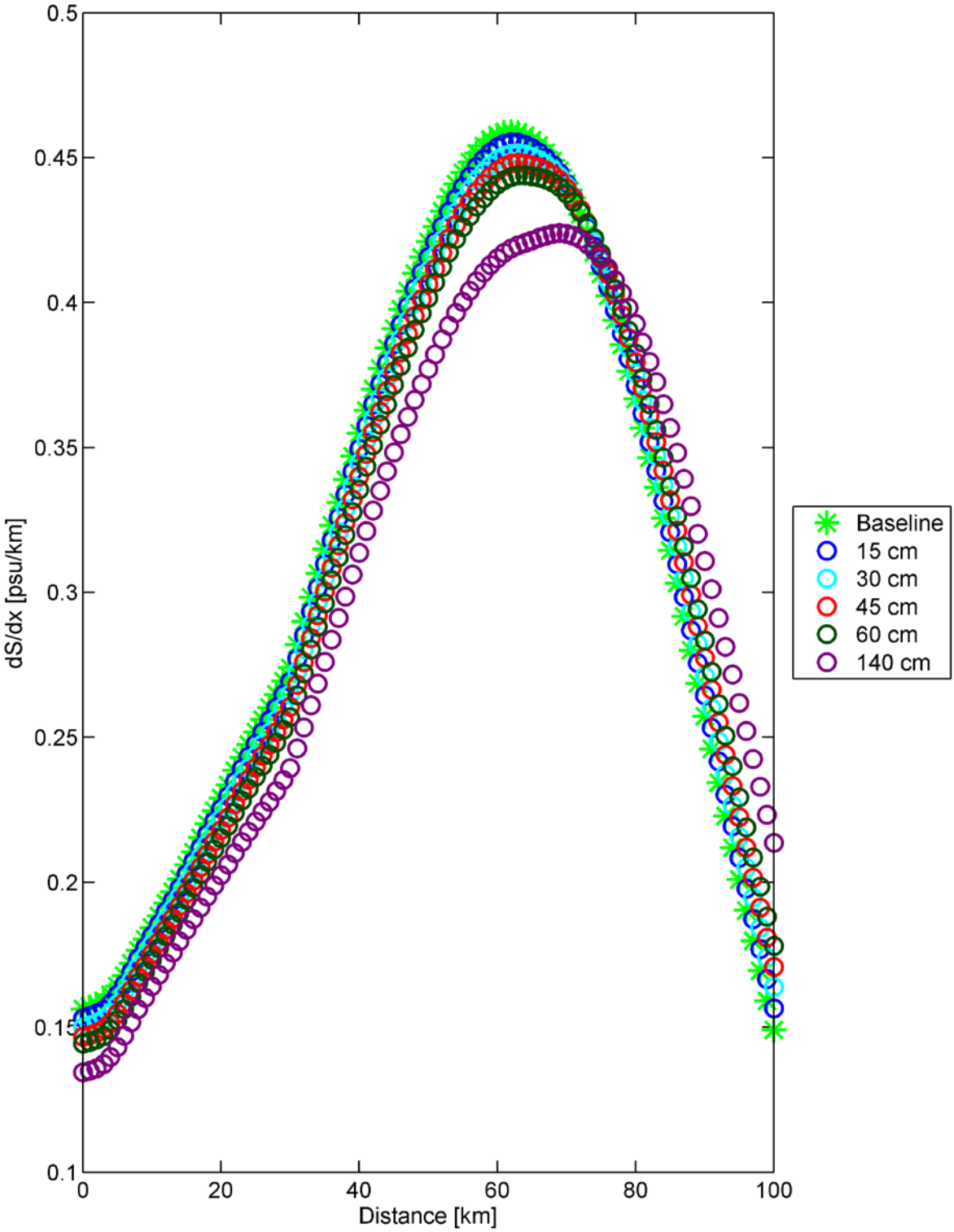

Figure 8.4-22 Estimated depth-averaged salinity gradient for the Baseline and SLR scenarios during the October 13, 2002 through November 10, 2002 analysis period. The horizontal scale is distance along the axis of the estuary from the Golden Gate.

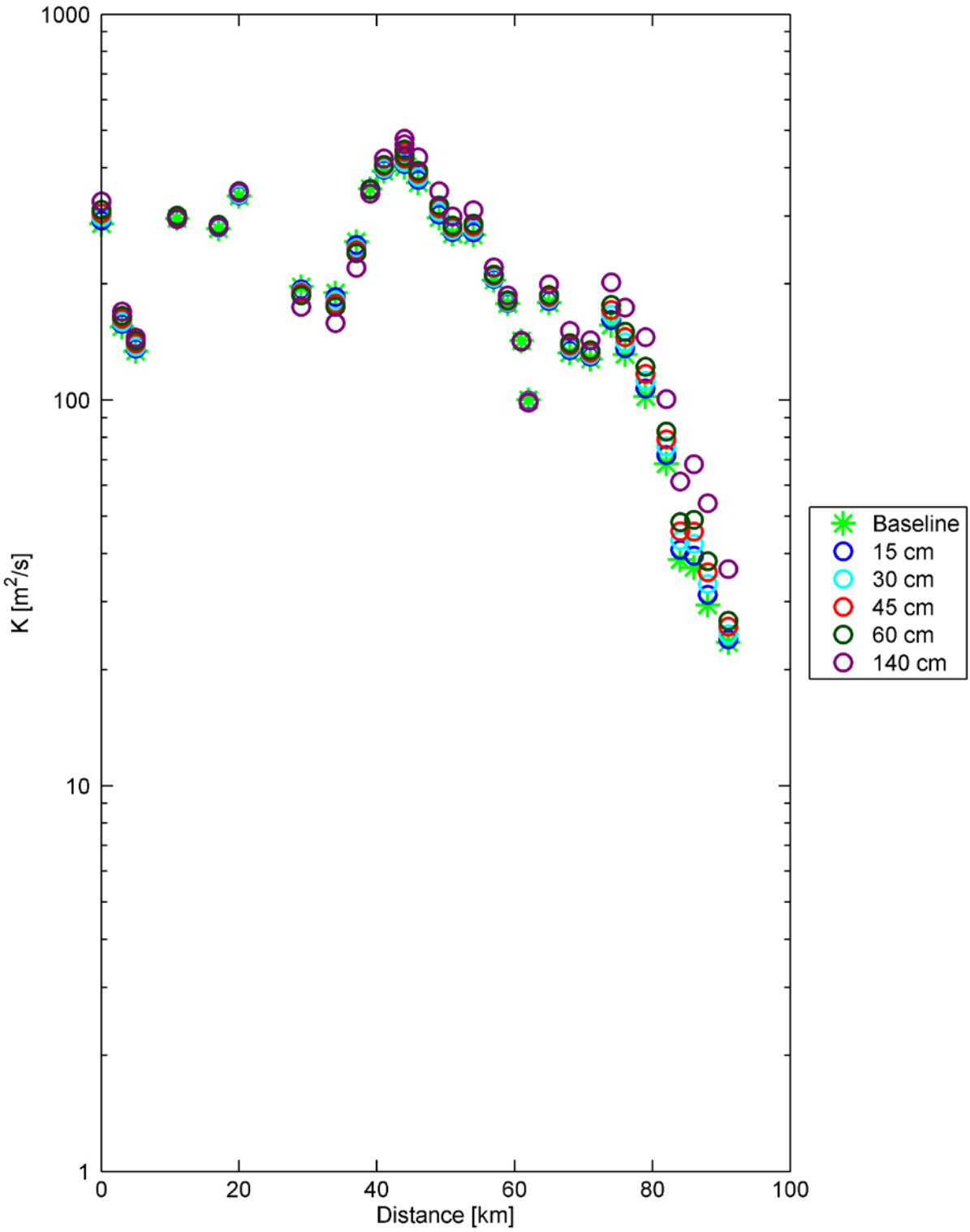

Figure 8.4-23 Estimated dispersion coefficient for the Baseline and SLR scenarios for the July 15, 2002 through August 12, 2002 analysis period. The horizontal scale is distance along the axis of the estuary from the Golden Gate.

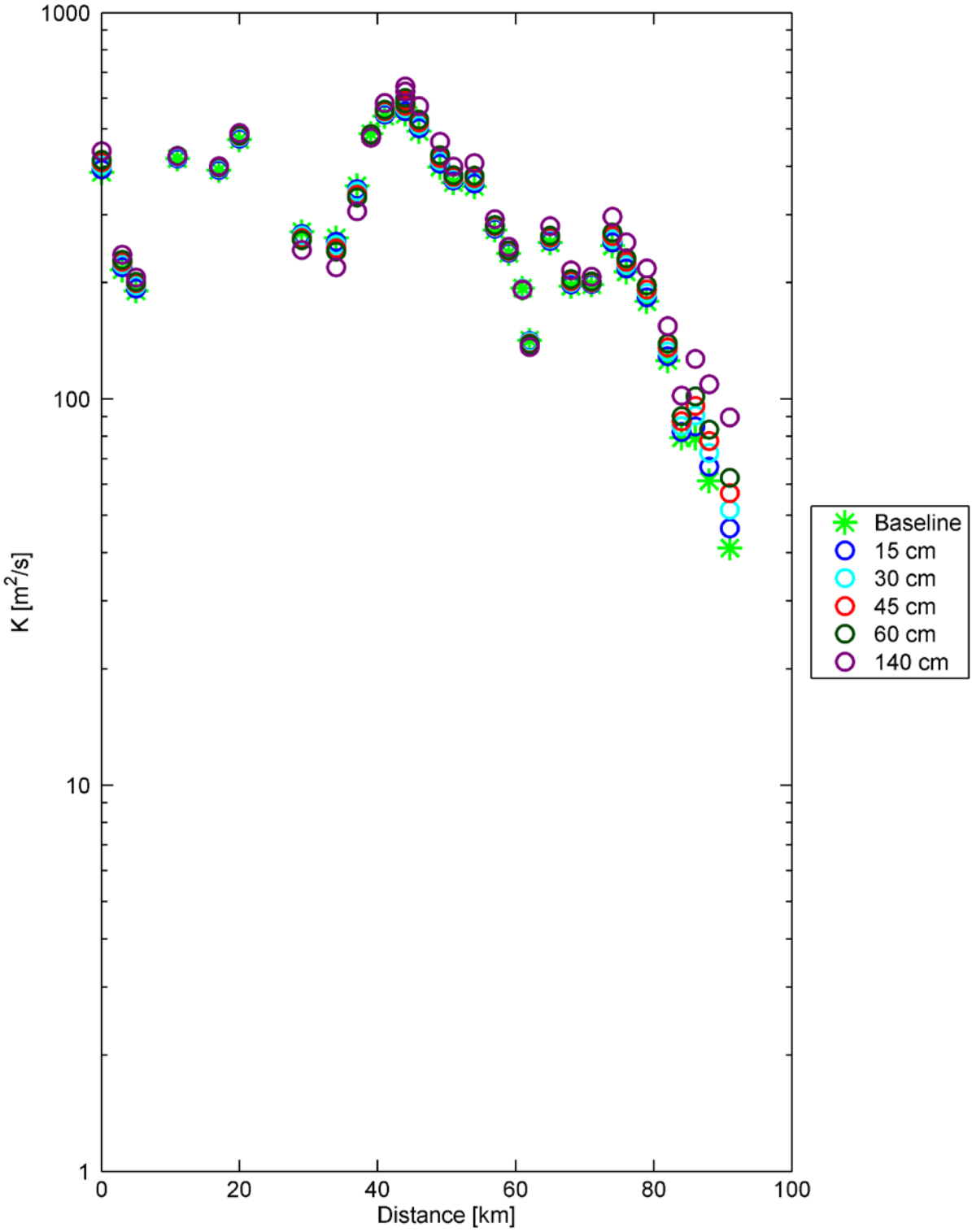

Figure 8.4-24 Estimated depth-averaged dispersion coefficient for the Baseline and SLR scenarios for the October 13, 2002 through November 10, 2002 analysis period. The horizontal scale is distance along the axis of the estuary from the Golden Gate.

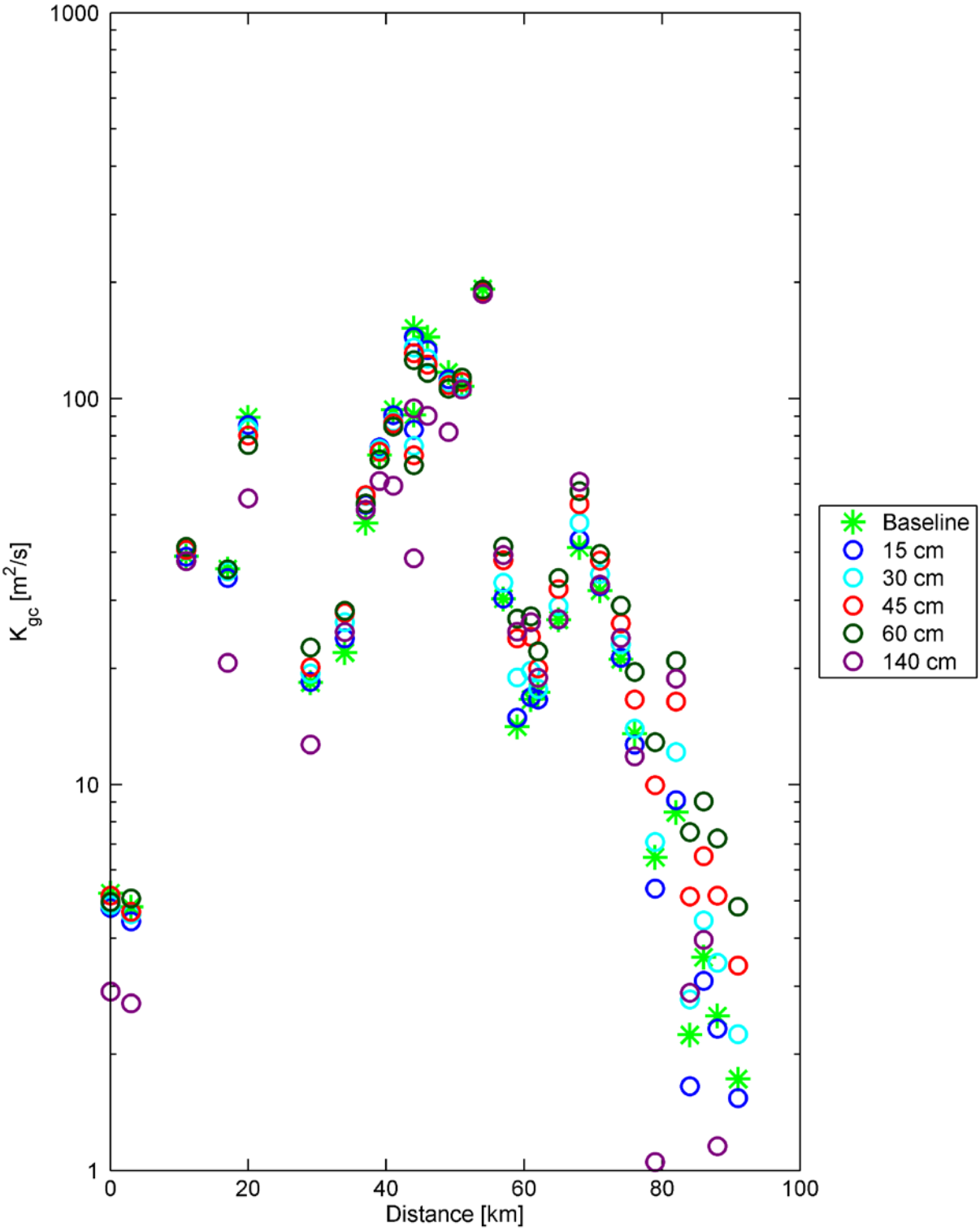

Figure 8.4-25 Estimated dispersion coefficient due to gravitational circulation for the Baseline and SLR scenarios for the July 15, 2002 through August 12, 2002 analysis period. The horizontal scale is distance along the axis of the estuary from the Golden Gate.

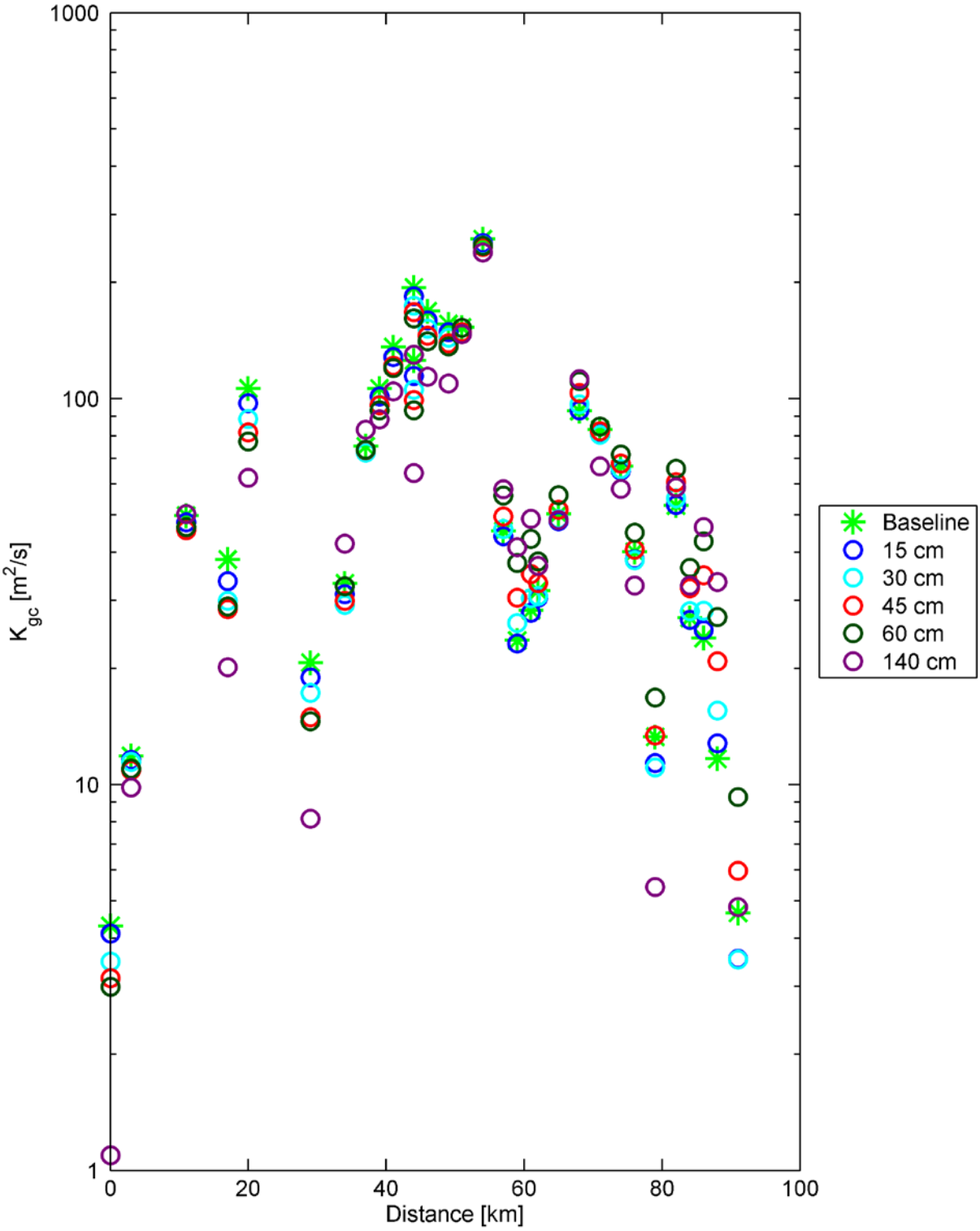

Figure 8.4-26 Estimated dispersion coefficient due to gravitational circulation for the Baseline and SLR scenarios for the October 13, 2002 through November 10, 2002 analysis period. The horizontal scale is distance along the axis of the estuary from the Golden Gate.

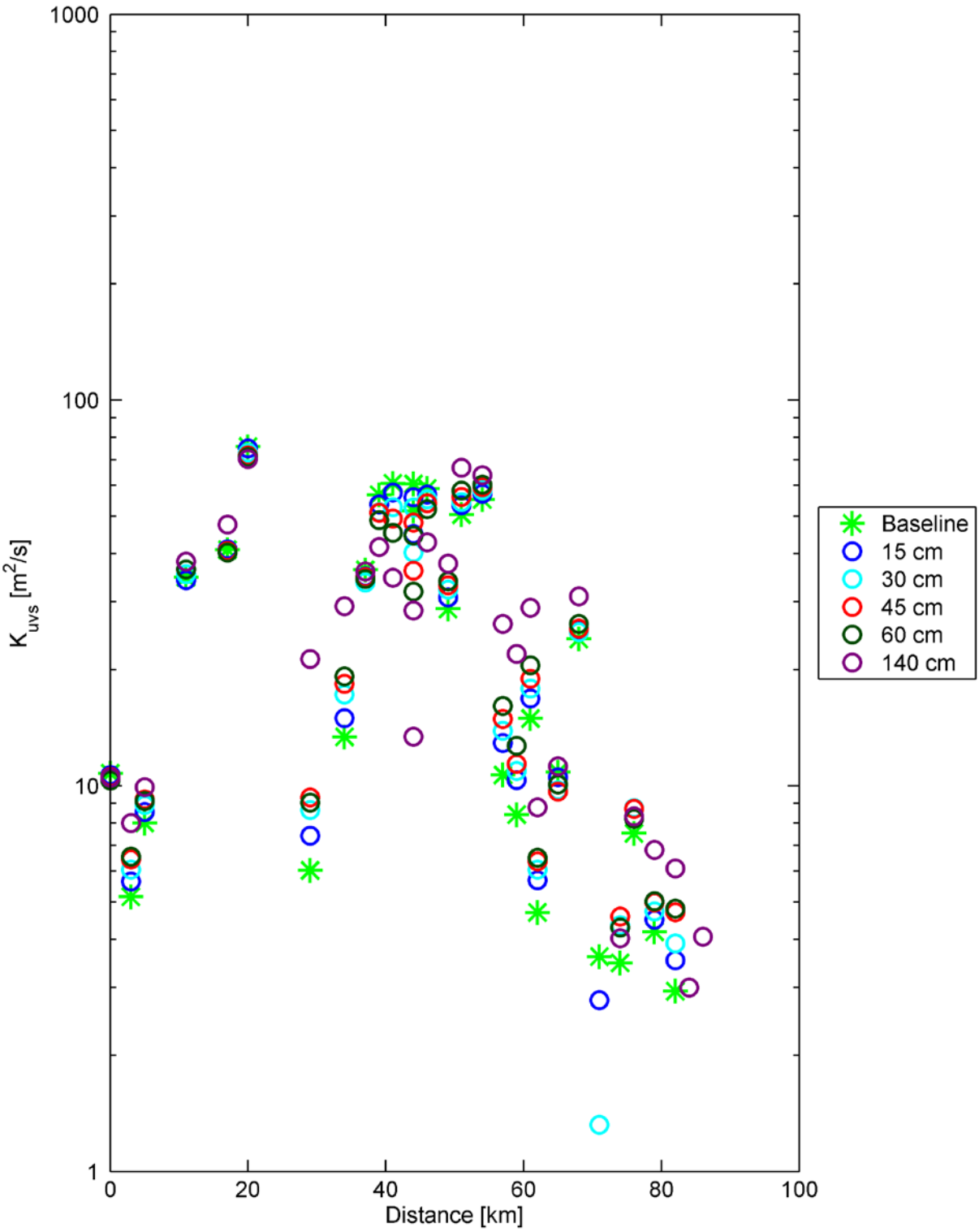

Figure 8.4-27 Estimated dispersion coefficient due to unsteady vertical shear for the Baseline and SLR scenarios for the July 15, 2002 through August 12, 2002 analysis period. The horizontal scale is distance along the axis of the estuary from the Golden Gate.

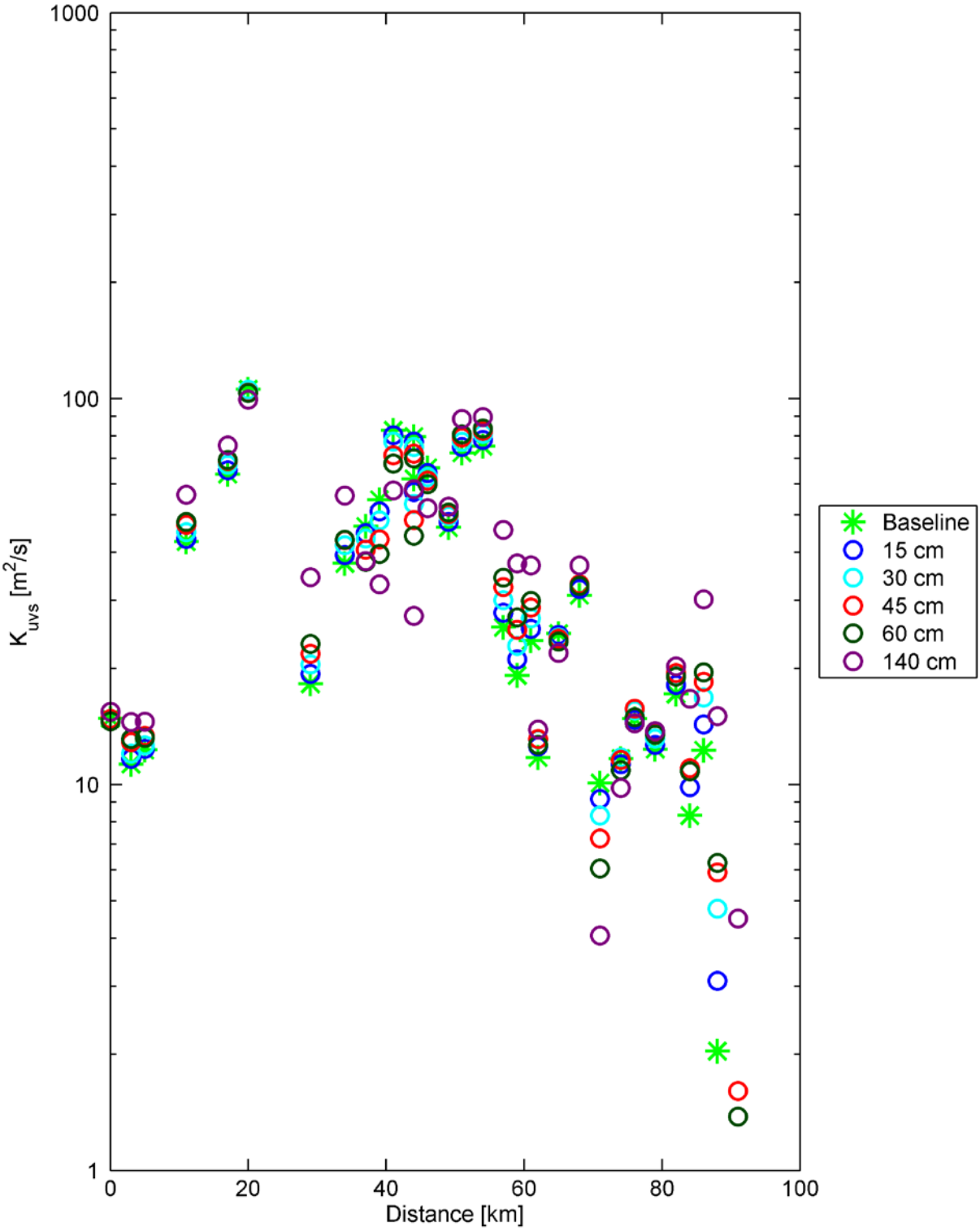

Figure 8.4-28 Estimated dispersion coefficient due to unsteady vertical shear for the Baseline and SLR scenarios for the October 13, 2002 through November 10, 2002 analysis period. The horizontal scale is distance along the axis of the estuary from the Golden Gate.

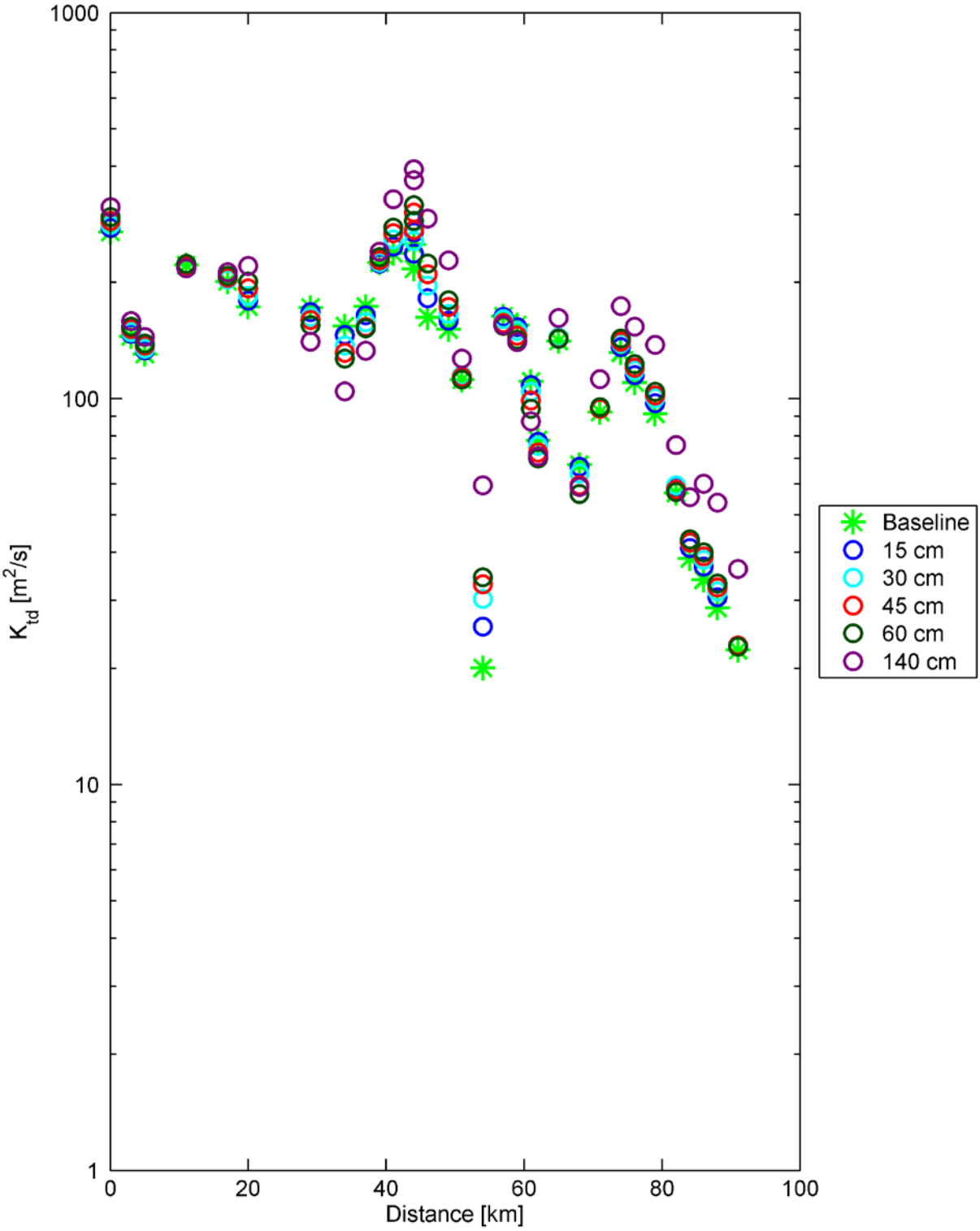

Figure 8.4-29 Estimated dispersion coefficient due to tidal dispersion for the Baseline and SLR scenarios for the July 15, 2002 through August 12, 2002 analysis period. The horizontal scale is distance along the axis of the estuary from the Golden Gate.

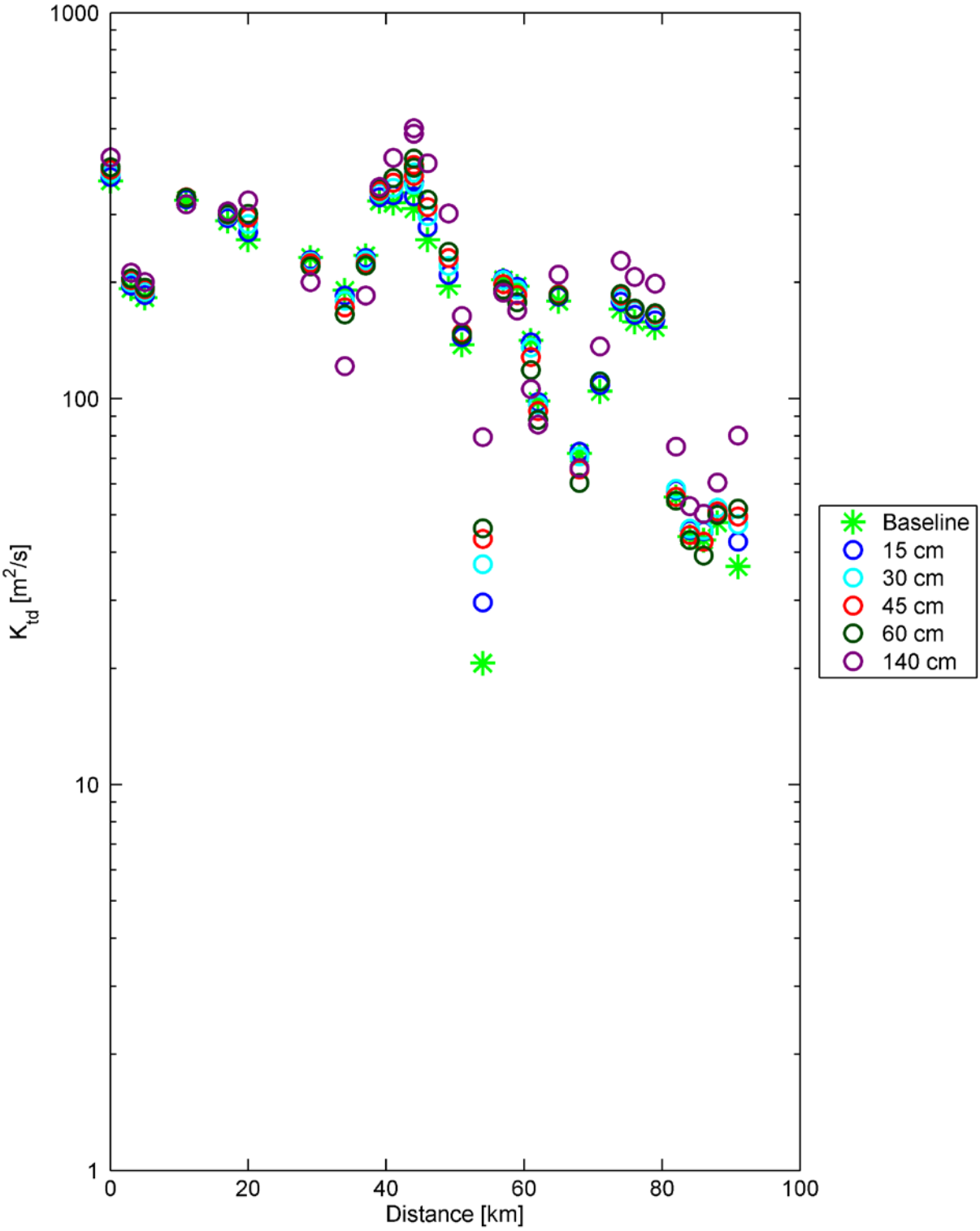

Figure 8.4-30 Estimated dispersion coefficient due to tidal dispersion for the Baseline and SLR scenarios for the October 13, 2002 through November 10, 2002 analysis period. The horizontal scale is distance along the axis of the estuary from the Golden Gate.

8.4.1 Central San Francisco Bay Cross-Sections

Dispersion coefficients and salt fluxes were estimated at the five cross-sections in Central Bay (cross-section 1 to cross-section 5) shown in Figure 8.3-1. In Figure 8.4-31 through **Error! Reference source not found.**, analysis results are provided for each cross-section that summarize the dispersion analysis at that location for a given analysis period. The top panel shows the contributions of individual processes to dispersive salt flux (advective salt flux is not shown) for each SLR scenario. The second type of figure shows the overall dispersion coefficient (K), the portion of the dispersion coefficient associated with gravitational circulation (K_{gc}), the portion of the dispersion coefficient associated with unsteady vertical shear dispersion processes (K_{uvs}), and the portion of the dispersion coefficient associated with tidal dispersion processes (K_{td}) for each SLR scenario. The bottom panel shows the period averaged velocity profile and salinity profile at the deepest point in the cross-section for each SLR scenario.

The dispersion coefficients are generally large in Central Bay. Tidal dispersion processes are the most important salt intrusion processes at all cross-sections in Central Bay for both analysis periods. The dispersion coefficients increase weakly with SLR in Central Bay due to increased tidal dispersion at most cross-sections. The increase in tidal dispersion is likely related to the increased tidal prism with SLR indicated by Figure 8.4-13 and Figure 8.4-14. The velocity profiles do not show clear evidence of gravitational circulation in Central Bay during either analysis period. In most sections the near surface layers are directed landward (up estuary), in the opposite direction expected for gravitational circulation, suggesting that wind forcing may be important and/or that the currents are likely to have strong lateral variability. The predicted stratification in Central Bay is weak during both analysis periods. As a result, the predicted fluxes from gravitational circulation and unsteady vertical shear are small at all sections for all scenarios. The salt flux term referred to as “gravitational circulation” in this report and other estuarine literature is more precisely referred to as “steady vertical exchange” (e.g. Fram et al. 2007). It can be substantially affected by wind. The negative fluxes associated with the steady vertical exchange term at some cross-sections in Central Bay suggest that wind effects are substantial in this region. Note that negative fluxes associated with the steady vertical exchange term result in negative dispersion coefficients that do not appear on the dispersion coefficient figures due to the use of a y-axis range from 1 to 1000 $m^2 s^{-1}$.

Salinity in Central Bay is higher in the October 13, 2002 through November 10, 2002 analysis period than the July 15, 2002 through August 12, 2002 analysis period. In addition, conditions are slightly more stratified during the October 13, 2002 through November 10, 2002 analysis period. This results in a slight increase in the predicted dispersion coefficient associated gravitational circulation during the October 13, 2002 through November 10, 2002 analysis period relative to the July 15, 2002 through August 12, 2002 analysis period.

The dispersive salt flux in the October 13, 2002 through November 10, 2002 analysis period is significantly lower than the dispersive salt flux in the July 15, 2002 through August 12, 2002 analysis period. This is surprising because the period averaged salinity is higher in the October 13, 2002 through November 10, 2002 analysis period is higher than period averaged salinity in the July 15, 2002 through August 12, 2002 analysis period and the Delta outflow is similar in the two periods. The lower dispersive salt fluxes are related to the higher unsteadiness in the October 13, 2002 through November 10, 2002 averaging period (Figure 8.4-2) relative to the July 15,

2002 through August 12, 2002 analysis period (Figure 8.4-1). The unsteadiness indicates that the total salt mass in the estuary decreased between October 13, 2002 and November 10, 2002. As seen in the salinity time series in Section 6, the salinity conditions are much more variable between October 13, 2002 and November 10, 2002 than between July 15, 2002 through August 12, 2002. It should be noted that the total dispersion coefficients are similar for the two periods indicating that the strength of mixing processes was similar for the two periods.

The results in Central Bay are generally consistent with the flux analysis of sea level rise scenarios performed as part of the DRMS studies (Gross et al., 2007b). However the DRMS scenarios were for higher Delta outflow and, therefore, showed a larger contribution of gravitational circulation and unsteady vertical shear. In addition, wind forcing was not included in the DRMS analysis of salt intrusion processes (Gross et al., 2007b) and negative fluxes were not estimated at any location for the steady vertical exchange term in that study. The flux analysis of various Delta outflows performed as part of the DRMS studies (Gross et al., 2007a) was consistent with these results for low Delta outflows and indicated that gravitational circulation becomes the dominant salt intrusion process at high Delta outflows.

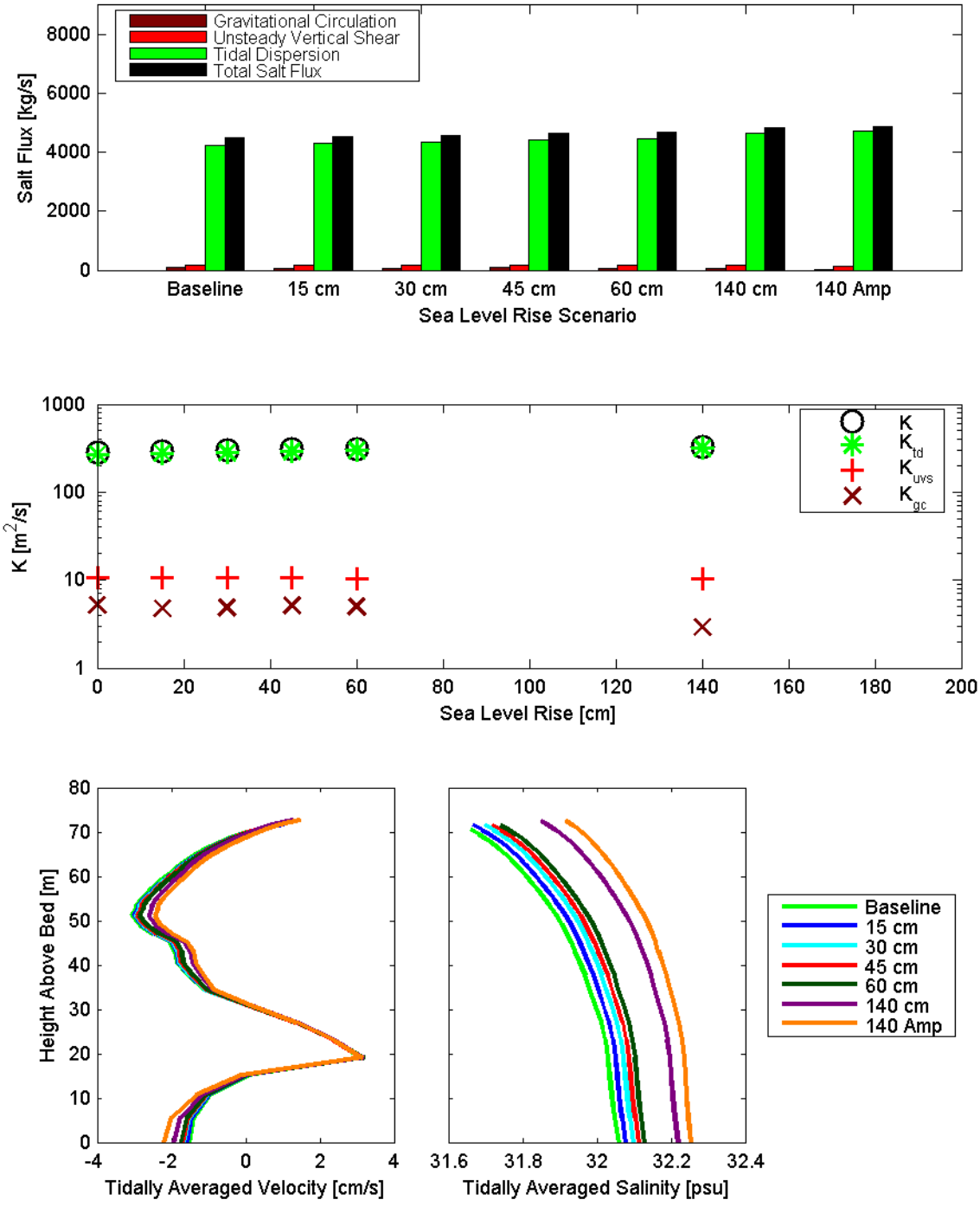

Figure 8.4-31 Dispersive salt flux (top), dispersion coefficients and dispersion coefficient components (middle) and tidally averaged velocity (bottom left) and tidally averaged salinity (bottom right) calculated for each SLR scenario at cross-section 1, located at the Golden Gate, for the July 15, 2002 through August 12, 2002 analysis period.

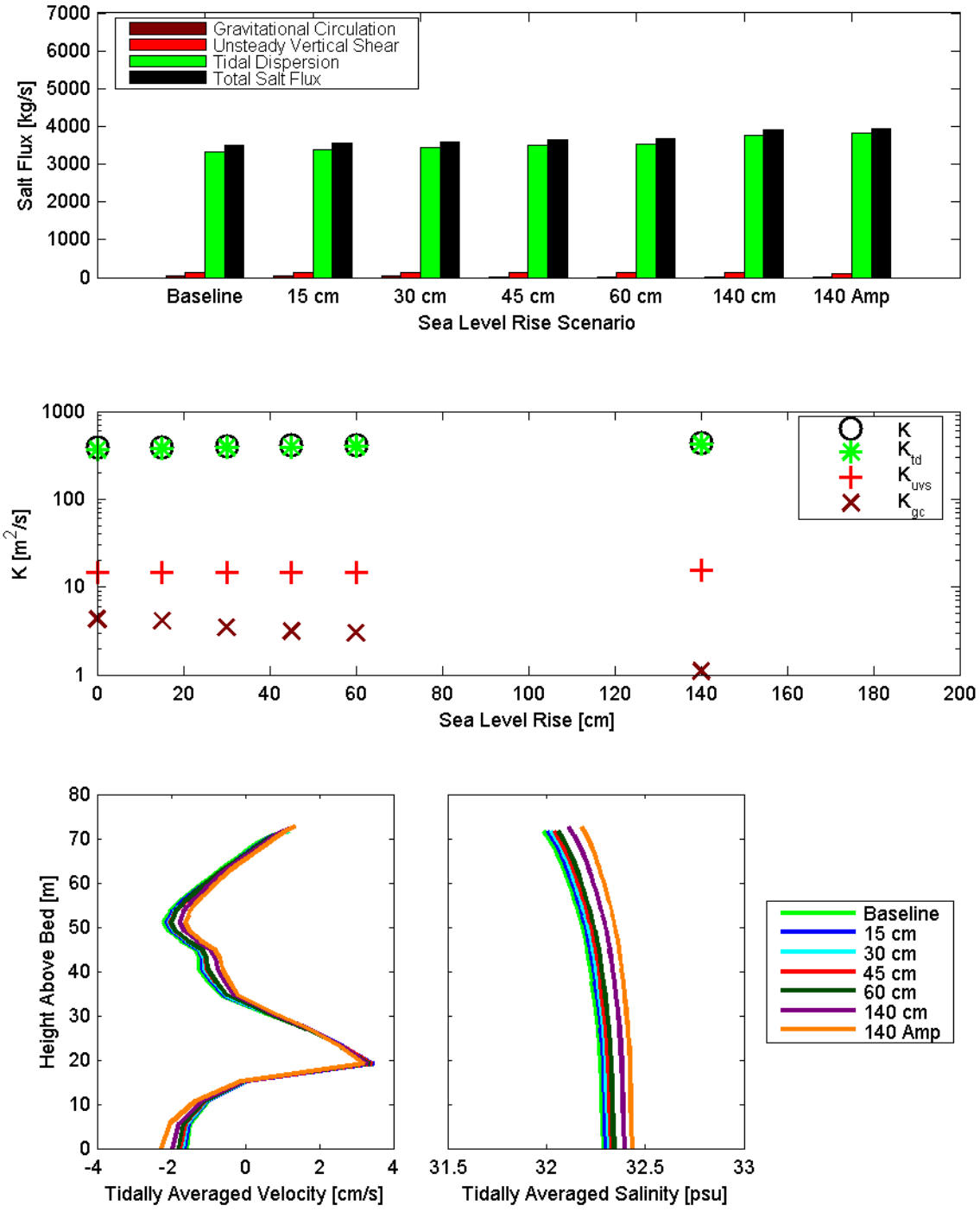

Figure 8.4-32 Dispersive salt flux (top), dispersion coefficients and dispersion coefficient components (middle) and tidally averaged velocity (bottom left) and tidally averaged salinity (bottom right) calculated for each scenario at cross-section 1, located at the Golden Gate, for the October 13, 2002 through November 10, 2002 analysis period.

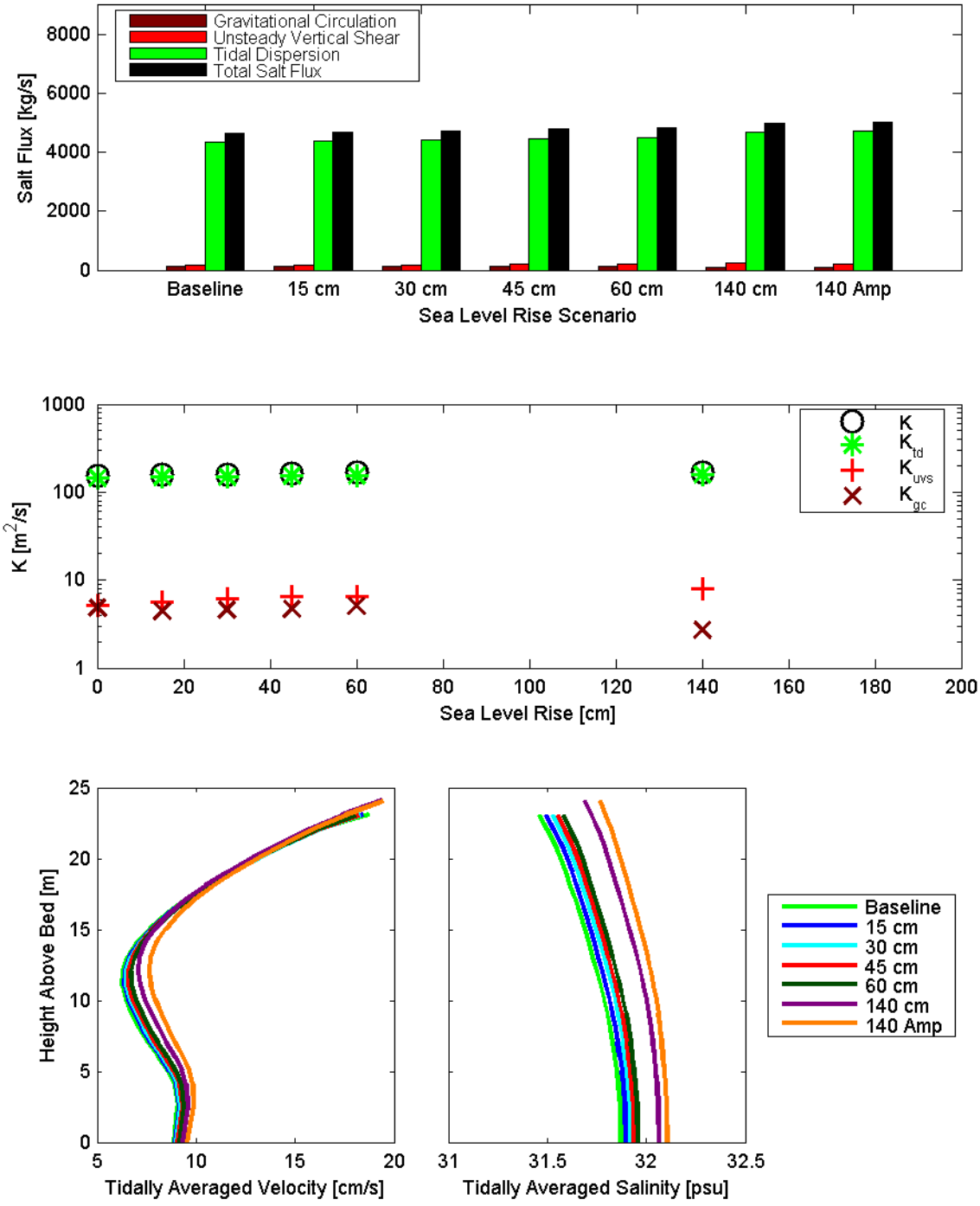

Figure 8.4-33 Dispersive salt flux (top), dispersion coefficients and dispersion coefficient components (middle) and tidally averaged velocity (bottom left) and tidally averaged salinity (bottom right) calculated for each scenario at cross-section 2, extending from North Point to Sausalito, for the July 15, 2002 through August 12, 2002 analysis period.

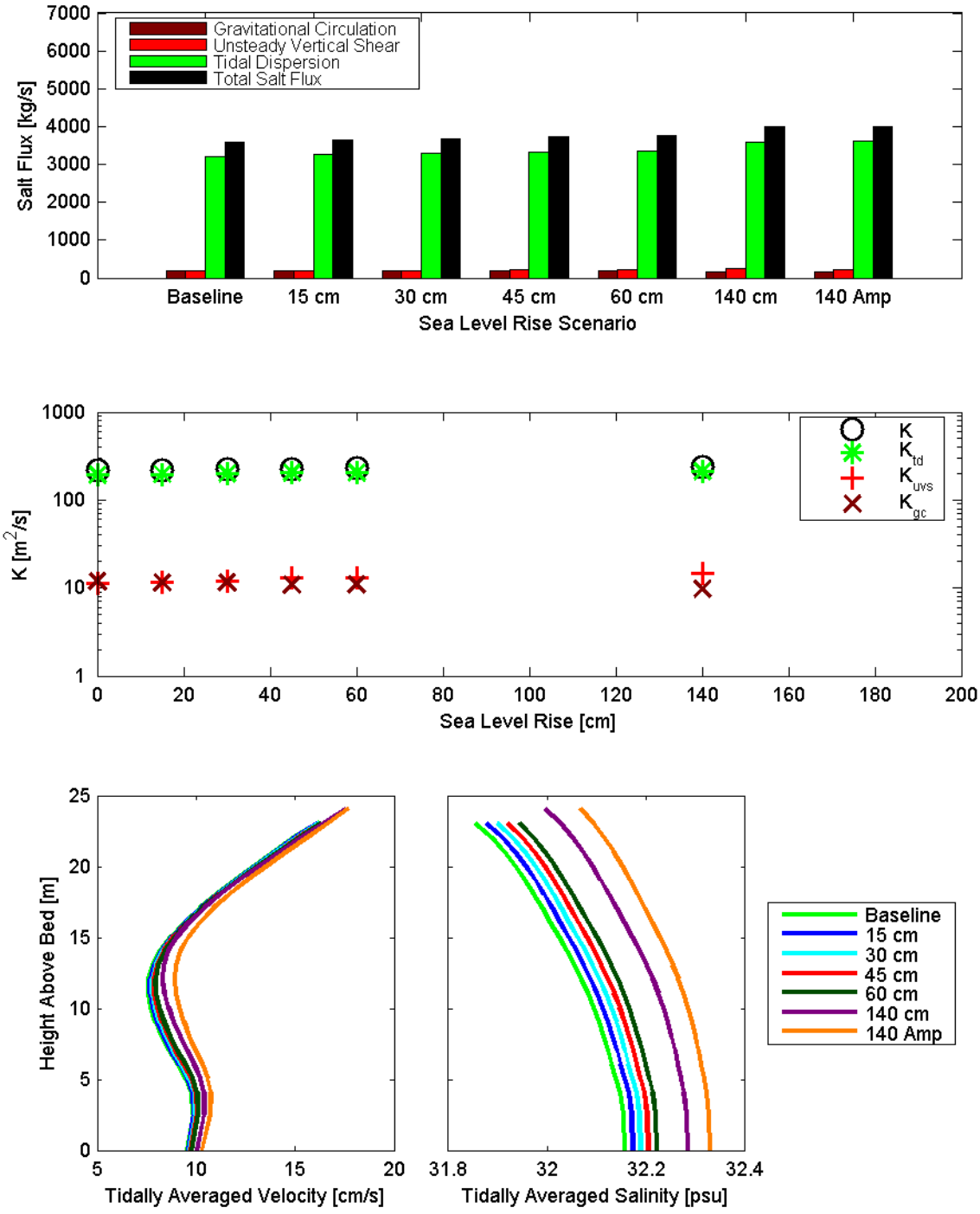

Figure 8.4-34 Dispersive salt flux (top), dispersion coefficients and dispersion coefficient components (middle) and tidally averaged velocity (bottom left) and tidally averaged salinity (bottom right) calculated for each scenario at cross-section 2, extending from North Point to Sausalito, for the October 13, 2002 through November 10, 2002 analysis period.

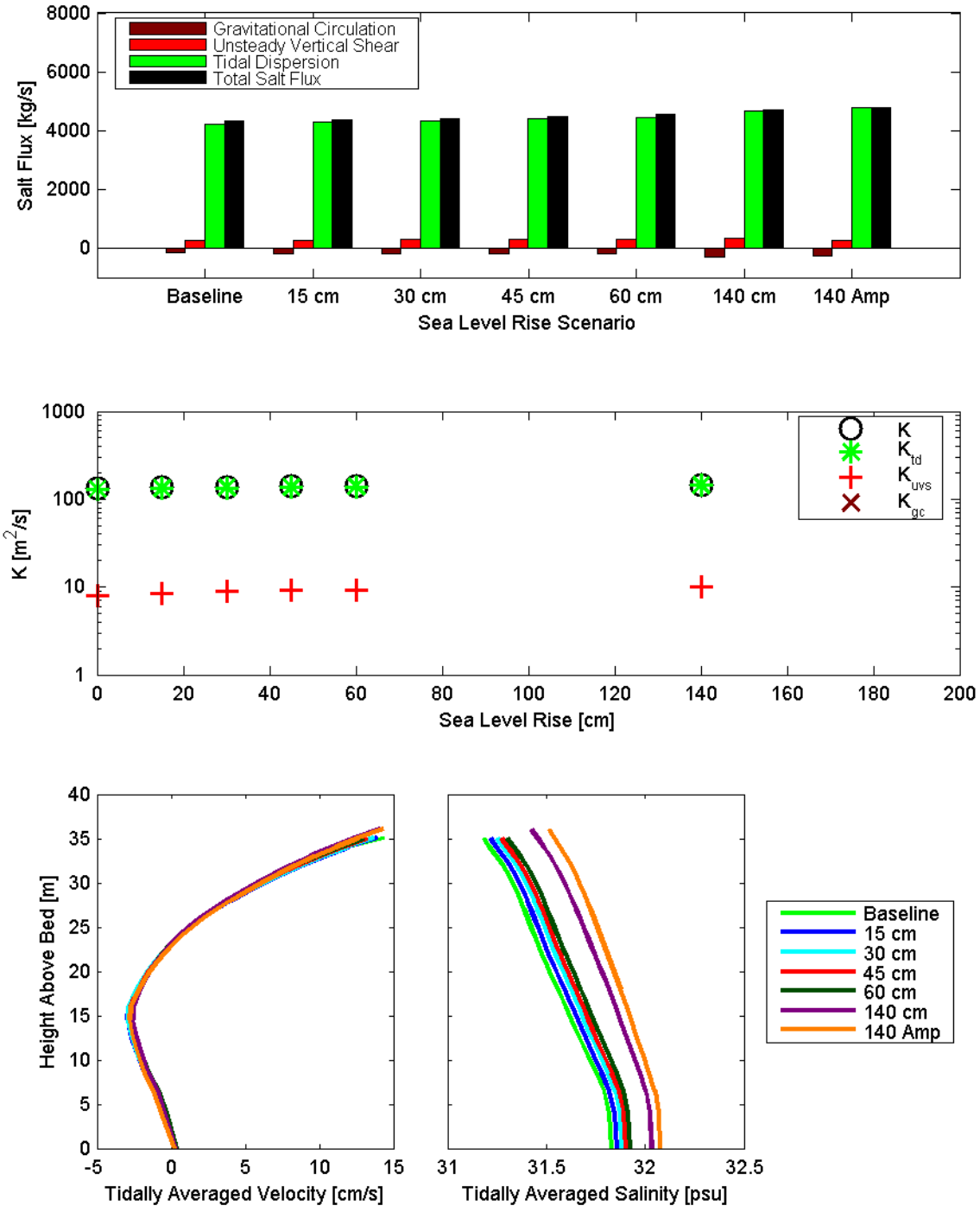

Figure 8.4-35 Dispersive salt flux (top), dispersion coefficients and dispersion coefficient components (middle) and tidally averaged velocity (bottom left) and tidally averaged salinity (bottom right) calculated for each scenario at cross-section 3, extending from San Francisco to Tiburon, for the July 15, 2002 through August 12, 2002 analysis period.

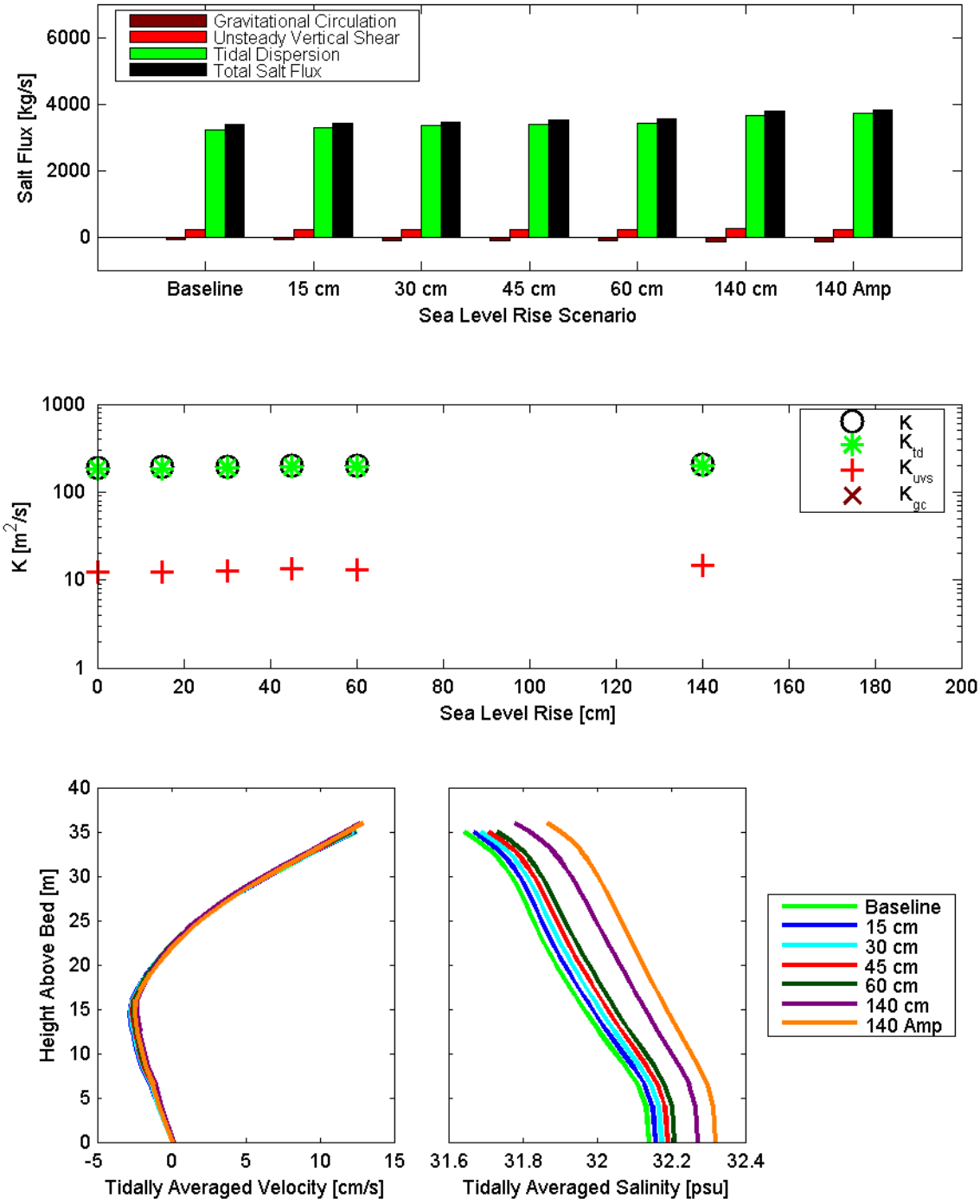

Figure 8.4-36 Dispersive salt flux (top), dispersion coefficients and dispersion coefficient components (middle) and tidally averaged velocity (bottom left) and tidally averaged salinity (bottom right) calculated for each scenario at cross-section 3, extending from San Francisco to Tiburon, for the October 13, 2002 through November 10, 2002 analysis period.

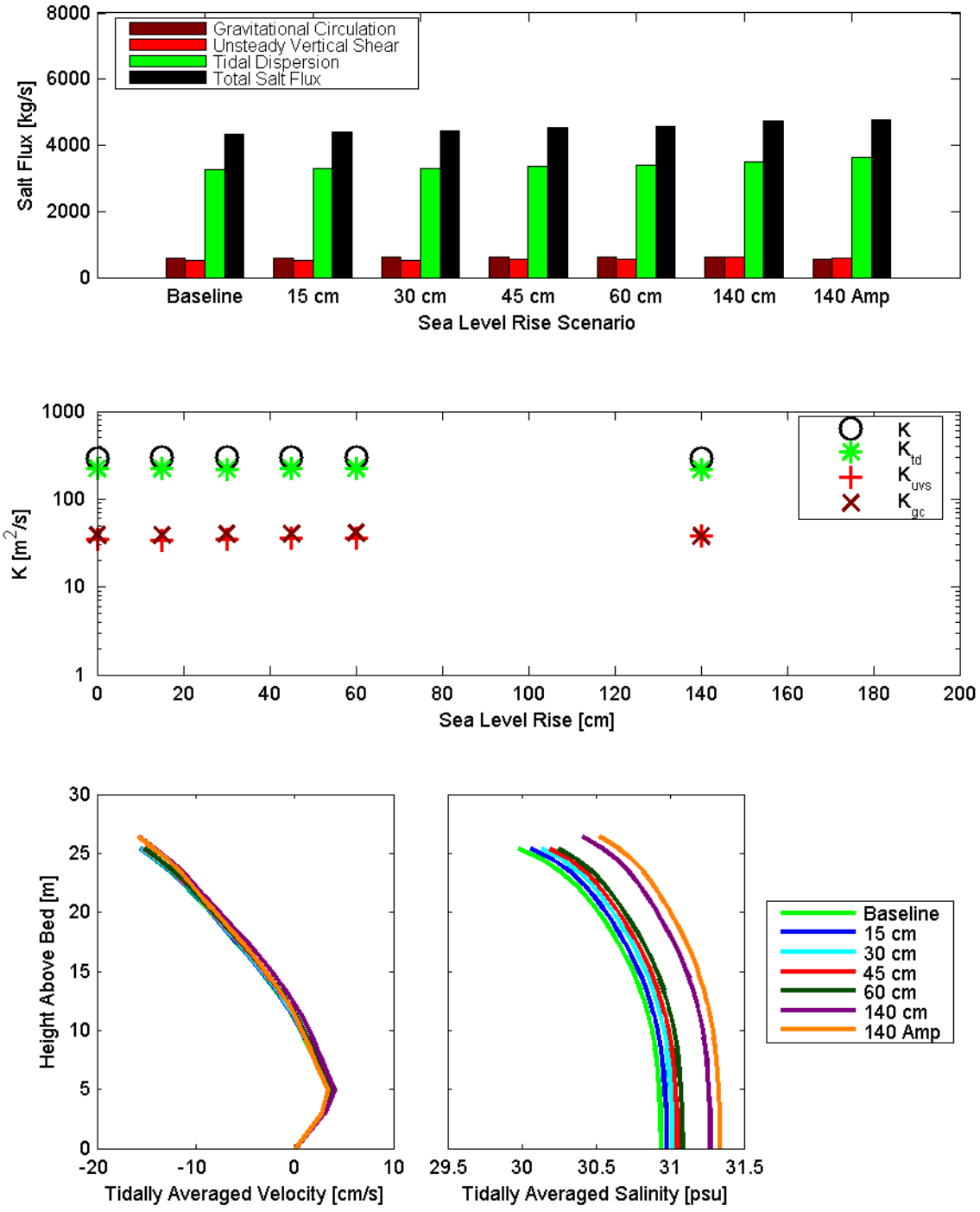

Figure 8.4-37 Dispersive salt flux (top), dispersion coefficients and dispersion coefficient components (middle) and tidally averaged velocity (bottom left) and tidally averaged salinity (bottom right) calculated for each scenario at cross-section 4, extending from Point Richmond to Bluff Point, for the July 15, 2002 through August 12, 2002 analysis period.

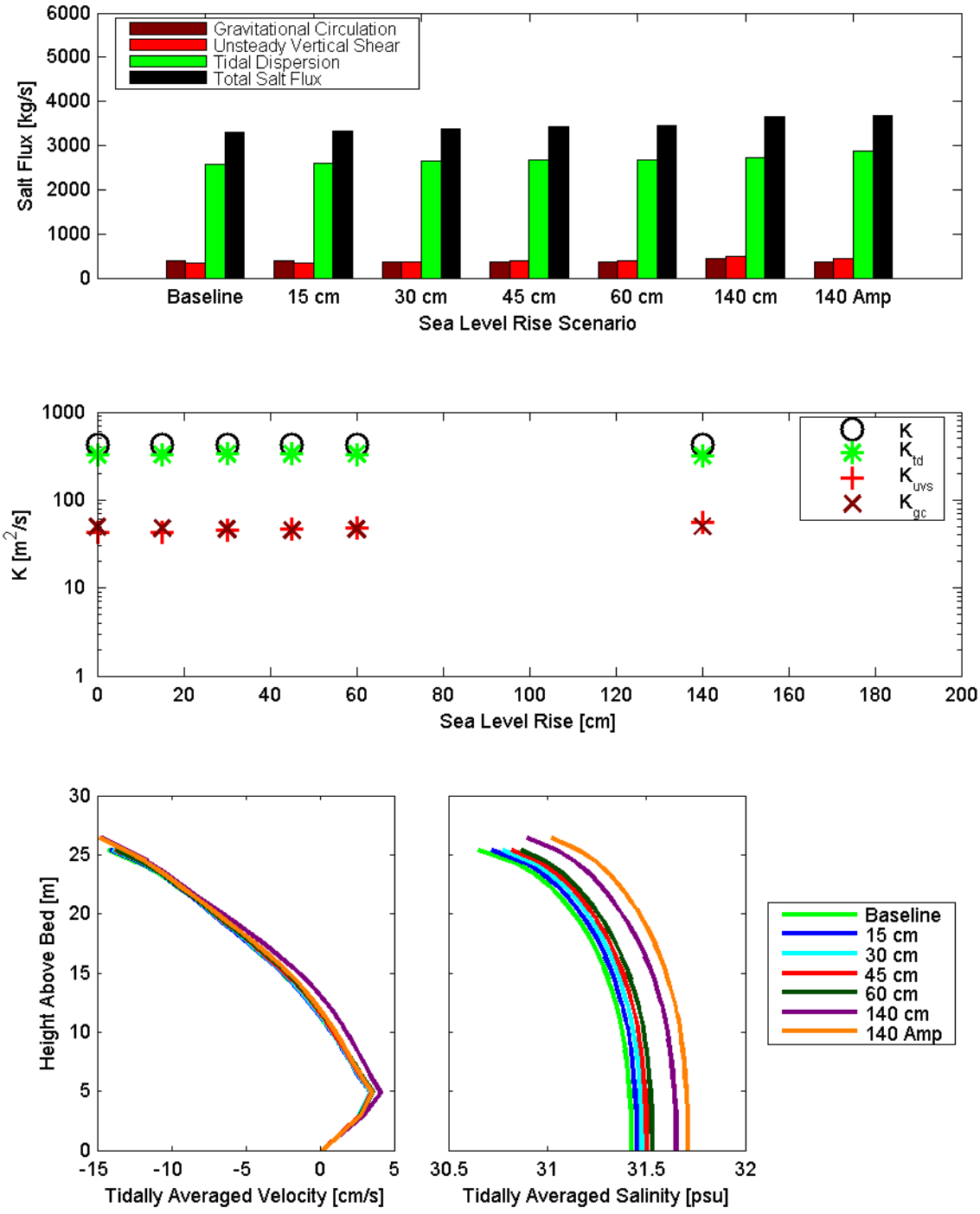

Figure 8.4-38 Dispersive salt flux (top), dispersion coefficients and dispersion coefficient components (middle) and tidally averaged velocity (bottom left) and tidally averaged salinity (bottom right) calculated for each scenario at cross-section 4, extending from Point Richmond to Bluff Point, for the October 13, 2002 through November 10, 2002 analysis period.

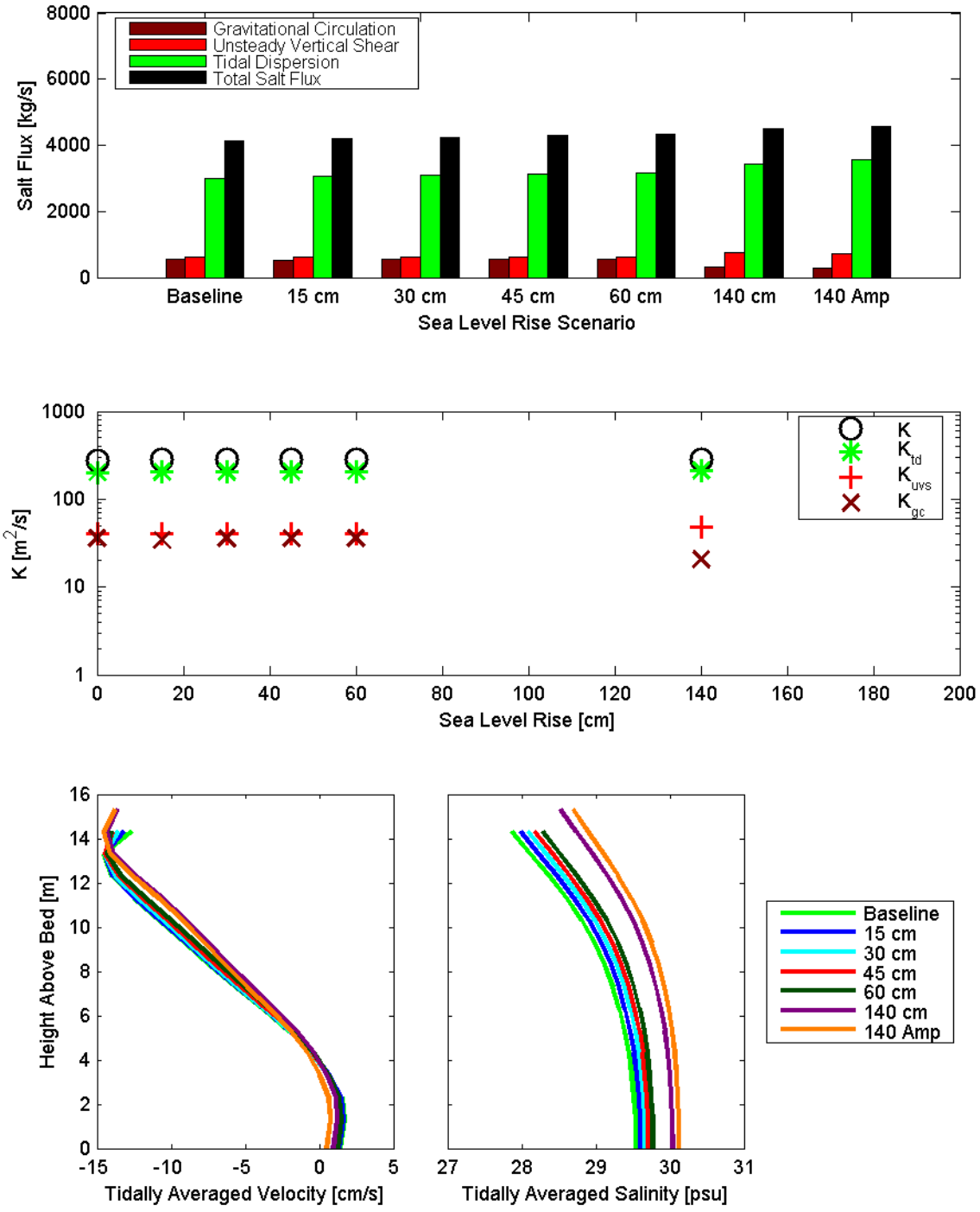

Figure 8.4-39 Dispersive salt flux (top), dispersion coefficients and dispersion coefficient components (middle) and tidally averaged velocity (bottom left) and tidally averaged salinity (bottom right) calculated for each scenario at cross-section 5, located at the Richmond-San Rafael Bridge, for the July 15, 2002 through August 13, 2002 analysis period.

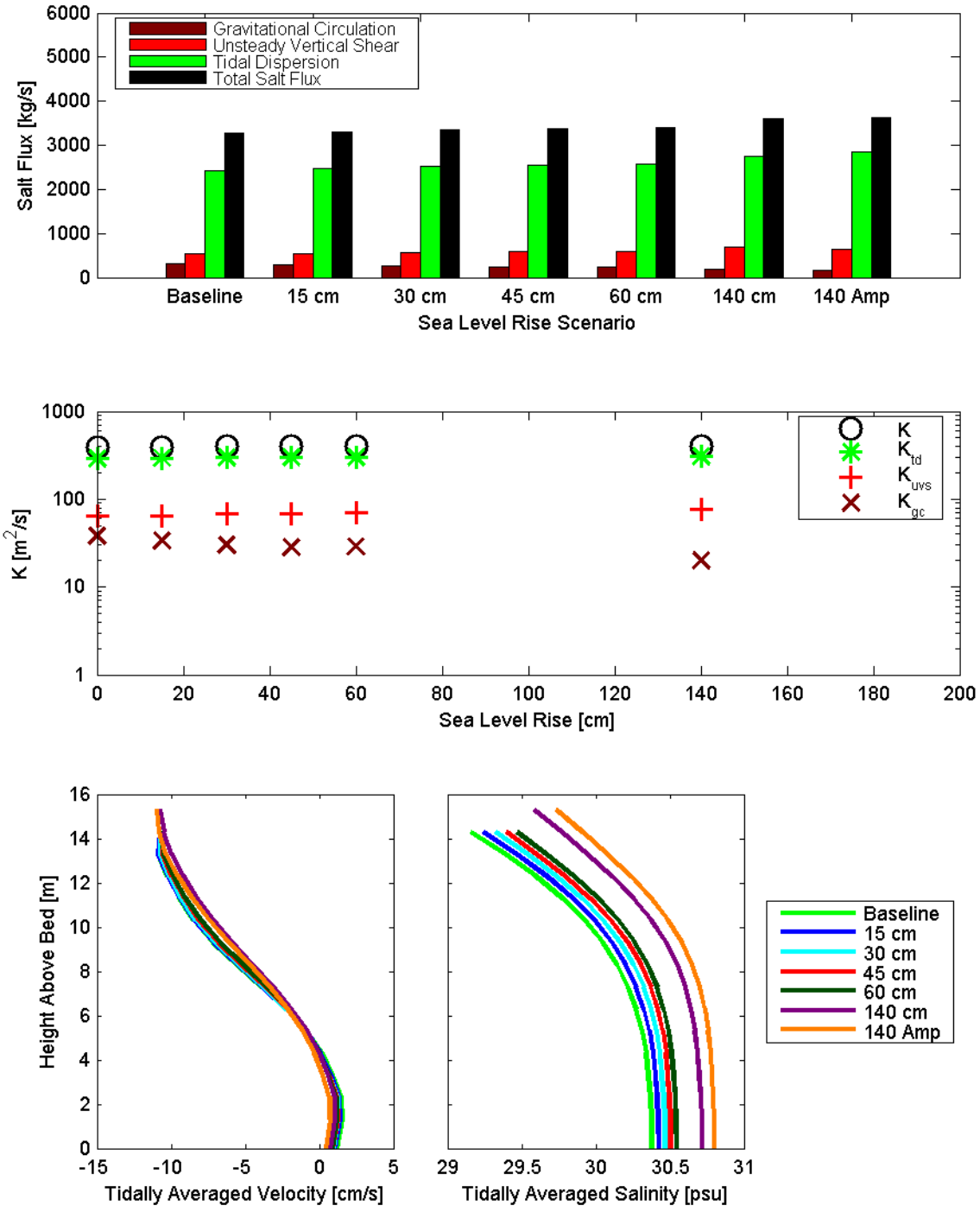

Figure 8.4-40 Dispersive salt flux (top), dispersion coefficients and dispersion coefficient components (middle) and tidally averaged velocity (bottom left) and tidally averaged salinity (bottom right) calculated for each scenario at cross-section 5, at the Richmond-San Rafael Bridge, for the October 13, 2002 through November 10, 2002 analysis period.

8.4.2 San Pablo Bay Cross-Sections

Dispersion coefficients and salt fluxes were estimated at the six cross-sections in San Pablo Bay (cross-section 6 to cross-section 11) shown in Figure 8.3-1. In Figure 8.4-41 through **Error! Reference source not found.**, analysis results are provided for each cross-section that summarize the dispersion analysis at that location for a given analysis period. The top panel shows the contributions of individual processes to dispersive salt flux (advective salt flux is not shown) for each SLR scenario. The second type of figure shows the overall dispersion coefficient (K), the portion of the dispersion coefficient associated with gravitational circulation (K_{gc}), the portion of the dispersion coefficient associated with unsteady vertical shear dispersion processes (K_{uvs}), and the portion of the dispersion coefficient associated with tidal dispersion processes (K_{td}) for each SLR scenario. The bottom panel shows the period averaged velocity profile and salinity profile at the deepest point in the cross-section for each SLR scenario.

The dispersion coefficients are generally large in San Pablo Bay. Tidal dispersion processes are the most important salt intrusion processes at all cross-sections in San Pablo Bay for both analysis periods. Gravitational circulation and unsteady vertical shear dispersion are both substantial at all locations in San Pablo Bay. The dispersive salt fluxes increase with sea level rise due to increased salinity in San Pablo Bay. However, the dispersion coefficients show little variability with SLR at most cross-sections indicating minimal changes in local mixing processes during low Delta outflow conditions. The velocity profiles show clear evidence of gravitational circulation in San Pablo Bay during both analysis periods but do not change substantially with sea level rise. The predicted stratification in San Pablo Bay is substantial during both analysis periods. Though salinity increases with sea level rise, the predicted stratification (e.g. difference between bottom and surface salinity) shows little variability with sea level rise.

The results in San Pablo Bay are generally consistent with the flux analysis of sea level rise scenarios performed as part of the DRMS studies (Gross et al., 2007b). However the DRMS scenarios were for higher Delta outflow and, therefore, showed a larger contribution of gravitational circulation and unsteady vertical shear. The flux analysis of various Delta outflows performed as part of the DRMS studies (Gross et al., 2007a) was consistent with these results for low Delta outflows and indicated that gravitational circulation becomes the dominant salt intrusion process at high Delta outflows.

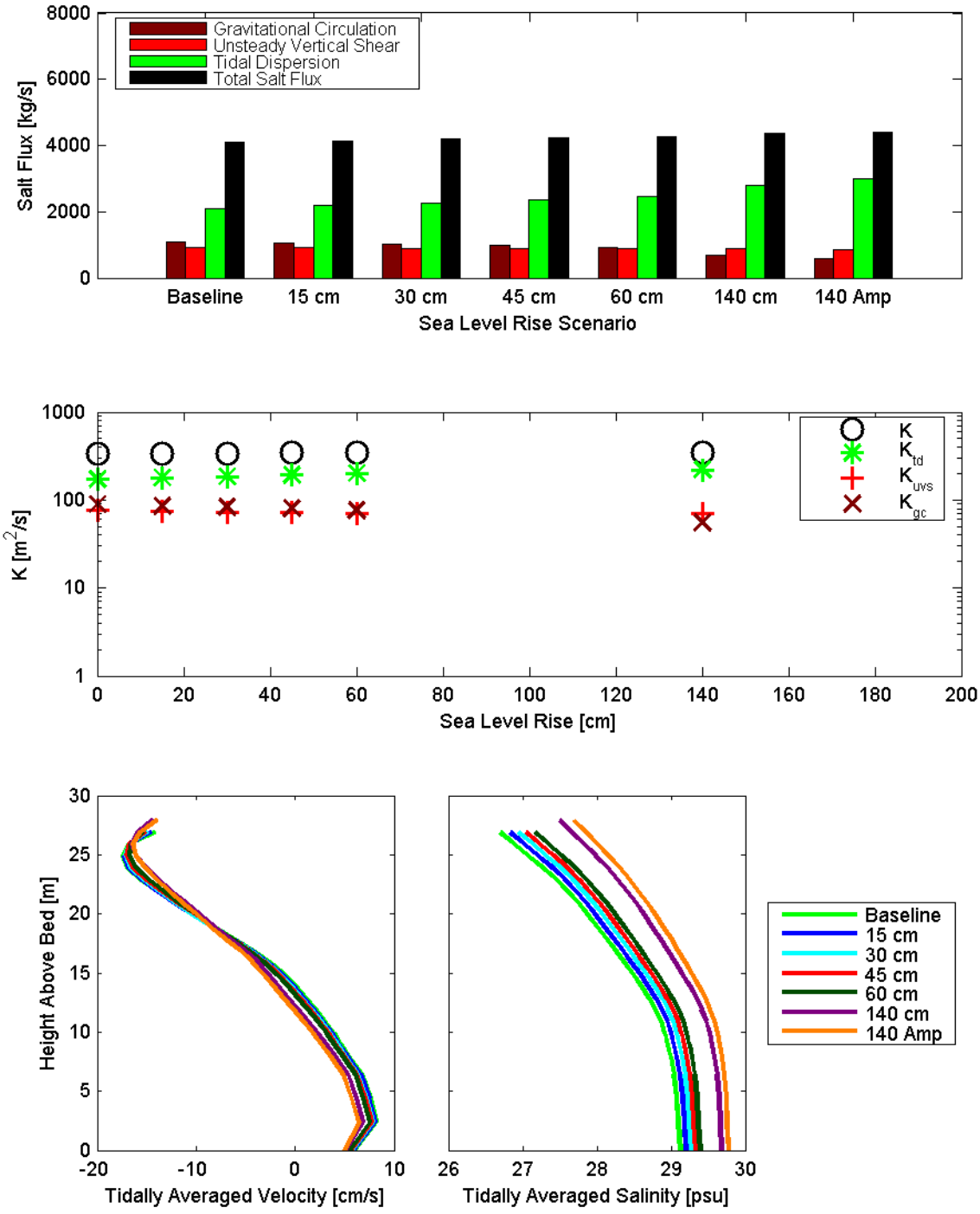

Figure 8.4-41 Dispersive salt flux (top), dispersion coefficients and dispersion coefficient components (middle) and tidally averaged velocity (bottom left) and tidally averaged salinity (bottom right) calculated for each scenario at cross-section 6, extending from Point San Pablo to Point San Pedro, for the July 15, 2002 through August 12, 2002 analysis period.

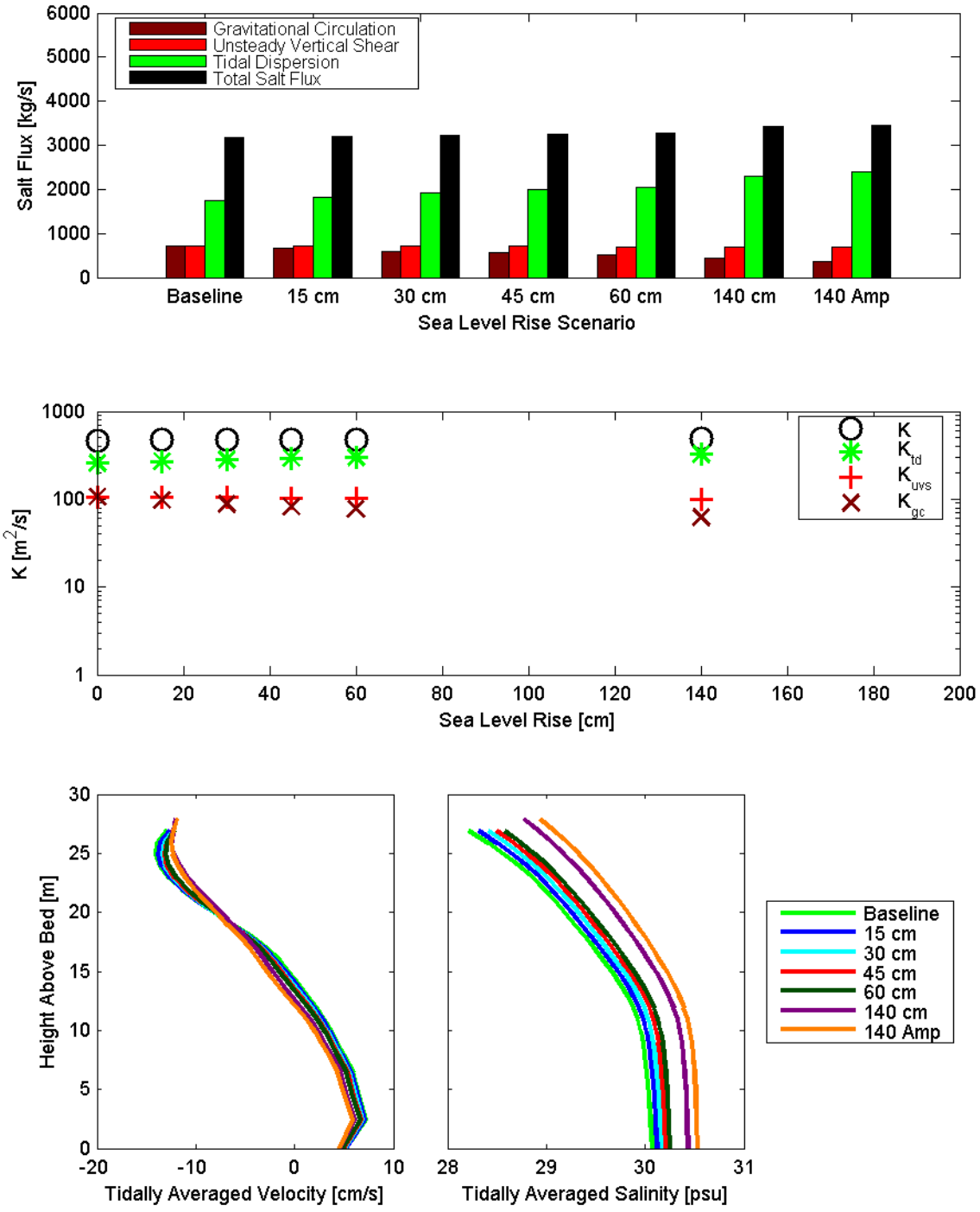

Figure 8.4-42 Dispersive salt flux (top), dispersion coefficients and dispersion coefficient components (middle) and tidally averaged velocity (bottom left) and tidally averaged salinity (bottom right) calculated for each scenario at cross-section 6, extending from Point San Pablo to Point San Pedro, for the October 13, 2002 through November 10, 2002 analysis period..

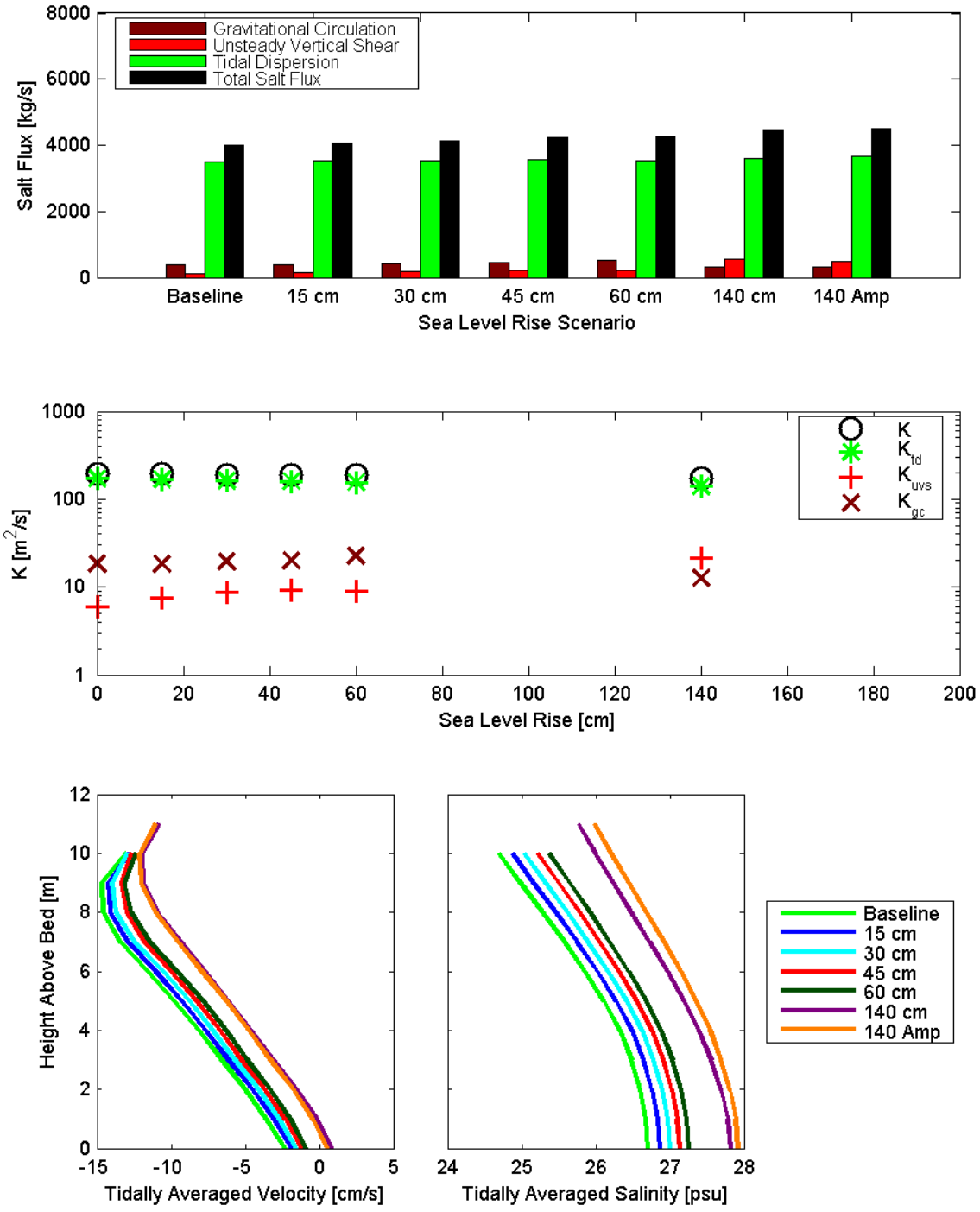

Figure 8.4-43 Dispersive salt flux (top), dispersion coefficients and dispersion coefficient components (middle) and tidally averaged velocity (bottom left) and tidally averaged salinity (bottom right) calculated for each scenario at cross-section 7, extending from Pinole Point to Tolay Creek, for the July 15, 2002 through August 12, 2002 analysis period.

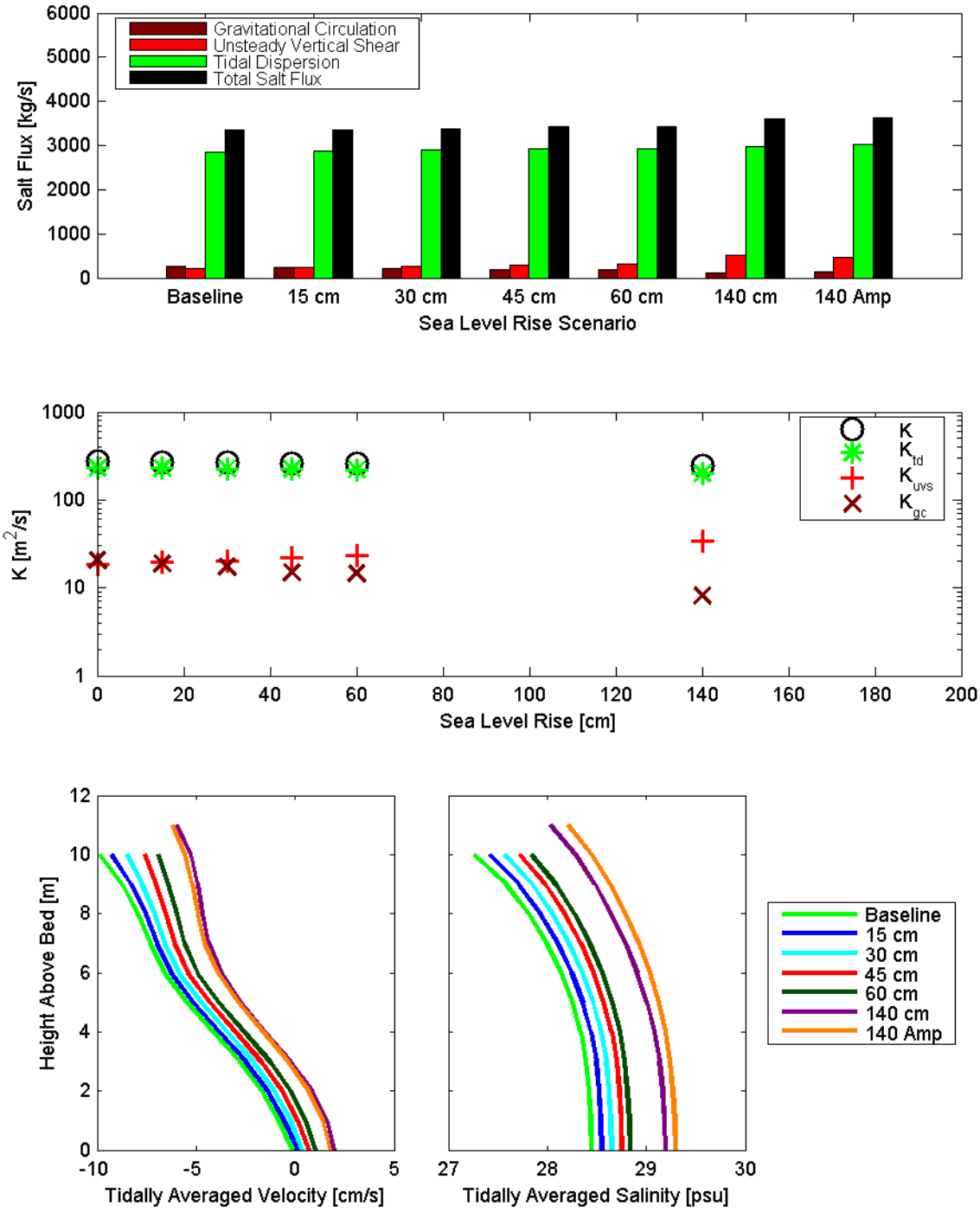

Figure 8.4-44 Dispersive salt flux (top), dispersion coefficients and dispersion coefficient components (middle) and tidally averaged velocity (bottom left) and tidally averaged salinity (bottom right) calculated for each scenario at cross-section 7, extending from Pinole Point to Tolay Creek, for the October 13, 2002 through November 10, 2002 analysis period.

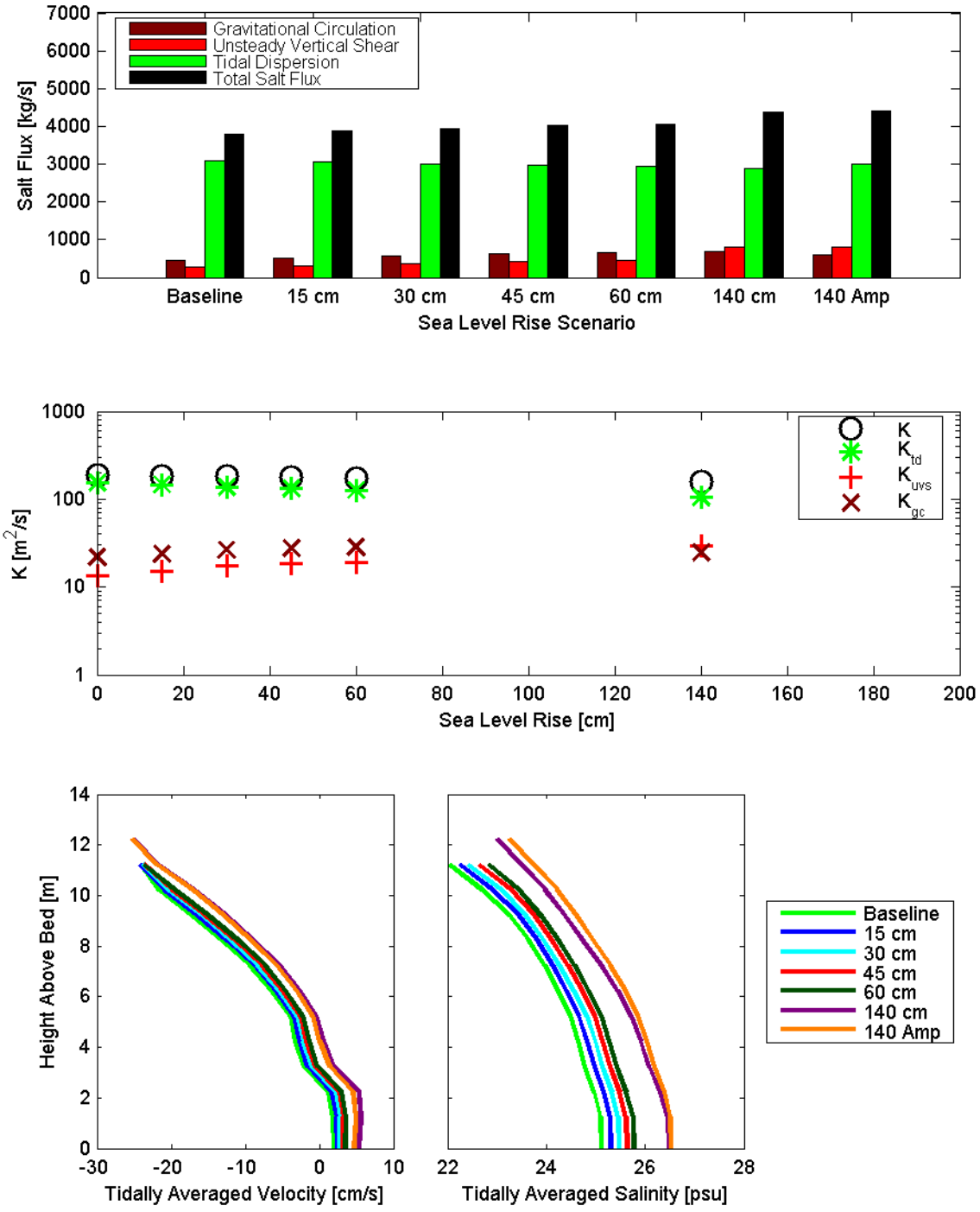

Figure 8.4-45 Dispersive salt flux (top), dispersion coefficients and dispersion coefficient components (middle) and tidally averaged velocity (bottom left) and tidally averaged salinity (bottom right) calculated for each scenario at cross-section 8, extending from Wilson Point to Sonoma Creek, for the July 15, 2002 through August 12, 2002 analysis period.

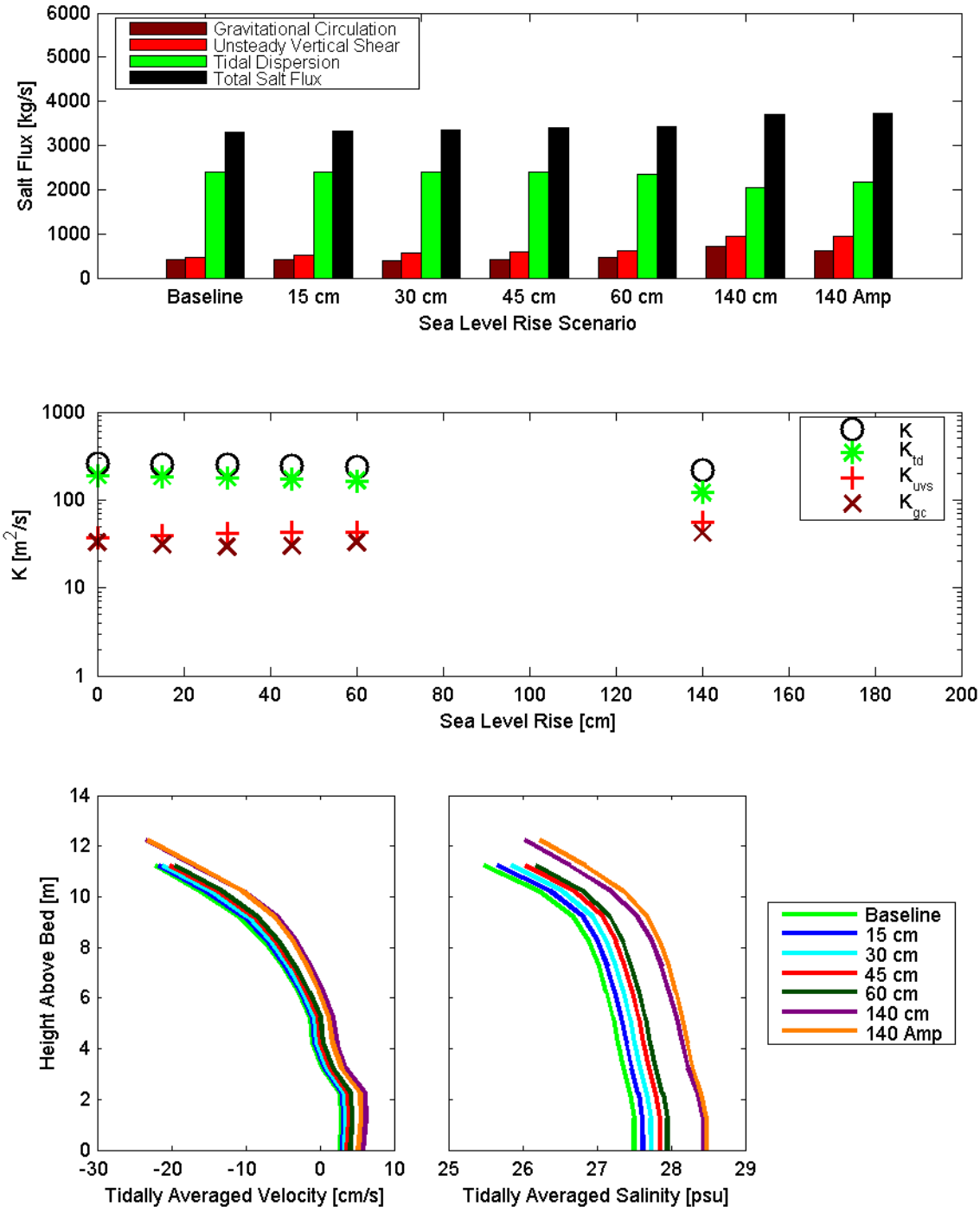

Figure 8.4-46 Dispersive salt flux (top), dispersion coefficients and dispersion coefficient components (middle) and tidally averaged velocity (bottom left) and tidally averaged salinity (bottom right) calculated for each scenario at cross-section 8, extending from Wilson Point to Sonoma Creek, for the October 13, 2002 through November 10, 2002 analysis period.

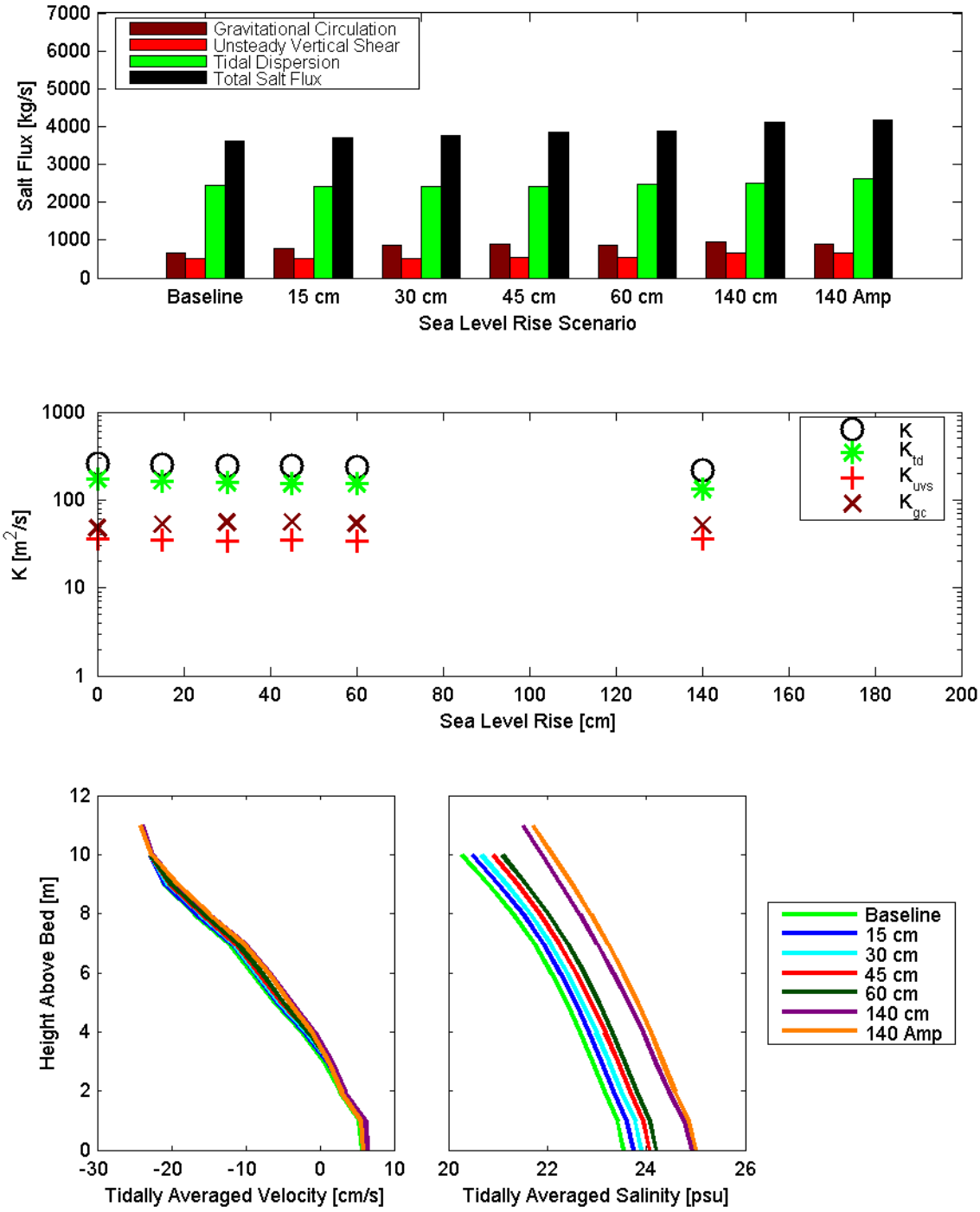

Figure 8.4-47 Dispersive salt flux (top), dispersion coefficients and dispersion coefficient components (middle) and tidally averaged velocity (bottom left) and tidally averaged salinity (bottom right) calculated for each scenario at cross-section 9, extending from Hercules to Mare Island for the July 15, 2002 through August 12, 2002 analysis period.

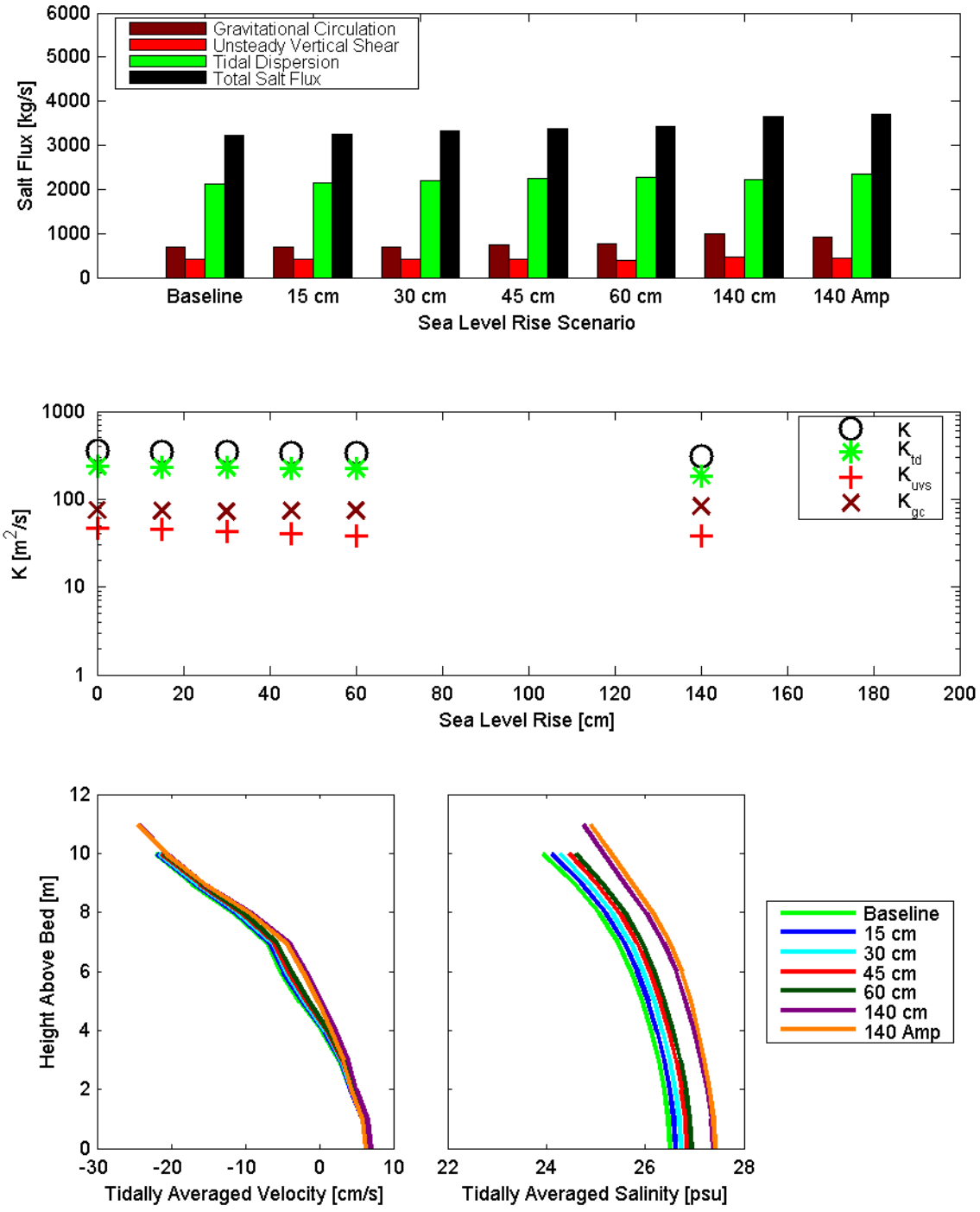

Figure 8.4-48 Dispersive salt flux (top), dispersion coefficients and dispersion coefficient components (middle) and tidally averaged velocity (bottom left) and tidally averaged salinity (bottom right) calculated for each scenario at cross-section 9, extending from Hercules to Mare Island, for the October 13, 2002 through November 10, 2002 analysis period.

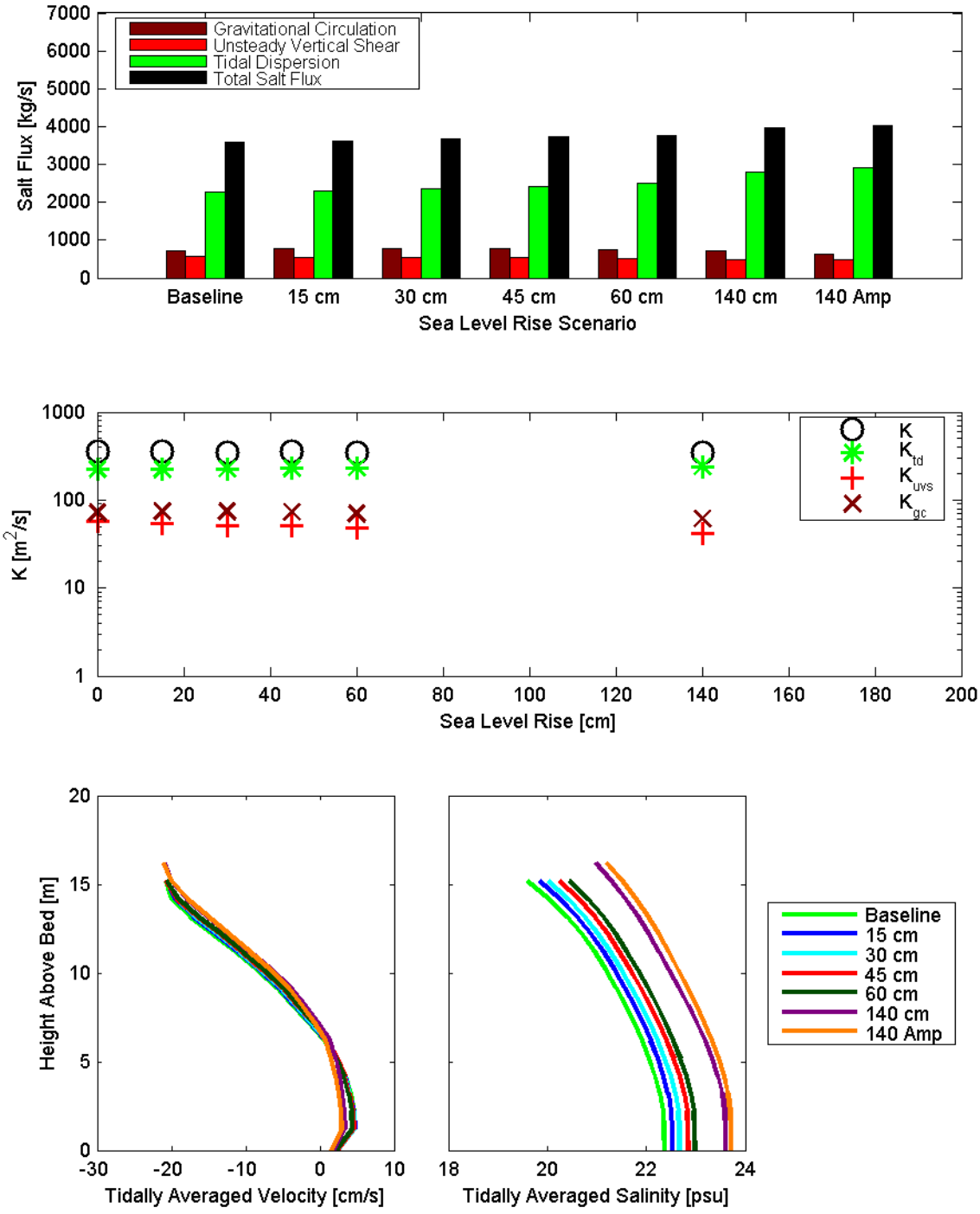

Figure 8.4-49 Dispersive salt flux (top), dispersion coefficients and dispersion coefficient components (middle) and tidally averaged velocity (bottom left) and tidally averaged salinity (bottom right) calculated for each scenario at cross-section 10, extending from Davis Point to Mare Island, for the July 15, 2002 through August 12, 2002 analysis period.

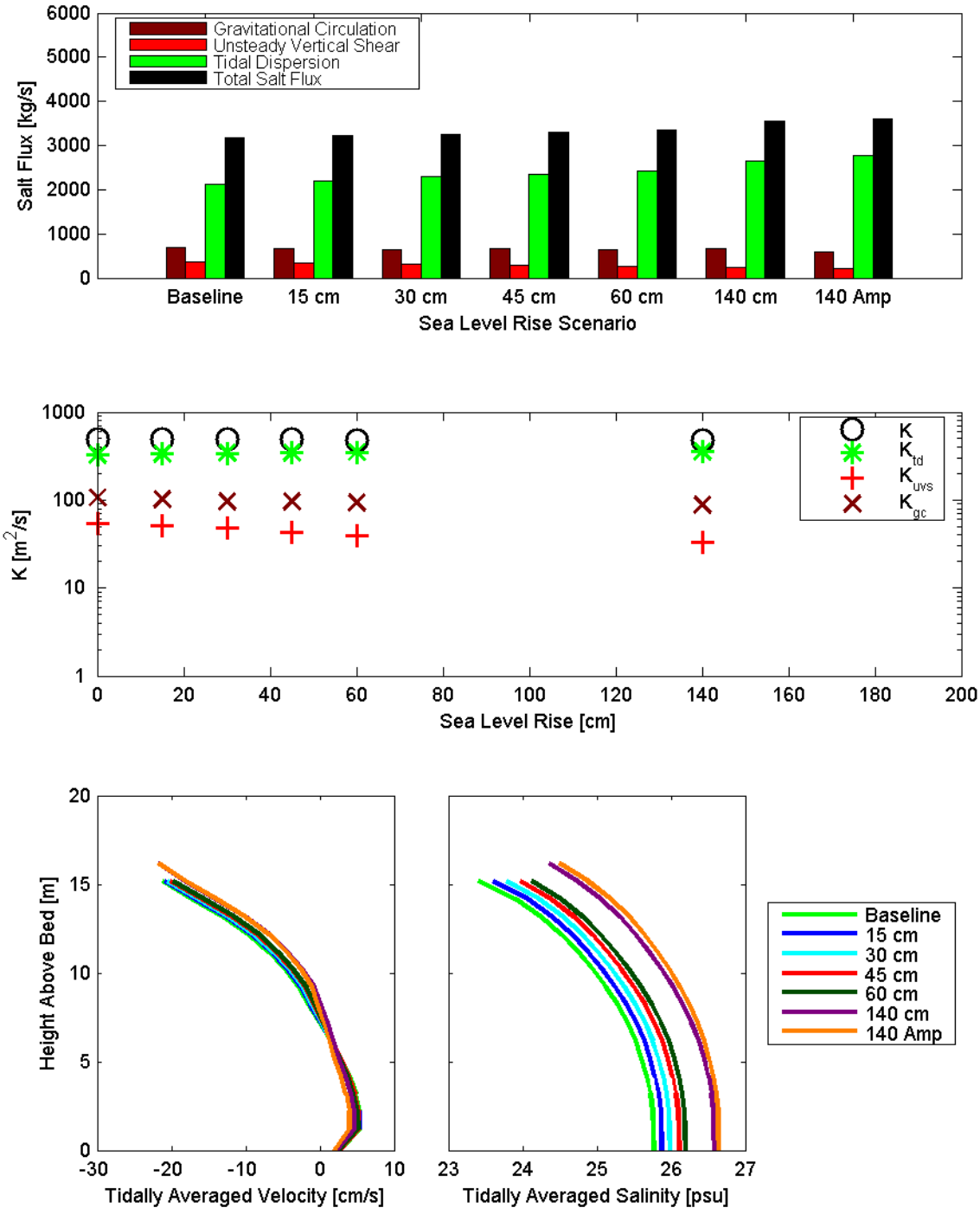

Figure 8.4-50 Dispersive salt flux (top), dispersion coefficients and dispersion coefficient components (middle) and tidally averaged velocity (bottom left) and tidally averaged salinity (bottom right) calculated for each scenario at cross-section 10, extending from Davis Point to Mare Island, for the October 13, 2002 through November 10, 2002 analysis period.

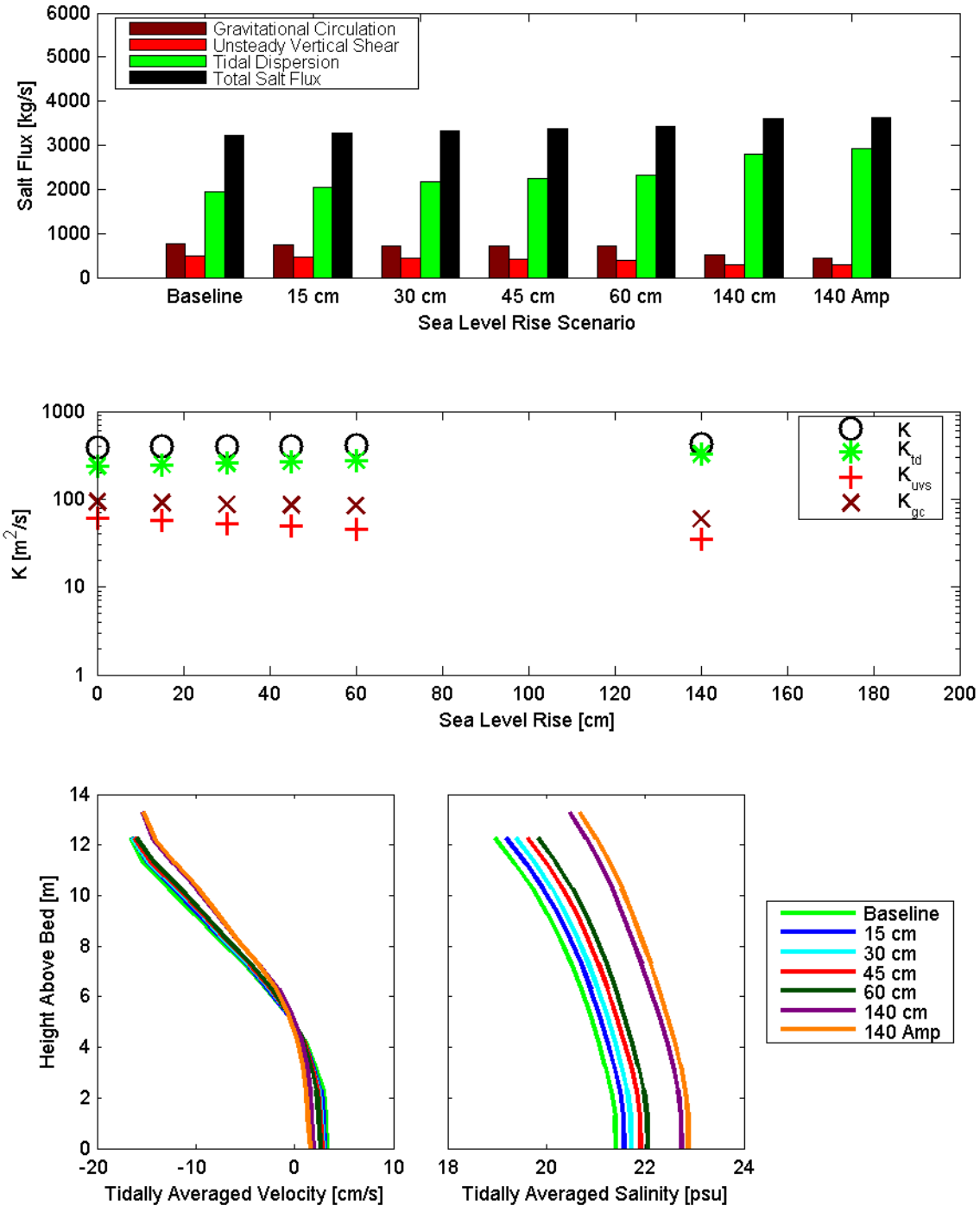

Figure 8.4-51 Dispersive salt flux (top), dispersion coefficients and dispersion coefficient components (middle) and tidally averaged velocity (bottom left) and tidally averaged salinity (bottom right) calculated for each scenario at cross-section 11, extending from Selby to Mare Island Strait, for the July 15, 2002 through August 12, 2002 analysis period.

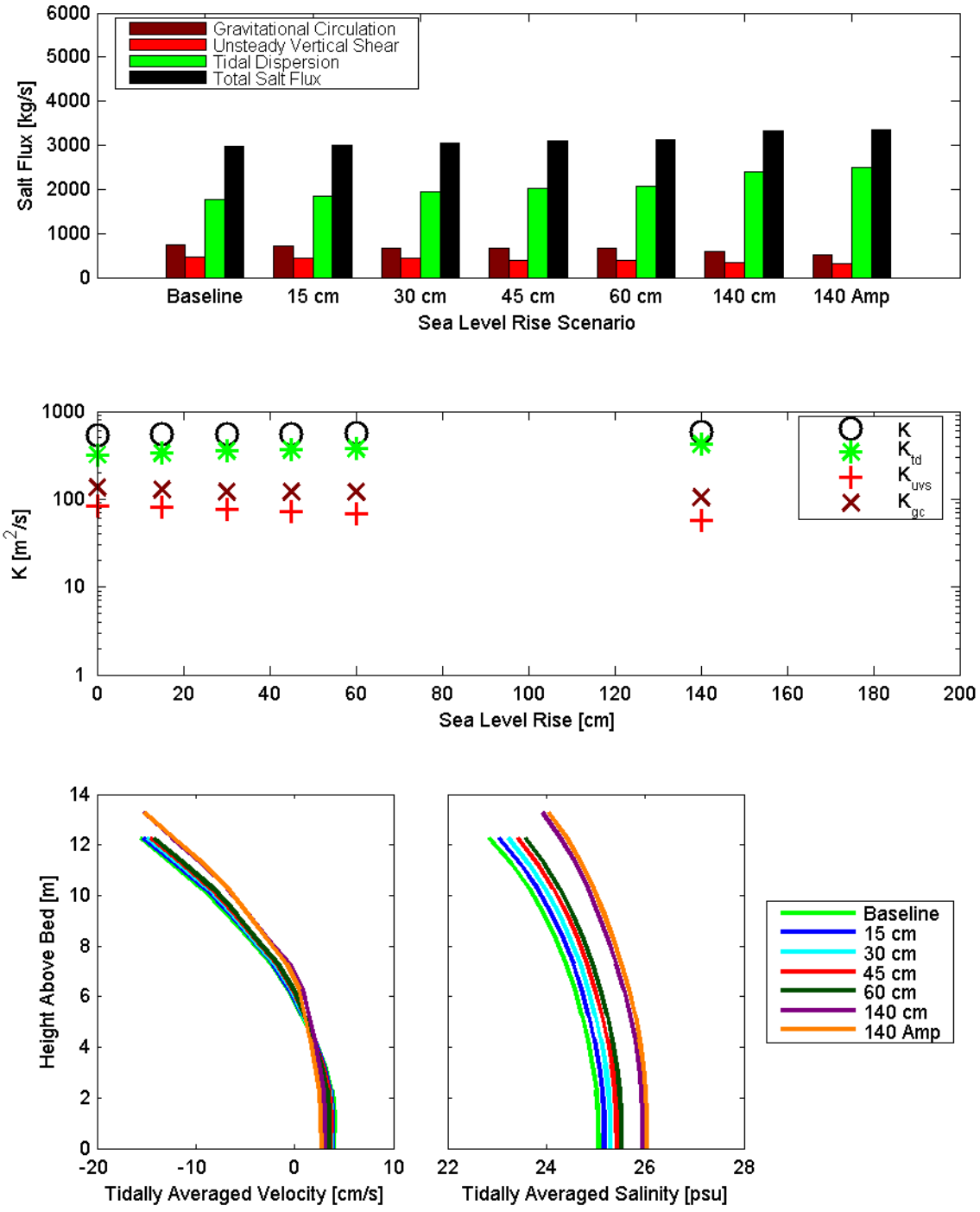

Figure 8.4-52 Dispersive salt flux (top), dispersion coefficients and dispersion coefficient components (middle) and tidally averaged velocity (bottom left) and tidally averaged salinity (bottom right) calculated for each scenario at cross-section 11, extending from Selby to Mare Island Strait, for the October 13, 2002 through November 10, 2002 analysis period.

8.4.3 Carquinez Strait Cross-Sections

Dispersion coefficients and salt fluxes were estimated at the five cross-sections in Carquinez Strait (cross-section 12 to cross-section 17) shown in Figure 8.3-1. In Figure 8.4-53 through Figure 8.4-64, analysis results are provided for each cross-section that summarize the dispersion analysis at that location for a given analysis period. The top panel shows the contributions of individual processes to dispersive salt flux (advective salt flux is not shown) for each SLR scenario. The second type of figure shows the overall dispersion coefficient (K), the portion of the dispersion coefficient associated with gravitational circulation (K_{gc}), the portion of the dispersion coefficient associated with unsteady vertical shear dispersion processes (K_{uvs}), and the portion of the dispersion coefficient associated with tidal dispersion processes (K_{td}) for each SLR scenario. The bottom panel shows the period averaged velocity profile and salinity profile at the deepest point in the cross-section for each SLR scenario.

The dispersion coefficients are generally large in Carquinez Strait. Tidal dispersion processes are the most important salt intrusion processes in cross-sections in the seaward (western) portion of Carquinez Strait for both analysis periods. Gravitational circulation and unsteady vertical shear dispersion are both substantial for all cross-sections in Carquinez Strait and increase with landward (up estuary) distance to become the dominant mechanisms at cross-section 17, located at the Benicia Bridge. The dispersive salt fluxes increase with sea level rise due to increased salinity in Carquinez Strait. However, the dispersion coefficients show little variability with SLR at most cross-sections indicating small changes in the strength of local mixing processes during low Delta outflow conditions. The relative contributions of individual salt flux mechanisms do change substantially with sea level rise. For example, at cross-section 12, located at the Carquinez Bridge, the importance of tidal dispersion increases with sea level rise and the importance of gravitational circulation and unsteady vertical shear decreases with sea level rise. It is likely that both trends are explained by the substantial predicted increases in tidal prism at this location (Figure 8.4-17 and Figure 8.4-18). Increased tidal prism can decrease the effect of gravitational circulation and unsteady vertical shear because vertical mixing increases with increased tidal current speed, resulting in less stratification and less vertical shear in tidally averaged velocity. Figure 8.4-53 and Figure 8.4-54 show that both stratification and tidally averaged vertical shear decrease with increased sea level rise at cross-section 12. In contrast to the results at cross-section 12, at cross-section 17, located at the Benicia Bridge, gravitational circulation and unsteady vertical shear are the dominant salt intrusion mechanisms for all of the scenarios (Figure 8.4-63 and Figure 8.4-64). Vertical shear in the tidally averaged velocity and stratification remain roughly constant with sea level rise.

The results in Carquinez Strait are generally consistent with the flux analysis of sea level rise scenarios performed as part of the DRMS studies (Gross et al., 2007b). However the DRMS scenarios were for higher Delta outflow and, therefore, showed a larger contribution of gravitational circulation and unsteady vertical shear. The flux analysis of various Delta outflows performed as part of the DRMS studies (Gross et al., 2007a) was consistent with these results for low Delta outflows and indicated that gravitational circulation becomes the dominant salt intrusion process at moderate to high Delta outflows.

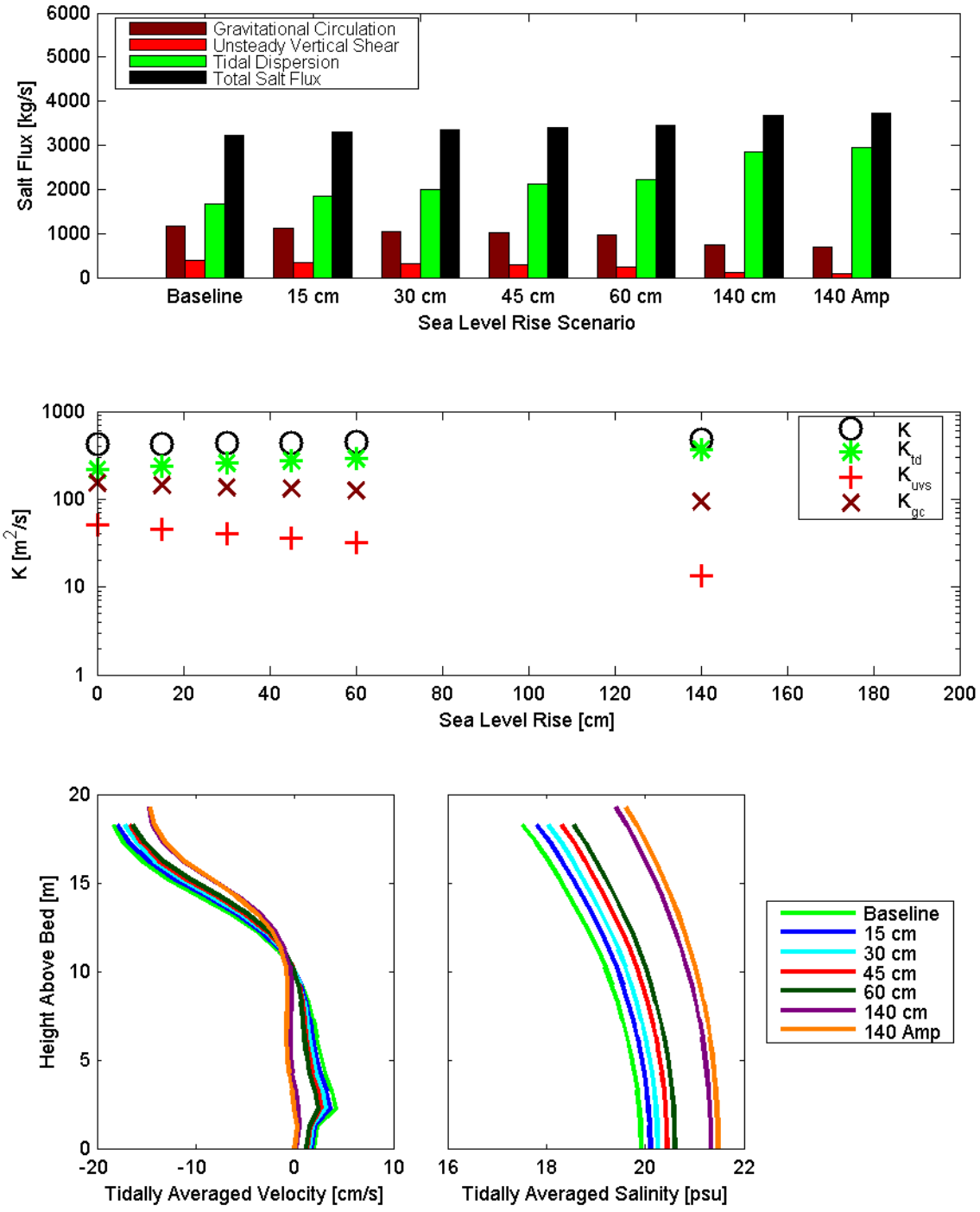

Figure 8.4-53 Dispersive salt flux (top), dispersion coefficients and dispersion coefficient components (middle) and tidally averaged velocity (bottom left) and tidally averaged salinity (bottom right) calculated for each scenario at cross-section 12, located at the Carquinez Bridge, for the July 15, 2002 through August 12, 2002 analysis period.

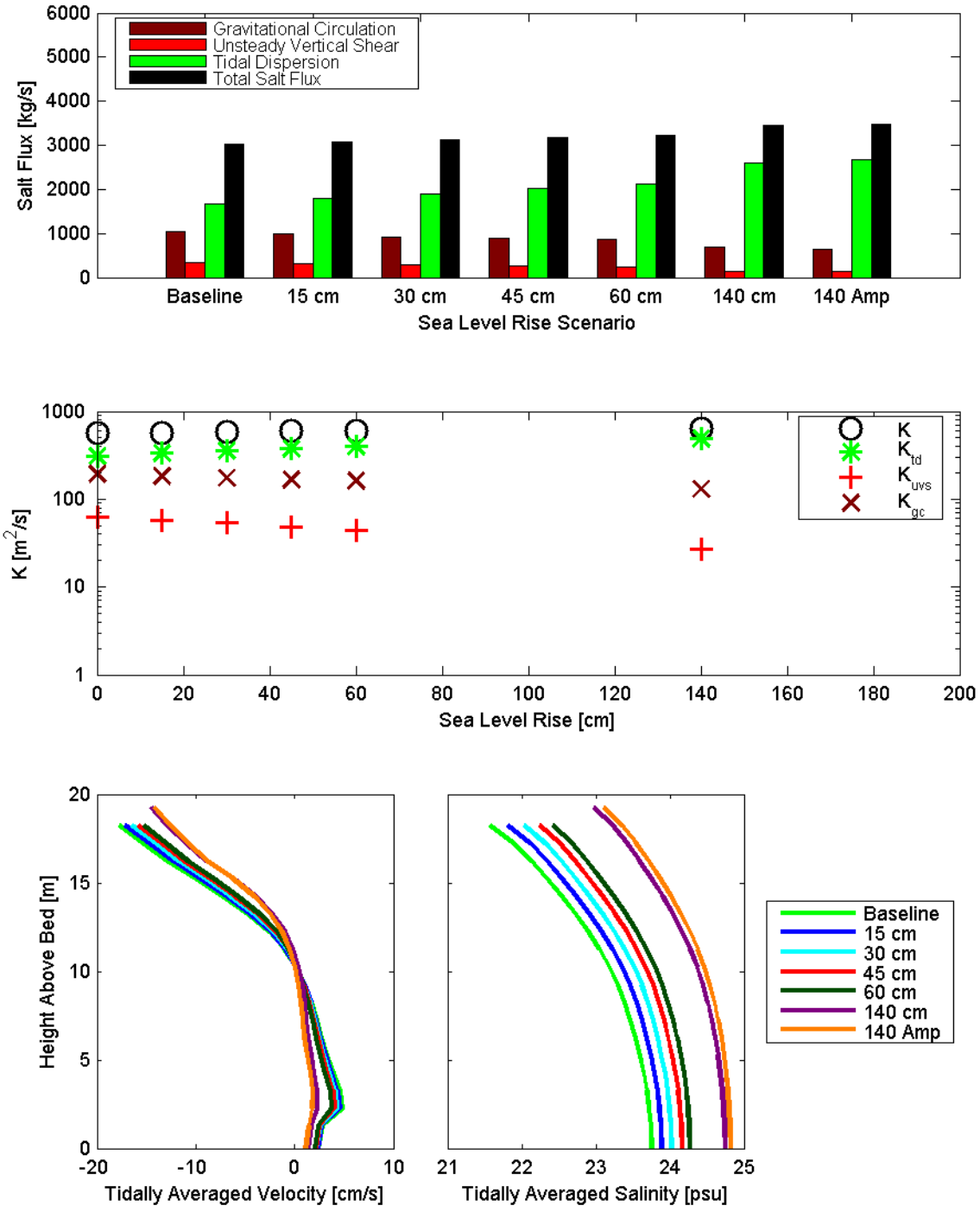

Figure 8.4-54 Dispersive salt flux (top), dispersion coefficients and dispersion coefficient components (middle) and tidally averaged velocity (bottom left) and tidally averaged salinity (bottom right) calculated for each scenario at cross-section 12, located at the Carquinez Bridge, for the October 13, 2002 through November 10, 2002 analysis period.

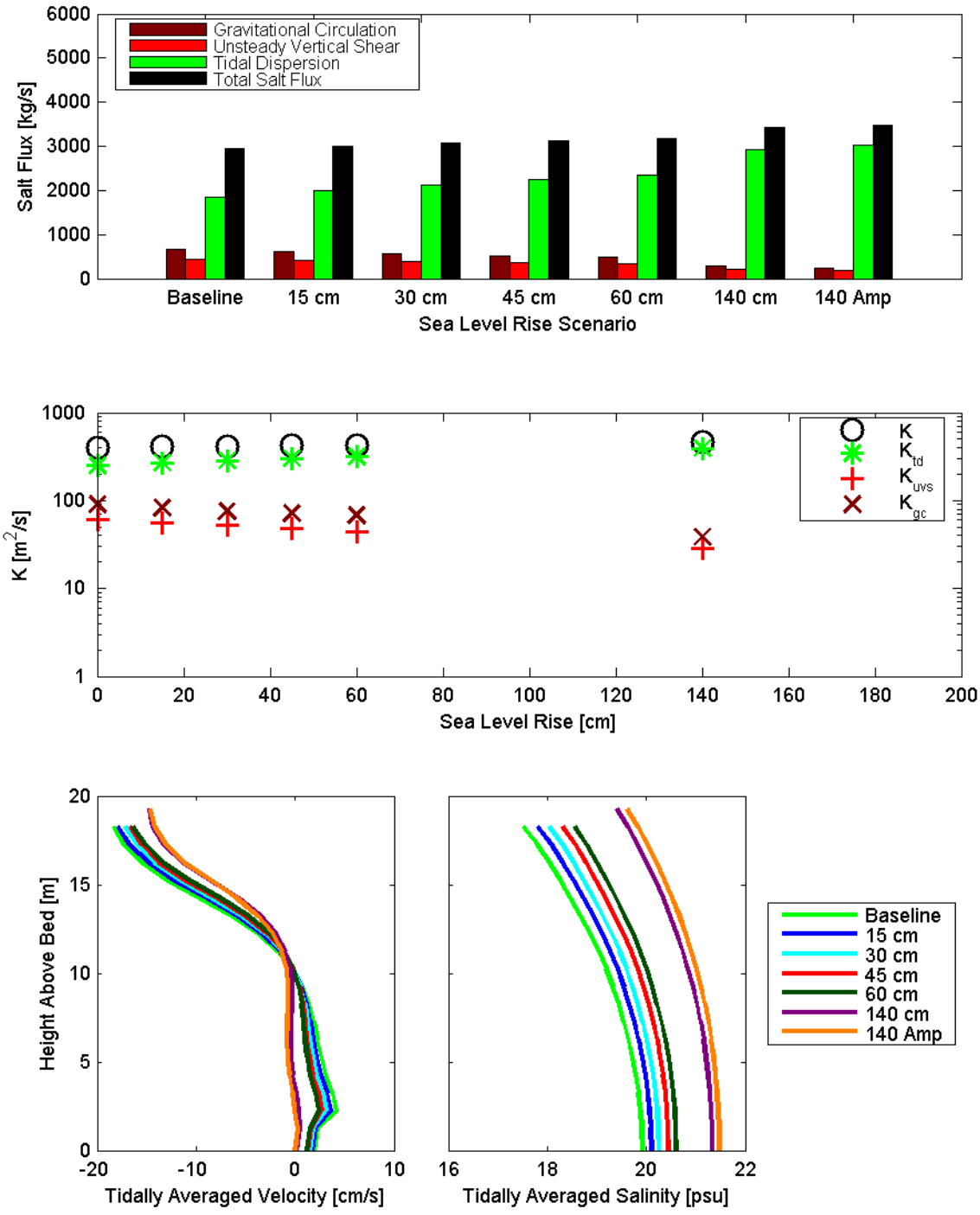

Figure 8.4-55 Dispersive salt flux (top), dispersion coefficients and dispersion coefficient components (middle) and tidally averaged velocity (bottom left) and tidally averaged salinity (bottom right) calculated for each scenario at cross-section 13, extending from Crockett to Elliot Cove, for the July 15, 2002 through August 12, 2002 analysis period.

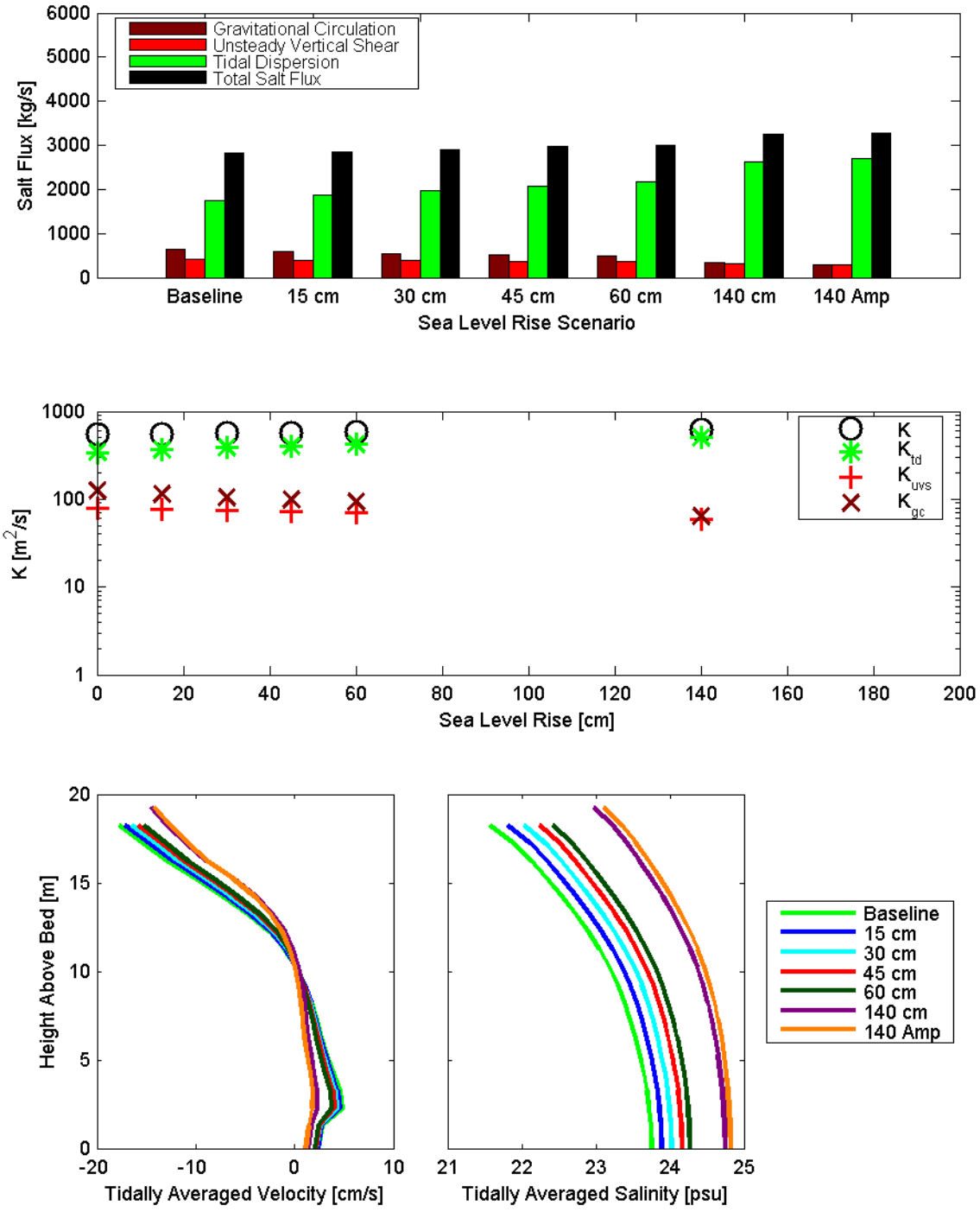

Figure 8.4-56 Dispersive salt flux (top), dispersion coefficients and dispersion coefficient components (middle) and tidally averaged velocity (bottom left) and tidally averaged salinity (bottom right) calculated for each scenario at cross-section 13, extending from Crockett to Elliot Cove, for the October 13, 2002 through November 10, 2002 analysis period.

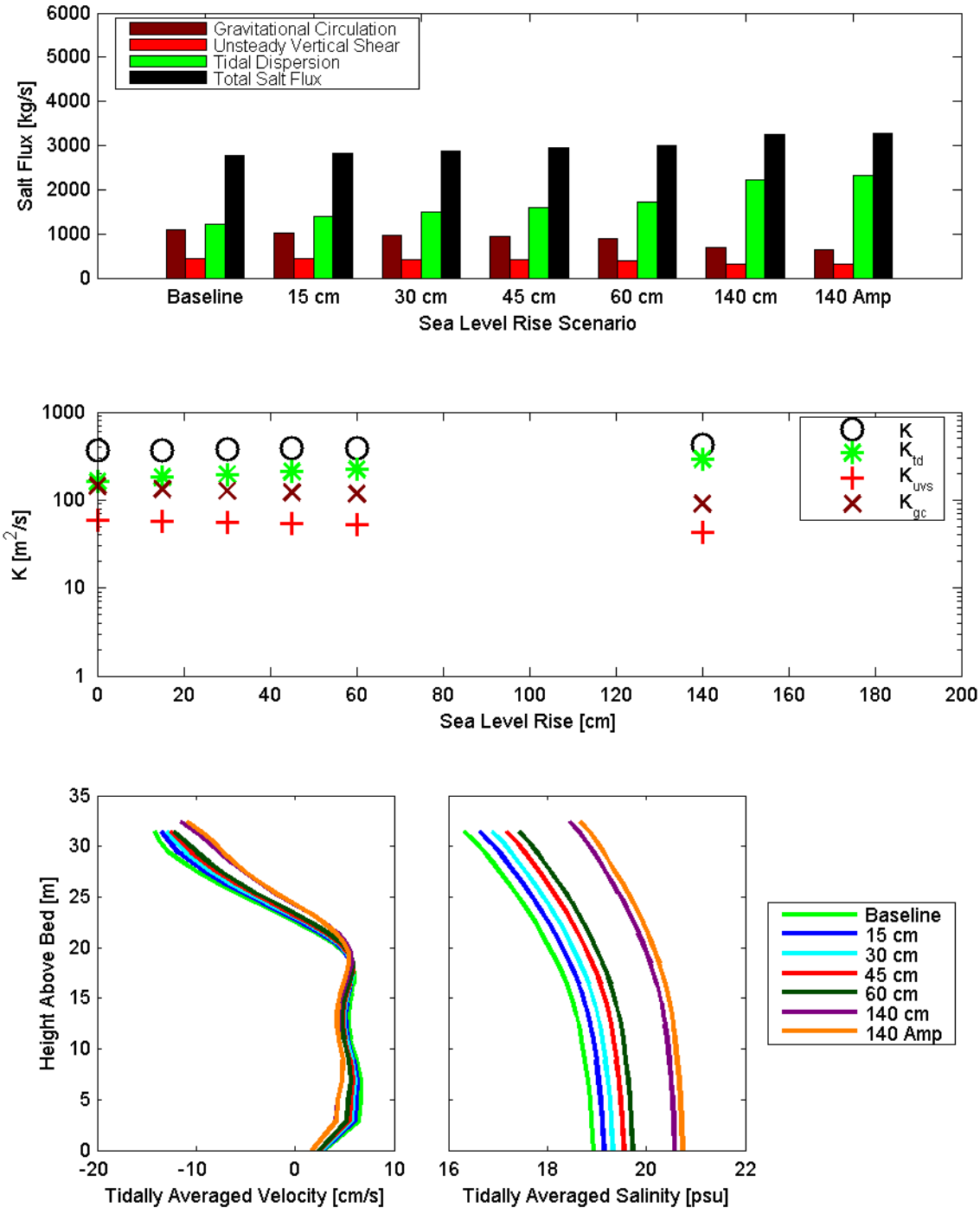

Figure 8.4-57 Dispersive salt flux (top), dispersion coefficients and dispersion coefficient components (middle) and tidally averaged velocity (bottom left) and tidally averaged salinity (bottom right) calculated for each scenario at cross-section 14, extending from Crockett to Dillon Point, for the July 15, 2002 through August 12, 2002 analysis period.

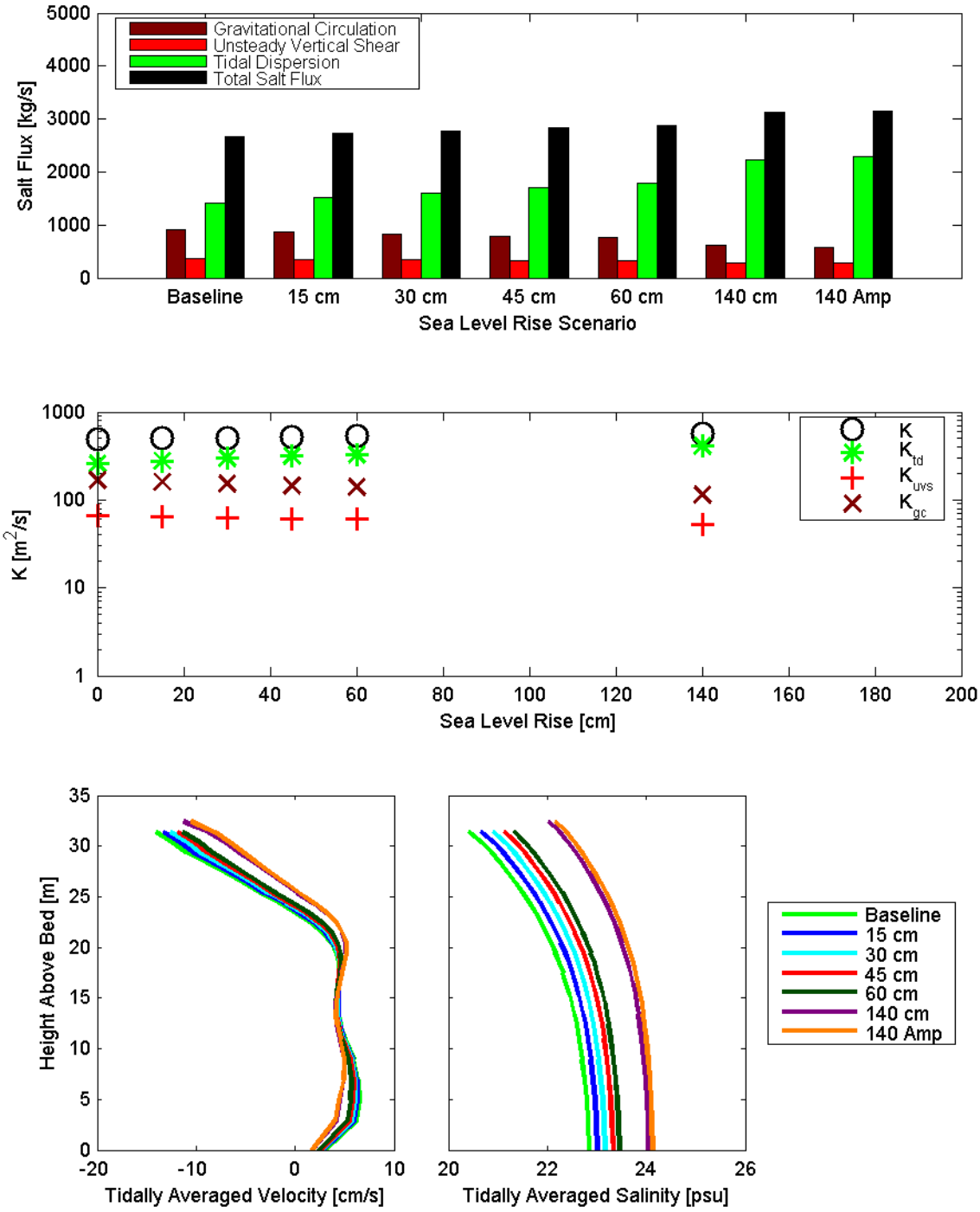

Figure 8.4-58 Dispersive salt flux (top), dispersion coefficients and dispersion coefficient components (middle) and tidally averaged velocity (bottom left) and tidally averaged salinity (bottom right) calculated for each scenario at cross-section 14, extending from Crockett to Dillon Point, for the October 13, 2002 through November 10, 2002 analysis period.

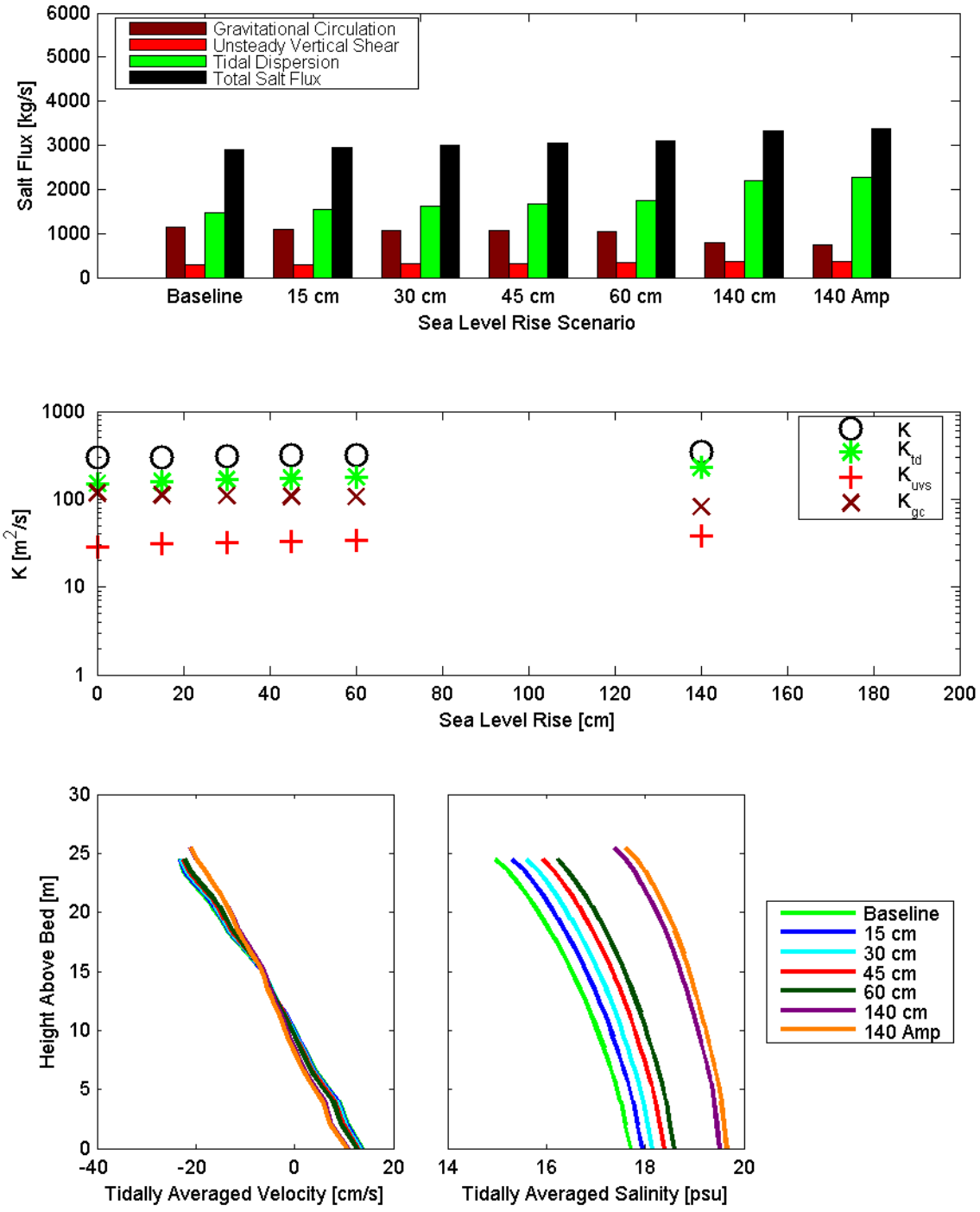

Figure 8.4-59 Dispersive salt flux (top), dispersion coefficients and dispersion coefficient components (middle) and tidally averaged velocity (bottom left) and tidally averaged salinity (bottom right) calculated for each scenario at cross-section 15, extending from Ozol to Benicia Point, for the July 15, 2002 through August 12, 2002 analysis period.

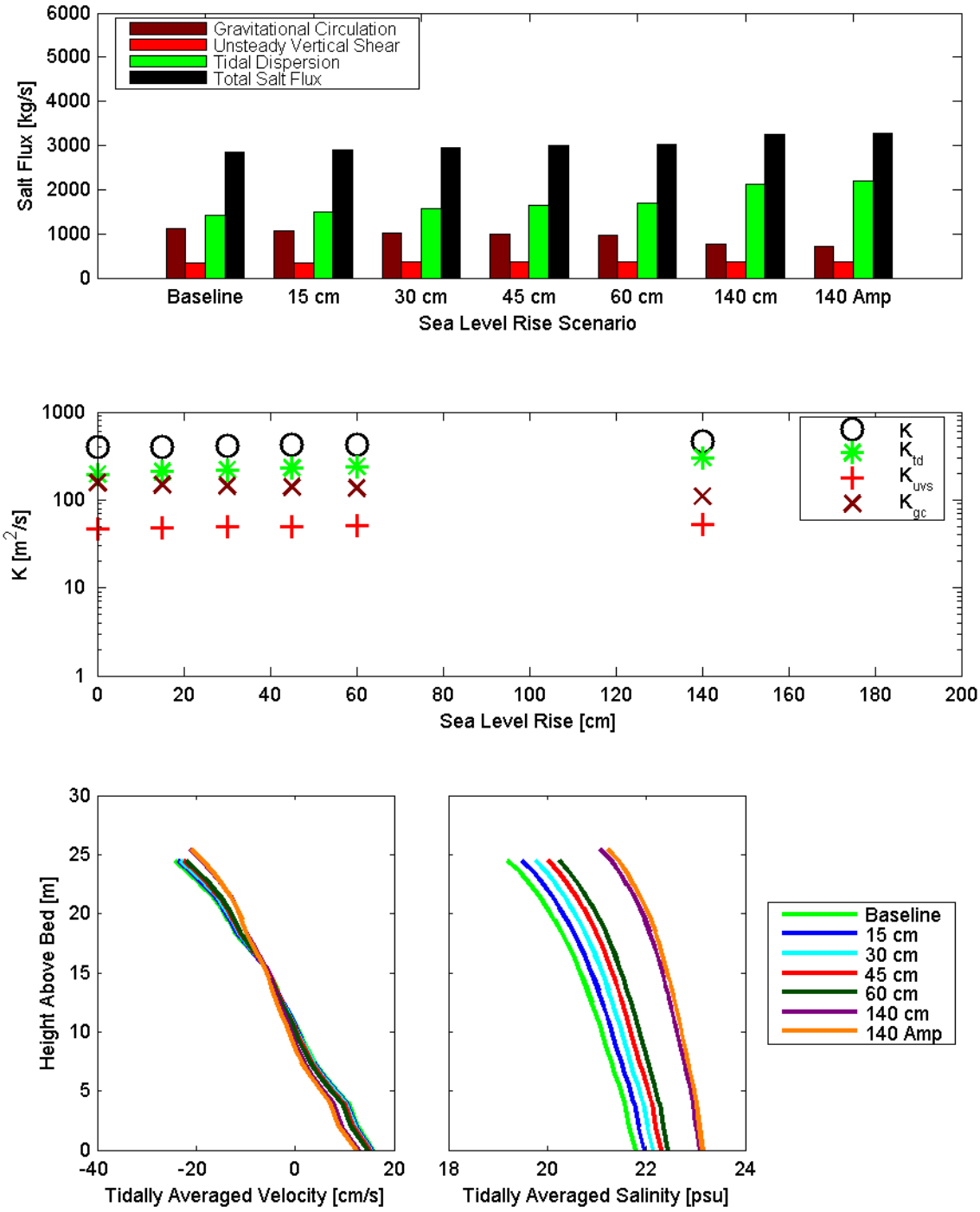

Figure 8.4-60 Dispersive salt flux (top), dispersion coefficients and dispersion coefficient components (middle) and tidally averaged velocity (bottom left) and tidally averaged salinity (bottom right) calculated for each scenario at cross-section 15, extending from Ozol to Benicia Point, for the October 13, 2002 through November 10 2002 analysis period.

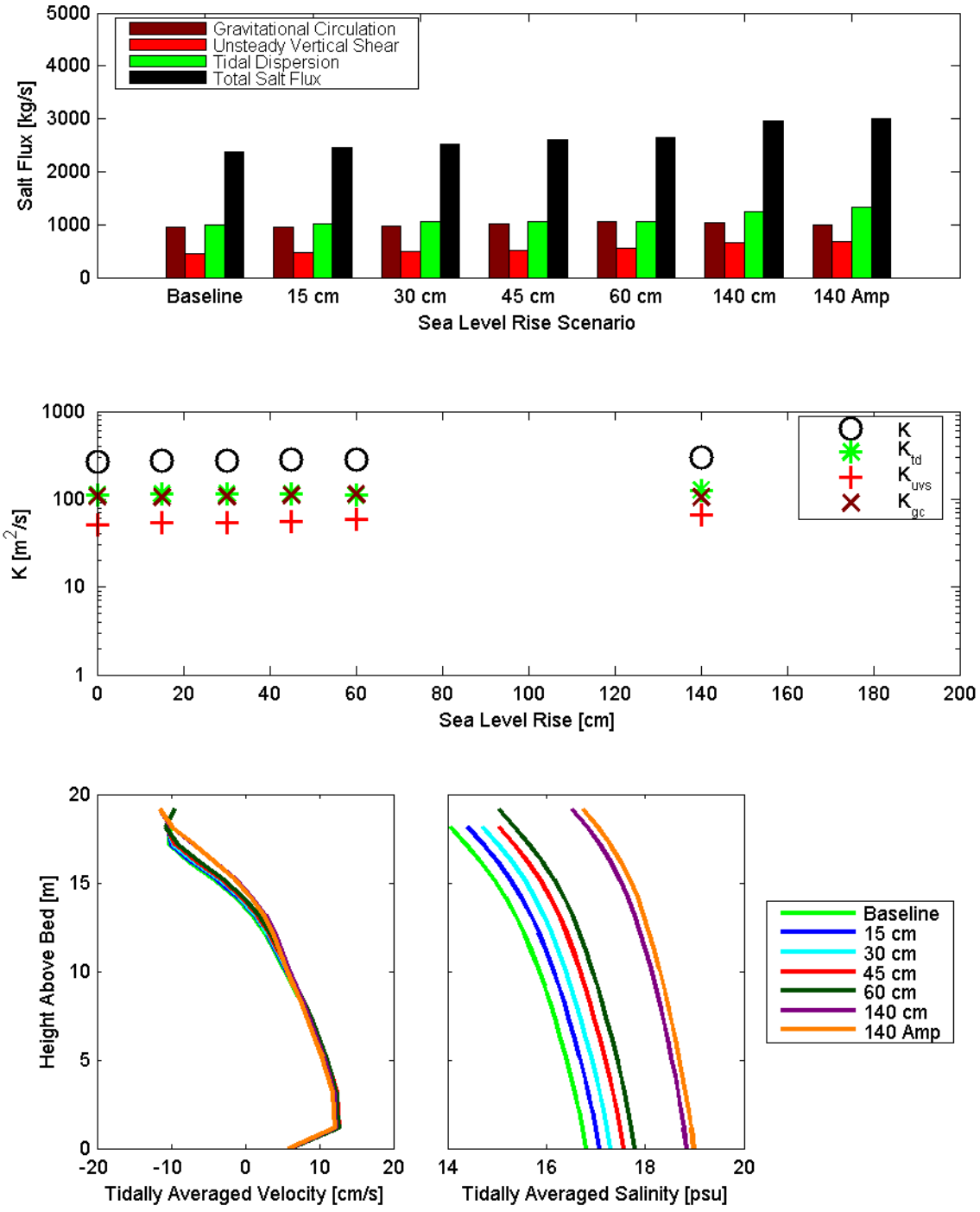

Figure 8.4-61 Dispersive salt flux (top), dispersion coefficients and dispersion coefficient components (middle) and tidally averaged velocity (bottom left) and tidally averaged salinity (bottom right) calculated for each scenario at cross-section 16, extending from Martinez to Benicia, for the July 15, 2002 through August 12, 2002 analysis period.

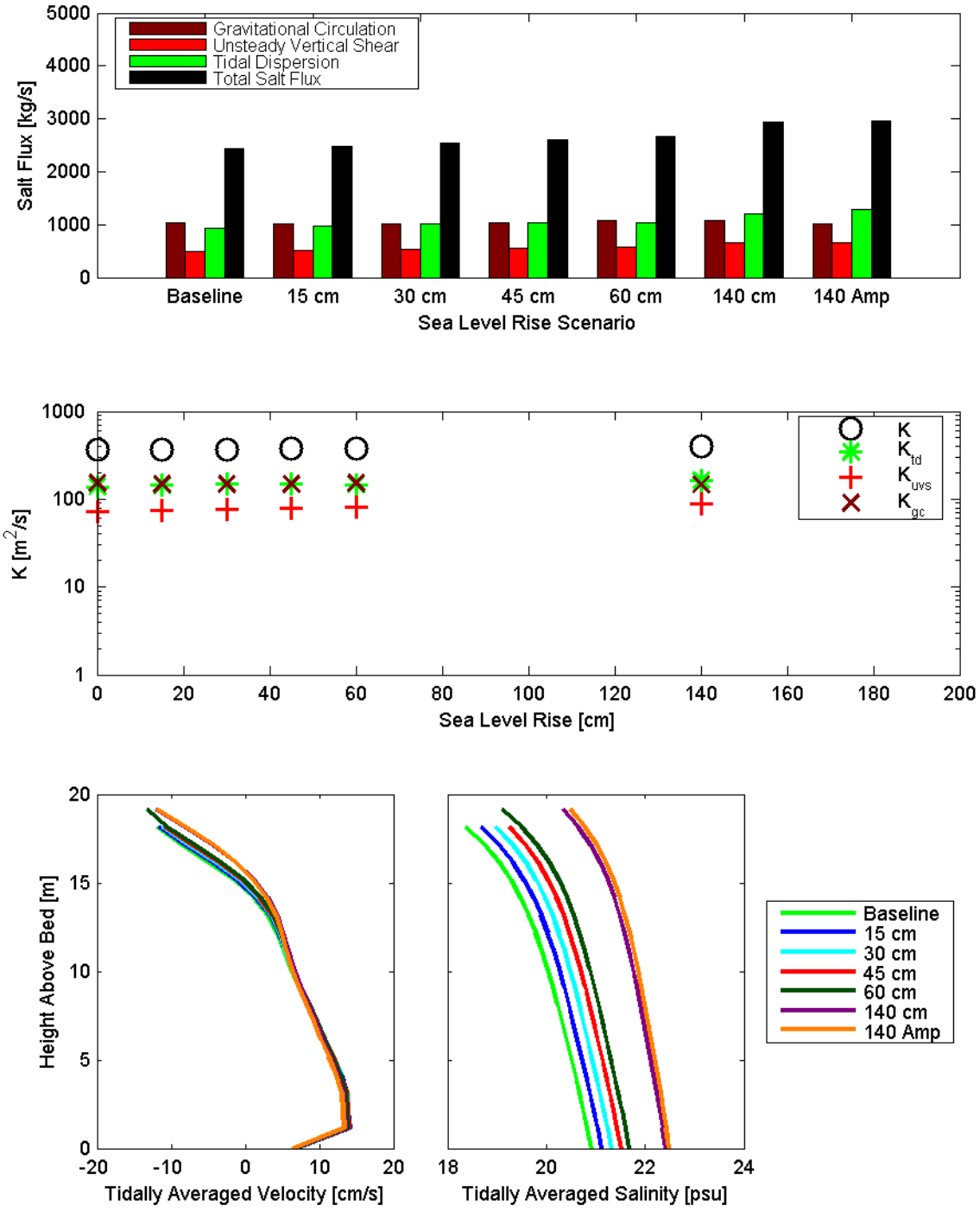

Figure 8.4-62 Dispersive salt flux (top), dispersion coefficients and dispersion coefficient components (middle) and tidally averaged velocity (bottom left) and tidally averaged salinity (bottom right) calculated for each scenario at cross-section 16, extending from Martinez to Benicia, for the October 13, 2002 through November 10, 2002 analysis period.

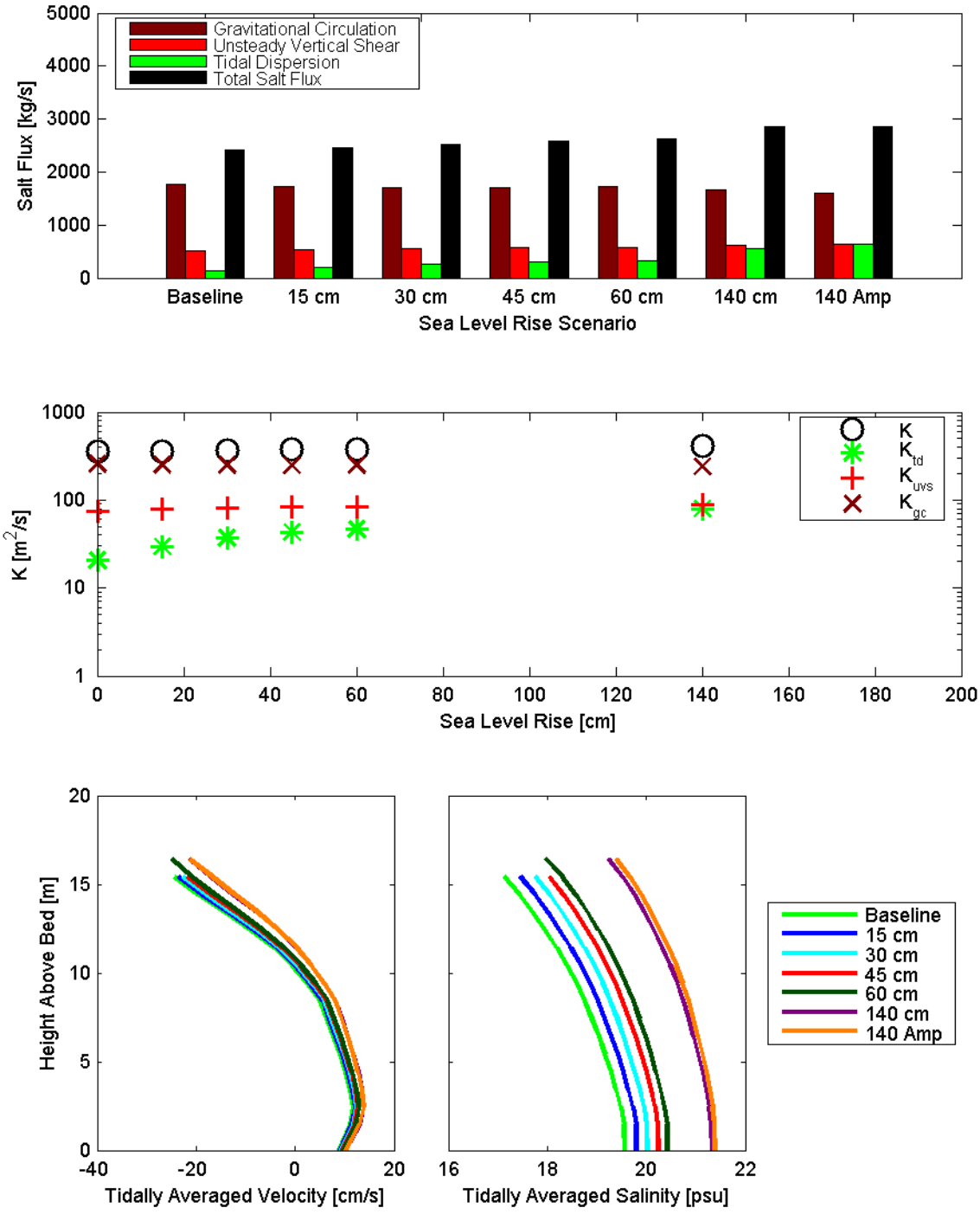

Figure 8.4-63 Dispersive salt flux (top), dispersion coefficients and dispersion coefficient components (middle) and tidally averaged velocity (bottom left) and tidally averaged salinity (bottom right) calculated for each scenario at cross-section 17, located at the Benicia Bridge, for the July 15, 2002 through August 12, 2002 analysis period.

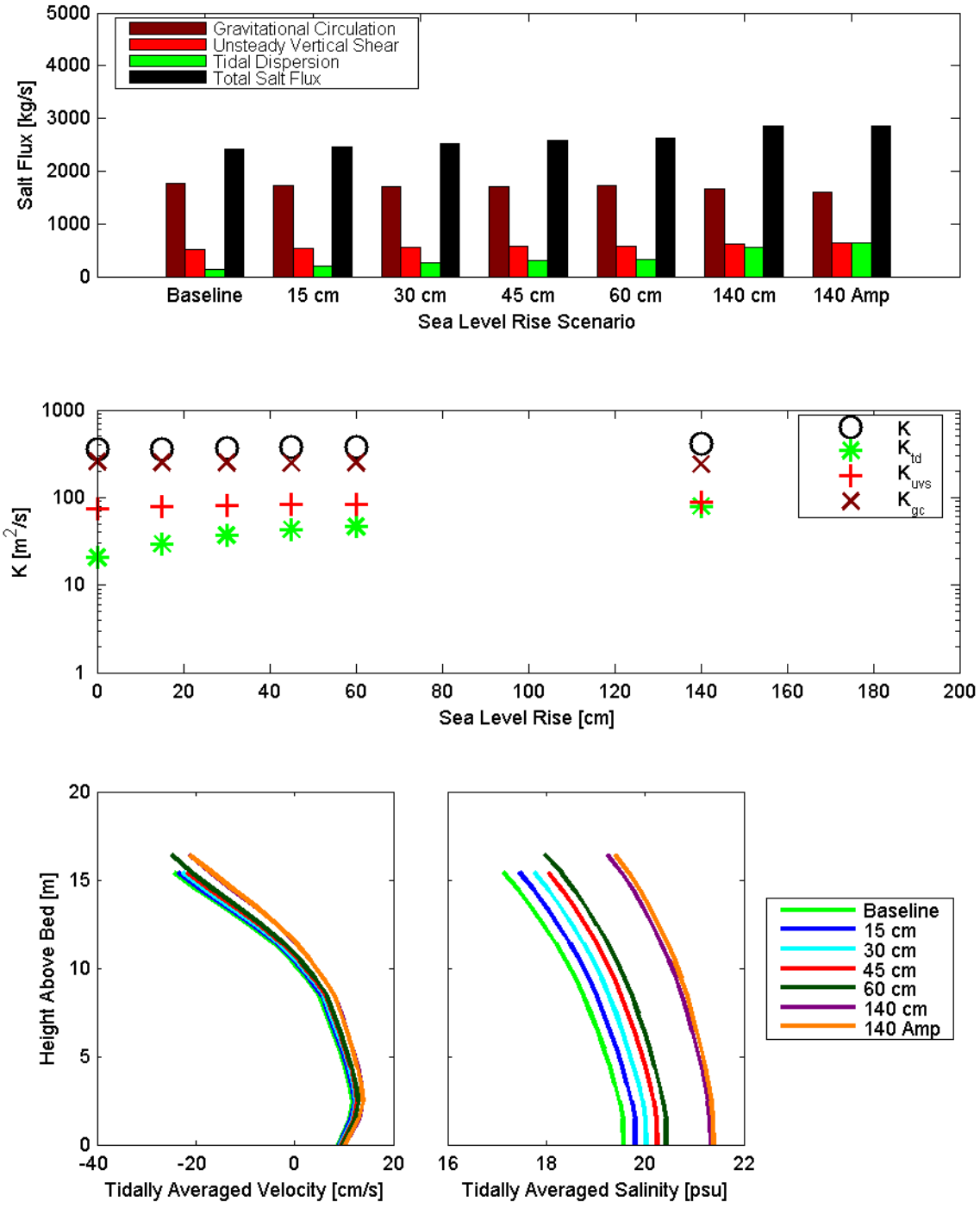

Figure 8.4-64 Dispersive salt flux (top), dispersion coefficients and dispersion coefficient components (middle) and October 13, 2002 through November 10, 2002 analysis period tidally averaged velocity (bottom left) and tidally averaged salinity (bottom right) calculated for each scenario at cross-section 17, located at the Benicia Bridge, for the October 13, 2002 to November 10, 2002 analysis period.

8.4.4 Suisun Bay Cross-Sections

Dispersion coefficients and salt fluxes were estimated at the eight cross-sections in Suisun Bay (cross-section 18 to cross-section 25) shown in Figure 8.3-1. In Figure 8.4-65 through Figure 8.4-80, analysis results are provided for each cross-section that summarize the dispersion analysis at that location for a given analysis period. The top panel shows the contributions of individual processes to dispersive salt flux (advective salt flux is not shown) for each SLR scenario. The second type of figure shows the overall dispersion coefficient (K), the portion of the dispersion coefficient associated with gravitational circulation (K_{gc}), the portion of the dispersion coefficient associated with unsteady vertical shear dispersion processes (K_{uvs}), and the portion of the dispersion coefficient associated with tidal dispersion processes (K_{td}) for each SLR scenario. The bottom panel shows the period averaged velocity profile and salinity profile at the deepest point in the cross-section for each SLR scenario.

The dispersion coefficients are smaller on average in Suisun Bay than in Central Bay and San Pablo Bay. Tidal dispersion processes are the most important salt intrusion processes in most cross-sections for both analysis periods. Gravitational circulation and unsteady vertical shear dispersion are both substantial for all cross-sections in Suisun Bay and gravitational circulation is the strongest salt intrusion process at cross-section 23, extending from Concord to Montezuma Slough, during the October 13, 2002 through November 10, 2002 analysis period (Figure 8.4-76). The dispersive salt fluxes increase with sea level rise due to increased salinity in Suisun Bay. The dispersion coefficients also increase with SLR at most cross-sections primarily due to increases in tidal dispersion. It is likely that this predicted increase results from substantial increases in tidal prism (Figure 8.4-19 and Figure 8.4-20). At most cross-sections in Suisun Bay vertical shear and stratification do not vary greatly with sea level rise.

The results in Suisun Bay are generally consistent with the flux analysis of sea level rise scenarios performed as part of the DRMS studies (Gross et al., 2007b). For example, the DRMS study also showed strong local importance of gravitational circulation in Suisun Bay near Concord. However the DRMS scenarios were for higher Delta outflow and, therefore, showed a larger contribution of gravitational circulation and unsteady vertical shear. The flux analysis of various Delta outflows performed as part of the DRMS studies (Gross et al., 2007a) was consistent with these results for low Delta outflows and indicated that gravitational circulation increases in the seaward (western) portion of Suisun Bay at moderate outflows. At higher Delta outflows, salt is almost entirely flushed out of Suisun Bay.

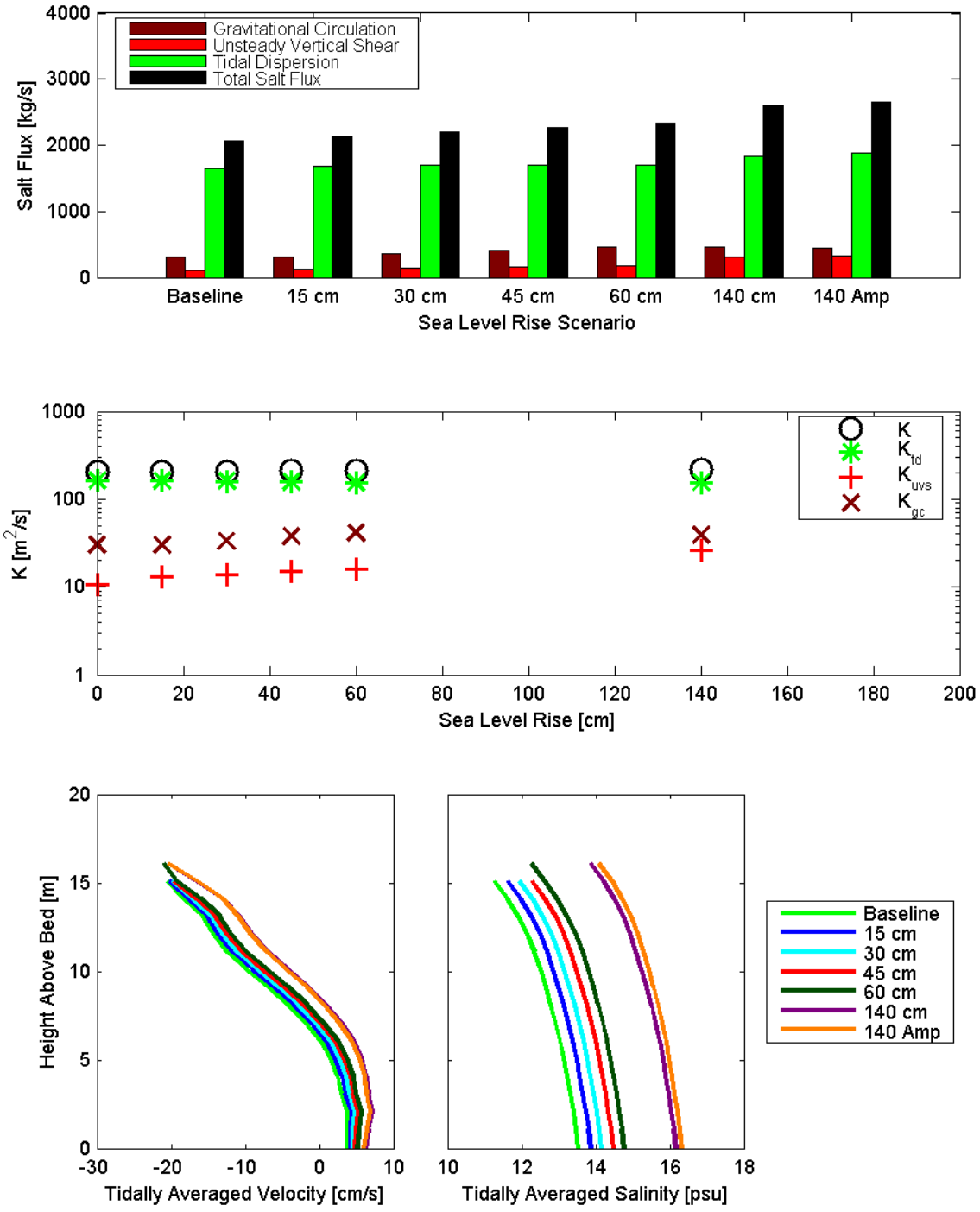

Figure 8.4-65 Dispersive salt flux (top), dispersion coefficients and dispersion coefficient components (middle) and tidally averaged velocity (bottom left) and tidally averaged salinity (bottom right) calculated for each scenario at cross-section 18, located east of the Mothball Fleet, for the July 15, 2002 through August 12, 2002 analysis period.

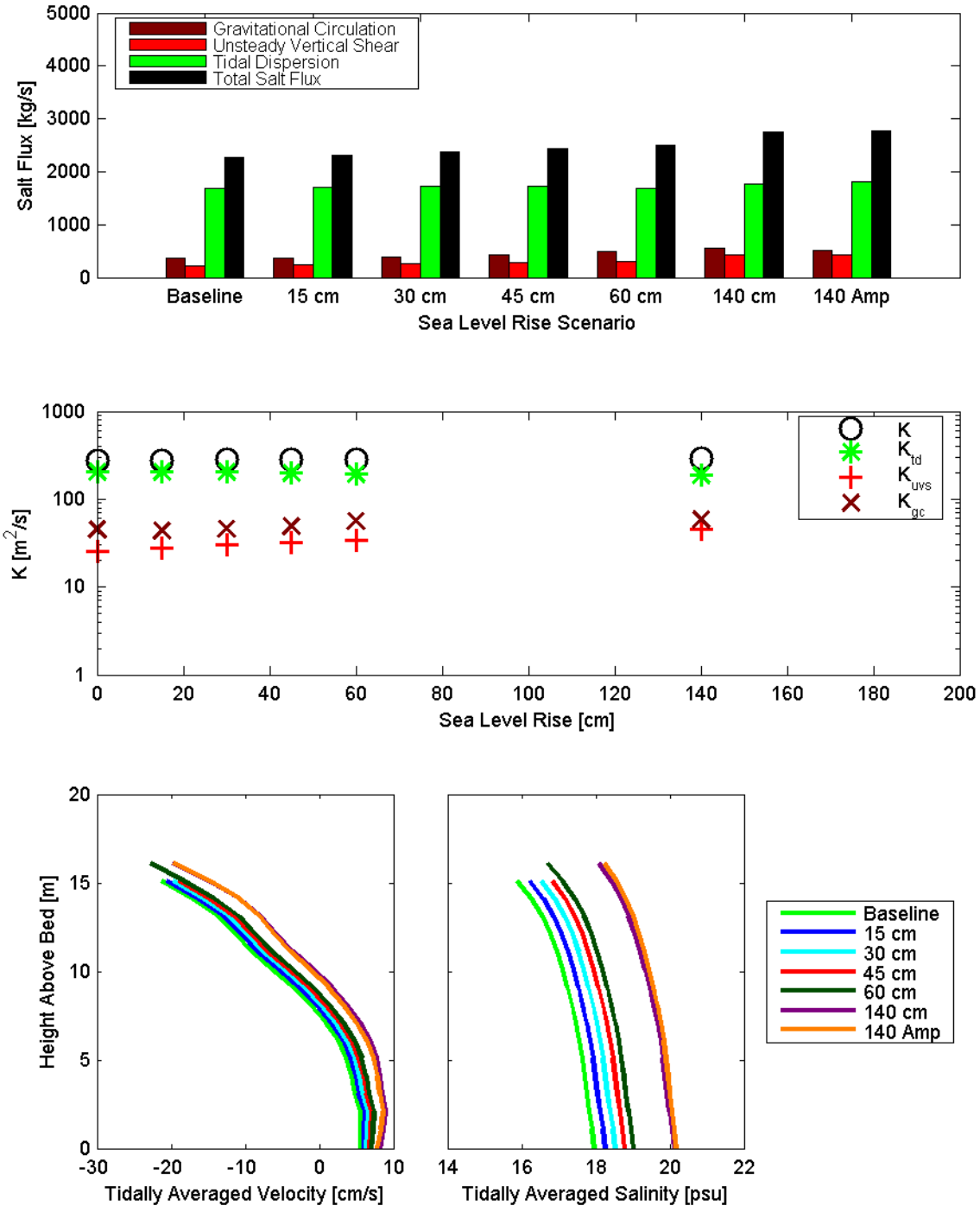

Figure 8.4-66 Dispersive salt flux (top), dispersion coefficients and dispersion coefficient components (middle) and tidally averaged velocity (bottom left) and tidally averaged salinity (bottom right) calculated for each scenario at cross-section 18, located east of the Mothball Fleet, for the October 13, 2002 through November 10, 2002 analysis period.

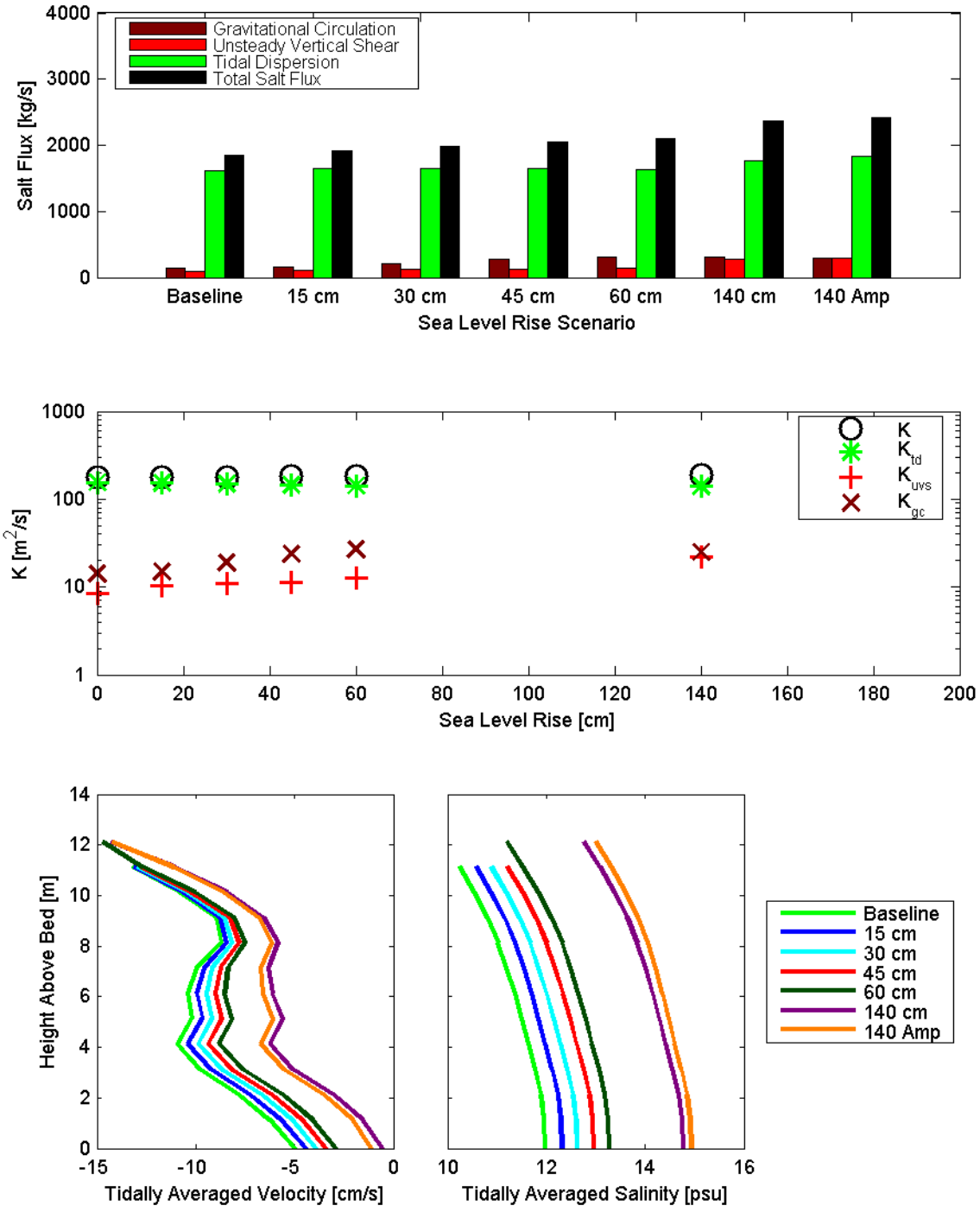

Figure 8.4-67 Dispersive salt flux (top), dispersion coefficients and dispersion coefficient components (middle) and tidally averaged velocity (bottom left) and tidally averaged salinity (bottom right) calculated for each scenario at cross-section 19, extending from Edith Point to Bahia, for the July 15, 2002 through August 12, 2002 analysis period.

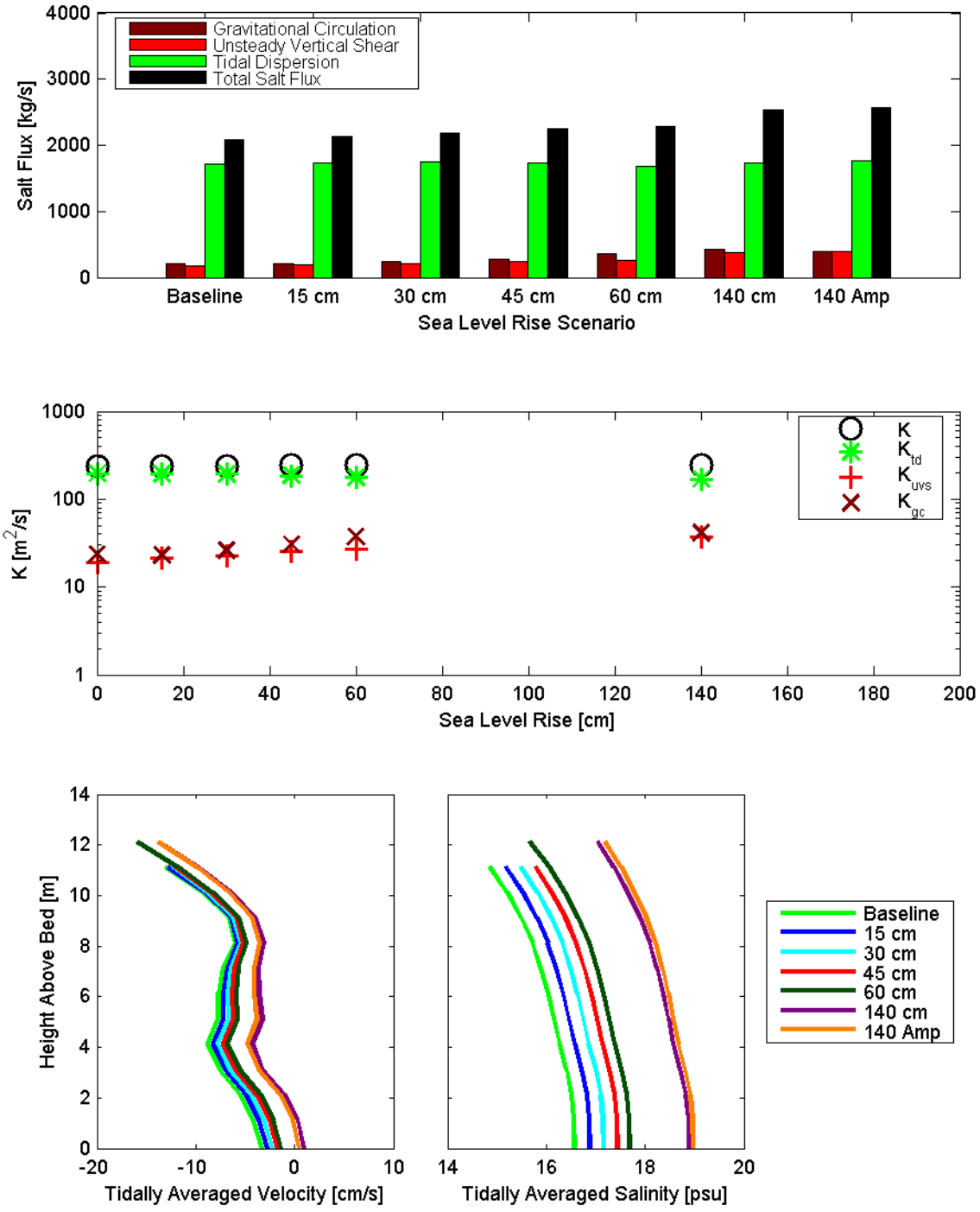

Figure 8.4-68 Dispersive salt flux (top), dispersion coefficients and dispersion coefficient components (middle) and tidally averaged velocity (bottom left) and tidally averaged salinity (bottom right) calculated for each scenario at cross-section 19, extending from Edith Point to Bahia, for the October 13, 2002 through November 10, 2002 analysis period.

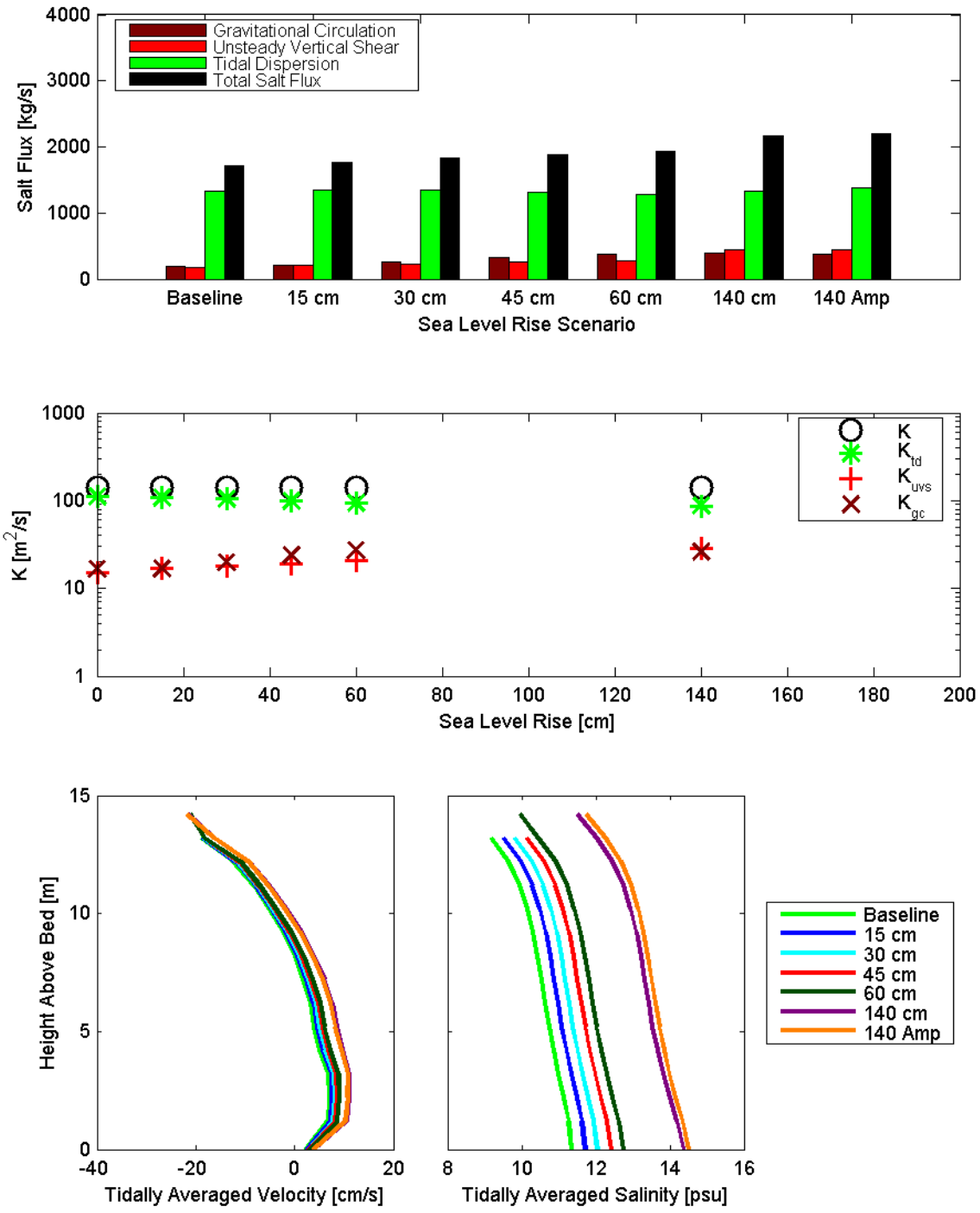

Figure 8.4-69 Dispersive salt flux (top), dispersion coefficients and dispersion coefficient components (middle) and tidally averaged velocity (bottom left) and tidally averaged salinity (bottom right) calculated for each scenario at cross-section 20, extending from Point Edith to Suisun Slough, for the July 15, 2002 through August 12, 2002 analysis period.

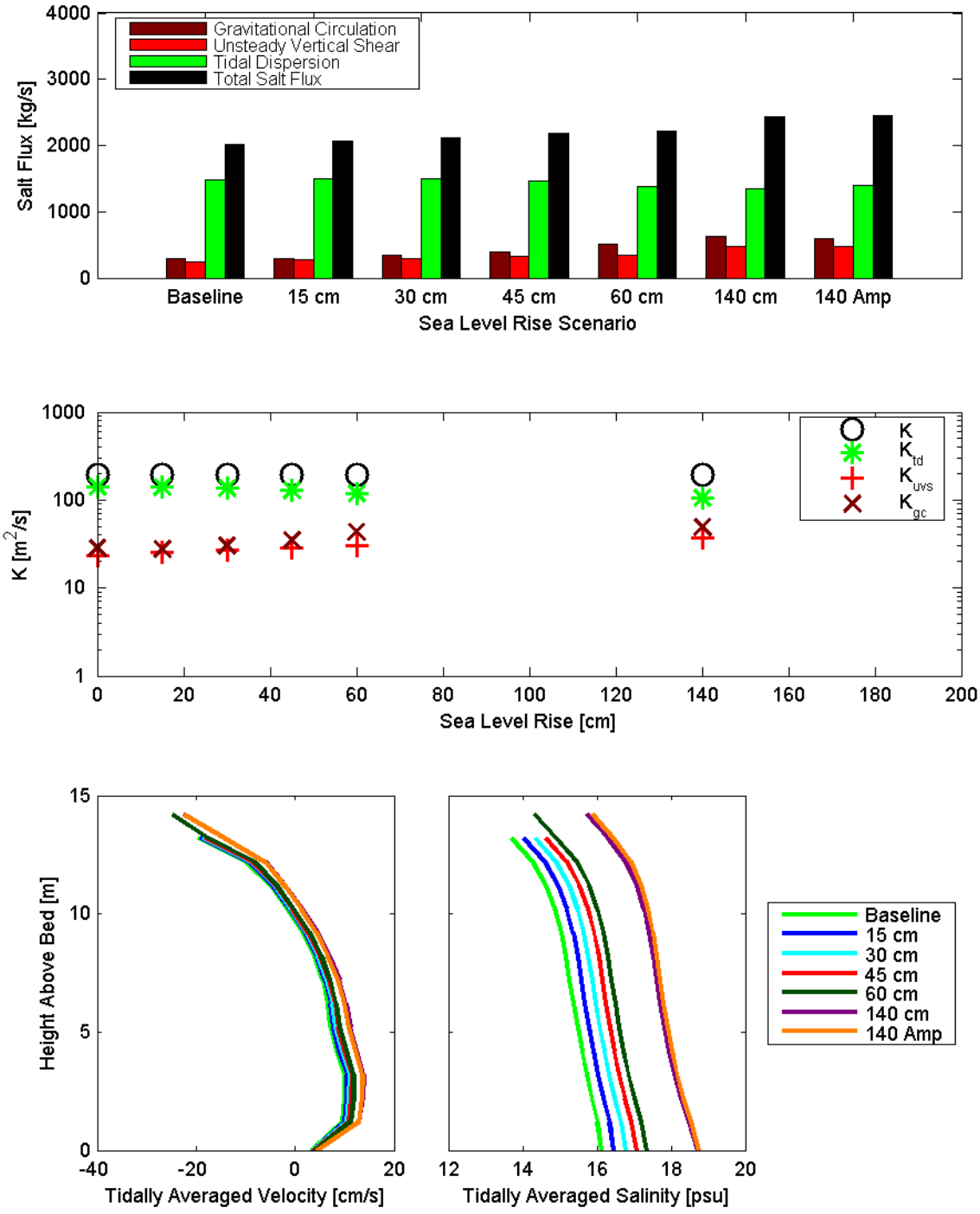

Figure 8.4-70 Dispersive salt flux (top), dispersion coefficients and dispersion coefficient components (middle) and tidally averaged velocity (bottom left) and tidally averaged salinity (bottom right) calculated for each scenario at cross-section 20, extending from Point Edith to Suisun Slough, for the October 13, 2002 through November 10, 2002 analysis period.

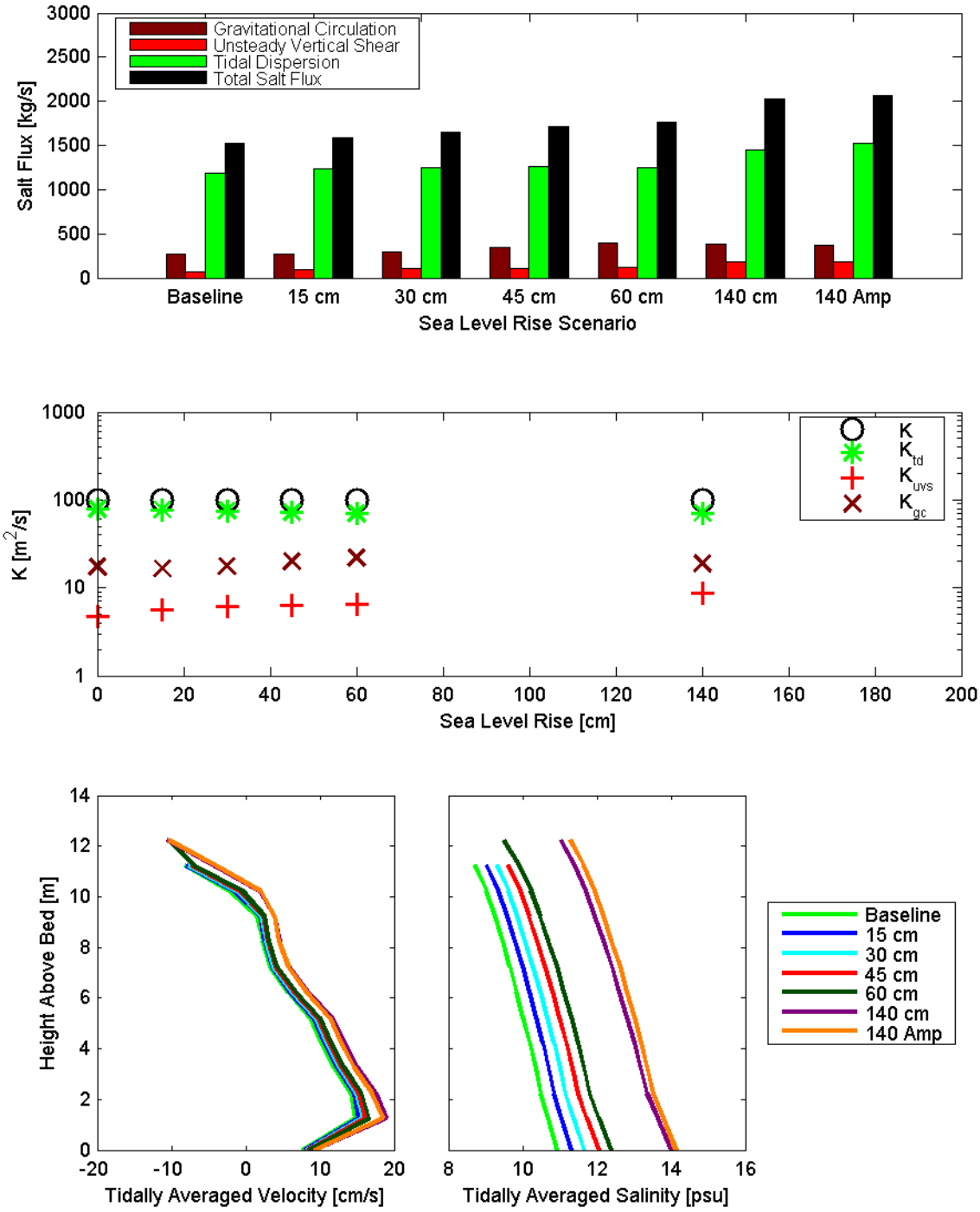

Figure 8.4-71 Dispersive salt flux (top), dispersion coefficients and dispersion coefficient components (middle) and tidally averaged velocity (bottom left) and tidally averaged salinity (bottom right) calculated for each scenario at cross-section 21, extending from Hastings Slough to Montezuma Slough, for the July 15, 2002 through August 12, 2002 analysis period.

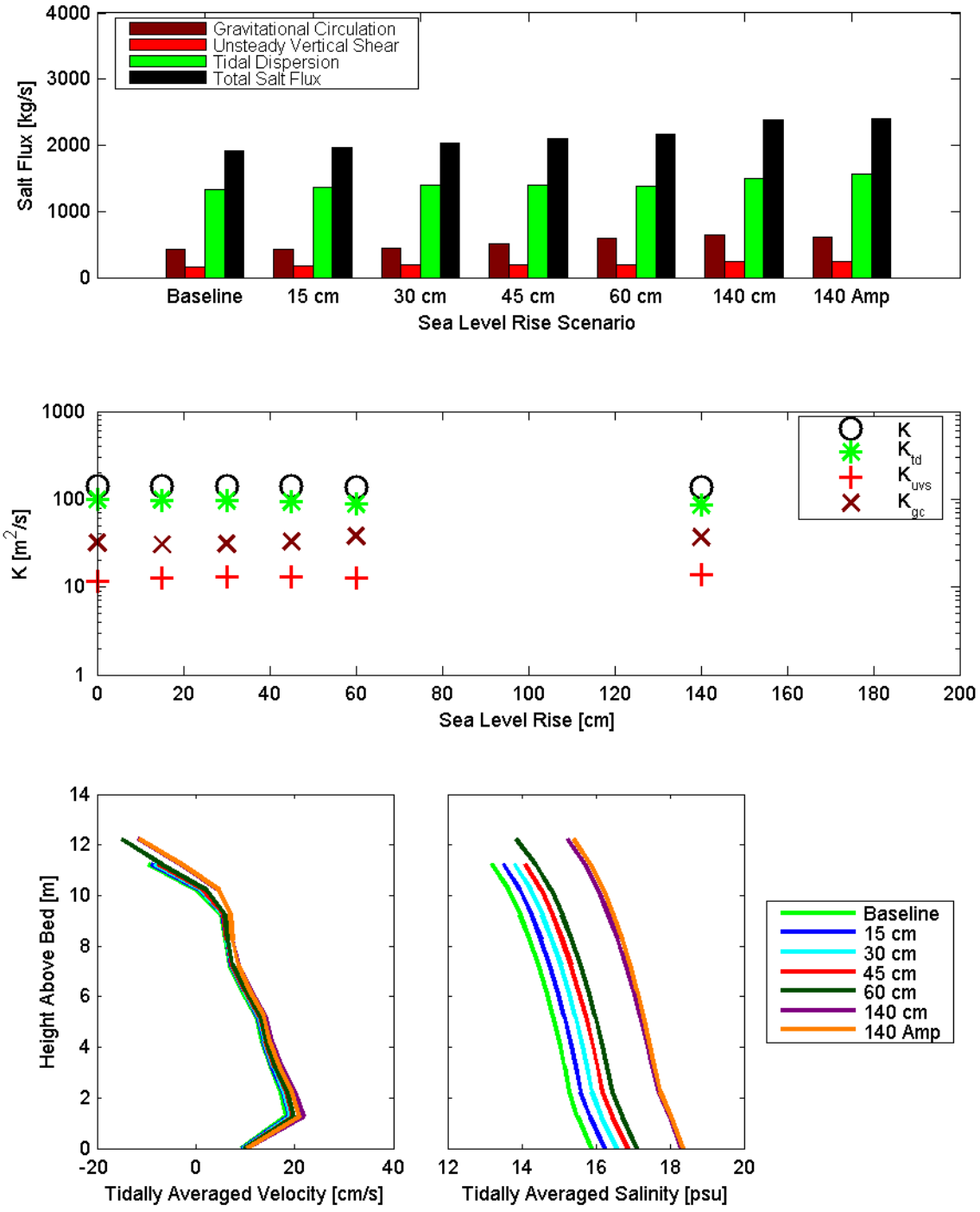

Figure 8.4-72 Dispersive salt flux (top), dispersion coefficients and dispersion coefficient components (middle) and tidally averaged velocity (bottom left) and tidally averaged salinity (bottom right) calculated for each scenario at cross-section 21, extending from Hastings Slough to Montezuma Slough, for the October 13, 2002 through November 10, 2002 analysis period.

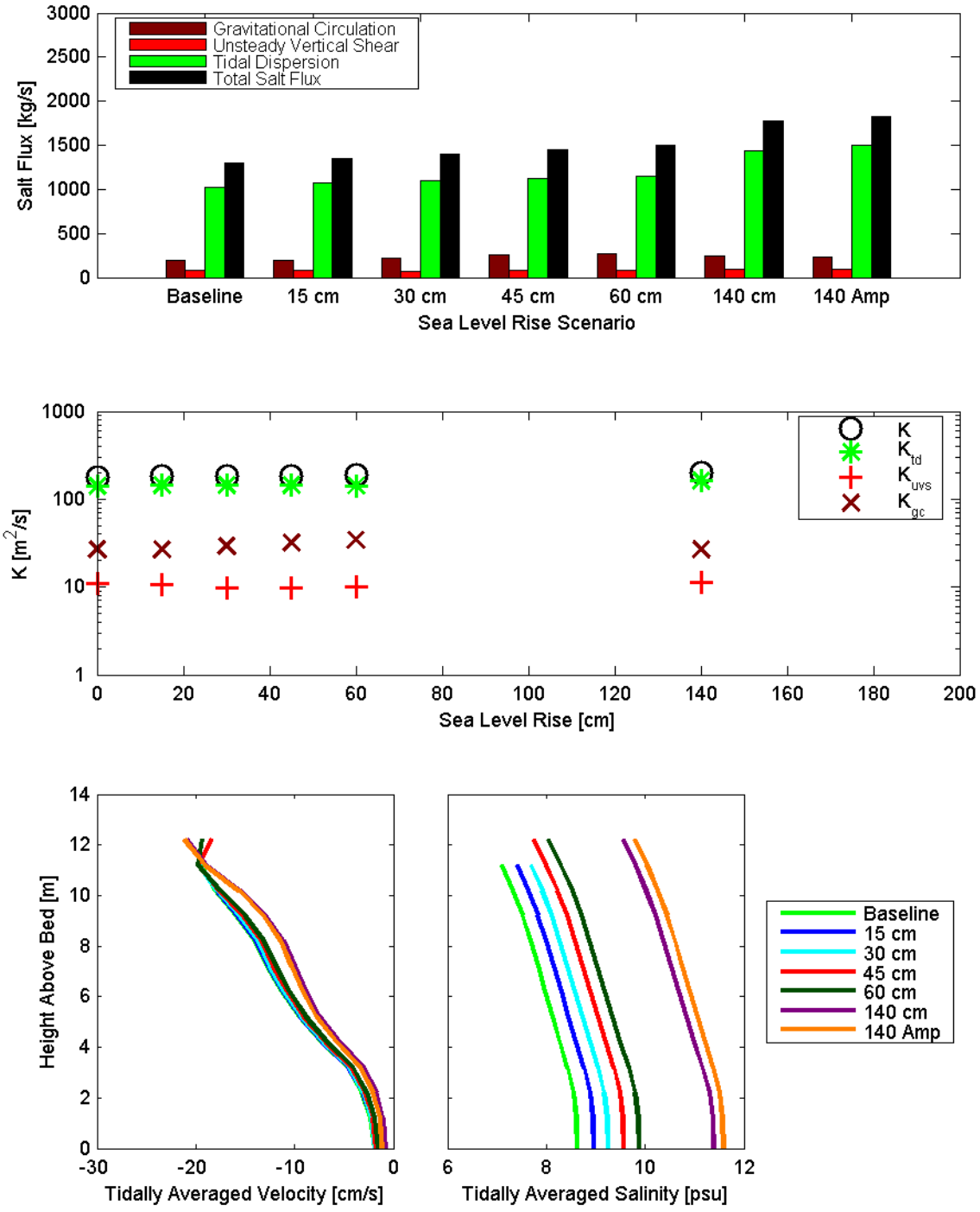

Figure 8.4-73 Dispersive salt flux (top), dispersion coefficients and dispersion coefficient components (middle) and tidally averaged velocity (bottom left) and tidally averaged salinity (bottom right) calculated for each scenario at cross-section 22, extending from Port Chicago to Montezuma Slough, for the July 15, 2002 through August 12, 2002 analysis period.

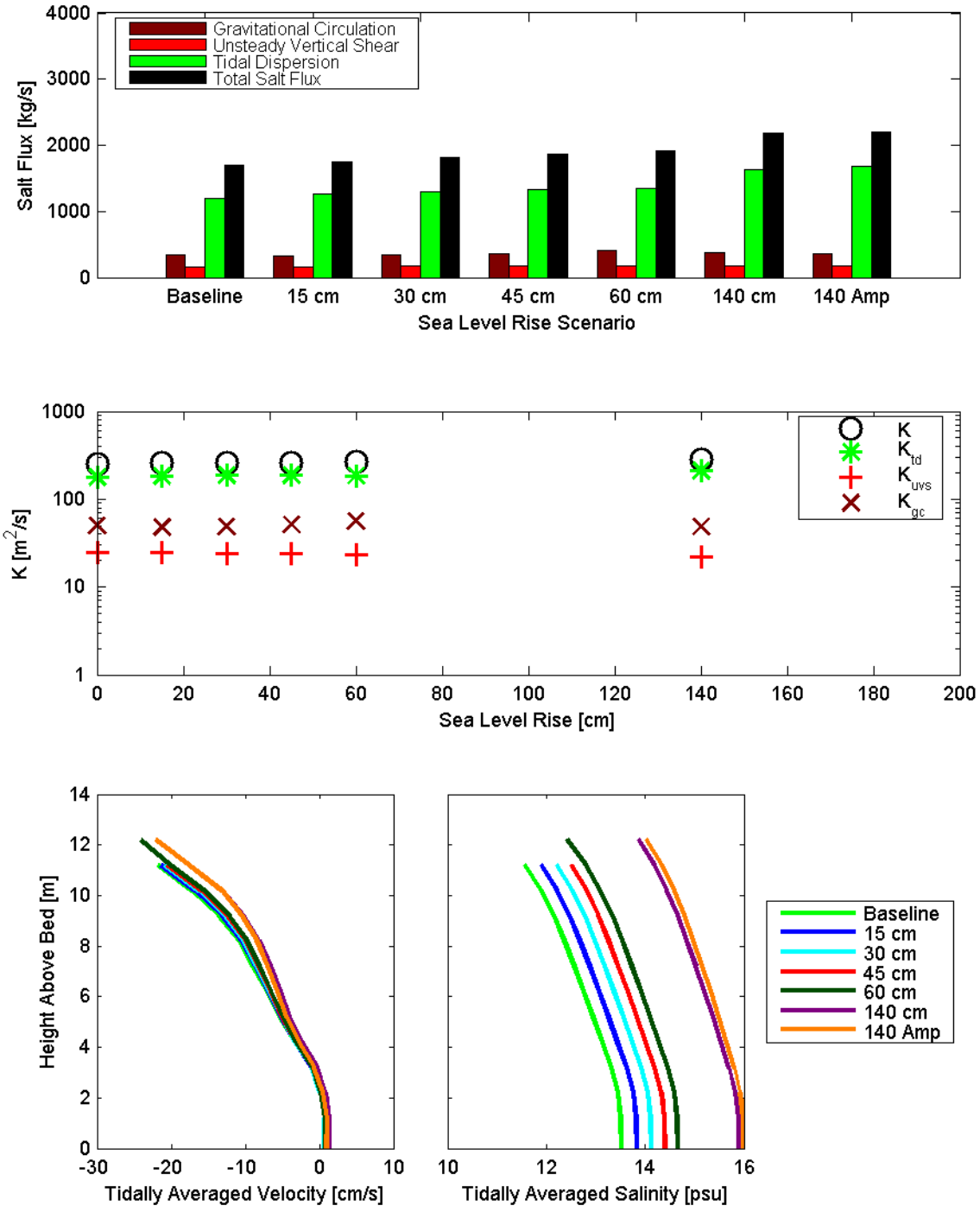

Figure 8.4-74 Dispersive salt flux (top), dispersion coefficients and dispersion coefficient components (middle) and tidally averaged velocity (bottom left) and tidally averaged salinity (bottom right) calculated for each scenario at cross-section 22, extending from Point Chicago to Montezuma Slough, for the October 13, 2002 through November 10, 2002 analysis period.

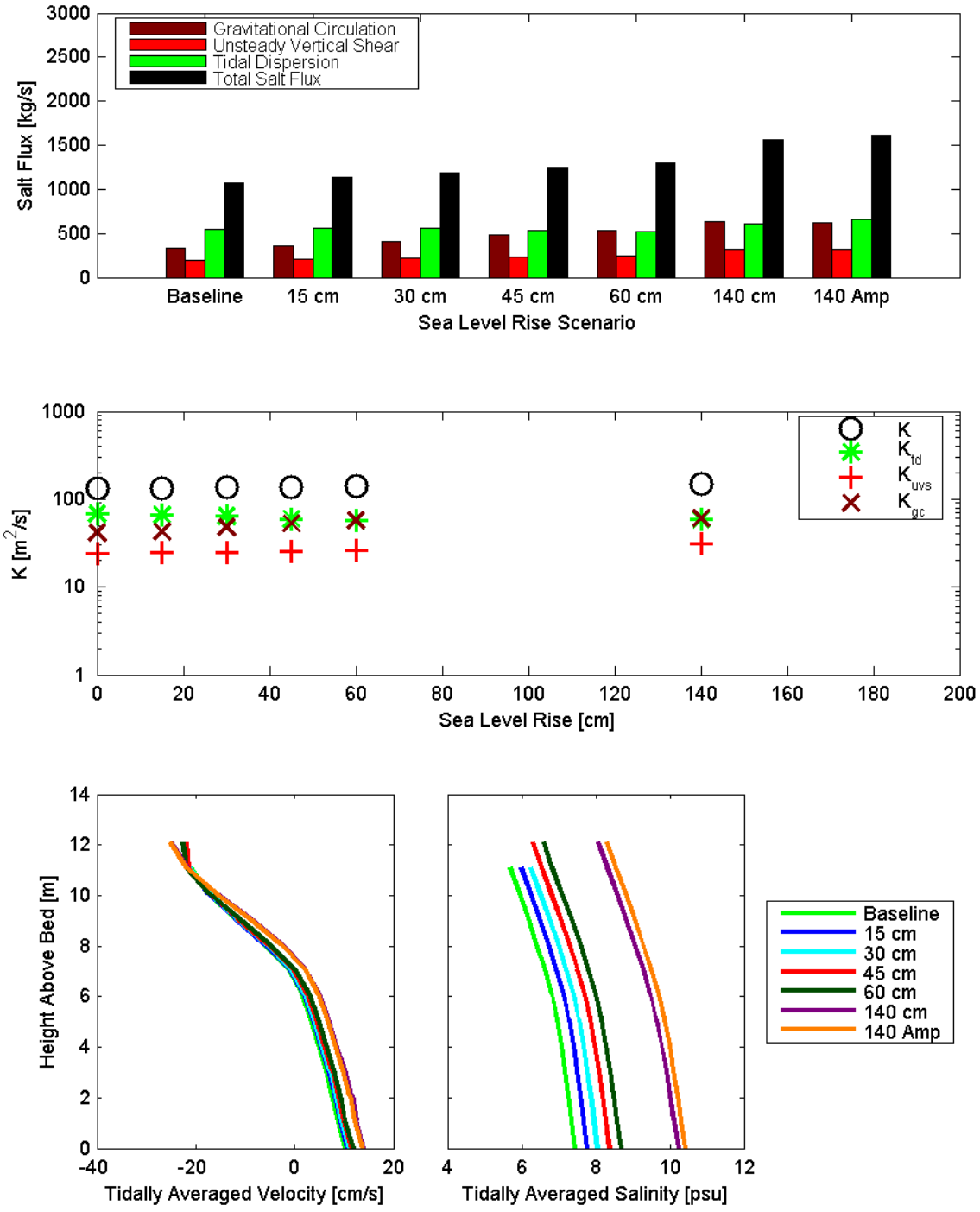

Figure 8.4-75 Dispersive salt flux (top), dispersion coefficients and dispersion coefficient components (middle) and tidally averaged velocity (bottom left) and tidally averaged salinity (bottom right) calculated for each scenario at cross-section 23, extending from Concord to Montezuma Slough for the July 15, 2002 through August 12, 2002 analysis period.

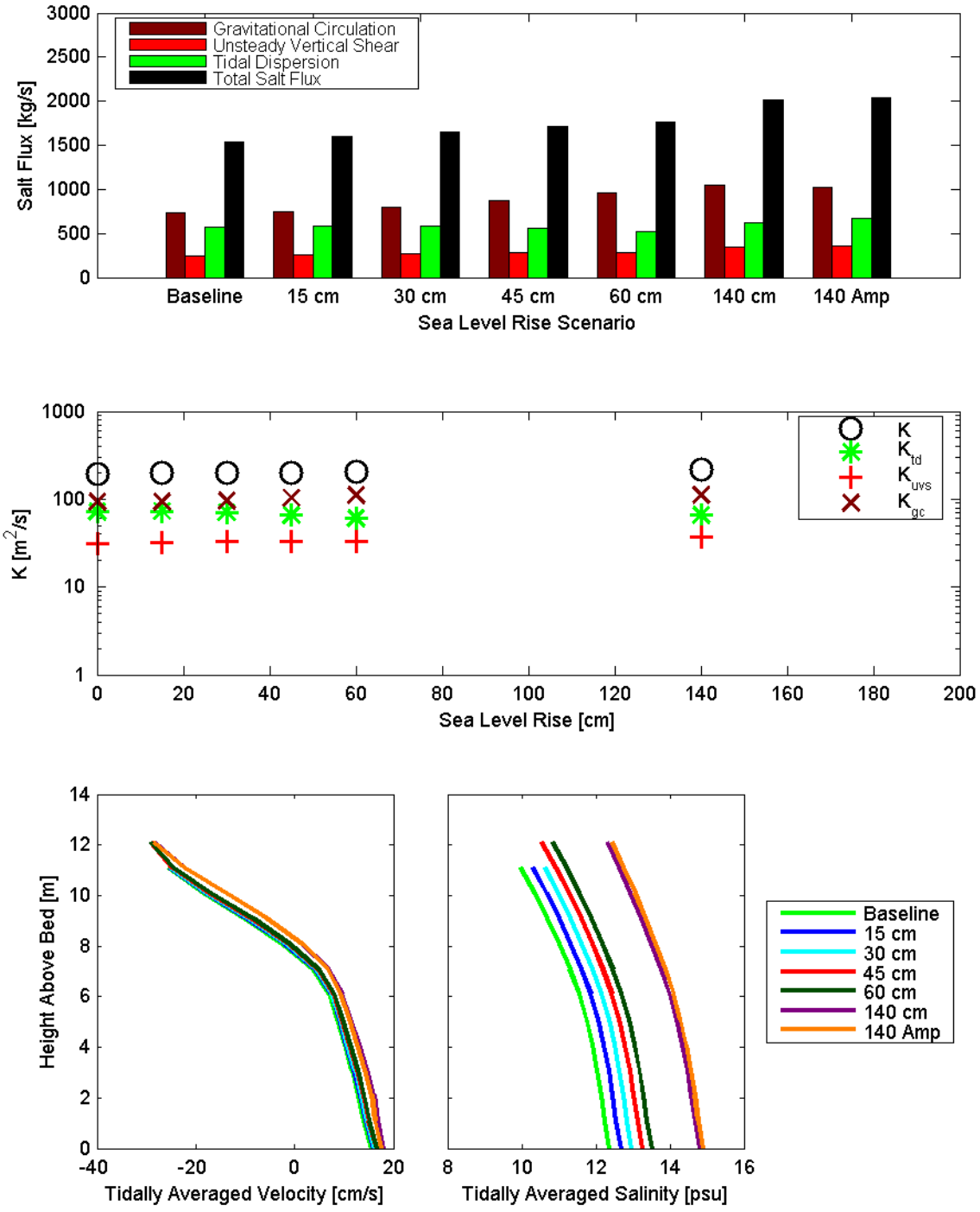

Figure 8.4-76 Dispersive salt flux (top), dispersion coefficients and dispersion coefficient components (middle) and tidally averaged velocity (bottom left) and tidally averaged salinity (bottom right) calculated for each scenario at cross-section 23, extending from Concord to Montezuma Slough, for the October 13, 2002 through November 10, 2002 analysis period.

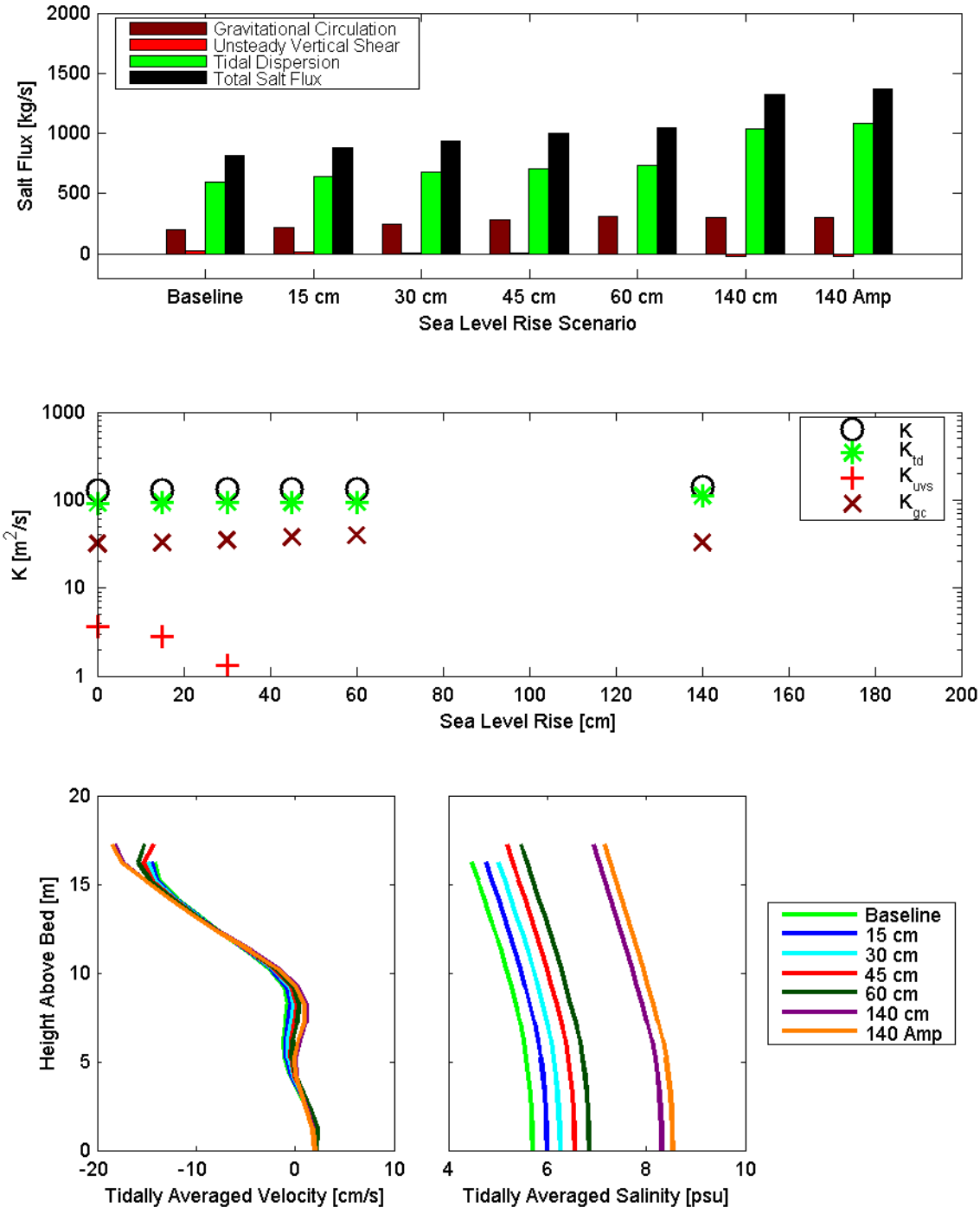

Figure 8.4-77 Dispersive salt flux (top), dispersion coefficients and dispersion coefficient components (middle) and tidally averaged velocity (bottom left) and tidally averaged salinity (bottom right) calculated for each scenario at cross-section 24, extending from Stake Point to Montezuma Slough, for the July 15, 2002 through August 12, 2002 analysis period.

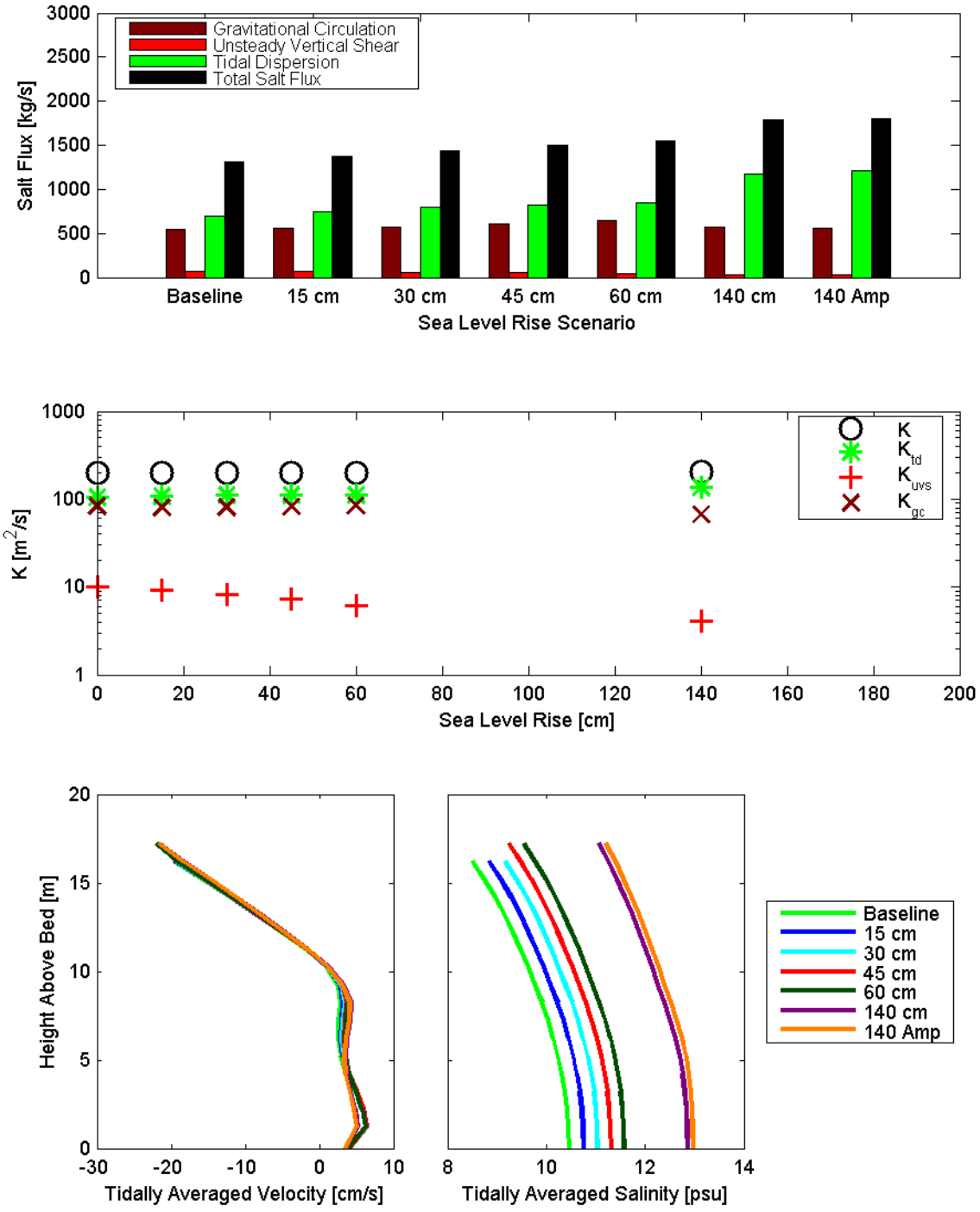

Figure 8.4-78 Dispersive salt flux (top), dispersion coefficients and dispersion coefficient components (middle) and tidally averaged velocity (bottom left) and tidally averaged salinity (bottom right) calculated for each scenario at cross-section 24, extending from Stake Point to Montezuma Slough, for the October 13, 2002 through November 10, 2002 analysis period.

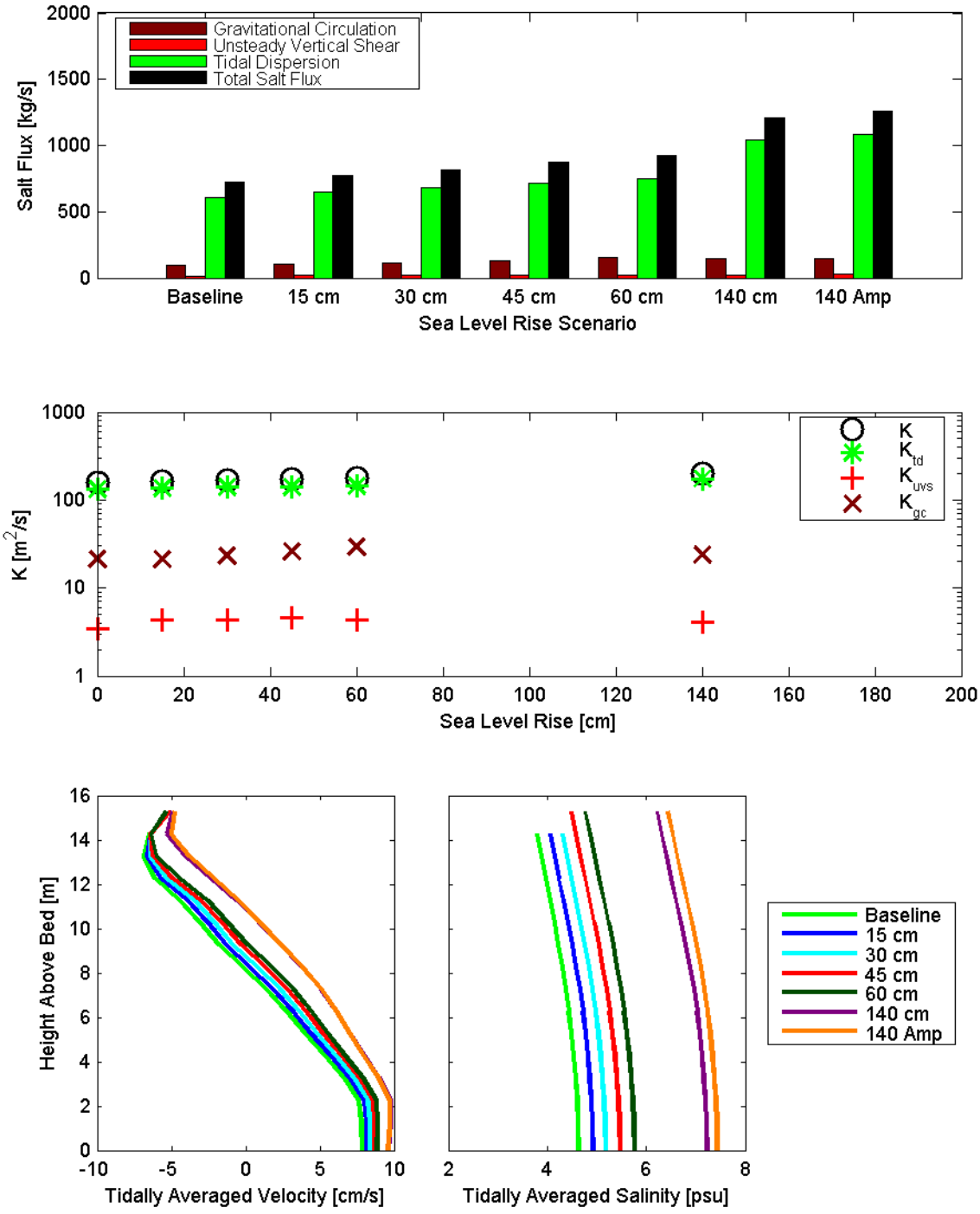

Figure 8.4-79 Dispersive salt flux (top), dispersion coefficients and dispersion coefficient components (middle) and tidally averaged velocity (bottom left) and tidally averaged salinity (bottom right) calculated for each scenario at cross-section 25, extending from Mallard Island to Montezuma Slough, for the July 15, 2002 through August 12, 2002 analysis period.

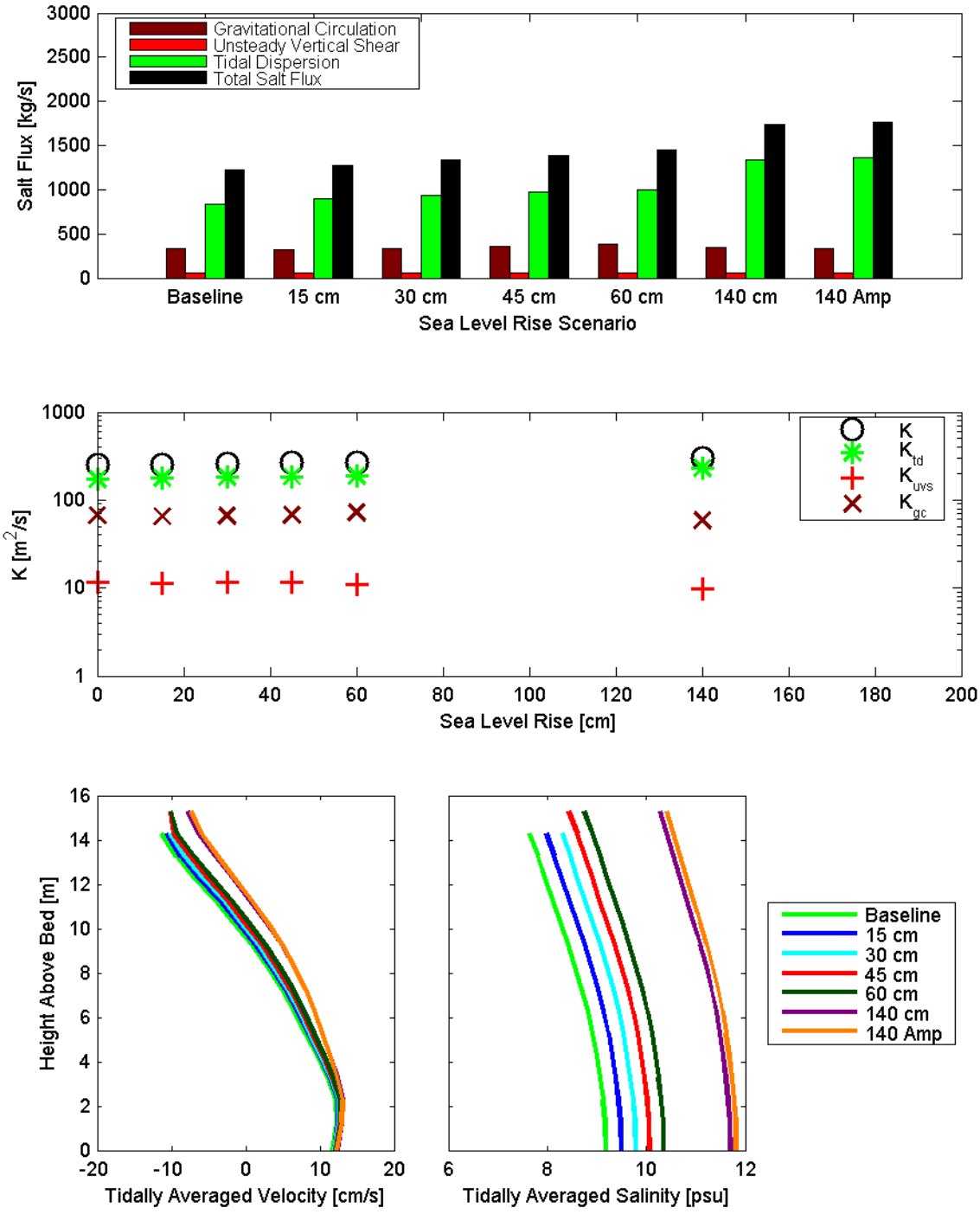

Figure 8.4-80 Dispersive salt flux (top), dispersion coefficients and dispersion coefficient components (middle) and tidally averaged velocity (bottom left) and tidally averaged salinity (bottom right) calculated for each scenario at cross-section 25, extending from Mallard Island to Montezuma Slough, for the October 13, 2002 through November 10, 2002 analysis period.

8.4.5 Western Delta Cross-Sections

Dispersion coefficients and salt fluxes were estimated at the seven cross-sections in the western Delta (cross-section 26 to cross-section 32) shown in Figure 8.3-1. In Figure 8.4-81 through Figure 8.4-94, analysis results are provided for each cross-section that summarize the dispersion analysis at that location for a given analysis period. The top panel shows the contributions of individual processes to dispersive salt flux (advective salt flux is not shown) for each SLR scenario. The second type of figure shows the overall dispersion coefficient (K), the portion of the dispersion coefficient associated with gravitational circulation (K_{gc}), the portion of the dispersion coefficient associated with unsteady vertical shear dispersion processes (K_{uvs}), and the portion of the dispersion coefficient associated with tidal dispersion processes (K_{td}) for each SLR scenario. The bottom panel shows the period averaged velocity profile and salinity profile at the deepest point in the cross-section for each SLR scenario.

The dispersion coefficients are smaller on average in the western Delta than in San Francisco Bay. Tidal dispersion processes are the most important salt intrusion processes in most cross-sections for both analysis periods. Gravitational circulation and unsteady vertical shear dispersion are both substantial for all cross-sections in the western Delta and gravitational circulation is the strongest salt intrusion process for some scenarios at cross-section 28, extending from Antioch to Montezuma Landing, during the October 13, 2002 through November 10, 2002 analysis period (Figure 8.4-86). Gravitational circulation is more pronounced in the October 13, 2002 through November 10, 2002 analysis period than the July 15, 2002 through August 12, 2002 analysis period, because salt has intruded further into the Delta by the time of the October 13, 2002 through November 10, 2002 analysis period, thereby allowing stratification to develop. In both analysis periods, the dispersive salt fluxes increase with sea level rise due to increased salinity in the western Delta. The dispersion coefficients also increase significantly with SLR at most cross-sections, primarily due to increases in tidal dispersion. It is likely that these predicted increases result from substantial increases in tidal prism (Figure 8.4-19 and Figure 8.4-20). At several cross-sections, the strength of gravitational circulation also increases with sea level rise, probably due to increased depth (Monismith et al., 2002). At most cross-sections in the western Delta, the predicted vertical shear and stratification increase with sea level rise, particularly during the July 15, 2002 through August 12, 2002 analysis period.

The results in the western Delta are generally consistent with the flux analysis of sea level rise scenarios performed as part of the DRMS studies (Gross et al., 2007b). One substantial difference in this analysis is that all cross-sections extend across the Delta, while in the salt flux analysis for DRMS (Gross et al., 2007b), some cross-sections extended only across the Sacramento River. The flux analysis of various Delta outflows performed as part of the DRMS studies (Gross et al., 2007a) was consistent with these results for low Delta outflows. At higher Delta outflows, the ocean derived salt is flushed out of the western Delta and the flux analysis could not be performed.

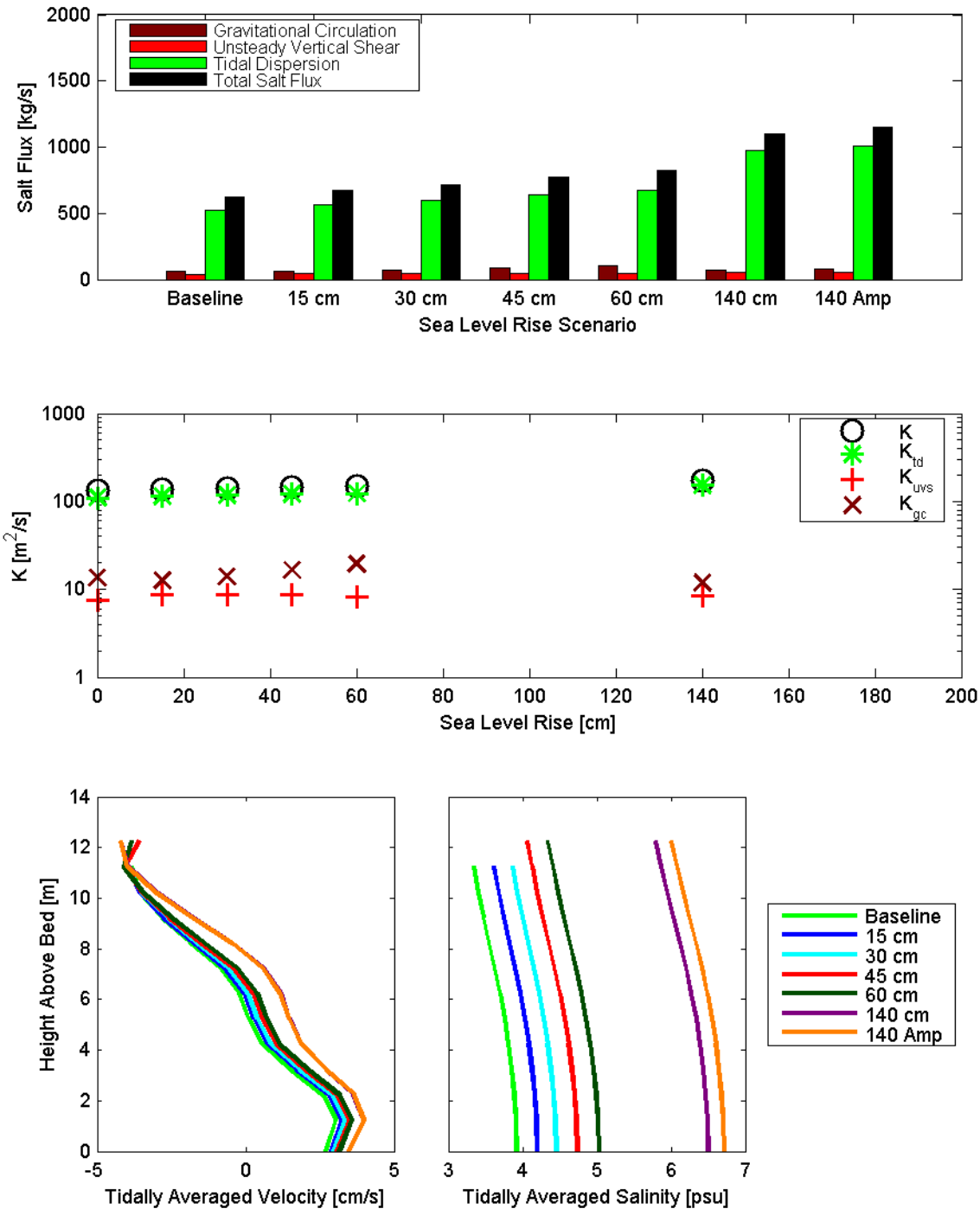

Figure 8.4-81 Dispersive salt flux (top), dispersion coefficients and dispersion coefficient components (middle) and tidally averaged velocity (bottom left) and tidally averaged salinity (bottom right) calculated for each scenario at cross-section 26, extending from Pittsburg to Montezuma Slough, for the July 15, 2002 through August 12, 2002 analysis period.

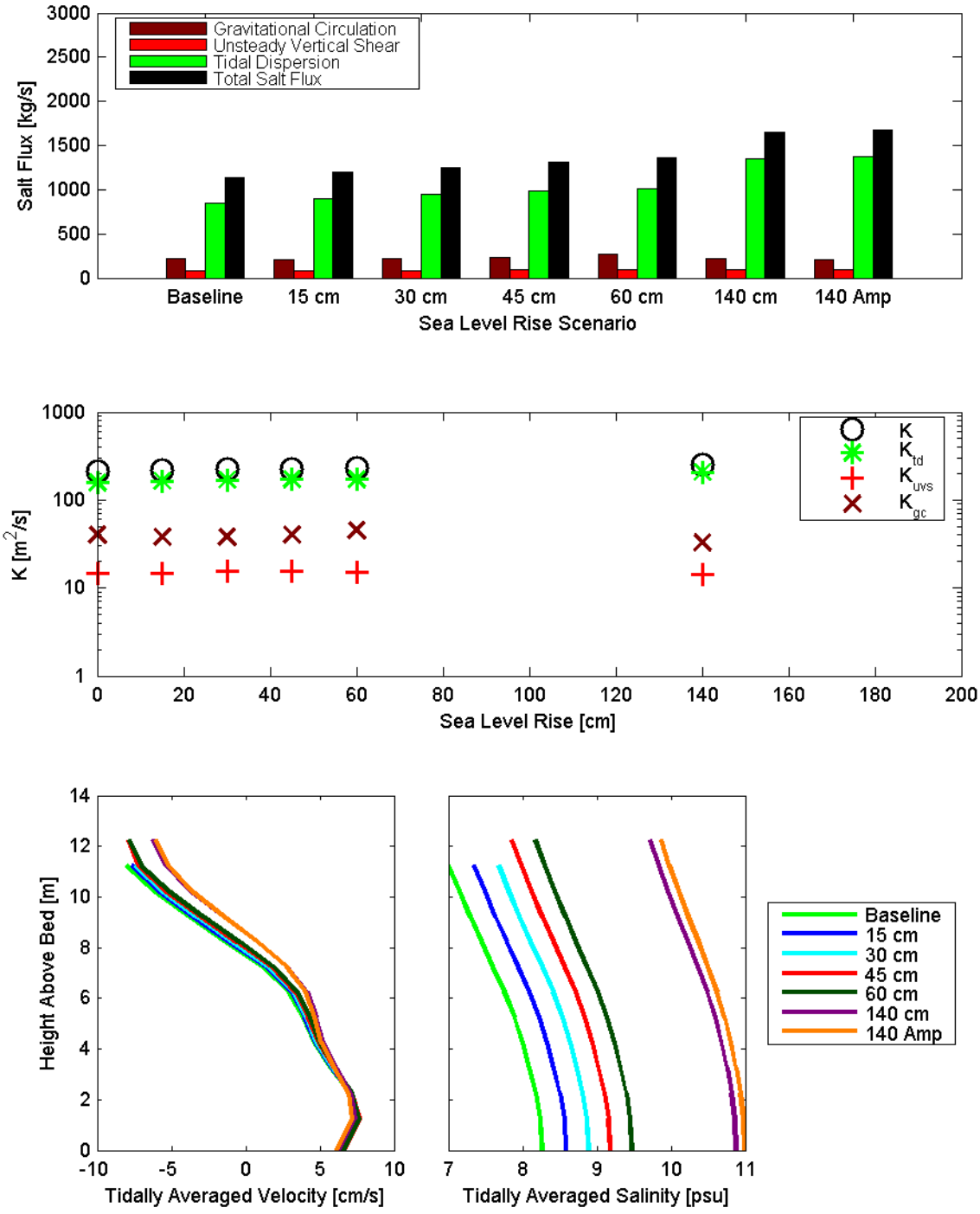

Figure 8.4-82 Dispersive salt flux (top), dispersion coefficients and dispersion coefficient components (middle) and tidally averaged velocity (bottom left) and tidally averaged salinity (bottom right) calculated for each scenario at cross-section 26, extending from Pittsburg to Montezuma Slough, for the October 13, 2002 through November 10, 2002 analysis period.

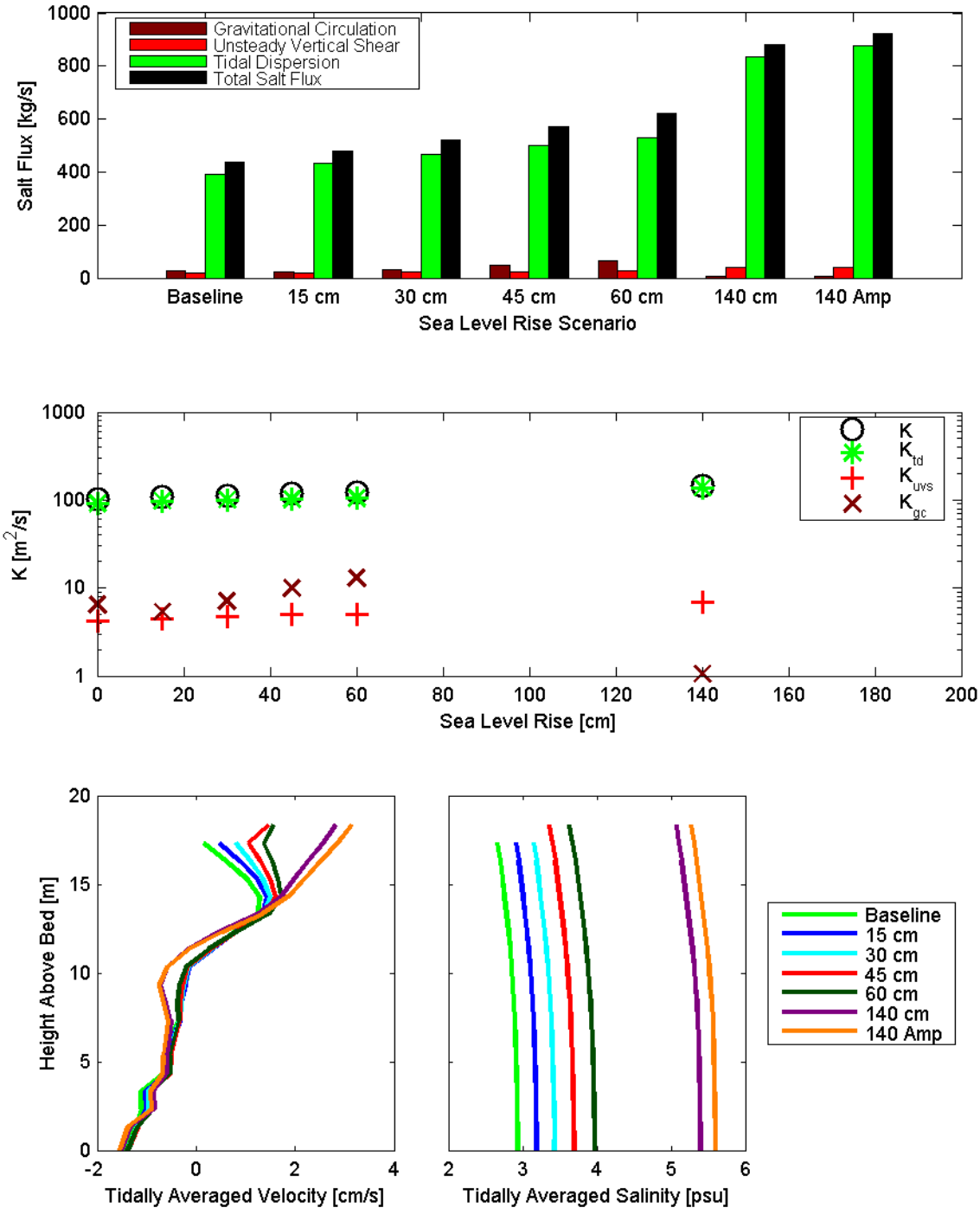

Figure 8.4-83 Dispersive salt flux (top), dispersion coefficients and dispersion coefficient components (middle) and tidally averaged velocity (bottom left) and tidally averaged salinity (bottom right) calculated for each scenario at cross-section 27, extending from Pittsburg to Collinsville. for the July 15, 2002 through August 12, 2002 analysis period.

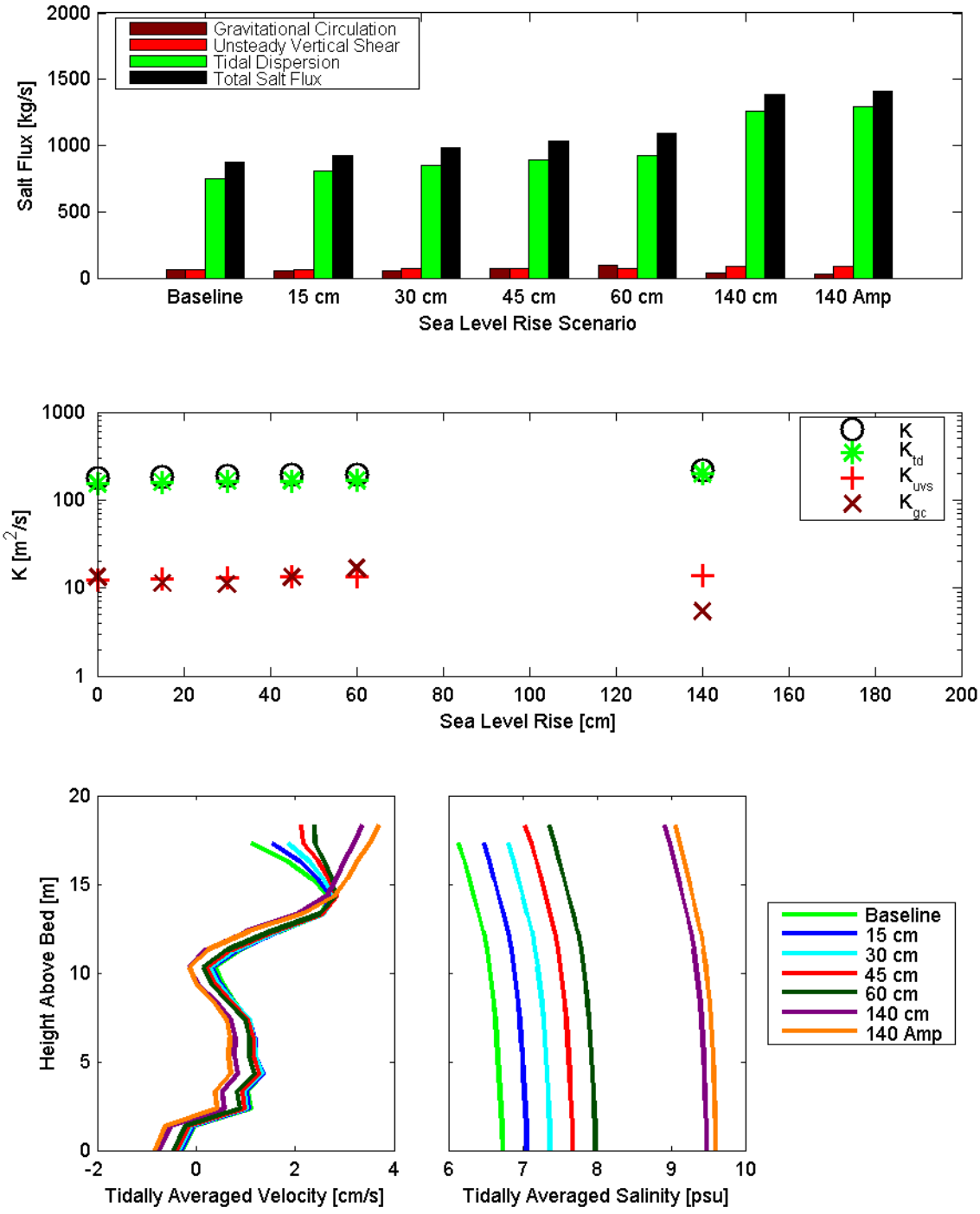

Figure 8.4-84 Dispersive salt flux (top), dispersion coefficients and dispersion coefficient components (middle) and tidally averaged velocity (bottom left) and tidally averaged salinity (bottom right) calculated for each scenario at cross-section 27, extending from Pittsburg to Collinsville, for the October 13, 2002 through November 10, 2002 analysis period.

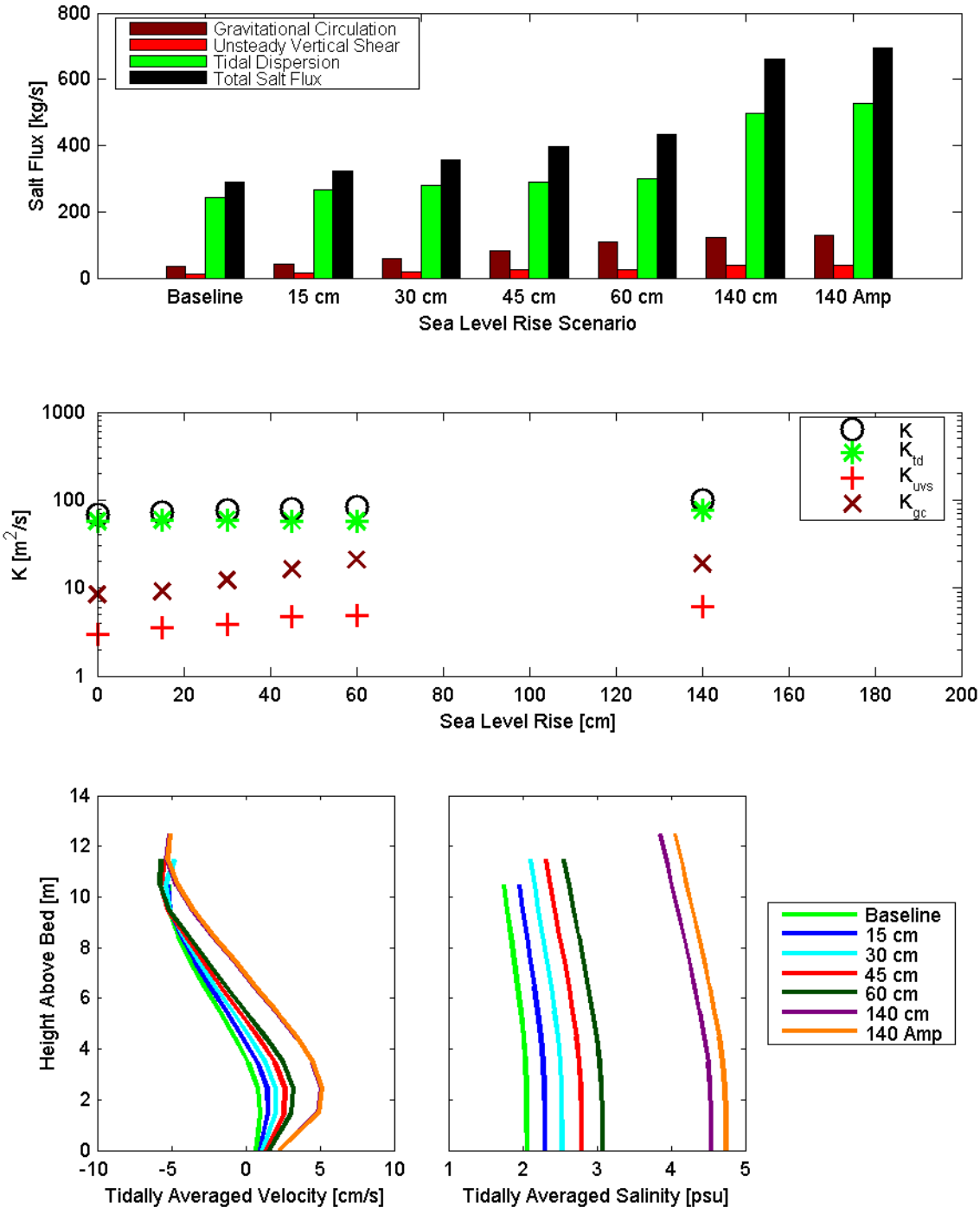

Figure 8.4-85 Dispersive salt flux (top), dispersion coefficients and dispersion coefficient components (middle) and tidally averaged velocity (bottom left) and tidally averaged salinity (bottom right) calculated for each scenario at cross-section 28, extending from Antioch to Montezuma Landing, for the July 15, 2002 through August 12, 2002 analysis period.

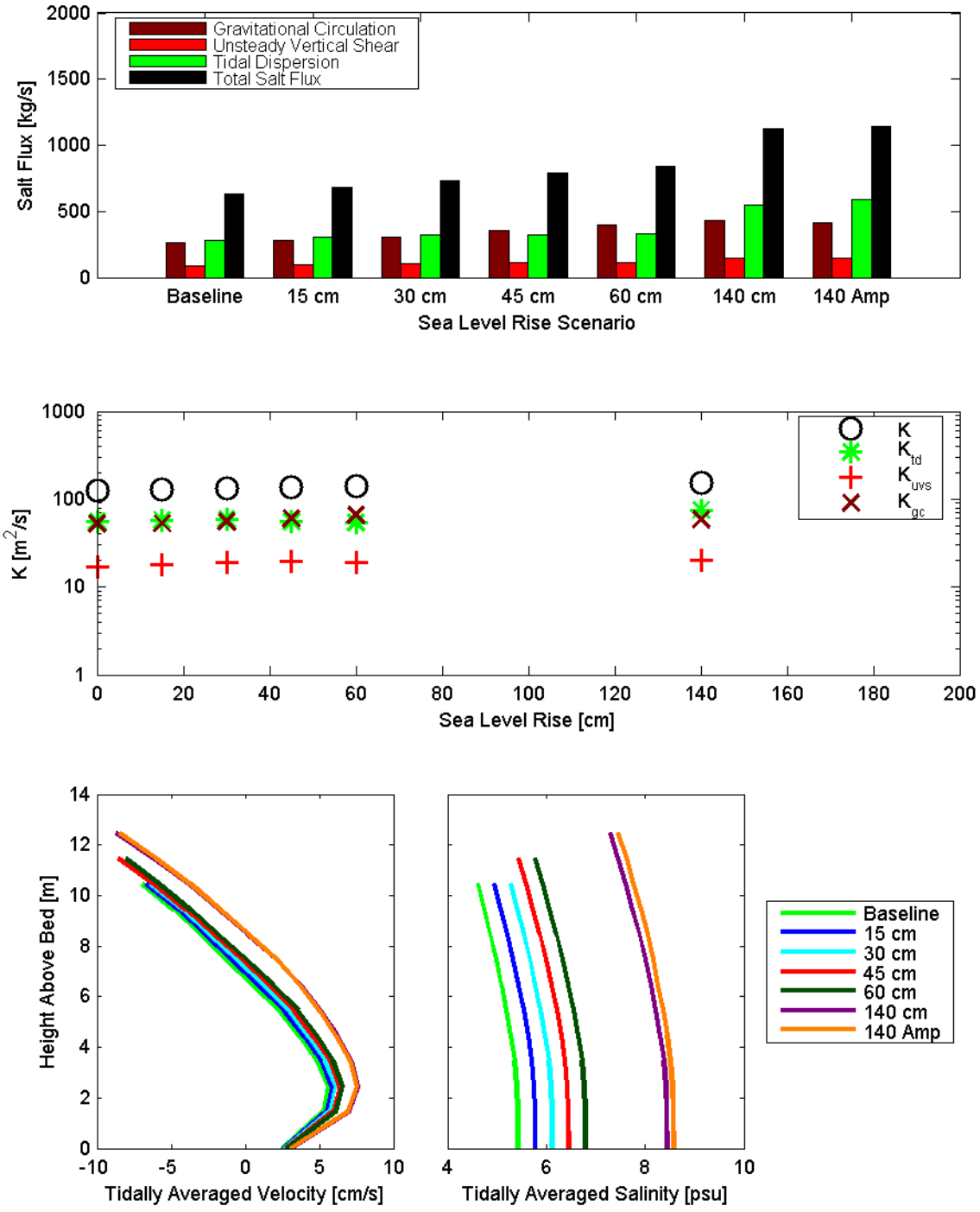

Figure 8.4-86 Dispersive salt flux (top), dispersion coefficients and dispersion coefficient components (middle) and tidally averaged velocity (bottom left) and tidally averaged salinity (bottom right) calculated for each scenario at cross-section 28, extending from Antioch to Montezuma Landing, for the October 13, 2002 through November 10, 2002 analysis period.

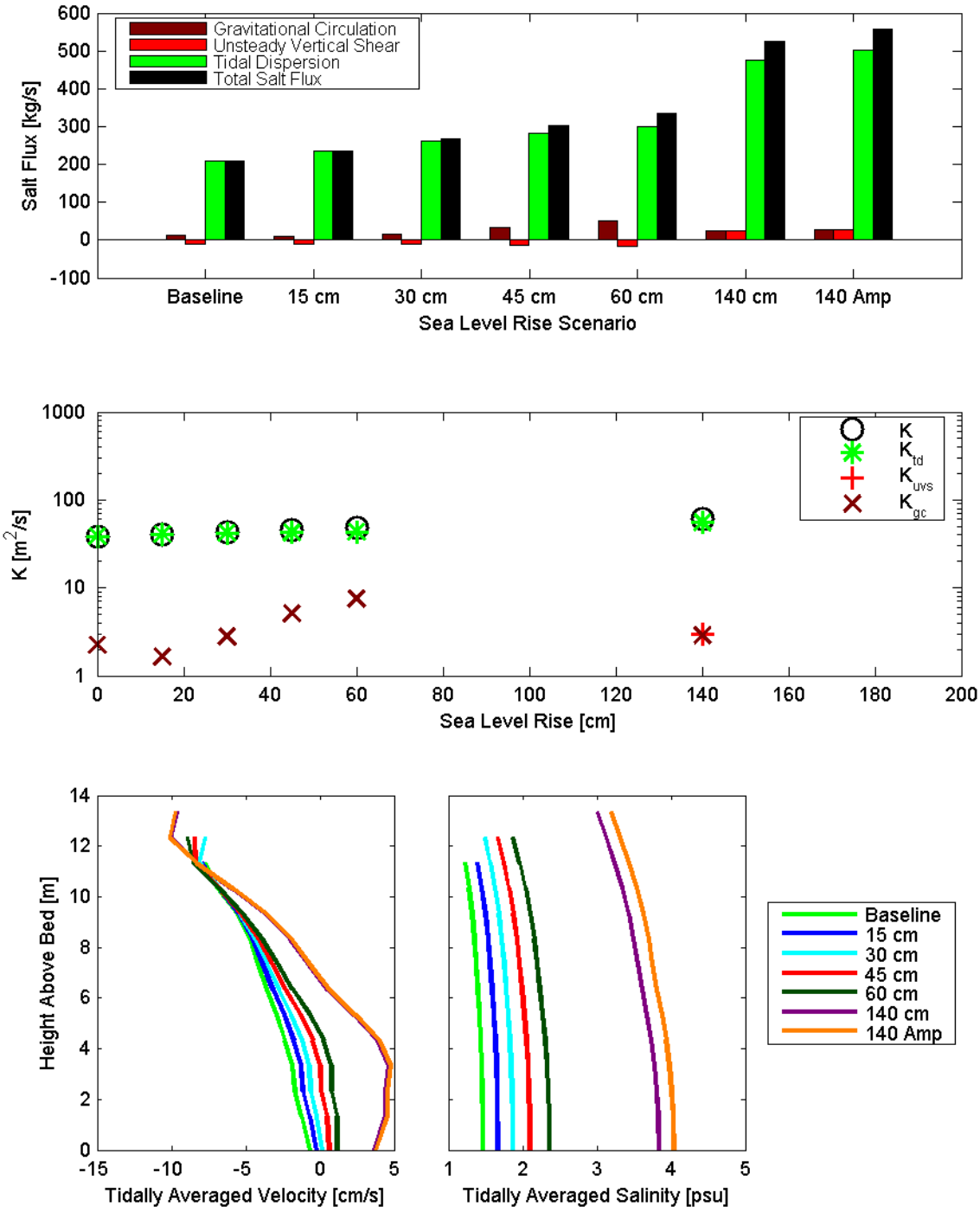

Figure 8.4-87 Dispersive salt flux (top), dispersion coefficients and dispersion coefficient components (middle) and tidally averaged velocity (bottom left) and tidally averaged salinity (bottom right) calculated for each scenario at cross-section 29, extending through Sherman Lake, for the July 15, 2002 through August 12, 2002 analysis period.

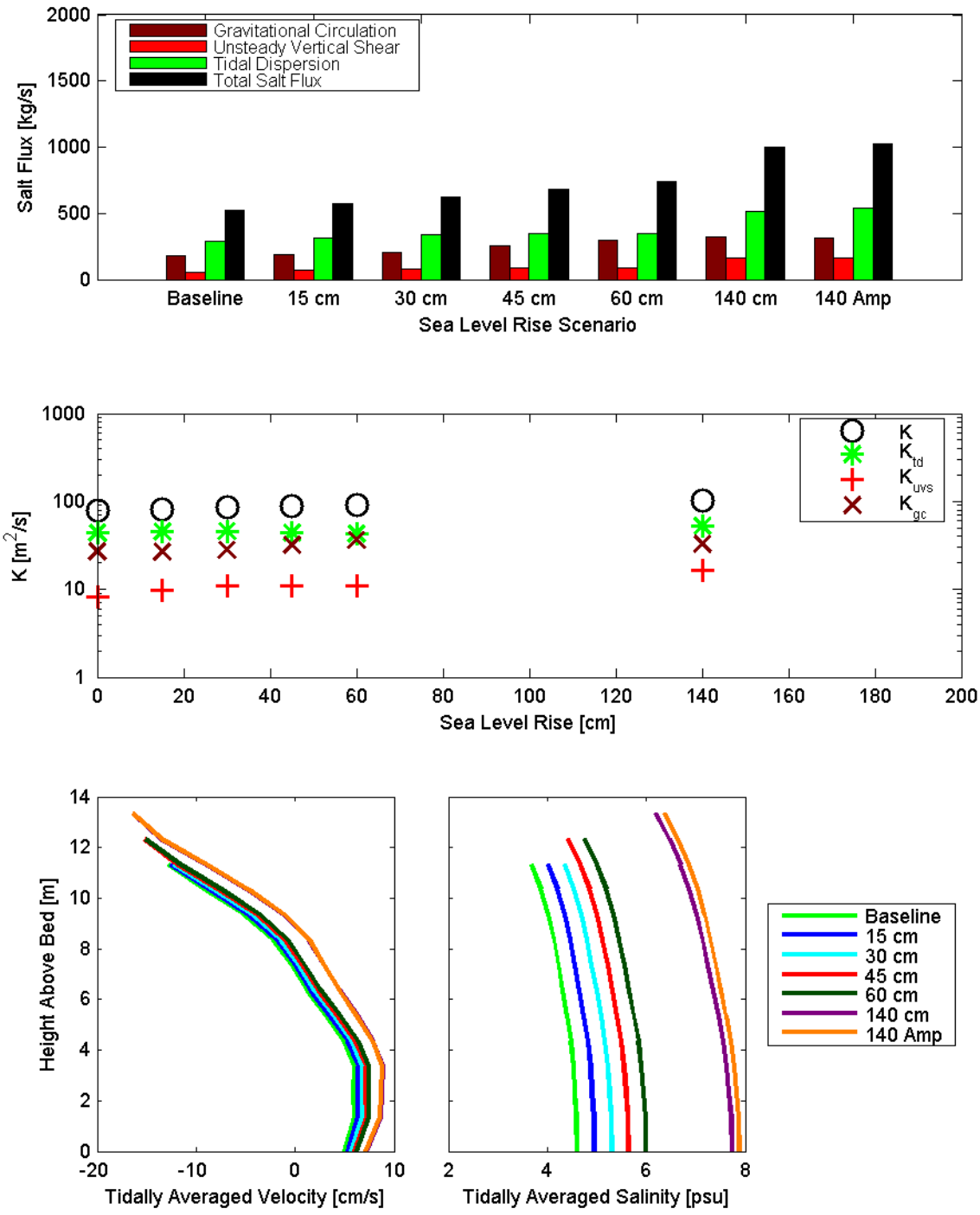

Figure 8.4-88 Dispersive salt flux (top), dispersion coefficients and dispersion coefficient components (middle) and tidally averaged velocity (bottom left) and tidally averaged salinity (bottom right) calculated for each scenario at cross-section 29, extending through Sherman Lake, for the October 13, 2002 through November 10, 2002 analysis period.

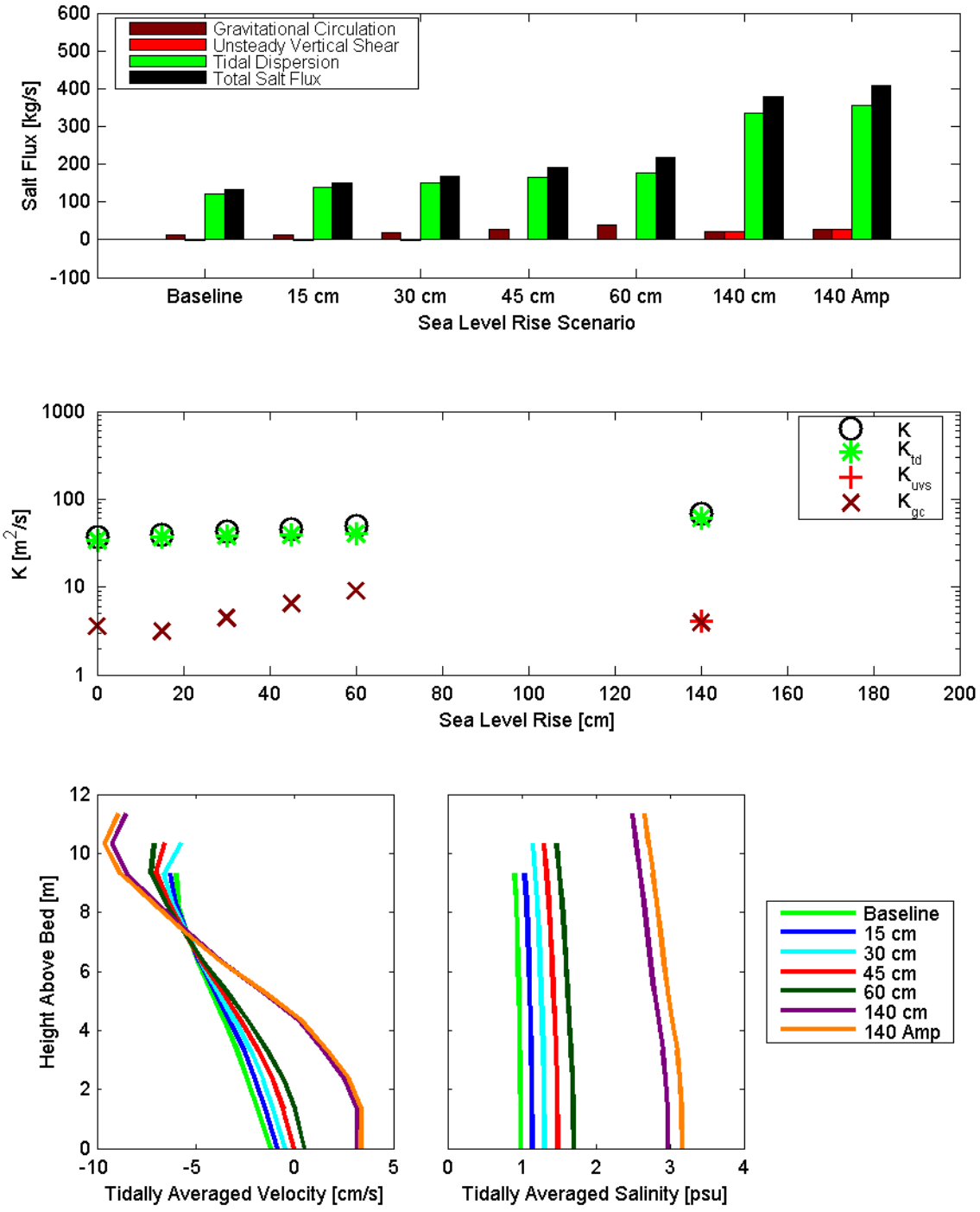

Figure 8.4-89 Dispersive salt flux (top), dispersion coefficients and dispersion coefficient components (middle) and tidally averaged velocity (bottom left) and tidally averaged salinity (bottom right) calculated for each scenario at cross-section 30, located near State Highway 160, for the July 15, 2002 through August 12, 2002 analysis period.

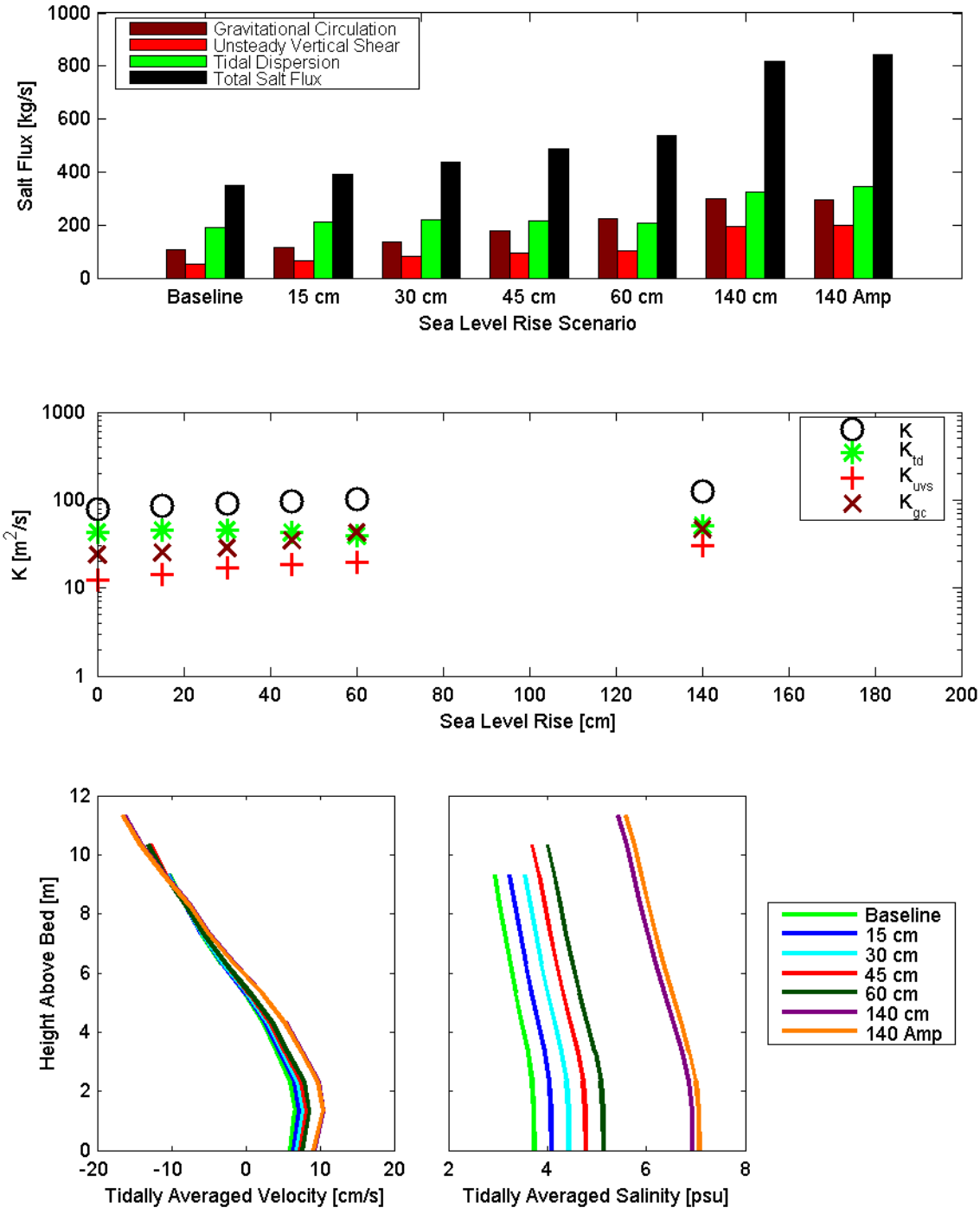

Figure 8.4-90 Dispersive salt flux (top), dispersion coefficients and dispersion coefficient components (middle) and tidally averaged velocity (bottom left) and tidally averaged salinity (bottom right) calculated for each scenario at cross-section 30, located near State Highway 160, for the October 13, 2002 through November 10, 2002 analysis period.

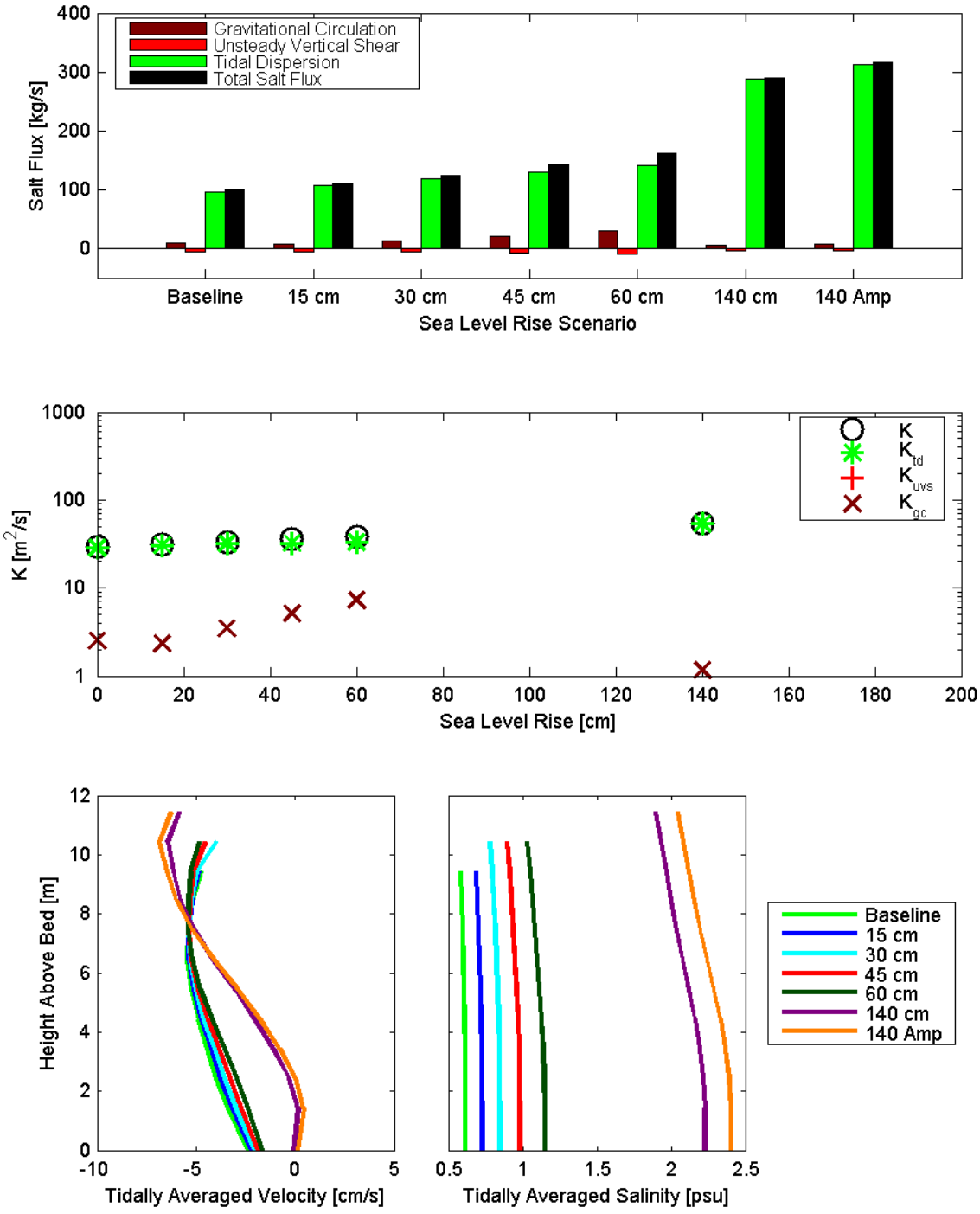

Figure 8.4-91 Dispersive salt flux (top), dispersion coefficients and dispersion coefficient components (middle) and tidally averaged velocity (bottom left) and tidally averaged salinity (bottom right) calculated for each scenario at cross-section 31, extending from Big Break to Toland Landing, for the July 15, 2002 through August 12, 2002 analysis period.

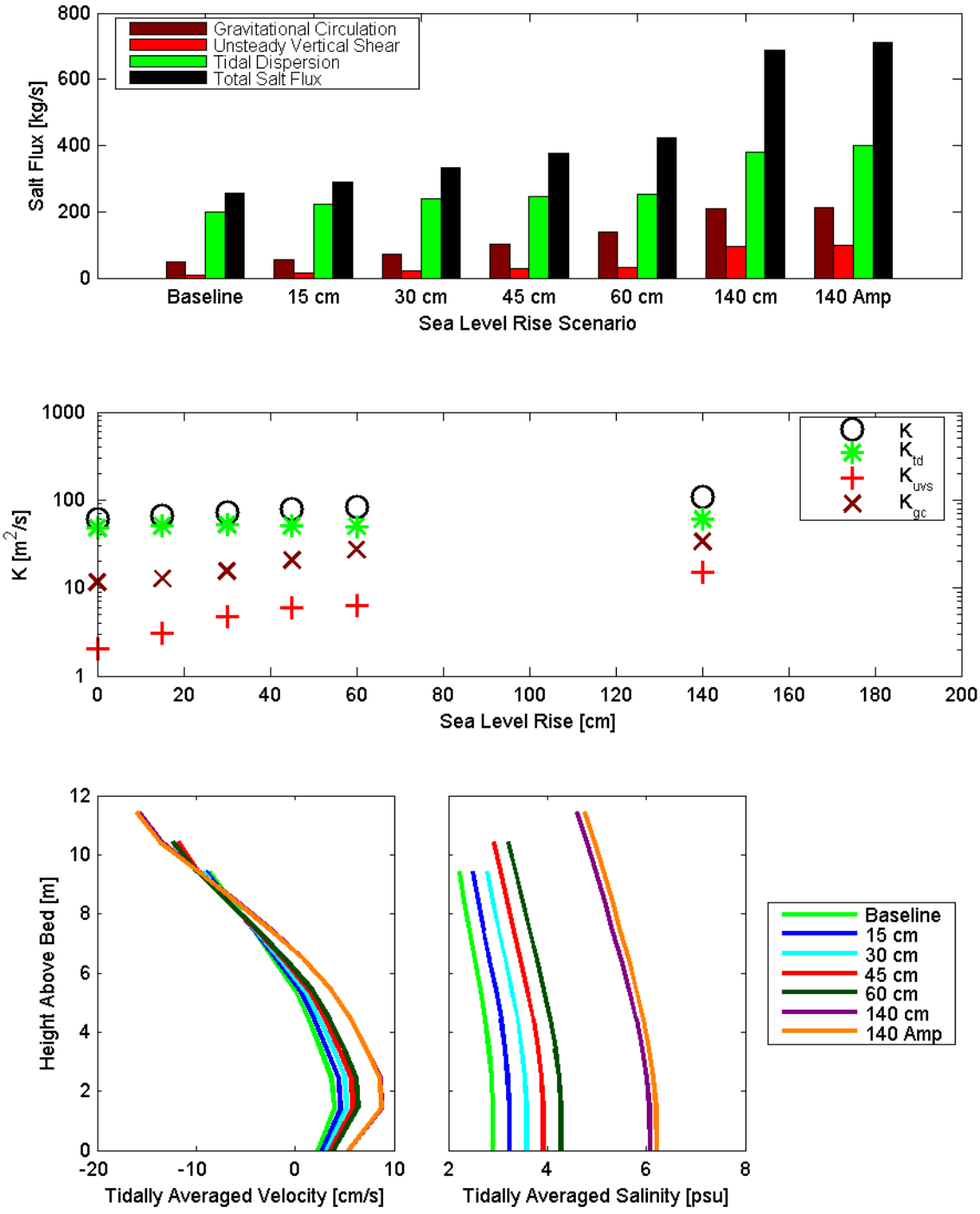

Figure 8.4-92 Dispersive salt flux (top), dispersion coefficients and dispersion coefficient components (middle) and tidally averaged velocity (bottom left) and tidally averaged salinity (bottom right) calculated for each scenario at cross-section 31, extending from Big Break to Toland Landing, for the October 13, 2002 through November 10, 2002 analysis period.

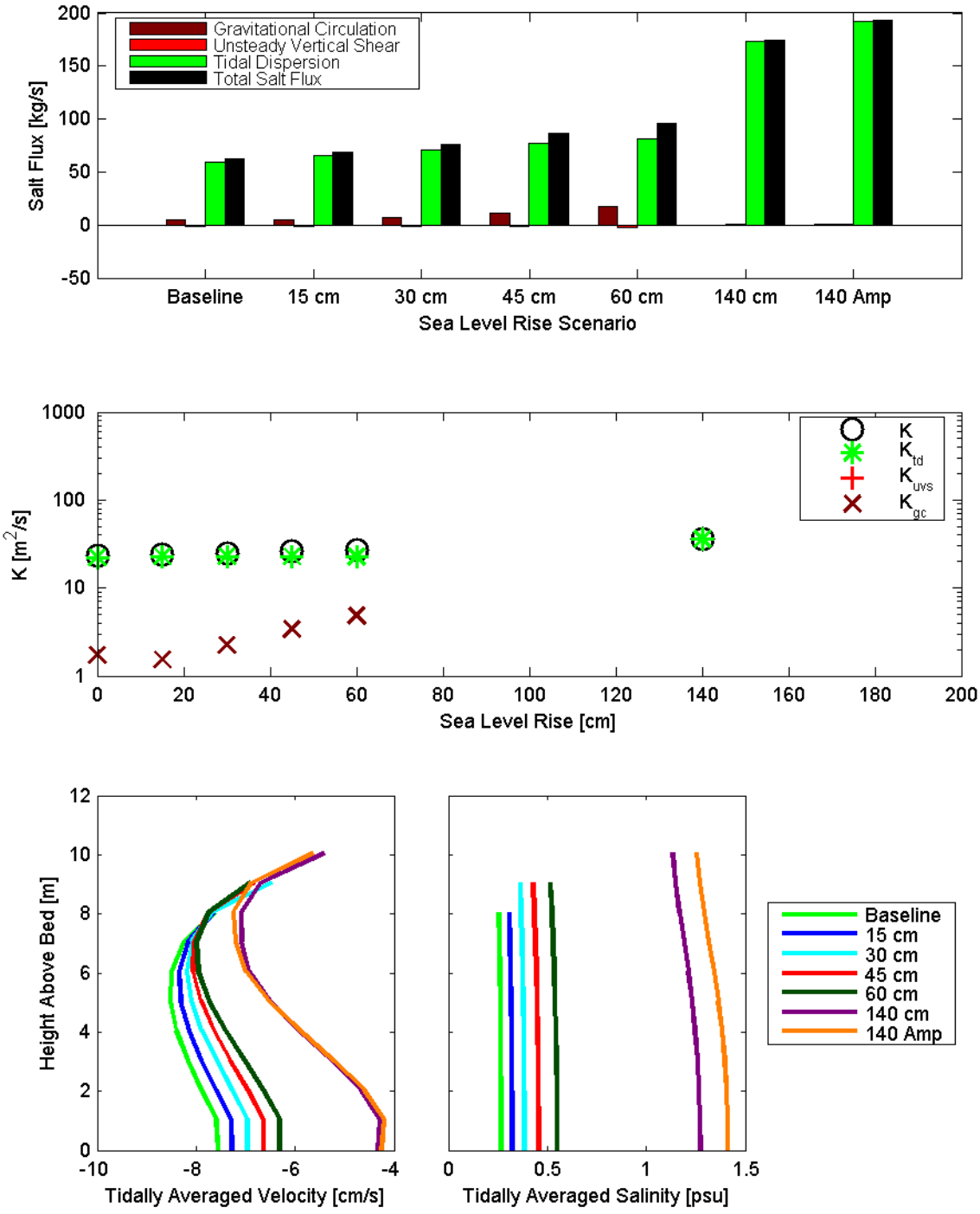

Figure 8.4-93 Dispersive salt flux (top), dispersion coefficients and dispersion coefficient components (middle) and tidally averaged velocity (bottom left) and tidally averaged salinity (bottom right) calculated for each scenario at cross-section 32, extending from Dutch Slough to Chinese Cut, for the July 15, 2002 through August 12, 2002 analysis period.

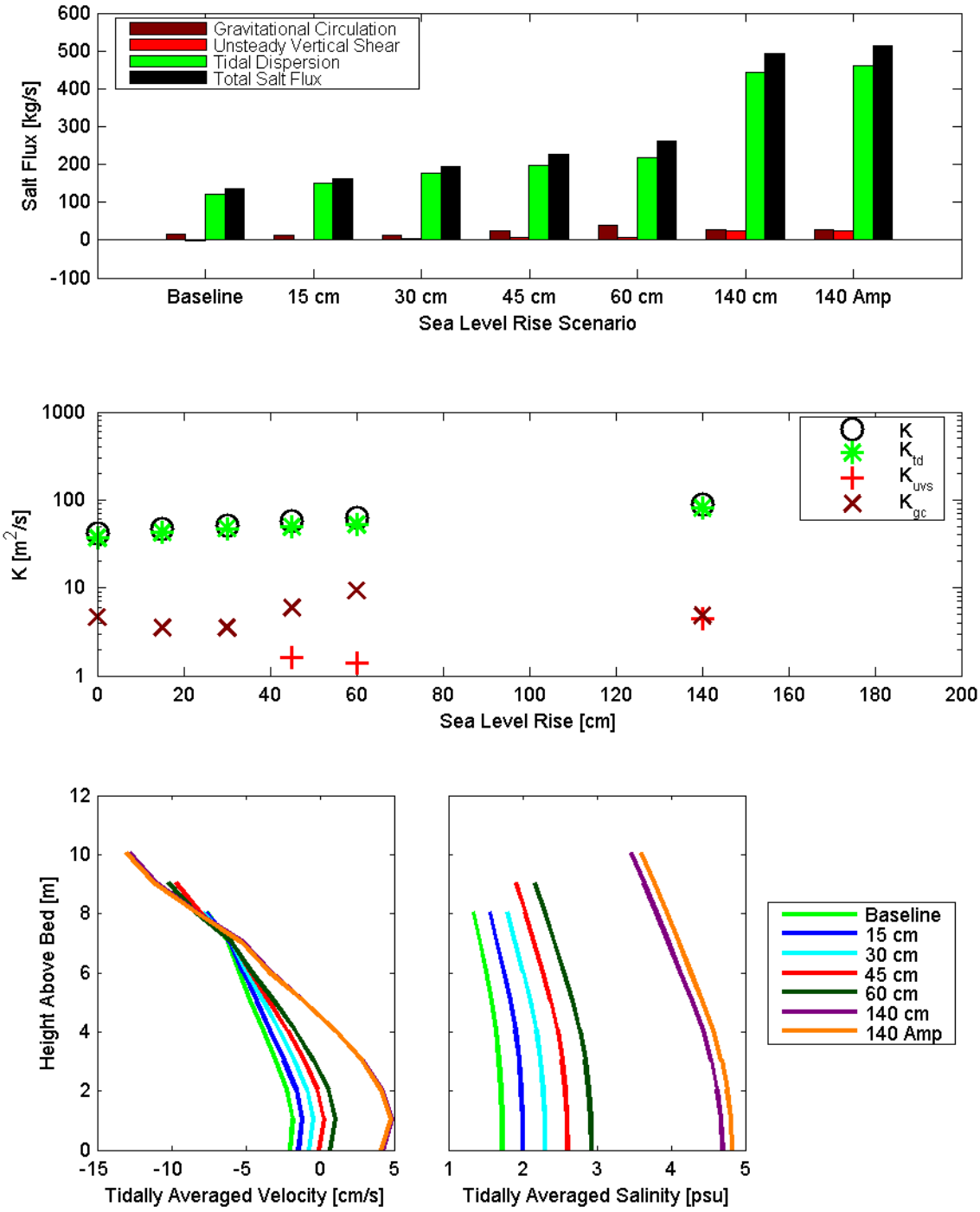

Figure 8.4-94 Dispersive salt flux (top), dispersion coefficients and dispersion coefficient components (middle) and tidally averaged velocity (bottom left) and tidally averaged salinity (bottom right) calculated for each scenario at cross-section 32, extending from Dutch Slough to Chinese Cut, for the October 13, 2002 through November 10, 2002 analysis period.

8.5 Tidal Amplification Scenario Salt Flux Analysis Results

This section evaluates the effect of the amplification of tidal range on salt flux through the comparison of the salt flux analysis for the 140 cm SLR scenario and the 140 cm SLR with 5% Amplification scenario.

As discussed in Section 8.3, analysis periods were chosen in part as periods in which advective and dispersive fluxes balance closely. In other words, the periods selected for the salt analysis have low to moderate variability in salinity conditions. The total dispersive, advective and net fluxes during each period are shown for both analysis periods of the 140 cm SLR scenario and the 140 cm SLR with 5% Amplification scenario in Figure 8.5-1 through Figure 8.5-4. The distance shown on the x-axis corresponds to the distances labeled on the Golden Gate to Rio Vista transect in Figure 5.1-2. For each scenario and analysis period, the advective and dispersive fluxes were bigger than the net fluxes at most or all cross-sections, indicating limited net change in salt mass in the estuary during the analysis period. The net fluxes, indicated with a black x, are generally quite close to the sum of the advective and dispersive fluxes, indicated with a green +. Differences between net fluxes and the sum of the advective and dispersive fluxes are associated with flux terms that are neglected in the flux analysis and other sources of inaccuracies in the analysis but are typically very small.

In Figure 8.5-5 through Figure 8.5-12, the average tidal prism predicted during each analysis period is provided for several cross-sections. The tidal prism increases significantly at all locations with 5% amplification of tidal amplitude. The increase in tidal prism with tidal range amplification is likely to explain several trends in the salt flux analysis. It should be noted that the scenarios assume “hard shorelines.” As a result of this assumption, the tidal prism is likely to increase more substantially with amplification of tides than is predicted in this analysis due to more frequent inundation of low elevation regions bordering the estuary.

In order to calculate dispersion coefficient using Equation 8-1, the variables Q, S and A are averaged through the analysis period at the individual cross-sections. Salinity is also period averaged along the centerline transect shown in Figure 8.3-1, and is shown the 140 cm SLR scenario and the 140 cm SLR with 5% Amplification scenario for both analysis periods in Figure 8.3-14 through Figure 8.3-17. In order to calculate the longitudinal salinity gradient (dS/dx) at each cross section, the period averaged salinity along the centerline transect is depth-averaged for each scenario, to calculate the predicted depth-averaged and period averaged salinity along the centerline of the estuary from the Golden Gate to Rio Vista. The longitudinal salinity gradient at each point is determined by a linear fit of the variability of depth-averaged salinity with distance along the centerline. The longitudinal salinity gradients along the centerline of the estuary for the 140 cm SLR scenario and the 140 cm SLR with 5% Amplification scenario are shown in Figure 8.5-13 and Figure 8.5-14, respectively.

Salt fluxes and dispersion coefficients were calculated for each cross-section shown in Figure 8.3-1 and for the 140 cm SLR scenario and the 140 cm SLR with 5% Amplification scenario. Increases in salt fluxes and dispersion coefficients with amplification indicate that increased Delta inflows will be required to meet salinity standards as a result of amplification of tidal range. The estimated dispersion coefficients (K) are shown in Figure 8.5-15 for the July 15, 2002 through August 12, 2002 analysis period and in Figure 8.5-16 for the October 13, 2002

through November 10, 2002 analysis period. The dispersion coefficients for the two periods show similar trends, but the dispersion coefficients for the October 13, 2002 through November 10, 2002 analysis period are higher in Suisun Bay and the western Delta than the respective dispersion coefficients for the July 15, 2002 through August 12, 2002 analysis period. The calculated dispersion coefficients have limited variability with amplification at most cross-sections in Central Bay and San Pablo Bay. However, dispersion coefficients in Suisun Bay and the western Delta generally increase significantly with amplification.

The salt flux analysis described in Section 8.2 was used to divide each dispersion coefficient into three components: K_{gc}, $K_{uvs,}$ and K_{td}. K_{gc} represents the strength of gravitational circulation, K_{uvs} represents the strength of all unsteady vertical shear dispersion processes and K_{td} represents the strength of all tidal dispersion processes.

The estimated dispersion coefficients associated with gravitational circulation (K_{gc}) for the 140 cm SLR scenario and the 140 cm SLR with 5% Amplification scenario are shown in Figure 8.5-17 for the July 15, 2002 through August 12, 2002 analysis period and in Figure 8.5-18 for the October 13, 2002 through November 10, 2002 analysis period. Note that the dispersion coefficient component associated with gravitational circulation is more variable with location than the overall dispersion coefficient. The dispersion coefficient components associated with gravitational circulation decrease with amplification at most locations. This was expected because tidal range amplification results in higher tidal currents and, therefore, stronger vertical mixing and less stratification.

The dispersion coefficients associated with unsteady vertical shear (K_{uvs}) for the 140 cm SLR scenario and the 140 cm SLR with 5% Amplification scenario are shown in Figure 8.5-19 for the July 15, 2002 through August 12, 2002 analysis period and in Figure 8.5-20Figure 8.4-28 for the October 13, 2002 through November 10, 2002 analysis period. The unsteady vertical shear component is highly variable but often of similar magnitude as the gravitational circulation component. Some of the dispersion associated with unsteady vertical shear is associated with the SIPS mechanism which is known to be active in portions of Suisun Bay (Stacey et al. 2001). The dispersion associated with unsteady vertical shear varies significantly with amplification. However, the sign and magnitude of change in this component with amplification varies from cross-section to cross-section.

The dispersion coefficients associated with all tidal dispersion processes (K_{td}) for the 140 cm SLR scenario and the 140 cm SLR with 5% Amplification scenario are shown in Figure 8.5-21 for the July 15, 2002 through August 12, 2002 analysis period and in Figure 8.5-22 for the October 13, 2002 through November 10, 2002 analysis period. K_{td} is similar between the two analysis periods and varies over slightly more than one order of magnitude spatially. Since this component of the dispersion coefficient is not expected to have strong variation with stratification, the less pronounced spatial variability was expected. The dispersion coefficient component associated with tidal dispersion generally increases with amplification. This increase is probably related to the increased tidal prism shown in Figure 8.5-6 through Figure 8.5-12.

The effects of amplification were shown individually at each cross-section in Section 8.4.

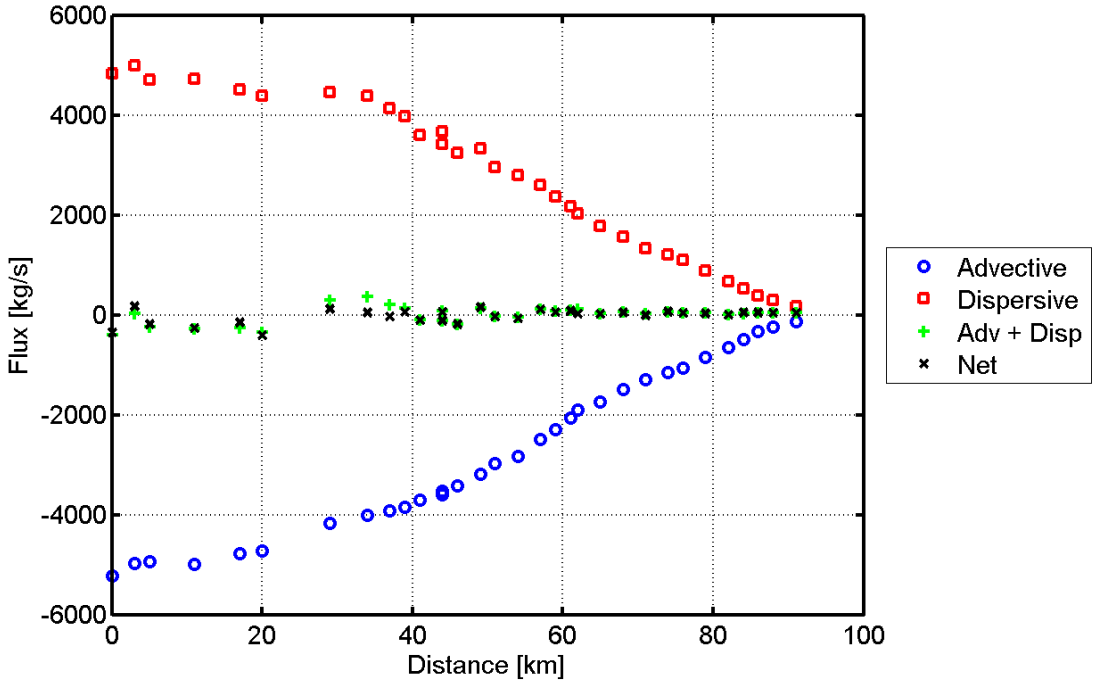

Figure 8.5-1 Predicted advective, dispersive and net salt fluxes for the 140 cm SLR scenario during the July 15, 2002 through August 12, 2002 analysis period.

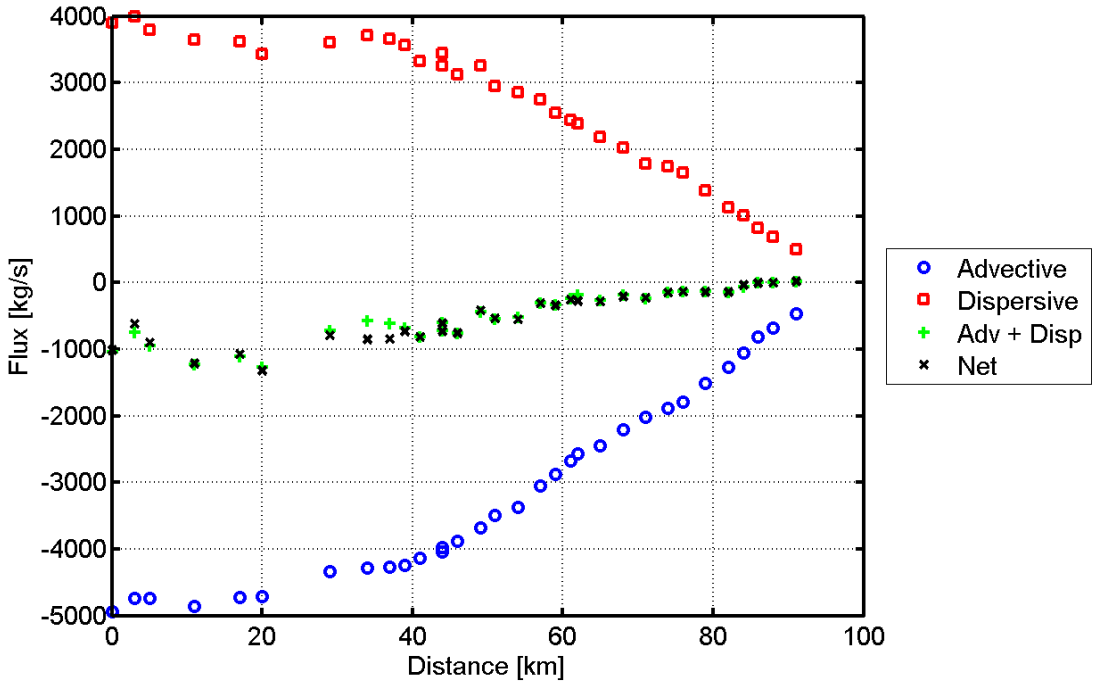

Figure 8.5-2 Predicted advective, dispersive and net salt fluxes for the 140 cm SLR scenario during the October 13, 2002 through November 10, 2002 analysis period.

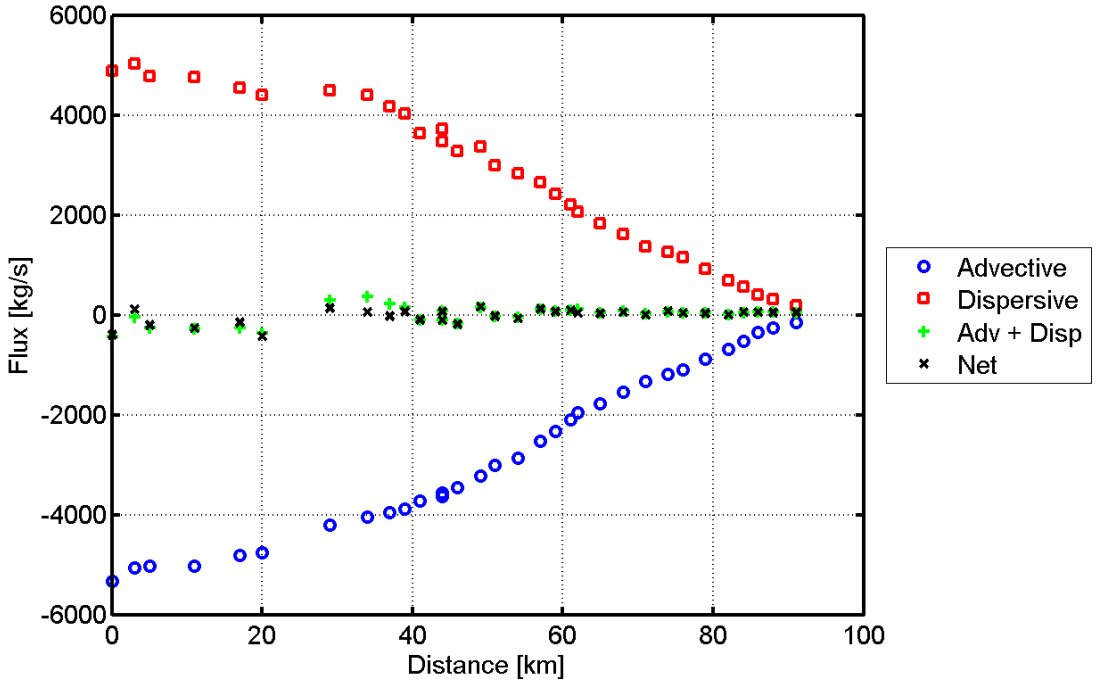

Figure 8.5-3 Predicted advective, dispersive and net salt fluxes for the 140 cm SLR with 5% Amplification scenario during the July 15, 2002 through August 12, 2002 analysis period.

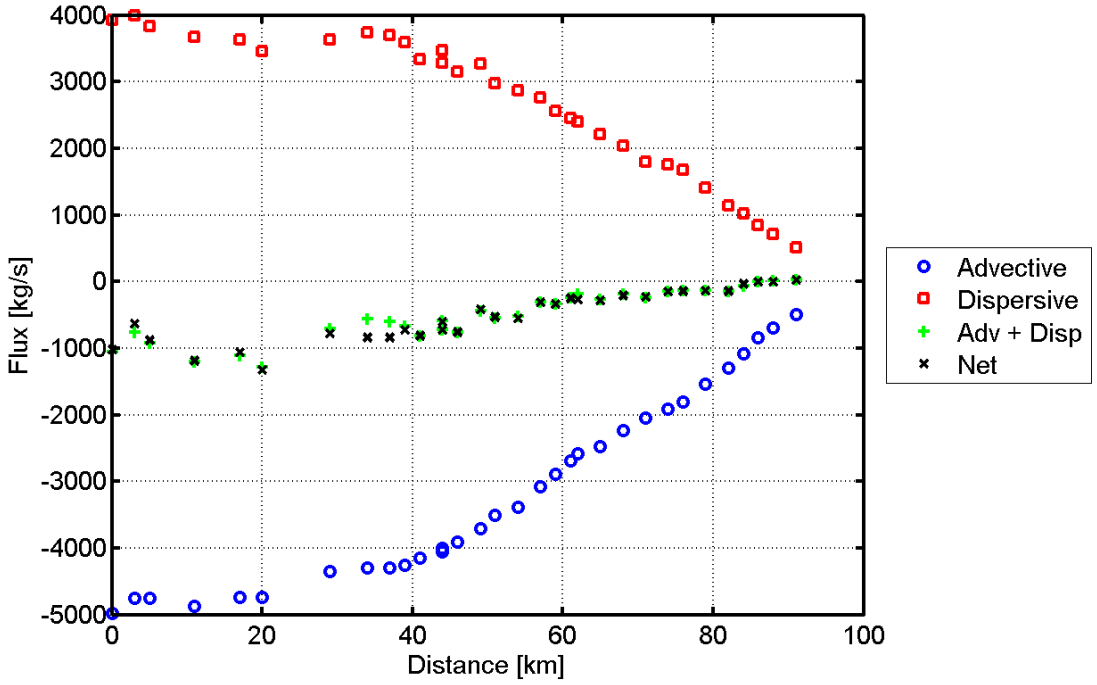

Figure 8.5-4 Predicted advective, dispersive and net salt fluxes for the 140 cm SLR with 5% Amplification scenario during the October 13, 2002 through November 10, 2002 analysis period.

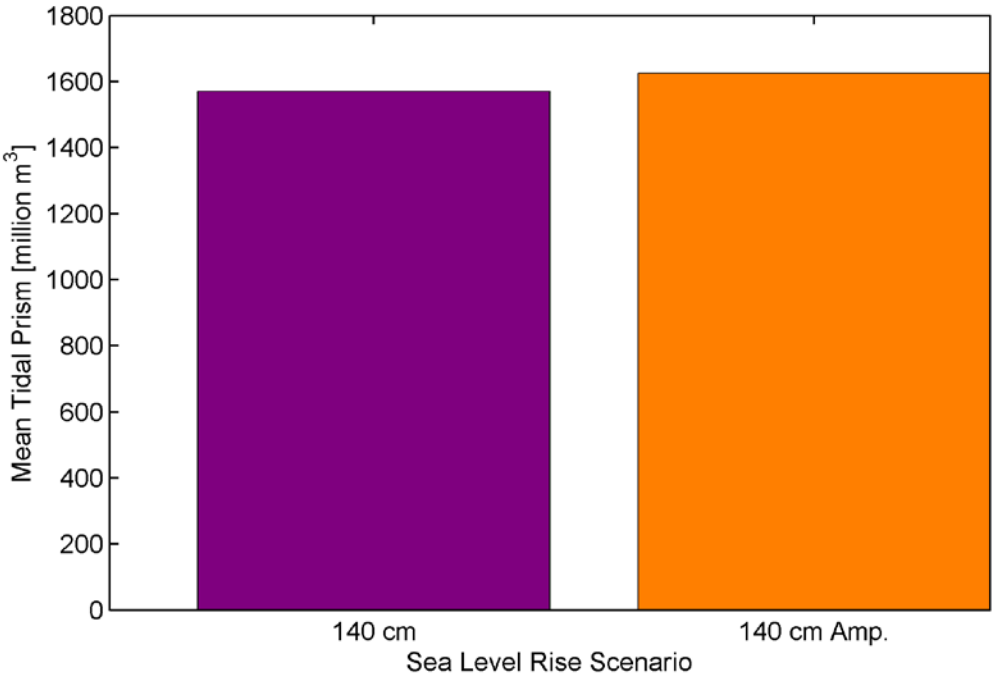

Figure 8.5-5 Average tidal prism at cross-section 1, located at the Golden Gate, for the 140 cm SLR and 140 cm SLR with 5% Amplification scenarios during the July 15, 2002 through August 12, 2002 analysis period.

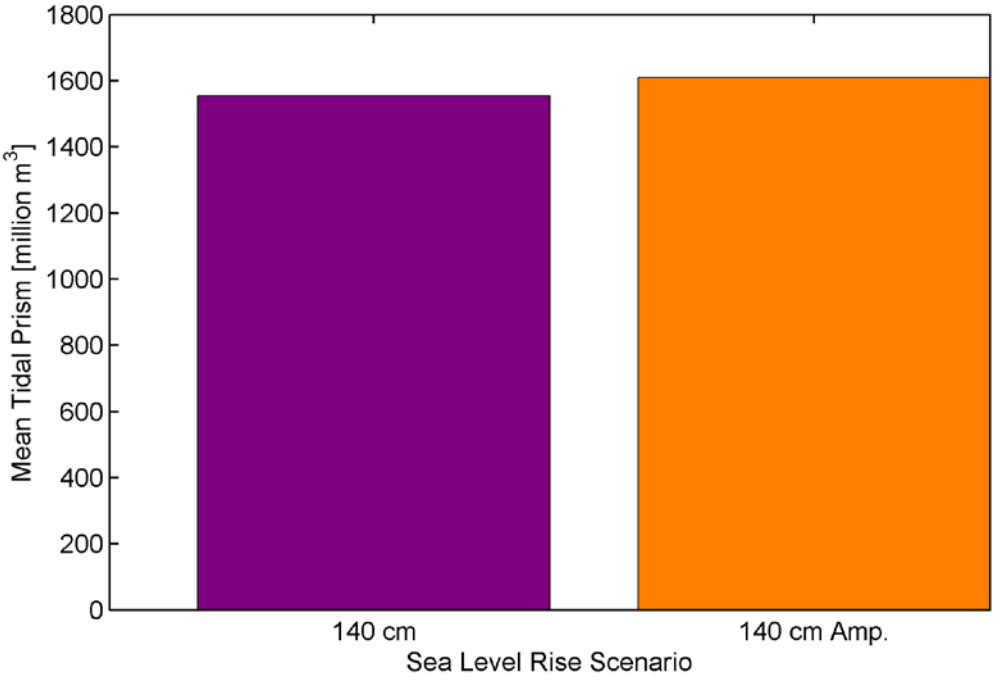

Figure 8.5-6 Average tidal prism at cross-section 1, located at the Golden Gate, for the 140 cm SLR and 140 cm SLR with 5% Amplification scenarios during the October 13, 2002 through November 10, 2002 analysis period.

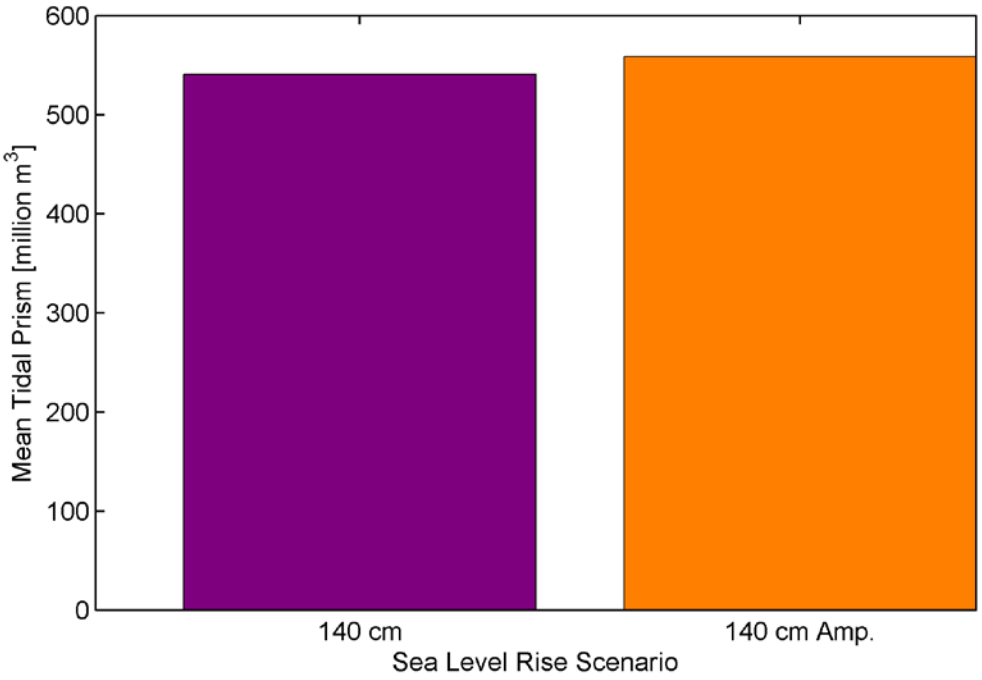

Figure 8.5-7 Average tidal prism at cross-section 5, located at the Richmond-San Rafael Bridge, for the 140 cm SLR and 140 cm SLR with 5% Amplification scenarios during the July 15, 2002 through August 12, 2002 analysis period.

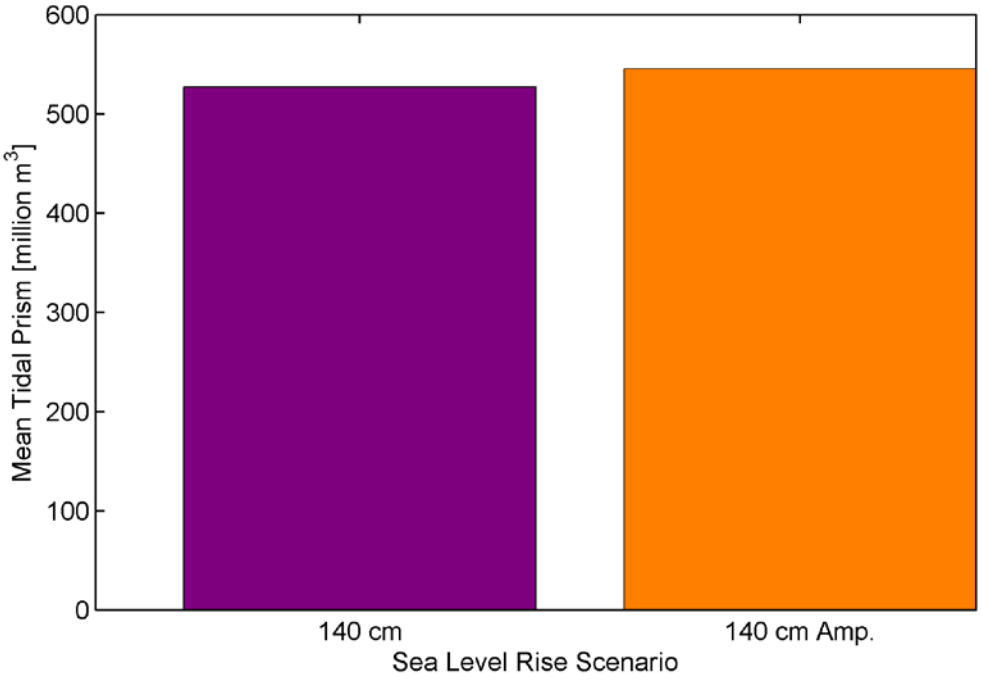

Figure 8.5-8 Average tidal prism at cross-section 5, located at the Richmond-San Rafael Bridge, for the 140 cm SLR and 140 cm SLR with 5% Amplification scenarios during the October 13, 2002 through November 10, 2002 analysis period.

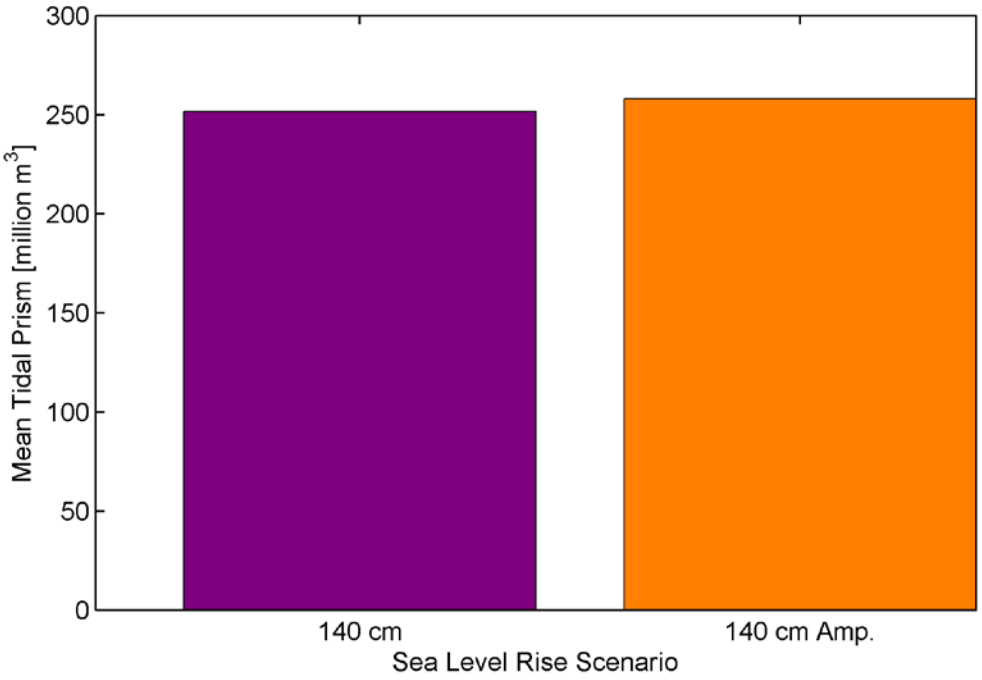

Figure 8.5-9 Average tidal prism at cross-section 12, located at the Carquinez Bridge, for the 140 cm SLR and140 cm SLR with 5% Amplification scenarios during the July 15, 2002 through August 12, 2002 analysis period.

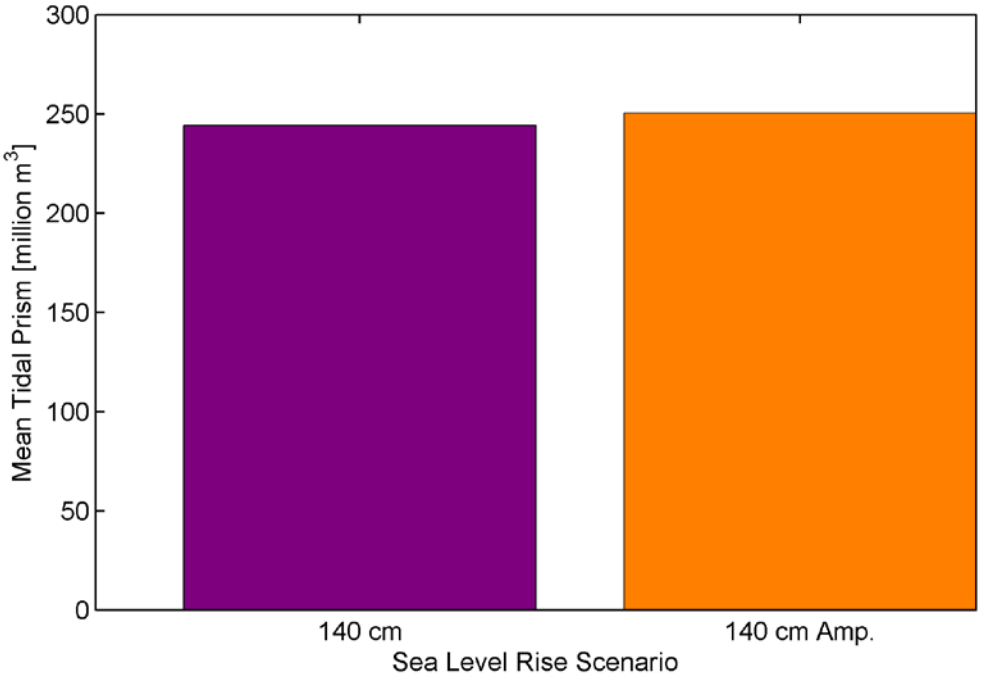

Figure 8.5-10 Average tidal prism at cross-section 12, located at the Carquinez Bridge, for the 140 cm SLR and 140 cm SLR with 5% Amplification scenarios during the October 13, 2002 through November 10, 2002 analysis period.

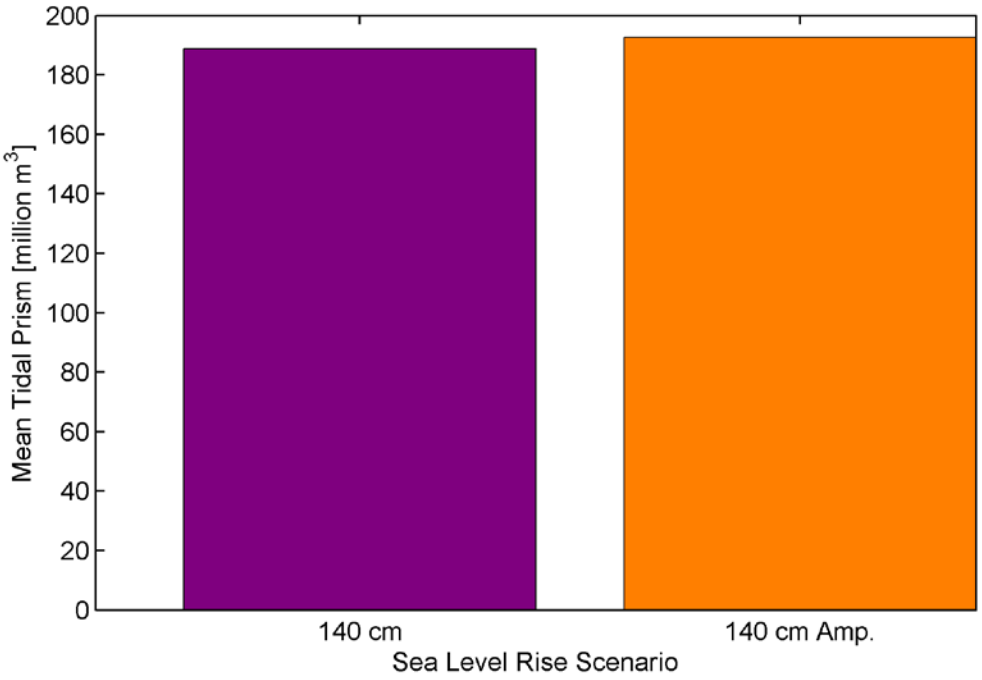

Figure 8.5-11 Average tidal prism at cross-section 25, located at Chipps Island, for the 140 cm SLR and 140 cm SLR with 5% Amplification scenarios during the July 15, 2002 through August 12, 2002 analysis period.

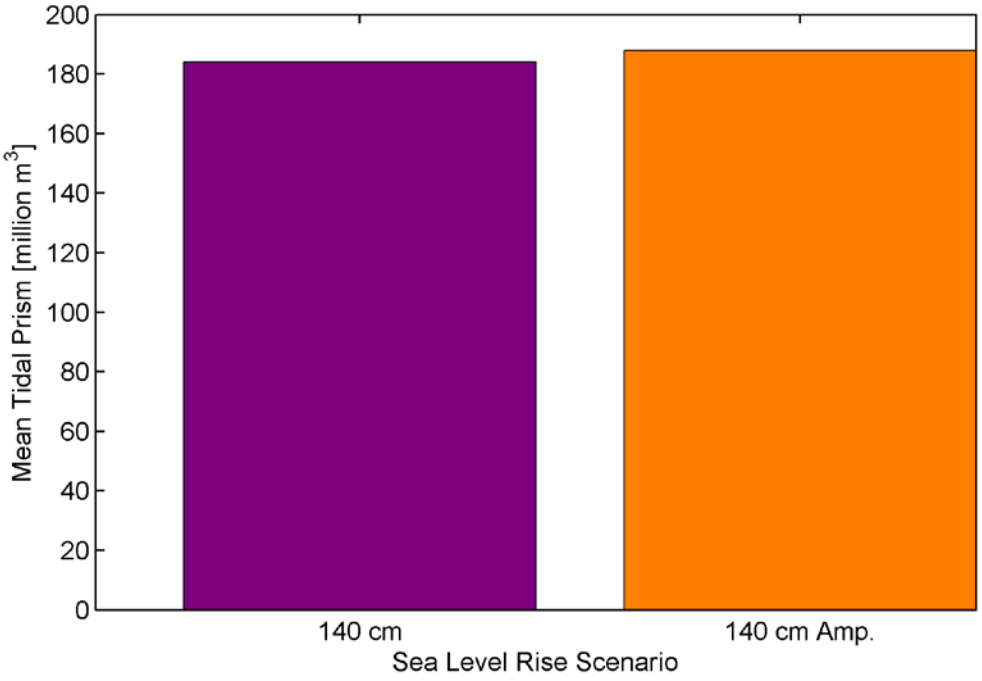

Figure 8.5-12 Average tidal prism at cross-section 25, located at Chipps Island, for the 140 cm SLR and 140 cm SLR with 5% Amplification scenarios during the October 13, 2002 through November 10, 2002 analysis period.

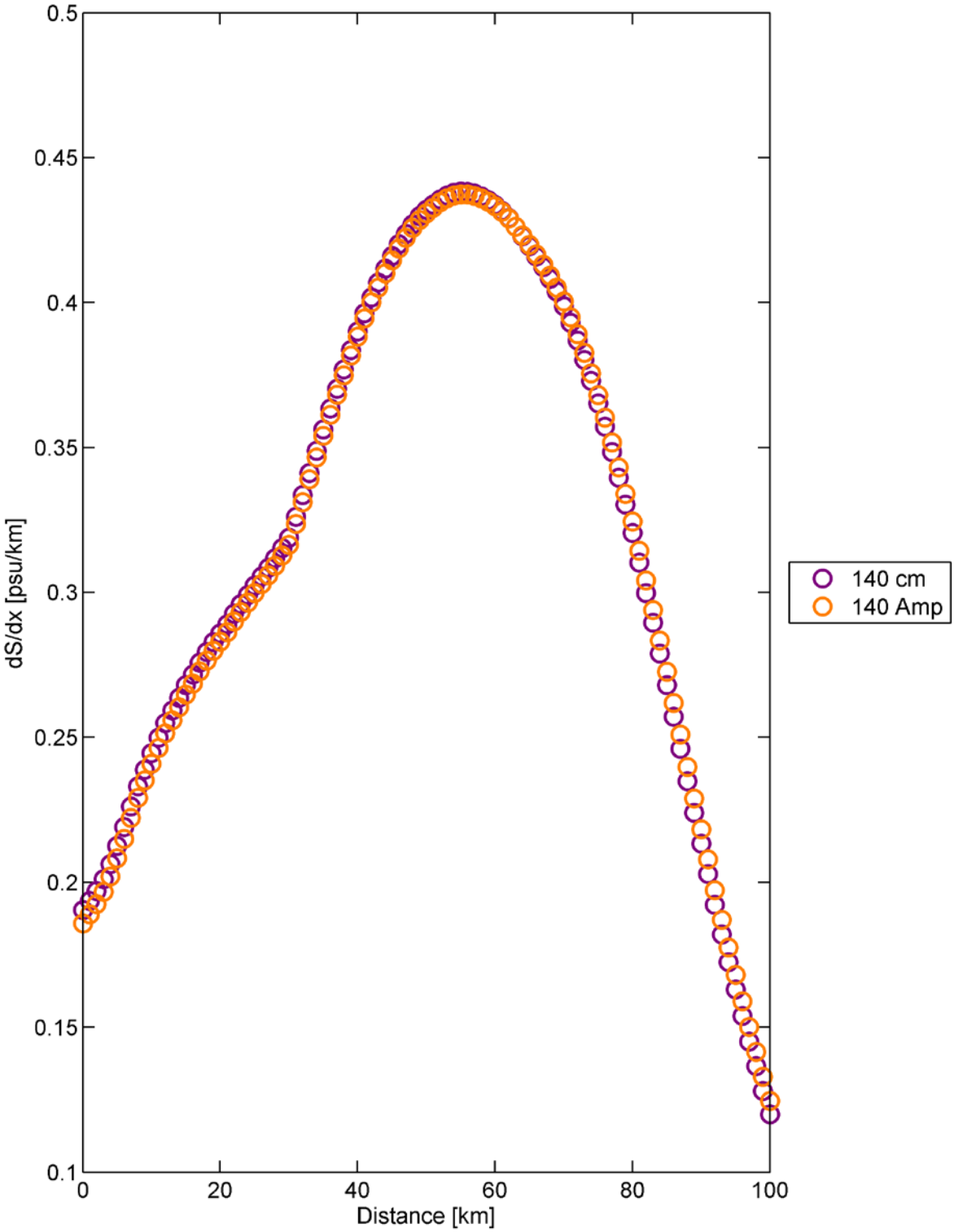

Figure 8.5-13 Estimated depth-averaged salinity gradient for the 140 cm SLR and 140 cm SLR with 5% Amplification scenarios for the July 15, 2002 through August 12, 2002 analysis period. The horizontal scale is distance along the axis of the estuary from the Golden Gate.

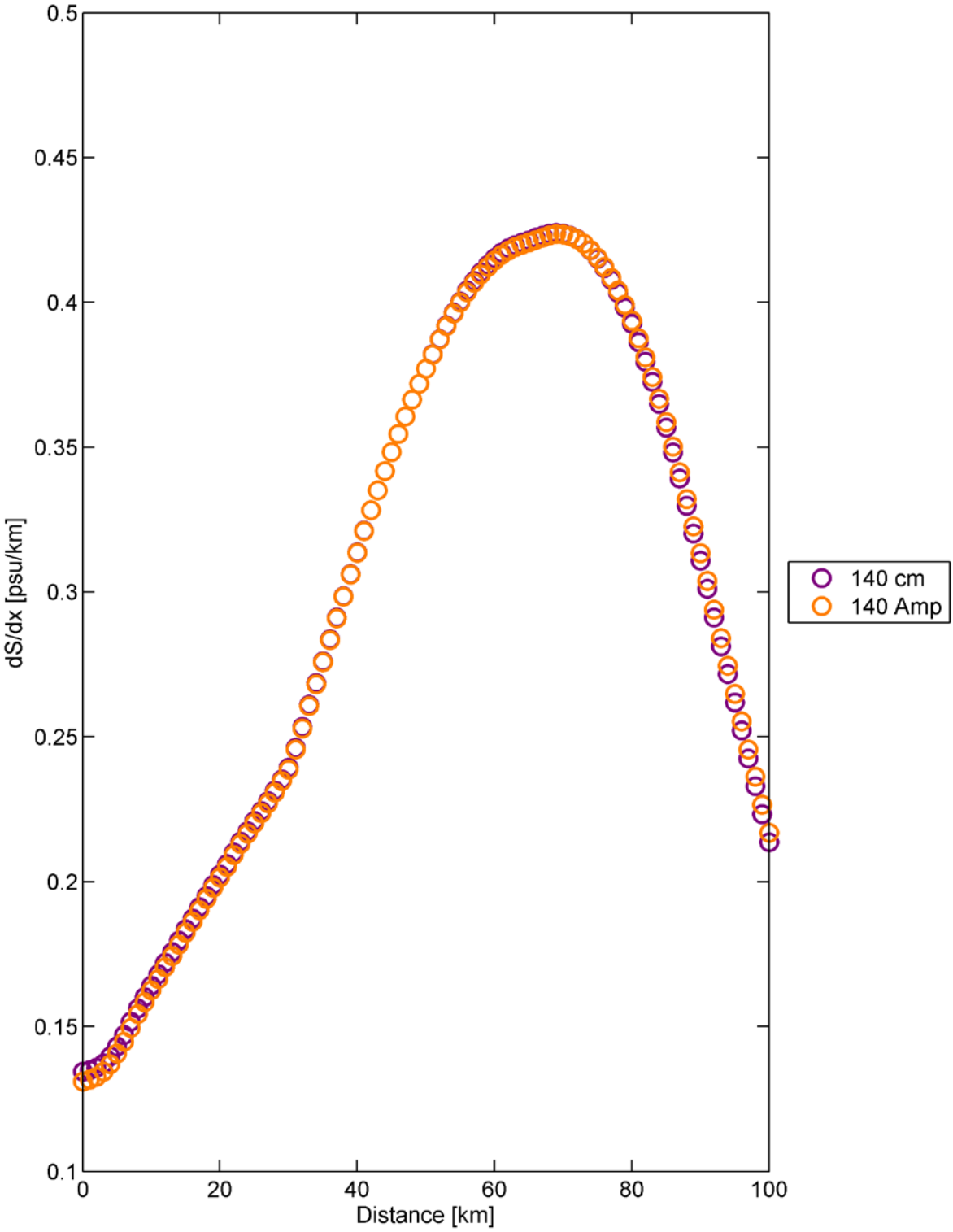

Figure 8.5-14 Estimated depth-averaged salinity gradient for the 140 cm SLR and 140 cm SLR with 5% Amplification scenarios for the October 13, 2002 through November 10, 2002 analysis period. The horizontal scale is distance along the axis of the estuary from the Golden Gate.

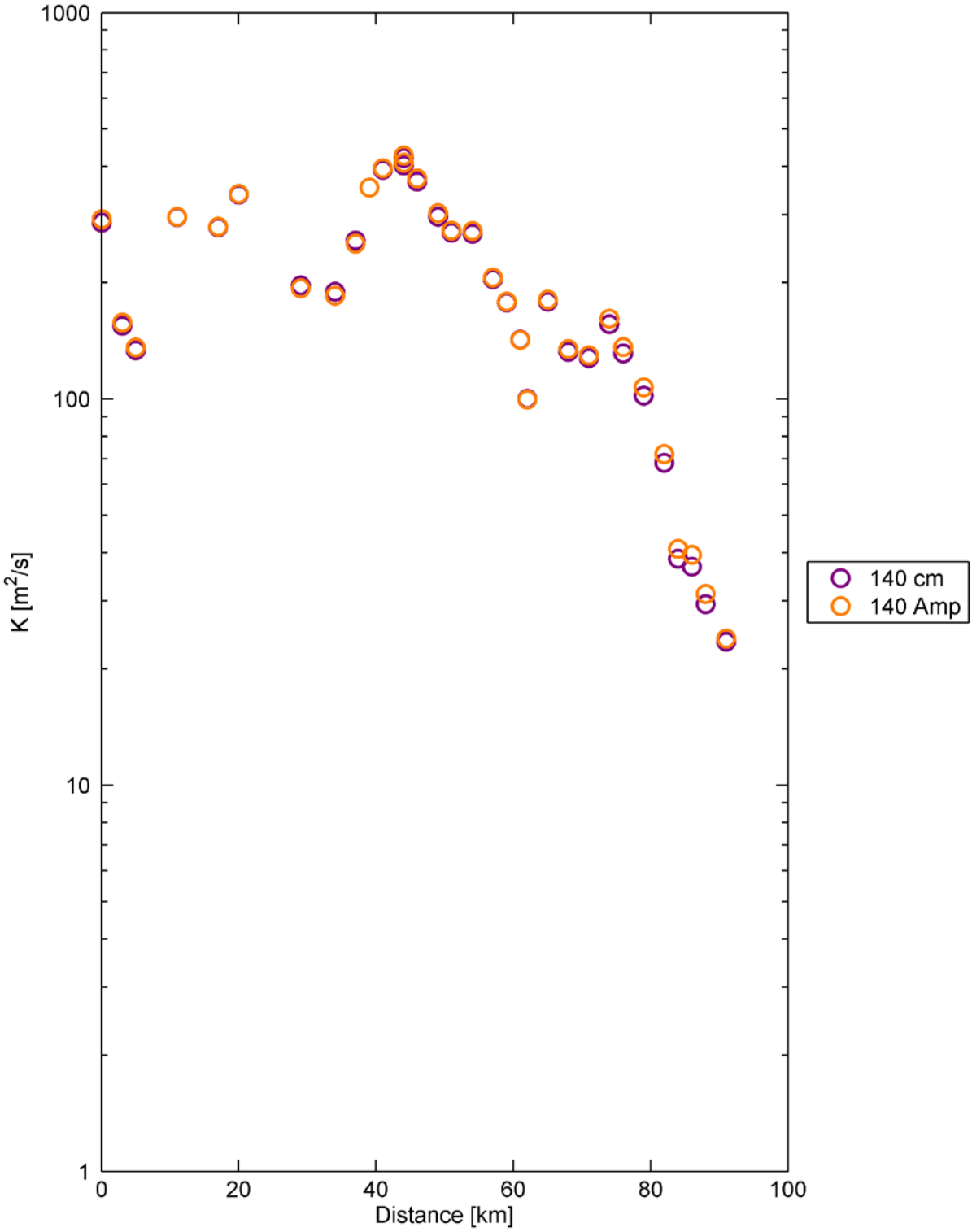

Figure 8.5-15 Estimated dispersion coefficient for the 140 cm SLR and 140 cm SLR with 5% Amplification scenarios for the July 15, 2002 through August 12, 2002 analysis period. The horizontal scale is distance along the axis of the estuary from the Golden Gate.

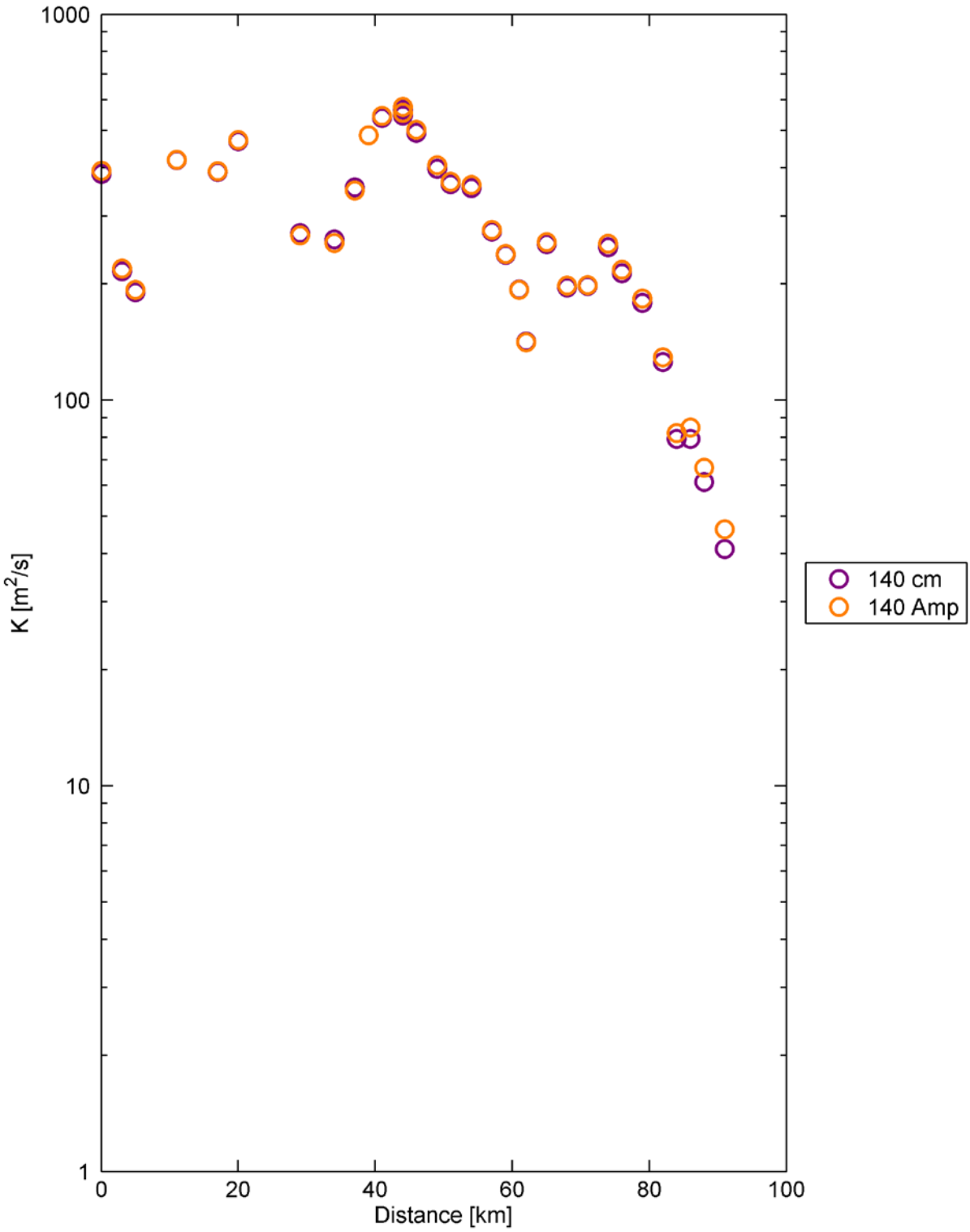

Figure 8.5-16 Estimated dispersion coefficient for the 140 cm SLR and 140 cm SLR with 5% Amplification scenarios for the October 13, 2002 through November 10, 2002 analysis period. The horizontal scale is distance along the axis of the estuary from the Golden Gate.

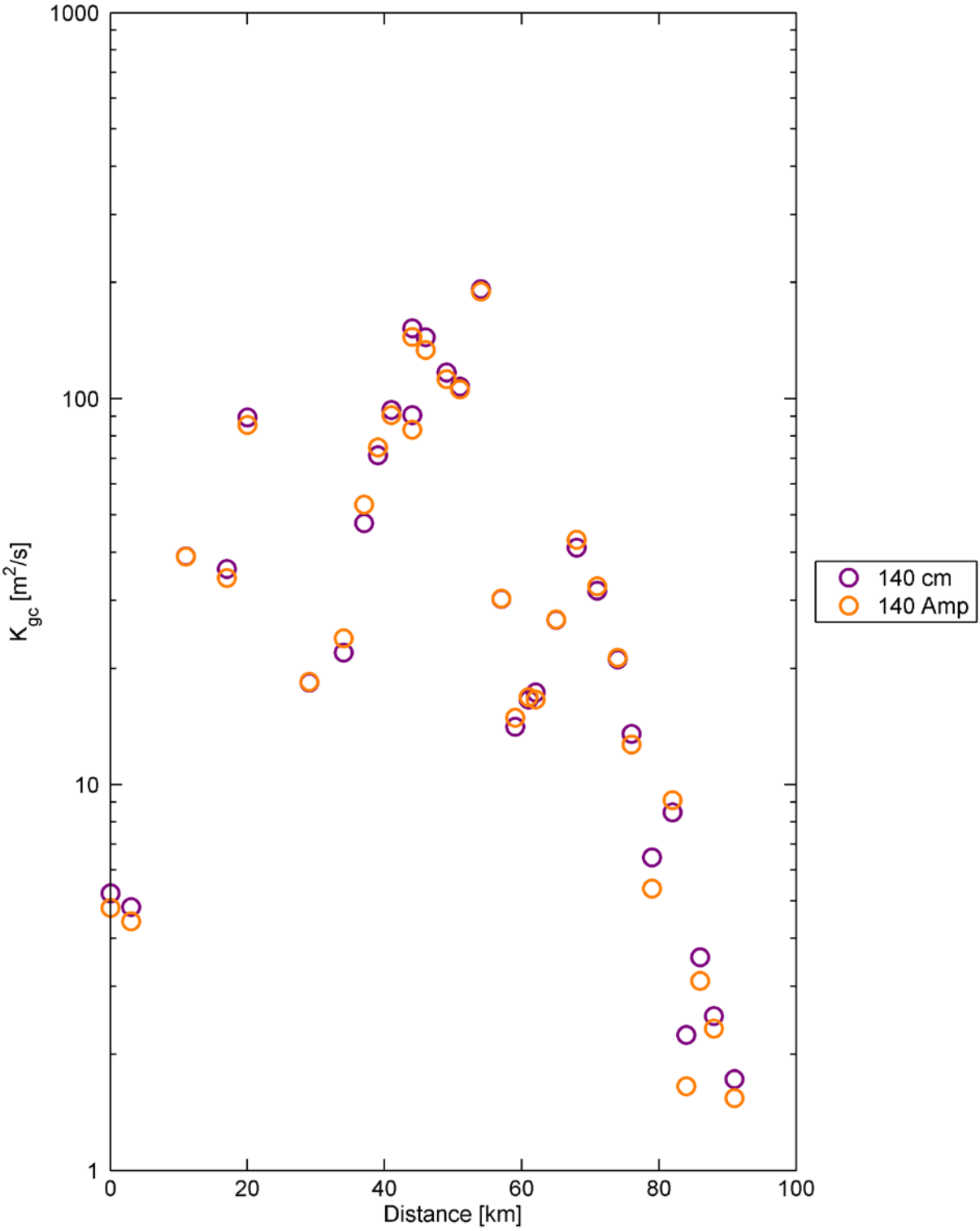

Figure 8.5-17 Estimated dispersion coefficient due to gravitational circulation for the 140 cm SLR and 140 cm SLR with 5% Amplification scenarios for the July 15, 2002 through August 12, 2002 analysis period. The horizontal scale is distance along the axis of the estuary from the Golden Gate.

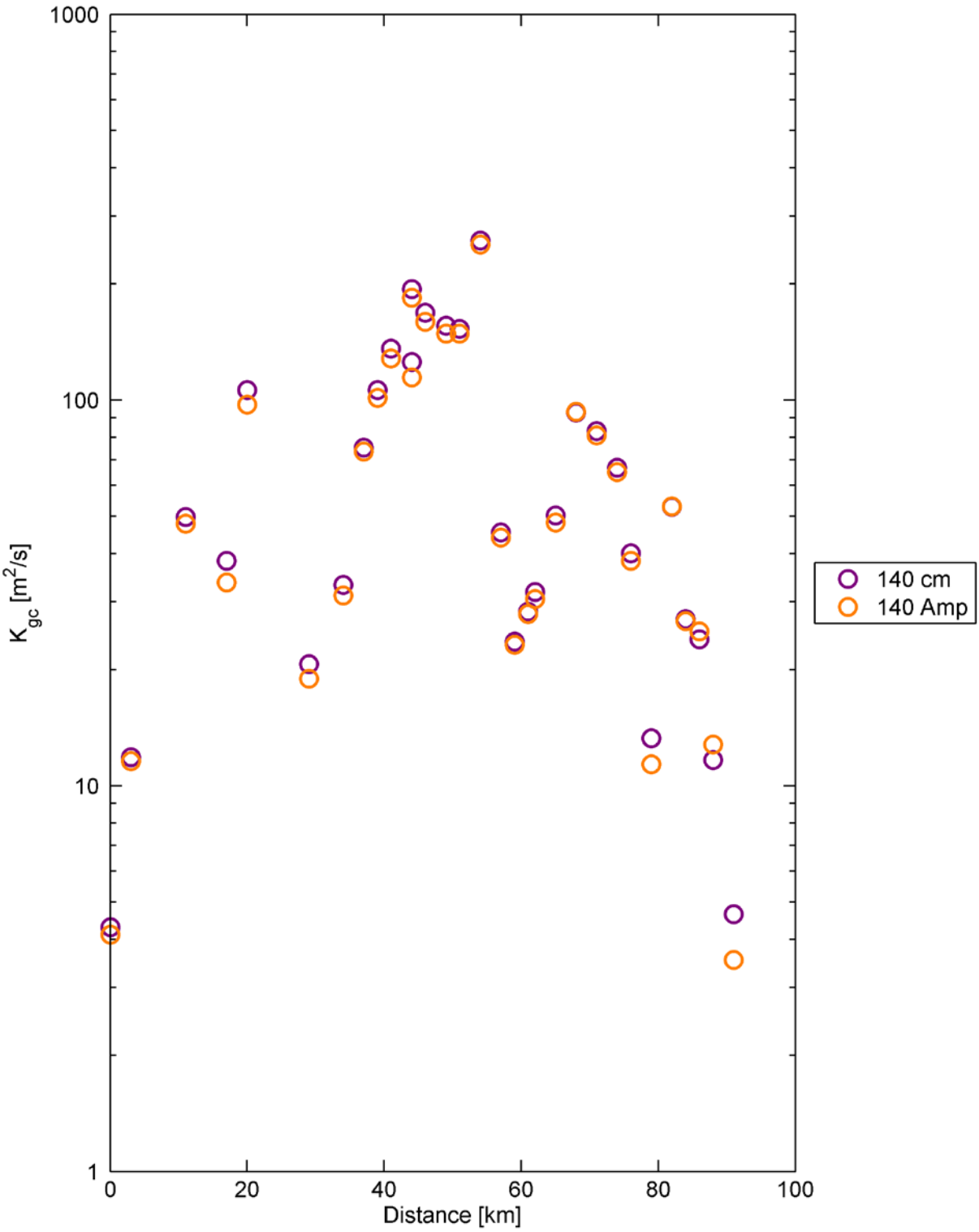

Figure 8.5-18 Estimated dispersion coefficient due to gravitational circulation for the 140 cm SLR and 140 cm SLR with 5% Amplification scenarios for the October 13, 2002 through November 10, 2002 analysis period. The horizontal scale is distance along the axis of the estuary from the Golden Gate.

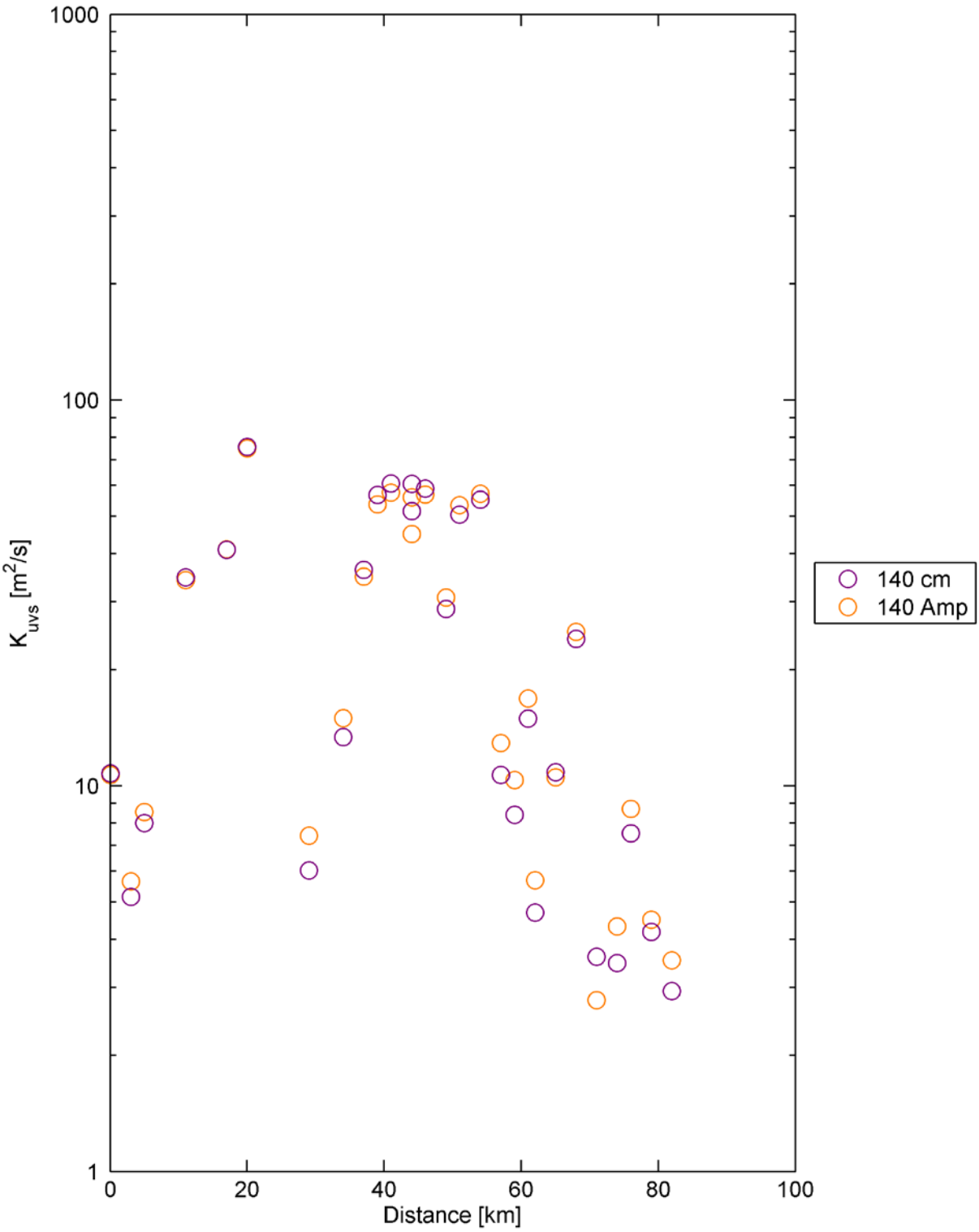

Figure 8.5-19 Estimated dispersion coefficient due to unsteady vertical shear for the 140 cm SLR and 140 cm SLR with 5% Amplification scenarios for the July 15, 2002 through August 12, 2002 analysis period. The horizontal scale is distance along the axis of the estuary from the Golden Gate.

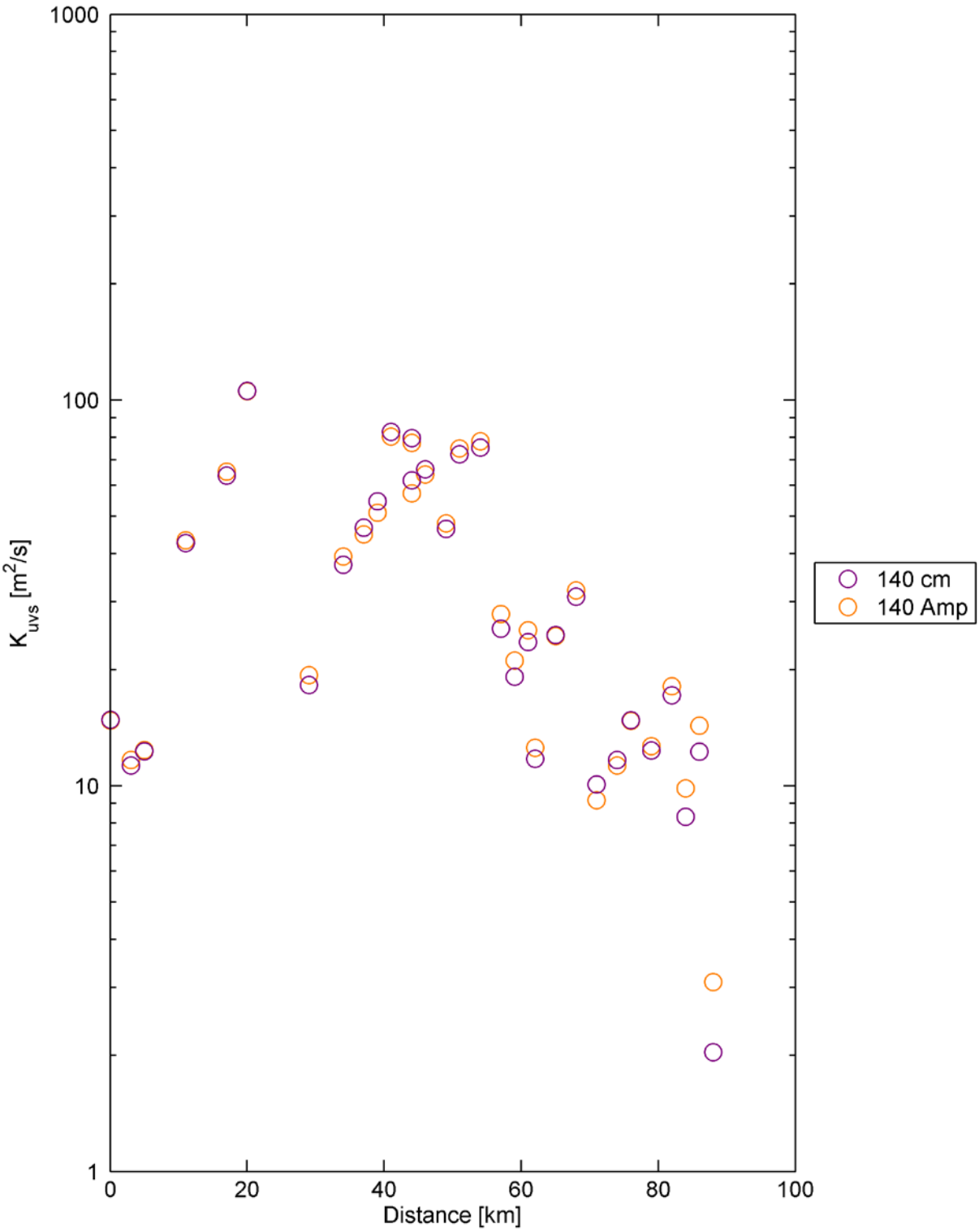

Figure 8.5-20 Estimated dispersion coefficient due to unsteady vertical shear for the 140 cm SLR and 140 cm SLR with 5% Amplification scenarios for the October 13, 2002 through November 10, 2002 analysis period. The horizontal scale is distance along the axis of the estuary from the Golden Gate.

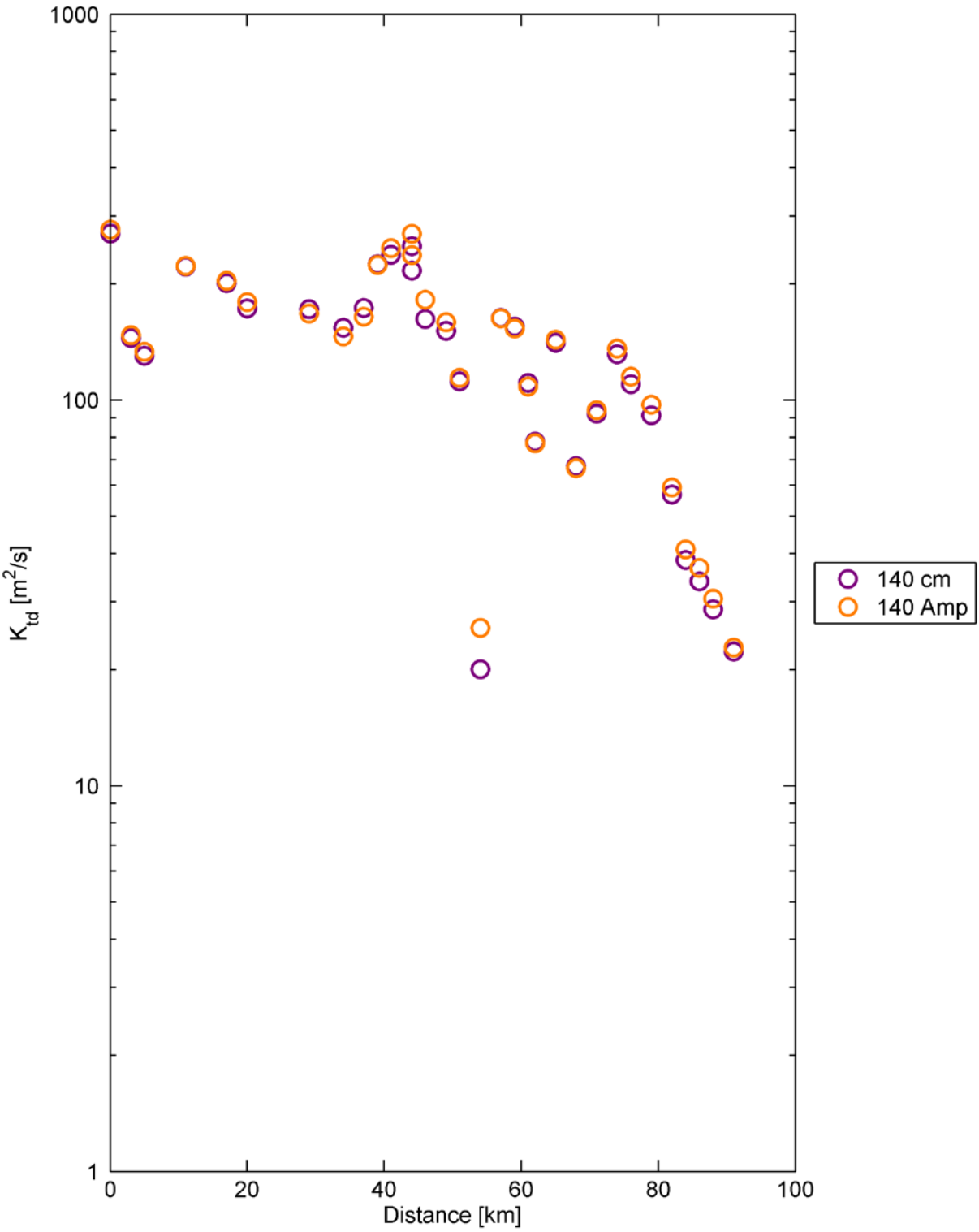

Figure 8.5-21 Estimated dispersion coefficient due to tidal dispersion for the 140 cm SLR and 140 cm SLR with 5% Amplification scenarios for the July 15, 2002 through August 12, 2002 analysis period. The horizontal scale is distance along the axis of the estuary from the Golden Gate.

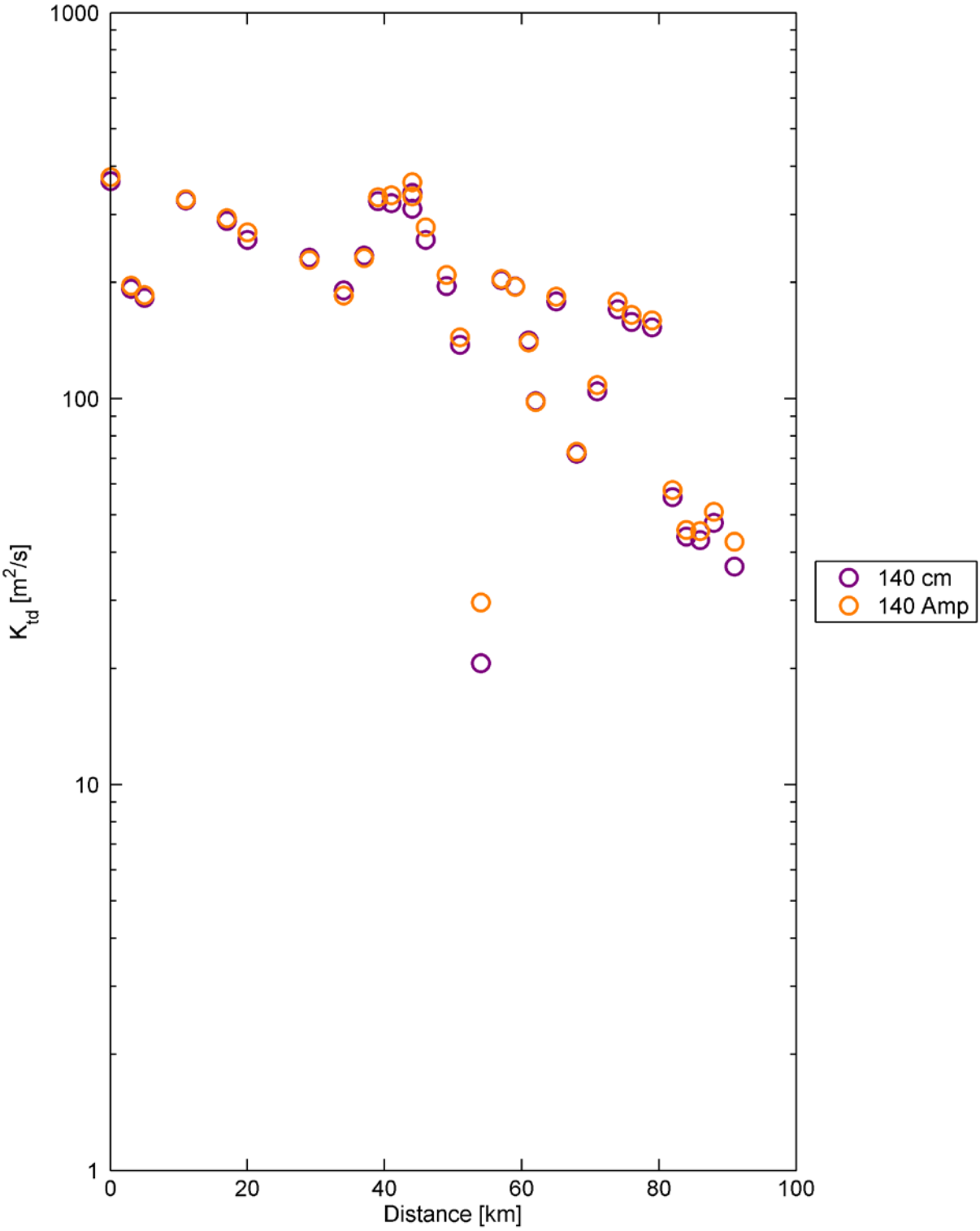

Figure 8.5-22 Estimated dispersion coefficient due to tidal dispersion for the 140 cm SLR and 140 cm SLR with 5% Amplification scenarios for the October 13, 2002 through November 10, 2002 analysis period. The horizontal scale is distance along the axis of the estuary from the Golden Gate.

8.6 Uncertainty of Salt Flux and Dispersion Analysis

The UnTRIM Bay-Delta model was calibrated for historical conditions and predicts salinity accurately during the calibration period. This calibration provides confidence that physical processes responsible for salt transport are represented adequately. The method used for the calculation of dispersion coefficients and the method used to distinguish fluxes from different physical processes are well-established (e.g. Fischer et al. 1979).

The results of the analysis for the Baseline (0 cm SLR) scenario are consistent with the conceptual model of transport developed through many field studies (e.g. Burau et al., 1998). The conceptual model is that gravitational circulation is a key transport mechanism in San Pablo Bay and Carquinez Strait and that the importance of gravitational circulation decreases sharply at the Benicia shoal due to limited depth. The DRMS analysis of dispersion coefficients at varying Net Delta Outflow (Gross et al. 2007a) indicated that the strength of gravitational circulation increased strongly with flow so that at higher flow rates it became the dominant mechanism in San Pablo Bay and Carquinez Strait, as expected. The salt flux and dispersion analysis conclusions from this analysis apply only to low flow rates similar to those during the two periods used in the analysis presented in this section. In Suisun Bay, due to complex bathymetry as well as less pronounced gravitational circulation, tidal dispersion processes are the dominant transport processes (e.g. Burau et al., 1998).

Though the accuracy of the estimated salt fluxes and dispersion coefficients is likely to be adequate, several limitations and uncertainties limit confidence in the estimated salt fluxes and dispersion coefficients. Some of this uncertainty is associated with the three-dimensional model predictions while additional uncertainty is associated with the analysis method. The three-dimensional model applied in this analysis provides a more detailed description of fluid motion in the San Francisco Estuary than depth-averaged or one-dimensional models. The model has been well-calibrated to water levels, tidal and tidally averaged flows and salinity. Comparison of model results to observed tidally averaged velocity profiles was not included in the calibration effort. Such a comparison would improve confidence in the model's ability to accurately predict gravitational circulation. Any future improvements to model calibration would result in some changes to calculated salt fluxes and dispersion coefficients.

Substantial uncertainty is associated with the analysis technique. Sources of uncertainty include:

- The model cross-sections are not perfectly aligned normal to tidal or tidally averaged flows.
- Only an approximate balance between advective fluxes and dispersive fluxes is achieved during the averaging period. Some of the imbalance is likely to occur due to varying Delta outflow during the analysis periods. Some of the imbalance is likely due to net tidal advection because the averaging period does not encompass an integer number of all tidal constituents (M2, K1, etc.). However, the imbalance could also affect the dispersive flux analysis to some extent.
- The salinity gradient in Equation 8-1 is the longitudinal gradient of cross-sectionally averaged and tidally averaged salinity. This salinity gradient was estimated based on centerline ("thalweg") salinity, not cross-sectionally averaged salinity, in our analysis.

- The order of spatial averaging can affect the flux decomposition. In an analysis of flux at the Golden Gate, Fram et al. (2007) report that changing from averaging laterally first to averaging vertically first changed individual flux components by approximately 10%.
- Some cross-sections are placed in branching channels. The locations where the cross-section crosses each individual channel were somewhat subjective. Adopting a different convention for orienting the cross-sections across branching channels could affect the flux decomposition.

8.7 Summary and Conclusions

The salt flux analysis presented in this section quantitatively estimated the contributions of individual transport processes to predicted increased salt intrusion resulting from sea level rise and tidal amplification. Salt fluxes and dispersion coefficients were estimated at 32 different cross-sections for seven different scenarios: Baseline, 15 cm SLR, 30cm SLR, 45 cm SLR, 60 cm SLR, 140 cm SLR, and 140 cm SLR with 5% Amplification. Two different periods, each spanning 29 days of historic tides and variable Delta outflows were analyzed for each scenario. Periods of fairly steady flows were chosen to simplify interpretation of the analysis results. For this reason, both periods were low flow periods, but the second analysis period, October 13, 2002 through November 10, 2002, had more variable flows and substantially higher salinity conditions than the first analysis period, July 16, 2002 through August 12, 2002. Therefore the two sets of results can be viewed two different realizations of flux analysis for fairly similar Delta outflows.

The salt flux analysis had not previously been applied in the San Francisco Estuary to simulations using historical tides. This analysis was successfully conducted, as evidenced by the close balance between computed dispersive flux and advective flux in the July 16, 2002 through August 12, 2002 analysis period and fairly good balance between computed dispersive flux and advective flux in the October 13, 2002 through November 10, 2002 analysis period. The second period was more challenging due to more variable Delta outflow and salinity.

The predicted salinity and salt fluxes increase at all locations with sea level rise. The estimated dispersion coefficients show little variability with sea level rise in Central Bay and San Pablo Bay and increase with sea level rise in Carquinez Strait, Suisun Bay and the Western Delta. Much of the predicted increase is attributed to increases in tidal dispersion associated with increased tidal prism for sea level rise scenarios and the tidal amplification scenario. Gravitational circulation was predicted to increase slightly with sea level rise at most cross-sections in Suisun Bay and the Western Delta but show little variation in other locations. At some locations in Central Bay, Suisun Bay and the western Delta, the salt flux and dispersion coefficient associated with gravitational circulation was negligible, so the predicted variability with sea level rise was not meaningful. The salt flux and dispersion coefficients for the unsteady vertical shear term varied substantially with sea level rise but did not show consistent trends from cross-section to cross-section as a result of sea level rise. The dispersion coefficient associated with unsteady vertical shear increased in many cross sections but also decreased significantly in some locations.

Amplification of tides increased salt intrusion at all locations. The 5% amplification of tidal range resulted in increased tidal prism at all locations and increased tidal dispersion at nearly all

cross-sections. In contrast, the 5% amplification of tidal range resulted in decreased gravitational at most cross-sections. There was no consistent trend of change in the magnitude of unsteady vertical shear with amplification of tidal range.

The salt flux results were generally consistent with previous analyses conducted as part of the DRMS studies (Gross et al., 2007a; Gross et al., 2007b). Since the Delta outflow conditions were higher for the SLR analysis conducted for DRMS (Gross et al., 2007a), gravitational circulation was estimated to be more substantial for those higher flow conditions. However, the spatial variability of dispersion components and variability with sea level rise predicted in the DRMS studies (Gross et al., 2007a) were generally similar to those predicted in this report. In this report, additional supporting analysis has been conducted showing variability in tidal prism, vertical shear in tidally averaged velocity and stratification between scenarios. These analyses help to explain predicted changes in salt flux processes and dispersion coefficients.

It should be emphasized that the results in this report apply only to low flow conditions typical of summer and fall when salt intrusion is most pronounced. Under higher flow conditions, gravitational circulation becomes dominant throughout most of the estuary (Gross et al., 2007a). Increases in gravitational circulation could result from the deepening associated with sea level rise. Those increases would result in less efficient flushing of salt during peak flow periods, as noted in Section 4.

Some of the results of the salt flux analysis in this report and the DRMS studies (Gross et al., 2007a) may be surprising to San Francisco Bay scientists. First, tidal prism increases significantly with sea level rise. Second, at least partially as a consequence of increases in tidal prism, tidal dispersion increases as a result of sea level rise. Third, in many locations, gravitational circulation is estimated to decrease with sea level rise. Increased depth, as an isolated factor, can be expected to cause increased gravitational circulation (e.g. Monismith et al., 2002). However, increases in tidal prism with sea level rise causes increased vertical mixing and less stratification, resulting in less gravitational circulation.

These salt flux analysis results have some important ramifications for simulation of salt intrusion in San Francisco Bay and the Delta. First, since dispersion coefficients at many locations change significantly with sea level rise, one-dimensional models should be “recalibrated” to account for this change in dispersion with sea level rise. Second, since dispersion coefficients change with tidal amplitude, it is reasonable to assume that they will change with tidal restoration, flooding of islands, inundation of low lying regions as sea level rises, or other changes to the Delta geometry that are likely to affect tidal range and/or tidal prism. Therefore, dispersion coefficients applied in a one-dimensional model for an existing geometry of the Delta may not be accurate for simulation of an altered geometry. Lastly, the gravitational circulation component of dispersion also changes with tidal prism, as clearly evidenced in the 140 cm SLR with 5% Amplification scenario. Therefore, this component of dispersion should also be expected to change as a result to changes in Delta geometry. For this reason, unless adjusted to account for changes to dispersion processes, the dispersion coefficients of both one-dimensional and two-dimensional models could lead to significant inaccuracies in simulations of salt intrusion for substantially altered Delta geometry. In order to assure appropriate representation of changes to salt intrusion processes for scenarios of substantially altered Delta geometry, three-dimensional simulations are preferable.

The salt flux analysis results also inform expectations of effects of restoration scenarios on salt intrusion. They suggest that increases in tidal prism associated with restoration are likely to result in increased salt intrusion during low Delta outflow conditions.

9. Summary and Conclusions

As part of the Bay Delta Conservation Plan (BDCP), future conditions simulations are planned which will need to incorporate the potential effects of sea level rise on salinity intrusion in the Sacramento-San Joaquin Delta. In support of this effort, three-dimensional hydrodynamic and salinity simulations using the UnTRIM Bay-Delta model were made to provide a reference condition for re-calibration of appropriate dispersion factors for the 1-D and 2-D models which are the primary tools being used in the BDCP planning process. The 3-D UnTRIM Bay-Delta model provides an already established and well-documented hydrodynamic model which is suitable for a detailed assessment of the potential salinity impacts of Sea Level Rise (SLR) in San Francisco Bay and the Sacramento-San Joaquin Delta.

This report presents the results of the sea level rise impacts on salinity in San Francisco Bay and the Sacramento-San Joaquin Delta that were predicted using the UnTRIM Bay-Delta model. A full set of hydrodynamic and salinity model results were also provided to CH2M Hill for use in recalibration of the DSM2 and RMA2 models to incorporate the effects of SLR into the lower dimensional models being used as part of the BDCP technical studies.

The UnTRIM Bay-Delta model used for this project builds on previous applications (e.g., MacWilliams et al., 2007; MacWilliams et al., 2008; MacWilliams et al., 2009), and was further refined as part of this study to increase the model grid resolution in Suisun Marsh. The UnTRIM Bay-Delta model was used to simulate hydrodynamics and salinity under Baseline conditions and for two levels of SLR. The Baseline simulation period spans from October 15, 2001 through January 1, 2003. The analysis of sea level rise impacts spans a one-year period from January 1, 2002 through January 1, 2003.

The sea level rise simulation results and salt flux analysis demonstrate that multiple different processes result in salinity impacts due to sea level rise. These processes include increased tidal dispersion, increased gravitational circulation in some regions, and decreased efficiency of flushing flows at pushing salt out of the Delta. In the south Delta, more frequent flow over agricultural barrier weirs with increasing SLR also results in some salinity differences. Additionally, increased water volume with SLR results in a slower response in the south Delta to inflow salinity increases, which results in decreases in salinity with SLR in some regions, particularly in the San Joaquin River near Stockton, during periods of increasing tributary inflow salinity.

The simulations with increased tidal amplitude suggest that increased tidal prism results in increased salt intrusion. These results are consistent with the salt flux analysis in indicating the importance of tidal dispersion processes in causing salt intrusion during low Delta outflow periods and suggest that tidal marsh restoration, flooding of Delta islands and any other actions which increase tidal prism in the Delta could increase salt intrusion.

The sea level rise simulations presented in this report assume a “hard shoreline,” which means that the current shoreline as represented by the edges of the UnTRIM Bay-Delta model grid is assumed to stay constant with SLR. Since additional areas—including in-channel islands, high marsh areas, and other regions that are expected to flood with increasing sea level or due to levee

failures—are expected to flood with increasing sea level rise, it is likely that the hard shoreline assumption results in an under prediction of salinity impact due to SLR. The effect of this under prediction is likely to increase with the level of SLR simulated. Furthermore, the salt flux analysis suggests that the dispersion coefficients used to represent unresolved salt transport processes in one-dimensional models may be inappropriate for future scenarios with substantially different tidal prism than current conditions.

The SLR simulations presented in this report assumed no operational response to the increased salinity intrusion. Incorporation of operational response into SLR simulations requires the incorporation of the predicted salinity impacts due to SLR into DSM2 and CALSIM II. The predicted salinity impacts from the UnTRIM Bay-Delta model simulations presented in this report are being used to incorporate the increases in salinity resulting from SLR into the DSM2 and CALSIM II models in order to allow for the simulation of operational response to predicted salinity impacts due to SLR in CALSIM II. This will allow for future SLR simulations that incorporate operational response, using either UnTRIM, RMA2, or DSM2.

Acknowledgments

The authors would like to acknowledge Armin Munevar (CH2M Hill) for project management and technical oversight. Additional technical expertise—particularly with regards to coordination of boundary conditions between UnTRIM, RMA2, and DSM2—was provided by Kyle Winslow (CH2M Hill), Chandra Chilmakuri (CH2M Hill), Richard Rachiele (RMA), Stacie Grinbergs (RMA), and John DeGeorge (RMA). Observation data were provided by Nick Leach (USGS) and Cathy Ruhl (USGS). Additional data and information was provided by Min Yu (DWR). The authors would like to acknowledge Sandy Chang and Rusty Holleman for their assistance with the analysis and figure preparation for the salt flux analysis. The UnTRIM code was developed by Professor Vincenzo Casulli (University of Trento, Italy). The authors would especially like to thank Richard Rachiele (RMA) and John DeGeorge (RMA) for sharing their vast experience and knowledge of modeling the Sacramento-San Joaquin Delta and providing guidance on the application of UnTRIM to the Bay-Delta. Additional technical input and expertise in the development of the UnTRIM Bay-Delta model was provided by Ralph Cheng (USGS, retired), Pete Smith (USGS, retired), and Jon Burau (USGS).

References

Anderson, J. and A. Miller, 2005. Estimation of Electrical Conductivity at Martinez for Sea Level Rise Conditions, Methodology for Flow and Salinity Estimates in the Sacramento-San Joaquin Delta and Suisun Marsh, 26th Annual Progress Report, Chapter 5.

Casulli, V. 1990. Semi-implicit finite difference methods for the two-dimensional shallow water equations. Journal of Computational Physics. 86, 56-74.

Burau, J.R., Gartner, J.W., and Stacey, M., 1998. Results for the hydrodynamic element of the 1994 Entrapment Zone Study in Suisun Bay. In Report of the 1994 Entrapment Zone Study, edited by Wim Kimmerer, 13-53. Interagency Ecological Program for the San Francisco Bay/Delta Estuary.

Casulli, V., 1999. A semi-implicit numerical method for non-hydrostatic free-surface flows on unstructured grid, in Numerical Modelling of Hydrodynamic Systems, ESF Workshop, pp. 175-193, Zaragoza, Spain.

Casulli, V. and R.A. Walters, 2000. An unstructured, three-dimensional model based on the shallow water equations, International Journal for Numerical Methods in Fluids 2000, 32: 331 - 348.

Casulli, V. and Zanolli, P., 2002. Semi-Implicit Numerical Modelling of Non-Hydrostatic Free-Surface Flows for Environmental Problems, Mathematical and Computer Modelling, 36: 1131 - 1149.

Casulli, V. and Zanolli, P., 2005. High Resolution Methods for Multidimensional Advection-Diffusion Problems in Free-Surface Hydrodynamics, Ocean Modelling, 2005, v. 10, 1-2, p. 137-151.

[CDWR] California Department of Water Resources, 1986. DAYFLOW program documentation and data summary user's guide. California Department of Water Resources, Sacramento.

CH2M Hill, 2009. DSM2 Recalibration, prepared for California Department of Water Resources, October.

Department of Water Resources, 2009. Chronological Reconstructed Sacramento and San Joaquin Valley Water Year Hydrologic Classification Indices, http://cdec.water.ca.gov/cgi-progs/iodir/wsihist

Dyer K.R., 1973. Estuaries: A Physical Introduction. Wiley-Interscience, New York and London.

Fischer, H.B., List, E.J., Koh, R.C.Y., Imberger, J., and N.H. Brooks, 1979. Mixing in Inland and Coastal Waters. New York: Academic Press.

Fram, J.P., Martin. M.A., and M.T. Stacey. 2007. Dispersive Fluxes between the Coastal Ocean and a Semienclosed Estuarine Basin, Journal of Physical Oceanography, 37: 1645-1660.

Gross, E.S., Nidzieko, N., and M.L. MacWilliams, 2007a. Parameterization of mixing using a three-dimensional hydrodynamic model, Delta Risk Management Study, prepared for CA Department of Water Resources, March 2007.

Gross, E.S., MacWilliams M.L., and N. Nidzieko, N. 2007b. Three-dimensional salinity simulations of sea level rise scenarios, Delta Risk Management Study, prepared for CA Department of Water Resources, March 2007.

Hill, K. D., T. M. Dauphinee, and D. J. Woods, 1986. The extension of the Practical Salinity Scale 1978 to low salinities. IEEE J. Oceanic Eng. OE-11: 109–112.

[IEP] Interagency Ecological Program, 2008. DSS database, http://iep.water.ca.gov/data.html

[IEP] Interagency Ecological Program, 2009. Dayflow Documentation, http://iep.water.ca.gov/dayflow/

Jassby, A.D., W.J. Kimmerer, S.G. Monismith, C. Armor, J.E. Cloern, T.M. Powell, J. R. Schubel, and T.J. Vendlinski,1995. Isohaline position as a habitat indicator for estuarine populations. Ecological Applications 5:272-289.

MacWilliams, M.L., and E.S. Gross, 2007. UnTRIM San Francisco Bay-Delta Model Calibration Report, Delta Risk Management Study, prepared for CA Department of Water Resources, March 2007.

MacWilliams, M.L., E.S. Gross, J.F. DeGeorge, and R.R. Rachiele, 2007. Three-dimensional hydrodynamic modeling of the San Francisco Estuary on an unstructured grid, IAHR, 32nd Congress, Venice Italy, July 1-6, 2007.

MacWilliams, M.L., Salcedo, F.G., and E.S. Gross, 2008. San Francisco Bay-Delta UnTRIM Model Calibration Report, POD 3-D Particle Tracking Modeling Study, Prepared for California Department of Water Resources, December 19, 2008, 344 p.

MacWilliams, M.L., Salcedo, F.G., and E.S. Gross, 2009 (in review). San Francisco Bay-Delta UnTRIM Model Calibration Report, Sacramento and Stockton Deep Water Ship Channel 3-D Hydrodynamic and Salinity Modeling Study, Prepared for US. Army Corps of Engineers, San Francisco District, July 14, 2009, 574 p.

Monismith, S.G., Kimmerer, W., Burau, J.B., and M.T. Stacey. 2002. Structure and flow-induced variability of the subtidal salinity field in Northern San Francisco Bay, *Journal of Physical Oceanography*, 32, 3,003-3,019.

[NOAA] National Oceanic & Atmospheric Administration, 2008. NOAA Tides & Currents http://tidesandcurrents.noaa.gov/

[RMA] Resource Management Associates, 2005. Flooded Islands Pre-Feasibility Study: RMA Delta Model Calibration Report, prepared for CA Department of Water Resources for submittal to California Bay-Delta Authority, June 30.

Schoellhamer, D, and P. Buchanan, 2010. Continuous Monitoring in the San Francisco Bay and Delta, Data Collection Methods and Procedures, http://sfbay.wr.usgs.gov/sediment/cont_monitoring/methods.html

Simpson, J.H., Brown, J., Matthews, J. and G. Allen. 1990. Tidal straining, density currents and stirring in the control of estuarine stratification, Estuaries, 13, 125-131.

Sommer T, Armor C, Baxter R, Breuer R, Brown L, Chotkowski M, Culberson S, Feyrer F, Gingras M, Herbold B, Kimmerer W, Mueller-Solger A, Nobriga M, Souza K. 2007. The collapse of pelagic fishes in the upper San Francisco Estuary. Fisheries 32:270-277.

Stacey, M.T., Burau, J.R, and S.G. Monismith, 2001. The creation of residual flows in a partially stratified estuary, Journal of Geophysical Research, 106(C8), 17,013-17,038.

[SWRCB] State Water Resources Control Board, California Environmental Protection Agency, 2000. Revised Water Right Decision 1641, In the Matter of: Implementation of Water Quality Objectives for the San Francisco Bay/Sacramento-San Joaquin Delta Estuary; A Petition to Change Points of Diversion of the Central Valley Project and the State Water Project in the Southern Delta; and A Petition to Change places of Use of the Central Valley Project, December 29, 1999; Revised in Accordance with Order WR 2000-02, March 15, 2000.

UNESCO, 1985. The International System of Units (SI) in Oceanography. Tech. Pap. Mar. Sci., 45: 124 pp.

USGS, 2009, USGS Water Quality of SF Bay, http://sfbay.wr.usgs.gov/access/wqdata

Walters, R.A., Cheng, R.T. and Conomos, T.J., 1985. Time scales of circulation and mixing processes of San Francisco Bay waters, *Hydrobiologia*, 129, 13-36.

Appendix A. Model Validation Figures for 2002 Simulation Period

The calibration of UnTRIM Bay-Delta model for flow, stage, and salinity has been thoroughly documented in previous studies (i.e., MacWilliams et al., 2008; MacWilliams et al., 2009). As a result, no additional calibration was conducted as part of this study. In this context, comparison of predicted water levels, flows, and salinity with observations during this simulation provides an additional validation of the previous calibration and validation studies.

Some aspects of the boundary conditions used in this application of the UnTRIM Bay-Delta model differ from the commonly used boundary conditions described by MacWilliams et al. (2008; 2009). In general, these modifications were made so that the boundary conditions used in this application of the UnTRIM Bay-Delta model were as close to identical as possible to the boundary conditions used in DSM2 for the DSM2 recalibration (CH2M Hill, 2009). The most significant change was that the flow though the radial gates into Clifton Court Forebay were applied using the exact flows calculated by DSM2. This modification results in a much lower level of agreement between observed and predicted water levels inside Clifton Court Forebay, than in previous applications of the UnTRIM Bay-Delta model (e.g., MacWilliams et al., 2009). In addition, the agreement between observed and predicted tidal time scale flows in Old River is decreased relative to the three periods simulated by MacWilliams et al. (2008) or the three periods simulated by MacWilliams et al. (2009). This largely results because the gate equations used in DSM2 are not nearly as accurate at determining the instantaneous flow through the radial gates as the historical SWP flow values which are based in part the daily change in volume inside Clifton Court Forebay. Additionally, the time interpolation of inflow boundaries was modified to reflect the stepwise application of these boundaries in DSM2. The effect of this change is evident in the stage comparisons at Verona and Vernalis, and some of the predicted phase differences in the calibration, but this change is not expected to have a significant impact on the overall model results. Lastly, additional inflows were applied in Suisun Marsh to be consistent with the flows used in the RMA2 model.

The hydrodynamic model validation presented in this section gives a measure of the ability of the UnTRIM Bay-Delta model to accurately predict water levels (stage), flows, and salinity in San Francisco Bay and the Sacramento-San Joaquin Delta. Accurate prediction of water levels in San Francisco Bay demonstrates that tides are accurately propagating through the Bay and into the Delta. Comparison of predicted flows to observations in the Delta demonstrate the degree that the model captures the instantaneous, tidally averaged, and net flows in specific channels within the Delta. Accurate prediction of salinity in San Francisco Bay and the western Delta demonstrate the degree to which the model is accurately predicting salinity intrusion due to gravitational circulation and other processes. Within the Sacramento-San Joaquin Delta, prediction of salinity is strongly dependent on consumptive use and the out flow salinity from agricultural diversions, both of which introduce a significant level of uncertainty.

This section presents the method used to assess the model validation, and provides an extensive set of comparisons between observed and predicted water levels, flows, and salinity at observation stations in San Francisco Bay and in the Delta for the model simulation period in 2002.

A.1 Model Assessment Method

The calibration dataset included water level observations collected by NOAA, USGS, and DWR, flow measurements made by USGS and DWR, salinity data from continuous monitoring sites operated by the USGS, United States Bureau of Reclamation (USBR), and the DWR, and synoptic salinity observations by the USGS, consisting of vertical profiles of salinity at 1 meter vertical resolution at 38 sampling locations along the axis of the San Francisco Estuary (USGS, 2009).

Predicted stage, flow, and salinity were compared to observation data at stations where data were collected by NOAA, USGS, and DWR. Data from NOAA were downloaded from the Tides and Currents webpage (NOAA, 2008) and are identified using the seven digit NOAA station identification number. USGS data were provided by Cathy Ruhl and Nick Leach from the USGS Sacramento office and are identified using the three letter USGS identifier. The DWR data were obtained both from the IEP DSS database (IEP, 2008) and from the California Data Exchange Center (CDEC) online database. Data extracted from the IEP DSS database are identified using the DSS B value field which consists of a string of letters and numbers, while data downloaded from CDEC are identified by the three letter CDEC identifier, which in some cases differs from the USGS three letter identifier for the same station.

The quality of fit between predicted model results and observed stage, flow, and salinity time series data are assessed following a cross-correlation procedure similar to that used by RMA (2005). This approach has also been used by MacWilliams and Gross (2007) and MacWilliams et al. (2008; 2009), and provides a thorough description of the differences between time series records through a quantitative measure of differences in terms of phase, mean, amplitude, and constant offsets. Statistics are derived to quantify the differences between predicted and observed time series data. Four types of statistics are presented in this report, following the approach used by RMA (2005):

- Mean – Comparison of simple mean values of the predicted and observed time series.

- Phase Shift – The average shift in time between the predicted and observed time series.

- Amplitude Ratio – Comparison of the time series range, which ideally would equal 1. This value is estimated after removing the phase shift between predicted and observed time series.

- Scatter – The remaining difference between predicted and observed time series after phase and amplitude errors are removed. One measure of the scatter is the goodness of fit parameter, R^2, from a linear regression performed on the observed and predicted time series with phase error removed. Note that this R^2 is a measure of the scatter around a best-fit line, not a 1:1 line, on the scatter plots.

For each stage, flow, and salinity time series comparison, a total of three different types of figures are shown. The top figure shows the tidal time scale variability for a period of approximately fifteen days. On the bottom left, a tidally averaged plot is shown for the full analysis period to evaluate spring-neap and longer time scale variability, as well as non-tidal forcing such as storm surge. Tidal averages are computed by filtering twice using a 24.75 hour running average filter. On the lower right, the scatter plot shows a comparison between the observed and predicted data over the analysis period. The scatter plot is produced by first running a cross-correlation between the observed data and model predictions to find the average phase lag over the entire record. The cross-correlation was performed following the procedure outlined by RMA (2005). The process entails repeatedly shifting the predicted time series record at one minute increments relative to the observed time series and computing the correlation coefficient at each time shift. The correlation has a maximum value when the shifted model time series best matches the observed time series. The time shift when the maximum correlation occurs represents the phase difference in minutes between the predicted and observed data, with positive values indicating that the predicted time series lags the observed time series. The linear regression is then performed between the time shifted model results and observed data record to yield the amplitude ratio, best-fit line, and correlation coefficient. In some cases, the cross-correlation procedure does not identify a local maximum correlation coefficient within a four hour analysis window (two hours forward and two hours backward). This can occur for water level comparisons when the data does not having a strong tidal time-scale signal (at upstream stations such as Verona on the Sacramento River or Vernalis on the San Joaquin River), or for upstream salinity stations where the inflow salinity is constant or nearly constant. For these stations, the phase lag is shown as "n/a", and the linear regression is performed with no phase correction. In summary, the statistics reported on each scatter plot include the following:

- Mean Obs – Average value of observed time series for analysis period
- Mean Pred – Average value of predicted time series for analysis period
- Lag – Phase difference in minutes between observed and predicted; a positive value indicates that the predicted time series lags behind the observed time series.
- Y = slope*X + offset – Best linear fit, where Y is predicted, X is observed. The slope value is used as the amplitude ratio.
- R^2 – Linear regression goodness of fit parameter.

The observed and predicted means, phase lag, amplitude ratio, and R^2 value are also summarized in tables for each simulation period and comparison type.

A.2 Description of 2002 Simulation Period

The 2002 simulation period, which spans from January 1, 2002 to January 1, 2003, was used as the primary analysis period in this study. This period was selected to provide the opportunity for comparison to the corroboration results from the RMA2 and DSM2 models which was

completed as part of the BDCP study. A subset of this period was used for flow and stage model calibration of the UnTRIM Bay-Delta model as part of the POD project (MacWilliams, et al., 2008). No previous salinity calibration or validation of the UnTRIM Bay-Delta model has been conducted for this simulation period.

The 2002 simulation period spans from water year 2002 to water year 2003. Water year 2002 (from October 1, 2001 through September 30, 2002) was classified as a "dry" year on both the Sacramento River and the San Joaquin River. Water Year 2003 (from October 1, 2002 through September 30, 2003) was classified as an "above normal" year on the Sacramento River and as a "below normal" year on the San Joaquin River (DWR, 2009).

A.3 Water Level Comparison Figures

Observed and predicted water levels were compared at seven stations in San Francisco Bay and at fifty-six stations in the Sacramento-San Joaquin Delta during the 2002 simulation period. At each station, observed and predicted water levels were plotted over a fifteen day period to show the water level agreement over tidal time scales. In addition, the observed and predicted stage are tidally averaged, to assess the accuracy of the model in predicting water level variability on spring-neap time scales, as well as non-tidal forcing such as storms. Lastly, the cross-correlation (as described in Section A.1) was used to determine the mean observed and predicted water level, the amplitude ratio, the phase lag, and the correlation coefficient squared (R^2). For each of the water level stations, these values are compiled in Table A-1.

A.3.1 San Francisco Bay

Water level comparisons were made at five NOAA and two DWR continuous observation stations in the San Francisco Estuary, at the locations shown in Figure A.3-1. Water level comparisons at these stations are shown in Figures A.3-2 through A.3-8.

A.3.2 Northern Sacramento-San Joaquin Delta

Water level comparisons were made at ten continuous water level observation stations in the northern portion of the Sacramento-San Joaquin Delta, at the locations shown in Figure A.3-9. Water level comparisons at these stations are shown in Figures A.3-10 through A.3-19.

A.3.3 Central Sacramento-San Joaquin Delta

Water level comparisons were made at nineteen continuous water level observation stations in the central portion of the Sacramento-San Joaquin Delta, at the locations shown in Figure A.3-20. Water level comparisons at these stations are shown in Figures A.3-21 through A.3-39.

A.3.4 Southern Sacramento-San Joaquin Delta

Water level comparisons were made at twenty continuous water level observation stations in the southern portion of the Sacramento-San Joaquin Delta, at the locations shown in Figure A.3-40. Water level comparisons at these stations are shown in Figures A.3-41 through A.3-60.

Table A-1 Predicted and observed stage and cross-correlation statistics for stage monitoring stations in San Francisco Bay and the Sacramento-San Joaquin Delta during the 2002 simulation period.

Location	Data Source	Figure Number	Mean Water Level		Cross Correlation		R^2
			Observed (m)	Predicted (m)	Amp Ratio	Lag (min)	
2002 San Francisco Bay Stage Stations (Figure A.3-1)							
San Francisco	NOAA	A.3-2	0.96	0.95	0.999	-1	0.999
Alameda	NOAA	A.3-3	0.96	0.99	1.003	13	0.998
Redwood City	NOAA	A.3-4	0.97	1.00	0.988	6	0.998
Richmond	NOAA	A.3-5	0.97	0.99	0.991	7	0.998
Sacramento River at Martinez	DWR	A.3-6	1.11	1.10	0.973	13	0.988
Port Chicago	NOAA	A.3-7	1.14	1.14	0.973	10	0.996
Sacramento River near Mallard Island	DWR	A.3-8	1.12	1.14	0.950	8	0.995
2002 North Delta Stage Stations (Figure A.3-9)							
Sacramento River South of Georgiana Slough	USGS	A.3-10	1.54	1.46	0.980	-6	0.985
Georgiana Slough near Sacramento River	USGS	A.3-11	1.45*	1.45	0.952	9	0.978
Delta Cross Channel	USGS	A.3-12	1.24	1.36	1.016	8	0.928
Sacramento River North of Delta Cross Channel	USGS	A.3-13	1.56	1.47	0.945	7	0.979
Mokelumne River near Thornton	DWR	A.3-14	1.35	1.33	0.884	-33	0.843
South Fork Mokelumne River at New Hope Bridge	DWR	A.3-15	1.34	1.30	1.097	7	0.986
Steamboat Slough between Sacramento River and Sutter Sl.	USGS	A.3-16	1.39	1.39	1.157	2	0.985
Sacramento River at Freeport	USGS	A.3-17	1.78*	1.78	0.789	-25	0.982
Sacramento River at I Street	DWR	A.3-18	2.27*	2.27	0.824	-4	0.994
Sacramento River at Verona	DWR	A.3-19	3.82	3.84	0.642	117	0.995
2002 Central Delta Stage Stations (Figure A.3-20)							
San Joaquin River at Antioch	DWR	A.3-21	1.19*	1.19	0.942	1	0.976
Sacramento River at Rio Vista	USGS	A.3-22	1.25	1.22	1.029	11	0.993
Threemile Slough at San Joaquin River	USGS	A.3-23	1.19*	1.19	1.082	1	0.989
San Joaquin River at Jersey Point	USGS	A.3-24	1.21	1.20	1.019	13	0.982
Dutch Slough at Jersey Island	USGS	A.3-25	1.20	1.20	1.015	13	0.990
False River	USGS	A.3-26	1.15	1.18	1.067	20	0.994
Taylor Slough	USGS	A.3-27	1.15	1.19	1.073	17	0.993
Sand Mound Slough	USGS	A.3-28	1.15	1.20	1.048	23	0.987
San Joaquin River at San Andreas Landing	DWR	A.3-29	1.29	1.22	1.043	10	0.982
Old River at San Joaquin River	USGS	A.3-30	1.16	1.22	1.068	23	0.994
Mokelumne River near San	USGS	A.3-31	1.21	1.21	1.028	11	0.987

Joaquin River							

North Fork of Mokelumne River at Georgiana Slough	DWR	A.3-32	1.32	1.24	1.055	3	0.990
San Joaquin River at Venice Island	DWR	A.3-33	1.23*	1.23	1.034	11	0.991
Franks Tract East	USGS	A.3-34	1.14	1.21	1.059	23	0.993
Franks Tract West	USGS	A.3-35	1.16	1.20	0.983	24	0.967
Old River at Mandeville Island	USGS	A.3-36	1.15	1.21	1.072	23	0.994
Holland Cut	USGS	A.3-37	1.18	1.20	1.011	23	0.974
San Joaquin River at Rindge Pump	DWR	A.3-38	1.23*	1.23	1.022	13	0.990
Middle River south of Columbia Cut	USGS	A.3-39	1.22*	1.22	1.038	-22	0.990
2002 South Delta Stage Stations (Figure A.3-40)							
Old River at Bacon Island	USGS	A.3-41	1.18	1.21	1.015	9	0.984
Middle River at Middle River	USGS	A.3-42	1.16	1.16	1.024	6	0.991
Middle River at Borden Highway	DWR	A.3-43	1.19	1.15	1.030	-1	0.986
Middle River at Tracy Blvd	DWR	A.3-44	1.21	1.20	1.006	-7	0.977
Middle River at Howard Road Bridge	DWR	A.3-45	1.23*	1.23	0.944	5	0.947
Middle River at Mowry Bridge	DWR	A.3-46	1.25	1.25	0.971	1	0.959
Old River near Byron	DWR	A.3-47	1.18	1.15	1.039	-15	0.986
Clifton Court Forebay Radial Gates	DWR	A.3-48	0.58	0.16	0.566	-99	0.499
Old River at Clifton Court Ferry	DWR	A.3-49	1.05	1.09	1.020	-17	0.979
Grant Line Canal at Tracy Blvd	USGS	A.3-50	1.12	1.15	0.911	19	0.960
Doughty Cut above Grant Line Canal	DWR	A.3-51	1.24	1.24	0.843	-4	0.901
Old River near Delta Mendota Canal (NW of Barrier)	DWR	A.3-52	1.04	1.08	1.018	-13	0.976
Old River near Delta Mendota Canal (SE of Barrier)	USGS	A.3-53	1.21	1.20	0.932	-22	0.944
Old River at Tracy Blvd	DWR	A.3-54	1.18	1.21	0.894	-6	0.944
Stockton Ship Channel at Burns Cutoff	DWR	A.3-55	1.29	1.23	1.005	10	0.983
San Joaquin River at Stockton	USGS	A.3-56	1.24	1.24	1.037	10	0.989
San Joaquin River below Old River near Lathrop	DWR	A.3-57	1.42*	1.42	1.066	11	0.937
Old River at Head	DWR	A.3-58	1.35	1.35	1.018	-11	0.917
San Joaquin River at Mossdale	DWR	A.3-59	1.57	1.57	1.423	-7	0.863
San Joaquin River at Vernallis	DWR	A.3-60	4.28*	4.28	0.756	23	0.994

* Observed data are measured relative to arbitrary vertical datum. Observed data are offset to match predicted mean water level for comparison plots.

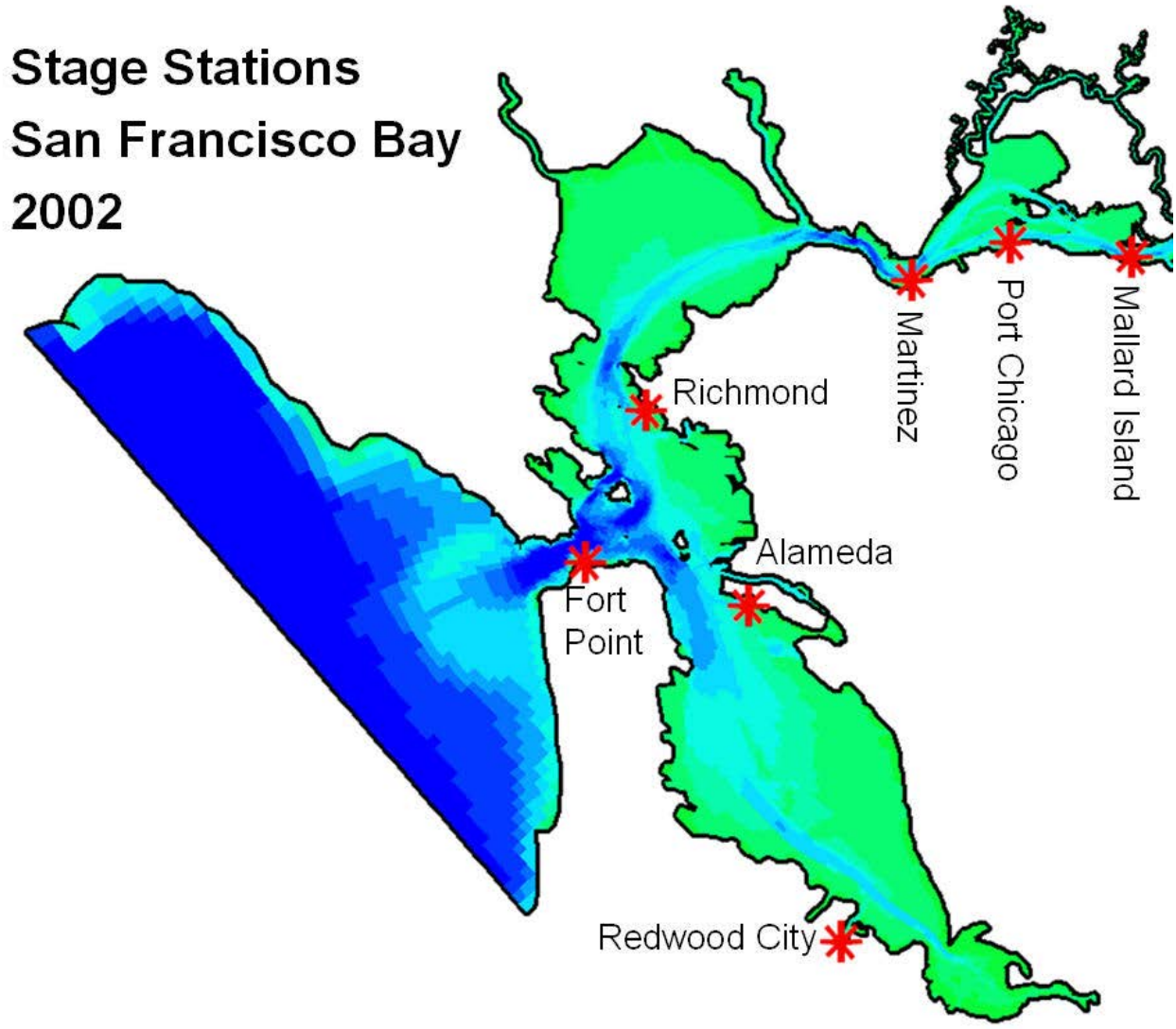

Figure A.3-1 Location of NOAA and DWR water level monitoring stations in San Francisco Bay used for 2002 water level comparisons.

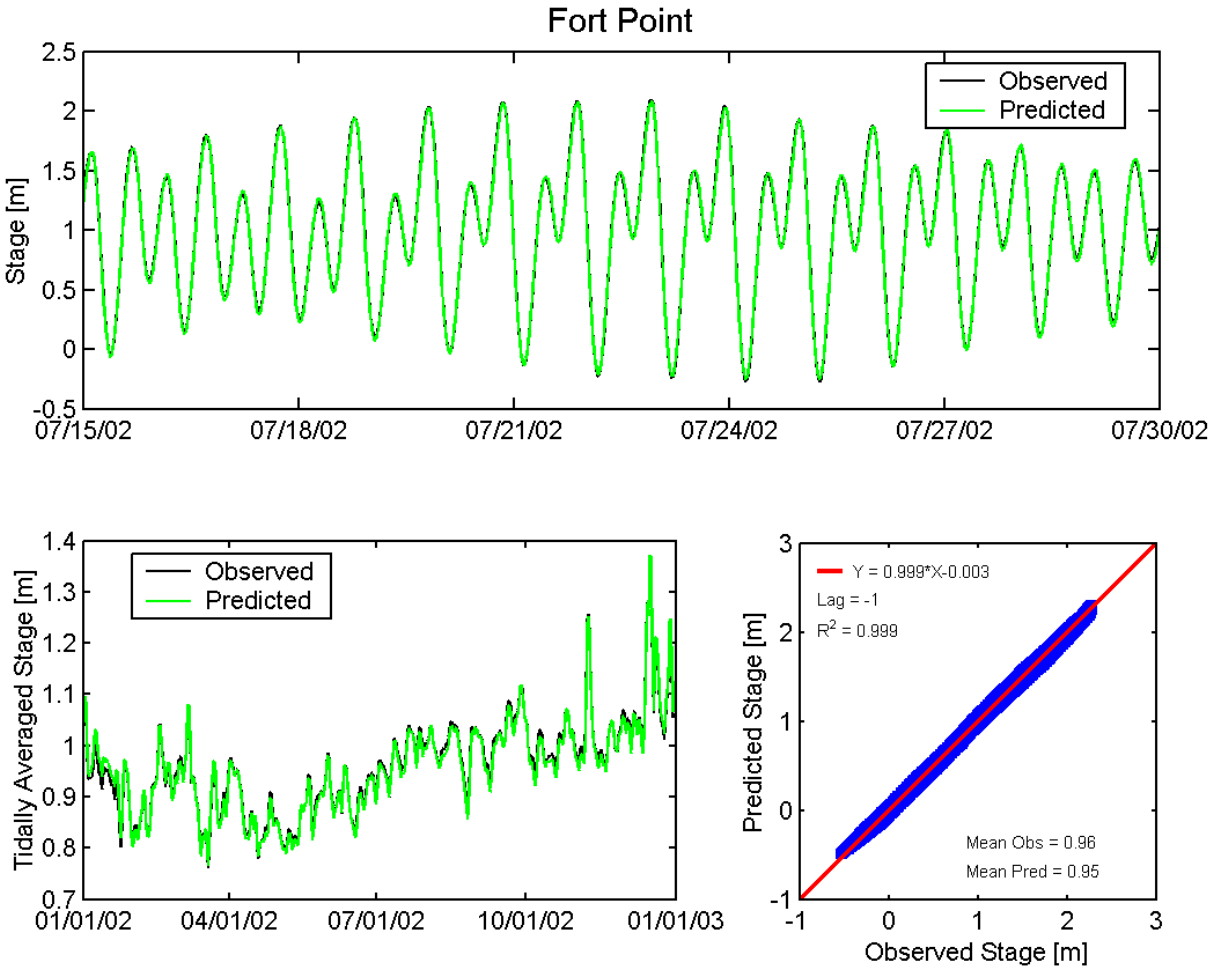

Figure A.3-2 Observed and predicted stage at San Francisco Fort Point NOAA station (9414290) during the 2002 simulation period.

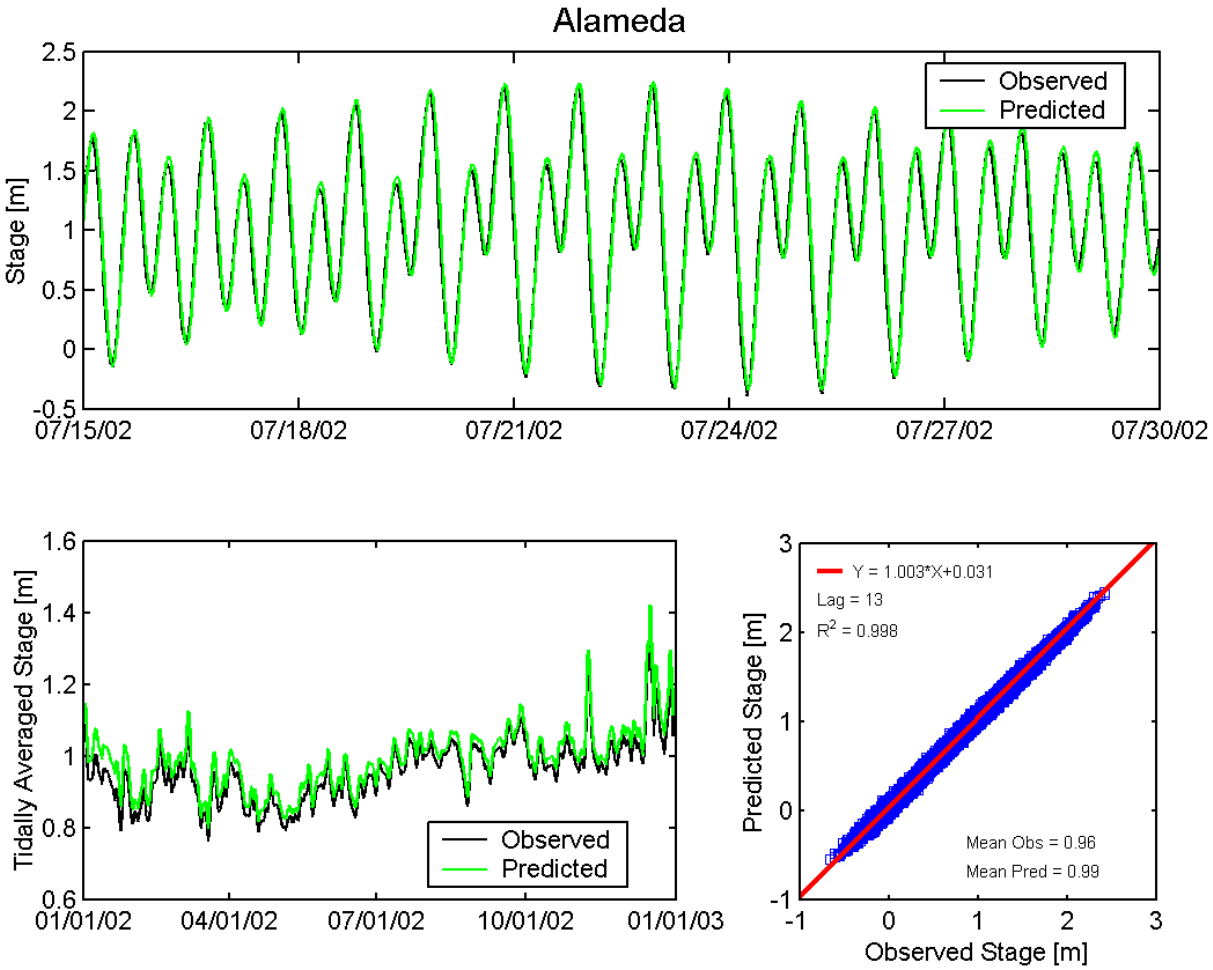

Figure A.3-3 Observed and predicted stage at Alameda NOAA station (9414750) during the 2002 simulation period.

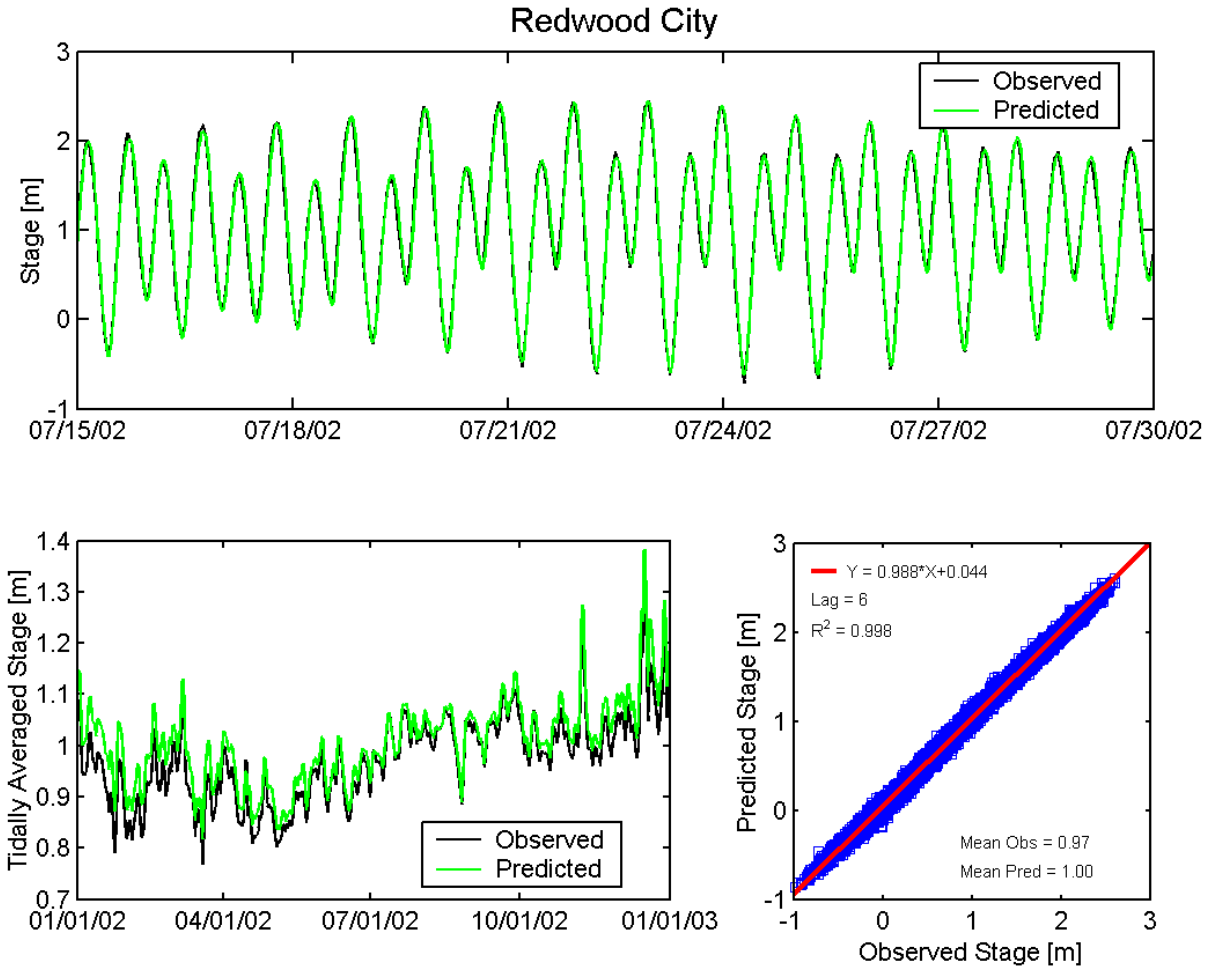

Figure A.3-4 Observed and predicted stage at Redwood City NOAA station (9414523) during the 2002 simulation period.

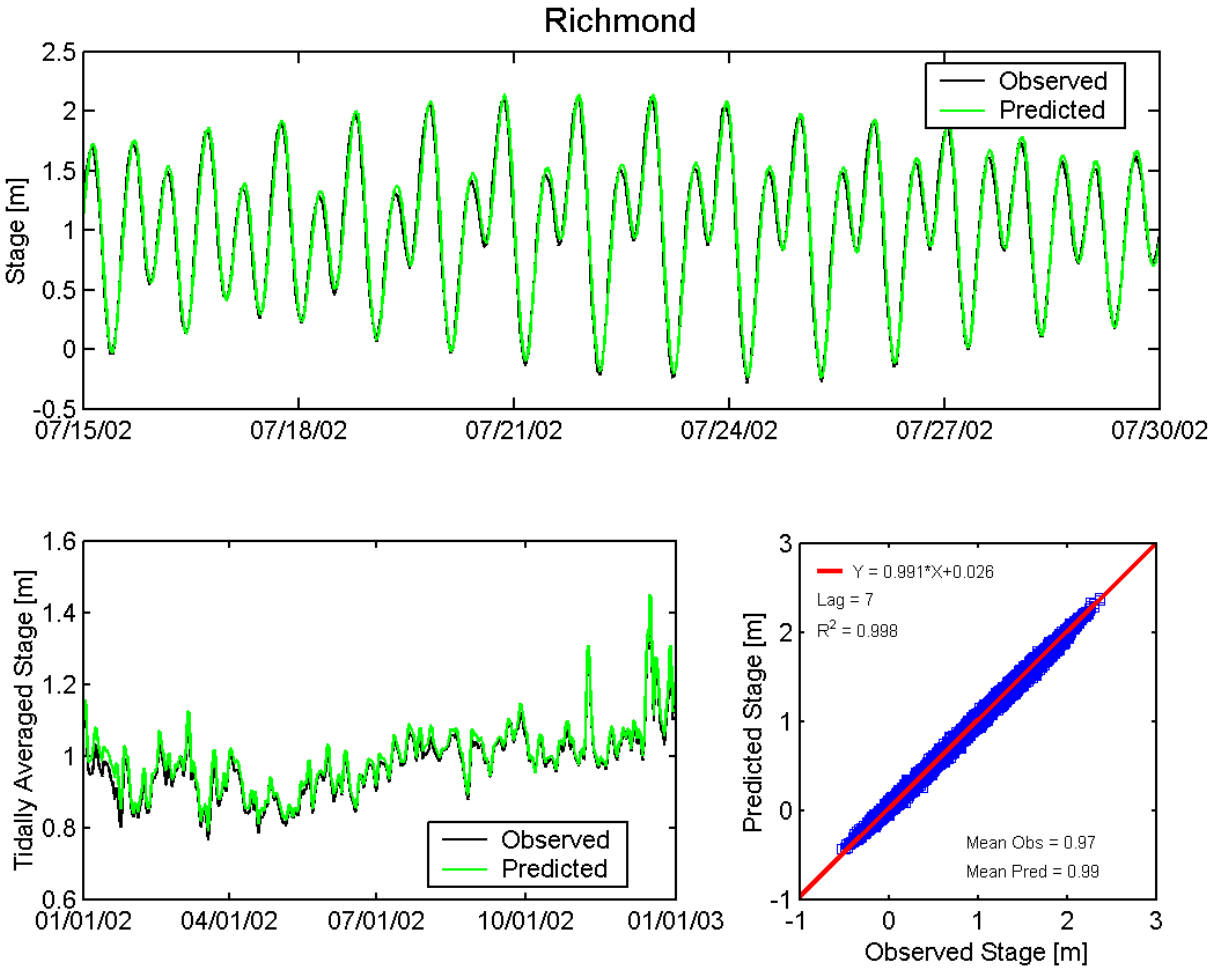

Figure A.3-5 Observed and predicted stage at Richmond NOAA station (9414863) during the 2002 simulation period.

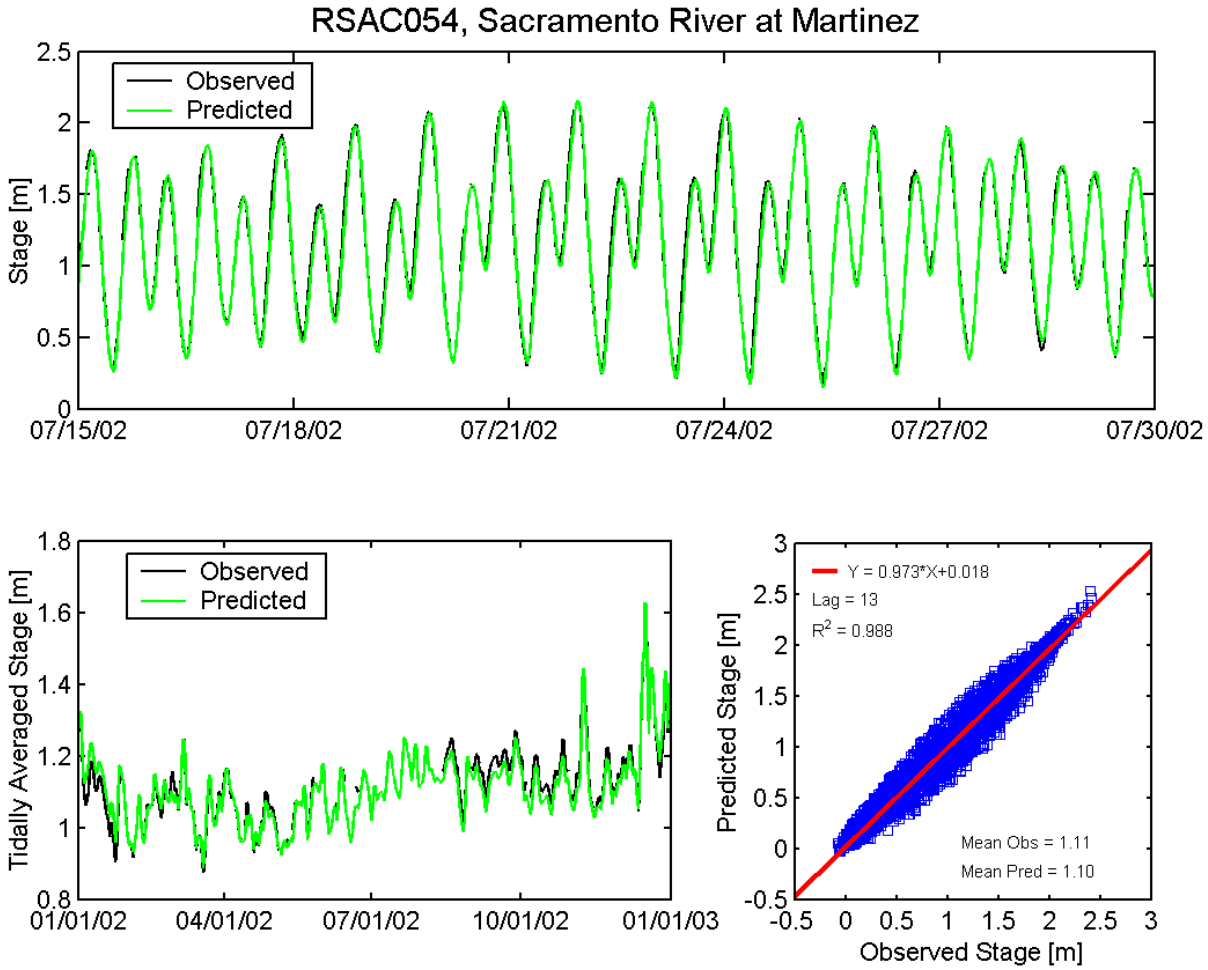

Figure A.3-6 Observed and predicted stage at Sacramento River at Martinez DWR station (RSAC054) during the 2002 simulation period.

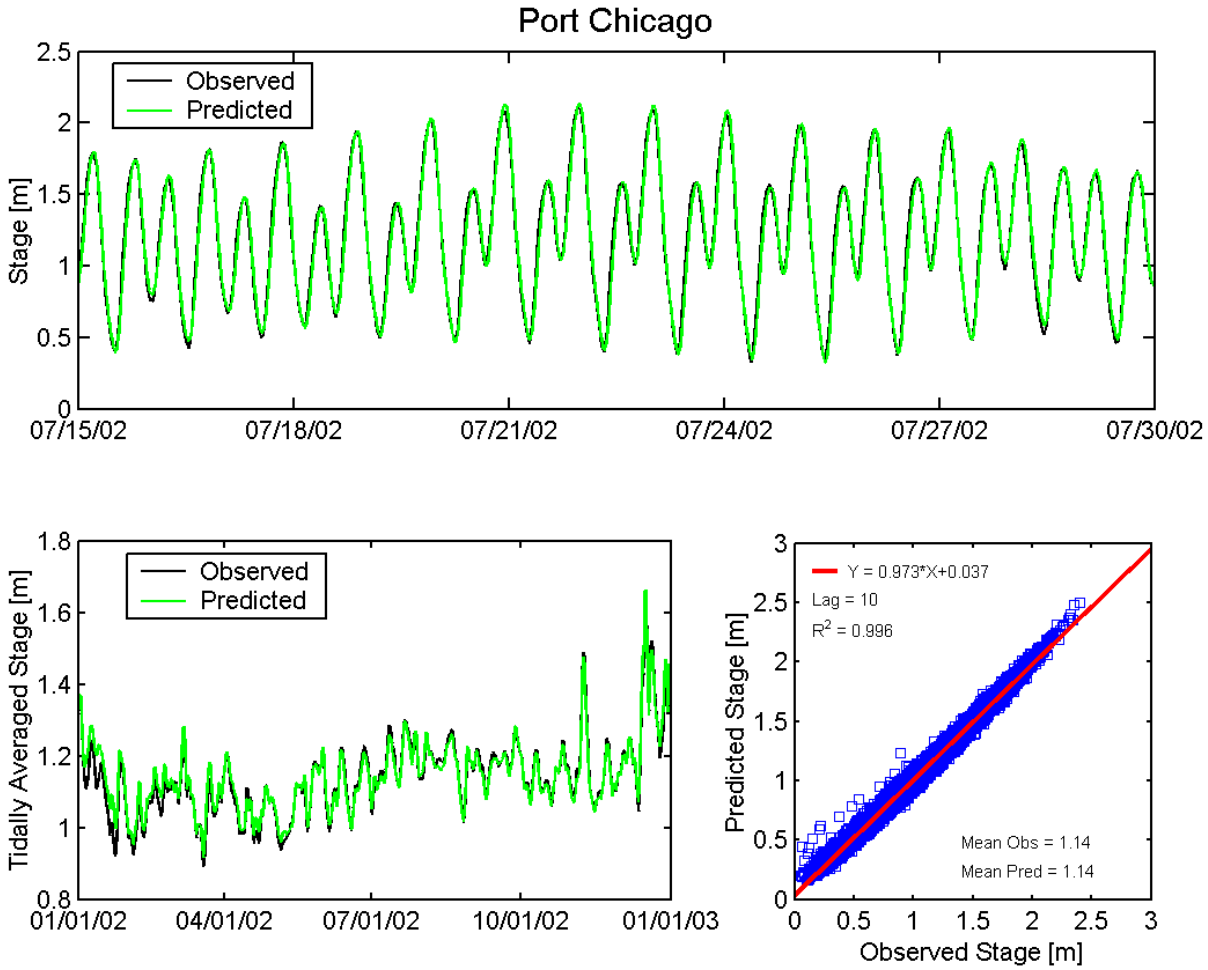

Figure A.3-7 Observed and predicted stage at Port Chicago NOAA station (9415144) during the 2002 simulation period.

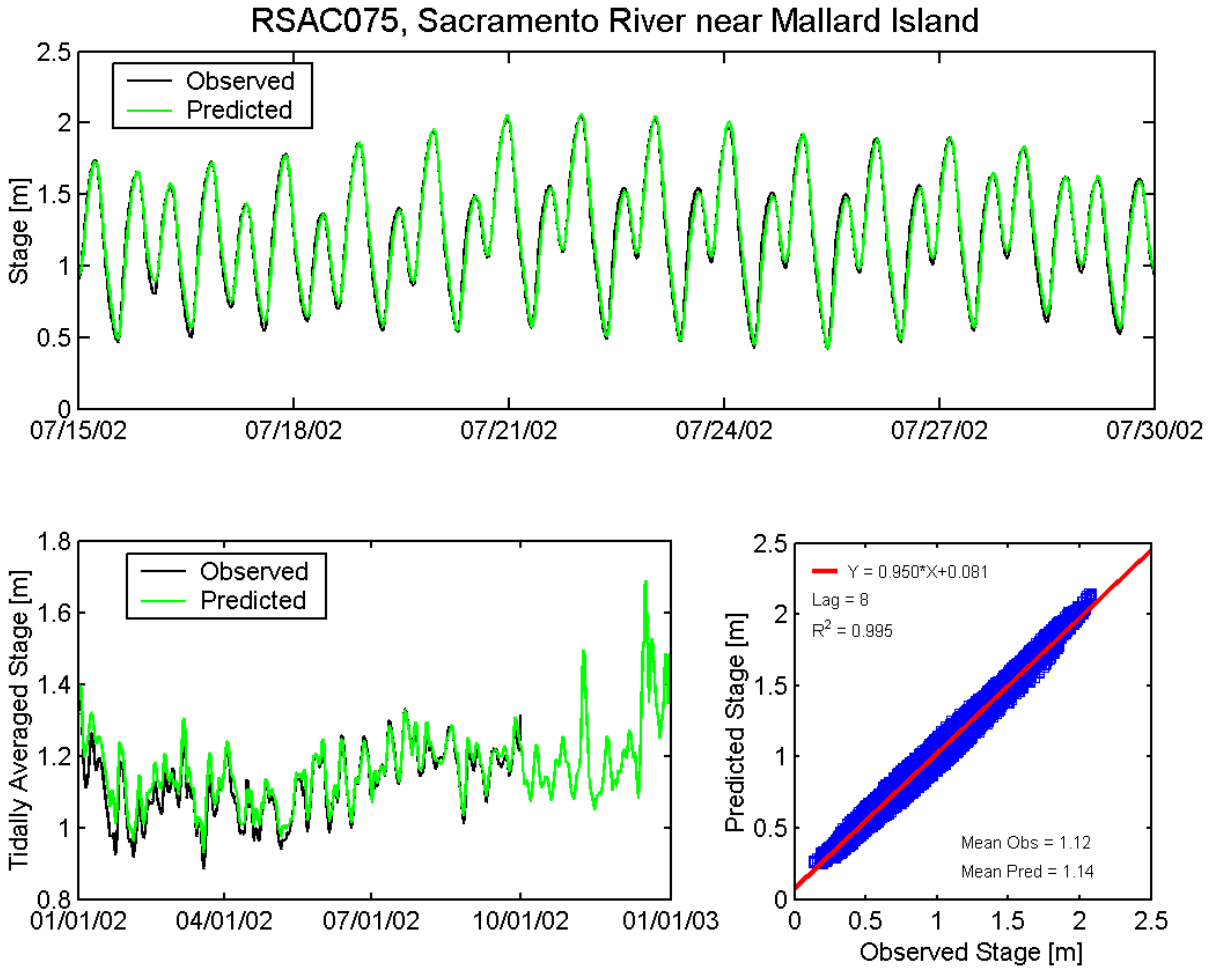

Figure A.3-8 Observed and predicted stage at Sacramento River near Mallard Island DWR station (RSAC075) during the 2002 simulation period.

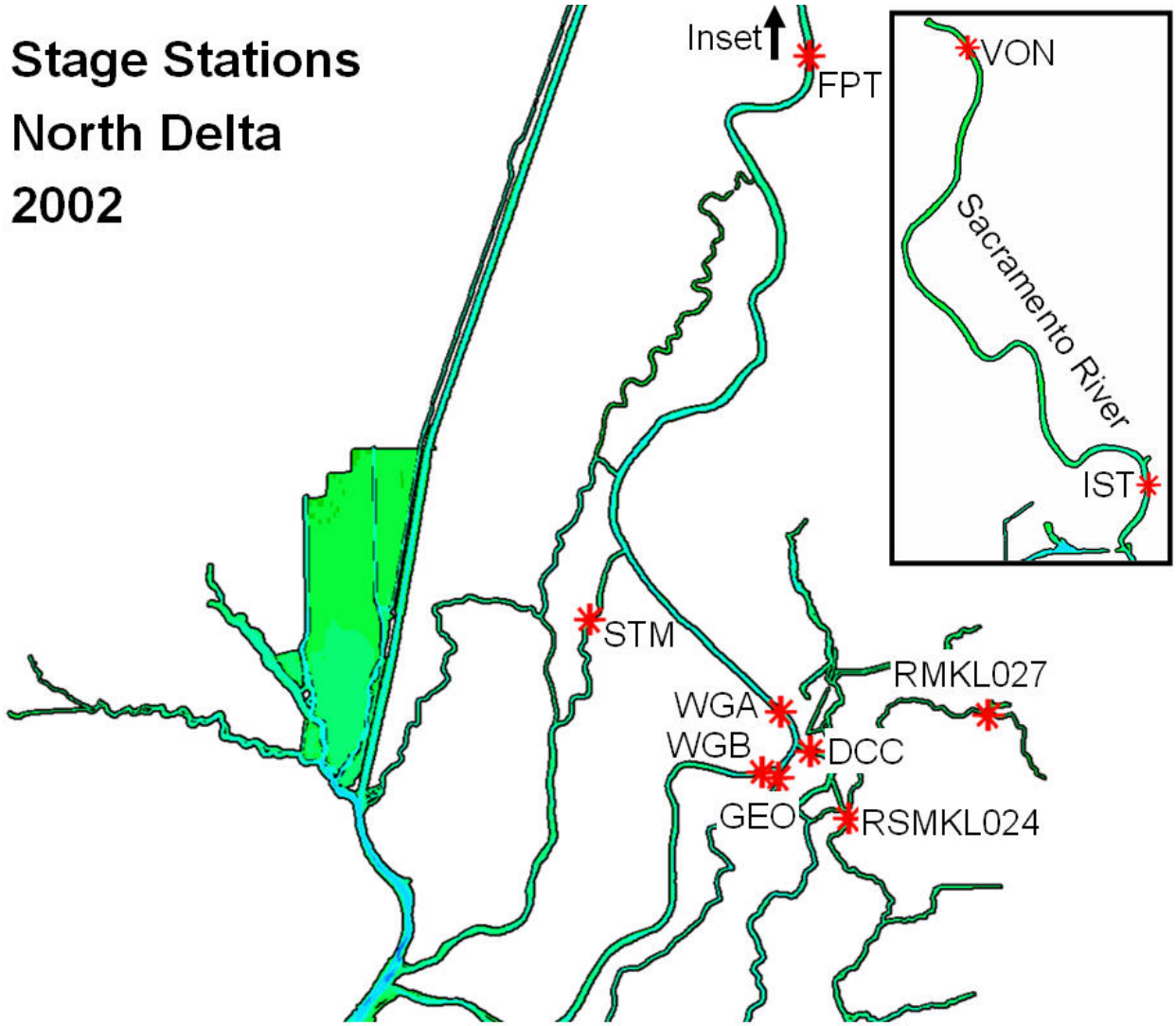

Station Names

WGB, Sacramento River South of Georgiana Slough

GEO, Georgiana Slough near Sacramento River

DCC, Delta Cross Channel

WGA, Sacramento River North of Delta Cross Channel

RMKL027, Mokelumne River near Thornton (Benson's Ferry)

RSMKL024, South Fork Mokelumne River at New Hope Bridge

STM, Steamboat Slough between Sacramento River and Sutter Sl.

FPT, Sacramento River at Freeport

IST, Sacramento River at I Street

VON, Sacramento River at Verona

Figure A.3-9 Location of water level monitoring stations in the northern portion of the Sacramento-San Joaquin Delta used for 2002 water level comparisons.

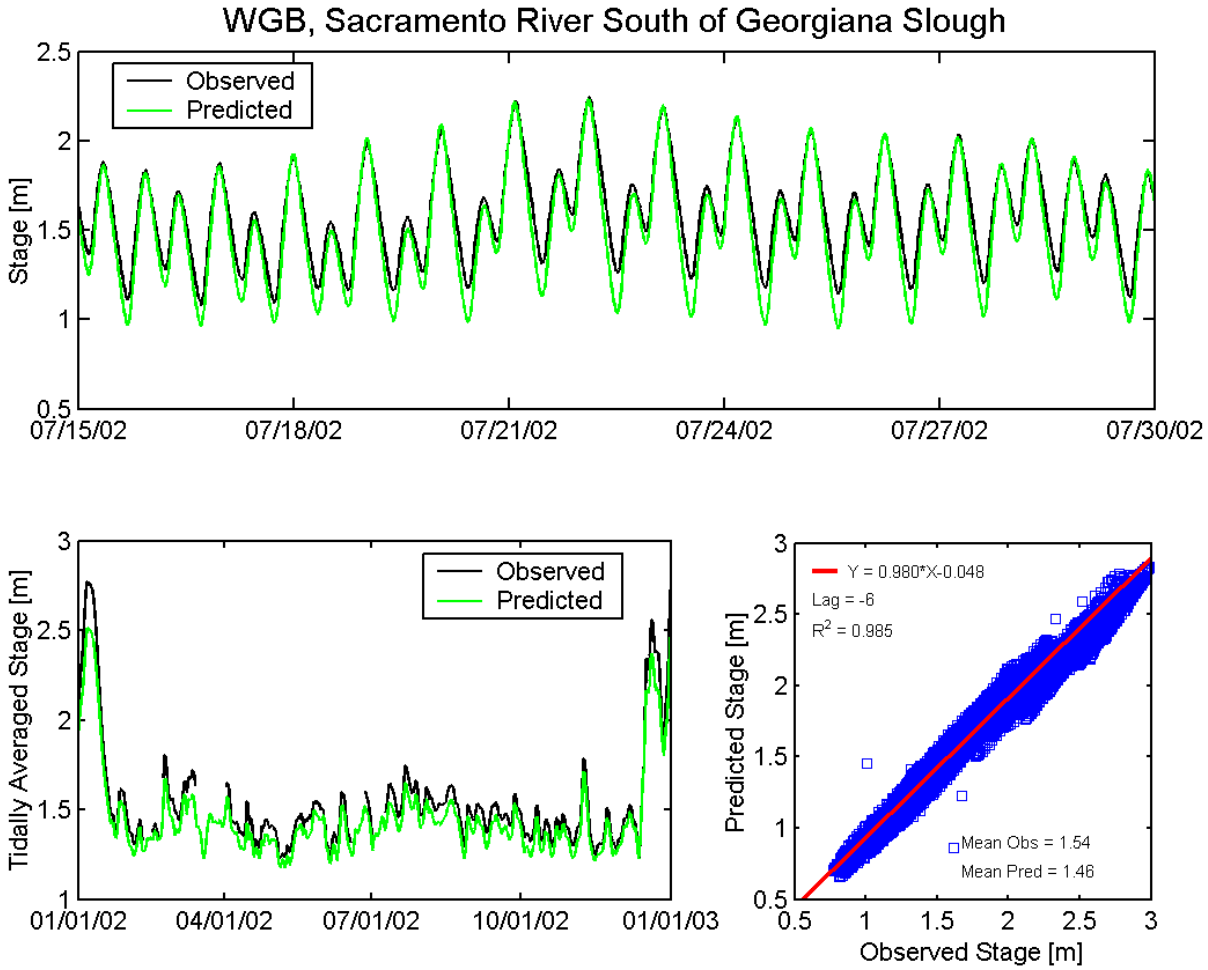

Figure A.3-10 Observed and predicted stage at Sacramento River South of Georgiana Slough USGS station (WGB) during the 2002 simulation period.

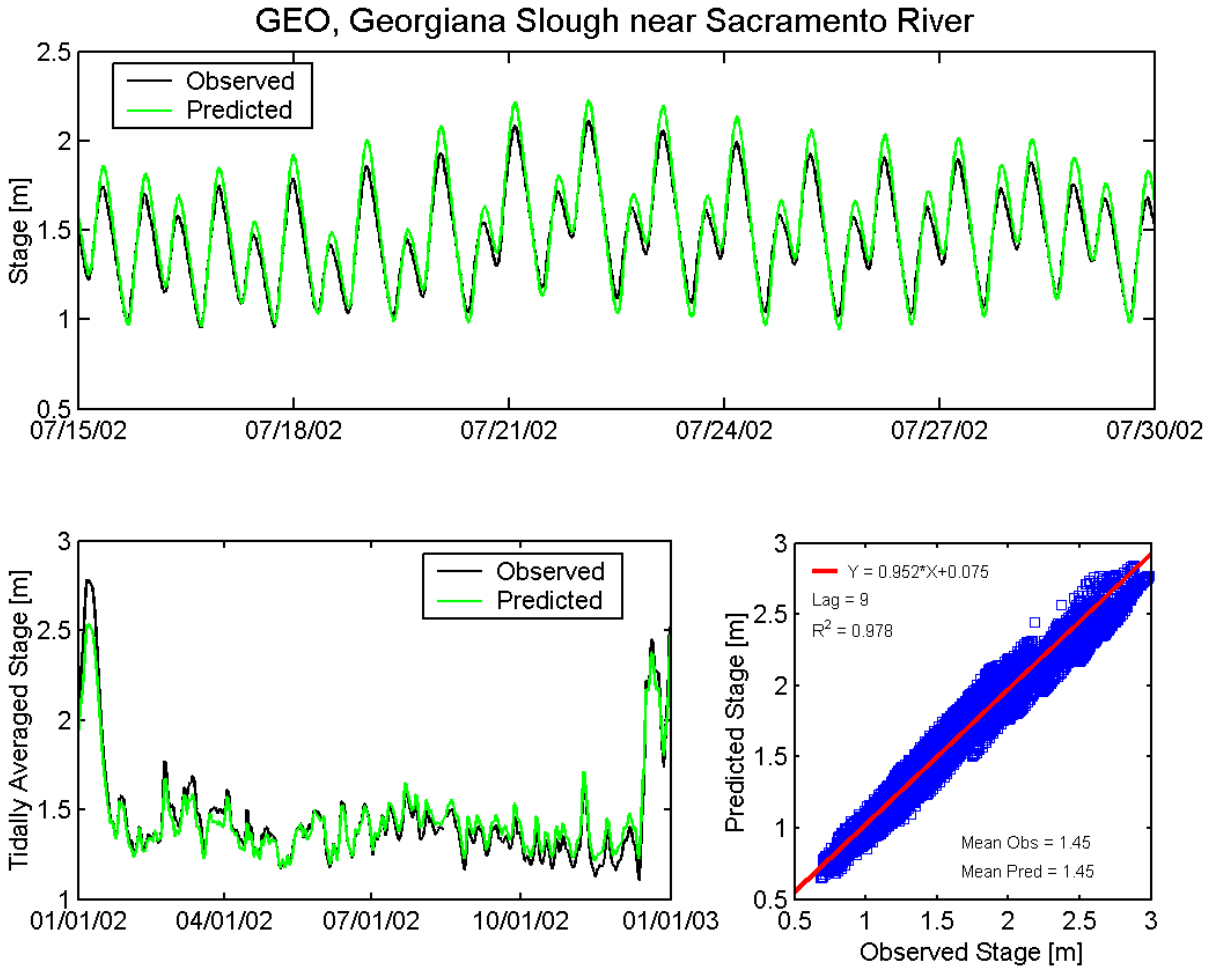

Figure A.3-11 Observed and predicted stage at Georgiana Slough near Sacramento River USGS station (GEO) during the 2002 simulation period.

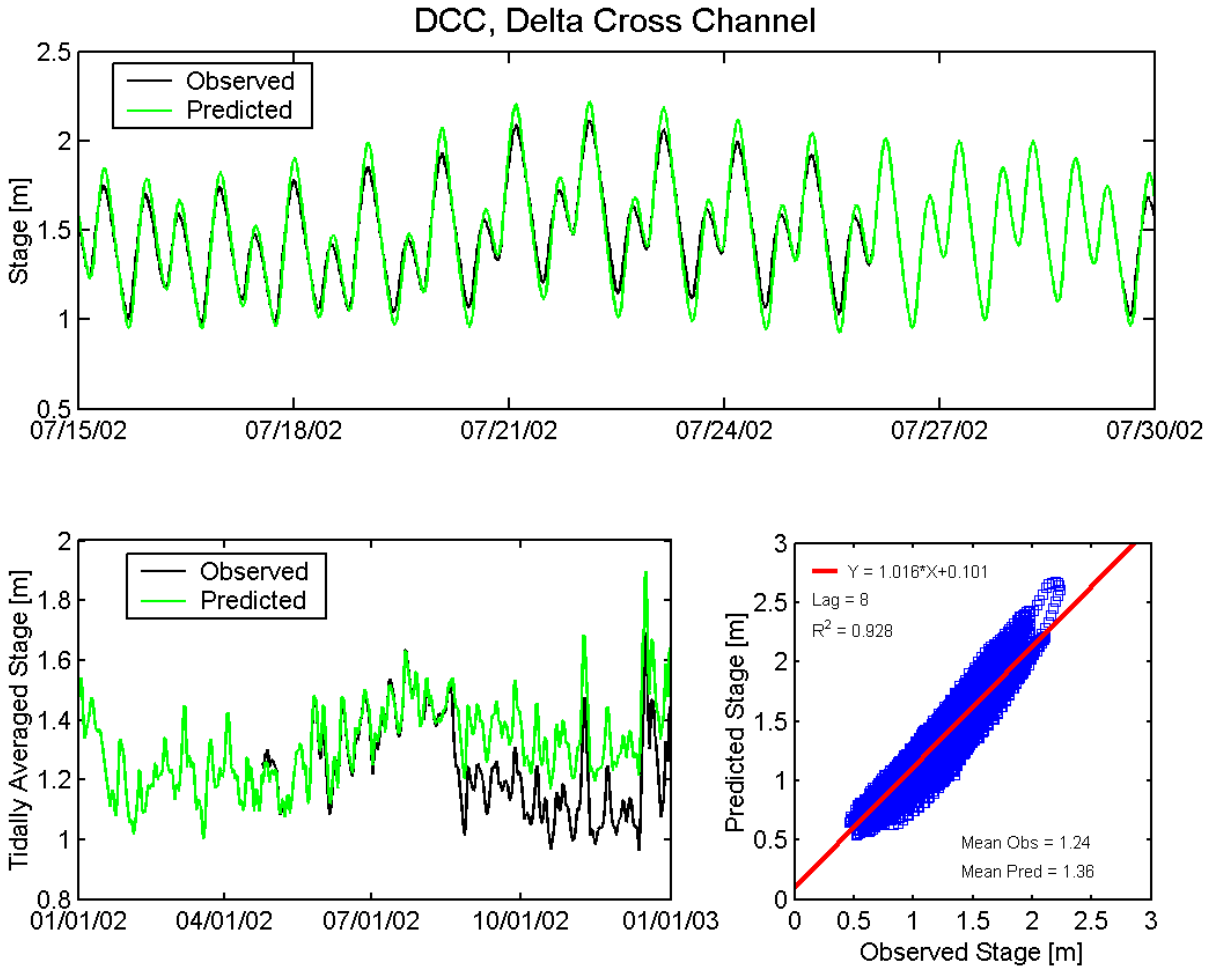

Figure A.3-12 Observed and predicted stage at Delta Cross Channel USGS station (DCC) during the 2002 simulation period.

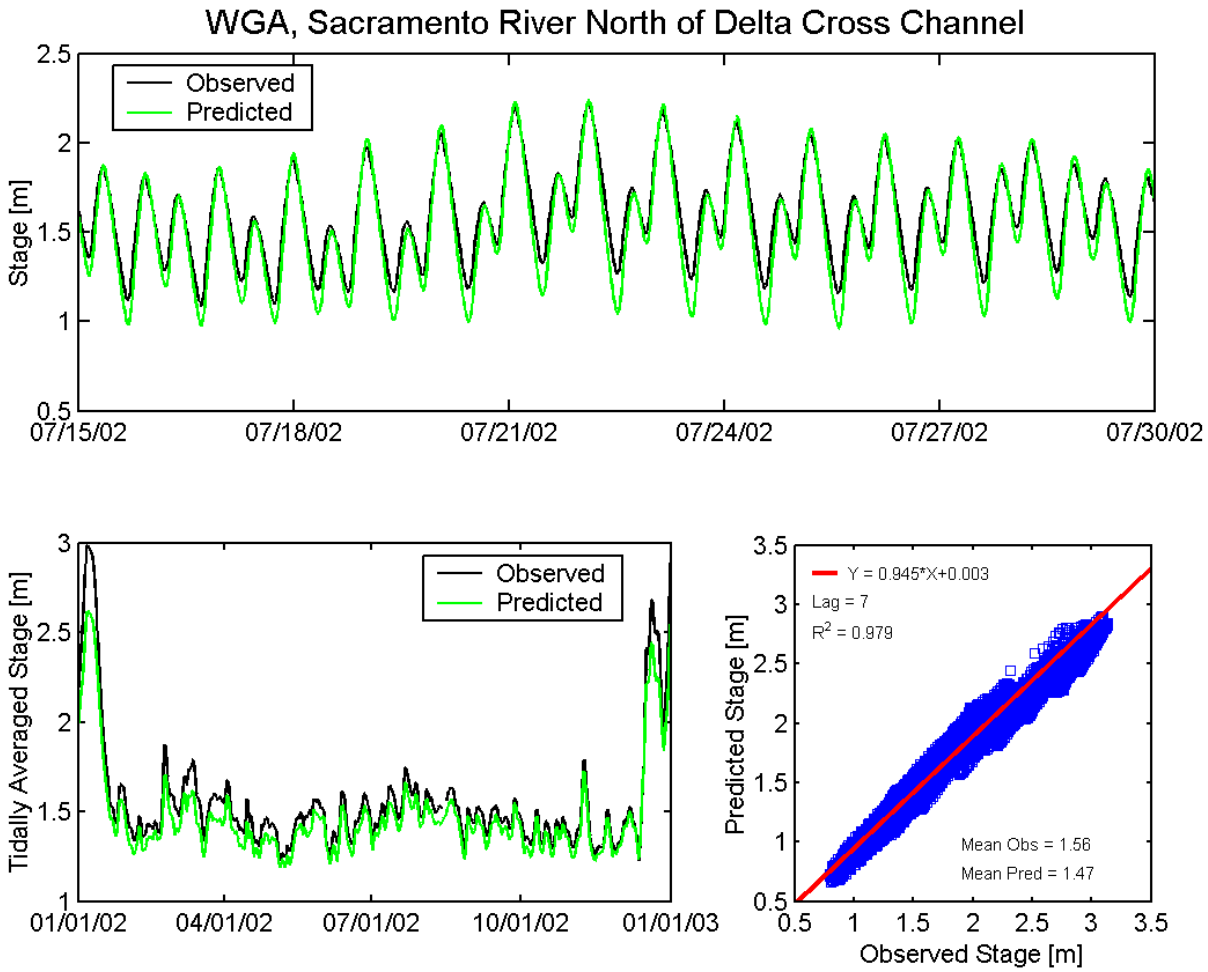

Figure A.3-13 Observed and predicted stage at Sacramento River North of Delta Cross Channel USGS station (WGA) during the 2002 simulation period.

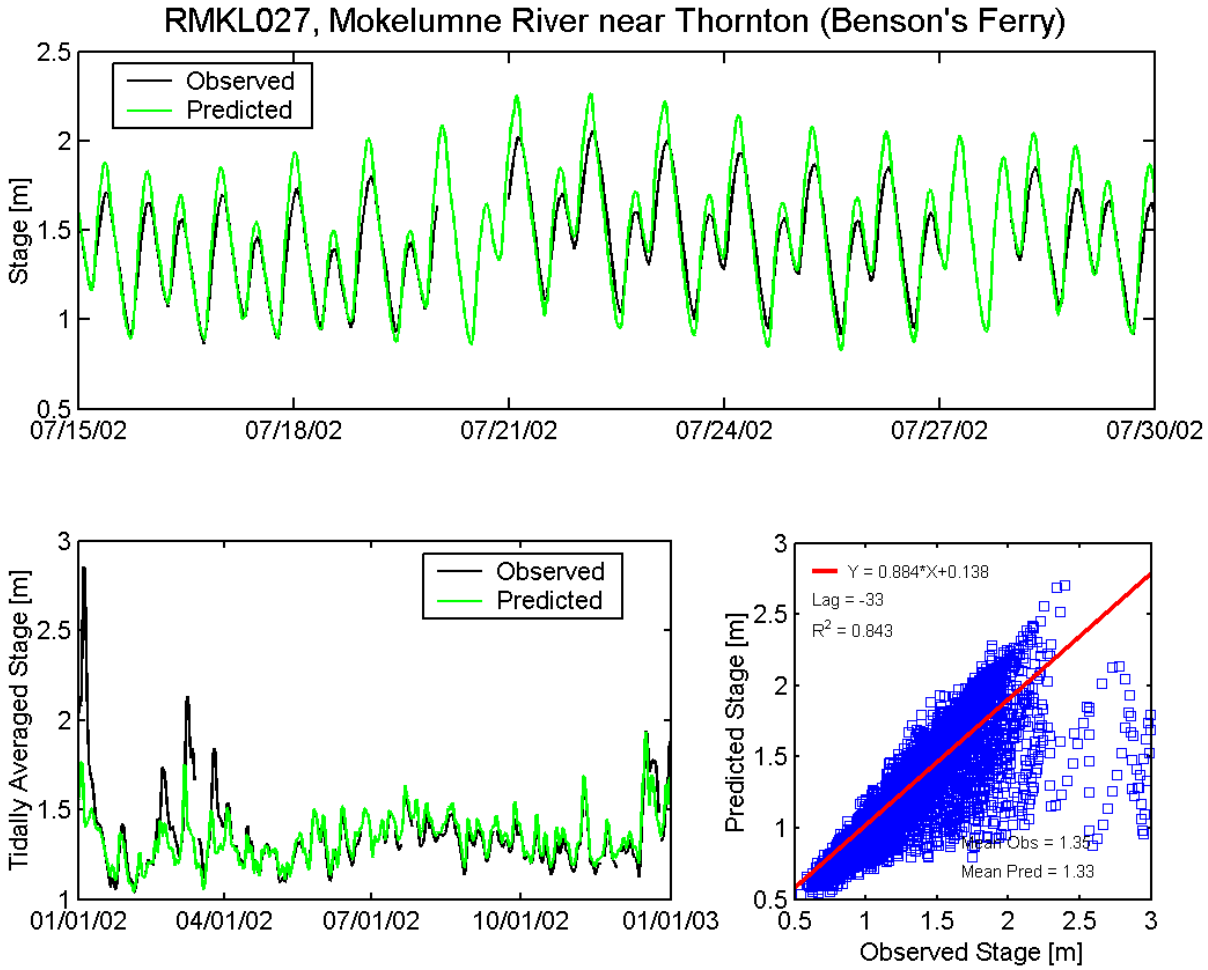

Figure A.3-14 Observed and predicted stage at Mokelumne River near Thornton (Benson's Ferry) DWR station (RMKL027) during the 2002 simulation period.

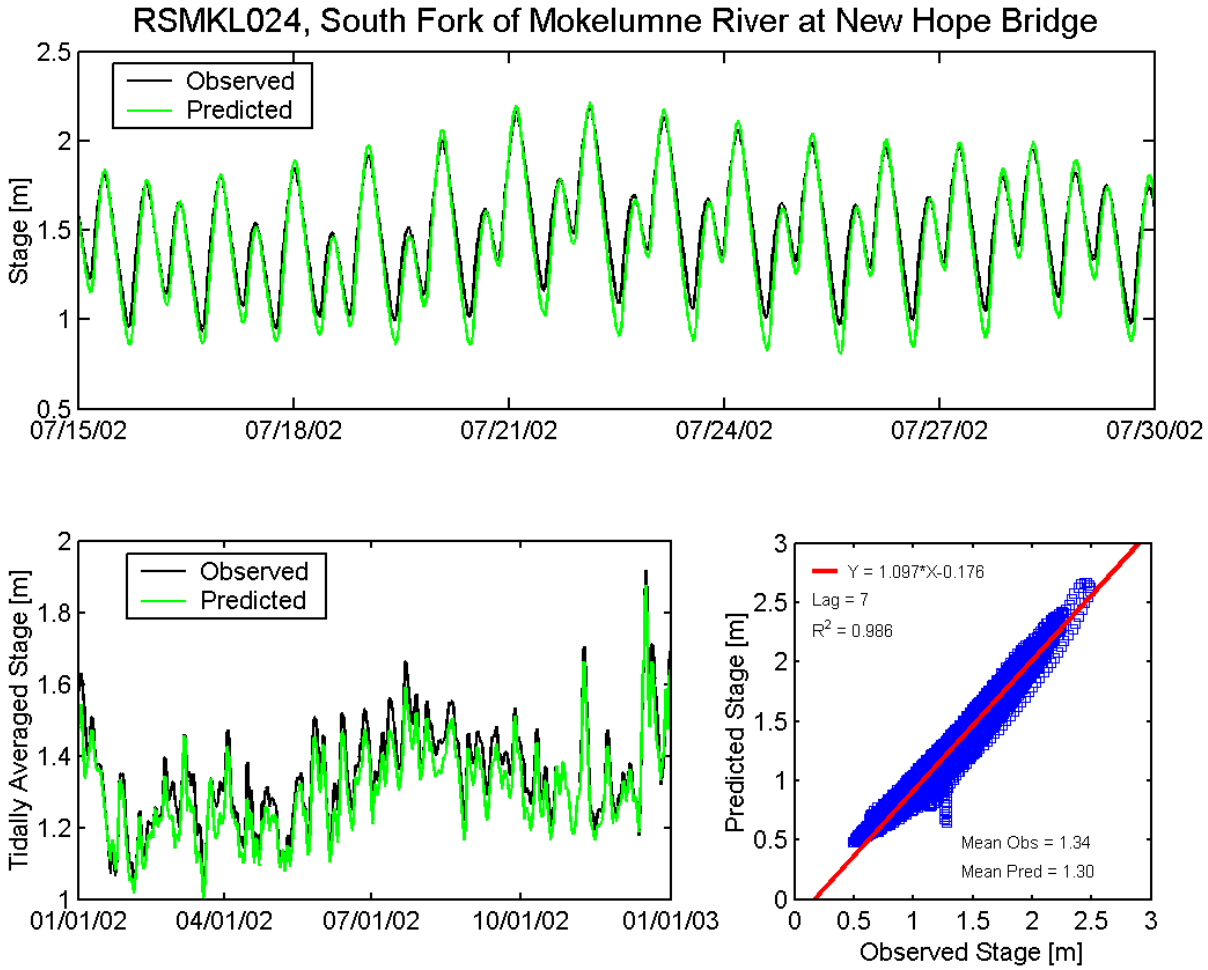

Figure A.3-15 Observed and predicted stage at Mokelumne River at New Hope Bridge DWR station (RSMKL024) during the 2002 simulation period.

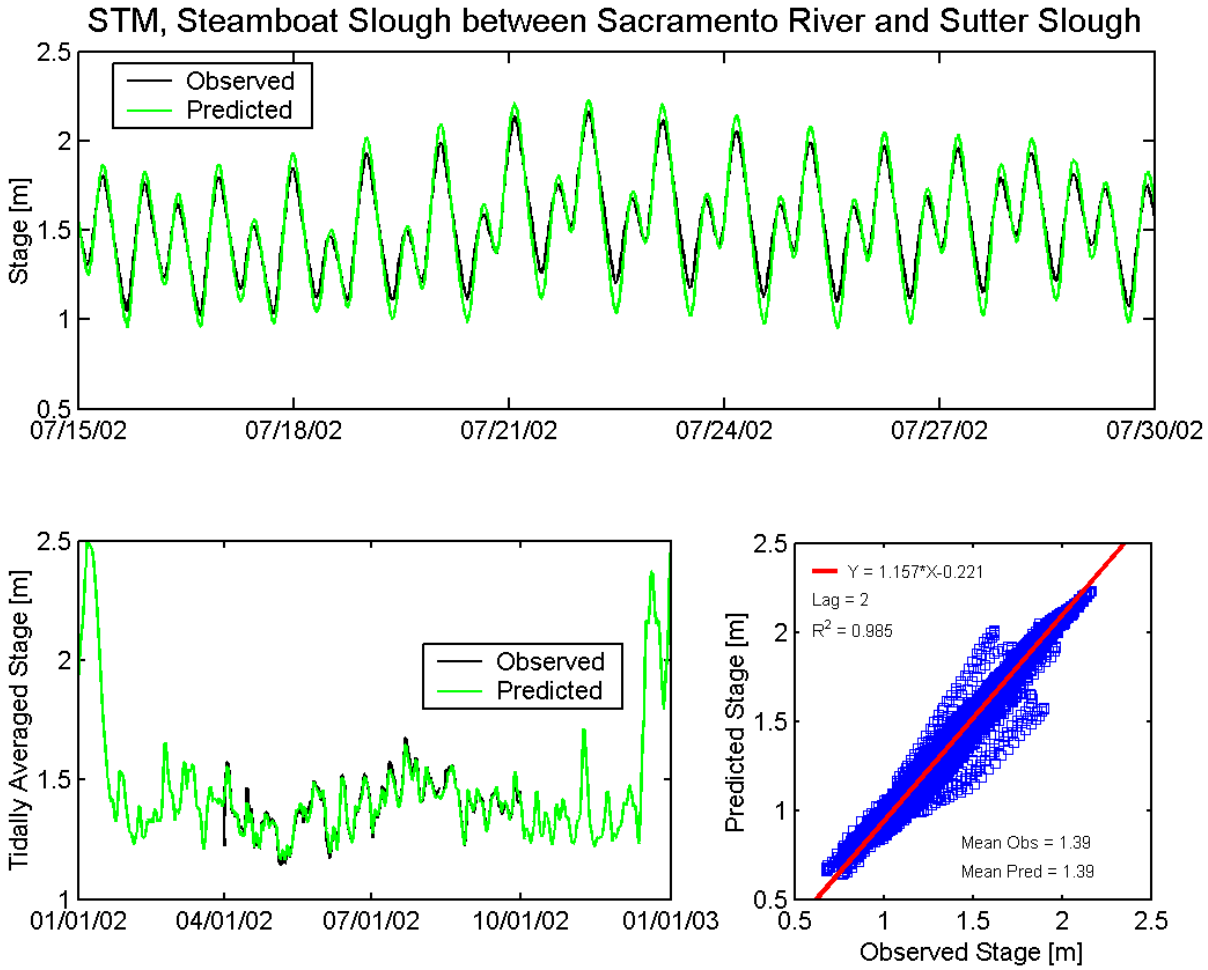

Figure A.3-16 Observed and predicted stage at Steamboat Slough between Sacramento River and Sutter Slough USGS station (STM) during the 2002 simulation period.

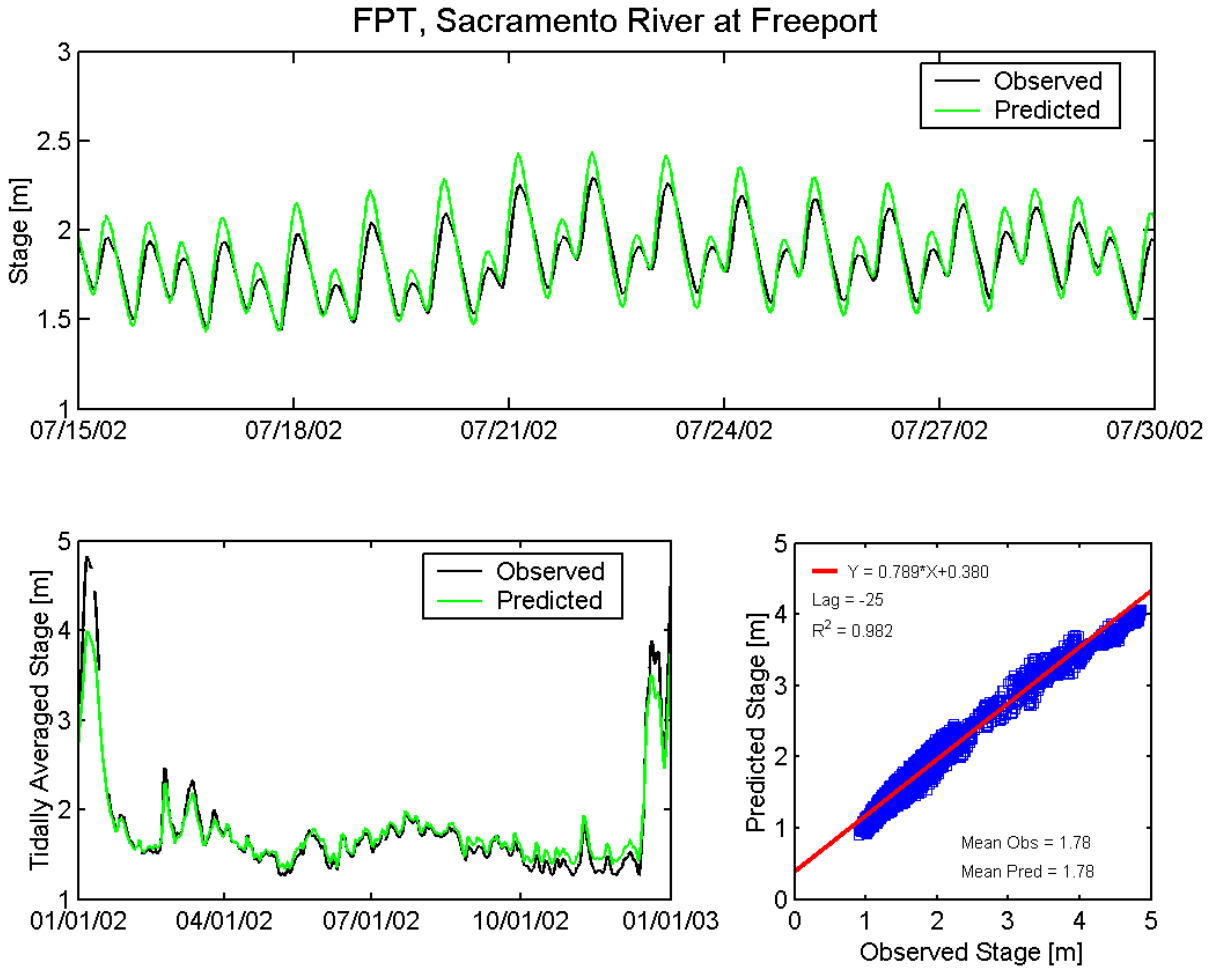

Figure A.3-17 Observed and predicted stage at Sacramento River at Freeport USGS station (FPT) during the 2002 simulation period.

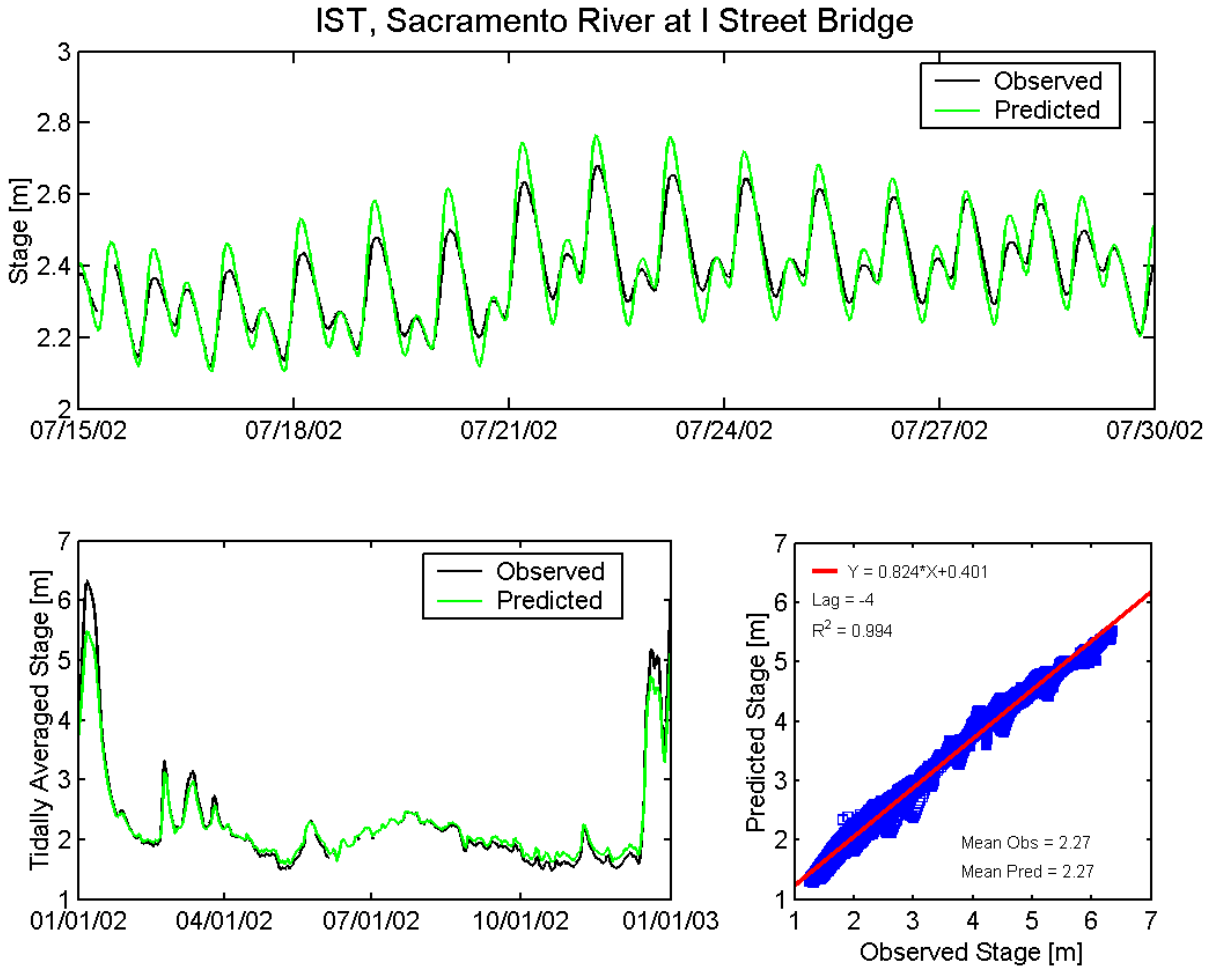

Figure A.3-18 Observed and predicted stage at Sacramento River at I Street Bridge DWR station (CDEC IST) during the 2002 simulation period.

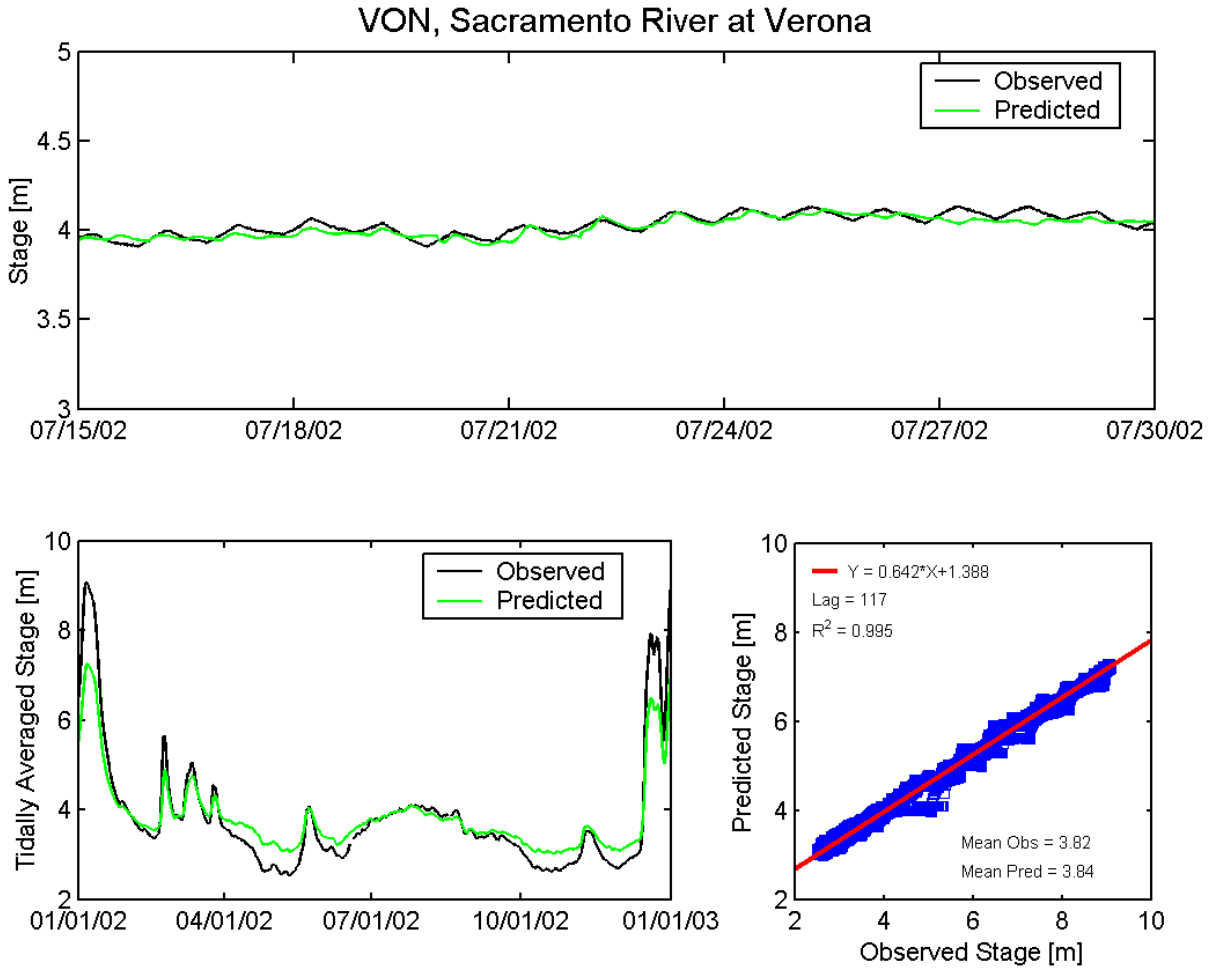

Figure A.3-19 Observed and predicted stage at Sacramento River at Verona DWR station (CDEC VON) during the 2002 simulation period.

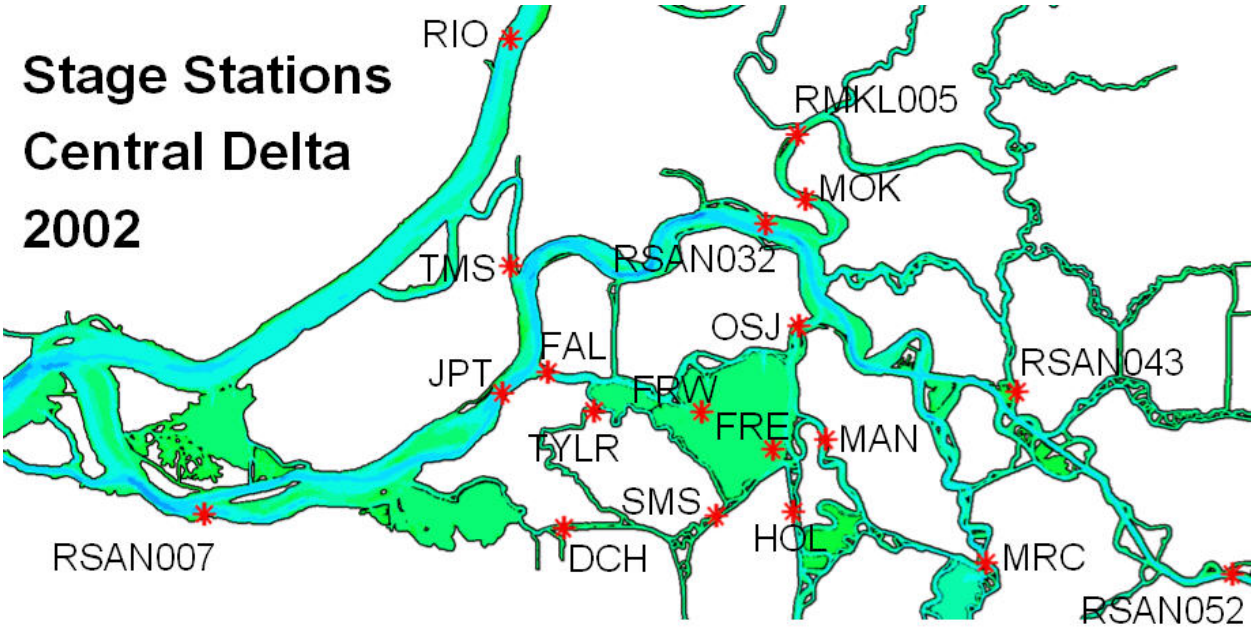

Station Names

RSAN007, San Joaquin River at Antioch

RIO, Sacramento River at Rio Vista

TMS, Threemile Slough at San Joaquin River

JPT, San Joaquin River at Jersey Point

DCH, Dutch Slough at Jersey Island

FAL, False River

TYLR, Taylor Slough

SMS, Sand Mound Slough

RSAN032, San Joaquin River at San Andreas Landing

OSJ, Old River at San Joaquin River

MOK, Mokelumne River near San Joaquin River

RMKL005, North Fork of Mokelumne River at Georgiana Slough

FRE, Franks Tract East

FRW, Franks Tract West

MAN, Old River at Mandeville Island

HOL, Holland Cut

RSAN043, San Joaquin River at Venice Island

RSAN052, San Joaquin River at Rindge Pump

MRC, Middle River South of Columbia Cut

Figure A.3-20 Location of water level monitoring stations in the central portion of the Sacramento-San Joaquin Delta used for 2002 water level comparisons.

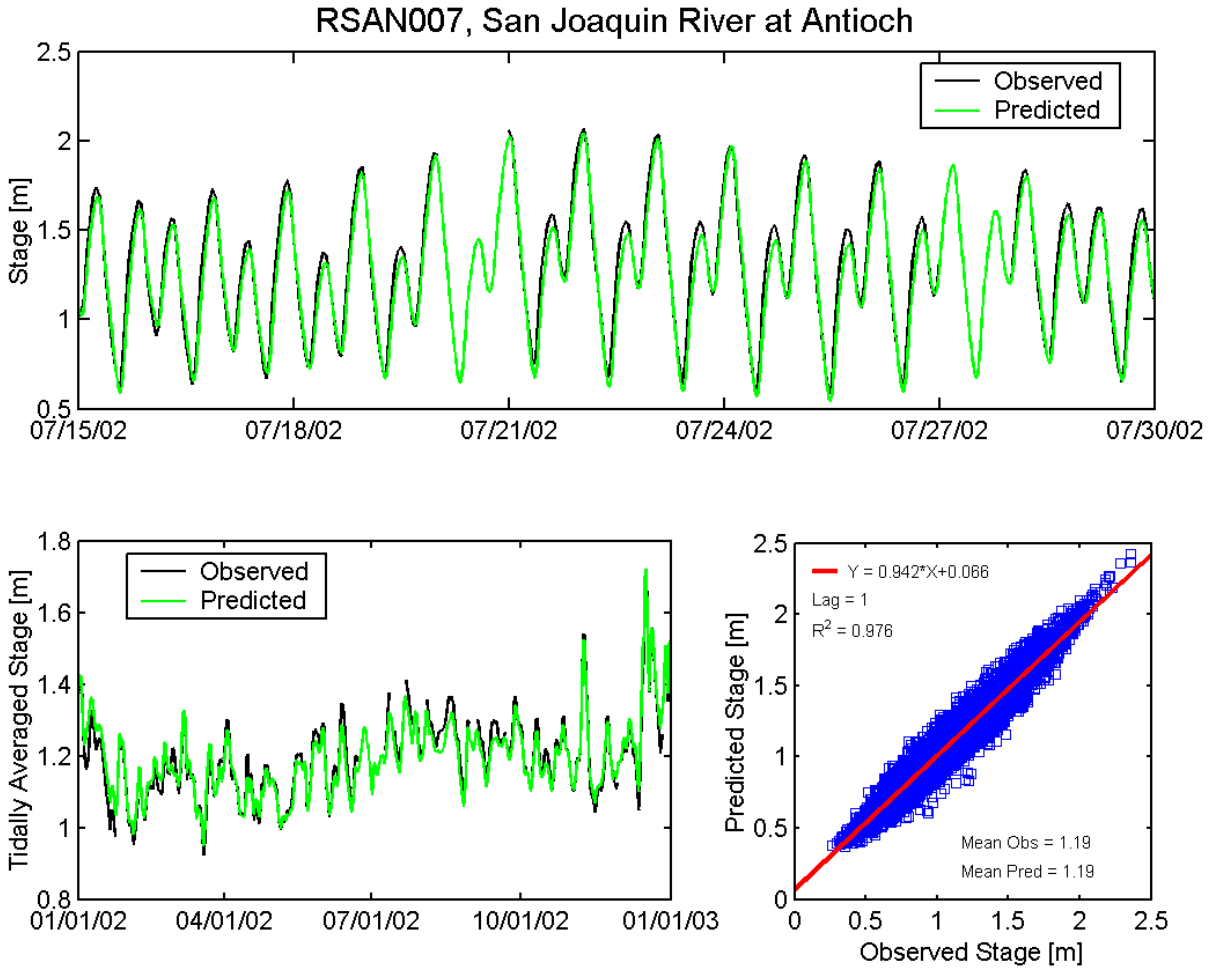

Figure A.3-21 Observed and predicted stage at San Joaquin River at Antioch DWR station (RSAN007) during the 2002 simulation period.

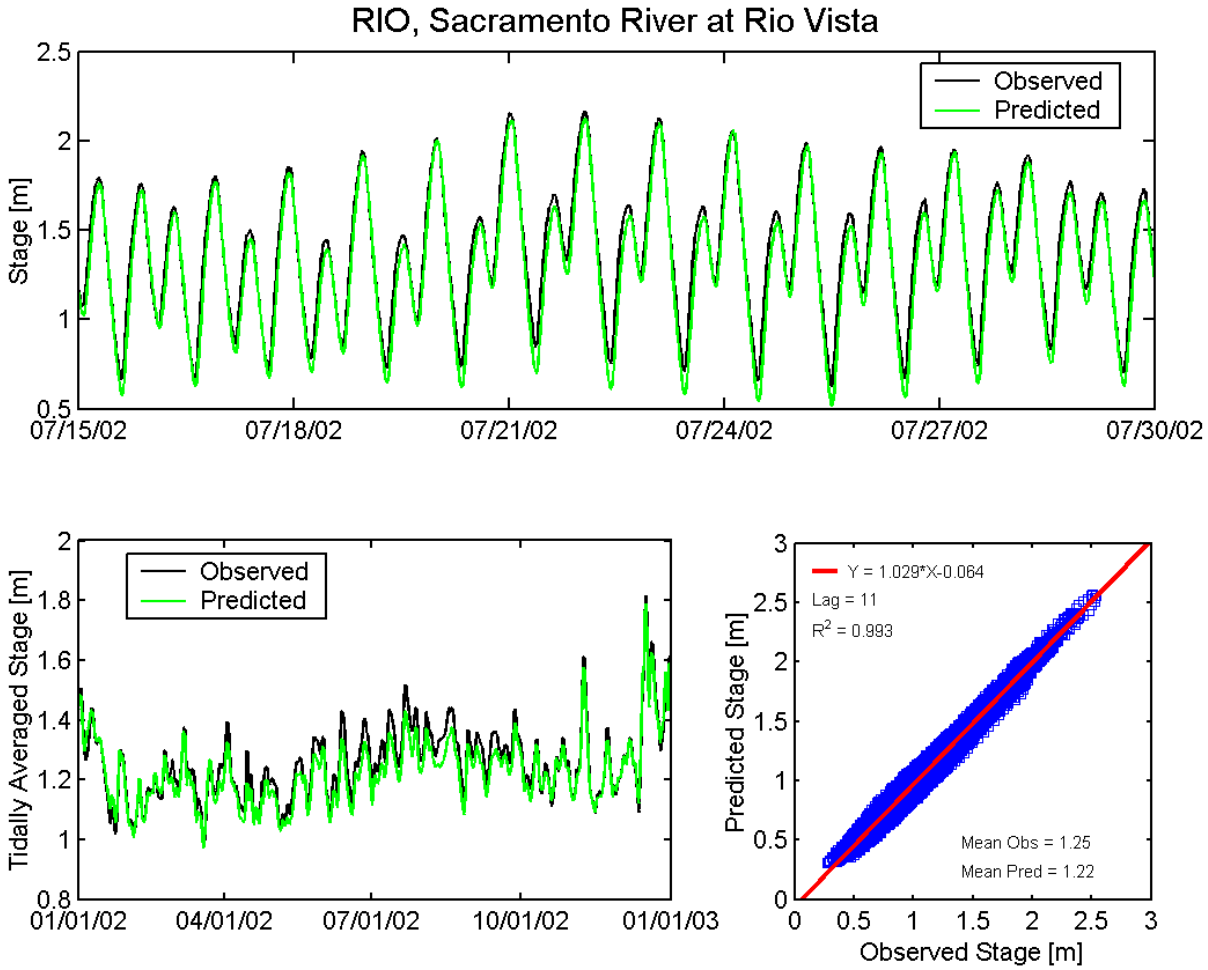

Figure A.3-22 Observed and predicted stage at Sacramento River at Rio Vista USGS station (RIO) during the 2002 simulation period.

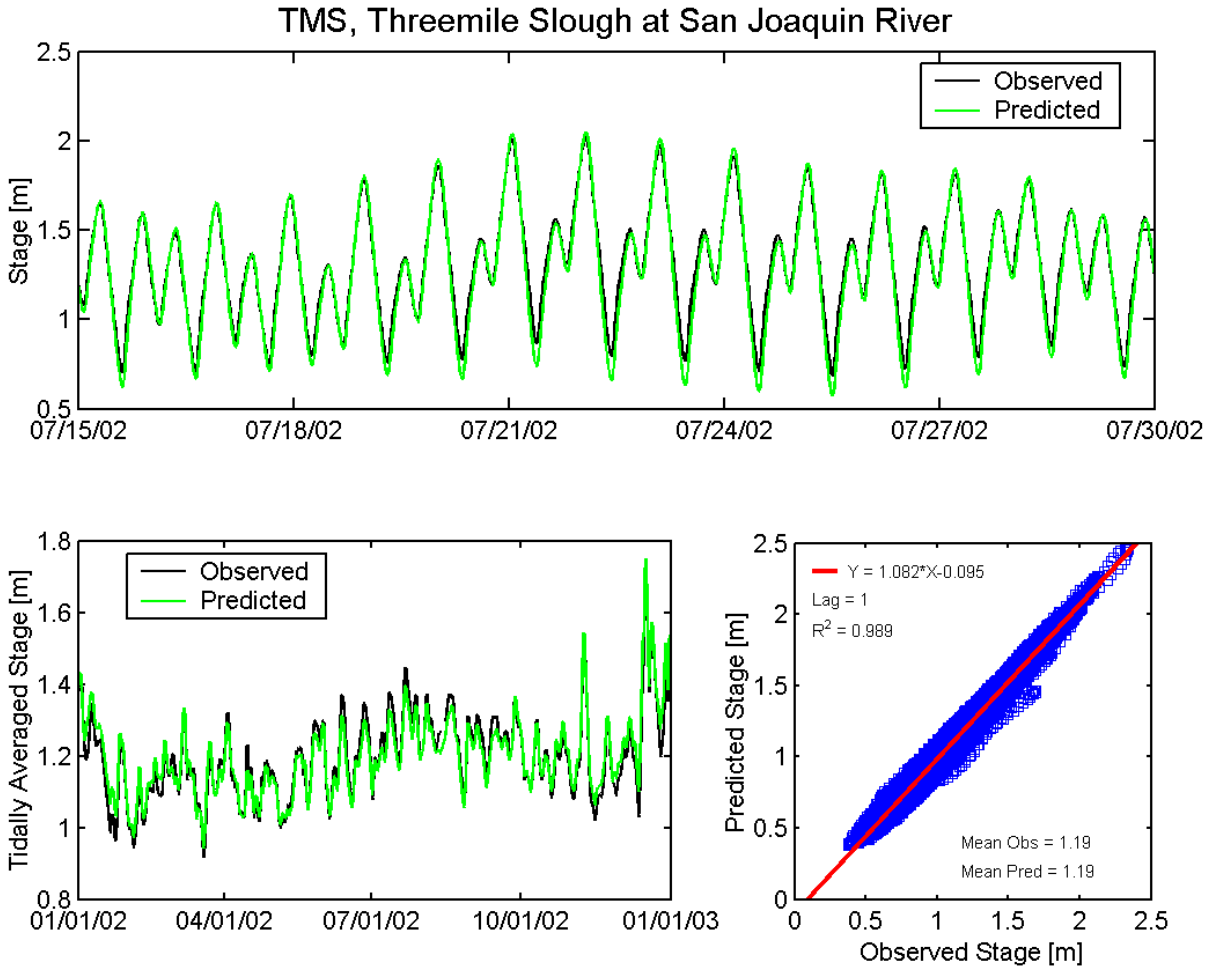

Figure A.3-23 Observed and predicted stage at Threemile Slough at San Joaquin River USGS station (TMS) during the 2002 simulation period.

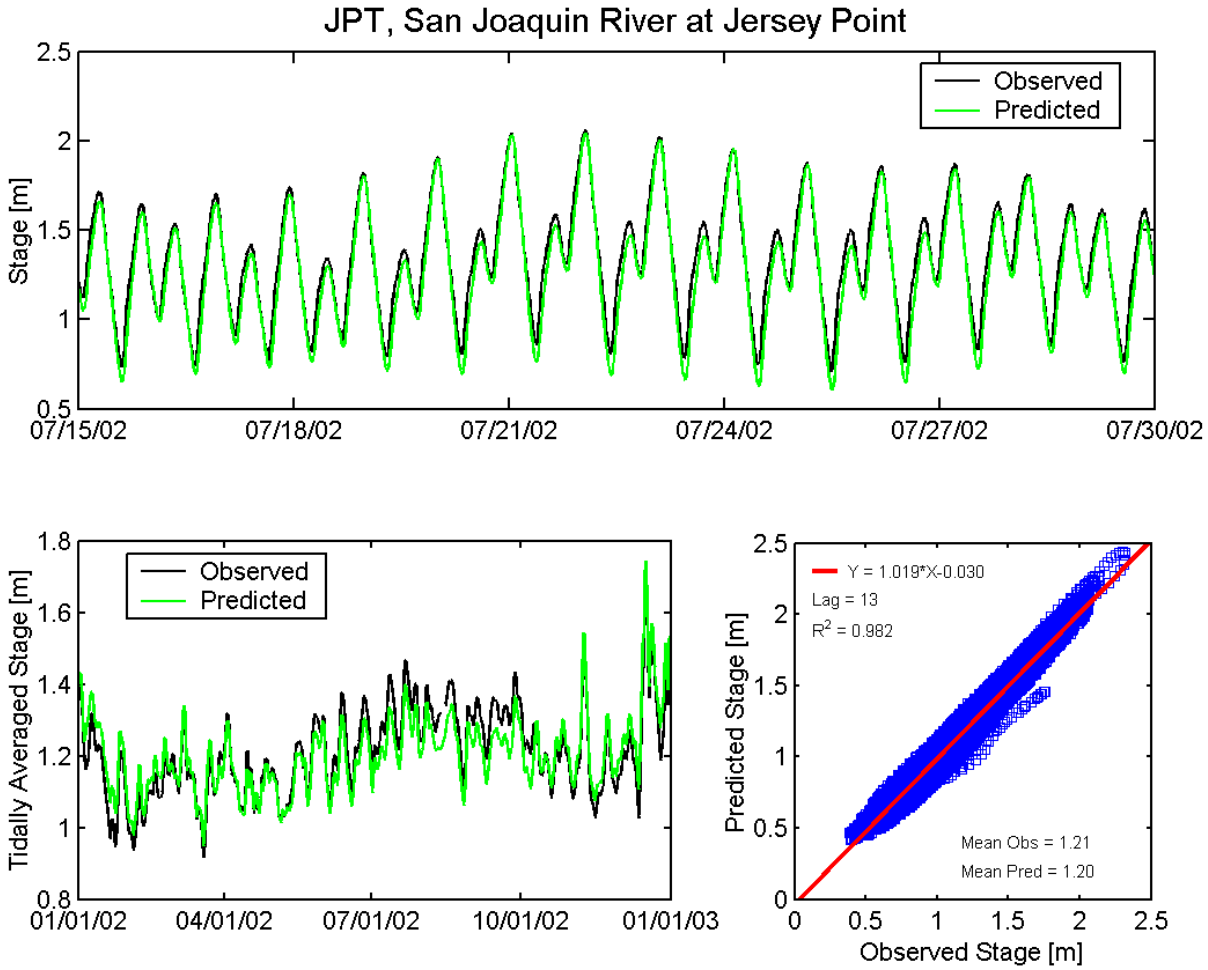

Figure A.3-24 Observed and predicted stage at San Joaquin River at Jersey Point USGS station (JPT) during the 2002 simulation period.

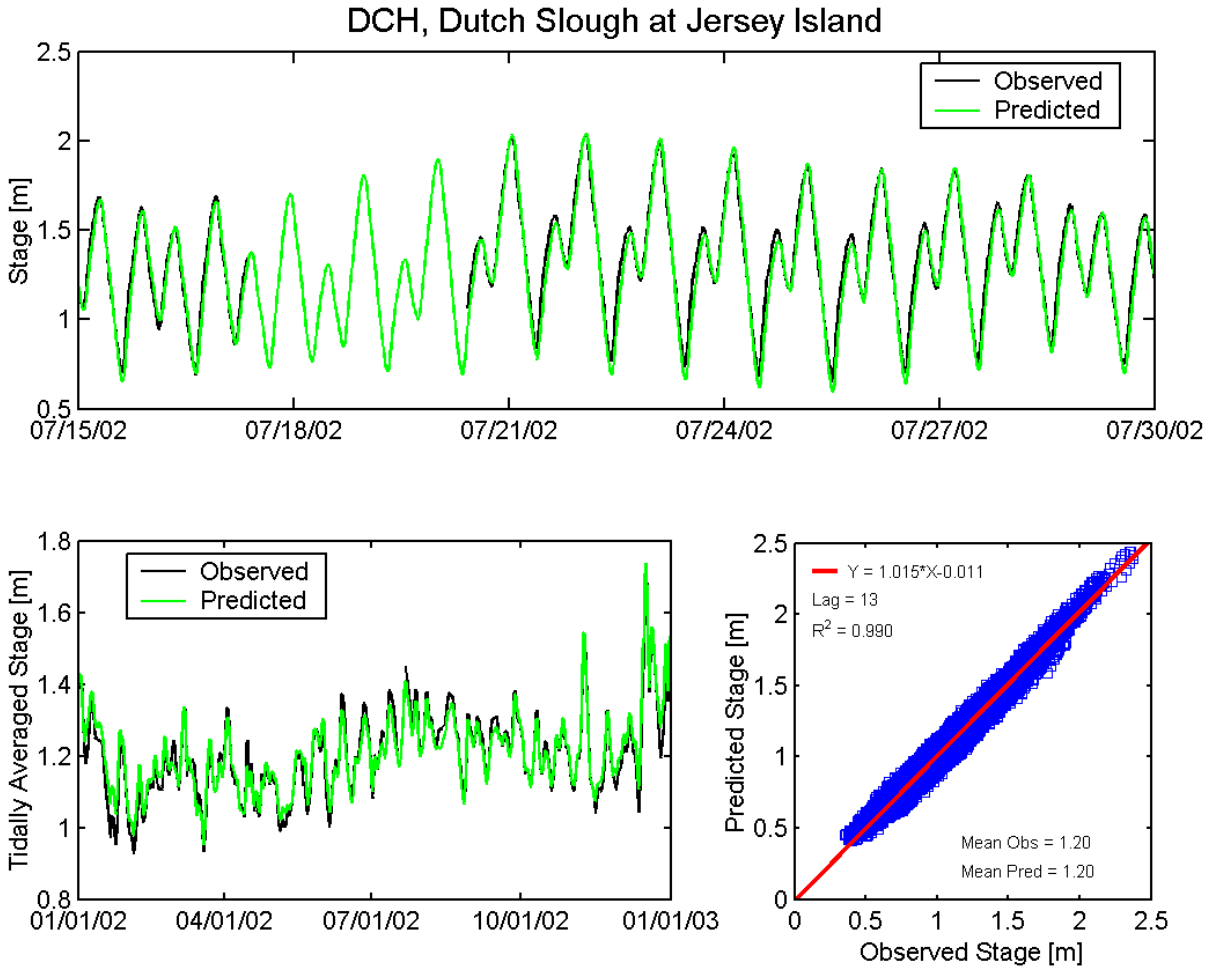

Figure A.3-25 Observed and predicted stage at Dutch Slough at Jersey Island USGS station (DCH) during the 2002 simulation period.

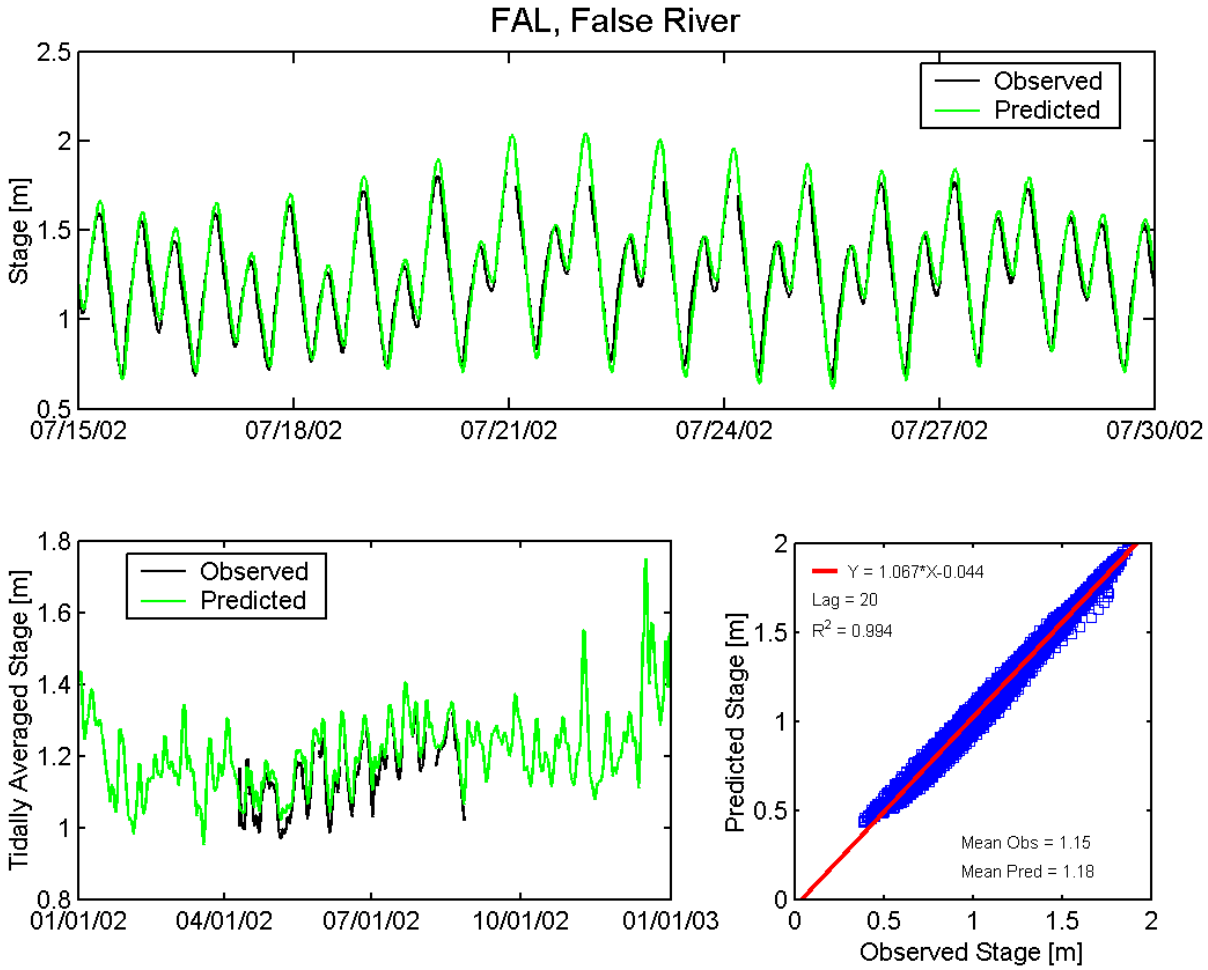

Figure A.3-26 Observed and predicted stage at False River USGS station (FAL) during the 2002 simulation period.

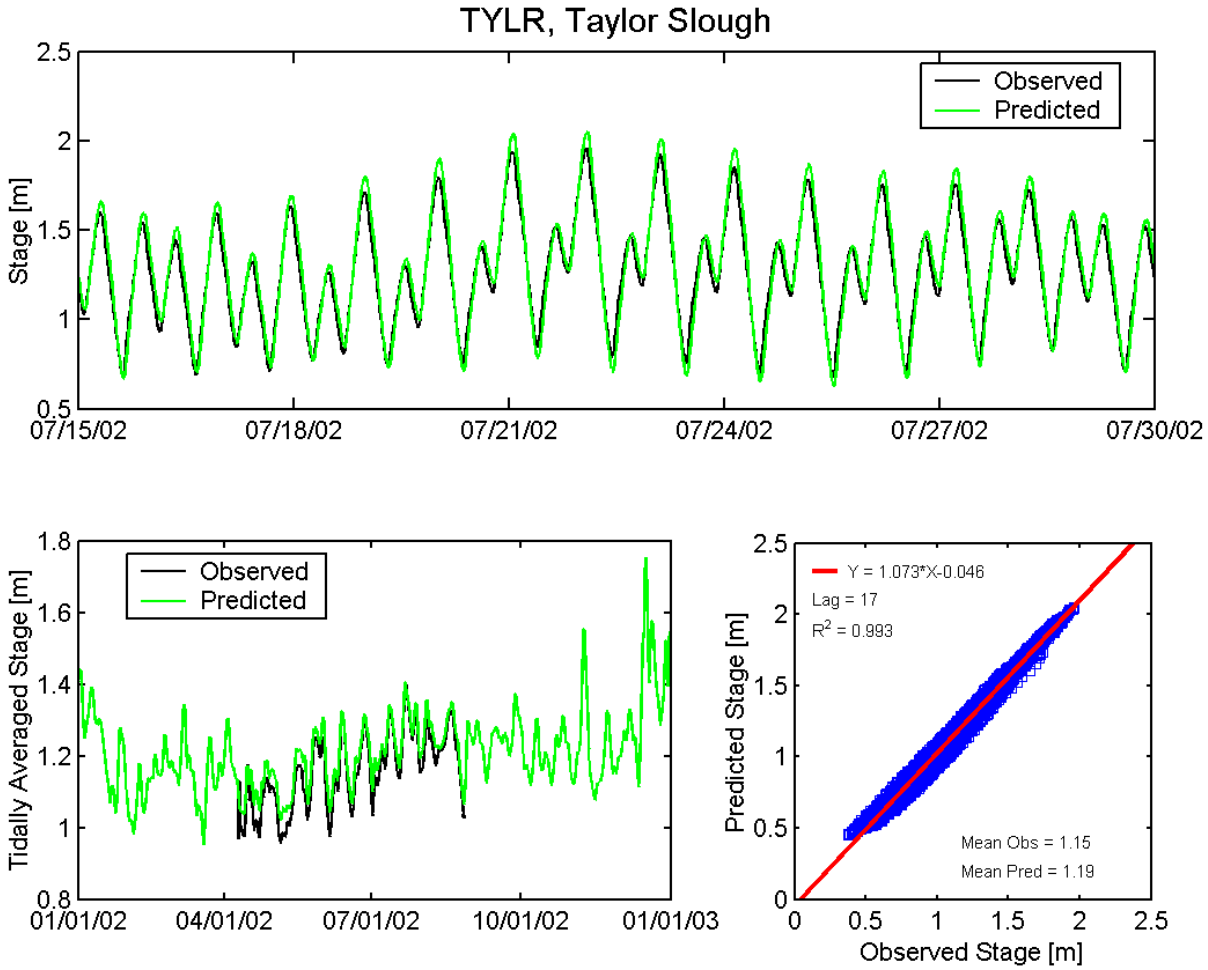

Figure A.3-27 Observed and predicted stage at Taylor Slough USGS station (TYLR) during the 2002 simulation period.

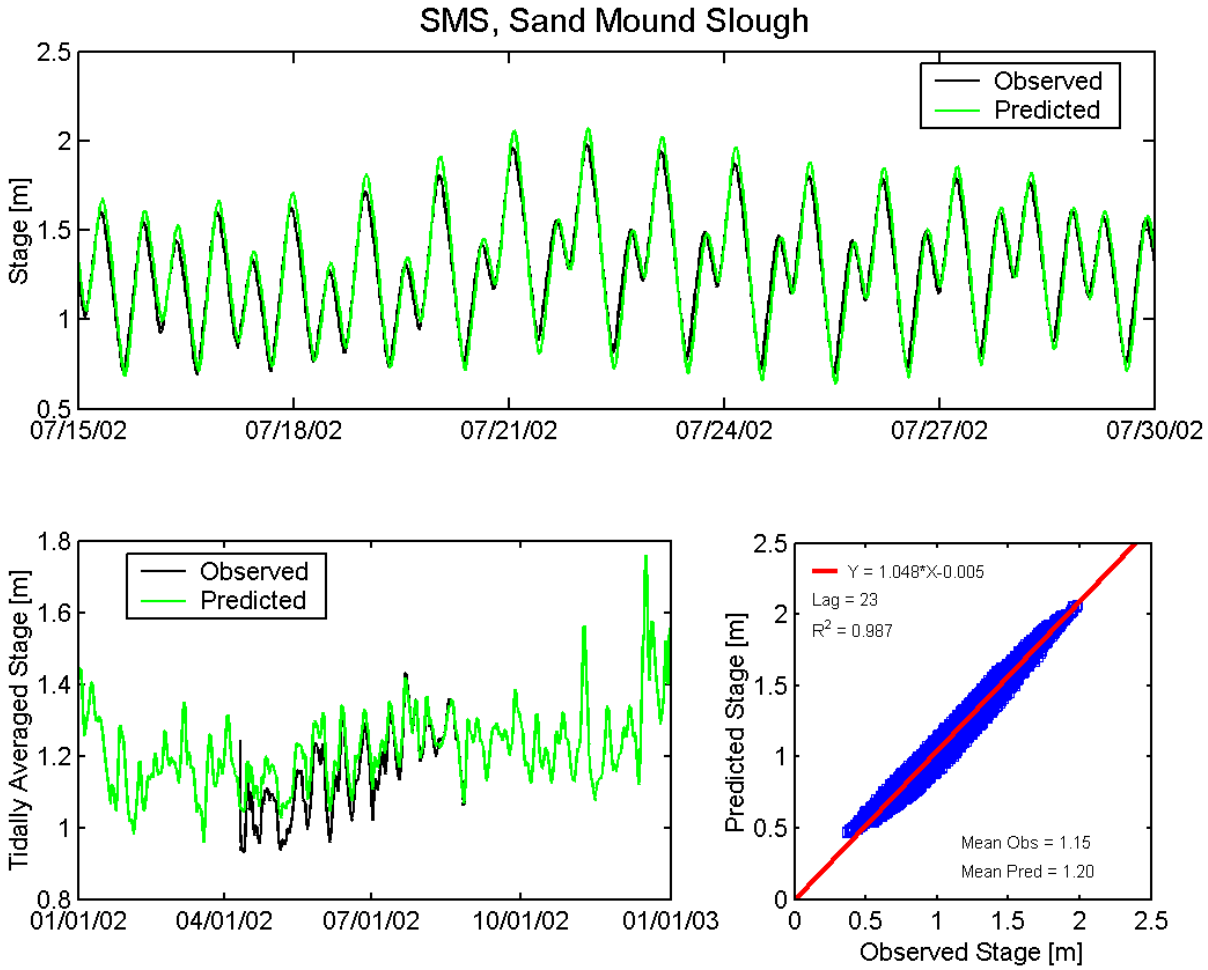

Figure A.3-28 Observed and predicted stage at Sand Mound Slough USGS station (SMS) during the 2002 simulation period.

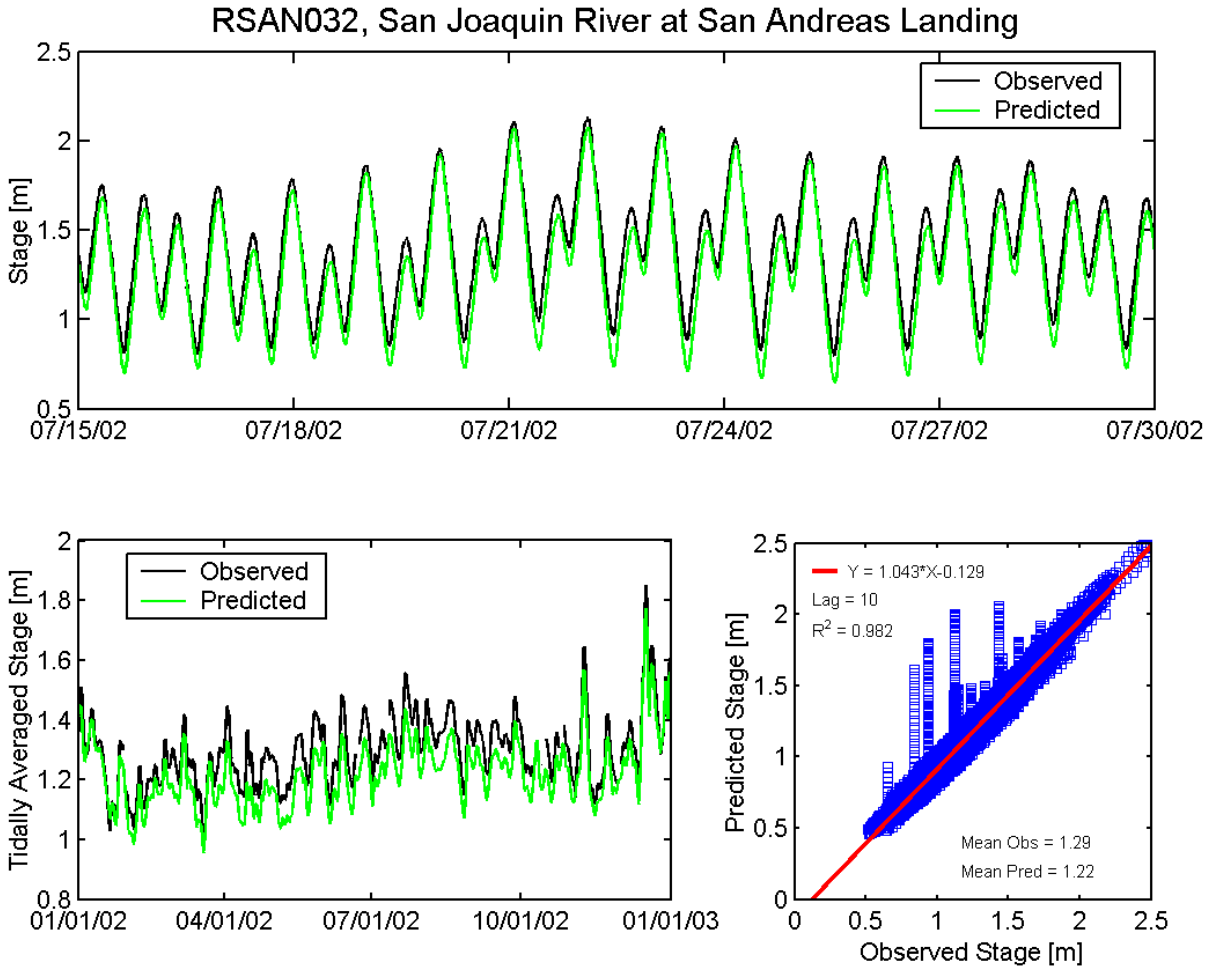

Figure A.3-29 Observed and predicted stage at San Joaquin River at San Andreas Landing DWR station (RSAN032) during the 2002 simulation period.

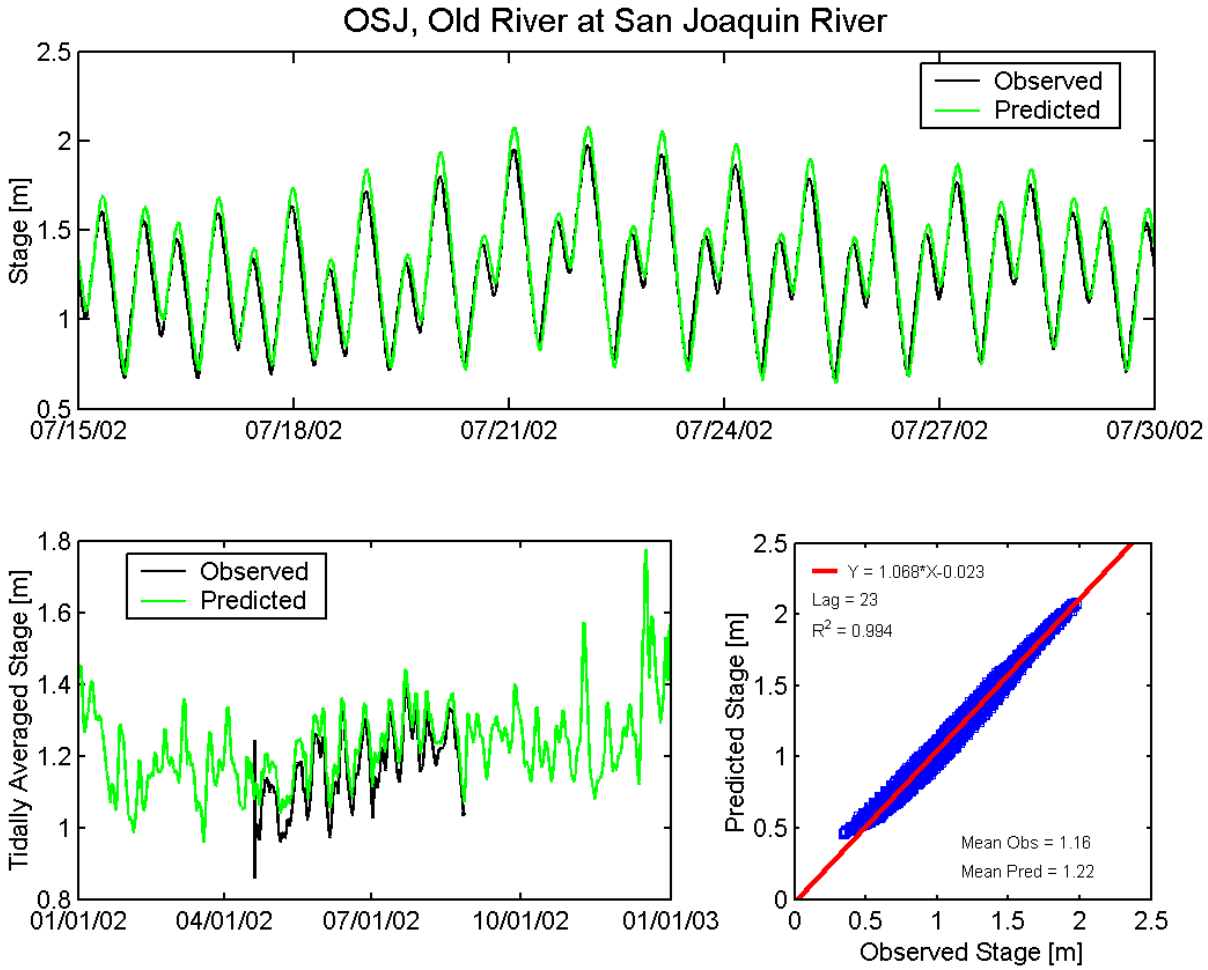

Figure A.3-30 Observed and predicted stage at Old River at San Joaquin River USGS station (OSJ) during the 2002 simulation period.

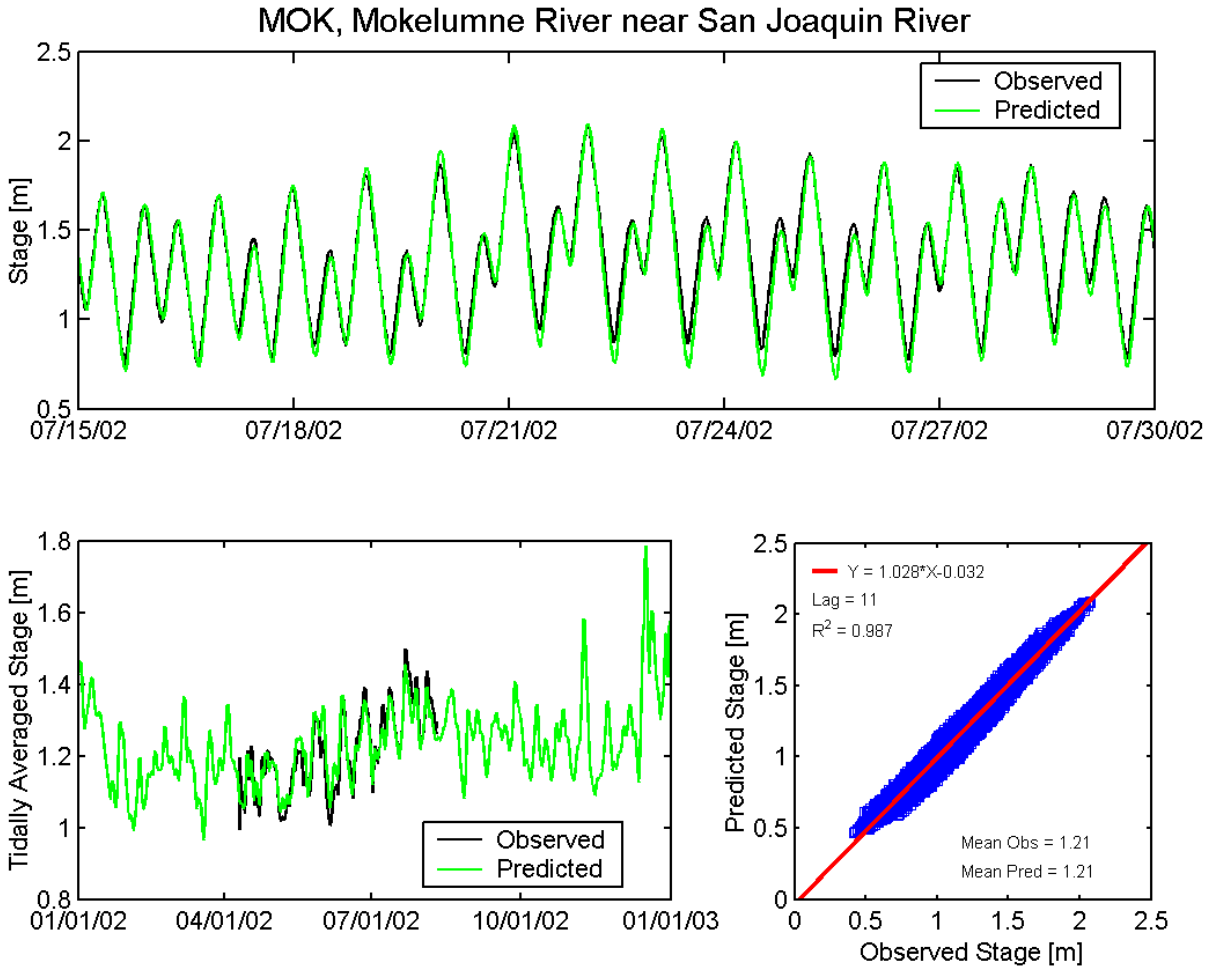

Figure A.3-31 Observed and predicted stage at Mokelumne River near San Joaquin River USGS station (MOK) during the 2002 simulation period.

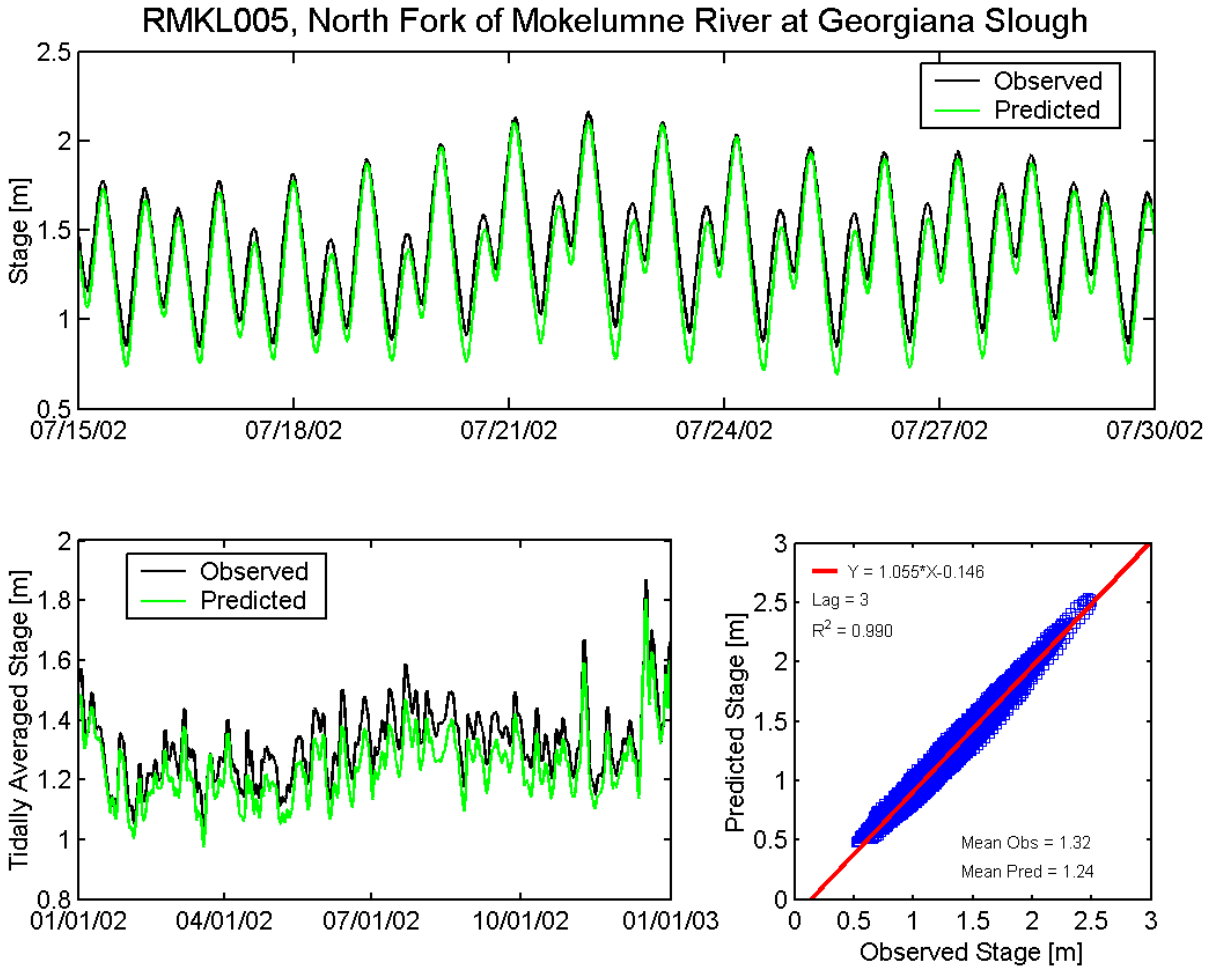

Figure A.3-32 Observed and predicted stage at North Fork of Mokelumne River at Georgiana Slough DWR station (RMKL005) during the 2002 simulation period.

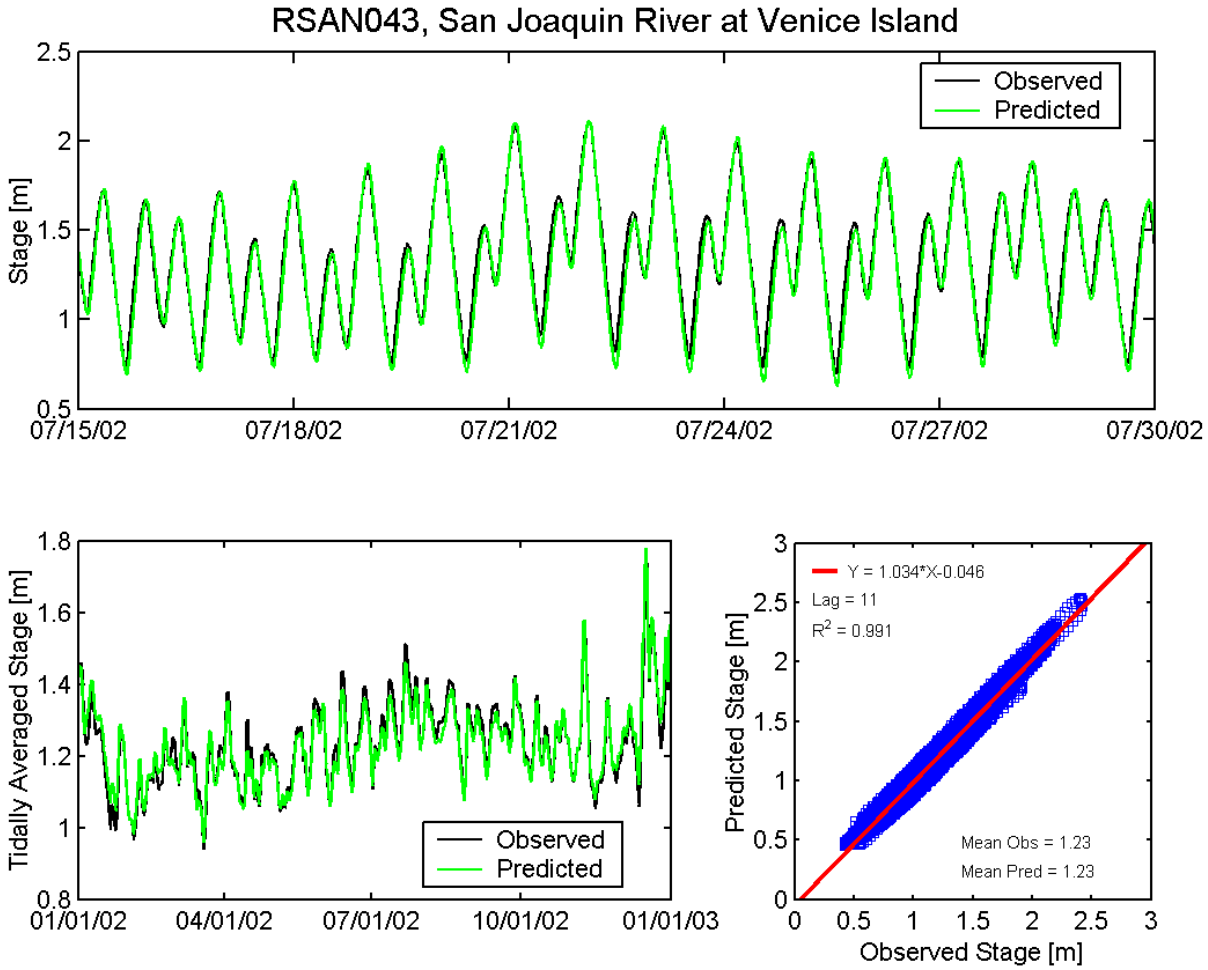

Figure A.3-33 Observed and predicted stage at San Joaquin River at Venice Island DWR station (RSAN043) during the 2002 simulation period.

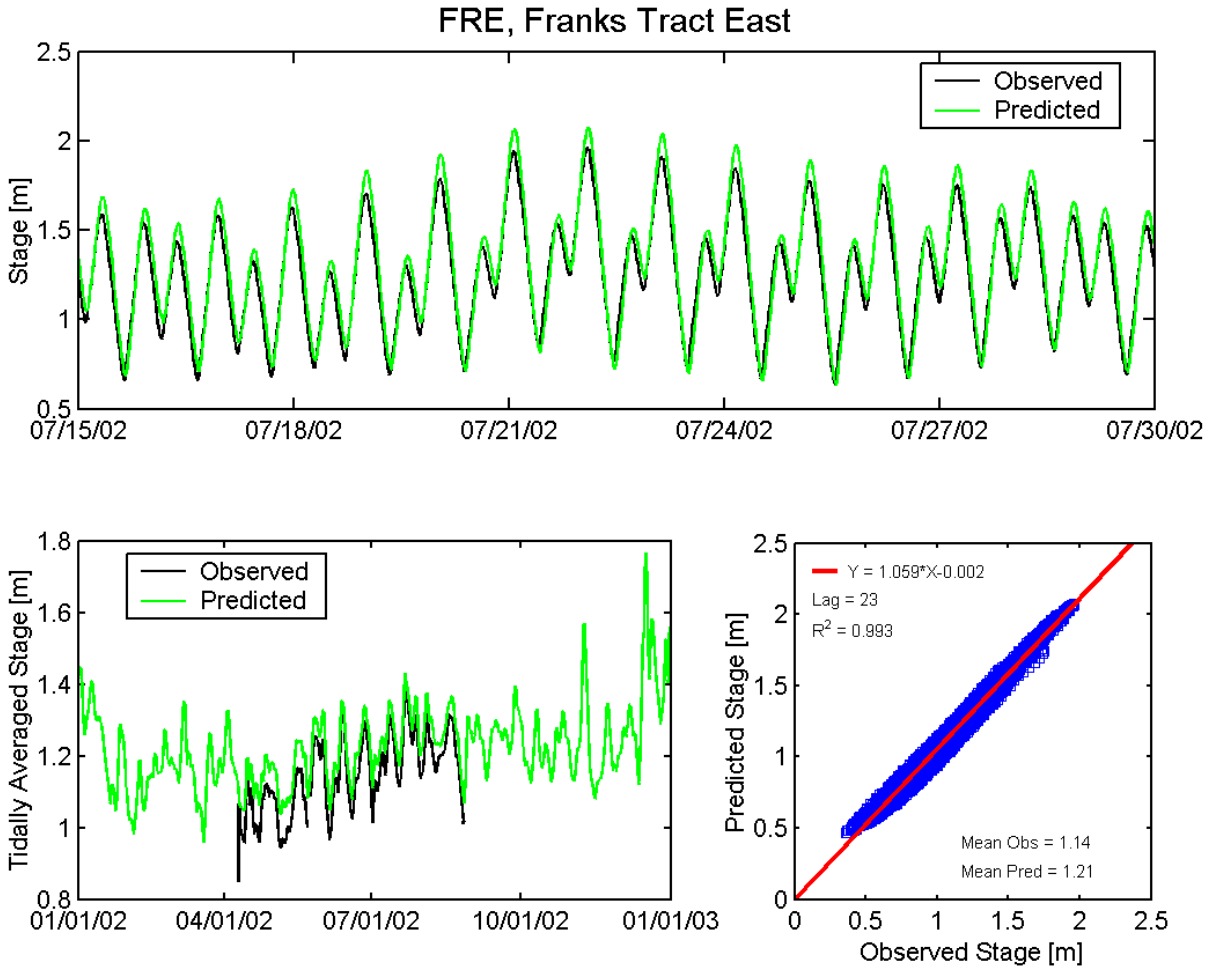

Figure A.3-34 Observed and predicted stage at Franks Tract East USGS station (FRE) during the 2002 simulation period.

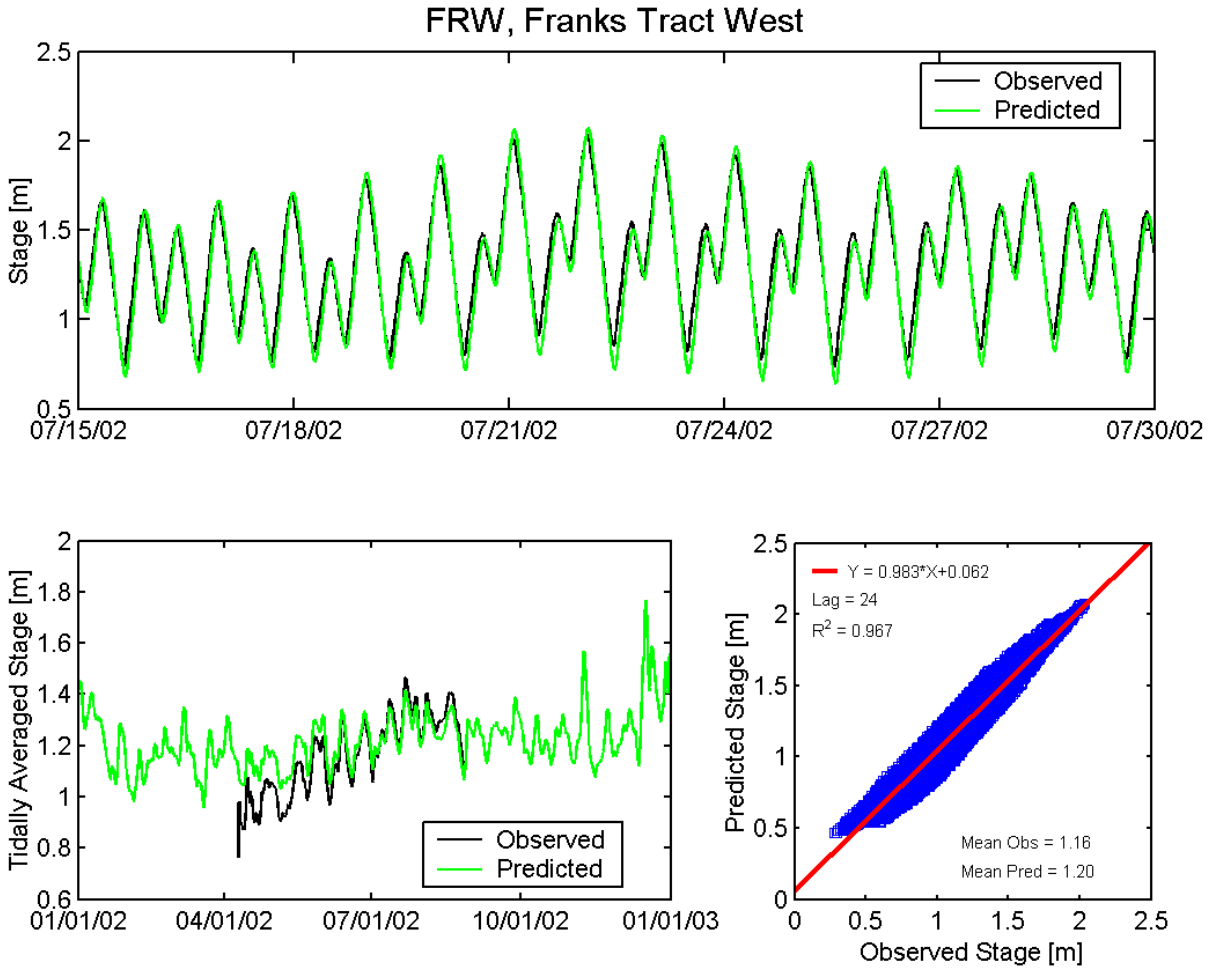

Figure A.3-35 Observed and predicted stage at Franks Tract West USGS station (FRW) during the 2002 simulation period.

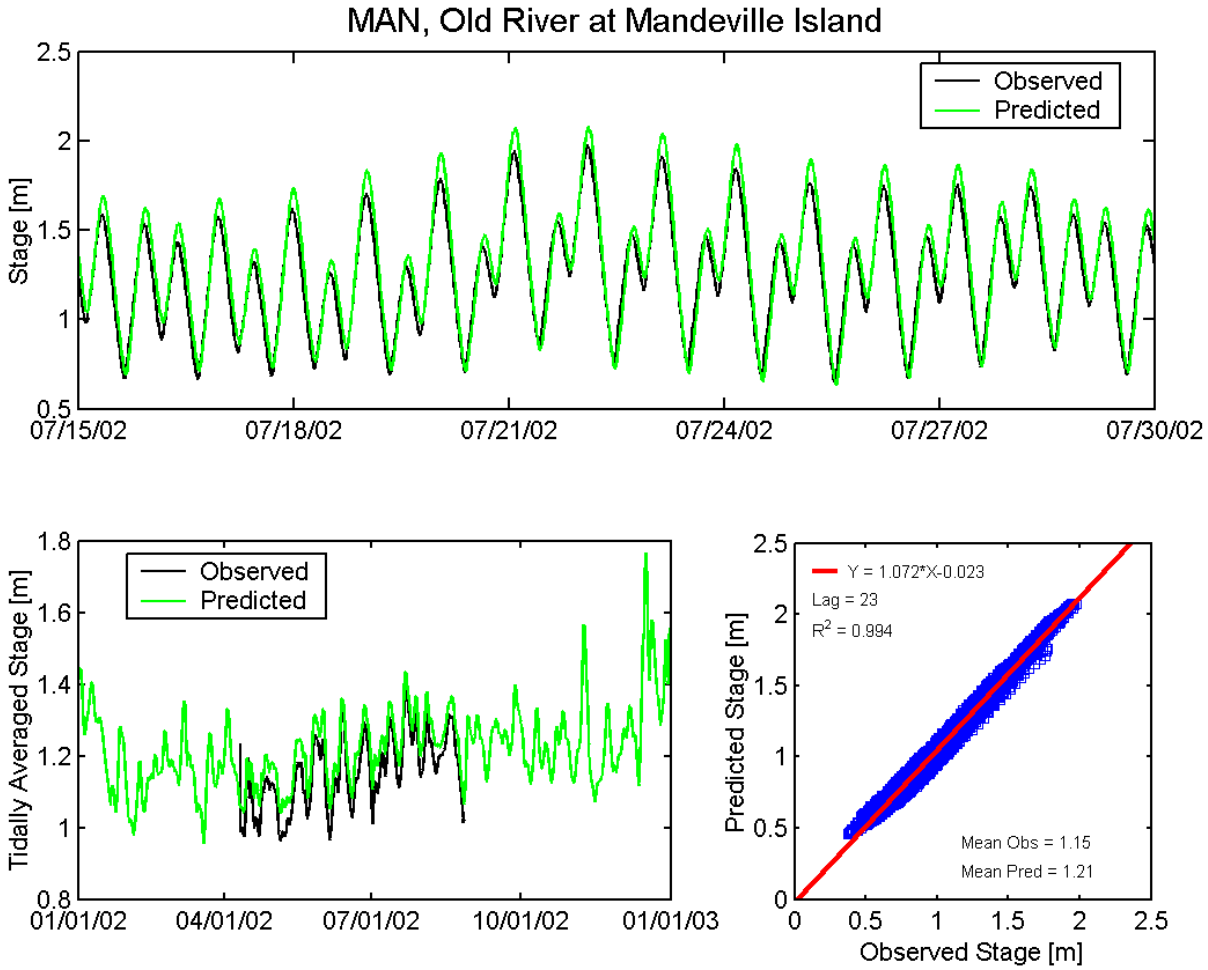

Figure A.3-36 Observed and predicted stage at Old River at Mandeville Island USGS station (MAN) during the 2002 simulation period.

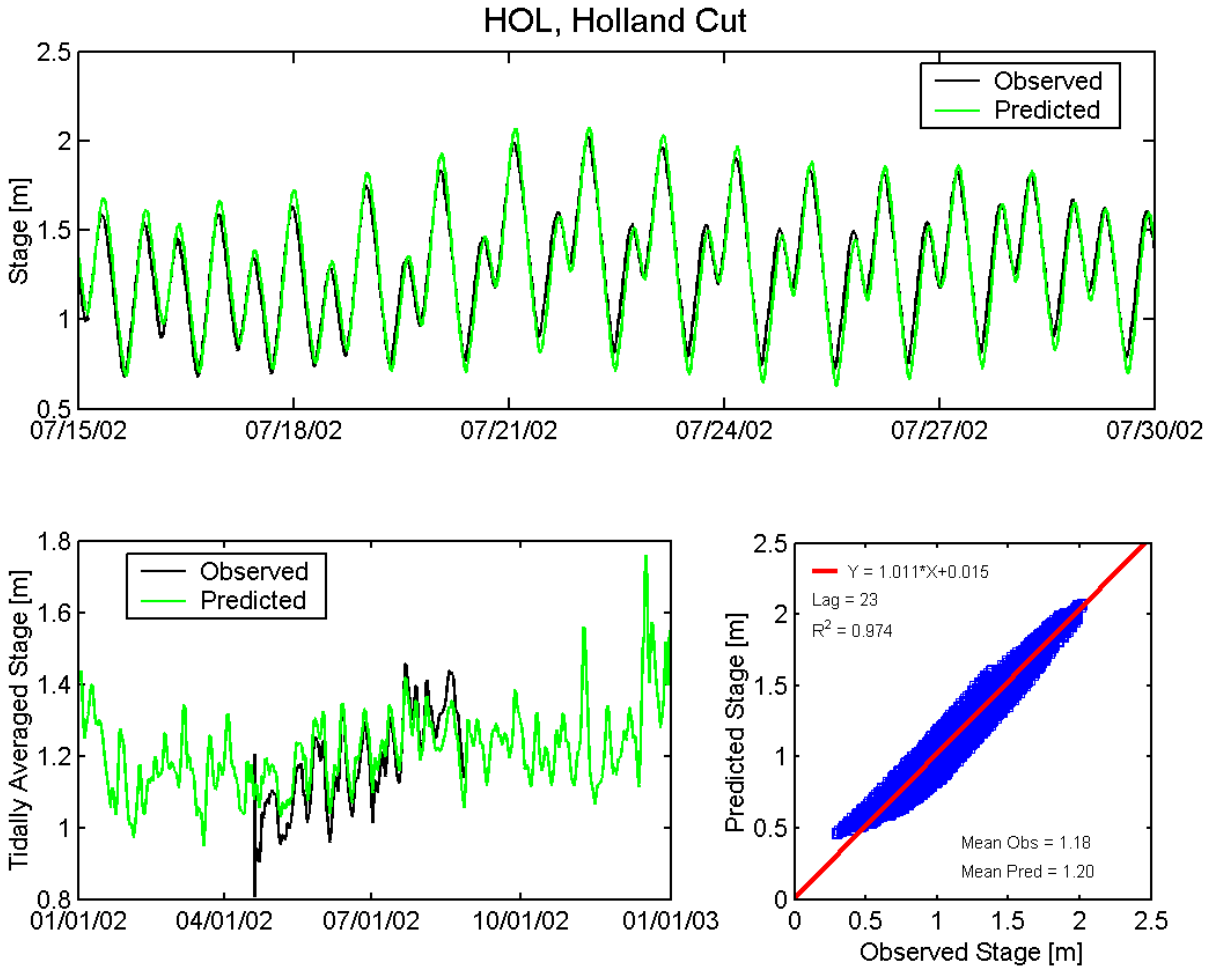

Figure A.3-37 Observed and predicted stage at Holland Cut USGS station (HOL) during the 2002 simulation period.

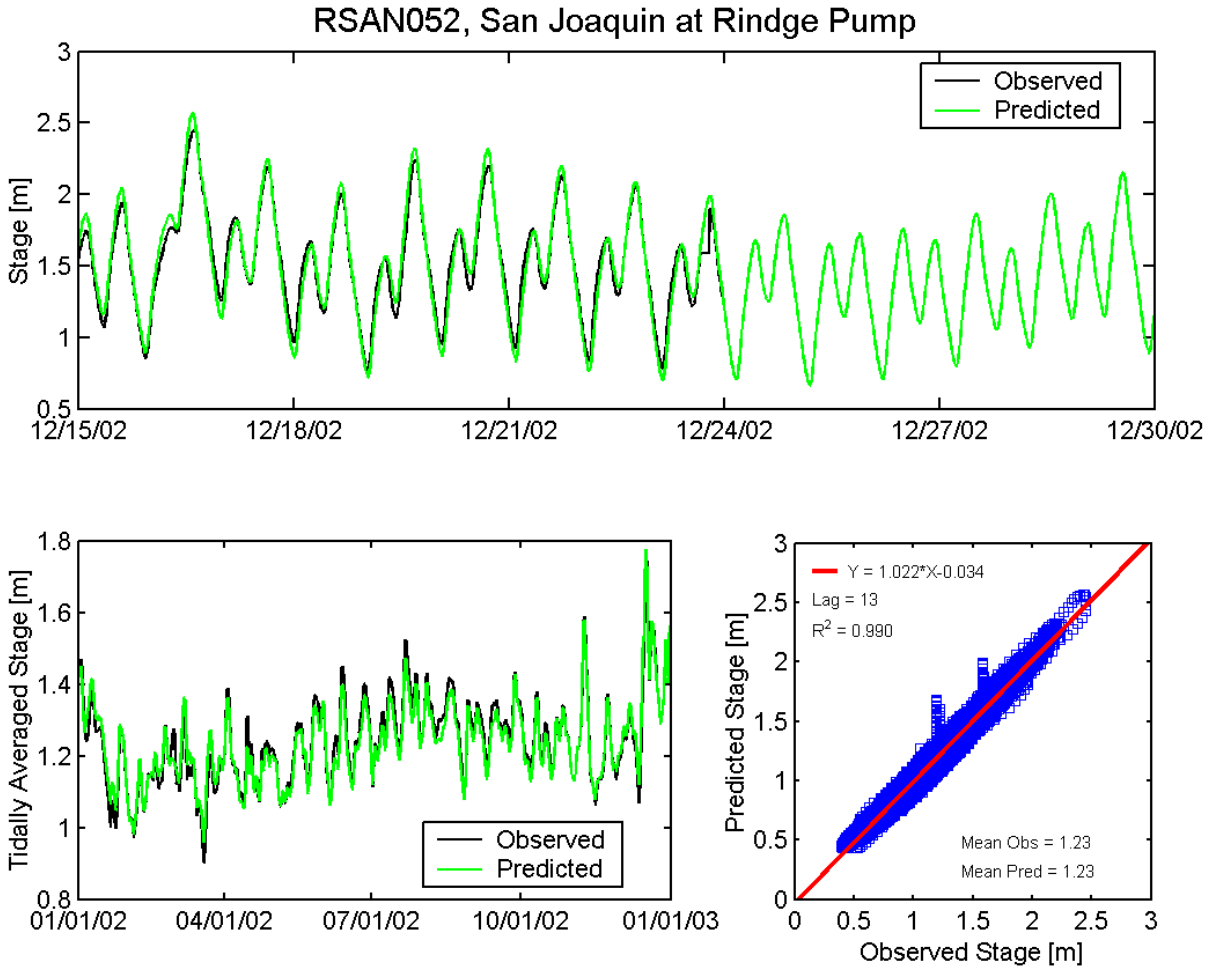

Figure A.3-38 Observed and predicted stage at San Joaquin River at Rindge Pump DWR station (RSAN052) during the 2002 simulation period.

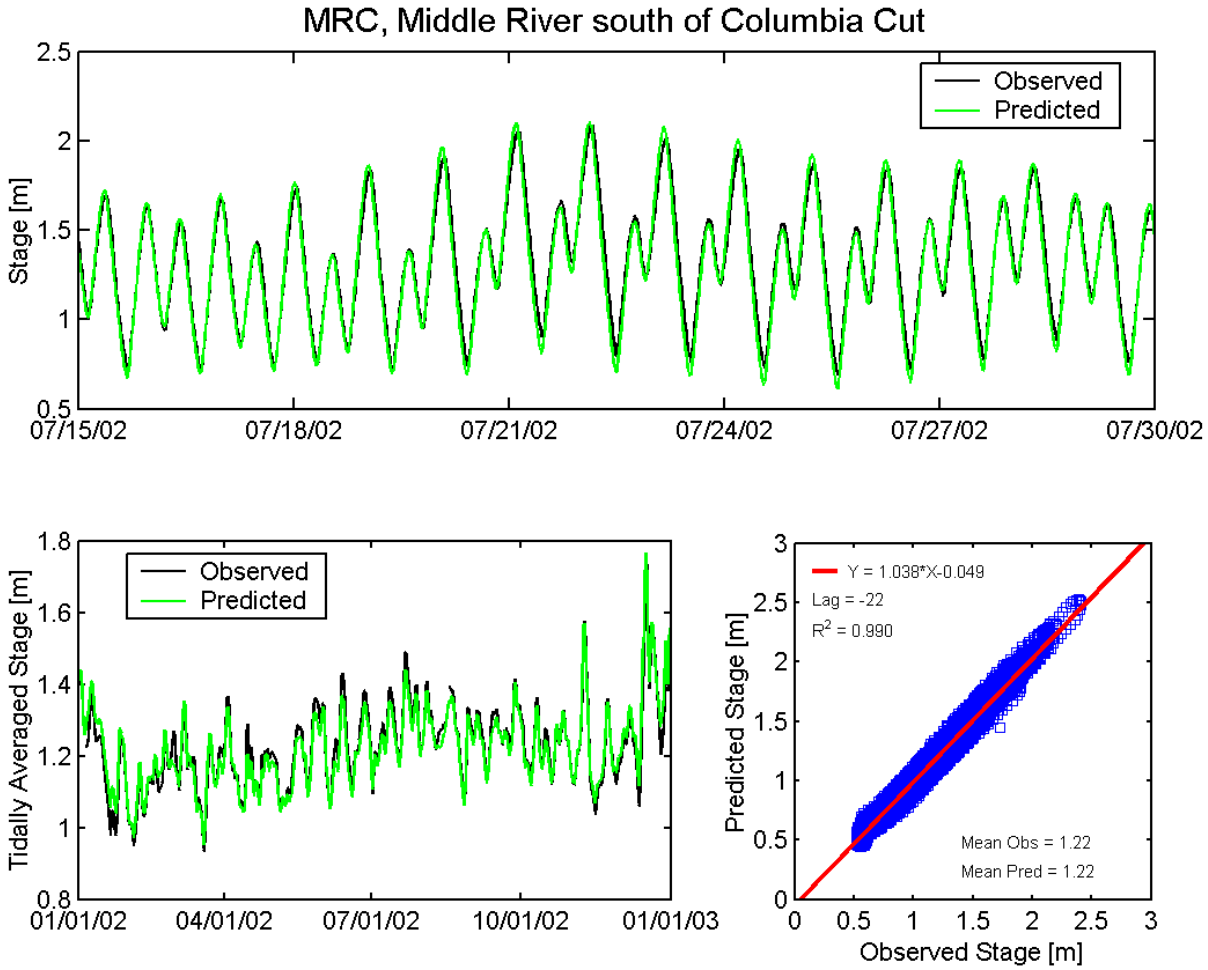

Figure A.3-39 Observed and predicted stage at Middle River south of Columbia Cut USGS station (MRC) during the 2002 simulation period.

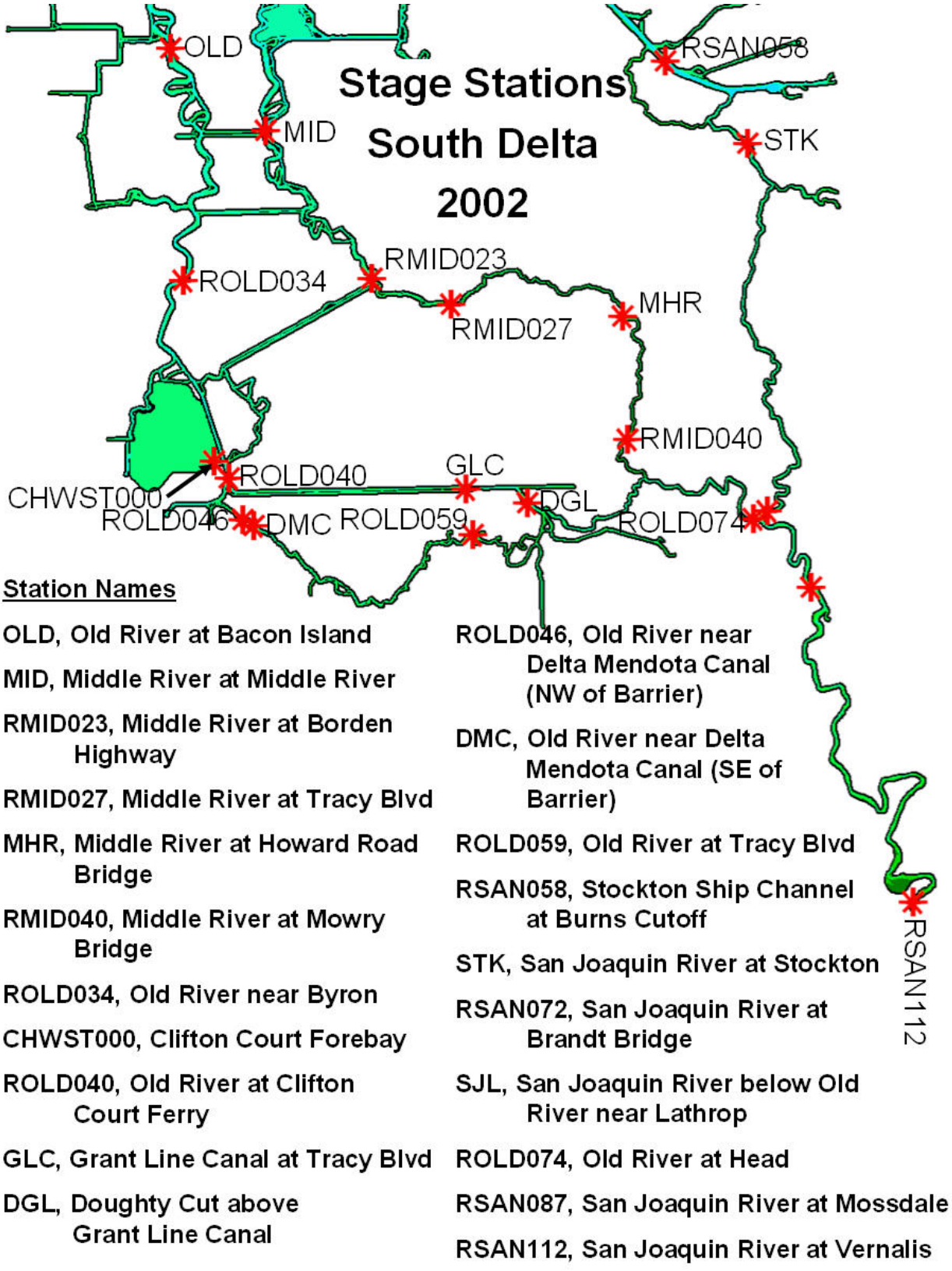

Figure A.3-40 Location of water level monitoring stations in the southern portion of the Sacramento-San Joaquin Delta used for 2002 water level comparisons.

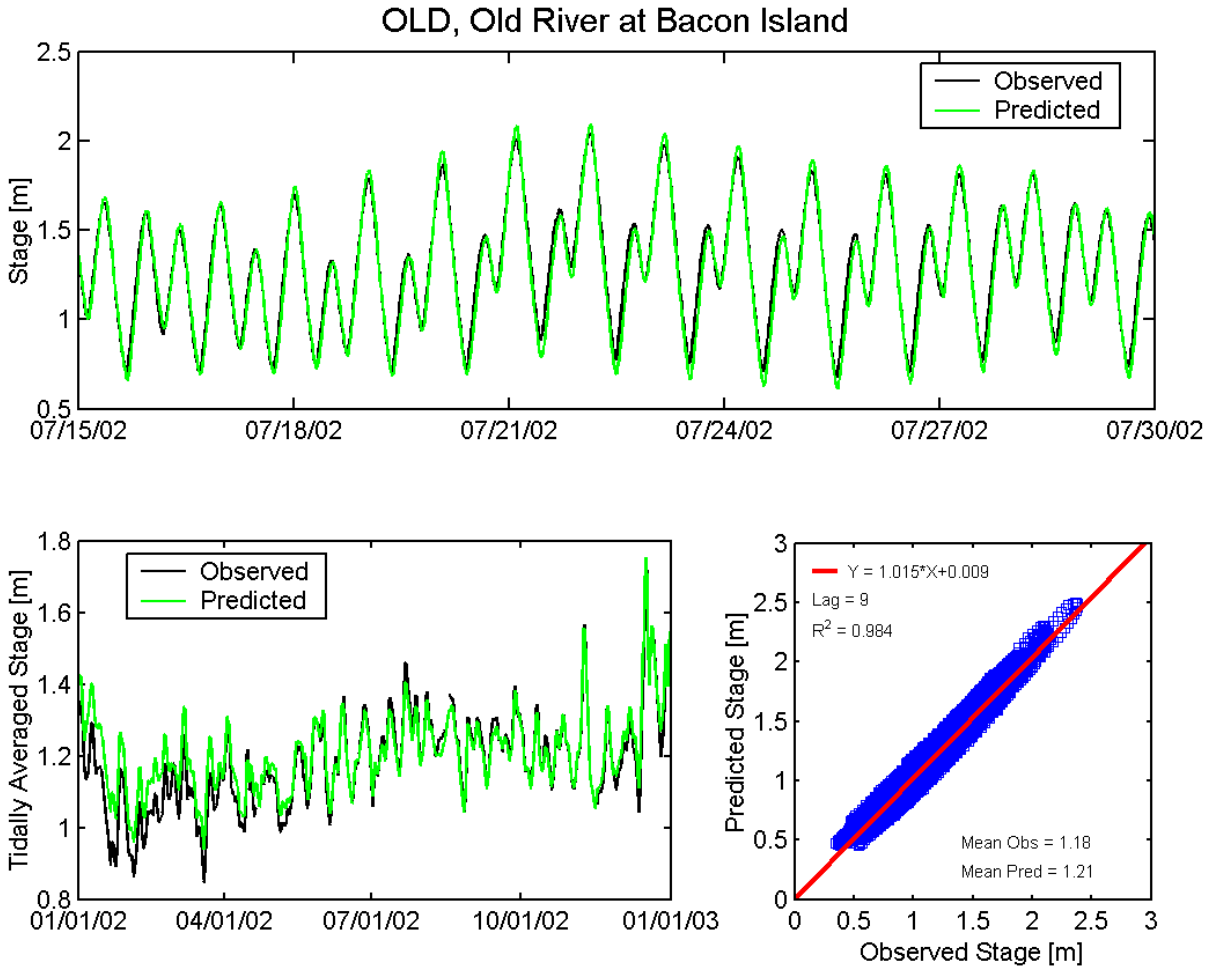

Figure A.3-41 Observed and predicted stage at Old River at Bacon Island USGS station (OLD) during the 2002 simulation period.

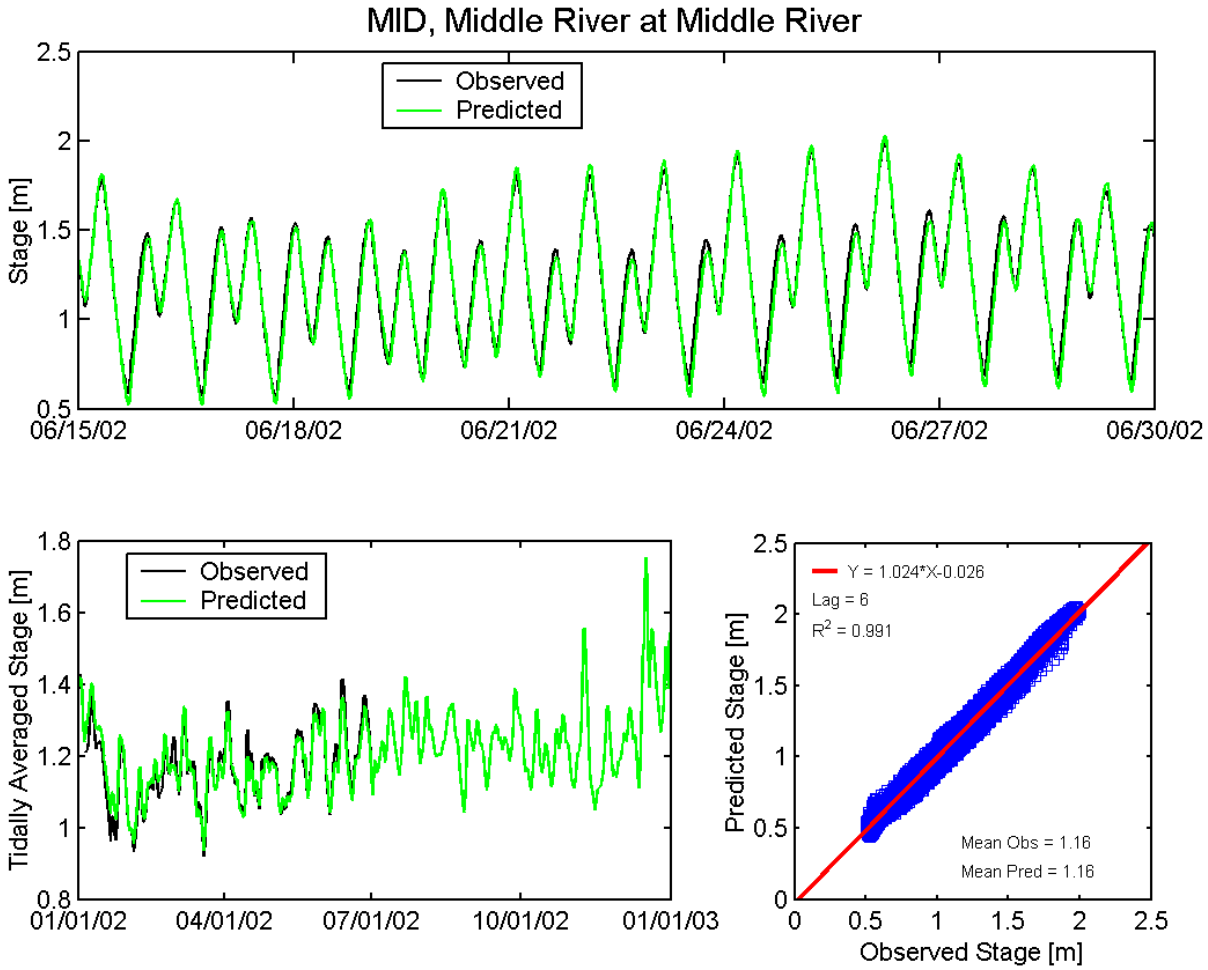

Figure A.3-42 Observed and predicted stage at Middle River at Middle River USGS station (MID) during the 2002 simulation period.

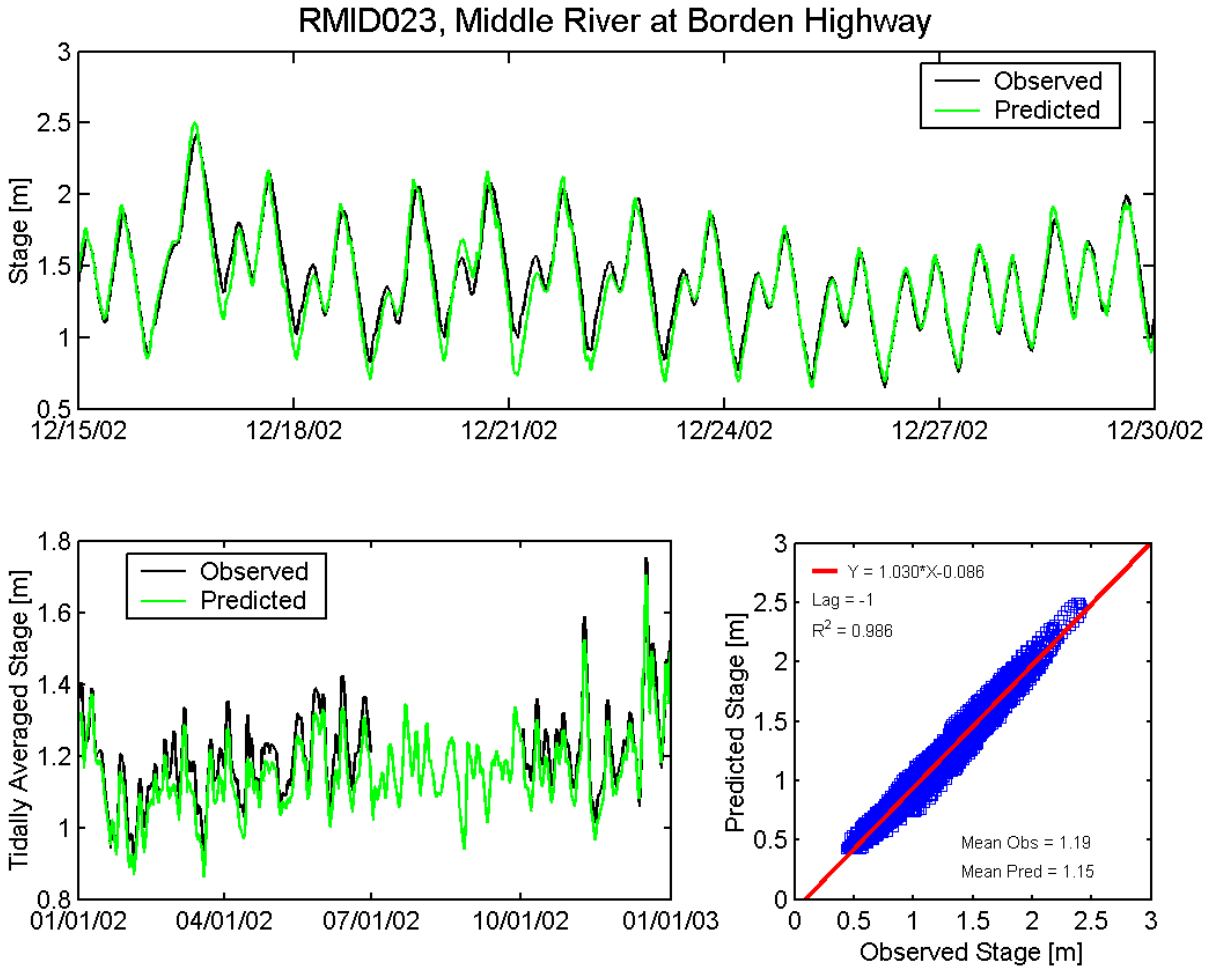

Figure A.3-43 Observed and predicted stage at Middle River at Borden Highway DWR station (RMID023) during the 2002 simulation period.

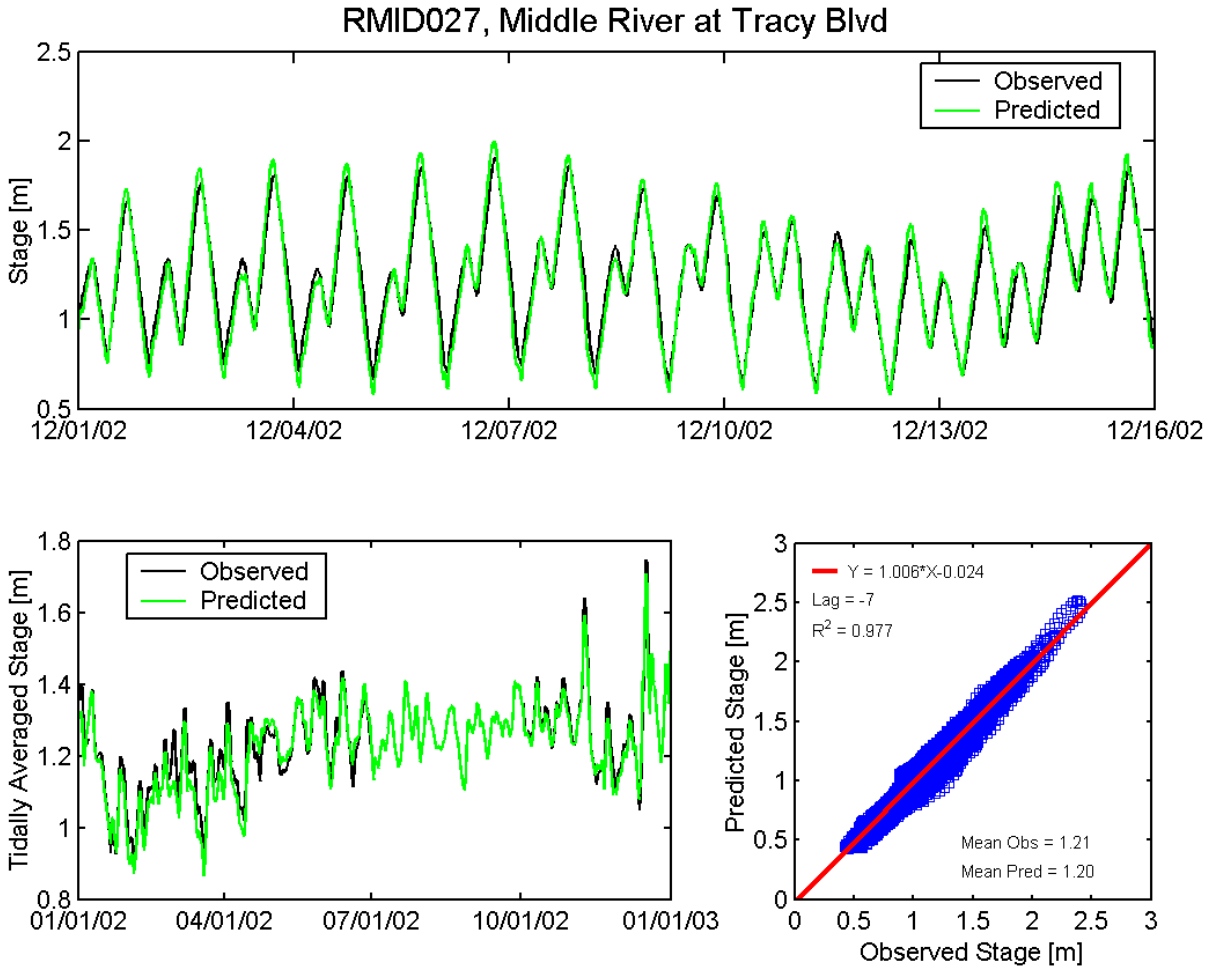

Figure A.3-44 Observed and predicted stage at Middle River at Tracy Boulevard DWR station (RMID027) during the 2002 simulation period.

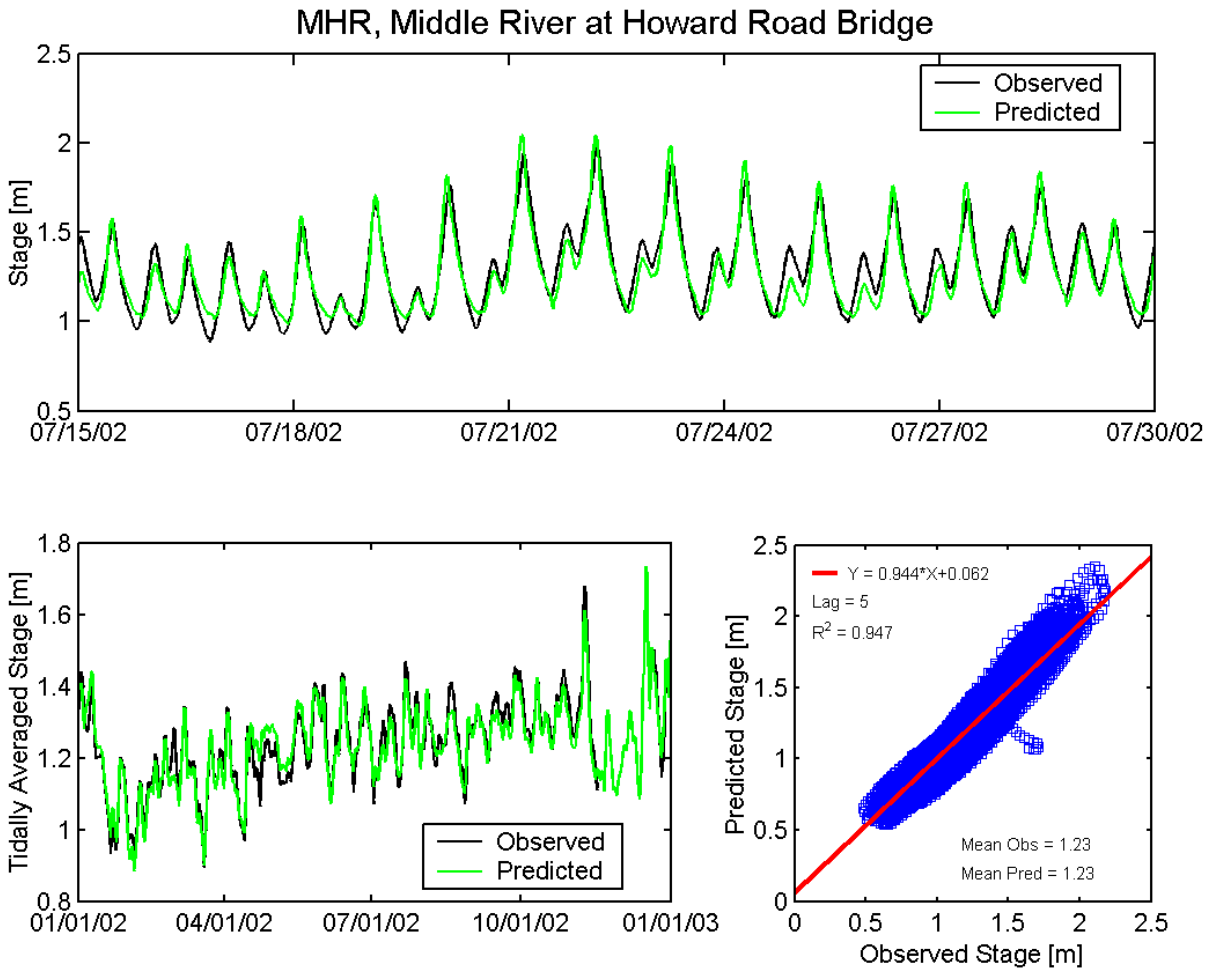

Figure A.3-45 Observed and predicted stage at Middle River at Howard Road Bridge DWR station (CDEC MHR) during the 2002 simulation period.

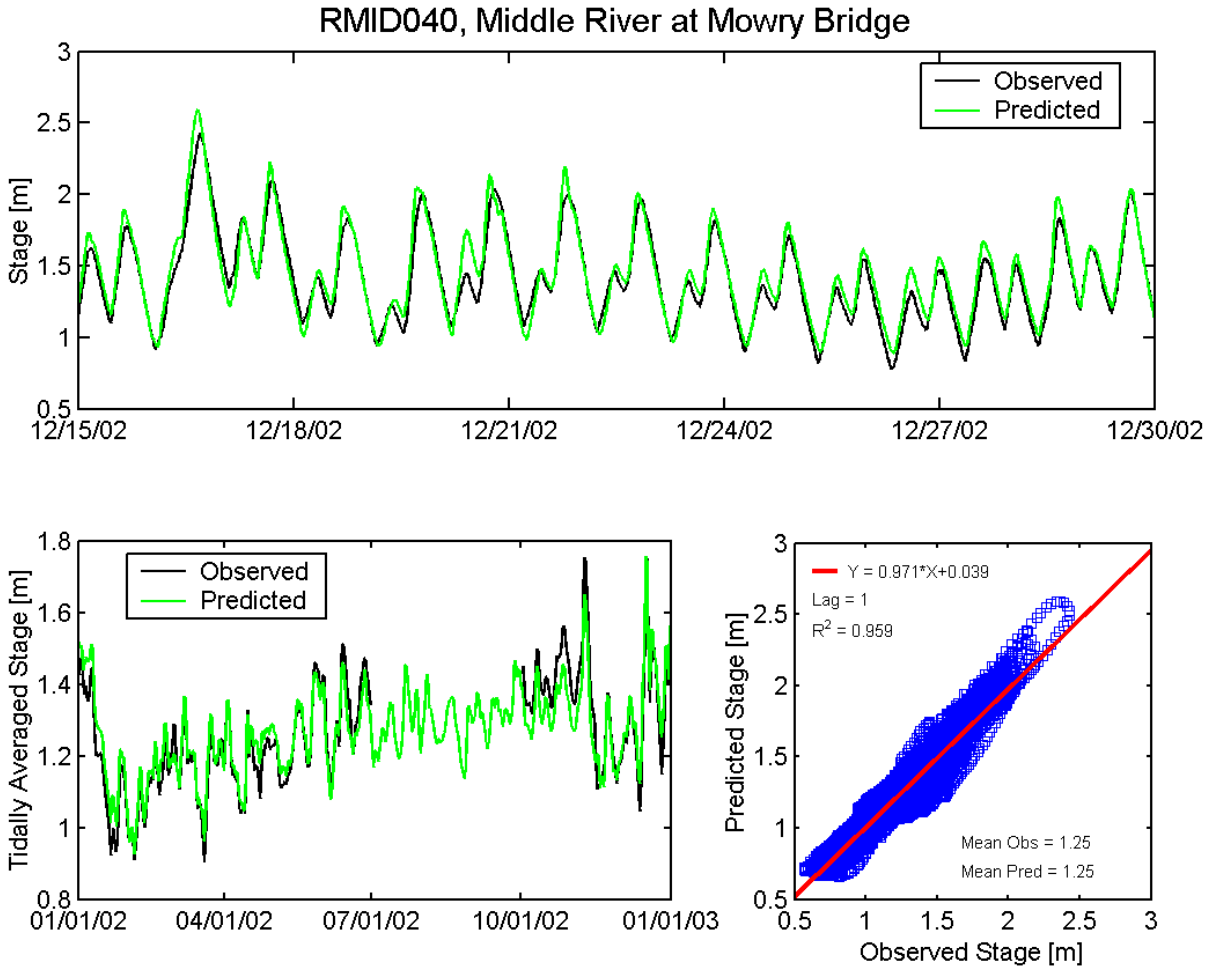

Figure A.3-46 Observed and predicted stage at Middle River at Mowry Bridge DWR station (RMID040) during the 2002 simulation period.

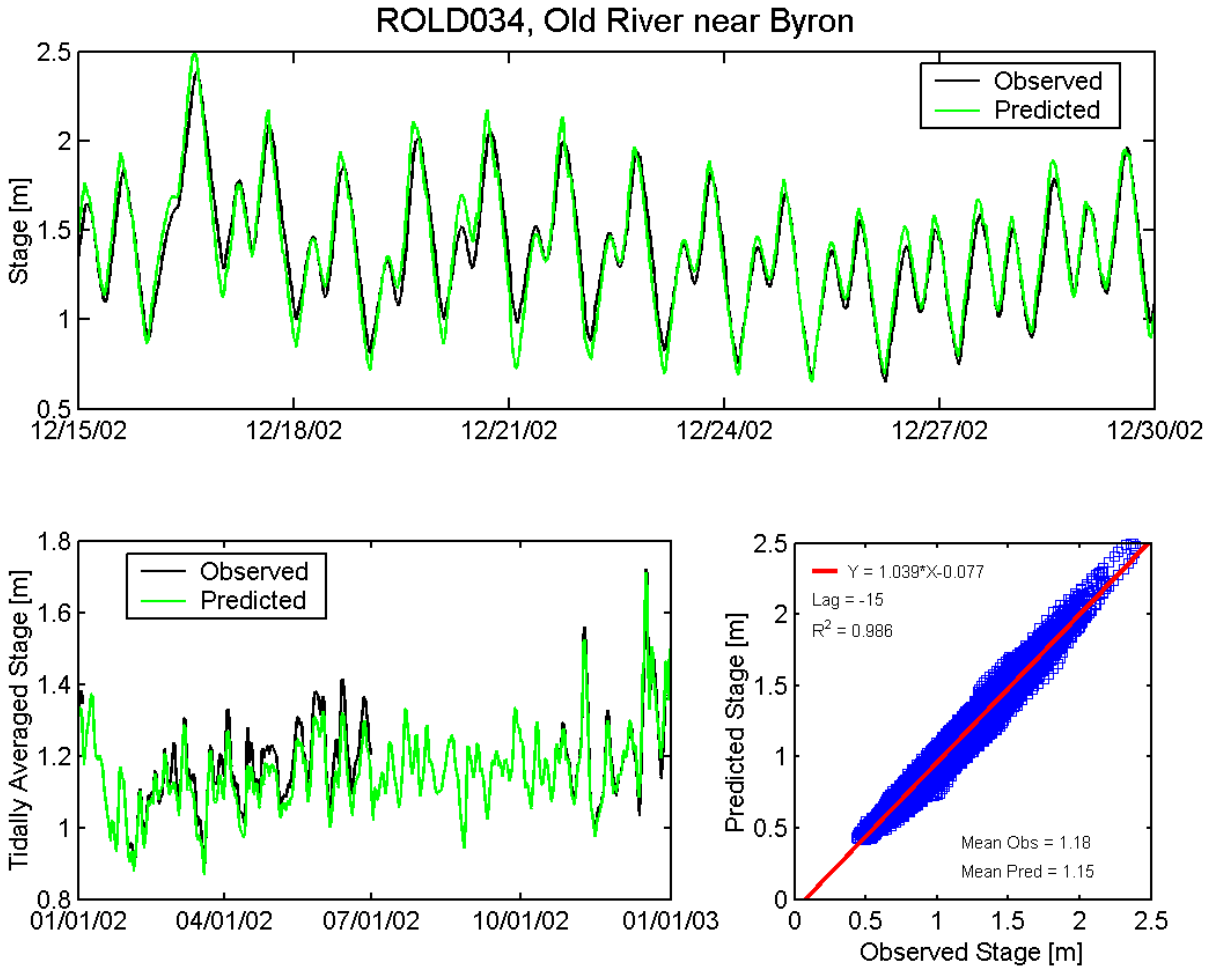

Figure A.3-47 Observed and predicted stage at Old River near Byron DWR station (ROLD034) during the 2002 simulation period.

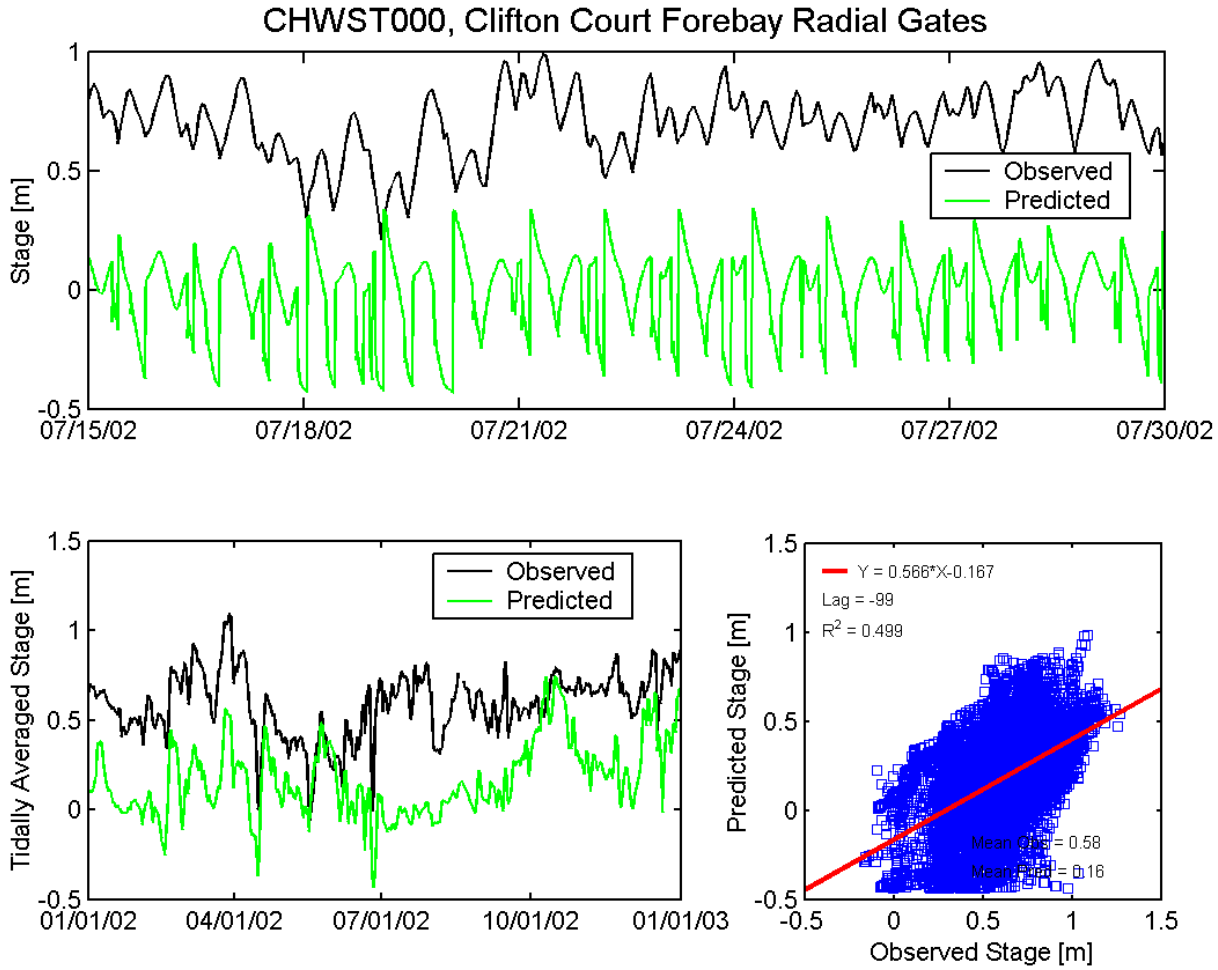

Figure A.3-48 Observed and predicted stage at Clifton Court Forebay Radial Gates DWR station (CHWST000) during the 2002 simulation period.

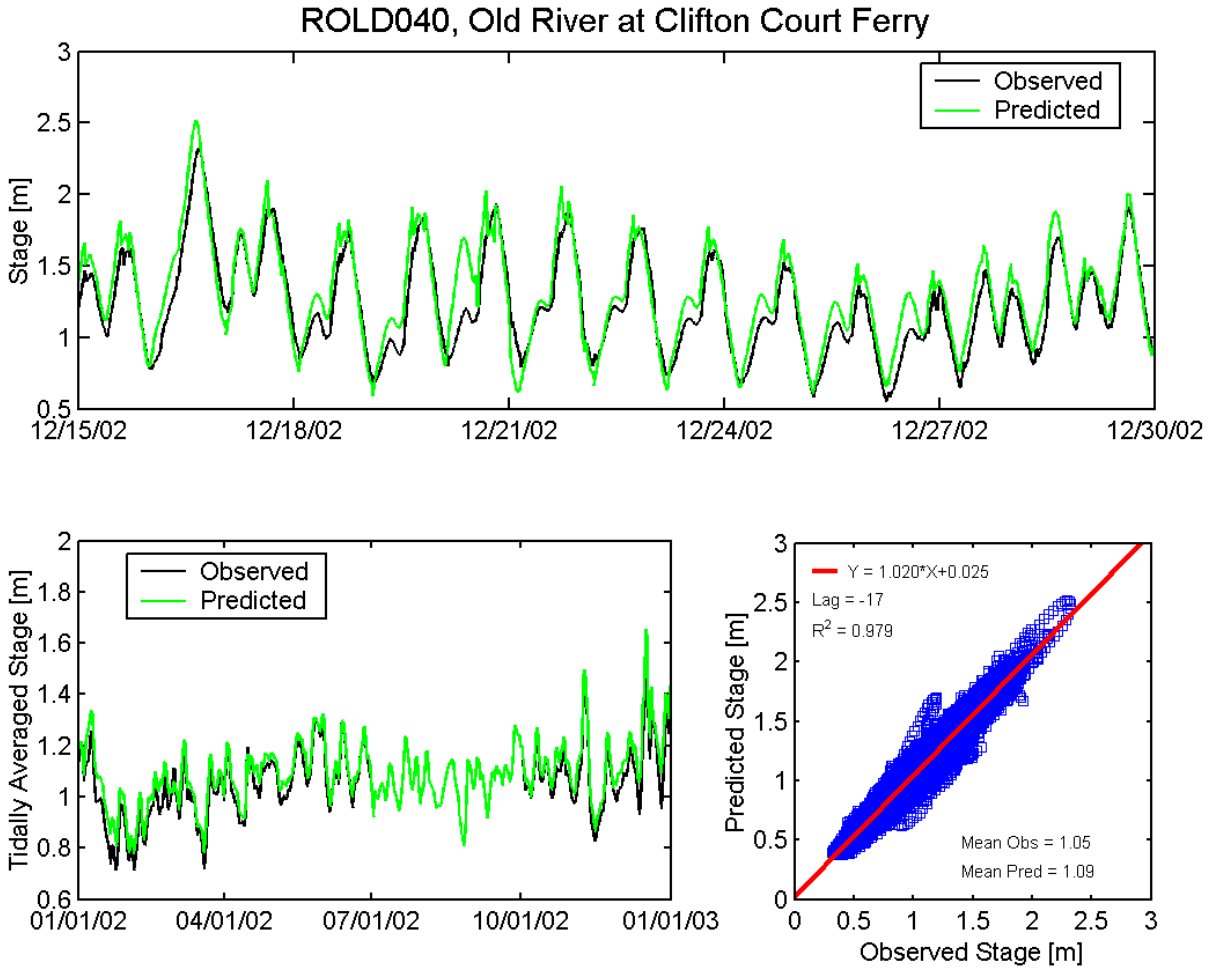

Figure A.3-49 Observed and predicted stage at Old River at Clifton Court Ferry DWR station (ROLD040) during the 2002 simulation period.

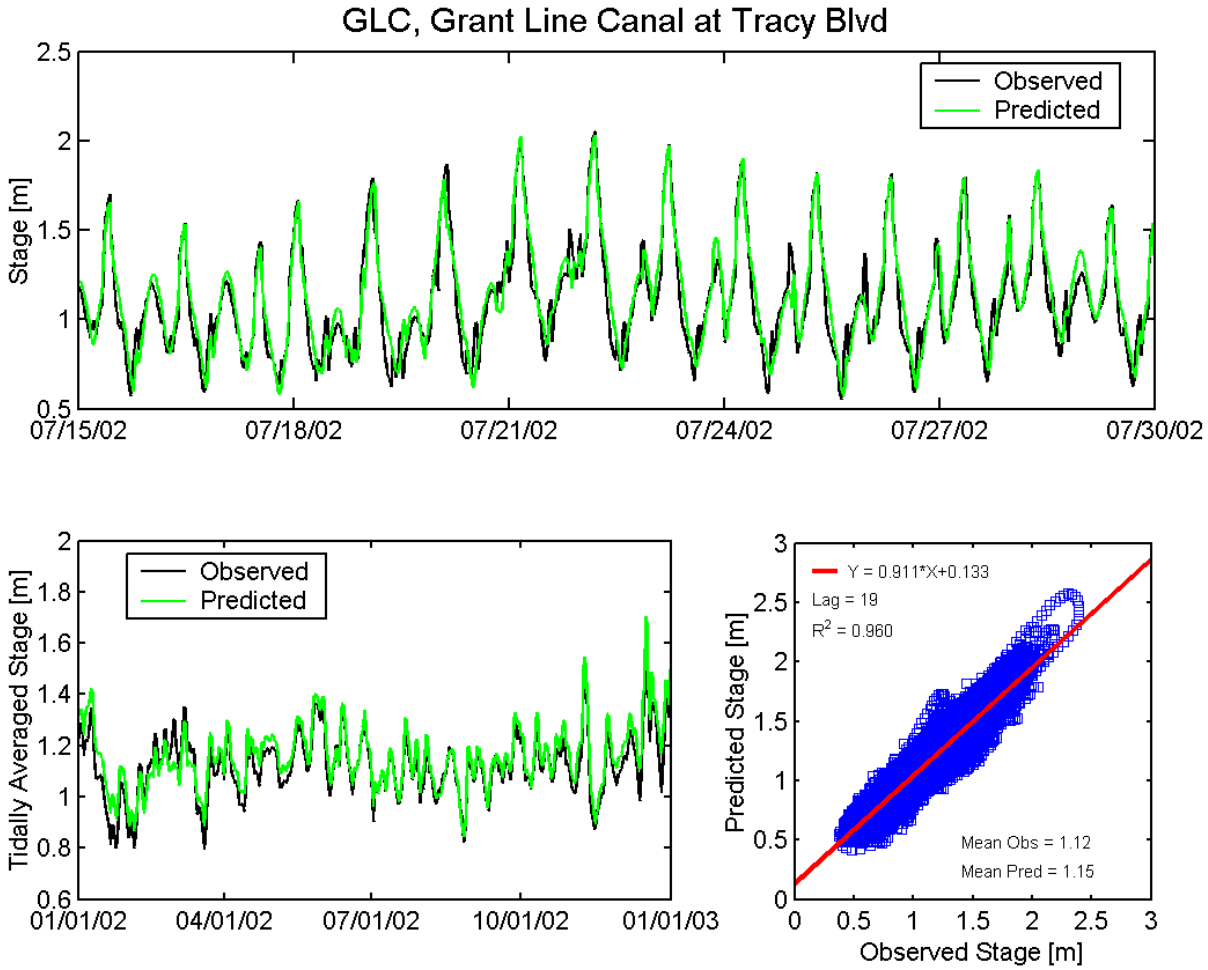

Figure A.3-50 Observed and predicted stage at Grant Line Canal at Tracy Boulevard USGS station (GLC) during the 2002 simulation period.

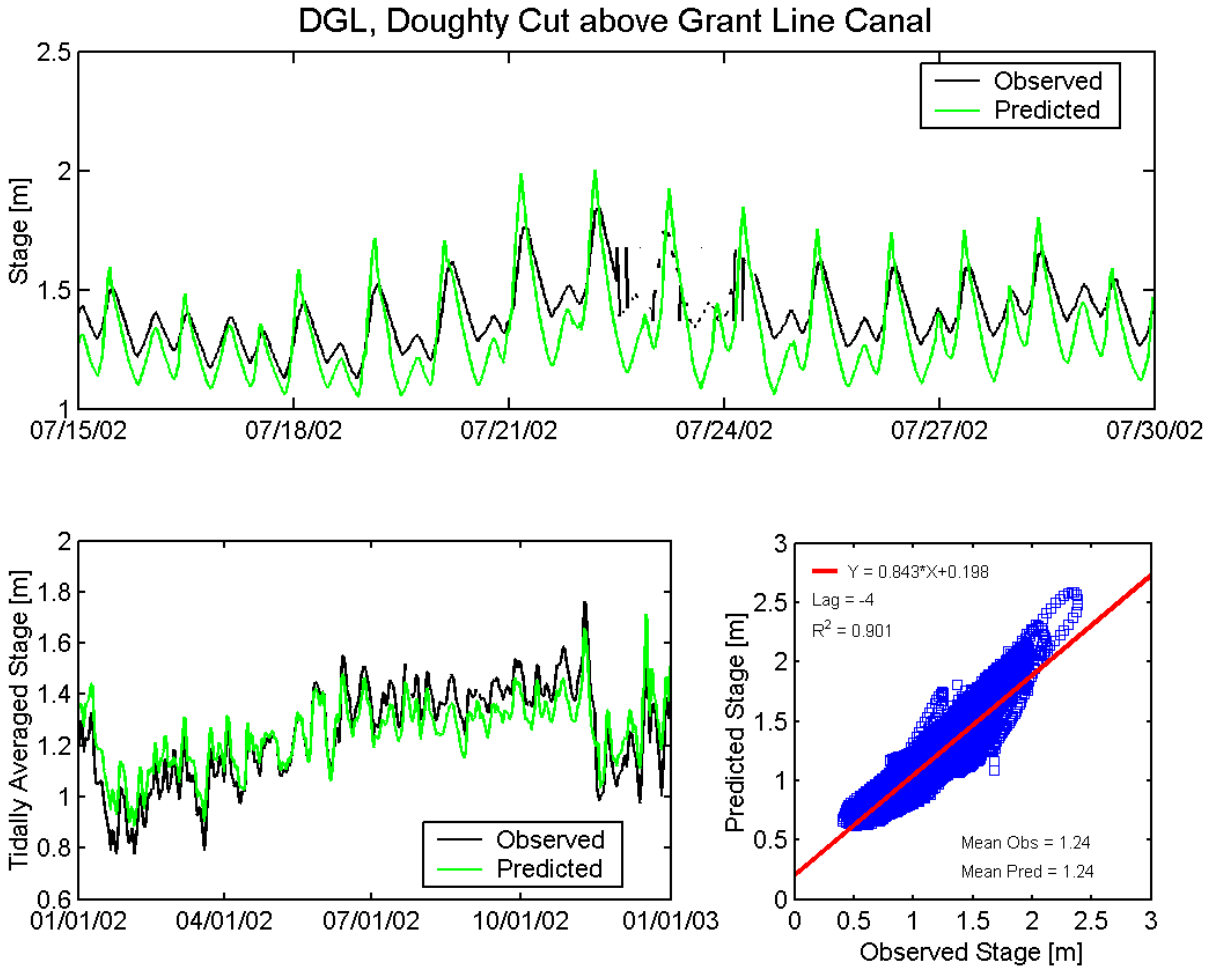

Figure A.3-51 Observed and predicted stage at Doughty Cut above Grant Line Canal DWR station (CDEC DGL) during the 2002 simulation period.

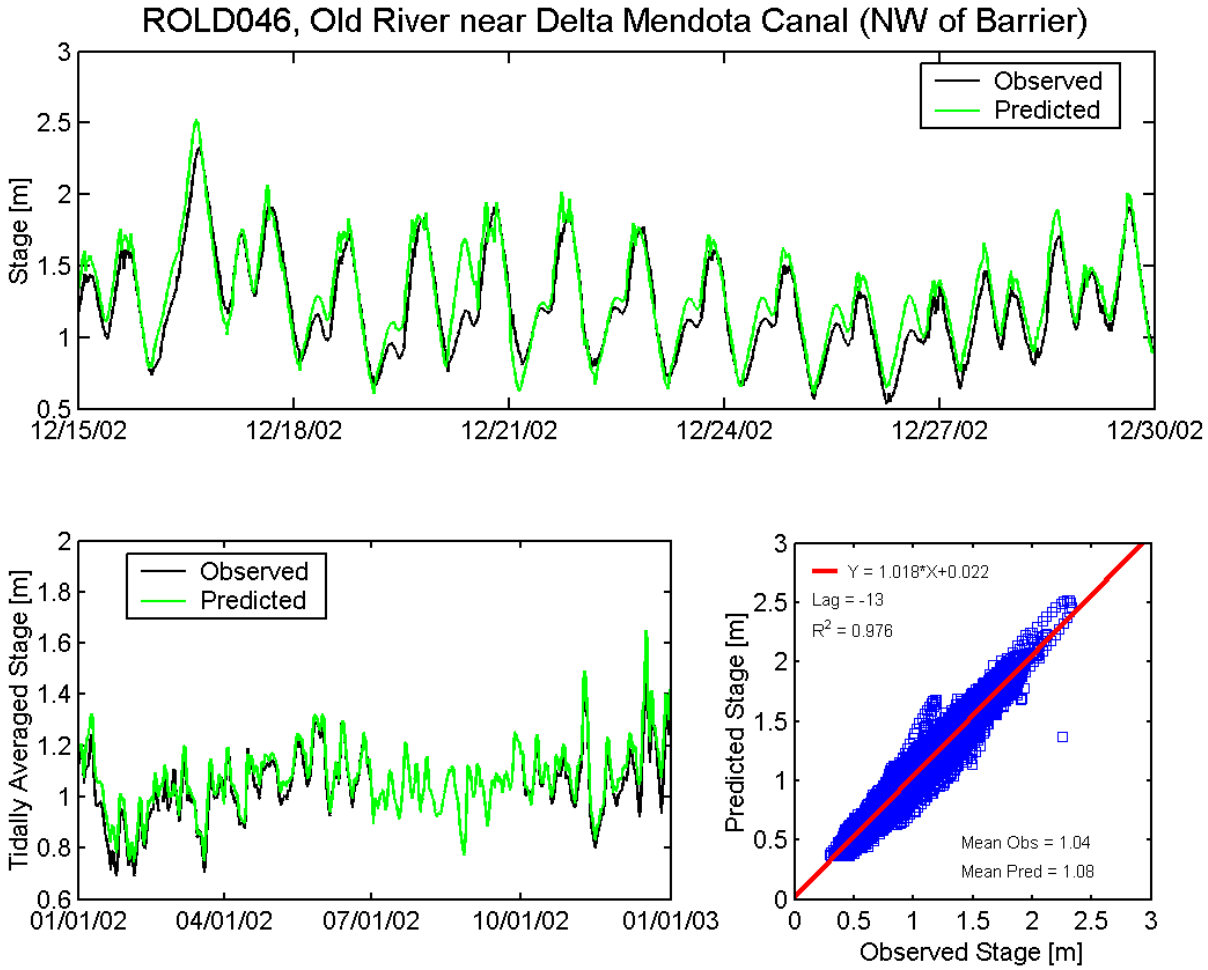

Figure A.3-52 Observed and predicted stage at Old River near Delta Mendota Canal NW of Barrier DWR station (ROLD046) during the 2002 simulation period.

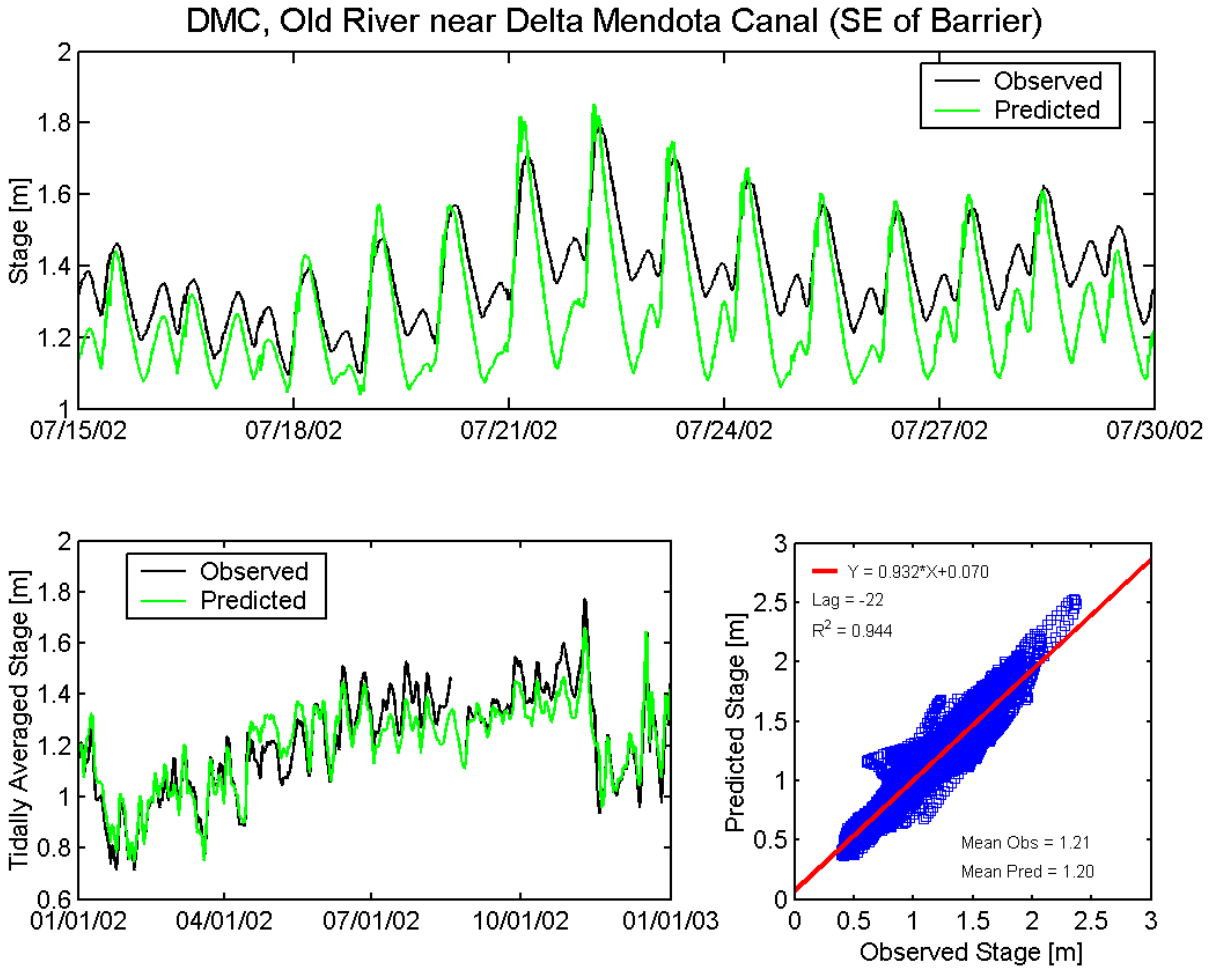

Figure A.3-53 Observed and predicted stage at Old River near Delta Mendota Canal SE of Barrier USGS station (DMC) during the 2002 simulation period.

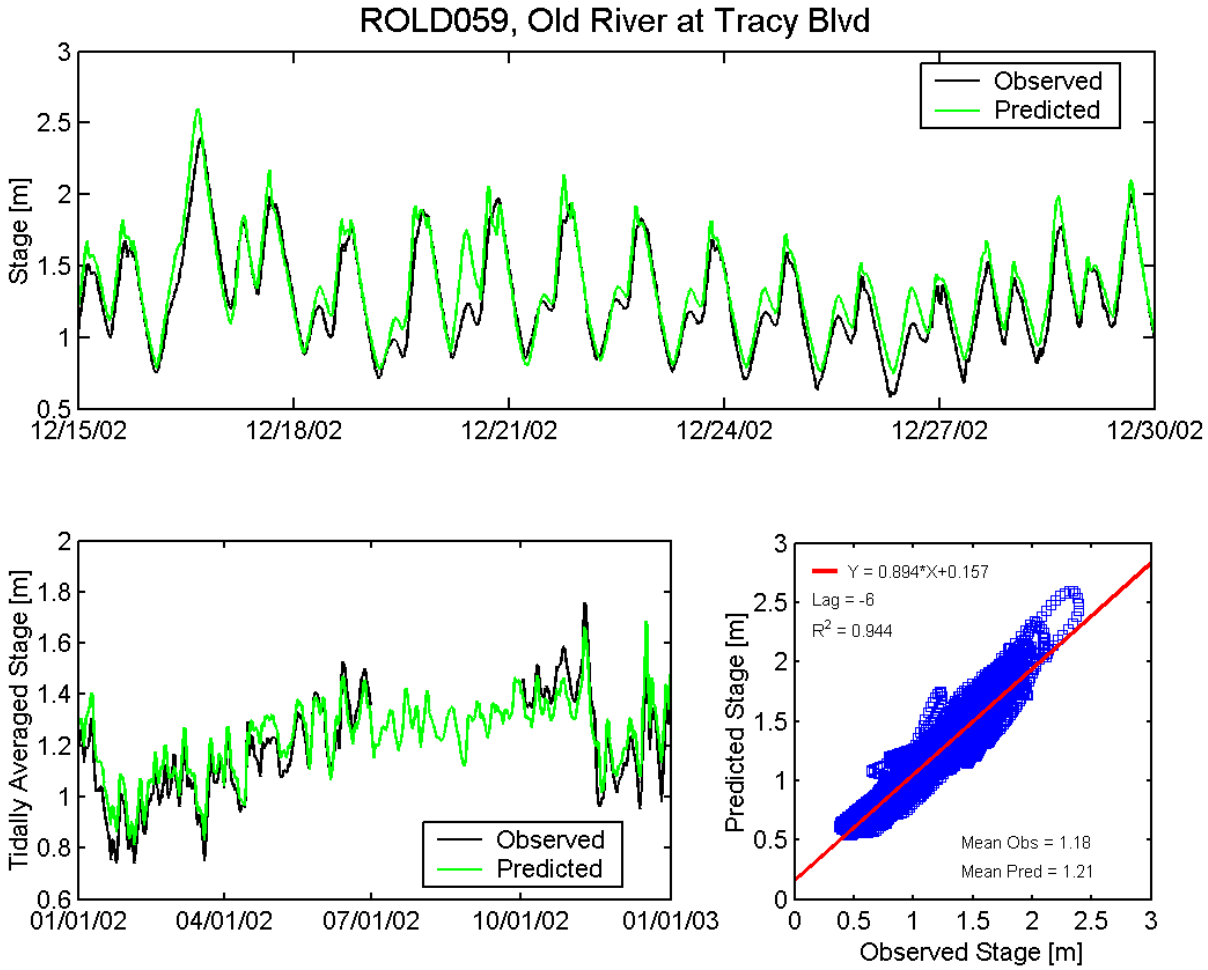

Figure A.3-54 Observed and predicted stage at Old River at Tracy Boulevard DWR station (ROLD059) during the 2002 simulation period.

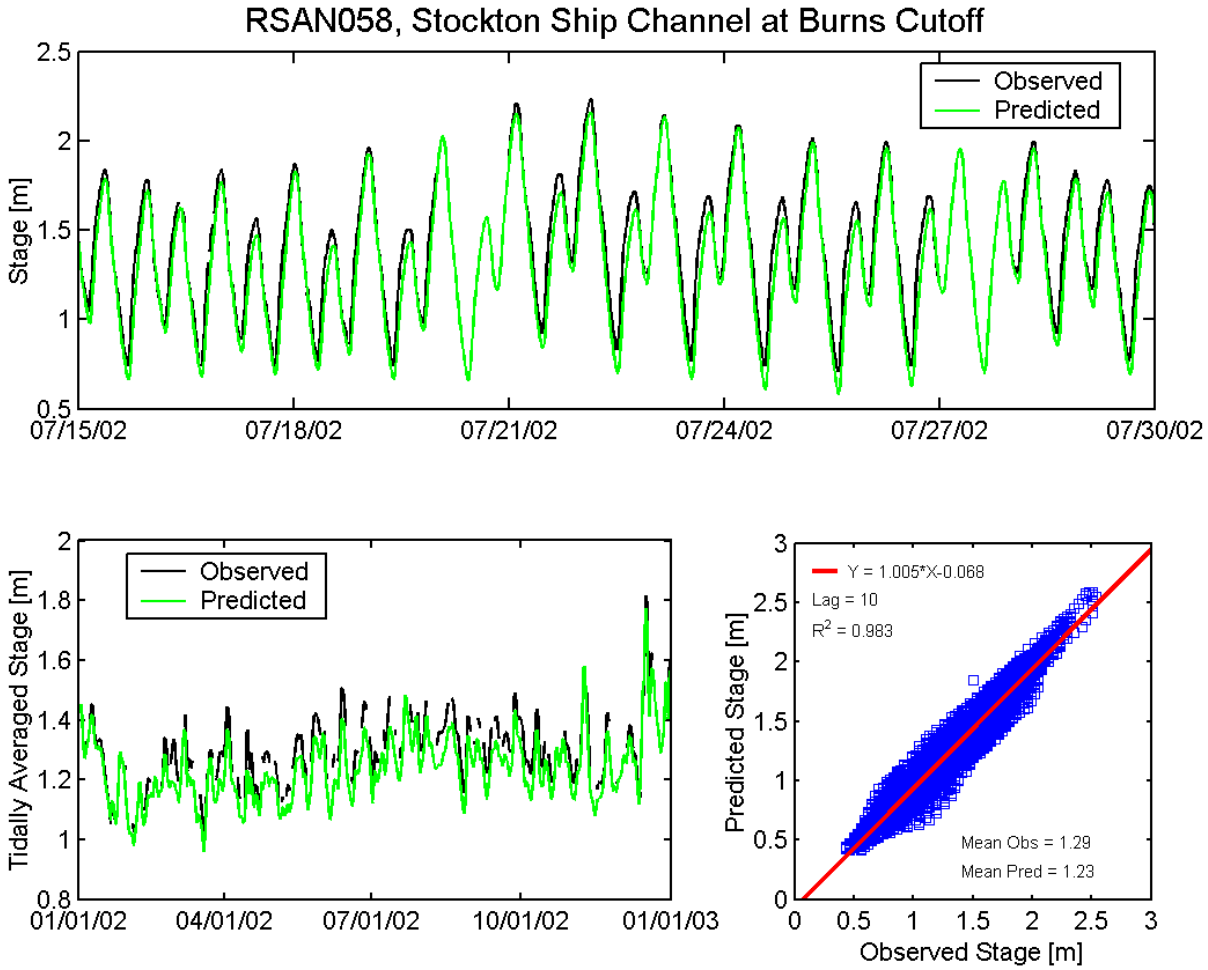

Figure A.3-55 Observed and predicted stage at Stockton Ship Channel at Burns Cutoff DWR station (RSAN058) during the 2002 simulation period.

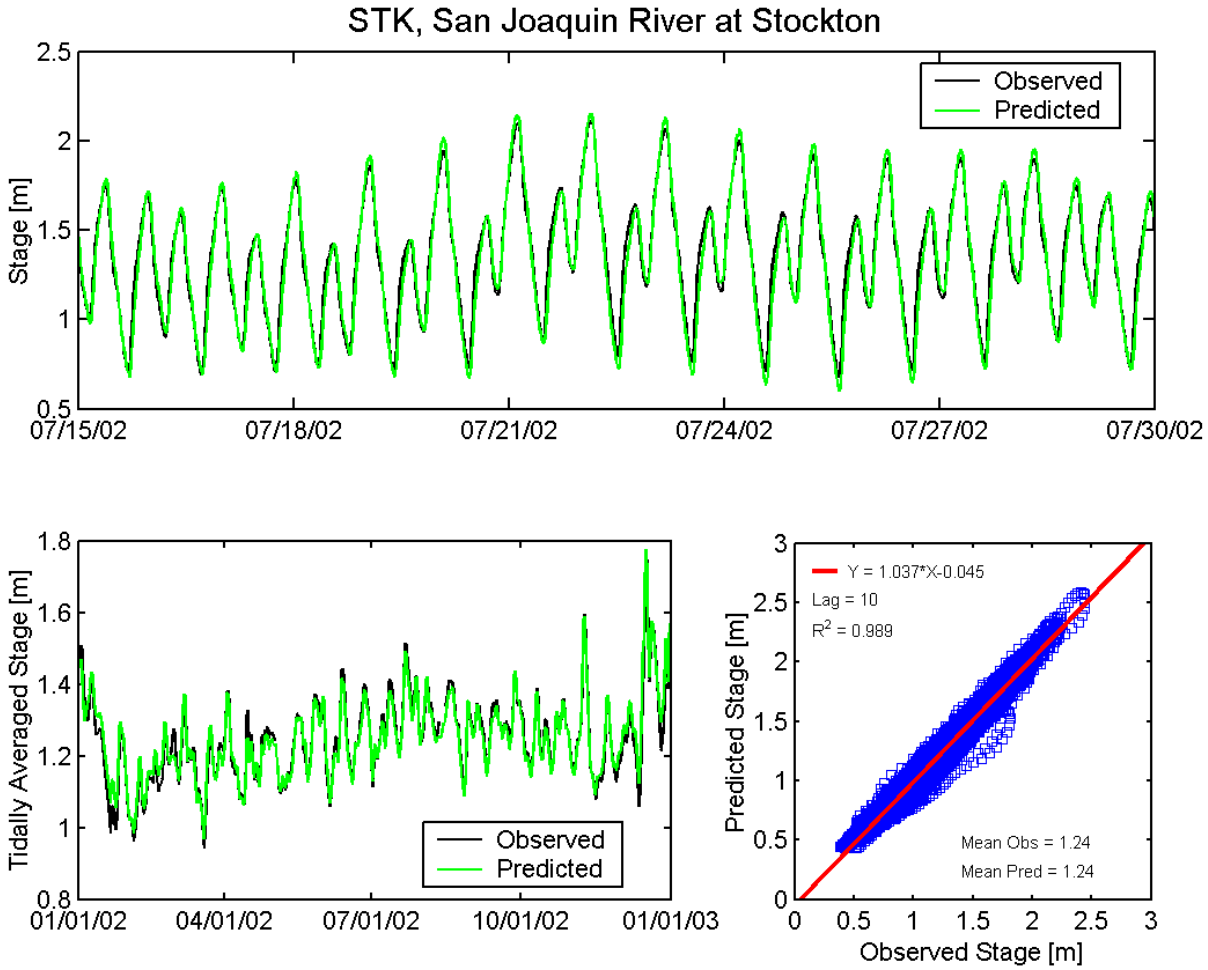

Figure A.3-56 Observed and predicted stage at San Joaquin River at Stockton USGS station (STK) during the 2002 simulation period.

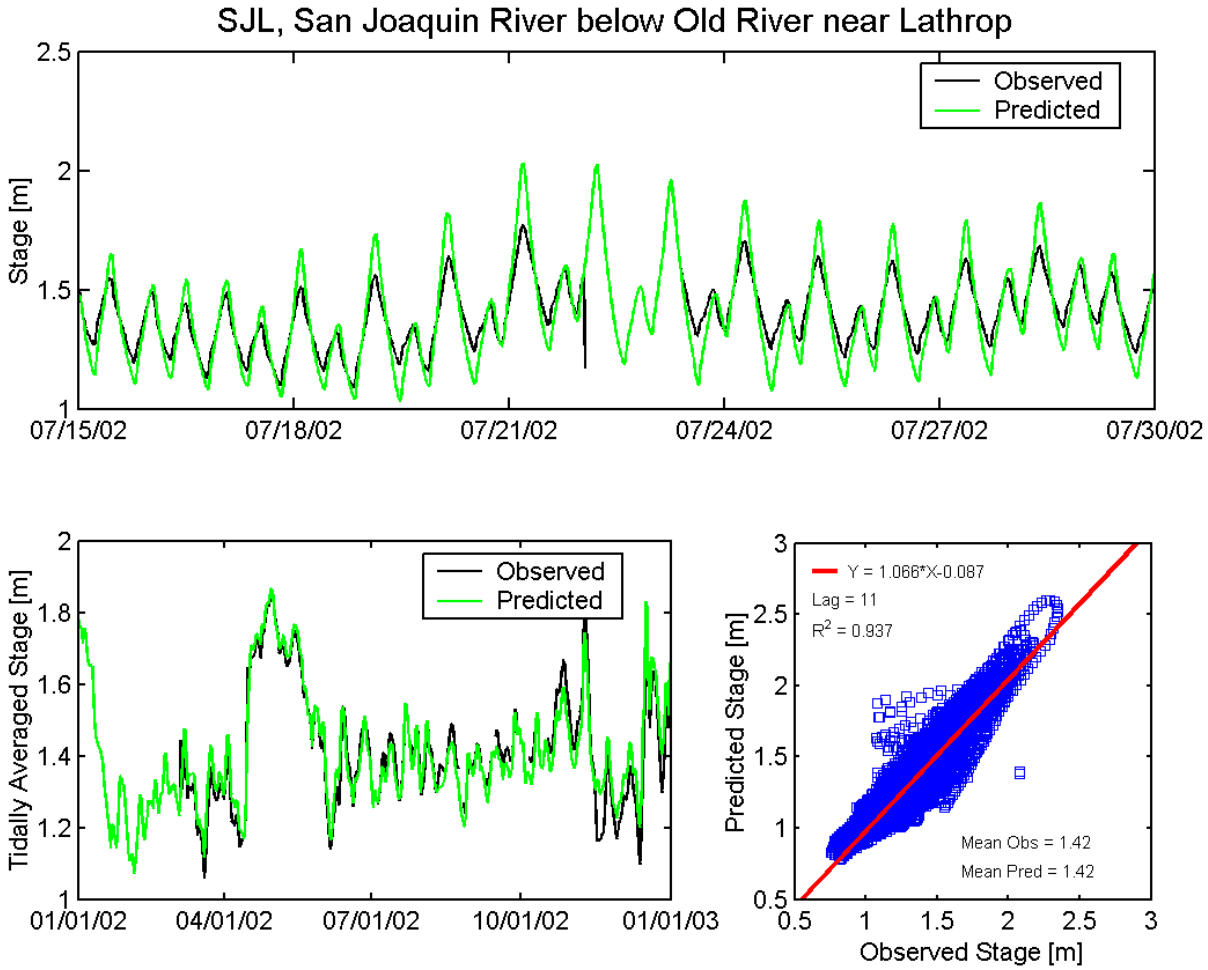

Figure A.3-57 Observed and predicted stage at San Joaquin River below Old River near Lathrop DWR station (CDEC SJL) during the 2002 simulation period.

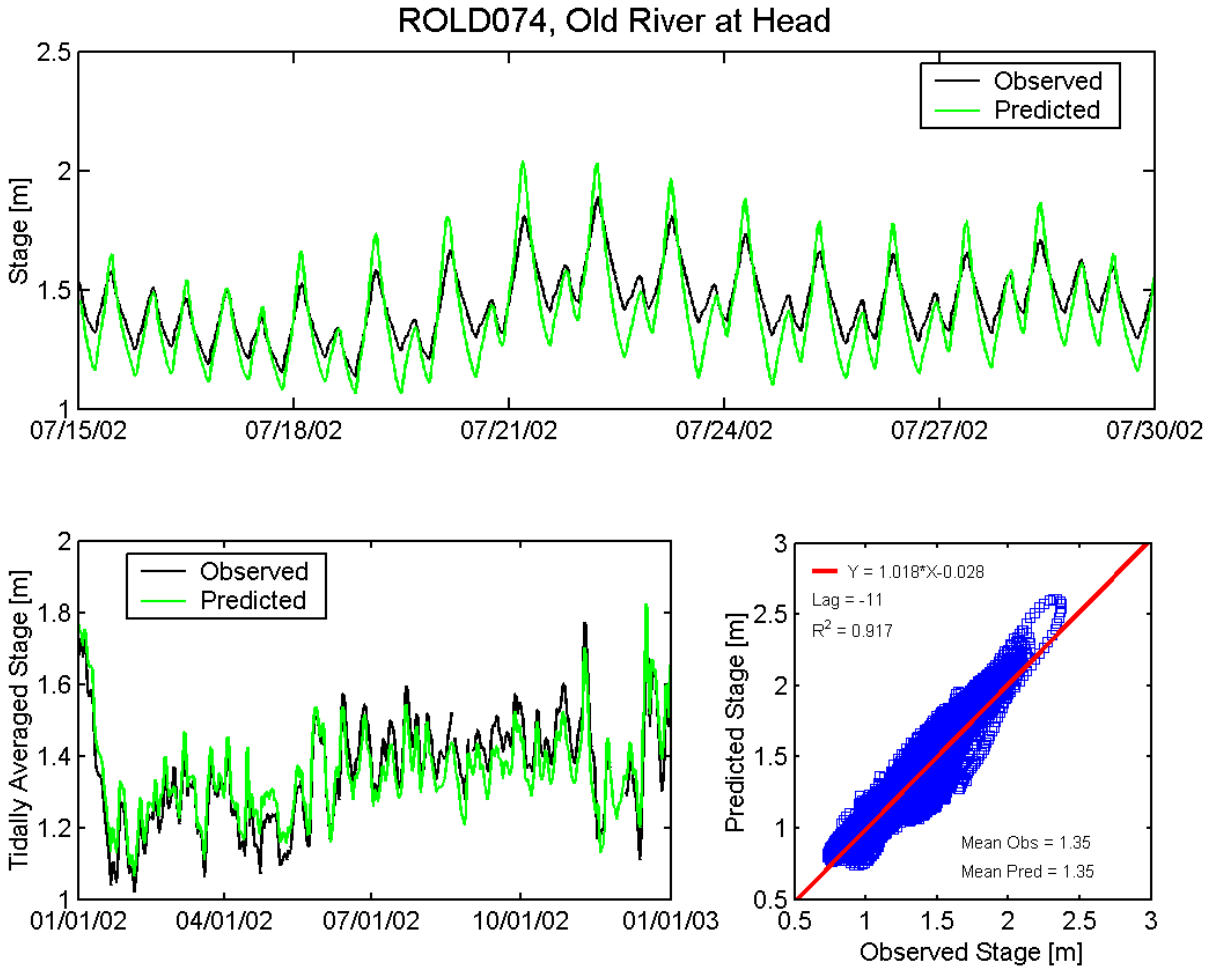

Figure A.3-58 Observed and predicted stage at Old River at Head DWR station (ROLD074) during the 2002 simulation period.

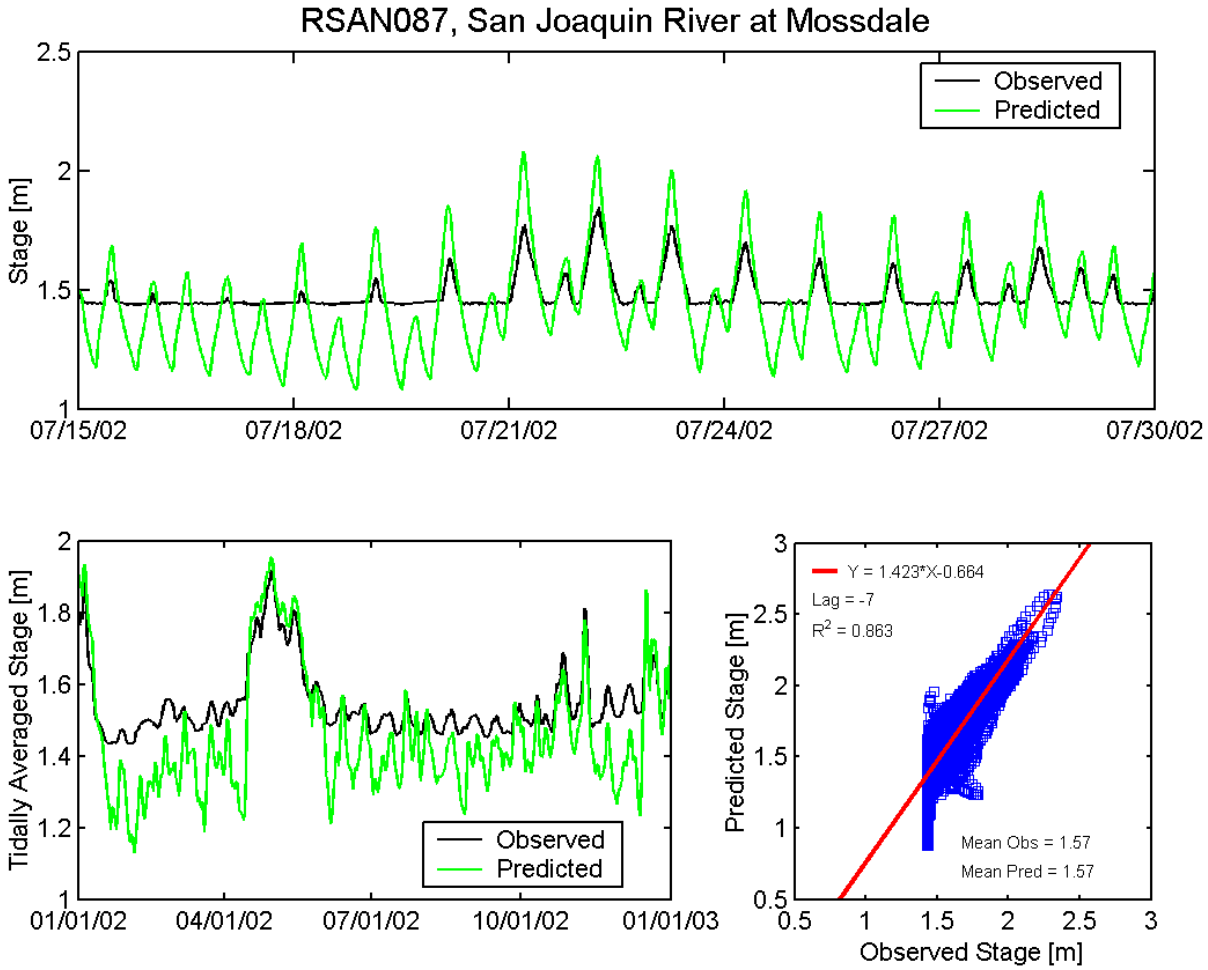

Figure A.3-59 Observed and predicted stage at San Joaquin River at Mossdale DWR station (RSAN087) during the 2002 simulation period.

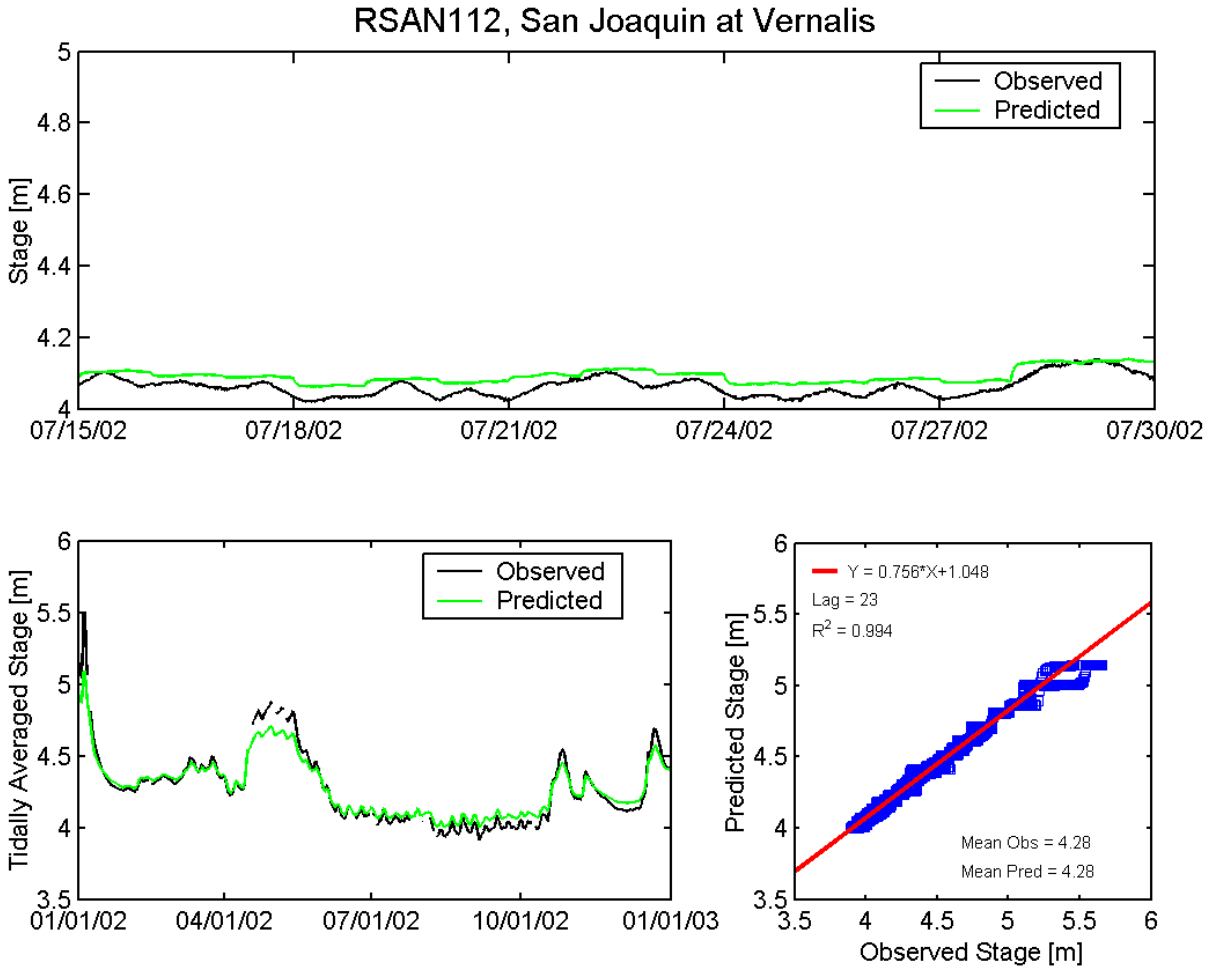

Figure A.3-60 Observed and predicted stage at San Joaquin River at Vernalis DWR station (RSAN112) during the 2002 simulation period.

A.4 Delta Flow Comparison Figures

During the 2002 simulation period, flow measurements are available at a total of twenty-five flow monitoring stations in the Sacramento-San Joaquin Delta. For each station, the mean observed and predicted net flow was calculated over the full simulation period, and the same cross-correlation procedure used in the water level analysis was applied to flow. Table A-2 gives the predicted and observed mean flow at each station as well as the corresponding amplitude ratio, phase lag, and R^2 for each station.

A.4.1 Northern Sacramento-San Joaquin Delta

Flow comparisons were made at six continuous flow monitoring stations in the northern portion of the Sacramento-San Joaquin Delta, at the locations shown in Figure A.4-1. Flow comparisons at these stations are shown in Figures A.4-2 through A.4-7.

A.4.2 Central Sacramento-San Joaquin Delta

Flow comparisons were made at twelve continuous flow monitoring stations in the central portion of the Sacramento-San Joaquin Delta, at the locations shown in Figure A.4-8. Flow comparisons at these stations are shown in Figures A.4-9 through A.4-20.

A.4.3 Southern Sacramento-San Joaquin Delta

Flow comparisons were made at seven continuous flow monitoring stations in the southern portion of the Sacramento-San Joaquin Delta, at the locations shown in Figure A.4-21. Flow comparisons at these stations are shown in Figures A.4-22 through A.4-28.

Table A-2 Predicted and observed stage and cross-correlation statistics for flow monitoring stations in the Sacramento-San Joaquin Delta during the 2002 simulation period.

Location	Data Source	Figure Number	Mean Flow		Cross Correlation		R^2
			Observed (m^3/s)	Predicted (m^3/s)	Amp Ratio	Lag (min)	
2002 North Delta Flow Stations (Figure A.4-1)							
Sacramento River South of Georgiana Slough	USGS	A.4-2	168	157	1.033	-11	0.992
Georgiana Slough near Sacramento River	USGS	A.4-3	98.3	102	0.974	33	0.989
Delta Cross Channel	USGS	A.4-4	87.9	84.1	0.936	-8	0.962
Sacramento River North of Delta Cross Channel	USGS	A.4-5	319	316	1.018	0	0.992
Sacramento River at Freeport	USGS	A.4-6	518	517	1.017	-15	0.992
Steamboat Slough between	USGS	A.4-7	61.2	61.9	1.290	2	0.983

Sacramento River and Sutter Sl.							
2002 Central Delta Flow Stations (Figure A.4-8)							
Sacramento River at Rio Vista	USGS	A.4-9	414	372	1.019	-2	0.995
Threemile Slough at San Joaquin River	USGS	A.4-10	-21.6	-76.0	1.031	7	0.994
San Joaquin River at Jersey Point	USGS	A.4-11	67.7	76.9	0.945	1	0.994
Dutch Slough at Jersey Island	USGS	A.4-12	0.26	-11.6	0.849	-1	0.993
False River	USGS	A.4-13	-4.64	-36.6	0.925	-37	0.982
Taylor Slough	USGS	A.4-14	-0.28	-7.21	0.672	-34	0.739
Fisherman's Cut	USGS	A.4-15	-21.2	-18.4	0.842	n/a*	0.439
Old River at San Joaquin River	USGS	A.4-16	-33.2	-2.96	0.965	-68	0.966
Mokelumne River near San Joaquin River	USGS	A.4-17	82.9	108	1.021	-35	0.973
Old River at Mandeville Island	USGS	A.4-18	-46.9	-34.6	0.820	-43	0.980
Holland Cut	USGS	A.4-19	-40.7	-40.9	0.901	-35	0.975
Middle River south of Columbia Cut	USGS	A.4-20	-117	-70.5	1.138	-58	0.978
2002 South Delta Flow Stations (Figure A.4-21)							
Middle River at Middle River	USGS	A.4-22	-93.8	-88.3	0.728	-2	0.974
Old River at Bacon Island	USGS	A.4-23	-81.5	-67.0	0.734	-1	0.984
Old River near Byron	USGS	A.4-24	-114	-122	0.960	-4	0.963
Old River near Delta Mendota Canal (SE of Barrier)	USGS	A.4-25	12.9	6.13	0.832	-14	0.938
Grant Line Canal at Tracy Blvd	USGS	A.4-26	39.6	41.6	0.801	-20	0.933
San Joaquin River at Stockton	USGS	A.4-27	21.5	14.8	1.089	-2	0.974
Old River at Head	DWR	A.4-28	15.6	33.1	1.119	-4	0.842

* n/a indicates that the cross-correlation procedure did not identify a local maximum correlation coefficient within the four hour analysis window. This can be indicative of the data not having a strong tidal time-scale signal.

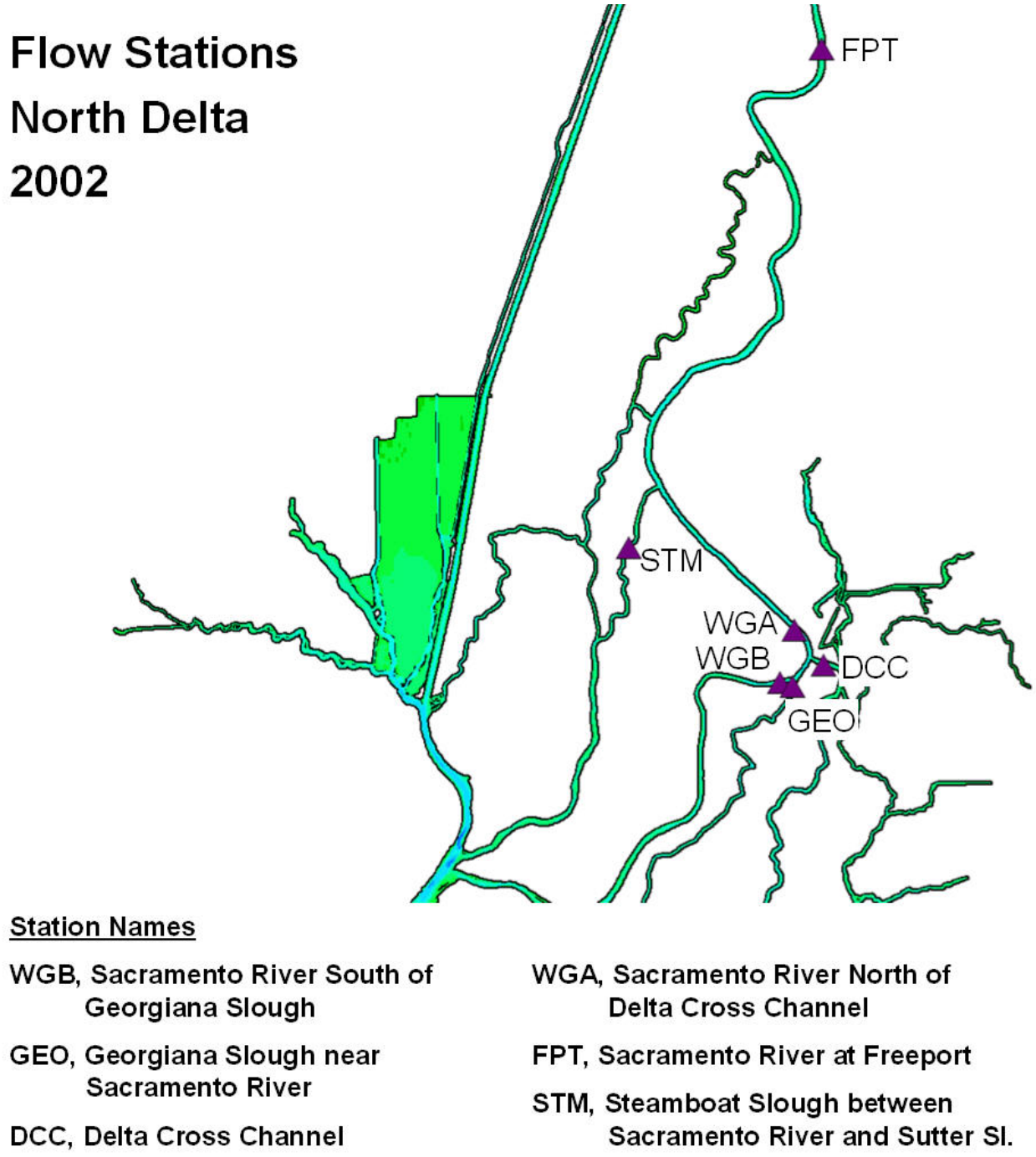

Figure A.4-1 Location of flow monitoring stations in the northern portion of the Sacramento-San Joaquin Delta used for 2002 flow comparisons.

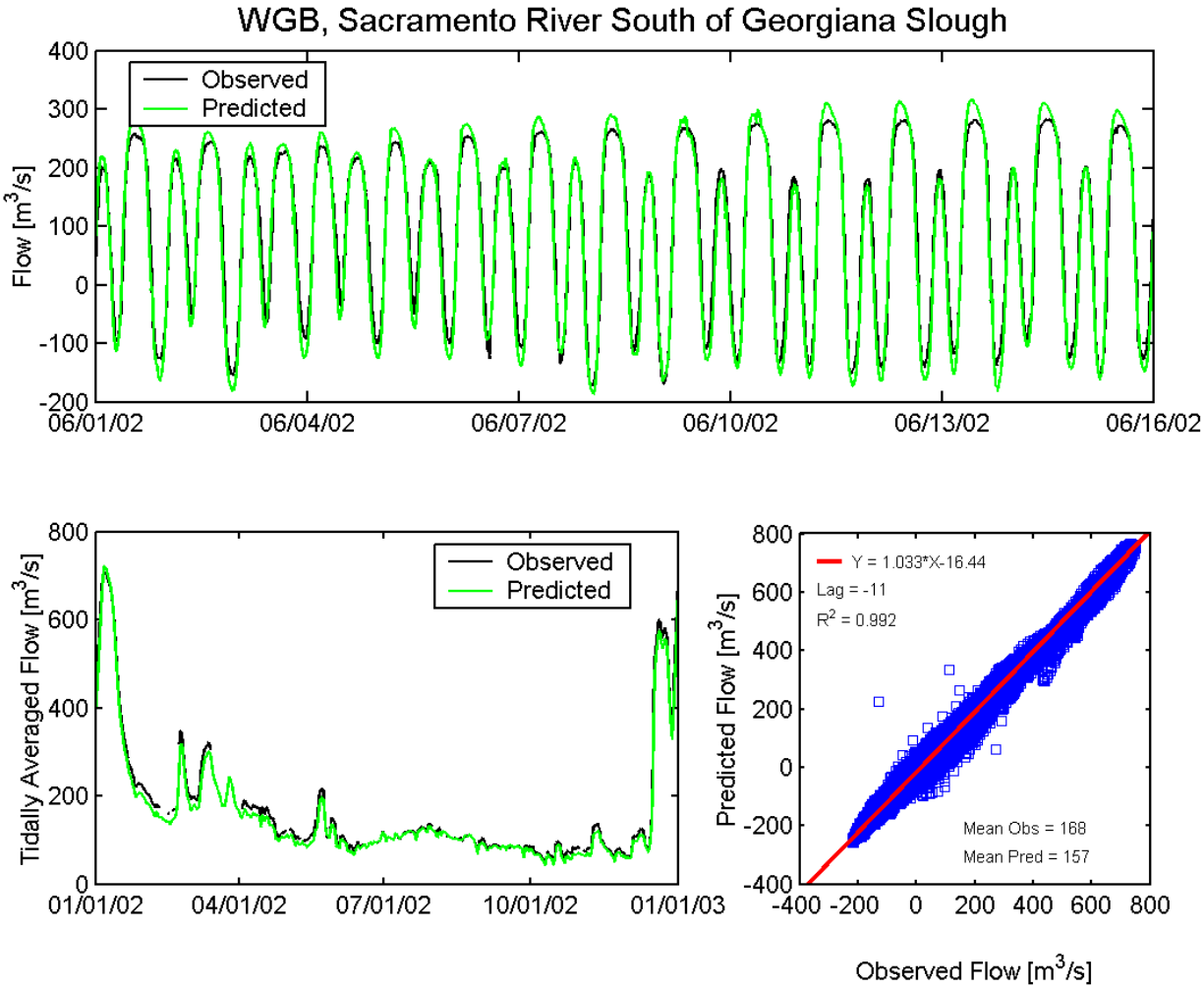

Figure A.4-2 Observed and predicted flow at Sacramento River South of Georgiana Slough USGS station (WGB) during the 2002 simulation period.

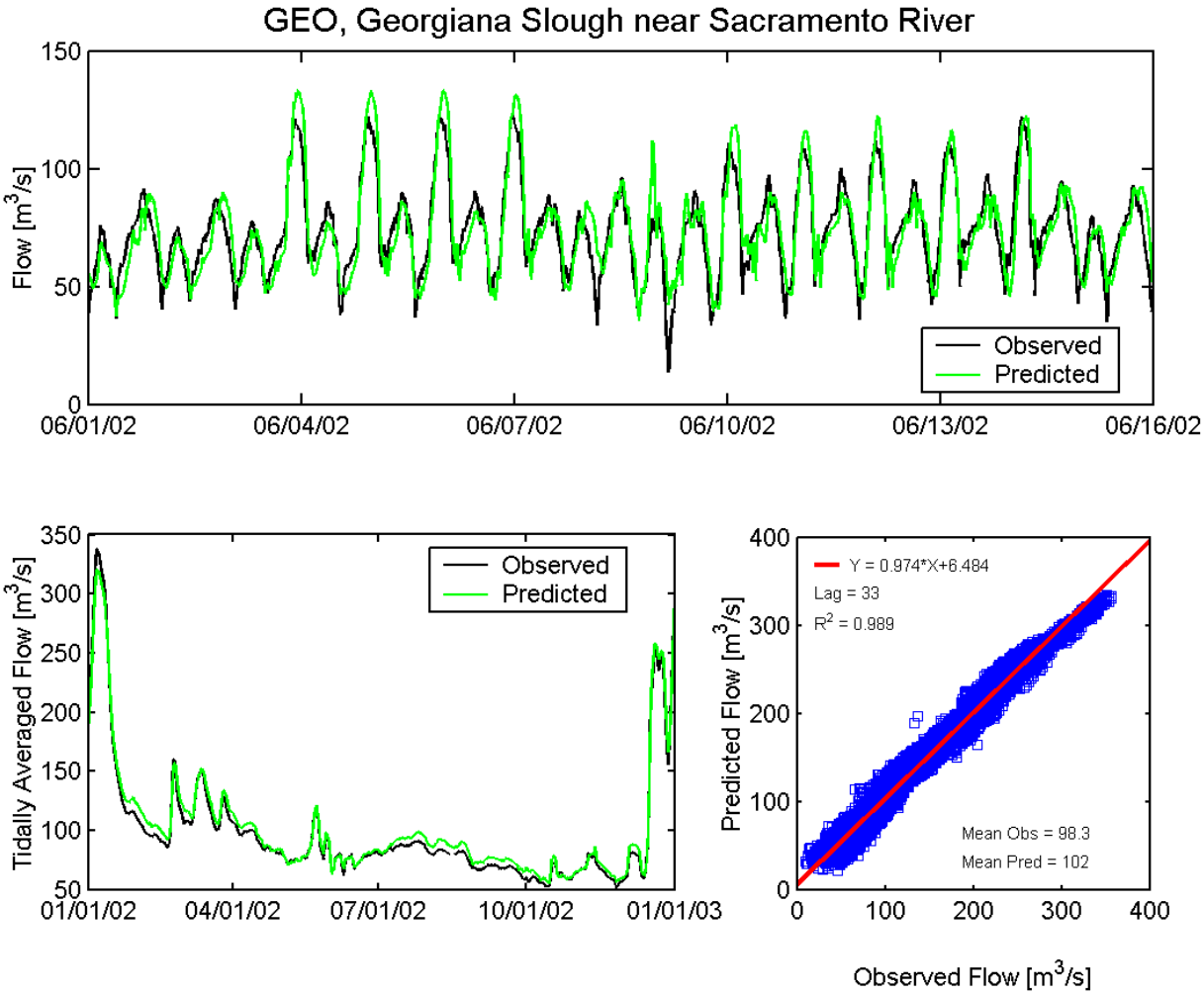

Figure A.4-3 Observed and predicted flow at Georgiana Slough near Sacramento River USGS station (GEO) during the 2002 simulation period.

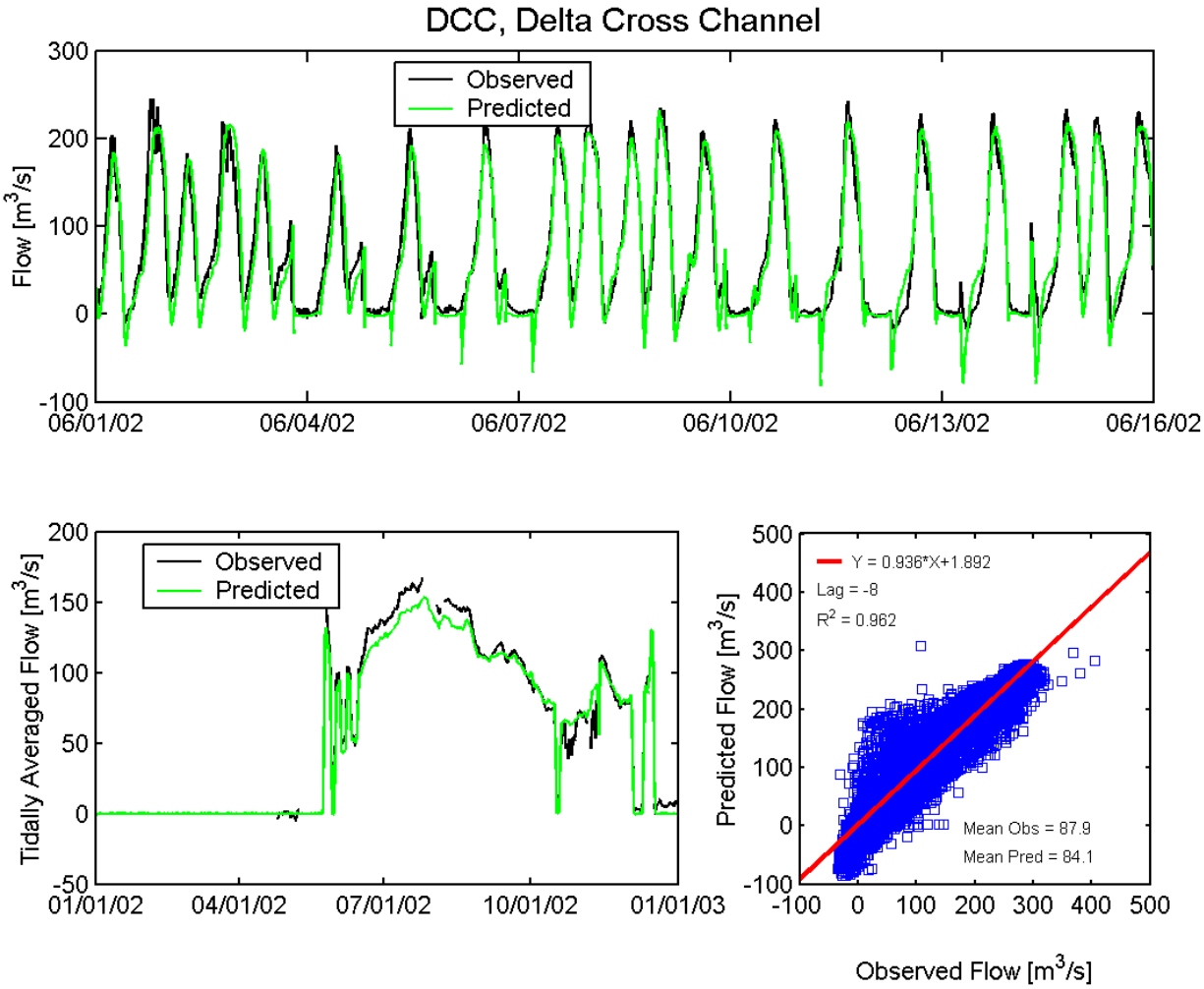

Figure A.4-4 Observed and predicted flow at Delta Cross Channel USGS station (DCC) during the 2002 simulation period.

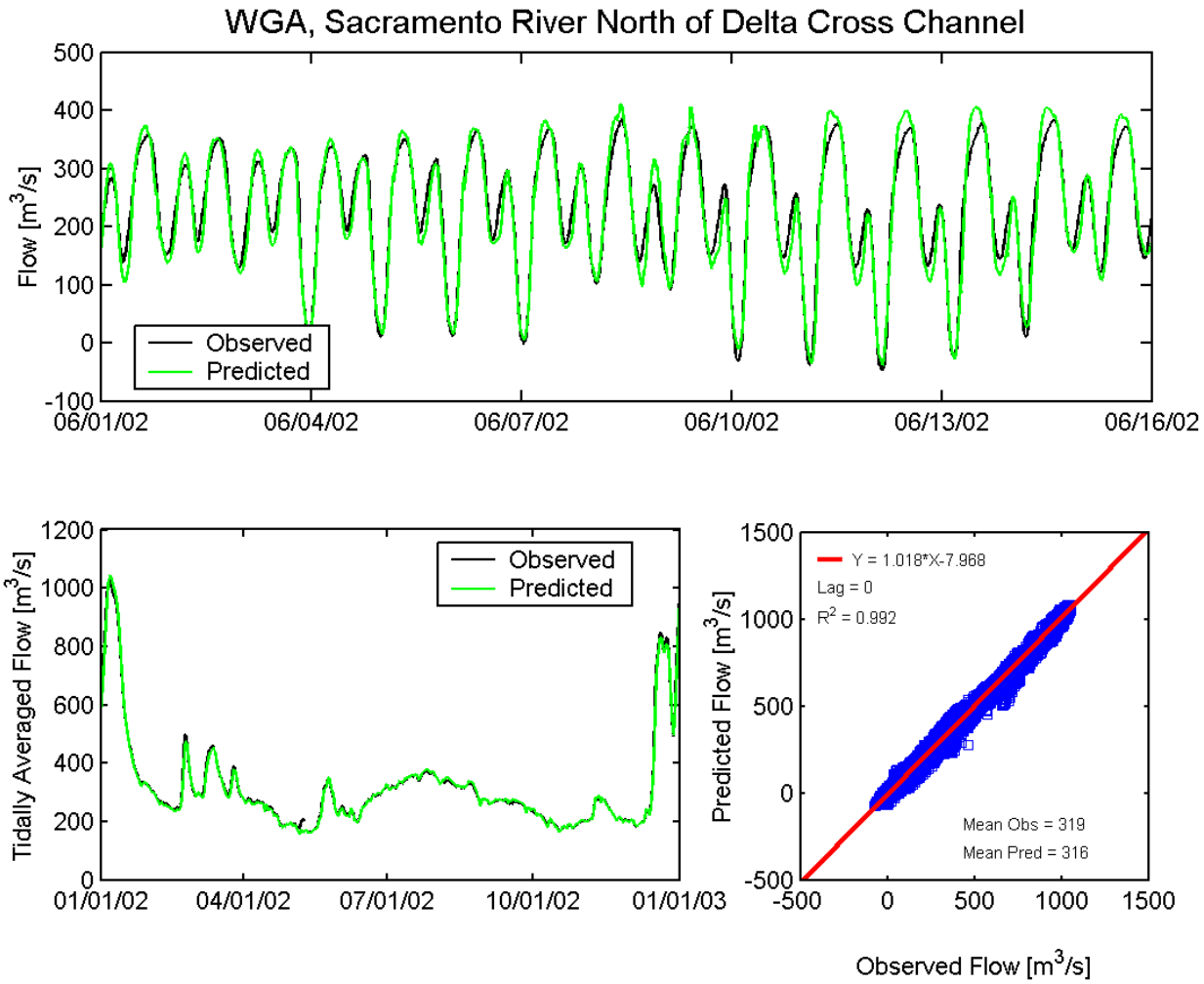

Figure A.4-5 Observed and predicted flow at Sacramento River North of Delta Cross Channel USGS station (WGA) during the 2002 simulation period.

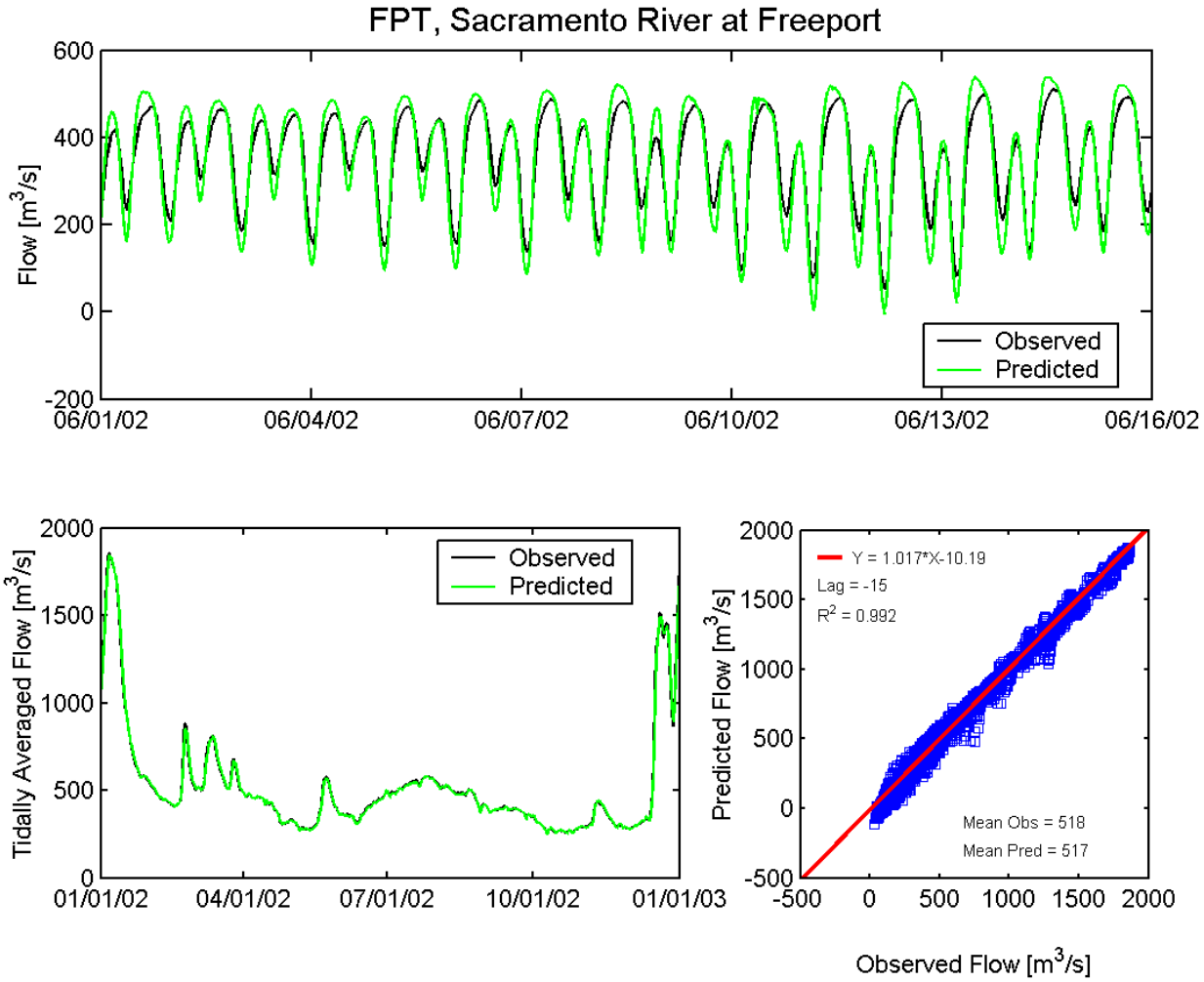

Figure A.4-6 Observed and predicted flow at Sacramento River at Freeport USGS station (FPT) during the 2002 simulation period.

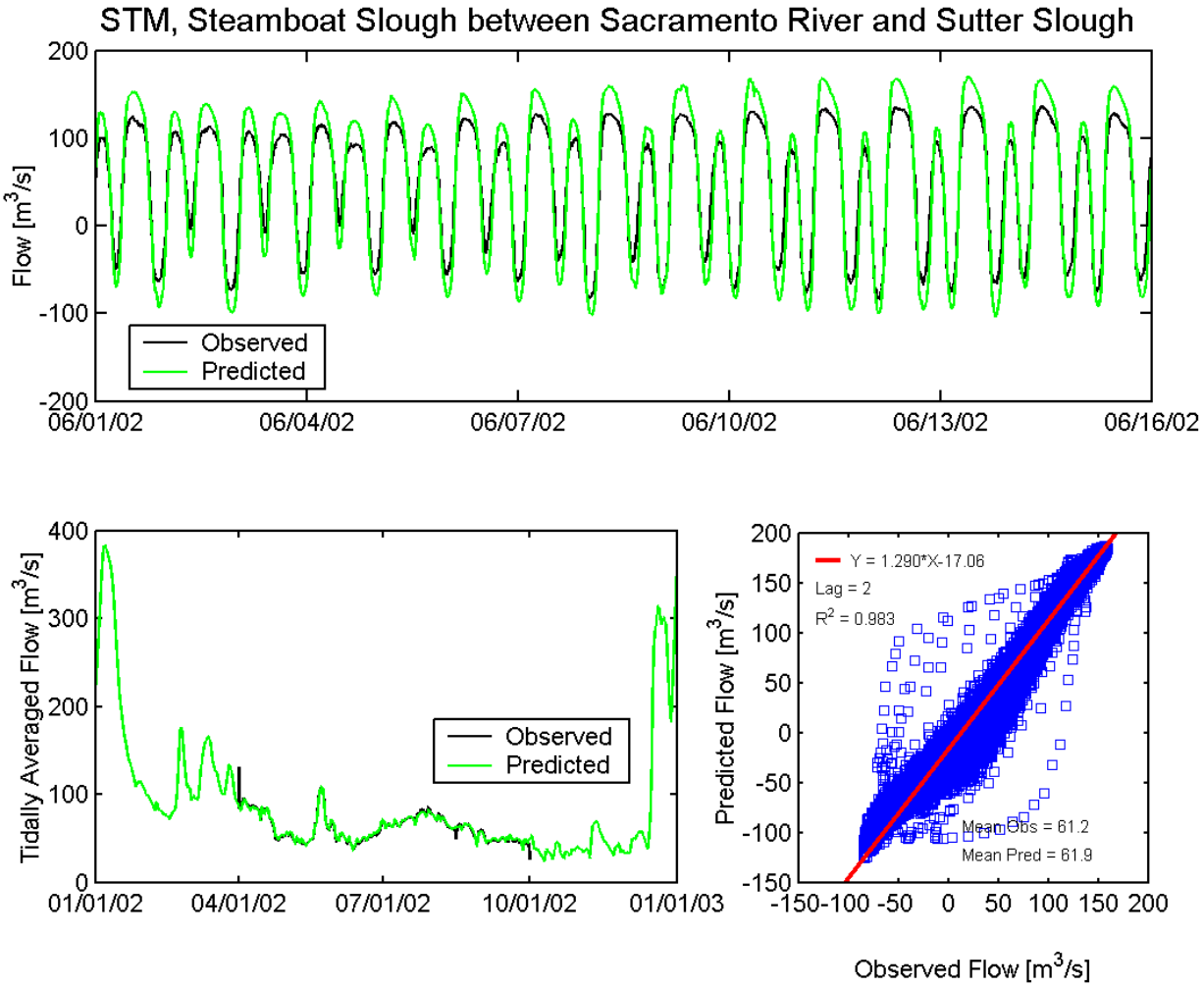

Figure A.4-7 Observed and predicted flow at Steamboat Slough between Sacramento River and Sutter Slough USGS station (STM) during the 2002 simulation period.

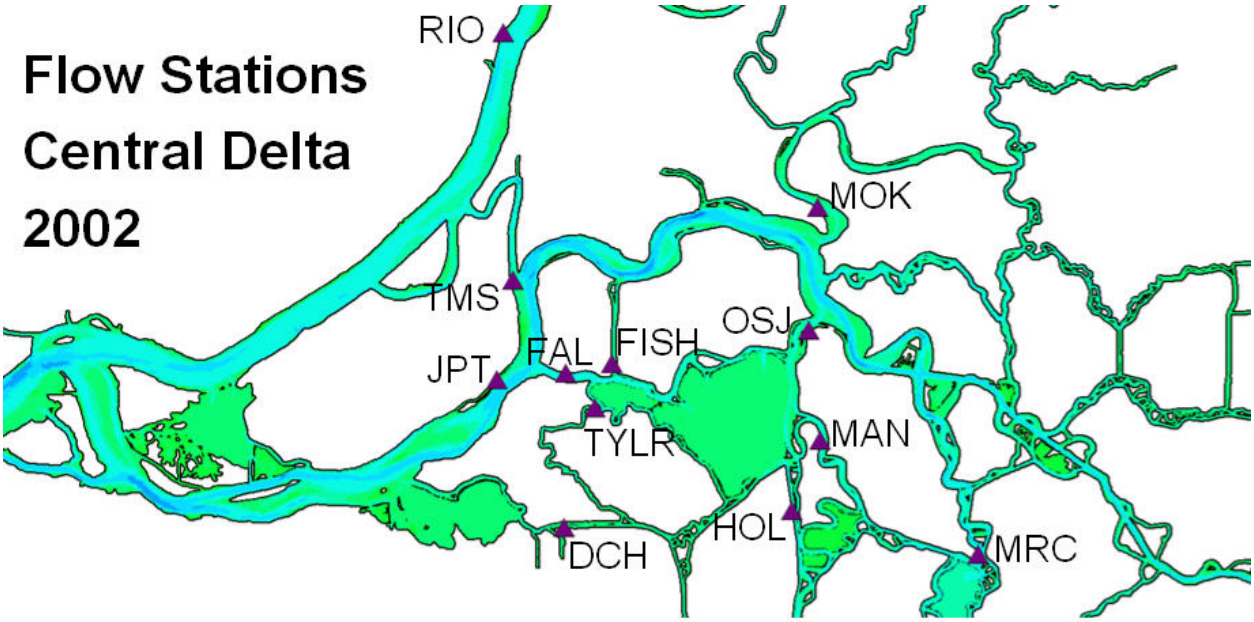

Station Names

RIO, Sacramento River at Rio Vista

TMS, Threemile Slough at San Joaquin River

JPT, San Joaquin River at Jersey Point

DCH, Dutch Slough at Jersey Island

FAL, False River

TYLR, Taylor Slough

FISH, Fisherman's Cut

OSJ, Old River at San Joaquin River

MOK, Mokelumne River near San Joaquin River

MAN, Old River at Mandeville Island

HOL, Holland Cut

MRC, Middle River South of Columbia Cut

Figure A.4-8 Location of flow monitoring stations in the central portion of the Sacramento-San Joaquin Delta used for 2002 flow comparisons.

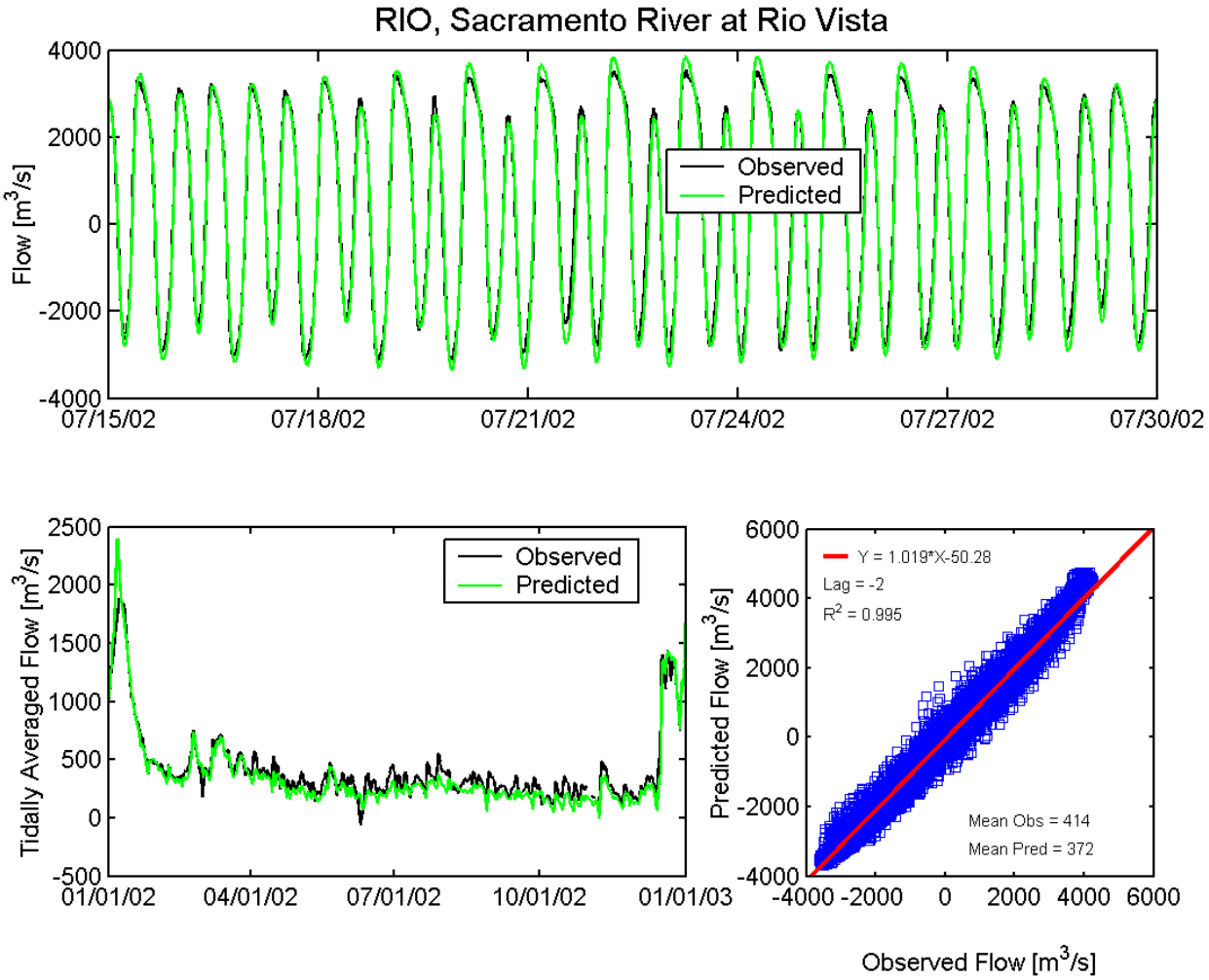

Figure A.4-9 Observed and predicted flow at Sacramento River at Rio Vista USGS station (RIO) during the 2002 simulation period.

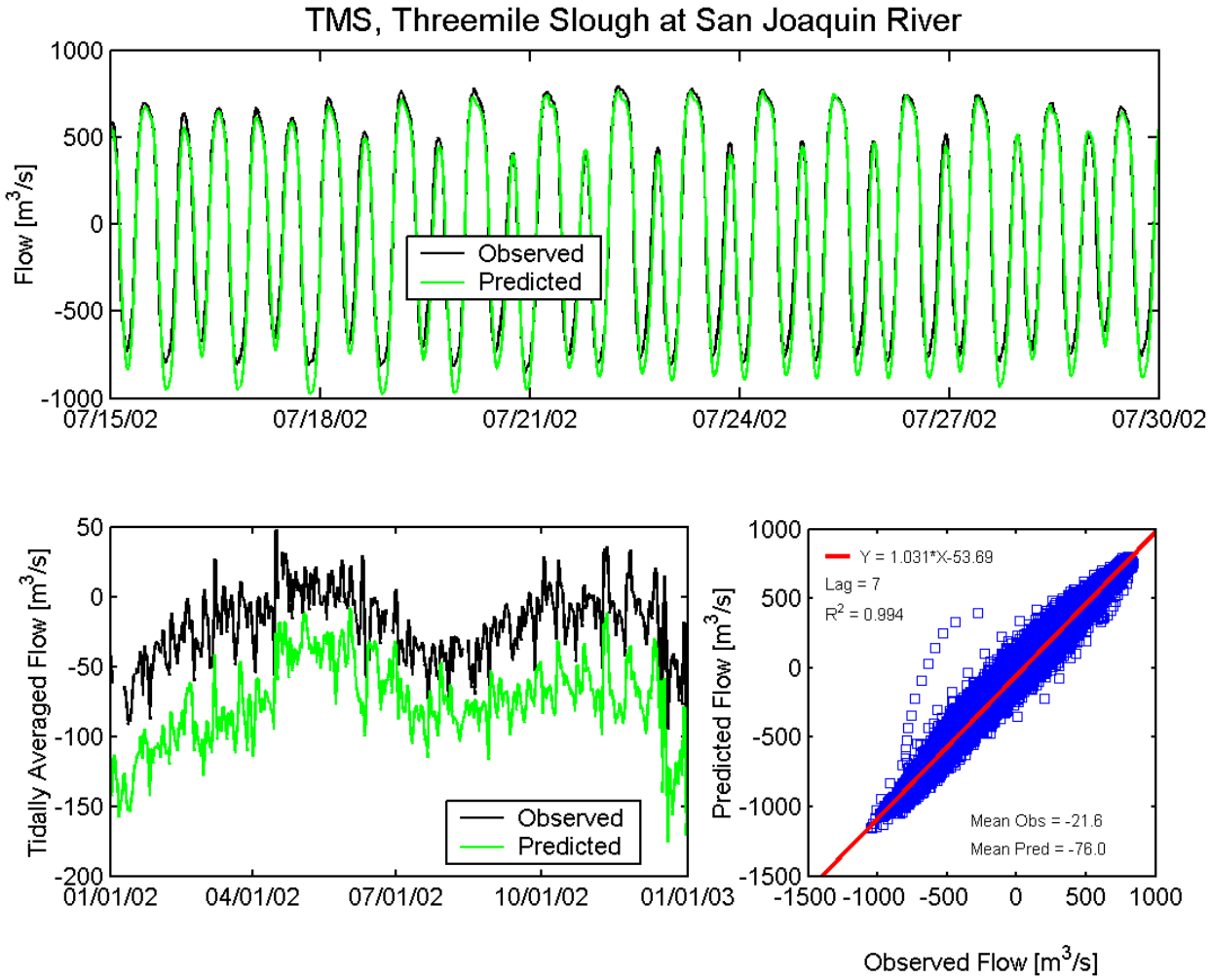

Figure A.4-10 Observed and predicted flow at Threemile Slough at San Joaquin River USGS station (TMS) during the 2002 simulation period.

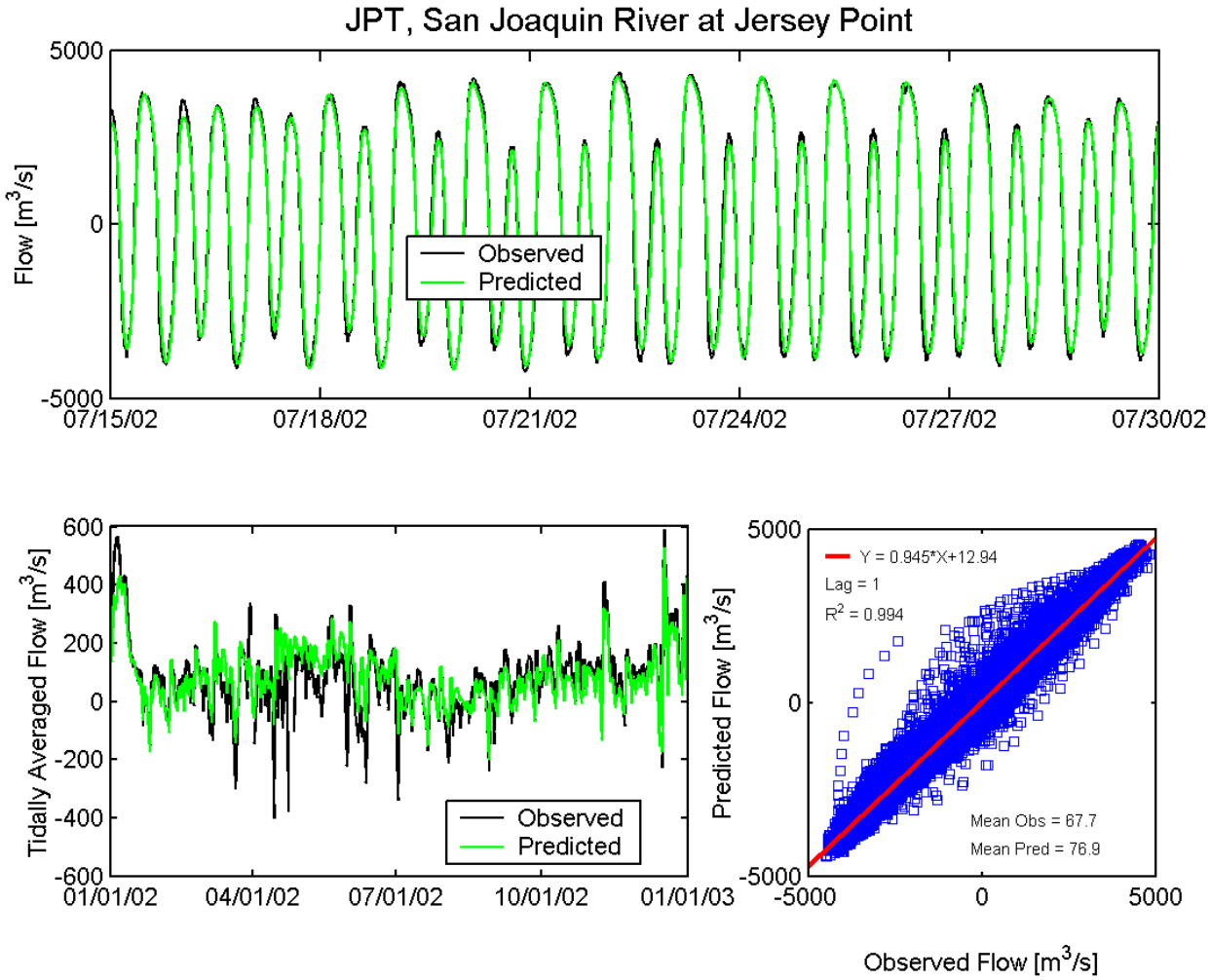

Figure A.4-11 Observed and predicted flow at San Joaquin River at Jersey Point USGS station (JPT) during the 2002 simulation period.

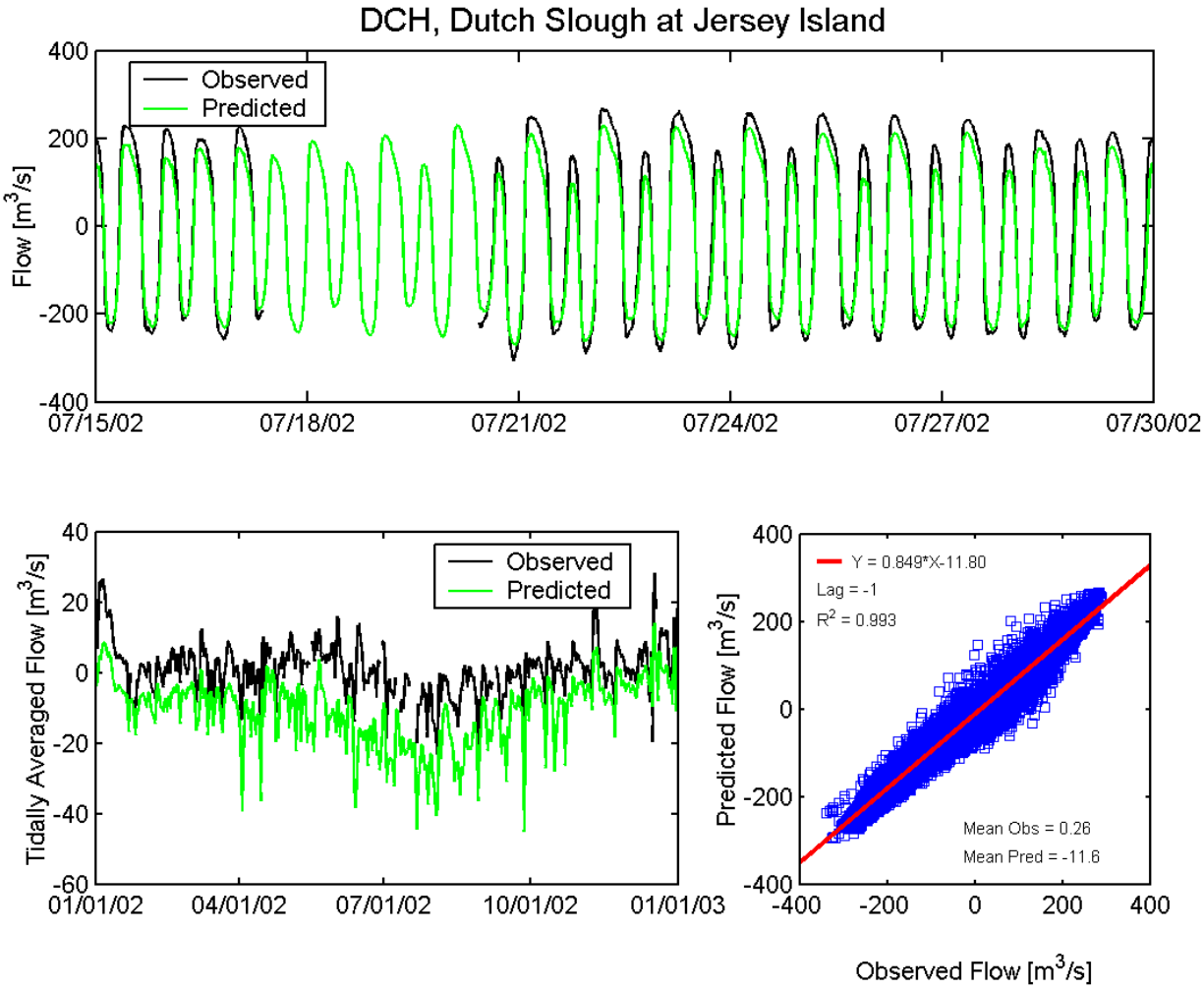

Figure A.4-12 Observed and predicted flow at Dutch Slough at Jersey Island USGS station (DCH) during the 2002 simulation period.

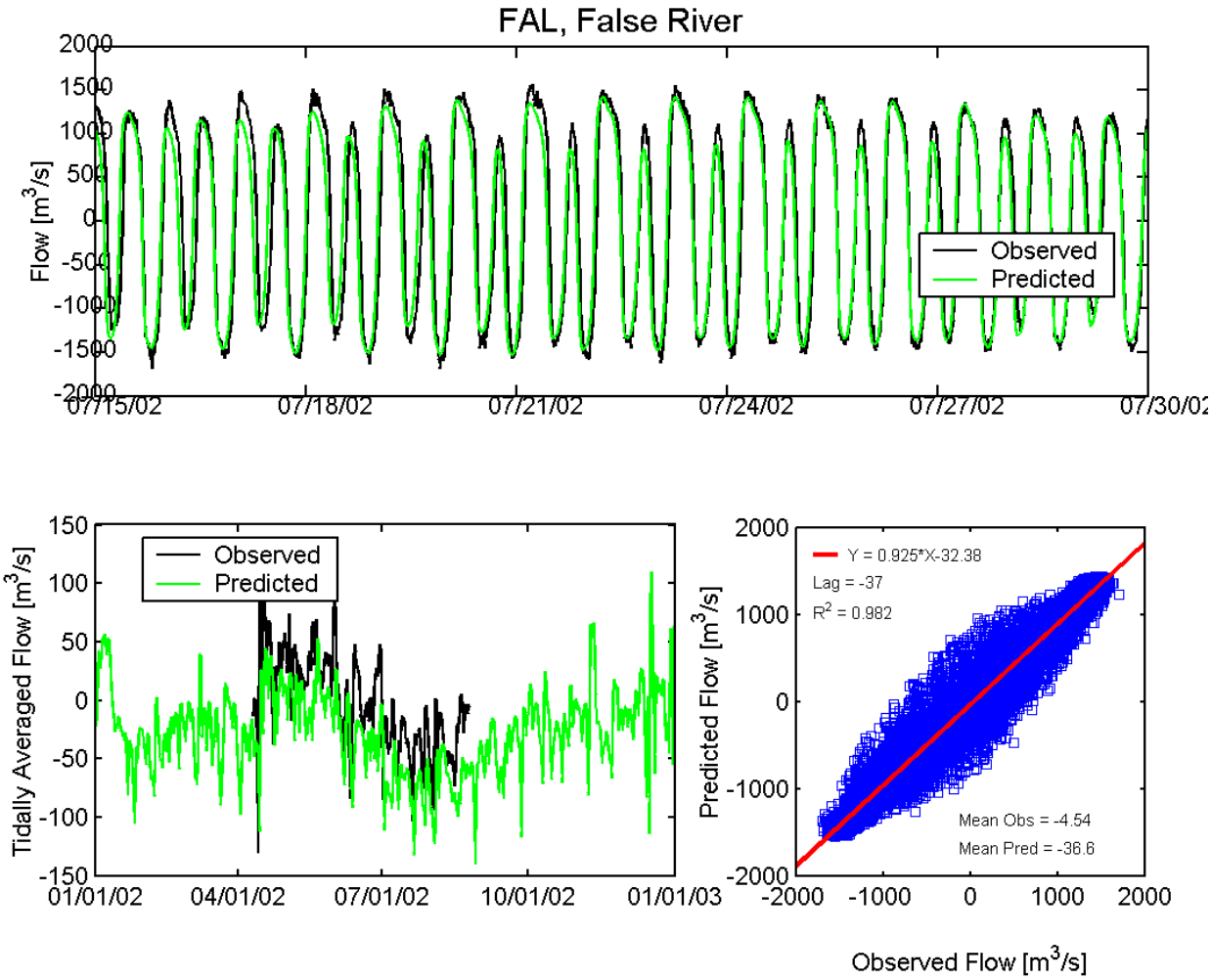

Figure A.4-13 Observed and predicted flow at False River USGS station (FAL) during the 2002 simulation period.

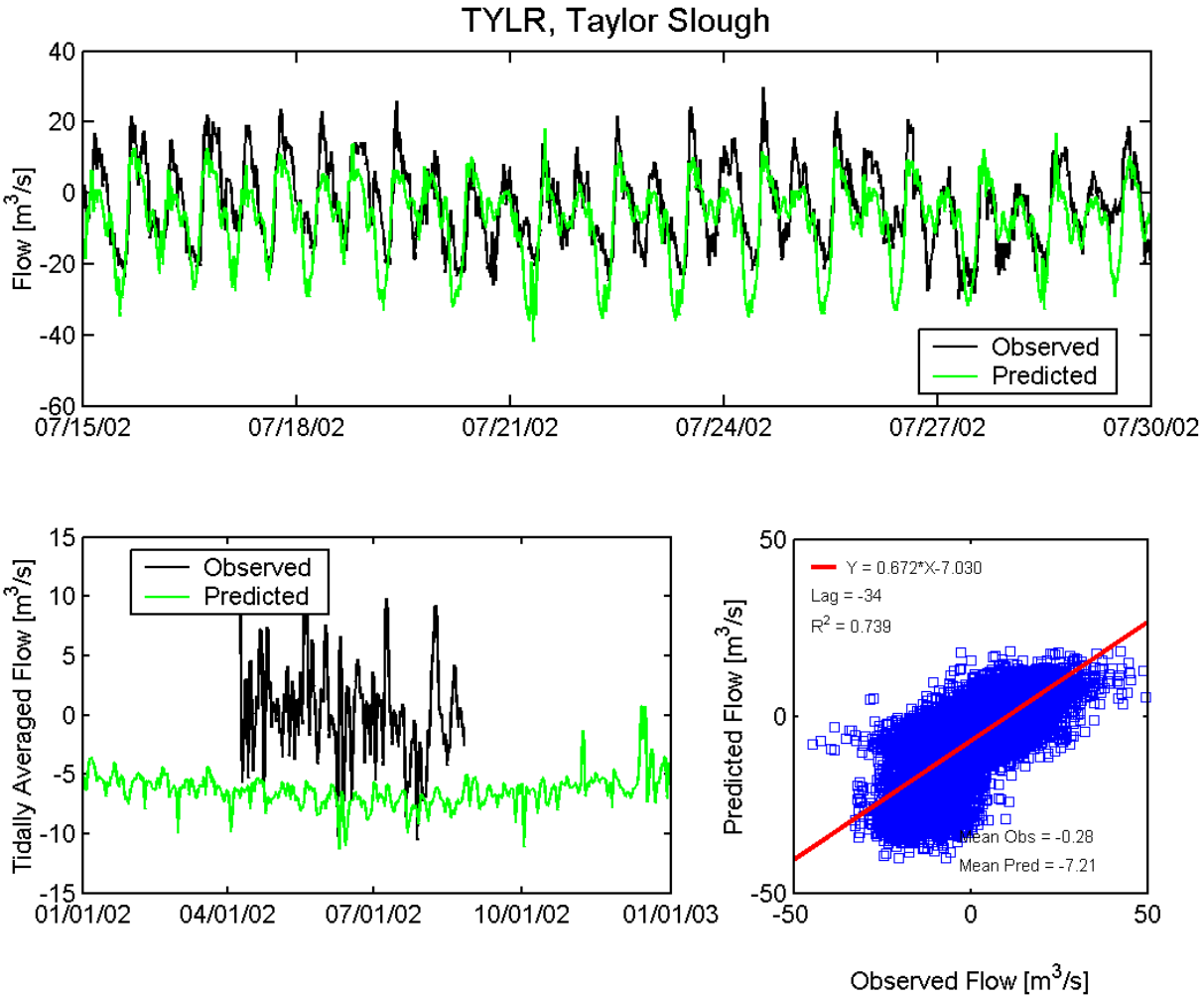

Figure A.4-14 Observed and predicted flow at Taylor Slough USGS station (TYLR) during the 2002 simulation period.

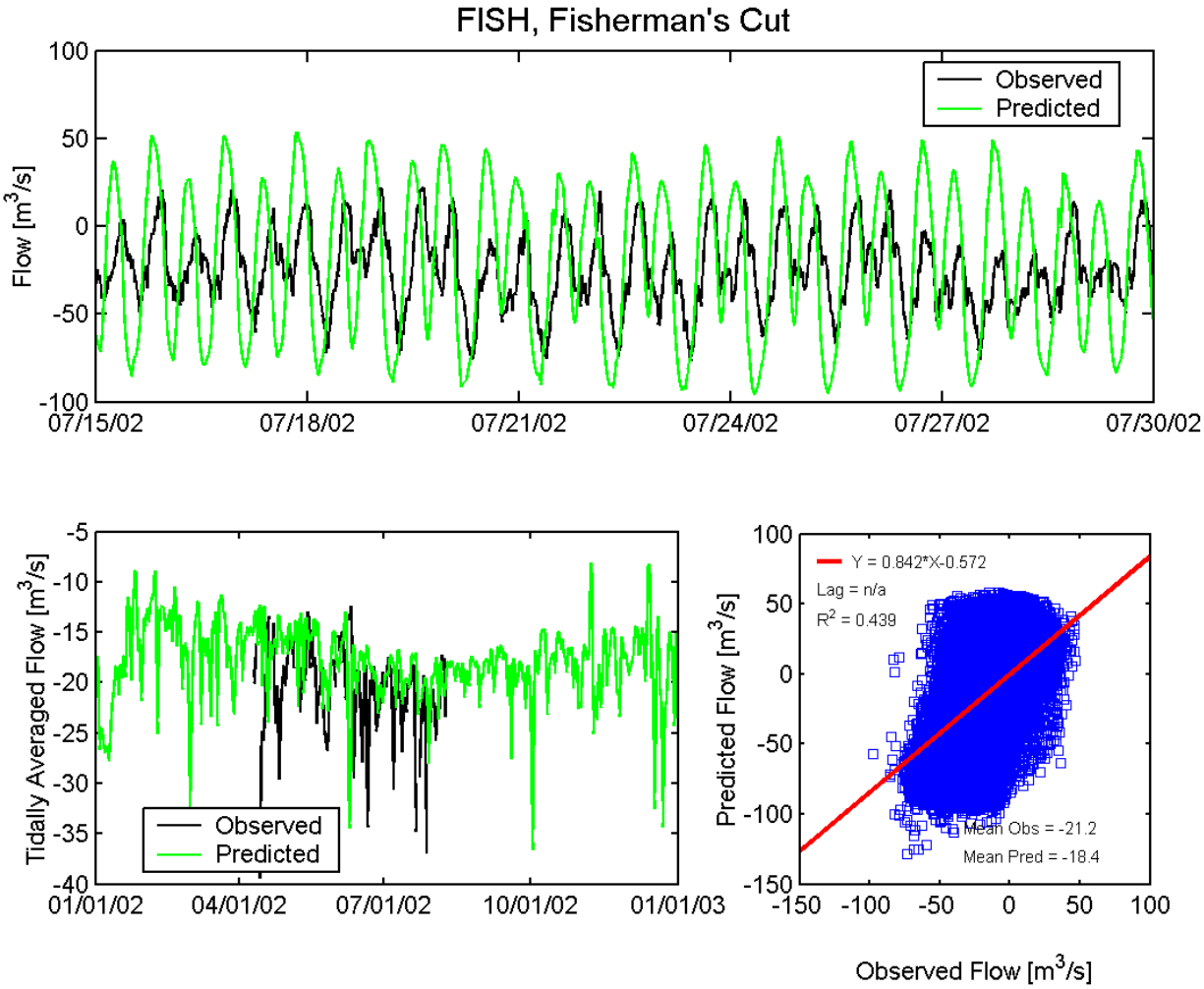

Figure A.4-15 Observed and predicted flow at Fisherman's Cut USGS station (FISH) during the 2002 simulation period.

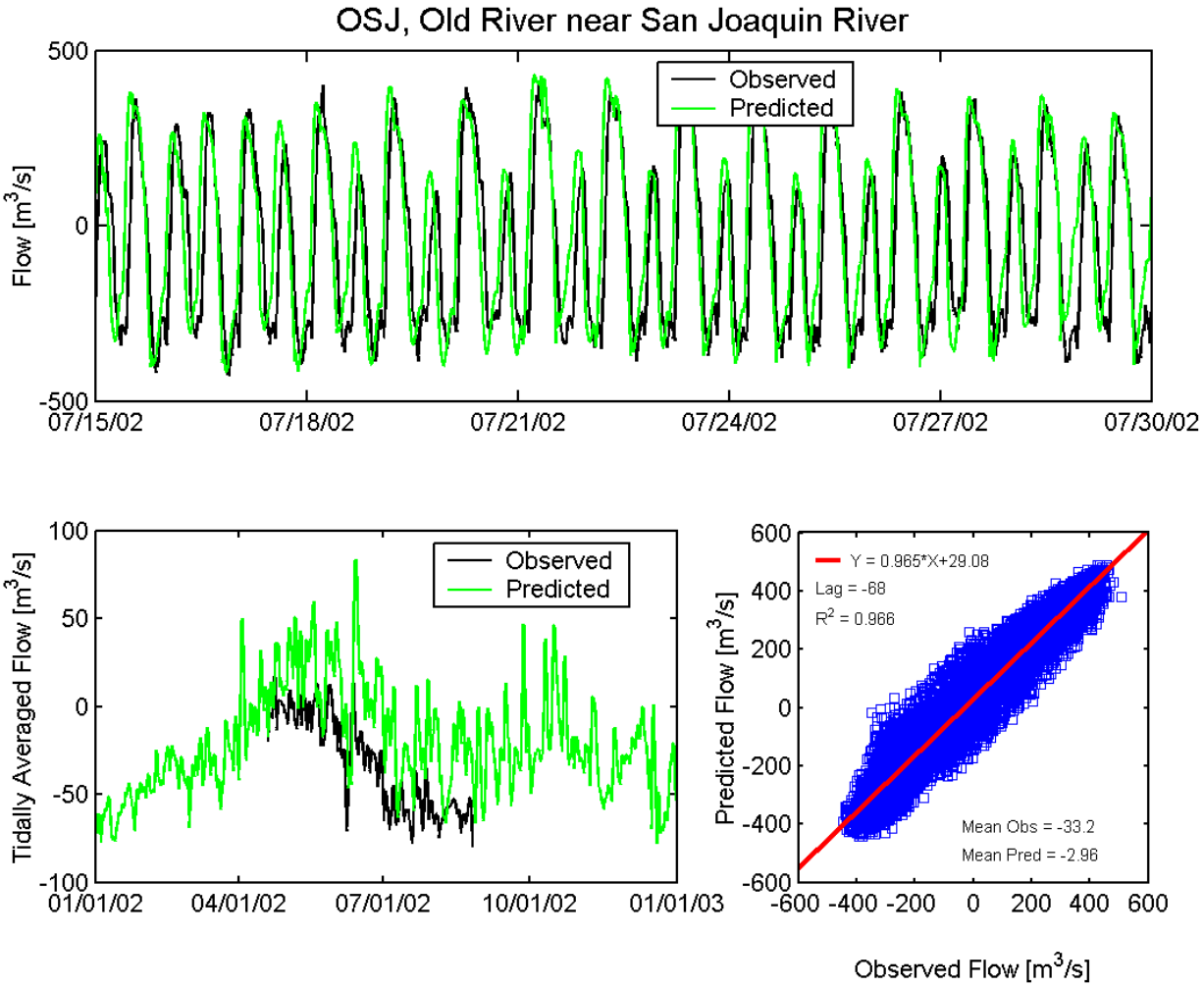

Figure A.4-16 Observed and predicted flow at Old River near San Joaquin River USGS station (OSJ) during the 2002 simulation period.

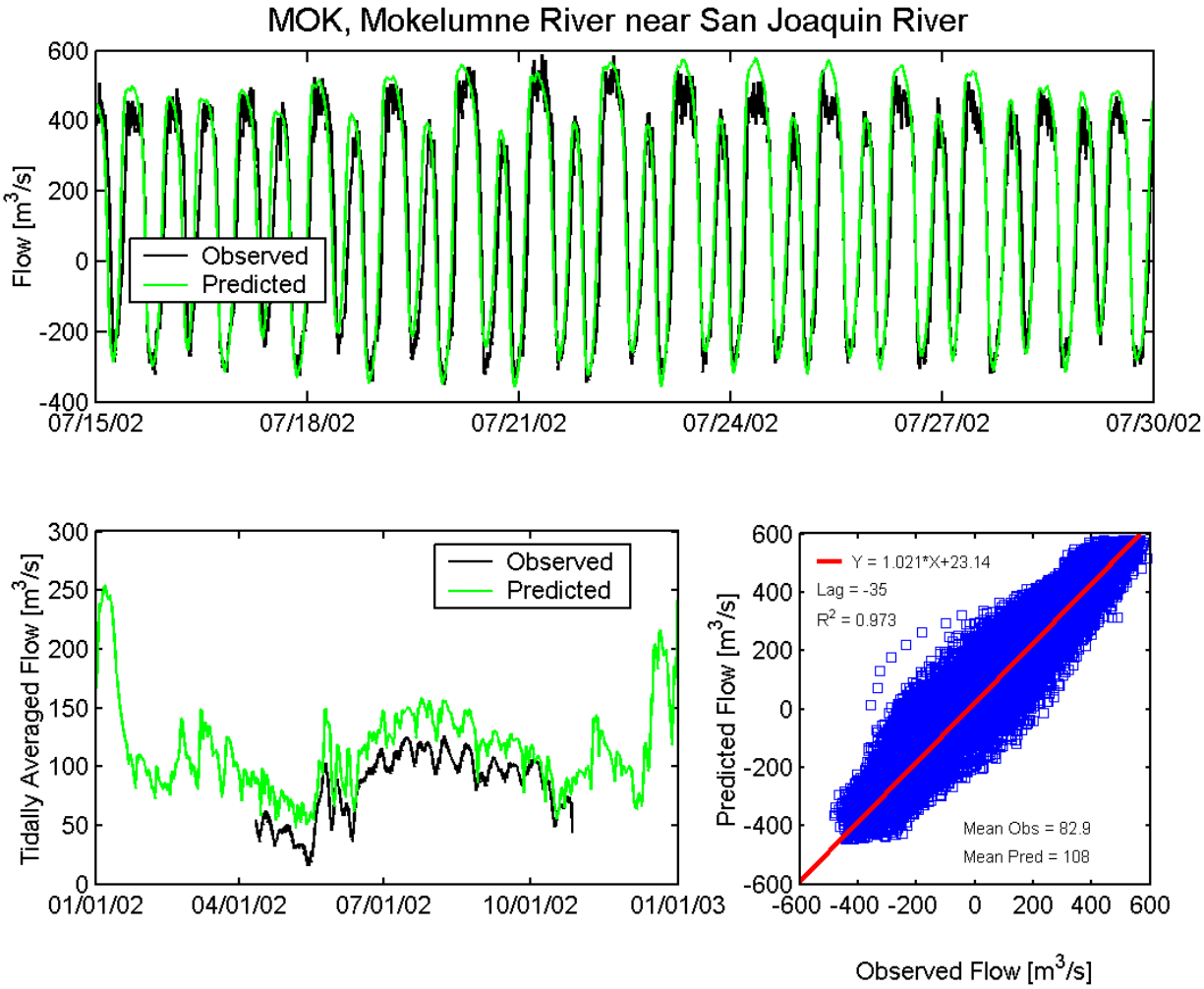

Figure A.4-17 Observed and predicted flow at Mokelumne River near San Joaquin River USGS station (MOK) during the 2002 simulation period.

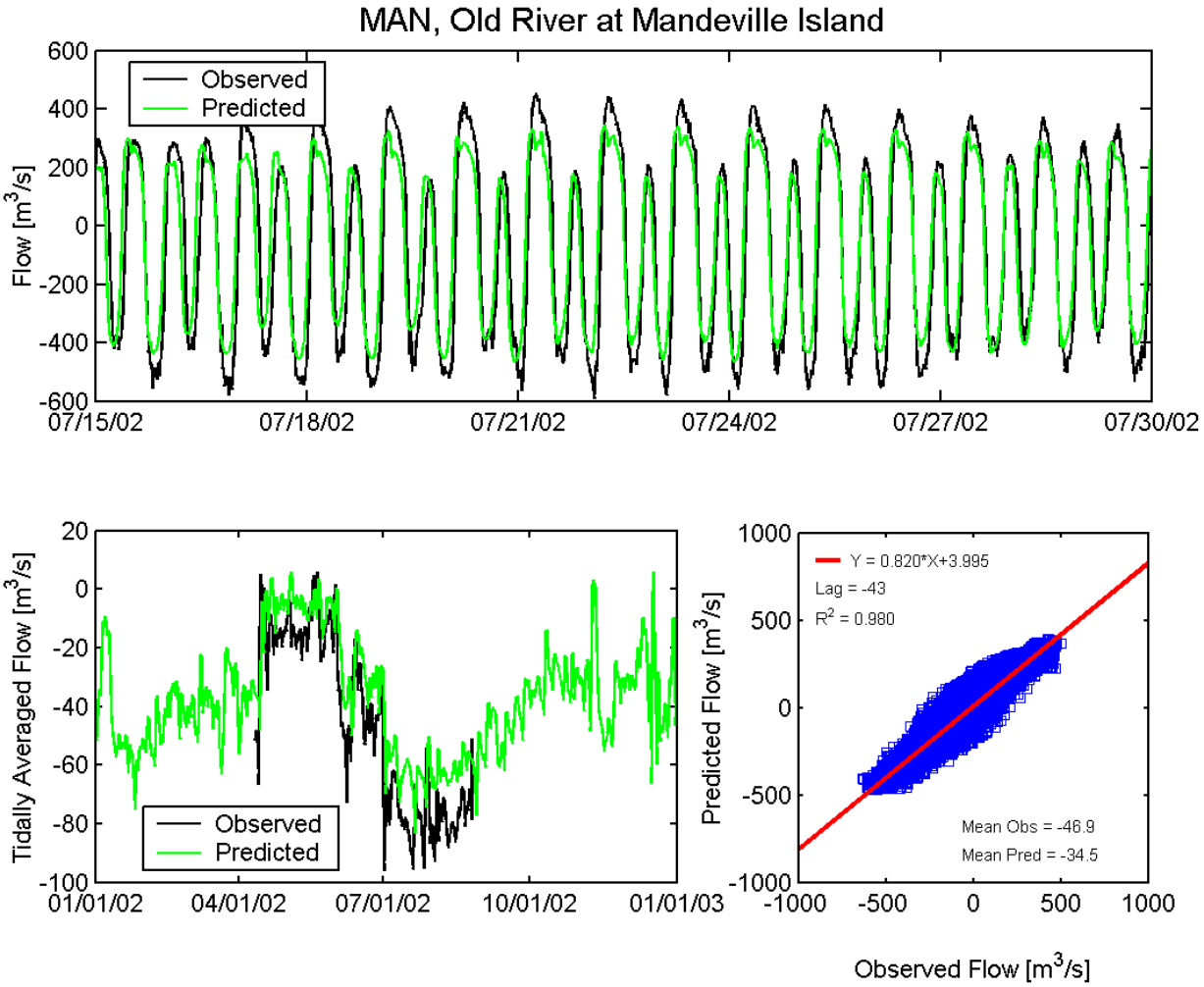

Figure A.4-18 Observed and predicted flow at Old River at Mandeville Island USGS station (MAN) during the 2002 simulation period.

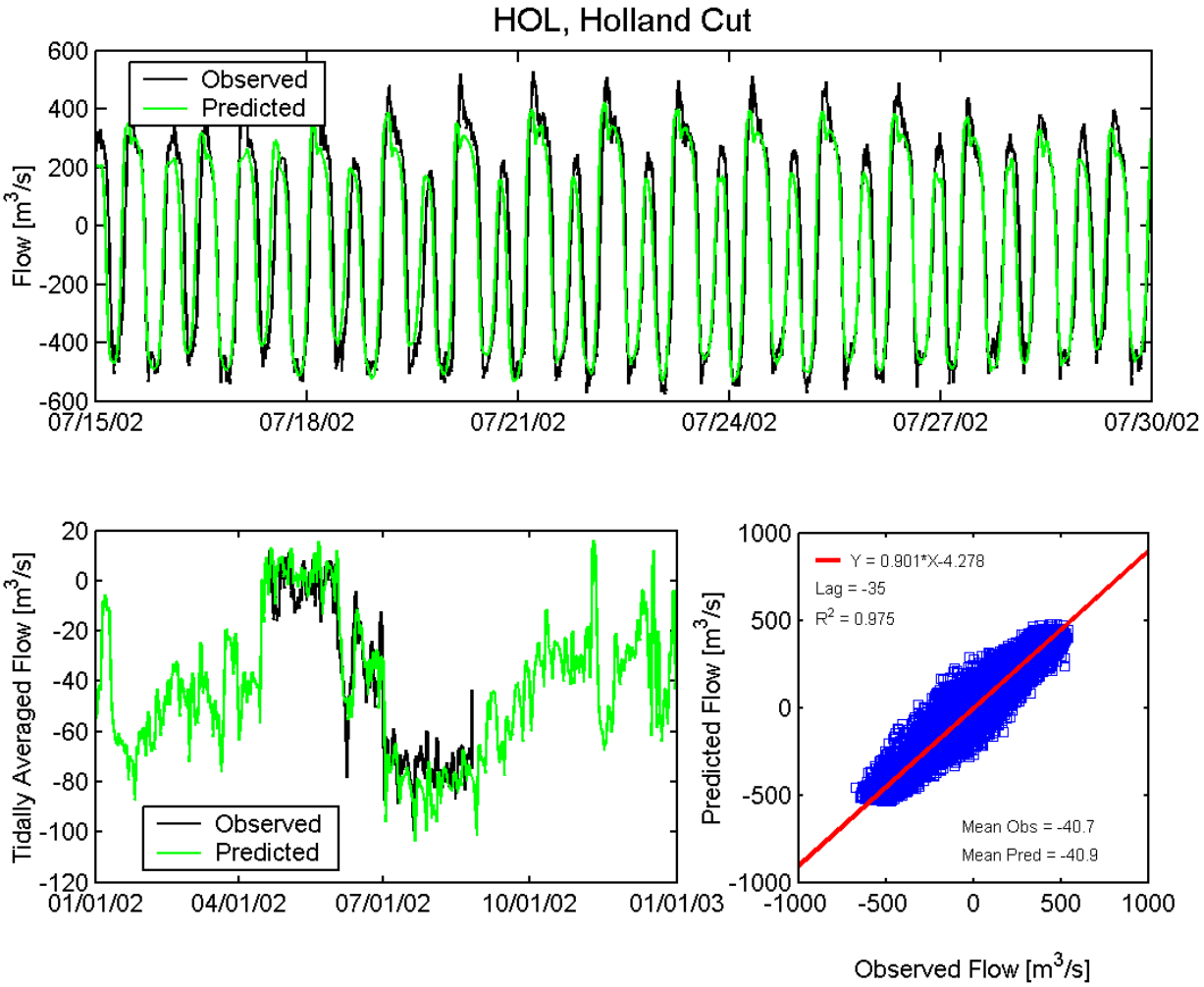

Figure A.4-19 Observed and predicted flow at Holland Cut USGS station (HOL) during the 2002 simulation period.

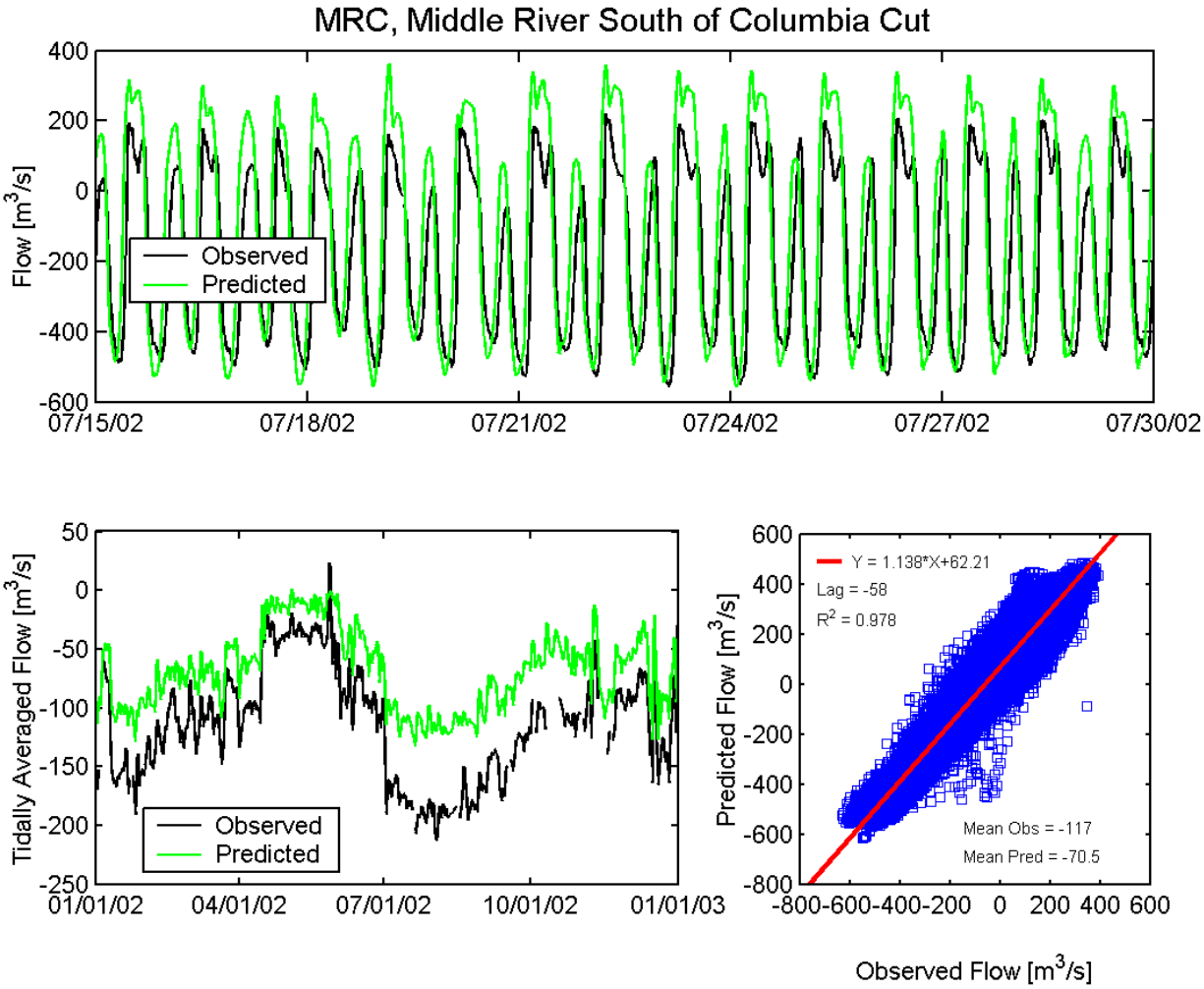

Figure A.4-20 Observed and predicted flow at Middle River South of Columbia Cut USGS station (MRC) during the 2002 simulation period.

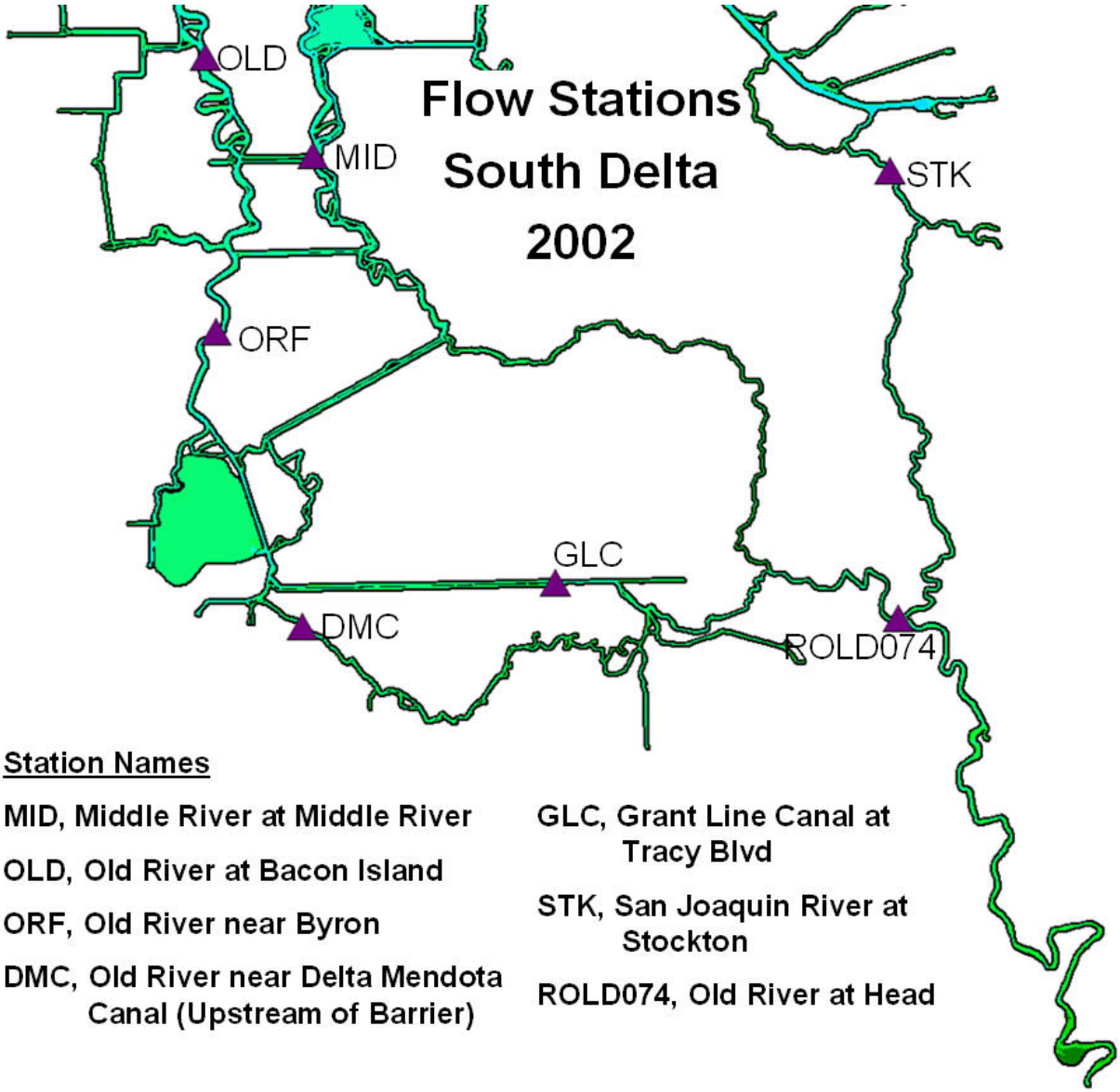

Figure A.4-21 Location of flow monitoring stations in the southern portion of the Sacramento-San Joaquin Delta used for 2002 flow comparisons.

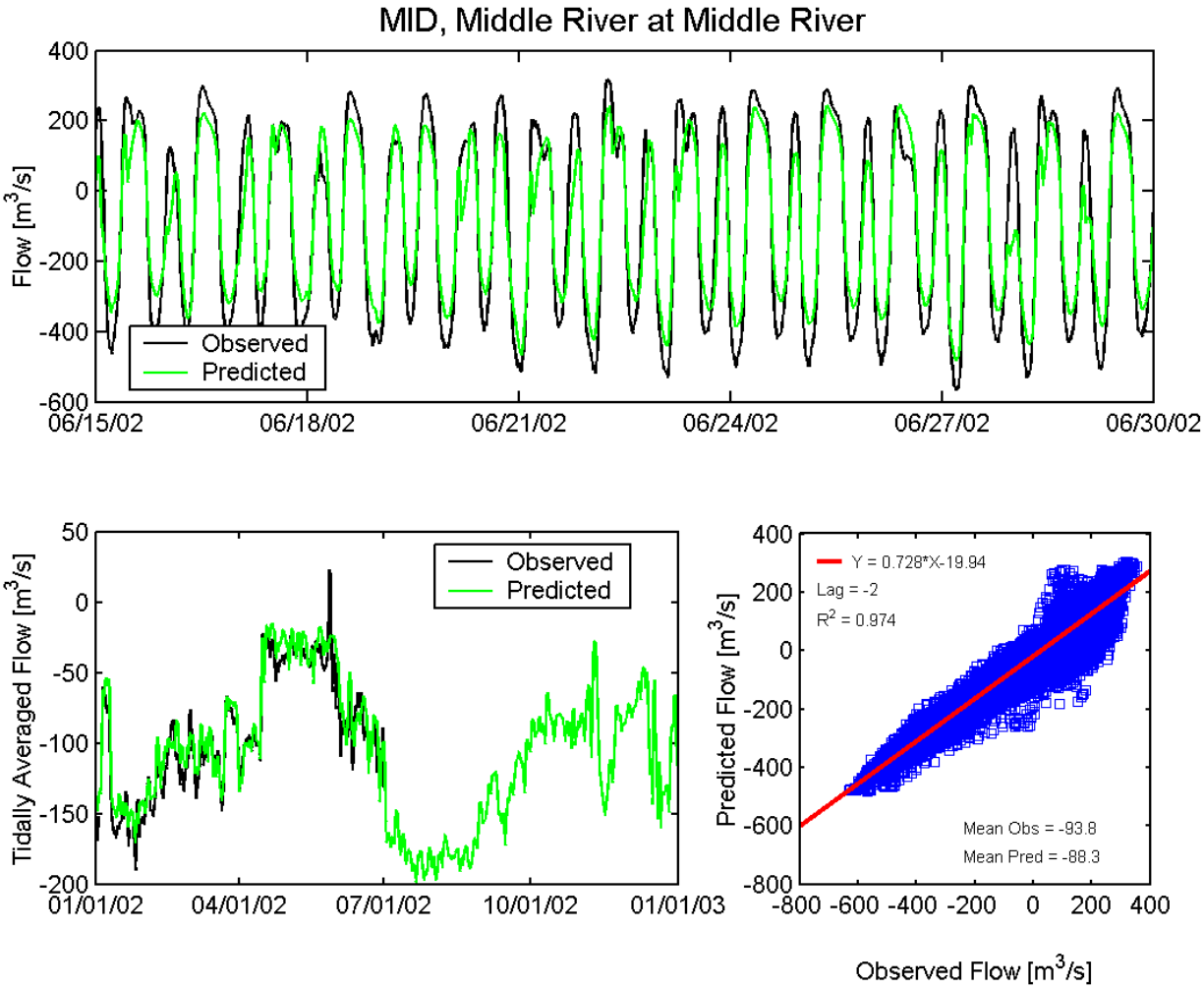

Figure A.4-22 Observed and predicted flow at Middle River at Middle River USGS station (MID) during the 2002 simulation period.

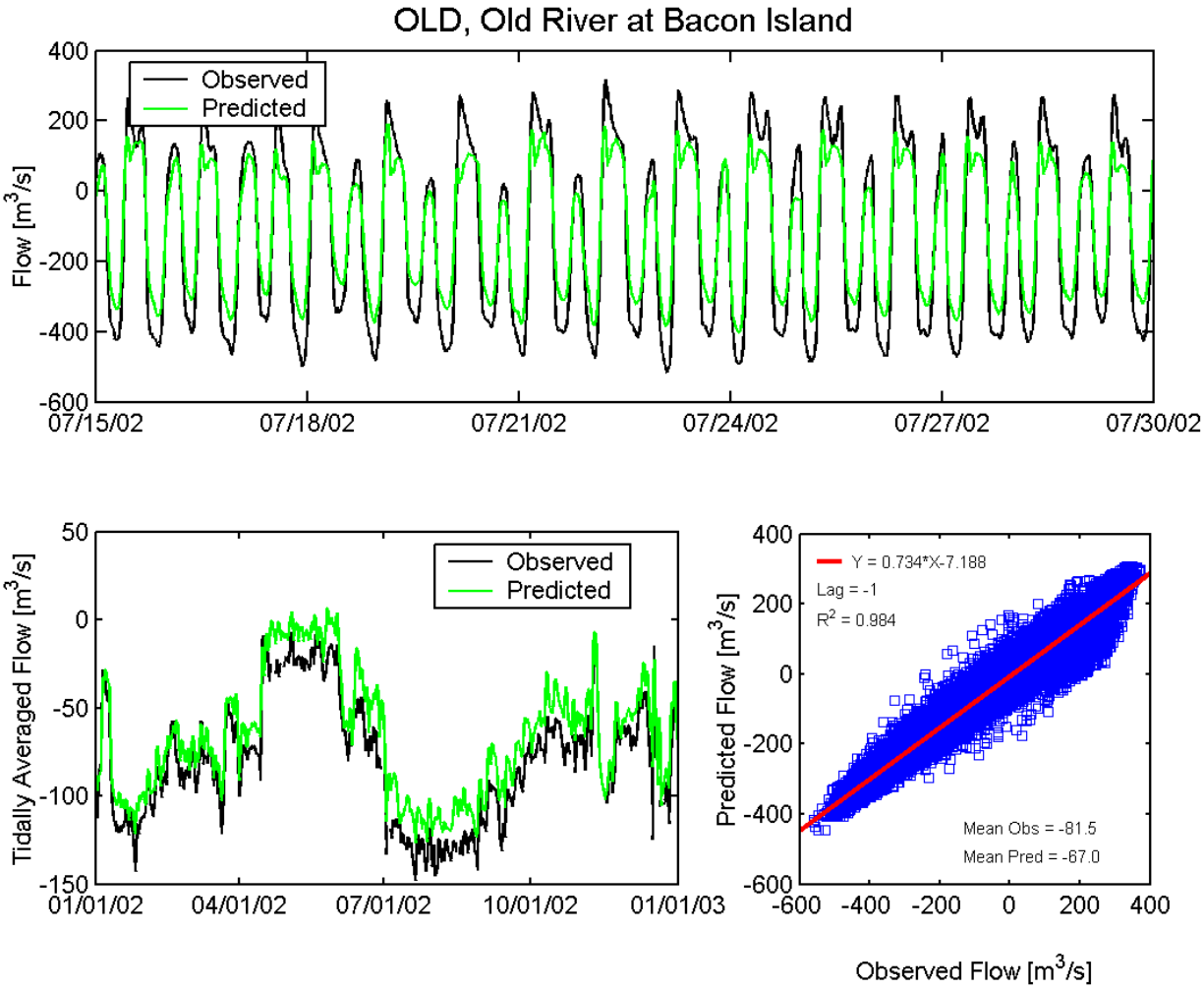

Figure A.4-23 Observed and predicted flow at Old River at Bacon Island USGS station (OLD) during the 2002 simulation period.

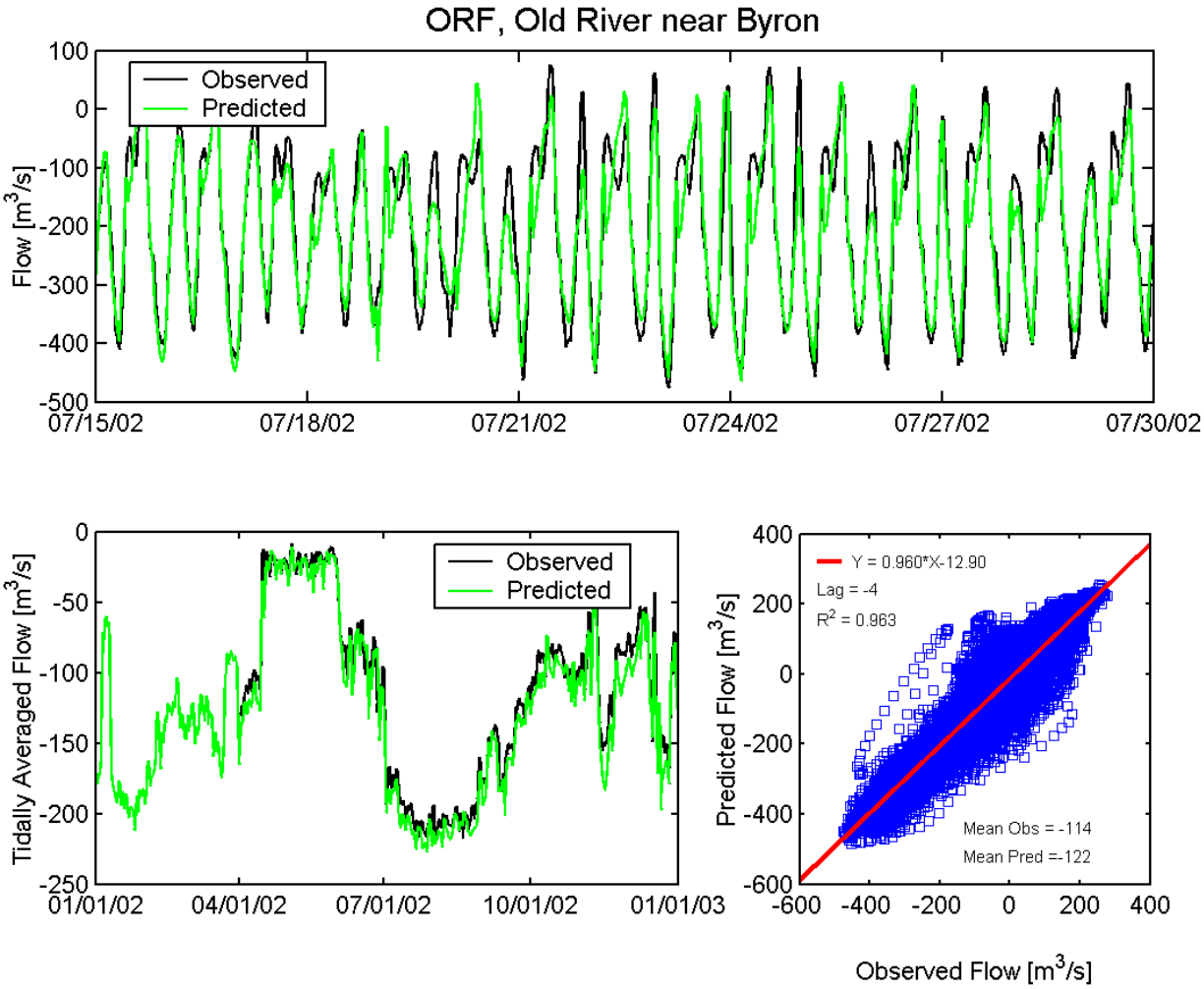

Figure A.4-24 Observed and predicted flow at Old River near Byron USGS station (ORF) during the 2002 simulation period.

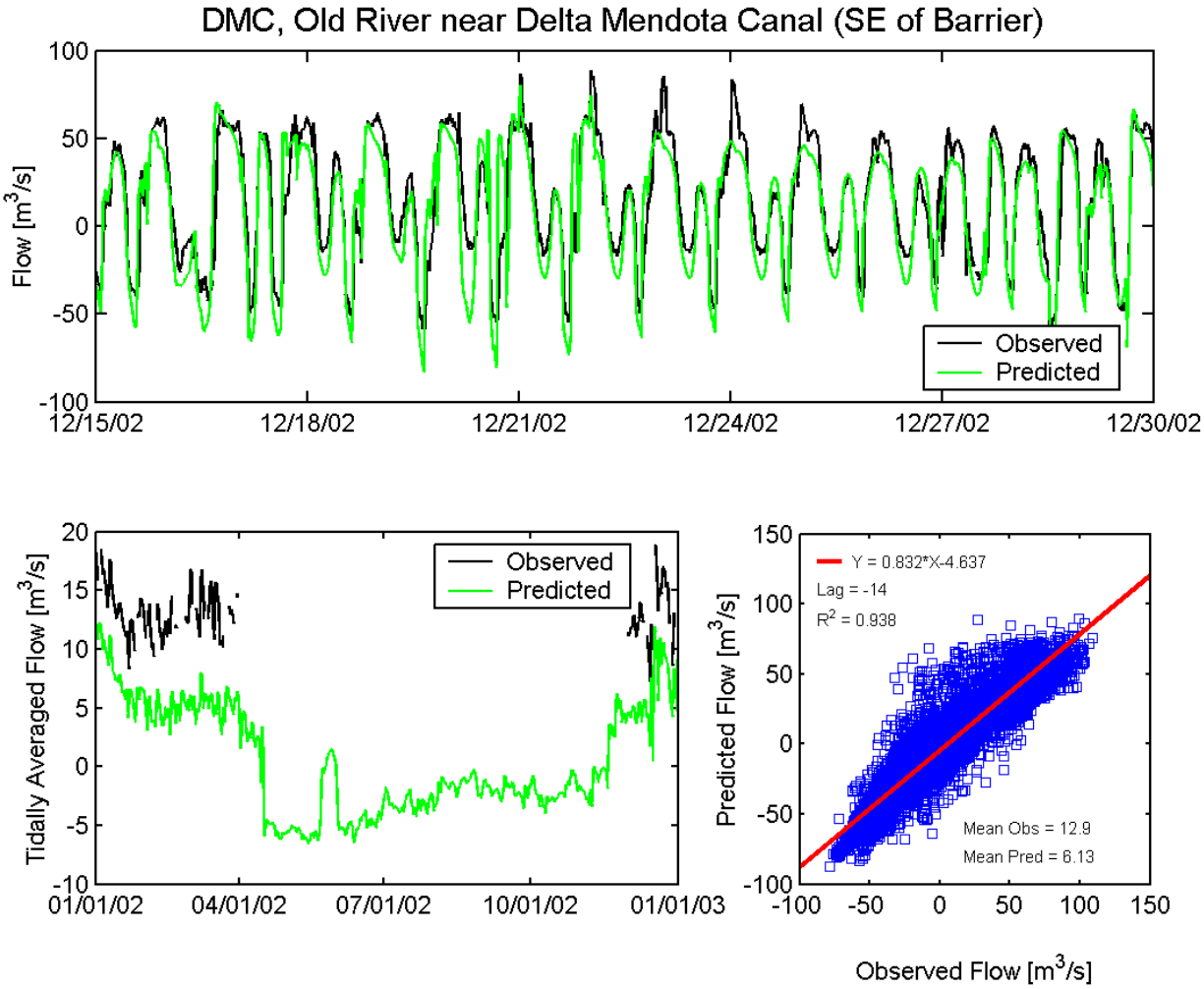

Figure A.4-25 Observed and predicted flow at Old River near Delta Mendota Canal SE of Barrier USGS station (DMC) during the 2002 simulation period.

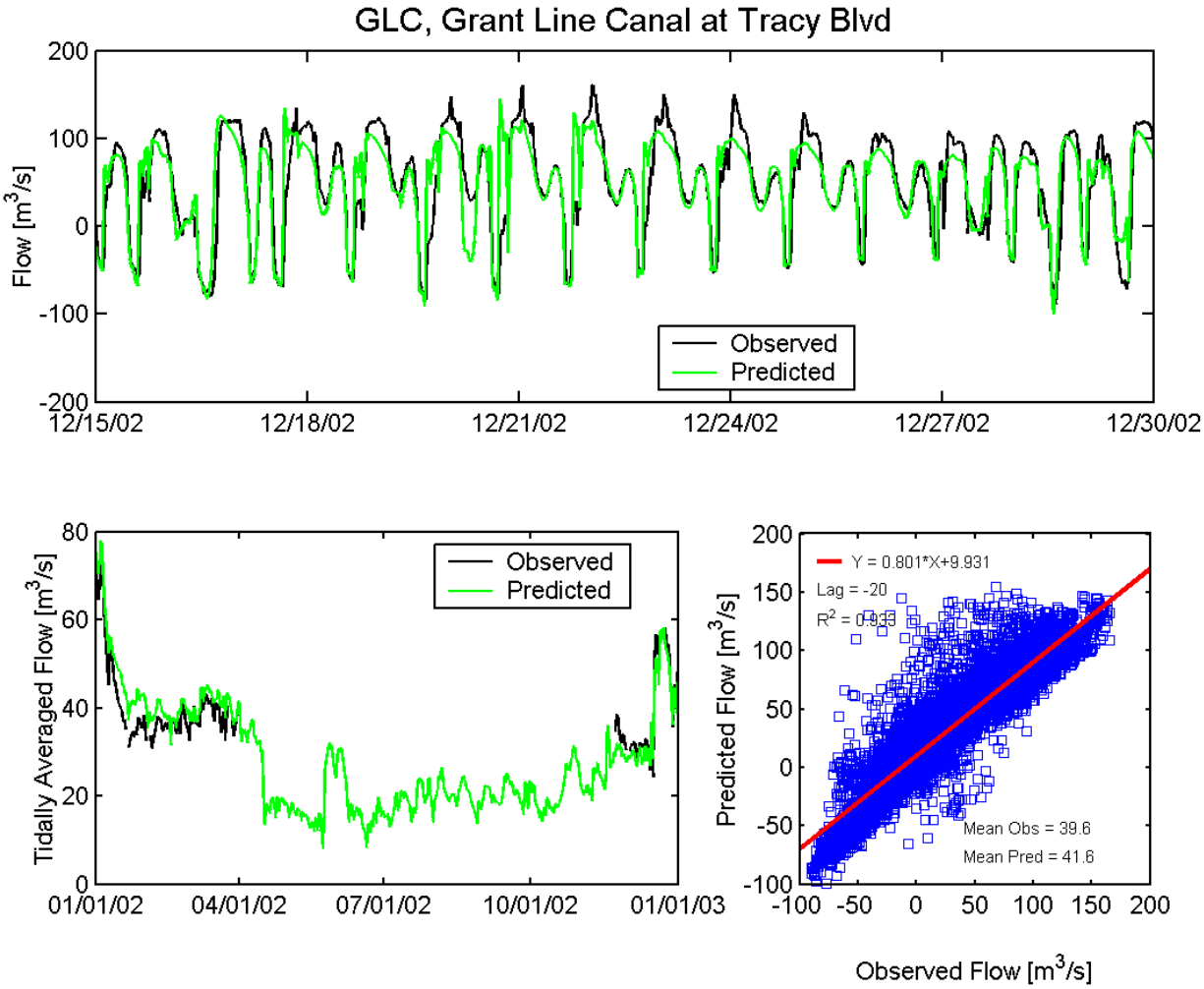

Figure A.4-26 Observed and predicted flow at Grant Line Canal at Tracy Boulevard USGS station (GLC) during the 2002 simulation period.

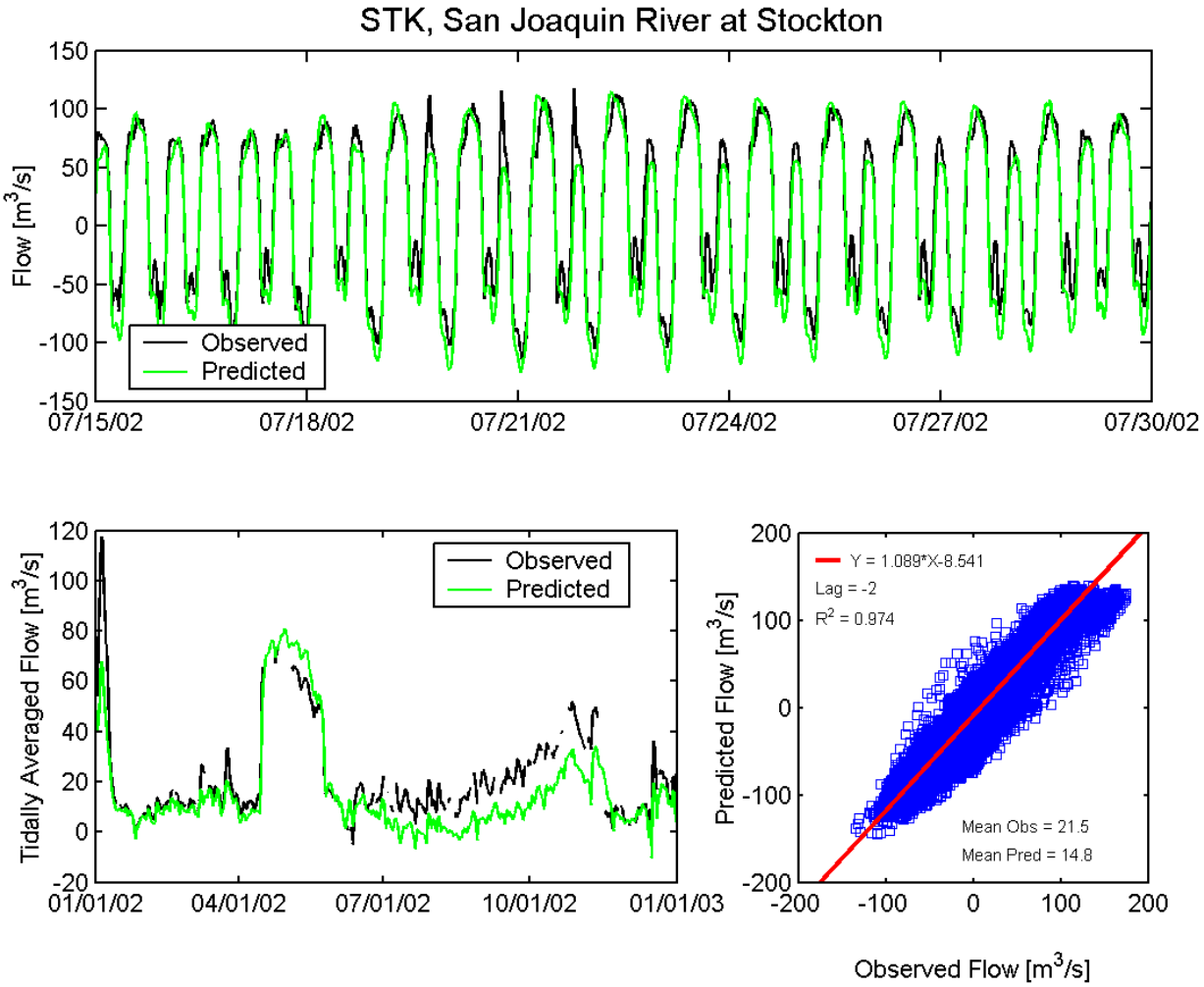

Figure A.4-27 Observed and predicted flow at San Joaquin River at Stockton USGS station (STK) during the 2002 simulation period.

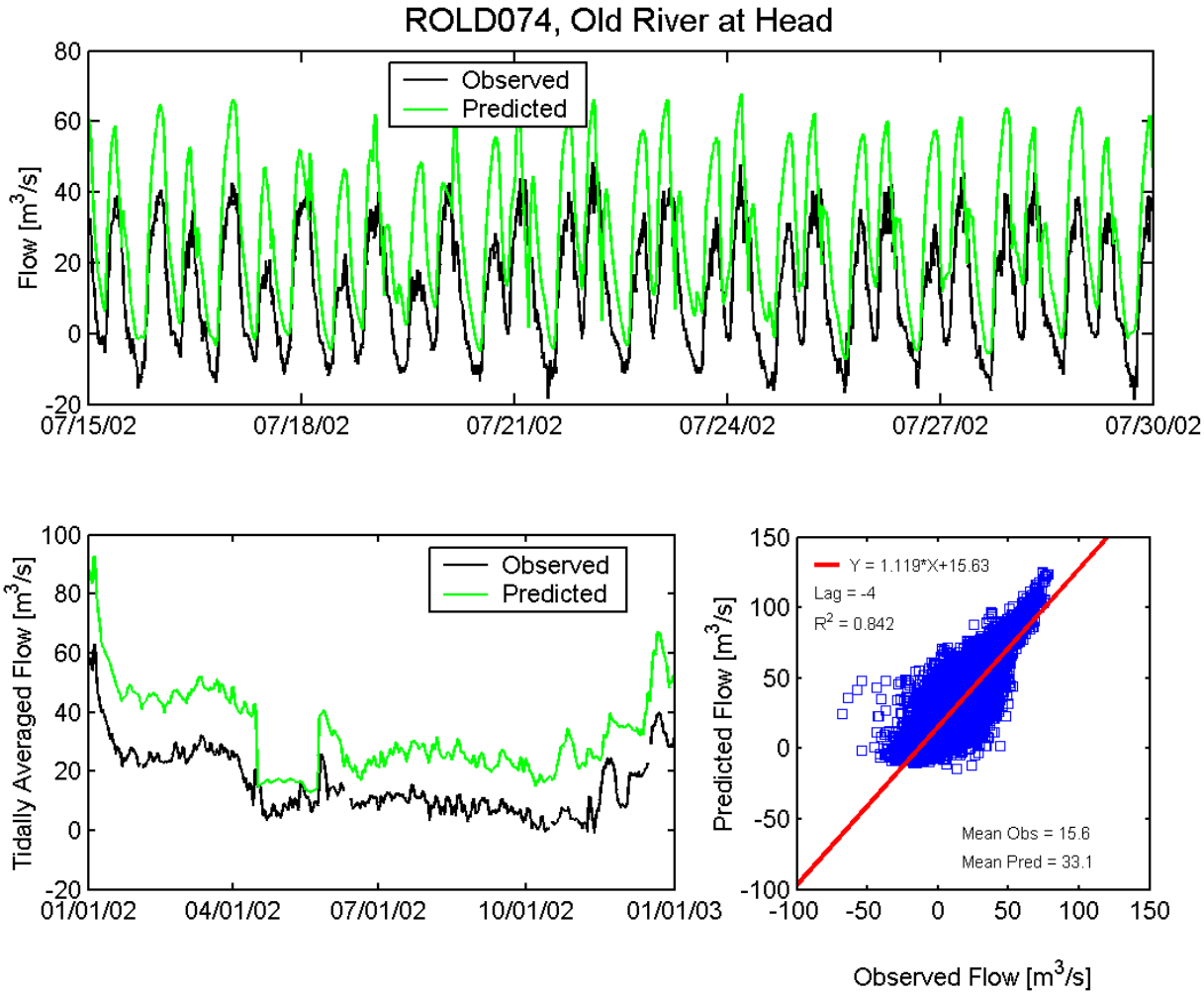

Figure A.4-28 Observed and predicted flow at Old River at Head DWR station (ROLD074) during the 2002 simulation period.

A.5 Synoptic Salinity Validation

The USGS maintains a program of research and observation in San Francisco Bay that includes regular measurements of water quality along a 145 kilometer transect spanning the length of the entire estuarine system (USGS, 2009). These data include synoptic salinity observations, consisting of vertical profiles of salinity at 1 meter vertical resolution at 38 sampling locations, along the axis of the San Francisco Estuary (USGS, 2009; Figure A.5-1). The synoptic salinity data are typically collected over a period of 10 to 12 hours, as the USGS research vessel travels along the channel of San Francisco Bay from the South Bay to the western Delta. The location of the synoptic monitoring stations are shown on Figure A.5-1.

A.6.1 USGS San Francisco Bay Synoptic Salinity Transects

The predicted salinity along the axis of the San Francisco Estuary was compared with USGS synoptic sampling observations (USGS, 2009) during all San Francisco Bay cruises between January 1, 2002 and January 1, 2002, except cruises that were limited to South San Francisco Bay. An additional comparison was made on November 27, 2001 (Figure A.5-2) during the model spin-up period.

Salinity was predicted accurately along the axis of the estuary by the UnTRIM Bay-Delta model on most dates (Figures A.5-2 through A.5-9), and the average errors and standard errors are small relative to the large range of salinity conditions that occurred during the calibration period (Table A-3).

Table A-3 Average error and standard error for each synoptic sampling cruise covering the axis of the San Francisco Estuary during the 2002 simulation period.

Date	Figure Number	Average Error (psu)	Standard Error (psu)	R^2
11/27/2001	A.5-2	0.54	0.87	0.99
05/13/2002	A.5-3	-0.11	0.57	0.79
07/16/2002	A.5-4	-1.40	1.11	0.97
08/20/2002	A.5-5	-1.01	0.91	0.98
09/10/2002	A.5-6	-0.79	1.15	0.98
10/08/2002	A.5-7	0.20	1.62	0.97
11/13/2002	A.5-8	0.30	0.98	0.99
12/10/2002	A.5-9	0.16	0.56	1.00

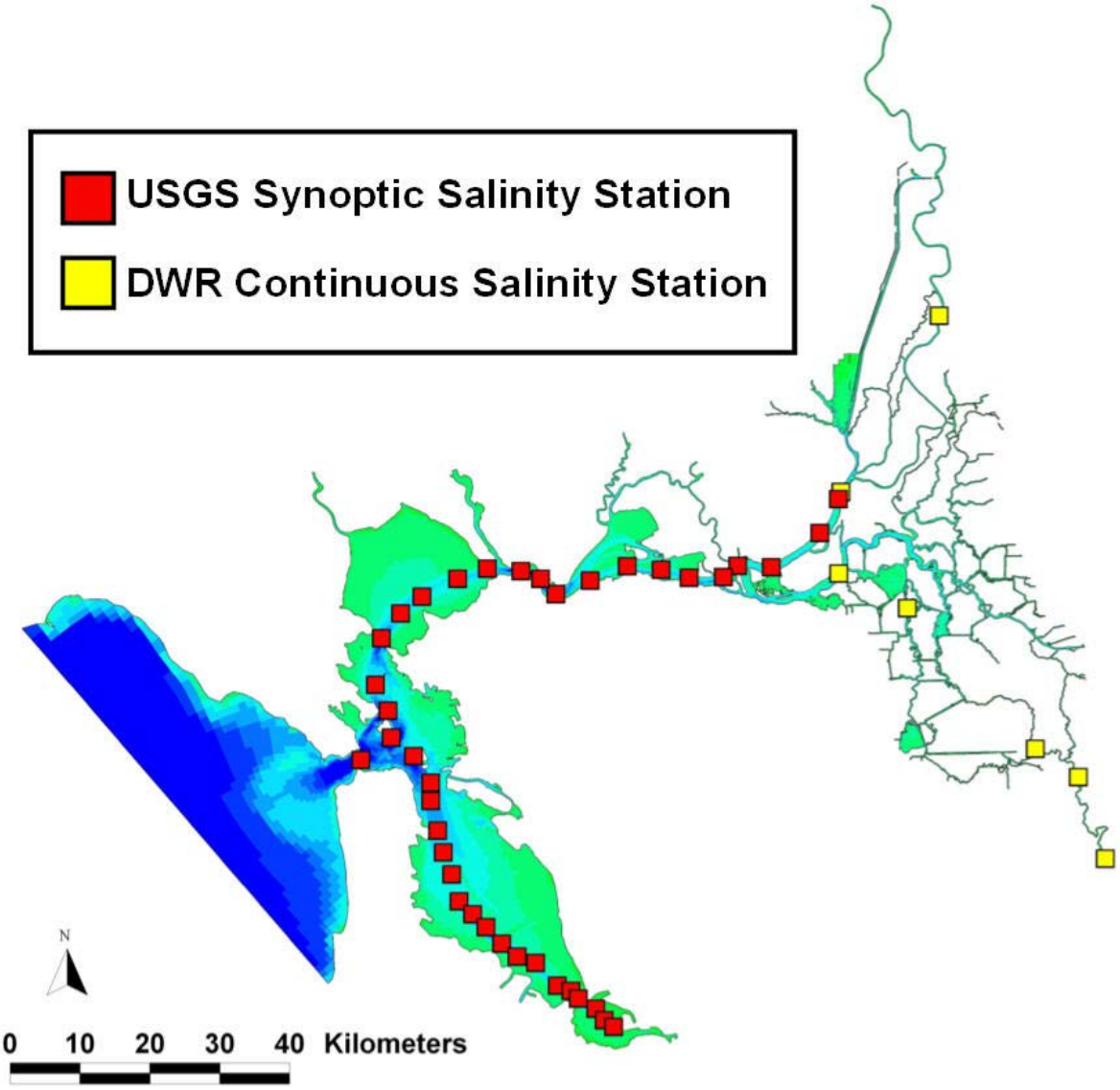

Figure A.5-1 Location of USGS synoptic monitoring stations along the axis of the San Francisco Estuary.

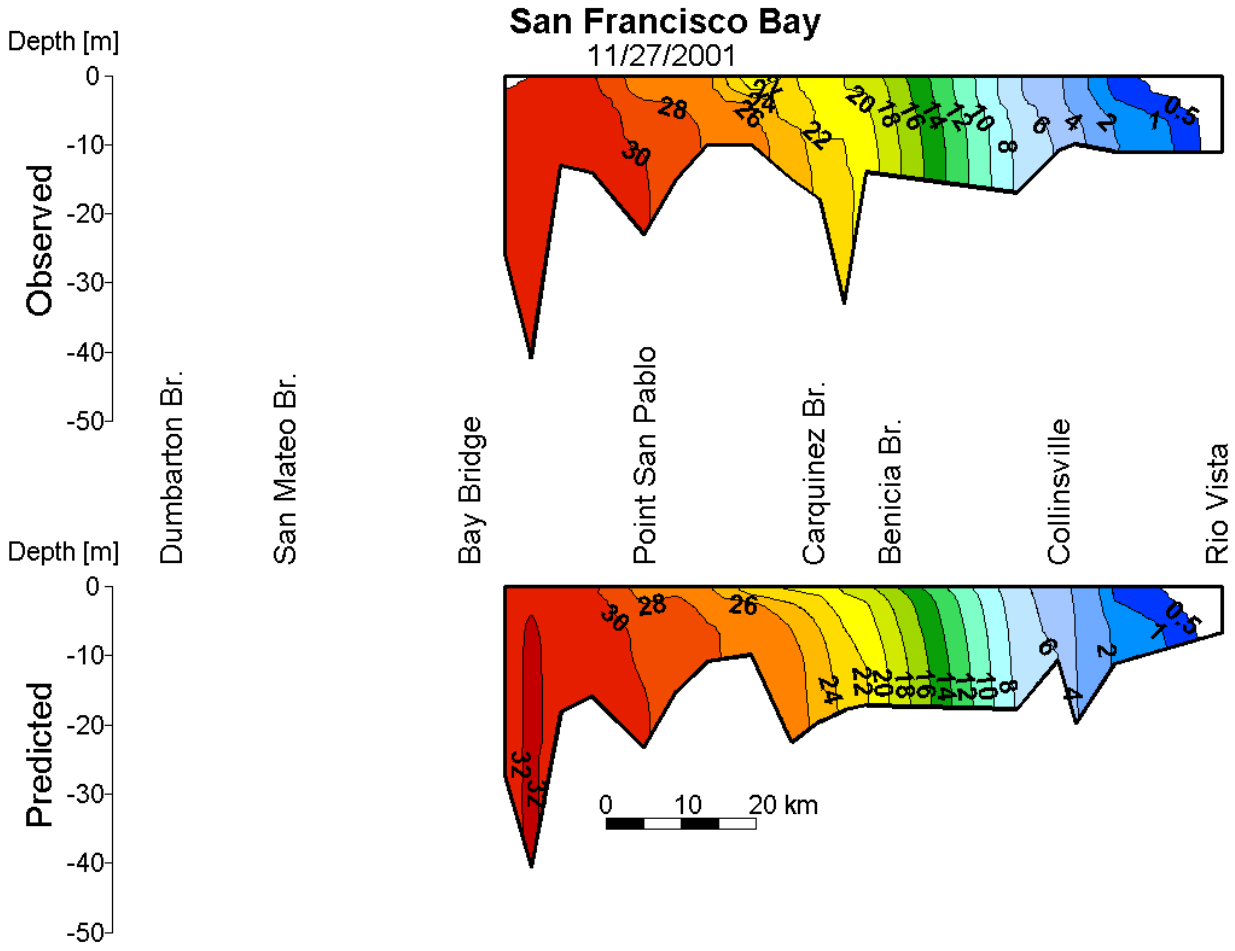

Figure A.5-2 Observed and predicted salinity profiles at synoptic sampling stations, interpolated along the axis of the San Francisco Estuary on November 27, 2001 during the model spin-up period.

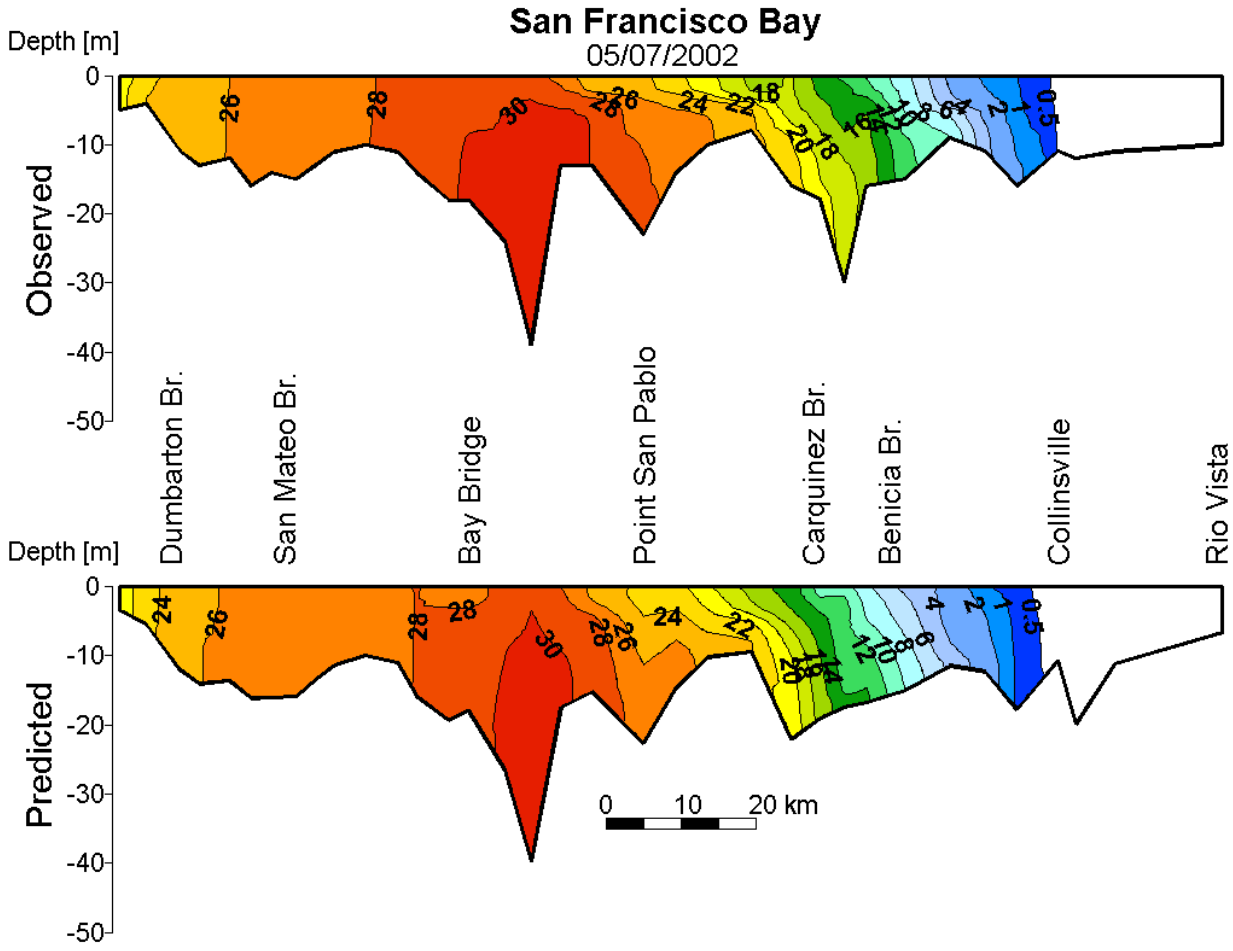

Figure A.5-3 Observed and predicted salinity profiles at synoptic sampling stations, interpolated along the axis of the San Francisco Estuary on May 7, 2002.

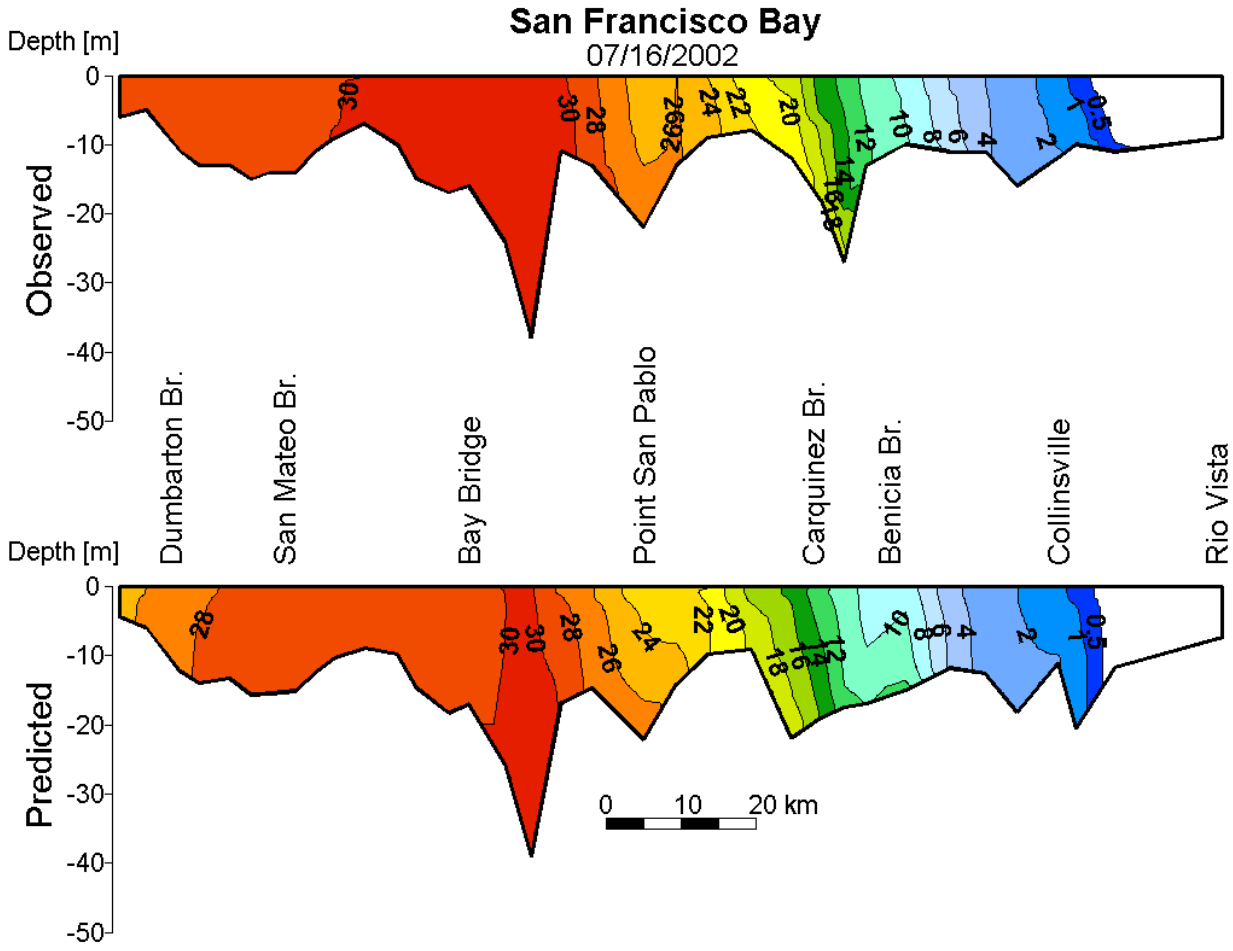

Figure A.5-4 Observed and predicted salinity profiles at synoptic sampling stations, interpolated along the axis of the San Francisco Estuary on July 16, 2002.

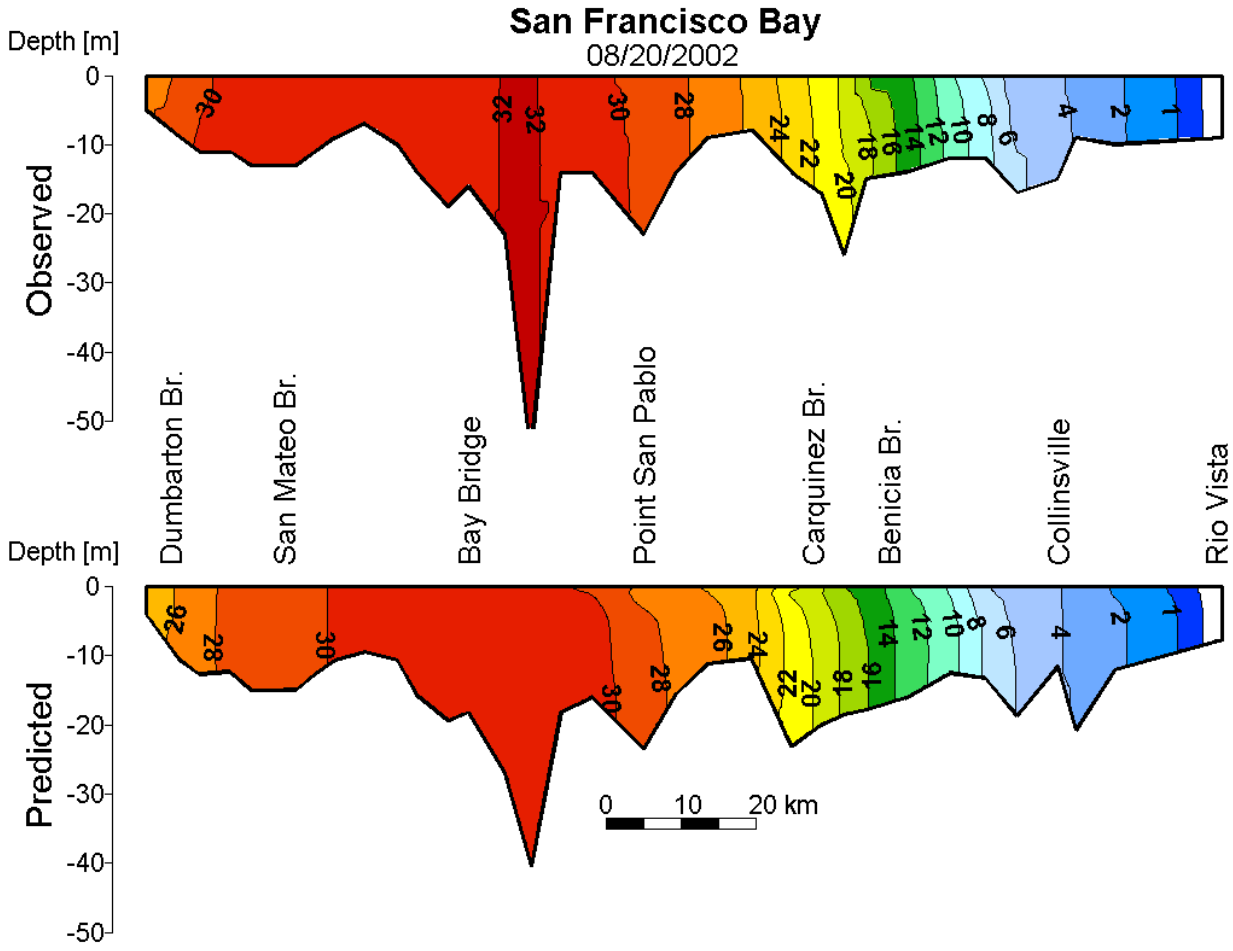

Figure A.5-5 Observed and predicted salinity profiles at synoptic sampling stations, interpolated along the axis of the San Francisco Estuary on August 20, 2002.

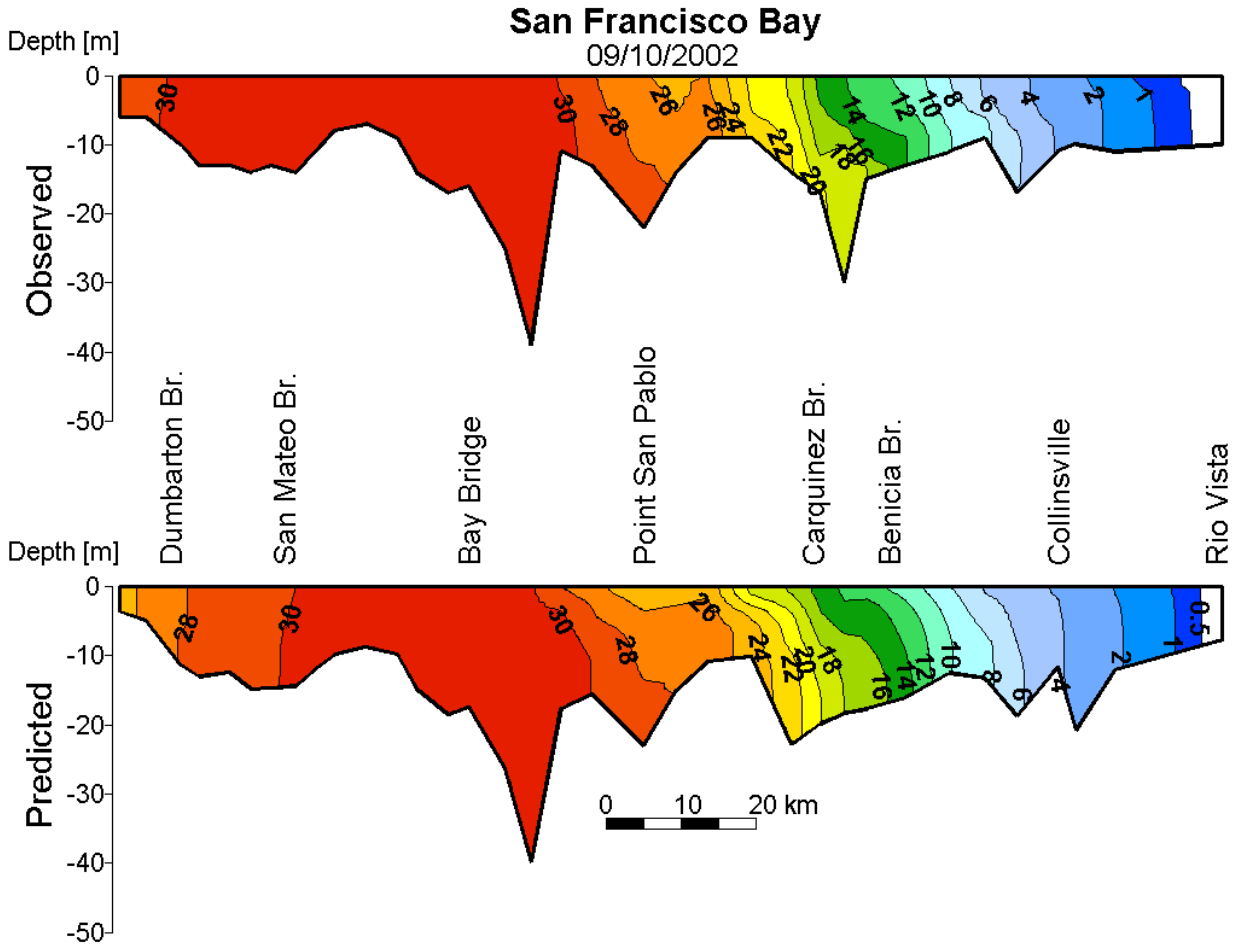

Figure A.5-6 Observed and predicted salinity profiles at synoptic sampling stations, interpolated along the axis of the San Francisco Estuary on September 10, 2002.

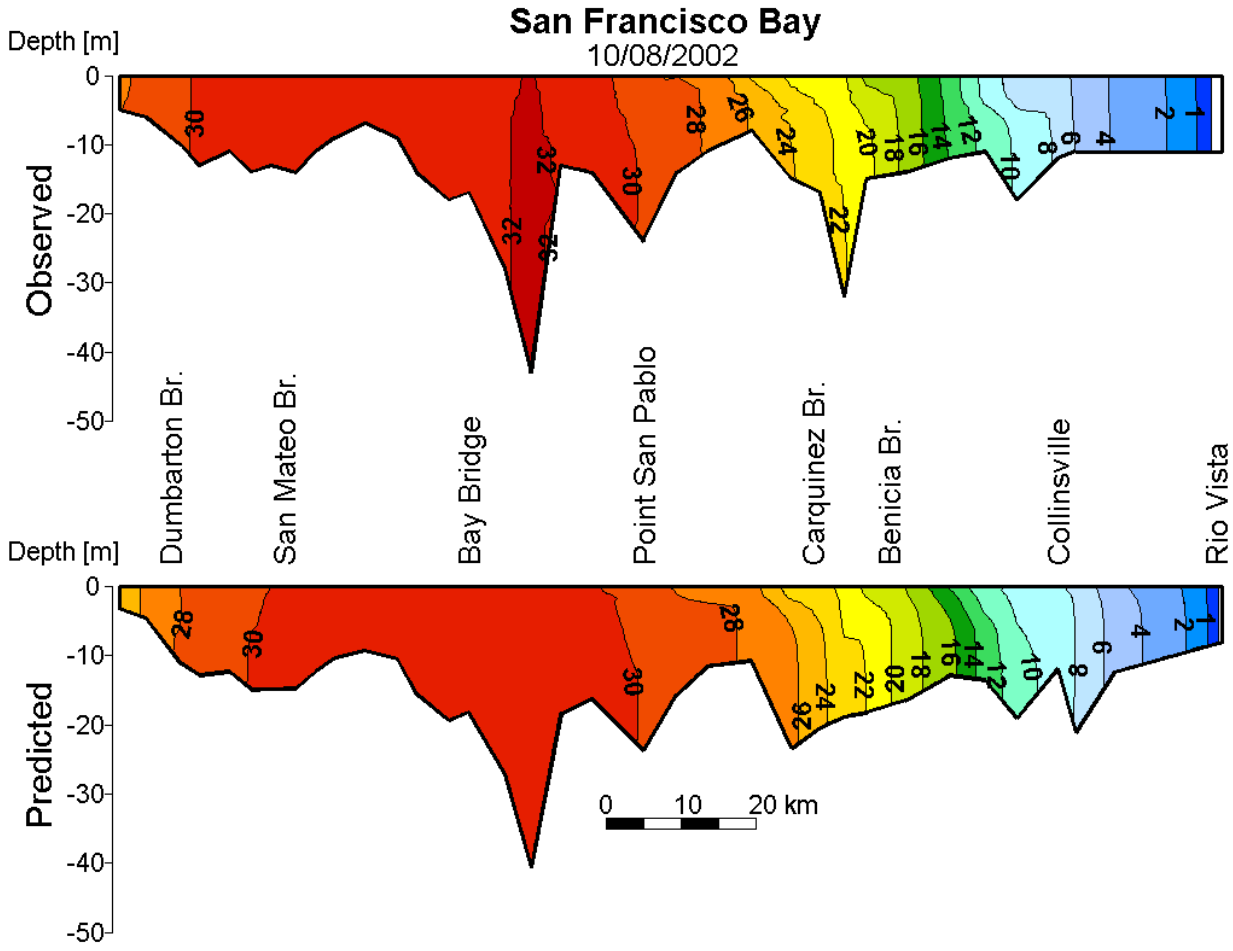

Figure A.5-7 Observed and predicted salinity profiles at synoptic sampling stations, interpolated along the axis of the San Francisco Estuary on October 8, 2002.

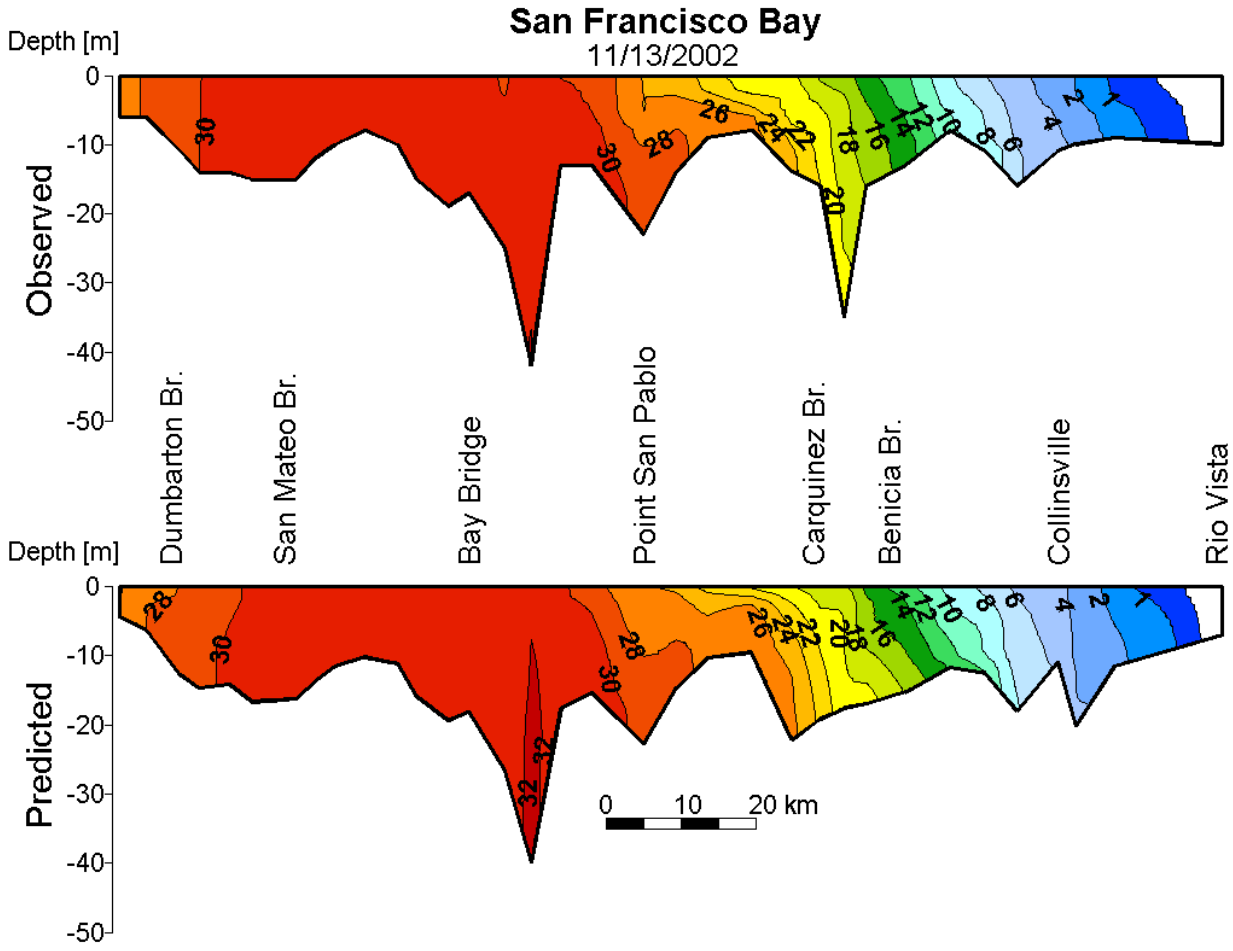

Figure A.5-8 Observed and predicted salinity profiles at synoptic sampling stations, interpolated along the axis of the San Francisco Estuary on November 13, 2002.

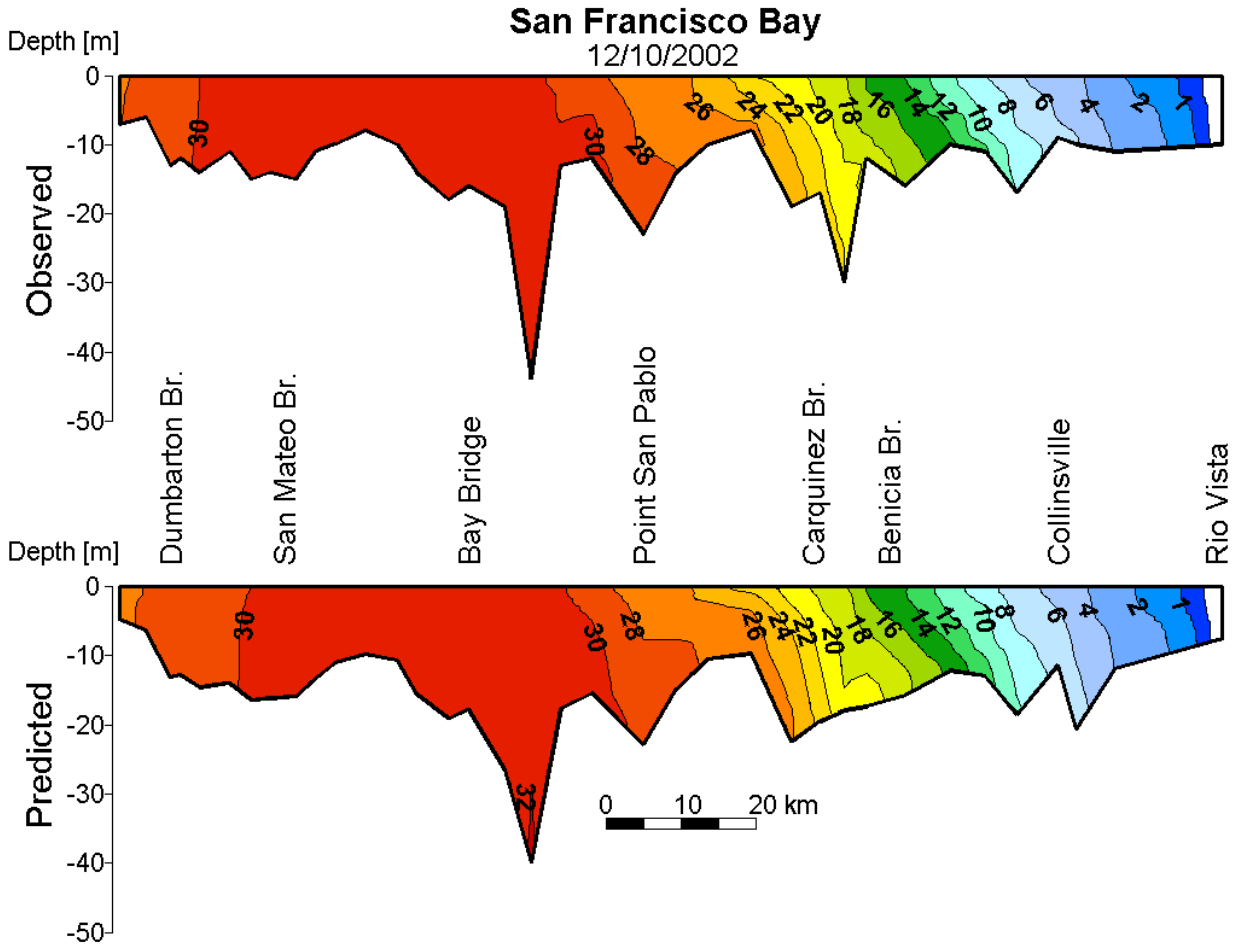

Figure A.5-9 Observed and predicted salinity profiles at synoptic sampling stations, interpolated along the axis of the San Francisco Estuary on December 10, 2002.

A.6 Salinity Comparison Figures

Observed and predicted salinity were compared at twenty-two locations in San Francisco Bay and at thirty-seven stations in the Sacramento-San Joaquin Delta during the 2002 simulation period. At each station (and at multiple depths at some stations), observed and predicted salinity were plotted over a fifteen day period to show the water level agreement over tidal time scales. In addition, the observed and predicted salinity are tidally averaged, to assess the accuracy of the model in predicting water level variability on spring-neap time scales, as well as during non-tidal forcing such as storms. Lastly, the cross-correlation (as described in Section A.1) was used to determine the mean observed and predicted salinity, the amplitude ratio, the phase lag, and the correlation coefficient squared (R^2). For each of the salinity monitoring stations, these values are compiled in Table A-4.

A.6.1 San Francisco Bay

Salinity comparisons were made at twenty-two continuous monitoring stations in the San Francisco Estuary, at the locations shown in Figure A.6-1. Salinity comparisons at these stations are shown in Figures A.6-2 through A.6-23.

A.6.2 Northern Sacramento-San Joaquin Delta

Salinity comparisons were made at three continuous monitoring stations in the northern portion of the Sacramento-San Joaquin Delta, at the locations shown in Figure A.6-24. Salinity comparisons at these stations are shown in Figures A.6-25 through A.6-27.

A.6.3 Central Sacramento-San Joaquin Delta

Salinity comparisons were made at twenty-three continuous monitoring stations in the central portion of the Sacramento-San Joaquin Delta, at the locations shown in Figure A.6-28. Salinity at these stations are shown in Figures A.6-29 through A.6-51.

A.6.4 Southern Sacramento-San Joaquin Delta

Salinity comparisons were made at eleven continuous monitoring stations in the southern portion of the Sacramento-San Joaquin Delta, at the locations shown in Figure A.6-52. Salinity comparisons at these stations are shown in Figures A.6-53 through A.6-63.

Table A-4 Predicted and observed salinity and cross-correlation statistics for salinity monitoring stations in San Francisco Bay and the Sacramento-San Joaquin Delta during the 2002 simulation period.

Location	Data Source	Figure Number	Mean Salinity		Cross Correlation		R^2
			Observed (psu)	Predicted (psu)	Amp Ratio	Lag (min)	

2002 San Francisco Bay Salinity Stations (Figure A.6-1)							
Presidio	USGS	A.6-2	30.6	30.6	0.667	-36	0.892
Pier 24 (Lower Sensor)	USGS	A.6-3	26.9	27.9	0.762	9	0.780
Pier 24 (Upper Sensor)	USGS	A.6-4	26.3	27.2	0.749	5	0.817
San Mateo Bridge (Lower Sensor)	USGS	A.6-5	27.5	28.1	0.750	17	0.983
San Mateo Bridge (Upper Sensor)	USGS	A.6-6	26.6	27.4	0.767	6	0.971
Point San Pablo (Lower Sensor)	USGS	A.6-7	25.3	25.6	0.781	14	0.925
Point San Pablo (Upper Sensor)	USGS	A.6-8	25.2	25.0	0.839	12	0.924
Channel Marker 9	USGS	A.6-9	18.5	18.7	0.856	12	0.932
Mare Island Causeway (Lower Sensor)	USGS	A.6-10	16.0	13.6	1.065	44	0.881
Mare Island Causeway (Upper Sensor)	USGS	A.6-11	14.9	13.5	1.047	35	0.944
Carquinez Bridge (Lower Sensor)	USGS	A.6-12	17.8	18.3	0.794	25	0.880
Carquinez Bridge (Upper Sensor)	USGS	A.6-13	17.3	18.6	0.893	-8	0.917
Sacramento River at Martinez (Bottom Sensor)	DWR	A.6-14	13.8	13.9	0.930	33	0.950
Sacramento River at Martinez (Surface Sensor)	DWR	A.6-15	11.4	10.8	0.961	-25	0.937
Benicia Bridge (Lower Sensor)	USGS	A.6-16	14.0	14.6	0.720	52	0.877
Benicia Bridge (Upper Sensor)	USGS	A.6-17	12.6	12.5	0.988	6	0.953
Sacramento River at Port Chicago (Bottom Sensor)	USBR	A.6-18	7.59	7.63	0.972	-54	0.962
Sacramento River at Port Chicago (Surface Sensor)	USBR	A.6-19	6.79	5.99	0.895	-71	0.941
Sacramento River near Mallard Island (Bottom Sensor)	DWR	A.6-20	3.65	4.03	1.118	24	0.974
Sacramento River near Mallard Island (Surface Sensor)	DWR	A.6-21	3.35	3.42	1.043	34	0.975
Sacramento River at Pittsburgh (Bottom Sensor)	USBR	A.6-22	2.86	3.01	0.966	-23	0.907
Sacramento River at Pittsburgh (Surface Sensor)	USBR	A.6-23	2.84	2.90	1.064	-12	0.960
2002 North Delta Salinity Stations (Figure A.6-24)							
Mokelumne River below Snodgrass Slough	DWR	A.6-25	0.08	0.08	0.139	-26	0.179
Sacramento River at Green's Landing	USBR	A.6-26	0.07	0.07	0.887	n/a*	0.905
Sacramento River at Hood	DWR	A.6-27	0.08	0.07	0.812	n/a*	0.914
2002 Central Delta Salinity Stations (Figure A.6-28)							
Sacramento River at Collinsville	USBR	A.6-29	1.88	2.03	0.955	-20	0.898
Sacramento River at Emmaton (Bottom Sensor)	USBR	A.6-30	0.33	0.33	1.170	1	0.964
Sacramento River at Emmaton (Surface Sensor)	USBR	A.6-31	0.40	0.46	1.282	-7	0.942
Sacramento River at Rio Vista	USBR	A.6-32	0.10	0.10	1.684	-7	0.760
Threemile Slough at San Joaquin River	DWR	A.6-33	0.24	0.21	0.940	-4	0.852

San Joaquin River at Antioch (Bottom Sensor)	DWR	A.6-34	0.82	0.66	0.875	8	0.987
San Joaquin River at Antioch (Surface Sensor)	DWR	A.6-35	0.73	0.63	0.882	-38	0.989
San Joaquin River at Jersey Point	USBR	A.6-36	0.40	0.30	0.807	-24	0.948
Dutch Slough at Jersey Island	USBR	A.6-37	0.33	0.29	0.752	-54	0.950
False River	USGS	A.6-38	0.25	0.17	0.573	28	0.961
Taylor Slough	USGS	A.6-39	0.22	0.18	0.704	38	0.966
Sand Mound Slough	USGS	A.6-40	0.20	0.19	0.905	-67	0.944
Piper Slough at Bethel	DWR	A.6-41	0.25	0.16	0.489	-20	0.960
San Joaquin River at San Andreas Landing	USBR	A.6-42	0.12	0.10	0.500	4	0.774
Old River at San Joaquin River	USGS	A.6-43	0.13	0.10	0.118	n/a*	0.125
San Joaquin River before Prisoner's Point	DWR	A.6-44	0.11	0.10	0.910	-99	0.942
Mokelumne River near San Joaquin River	USGS	A.6-45	0.07	0.07	0.819	-5	0.874
Mokelumne River (South Fork) at Staten Island	USBR	A.6-46	0.07	0.08	0.356	n/a*	0.534
Franks Tract West	USGS	A.6-47	0.20	0.14	0.423	37	0.954
Franks Tract East	USGS	A.6-48	0.19	0.14	0.425	117	0.930
Holland Cut	USGS	A.6-49	0.18	0.15	0.547	113	0.950
Old River near Mandeville Island	USGS	A.6-50	0.16	0.13	0.400	35	0.895
Old River and Holland Cut at Mandeville Island	USBR	A.6-51	0.22	0.16	0.522	n/a*	0.907
2001 South Delta Salinity Stations (Figure A.6-52)							
Old River at Bacon Island	USGS	A.6-53	0.16	0.15	0.657	68	0.844
Middle River at Borden Highway	DWR	A.6-54	0.21	0.16	0.242	-3	0.188
Middle River at Tracy Blvd	DWR	A.6-55	0.33	0.23	0.467	-110	0.463
Clifton Court Forebay Radial Gates	DWR	A.6-56	0.23	0.17	0.367	-8	0.637
Grant Line Canal at Tracy Blvd	DWR	A.6-57	0.39	0.33	1.083	6	0.926
Old River near Delta Mendota Canal (NW of Barrier)	DWR	A.6-58	0.35	0.24	0.182	-15	0.322
Old River near Delta Mendota Canal (SE of Barrier)	DWR	A.6-59	0.50	0.24	-0.445	-105	-0.294
Old River at Tracy Blvd	DWR	A.6-60	0.45	0.34	0.634	-110	0.733
Middle River near Old River	USBR	A.6-61	0.35	0.33	0.797	119	0.898
Stockton Ship Channel at Burns Cutoff	DWR	A.6-62	0.33	0.26	0.743	118	0.641
San Joaquin River at Mossdale	DWR	A.6-63	0.36	0.32	0.930	n/a*	0.966

* n/a indicates that the cross-correlation procedure did not identify a local maximum correlation coefficient within the four hour analysis window. This can be indicative of the data not having a strong tidal time-scale signal.

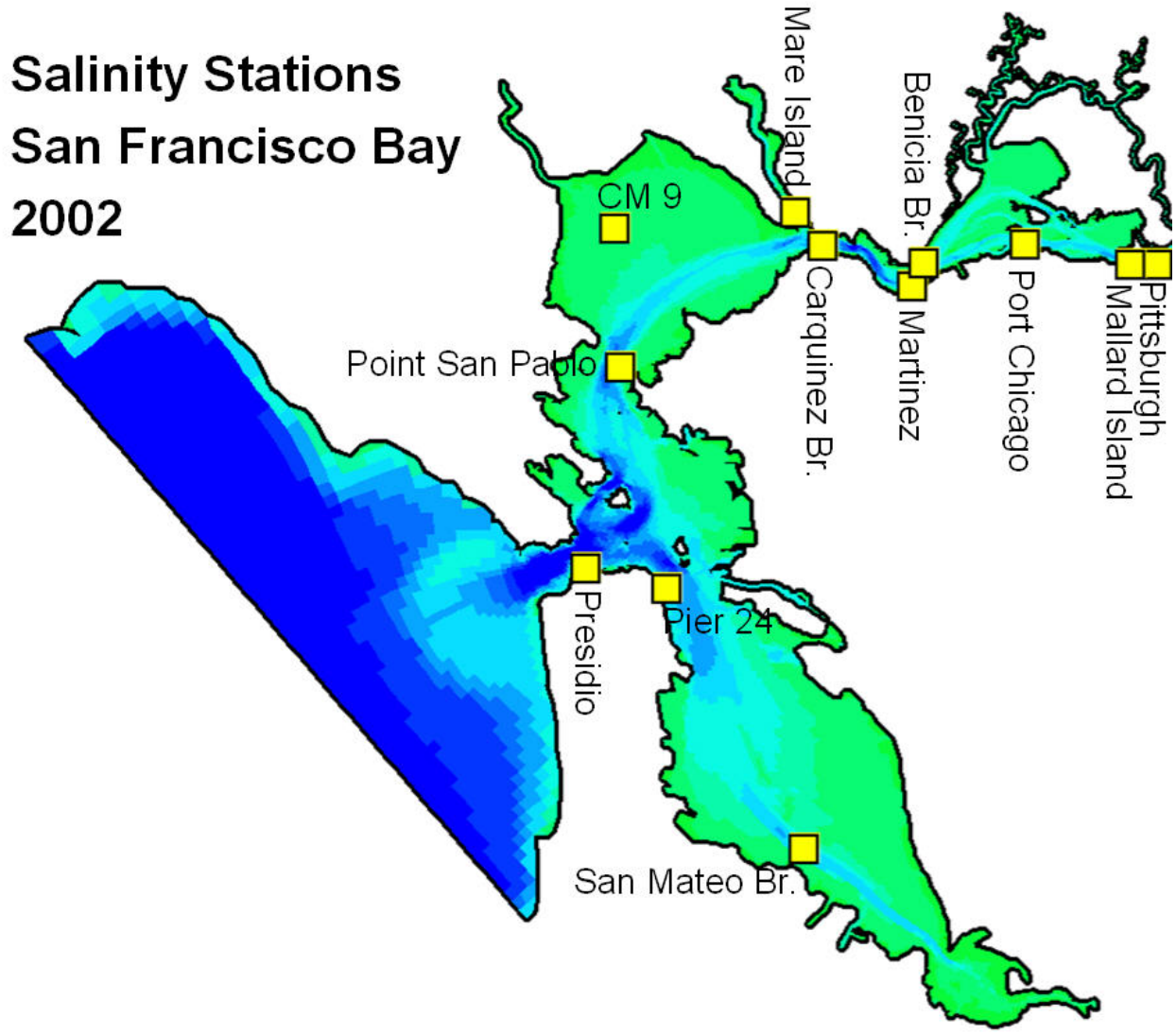

Figure A.6-1 Location of salinity monitoring stations in San Francisco Bay used for 2002 salinity comparisons.

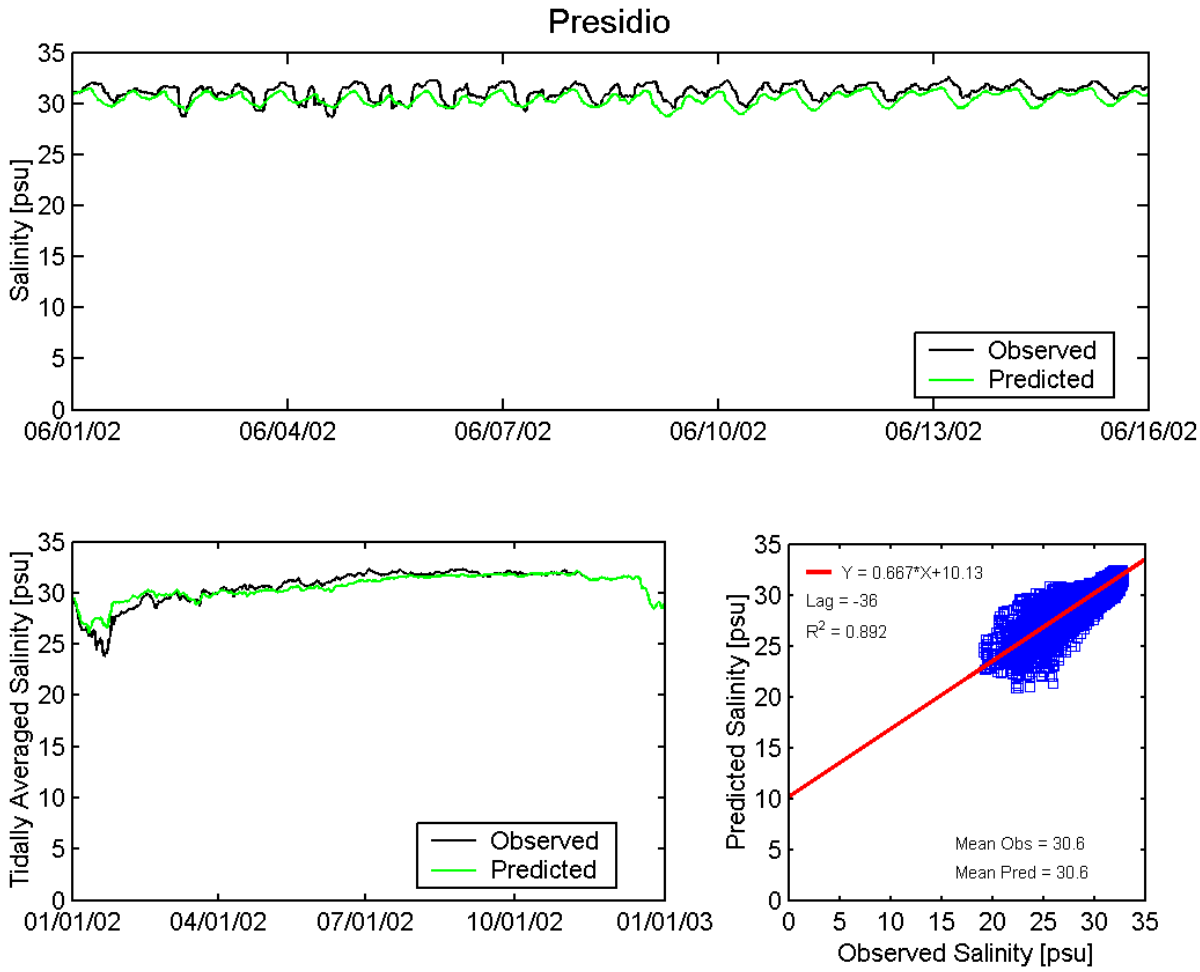

Figure A.6-2 Observed and predicted salinity at Presidio USGS station during the 2002 simulation period.

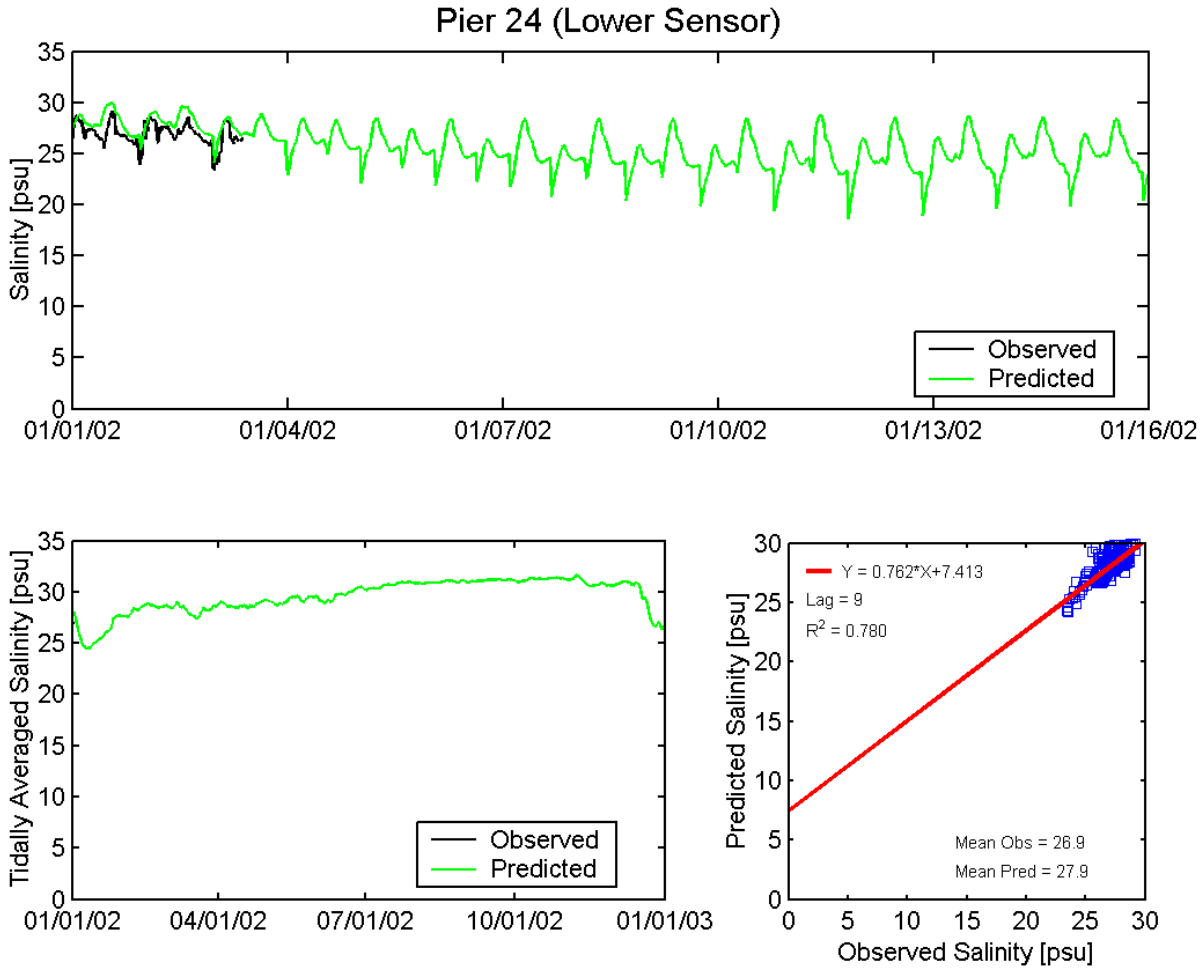

Figure A.6-3 Observed and predicted salinity at Pier 24 USGS station (Lower Sensor) during the 2002 simulation period.

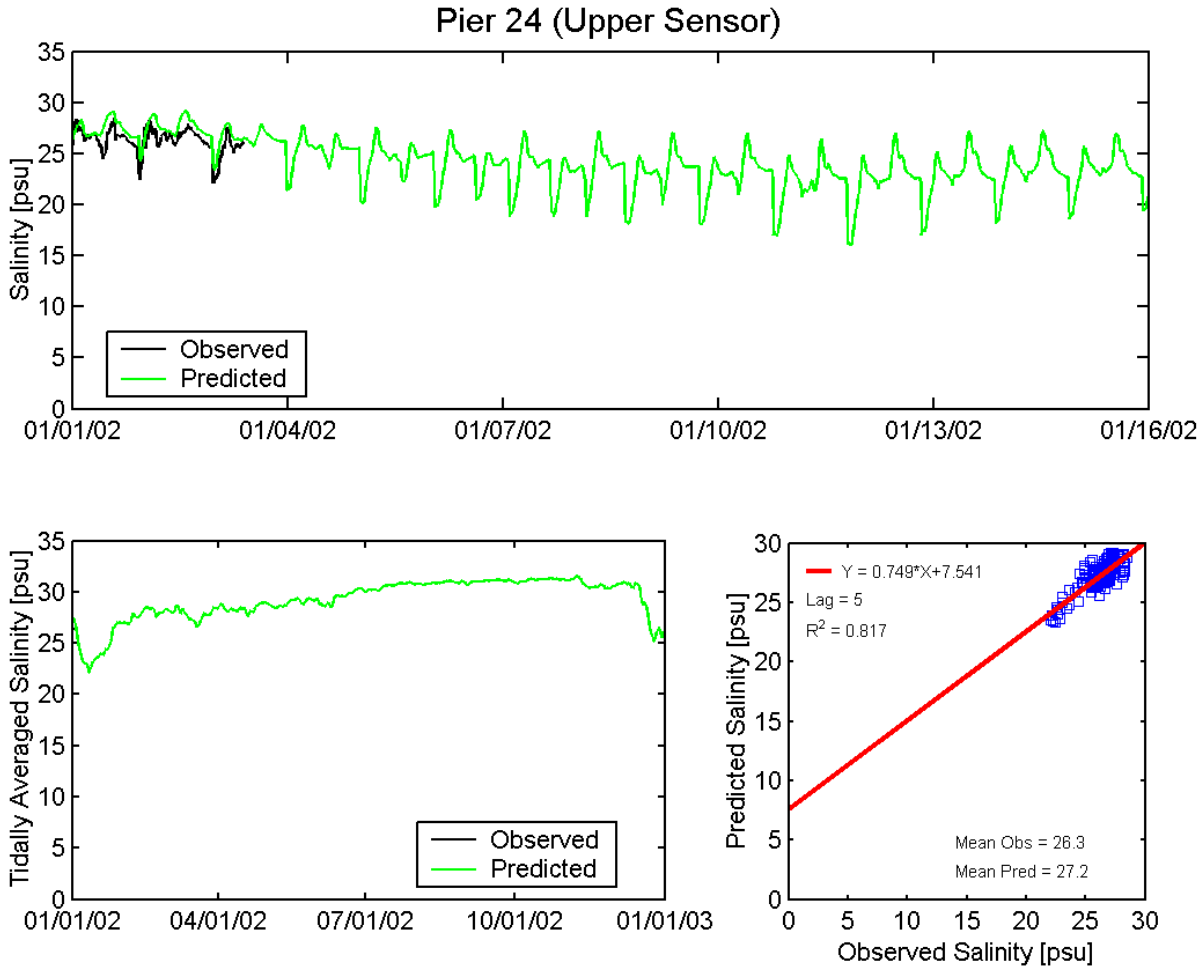

Figure A.6-4 Observed and predicted salinity at Pier 24 USGS station (Upper Sensor) during the 2002 simulation period.

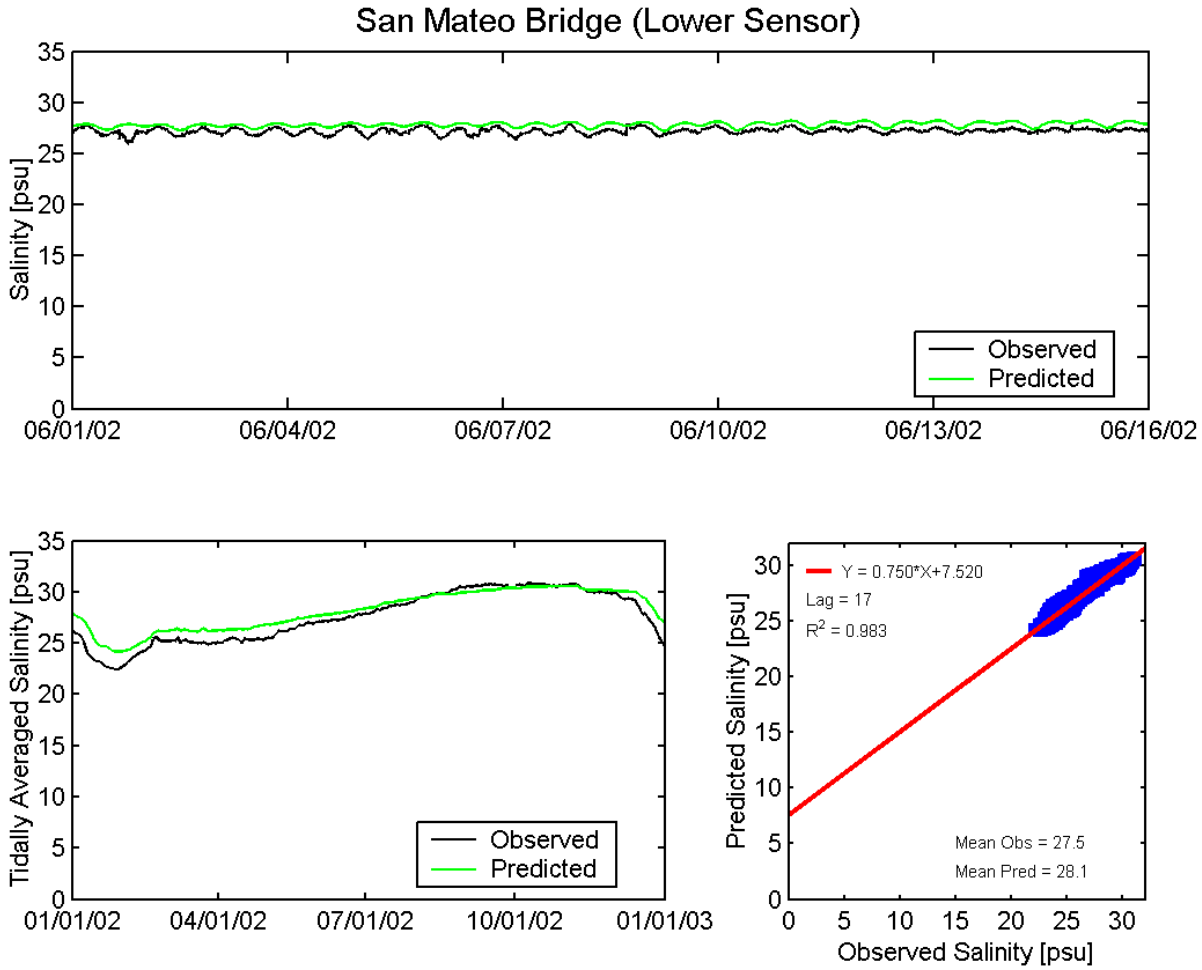

Figure A.6-5 Observed and predicted salinity at San Mateo Bridge USGS station (Lower Sensor) during the 2002 simulation period.

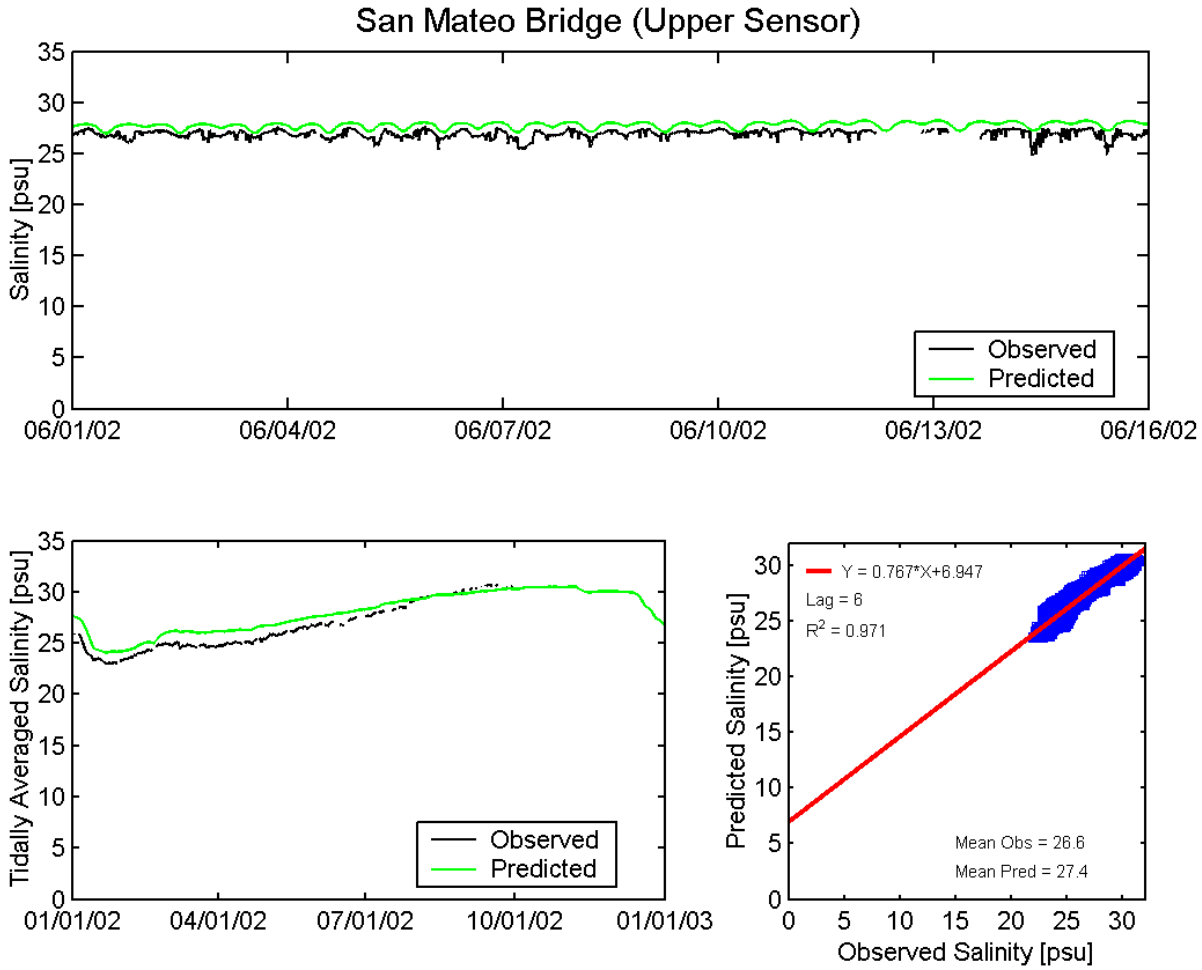

Figure A.6-6 Observed and predicted salinity at San Mateo Bridge USGS station (Upper Sensor) during the 2002 simulation period.

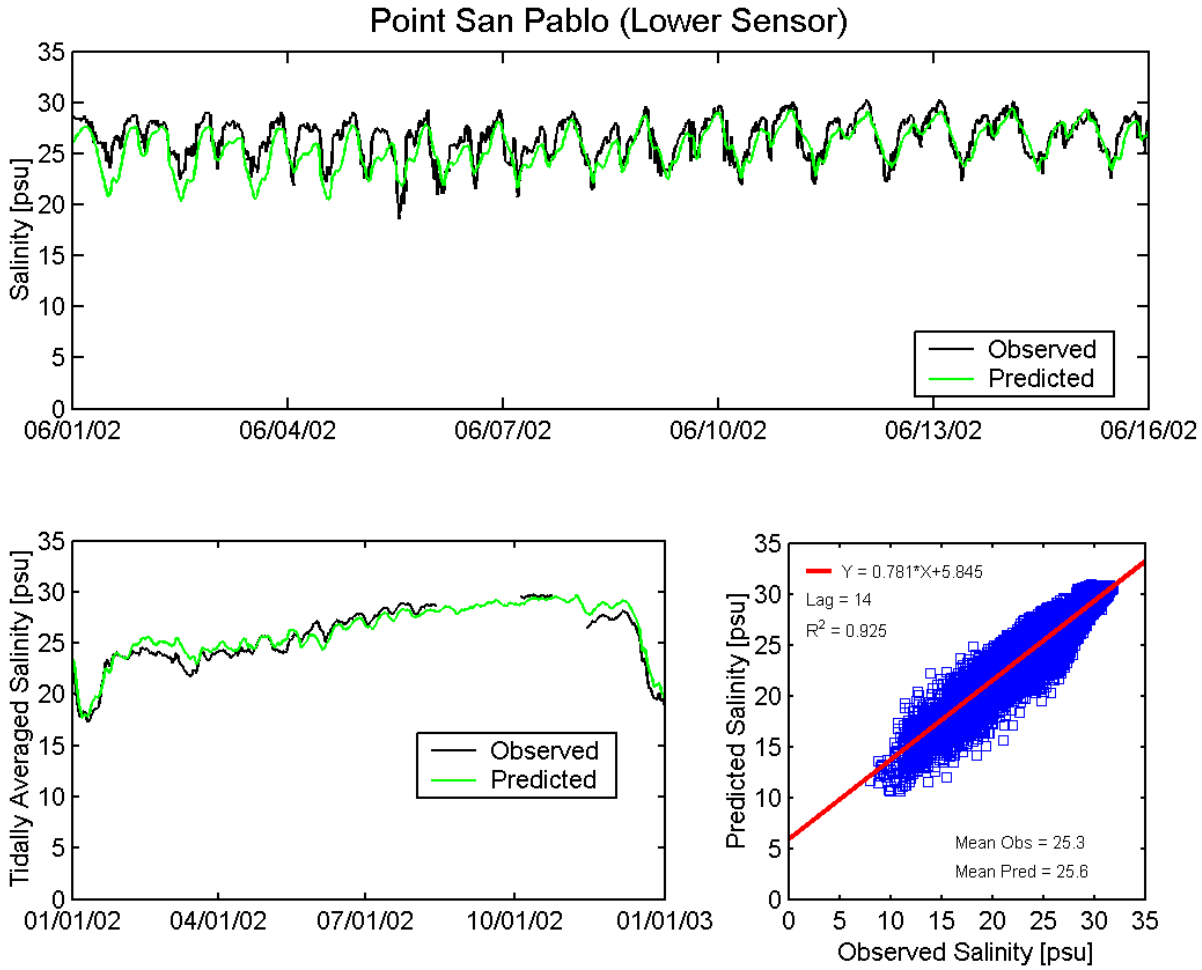

Figure A.6-7 Observed and predicted salinity at Point San Pablo USGS station (Lower Sensor) during the 2002 simulation period.

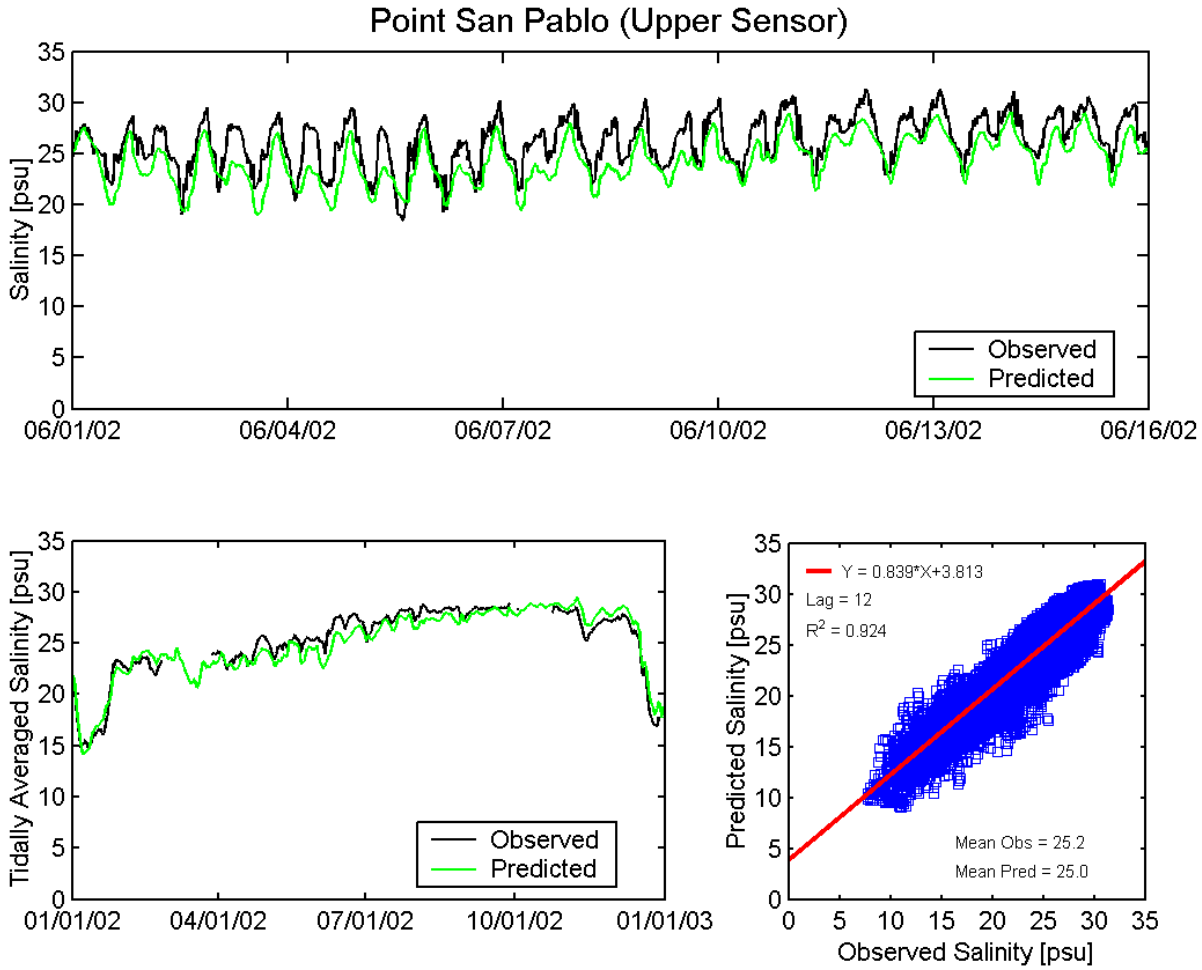

Figure A.6-8 Observed and predicted salinity at Point San Pablo USGS station (Upper Sensor) during the 2002 simulation period.

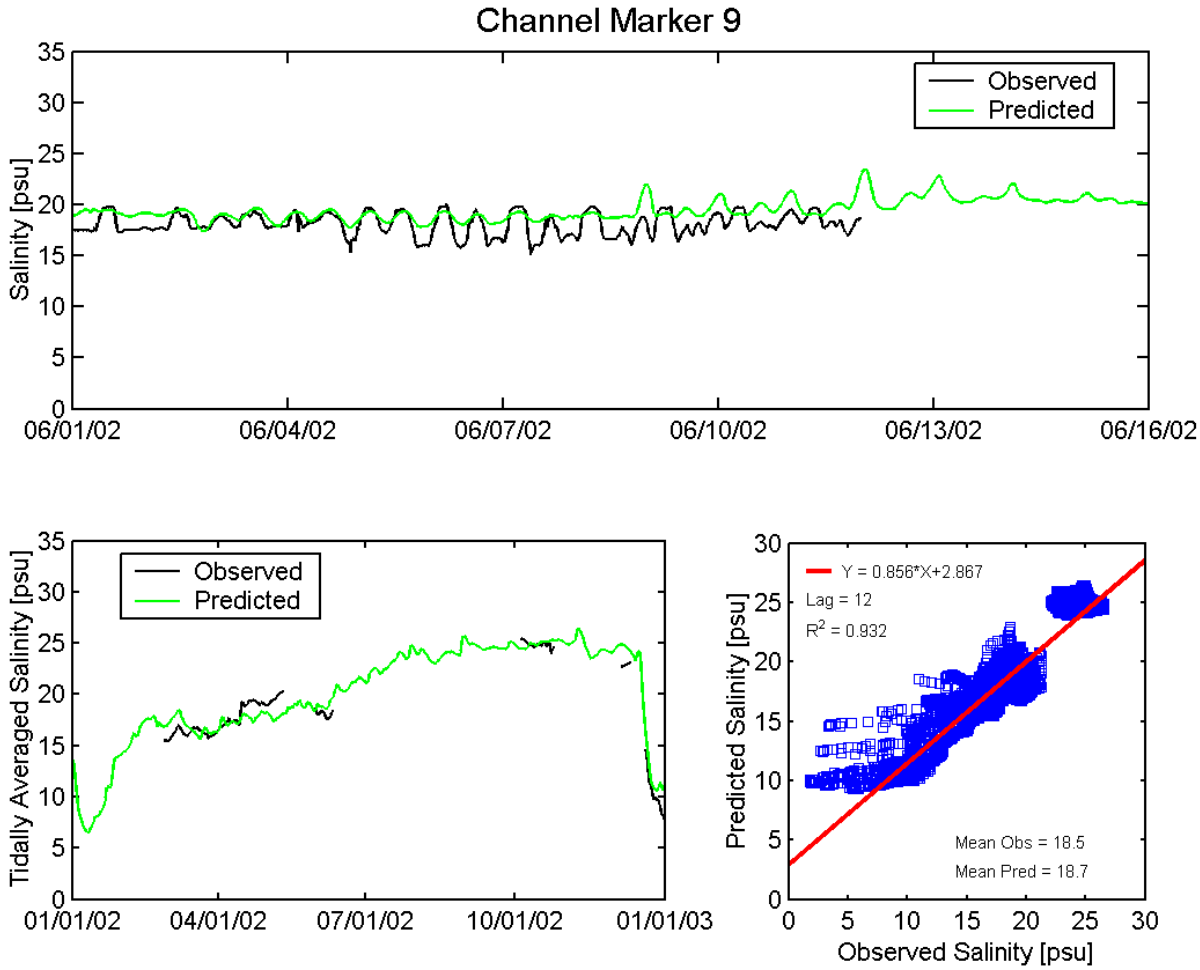

Figure A.6-9 Observed and predicted salinity at Channel Marker 9 USGS station during the 2002 simulation period.

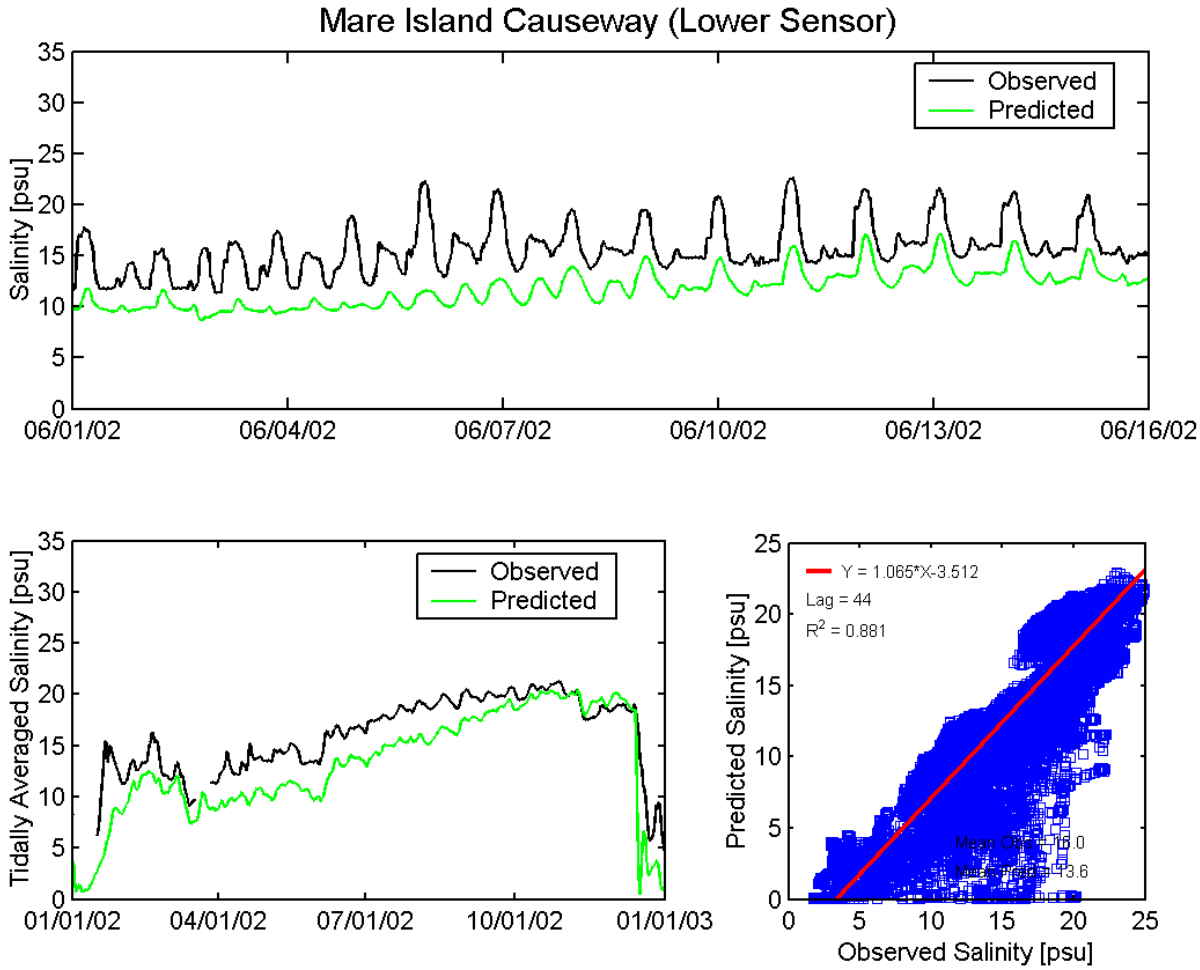

Figure A.6-10 Observed and predicted salinity at Mare Island Causeway USGS station (Lower Sensor) during the 2002 simulation period.

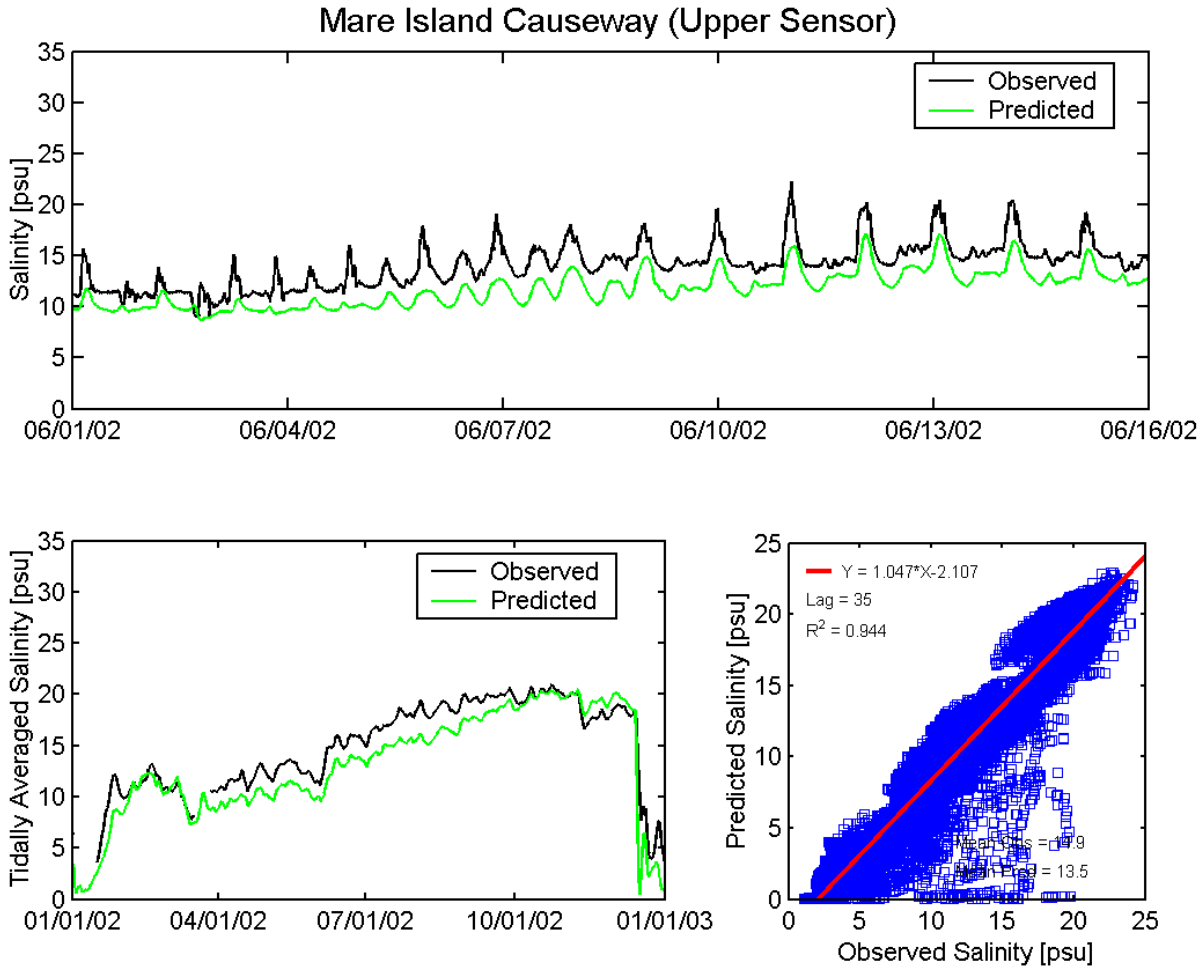

Figure A.6-11 Observed and predicted salinity at Mare Island Causeway USGS station (Upper Sensor) during the 2002 simulation period.

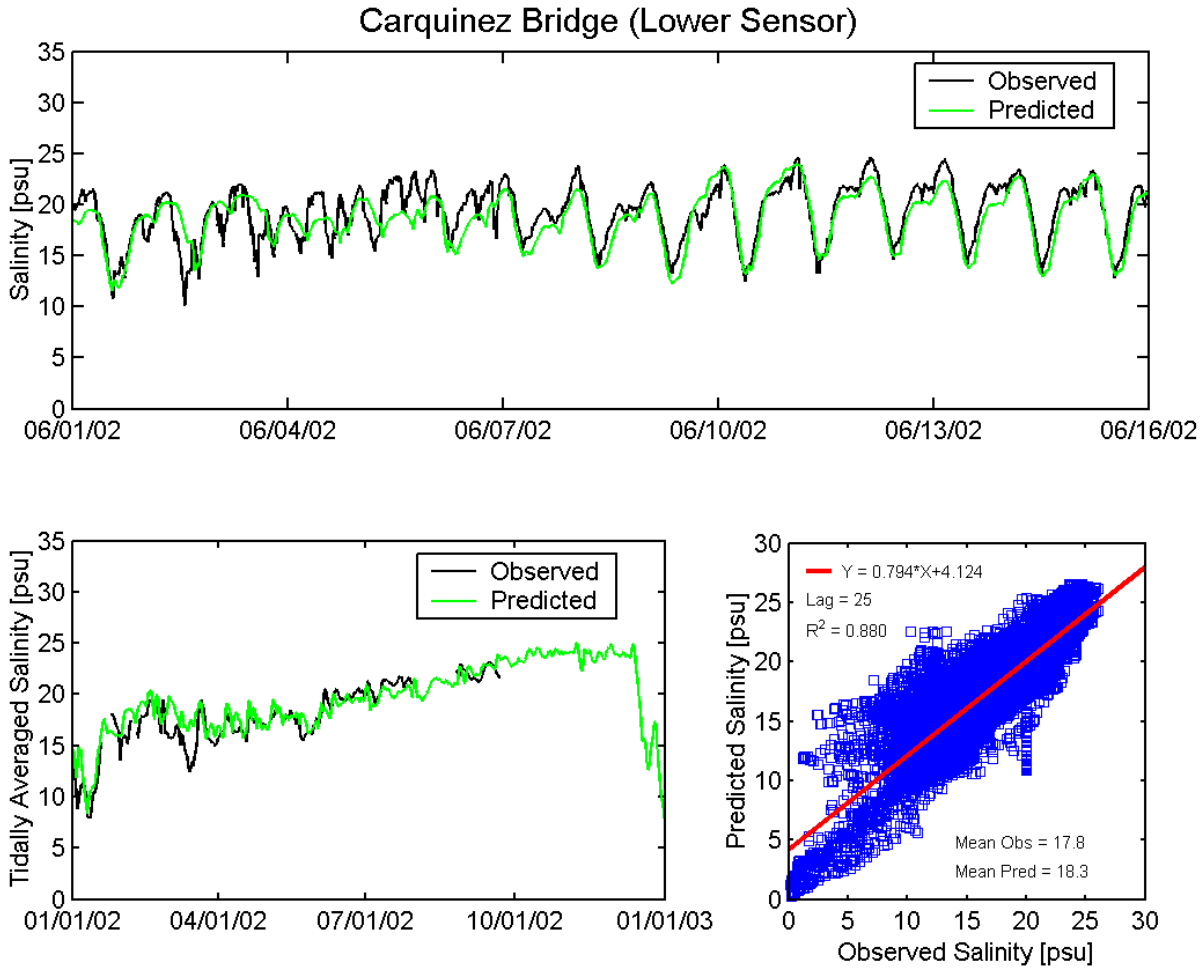

Figure A.6-12 Observed and predicted salinity at Carquinez Bridge USGS station (Lower Sensor) during the 2002 simulation period.

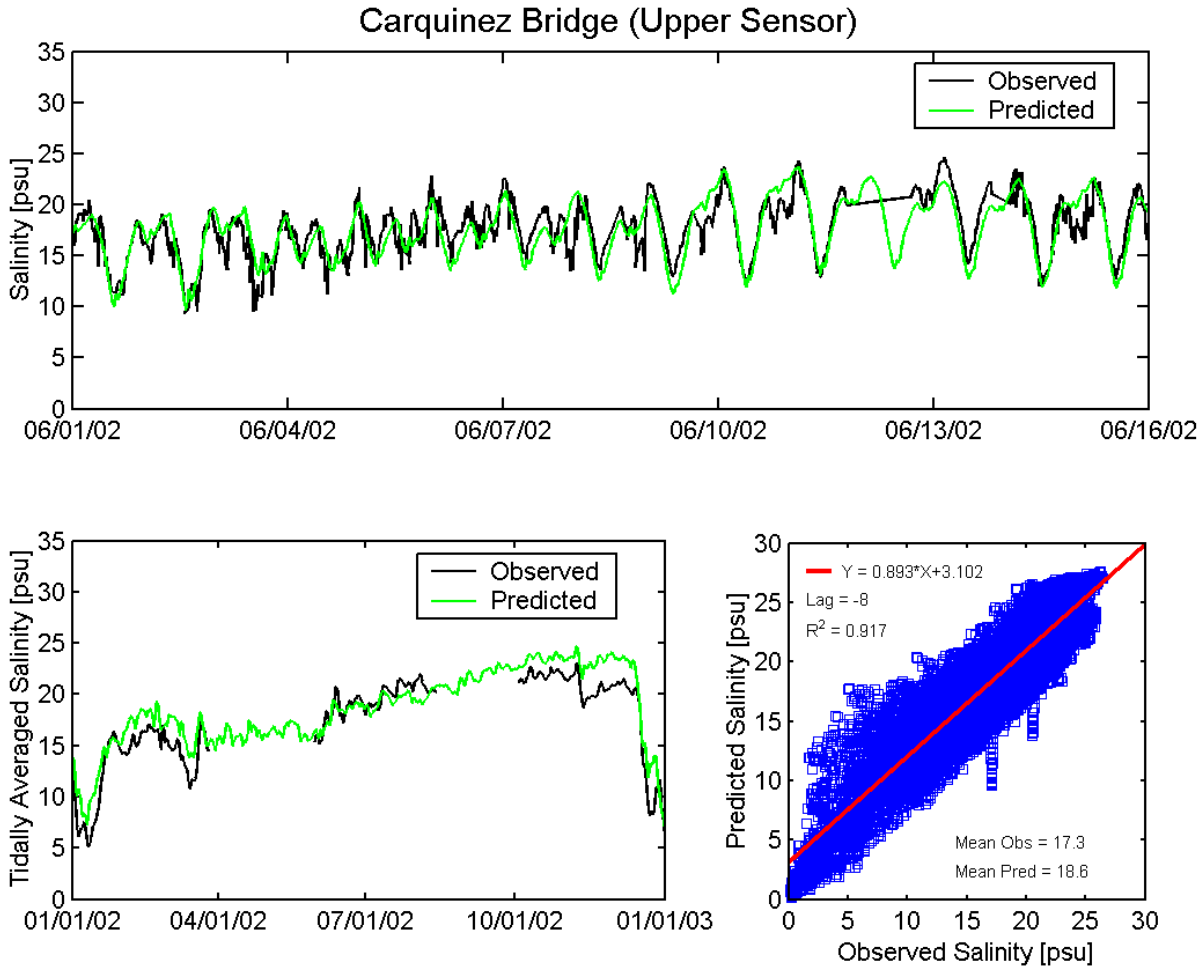

Figure A.6-13 Observed and predicted salinity at Carquinez Bridge USGS station (Upper Sensor) during the 2002 simulation period.

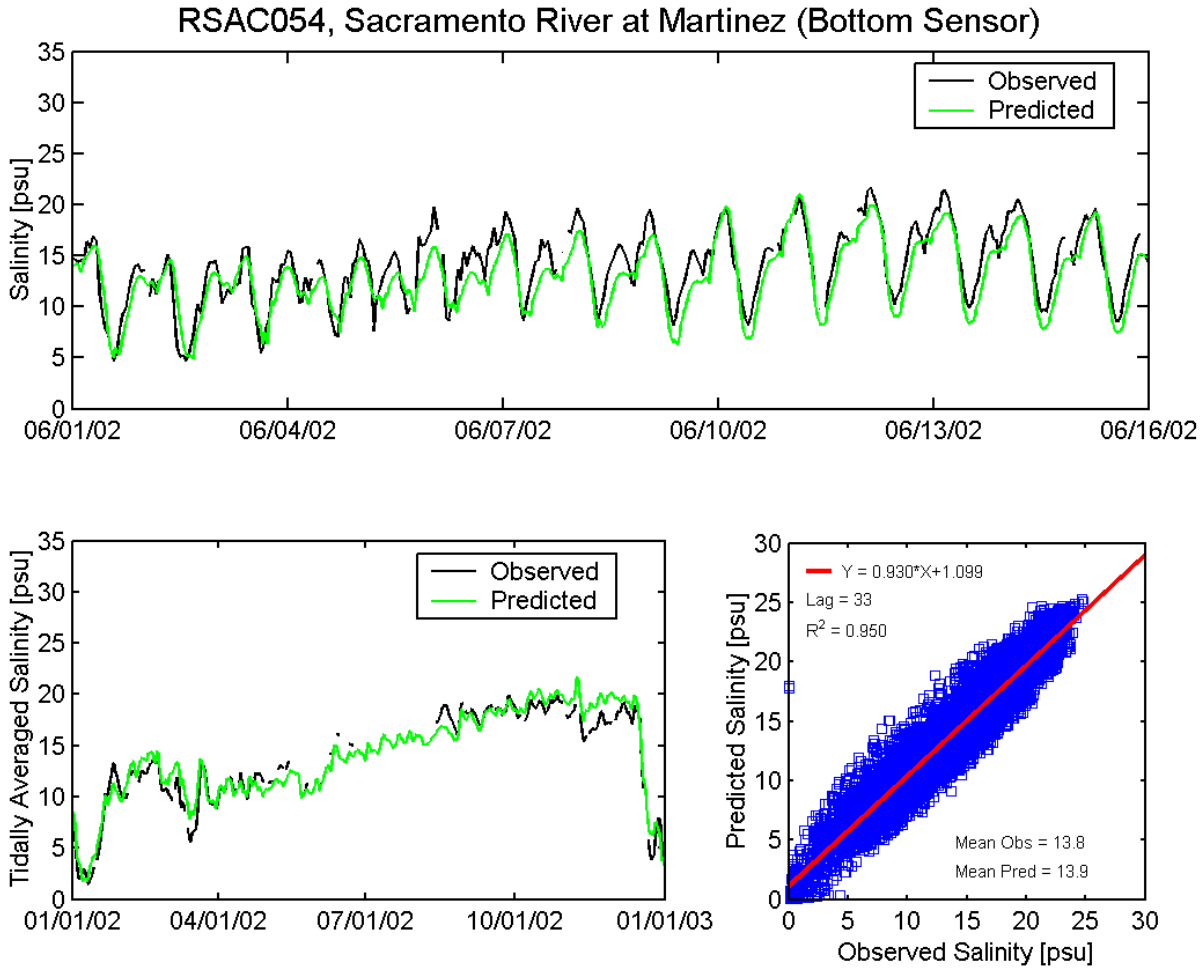

Figure A.6-14 Observed and predicted salinity at Sacramento River at Martinez (Bottom Sensor) DWR station (RSAC054) during the 2002 simulation period.

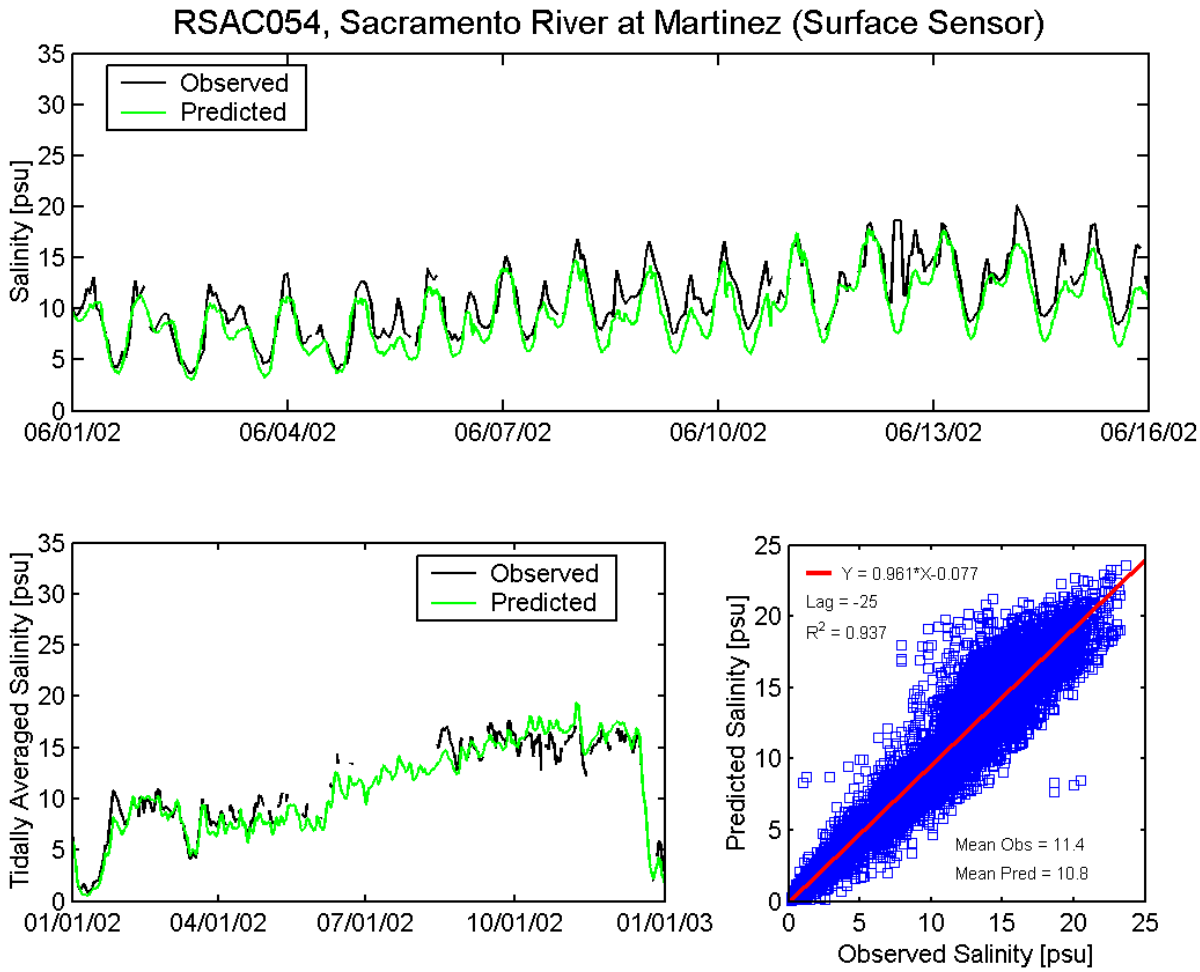

Figure A.6-15 Observed and predicted salinity at Sacramento River at Martinez (Surface Sensor) DWR station (RSAC054) during the 2002 simulation period.

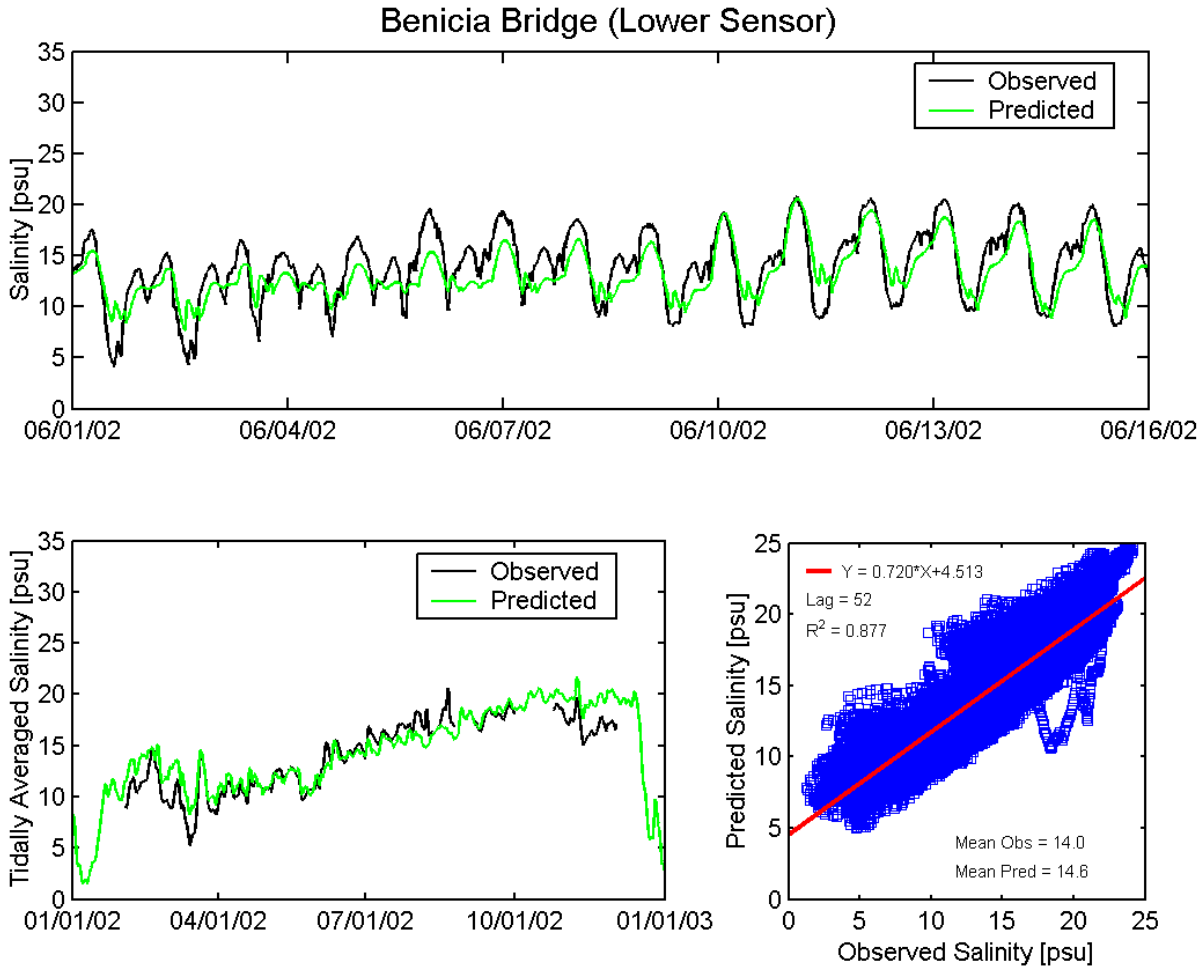

Figure A.6-16 Observed and predicted salinity at Benicia Bridge (Lower Sensor) USGS station during the 2002 simulation period.

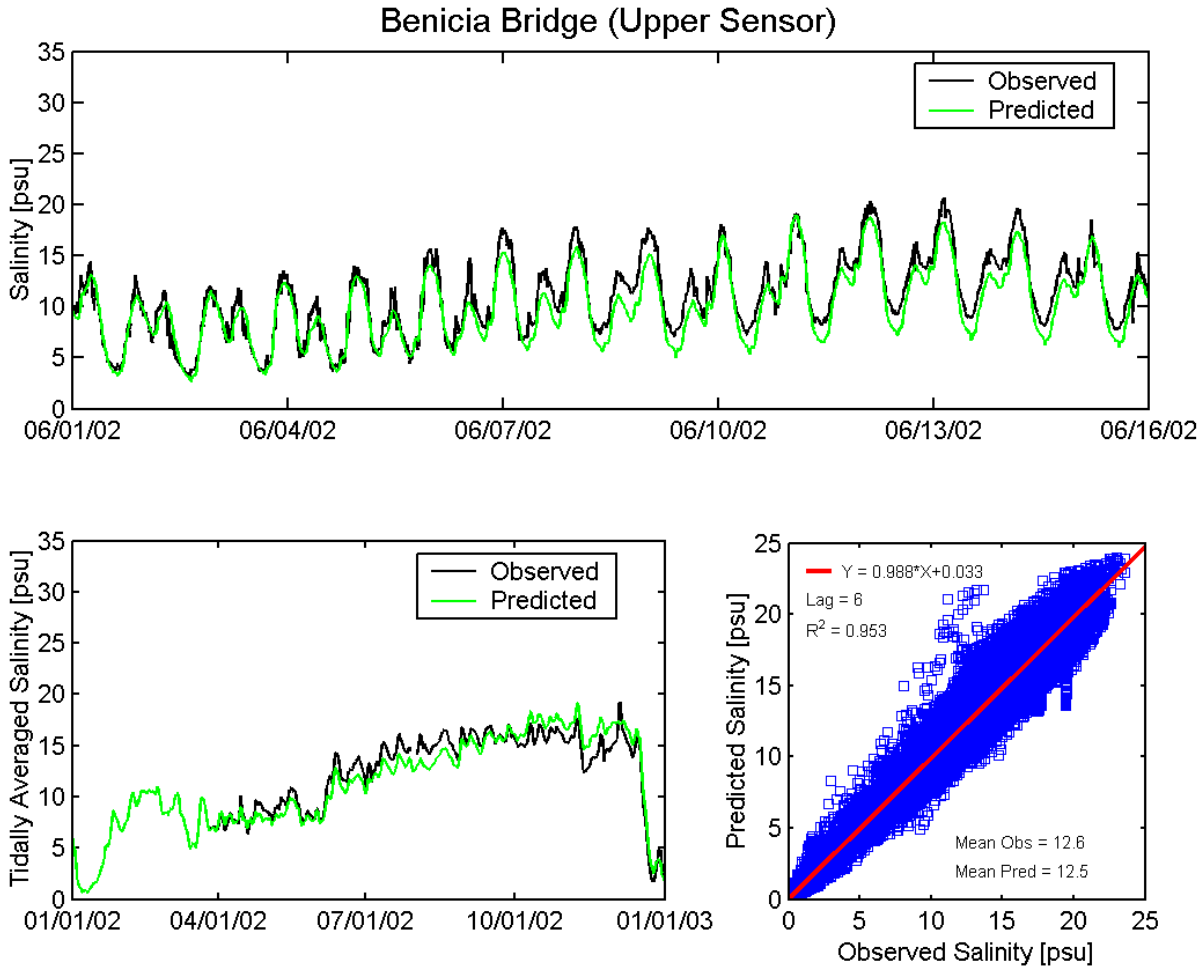

Figure A.6-17 Observed and predicted salinity at Benicia Bridge (Upper Sensor) USGS station during the 2002 simulation period.

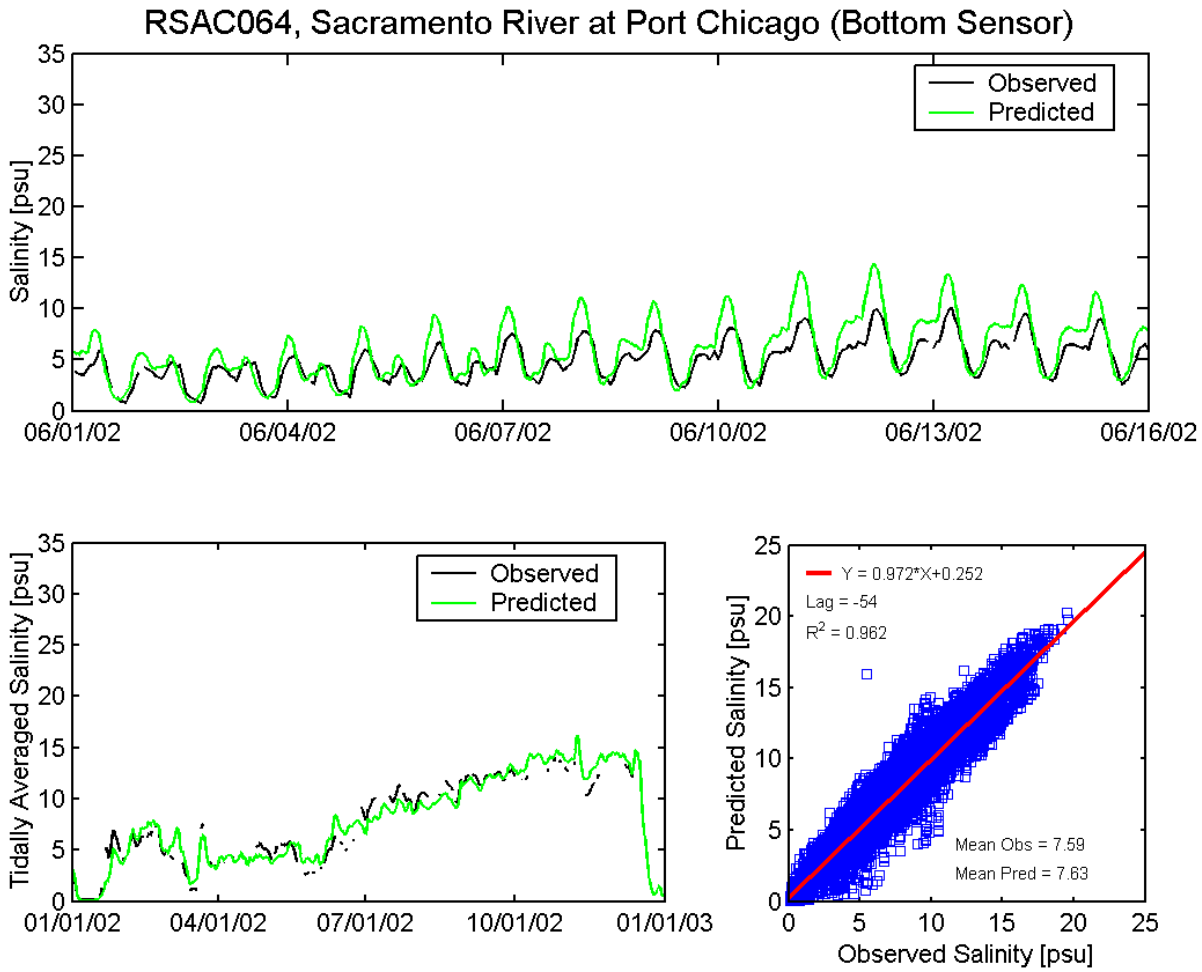

Figure A.6-18 Observed and predicted salinity at Sacramento River at Port Chicago (Bottom Sensor) DWR station (RSAC064) during the 2002 simulation period.

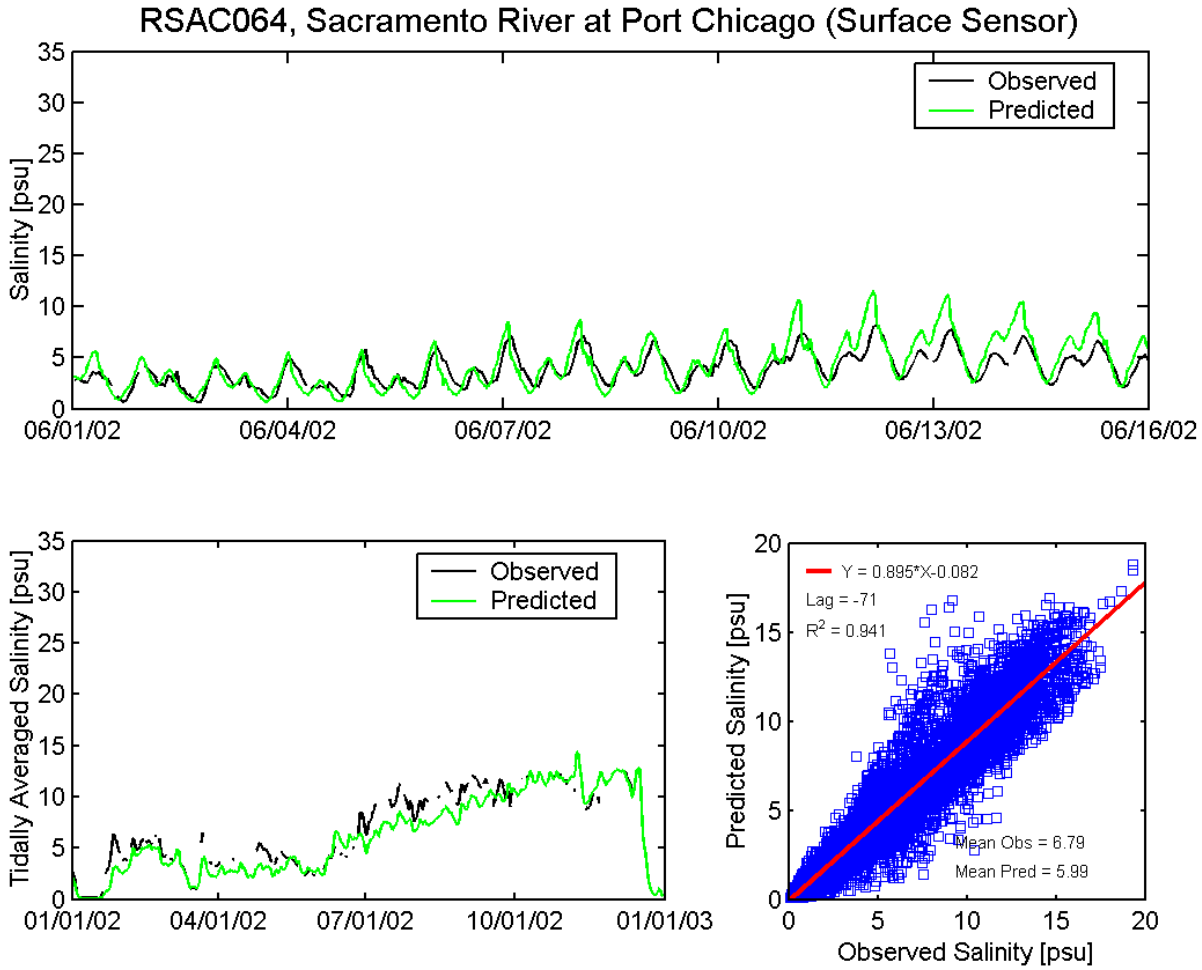

Figure A.6-19 Observed and predicted salinity at Sacramento River at Port Chicago (Surface Sensor) DWR station (RSAC064) during the 2002 simulation period.

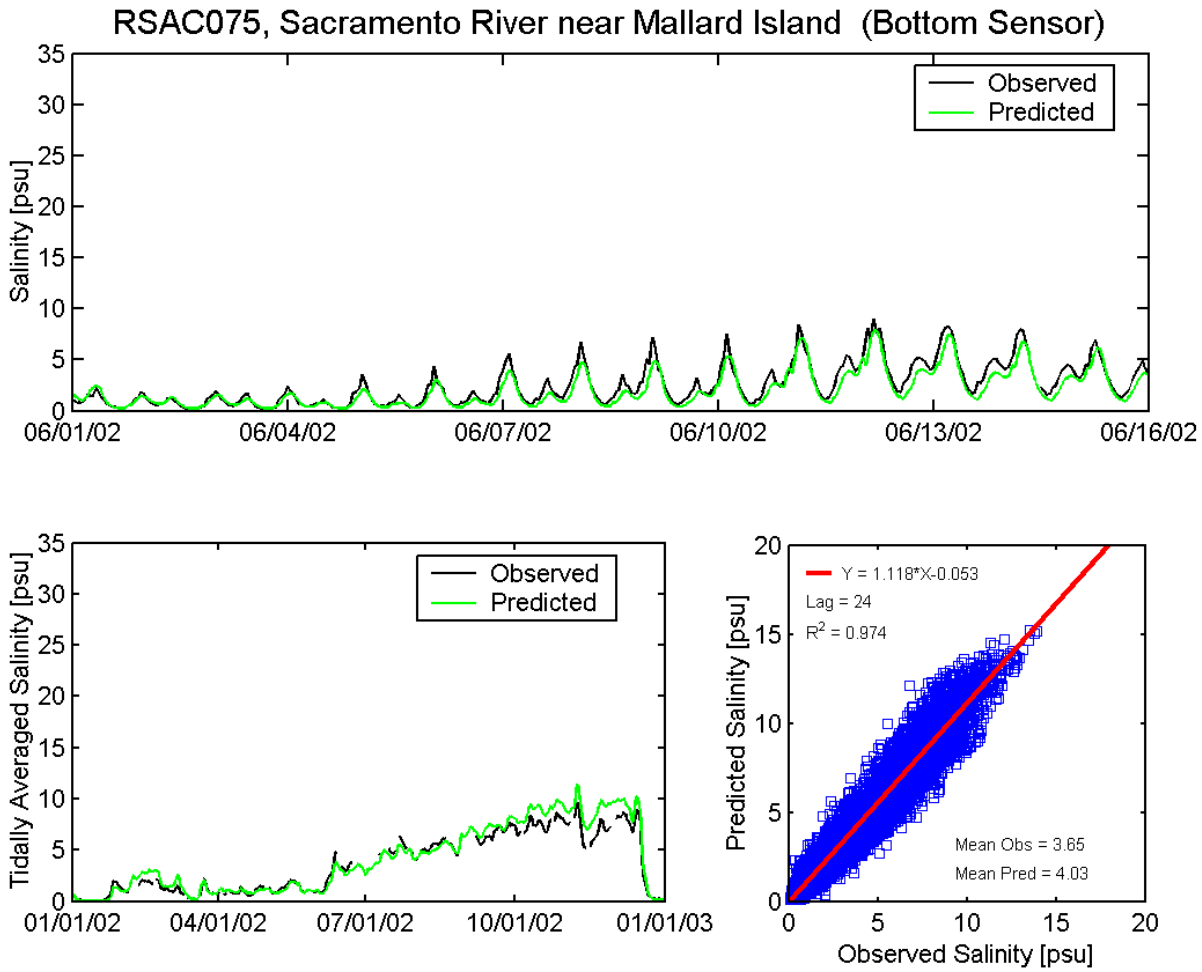

Figure A.6-20 Observed and predicted salinity at Sacramento River near Mallard Island (Bottom Sensor) DWR station (RSAC075) during the 2002 simulation period.

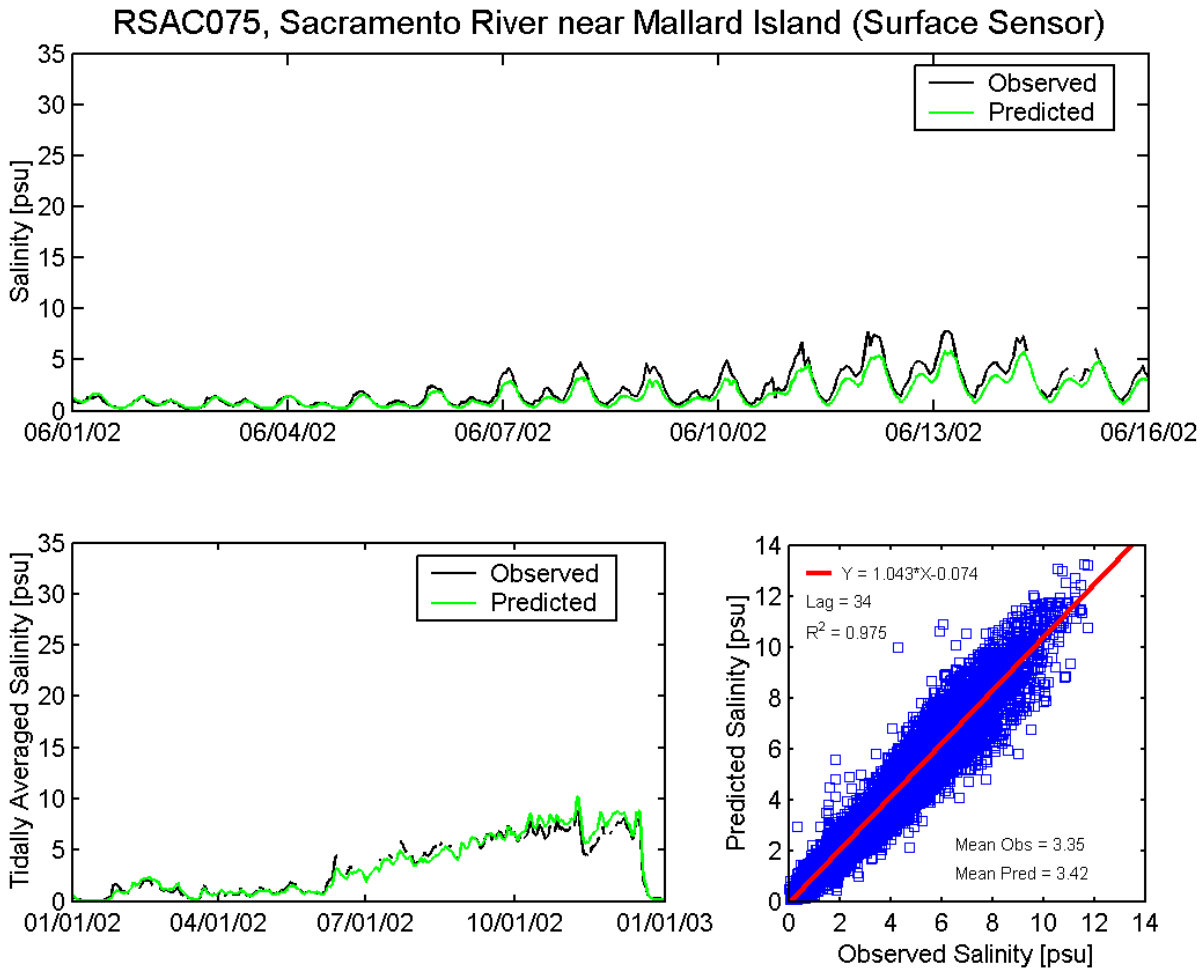

Figure A.6-21 Observed and predicted salinity at Sacramento River near Mallard Island (Surface Sensor) DWR station (RSAC075) during the 2002 simulation period.

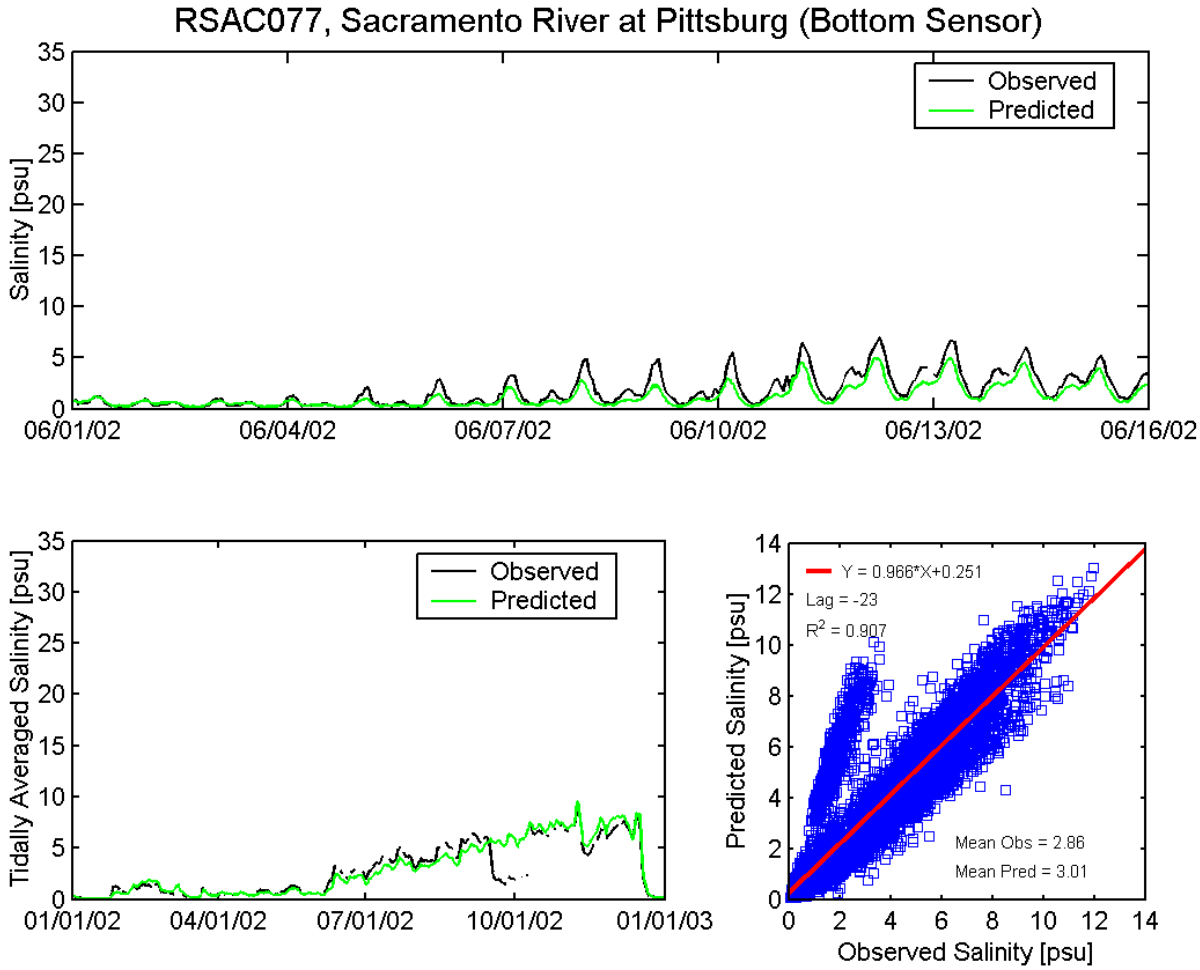

Figure A.6-22 Observed and predicted salinity at Sacramento River at Pittsburgh (Bottom Sensor) DWR station (RSAC077) during the 2002 simulation period.

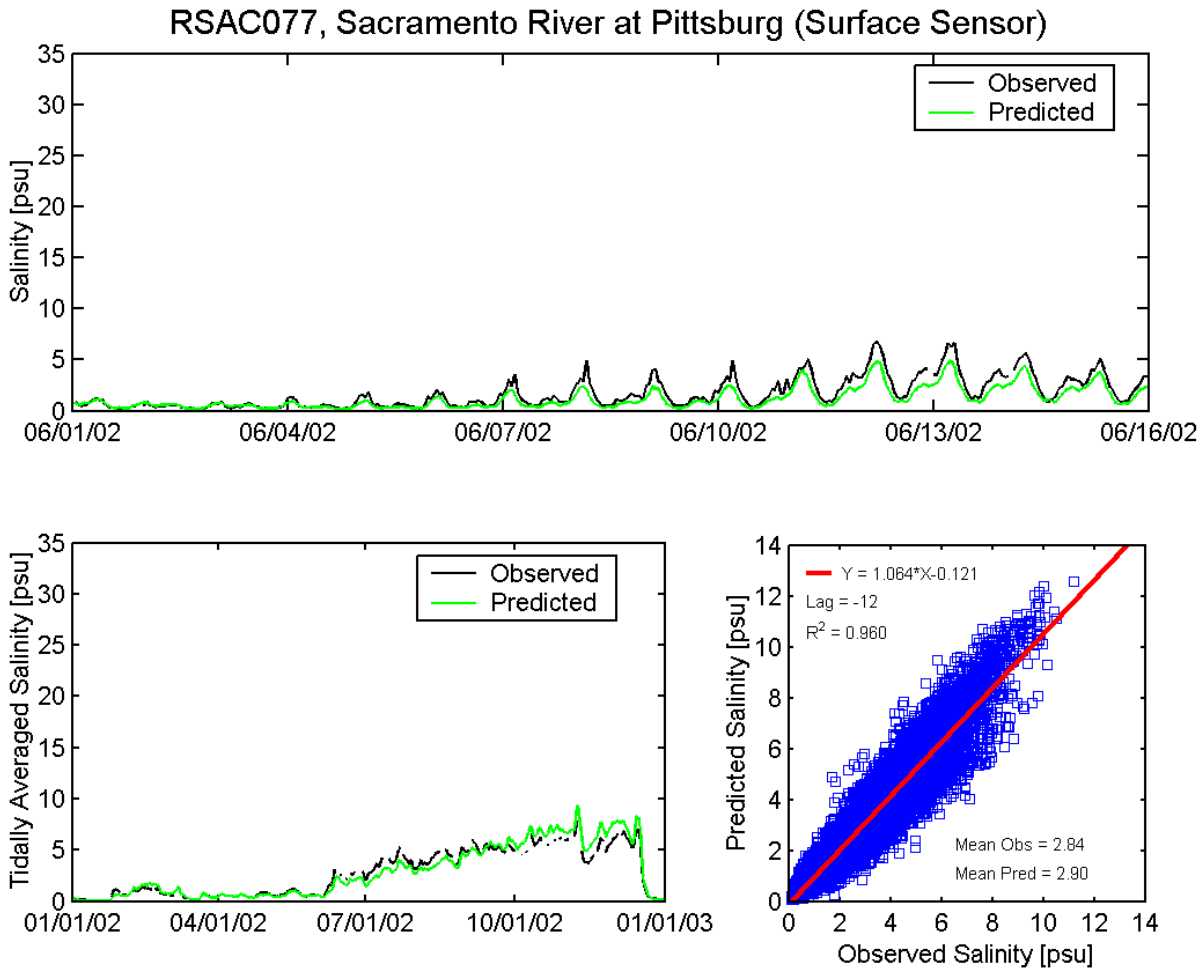

Figure A.6-23 Observed and predicted salinity at Sacramento River at Pittsburgh (Surface Sensor) DWR station (RSAC077) during the 2002 simulation period.

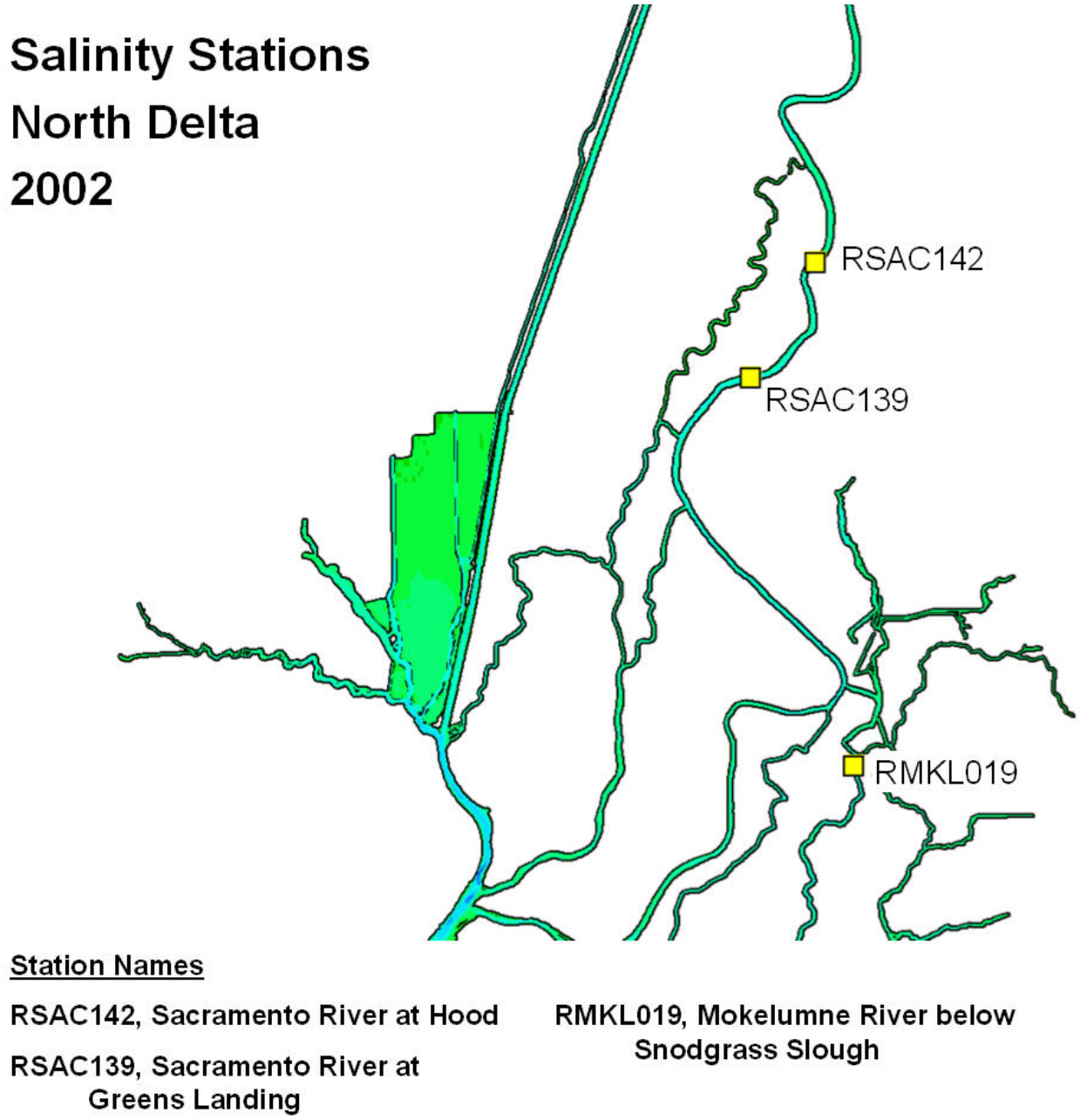

Figure A.6-24 Location of salinity monitoring stations in the northern portion of the Sacramento-San Joaquin Delta used for 2002 salinity comparisons.

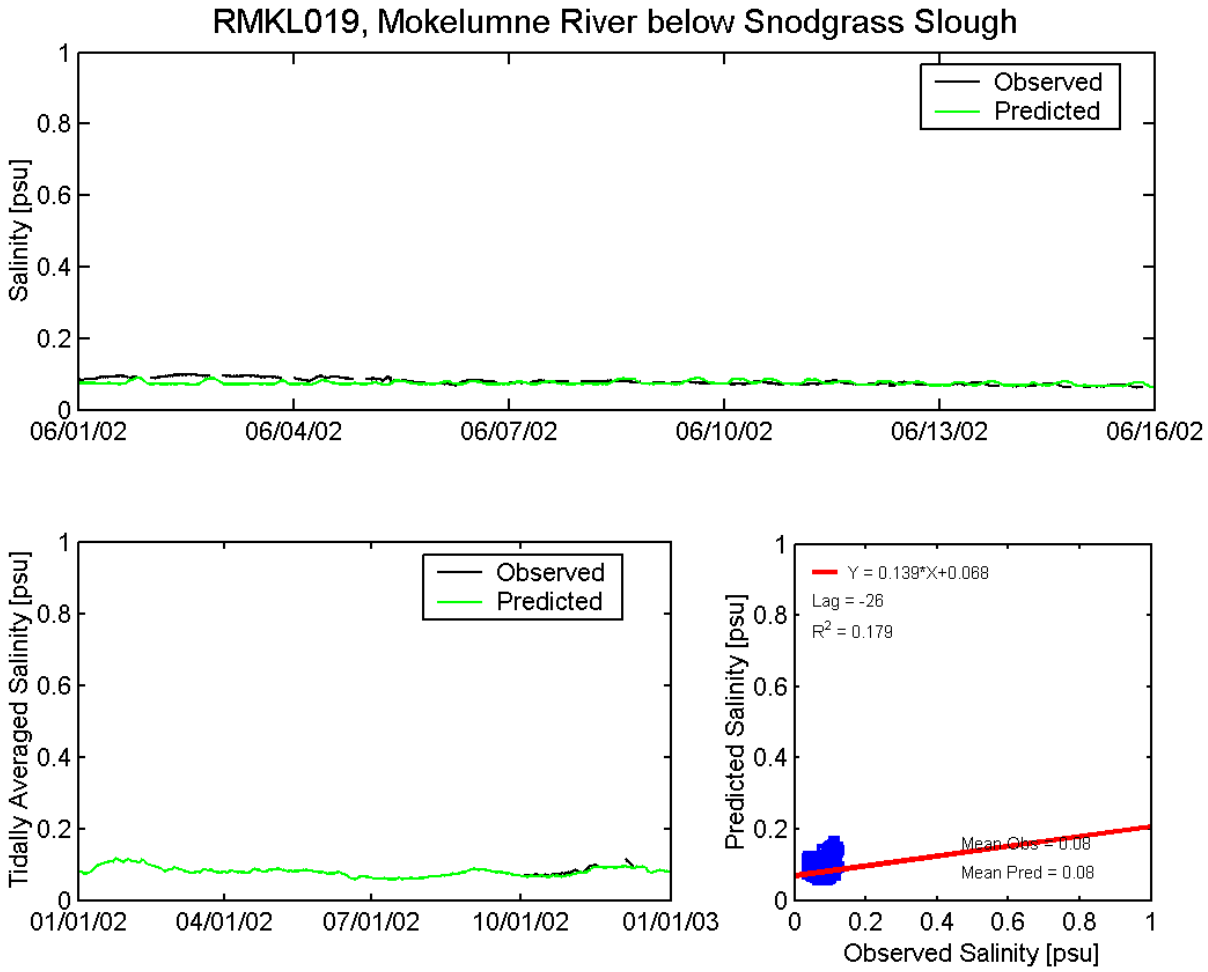

Figure A.6-25 Observed and predicted salinity at Mokelumne River below Snodgrass Slough DWR station (RMKL019) during the 2002 simulation period.

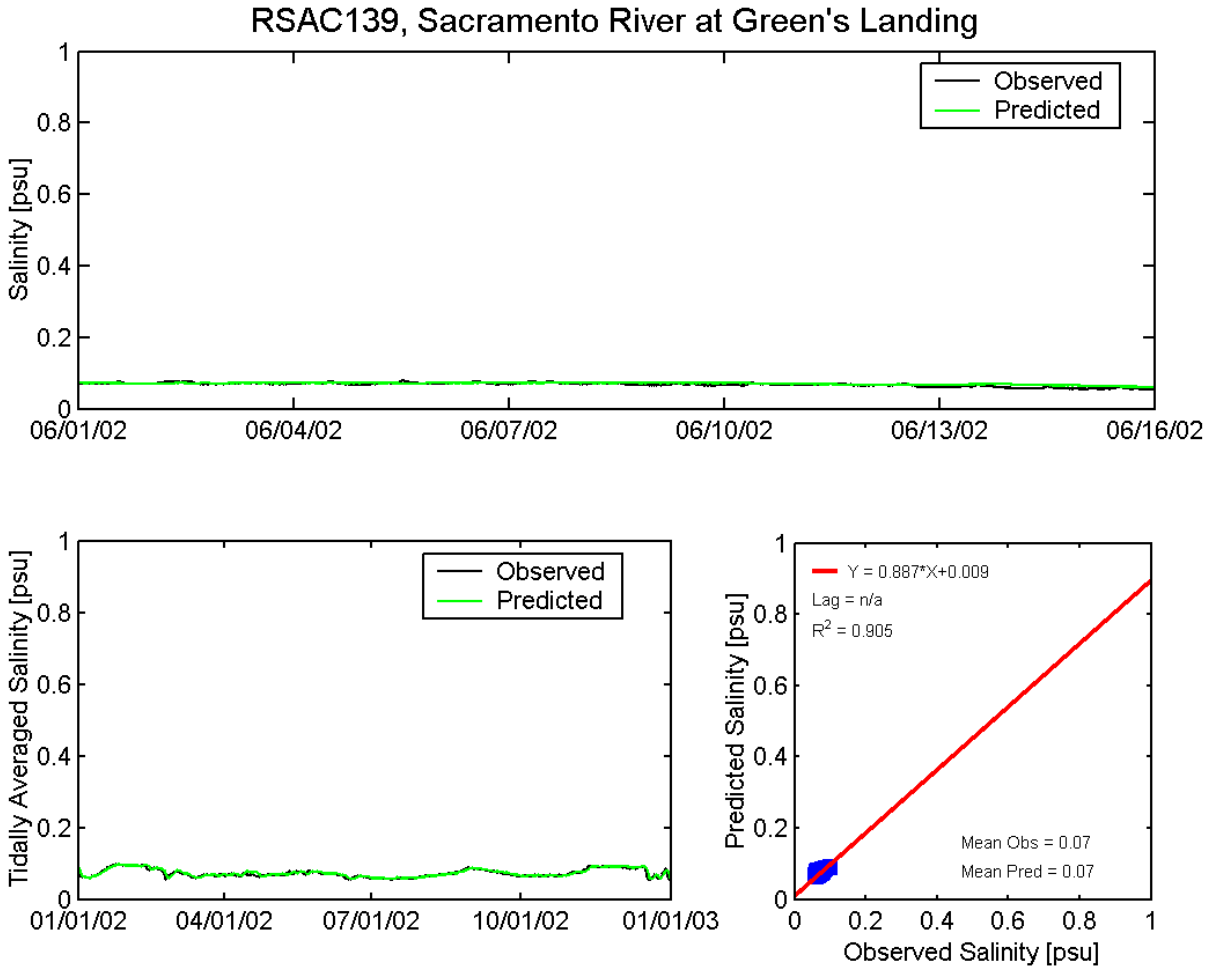

Figure A.6-26 Observed and predicted salinity at Sacramento River at Green's Landing DWR station (RSAC139) during the 2002 simulation period.

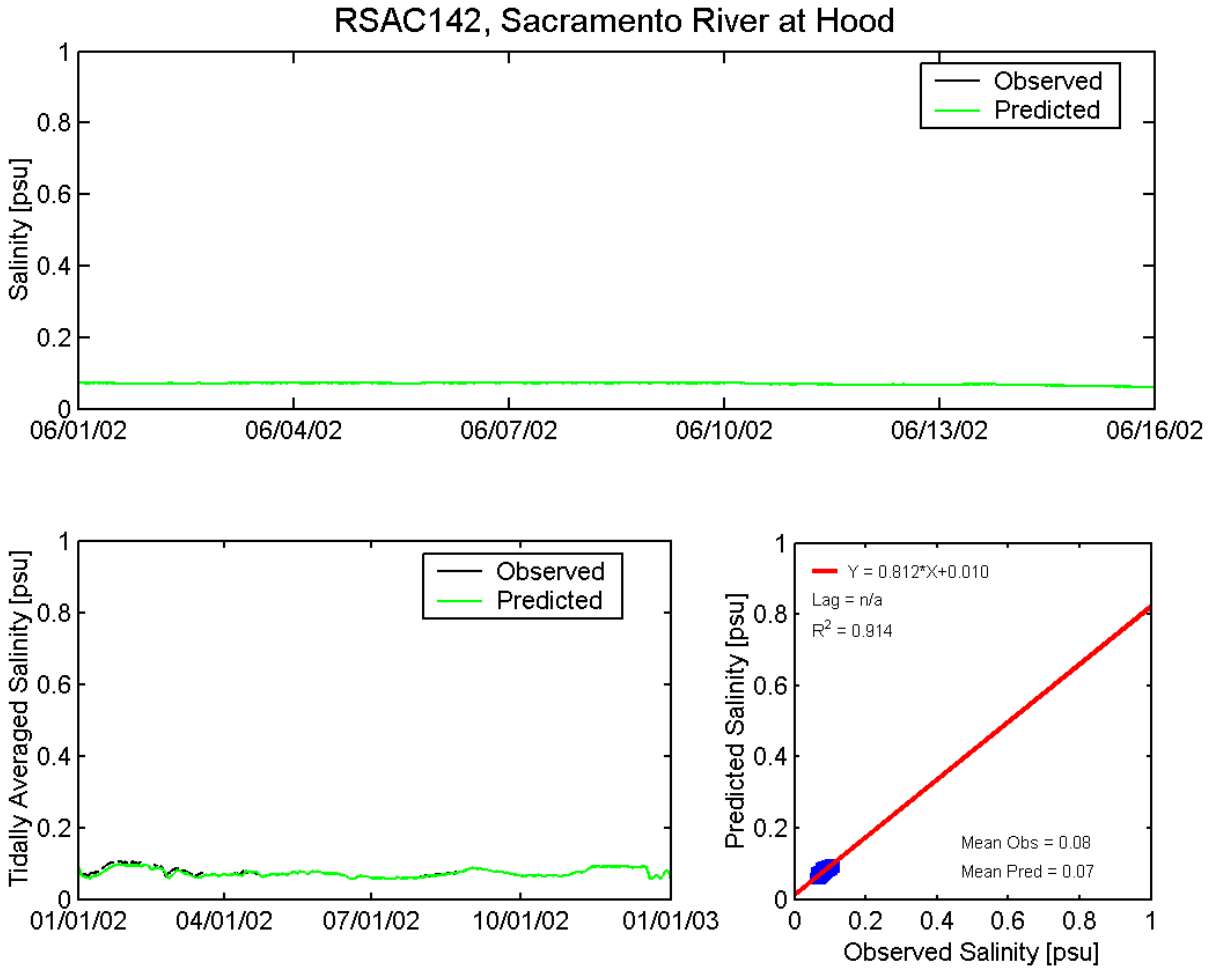

Figure A.6-27 Observed and predicted salinity at Sacramento River at Hood DWR station (RSAC142) during the 2002 simulation period.

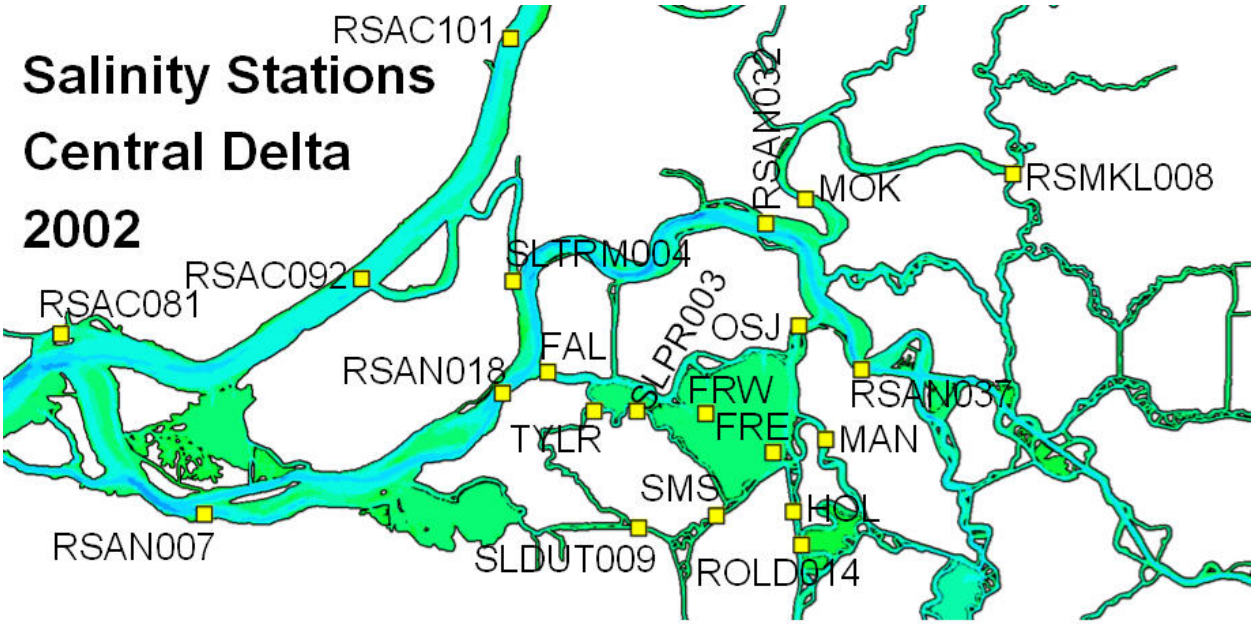

Station Names

RSAC081, Sacramento River at Collinsville

RSAC092, Sacramento River at Emmaton

RSAC101, Sacramento River at Rio Vista

SLTRM004, Threemile Slough at San Joaquin River

RSAN007, San Joaquin River at Antioch

RSAN018, San Joaquin River at Jersey Point

SLDUT009, Dutch Slough at Jersey Island

FAL, False River

TYLR, Taylor Slough

SMS, Sand Mound Slough

SLPR003, Piper Slough at Bethel

RSAN032, San Joaquin River at San Andreas Landing

OSJ, Old River at San Joaquin River

RSAN037, San Joaquin River before Prisoners Point

MOK, Mokelumne River near San Joaquin River

RSMKL008, South Fork Mokelumne River at Staten Island

FRE, Franks Tract East

FRW, Franks Tract West

MAN, Old River at Mandeville Island

HOL, Holland Cut

ROLD014, Old River and Holland Cut at Mandeville Island

Figure A.6-28 Location of salinity monitoring stations in the central portion of the Sacramento-San Joaquin Delta used for 2002 salinity comparisons.

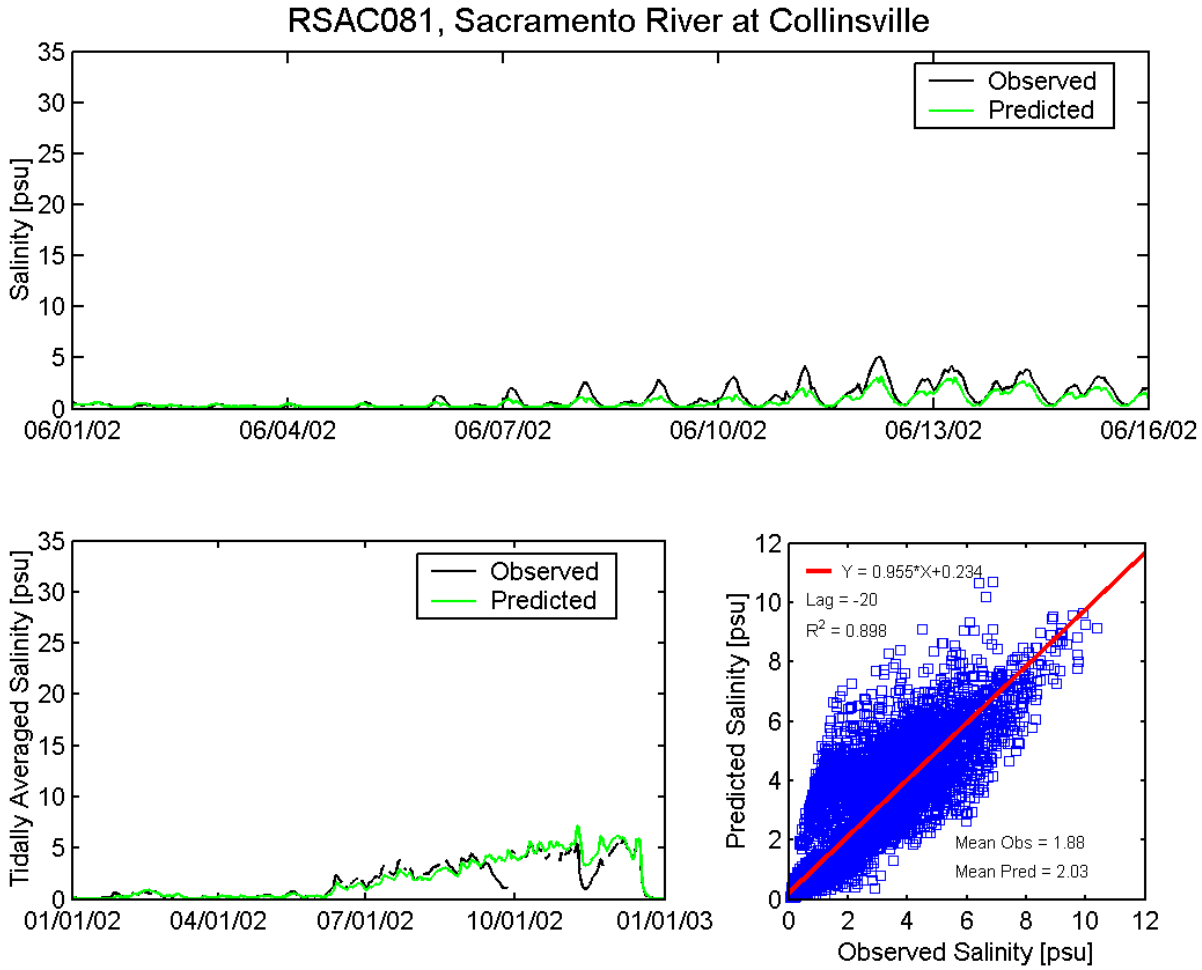

Figure A.6-29 Observed and predicted salinity at Sacramento River at Collinsville DWR station (RSAC081) during the 2002 simulation period.

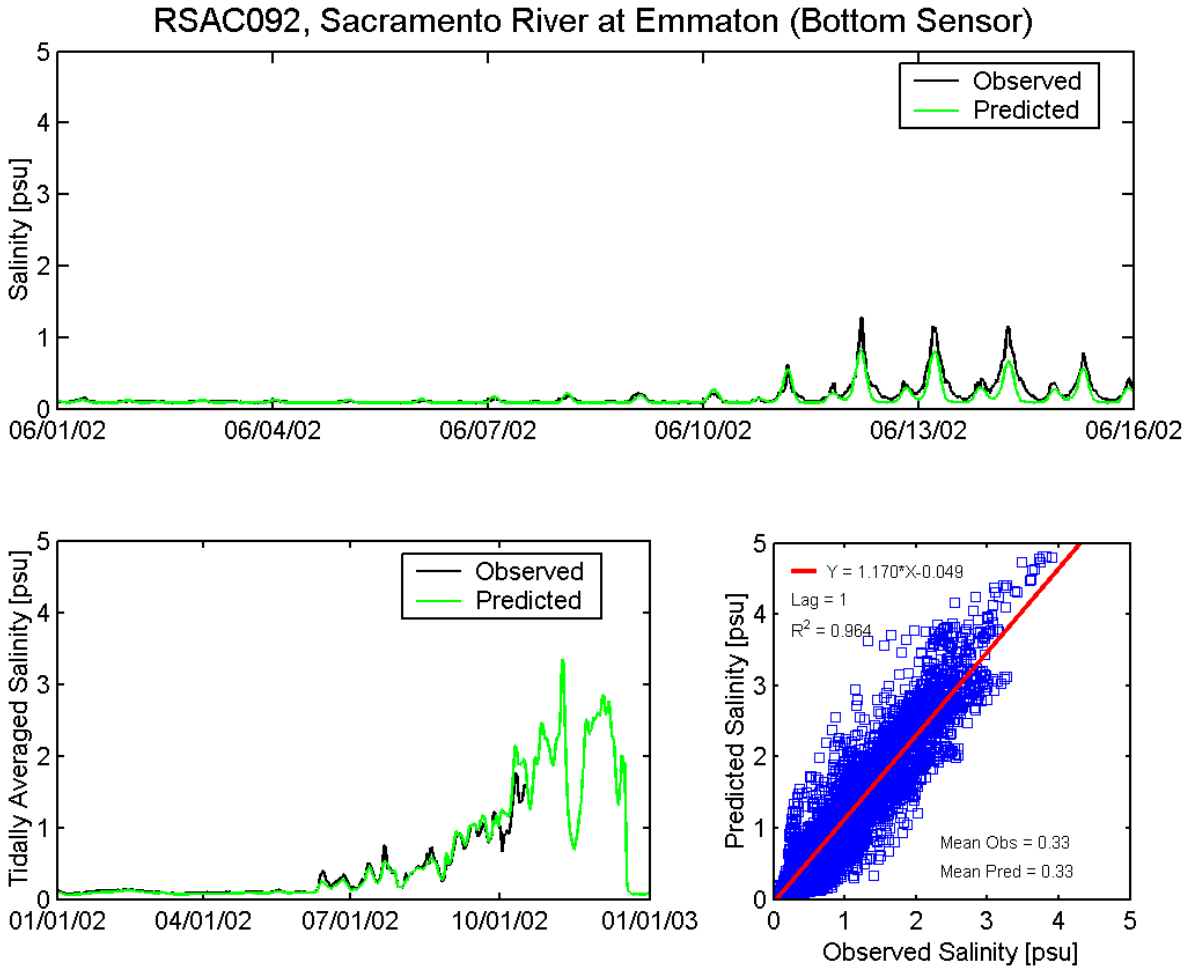

Figure A.6-30 Observed and predicted salinity at Sacramento River at Emmaton (Bottom Sensor) DWR station (RSAC092) during the 2002 simulation period.

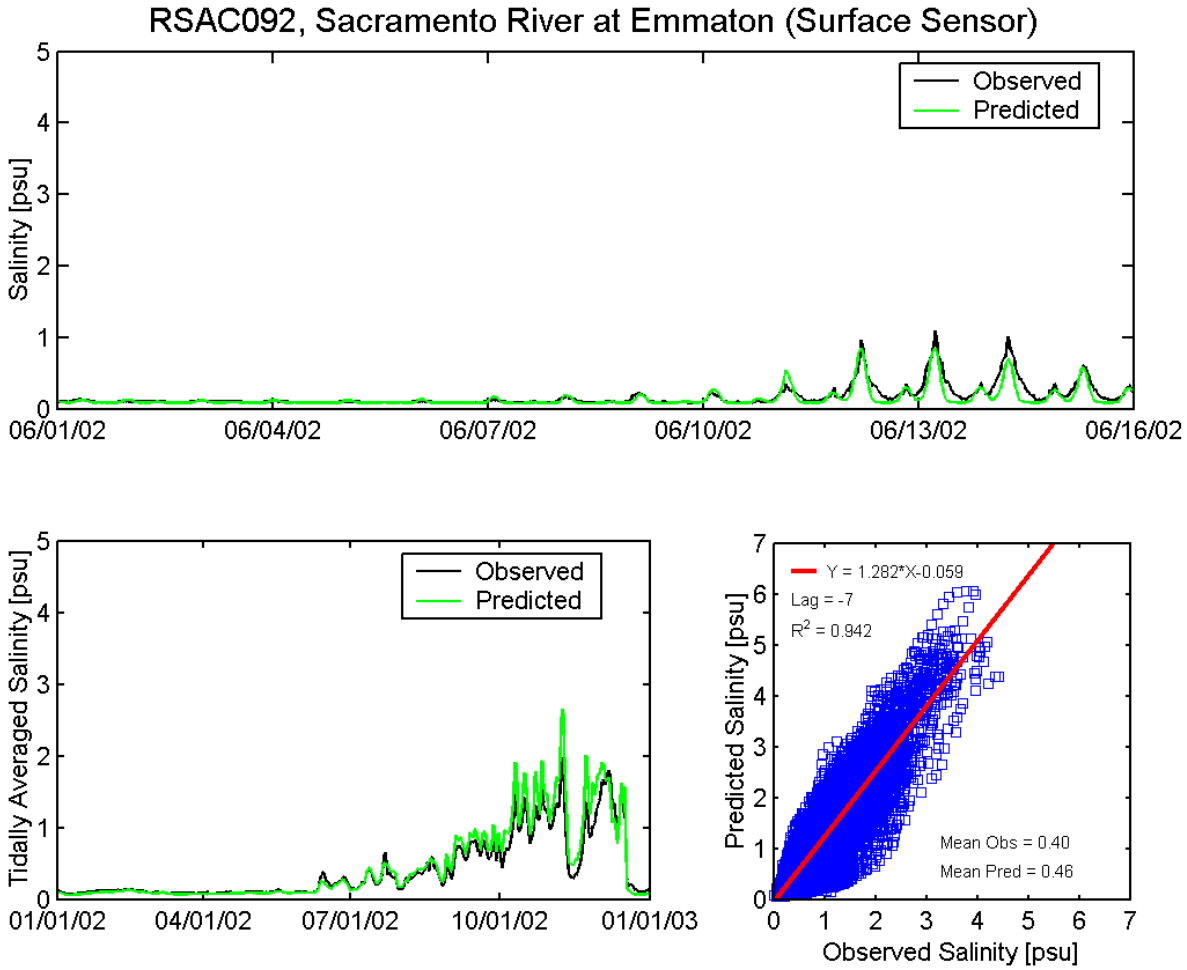

Figure A.6-31 Observed and predicted salinity at Sacramento River at Emmaton (Surface Sensor) DWR station (RSAC092) during the 2002 simulation period.

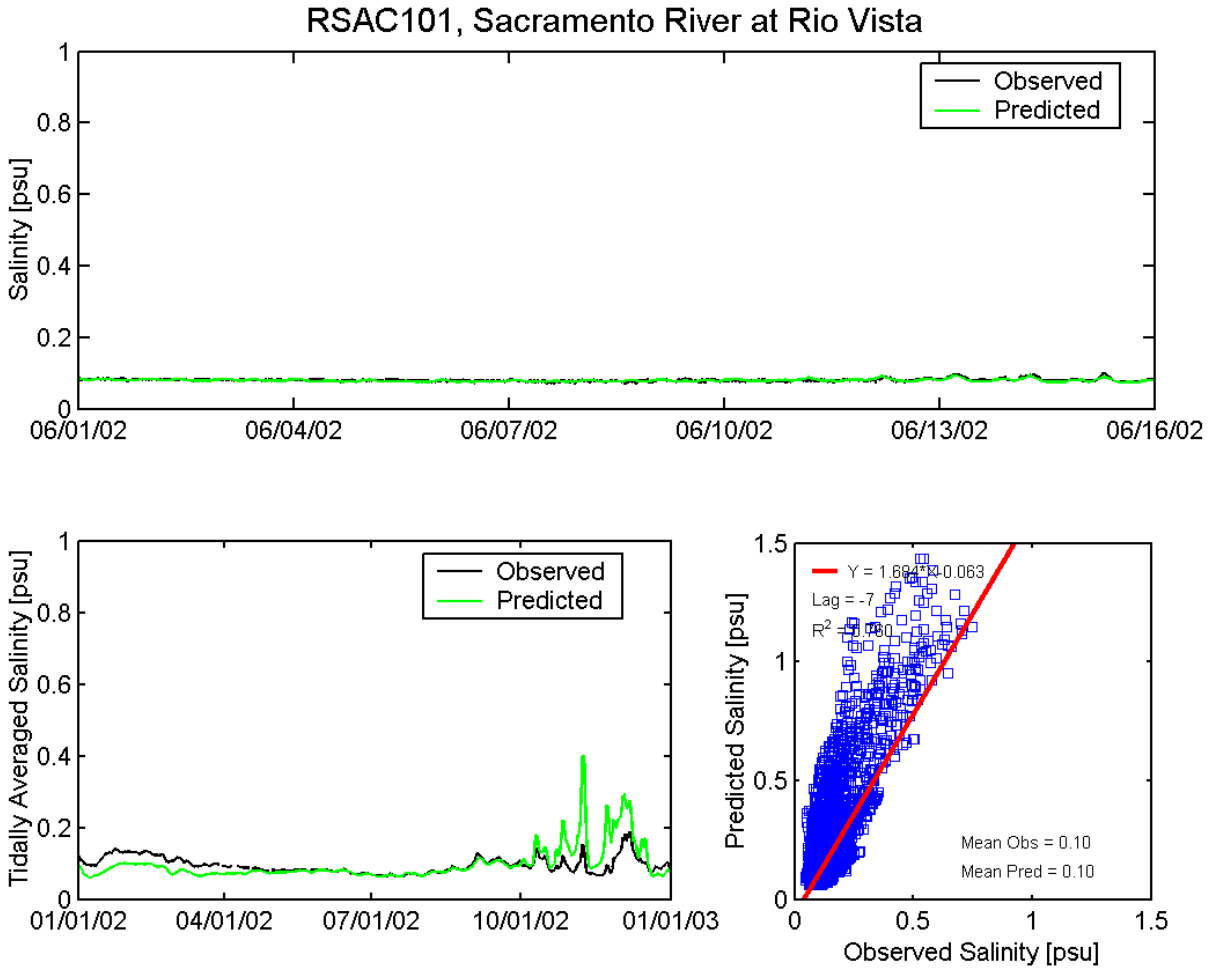

Figure A.6-32 Observed and predicted salinity at Sacramento River at Rio Vista DWR station (RSAC101) during the 2002 simulation period.

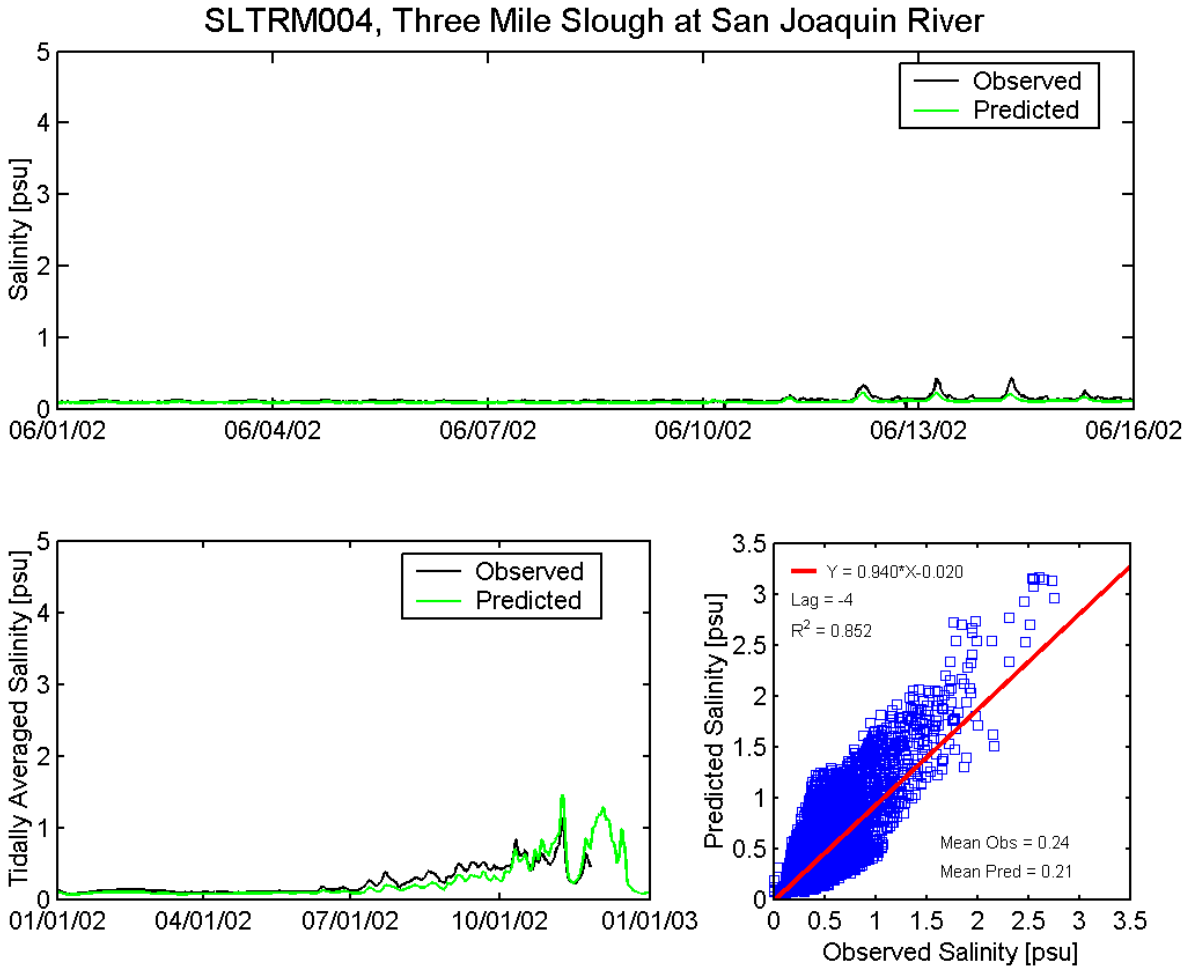

Figure A.6-33 Observed and predicted salinity at Threemile Slough at San Joaquin River DWR station (SLTRM004) during the 2002 simulation period.

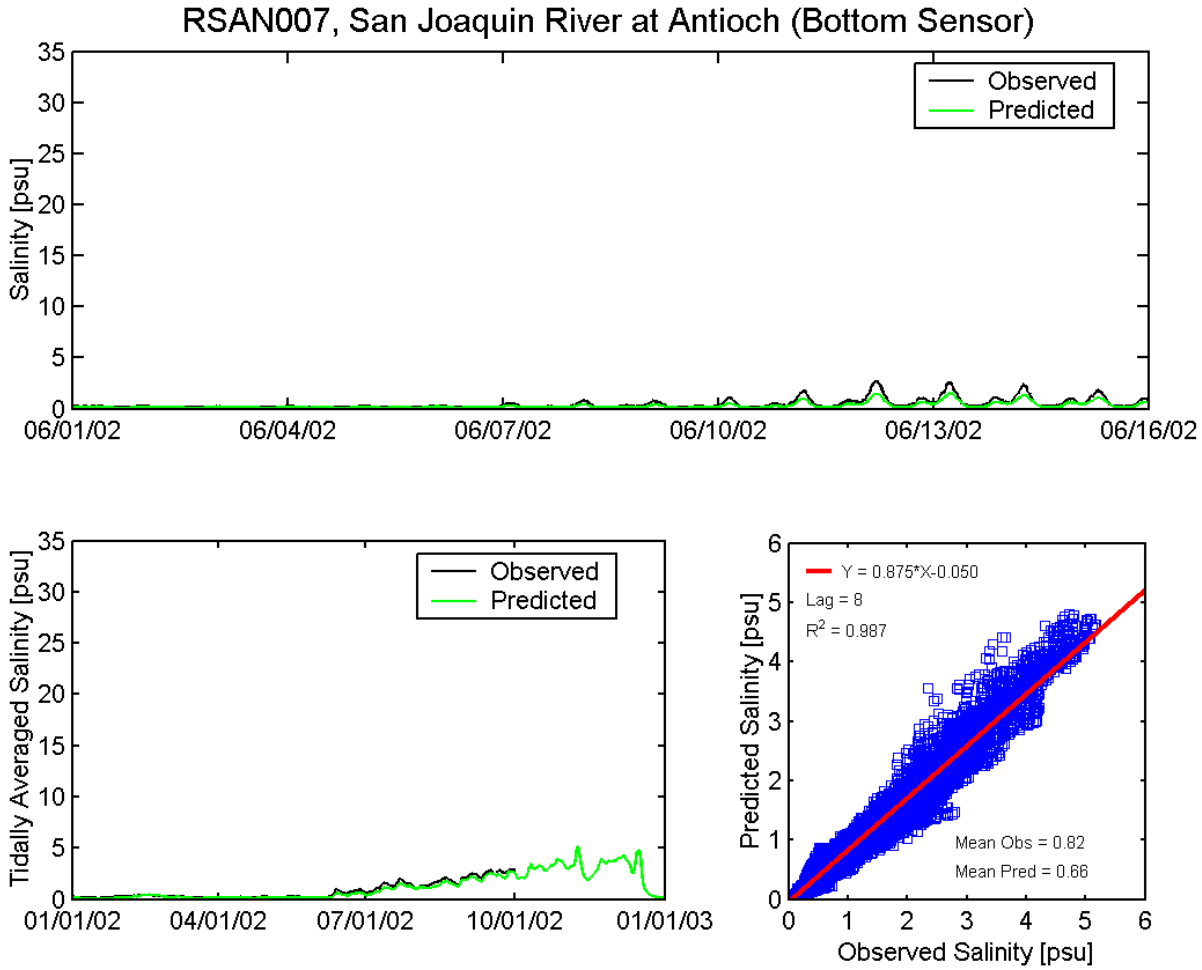

Figure A.6-34 Observed and predicted salinity at Antioch (Bottom Sensor) DWR station (RSAN007) during the 2002 simulation period.

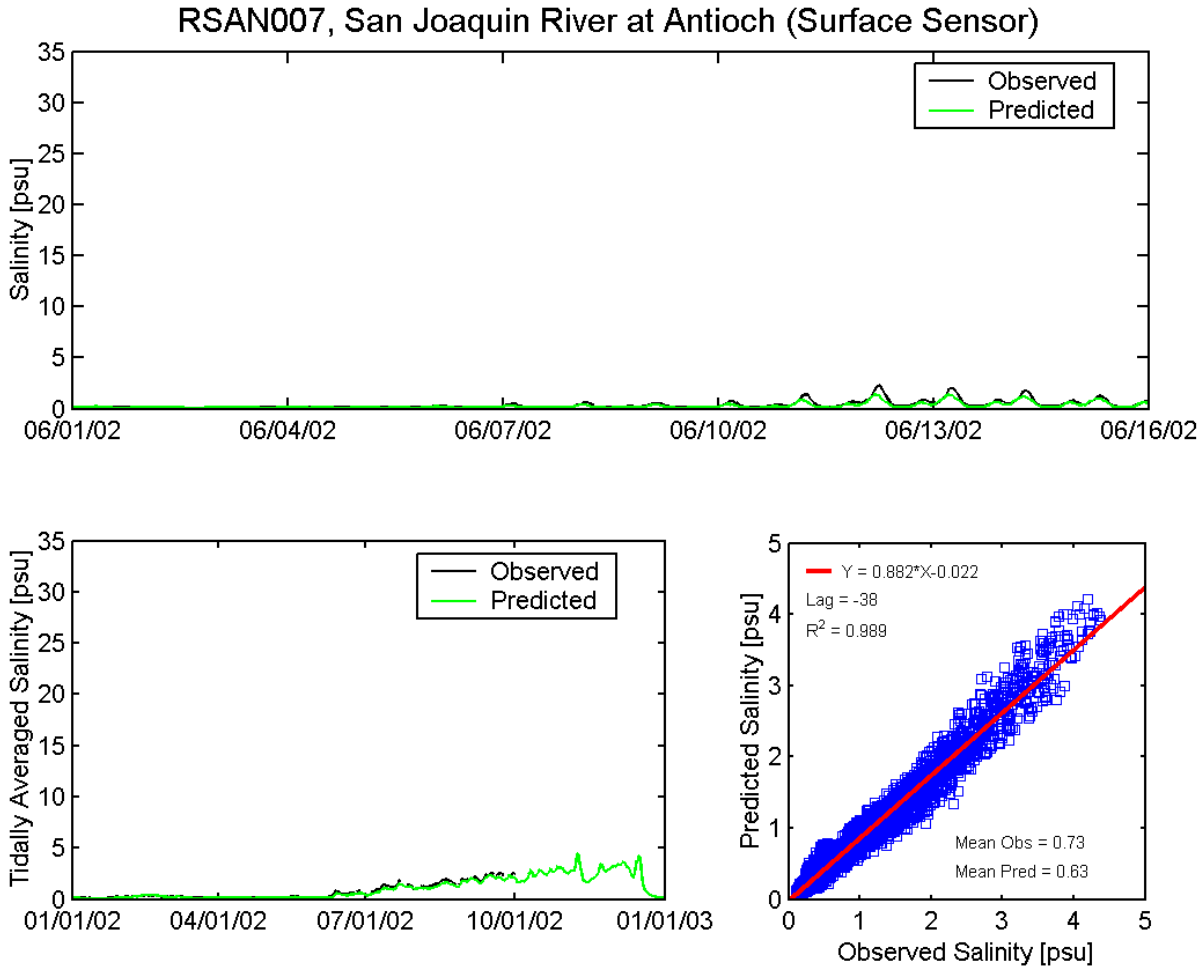

Figure A.6-35 Observed and predicted salinity at Antioch (Surface Sensor) DWR station (RSAN007) during the 2002 simulation period.

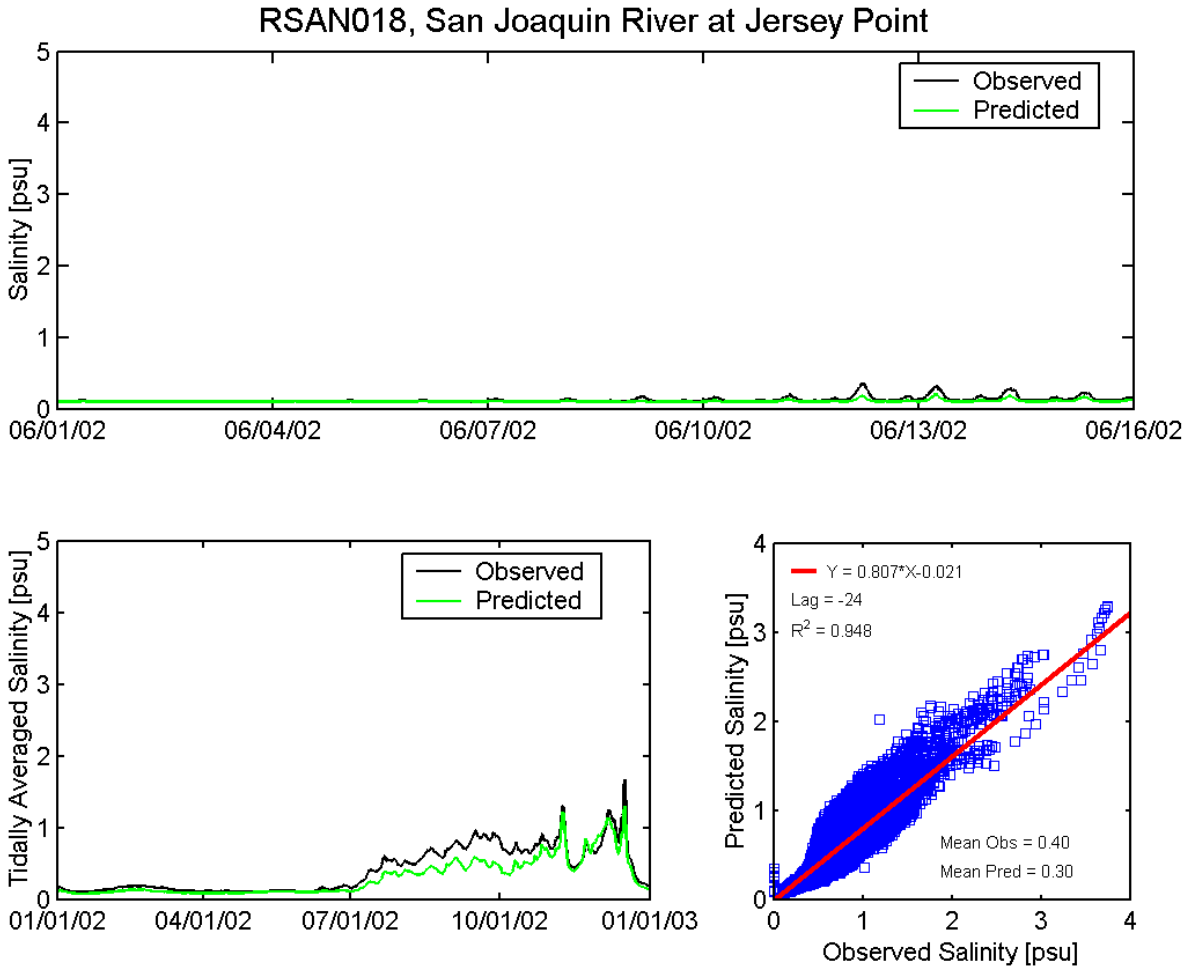

Figure A.6-36 Observed and predicted salinity at San Joaquin River at Jersey Point DWR station (RSAN018) during the 2002 simulation period.

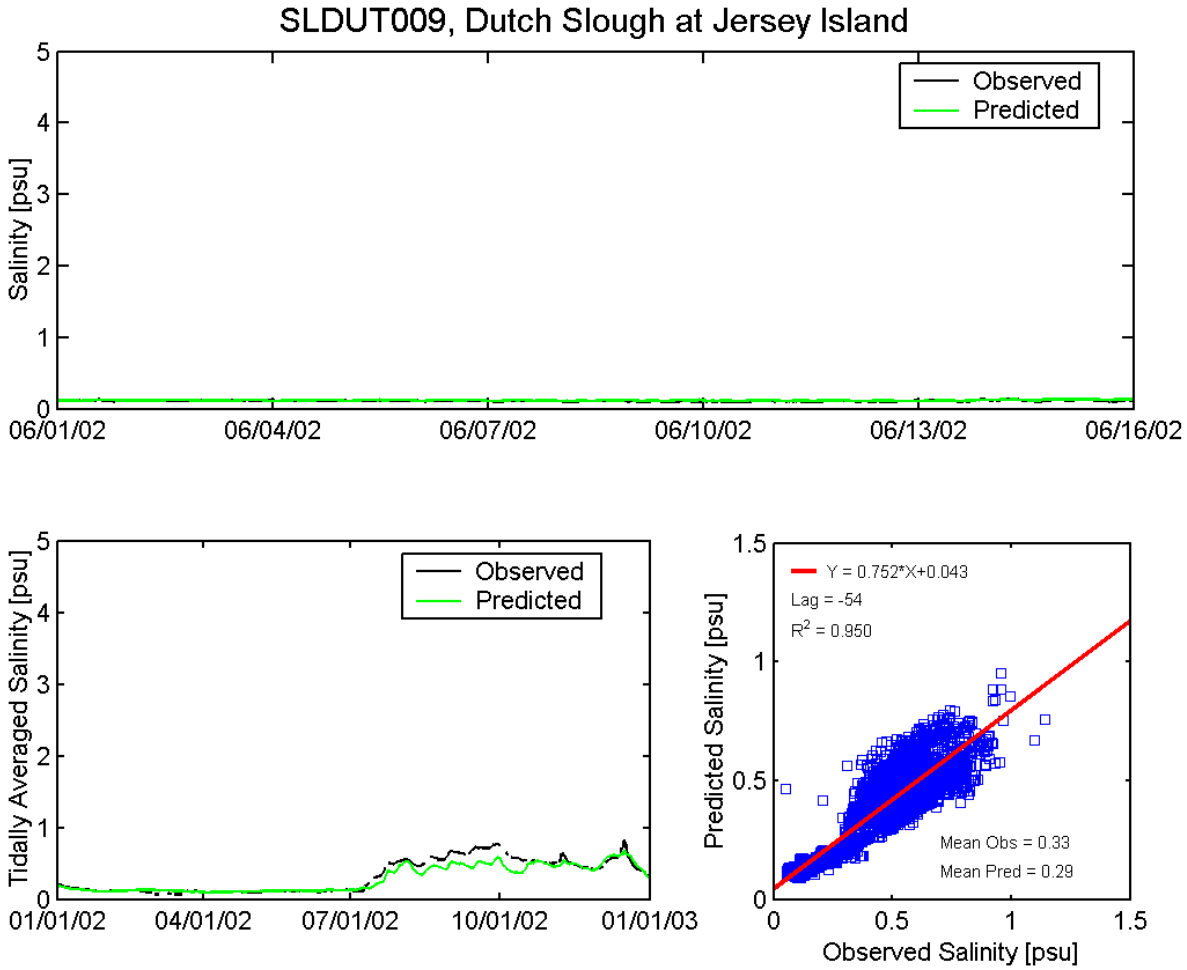

Figure A.6-37 Observed and predicted salinity at Dutch Slough at Jersey Island DWR station (SLDUT009) during the 2002 simulation period.

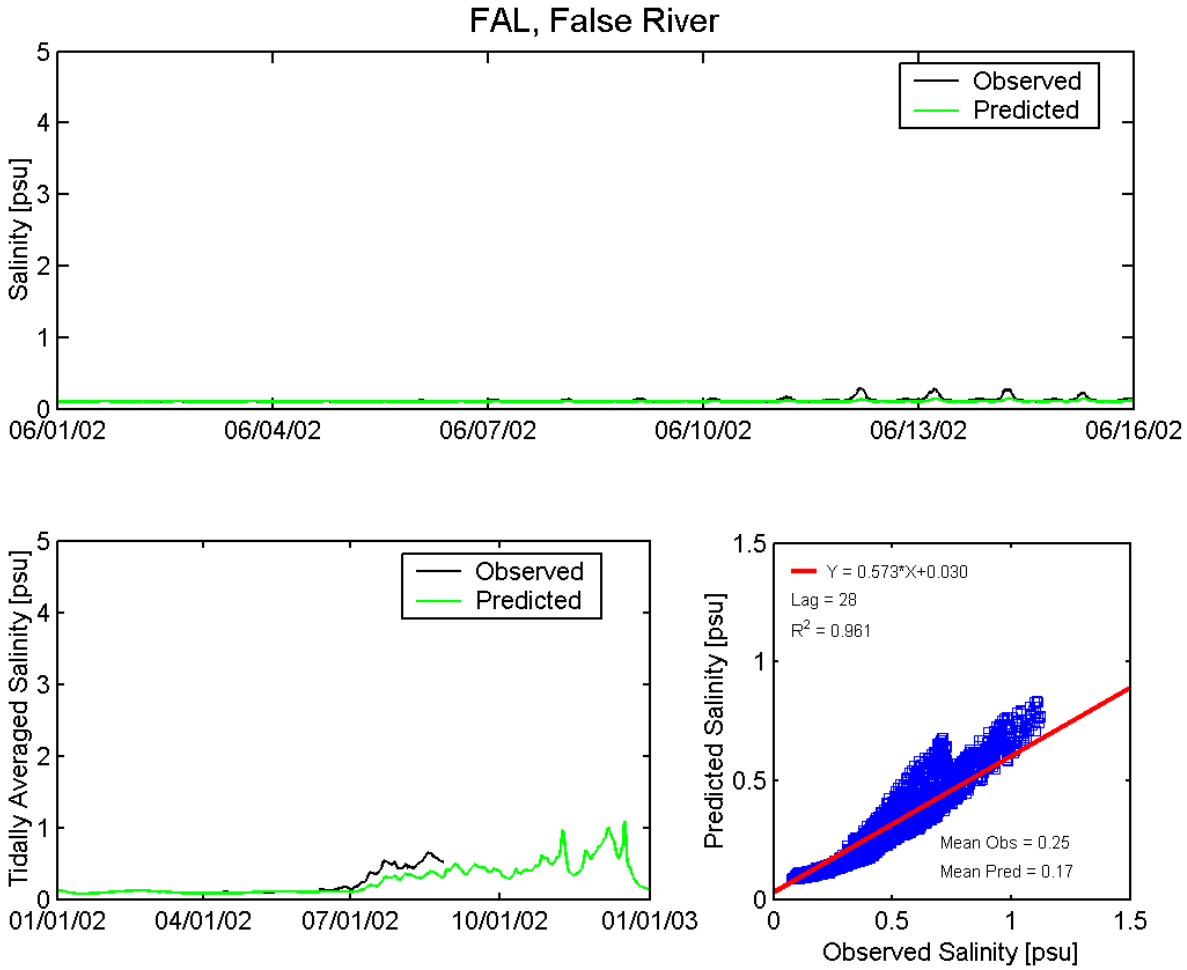

Figure A.6-38 Observed and predicted salinity at False River USGS station (FAL) during the 2002 simulation period.

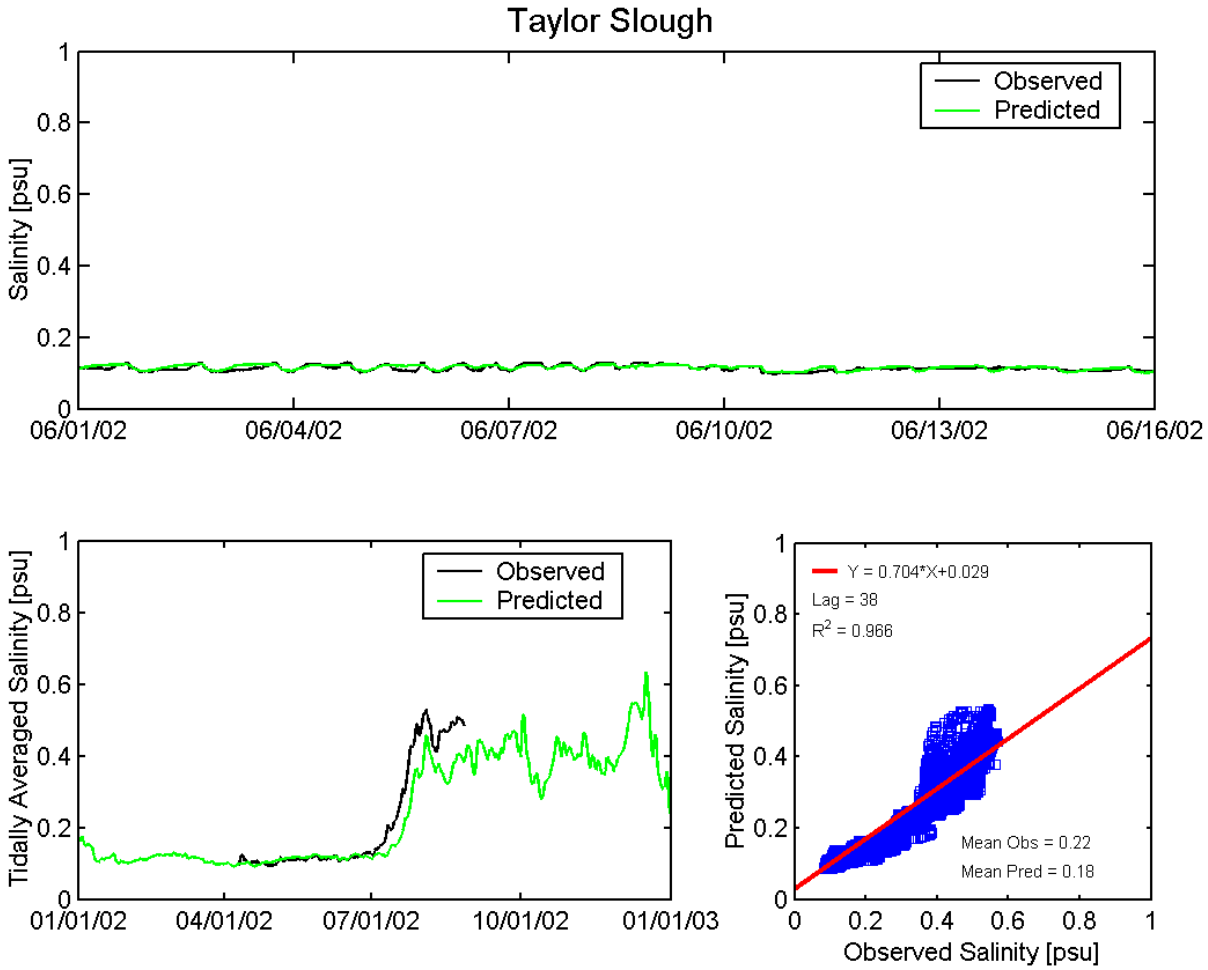

Figure A.6-39 Observed and predicted salinity at Taylor Slough USGS station (TYLR) during the 2002 simulation period.

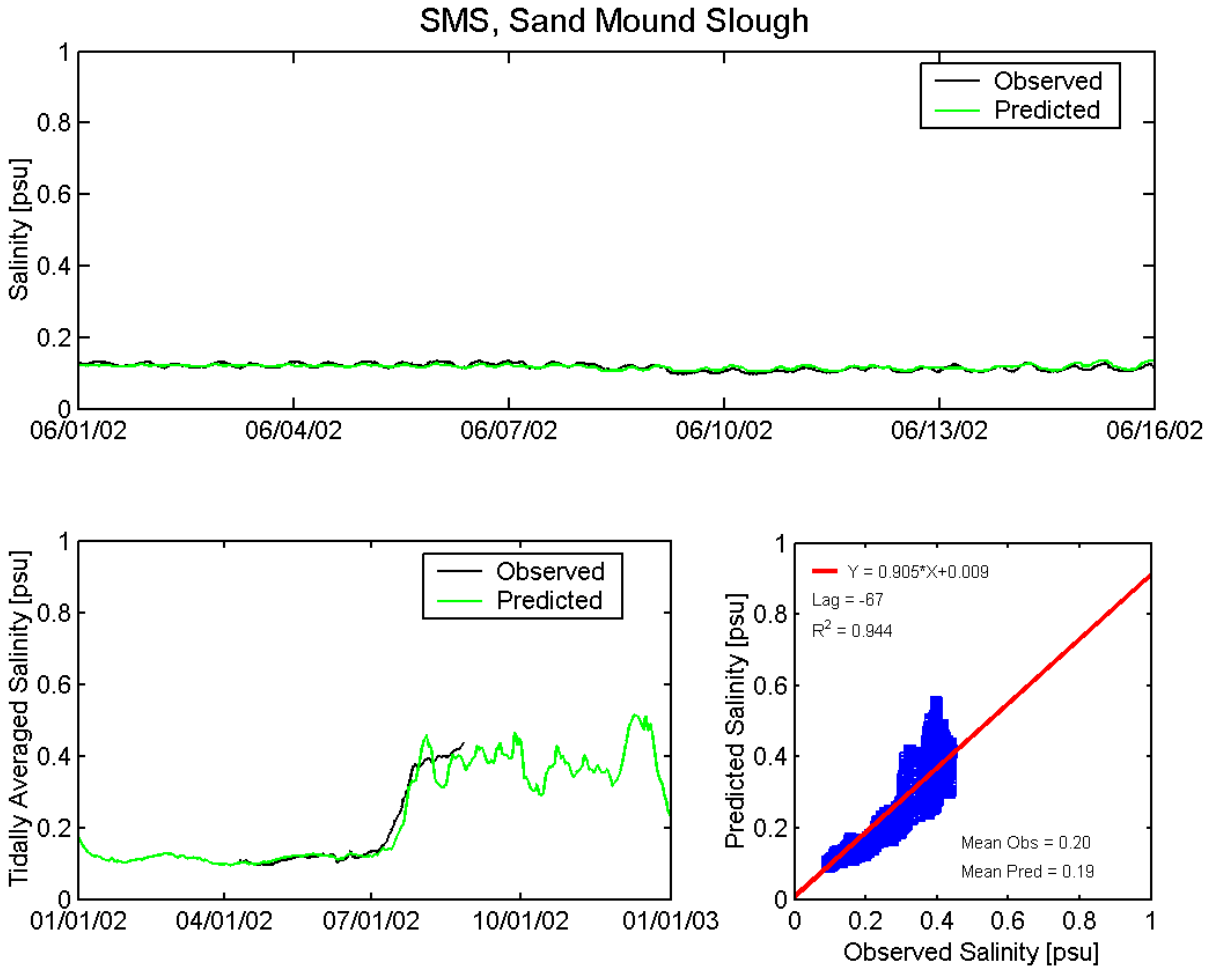

Figure A.6-40 Observed and predicted salinity at Sand Mound Slough USGS station (SMS) during the 2002 simulation period.

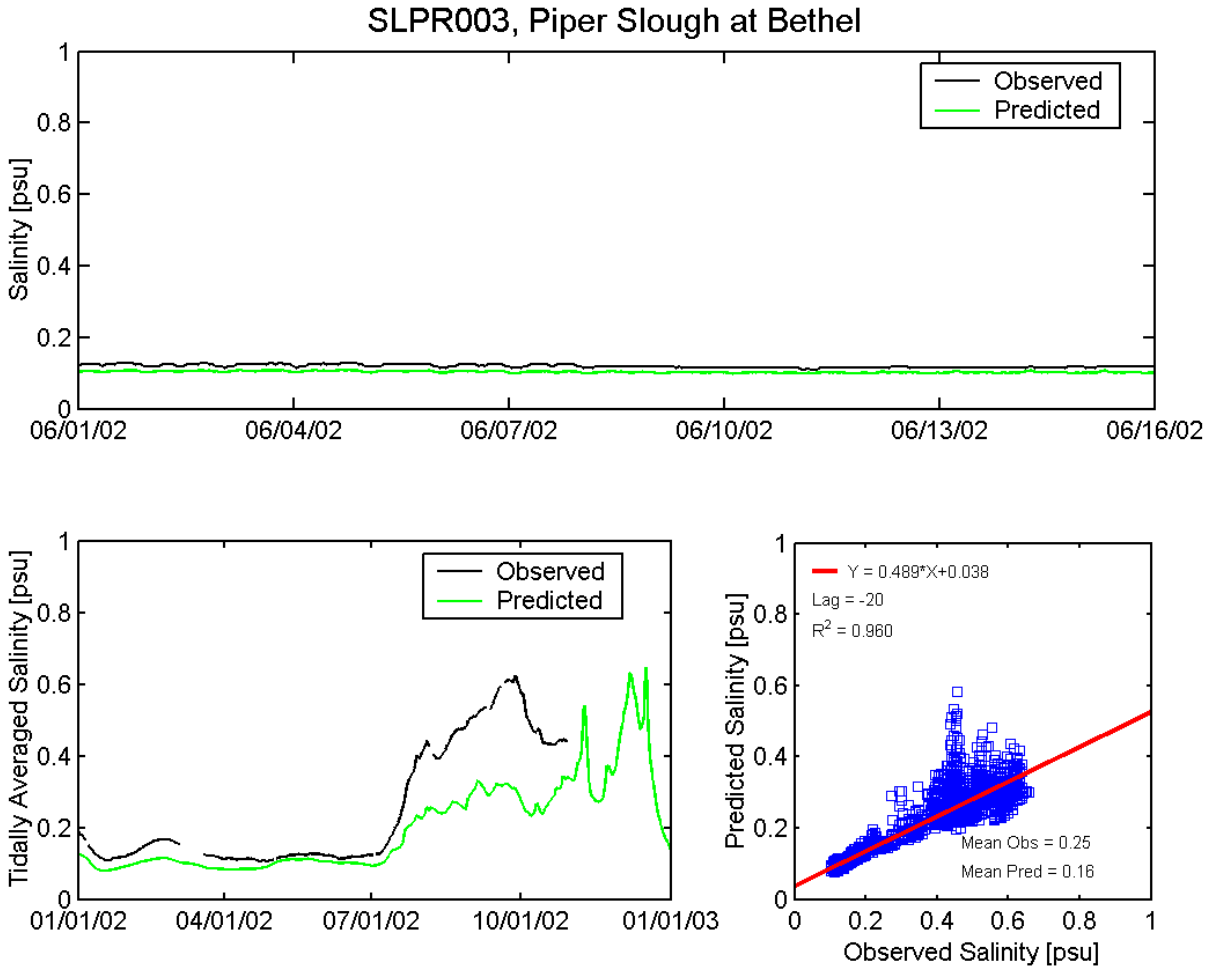

Figure A.6-41 Observed and predicted salinity at Piper Slough at Bethel Tract DWR station (SLPR003) during the 2002 simulation period.

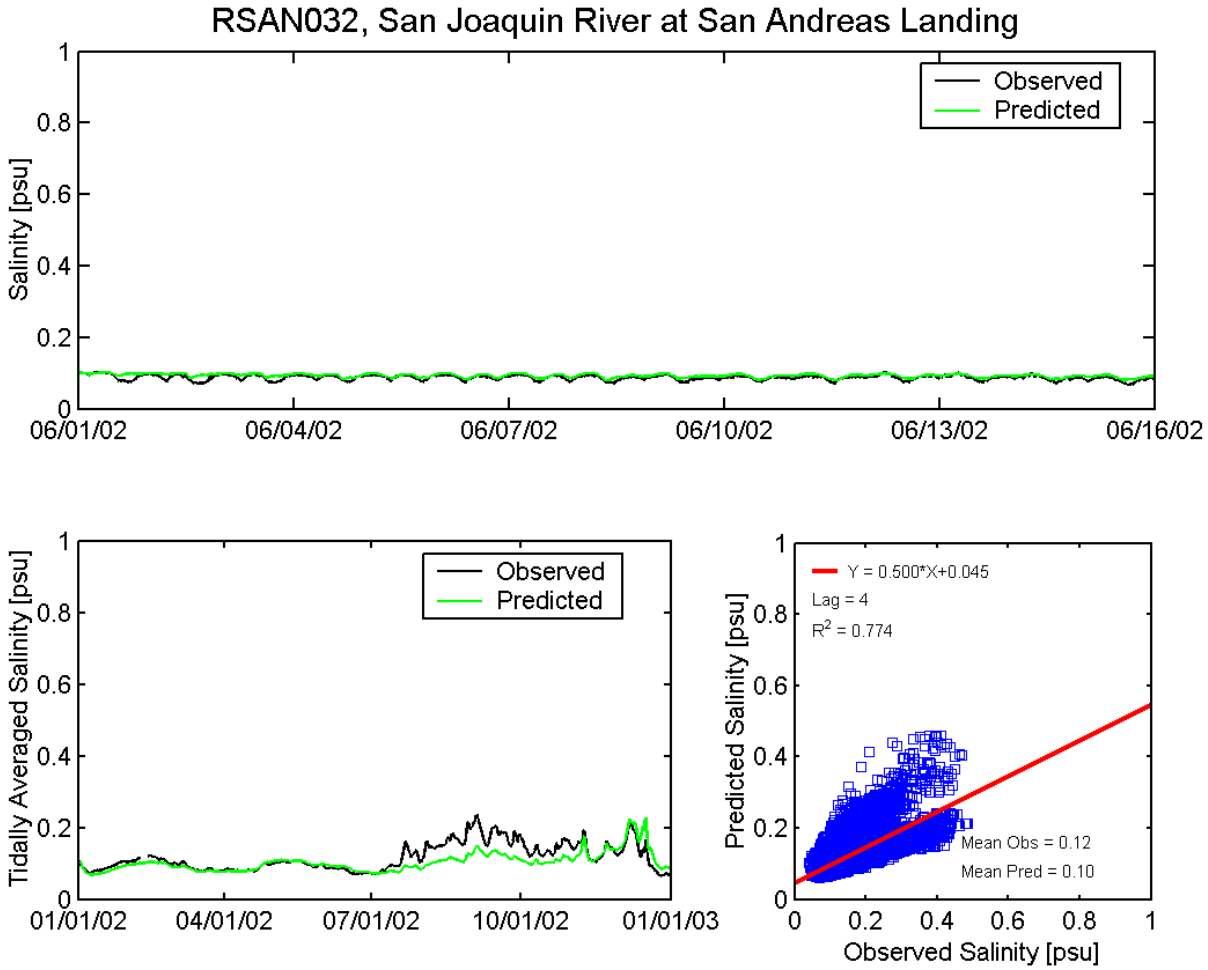

Figure A.6-42 Observed and predicted salinity at San Joaquin River at San Andreas Landing USBR station (RSAN032) during the 2002 simulation period.

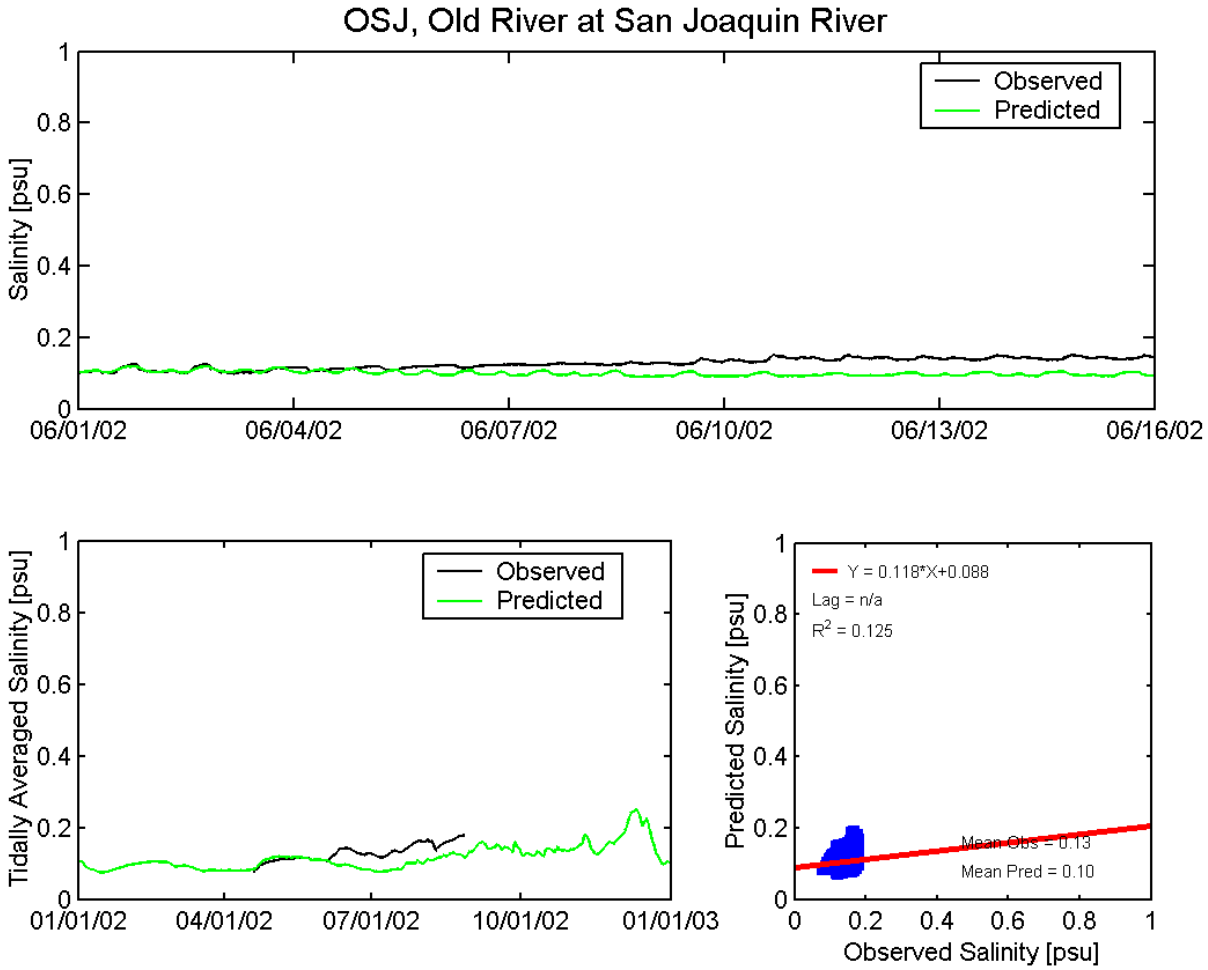

Figure A.6-43 Observed and predicted salinity at Old River at San Joaquin River USGS station (OSJ) during the 2002 simulation period.

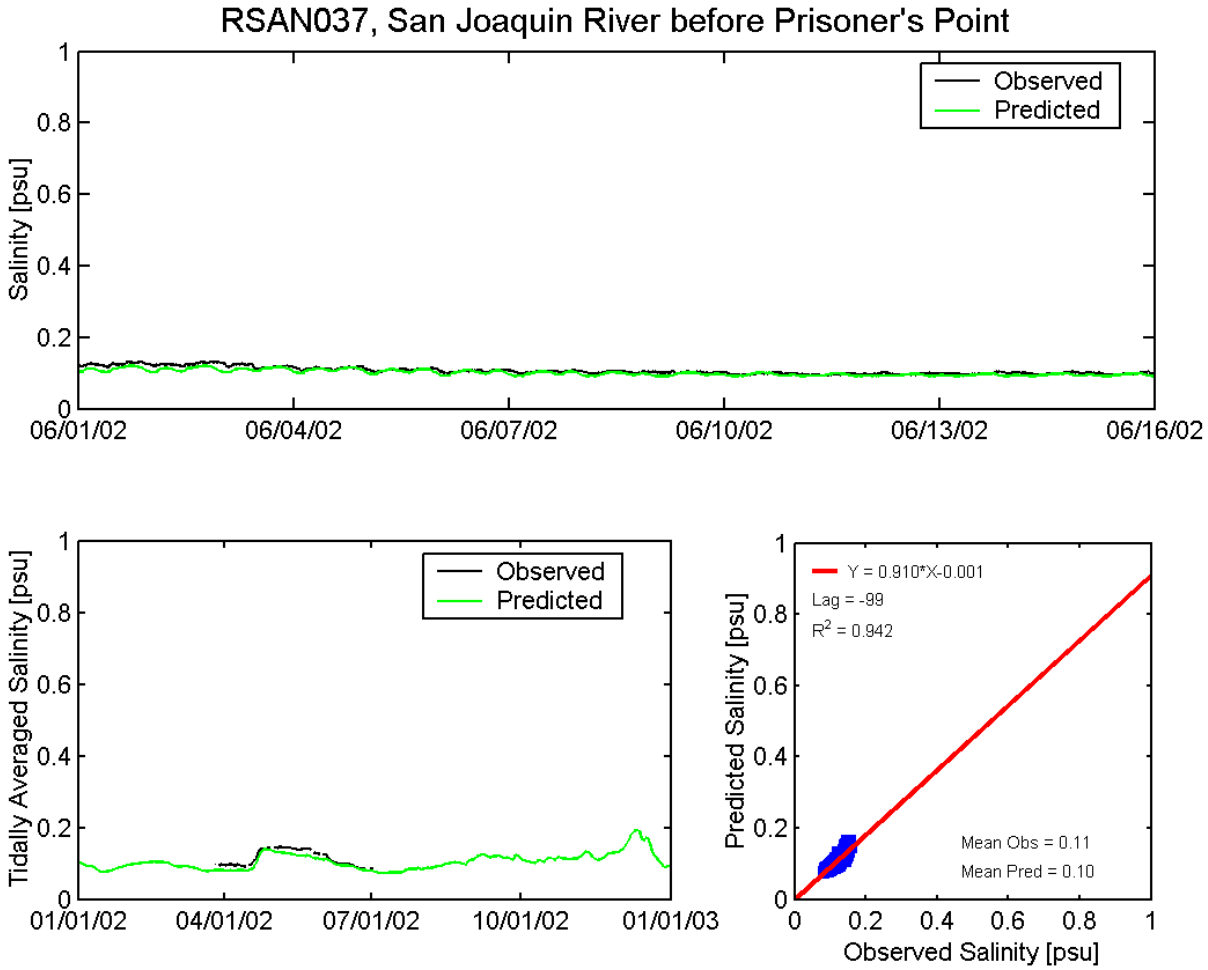

Figure A.6-44 Observed and predicted salinity at San Joaquin River before Prisoner's Point DWR station (RSAN037) during the 2002 simulation period.

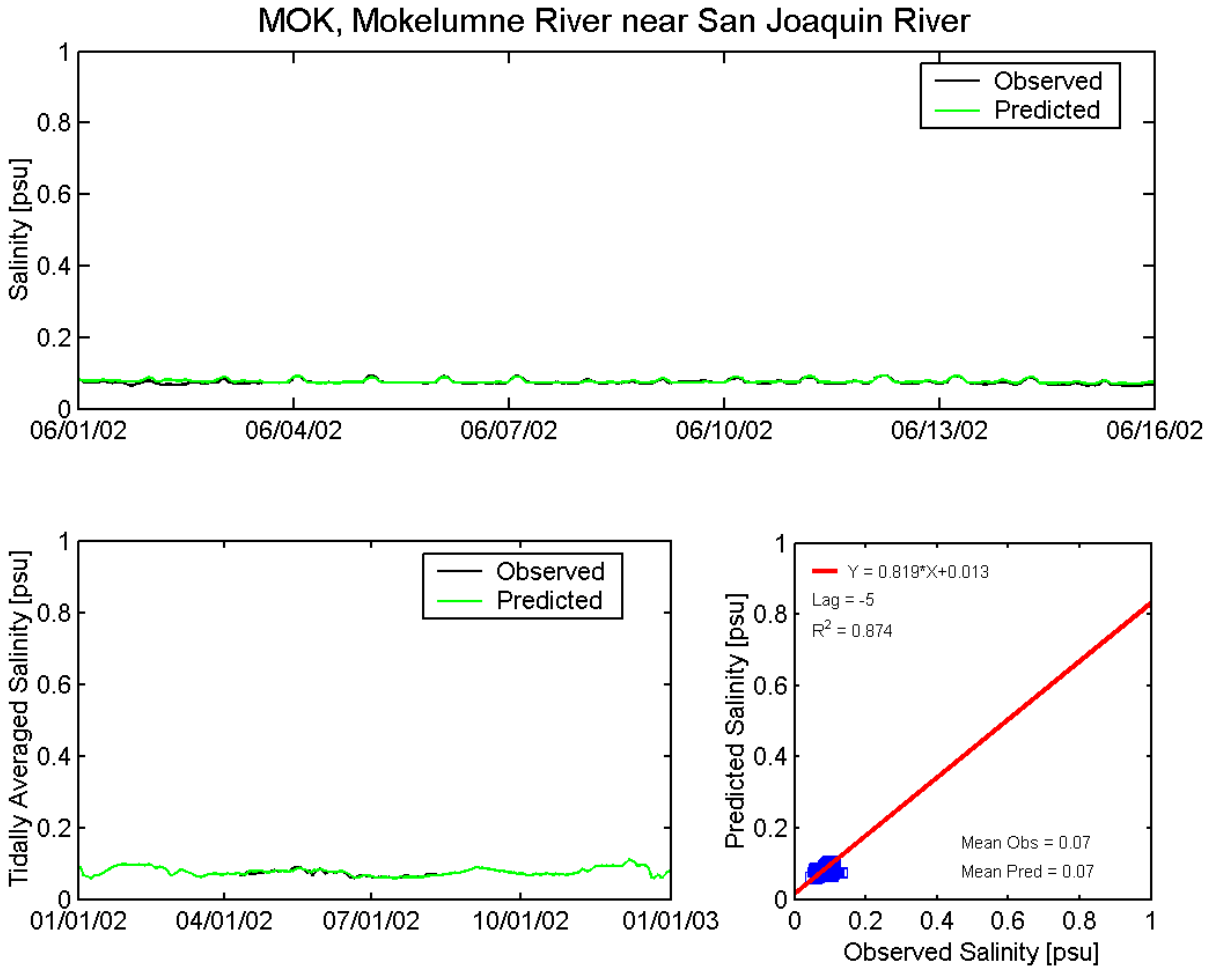

Figure A.6-45 Observed and predicted salinity at Mokelumne River near San Joaquin River USGS station (MOK) during the 2002 simulation period.

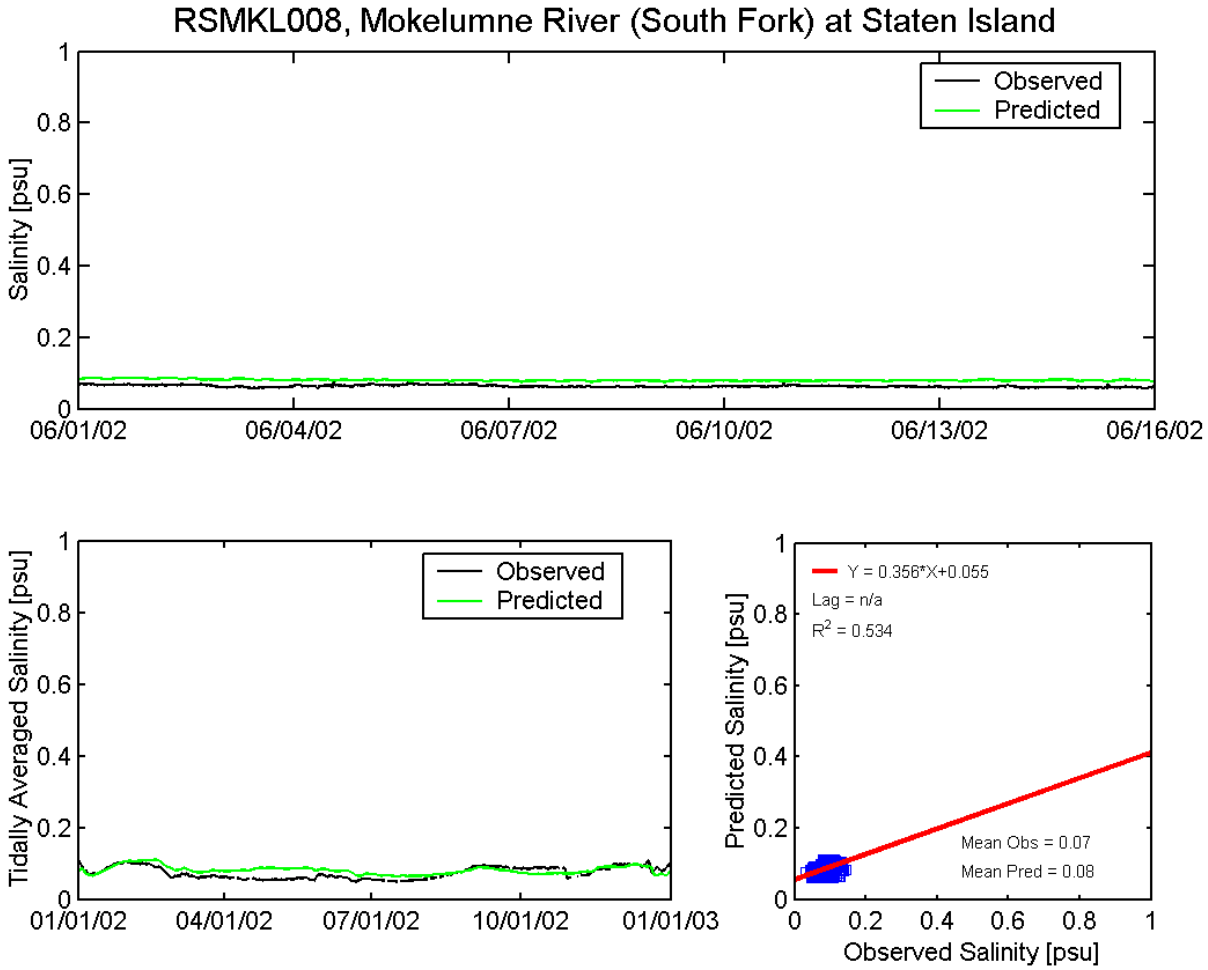

Figure A.6-46 Observed and predicted salinity at Mokelumne River (South Fork) at Staten Island DWR station (RSMKL008) during the 2002 simulation period.

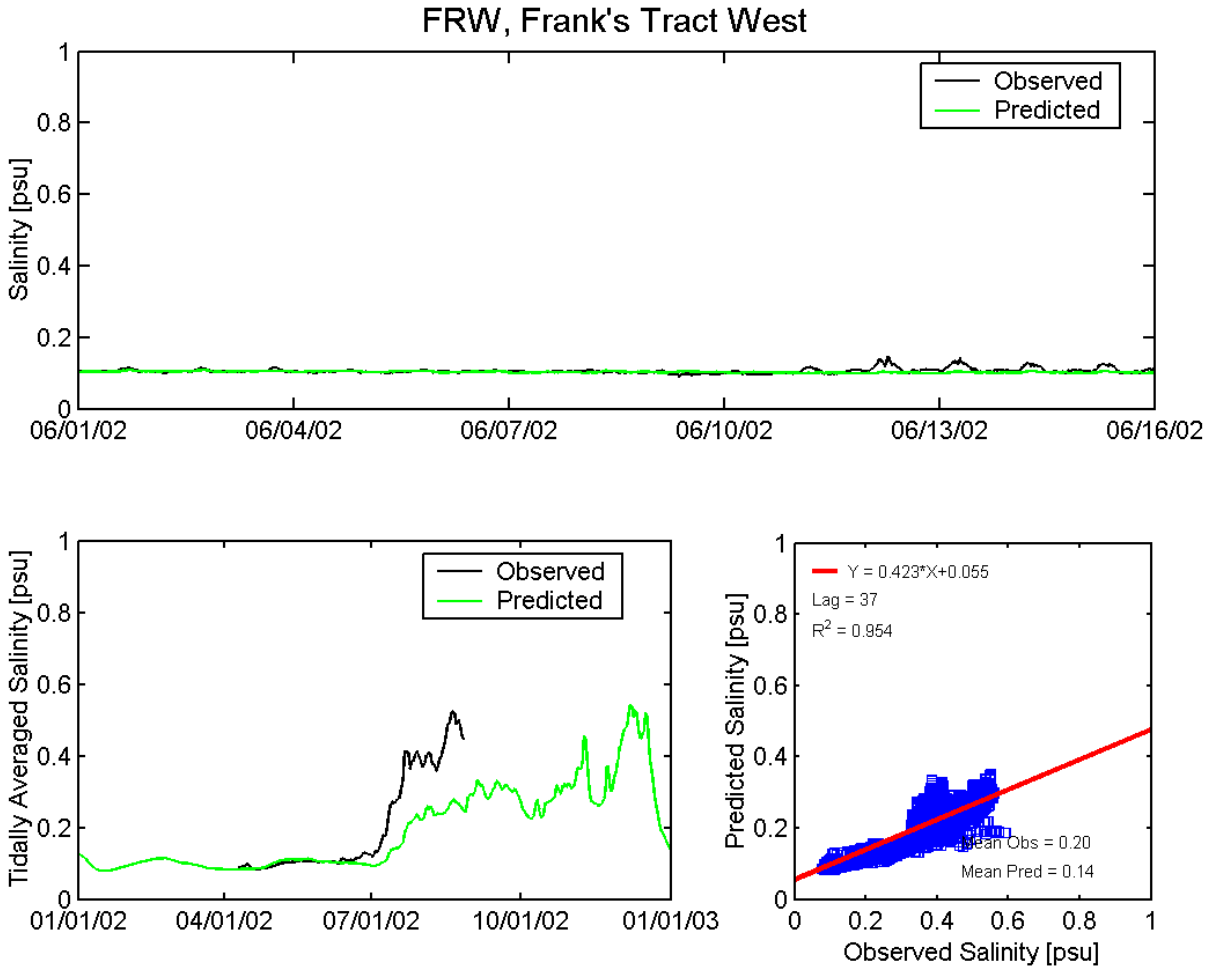

Figure A.6-47 Observed and predicted salinity at Franks Tract West USGS station (FRW) during the 2002 simulation period.

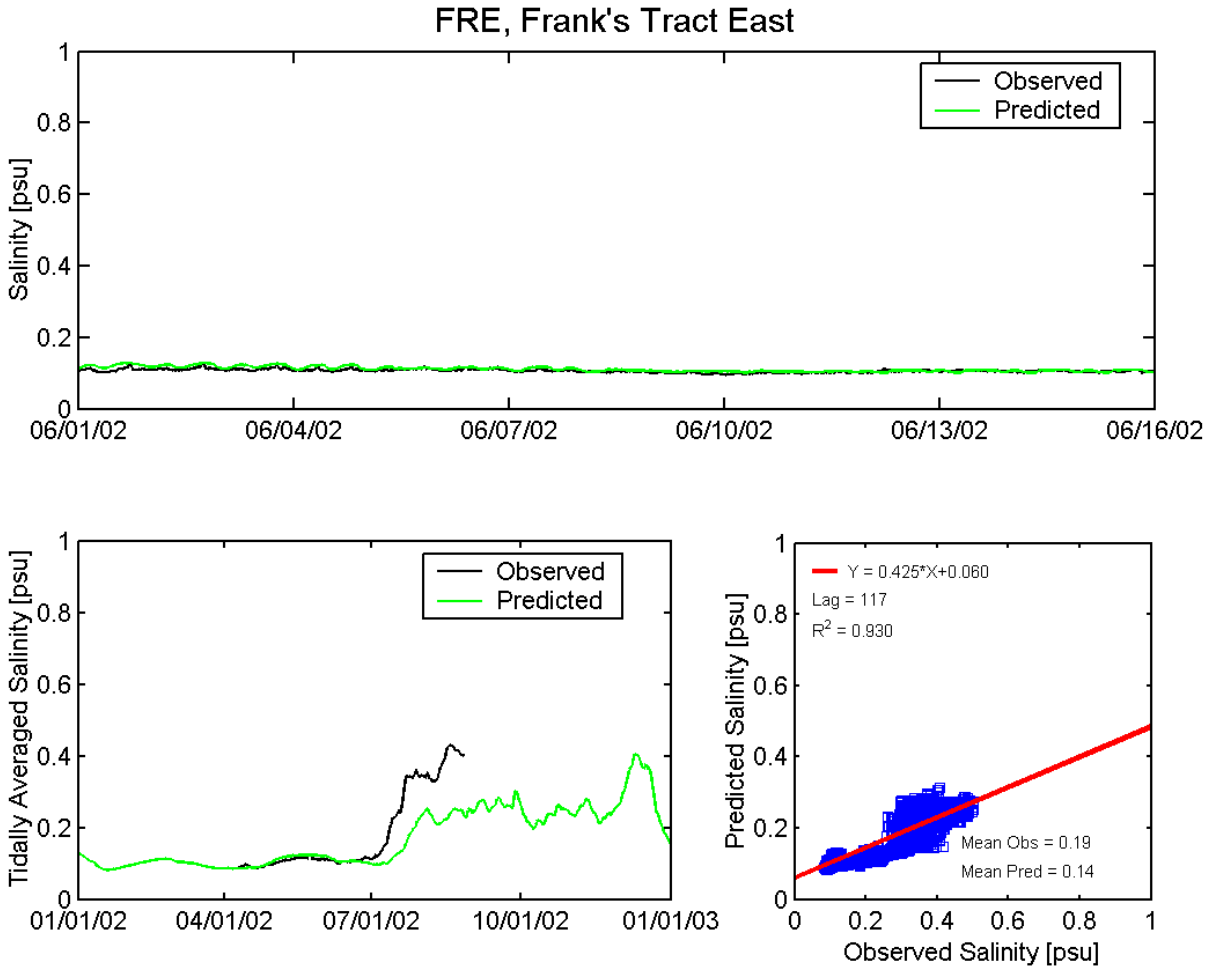

Figure A.6-48 Observed and predicted salinity at Franks Tract East USGS station (FRE) during the 2002 simulation period.

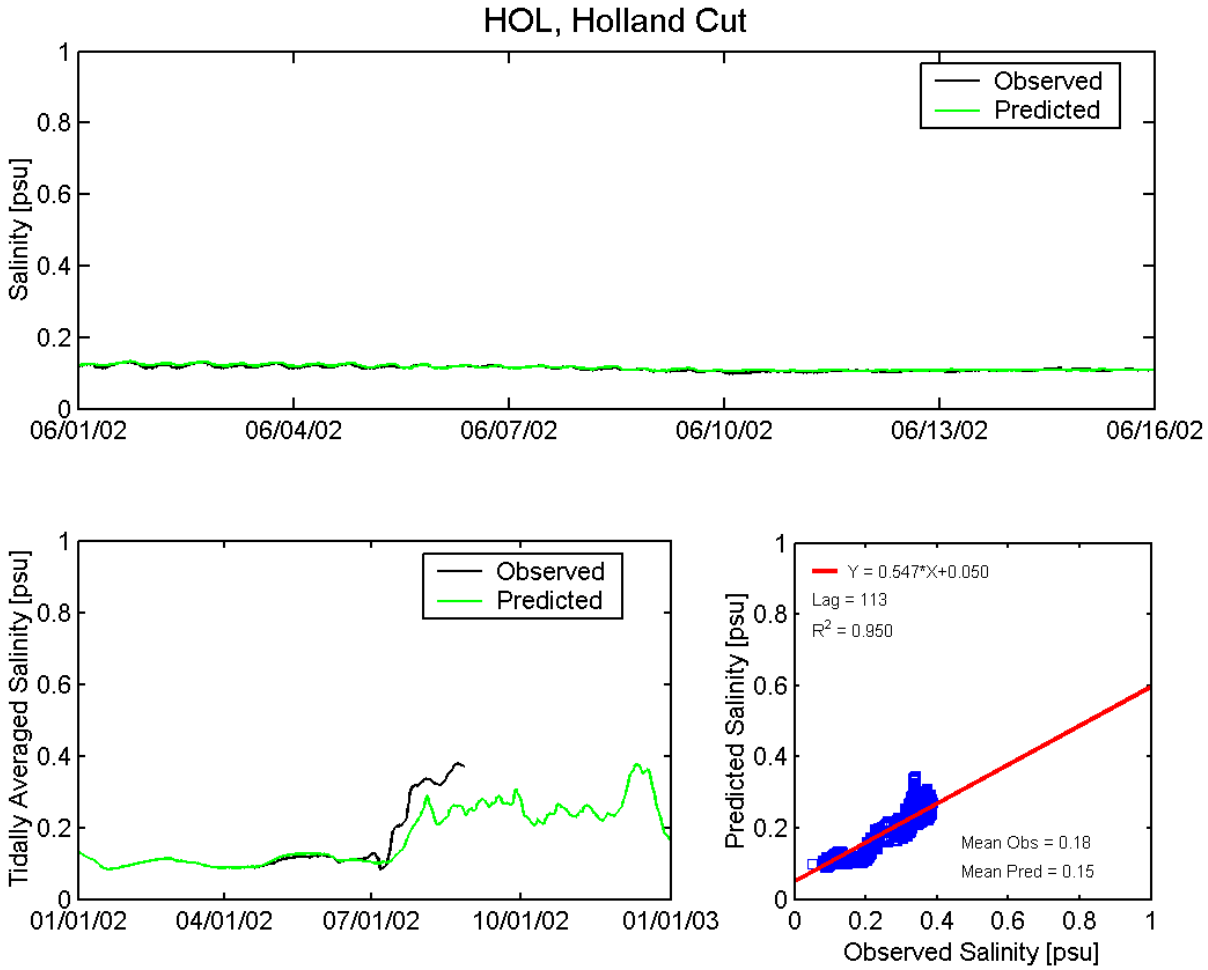

Figure A.6-49 Observed and predicted salinity at Holland Cut USGS station (HOL) during the 2002 simulation period.

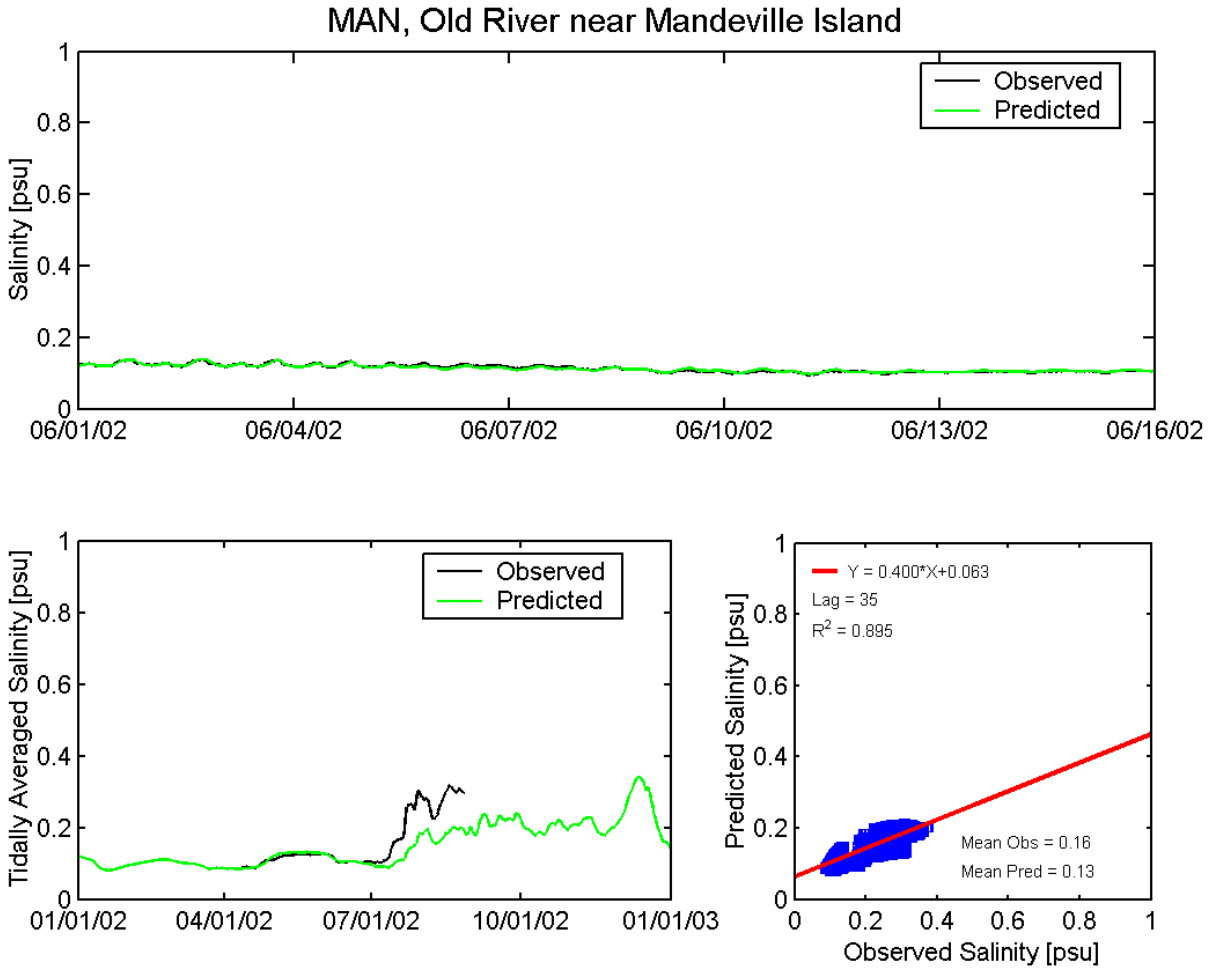

Figure A.6-50 Observed and predicted salinity at Old River near Mandeville Island USGS station (MAN) during the 2002 simulation period.

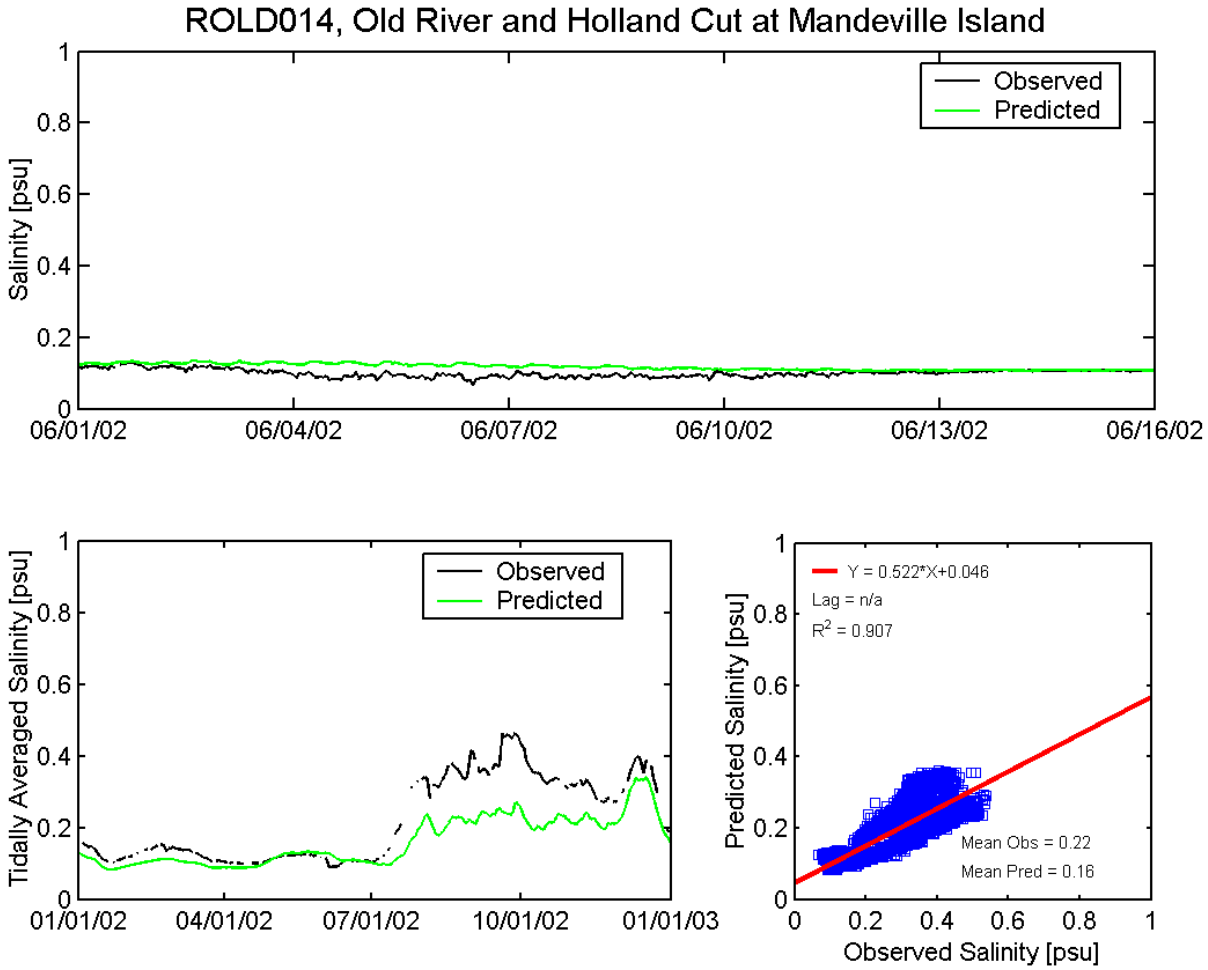

Figure A.6-51 Observed and predicted salinity at Old River and Holland Cut at Mandeville Island USBR station (ROLD014) during the 2002 simulation period.

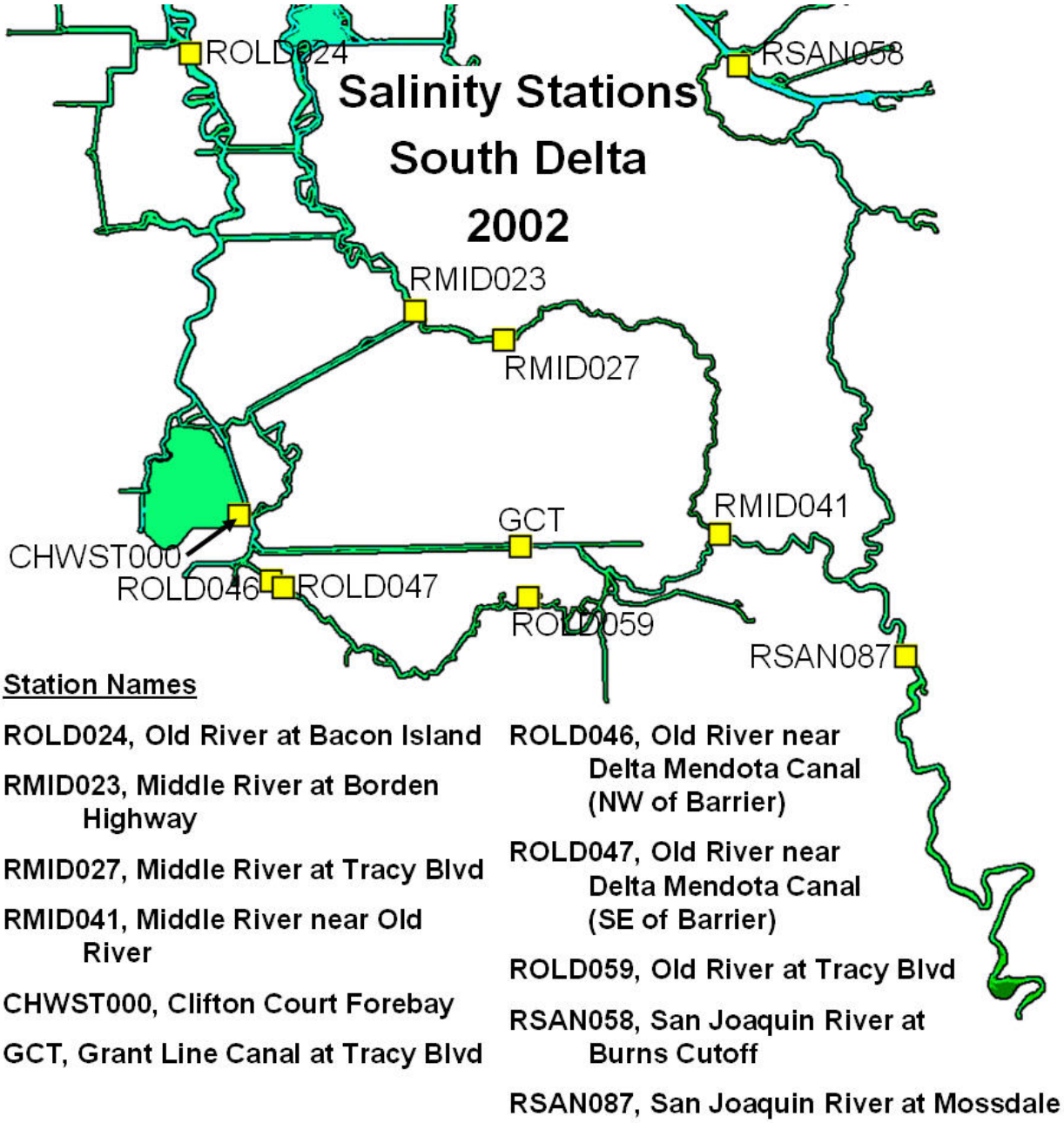

Figure A.6-52 Location of salinity monitoring stations in the southern portion of the Sacramento-San Joaquin Delta used for 2002 salinity comparisons.

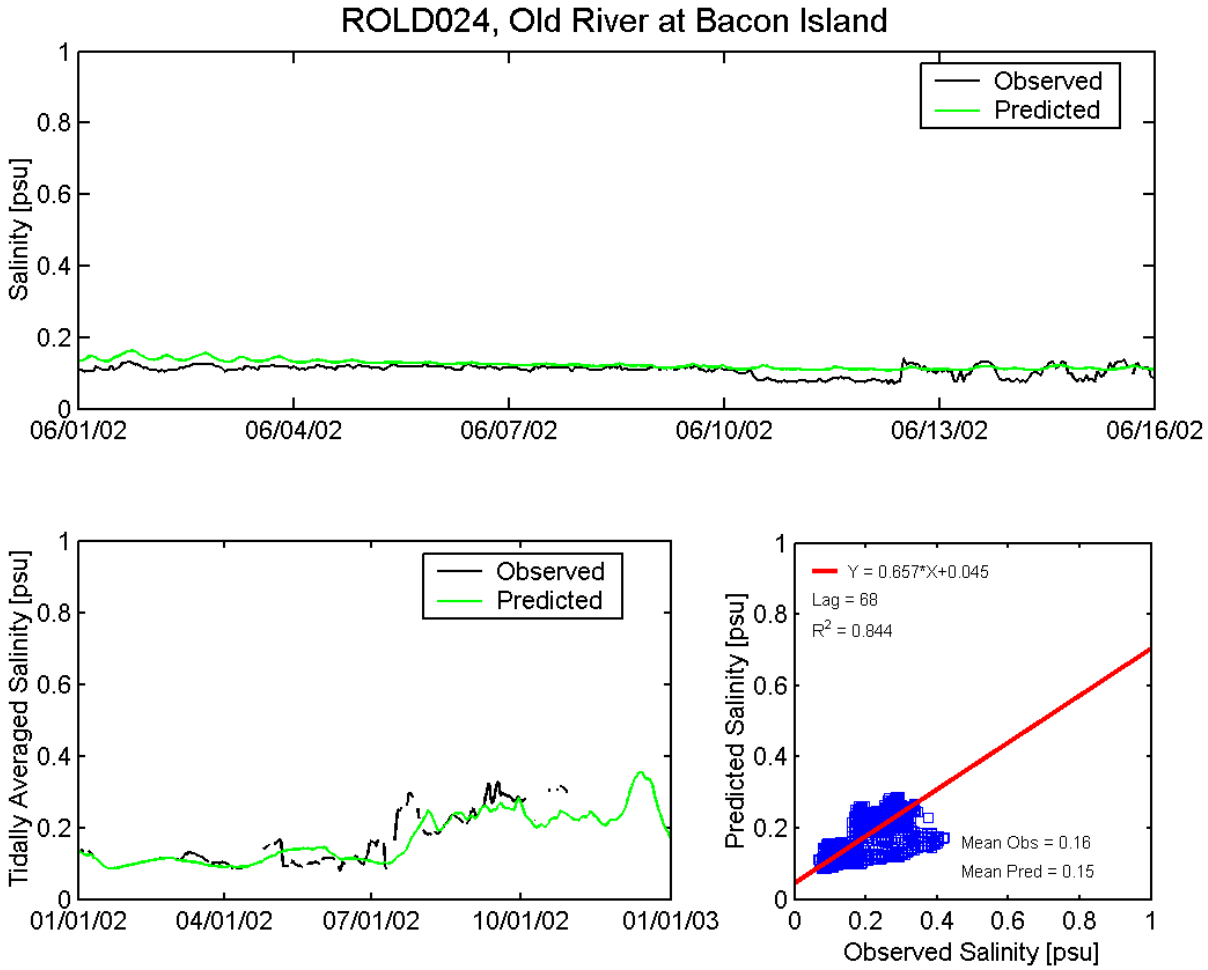

Figure A.6-53 Observed and predicted salinity at Old River at Bacon Island DWR station (ROLD024) during the 2002 simulation period.

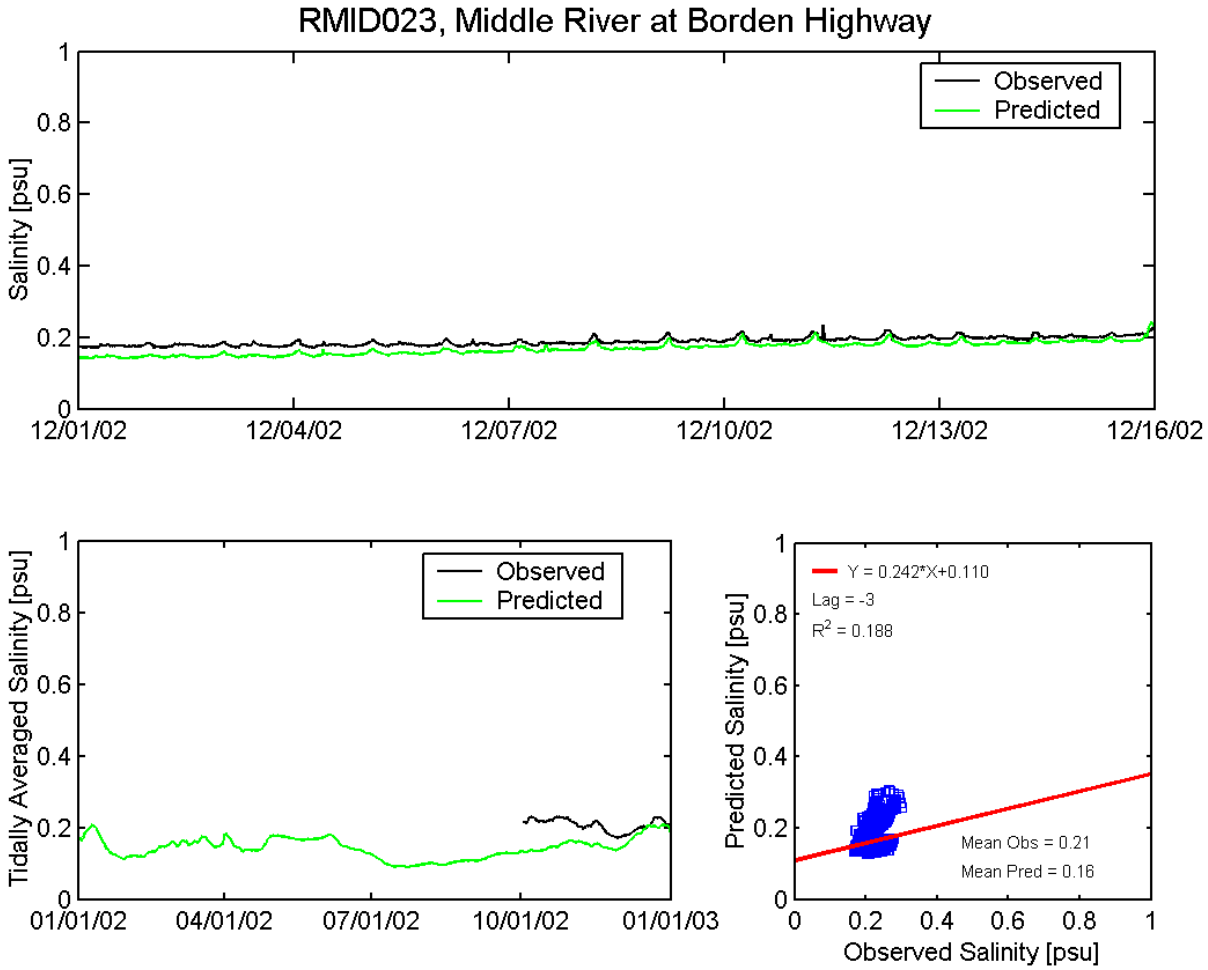

Figure A.6-54 Observed and predicted salinity at Middle River at Borden Highway DWR station (RMID023) during the 2002 simulation period.

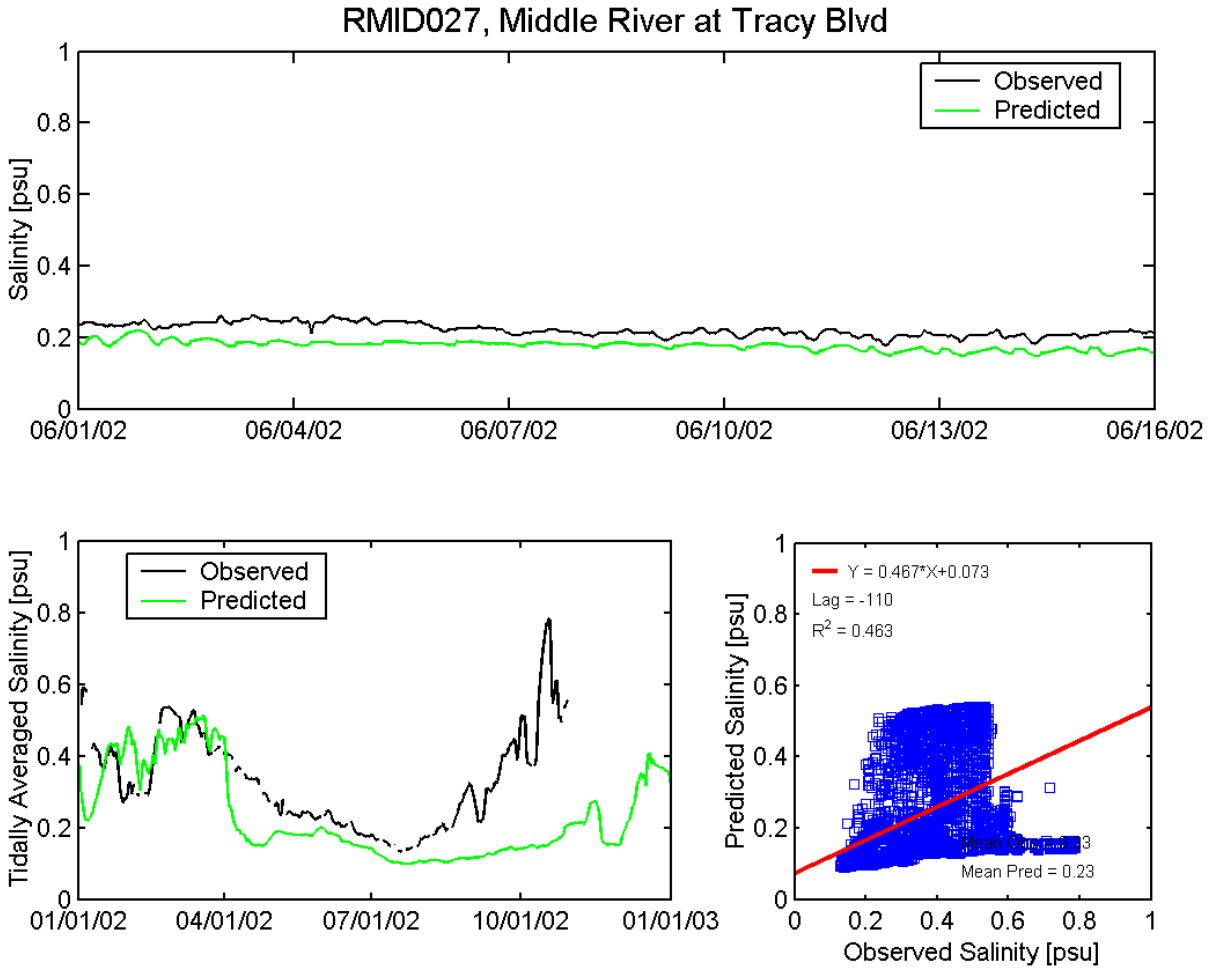

Figure A.6-55 Observed and predicted salinity at Middle River at Tracy Boulevard DWR station (RMID027) during the 2002 simulation period.

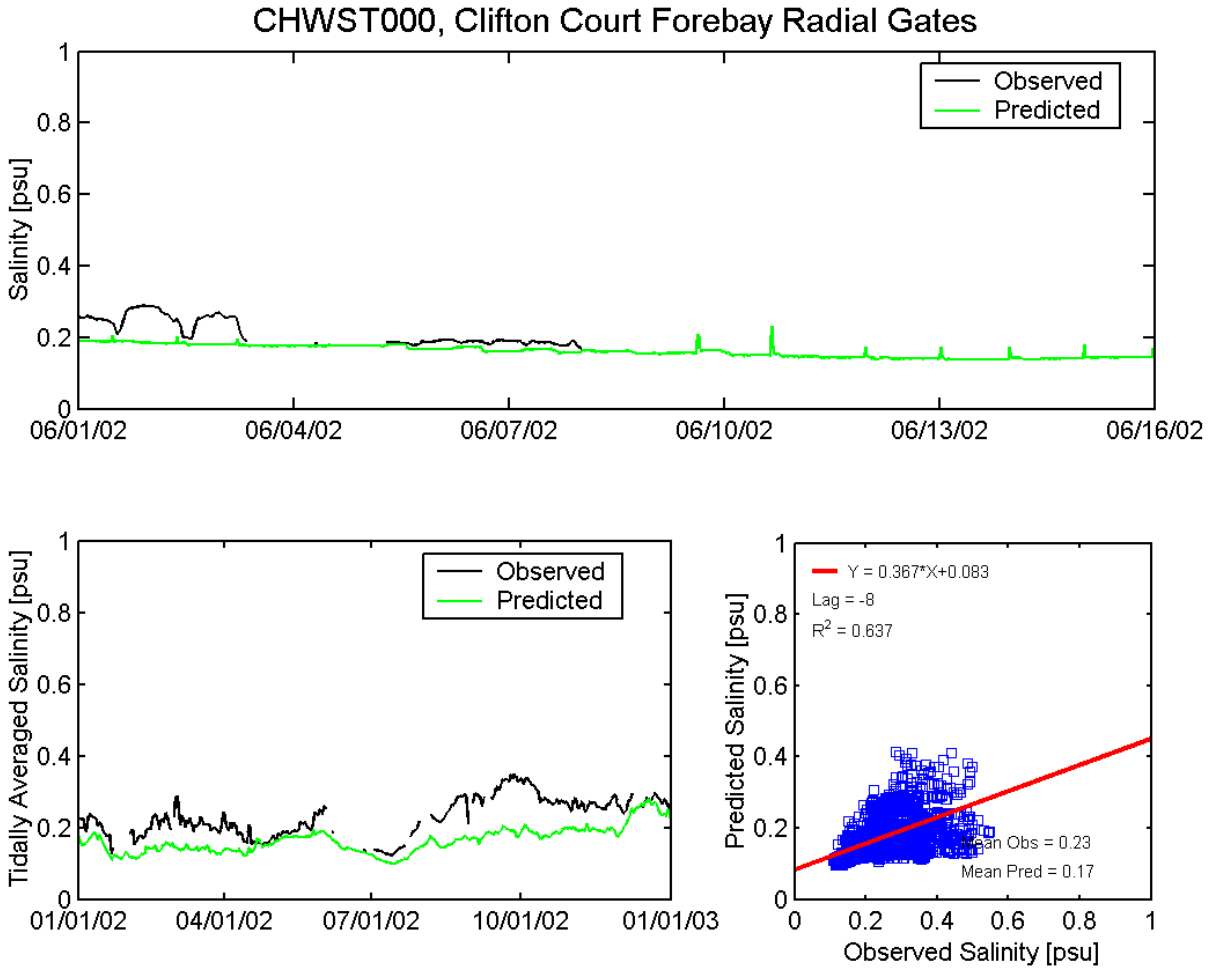

Figure A.6-56 Observed and predicted salinity at Clifton Court Forebay Radial Gates DWR station (CHWST000) during the 2002 simulation period.

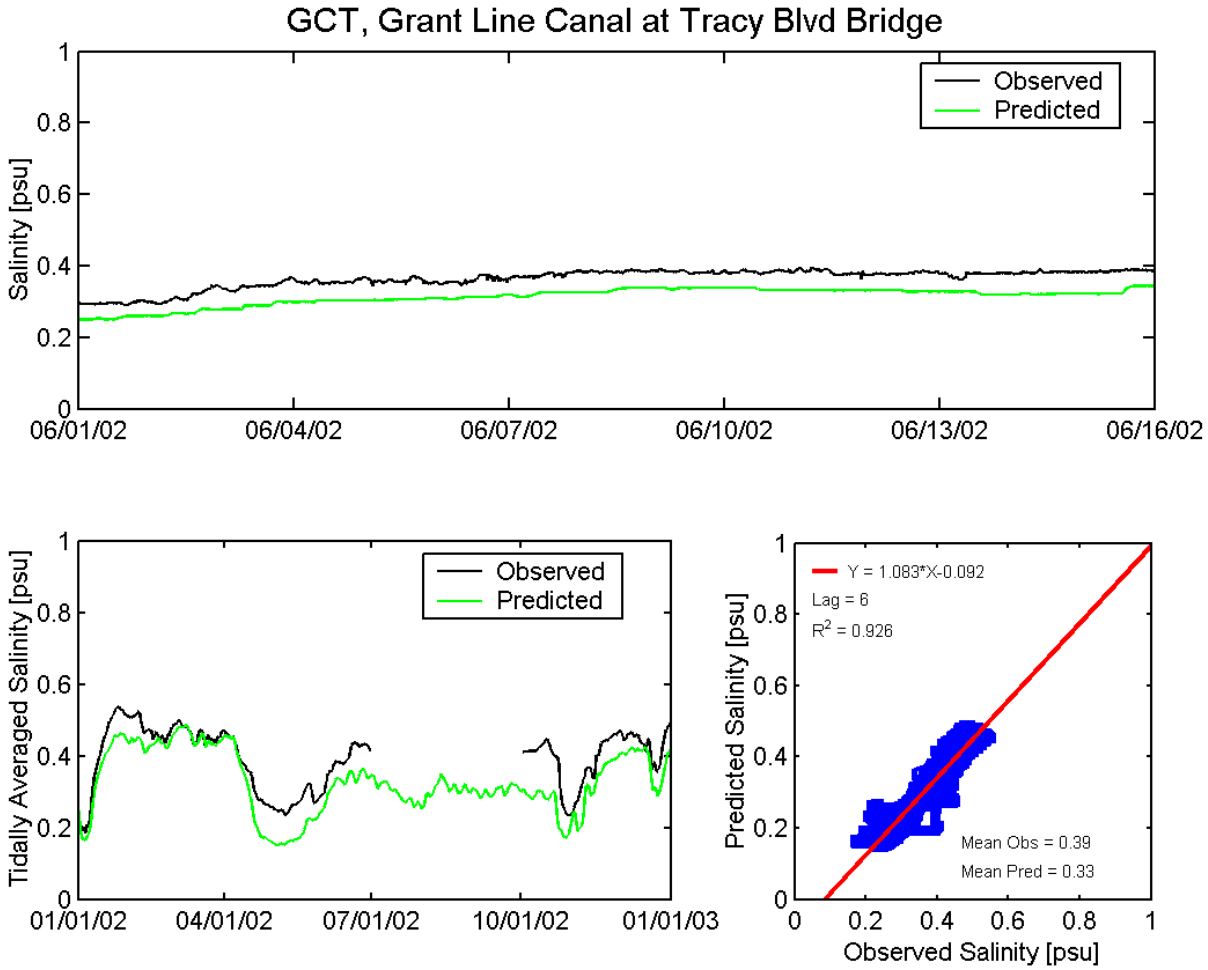

Figure A.6-57 Observed and predicted salinity at Grant Line Canal at Tracy Boulevard DWR station (CDEC GCT) during the 2002 simulation period.

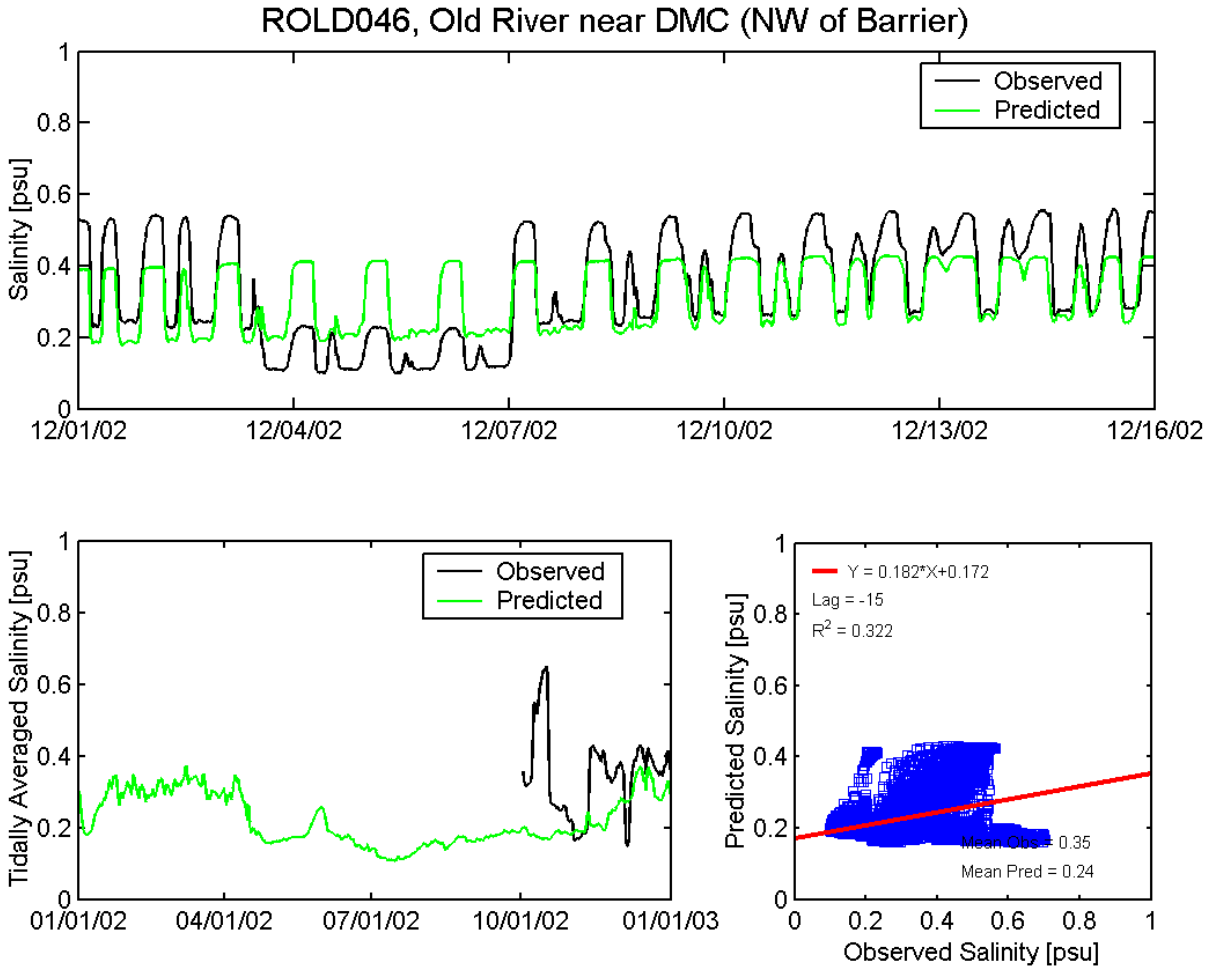

Figure A.6-58 Observed and predicted salinity at Old River near Delta Mendota Canal NW of Barrier DWR station (ROLD046) during the 2002 simulation period.

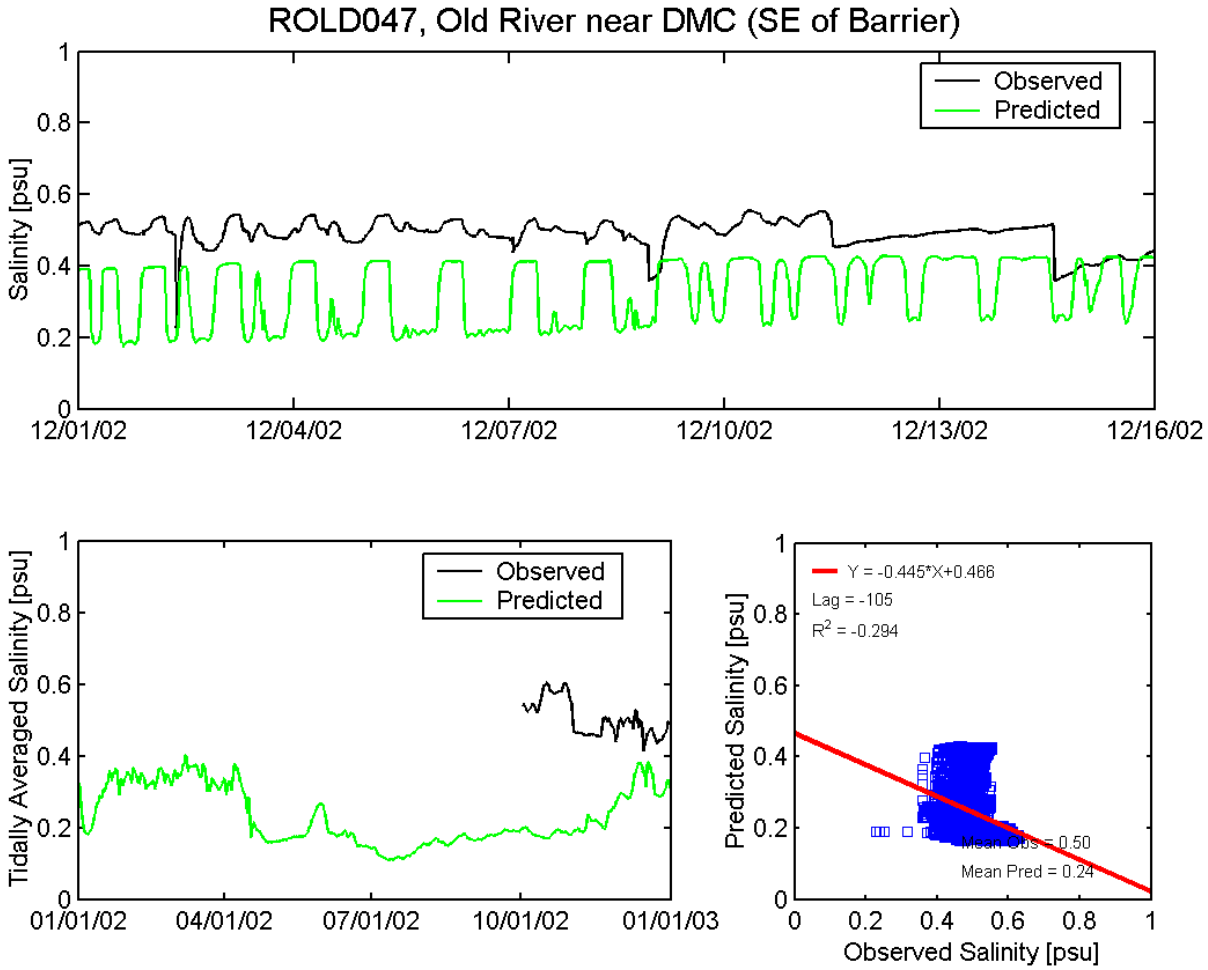

Figure A.6-59 Observed and predicted salinity at Delta Mendota Canal SE of Barrier DWR station (ROLD047) during the 2002 simulation period.

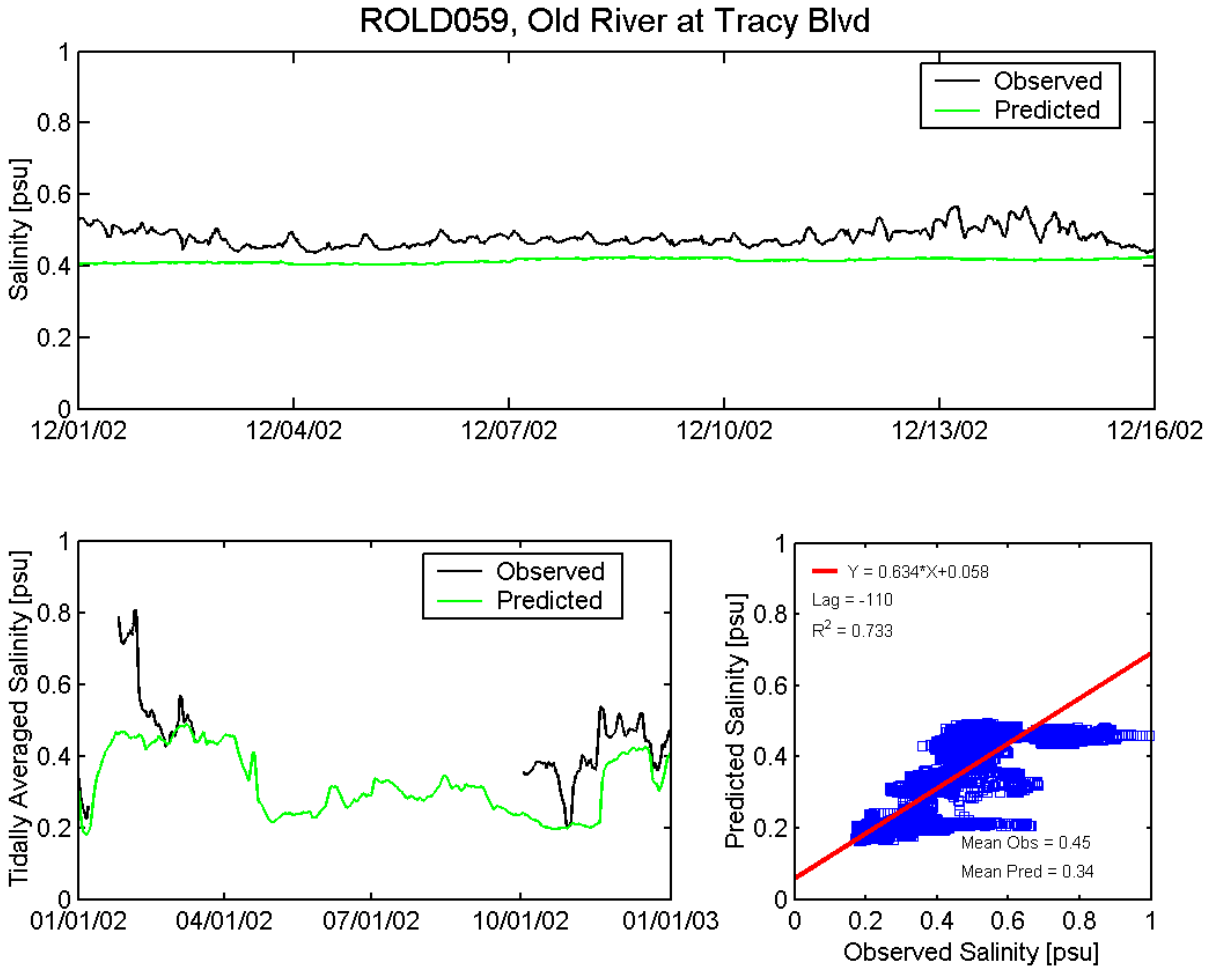

Figure A.6-60 Observed and predicted salinity at Old River at Tracy Boulevard DWR station (ROLD059) during the 2002 simulation period.

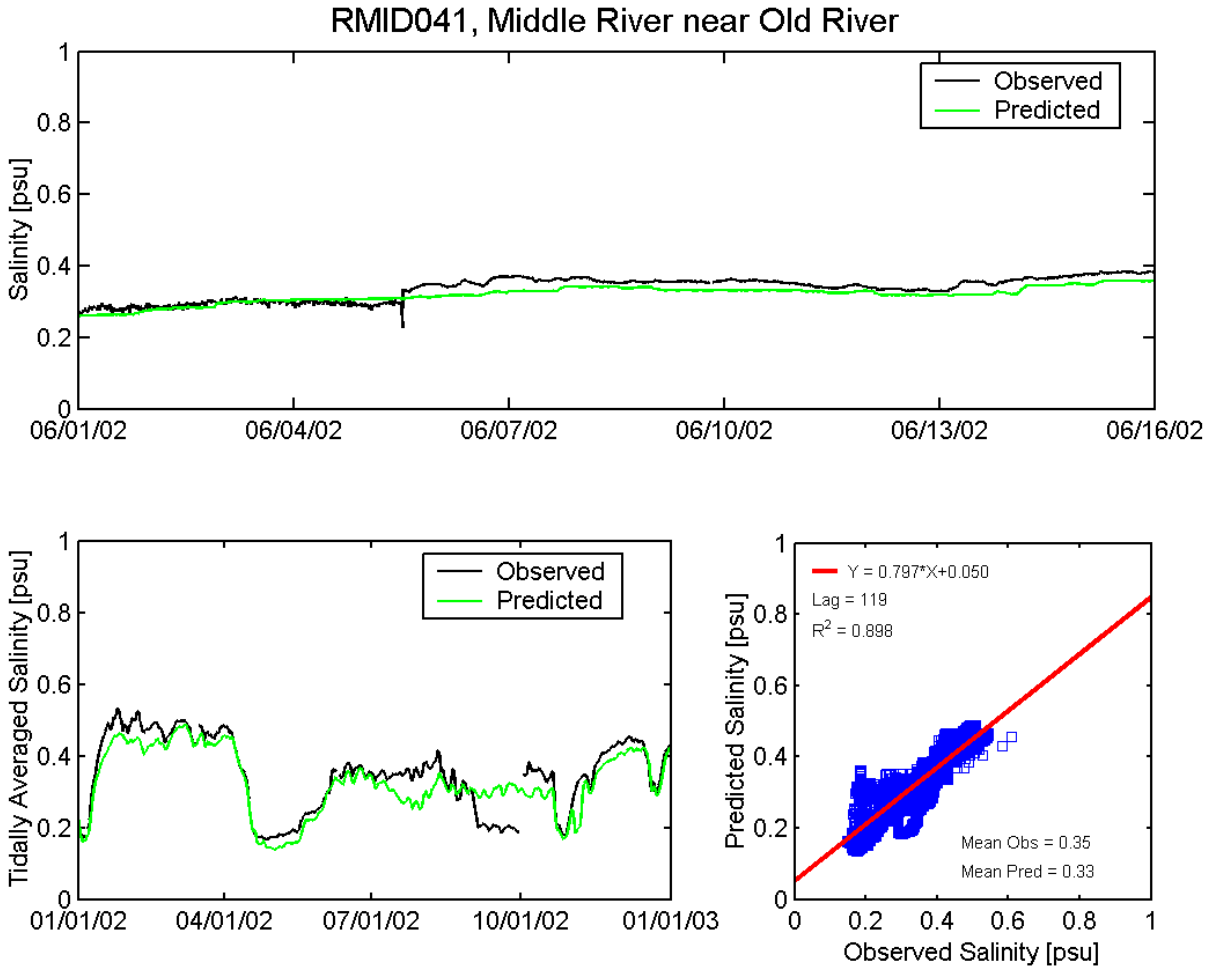

Figure A.6-61 Observed and predicted salinity at Middle River near Old River DWR station (RMID041) during the 2002 simulation period.

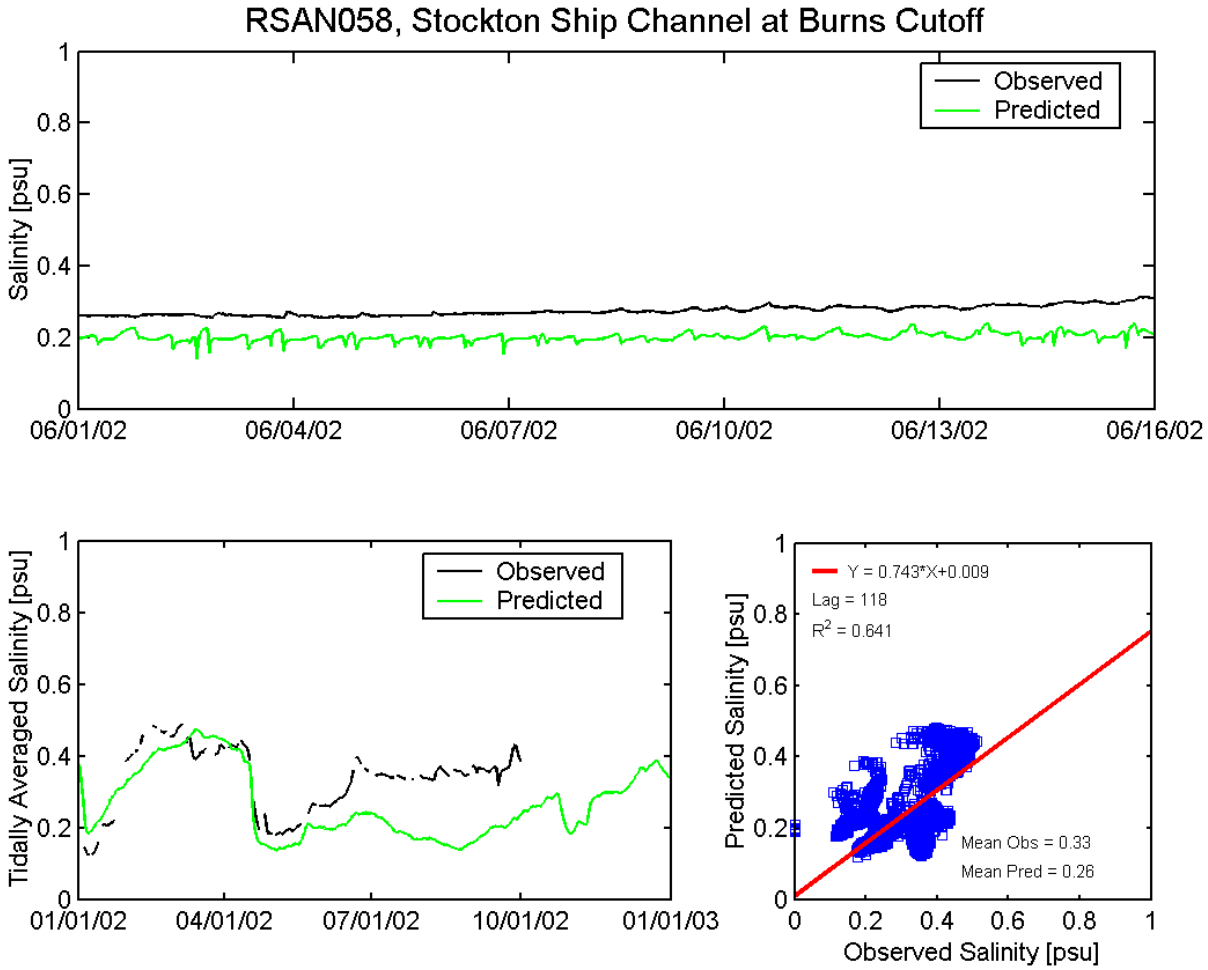

Figure A.6-62 Observed and predicted salinity at Stockton Ship Channel at Burns Cutoff DWR station (RSAN058) during the 2002 simulation period.

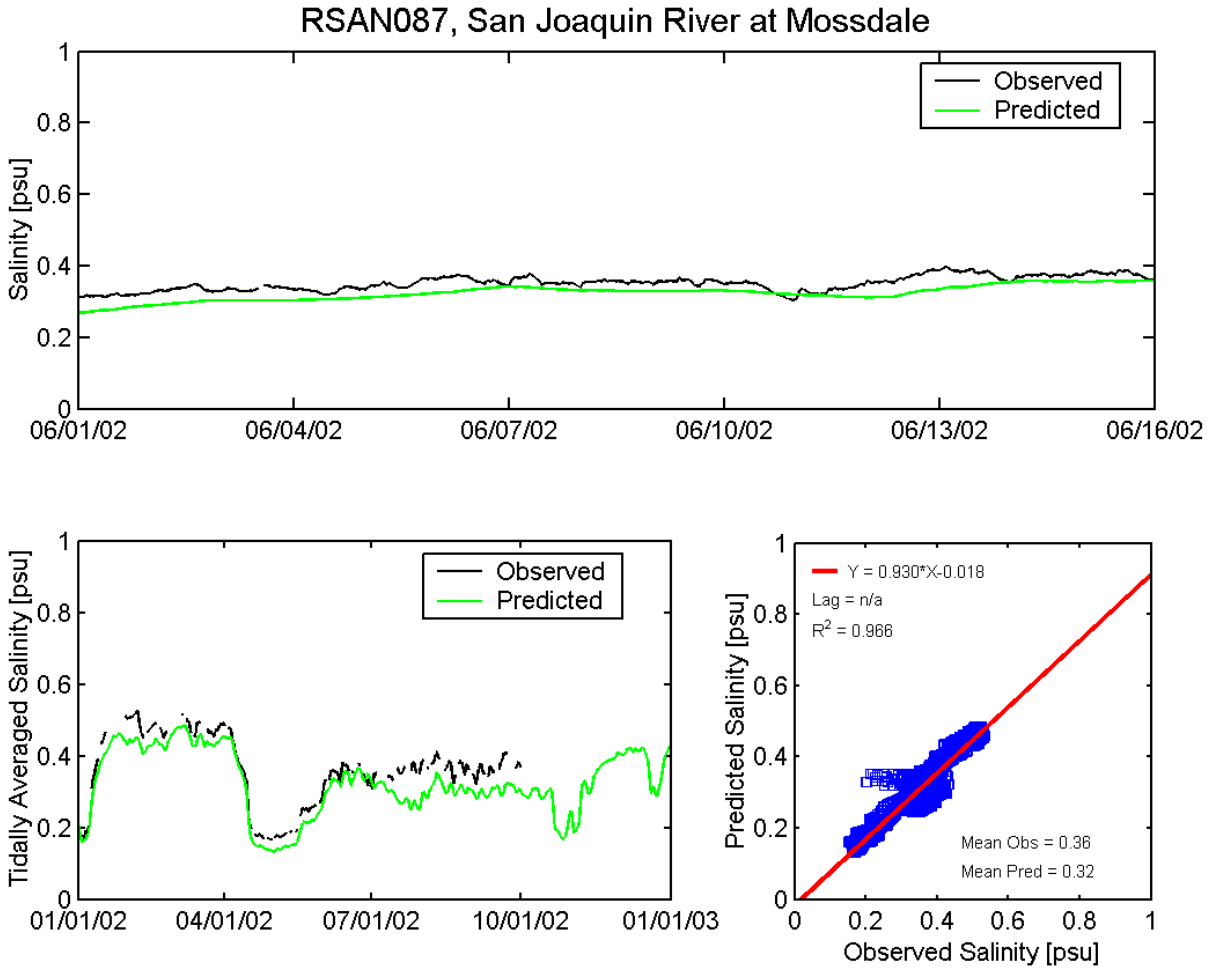

Figure A.6-63 Observed and predicted salinity at San Joaquin River at Mossdale DWR station (RSAN087) during the 2002 simulation period.